RRFM

EUROPEAN RESEARCH REACTOR CONFERENCE 2015

Conference Proceedings

Bucharest, Romania
19-23 April 2015

EUROPEAN NUCLEAR SOCIETY

ENS CONFERENCE

RRFM 2015 Silver Sponsor

EDF

organised in collaboration with:

IAEA
International Atomic Energy Agency

ASOCIAȚIA ROMÂNĂ "ENERGIA NUCLEARĂ"

European Nuclear Society
Avenue des Art 56
1000 Brussels, Belgium
Phone + 32 2 505 30 54
Fax +32 2 502 39 02
E-mail ens@euronuclear.org
Internet www.euronuclear.org

ISBN 978-92-95064-23-2

TABLE OF CONTENTS

International Topics

LEU Fuel Development & Qualification

RRFM2015-A0025	MICROSTRUCTURAL CHARACTERIZATION OF IRRADIATED U-7MO: REGIONS AROUND GRAIN BOUNDARIES AND REGIONS WITH DIFFERENT MO CONCENTRATIONS	Keiser, D. (1); Jue, J.-F. (1); Gan, J. (1); Miller, B. (1); Robinson, A. (1); Williams, W. (1); Medvedev, P. (1) 1 - Idaho National Laboratory, United States
RRFM2015-A0058	OPTIMIZATION OF A THIN U-10MO FUEL PLATE CASTING BY MODELING AND EXPERIMENT	Aikin, R. (1); Dombrowski, D. (1) 1 - Los Alamos National Laboratory, United States
RRFM2015-A0070	IMPROVEMENTS OF U-MO/AL DISPERSION FUEL PERFORMANCE	Kim, Y. S. (1); Jeong, G. Y. (2); Park, J. M. (3); Leenaers, A. (4) 1 - Argonne National Laboratory, United States 2 - Ulsan National Institute of Science and Technology, Korea, Republic of 3 - Korea Atomic Energy Research Institute, Korea, Republic of 4 - SCK-CEN, Belgium
RRFM2015-A0090	THE THERMAL PROPERTIES OF FRESH AND SPENT U-MO FUELS: AN OVERVIEW	Huber, T. (1); Breitkreutz, H. (1); Petry, W. (1); Reiter, C. (1); Elgeti, S. (2); Burkes, D. (3); Casella, A. (3); Casella, A. (3); Smith, F. (3); Wachs, D. (4) 1 - Forschungs-Neutronenquelle Heinz Maier-Leibnitz (FRM II), Technische Universität München, Germany 2 - Max-Planck-Institute for Plasma Physics, Germany 3 - Pacific Northwest National Laboratory, United States 4 - Idaho National Laboratory, United States
RRFM2015-A0099	THERMODYNAMIC AND KINETIC STUDY OF NITRIDES AND TRANSITION-METALS AS DIFFUSION BARRIERS FOR U-MO/AL DISPERSION FUEL	Mei, Z.-G. (1); Yacout, A. (1); Kim, Y. S. (1); Hofman, G. (1) 1 - Argonne National Laboratory, United States

RRFM2015-A0102	84 MEV XE IRRADIATION ON U-MO/AL DISPERATION FUEL	Ye, B. (1); Bhattacharya, S. (2); Mo, K. (1); Yun, D. (1); Mahomed, W. (1); Kim, Y. S. (1); Hofman, G. (1); Fortner, J. (1); Yacout, A. (1); Pellin, M. (1); Van den Berghe, S. (3); Leenaers, A. (3); Jamison, L. (1) 1 - Argonne national laboratory, United States 2 - Northwestern University, United States 3 - SCK CEN, Belgium
RRFM2015-A0146	THE POTENTIAL FOR DIFFERENCES IN AS-FABRICATED MONOLITHIC FUEL PLATE MICROSTRUCTURE TO AFFECT FUEL PERFORMANCE	Keiser, D. (1); Jue, J.-F. (1); Perez, E. (1); Rice, F. (1); Robinson, A. (1); Williams, W. (1); Meyer, M. (1) 1 - Idaho National Laboratory, United States
RRFM2015-A0052	FOUR-POINT BEND TESTING OF IRRADIATED MONOLITHIC U-10MO FUEL	Rabin, B. (1); Lloyd, R. (1); Schulthess, J. (1); Wright, J. (1); Lind, P. (1); Scott, L. (1); Wachs, K. (1) 1 - Idaho National Laboratory, United States
RRFM2015-A0179	UMO FUEL-POWDER PRODUCTION PROCESS AND RESULTS	Schenk, R. (1); Schauer, R. (1); Petry, W. (1); Stepnik, B. (2); Moyroud, C. (2); Grasse, M. (2); Coullomb, C. (2); Bourdat, G. (2); Jarousse, C. (2) 1 - Forschungs-Neutronenquelle Heinz Maier-Leibnitz (FRM II), Technische Universität München (TUM), Germany 2 - AREVA NP, France

Utilisation of Research Reactors

RRFM2015-A0028	NEUTRON SCATTERING IN VERY HIGH MAGNETIC FIELDSTHE NEW HYBRID MAGNET AT HELMHOLTZ CENTRE BERLIN	Smeibidl, P. (1); Bird, M. (2); Ehmler, H. (1); Prokhnenko, O. (1); Lake, B. (1) 1 - Helmholtz Centre Berlin, Germany 2 - National High Magnetic Field Laboratory, United States
RRFM2015-A0030	CHARACTERIZATION OF A QUASI-VERTICAL NEUTRON BEAM FROM THE BRAZILIAN TRIGA IPR-R1 REACTOR	Leal, A. (1); Guerra, B. (2); Lemos, B. (1) 1 - Centre for Development of Nuclear Technology (CDTN), Brazilian Nuclear Energy Commission (CNEN), Brazil 2 - Federal University of Minas Gerais, Dept. of Nuclear Engineering , Brazil
RRFM2015-A0043	RECENT IRRADIATION TESTS FOR FUTURE NUCLEAR SYSTEM AT HAHARO	Cho, M. S. (1); Choo, K. N. (1); Yang, S. W. (1); Park, S. J. (1) 1 - Korea Atomic Energy Research Institute (KAERI), Korea, Republic of
RRFM2015-A0050	EXPERIMENTAL POSSIBILITIES OF RESEARCH FAST REACTOR BOR-60	Kalygin, V. (1); Izhutov, A. (1); Krasheninnikov, Y. (1); Zhemkov, I. (1); Naboyshchikov, Y. (1); Varivtsev, A. (1) 1 - JSC "State Scientific Center Research Institute of Atomic Reactor", Russian federation
RRFM2015-A0161	OVERVIEW OF RESEARCH REACTOR UTILIZATION AND RELATED TECHNOLOGY DEVELOPMENT IN KAERI	Lim, I.-C. (1); Lee, C.-H. (1); Seong, B.-S. (1); Park, S.-J. (1); Lee, C.-S. (1) 1 - Korea Atomic Energy Research Institute, Korea, Republic of

RRFM2015-A0015	RESEARCH REACTORS FOR REGIONAL NUCLEAR EDUCATION: EXPANDING THE EASTERN EUROPEAN RESEARCH REACTOR INITIATIVE MODEL.	Ames, C. (1); Boeck, H. (2); Villa, M. (2); Vyshniauskas-Gomez, J. (1); Borio di Tigliole, A. (1); Bradley, E. (1); Sklenka, L. (3) 1 - Department of Nuclear Energy, International Atomic Energy Agency, Austria 2 - Atominstitut, Vienna University of Technology, Austria 3 - Department of Nuclear Reactor, Czech Technical University in Prague, Czech Rep.
RRFM2015-A0056	JULES HOROWITZ REACTOR: UPDATE OF THE EXPERIMENTAL CAPACITY	Blandin, C. (1); Jaecki, P. (1); Colin, C. (1); Dousson, T. (1); Ferry, L. (1); Pierre, J. (1); Gonnier, C. (1); Estrade, J. (1) 1 - CEA Cadarache/DEN/DER/SRJH, France
RRFM2015-A0084	ACTIVITIES AT TRIGA RC-1 ENEA REASERCH REACTOR	Falconi, L. (1); Innarella, C. (1); Palomba, M. (1); Carta, M. (1); Sepielli, M. (1) 1 - ENEA, Italy
RRFM2015-A0171	STATUS OF THE FLUORIDE SALT HIGH TEMPERATURE REACTOR MATERIALS IRRADIATION TESTS AT THE MIT RESEARCH REACTOR	Carpenter, D. (1); Ames, M. (1); Ostrovsky, Y. (1); Kohse, G. (1); Hu, L.-W. (1) 1 - Nuclear Reactor Laboratory, Massachusetts Institute of Technology, USA

Innovative Methods in Research Reactor Analysis and Design

RRFM2015-A0017	ESTIMATING BURNUP OF MTR FUEL USING THE LEAST SQUARE FITTING METHOD	Alawneh, L. (1); Khafaji, S. (1); Abu Saleem, K. (1); Park, C. J. (2) 1 - Jordan Atomic Energy Commission, Jordan 2 - Sejong University, Korea, Republic of
RRFM2015-A0029	VALIDATION OF THE MCNP6 MODEL AT THE ATOMINSTITUT TRIGA REACTOR	Cagnazzo, M. (1); Stummer, T. (1); Villa, M. (1); Böch, H. (1) 1 - Vienna University of Technology, Austria
RRFM2015-A0035	BR2 REACTOR COUPLED MCNPX & MURE SIMULATIONS FOR THE SOLID EXPERIMENT	Giot, L. (1); Fallot, M. (1); Kalcheva, S. (2); Koonen, E. (2) 1 - SUBATECH, Ecole des Mines de Nantes - CNRS/IN2P3 - Université de Nantes, France 2 - SCK.CEN, BR2 Reactor Department, Belgium
RRFM2015-A0037	THERMAL HYDRAULIC AND NEUTRON KINETIC SIMULATION OF THE TRIGA IPR-R1 RESEARCH REACTOR USING A RELAP5-PARCS COUPLED MODEL	A. l. Reis, P. (1); Pereira, C. (1); González-Mantecón, J. (1); L. Costa, A. (1); F. Veloso, M. A. (1); V. Soares, H. (1); Miró , R. (2) 1 - UNIVERSIDADE FEDERAL DE MINAS GERAIS, Brazil 2 - UNIVERSITAT POLITÈCNICA DE VALÈNCIA, Spain
RRFM2015-A0038	THERMAL-HYDRAULIC SIMULATION OF SINGLE PIN AND ASSEMBLY SECTOR GEOMETRIES FOR THE IVG.1M RESEARCH REACTOR	Kraus, A. (1); Garner, P. (1); Hanan, N. (1) 1 - Argonne National Laboratory, United States
RRFM2015-A0049	IAEA CRP ON "BENCHMARKS OF COMPUTATIONAL TOOLS AGAINST EXPERIMENTAL DATA ON FUEL BURNUP AND MATERIAL ACTIVATION FOR UTILIZATION, OPERATION AND SAFETY ANALYSIS OF RESEARCH REACTORS": UPDATE AFTER THE FIRST RESEARCH COORDINATION MEETING	Ridikas, D. (1); Marshall, F. (2); Kennedy, W. (3) 1 - NA/IAEA, Austria 2 - NE/IAEA, Austria 3 - NS/IAEA, Austria
RRFM2015-A0051	PROPAGATION OF UNCERTAINTY FROM FINE-GROUP CROSS-SECTION DATA THROUGH LATTICE PHYSICS CALCULATIONS FOR THE SAFARI-1 RESEARCH REACTOR	Groenewald, S. (1); Bokov, P. (1) 1 - South African Nuclear Energy Corporation (Necsa), South Africa

RRFM2015-A0055	SAFETY ANALYSIS ON BRAZILIAN MULTIPURPOSE REACTOR USING THE RELAP5-3D CODE	V. Soares, H. (1); González-Mantecón, J. (1); L. Costa, A. (1); Pereira, C. (1); A. l. reis, P. (1); F. Veloso, M. A. (1); D. Aronne, I. (2) 1 - UNIVERSIDADE FEDERAL DE MINAS GERAIS, Brazil 2 - CENTRO DE DESENVOLVIMENTO DA TECNOLOGIA NUCLEAR CDTN/CNEN, Brazil
RRFM2015-A0071	A FULL CORE HOMOGENIZATION APPROACH USING SERPENT AS A CROSS SECTION GENERATION TOOL FOR THE OSCAR-4 CODE SYSTEM	Erasmus, B. (1); Prinsloo, R. (1); Van Heerden, F. (1); Groenewald, S. (1); Jacobs, C. (1); Mashau, M. (2) 1 - South African Nuclear Energy Corporation (Necsa), South Africa 2 - University of Johannesburg, South Africa

RRFM2015-A0123	NEUTRONIC ANALYSIS OF MTR REACTOR CORE USING MONTE CARLO TECHNIQUES	Khan, R. (1); Ali, R. (1); Boeck, H. (2); Stummer, T. (2) 1 - Pakistan Institute of Engineering and Applied Sciences (PIEAS), Pakistan 2 - Vienna University of Technology/Atominstitute , Austria
RRFM2015-A0135	ASSESSMENT OF THE BURNOUT PHENOMENON IN THE SAFARI-1 RESEARCH REACTOR	Belal, M. (1); D'arcy, A. (1) 1 - South African nuclear energy corporation, South Africa

LEU Fuel Fabrication & Conversion

RRFM2015-A0106	FABRICATION OF PIN-TYPE MINI-ELEMENTS CONTAINING U-MO/MG DISPERSION FUEL FOR TEST IRRADIATION IN NRU	Wang, N. (1); Kulakov, M. (2); Hibbins, S. (1) 1 - Canadian Nuclear Laboratories - Nuclear Fuel Fabrication Facility, Canada 2 - Canadian Nuclear Laboratories - Fuel Development, Canada

RRFM2015-A0167	UMO FOIL FABRICATION DEMONSTRATION LINE AT BABCOCK & WILCOX	Johnson, R. E. (1); Navolio, D. W. (1); Wight, J. M. (1) 1 - Babcock & Wilcox, Nuclear Operations Group, United States

Moly99 production

RRFM2015-A0079	THE ROLE OF THE IAEA IN SUPPORTING PRODUCTION OF MO-99 AND/OR TC-99M WITHOUT THE USE OF HEU	Osso Junior, J. A. (1); Venkatesh, M. (1); Duatti, A. (1); Dix, J. (1); Bradley, E. (1) 1 - International Atomic Energy Agency - IAEA, Austria
RRFM2015-A0085	U.S. DEPARTMENT OF ENERGY NATIONAL LABORATORY RESEARCH AND DEVELOPMENT ACTIVITIES DIRECTED TOWARD MINIMIZING THE USE OF HIGH ENRICHED URANIUM FOR MO-99 PRODUCTION AND DEVELOPING A DOMESTIC SUPPLY	Vandegrift, G. (1) 1 - Argonne National Laboratory, United States
RRFM2015-A0088	Mo-99 PRODUCTION AT FRM II – STATUS OF THE PROJECT	Müller, C. (1); Gerstenberg, H. (1); Röhrmoser, A. (1); Kastenmüller, A. (1) 1 - Technische Universität München, ZWE FRM II, Germany
RRFM2015-A0118	COATING OF LEU FOIL WITH ELECTRODEPOSITED NICKEL FOR Mo-99 PRODUCTION	Lisboa, J. (1); Olivares, L. (1); Marin, J. (1); Barrera, M. (1) 1 - Chilean Commission for Nuclear Energy, Chile
RRFM2015-A0163	STATUS AND FUTURE OF MO-99 SUPPLY	Ponsard, B. (1) 1 - SCK.CEN - BR2 REACTOR, Belgium

LEU Fuel Conversion

RRFM2015-A0136	CONVERSION STUDY FOR FRM II WITH BACKUP FUEL U3SI2	Röhrmoser, A. (1) 1 - Technische Universität München, Germany
RRFM2015-A0139	REPLACEMENT FUEL FOR THE VIENNA AUSTRIA TRIGA RESEARCH REACTOR	Luke, D. (1); Robb, A. (1) 1 - CH2M*Washington Group Idaho, LLC (CWI), United States
RRFM2015-A0174	THE PHYSICS EXPERIMENTAL STUDY FOR PROTOTYPE MNSR WITH LEU CORE	Li, Y. (1); Peng, D. (1); Wu, X. (1); Zou, S. (1); Lu, J. (1); Zhang, Y. (1); Hao, Q. (1) 1 - China Institute of Atomic Energy , China

Safety and Security of Research Reactors

RRFM2015-A0024	ENHANCEMENT OF THE SAFETY REQUIREMENTS FOR RESEARCH REACTOR FACILITIES IN THE LIGHT OF THE ACCIDENT AT THE FUKUSHIMA DAIICHI NUCLEAR POWER PLANT	Poliakov, D. (1) 1 - Scientific Engineering Center for Nuclear and Radiation Safety, Russian federation

RRFM2015-A0074	SEISMIC IMPACT ON MARIA REACTOR REACTIVITY AND POWER CHANGES	Lipka, M. (1) 1 - National Centre for Nuclear Research, Poland
RRFM2015-A0087	A SAFETY ANALYSIS REPORT FOR THE CONVERSION OF THE NIST RESEARCH REACTOR	Diamond, D. (1); Baek, J.-S. (1); Hanson, A. (1); Cheng, L.-Y. (1); Cuadra, A. (1); Brown, N. (1) 1 - Brookhaven National Laboratory, United States
RRFM2015-A0153	LESSONS LEARNED FROM HIGHLY ENRICHED URANIUM SOLIDIFICATION AND SHIPMENT PROJECT	Pfennigwerth, G. (1); Andes, T. (1); Di gasbarra , F. (2); Proietti , A. (2) 1 - Y-12 National Security Complex, United States 2 - Societa' Gestione Impianti Nucleari, Italy

Back-end of the Fuel Cycle

RRFM2015-A0004	6 YEARS OPERATION OF THE NCS 45 PACKAGE FOR IRRADIATED FUEL RODS	Lefebvre, P. (1); Hilbert, F. (1) 1 - DAHER-NCS, Germany
RRFM2015-A0012	COATINGS TO PROTECT SPENT ALUMINIUM-CLAD RESEARCH REACTOR FUEL DURING WET STORAGE	Fernandes, S. M. (1); Correa, O. (1); De souza, J. A. (1); Ramanathan, L. (1); Antunes, R. (2); Oliveira, M. (3) 1 - Instituto de Pesquisas Energéticas e Nucleares, Brazil 2 - Engineering, Modeling and Applied Social Sciences Center (CECS), Federal University of ABC, Brazil 3 - Electrocell Ind. Com. Equip. Elet. LTDA, CIETEC, Brazil
RRFM2015-A0086	IAEA CRP ON "OPTIONS AND TECHNOLOGIES FOR MANAGING THE BACK END OF THE RESEARCH REACTOR NUCLEAR FUEL CYCLE" CURRENT STATUS	Marshall, F. (1); Ames , C. (1); Gouzy-portaix, S. (1); Mayer, S. (1) 1 - International Atomic Energy Agency, Austria
RRFM2015-A0093	STATUS ON SILICIDE FUEL REPROCESSING AT AREVA LA HAGUE	Domingo, X. (1); Valery, J.-F. (1); Landau, P. (1); Alameda angulo, C. (2); Pechard, C. (1); Laloy, V. (3) 1 - AREVA NC, France 2 - AREVA E&P, France 3 - AREVA TN, France

RRFM2015-A0054	REMOVAL OF FRESH HEU TRIGA FUEL	Wilhoit, B. (1); Andes, T. (1); Hanlon, T. (1) 1 - Y-12 National Security Complex , United States
RRFM2015-A0089	HANDLING THE TYPE C PACKAGE TUK-145/C DURING SPENT FUEL REMOVAL FROM DNRI RESEARCH REACTOR, VIETNAM	Ivashchenko , A. (1); Komarov, S. (1); Kashkirov, S. (1); Dien, N. N. (2); Moses, S. (3) 1 - SOSNY R&D Company, Russian federation 2 - Dalat Nuclear Research Institute , Vietnam 3 - Oak-Ridge National Laboratory, United States
RRFM2015-A0091	AVAILABLE REPROCESSING AND RECYCLING SERVICES FOR RESEARCH REACTOR SPENT NUCLEAR FUEL - A NEW IAEA REPORT	Budu, M. (1); Bradley, E. (2); Adelfang, P. (2); Marshall, F. (2); Tozser, S. (2); Chiguer, M. (3) 1 - SOSNY R&D Company, Russian Fed. 2 - International Atomic Energy Agency, Austria 3 - AREVA, France
RRFM2015-A0103	AREVA TN TRANSPORTS AND LOGISTICS ACTIVITIES -FLEET OF TRANSPORT CASKS FOR INTERNATIONAL SHIPMENTS IN SUPPORT OF RESEARCH REACTOR AND LABORATORIES	Guibert, N. (1); Thomas, J. (1); Laloy, V. (2) 1 - AREVA TN Americas, United States 2 - AREVA TN Europe, France
RRFM2015-A0141	DESCRIPTION OF THE PROCESS FOR FUTURE RETURNS OF IRRADIATED TRIGA FUEL FROM RESEARCH REACTORS TO IDAHO	Luke, D. (1); Robb, A. (1) 1 - CH2M*Washington Group (CWI), LLC, United States
RRFM2015-A0147	REMOVAL OF LEGACY PLUTONIUM MATERIALS FROM RESEARCH FACILITIES IN ITALY	Di Gasbarro, F. (1); Proietti, A. (1); Iyer, N. (2); Dunn, K. (2); Hackney, E. (2); Dickerson, S. (3) 1 - SOGIN S.p.A, Italy 2 - Savannah River National Laboratory, USA 3 - U.S. Department of Energy - National Nuclear Security Administration, USA

Decommissioning and dismantling of research reactors and waste management

RRFM2015-A0016	THE DISMANTLING OF THE MONTECUCCOLINO RB3 RESEARCH REACTOR: RADIOLOGICAL CHARACTERISATION OF MATERIALS FOR FREE RELEASE	Capone, M. (1); Cherubini, N. (1); Compagno, A. (1); Dodaro, A. (1); Rocchi, F. (1) 1 - ENEA, Italy
RRFM2015-A0046	THE DECOMMISSIONING PROGRAM OF THE RESEARCH REACTOR RTS-1 "G. GALILEI - ITALY"	Baldassarre, L. (1); Russo, M. (2); Dodaro, A. (1); Cimini, E. (2) 1 - Nucleco SpA, Italy 2 - Interforce Center for Studies and Military Applications (CISAM), Italy
RRFM2015-A0092	DECOMMISSIONING THE IFIN-HH VVR-S NUCLEAR RESEARCH REACTOR DISMANTLING THE PRIMARY COOLING CIRCUIT	Dragusin, M. (1); Zorliu, A. (1); Deju, R. (1); Dragolici, C. A. (1); Mincu, I. (1); Stanga, D. (1); Gurau, D. (1); Petran, C. (1); Stoian, I. (1); Mustata, C. (1) 1 - National Institute for R&D in Physics and Nuclear Enginering-Horia Hulubei-IFIN-HH, Romania
RRFM2015-A0119	LEGAL AND CONTRACTUAL FRAMEWORK FOR SPENT FUEL BACK-END MANAGEMENT IN CONNECTION TO THE DECOMMISSIONING OF THE FINNISH TRIGA FIR 1	Auterinen, I. (1) 1 - VTT Technical Research Centre of Finland, Finland
RRFM2015-A0148	SAFETY REGULATION OF DECOMMISSIONING OF NUCLEAR RESEARCH FACILITY IN RUSSIA	Sapozhnikov, A. (1) 1 - Federal Environmental, Industrial and Nuclear Supervision Service of Russia, Russian Federation

Research Reactor Operation and Maintenance

RRFM2015-A0003	NEW CORE CONFIGURATIONS FOR THE IPEN/CNEN-SP IEA-R1 RESEARCH REACTOR USING HIGHER DENSITY FUELS	Garcia Joao, T. (1); Rossi, P. (1); Teixeira e Silva, A. (1) 1 - IPEN/CNEN-SP, Brazil
RRFM2015-A0014	EFFECT OF THERMAL GRADIENT ON IN REACTOR OXIDATION OF MTR FUEL PLATES.	Valdez Tordoya, D. (1); Haddad Andalaf, R. (1) 1 - CNEA, Argentina
RRFM2015-A0081	SAFARI-1 POOL LINER LEAKS	Steynberg, B. (1) 1 - SAFARI-1 Research Reactor, South African Nuclear Energy Corporation, South Africa
RRFM2015-A0126	INTERNET PRACTICAL COURSES FROM THE ISIS RESEARCH REACTOR	Foulon, F. (1); Lescop, B. (1); Badeau, G. (1); Ivanovic, S. (1); Wohleber, X. (1); Huot, N. (1) 1 - CEA, France

RRFM2015-A0133	MANUFACTURING CONDITIONS OF FRENCH REACTOR PRESSURE VESSEL STEELS TO AVOID THE OCCURRENCE OF FLAKES	Buisine, D. (1); Champigny, F. (1); Miller, C. (1); Frund, J.-M. (1); Berger, T. (2); Joly, P. (2) 1 - Electricité de France, CEIDRE, France 2 - AREVA NP, France
RRFM2015-A0159	MODERNIZATION OF I&C SYSTEMS IN NUCLEAR RESEARCH REACTORS	Avila, A. (1) 1 - INVAP S.E., Instrumentation & Control Department, Argentina

New Research Reactor Projects

RRFM2015-A0013	OYSTER REACTOR UPGRADE PROJECT: COLD NEUTRONS FOR COOL SCIENCE	Molag, A. (1); Kaaijk, C. (1) 1 - Reactor Institute Delft, Technical University Delft, Netherlands
RRFM2015-A0032	THE JULES HOROWITZ REACTOR: A NEW HIGH PERFORMANCE MTR (MATERIAL TESTING REACTOR) WORKING AS AN INTERNATIONAL USER FACILITY IN SUPPORT TO NUCLEAR INDUSTRY, PUBLIC BODIES ANDRESEARCH INSTITUTES	Estrade, J. (1); Bignan, G. (1); Bravo, X. (1) 1 - French Atomic Energy and Alternatives Energies Commission, France
RRFM2015-A0039	THE TUNISIAN SUBCRITICAL ASSEMBLY PROJECT: PRELIMINARY MONTE CARLO RESULTS OF A FIRST PROPOSAL CORE DESIGN	Dridi, W. (1); Romdhani, I. (1); Benismaïl, A. (1) 1 - National Center of Nuclear Sciences and Technology, Tunisia
RRFM2015-A0082	IAEA INTEGRATED RESEARCH REACTOR INFRASTRUCTURE ASSESSMENT (IRRIA) MISSION	Borio di Tigliole, A. (1); Bradley, E. (1); Shokr, A. (2); Ridikas, D. (3) 1 - International Atomic Energy Agency - Research Reactor Section (NEFW-NE), Austria 2 - International Atomic Energy Agency - Research Reactor Safety Section (NSNI-NS), Austria 3 - International Atomic Energy Agency - Physics Section (NAPC-NA), Austria
RRFM2015-A0143	BUILDING CAPABILITIES FOR NEW REACTORS	Pavel, G. L. (1); Ghitescu, P. (1); Fosca, D. G. (2) 1 - University Politehnica of Bucharest, Romania 2 - Research Centre Rez, Czech Republic
RRFM2015-A0158	NEUTRONIC DESIGN OF THE COQUI REACTOR	Ferraro, D. (1); Boschetti, F. (2); Villarino, E. (2); Sardella, F. (2) 1 - INVAP S.E., Nuclear Engineering Department, Buenos Aires, Argentina 2 - INVAP S.E., Nuclear Engineering Department, Rio Negro, Argentina
RRFM2015-A0164	DESIGNS OF MEDICAL ISOTOPE PRODUCTION FACILITIES	Mazufri, C. M. (1) 1 - INVAP S.E., Nuclear Project Division, Argentina

Poster

RRFM2015-A0021	MULTI-CHANNEL THERMAL HYDRAULIC ANALYSIS OF PLATE TYPE RESEARCH REACTOR	Albati', M. (1); Alkhafaji, S. (1); Abusaleem, K. (2); Jo, D. (3); Alfandi, A. (1) 1 - Jordan Atomic Energy Commission (JAEC), Jordan 2 - The University of Jordan, Jordan 3 - Kyungpook National University, Korea, Republic of
RRFM2015-A0022	DEVELOPMENT OF PERFORMANCE ANALYSIS CODE FOR RESEARCH REACTOR FUEL	jeong, G. Y. (1); Sohn, D.-S. (1); Lee, K. H. (2); Park, J. M. (2) 1 - Ulsan National Institute of Science and Technology, 50 UNIST-gil, Eonyang-eup, Korea, Republic of 2 - Korea Atomic Energy Research Institute, Korea, Republic of
RRFM2015-A0027	EVALUATION OF PERFORMED EXPERIMENTS ON FAST MULTIPLYING SYSTEMS WITH HEU FUEL FOR RECEIVING BENCHMARK DATA ON CRITICALITY	Sikorin, S. (1); Mandzik, S. (1); Polazau, S. (1); Kuzmin, A. (1); Damarad, Y. (1); Soltan, I. (1) 1 - The Joint Institute for Power and Nuclear Research – Sosny of the National Academy of Sciences of Belarus, Belarus
RRFM2015-A0034	JRTR INITIAL CRITICALITY CALCULATIONS AND NUCLEAR COMMISSIONING TESTS	Jaradat, M. (1); Alkhafaji, S. (1); Abu saleem , K. (1); Park, C. J. (2) 1 - Jordan Atomic Energy Commission, Jordan 2 - Korea Atomic Energy Research Institute, Korea, Republic of
RRFM2015-A0047	A COMPREHENSIVE ANALYSIS OF THE TECHNICAL FEASIBILITY OF THE MIR RESEARCH REACTOR CONVERSION TO LOW-ENRICHED URANIUM FUEL	Izhutov, A. (1); Starkov, V. (1); Pimenov, V. (1); Maynskov, S. (2); Osipova, T. (2); Uzikov, V. (1); Fedoseev, V. (1) 1 - JSC "SSC Research Institute of Atomic Reactors", Russian federation 2 - National Nuclear University MEPhI (Moscow Engineering Physics Institute), Russian Federation
RRFM2015-A0053	NEUTRONIC COMPARISON OF HIGH DENSITY FUELS (U-MO-AL AND U3SI2-AL) FOR RESEARCH REACTORS	Oliveira rondon muniz, R. (1); Teixeira e silva, A. (1); Borges domingos, D. (1); Dos santos, A. (1); Yamaguchi, M. (1) 1 - IPEN/CNEN-SP, Brazil
RRFM2015-A0057	COMPARISON OF LOW ENRICHED URANIUM (UALX-AL AND U-NI) TARGETS WITH DIFFERENT GEOMETRIES FOR THE PRODUCTION OF MOLYBDENUM-99	Teixeira e silva, A. (1); Borges domingos, D. (1); Garcia joão, T. (1); Oliveira rondon muniz, R. (1) 1 - IPEN/CNEN-SP, Brazil

RRFM2015-A0059	NEUTRONIC AND THERMAL-HYDRAULICS CALCULATIONS FOR THE PRODUCTION OF MOLYBDENUM-99 BY FISSION IN LOW ENRICHED URANIUM UALX-AL TARGETS	borges domingos, D. B. D. (1); Teixeira e silva, A. (1); Garcia joão, T. (1); J.B. de o. Nishiyama, P. (2); Giovedi, C. (2) 1 - IPEN-CNEN/SP, Brazil 2 - CTMSP, Brazil
RRFM2015-A0060	LOW ENRICHED URANIUM FOIL TARGETS WITH DIFFERENT GEOMETRIES FOR THE PRODUCTION OF MOLYBDENUM-99	Borges Domingos, D. (1); Teixeira e Silva, A. (1); Garcia João, T. (1) 1 - IPEN/CNEN-SP, Brazil

RRFM2015-A0063	HORUS3D NEUTRON CALCULATION TOOL DEDICATED TO JHR DESIGN AND SAFETY STUDIES – DEVELOPMENT, VALIDATION, BIASES AND UNCERTAINTIES QUANTIFICATION	Vaglio-gaudard, C. (1); Jeury, F. (1); D'aletto, C. (1); Vidal, J.-F. (1); Vidal, J.-M. (1); Gaubert, L. (1); Politello, J. (1) 1 - CEA, France

RRFM2015-A0066	UNCERTAINTY ASSESSMENT FOR REACTIVITY INDUCED ACCIDENT OF 5-MW POOL-TYPE RESEARCH REACTOR	Yum, S. (1); Park, S. (1) 1 - Korea Atomic Energy Research Institute, Korea, Republic of
RRFM2015-A0072	CONTRIBUTIONS TO PROBABILISTIC SAFETY ASSESSMENT STUDIES FOR TRIGA RESEARCH REACTORS	Mladin, D. (1); Mladin, M. (1) 1 - Institute for Nuclear Research, Romania
RRFM2015-A0073	INVESTIGATING THE SETUP FOR IRRADIATION OF MATERIAL SAMPLES IN TRIGA ROMANIA	Mladin, M. (1); Dulugeac, S. (1); Budriman, G. (1); Barbos, D. (1); Ciocanescu, M. (1) 1 - Institute for Nuclear Research, Romania
RRFM2015-A0075	STUDY OF MOLYBDENUM-99 PRODUCTION POSSIBILITIES IN TRIGA 14 MW REACTOR	Dulugeac, S. (1); Mladin, M. (1); Budriman, G. (1) 1 - Institute for Nuclear Research, Romania
RRFM2015-A0076	THE 14 MEV NEUTRON IRRADIATION FACILITY IN MARIA REACTOR	Prokopowicz, R. (1); Pytel, K. (1); Dorosz, M. (1); Zawadka, A. (1); Lechniak, J. (1); Lipka, M. (1); Marcinkowska, Z. (1); Wierzchnicka, M. (1); Małkiewicz, A. (1); Wilczek, I. (1); Krok, T. (1); Migdal, M. (1); Kozieł, A. (1) 1 - National Centre for Nuclear Research, Poland

RRFM2015-A0094	OVERVIEW ON A RRSF REPROCESSING, FROM SPENT FUEL EVACUATION TO VITRIFIED RESIDUES STORAGE	Domingo, X. (1); Valery, J.-F. (1); Landau, P. (1); Dupeyrat, A. (1); Deschamps, P. (1); Pechard, C. (1); Laloy, V. (2); Kalifa, M. (2) 1 - AREVA NC, France 2 - AREVA TN, France

RRFM2015-A0104	COMPARISON BETWEEN U(Mo)/Al(Si) MINIPLATE AND U3Si2/Al MINIPLATE AFTER THE SAME FABRICATION PROCESS.	Mirandou, M. (1); Aricó, S. (1); Balart, S. (1); Fabro, J. (1); Podestá, D. (1) 1 - Comisión Nacional de Energía Atómica , Argentina

RRFM2015-A0130	ANALYSIS OF MICROSTRUCTURE AND PRECIPITATIONS IN THE U-ZR METALLIC FUEL	Lee, C.-T. (1); Kim, H. L. (1) 1 - Korea Atomic Energy Research Institutes (KAERI), Korea, Republic of

RRFM2015-A0145	NEUTRONIC COMPARISON OF RELAP5-3D AND MCNP5 MODELS FOR THE TRIGA IPR-R1	A. F. Mesquita, P. (1); L. Costa, A. (1); A. M. Silva, C. (1); A. l. Reis, P. (1); Pereira, C. (1); F. Veloso, M. A. (1); V. Soares, H. (1) 1 - UNIVERSIDADE FEDERAL DE MINAS GERAIS, Brazil
RRFM2015-A0166	TRANSPORT OF IRRADIATED FUEL RODS AND SEGMENTS OF IRRADIATED FUEL RODS	Boeckx, W. (1) 1 - Transnubel, Belgium

RRFM2015-A0173	Y-12 NATIONAL SECURITY COMPLEX U-MO FABRICATION	Gambrell, M. (1); Langham, C. (1); Moore, A. (1); Demint, A. (1); Henkel, J. (1); Longmire, H. (1) 1 - Y-12 National Security Complex, United States

International Topics

IAEA DESIGNATED INTERNATIONAL CENTRE BASED ON RESEARCH REACTOR (ICERR)

A. BORIO DI TIGLIOLE*, E. BRADLEY,
M. KHOROSHEV, F. MARSHALL,
C. MORRIS, S. TOZSER.

Research Reactor Section
Division of Nuclear Fuel Cycle and Waste Technology
Department of Nuclear Energy
International Atomic Energy Agency
PO Box 100, Vienna, AUSTRIA

*Corresponding author: A.Borio@iaea.org

ABSTRACT

The IAEA designated "International CEntre based on Research Reactor" (ICERR) scheme, recently developed by the IAEA, is intended to enable IAEA Member States to gain timely access to relevant nuclear infrastructure based on research reactors. ICERRs will make available their research reactors and ancillary facilities and resources to organizations/institutions of IAEA Member States seeking access to such nuclear infrastructure (named Affiliates). For Affiliates, ICERRs will provide an opportunity to access research reactor capabilities much sooner and, probably, at a lower cost.

The implementation of the ICERR scheme will also contribute to enhance the utilization of some existing research reactor facilities and, by fostering wider utilization in cooperative manner of research reactors and associated facilities capabilities, could also effectively contribute to the development and deployment of innovative nuclear technologies.

1. INTRODUCTION

Many International Atomic Energy Agency (IAEA) Member States are initiating or increasing their interest in the broader applications of nuclear science and technology, including nuclear power. They typically develop national competencies as well as a framework of research and development (R&D) strategies along with plans to effectively support implementation. To achieve these goals, they often require access to research reactor (RR) facilities to conduct nuclear R&D projects and to educate and train the young generation of nuclear scientists, engineers, and technicians. Accessing such facilities can present significant challenges for IAEA Member States without RRs. Though access to such nuclear infrastructure at various research organizations and/or universities is available, it is often both expensive and cannot be quickly realized.

World-wide there are RRs facilities that have established long-standing nuclear R&D and capacity building programmes at an international/regional level. IAEA Member States' interest in nuclear science and technology programmes, as well as the expected growth of nuclear power programmes, could benefit from the direct use of these facilities, as well as

from the expertise of their staff, from the processes and practices which have been established and adopted to operate these facilities, and from continued and/or expanded international collaboration to more fully exploit the combined infrastructure.

The IAEA designated “International CEntre based on Research Reactor” (ICERR) scheme is intended to enable IAEA Member States to gain timely access to relevant nuclear infrastructure based on RRs. ICERRs will make available their RRs, ancillary facilities (AFs), and resources to organizations/institutions of IAEA Member States seeking access to such nuclear infrastructure (named Affiliates). For Affiliates, ICERRs will provide an opportunity to access RR capabilities much sooner and, probably, at a lower cost.

An IAEA Member State organization and/or institution is eligible to be designated by the IAEA as ICERR if it operates or is constructing one or more RR(s) and it can demonstrate experience in hosting activities based on the RR with significant international/regional participation. The criteria for designation address logistical capability, technical capability and sustainability. To enhance the collaboration among ICERRs, a network will be established by the IAEA (named ICERRNet).

The implementation of the ICERR scheme will also contribute to enhance the utilization of some existing RR facilities and, by fostering wider utilization in cooperative manner of RRs and associated facilities capabilities, could also effectively contribute to the development and deployment of innovative nuclear technologies.

2. The ICERR scheme

The principal objective of the ICERR scheme is to recognize and incentivise the following outcomes:

1. To make available existing RRs and their AFs to IAEA Member States that don’t have access to such nuclear infrastructure;
2. To provide a scientific hub for IAEA Member States (operating RRs or not) to support nuclear R&D and capacity building objectives relevant to their identified national priorities;
3. To improve accessibility of existing RRs and thereby optimizing the need for new RRs and/or orienting the IAEA Member States for appropriate facility investments;
4. To facilitate joint activities of IAEA Member States targeting the development of innovative nuclear technologies for various applications;
5. To enhance the utilization of existing RRs while supporting IAEA Member States to develop their nuclear R&D and capacity building programmes.

ICERRs are IAEA Member States organizations and/or institutions operating or constructing one or more RR(s) and AFs that, upon request, have been designated by the IAEA on the basis of established criteria.

The ICERR designation is limited to area(s) of activities (e.g. education and training, reactor physics, neutron beams science, material testing, operation & maintenance, facility

management, emergency preparedness and response, etc.) in which the compliance with the designation criteria is demonstrated.

To enhance the collaboration among ICERRs, a network will be established by the IAEA (named ICERRNet); the network will allow ICERRs to share experience and lessons learned, to coordinate and to rationalize their offer of facilities, resources and services to interested IAEA Member States; the platform will also be a gateway to exchange information between ICERRs, Affiliates, and the IAEA.

The ICERR-Affiliate relationship is established on contractual basis (commercial or in-kind) through a bilateral agreement. The IAEA, upon request, may provide support to an Affiliate, including financial and/or for the identification and selection of the ICERR, through IAEA established mechanisms and according to the IAEA rules and regulations; in this case, ICERR-Affiliate relationship remains on bilateral agreement and the IAEA doesn't own any legal and financial liability.

ICERR designation/re-designation process is at ICERR candidate's own cost, including the costs for the meeting of the Selection Committee and of the assessment mission at ICERR candidate's site; where the IAEA established mechanisms permit, the IAEA, upon request, may provide financial support for the designation of an ICERR according to the IAEA rules and regulations.

In the ICERR scheme (see Fig. 1), the functions of the IAEA are the following:

- Facilitator in the development of the relationship between an ICERR and Affiliates (e.g., through a dedicated web-based platform);
- Facilitator in fostering the collaboration among ICERRs (e.g., promoting and supporting ICERRNet);
- Promoter for enhancing utilization of existing RR facilities;
- Designating body responsible for ensuring that an ICERR candidate meets the establish criteria for the ICERR designation (and re-designation).

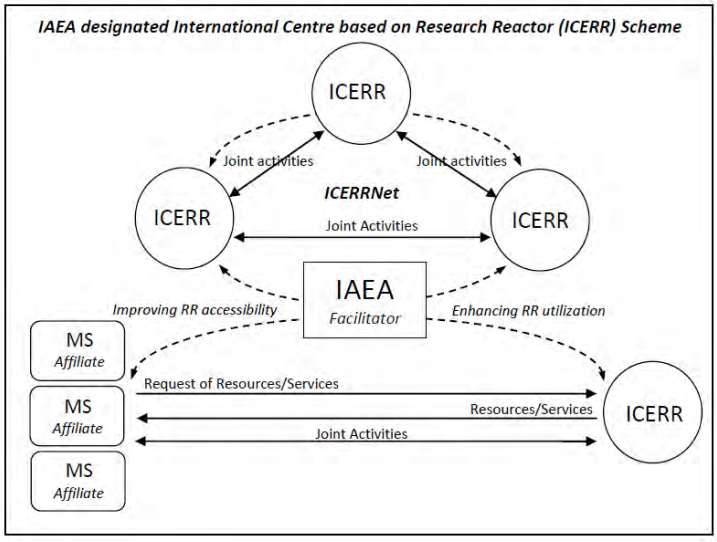

Fig. 1. ICERR scheme

3. Eligibility and criteria for designation

An IAEA Member State organization and/or institution is eligible to be designated by the IAEA as ICERR if:

1. It operates or is constructing one or more RR(s);
2. It can demonstrate experience in hosting activities based on the RR with significant international/regional participation (these activities are not required to involve the IAEA).

The criteria for designation, presented below, address logistical capability, technical capability, and sustainability.

3.1 Logistics criteria

The proposing organization must have an established, demonstrated process, adequate infrastructure, internal organization, and experience to host international/regional scientists, engineers, technicians and students, including:

- Demonstrated capacity and adequate internal organization to provide training at international/regional level (i.e., with a significant number of trainees from outside of the host country), including by secondment of staff, also to fill the gap between academic education and product-oriented training;
- Demonstrated experience in hosting international/regional events such as conferences, workshops, symposia, seminars, etc., with a significant number of participants from outside of the host country;

3.2 Technical criteria

The proposing organization must have demonstrated experience in promoting and participating in collaborations at international/regional level, including:

- Demonstrated capability to accomplish the requests of international/regional potential users (with possibility to communicate in regional languages and/or selected languages) in specific areas of the research reactors field of activities;
- Demonstrated transparent selection and decision mechanisms to evaluate the requests of potential users, prioritize the activities and provide the feedback to the applicants; for this purpose, when a dedicated access to the reactor or to its ancillary facilities is required, the ICERR candidate should have in place some type of an advisory board (e.g. Scientific Committee) while, for human resources development requests, the ICERR candidate should have in place adequate managerial measures;
- Demonstrated capability to provide potential users with access to relevant technology, methodology and standards in the area(s) of the RR activities for which designation is requested.

3.3. Sustainability criteria

The proposing organization must have a

- Demonstrated mid-term commitment (3-5 years) in terms of financial and human resources availability to assure continuous and reliable support to Affiliates;
- Demonstrated mid-term (3-5 years) capability to maintain sustainability for operation, training, licensing, waste management, etc.;
- Continuous improvement plan in place to provide potential users with access to relevant technology, methodology and standards in the area(s) of the RR activities for which designation is requested.

4. Process for designation

The designation process will take into account, and be limited to, the specific area(s) of RR(s) activities for which the designation is requested. The assessment of the ICERR candidate will cover the period of five (5) years immediately preceding the date of the submission of the application. The ICERR designation will last for a period of five (5) years starting from the date of the designation.

The ICERR candidate will submit to the IAEA, through the Permanent Mission of the IAEA Member State in which the ICERR candidate is sited, a request for designation which shall include:

- A profile of the ICERR candidate, including a description of the relevant activities over the past five (5) years;
- A self-assessment report prepared on the basis of the ICERR Eligibility and Designation criteria and of the Guidelines for Designation [1];
- A statement in which the ICERR candidate ensures that the RR(s) and its AFs are safely and securely operated in accordance to national regulations, international standards and good practices, as applicable;
- A statement clearly identifying the activity/activities for which the ICERR designation is requested;
- A letter of endorsement of the request issued by the relevant Governmental Authority/Institution.

Upon receipt of one or more requests, the IAEA will appoint a Selection Committee to review the request(s), including the self-assessment report(s), and to provide recommendations to the IAEA. A review mission at each ICERR candidate site will be performed by designated members of a Selection Committee.

The designation process is expected to be completed within six (6) months from the date of receipt of the request for designation (unless delay is caused by the ICERR candidate in providing any requested additional information). The IAEA will inform the ICERR candidate of the result of its decision based on the candidate's self-assessment and on the recommendation of the Selection Committee.

In case of positive outcome, the ICERR status is awarded through an official communication from the IAEA which contains, inter alia:

- The undertakings of the ICERR and the IAEA;
- The duration of the designation;
- Functions and clauses on termination, suspension, confidentiality, public information, liability, settlement of disputes, etc.

In case of a negative outcome, the IAEA will provide recommendations to the ICERR candidate to meet the criteria for designation and the time frame to implement them. If the recommendations are not satisfactorily implemented within the time frame indicated by the IAEA, the application will be considered lapsed.

5. Conclusion

The ICERR concept was developed through several IAEA meetings. Criteria and process for ICERR's designation were developed during a consultancy meeting attended by international experts representing institutions of different type (Universities, Research Centres, National Laboratories, etc.) and research reactor facilities of different sizes and utilization.

The ICERR scheme will contribute as an additional opportunity provided by the IAEA, complementary to others (e.g. Coordinated Research Projects, Technical Cooperation Projects, Joint Initiatives, Collaborating Centres, etc.) to support Member States engaged in nuclear R&D and capacity building programmes.

Time schedule for the implementation of the ICERR scheme is expected to be the following:

- Q1/Q2-2015: Expected first ICERR candidate(s) application(s) submittal;
- Q1/Q2-2015: Appointment of the Selection Committee;
- Q2/Q3-2015: Review mission(s) at ICERR candidates' site(s) performed by designated members of the Selection Committee;
- Q3-2015: Designation process finalized by the IAEA;
- Designation of the ICERR status and award of an official plaque during the 59th IAEA General Conference (14-18 Sept. 2015) or the IAEA International RR Conference (16-20 Nov. 2015).

6. References

[1] ICERR Terms of Reference (September 2014), IAEA web-page: *http://www.iaea.org/OurWork/ST/NE/NEFW/Technical-Areas/RRS/documents/ICERR_Concept_ToR_Final.pdf*

A New IAEA Document on Managing the Interface between Safety and Security for Research Reactors

[1]A. M. Shokr, [1]C. Torres Vidal, [2]J. Lolich and [1]M. Clarke

[1]Department of Nuclear Safety and Security
International Atomic Energy Agency, Wagramerstrasse 5, PO Box 100
A-1400 Vienna, Austria

[2] Instituto Balseiro/Universidad Nacional de Cuyo
Av. Bustillo km 9.5, 8400 Bariloche, Argentina

ABSTRACT

The activities that address nuclear safety and security have different focus and sometimes actions that are taken in one area can have implications for the other one. Recognizing that nuclear safety and nuclear security share the same ultimate goal – to protect individuals, the public, and the environment from harmful effects of ionizing radiation, a well-coordinated approach is mutually beneficial, and safety and security measures should be established and implemented in a manner that they do not compromise (but mutually enhance) one another. The interfaces between nuclear safety and security should be addressed throughout the research reactor lifetime.

The feedback from the IAEA activities on research reactors, including nuclear safety and security review missions, implemented during the past few years indicated the need in many Member States to enhance and improve the awareness and understanding of the interface between nuclear safety and security. In particular, there is a need to identify interfaces and, as necessary, integrate nuclear safety and nuclear security measures in the design process (including research reactor experiments) as well as during the operational phase of the reactor facilities, and to develop the regulatory authorities' capabilities and methodologies for assessment and addressing interfaces between nuclear safety and nuclear security.

Managing the interface between safety and security for research reactors is addressed in this paper together with the IAEA activities in this area including a progress report on the status of development of a new IAEA publication in this area.

1. Introduction

Research reactor organizations are giving increased attention to ensuring adequate nuclear security of their research reactor facilities and are currently planning or implementing nuclear security upgrade measures. Parallel to these efforts, the majority of research reactor organizations continue to implement refurbishment and modernization projects to address ageing of reactor facilities [1]. In addition, more than 20 countries are currently implementing (or planning) new research reactors [2].

The activities that address nuclear safety and security have different focus and sometimes actions that are taken in one area can have implications for the other one. On the other hand, as nuclear safety and security share the same ultimate goal – to protect individuals, the public, and the environment from harmful effects of ionizing radiations, many of these activities could serve to enhance both areas simultaneously [3]. It is therefore essential to establish a well-coordinated approach for the mutual benefit of nuclear safety and security so

that relevant measures are implemented in a manner that they do not compromise, but mutually enhance, one another. Analysis and understanding of the similarities and differences between nuclear safety and security are a corner stone for achieving this goal. These will also provide for identification of necessary engineering measures and administrative actions to address potential conflicts.

All these aspects are covered by a new IAEA publication on managing the interface between safety and security for research reactors, which is currently under development. The following sections addressed the main topics to be covered by this publication along with discussions.

2. Similarities and differences between nuclear safety and security for research reactors

Nuclear safety is the achievement of proper operating conditions, prevention of accidents or mitigation of accident consequences, resulting in protection of workers, the public and the environment from undue radiation hazards. The concern is, therefore, the radiological risk to human and environment, whatever the cause (initiating event) of this risk. For research reactors, causes could be human errors, equipment failure and internal events (fire, pipe break, etc.) and external events (earthquakes, flooding, etc.) [4]. Nuclear Security is the prevention and detection of, and response to, theft, sabotage, unauthorized access, illegal transfer or other malicious acts involving nuclear materials, other radioactive substances, or their associated facilities. For research reactors, the main concern is sabotage of the large inventories of fission and activation products and theft of high security-risk targets such as highly enriched uranium fuel [5].

The acceptable risk should be the same whether the initiating event of a radiological release is due to human error or equipment failures, internal or external events or an event of malicious origin, which is a major area of similarity between nuclear safety and security and is the basis for measures to be implemented for addressing the interfaces between nuclear safety and security.

2.1. Legislative and regulatory framework

Legislative and regulatory framework should be in place to ensure oversight of the facility and activities of potential radiological risk. For both nuclear safety and security, the role of the regulatory body is paramount to assuring that site evaluation, design, construction, operation, and decommissioning of a research reactor will be performed safely and in a secured manner [6, 7]. Although the regulatory bodies for nuclear safety and for nuclear security may be different, the functions of these bodies are similar: Establishment of nuclear safety or security regulations, authorize facilities and activities of safety or security significance; perform assessment of safety or security submittals, establish and implement regulatory safety and security inspection programmes to enforce applicable regulations. To be effective, the regulatory bodies for nuclear safety and security need adequate authority and independence, as well as effective coordination to avoid contractor requirements.

2.2. Radiation protection principles and use of a graded approach

Another major technical area of similarity between nuclear safety and security is the principle of optimization of protection - radiation risk should be as low as reasonably achievable,

taking social and economic factors into account [8], which is applicable to both areas. The risks, including those resulting from security events, need to be assessed taking into account the use of a graded approach that commensurate with the potential hazard of the research reactor facilities. The approach is applied for both safety and security but its application may be different.

Most of the factors to be considered in the use of a graded approach in the design of the reactor safety systems [9] are also used in the design of the physical protection systems. These factors include reactor power level, inventories of radioactive material, radiological source term, amount and enrichment of fissile and fissionable material, type of fuel and its chemical composition, amount of reactivity that could be introduced in the reactor core and rate of its insertion, quality of containment, location of the reactor site and proximity of the site to population, and feasibility for implementing emergency plans. For security, other factors are considered such as the current evaluation of threat, relative attractiveness and nature of nuclear materials.

2.3. Management of nuclear safety and security

The operating organization has the prime responsibility for the reactor safety. However, in case of nuclear security the responsibility of the operating organization is limited to the protection measures within the design basis threat. It is normal that other organizations within the country perform assessment of the risk of sabotage and other security-related events and define the design basis threat that should be complied with by the research reactor operating organization.

An integrated management system should be established and implemented in different stages of research reactor lifetime. This system should integrate all quality, health, economic and environmental aspects as well as safety and security [10]. The system should be the basis for establishing safety and security cultures. However, the safety culture is different from security culture. Safety culture pursues transparency and sharing of knowledge and information while for nuclear security information should be restricted to a small number and selected individuals.

The functional categories of the management system for safety and security are the same (management responsibility, resources management, process implementation, and review and improvement). However, there are major differences in the management system processes for nuclear safety and security. Typical processes for nuclear safety include safety analysis, fuel handling and core management, reactor operation, experiments, maintenance of systems and components important to safety. Typical nuclear security processes include management of classified information, assessment of threat, target identification, design of security system, including intrusion detection, access control, search, surveillance, and response.

2.4. Prevention of accidents and security events

Defence in depth is a fundamental concept in nuclear safety and security. However, there are differences in application of the concept in both areas [7, 11]. For nuclear safety, there are five levels for the defence in depth that are aimed at preventing deviation from normal operation; controlling deviation from operational states; controlling of accidents within design basis; controlling severe accidents; and mitigating accident conditions.

In nuclear security, the first line of the defence in depth concept is preventing; with measures to avoid and discourage an adversary from attempting an attack, the second line of defence is protection; with implementation of security measures that prevents an adversary from succeeding in an attack or delaying for a sufficient period to allow for external support. The second line in defence includes several measures like many layers of barriers (around potential targets), mechanism for detection, rejecting unauthorized entry, surveillance and monitoring, etc. Planning against events beyond the design basis threat needs the participation of many organizations within the country. The third line of defence includes measures to mitigate or minimize the radiological consequences.

2.5. Operational aspects

The major similarities between nuclear safety and security during the operational phase of a research reactor include the need for access control measures and procedures, respectively, for protection against radiological exposure and for prevention of unauthorized access to nuclear material. Maintenance and in-service inspection programmes for the reactor safety systems and for the physical protection system are also required. Modification, refurbishment and upgrade of the reactor systems are also usual during the reactor lifetime for ageing management and utilization purposes. These also apply for the physical protection systems. Although these activities have similarities, they are different in nature and the associated procedures may have potential conflicts, as discussed in Section 4.

2.6. Emergency and contingency plan

Research reactors are establishing emergency plans to mitigate the consequences of a radiological accident, which covers both safety and security events [12]. However, the emergency plan for security events (usually called a contingency plan) requires involvement of a greater number of entities within the country. Contingency plans are established to respond to both “unauthorised Removal of material” and “sabotage of nuclear facilities or material” Contingency plans should be prepared to counter malicious acts effectively and to provide for appropriate response. The contingency plan should include measures for the location and recovery of missing or stolen nuclear material, in terms of unauthorised removal, and it should also include measures which focus on preventing further damage, on securing the nuclear facility and on protecting emergency equipment and personal. The emergency plan consists of measures to ensure the mitigation or minimization of the radiological consequences of sabotage as well as human errors, equipment failures and natural disasters. [3].

3. Maximizing the coordination between safety and security

3.1. Design phase and modification projects

Ideal approach is to consider the interfacing between nuclear safety and security in the reactor design. Table 1 presents design safety provisions that also result in security enhancement for research reactors.

Table 1: Safety design provisions result in security enhancement

Design safety provisions	Benefits to security
Design for reliability of safety systems (use of redundant, diverse, physical separation and fail-safe systems and components)	Enhancing protection against sabotage – adversaries have to attack simultaneously several components located in different places in the reactor building.
Use of passive components and robustness against human errors to avoid or minimize human errors.	Providing additional protection against malicious acts, and protection against internal threat.
Use of physical barriers for radiation shielding and protection purposes	Preventing or delaying malicious acts or unauthorized access
Use of verified and validated software in control systems	Providing protection against hackers and malicious intruders.
Use of containment and construction concept of the reactor building minimizing release of radioactive material	Providing additional protection of the reactor from an attack.
Use of surveillance equipment (e.g. CCTV) for monitoring of physical status of the reactor systems	Used also for security surveillance.

Although the provisions included in Table 1 are used in the design phase of a new research reactor, they can be also used in any modification project (including refurbishment, upgrading and modernization of the reactor facilities). In this regard, the design requirements for proposed upgrades in the security systems, including physical protection systems, and the associated installation and operation processes, should be carefully analysed so that the foreseen upgrade does not adversely affect the reactor operational safety. Equally important, any proposed safety upgrades should be carefully analysed to ensure that the security is not affected.

It is also important to note that safety knowledge and information of the reactor systems are important for evaluation of the consequences of malicious acts and target identification, and therefore coordination between safety and security specialists is mutually beneficial for both nuclear safety and security.

3.2. Operation

Establishment of an integrated management system for the operation phase is an important step toward enhancing the coordination between safety and security. The system provides for integrated approach of safety and security objectives in the reactor processes. The system allows for information exchange on security aspects without breaching confidentiality. Safety and security specialists should be involved in development of the processes with potential safety and security implications as well as the associated operating procedures. This includes access control procedures, procedures for evaluation of malicious acts, and procedures for experiments.

It is also a good practice to use sets of performance indicators for safety and for security. Although both sets may be different, they can include indicators to measure the interface between safety and security. Analysis of such indicators would provide for identification of actions to be implemented for further improvements along the facility operation lifetime.

Access control procedures are required for both safety and security. Although potential conflicts would occur, they could be used to enhance both areas by providing protection to personnel against radiation exposure and preventing unauthorized access to nuclear materials and systems important to safety. This classification should be subjected to periodic review to ensure the continuity of meeting these criteria in view of possible changes on the characteristics of these areas.

The operating procedures usually include a routine walkthrough of the facility. The procedures are mainly for safety consideration. The procedures can be revised to account for items important to security or similar procedures with a security focus should be established. Additionally, in-service inspection activities performed in the framework of a maintenance programme and the associated procedures should also cover items important to security.

Another important aspect that would enhance the coordination between nuclear safety and security is the training and qualification programme for operating personnel. The programme can be revised to provide for enhancement of the understanding of the operators and maintenance personnel of the security risks and the effect on the programme and activities they are implementing on security. It is also advisable vice-versa that security training address nuclear safety implications of security practices and procedures.

Although the emergency response to a safety event and to a security event is not the same, measures can be taken to mutually enhance the emergency plan and contingency plan. This can be achieved mainly by considering the attributes for both nuclear safety and security in developing these plans. Coordinated emergency exercises can be also organized in order to be able to evaluate the adequacy of the emergency plan and contingency plan and their interface.

Additionally, regulatory practices could also contribute to maximizing the coordination between safety and security. Despite the fact that safety and security regulators could be subjected to different organizational settings, conduct of joint regulatory inspections would contribute to enhancing both safety and security. Though licensing process for safety and security may be differ for each, it needs to be coordinated during every stage of the research reactor lifetime.

4. Addressing potential conflicts between nuclear safety and security

The activities of nuclear safety and security have different focus and potential conflicts may arise from the implementation of these activities. The technical areas that have potential conflicts between nuclear safety and security are safety and security culture (transparency versus security of information), access control, utilization, maintenance, modifications, and managing of long reactor shutdown periods.

Addressing potential conflicts in these areas requires a well-coordinated approach. However, in some cases conflicts are unavoidable. In this case these conflicts should be treated on the basis of minimizing the likelihood of radiation exposure to the reactor operators and public. Table 2 shows the areas of potential conflicts, consequences of these conflicts and a proposed strategy to address them.

Table 2: Areas of potential conflicts between nuclear safety and security and strategy to address them

Potential conflict	Consequences	Strategy for addressing conflicts
Management of information: Transparency is required for safety improvements while information should be confidential for security purposes.	Information on safety weakness could be used by potential adversary for malicious acts. Insufficient protection of the security information increases the vulnerability of safety systems to malicious acts.	Coordinated involvement of safety and security specialists in establishing an integrated management system which needs to take into account the specifics of management of information in each area.
Access control: The necessity for rapid access during emergencies can create vulnerability from the security point of view.	A lack of balance between security provisions and safety can lead to delays in responding to emergencies situations or can create security vulnerability.	Access control procedures should ensure balanced considerations between safety and security, and should be developed jointly by safety and security specialists.
Utilization of the reactor: The need to use the reactor by experimenters external to the organization may constitute a risk of sabotage (e.g. introduction of dangerous materials into the reactor core through the rabbit system, or damaging beam tube isolation windows).	Damage to core components caused by safety or security problems results in significant radiological consequences to the people and to the environment. Prohibiting use of the reactor by experimenters external to the organization limits the usefulness of the reactor.	Application of strict quality control rules to ensure that characteristics of the samples to be irradiated are in conformance with approved specifications, and that experimenters are those approved to perform the irradiations.
Maintenance: Change or modification of the reactor configurations during maintenance (e.g. cut of electrical power supply) affect operability of safety (e.g. doors opened) and security items (surveillance cameras)	Configuration changes during maintenance could introduce vulnerability from the security point of view (may be increased if the activities are performed by contractors).	Coordination with the security specialists concerning the temporary changes planned during maintenance activities as well as the associated compensatory measures.
Modifications: May affect negatively security equipment and vice versa.	Degradation or loss of safety or security function.	Modifications need to be assessed from the safety and security perspective before implementation.
Long shutdown periods: Safety requires partial or full unload of fuel from core. This may increase the vulnerability of the facility from the security point of view.	Vulnerability increases due to change of access control rules and the number of operating personnel present in comparison with the operation periods of the reactor.	Involvement of security specialists in planning for ensuring adequate surveillance and periodic testing and maintenance of the security equipment.

5. Conclusions

The activities that address nuclear safety and security have different focus and sometimes actions that are taken in one area can have implications for the other one. Challenges in managing the interface between safety and security are mainly due to differences between safety culture and security culture, traditional separation between safety and security organizations and groups, inadequate regulatory guidance, lack of an integrated approach of safety and security measures in the reactor designs, and inadequate coordination during the reactor operation phase.

Recognizing that nuclear safety and nuclear security share the same ultimate goal, a well-coordinated approach is mutually beneficial, and safety and security measures should be established and implemented in a manner that they do not compromise, but mutually enhance, one another. There are more similarities than differences between nuclear safety and security and use of appropriate safety design concepts and principles, and adherence to administrative requirements including use of approved procedures would also result in security enhancement.

It is also important to note that specific attributes in some areas may lead to conflicts between safety and security. This should be managed through effective coordination and harmonization of methods and approaches and by following proven operating practices. When conflicts are unavoidable, the issue should be resolved on the basis of minimizing the overall radiological risk to the workers and public.

The new IAEA publication on the interface between safety and security of research reactors, which is at present under development, is intended to provide guidance on the programmes and activities discussed in this paper, along with practical examples on their application to different research reactor types and sizes. The IAEA is also planning technical meetings and workshops, as well as advisory missions, upon requests from Member States, on enhancing the interface between safety and security for research reactors

References

[1] International Atomic Energy Agency, Project Experience in Research Reactor Ageing Management, Modernization and refurbishment, IAEA TECDOC Series No. 1748, IAEA, Vienna, 2014.

[2] A. Borio Di Tiglioe, E. Bradly, A. Zhukova, P. Adelfang, A. Shokr, and R. Ridikas, IAEA Assistance in the Development of New Research Reactor Projects, Proceedings of the Research Reactor Fuel Management Meeting, 30 March – 3 April 2014, Ljubljana, Slovenia, pp 40-46, ENS, 2014.

[3] International Nuclear Safety Advisory Group, The Interface between Safety and Security for Nuclear Power Plants, INSAG-24, IAEA, Vienna, 2010.

[4] International Atomic Energy Agency, Safety of Research Reactors, IAEA Safety Standards Series No. NS-R-4, IAEA, Vienna, 2005.

[5] G. Bunn, C. Braun, A. Glaser, E. Lyman, and F. Steinhausler, Research Reactor Vulnerability to Sabotage by Terrorists, Science and Global Security, 11:pp 85-107, Tylor & Francis Inc. 2003.

[6] International Atomic Energy Agency, Governmental, Legal and Regulatory Framework for Safety, IAEA Safety Standards Series No. GRS Part 1, IAEA, Vienna, 2010.

[7] International Atomic Energy Agency, Nuclear Security Recommendations on Physical Protection of Nuclear Material and Nuclear Facilities, IAEA Nuclear Security Series no. 13, IAEA, Vienna, 2011.

[8] International Atomic Energy Agency, Use of a Graded Approach in the Application of the Safety Requirements for Research Reactors, IAEA Safety Standards Series No SSG-22, IAEA, Vienna, 2012.

[9] EC, FAO, IAEA, ILO, OECD/NEA, PAHO, OCHA, and WHO, Radiation Protection and Safety of Radiation Sources: International Basic Safety Standards, IAEA Safety Standards Series No. GSR Part 3, IAEA, Vienna, 2014.

[10] International Atomic Energy Agency, The Management System for Facilities and Activities, IAEA Safety Standards No GS-R-3, IAEA, Vienna, 2006.

[11] International Nuclear Safety Advisory Group, Defence in Depth in Nuclear Safety, INSAG-10, IAEA, Vienna, 1996.

[12] FAO, IAEA, ILO, OECD/NEA, PAHO, OCHA, and WHO, Preparedness and Response for a Nuclear or Radiological Emergency, IAEA Safety Standards Series No. GS-R-2, IAEA, Vienna, 2002.

ALFRED AND THE LEAD TECHNOLOGY RESEARCH INFRASTRUCTURE

A. ALEMBERTI, M. FRIGNANI, G. VILLABRUNA
ANSALDO Nucleare
Corso F. M. Perrone 25, 16152 Genova – Italy)

P. AGOSTINI, G. GRASSO, M. TARANTINO
ENEA
C.R. ENEA Brasimone, 40032 Camugnano (BO) – Italy

I. TURCU, M. CONSTANTIN, D. DIACONU
Institute for Nuclear Research
Str. Campului no 1, 115400 Mioveni, Jud. Arges – Romania

F. DI GABRIELE, N. WITZANYOVÁ, M. KRYKOVÁ
Centrum Výzkumu Řež s. r. o., CVR,
Hlavní 130, 250 68 Husinec-Řež – Czech Republic

ABSTRACT

ALFRED, the Advanced Lead Fast Reactor European Demonstrator, has emerged from a European research effort, in the frame of Lead cooled next generation nuclear power plants. The main goal behind ALFRED and Lead technology development is to maintain the nuclear energy source as an important contributor to the development of a secure and low carbon European energy system. ALFRED, as one of the projects supported by the European Sustainable Nuclear Industrial Initiative (ESNII), brings together industry and research partners in the development of so-called Generation IV Fast Neutron Reactor technology, as part of the EU's Strategic Energy Technology Plan (SET-Plan).
The paper presents briefly the design status of ALFRED as part of a future technology park to be built in Romania, with open access to European scientists and students for extensive research on operating conditions in a realistic environment. Also included is an overview of the main aspects of the design concerning: system design, safety features and core design. The main design parameters are briefly summarized.
In addition to the above described technical overview of ALFRED design, the paper reports about the activities carried out by the FALCON (Fostering ALfred CONstruction) Consortium established in Bucharest on December 18th 2013 by ANSALDO, ENEA, RATEN-ICN, and joined by CVR in December 2014. The main results of the FALCON activities are presented and the present status of the consortium, technical and management activities are summarized. One of the main results of FALCON in this first period of activities is highlighted by the development of the technological roadmap, divided in two main steps: the Lead Technology Development and the ALFRED construction. The first, preparatory step is deemed necessary in order to reach the technology readiness level that is required to build ALFRED. Such development relies on the realization of a number of experimental facilities dealing with the main aspects of lead technology such as: lead corrosion and erosion mechanisms, fuel handling, lead-water and lead-fuel interactions and so on. All these facilities themselves represent the basis of a Distributed Research Infrastructure having its focus on ALFRED, so that an extensive reflection on the challenges and opportunities offered by this approach for LFR development and demonstration is outlined as a conclusion.

1. Introduction

1.1. ALFRED as a Strategic Research Reactor

Internationally, Lead Fast Reactor (LFR) technology is considered as a very promising candidate option by the Generation-IV International Forum (GIF) [1]. The favourable physical features of lead as primary coolant, allows the fulfilment of the main goals of the next-generation power reactors [2]: LFR is based on a closed fuel cycle, thus aiming at a sustainable exploit of natural resources; the inert nature of the coolant provides important

design simplification, i.e. added economics and competitiveness, and is shown compatible with decay heat removal systems based on light water technology as well as with passive features, hence providing a safety level at least comparable with current nuclear technology (so called Gen-III+ [1]); additionally, the LFR fuel, taken as a reference in the European Projects, constitutes a very unattractive route for diversion or theft of weapons-grade materials, thus providing increased proliferation resistance and physical protection.
At European level, the LFR concept was selected by the European Sustainable Nuclear Industrial Initiative (ESNII), in order to support the development of innovative Nuclear Energy Systems (NES) that will represent a breakthrough improvement for a more sustainable and safer nuclear option in the long term, as formalized in the in the Strategic Energy Technology Plan (SET-Plan) by the Sustainable Nuclear Energy Technology Platform (SNETP) [3]. In this framework, ALFRED (Advanced Lead Fast Reactor European Demonstrator) is envisaged with the role of European Technology Demonstrator Reactor (ETDR) of the LFR technology, in the Strategic Research and Innovation Agenda (SRIA), issued by SNETP in 2013 [4].
Excluding Russian experience from the development of Class α nuclear submarines [5], the HLM technology is a relatively new technology and requires further Research, Development, Qualification and Demonstration (RDQ&D) steps, in view of the deployment of a fleet of Gen-IV lead-cooled reactors. In particular, EURATOM Framework Programme (FP7) projects identified the R&D needs and set the basis of a Roadmap (ADRIANA [6]), are reviewing such roadmap while identifying the synergies with other technologies (ESNII+ [7]), supported the definition of an applicable regulatory framework (SARGEN-IV [8]), identified gaps in the available competences and suitable Education and Training (E&T) schemes (ARCADIA [9]).
Since its conceptual design, carried out in the 3-years long LEADER (Lead-cooled European Advanced Demonstration Reactor) FP7 project [10], ALFRED has gradually been reckon as part of a necessary Distributed Research Infrastructure (DRI) of pan-european interest. Through the upgrade of existing facilities, the construction of new ones and the licensing, construction and operation of the first European LFR, the DRI is aimed at tackling the gaps and challenges in RDQ&D, increasing the readiness of HLM technology to a level attracting the interest of industry and investors.
In particular, the main LFR technological challenges and needs range from qualification of structural materials and development of coatings operating at high temperature in a corrosive/erosive HLM environment, to uniform chemistry control of molten lead in a pool; from qualification of sub-systems and components important to safety and subject to stressful conditions to development of reliable components requiring extensive test campaigns; from characterization of the phenomenology of HLM-fuel interaction to the validation of neutronic parameters for computational tools.
The structure of the DRI addresses the needs identified in the European landscape of existing research facilities, mostly due to the limitations in terms of possible commitments at single organization or member state level. Being one of the nodes of such a DRI, ALFRED will represent a strategic research reactor for education, training, development, qualification and demonstration, of interest for research centres, universities, safety authorities and Technical Safety Organizations (TSOs).

1.2. ALFRED in the International Context

The LEADER project, started in March 2010, was carried out in synergy with more than twenty other FP projects devoted to Heavy Liquid Metal (HLM) technology, covering an overall total cost of at least 100 M€ [11]. The increasing interest in HLM technology in the past 20 years is demonstrated by a scientific community, made of approximately 500 individuals from more than 15 European countries, gathering experts from universities, research organizations, industries, safety authorities and technical safety organizations.
The development of the LFR technology, and, in particular, the deployment of ALFRED, is also sustained at national level, through endorsements and financial commitments. In particular, Italy has invested approximately 2 M€/year on HLM technology research activities, since 2006. The ENEA Italian Research Centre has implemented large competencies and capabilities on LFRs and HLM coolant technology. Several experimental facilities (6 in

operation, 2 under construction) were designed and operated in the last 20 years in Brasimone, involving approximately 40 peoples full-time, out of which 10 researchers. Recently, Romania underlined the necessity of a continuous development of nuclear power, as a stable and sustainable component of the energy mix. The Romanian Minister of Economy, Trade and Business Environment expressed the interest in hosting ALFRED and supporting the implementation of the demonstrator, being a crucial stage for the LFR deployment process [12]. The Mioveni nuclear platform was selected in 2011 as candidate site for a new Centre of Excellence, including the ALFRED reactor, thanks to its strategic role for the development of nuclear energy in Romania, since 1971. Currently, the platform gathers four organizations (RATEN, ICN, FCN, and AN&DR branch) and hosts important nuclear facilities, with approximately 1200 people employed.

The Italian company Ansaldo Nucleare S.p.A. has been deeply involved in the LFR development and, in particular, in the ALFRED design, as coordinator of the LEADER project. The strong commitment of Ansaldo Nucleare, ENEA and ICN was formalized through the signature of an unincorporated Consortium, namely FALCON (Fostering ALfred CONstruction) [12], aimed at managing the R&D strategic needs and securing the necessary funding for siting, licensing and construction. Through the ingress of CVR from Czech Republic as a full-member and the signature of multiple Memoranda Of Agreement (MOA), the FALCON Consortium has further strengthened the LFR European community, aiming at providing the stability required for the long-term program. In fact, the involvement of the CVR is mainly based on its experience from the SUStainable ENergy project and the fact that, in the frame of this, many RI were built and are being built in support of research for Gen IV. Therefore, it is a strategic step to use RI already implemented with the support of the EU and ready available, as a solid base, for the further development of the HLM technology.

Thanks to the leadership of GIF in the next-generation nuclear reactors, the intrinsic cooperative nature of European FPs and the role played by the FALCON Consortium in promoting the initiative, ALFRED project has raised international interest, as demonstrated by the links and bilateral collaborations with many research centre operating in the field (e.g. CRS4, IIT, CIRTEN in Italy; NRG in Netherlands; KIT and GRS in Germany). In addition, ALFRED is explicitly mentioned in the documents of the LFR System Steering Committee of the GIF, and was chosen as the Generation IV reference system for a white paper on the Risk and Safety Assessment performed by the corresponding GIF Working Group [13]. ALFRED and its R&D supporting program were also thoroughly presented to the Technical Working Group on Fast Reactors of the International Atomic Energy Agency, for advice and support on program implementation [14]. Recently, an international collaboration on the project was ensured through a Cooperation Agreement (CooA) signed between the ALFRED and BREST communities, for information exchange and reciprocal advice about technology, design and safety aspects.

Integrating the existing experimental facilities in Italy (node 1) and the ones under construction and commissioning for the SUSEN project in Czech Republic (node 2) with the additional ones (node 3) and the ALFRED reactor (node 4) planned in Romania, the DRI will coordinate the RDQ&D efforts at a pan-European level: the complementarities offered by the HLM community in terms of developed background, relevant facilities and experienced professionals will be exploited in a synergic and comprehensive way, avoiding duplication of effort. A DRI including a lead-cooled research reactor will have a two-fold leveraging effect: it will strengthen the role of Europe favouring worldwide cooperation and will improve national economies through a relevant return of investment. Additionally, by re-investing all revenues from electricity production, to grant the open trans-national access and finance student and post-doc positions, ALFRED will contribute to the sustainability of the infrastructure itself and will attract scientists promoting the brain gain in the region.

2. Technical Overview

2.1. ALFRED Conceptual Design and On-going Improvements

In the role of a LFR demonstrator, ALFRED was designed to be fully representative of the ELFR, but with a reduced thermal power of 300 MW_{th}. Specific design solutions (e.g. no intermediate circuit, simplified and robust component design, compact size), combined with

an efficient thermal cycle, will allow the demonstration of the Gen-IV economic principle, through the connection to the electrical grid (125 MWe generated power).
Safety of ALFRED is extensively based on the use of the defence in depth criteria, enhanced by the use of passive safety systems. Preliminary enveloping safety analyses [15][16] have demonstrated the inherent safety of ALFRED, meaning no external radioactivity release will occur even in severe conditions, without the need of off-site or emergency AC electrical power supply. Safety has been implemented in all the design choices since the beginning, leading to the current baseline configuration of ALFRED [17], shown in Figure 1, based on the following main features:

- Pool type configuration for a compact and robust design, to avoid out-of-vessel primary coolant recirculation;
- Reactor vessel and safety liner, to ensure the Decay Heat Removal (DHR) flow-path in case of vessel break;
- Core and internals layout to promote natural circulation maximizing the grace time in case of loss of flow;
- Hexagonal wrapped Fuel Assemblies (FA), extended above the lead free level to simplify fuel handling;
- MOX hollowed fuel pellets, to mitigate maximum fuel temperature and reach the target peak burn-up;
- Combination of a lower core support plate and of a FA spike with coolant inlet holes and equalizer holes to avoid the FA sudden flow blockage;
- Two diverse and redundant safety shutdown systems, the first one actuated by buoyancy, while the second one actuated by a pneumatic system;
- Once-through SGs made of Double-Walled straight Bayonet-type Tubes (DWBT), ensuring a continuous monitoring of tube leakages
- Axial flow pumps, running at constant speed, combined with SGs in an integrated compact removable unit;
- Two diverse, redundant and fully passive DHR systems, based on water/steam as cooling medium and on a water pool as heat sink, able to ensure a grace time of 72 hours.

Recent advancements in the R&D activities funded by national and European programs are constantly supervised by the FALCON Consortium and will be integrated in a new conceptual configuration, which will represent the baseline to enter in the preliminary design stage. The main features currently under development are:

- Supported Safety Vessel, surrounded by a heat-resistant material, combined with a fully passive concrete cooling system, in order to ensure the pit integrity and exclude thermal stratification in the primary system, in any design condition;
- Revised primary system configuration, including a new concept of screw pump, aimed at improving natural circulation, avoiding regions of stagnant lead and excluding thermal stratification in the pool, in any design condition;
- Additional row of dummy assemblies for added flexibility in view of future needs, margin for compensation of uncertainties on nuclear data, as well as additional shielding protecting the inner vessel structure;
- Study and selection of ex-core instrumentation for on-line neutron flux monitoring and potential detection of failed FAs;
- Diversification of the heat transfer principles of the DHR systems, as an improvement suggested by safety authorities and TSOs, to reduce uncertainties related to long-term performances degradation of heat exchangers in liquid lead;
- Prevention of lead freezing in long-term post-accident scenario, by an intrinsically regulated insertion of non-condensable gases in the DHR system, able to inhibit the heat exchange performances, in a fully reversible way.
- Low (10^{-6}-10^{-8} w%) oxygen strategy for coolant chemistry in order to minimize the risk of lead-oxide formation, potentially inducing dangerous plugging or reducing heat exchange performances.

As offered by the above listed improvements, the increased safety and robustness, combined with the added flexibility and control, is intended to smooth the licensing process of the demonstrator and to widen the range of applications in support of strategic research activities.

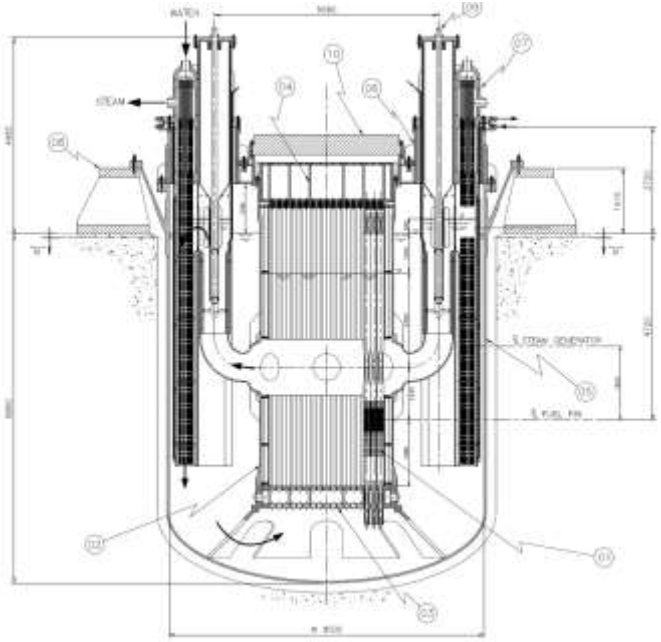

Parameter	Value
Lead coolant inventory	~416 m^3
Gap between Vessels	0.2 m
Pins bundle pitch/diameter	1.35
Primary pressure drops	1.5 bar
Pressure drops through the core	1 bar
MOX fuel enrichment (average)	25.77 at%
Target peak burn-up	100 MW_d/kg
Control rods worth	6800 pcm
Safety rods worth	3300 pcm
SG number of tubes	542
Thermal power	300 MW_{th}
Primary coolant temperature	400-480°C
Secondary side temperature	335-450°C
Efficiency	~42%

Fig 1. ALFRED reactor conceptual configuration and parameters: (01) Fuel assembly; (02) Inner vessel; (03) Core lower grid; (04) core upper grid; (05) Reactor vessel; (06) Reactor cover; (07) Steam Generator; (08) Vessel support; (09) Primary pump; (10) Reactor FAs cover

2.2. ALFRED as Part of a Pan-European Technology Park

Although not offering neither in-core irradiation channels nor beam ports, ALFRED will serve two main purposes typical of a research reactor: irradiation for testing and human resource development [18].

ALFRED design is suited for testing, calibration and irradiation applied to instrumentation, as well as to materials for nuclear fuels and structural components. Proper characteristics and accurate readings for both off-the-shelf or newly developed instruments (e.g. fission chambers, SPNDs, nuclear heating calorimeters) are ensured through testing and calibration (both in and out of reactor). Compatibly with core design and fuel management, ALFRED is intended to be used for ageing tests and qualification of mechanical properties of materials and fuels for next generation fast reactors. Design improvements aimed at a safe operation of the reactor for experimental studies on fuel aging at steady state power conditions, as well as on fuel and cladding behaviour under power transient conditions, are currently under investigation.

Educational tours, at different levels, should not be considered a trivial or unprofitable mission, since making the public more familiar with nuclear and safety culture results in less opposition and potentially more support. Awareness in the facility activities and services develops interest in the scientific and industrial communities, attracting students, future customers and potential users. ALFRED size offers more possibilities in terms of teaching radiation protection, radiological engineering, nuclear engineering: exercises on principles of radiation protection can take advantage of the production of activated materials and radioactive effluents, while rather complex reactor physics experiments can be performed thanks to the high neutron flux (including measures of static and kinetic reactor parameters, operation experiments at zero power and above, instrumentation and control systems).

Due to innovative aspects of LFR technology, operator training in a fully representative environment is of paramount importance for operational, maintenance and inspection

aspects. Covering a potential range of experiments from basic reactor controls and measurements to very specific tasks (e.g. fuel manipulation), ALFRED is intended to provide hands-on experience from understanding of basic principles to plant operation training for the safe management of next generation reactors. Experiences on administrative and organizational topics (e.g. regulatory requirements, code of conduct, physical security, emergency procedures, radiation protection and dosimetry, fuel management, waste management and decommissioning planning) are less specific, but undoubtedly important.
In these respect, the presence of other research facilities close to the ALFRED site, as well as continuous exchanges with the other nodes of the pan-european DRI, are considered a very desirable and advantageous feature for a research reactor. The main experimental facilities foreseen in support of ALFRED design, licensing, construction and operation are aimed at addressing the main LFR technological challenges and needs, still requiring RDQ&D efforts:

1. HLM thermal-hydraulic (natural circulation, transition from/to forced circulation, heat exchange correlations, stratification, stagnant zones, level oscillations,…):
   a. code development and validation (including Computational Fluid Dynamics)
   b. testing of components (DWBT heat exchangers, pin assemblies, integral tests…);
   c. HLM freezing, counter-measures and plant recovery procedures.
2. Structural material studies and HLM physical-chemistry:
   a. chemical interaction (dissolution of alloying elements, protection by oxide layers);
   b. physical interaction (erosion, stress corrosion cracking, fretting);
   c. chemistry control (temperature gradients, circulation patterns, dosing elements, inhibitors, impurities).
3. Heat exchanger functionality and safety demonstration:
   a. HLM interaction with water/steam (pressure waves, steam entrainment, sloshing,…);
   b. measures to mitigate and prevent interaction by design (detection, isolation, over-pressure protection,…);
   c. qualification against potential degradation or rupture of components important to safety (DHR heat exchangers).
4. Primary Pump development based on innovative concepts:
   a. materials performances (erosion on impeller, cavitation, vibrations,…);
   b. safety design requirements (pressure drops, coast-down, codes validation);
   c. performance and endurance tests (long-term reliability).
5. Equipment for In-Service-Inspection and Repair (ISI&R), maintenance and refuelling:
   a. monitoring instrumentation (oxygen sensors, in-core instrumentation);
   b. devices ISI&R (ultrasonic devices) in a dense and opaque medium;
   c. refuelling manipulators, recovery actions in HLM (feasibility, test, long-term reliability);
6. Nuclear fuel development and waste management:
   a. irradiation by fast neutrons (embrittlement, creep, swelling, development of coatings);
   b. fuel-cladding and fuel-(clad)-coolant interactions;
   c. fuel enrichment, fuel cycle, waste processing and disposal.
7. Neutronics:
   a. validation measurements for nuclear data improvement;
   b. validation measurements for licensing and operation.

The existing and planned experimental facilities of the DRI, aimed at improving the HLM Technology Readiness Level (TRL) [21], are listed in Table 1 and cross-linked to the above gaps and needs (from 1 to 11). The international interest on the wide range of possible experimental activities and the strong synergy between the 3 nodes and ALFRED (node 4) are big assets for the sustainability of the DRI, as well as for the efficient implementation of a strategic research program for the deployment of LFRs.

3. FALCON Consortium and Strategic Roadmap

3.1. Status of FALCON Consortium Activities

All the strategic actions and technical work towards ALFRED construction and operation are coordinated by the FALCON Consortium. Since the signature on December 18th, 2013, with the support of the Italian Ministry of Economic Development and the Romanian Ministry of

Energy, the unincorporated Consortium was joined by the CVR (CZ) as full-member, and supported by a number of organizations through MOAs or expressions of interest (LeadCold

Node	Facility	Status	Description	Target
ENEA Brasimone (node 1 – IT)	LIFUS 5	O	Small pool, water injection system	3.a, 3.b
	HELENA-I	O	Lead loop (500°C, 2 m/s)	1.a, 4.a
	LECOR	O	Lead loop (500°C, 1 m/s)	2.b
	NACIE-UP	O	Lead loop, forced and natural circulation	1.a, 1.b, 2.c
	GIORDI	O	Fretting equipment facility in HLM (550°C)	2.b
	RACHELE	O	Experimental muffles and furnace	2.c
	SOLIDX	P	Lead pool (20 dm^3), cooling and heating circuits	1.c
CV-Rez (node 2 – CZ)	LR-0	O	Pool type research reactor (1 kW, $10^{13}n/m^2s$)	6
	LVR-15	O	Tank research reactor (10 MW, $10^{13}n/m^2s$ fast, 0.1 dpa/month)	6
	COLONRI-1	O	Loop for material testing (500°C, 2 cm/s)	2.a, 2.b
	COLONRI-2	O	Loop for material testing (550°C, 2 cm/s)	2.a, 2.b
	MATLOO	C	Loop for material testing (550°C, 1.5 m/s, 10^{-6}-10^{-8} O_2 w%)	2.a, 2.b, 2.c
	CMT	T	Cold Material testing	2.b
	HMT	C	Hot Material Testing (hot cells, max 300 TBq)	2.b, 6.a
	NDL	T	Non-destructive Lab	2.a, 2.b
	SAL	C	Severe Accident Lab	6.b
ICN Pitesti (node 3 – RO)	HELENA-II	E	Lead loop (650°C, 20 m/s)	1.a, 4
	ATHENA	E	Large pool, in forced or natural circulation	1, 5.a, 5.b
	Meltin'Pot	E	Small pool	6.b
	Hands-ON	E	Cold facility, remote handling equipment	5.c
	ChemLab	E	Chemical Laboratory	2.a, 2.c
	ELF	E	Electrical Long-running Facility	1.c, 3.c, 4.b, 4.c, 5.a, 5.b

Tab 1: Experimental facilities of the DRI grouped by node. Current status (O – Operation; P – Procurement; C – Construction; T – Commissioning; E – Engineering) and short description of the facility are provided. RDQ&D target is cross-linked to the gaps and needs of current HLM TRL, as listed in the text of Section 2.2.

(SE) and SRS (IT) as industries, KIT (DE), NRG (NL), CRS4 and IIT (IT) as research organizations, GRS (DE) as Technical Safety Organisation, SYMLOG (FR) as institute for social studies, and CIRTEN and UniGE (IT) as universities).
All the associated partners are called to provide 18 equivalent person-months as in-kind contribution for supporting the identified necessary steps in the development and preparation of the ALFRED project. The activities are grouped in 5 thematic areas, namely sharing of information and technical review, licensing and siting preliminary review, assessment of financial instruments, strategic roadmap and implementation plan, promotion of initiatives and coordinated actions.
Preliminary contacts were established with the Romanian national competent authority in nuclear field (CNCAN). The legal framework for the stepwise licensing process [19] was thoroughly analysed, considering the contents of the Initial Safety Report (ISR), the needs of an Environmental Impact Assessment (EIA) [20] and public consultations, the management structure requirements for a licensable body and all the other involved authorities. On the other hand, the selected site of Mioveni in Pitesti was demonstrated to provide advantages, both in the short and long term perspective (hosting two others nuclear research reactors, post irradiation laboratories, fuel fabrication, waste treatment plant).
FALCON promoted the inclusion of ALFRED in the Romanian energy smart specialization of the National Strategy for Research, Development and Innovation (NSRDI), as well as in the South-Muntenia regional Strategy (S3I). Other coordinated actions were aimed at widening the Romanian Partnership Agreement towards the added sustainability of nuclear energy and at including ALFRED in the national Operational Program-Competitiveness (PO-C).

Consultations with an ad-hoc Inter-ministerial Working Group (IWG) were held in order to assess the eligibility of the DRI construction phase for the European Structural and Investment Funds (ESIF). Letters of endorsement were exchanged between the competent Italian and Romanian ministries, while financial commitments were obtained for covering the costs of the preparatory phase and operation of the facilities through the allocated national budgets (approximately 60 M€). These, combined with other in-kind contributions currently under discussion and with synergies with H2020 funds [22], are expected to cover more than 15% of the present cost estimate for the preparatory activities and construction of ALFRED.
Considering recent studies [23] about the barriers to fund raising for First Of A Kind (FOAK) demonstration projects, FALCON decided not to exploit the possibility to apply for loans of the European Investment Bank (EIB) or any other equivalent national credit system, despite the expected incomes resulting from selling the electricity generated by ALFRED. The strategy is aimed at guaranteeing the sustainability of the DRI, while removing any obstacle to trans-national open-access, by offering grants to MS and PhD students, post-doctoral or young researchers.
Based on this view and as foreseen in the FALCON statute, the Consortium Agreement will evolve towards a legal entity with an explicit non-profit commitment (e.g. “International Organization” or “Sans but lucratif”) and a more articulated governance and management structure (general assembly, director, secretariat, advisory committees, executive and technical offices).

3.2. Implementation Plan and Socio-economic Impacts

As part of the FALCON activities, a strategic roadmap and implementation plan were conceived towards the achievement of TRL7 (“system prototype demonstration in operational environment”, i.e. the ALFRED reactor operation. A preparatory phase was recognized as a mandatory step, in order to align to the same level of maturity (TRL6) all the identified relevant aspects. As shown in Table 1, while part of the needed facilities are already in operation or under construction (nodes 1 and 2), others (node 3) have entered an engineering and design phase, relying on available results from past and on-going research activities. As shown in Table 2, node 3 is planned to reach full capacity in approximately 6.5 years, thus allowing extensive testing up to complete qualification of components and procedures. The stepwise licensing of ALFRED will be carried out in parallel (preparatory phase of node 4). One year for procurement before entering a 5 years long construction phase, will lead to commissioning and pre-operational tests of ALFRED in about 13 years from now. The costs of the DRI are split in operational and construction costs, taking into account the current status of the different nodes. While funding for refurbishment and construction of nodes 1 and 2 are already allocated, associated costs were accounted for the preparatory phase of nodes 3 and 4 (still on-going and), as well as of a central hub aimed at governing and coordinating the DRI. An extract of the cost-plan on a node and phase basis is proposed in Table 3; the overall cost of the preparation and construction is estimated in 1.7 b€, contingencies included, while the operational costs of the DRI would amount approximately to 110 M€/year.
As a combination of likelihood and impact indicators, the highest risks identified so far are related to management (inadequate communications, underestimate of time needed for critical tasks) and financial (inadequate funding sources, underestimate of costs) sectors. Additionally, availability of highly qualified personnel or delay in the supply chain of nuclear components could represent bottlenecks for the accomplishment of the ambitious implementation plan. The involvement of educational organizations and continuous exchange with industries will be guaranteed during the operation of the DRI nodes 1 and 2 to engage the main stakeholders and constantly review the forecasts. Attractive salaries and a dynamic and multi-cultural environment will be at a basis of a brain gain for the involved regions. Inter-disciplinarily researches hosted by the DRI will produce meaningful results in the area of HLM, with impacts in increasing innovation and developing new applications, products, and services. The open access to the facilities will boost the cooperation between different centres, will allow an efficient use of the resources and a better exchange of expertise and competences. The four proposed nodes (Brasimone, Řež, and two nodes in

Mioveni) will be connected not only by the management of the open access capacity, but also by a strong exchange of knowledge, expertise and results in order to speed up the development of the researches.

Timing	Milestone	Verification
T0+3months	Set-up of the Consortium Agreement	1 IR
T0+6 months	Arrangement of peripheral management structure for Node 1 and 2	-
T0+9 months	Set-up of governance, management and execution structures	1 IR
T0+1.5 years	Full capacity of Node 2	4 TR
T0+2 years	Infrastructure hosting the central offices and ICT services	4 TS
T0+2 years	Procurement of components for Node 3	2 PV
T0+3 years	Restructuring of the Consortium Agreement into a legal entity	2 IR
T0+3.5 years	Start operation of Node 3	2 PV, 8 TS
T0+4 years	Settlement of Node 4	4 PV
T0+6 years	Verification, validation and qualification of codes	2 SA, 2 TA
T0+6.5 years	Full capacity of Node 3	16 TS
T0+7 years	Completion of ALFRED design and licensing/siting procedures	3 PV
T0+8 years	Procurement of main components and site preparation	4 PV
T0+13 years	Completion of ALDRED construction (node 4)	20 TS

Tab 2: Main milestones of the implementation plan and means put in place to monitor the advancement of the activities (IR – Intermediate Review; TS – Trimestral Survey; PV – Progress Verification; SA – Scientific Assessment; TA – Technical Assessment).

	Preparation	Construction	Operation
Central hub	-	9 M€ (14%)	2.5 M€/y (11%)
Node 1 (IT)	-	-	5.0 M€/y (18%)
Node 2 (CZ)	-	-	12.0 M€/y (19%)
Node 3 (RO)	40 M€ (11%)	127 M€ (19%)	9.0 M€/y (17%)
Node 4 (RO)	512 M€ (20%)	1011 M€ (17%)	79 M€/y (16%)

Tab 3: Costs (including average contingencies in parentheses) of the DRI, split by node and phase.

Based on the extrapolation of available data from operating nodes, approximately 620 highly specialized new jobs will be created for researchers, PhD, post-docs positions, as well as for technicians. During the implementation and construction phase, more than 1200 jobs will be needed. Significant impacts will be produced at local level by stimulating the local economy. The magnitude of the investment and the level of the turnover will influence the local budget by local taxes. On the other hand indirect creation of jobs will occur (for example in the sector of services). A significant impact will consist of the increase of the qualification of research staff and of the development of the E&T sector aimed at preparing the labour force for the operation of the DRI. An increase of the number of patents and scientific papers is expected, contributing to the improvement of the current situation in Romania and Czech Republic.

4. Concluding Remarks

The synergies of a lead-cooled strategic research reactor (ALFRED) and a number of experimental facilities and laboratories distributed over three European countries are presented as an unique feature in the international context of LFR technology. The construction of a DRI is a unique opportunity to achieve fundamental objectives, needed by the European nuclear system to stay aligned with the technology readiness advancement by:

- mastering the specificities of innovative systems for the licensing authorities, with a beneficial effect also on the safety of Gen-III systems,
- practicing of the nuclear industry on innovative solutions, increasing the European competitiveness in the nuclear market with the required quality standards;
- performing education and training of a new generation of nuclear experts, able to operate in all phases of the nuclear design, supply and authorization chains.

National, regional, and local impacts are expected by the settlement and operation of the DRI, with a socio-cultural impact, a demographic impact and an impact on the visibility and

reputation of the regions and local communities. Moreover, thanks to the cooperative, fully open approach followed since the beginning in the development of the project itself, and due to the decision to pursue a Gen-IV LFR concept, Europe will be acknowledged to be at the forefront in an energy policy which embeds social concerns as a design mandate so as to meet the public acceptability.

Aknowledgments

This work has been supported by the SUSEN Project CZ.1.05/2.1.00/03.0108 realized in the framework of the European Regional Development Fund (ERDF) and by Italy and Romania National Research Funds.

5. References

[1] Generation IV International Forum, "Technology Roadmap Update for Generation IV Nuclear Energy Systems", OECD-NEA (Jan. 2014), www.gen-4.org

[2] A. Alemberti, V. Smirnov, C. F. Smith, M. Takahashi, "Overview of lead-cooled fast reactor activities", Progress in Nuclear Energy, Vol. 77, Pages 300-307 (Nov. 2014)

[3] European Commission Staff Working Document, "A Technology Roadmap for the Communication on Investing in the Development of Low Carbon Technologies (SET-Plan)", (Oct. 2009), setis.ec.europa.eu

[4] SNE-TP, "Strategic Research and Innovation Agenda" (Feb. 2013), www.snetp.eu

[5] IAEA Nuclear Energy Series, "Liquid Metal Coolants for Fast Reactors Cooled By Sodium, Lead, and Lead-Bismuth Eutectic", NP-T-1.6 (2012).

[6] I. Vasa, "ADRIANA Project Presentation", Project n. 249687 (Apr. 2010), adriana.ujv.cz

[7] FP7, "ESNII+: Preparing ESNII for H2020", Project number 605172, cordis.europa.eu

[8] FP7, "SARGEN-IV: Proposal for a harmonized European methodology for the safety assessment of innovative reactors with fast neutron spectrum planned to be built in Europe", Project number 295446, cordis.europa.eu

[9] FP7, "ARCADIA: Assessment of Regional Capabilities for new reactors Development through an Integrated Approach", Project number 605116, projectarcadia.eu

[10] FP7, "LEADER: Lead-cooled European Advanced DEmonstration Reactor", Project number 249668, www.leader-fp7.eu

[11] G. Van Goethem, "Euratom scientific and political challenges in Generation IV / Partitioning & Transmutation / Geological Disposal", STC Working Group(s) Generation IV / Partitioning & Transmutation / Geological Disposal, Brussels, (Mar. 2015)

[12] A. Alemberti, et al., "ALFRED and the FALCON Consortium", ISTC NIKIET-2014 (Oct. 2014)

[13] A. Alemberti, et al., "Lead-cooled Fast Reactor (LFR) Risk and Safety Assessment White Paper", GIF RSWG White Paper (Apr. 2014), www.gen-4.org

[14] P. Agostini, et al., "Progress report on the Italian national program on fast reactors",47th Fast Reactors Technical Working Group meeting 5/2014 www.iaea.org

[15] E. Bubelis, et al., "Safety analysis results of DBC transients performed for the ALFRED reactor", FR13, Paris France (2013)

[16] G. Bandini, et al., "Safety Analysis Results of Representative DEC Accidental Transients for the ALFRED Reactor", FR13, Paris, France (2013)

[17] M. Frogheri, et al., "The Lead Fast Reactor: Demonstrator (ALFRED) and ELFR Design", FR13, Paris, France (2013)

[18] IAEA Nuclear Energy Series, "Applications of Research Reactors", NP-T-5.3 (2014)

[19] FP7-ARCADIA, Deliverable D2.1, "Definition of Licensing Procedure", (Nov. 2014)

[20] FP7-ARCADIA, Deliverable D2.3, "Definition of Siting Procedure", (Nov. 2014)

[21] HORIZON 2020, WORK PROGRAMME 2014-2015, "Technology readiness levels (TRL)", Annex G, Extract from Part 19 - Commission Decision C(2014) 4995

[22] Enabling synergies between European Structural and Investement Funds, Horizon 2020 and other research, innovation and competitiveness-related Union programmes – Guidance for policy-makers and implementing bodies (2014)

[23] J. Burnham, et al., "Report on Innovative Financial Instruments for the Implementation of the SET Plan, First-Of-A-Kind projects", JRC (2013)

DEVELOPING STRATEGIC PLANS FOR EFFECTIVE UTILIZATION OF RESEARCH REACTORS

D. RIDIKAS
Department of Nuclear Sciences and Applications
International Atomic Energy Agency, Vienna International Centre, PO Box 100
1400 Vienna, Austria

E-mail: d.ridikas@iaea.org

ABSTRACT

Strategic plans are indispensable documents for research reactors (RRs) to ensure their efficient, optimized and well managed utilization. A strategic plan provides a framework for increasing utilization, while helping to create a positive safety culture, a motivated staff, a clear understanding of real costs and a balanced budget. A strategic plan should be seen as an essential tool for a responsible manager of any RR, from the smallest critical facility to the largest reactor. In fact, not only is it a document that can provide justification for the operational funding required for the facility, but it is also a powerful means of management control for all activities relating to the facility. A well prepared strategic plan will also provide on-going benefits to the facility management. However, due to its evolutionary nature, a strategic plan is a dynamic process, and therefore the plan will require monitoring and regular update to be truly successful.

In conjunction with this year's planned revision of IAEA TECDOC-1212 on "Strategic Planning for RRs" (2001), and in order to reflect the current status and trends in RR utilization and management, a group of international experts has reviewed 37 strategic plans submitted by RR managers in 2013-2014. The resulting suggestions and recommendations were communicated to the originators for their consideration. Each strategic plan document was reviewed against the requirements of TECDOC-1212. Results were tabulated for each document individually and recommendations for improvement were communicated to the originators. The detailed review also indicated a scoring range from well-prepared strategic plans that required only a limited amount of attention and others which were notably insufficient in their preparation.

As a follow up to the review, two interregional workshops were organized in July 2013 and October 2014. They gave for the a great number of participating RR facility managers from close to 30 Member States the chance to share experiences, lessons learned and good practices in developing and implementing strategic plans at their facilities. The lively meetings, packed with experts' lectures, country presentations and round table discussions, resulted in tangible suggestions and recommendations regarding how strategic plans should be prepared, revised and implemented. The concrete examples and case studies also provided additional input to how the TECDOC-1212, presently under revision, needs to be improved.

This paper will present in detail the results and lessons learned from the IAEA efforts to help the RR facilities developing strategic plans for effective utilization, provide review and advise services, organize national and regional stakeholder/user workshops, prepare further guidance and recommendations, document and publish guidance documents and other supporting materials.

1. Introduction

The IAEA is convinced of the need for Research Reactors (RRs) to have strategic plans (SPs) for their utilization and has regularly issued a series of publications to encourage facility managers, operators and stakeholders in this regard. The first publication of "Strategic Planning for Research Reactors" was released as TECDOC-1212 in 2001 [1]. In the meantime, planning the utilization and administration of RRs has changed according to how new technologies, business strategies and organizational structures have developed.

The IAEA has also sponsored several meetings and workshops to facilitate the exchange of expert advice and local circumstances in order to improve the concept of research reactor strategic plans and their implementation. The outcomes of these meetings identified the need to revise the original TECDOC-1212 and to publish a new version that will provide an improved approach to assist both existing and new research reactor operating organizations. Such an approach would enable reactor management to determine more accurately the state of existing reactors or the intended operation of new facilities. At the same time, management could identify the capabilities of their research reactors and match these to stakeholders' needs and establish the feasibility of supplying such needs. Management could then also establish a long term vision that would not only accomplish optimized utilization of the research reactor but would also promote the sustainability of the reactor and its ancillary facilities.

The review of the original TECDOC-1212 was also strongly recommended by the Technical Working Group on Research Reactors (TWGRR). Although the original TECDOC-1212 only focused on enhancing the utilization of existing RRs, this updated version now also provides guidance on how to develop a strategic plan for a new RR and will be of particular interest for organizations which are preparing a feasibility study to establish such a new facility. This revised publication, therefore, now complements the recently published RR Milestones document [2] and contributes to the important set of technical documents and guidelines recommended for new RR facilities. In addition, the concepts of the recently issued document on RR applications and utilization [3] are incorporated in this revision. The latter report brings together many of the current uses of RR and enables a reactor owner or operator to evaluate which applications might be possible with a particular research reactor facility. An analysis of a research reactor's capabilities, both existing and potential, is an early phase in the strategic planning process.

This paper presents some major results and lessons learned from the IAEA efforts to help the RR facilities developing strategic plans for effective utilization, provide review and advise services, organize national and regional stakeholder/user workshops, prepare further guidance and recommendations, document and publish guidance documents and other supporting materials.

2. Review of SP documents

Assistance in preparation and review of SP documents is available as an IAEA service provided to the RR facilities. Indeed, SPs for RRs are key documents to ensure their efficient, optimized and well managed utilization - this applies to both existing and newcomer RRs. Newcomers benefit from a strategic plan by the justification of the project and by clarified definition of the specification of the RR and its ancillary facilities in order to optimize its future utilization. On the other hand, existing RR could benefit by re-evaluation of stakeholder needs in order to both continue operation and to optimally increase its utilization.

In conjunction with this year's planned revision of TECDOC 1212 and in order to reflect the current status and trends in RR utilization and management, a group of international experts has reviewed 37 strategic plans submitted by RR managers around the world. The resulting suggestions and recommendations were communicated to the originators for their consideration. Each strategic plan document was reviewed against the requirements of TECDOC 1212. Results were tabulated for each document individually and recommendations for improvement were communicated to the originators. The detailed review also indicated a scoring range from well-prepared strategic plans that required only a limited amount of attention and others which were notably insufficient in their preparation.

In practice, the review of each individual SP document was completed according to a sufficiency scale (0 to 10) of section content according to the IAEA TECDOC-1212 proposals with the results tabulated for each SP. The outcome of this allocated review also indicated a range from "well-prepared SPs that required some attention with overall average, say, above 5" to some SPs which were "totally insufficient in their preparation with overall average, say, below 5".

A selective ranking system based purely on average of un-weighted scores is given in Table 1 for comparison of the levels of SP sections-areas completed by the various facilities. The numbers are the granted points (from 0 to 10). Table 1 also includes specific country average for all required sections-areas (grey column), number of zeros for not included chapters-areas (bright-blue column) and section-area averaged score by all considered countries (last line).

Table 1: The levels of SP sections-areas completed by the various facilities

Required sections or areas	MS	Exec Stat	Intro	Fac Desc	Capab (Exist)	Capab (Pot)	Stake-H (Exist)	Stake-H (Pot)	SWOT	Mission	Strat Consid	Struct & Pers	P Object	Sp Object	Action Pl	Stat & Rev	Market	Fin		# of zeros
Country 1		9	10	10	8	9	8	10	10	10	10	9	8	10	7	10	0	10	8.71	1
Country 2		10	10	8	8	8	10	10	10	10	10	8	5	9	8	10	0	10	8.47	1
Country 3		9	10	8	7	4	7	6	7	10	8	7	9	6	7	8	0	10	7.24	1
…		0	9	10	10	8	5	5	9	7	10	9	8	9	1	10	0	10	7.06	2
		9	9	7	6	4	6	4	8	10	7	10	9	8	0	0	0	0	5.71	4
		9	10	8	10	10	9	7	10	10	0	6	0	0	0	0	0	0	5.24	7
		0	0	0	0	0	0	0	10	10	10	0	8	8	8	8	0	0	3.65	10
		0	0	7	6	6	6	6	7	7	0	0	6	6	0	0	0	0	3.35	8
		0	0	0	0	0	0	0	0	0	0	0	8	9	9	0	0	0	1.53	14
Average		5.1	6.4	6.4	6.1	5.4	5.7	5.3	7.9	8.2	6.1	5.4	6.8	7.2	4.4	5.1	0.0	4.4	Average	

The involved experts recommended that the IAEA provide suitable feedback to each individual facility regarding the level of the SP preparation to still receive attention before the forthcoming workshop and then to address any outstanding shortcomings at the workshop and assist the applicable RR managers to complete their SPs to the required levels of sufficiency.

From Fig. 1 one can clearly observe that "Marketing", "Finances", "Action plans" and "Potential stakeholder needs" are the areas where the most attention is required by all.

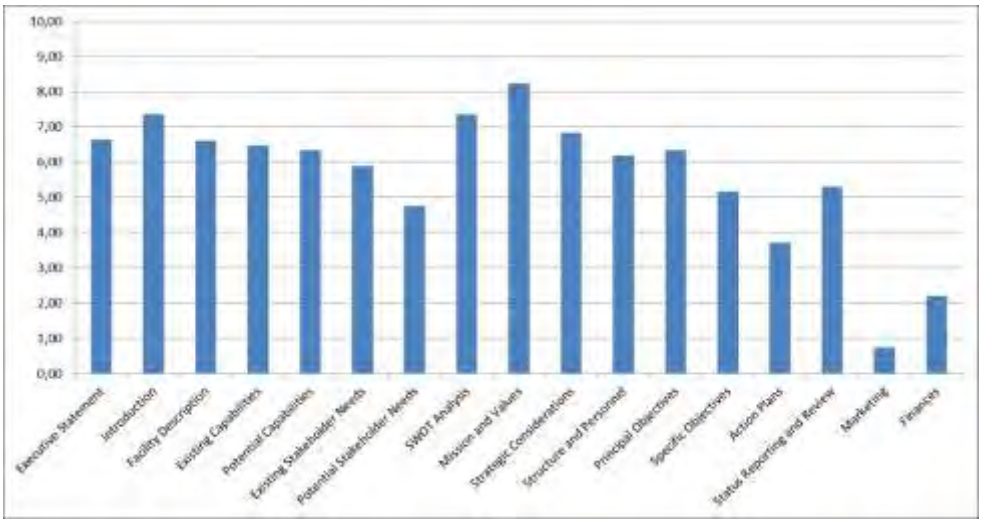

Figure 1: Un-weighted performance of SP sections-areas, averaged over all RR facilities which submitted their SP for review.

Other observations by the experts were:

- Most reports were submitted following the IAEA template – but
  - A few countries provided strategic plans in a different layout to that requested;
  - The general recommendation remains that these countries adapt their information to the IAEA TECDOC-1212 and provided format.
- Most countries completed several of the seventeen sections, but not all countries provided all information requested;
- Several countries referred to Annexes to their report but these were not received by the IAEA (and subsequently not made available to the reviewing experts);
- Although several SPs had been dated as prepared in 2012 or later, many of the others were outdated, some very much so and had obviously not received the necessary managerial controls to ensure implementation;
- Although several of the SPs reviewed applied the IAEA template there were very few that satisfactorily addressed all the review requirements of the performance indicators;
- The current status of the facility was generally well described in the SPs, as well as the analysis of Strengths, Weaknesses, Opportunities and Threats (SWOT) of the facility;
- Potential capabilities, strengths and opportunities on one hand and potential stakeholder needs are not always clearly correlated to one another;
- Quantitative information on existing capabilities and existing stakeholder needs is often absent;
- Operating schedules are missing, as are characteristics of facilities (e.g. neutron fluxes, maximum source strengths that can be handled), presence of auxiliary facilities such as hot cells or radioisotope processing plants;
- It is difficult to draw conclusions on existing stakeholders' needs if no information is given on, e.g. how often irradiations have to be provided, how many students are trained, how many samples are irradiated for NAA, etc.
- The principal objectives – and derived specific objectives - mostly are based on the strengths and opportunities. However, many facilities report concerns in their SPs how the existing experience can be fostered, or expanded, but such weaknesses or even threats are considered only in a few cases as a principal objective for actions;

- Both the specific objectives and derived action plans often contain sufficient detail, but the ones drafted using the Template's tables demonstrate that they were drafted with attention to realization;
- It is at least remarkable that only one facility explained in detail their outreach and marketing strategy and actions. This component was not specifically addressed as a mandatory item in the IAEA Template;
- It is regrettable that facilities did not take the initiative of adding marketing strategy to their SPs. This, together with the fact that almost all facilities literally copied the IAEA template text for the executive management statement, i.e. without any facility-specific notes, may raise the question whether the SPs have been reviewed at the highest executive level.

3. Follow up workshops

As a follow up to the review process of the received SPs, two interregional workshops were organized in July 2013 and October 2014. Altogether, they gave for the a great number of participating RR facility managers from close to 30 Member States the chance to share experiences, lessons learned and good practices in developing and implementing strategic plans at their facilities (Fig. 2). The concrete examples and case studies also provided additional input to how the TECDOC-1212, presently under revision, needs to be improved.

Figure 2: Photo of participants and experts attending the IAEA Training Workshop on "Development of Research Reactor User Communities and Industrial Partnerships" IAEA Headquarters, Vienna, Austria, 13–17 October 2014.

The workshops also allowed facilitating the exchange of experts' advice and local circumstances in order to improve the concept of RR strategic plans and their implementation. Such an approach enables reactor management to determine more accurately the state of existing RRs or the intended operation of new facilities. At the same time, management could identify the capabilities of their RRs and match these to stakeholders' needs and establish the feasibility of supplying such needs. Management could then also establish a long term vision that would not only accomplish optimized utilization of the RR but would also promote the sustainability of the reactor and its ancillary facilities.

The following is a summary of the issues raised during the feedback session from the workshop participants regarding lessons learned during the expert and participant presentations and discussions.

- The topics effectively covered SPs over the full range of RRs:
    - From “Small” to “Big”, and of various statuses from
    - Planned, Under construction, Operational (both well-utilised and under-utilised), Shutdown, to Being Decommissioned
- There was in most cases a need for a national strategy and vision to enable the RR SP to be effectively applied
- Most (all) RRs were dependent on Government funding
- Assistance is readily available to help RR management - but managers need to be proactive
- The choices among E&T / R&D / and Irradiation Services (IS) and Isotope Production (IP) are not always that simple
    - The preferred government strategy is rather E&T than R&D
    - There is often insufficient funding to carry on these activities
    - IS and IP are generally considered for income generation
    - The RR remains as a service provider for the above and is not the service/product originator
- Common problems experienced across the RR SP profiles presented:
    - Funding
    - Loss of Personnel and expertise – Retirement, Relocation to industry
    - Ageing of staff and systems
    - Ability to find stakeholders/users and increase utilisation
    - Extended shutdown situation.

The workshop participants together with the experts also formulated a number of follow up recommendations to the teams involved in drafting facility SPs, namely they should:

- Revise their SPs according to the expert review comments and the lessons learned during the workshop;
- Follow-up the draft SPs by implementation, progress monitoring and evaluation, and review by facility’s own committee;
- Share the lessons learned with relevant staff, top down and bottom-up;
- Quantify capabilities, existing and future stakeholder’s needs; the latter in close communication with those stakeholders. If applicable, make an inventory of radionuclides and sources (and their strengths) imported and in use in the country;
- Establish and quantify the performance indicators for monitoring progress and provide baseline values for the status in the reference year;
- If applicable, initiate awareness building on RR utilization at universities and the public. If applicable, publish in the social media success stories of social-economical relevance;
- Consider professional help in marketing, advertisement and sales;
- Consider finding stakeholders also outside the country.

4. Review of the IAEA TECDOC-1212

As one of the key outcomes of the SP review meetings/workshops, it was identified that there is a need to revise the original TECDOC-1212 and to publish a new version that will provide an improved approach to assist both existing and new RR operating organizations. The review of the original TECDOC-1212 was also strongly recommended by the Technical Working Group on Research Reactors (TWGRR). The Agency, in addition to the above mentioned follow up workshops, has organized a dedicated consultancy meeting (in May 2014 in Vienna), where a group of international experts have proposed and provided inputs to the following new structure of the future IAEA publication:

Part 1 – Guidelines: The purpose of this part is to put the formulation of a strategic plan into perspective, to provide a rationale for the development of a strategic plan and to give an overview of the process.

Part 2 – Preparation of a Strategic Plan: The second part of the document is a more detailed guide. It gives a suggested format for the plan and describes the considerations and content of each section. Selected question sets are used which aim at assisting the facility management in tailoring the plan to meet its needs.

Part 3 – Guidance on Specific Topics: The third part contains guidance on how to evaluate the financial implications to operate the facility, increase stakeholder awareness of the existence of the facility and how to attract stakeholder utilization. As mentioned above, a change in management and personnel mind-set is sometimes necessary - this is also described in this part of the document.

In addition, several Annexes have been added to this revised version of the document and include examples to clarify the methodologies discussed in the document and to thereby assist the preparers of the strategic plan:

- Annex 1: Some strategic considerations that could be taken into account for the strategic plan's preparation;
- Annex 2: A template as an example of a typical strategic plan's layout;
- Annex 3: Clarification of the application of Strength-Weakness-Opportunity-Threat (SWOT) analysis and the relevant Probabilistic Risk Assessment (PRA) evaluation;
- Annex 4: A typical questionnaire as an example of surveys required to determine capabilities and competencies required for a new nuclear center;
- Annex 5: An example of evaluation methodologies for Key Performance Indicators (KPIs) required for a research reactor's utilization;
- Annex 6: Clarification of the concept of Eliminate-Reduce-Create-Raise (ERCR) analysis for achievement of an objective with a typical example; and
- Annex 7: A completed (but filtered) strategic plan from an operational research reactor.

The schematic structure outlined below in Figure 3 is an illustration of the revised approach that should be considered when regarding the development of a strategic plan and its intended outcome. The outcome (roof) of a successfully implemented SP must result in optimized Utilization and Sustainability of the RR during its lifetime. This can only be achieved if the support system (pillars) of the applicable Stakeholders are sufficiently well developed to ensure implementation – e.g. by utilization of irradiation services, existence of R&D projects, and need for Education and Training (E&T) activities. A sound basis (foundation) for the structure is built according to the Stakeholder Engagement (through their needs and interests) which ensures that the resources are made available. These resources are normally the facility itself, funds required and the staff operating and supporting the on-going activities.

Finally, it must be emphasized that the methodology for the preparation of a strategic plan as identified in this revised document is purely a guideline and is not mandatory – unless it is a specific requisite by the IAEA when evaluating requests for technical/financial assistance. The IAEA does not expect general publication of plans or public disclosure of the information contained therein. The IAEA, however, recommends that it will prioritize support requests for new ancillary facilities or equipment for RR utilization if they are accompanied by a strategic plan clearly demonstrating that the items requested are necessary to achieve the objectives of the plan.

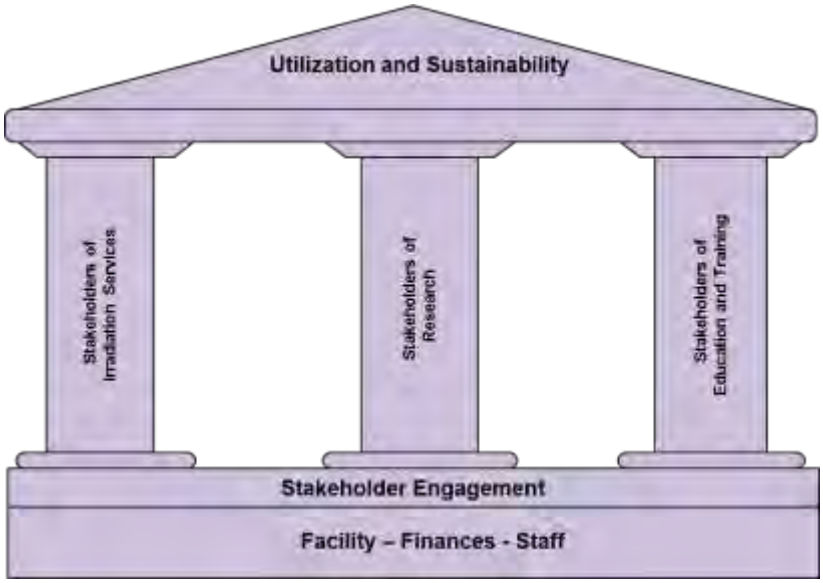

Figure 3: Modular approach for the strategic plan of a research rector.

6. Conclusions

The IAEA is convinced that the long-term sustainability of many RRs around the world depends upon the development and implementation of an effective and achievable SP for their utilization. It is hoped that the revised guidelines on how to prepare, efficiently monitor and successfully implement the SPs for RR facilities together with the offered IAEA services in preparation and review of SP documents will prove to be a key element to enhance RR utilization and ensure long term sustainability of the products and services these facilities can provide.

References

[1] INTERNATIONAL ATOMIC ENERGY AGENCY, Strategic Planning for Research Reactors — Guidance for Reactor Managers, IAEA TECDOC Series No. 1212, IAEA, Vienna (2001); presently under review with the new publication expected in 2015.

[2] INTERNATIONAL ATOMIC ENERGY AGENCY, Specific considerations and milestones for a Research Reactor project, IAEA Nuclear Energy Series No. NP-T-5.1, IAEA, Vienna, (2012).

[3] INTERNATIONAL ATOMIC ENERGY AGENCY, Applications of Research Reactors, IAEA Nuclear Energy Series, NP-T-5.3, IAEA, Vienna (2014).

LESSONS LEARNED IN THE PACKAGING AND REMOVAL OF LEGACY PLUTONIUM MATERIALS

L. D'Andrea, P. Negrini, M. Pietrobon, A. Proietti, F. Di Gasbarro
SOGIN S.p.A. Italy

D. Maertens, M. Gysemans, L. Noynaert
SCK•CEN, Belgium

K.A. Dunn and N.C. Iyer
Savannah River National Laboratory, USA

ABSTRACT

Significant fuel cycle research using research reactors and associated facilities were conducted in Europe during the 1970s and early 1980s to assess technologies for the reprocessing of spent fuel and the development of new mixed oxide fuel using the separated plutonium from the reprocessing activities. The pace of this research significantly diminished in the last two decades and as a result, legacy separated plutonium materials have been stored in various research facilities during the past several decades with no obvious disposition path. The U.S. Department of Energy – National Nuclear Security Administration (DOE-NNSA) has been working with a number of countries in Europe to package and dispose the separated plutonium materials in the context of global threat reduction and the Nuclear Security Summit process. Since much of the infrastructure for handling plutonium materials in these research facilities had been dismantled, the handling of the legacy plutonium materials to facilitate stabilization and repackaging for transport have entailed development of new glove box facility in various European countries. This paper will detail the lessons learned during the development of new glove box line at SOGIN, Italy and the implementation of the repackaging operations. The development of a new facility not only had to meet the stringent regulatory requirements for the handling of alpha plutonium materials but also had to adapt plutonium stabilization and packaging flow sheets to meet the package and transport requirements. Key elements of the plutonium stabilization and repackaging involve high temperature stabilization treatment in a furnace within the glove box, packaging the stabilized materials within the glove box and analytical characterization of the material. Lessons learned during the stabilization and glove box handling activities resulted in improvements and modifications in the design of the plutonium glove box systems, optimization of operation processes and refinements in packaging flow sheets. The cooperative efforts between SOGIN, Italy, U.S. DOE-NNSA and SCK•CEN, Belgium is described and key lessons learned in the effective packaging of plutonium in transport-ready packages highlighted.

1. Introduction

Nuclear materials from the past reprocessing and plutonium fuel research/pilot operations were stored at the EUREX (Enriched Uranium Extraction) plant at Saluggia Research Center, Vercelli, Italy and the IPU (Impianto Plutonio) plant at Casaccia Research Center, Rome, Italy. These plants were previously operated by ENEA (Agenzia nazionale per le nuove tecnologie, l'energia e lo sviluppo economico sostenibile). Since 2003, SOGIN has managed these plants with the mission to perform the decommissioning of the facilities in order to achieve "green field" status. The first step in decommissioning is the removal of the high enriched uranium (HEU) and separated plutonium materials. SOGIN has worked with the U.S. Department of Energy (DOE) – National Nuclear Security Administration's (NNSA) to repatriate the legacy HEU and plutonium materials to the U.S. The characterization, packaging and removal of plutonium materials presented many unique challenges some of which will be reviewed in this paper.

The plutonium bearing materials had to be thermally stabilized prior to packaging in order to comply with the DOE requirements and safety standards for the removal and transfer of the plutonium materials. The materials content and packaging configuration also had to comply with the conditions of the 9975 Type B transport package certificate. For this reason a new line of gloveboxes was designed, constructed, assembled and made operational at the IPU plant in a very short time frame in order to implement the plutonium packaging and removal project. The glovebox system had the capability to support unpackaging of storage containers, high temperature stabilization, analytical characterization and repackaging in inert environment of the plutonium oxide materials in order to meet the U.S. DOE requirements for the acceptance of these materials. The project had an aggressive schedule in order to complete the packaging, transport and removal mission prior to the 2014 Nuclear Security Summit. Numerous emerging technical issues had to be solved without compromising the safety imperatives and the schedule goal. This paper will outline the lessons learned during the packaging operation using the new gloveboxes system.

2. Glove Box Facility and Plutonium Materials Stabilization Process

The system installed at the IPU plant consisted of a train of three gloveboxes, designed to permit the safe handling of nuclear materials (uranium and plutonium oxides), while providing capability to perform the following tasks:

- Glovebox 1 (GB1): Introduction and opening of canisters containing nuclear materials, sieving, weighing and mixing
- Glovebox 2 (GB2): Crushing, stabilization at high temperature (950°C) of the plutonium materials/ powder in the furnace
- Glovebox 3 (GB3): Thermo-gravimetric analysis (TGA) to measure moisture content and confirm the effectiveness of the thermal stabilization.

Figure 2.1 Glovebox system and operators

The glovebox design did not include leaded glass because of SOGIN IPU plant familiarity with conventional glass gloveboxes. However, the operators used lead coats and portable shielding to minimize the dose to the operators.

The GB1 was dedicated for the inspection and opening of the legacy plutonium storage containers, extraction of plutonium bearing materials, identification of the material condition, eventual homogenization of the material, distribution of the material in a convenience can able to contain the process batch identified in the packaging matrix. After the preparation of the batch, the convenience can, was transferred from GB 1 to GB 2 through the transfer channels which had connection doors.

The GB2 was established to characterize the powder particle size, perform sieving and grinding operations as necessary in order to obtain homogeneous powder mixture. The material was transferred to an alumina tray and loaded into the furnace to perform the thermal stabilization. Each operation was always preceded by weighing operations to ensure materials accountability and control. Upon completion of the stabilization thermal cycle, the material was extracted from the furnace and transferred into the special container to be homogenized using the manual mixer. Subsequently the material was loaded into the slip lid can prior to transfer from the GB2 to GB3.

The GB3 operations included extraction of a small portion of the mixture for TGA (Thermo Gravimetric Analyser) analyses to measure moisture content through the change in weight of the sample. If the measured value was higher than the 0.42% by weight, the material had to be subjected again to the thermal treatment cycle.

3. Lesson Learned from Plutonium Glove Box Operations

3.1 Bag out system modification

The geometric characteristics of the bag ports were defined during the design stage in collaboration with the DOE technical team. The port external diameter was 156 mm. The filter bags were manufactured by Nuclear Fuel Technology, U.S. (NFT) for a direct connection to the 156 mm diameter bag port and provided by the DOE team to the IPU Plant. A back-up option, which included the adoption of a transition piece between the bag-out port and the filter bag was planned, as the solution was already implemented in the USA and other European sites.

The verification of the tightness between glove box bag port and filter bags was possible only during the glovebox site acceptance tests (SAT). The direct connection did not assure the tightness of the system for the following reasons:

- Bag port grooves were too close to each other and to the terminal part of the port; the bag port grooves were also not sufficiently deep. These two issues were deemed critical, especially during the substitution of the filter bag.

- The bungee cord of the filter bag was not strong enough to prevent the detachment of the bag. The bags normally used at the IPU plant have an O-ring made of a rigid rubber band.

Figure 3.1 Details of the bag port with filtered bag

The back-up solution immediately explored was the use of a transition piece as was planned during the design stage. This approach was adopted by SCK•CEN in similar operations. However it was not possible to adopt it because the bag port grooves of the glove boxes were not deep enough and not properly positioned.

The solution investigated by SOGIN was to use just one bag (modified) that would assure the same level of tightness assured by the bag-out system of the other glove boxes. The solution analysed included the modification of the PVC filter bag and the application of a special adapter mounted on the 156 mm diameter bag port to assure direct connection between the bag and the port.

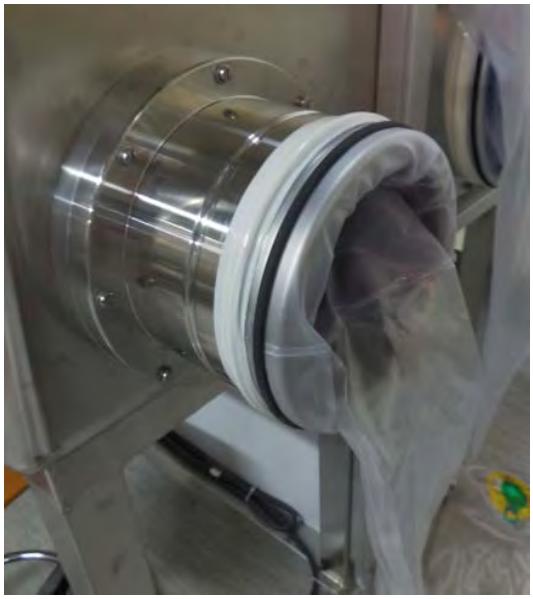

Figure 1.2 View of the bag port modified with the adaptor

The bag was modified by cutting the terminal part of the bag with the bungee cord and replacing it with a piece of PVC welded to the DOE supplied filter bag having the same diameter. The O-ring fixed to the added piece of PVC is made of rigid rubber, stronger than the bungee cord thus assuring a better tightness of the bags with the bag ports.

The modification of the filter bag was reviewed with a SOGIN qualified supplier of PVC bags and, before implementing it, several tests were carried out in order to verify the quality and accuracy of the welding, using different types of PVC and defining the external diameter of the adapter to be mounted on the 156 mm diameter port.

Figure 3.3 A filtered bag modified with rubber O-ring

The modified filter bag had a diameter of 177 mm and could be directly mounted on the 190 mm diameter bag port. The characteristics and dimensions of the adapting device were analysed with the glovebox manufacturer. Two options were considered:

- Replace the 156 mm diameter bag port with a new 190 mm diameter port with adequate grooves
- Install an adapter and maintain the existing bag port as-is in place.

The second option was selected because it had the advantage of not having to drill holes or modify (machine) any of the glovebox components. It was only necessary to replace the existing screws of the bag port with longer ones.

The adapter consisted of a flange and a new port. The flange was fixed to the sidewall of the glovebox. It included an O-ring on each end to ensure that the new port was leak tight. The new port was fixed to the flange and sealed with one O-ring on the flange and with a second one to the existing bag port. The solution eventually implemented is illustrated in the following drawings and pictures.

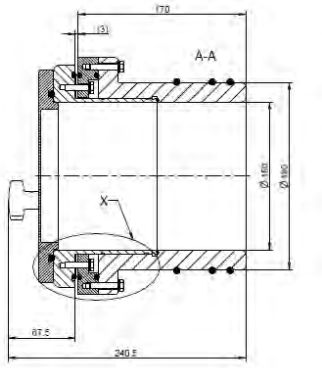

Figure 3.4 Sectional view of the adapter

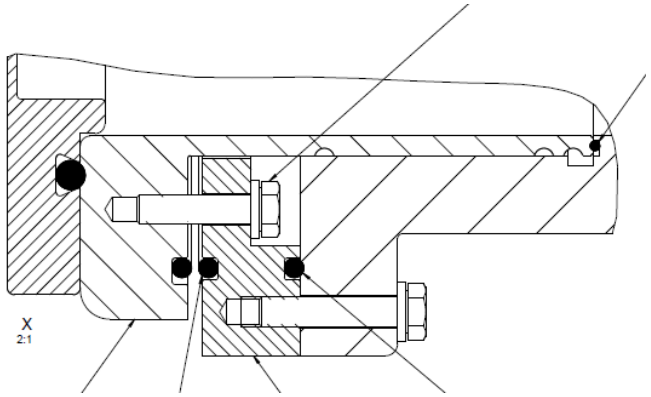

Figure3.5 Adapter design

The analysis and implementation of the solution adopted by SOGIN required significant cooperation between SOGIN, glovebox manufacturer and the SOGIN PVC bag supplier, due to the stringent time schedule of the Project. Furthermore, since the glove port adapter was installed after the glove boxes site acceptance tests, the leak tightness test of the entire glovebox system had to be revalidated. The entire plutonium stabilization and packaging campaign was completed safely using the glove port arrangement described herein.

3.2 Thermal treatment cycle optimization for nuclear material stabilization

The plutonium packaging operations plan was based on thermal cycles of 24 hours as established during the execution of the furnace acceptance tests with cerium oxide. However the thermal treatment cycle carried out with the plutonium materials lasted over 30 hours. The cooling phase of the furnace showed a gradual decrease from 200°C to 150°C however the cool down duration from 150°C to 45°C, the temperature value at which the furnace door was permitted to be opened for materials extraction, lasted more than 10 hours. The furnace was constructed with high insulation characteristics in order to fulfil the IPU plant requirement to limit glovebox ambient temperature to less than 50°C.

Options to reduce the total thermal cycle time were considered to minimize the impact on the overall project schedule. Following consultation with the DOE team, the experiences and procedure applied at SCK•CEN was adopted. It included a reduction in the cooling phase duration by partially opening the furnace door at 150°C to have a more effective heat exchange between the chamber of the furnace and the internal volume (space) of the glovebox. Adoption of this practice learned through the experience at SCK•CEN offered the best opportunity to manage the packaging window for the plutonium materials packaging and removal campaign.

A numerical simulation based on conservative assumptions was performed to analyse the temperature field inside the glovebox in order to ensure a defensible and credible technical basis for the modification of the packaging procedure. The case for when the furnace door is left slightly opened to enhance the heat exchange was analysed in order to demonstrate that the glovebox interior and surface temperatures were sufficiently low so as not to compromise the leak tightness and the structural integrity of the glovebox.

A three dimensional (3-D) stationary finite element model (FEM) simulation was performed using

the COMSOL multiphysics software. The heating source was assumed to be in the frontal chamber of the furnace rather the interior in this model. The following characterize primary assumptions and characteristics of the model:

- Stationary simulation, equivalent to a solution after an infinite time with the heating source at fixed temperature of 423 K (150°C)
- The oven and the glovebox surfaces are modelled as adiabatic walls
- The cover door is considered open and rotated of 90 degrees respect to its resting position to consider the minimum distance between the cover and the glove connections.
- Simulation was carried out on a 1:1 scale;
- Thermo-physical fluid properties are function of temperature and pressure;

The model included a coarse mesh of almost 220,000 cells (boundary layer thickness of 5 mm for the inlet and outlet ducts and of 2.5 cm for the other surfaces). The furnace door was assumed to be 3 cm wide and positioned 5 cm far from the frontal chamber surface.

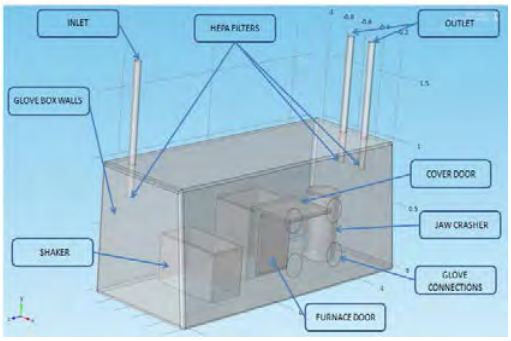

Figure 3.6 Glovebox geometry

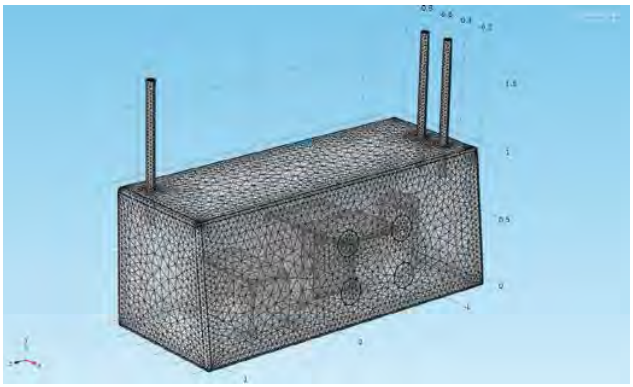

Figure 3.7 Glovebox model meshes

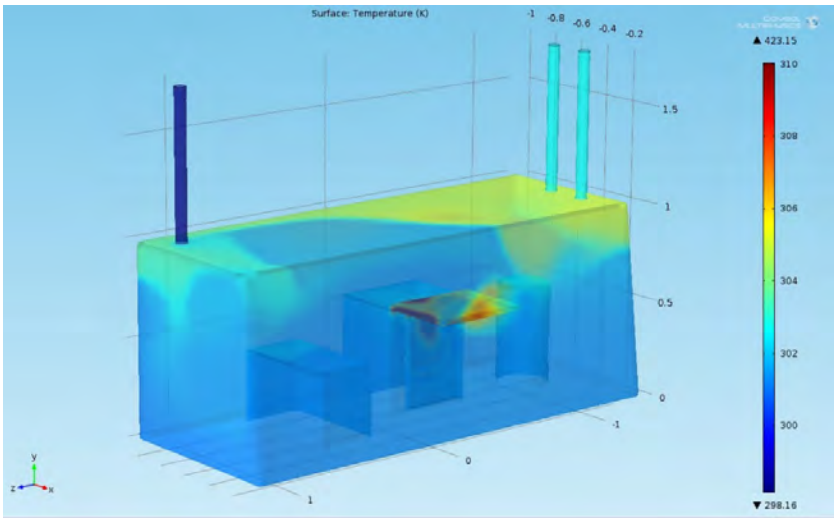

Figure 3.8 Glovebox surface temperature - front view

The modelling results showed that the thermal plume rises up due to the temperature difference between the front portion of the chamber surface and the “colder” air in the glovebox interior. The glovebox surface temperatures were analysed to be:

- The maximum temperature is 306.9 K (33.8°C).
- The average temperature is 302.2 K (29.1°C)
- The minimum temperature is 301.1 K (28.0°C)

The maximum temperature of the glove connections was analysed to be 305 K (31.9°C). Furthermore, the maximum temperature close to the surface of the outlet HEPA filters was analysed to be 303.8 K (30.7°C) and the average temperature inside the Glove Box was 302.2 K (29.1°C). A very limited higher temperature zone was identified in the furnace casing as expected close to the front surface of the furnace chamber near the location of the heating source in the model.

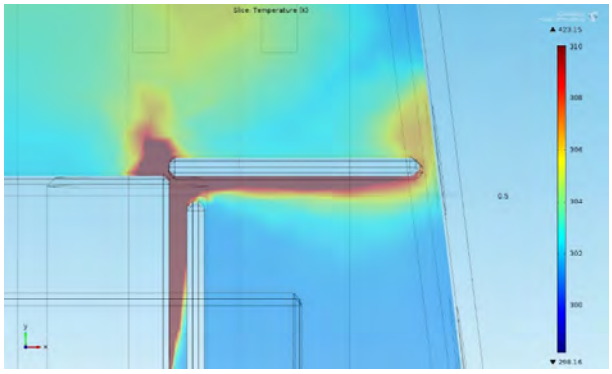

Figure 3.9 Model of the thermal plume

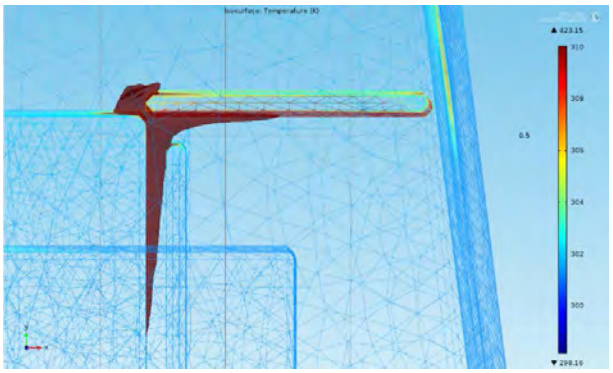

Figure 3.10 Isothermal surface at T=~318 K (45°C)

Independent analyses by the glovebox manufacturer confirmed that neither the structural integrity nor the leak tightness of the containment would be compromised if the furnace door were opened prior to reaching ambient temperatures. Some modifications on the interlocks were also implemented to enable the partial opening of the furnace door at 150°C. The designed safety level of the glovebox system was maintained to those approved by the regulator.

The safety case and the revised operation procedure were subject to the approval of the Nuclear Authority (regulator). The full implementation of the above procedure modification was validated by three cycles of tests with plutonium materials carried out under the supervision of the Nuclear Authority. The results of the tests are shown in the Table below and compared to numerical outputs of the finite element (F.E) analytical model.

	Temperatures [°C]	
	F.E. Model	Test
Tmax GB	33,9	27,2
Tmax Glove	32,0	27,0
Tmax Cover	64,6	33,9

3.3 Other lessons learned examples

Other important lessons learned were acquired from the GB equipment and packaging operation. The alumina tray used to hold the plutonium materials in the furnace was sized in order to contain one process batch of plutonium materials assuming a material density of 2.5 g/cm^3. Because of a different separation and calcination process, plutonium materials from the EUREX plant had a density of about 1 gm/cm^3 due to some particular resins that enlarged the grain size of the materials in microspheres. For this reason it was not possible to load the EUREX materials batch in one alumina tray because of limited volume of the tray. The treatment of all the EUREX materials would have required twice the number of planned furnace cycles. This fact would have negatively affected the time schedule of the activities and timely completion of the removal activities prior to the 2014 Nuclear Security Summit. The team analyzed multiple options and determined that the best way to solve the problem was to procure a larger volume alumina tray able to contain an entire batch of EUREX materials. Unfortunately the lead time for procurement of alumina trays and the incompatibility of plutonium materials with metal trays precluded ready implementation of the option. SCK•CEN, the Belgian Research Center, which performed similar plutonium stabilization activities in conjunction with DOE-NNSA had already qualified use of larger size stabilization trays. The SOGIN, DOE and SCK•CEN team work cooperatively to quickly implement the Belgian lessons learned at SOGIN to qualify and implement the use of larger trays for the EUREX materials in a timely manner and meet schedule goals. Implementation of the larger trays at SOGIN required requalification of the furnace operations by DOE to assure that the entire bed of the larger batch of EUREX materials was exposed to the 950°C thermal cycle. Requalification of the furnace using a plutonium contaminated glove box system presented significant challenges and was closely coordinated with the appropriate authorities.

Figure 3.11 Large size alumina tray furnace test

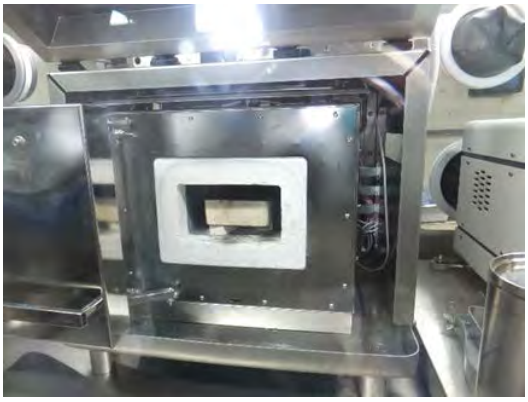

Figure 3.12 Tray in the furnace

There were many other more routine lessons learned adopted throughout the packaging campaign. For example, although the gloveboxes were procured with an electronic sieve to separate the powder materials with different particle size, the glovebox operators developed a sieving method using manual sieves which was more ergonomically efficient.

Figure 3.13 Sieve used during operations in the glovebox

The extraordinary teamwork and cooperation using a multinational team including SOGIN, DOE, SCK•CEN, glovebox manufacturer and the Italian Nuclear Authority enabled SOGIN to meet the challenging packaging and materials removal goal.

4. Conclusions

SOGIN completed a very challenging plutonium characterization, packaging and removal/shipping project in support of global threat reduction initiatives and as part of its decommissioning activities of legacy research facilities. Partnership with DOE and multinational cooperation with Belgium and other European organizations was a key to success. The project was completed in less than 540 calendar days including the design, construction, installation and start-up of a plutonium characterization and packaging facility. The packaging operations were safely performed in 72 calendar days without registering any anomaly or deviation from the approved procedures. .

The key success factors are summarized as follows:

- The lessons learned in similar projects e.g. through AB SVAFO in Sweden were very useful to identify the right path for this project during the planning phase.

- Cooperation with SCK•CEN and glovebox manufacturer was important to solve emerging issues during the packaging campaign.

- The strong collaboration between SOGIN and the DOE team enabled identification of the most appropriate solutions to the many technical and management issues of the Project and enabled timely coordination with the Nuclear Authority.

- The comprehensive project planning process, SOGIN and DOE-NNSA management support and their empowerment of the project team enabled effective project execution. .

LEU Fuel Developmet & Qualification

MICROSTRUCTURAL CHARACTERIZATION OF IRRADIATED U-7MO: REGIONS AROUND GRAIN BOUNDARIES AND REGIONS WITH DIFFERENT MO CONCENTRATIONS

J. GAN, D. KEISER, JR., B. MILLER, J. JUE, A. ROBINSON, P. MEDVEDEV, AND J. MADDEN

Nuclear Fuels and Materials Division, Idaho National Laboratory
P. O. Box 1625, Idaho Falls, ID 83415-6188 U.S.A.

Corresponding Author Contact Information:
Dennis D. Keiser, Jr.
Idaho National Laboratory
P.O. Box 1625
Idaho Falls, ID, 83415-6146 U.S.A.
Phone: 1 (208) 533-7298
Fax: 1 (208) 533-7863
E-mail: Dennis.Keiser@inl.gov

For Publication in the Proceedings of the Research Reactor Fuel Managment Conference
(April, 2015 in Bucharest, Romania)

MICROSTRUCTURAL CHARACTERIZATION OF IRRADIATED U-7MO: REGIONS AROUND GRAIN BOUNDARIES AND REGIONS WITH DIFFERENT MO CONCENTRATIONS

J. GAN, D. KEISER, JR., B. MILLER, J. JUE, A. ROBINSON, P. MEDVEDEV, AND J. MADDEN

Nuclear Fuels and Materials Division, Idaho National Laboratory
P. O. Box 1625, Idaho Falls, Idaho 83403 USA

ABSTRACT

During irradiation, the microstructure of U-7Mo evolves until at a fission density near $5x10^{21}$ f/cm^3 a high-burnup microstructure exists that is very different than what was observed at lower fission densities. This microstructure is dominated by randomly distributed, relatively large, homogeneous fission gas bubbles. It is of interest to determine how microstructural development at the grain boundaries and at low-Mo-content regions impact the development of this high burnup microstructure. It has been observed that relatively large fission gas bubbles develop on grain boundaries before the intergranular regions, and relatively large fission gas bubbles initiate in the low Mo regions of the fuel particles before the higher Mo regions. Potentially, a heat treatment of the starting fuel powder could be employed to grow the grains, resulting in fewer grain boundaries, and to homogenize the Mo content, thereby reducing the fraction of low-Mo areas in the fuel particles. A microstucture with these characteristics could potentially exhibit improved fuel performance (i.e., postpone the development of the high-burnup microstructure). This paper discusses the irradiated fuel microstructures that have been observed around grain boundaries and in microstructural regions with different Mo contents. This information is beneficial for improving the understanding of how heat-treated fuel particles may behave during irradiation.

1. Introduction

The Material Management and Minimization (also known historically as the Reduced Enrichment for Research and Test Reactor) Fuel Development program is developing low-enriched uranium (LEU) fuel to reduce the demand of highly-enriched uranium (HEU) fuels currently used in research and test reactors throughout the world [1,2]. During reactor testing, it has been observed that a relatively large change in swelling behavior can occur above 4.6 $\times 10^{21}$ f/cm^3 [3], and one potential cause of this behavior is a significant change in the swelling behavior of the U-7Mo fuel particles themselves at fission densities above this value. It has been observed that at higher fission densities significant changes have occurred in the observed microstructure of the fuel such that it consists of relatively large fission gas bubbles and metallic fission product precipitates [4].

It is of interest to determine how the microstructural development at grain boundaries and low Mo content regions contribute to the devleopment of this "high-burnup" microstructure. Typically, relatively large fission gas bubbles develop first on grain boundaries and in low Mo content regions [5]. As a result, it has been determined that by heat treating the fuel particles the grain size could be increased (to reduce the amount of high angle grain boundaries in a fuel particle) and the Mo content could be more evenly distributed (to reduce the amount of low Mo regions). To better understand the impact of having grain boundaries and low Mo regions in the fuel particle microstructure, detailed microstructural characterization has been performed on U-7Mo fuel irradiated under different conditions. These fuel plates were characterized using a scanning electron microscopy (SEM) and a focused ion beam (FIB) in-situ lift out (INLO) technique for sample preparation. SEM analysis of FIBINLO samples was performed to investigate the size, morphology, and distribution of fission gas bubbles and

solid fission product phases. TEM characterization was also conducted using the generated FIB lamella samples. This paper focuses on TEM results.

2. Experimental

The dispersion fuel plates that were characterized were irradiated in the Advanced Test Reactor, and the fuel particles used in the fuel plates were produced using a Rotating Electrode Process (REP) with a cast U-7Mo alloy rod. During irradiation, the plates were oriented edge on facing the core. This led to a significant fission rate variation across the plates. This provided a variation in fission densities across individual plates. Samples were produced from four fuel plates (see Table 1) at the Hot Fuels Examination Facility (HFEF) at the Idaho National Laboratory in the form of 1-mm-diameter by 1.4-mm-long fuel punchings. The samples were mounted and polished at the Electron Microscopy Laboratory for sample preparation and analysis in the scanning electron microscope (SEM). Both secondary electron (SE) and backscattered electron (BSE) images were produced from the polished samples. Additional characterization samples were produced from the mounted samples using a FEI Quanta3D Dualbeam FIB. The first step when generating a FIB sample is to deposit a Pt protective layer on the sample surface to reduce curtaining and minimize damage to the specimen surface during milling operations. This is followed by the generation of "lift-outs", which are ultimately obtained at specific locations by coarse trenching a 20 μm x10 μm x 1 μm sample. Figure 1 shows a polished surface for the R2R040 sample where six FIBINLO samples were produced for characterization. SE imaging was employed to evaluate the size, morphology, and distribution of fission gas bubbles and solid fission product phases present in these samples. TEM characterization was peformed using FIB-produced samples. Composition analysis of TEM lamella samples was carried out using a Brukers Si Drift Detector (SDD) in Scanning TEM mode (STEM) or a Si(Li) detector in TEM mode (before EDS upgrade in 2012).

Table 1: Irradiation parameters of TEM samples.

Fuel Composition	U-7Mo	U-7Mo*	U-7Mo*	U-7Mo*	U-7Mo*
Matrix	Al-2Si	Al-2Si	Mg	Mg	Pure Al
Fuel Plate ID	R2R040 (Low)	R2R040 (High)	R9R010 (Low)	R9R010 (High)	R0R010 (High)
U^{235} % Enrichment	58%	58%	58%	58%	58%
Local Fission Density (10^{21} fiss/cm^3)	3.3	6.3	3.7	5.5	5.6
Time Avg. Fission Rate (10^{14} fiss/cm^3-sec)	4.3	8.1	7.4	11.0	7.2
Temperature (˚C)	90	120	123	158	125

*FIB-TEM lamella are used for characterization.

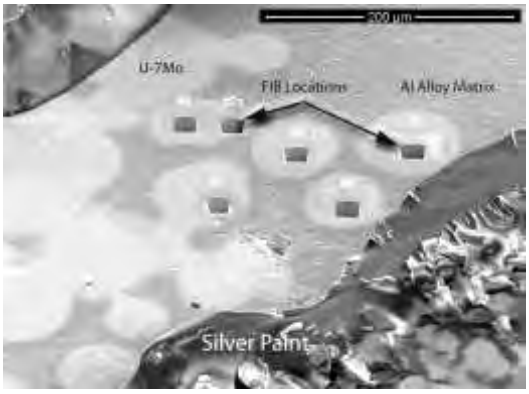

Figure 1. SEM image of the locations where FIBINLO samples were produced from an irradiated fuel plate (R2R040). Samples were produced to capture U-7Mo microstructure.

3. Results

3.1 Microstructures Around Grain Boundaries

Figure 2 shows the SEM images, left, of the FIB sectioned pristine surface from different fuel particle location (site A and B) along with the STEM images, right, of the corresponding TEM samples. It is for the irradiated fuel plate (R9R010) with a fission density of 3.7E+21 fissions/cm^3. The site-A sample (top) reveals an irradiated microstructure with more aggressive bubble development than a typical microstructure as shown in the site-B sample (bottom) at this fission density. The latter image shows significant fraction of “clean” areas consisting of fine fission gas bubble (3 - 4 nm) superlattice and the areas filled with large bubbles (> 100 nm) likely developed from grain boundaries. Note that grain subdivision does not occur at this burnup. It is well known that grain boundaries (g.b.) are the preferential sites for the devlopment of gas bubbles due to the high mobility for fission gas atoms on grain boundaries.

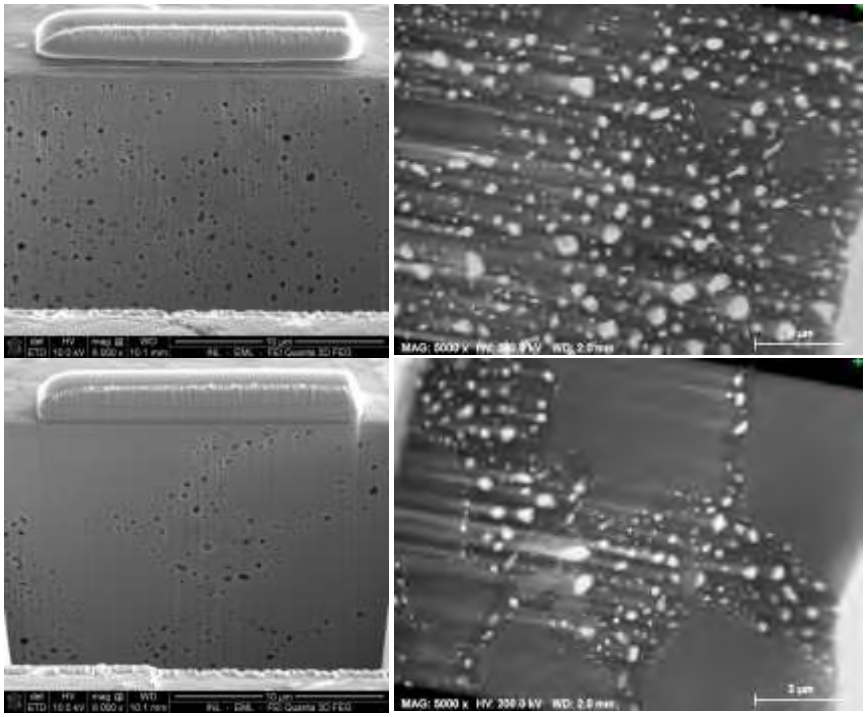

Figure 2. FIB-SEM images (left)) and STEM inages (right) of irradiated U-7Mo fuel particle (plate ID: R9R010) at a fission density of 3.7E+21 fissions/cm^3 from site “A” (top) and “B” (bottm). Note the orientation and magnification between SEM and STEM images are different.

The microstructure of the high flux side of the same irradiated fuel plate (R9R010) is shown in Figure 3 with a local fission density of 5.5E+21 fissions/cm^3. The STEM image at low magnification on the left reveals a bubble microstructure not significantly different from that of site-A in Figure 2. A high magnification STEM image of the boxed area on the right shows the complex subdivided grains of submicron size. This complex grain texture along with high density large bubbles (> 200 nm) is the characteristic high fission density microstructure for U-Mo fuel. Although at this condition the linkage of large bubbles is not evident, but the closeness between some large bubbles indicates the interlinking of these large bubbles can occur rather quickly as the fission density increases. Only few scattered small pockets of the residual gas bubble superlattice can be found in some crystalline areas at this fission density.

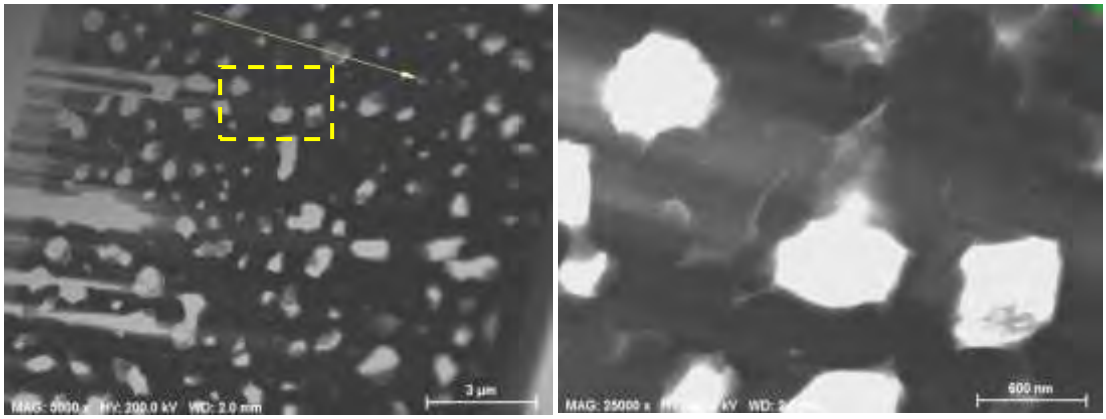

Figure 3. STEM image of irradiated U-7Mo fuel particle (plate ID: R9R010) at a fission density of 5.5E+21 fissions/cm^3 from site "C". A high magnification view of the boxed area is shown on the right where the subdivided grains with submicron grain size are discernable.

3.2 Changes in Microstructure as a Function of Mo Content

It is always a challenge to measure the absolute content of a specific element in U-Mo fuel in microstructural characterization. WDS in SEM or Electron Probe Micro Analysis (EPMA) can provide a composition profile for a specific element with a spatial resolution approximately 1 μm in diameter if the sample surface is not disturbed from smearing. For irradiated fuel with a large volume fraction of bubbles at micron size, smearing is inevitable as a result of mechanically polishing the surface, and it can disturb the elemental distribution in the original irradiated microstructure. EDS in TEM has advantage of high spatial resolution and no smearing effect from the sample preparation. It is ideal to fully evaluate the Mo fluctuation and distribution in U-Mo fuel before and after a reactor test from the fuel plate fabricated from the same batch. To evaluate the Mo content in a nominal U-7wt%Mo fresh dispersion fuel particle, a FIB lamella was prepared from a KAERI-produced fuel particle contained in a fuel plate that was fabricated in the same manner as those tested in the SELENIUM experiment. The results of EDS measurements in STEM mode with a SDD in line scan are shown in Figure 4. EDS in spot mode is marked where the data from spot 5 through 10 were from the same location to check the statistics of the measurement. The Mo content on average is 7.2 ± 1.5 wt% and on the same spot of 5 - 10 is 6.8 ± 0.8 wt%. The Mo content at the grain boundary and grain interior are 4.0 ± 1.1 and 8.7 ± 1.1, respectively.

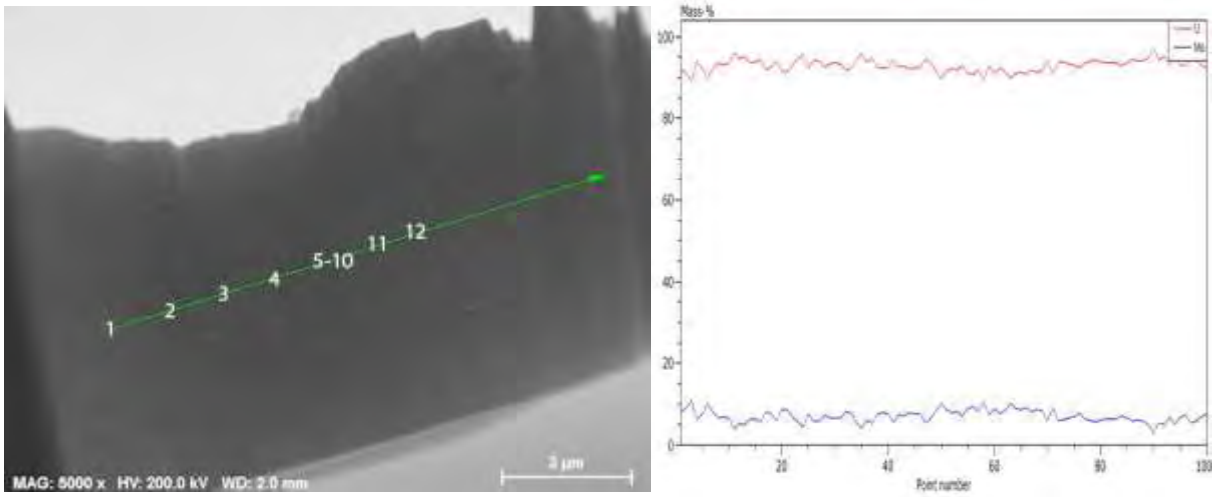

Figure 4. STEM image showing an EDS line scan (left) and the plot of the measured Mo and U content for a fresh U-7Mo fuel as a function of distance along the green line (right). The number indicates where an EDS measurement in spot mode was performed.

The locations of EDS measurements performed on the irradiated fuel plate R9R010 sample B are marked in Figure 5 where measurements 1 – 10 were taken from the clean areas with fine gas bubble superlattice (< 4 nm) and the measurements 11 – 20 were taken from the areas with large bubbles (> 100 nm). The average Mo content is 11.7 ± 0.7 wt% for the clean areas and 7.3 ± 2.4 for the bubble areas. The EDS measurement for sample A from the same fuel plate and irradiation condition shows an average Mo content of 9.8 ± 1.1 wt%. The relatively clean area has a slightly higher Mo content (10.8 wt%) than the area with many bubbles (9.2 wt%).

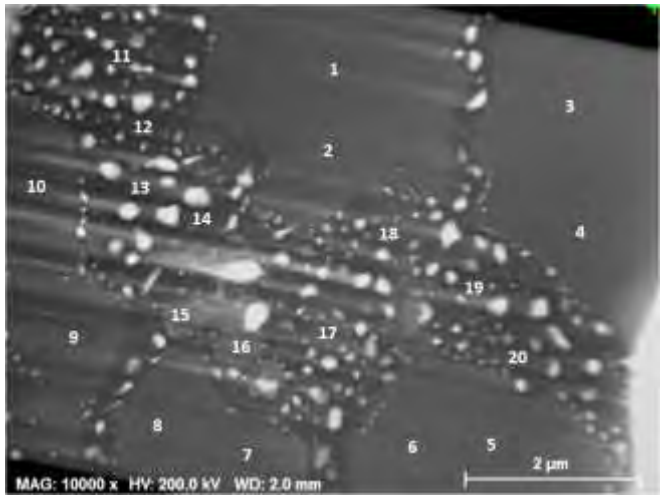

Figure 5. STEM image of U-7Mo fuel particle (R9R010: 3.7E+21 fission/cm^3) showing the positions of EDS measurements in spot mode. The average Mo content is 11.7 ± 0.7 wt.% for the clean areas (1-10) and 7.3 ± 2.4 wt.% for the areas with bubbles (11-20).

The EDS measurements for a fuel particle in an irradiated fuel plate (R2R040, U-7Mo/Al-2Si) at the high flux condition are shown in Figure 6, and the results are listed in Table 2. The measured average Mo content is 8.3 wt.%, lower than 9.6 wt.% calculated for U-7Mo at this fission density. Note that this set of EDS data was generated using a Si(Li) EDS detector in TEM mode before the EDS upgrade to a Brukers Silicon Drift Detector (SDD) took place in February 2012. Since then, the EDS measurements were performed in S-TEM mode with a SDD.

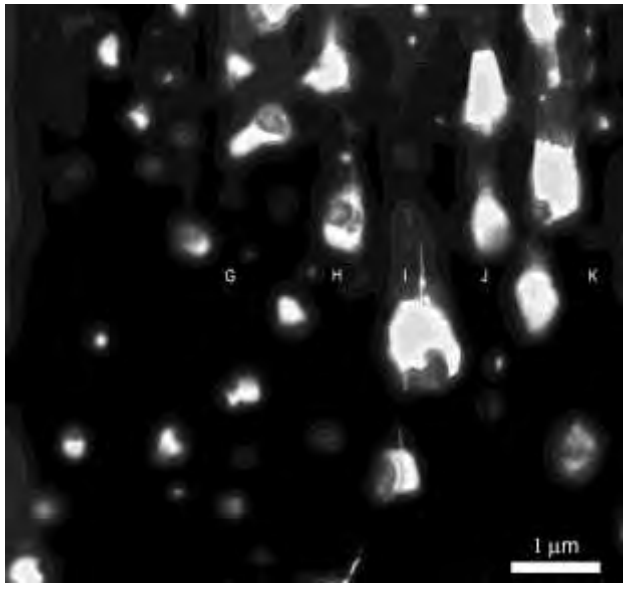

Figure 6. TEM image of Irradiated microstructure of fuel particle in R2R040 fuel plate at 6.3E+21 f/cm^3 fission density with areas labeled for EDS measurements.

Table 2: EDS measurement of the areas marked in Figure 6. (wt%) [Si(Li) detector in TEM]

Spot	U	Mo	Si	Al
G	92.3	7.6	0.2	0
H	91.0	8.7	0.1	0.1
I	90.0	9.1	0.3	0.5
J	91.7	8.1	0.2	0.1
K	91.9	8.0	0	0.1

The irradiated microstructure of the fuel particle for R0R010 (U-7Mo/Al) at the high fission density of 5.6E+21 f/cm^3 is shown in Figure 7 where labels are the spots for the EDS measurement listed in Table 3. The average Mo content for these 7 measurements is 8.8 ± 1.1 wt%. This is lower than 9.3 wt% calculated for U-7Mo at this fission density. Grain subdivision is evident, as shown in the picture. The attachment of the solid fission product precipitates to the large bubbles is clearly shown. A narrow amorphous layer consisting of solid fission product on the inner wall of the large bubbles can also be seen.

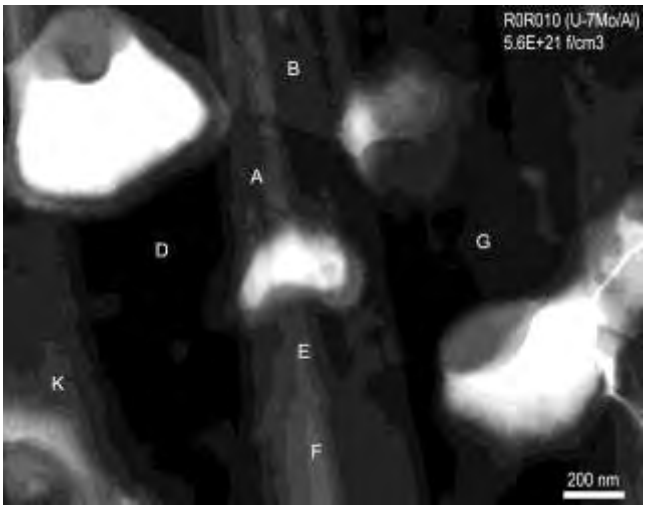

Figure 7. Irradiated microstructure of the fuel particle at a fission density of 5.6E+21 f/cm^3 with areas labeled for EDS measurement.

Table 3: EDS measurement of the locations marked in Figure 7. (wt%)

Spot	U	Mo
A	91.6	8.4
B	91.3	8.7
D	92.4	7.6
E	91.9	8.1
F	89.8	10.2
G	91.7	8.3
K	89.4	10.6

4. Discussion

4.1 Comparison of Grain Boundaries and Intergranular Regions

At a low fission density of less than 4.0E+21 fissions/cm^3, as shown in the site-B sample in Figure 2, the U-Mo fuel interior is dominated with fine gas bubble superlattice with large bubbles only seen at grain boundary regions. This preferential development of large bubbles at the grain boundary is well known as a result of high mobility of fission gas atoms. Since the high-angle grain boundary has a higher sink strength and a higer defect mobility than

does the low-angle grain boundary, defects are more easily trapped, including fission gas atoms. Therefore, the development of large bubbles at a grain boundary is anticipated to be dependent on the energy state of the grain boundary. As is clearly shown in the FIB-SEM image for site-B, the development of visible bubbles along the grain boundary under SEM imaging appears to be non-uniform. Note that the orientation of the STEM image is rotated nearly 100 degrees clockwise from the FIB-SEM image. The STEM image of the site-B sample shows noticeble differences in the developmeht of large bubbles at different grain boundaries. The narrow bubble region shown on the upper-right and lower-left likely originated from the low-angle boundaries, and the broad regions from the upper-left to the lower-right likely originated from high-angle grain boundaries, the preferential site for the development of large bubbles.

Another important factor influencing the nucleation and growth of large bubbles at a grain boundary is the Mo depletion at the grain boundary that has been reported in the fresh U-Mo fuel particles. It is believed that Mo depletion also depends on the type of grain boundary with high-angle boundaries having more significant Mo depletion. It is known that Mo depletion can reduce the γ-phase (bcc) stability for U-Mo and promote bubble devolopment in that region. It appears that the high-angle grain boundary is not only the preferential region for large bubble development, but is also a problematic region where large bubbles extend into the grains on both sides. It is like a percolation. The leading front of this expanding region is decorated with smaller bubbles in lenticular shape to begin with. The collapse of the gas bubble superlattice in the vicinity of this leading front provides a source term to feed those smaller bubbles and make them grow in size as the leading front proceeds into the grain interior.

To delay the early development of large bubbles at original grain boundaries in a UMo fuel particle, it is desired to reduce the number of high angle grain boundaries. This is called grain boundary structural engineering (GBSE) that has been proven effective in mitigating irradiation assisted stress corrosion cracking (IASCC) of stainless steels for nuclear reactor structural materials. However, it is not practical to apply thermal mechanical heat treatment to the U-Mo fuel particles to reduce the high-angle grain boundary. One option is to reduce the grain boundary surface area by grain growth at high temperature, but the risk is that this may result in the decomposition of the γ-phase (which is unlikely if substantially high heat treatment temperatures are used), although it is postulated that the decomposed phase would quickly return to the γ-phase under fission. Nevertheless, it is desired to have large-grain fuel particles in the fresh fuel to delay the development of large bubbles at grain boundaries.

At high fission density, however, in addition to the mechanism described above on the percolation of the large bubble regions from the original high-angle grain boundaries into the grain interior, the collapse of the gas bubble superlattice itself can also develop large bubbles in the grain interior through coalescence of fine bubbles [4]. As a result, these two processes produce an irradiated U-Mo microstructure with a relatively uniform distribution of the large bubbles throughout the entire U-Mo fuel particle. Although original large grains (5 – 10 μm) subdivide into numerous submicron grains under the stress from fission products in the solution, there is no evidence showing the preferential development of bubbles at these new subdivided grain boundaries largely because most of these subdivided grain boundaries are low angle grain boundaries and high concentration of the large bubbles provide effective sinks for the fission gas in the U-Mo. It is known that fine fission gas bubbles (< 4 nm) can maintain much higher pressure than the large bubbles. A transition from small to large bubbles, plus the linking of large bubbles, may eventutally lead to breakaway swelling in U-Mo fuel.

4.2 Changes in Microstructure as a Function of Mo Concentration

To facilitate the discussion on Mo content vs. U content as a function of fission density, the Mo content in wt% is calculated for U-Mo at four different initial Mo contents (5, 7, 10 and 12 wt.% Mo) assuming the sum of Mo and U atoms in a bcc U-Mo cell equals 100 wt%. Mo is a high yield solid fission product (~ 25% atomic yield per fission with two atoms generated). As a result of fissioning, the number of U-235 atoms in U-Mo decreases and the number of Mo atoms increases. The fission from Pu-239 as a transmutation of U-238 by capturing epithermal neutrons (10 – 20,000 eV) is not included for this simple calculation. The actual Mo wt% for a given fission density should be higher than the number listed in Table 4 if fission from Pu-239 is also included which also increases Mo and decreases U.

Table 4. Calculated Mo content (wt.%) vs fission density for low enrichment (19% U-235) U-Mo.

Fission Density (10^{21} f/cm^3)	U-5Mo (wt% Mo)	U-7Mo (wt% Mo)	U-10Mo (wt% Mo)	U-12Mo (wt% Mo)
3.0	6.0	8.2	11.5	13.6
4.0	6.4	8.6	12.0	14.2
5.0	6.7	9.1	12.5	14.7
6.0	7.1	9.5	13.0	15.3
7.0	7.5	10.0	13.6	16.0
F.D. at 100%BU	8.2E+21 f/cm^3	7.9E+21 f/cm^3	7.5E+21 f/cm^3	7.2E21 f/cm^3

The EDS measurements in STEM mode for a fresh SELENIUM fuel particle (that was produced using the KAERI atomization process) of nominal 7 wt.% Mo composition in Figure 4 gives a Mo content in general agreement with its nominal composition. Local fluctuation of Mo is evident as shown by the line scan. The grain boundary Mo depletion is quite significant with an average of 4.0 wt%. Note that this is a somewhat averaged value considering the STEM probe size is 25 nm. Higher average Mo content in grain interior (8.7 wt%) clearly shows the challenge to obtain a uniform Mo distribution when the grain size is small and the volume fraction of grain boundaries is high. The measurement in spot mode and line scan is in general agreement. The 6 measurements on a single spot (5 - 10) indicate the statistics of Mo measurement for a single spot (6.8 $\pm$ 0.8 wt%) is consistent with the standard deviation estimated by the EDS software (~ 10%). Since the line scan was terminated when there was no further change in the Mo profile, it is believed that the local Mo fluctuation shown in the EDS line scan is real from 2 to 11 wt% across a distance of ~ 10 μm. The large local fluctuation of Mo within a single fuel particle could be responisble for the heterogeneous irradiated microstructure at intermediate fission density.

The effect of Mo content and its fluctuation on the development of irradiated microstructure in U-Mo fuel is complicated. This is due to multiple reasons. One is the difficulty in EDS measurement with high confidence, particularly in the irradiated fuel where the presence of fission products results in x-ray peak overlap. A relative error of up to 10% on EDS composition measurement can be expected. If the spectrum collection time is short and the statistics are poor, the error could be even higher. Another reason is the potentially large fluctuation in Mo content on a local scale within a fuel particle and on a global scale from particle to particle in a single fuel plate. For the case where a U-7Mo alloy rod is used as a discharge eletrode in REP to produce fuel particles, the inhomogeneity of Mo distribution in the U-Mo rod can result in a global Mo fluctuation from particle to particle. The grain texture and size resulted from rapid quench during atomization can affect local Mo fluctuation as discussed previously. If a large number of FIB-TEM samples are analyzed for both fresh fuel and the irradiated fuel, the uncertainty on Mo wt% may be reduced.

The correlation between local Mo content and local irradiated microstructure is clearly demonstrated in Figure 5 and the corresponding EDS measurements. The initial Mo content

in the low Mo and high Mo areas could be less than 6 wt% and higher than 9 wt%, respectively, according to the calculated Mo contents in Table 4. The early development of large bubbles for the low Mo region at 3.7E+21 f/cm^3 clearly shows the problem with initial low Mo content. Although the overall Mo content over the spot 1 through 20 is 9.5 wt%, indicating a high initial average Mo content (> 7wt%) for the entire sample area, the large fluctuation in Mo distribution has a direct impact on the irradiated microstructure. In addition to the non-uniform Mo distribution from U-Mo alloy fabrication, part of this large Mo flucatuation is the result of Mo depletion at grain boundaries from atomization. This is confirmed in the EDS measurements for the U-7Mo fresh fuel particle contained in the SELENIUM as-fabricated fuel plate. Since a nonuniform Mo distribution is observed in both fresh fuel and the high fission density condition, it appears that the chemical driving force for Mo homogenization in U-Mo is weak, even under severe atomic displacement from energetic fission fragments.

The EDS data in Table 2 shows an average of 8.3 wt% Mo at a fission density of 6.3E+21 f/cm^2, which is lower than 9.6 wt% calculated following Table 4. It suggests that the initial Mo content in this region is probably ~ 6 wt%. This set of data was generated using an Si(Li) EDS detector in TEM mode. EDS data in Table 3 shows an average of 8.8 $\pm$ 1.1 wt% Mo at a fission density of 5.6E+21 f/cm^2, which is in general agreement with the 9.3 wt% Mo measured for a nominal U-7Mo fuel particle at this fission density following the same calculation. The large spread of the measured Mo content in the irradiated U-Mo fuel reflects the challenge in evaluating the effect of Mo content on the irradiated microstructure, particularly when the data on Mo distribution in the fresh fuel condition of the same fabrication batch is missing. Nevertheless, it is expected that U-Mo fuel particles with big grains, with low volume fraction of grain boundaries and with uniform Mo distribution, if achievable, may effectively delay the onset of the development of large bubbles.

5. Conclusions

The effects of grain boundaries and Mo distribution on irradiated microstructures in nominal U-7Mo fuel particles have been evaluated. The adverse effect of high angle grain boundaries on the early development of large bubbles is evident. The heterogeneous Mo distribution, the large fluctuation in local scale and the severe Mo depletion in grain boundary regions are all responsible for the early development of large bubbles in U-Mo fuel. The EDS measurements for a fresh SELENIUM U-7Mo fuel sample shows a large Mo fluctuation on a local scale from 2 to 11 wt% across a distance of ~ 10 microns.

Acknowledgments

This work was supported by the U.S. Department of Energy, Office of Nuclear Materials Threat Reduction (NA-212), National Nuclear Security Administration, under DOE-NE Idaho Operations Office Contract DE-AC07-05ID14517. Hot Fuel Examination Facility personnel are recognized for their contributions in destructively examining fuel plates. Sven Van den Berghe and Ann Leenaers from SCK CEN are recognized for providing the SELENIUM sample used to measure the starting fuel particle Mo content in an as-fabricated fuel plate.

References

[1] J.L. Snelgrove, et al., Nucl. Eng. Des. 178 (1977) 119.
[2] D. Wachs, et al., Proc. of GLOBAL 2007, Boise, Idaho, September 9-13, 2007.
[3] S. Van den Berghe, et al., J. Nucl. Mater., 442 (2013) 60-68.
[4] J. Gan, et al., J. Nucl. Mater., 454 (2014) 434-445.
[5] S. Van den Berghe and P. Lemoine, Nuc. Engr. and Tech. 46(2) (2014) 125-146.

OPTIMIZATION OF A THIN U-10MO FUEL PLATE CASTING BY MODELING AND EXPERIMENT

R. M. AIKIN JR. AND D. DOMBROWSKI
Materials Science and Technology: Metallurgy, Los Alamos National Laboratory
P.O. Box 1663, Los Alamos, NM 87544

ABSTRACT

LEU U-10%Mo fuel fabrication begins with a molten metal casting process which is feedstock for fuel foil fabrication by rolling. This work describes the experiments and modeling that have been performed to optimize the casting of long thin (28 cm x 20 cm x 0.5 cm) plates of U-10%Mo using vacuum induction melting (VIM). Three casting trials where used to evaluate a preliminary design and two revised designs. The mold and casting cavity were instrumented with a number of thermocouples to determine the thermal history of the mold and casting. The resulting cast plates were analyzed for filling and solidification defects using radiography. The goal was to develop a refined mold design and casting process parameters that maximized casting yield and minimized casting defects such as porosity and Mo segregation.

1. Introduction

The production of low enriched U-10wt%Mo fuel begins by the vacuum induction melting (VIM) and casting of a rolling billet. Production options include i) casting a thicker (~2 to 3 cm) billet and then hot rolling to an intermediate thickness (0.3 cm), or ii) casting intermediate thickness billets directly. The trade off is between additional processing (rolling) versus the difficulty of casting a thin part. The mold design, casting, and process optimization of a thicker billet has previously been reported [1]. This work examines the second option with the simultaneous casting of three thin 28 cm by 20 cm by 0.5 cm billets.

2. Initial Mold Design and Casting

2.1 Casting Procedure

The initial mold design and process parameters were supplied by Y-12 [2]. This design to simultaneously cast 3 thin billets is shown in Fig. 1. The mold stack is comprised of 7 parts: a bottom and top clamp, the 4 parts of the book mold body, and a crucible on top. The 4 parts of the book mold are held together by the top and bottom mold clamps. The clamps also serve as a heat source on top and a chill on the bottom. The mold forms 3 cavities that are 28.4 cm tall by 20.3 cm wide by 0.5 cm thick. A standard 35 cm OD by 30 cm ID by 14 cm tall bottom pour crucible is used. When cast at Y-12, this crucible would be used with a knockout/rupture disk, but because of furnace differences, a stopper rod with 1.52 cm diameter pour hole was used in this study.

The mold was machined from HLM grade graphite [3]. HLM is a medium-grain extruded graphite commonly used for molds and crucibles for the casting of uranium. To prevent chemical reaction between molten uranium and the graphite mold, those parts of the mold and crucible that come in contact with the molten uranium were coated with a yittrium-oxide mold coating [4]. The mold coating was applied with an automotive style paint sprayer and allowed to dry prior to mold assembly.

Stainless steel sheathed type-K thermocouples (chromel – alumel) were inserted into holes drilled in the graphite mold. Alumina sheathed type-C thermocouples (W-5%Re – W-26%Re) with a bare-bead tip were placed in the casting cavity and cemented in place. Locations of the thermocouples are shown in Fig. 1 along with the thermocouple number. The blue dots represent the location of the type-K thermocouples in the mold, while the red dots represent the location of the type-C thermocouples in the casting cavity.

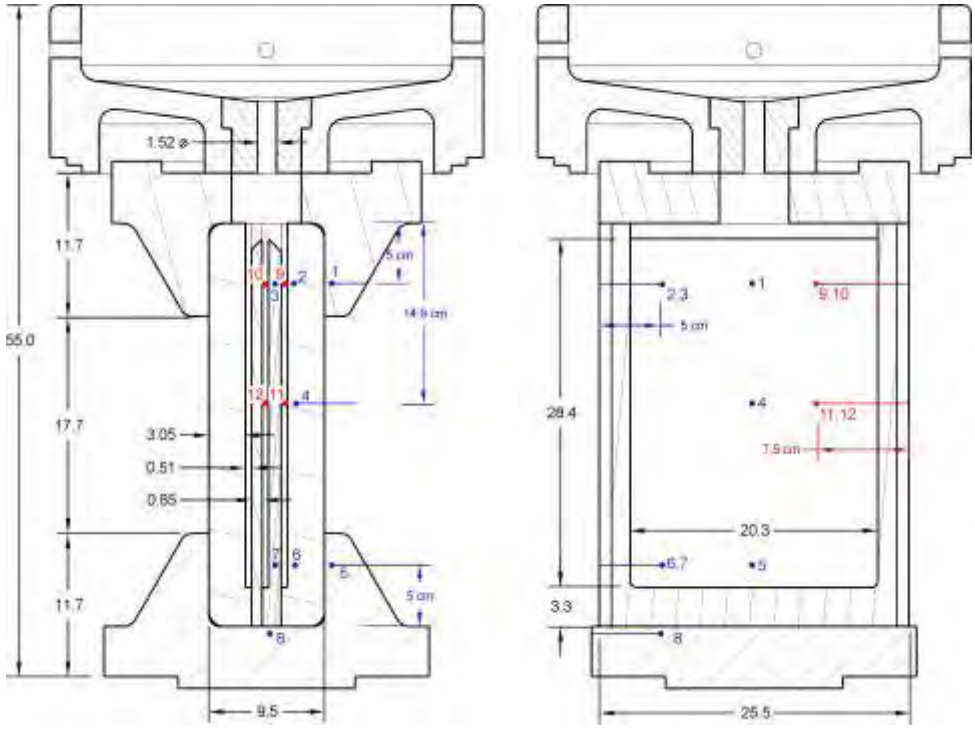

Fig. 1 Front and side views of the initial mold design. The location of thermocouples is shown with blue for thermocouples imbedded in the graphite and red for thermocouples in the casting cavity. Dimensions are in centimeters.

The crucible was charged with 17270 g of U-10Mo buttons produced by non-consumable arc-melting. The buttons were produced from high purity depleted uranium plate with approximately 65 ppm carbon and 99.95% pure molybdenum. The metal was arc-melted in a copper tundish with a tungsten electrode. Each button was melted and flipped 3 times prior to charging into the VIM crucible.

The mold stack was placed in a vacuum induction furnace. The furnace has a single induction coil 46 cm in diameter by 91 cm long. Between the mold stack and induction coil is a 4 cm thick layer of refractory insulation. The mold stack was placed with the bottom of the casting cavity at the same level as the bottom of the coil. The mold stack was supported by a 28 cm diameter graphite pedestal that was below the bottom of the coil. The coil was powered by a 100kW / 3kHz solid-state power supply. Furnace vacuum was supplied by a blower backed by a rotary-vane vacuum pump.

2.2 Casting with Initial Mold Design (1st Casting)

The initial casting followed the Y-12 recommended processing procedure. Induction power of 60 kW was applied until the metal melted and the molten metal temperature reached 1350°C. The molten metal temperature was determined by a two-color pyrometer looking in though the furnace lid and aimed on the metal surface near the stopper rod. Once the metal reached 1350°C (38 minutes), power was reduced and the metal was held at 1350°C for an additional 10 minutes. The stopper rod was removed and the molten metal was allowed to flow into the mold cavity.

The liquidus of U-10Mo is 1230°C [5-6], thus the 1350°C pouring temperature represents 120°C of superheat above the liquidus. Figure 2 shows the temperature in the mold, as a function of position, just prior to the removal of the stopper rod. The mold is quite cool at pouring time with 700°C at bottom and 1050°C at top.

Figure 3 shows the resulting cooling curves for the thermocouples in the mold and in the casting cavity. The liquidus and solidus temperatures are indicated by dotted lines. Filling time is estimated from these curves to be 15 seconds. The fact that the thermocouple traces in the casting cavity either do not reach, or barely reach the liquidus, indicates that the loss

of all of the super head and the beginning of solidification has occurred prior to the complete filling of the mold.

Comparison of thermocouples 9 and 10 and thermocouple 11 and 12 in Fig. 3(b) shows dissimilar cooling rates between the center and outer cast plates. This uneven cooling is due to the fact that the outer plates are in contact with a greater thickness (or volume) of graphite for heat to diffuse away from the casting/mold interface than the center plate. This thermal mass effect can be seen by the fact that the thermal spike is much greater in the thermocouples in the inner mold plates (TC 3 and 7) than those of the outer mold (TC 2 and 6).

The castings were joined by a very small common section connecting the three plates at the top. This connection caused the top of the plates to contract and clamp onto the inner mold sections. The inner graphite mold sections had to be broken to separate the mold and casting. The common section was then sawed off to separate the plates and allow for radiographic inspection.

The radiographic results of these 3 plates from are shown in Figure 4(a). The two dark horizontal lines in the center and right plates are the sheaths for the thermocouples imbedded in the casting cavity. The radiographs show numerous areas of "porosity" especially in lower half of castings indicated as dark bands. Also visible in Figure 4(a) is a region of non-filling on the right plate associated with a thermocouple sleeve (0.32 cm diameter sleeve vs. 0.5 cm thick cavity). This implies very marginal filling and emphasizes how cold the mold and filling conditions were.

Figure 5 shows the results of sectioning and metallographic examination of one of the dark banded region. Metallography performed on samples cut from these regions show the presence of microporsity (Fig. 5(b) and 5(c)) confirming that the dark radiographic bans are microporosity. It is likely that this microporosity was due solidification shrinkage.

3. Mold Redesign

3.1 Mold Design

As demonstrated in the initial casting, plates with a long thin nature are a challenge to cast without defects. For the purpose of this study the plate dimensions are is a design constraint that can’t be altered. So the goal is to develop a mold design and corresponding process parameters that minimize or eliminates the defects for this given geometry.

The defects are principally of two kinds:

1) Filling defects - areas were liquid metal become isolated by premature freezing of the metal or areas were molten metal flows against already frozen solid.
2) Solidification shrinkage defects - areas were porosity forms because of a lack of feed metal to accommodate the contraction that occurs during solidification.

To avoid filling defects the mold needs to be filled before significant solidification can occur. To help accomplish this filling goal the following modifications were made to the original mold design -

a) Increase the mold temperature so that the hot top section of the mold is near the solidus temperature.
b) The casting cavity was rotated from being 28 cm tall by 20 cm wide to 20 cm tall and 28 cm wide. This long horizontal dimension and short vertical dimension minimizes the filling length.
c) A distributor was added to provide simultaneous and equal volume filling of all 3 plates in a controlled manner.

The distributor has an added benefit of maintaining physical separation between plates for ease of breakout.

To minimize shrinkage porosity in an alloy casting the thermal gradient should be maximized to minimize the length of the dendrites and improve flow from the hot top to the dendrite roots [7].

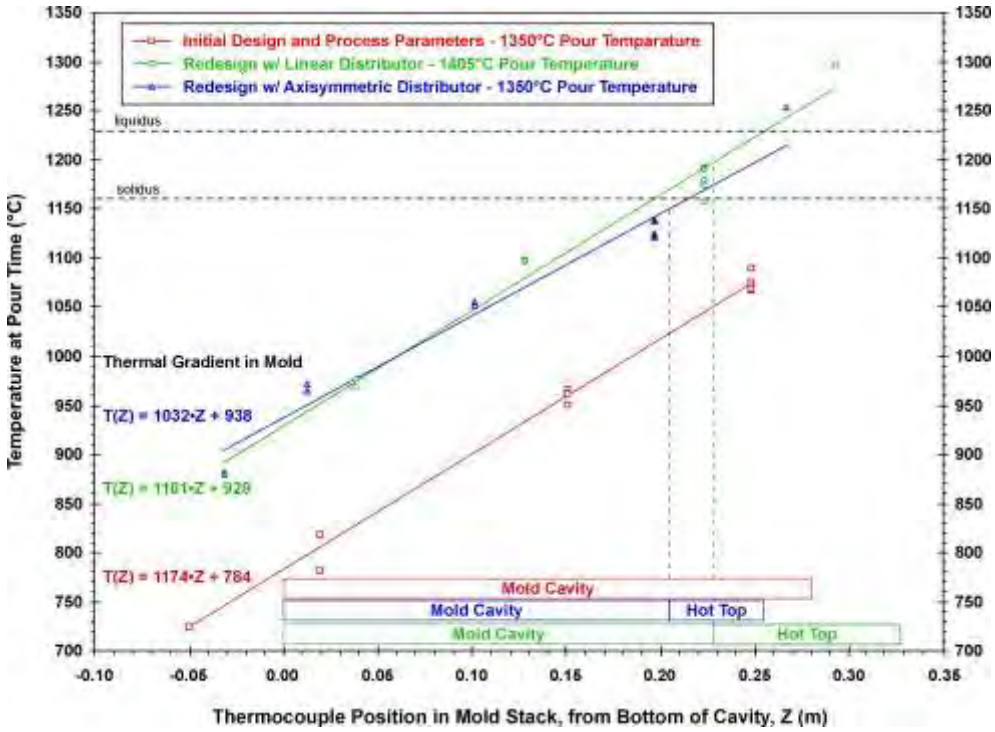

Fig. 2 Temperature as a function of position in the mold just prior to removal of the stopper rod showing initial thermal gradient in the mold for the 3 castings considered.

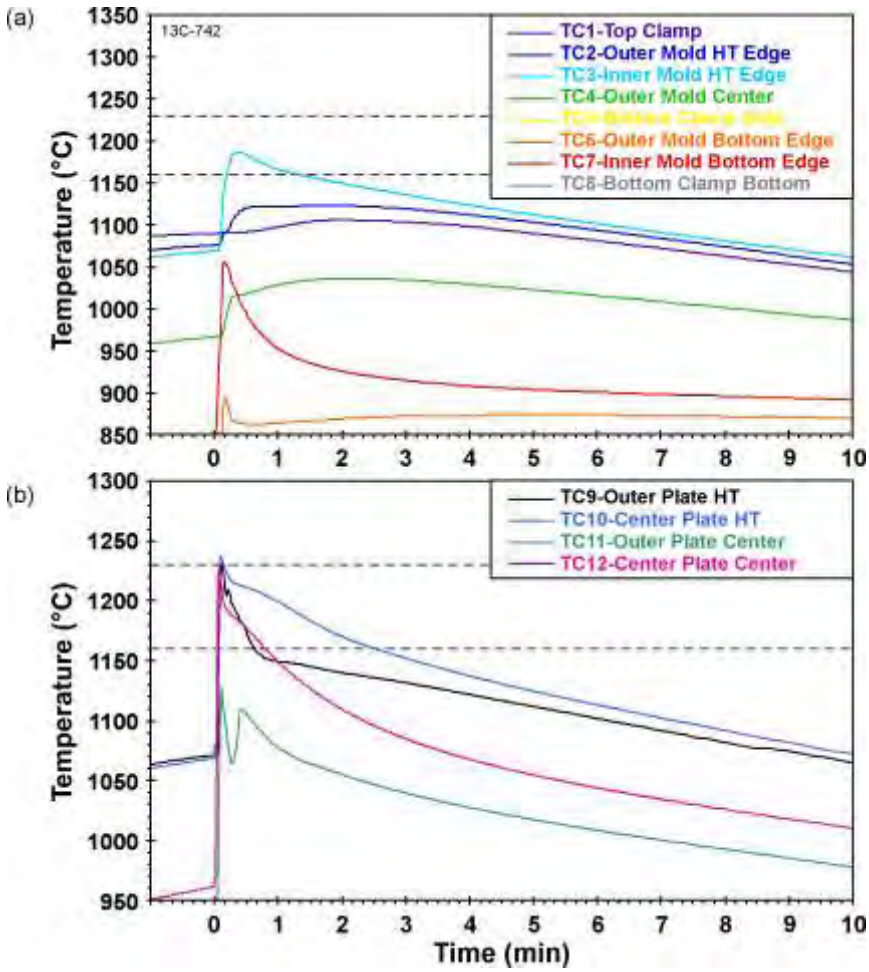

Fig. 3 Thermal history of initial mold poured at 1350°C; (a) thermocouples in mold and (b) thermocouples in casting cavity.

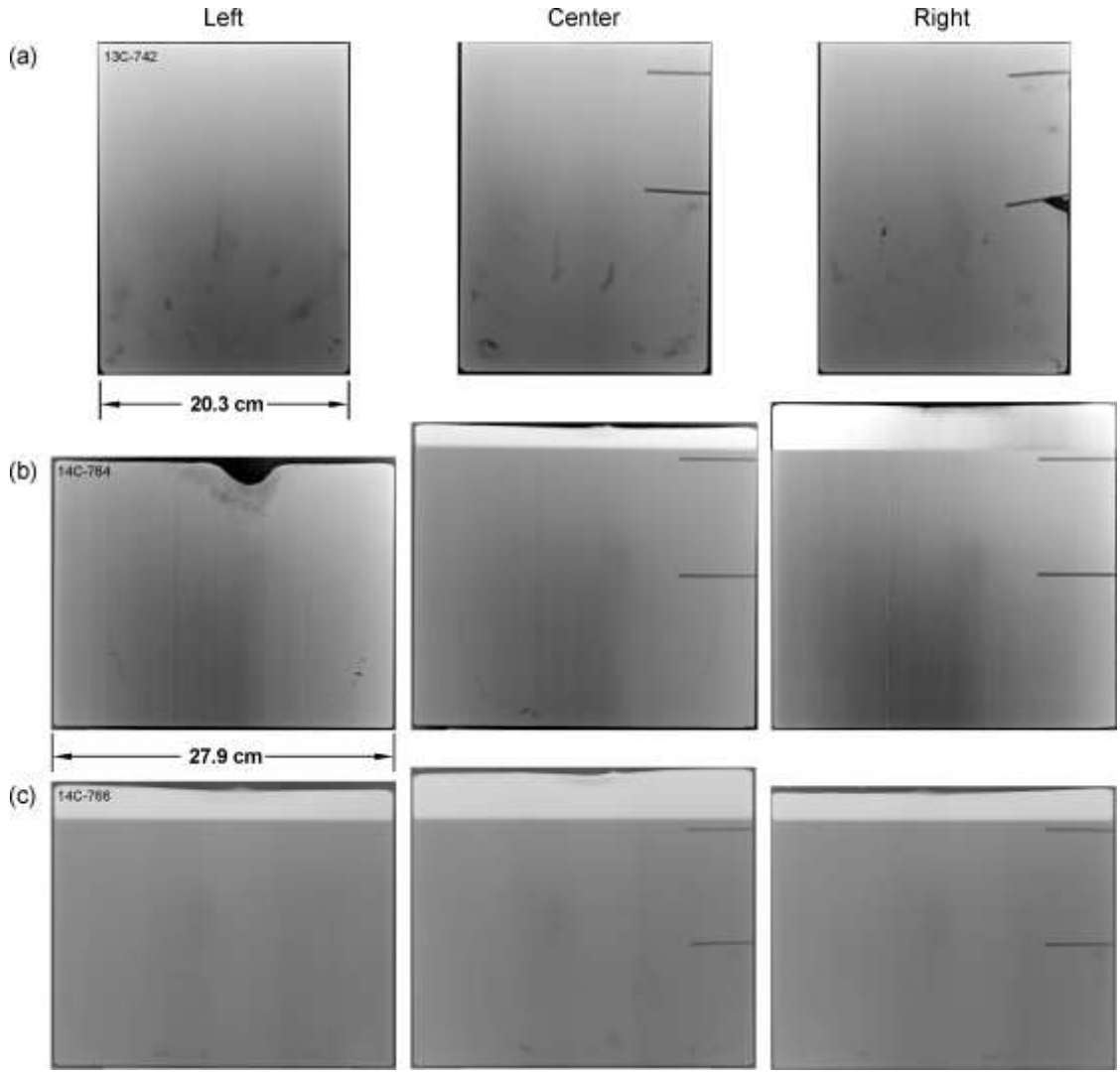

Fig. 4 Radiographic results of the three castings; (a) initial mold design, (b) redesigned mold with linear distributor, and (c) redesigned mold with axisymmetric distributor.

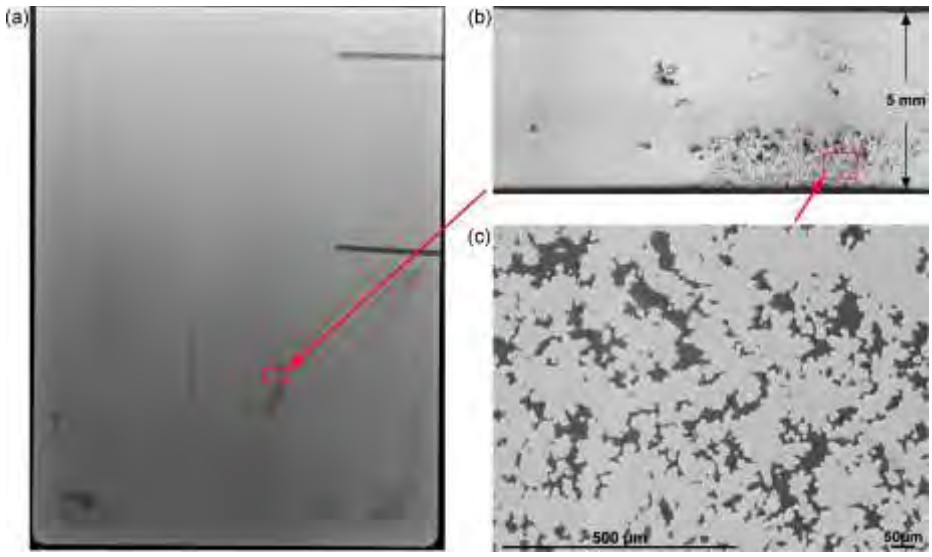

Fig. 5 Sectioning from the center plate of the 1st casting showing that radiographic indications are porosity; (a) radiograph image showing origin of metallographic section in red box, (b) through-thickness micrograph, and (c) higher magnification image of a near surface area showing shrinkage porosity.

In addition, there must be a hot top that:
- solidifies at the same time or later than the casting,
- contains sufficient liquid to compensate for the volume-contraction of the freezing metal,
- there must be a path from the hot top to allow feed metal to reach regions that need it.

Following these rules the following modifications where made to the original mold design -
d) Added a hot top with sufficient thermal mass and metal volume to feed solidification shrinkage.
e) Rotating the casting cavity was from being 28 cm tall by 20 cm wide to 20 cm tall and 28 cm wide also reduces the mold height, which can help increase the thermal gradient and decrease the molten metal feeding length from the hot top.

An additional goal is to try to ensure similar solidification time for the plates regardless of which casting cavities (center or edge) they originated from. To accomplish this, the mold thickness was "balanced" to make heat extraction rates of inner and outer plates similar by -
f) Make the outer mold wall thickness (casting to edge) to be one-half the thickness of the inner mold walls.

This revised mold design incorporating these changes is shown in Fig. 6.

3.2 Casting with Redesigned Mold with Linear Distributor (2nd Casting)

This second casting was cast quite similar to the first casting. As before, the mold was machined from HML graphite and coated with a yittrium-oxide mold coating. The type-K and type-C thermocouples were placed in the casting at locations indicated in Fig. 6. It was not discovered until casting was complete that the mold had been mistakenly machined with a 22.9 cm tall cavity, rather than the desired 20.3 cm tall cavity. This mistake was corrected in the 3rd casting and the as-built drawings are shown in Fig. 6.

The crucible was charged with 20900 g of U-10Mo buttons produced by non-consumable arc-melting. Induction power of 60 kW was applied until the metal melted and the molten metal temperature reached 1400°C. Once the metal reached 1400°C (51 minutes), power was reduced that the metal was held at 1400°C for an additional 10 minutes. The stopper rod was then removed and the molten metal allowed to flow into the mold cavity. The higher metal/crucible temperature was to try to further slow solidification and defects caused by solidification during filling.

Figure 2 shows the temperature in the mold as a function of position just prior to the removal of the stopper rod. Compared to the initial design and process parameters, the mold was significantly warmer with the hot top portion of the mold above the solidus temperature and the distributor above the liquidus temperature. This is advantageous because it minimized metal solidification and heat loss in the distributor and helped keep the metal in the hot top molten longer (while the rest of the casting solidifies).

Figure 7 shows the resulting cooling curves for the thermocouples in the mold and in the casting cavity. Thermocouple 11, in the center of the outer plate, did not return useful data. Overall, the warmer metal, mold, and mold redesign had the desired result of longer solidification times and filling was complete prior to significant solidification. Thermocouples 9 and 10 show similar solidification behavior for the center and edge plates demonstrating that balancing the mold thickness resulted in similar solidification times.

The resulting three plates had individual weights of 5153 g, 6485 g, and 7938 g for the left, center, and right plates respectively. This corresponded to no hot top, a 1.6 cm tall hot top, and a 2.5 cm tall hot top respectively. Clearly the distributor failed to deliver the same volume of metal to each of the 3 casting cavities. This is a flaw in the distributor design that needs to be corrected.

The failure of the distributor to fill the castings evenly had the unintentional consequence of providing a measure of casting soundness versus hot top size. Figure 4(b) shows the radiographs of the 3 plates. The right plate, with large (1.5" tall) hot top, appears sound with

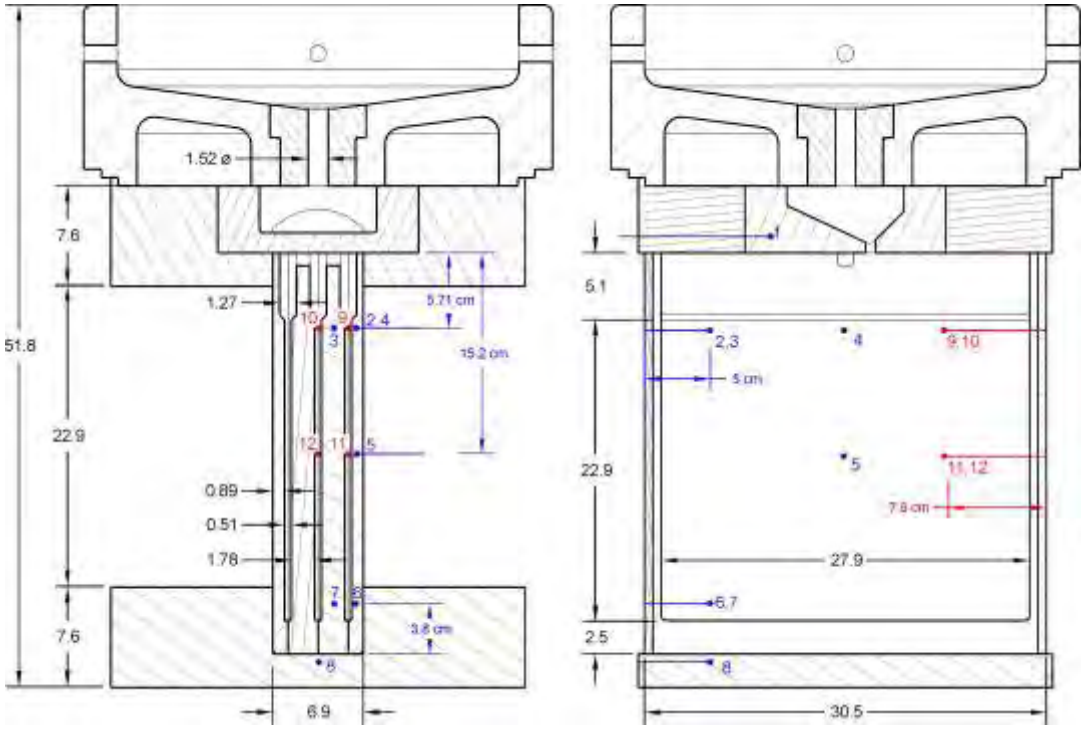

Fig. 6 Front and side views of the revised mold design with the linear distributor along with the location of thermocouples. Dimensions are in centimeters.

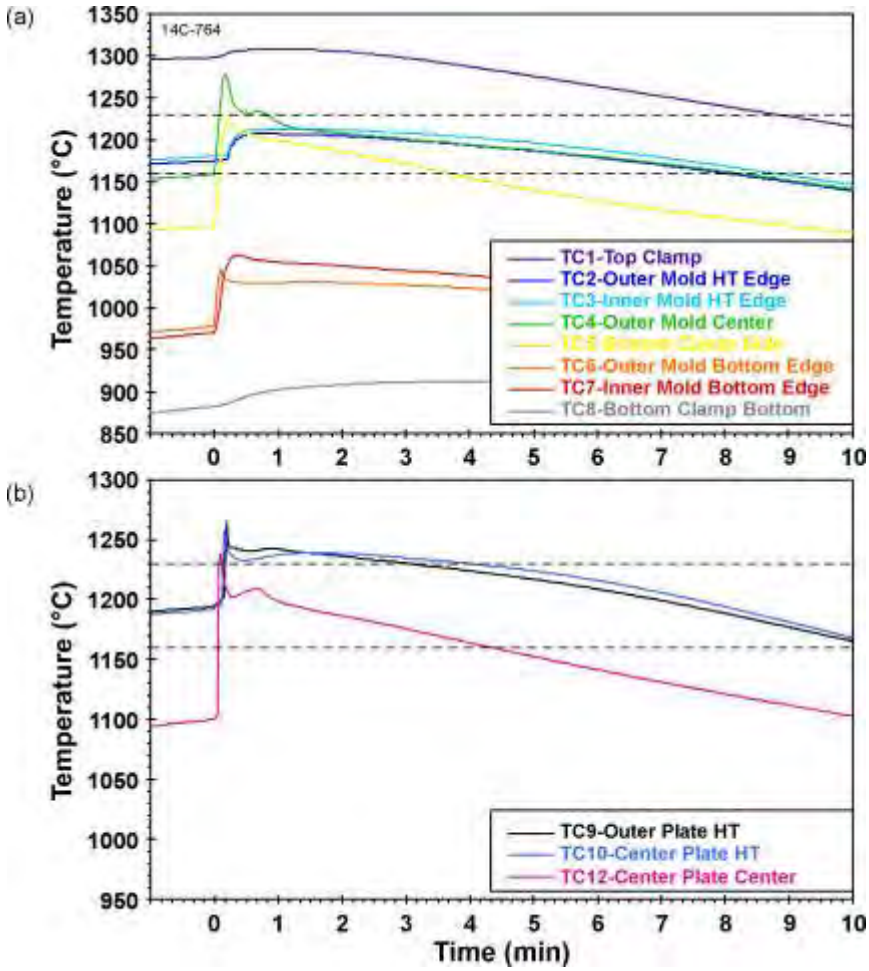

Fig. 7 Thermal history of revised mold design with the linear distributor poured at 1400°C; (a) thermocouples in mold and (b) thermocouples in casting cavity.

no defects in the plate. The center plate with medium (1.6 cm tall) hot top, and the left plate with no hot top both show a faint concave band of porosity in lower section of the casting. It is unclear if this is a filling or feeding defect. The left plate, with no hot top, has shrinkage porosity and surface shrink where top of plate subsided and fed the casting.

4. Distributor Redesign

The fact that the distributor did not evenly distribute the molten metal into the 3 cavities of the redesigned mold was unexpected and it was initially not evident why filling was unequal. To understand this unexpected filling behavior, the mold filling was simulated using the commercial computational fluid dynamics code Flow-3D [8]. FLOW-3D solves relevant time-dependent heat and fluid flow free-surface problems in three dimensions. The experimentally determined temperature of the mold at pour time was used as the initial conditions and the experimentally determined cooling curves were used to validate the code and parameters used. Only a portion of the results are presented here.

4.1 Simulation of the Linear Distributor

The details of the linear distributor used in the 2nd casting (and Fig. 6) is shown in Figure 8(a). The three holes are linear with a spacing equal to the 2.26 cm center-to-center spacing of the individual plates. The 0.76 cm diameter discharge hole was sized such that a hole of this diameter has 1/4 the cross-sectional area of the crucible's 1.52 cm diameter discharge hole. This hole is smaller than the 1/3 size that would give equal crucible to distributor sizes so that the metal backs up a bit in the distributor resulting in choked flow.

In Figure 8(b) horizontal and vertical sections though the distributor are shown at 10 seconds into the 15 second pour. The molten metal is colored by velocity magnitude (in m/s). Metal has backed up in the crucible but as shown in the horizontal section, the 3 discharge holes are not choked. The vertical section shows a stream of high velocity flow from the input stream cutting across the bottom of the distributor (below the backed up liquid). This flow causes the flow out of the 3 discharge holes to detach on the one side and results in uneven flow out of the 3 holes. The result, as shown in Fig. 8(c), is that the center plate fills to a greater extent than the two side plates. This is consistent with the observed behavior of the 2nd casting.

4.2 Simulation of an Improved Distributor Design

To avoid the unequal flow observed in the linear distributor design, 12 different distributor redesigns were considered. The redesign concepts were used to simulate the filling process. The goal was to produce even filling. For the most part the focus was on eliminating the strong flow that prevented choking of the discharge holes in the linear design of Fig. 8.

Of the dozen concepts considered the design shown in Figure 9(a) was chosen. In Figure 9(b) horizontal and vertical sections though the distributor are shown at 10 seconds into the 15 second pour. Again, the molten metal is colored by velocity magnitude (in m/s). Metal has backed up in the distributor and, as shown in the horizontal section, the 3 discharge holes are choked. The vertical section shows the there is no longer a strong sheer flow across the bottom toward the discharge holes. The result, as shown in Fig. 9(c), is that the 3 plates fill evenly in the simulation.

4.3 Casting with Redesigned Mold and Axisymmetric Distributor (3rd Casting)

This third casting was cast quite similar to the second casting. The differences were in the distributor and the height of the mold cavity. As before, the mold was machined from HML grade graphite and coated with a yittrium-oxide mold coating. The type-K and type-C thermocouples were placed in the casting at locations indicated in Fig. 10.

The crucible was charged with 21280 k of U-10Mo buttons produced by non-consumable arc-melting. In an effort to slightly reduce the solidification time of the plates, the pouring temperature of the metal was reduced from 1400 to 1350°C. Induction power of 60 kW was applied until the metal melted and the molten metal temperature reached 1350°C. Once the

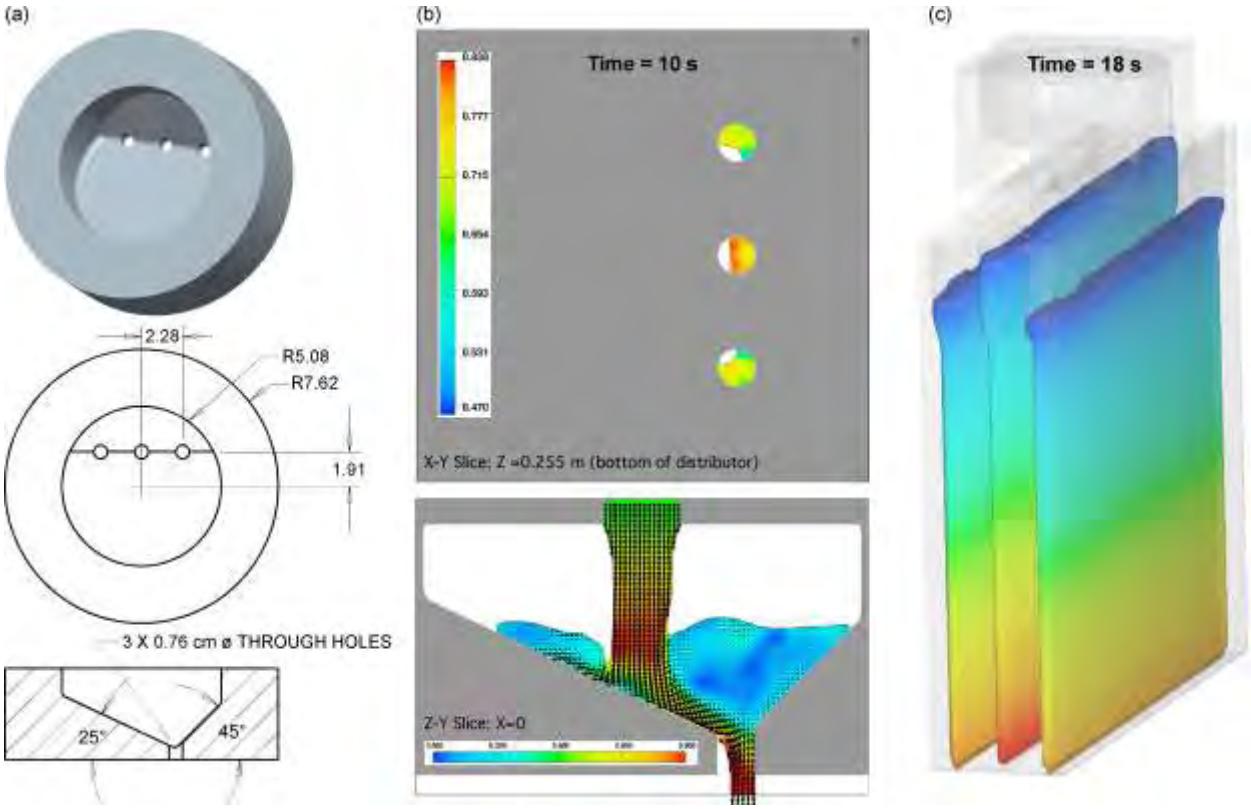

Fig. 8 Mold filling simulation of revised mold design with the linear distributor; (a) distributor geometry, (b) sections though the distributor during filling (metal colored by velocity magnitude), and (c) final unequal metal distribution in the three casting cavities.

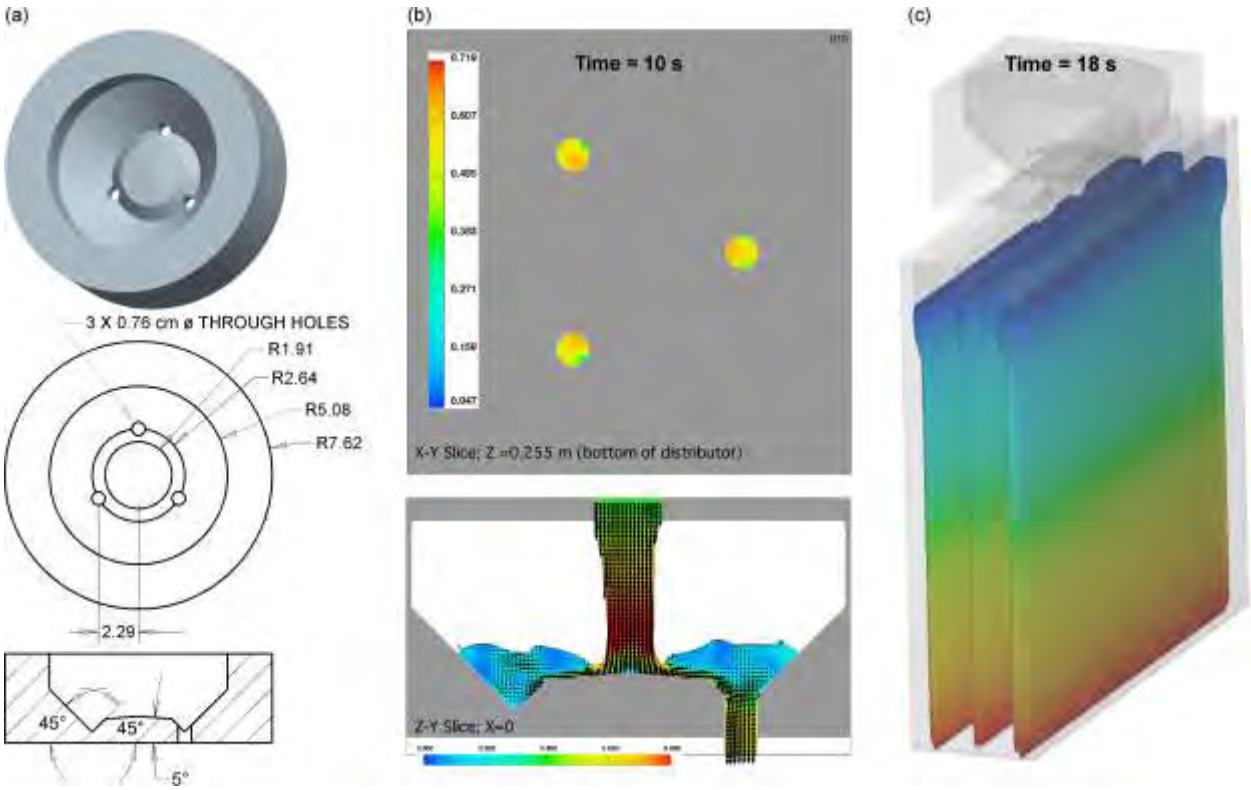

Fig. 9 Mold filling simulation of revised mold design with the axisymmetric distributor; (a) distributor geometry, (b) sections though the distributor during filling (metal colored by velocity magnitude), and (c) final nearly equal metal distribution in the three casting cavities.

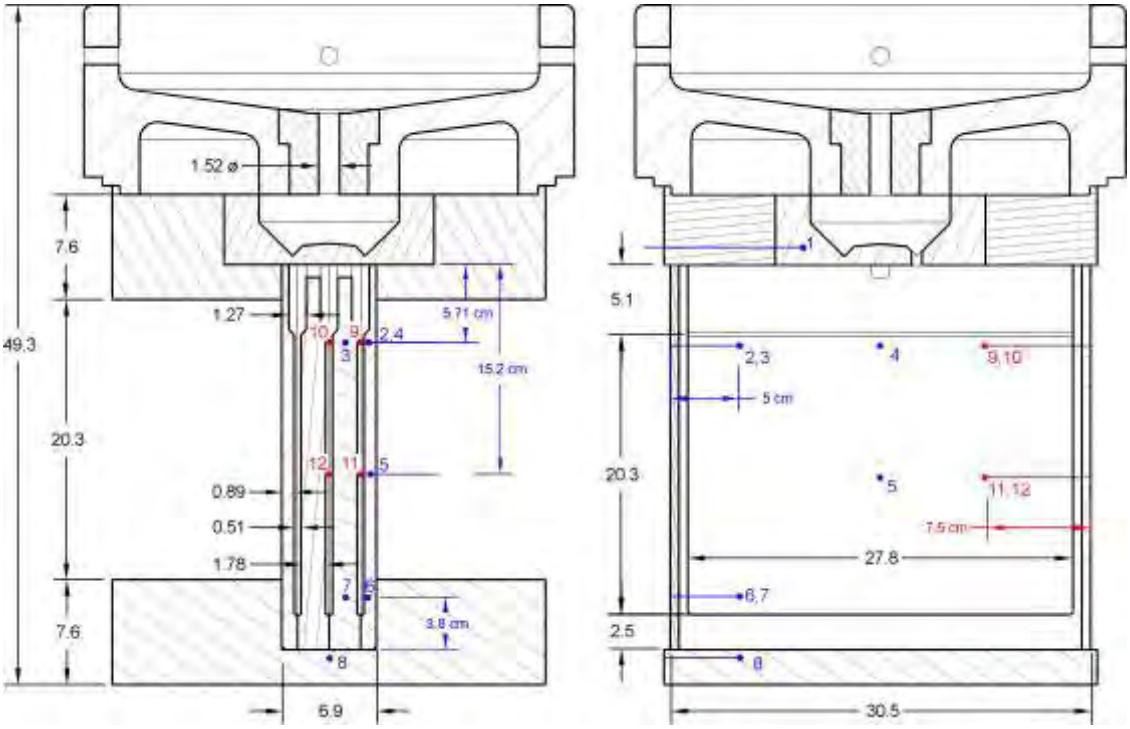

Fig. 10 Front and side views of revised mold design with the axisymmetric distributor along with the location of thermocouples. Dimensions are in centimeters.

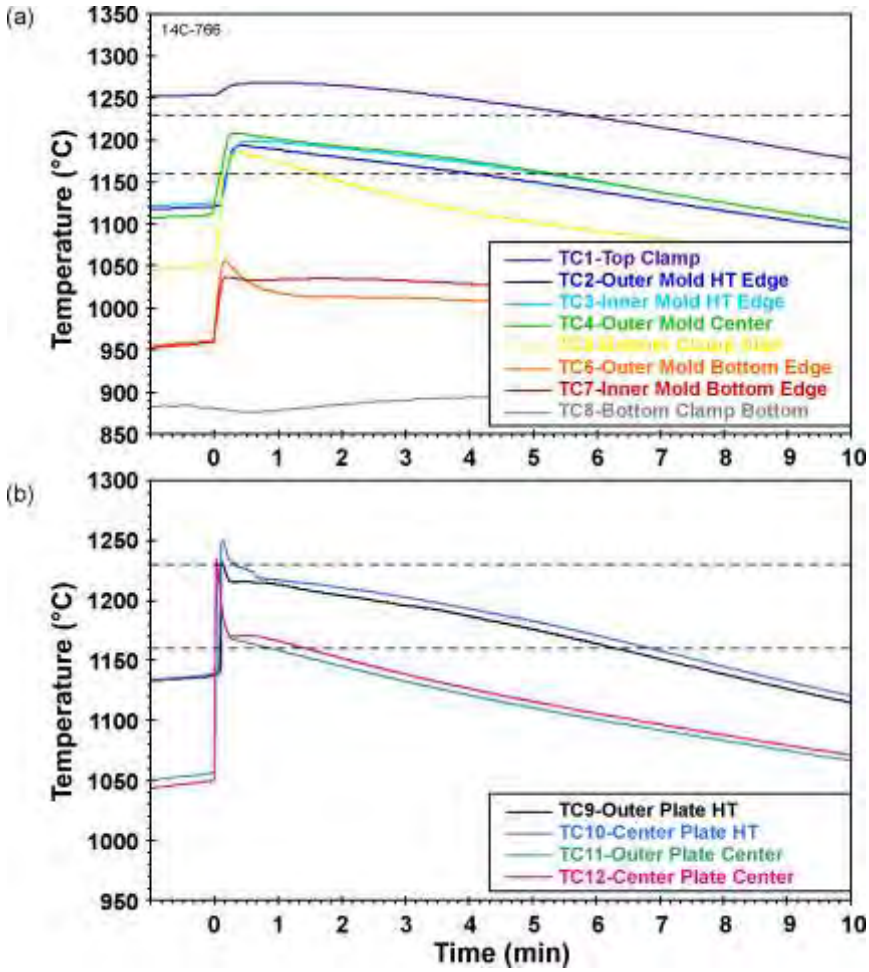

Fig. 11 Thermal history of revised mold design with the axisymmetric distributor poured at 1350°C; (a) thermocouples in mold and (b) thermocouples in casting cavity.

metal reached 1350°C (45 minutes), power was reduced that the metal was held at 1350°C for an additional 10 minutes. The stopper rod was then removed and the molten metal allowed to flow into the mold cavity.

Figure 2 shows the temperature in the mold as a function of position just prior to the removal of the stopper rod. The mold temperature is quite similar to the 2nd casting. Again hot top portion of the mold was above the solidus temperature and the distributor above the liquidus temperature.

Figure 11 shows the resulting cooling curves for the thermocouples in the mold and in the casting cavity. The solidification times are longer than the initial casting and shorter than the 2nd casting. Thermocouples 9 and 10 (and TC 11 and 12) show similar solidification behavior for the center and edge plates demonstrating that balancing the mold thickness resulted solidification times.

The resulting three plates had individual weights of 6637 g, 7179 g, and 6338 g for the left, center, and right plates respectively. The corresponding hot top heights were 2.5 cm, 3.8 cm and 2.5 cm. Although the weights were not exactly the same, this axisymmetric distributor was a significant improvement over the linear design used in the 2nd casting.

Figure 4(c) shows the radiographs of the 3 plates for the 3rd casting. Although there are a few faint concave bands of porosity in lower section of the casting, the defect content this set of 3 plates look the best of the 3 casting trials. The presence of the faint lower section defects in these castings means they are not quite as good as the best of the 2nd casting plates (the right plate with the largest hot top). It is believed that the decrease of the casting temperature from 1400 to 1350°C was a bit too much and a pouring temperature of 1400°C would be preferable for future castings.

5. Conclusions

The long (20 cm) and thin (0.5 cm) nature of the geometry of this casting makes it very difficult to cast without casting defects. Mold design and casting parameters were developed to minimize casting defects in the triple plate geometry. Care must be taken to make sure that the mold temperature is quite warm to ensure that filling can occur without significant solidification and the corresponding casting defects. Because of the very high rate of solidification, segregation of Mo during solidification is not believed to be a major concern.

Acknowledgement

The authors would like to acknowledge the financial support of the US Department of Energy Global Threat Reduction Initiative Reactor Convert program. Los Alamos National Laboratory, an affirmative action equal opportunity employer, is operated by Los Alamos National Security, LLC, for the National Nuclear Security Administration of the U.S. Department of Energy under contract DE-AC52-06NA25396.

7. References

[1] R.M. Aikin Jr. and D. Dombrowski, “Process Optimization of U-10Mo Casting by Modeling and Experiment”, European Research Reactor Conference 2014, RRFM2014-A0128 (2014).

[2] Baseline mold design and process parameters private communication H.A. Longmire, Y-12 Nat. Secruity Complex, Oak Ridge, TN, USA.

[3] HML grade graphite by SGL Carbon, LLC., St. Marys, PA USA.

[4] Type YK nonaqueous-based yttrium oxide paint by ZYP Coatings, Oak Ridge, TN USA.

[5] P.C.L. Pfeil, J. Inst. Metals, v 77, pp. 553-570 (1950).

[6] S.P. Garg and R.J. Ackermann, J Nucl. Mater., v. 64, pp. 265-274 (1977).

[7] John Campbell, Complete Casting Handbook, Butterworth, Oxford UK (2011).

[8] Flow-3D by Flow Science Inc., Santa Fe, NM USA.

IMPROVEMENTS OF U-Mo/Al DISPERSION FUEL PERFORMANCE

YEON SOO KIM [1], G.Y. JEONG [2], J.M. PARK [3]

1: Argonne National Laboratory, 9700 S. Cass Ave, Argonne, IL 60439 – USA

2: UNIST, 50 UNIST-gil, Eonyang-eup, Ulju-gun, Ulsan 689-798 – Republic of Korea

3: KAERI, 989-111 Daedeok-daero, Yuseong-gu, Daejeon 305-353 – Republic of Korea

ABSTRACT

Performance improvement parameters for U-Mo/Al dispersion fuel have been quantitatively studied. The effects of the particle size, Mo content, and high-temperature heating of U-Mo particles on the performance of U-Mo/Al dispersion fuel were studied. The effect of U-Mo particle size on the performance of the U-Mo/Al fuel was examined using KAERI's KOMO-4 test results. The effect of the Mo content in the U-Mo particles on fuel swelling was also analyzed using PIE data. The effect of using large grains in U-Mo, i.e., the effect of an intentional heating of the U-Mo particles, on U-Mo/Al fuel swelling was assessed. By using a model developed for dispersion fuel meat swelling, the benefit of each performance improvement parameter was estimated.

1. INTRODUCTION

In order to improve U-Mo/Al dispersion fuel performance, increases in U-Mo particle size, Mo content in U-Mo alloy, and grain size in U-Mo have been shown to be important by the RERTR tests and KAERI's KOMO tests [1]. Quantitative analyses were performed to assess the effectiveness of each improvement parameter. Specifically, in this study, the benefit of each proposed parameter was evaluated in terms of U-Mo/Al meat swelling.

By using a recently developed model [2], the advantage in meat swelling achieved for each parameter change was quantified. Specifically, the meat swelling for a plate with and without the proposed performance improvement parameter was calculated and compared.

2. U-Mo PARTICLE SIZE INCREASE

KAERI has systematically tested the effect of U-Mo particle size on the performance of U-Mo/Al dispersion fuel in the KOMO-3, -4 and -5 tests [3]. The use of larger U-Mo particles was proved to be beneficial owing to the reduced IL volume between U-Mo and Al even at the same IL thickness. For the larger U-Mo particle case, the U-Mo particle-to-volume ratio in the dispersion fuel meat was reduced.

In the KOMO-4 irradiation test, fuel test rods with different fuel particle size were tested. The test data are given in **Table 1**. The test rods were loaded with U-Mo particles larger than the typical size of ~70 μm used in the RERTR tests. The test rod 557-LD3 had larger-sized U-Mo particles than did the 557-SD3. The optical microscopy images shown in **Fig. 1** indicate the IL thickness was slightly larger in 557-SD3. The reason for the increased IL growth kinetics may be due to reduced thermal conductivity of the fuel meat stemming from the increased IL volume. It is worth noting that the meat swelling of 557-SD3 was larger, despite the similar power and burnup. A comparison of the measured volume fractions between 557-SD3 and 557-LD3 indicates that the IL volume increased more in 557-SD3. The fuel volume fractions for both

samples were slightly reduced from the as-fabricated value although fission induced swelling was substantial, which means the U-Mo consumption by IL growth was even larger.

One important aspect of using larger fuel particles is that even at the same IL thickness, the smaller fuel particle case gives the larger IL volume [4] and, hence, the larger meat swelling.

Table 1 KOMO-4 in-pile test data for samples with different U-Mo particle sizes

Specimen ID		557-LD3	557-SD3
U-Mo size (μm)		300 - 425	105 - 210
Fuel (wt%)		U-7Mo	U-7Mo
Matrix		Al	Al
U-loading (gU/cm^3)		4.5	4.5
Burnup (%)		53	54
Fuel volume fraction (%)		28	28
LHR (kW/m)		87	87
T_{BOL} (^oC)		168	169

Volume fraction (%)	As fabricated	PIE 557-LD3	PIE 557-SD3
U-Mo	27	26	23
Al	73	55	50
IL	0	19	27

Measured meat swelling (%)		4	7

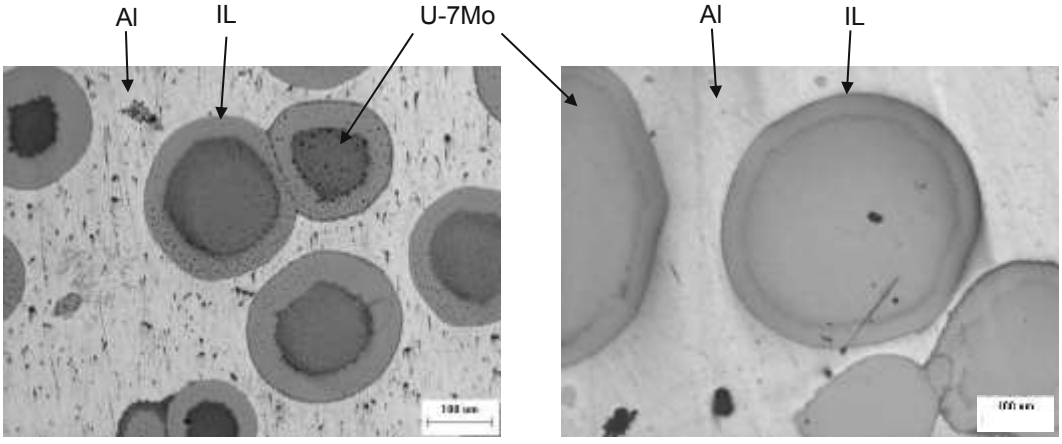

557-SD3 557-LD3

Fig. 1 Optical micrographs of cross sections of post-irradiation KOMO-4 test rods with different U-Mo particle sizes taken at the meat center regions.

The benefit of using the large fuel particles was quantitatively estimated by comparing the meat swelling of V8006B from the RERTR-4 test having U-Mo size of 70 μm with a hypothetical case that has the fuel particle size of 120 μm. The same IL thickness was used for both cases.

The results given in **Table 2**, however, show an insignificant benefit of using increased U-Mo size. This outcome contradicts with the KOMO test results. The possible reason was attributed to the high fuel loading in the RERTR case. The benefit of using larger U-Mo particles is

obtained by reducing the IL volume fraction in the meat. However, when fuel loading becomes high such as 8 gU/cm^3, the fuel volume itself becomes dominant and the influence of IL diminishes.

Table 2 Comparison of meat swelling of V8006B [4] with a hypothetical case with U-Mo particle size of 120 μm at the same irradiation condition

	V8006B	Hypothetical case
U-Mo size (μm)	70	120
Mo content in U-Mo (wt.%)	10	10
U-loading (gU/cm^3)	8	8
Fission density (10^{21} f/cm^3)	5.4	5.4
Measured meat swelling (%)	19	-
Predicted meat swelling (%)	20	20

The above comparison was made on the same IL growth condition, i.e., the same thermal conductivity. However, because the U-Mo/Al fuel meat with larger U-Mo particles will result in higher thermal conductivity, a lower IL growth is expected. Another more important benefit of using larger U-Mo size is perhaps to reduce fission gas release from the fuel particles to the matrix, whereby decreases pore-formation in the matrix. If these factors are considered, the use of larger U-Mo is still deemed beneficial. The drawback of using large U-Mo dispersants is to decrease the homogeneity of U-Mo particle distribution in the meat. Therefore, an optimization is needed to best take advantage of this effect.

3. MO CONTENT INCREASE IN U-Mo

As for the fuel swelling of U-7Mo, only a batch of data from the RERTR-6 test was available. The measured data are plotted in **Fig. 2**. Also included are the predictions for fuel swelling of U-10Mo by the model that was documented previously [5]. The measured swelling data for U-7Mo appear to be on average about 22% higher than that of U-10Mo. Since fuel swelling by solid fission products should be similar for both alloys [5], the augmentation is probably due to fission gas bubble (FGB) swelling.

FGB swelling is closely dependent on the grain subdivision (also known as recrystallization) kinetics as FGB grows on grain boundaries. As grain subdivision progresses, grain boundaries additionally become available to facilitate FGB to grow [7]. Hence fuel swelling is enhanced.

Fig. 3 shows grain subdivision kinetics as a function of fission density (FD). Fuel grain subdivision increases with FD. The alloy with a lower Mo content tends to have a higher kinetics and earlier start maybe due to enhanced diffusion in the reduced Mo content in the grain boundaries.

The data fit gives a correlation as a function of FD as follows:

$$\left(\frac{\Delta V}{V_0}\right)_f = 5.0\, f_d, \quad \text{for } f_d \le 2.0\times 10^{21} \text{ fissions / cm}^3 \tag{1}$$

$$\left(\frac{\Delta V}{V_0}\right)_f = 10 + 6.7\left(f_d - 2.0\right) + 0.58\left(f_d - 2.0\right)^2, \quad \text{for } 2.0\times 10^{21} < f_d \text{ fissions / cm}^3 \tag{2}$$

where fuel swelling is in percent and f_d is in 10^{21} f/cm^3.

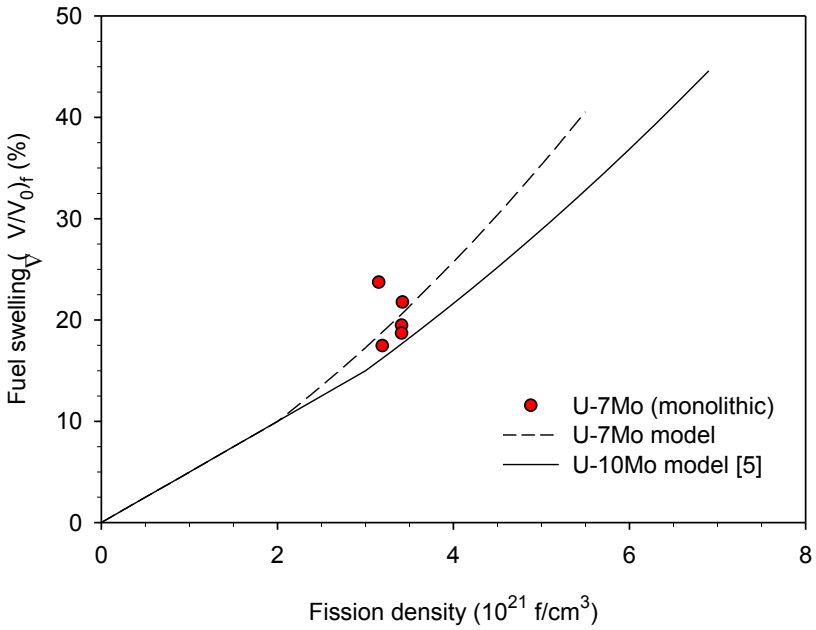

Fig. 2 U-Mo fuel swelling vs fission density showing the effect of the Mo content.

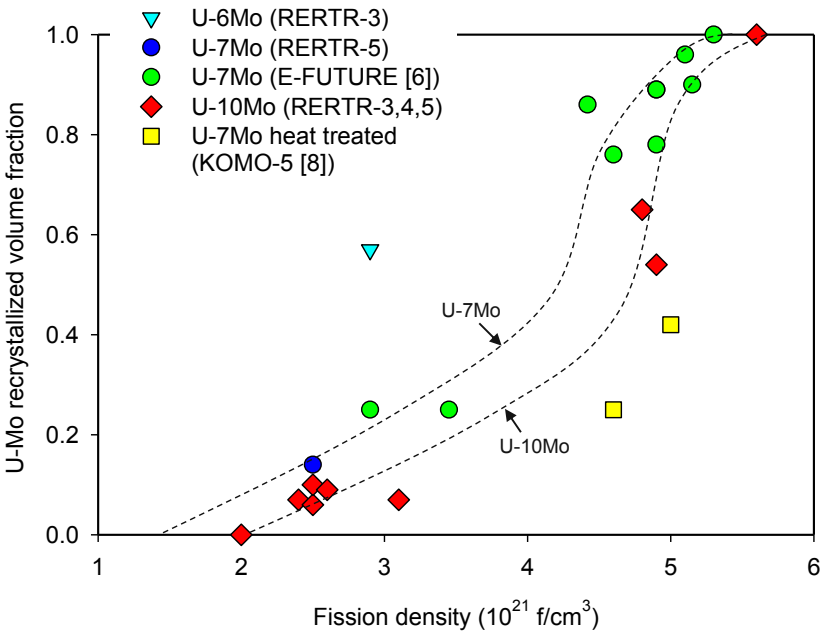

Fig. 3 Mo content effect on grain subdivision kinetics. The guiding lines for U-7Mo and U-10Mo are also shown.

The benefit of increasing the Mo content from 7wt% to 10wt% was estimated in terms of fuel meat swelling. R2R088 from the RERTR-9B test was taken as an example. A hypothetical case with the same fabrication parameters and irradiation condition as R2R088, except for 10 wt% Mo, was also assumed. The meat swelling of the hypothetical case with U-10Mo given in **Table**

3 is much lower than U-7Mo, which is a clear benefit of using the higher Mo content. It is also suspected that the use of U-10Mo is beneficial in terms of IL growth compared to U-7Mo [4].

Table 3 Comparison of meat swelling of R2R088 (U-7Mo/Al-2Si) [4] with a hypothetical case with U-10Mo/Al-2Si at the same irradiation condition

	R2R088	Hypothetical case
Mo content (wt.%)	7	10
U-Mo size (μm)	50	50
U-loading (gU/cm^3)	8.5	8.5
Fission density (10^{21} f/cm^3)	5.6	5.6
Fuel volume fraction (%)	52	52
Measured meat swelling (%)	25.6	-
Predicted meat swelling (%)	26.4	22.5

The disadvantage of increasing the Mo content is the reduction in U-loading in the meat. The increased Mo content from 7wt% Mo to 10wt% Mo decreases the U-loading in the meat by about 0.5 gU/cm^3-meat.

4. GRAIN SIZE INCREASE IN U-Mo

The kinetics of the formation and growth of FGB depends on the number density of grain boundaries [8]. The FGB are larger than the nanosize intragranular bubbles [9][10] by about two orders of magnitude, so the effect on fuel swelling is more prominent.

The image in **Fig. 4**(a) shows the cross section of an atomized U-7Mo sphere, in which the grain boundaries are shown brighter. The image in **Fig. 4**(b) is a cross section of U-nitride coated U-7Mo spheres that were heated at 1000 °C for an hour. The grain growth was substantial: the as-atomized grain size of about 2 – 5 μm has grown to 10 – 20 μm.

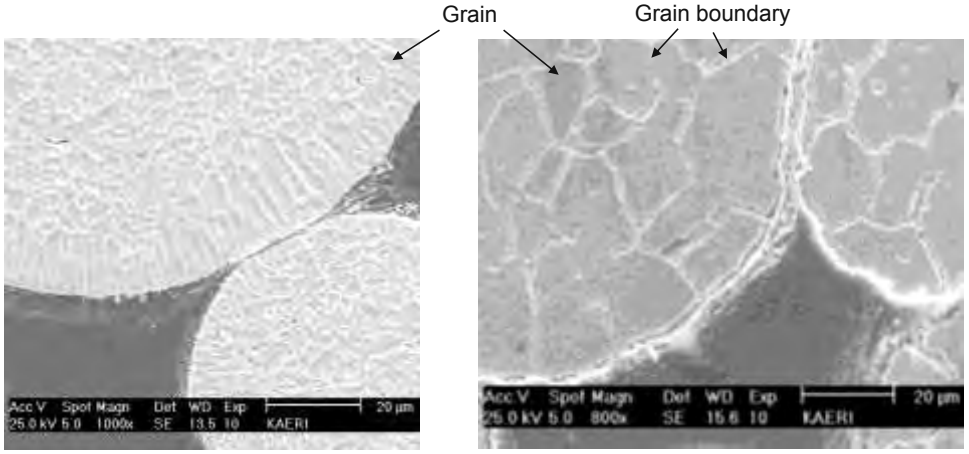

(a) Cross section of as-atomized U-Mo spheres (b) Cross section of heated U-Mo spheres

Fig. 4 Comparison of grain size between as-atomized U-7Mo spheres and U-nitride coated U-7Mo spheres. The U-Mo particles were heated at 1000 °C for an hour to apply U-nitride coating [11].

The image in **Fig. 5** is a cross section of an irradiated U-7Mo sphere (676-NI1) that was U-nitride coated at 1000 °C for an hour before irradiation [11]. The intergranular fission gas bubbles on the grain boundaries highlight the grain boundares in the SEM image. The fuel particle has much larger grains than the as-fabricatded grains shown in **Fig. 4**(a). Another observation is that the fuel particle was barely in the grain subdivision stage. The FD of 62%

burnup is approximately $4.6x10^{21}$ f/cm^3, at which nearly a complete grain subdivision is typically observed [6] (see **Fig. 3**). This low grain subdivision can be attributed to the heating treatment.

The lack of grain subdivision and low extent of intergranular FGB suggest that fuel swelling by FGB is negligible. For this situation, the parabolic term in the fuel swelling correlation given in Eq. (2) can be turned off.

Table 4 contains a comparison between the measured meat swelling of 676-NI1 and the prediction excluding intergranular FGB swelling. Both are close to each other. However, if the intergranular FGB swelling is included, the result is higher by 5%. Therefore, this is the benefit of grain growth occurred by the heating.

A hypothetical case that had the same test parameters and irradiation condition as R2R088 but large assumed grain size was considered to estimate the effect of grain size. The prediction was made by the same way for 676-NI1 above. The result given in **Table 5** presents a considerable effect. A heating process may have an additional positive effect that modifies U-Mo fuel to reduce fission gas release to the matrix due to annealing of the defects in the U-Mo. This effect increases with U-Mo loading and burnup.

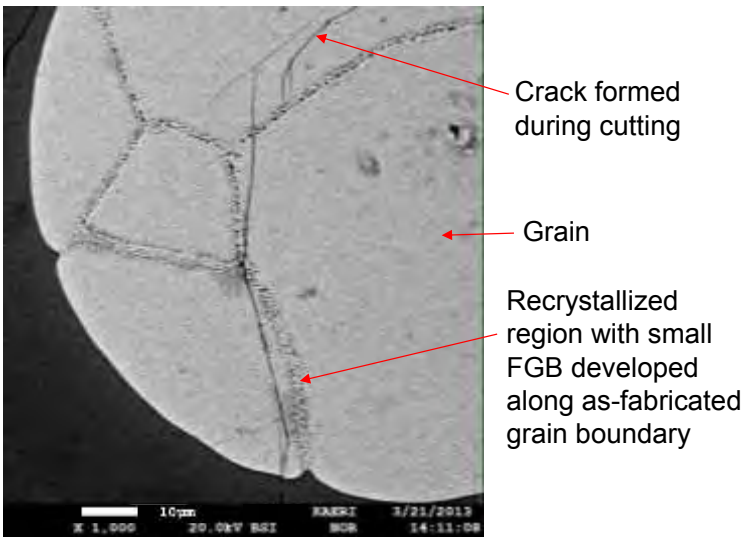

Fig. 5 SEM image of pre-irradiation heated U-7Mo fuel particle after irradiation to a burnup of 62% of U-235 with 19.75% enrichment.

Table 4 Comparison of measured meat swelling of 676-NI1

	676-NI1
Mo content (wt.%)	7
U-loading (gU/cm^3)	5
Average U-Mo size (μm)	175
Fission density (10^{21} f/cm^3)	4.6
Measured meat swelling (%)	9
Predicted meat swelling (%) without intergranular FBG	10
Predicted meat swelling (%) with Intergranular FGB	15

Table 5 Comparison of meat swelling of R2R088 with a hypothetical case at the same irradiation condition but having large grains

	R2R088	Hypothetical case
Mo content (wt.%)	7	7
U-loading (gU/cm^3)	8.5	8.5
Average U-Mo size (μm)	50	50
Fission density (f/cm^3)	5.6	5.6
Grain size (μm)	5	20
Measured meat swelling (%)	25.6	-
Predicted meat swelling (%)	26.4	21.3

The drawback to adopt larger grain-sized U-Mo is to have a heat treatment as an extra manufacturing step. Hence, a higher manufacturing cost is inevitable.

5. CONCLUSIONS

To improve the performance of U-Mo/Al dispersion fuel the use of larger fuel particles, higher Mo content in U-Mo and larger grain size in U-Mo were proposed. The effect of these modifications were analyzed using PIE data. The benefit of each modification was quantitatively assessed by comparing the porposed case with a real test plate.

For reasonably achievable changes, the increase in the Mo content and the use of larger grain size by a heat treatment were assessed to be most effective. However, the effect of using larger U-Mo particles was predicted to be negligible for high fuel loading and high burnup conditions.

In addition to the benefits related to fuel meat swelling, the use of larger U-Mo particles can reduce fission gas release from the fuel particles to the matrix. Hence, it can reduce pore formation in the matrix. The modification for a higher Mo content may have a secondary positive effect in reducing the IL growth rate. The large grain size option also has the benefit of reducing fission gas release to the matrix.

ACKNOWLEDGMENTS

This study was supported by the UChicago Argonne, LCC as Operator of Argonne National Laboratory under Contract No.DE-AC-02-06CH11357 between UChicago Argonne, LLC and the US Department of Energy, and in part by the National Nuclear R&D Program of Ministry of Education, Science and Technology (MEST) of Republic of Korea.

REFERENCES

[1] Yeon Soo Kim, ANL-INL workshop on U-Mo/Al dispersion fuel development, Argonne National Laboratory, Aug. 28, 2013.
[2] Yeon Soo Kim, G.Y. Jeong, J.M. Park, J. Nucl. Mater., submitted, 2015.
[3] C.K. Kim, K.H. Kim, J.M. Park, H.J. Ryu, Y.S. Lee, D.B. Lee, S.J. Oh, H.T. Chae, C.G. Seo, C.S. Lee, Proc. Inter. Meeting on RERTR-2005, Boston, USA, Nov. 6-10, 2005.
[4] Yeon Soo Kim, G.L. Hofman, H.J. Ryu, J.M. Park, A.B. Robinson, D.M. Wachs, Nucl. Eng. Technol., 45 (2013) 827.
[5] Yeon Soo Kim, G.L. Hofman, J. Nucl. Mater., 419 (2011) 291.
[6] A. Leenaers, Sc.D. Thesis, Univ. of Ghent, Belgium, 2014.
[7] Yeon Soo Kim, G.L. Hofman, J.S. Cheon, J. Nucl. Mater., 436 (2013) 14.
[8] J. Rest, J. Nucl. Mater., 346 (2005) 226.
[9] S. Van den Berghe, W. Van Renterghem, A. Leenaers, J. Nucl. Mater., 375 (2008) 340.
[10] J. Gan, D.D. Keiser Jr, D.M. Wachs, A.B. Robinson, B.D. Miller, T.R. Allen, J. Nucl. Mater., 396 (2010) 234.
[11] Yeon Soo Kim, J.M. Park, K.H. Lee, B.O. Yoo, H.J. Ryu, B. Ye, J. Nucl. Mater., 454 (2014) 238.

THE THERMAL PROPERTIES OF FRESH AND SPENT U-MO FUELS: AN OVERVIEW

T.K. Huber, H. Breitkreutz, W. Petry, C. Reiter
Forschungs-Neutronenquelle Heinz Maier-Leibnitz (FRM II), Technische Universität München
Lichtenbergstrasse 1, 85748 Garching – Germany

S. Elgeti
Max-Planck-Institute for Plasma Physics
Boltzmannstraße 2, D-85748 Garching – Germany

D.E. Burkes, A.J. Casella, A.M. Casella, F.N. Smith
Pacific Northwest National Laboratory
P.O. Box 999, Richland, WA 99352 – USA

D.M. Wachs
Idaho National Laboratory
P.O. Box 1625, Idaho Falls, ID 83415 – USA

ABSTRACT

The evolution of the thermal conductivity of research reactor fuel during in-pile irradiation plays a significant role for the performance of the fuel element. To correctly simulate the heat fluxes and temperatures in the fuel meat during normal reactor operation and also off-normal scenarios, it is crucial to investigate the change in thermal properties, especially the thermal conductivity, depending on the fission density and temperature.
Two different U-Mo fuel types, dispersion and monolithic design, have to be considered. The thermal conductivity of fresh dispersion fuel lies between 40 and 80 W/mK depending on the particle size and shape, matrix material composition and U-loading. In contrast, the thermal conductivity of non-irradiated monolithic fuel is already below 15 W/mK due to the lack of the highly conductive aluminum matrix.
The thermal conductivity is a composition of the thermal diffusivity, specific heat capacity and density. The specific heat capacity does not change significantly during irradiation. The density decreases slightly due to the formation of fission gas bubbles. The thermal diffusivity is strongly dependent on the materials structure. During irradiation this structure is destroyed by the fission products and fission gas bubbles. This decreases the thermal diffusivity of the irradiated material drastically down to 20% of the fresh material and has therefore the highest impact on the change of the thermal conductivity during irradiation.
Therefore, during irradiation, the thermal conductivity of the dispersion fuel strongly deceases down to about 15% of the original value. The measurement of a dispersion segment from AFIP-1 with a burn-up of $6 \cdot 10^{21}$f/cc yielded a thermal conductivity of 7 W/mK. The low thermal conductivity of monolithic fuel further decreases as well with increasing burn-up. At a burn-up of $3 \cdot 10^{21}$f/cc, the thermal conductivity is already below 10 W/mK.

1 Introduction

For the design of the cooling system, it is mandatory to calculate the heat fluxes and the overall temperature in the fuel element during reactor operation. For the calculation, the thermal conductivity of the used reactor fuel is required.
Currently, research reactors that are operated with highly enriched fuel are in the process to convert to lower enriched fuel. Therefore a new kind of fuel, based on a uranium-molybdenum (U-Mo) alloy, has been developed. Accordingly, the thermal conductivity of this new fuel type has to be investigated for the thermal hydraulic calculations.
First, two types of this new fuel need to be distinguished. On the one hand, there is dispersion fuel which is U-Mo particles in a matrix material and on the other hand there is monolithic fuel which consists of bulk U-Mo alloy without matrix material.
Pure U-Mo has a comparably low thermal conductivity of 15W/mK at room temperature. This leads to the fact that the heat originating from the fission during reactor operation is transferred to the cladding and the cooling agent rather slowly, ending up in relatively high operating temperatures in the fuel meat (~150°C). Mixing the U-Mo with a high conductive material, like aluminum (Al), as it is done in dispersion fuels, increases the thermal conductivity and the heat transfer from the fuel meat to the cladding and coolant happens faster. This way, the meat temperature during reactor operation is lower for dispersion fuels (~100°C). In some cases, for metallographic reasons, the matrix material does not only consist of pure Al, but silicon (Si) is added to the matrix. In other cases, the fuel particles are coated with Si or zirconium-nitride (ZrN).
As the thermal conductivity of such composites cannot be obtained by calculation alone, it is mandatory to measure the thermal conductivity of the different types of dispersion fuel.
Further, during irradiation, solid and gaseous fission products are generated. Especially, the gaseous fission products conglomerate in voids, which decrease the thermal conductivity of the fuel. Additionally, some dispersion fuels grow an inter-diffusion layer (IDL) during irradiation, which mainly consists of UAl_x compounds, around the fuel particles. It is therefore currently only to a very limited extent possible to predict the evolution of the thermal conductivity of the fuel during irradiation with mathematical models. Thus, measurements on both monolithic and dispersion fuels with different burn-up have been performed.
In the following the thermal properties measurements of several different non-irradiated dispersion fuels, as well as irradiated dispersion and monolithic fuels will be presented.

2 Measurement

2.1 Measurement Techniques

The thermal conductivity λ cannot be accessed directly, rather it is a composition of the material's density ρ, thermal diffusivity α and specific heat capacity Cp, according to eqn. 1. Each of these parameters can be measured separately.

$$\lambda = \rho \cdot \alpha \cdot C_p \tag{1}$$

The density can be measured by immersion or pycnometry. The fresh fuel specimens have been measured using the immersion technique that is based on Archimedes' principle. The specimen's weight is measured on air and in a liquid like water or ethanol. Finally, the density can be calculated from the different masses via the balance of forces. This method is simple and cost-efficient for fresh fuel for handling on the benchtop or fume hood, but it is not practical for hot cells. So, the in-pile irradiated fuels have been measured using gas pycnometry. Simultaneously, measurements performed with this method have a reduced uncertainty, as minimal voids with air adhere on the sample surface during immersion in the liquid and create a buoyant force that marginally falsifies the measurement. Using this method, first, the volume of the specimen is determined by Boyle's law, i.e. volume displacement. Together with the specimen's mass, the density can be calculated.

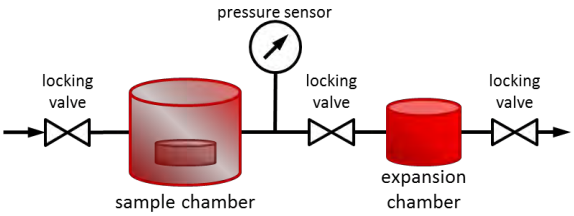

Fig 1. Pycnometry setup to measure the density using Boyle's law.

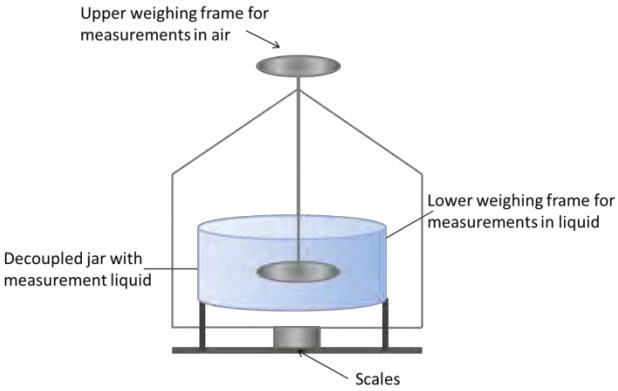

Fig 2. Immersion setup to measure the density using Archimede's principle.

The laser flash method (LFA) is the standard technique to measure the thermal diffusivity. A very short laser pulse with high intensity hits the rear side of the specimen. The heat is transferred through the material and heats up the opposite surface. There, an infrared detector measures the time dependent temperature rise. The thermal diffusivity can finally be calculated from the slope of the temperature rise. The sample is located in a sealed chamber for measurements in inert gas atmospheres or vacuum to reduce the risk of oxidation. Heating elements around the sample chamber allow measurements up to more than 1000°C. This technique has been used for all thermal diffusivity measurements.

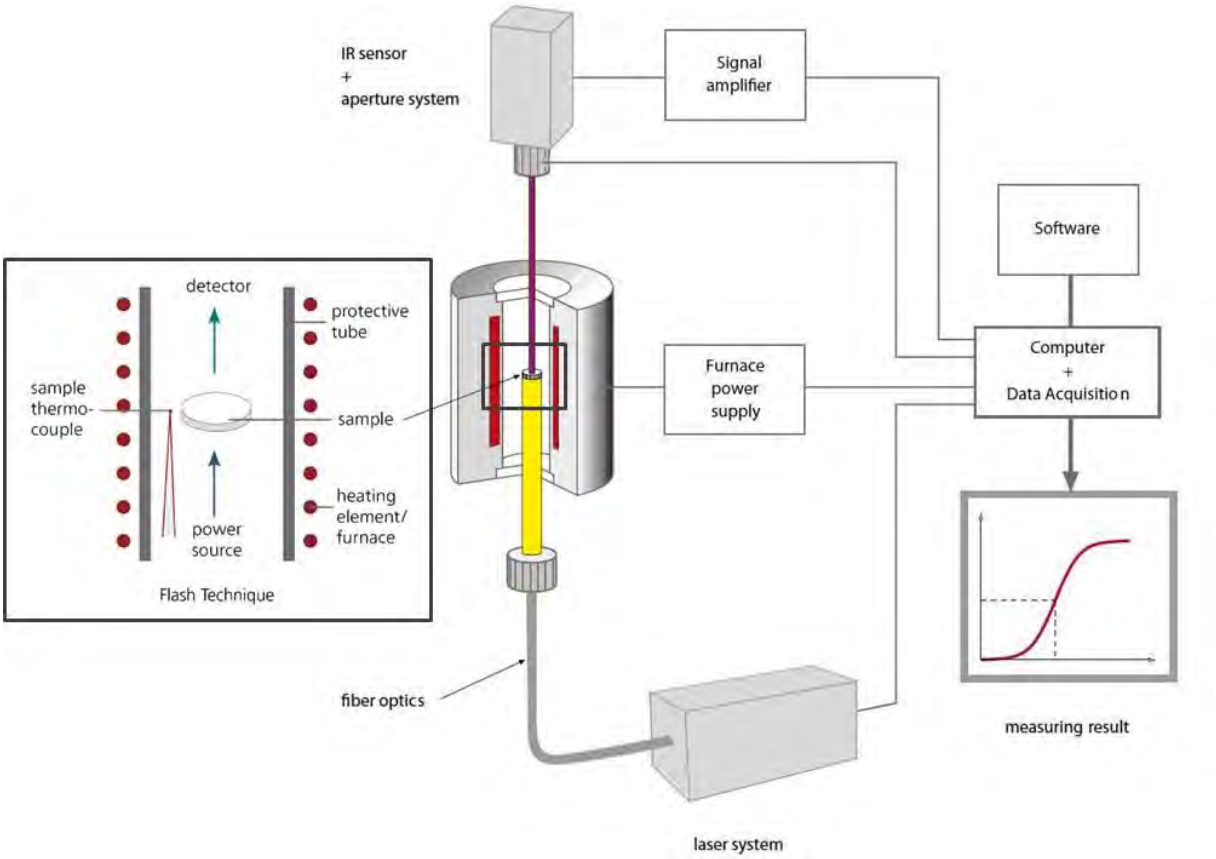

Fig 3. Laser Flash setup for the measurement of the thermal diffusivity [LFA467].

The specific heat capacity can be obtained with a power compensating differential scanning calorimeter (DSC). It consists of two crucibles with heating elements and temperature sensors. The specimen is placed into one of the crucibles and the same amount of heat is added to both crucibles. The crucible with the specimen heats up less due to the additional mass and its specific heat capacity. So, more heat is added to the crucible with the specimen

until it has the same temperature as the empty crucible. The additional amount of heat that was necessary to adjust the temperature of the crucible with the specimen is proportional to the specific heat capacity of the specimen.

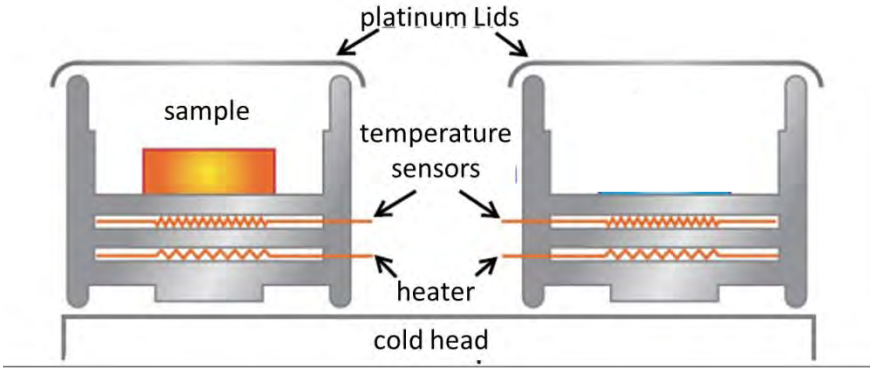

Fig 4. Schematic setup of a power compensating Differential Scanning Calorimeter for the measurement of the specific heat capacity [Rei13].

2.2 Investigated Materials

The main focus lies on the various dispersion fuel types. For dispersion fuels usually an alloy of uranium with 7wt% molybdenum is used for powder production, except for IRIS-TUM, which is fabricated from U-8wt%Mo. Two different U-Mo powder types need to be distinguished: ground and atomized powder. The ground powder has an irregular shape tending to higher porosities than the almost perfect spherical shape of the atomized powder. Different kinds of sputter-coating can be applied on atomized powder, like Si or ZrN, to prevent the disadvantageous reaction of the U-Mo particles with the aluminum of the matrix. Another way of coating is simply oxidation of the particle surface, as uranium-oxide does not react with the aluminum of the matrix in the same way as metallic U-Mo does. If no coating is applied on the UMo powder, the most convenient way is to mix the aluminum of the matrix with silicon, which forms a silicon rich layer around the U-Mo particles during annealing at 400-450°C. Tab 1 gives an overview over the investigated U-Mo fuels chosen from siblings of plates tested during in-pile experiments.

Fuel Name	Powder Type	Particle Coating	Uranium Loading	Matrix Material
E-FUTURE 4112	atomized	---	8gU/cm³	Al + 4wt%Si
E-FUTURE 6101	atomized	---	8gU/cm³	Al + 6wt%Si
E-FUTURE II 701	atomized	---	8gU/cm³	Al + 7wt%Si
E-FUTURE II 1203	atomized	---	8gU/cm³	Al + 12wt%Si
E-FUTURE II 1212	atomized	---	8gU/cm³	Al + 12wt%Si
IRIS-4 UMo/Al	atomized	oxide	8gU/cm³	Al
IRIS-4 UMo/AlSi	atomized	oxide	8gU/cm³	Al + 2wt%Si
IRIS-TUM 7001	ground	---	7gU/cm³	Al
IRIS-TUM 8003	ground	---	8gU/cm³	Al
IRIS-TUM 8502	ground	---	8gU/cm³	Al + 2wt%Si
SELENIUM A	atomized	300nm Si	8gU/cm³	Al
SELENIUM B	atomized	600nm Si	8gU/cm³	Al
SELENIUM C	atomized	1000nm ZrN	8gU/cm³	Al
AFIP-1	atomized	---	8gU/cm³	Al + 2wt%Si

Tab 1. Overview of investigated fresh fuels from European irradiation tests.

Additionally, two in-pile irradiated segments of the AFIP-1 fuel with different burnup have been investigated. This full size test plate was irradiated in the Advanced Test Reactor (ATR) at the Idaho National Laboratory (INL) in Idaho, USA, in three reactor cycles in 2008 and 2009.

Segment	Fission Density	Surface Heat Flux	U-235 Depletion
AFIP-1 TL	4.86E21 f/cm³	116.3 W/cm²	65.5%
AFIP-1 TK	6.12E21 f/cm³	124.9 W/cm²	81.6%

Tab 2. AFIP-1 irradiation conditions [Per11].

Besides the dispersion fuel, monolithic fuel and its behavior during irradiation has been investigated. Usually the monolithic fuels contain 10wt% molybdenum in the uranium alloy. The in-pile irradiated fuel investigated here originates from the AFIP-2BZ full size test plate. The average surface heat flux was 237W/cm². The fission density of the fuel segment was 3.25E21 f/cm³.

3 Results and Discussion

3.1 Density

Fig 5 shows a summary of the density ρ of fresh and irradiated dispersion and monolithic fuels. The density of fresh dispersion fuels lies in a narrow band around 10g/cm³. Small deviations in the porosity and uranium loading cause the small variations. The AFIP-1 sample shows the impact of irradiation on the density. With increasing burnup, more fission products are generated, of those mainly the gaseous products increase the fuels volume, leading to a decrease of the density.

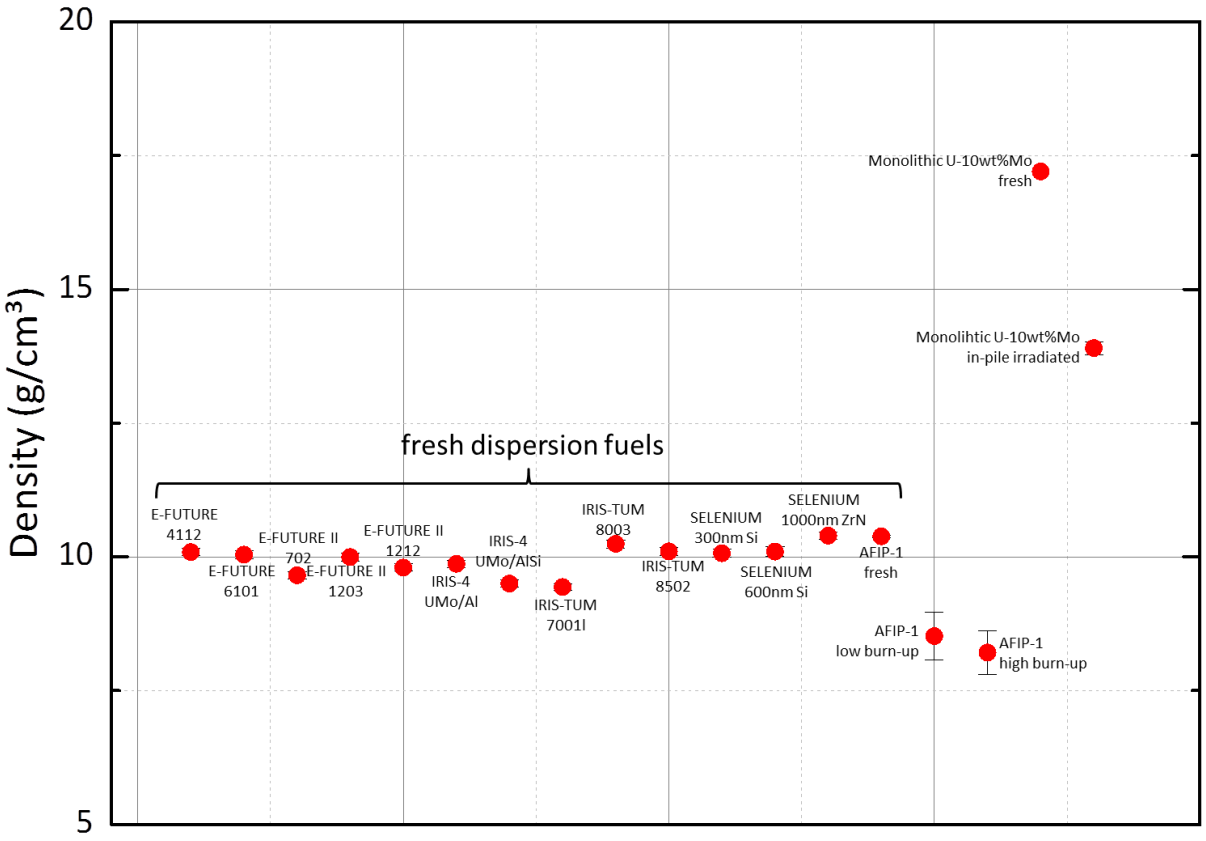

Fig 5. Summary of the density of fresh and irradiated dispersion and monolithic U-Mo fuels

The monolithic fuel has a significantly higher density than the dispersion fuels due to the lack of matrix material, which mainly consists of aluminum with a density of 2.7g/cm³. During irradiation, again mainly the generation of the gaseous fission products lead to a decrease of the fuels' density.

3.2 Thermal Diffusivity

In contrast to the density, the thermal diffusivity α for fresh dispersion fuels has a much higher variation, see Fig **6**. Already dispersion fuels containing atomized powder vary within a band between 20mm²/s to 30mm²/s, but dispersion fuels containing ground powder have a significantly lower thermal diffusivity between 10mm²/s and 15mm²/s. The heat is mainly transferred through the high conductive aluminum in the matrix material. Depending on the silicon content in the aluminum alloy, its thermal diffusivity lies between 60mm²/s to 100mm²/s [Wol14]. The thermal diffusivity of U-8wt%Mo is much lower at 5mm²/s [Hen10]. So, the particles are a thermal resistance, same as porosities. Therefore, the thermal diffusivity is very sensitive on uranium loading and the amount of porosities.

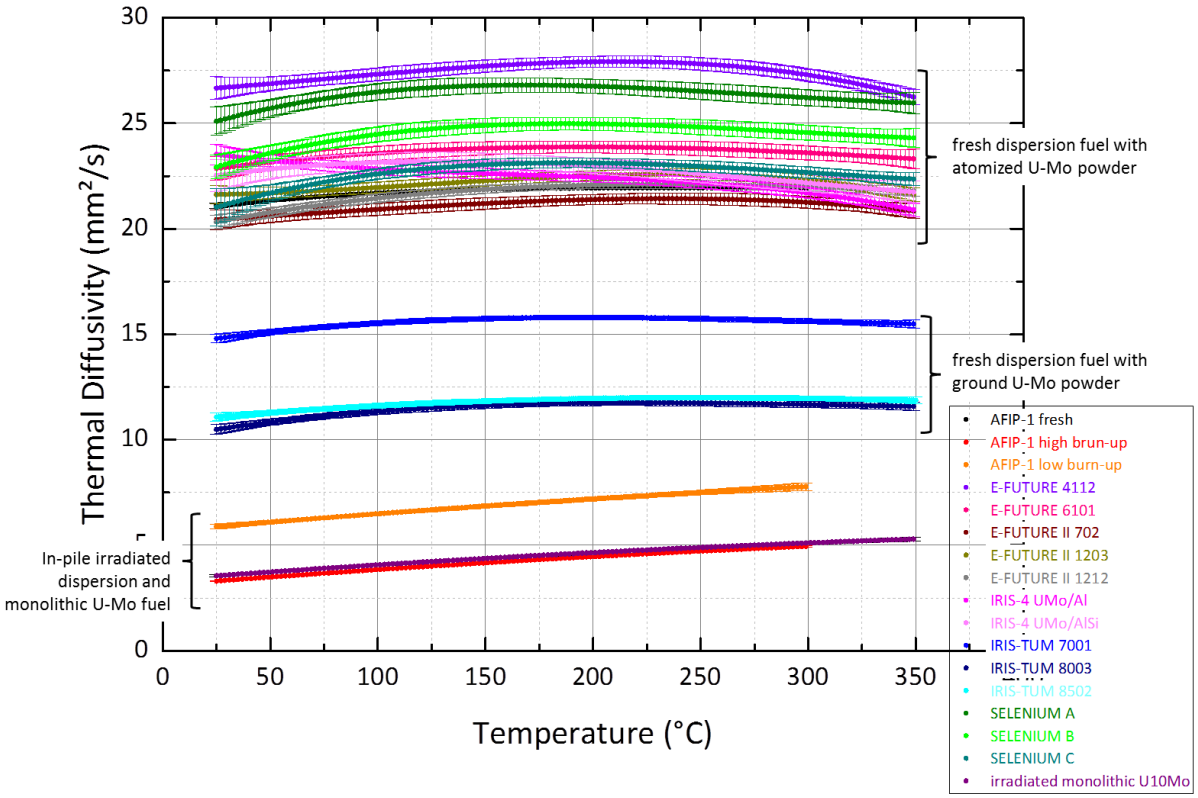

Fig 6. Summary of the thermal diffusivity of the different fuel types, also comparing fresh and in-pile irradiated fuels.

In the case of the atomized powder dispersion fuels, additionally, the amount of Si in the matrix material leads to deviations in the thermal diffusivity. But also small differences in uranium loading and porosities have an impact.

Due to the irregular particle shape of the ground powder, in general a higher amount of porosities is generated in the fuels during fabrication. Further, the irregular particle shape itself creates a higher thermal resistance than the perfectly round particles in fuels with atomized powder. So, the higher amount of porosities and the higher thermal resistance lead to a further decrease of the thermal diffusivity of ground powder fuels, compared to atomized powder fuels.

During irradiation, the gaseous fission products form bubbles. So, more porosity is created that lead to a decrease of the thermal diffusivity. Further, due to the high energy of the fission products (~80MeV) the crystal lattice of the fuel is destroyed in parts. As the heat is partly transferred via phonons and electrons, defects in the crystal lattice additionally lead to a higher thermal resistance.

3.3 Specific Heat Capacity

Fig 7 shows that the specific heat capacity C_p of the fresh dispersion fuels lies in a narrow band between 0.2 J/gK and 0.3 J/gK with only very small variation between the different fuels. The particle shape or porosities do not impact the specific heat capacity. It is mainly dependent on the material composition. The dispersion fuels do not significantly vary in composition, so that the specific heat capacity has no big variations between the fresh as well as the irradiated fuels. Also here, the specific heat capacity is not impacted by most of the changes that happen to the material during irradiation except a small change in the material composition that results from the solid fission products. But the fraction of generated fission products is below 1% of the fuels atomic composition, which is too low for the sensitivity of the DSC. Another rather small impact comes from the change in the crystal lattice, which is partially destroyed during irradiation. The energy that is stored in the materials crystal lattice is part of the materials specific heat capacity and changes in the lattice have accordingly an impact on this property.

The specific heat capacity of monolithic fuel [Bur10] is significantly lower than the specific heat capacity of dispersion fuels. This is caused by the lack of matrix material, which mainly consists of materials with high specific heat capacities, like pure aluminum with about 0.9 J/gK [Tou70a]. Irradiation has in this case about the same impact as on dispersion fuels.

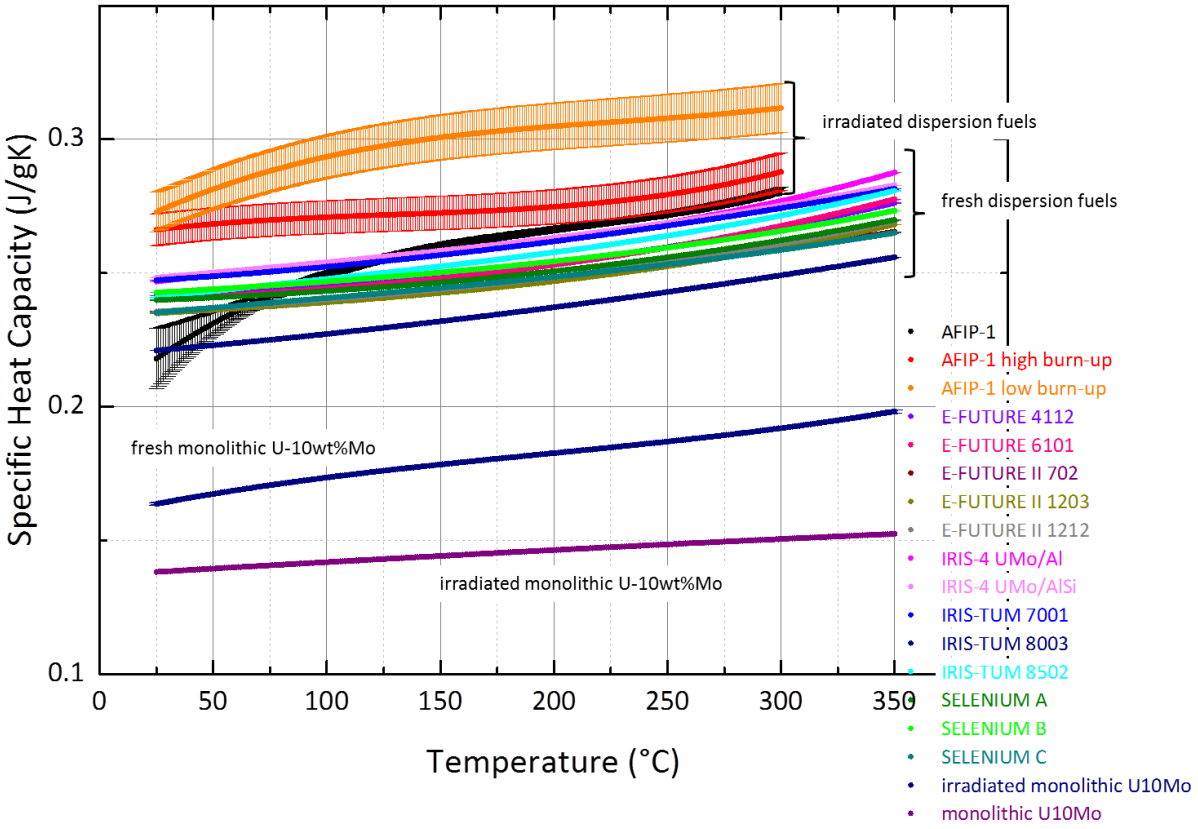

Fig 7. Summary of the specific heat capacity.

3.4 Thermal Conductivity

The thermal conductivity λ is finally the product of the density, thermal diffusivity and specific heat capacity, as shown in equation 1. In the following, the fuels will be discussed separately according to their type and differentiating fresh and irradiated fuel.

3.4.1 Dispersion Fuel with Atomized Powder and Si-Matrix

Fig 8 shows the thermal conductivity of fresh dispersion fuels with Al-Si matrix materials with differing Si content. E-FUTURE and E-FUTURE II are dispersion fuels containing atomized powder with a uranium loading of 8gU/cm³. The matrix materials consist of Al-Si alloys with 4wt% to 12wt.% Si content. Pure Al has a thermal conductivity of about 250W/mK [Tou70b] at room temperature, which is significantly higher than the thermal conductivity of Si with about 150W/mK [Tou70b] at room temperature. So, the thermal conductivity of these fuels is expected to be only dependent on the Si content, as the uranium loading and composition is constant. Consequently, the thermal conductivity of the fuels should decrease with increasing Si content. But a deviation from this expected behavior can be observed regarding the 7wt% and 12wt% Si E-FUTURE II fuel. The 12wt% Si fuels thermal conductivity is higher than the 7wt% fuels thermal conductivity. Reference measurements of Al-Si alloys with similar composition show exactly the same behavior, the thermal conductivity of an Al-12wt%Si alloy is higher than a Al-8wt%Si alloy [Wol14]. First scanning electron microscopy images and the examination of the Al-Si phase diagram do not show indications for this behavior.

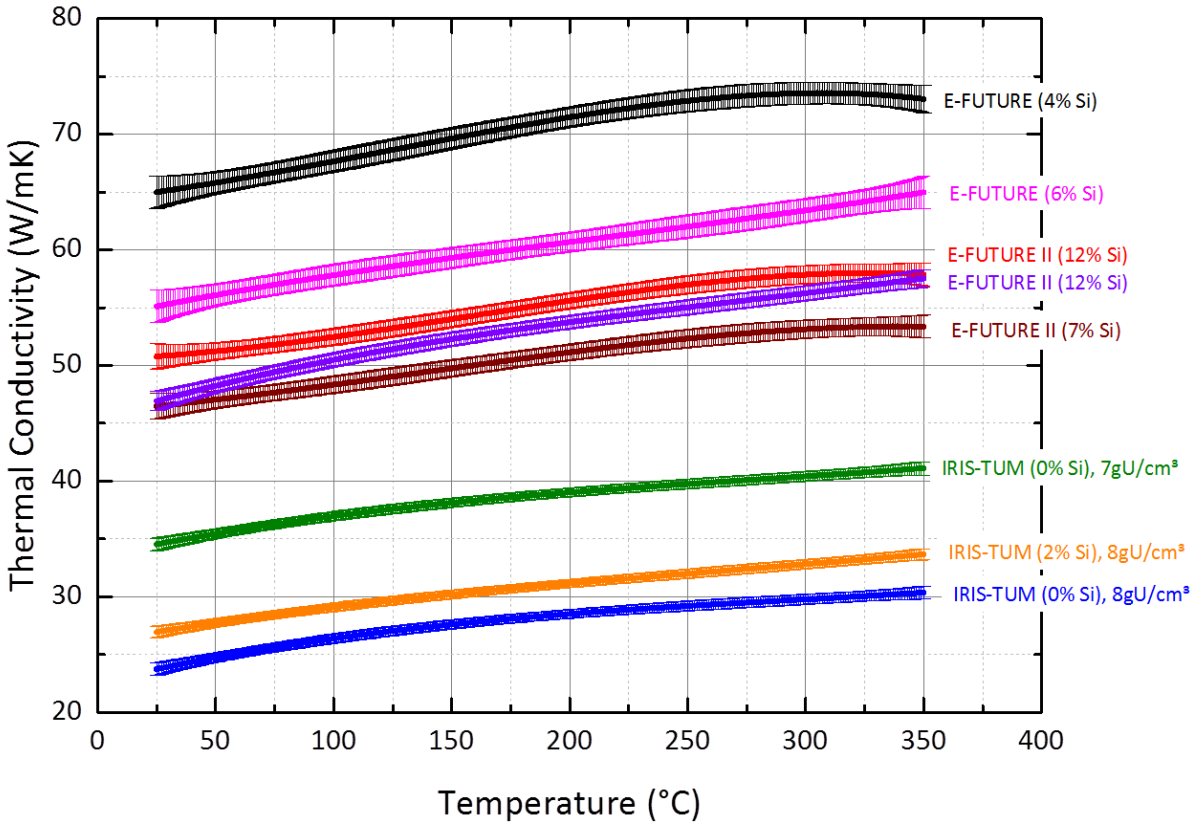

Fig 8. Thermal conductivity of fresh dispersion fuels with Al-Si matrix material.

3.4.2 Dispersion Fuel with Ground Powder and Si-Matrix

The IRIS-TUM fuels consist of ground powder. As already seen in Fig 6, the thermal diffusivity is strongly impacted by the particle shape, and is simultaneously the parameter with the highest impact on the thermal conductivity. Accordingly, the thermal conductivity of

the ground powder fuel is lower than the thermal conductivity of the atomized powder fuel. Additionally, the impact of the uranium loading can be observed. Due to the low thermal conductivity of U-Mo, the fuel with higher uranium loading has a significantly lower thermal conductivity. Here, it is conscious that the thermal conductivity of the IRIS-TUM fuel without Si in the matrix is higher than the thermal conductivity of the fuel with 2wt% Si. But here, the uranium loading of the 2wt%Si plate is also 0.2gU/cm³ higher than the fuel without Si. So, the uranium loading has a higher impact on the thermal conductivity than the Si content, as the thermal conductivity of Si is closer to the thermal conductivity of the Al than the uranium.

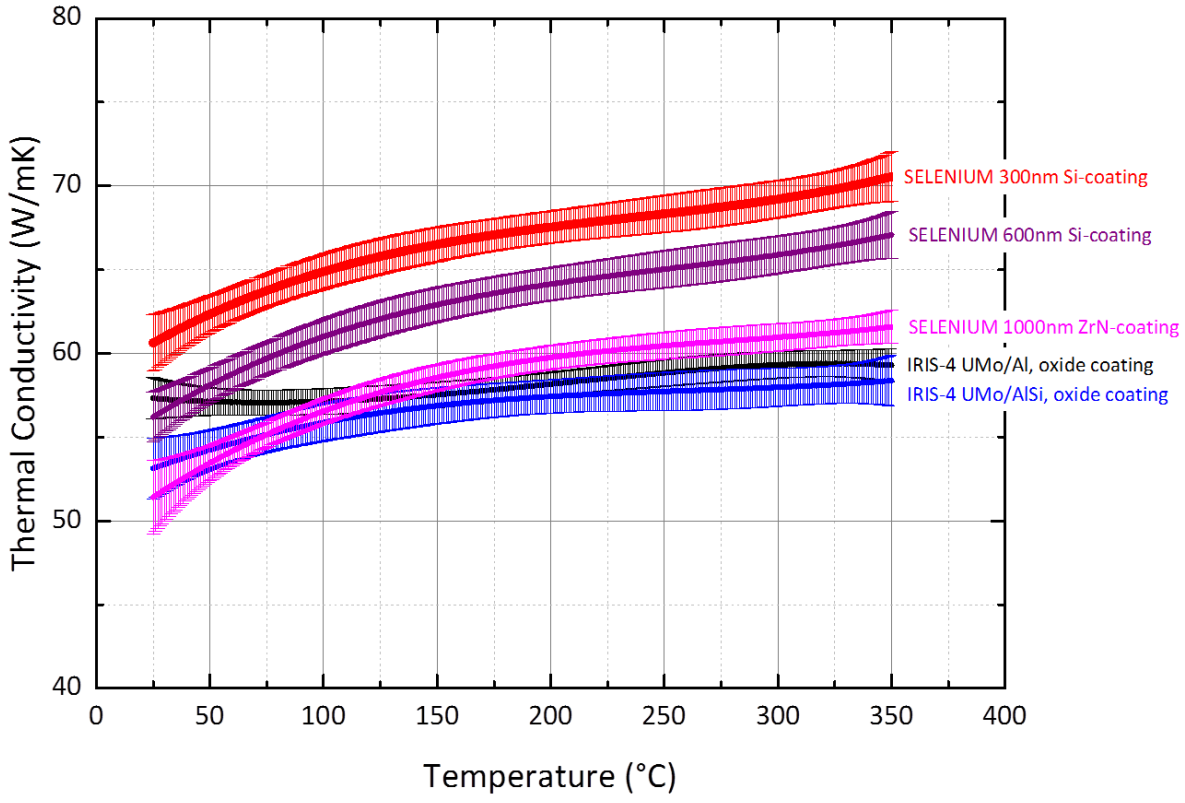

Fig 9. Thermal conductivity of dispersion fuels with different coatings.

3.4.3 Dispersion Fuel with Coated Powder

Fig 9 shows the thermal conductivity of dispersion fuels fabricated from atomized powder with different coatings. The thermal conductivity of the Si coated fuels is analogous to the fuels with Si in the matrix material in the same region. Consistently, the fuel with thicker Si coating has a lower thermal conductivity.

The fuel with oxide and ZrN coating have a similar thermal conductivity which is lower than the Si coated particle fuels thermal conductivity. Both coatings are ceramics, which have a generally low thermal conductivity below 10W/mK [Fin00].

3.4.4 In-pile Irradiated Fuels

Fig 10 shows a comparison of fresh and in-pile irradiated dispersion fuels in relation to fresh and in-pile irradiated monolithic fuels. The thermal conductivity of the fresh dispersion fuel containing atomized powder in Al-2wt%Si matrix is in the same range as the other investigated dispersion fuels. But during irradiation with increasing burnup to 4.86E21 f/cm³, the thermal conductivity strongly decreases from ~50W/mK down to ~15W/mK comparable with fresh monolithic U-10wt%Mo [Bur10] at room temperature. With further irradiation to a

burnup of 6.12E21 f/cm³ the thermal conductivity further decreases down to ~8W/mK which is about 15% of the original value of the fresh fuel. In contrast, the thermal conductivity of irradiated monolithic fuel only decreases from ~12W/mK to ~9W/mK, which is about 75% of the original value of the fresh fuel at a burnup of 3.25E21f/cm³ [Bur13].

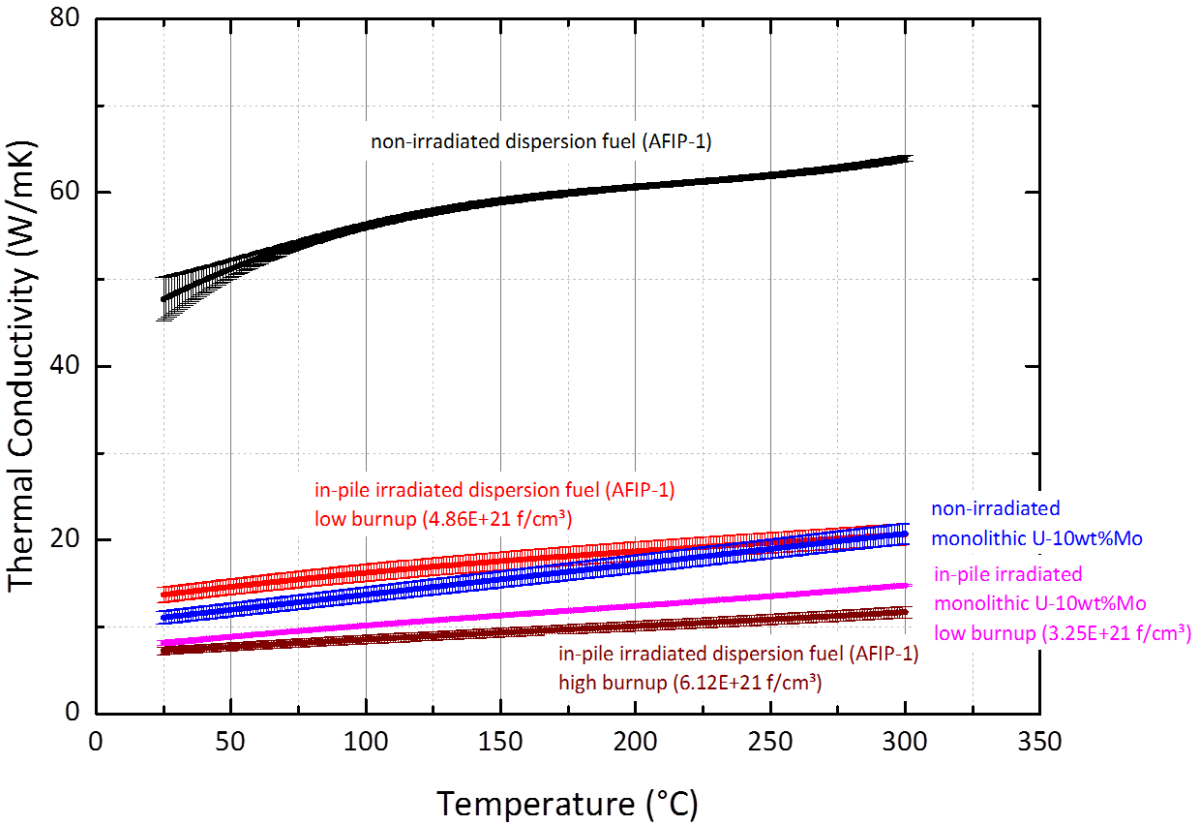

Fig 10. Thermal conductivity of fresh and in-pile irradiated dispersion and monolithic U-Mo fuels.

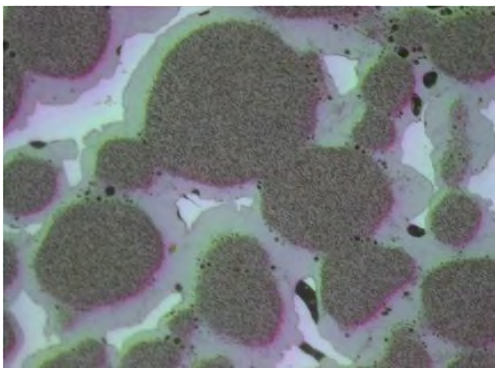

Fig 11. Optical microscope image of the low burnup dispersion segment.

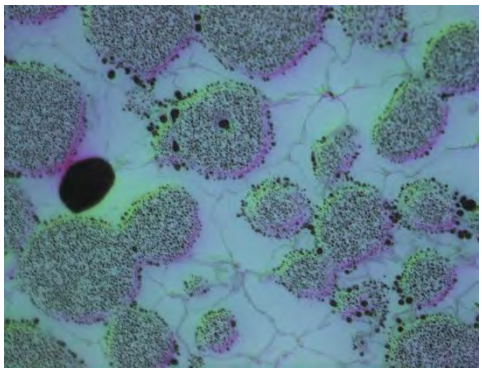

Fig 12. Optical microscope image of the high burnup dispersion segment.

In both fuels, monolithic and dispersion, the fission-induced formation of fission gas bubbles and the decomposition of the U-Mo crystal lattice lead to a decrease in the thermal conductivity. But, in the case of the dispersion fuel, additionally, the matrix material is more and more consumed by inter-diffusion layer (IDL) that is generated during irradiation due to the reaction of uranium with the aluminum matrix. Fig 11 is an optical microscopy image of the low burnup dispersion fuel segment. The formation of the IDL has already started, which can be seen at the dark grey areas around the fuel particles. The black spots in the fuel

particle are the fission gas bubbles. The few light grey areas represent the remaining Al matrix material. Fig 12 is an optical microscopy image of the high burnup fuel segment. The fission gas bubbles increased and the dark gray IDL has completely consumed the matrix.

Consequently, this inter-diffusion layer has a very low thermal conductivity, so that the high conductive matrix material is successively replaced by low conductive IDL material, leading to a decrease of the thermal conductivity of the entire fuel meat.

4 Conclusion

The thermal diffusivity has the highest impact on the thermal conductivity, as it is the parameter with the largest variation. It strongly decreases during irradiation with increasing burnup. In contrast, the specific heat capacity has only a small variation between the different dispersion fuels and even irradiation has only a small impact. The density does not vary much for fresh dispersion fuels as well, but decreases during irradiation, mainly due to the formation of gaseous fission products.

The thermal conductivity of monolithic fuel decreases from ~12W/mK down to ~9W/mK (at room temperature), which is a decrease of about 25% for fresh fuel during irradiation due the formation of fission gas bubbles and crystal defect from the solid fission products. In contrast, the thermal conductivity of dispersion fuels decreases from ~50W/mK down to ~15W/mK (at room temperature), which is a total decrease of 85%. In this case, the thermal conductivity of fresh dispersion fuel is in general higher than the thermal conductivity of monolithic fuel due to the high conductive matrix material. But during irradiation the high conductive material is successively consumed by low conductive IDL material, which finally leads to a drastic drop of the entire fuel meats thermal conductivity.

5 Acknowledgements

The authors would like to thank Idaho National Laboratory (INL) for providing the AFIP-1 fuel and Pacific Northwest National Laboratory (PNNL) for providing the equipment, instruments and manpower for the measurements. The dispersion fuels have been provided by AREVA CERCA, CEA and SCK CEN.

The DSC measurements on the fresh fuel have been performed at Materials Science Lab of Heinz Maier-Leibnitz Centre (MLZ), Technische Universität München (TUM) in collaboration with Armin Kriele, Helmholtz-Zentrum Geesthacht (HZG). The LFA measurements have been performed at the Max-Planck Institute for Plasma Physics.

This work was supported by a combined grant (FRM 0911) of the Bundesministerium für Bildung und Forschung (BMBF) and the Bayrisches Staatsministerium für Wissenschaft, Forschung und Kunst (StMWFK).

6 References

[Bur10] D. E. Burkes, G. S. Mickum, Dm. M. Wachs, Thermophysical Properties of U-10Mo Alloy, 2010.

[Bur13] D. E. Burkes, A. M. Casella, E.C. Buck, A. J. Casella, M. K. Edwards, P. J. MacFarlan, K. N. Pool, B. D. Slonecker, F. N. Smith, F. H. Steen, R. E. Thornhill, Fuel Thermo-physical Characterisation Project: Fiscal Year 2013 Final Report, 2013.

[Fin00] J.K. Fink, Thermophysical properties of uranium dioxide, J. Nucl. Mat. 279 (2000), p. 1 – 18.

[Hen10] R.M. Hengstler, L. Beck, H. Breitkreutz, C. Jarousse, R. Jungwirth, W. Petry, W. Schmid, J. Schneider, N. Wieschalla, Physical Properties of monolithic U8wt.%-Mo, J. Nucl. Mat. **402** (2010), p. 74 – 80.

[LFA467] Netzsch-Gerätebau GmbH, Light Flash Apparatus LFA 467 HyperFlash, Brochure.

[Per11] D. M. Perez, M. A. Lillo, G. S. Chang, G. A. Roth, N. E. Woolstenhulme and D. M. Wachs, AFIP-1Irradiation Summary Report, 2011.

[Rei13] C. Reiter, Methodenentwicklung, Kalorimetrie und Messung der Dichte von hochdichten Kernbrennstoffen, diploma thesis, Technische Universität München, 2013.

[Tou70a] Y. S. Touloukian, Specific Heat: Metallic elements and alloys. IFI-Plenum, 1970.

[Tou70b] Y. S. Touloukian, Thermal Conductivity: Metallic elements and alloys. IFI-Plenum, 1970.

[Wol14] A. Wolf, Einfluss des Si-Anteils im Matrix-Material hinsichtlich der Wärmeleitfähigkeit von dispersen UMo-Brennstoffen, bachelor thesis, Technische Universität München, 2014.

THERMODYNAMIC AND KINETIC STUDY OF NITRIDES AND TRANSITION-METALS AS DIFFUSION BARRIERS FOR U-MO/AL DISPERSION FUEL

ZHI-GANG MEI, ABDELLATIF M. YACOUT, YEON SOO KIM, GERARD L. HOFMAN
Nuclear Engineering Division, Argonne National Laboratory
9700 South Cass Avenue, Argonne, IL 60439 - USA

ABSTRACT

Recent irradiation experiment at the BR-2 research reactor confirmed the effectiveness of adding a ZrN coating layer on U-Mo fuel particles in reducing the impact of fuel-matrix interaction layer (IL) formation on dispersion U-Mo fuel swelling. Post-irradiation examination studies indicated the possibility of Al atoms diffusion through ZrN coating layer at high burnups, forming an interaction layer inside the fuel particles. To evaluate the performance of ZrN as a diffusion barrier and search for new candidate barriers, we studied the thermodynamic and kinetic stability of TiN and ZrN using first-principles calculations. Both TiN and ZrN were found to be thermodynamically unstable with respect to Al at high temperatures. The decomposition of transitional-metal nitride coating is controlled by the diffusion of Al atoms in nitrides. The diffusion mechanisms of Al in TiN and ZrN were investigated and the effect of no-stoichiometry on the migration of Al was discussed. The thermodynamic stability of two transition-metals, i.e., Mo and Nb, were also studied as diffusion barriers against Al.

1. Introduction

Uranium-Molybdenum alloy is one of the most promising fuels for future high performance research and test reactors [1, 2]. Low-enriched uranium alloys with 6-10 wt% Mo content are under consideration by the Global Threat Reduction Initiative program (GTRI) as very high density fuels that allow nuclear research and test reactors conversion from use of highly-enriched uranium to low-enriched uranium fuels. When used in dispersion with aluminum, the growth of inter-diffusion layers (ILs) between the dispersed U-Mo fuel particles and the surrounding Al matrix strongly limits the fuel's performance [3]. Recent studies show that Al matrix alloyed with Si can improve the performance of U-Mo dispersion fuel by reducing the formation of ILs [4]. The irradiation induced IL not only decreases the thermal conductivity of fuel, but is also responsible for the anomalous swelling of fuel plates at high burnups. One major goal of U-Mo fuel development is to suppress the formation of IL. Among these, modification of Al matrix or U-Mo alloys by adding alloying elements has been proposed [4]. Adding Si to Al matrix was found to improve the U-Mo fuel performance at high burnups. It was suggested that a silicon rich layer formed at the interface between U-Mo and Al prevents the conventional U-Mo/Al inter-diffusion during irradiation. However, an excessive plate swelling can be still observed in very aggressive irradiation conditions. Using a similar idea, the application of coating a diffusion barrier on U-Mo fuel particles could be more efficient in retarding the inter-diffusion. Heavy ion irradiation experiments [2] suggested that Si coating do provide a good protection of U-Mo fuel particles by reducing the formation of IL. Meanwhile, transitional-metal nitride coatings have been widely used to protect surfaces from diffusion against Al and Cu in microelectronics. Recently ZrN was tested as a diffusion barrier for UMo/Al dispersion fuel. However, experiments reveal that ZrN coating layers show microcracks during fuel plate fabrication, which could be due to the high thermal expansion mismatch between U-Mo alloy and ceramic ZrN [5]. These microcracks in the coating layer provides fast diffusion channels for Al migration and therefore fails to protect the fuel particle from direct contact with Al matrix. For this reason, transitional metals (TM) and their alloys should be thermally/mechanically more stable as coating layer for U-Mo than ceramic materials.

According to Nicolet et al. [6], a good diffusion barrier should satisfy several criteria: (1) the barrier layer should be both thermodynamically and kinetically stable with respect to

contacted materials; (2) the barrier layer should adhere well to substrate and be resistant to thermal and mechanical stresses. In practice, these criteria cannot be satisfied simultaneously. Chemically inert transitional-metal nitrides (TMNs) might satisfy the first requirement but fail the latter one, while TMs and their alloys may not be thermodynamically stable with respect to Al. To this end, we will investigate thermodynamic and kinetic stability of two TMNs and two TM, i.e., TiN, ZrN, Mo and Nb, using first-principles calculations. This information is expected to be useful to identify new diffusion barrier materials for U-Mo/Al dispersion fuels in the future. The following paper is organized as following. A brief description of the computational methods will be provided in section 2. The thermodynamic and kinetic stability of the four materials as diffusion barriers will be discussed in section 3. In section 4 we will give a summary of this work.

2. Computational methodology

All density functional theory (DFT) based first-principles calculations were performed by the projector augmented wave method as implemented in VASP [7, 8] within generalize gradient approximation (GGA) parameterized by Perdew, Burke, and Ernzerhof [9]. During the total energy calculations, a plane-wave energy cutoff of 500 eV was employed. Accurate total energy calculations are performed by means of the linear tetrahedron method with Blöchl's correction [10]. In all cases the total energies are converged to 10^{-7} eV/cell. The obtained lattice parameters are then used to generate 3x3x3 supercells (216 atoms) to study defect formation energies in TMN. A Monkhorst-Pack mesh of 3x3x3 k-points in the Brillouin zone is sufficient to satisfy the convergence criterion. The atomic position and cell volume were fully relaxed for all the structures. The nudged elastic band method has been used to determine the migration barriers that impurity or intrinsic atoms in TMNs.

3. Results and discussion

3.1 Thermodynamic stability of TMs and TMNs

In order to evaluate the thermodynamic stability of TMN with respect to U-Mo fuel and Al, we calculated the enthalpy of formation for all the possible binary compounds in the U-Mo-Al-N-TM (TM=Ti, Zr) systems. Our calculations show that most of the compounds exhibit negative formation energies. Only two binary compounds, i.e., UZr_2 and U_2Mo, show slightly positive formation energy, indicating that they are thermodynamically unstable with respect to its pure elements. Figure 1 shows that the enthalpy of formation of binary compounds in Mo-Al and Nb-Al systems calculated by DFT. Both of Mo and Nb show negative formation energy in the whole composition range, indicating that they are thermodynamically unstable against Al. Therefore, transitional-metals Mo and Nb may not be appropriate as a diffusion barrier for Al. Among all the studied binary compounds, TiN and ZrN show the lowest formation energy, i.e., -1.74 eV/atom and -1.75 eV/atom, respectively. This is consistent with previous studies showing that TMNs are chemically very stable. Therefore, we believe that TiN will show a similar stability as ZrN when used as a diffusion barrier coating for U-Mo/Al dispersion fuel. We want to point out that the formation energies of all compounds were calculated at zero temperature. Relative phase stability can be different at high temperatures. We also notice that the formation energy of AlN is close to that of TiN and ZrN. Therefore, at high temperature, Al might react with TMNs and form AlN and TM-Al intermetallic compounds.

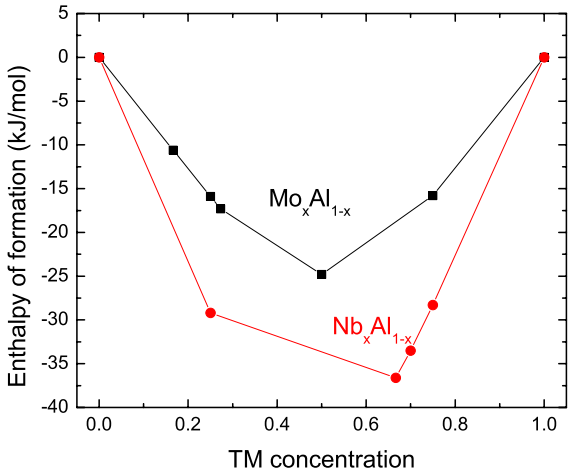

Figure 1 DFT calculated enthalpy of formation of intermetallic compounds in binary Mo-Al and Nb-Al systems.

Phase equilibria in the ternary system Zr-Al-N and Ti-Al-N has been studied by Schuster et al. two decades ago [11, 12]. The isothermal sections at 1000 °C and 1300 °C indicate that ternary compounds TM_3AlN and TM_5Al_3N are stable at high temperatures. Experiment by Krusin-Elbaum et al. [13] shows that $ZrAl_3$ forms at the interface between ZrN and Al at 550 °C. TiN has also be observed to be decomposed by Al at high temperatures in several experiments [14]. However, it is not clear if TiN or ZrN is stable against Al at low temperatures, such as 150 ~ 200 °C, a typical operating temperature range of research reactors.

From the ternary phase diagrams of Ti-Al-N and Zr-Al-N by Schuster et al. [11, 12], we proposed following two potential reactions between TMN and Al,

$\mathrm{TMN} + \mathrm{Al} \rightarrow \frac{2}{3}\mathrm{AlN} + \frac{1}{3}\mathrm{TM_3AlN}$, (1) and

$\mathrm{TMN} + 4\mathrm{Al} \rightarrow \mathrm{AlN} + \mathrm{TMAl_3}$. (2)

The heats of chemical reactions were predicted by DFT, as shown in Table 2. From the calculated heat of reaction, the following conclusions can be made: (1) The first reaction is not energetically favorable; (2) the second reaction is notably exothermic for TiN and ZrN, indicating that their reaction with Al is thermodynamically spontaneous; and (3) TiN is less reactive with Al compared to ZrN due to its lower heat of reaction. Consistent with previous experiment, Lee et al. [14] shows that TiN diffusion barrier fails at temperature above 550 °C due to reaction with Al. Based on the formed new compounds AlN and TiAl3, the decomposition reaction of TiN was proposed as the second reaction. As to ZrN, Krusin-Elbaum et al. [13] shows that a new compound $ZrAl_3$ forms due to the reaction between Al and ZrN at 550 °C. It has been reported that high temperature is required for the reaction between Al and TMN [13]. We believe the rate of this reaction is controlled by the diffusion of Al in TMN and the newly formed AlN layers. Although the diffusion of Al in TMN and AlN is negligible at temperatures below 200 °C, the radiation-induced defects and local temperature gradient can significantly enhance the diffusion of Al in TMN.

Chemical reactions	ΔH_{TiN} (kJ/mol)	ΔH_{ZrN} (kJ/mol)
$\mathrm{TMN} + \mathrm{Al} \rightarrow \frac{2}{3}\mathrm{AlN} + \frac{1}{3}\mathrm{TM_3AlN}$	0.7	-2.2
$\mathrm{TMN} + 4\mathrm{Al} \rightarrow \mathrm{AlN} + \mathrm{TMAl_3}$	-89.7	-120.2

Table 1. Heat of potential reactions between TMN and Al calculated by DFT.

A potential solution for TMN is to add additional layer of immiscible material between ZrN and Al. Since AlN is thermodynamically stable with respect to both Al and ZrN, it can be deposited as a second layer on top of ZrN to prevent their reaction. It has been suggested that layered interface promote the recombination of opposite type of point defects and

therefore reduce the accumulative defect density, swelling, and lattice distortion [15]. Additionally, interface can effectively reduce the perpendicular crack propagation and plastic deformation in the coating. The chemical stability of interface is an important issue when considering the radiation tolerant multilayer design. To investigate the possible formation of solid solution phase, we calculated the enthalpy of solution between TMN and AlN by DFT calculations. The calculated positive solution energy indicates that no solution phases will form at the interface between TMN and AlN layers. Therefore, TMN and AlN multilayer satisfies the critical thermodynamic requirement. We also expect that Al atom diffusion rate into AlN layer would be low and the loss rate of N into Al would be small due to strong bonding between Al and N.

Due to the thermodynamic instability of Mo and Mb against Al, we will limit our following study of kinetic stability to TMNs, i.e., TiN and ZrN.

3.2 Kinetic stability of TMNs

Recent in-pile experiments on ZrN coated U-Mo/Al dispersion fuel by Leenaers et al. [16] show three types of interaction layers formed: (1) double coating layer; (2) “volcano” IL; and (3) IL covered with coating. The first type of IL could be due to the reaction between Al and ZrN, and the additional layer might be the newly formed AlN. The second type of IL forms at the surface of U-Mo particle without coverage of ZrN coating. It is the classical $(U,Mo)Al_x$ IL formed at direct contact between U-Mo and Al. The formation of the third type IL is due to radiation-enhanced diffusion of Al through ZrN and forms $(U,Mo)Al_x$ below ZrN coating layer. To understand the formation of last type of IL, it is important to provide an atomistic study of defects formation and migration of Al atoms in TMNs.

In defect-free TiN or ZrN, the most stable configuration of Al interstitial occupies the center of a TMN cell. The introduction of Al interstitial atom expands the surrounding lattice by 24.5% and 21.8%, respectively for TiN and ZrN. The higher lattice distortion of TiN after adding Al is due to the smaller lattice constant of TiN compared to ZrN. The Al interstitial formation energy for TiN and ZrN is predicted to be 3.81 and 4.25, respectively. The migration of interstitial Al to a neighboring interstitial site proceeds via the transition state, in which Al atom lies in a (001) plane. The predicted migration energy of interstitial Al in TiN and ZrN is 2.42 eV and 2.19 eV, respectively, as shown in Table 2. The higher migration energy of interstitial Al in TiN is consistent with its smaller lattice constant. For this reason, TiN is a more efficient diffusion barrier against Al than ZrN. We also compared our current results with the previous study of Cu diffusion in TiN and ZrN by Tsetseris et al [17]. Cu interstitial also shows higher migration energy in TiN than that in ZrN. However, Cu diffuses much faster than Al in TMNs due to its smaller atom size.

TMN	a (Å)	$r(TM^{4+})$	E_f (eV)	E_{mig}-Al (eV)	E_{mig}-Cu (eV) [1]
TiN	4.237	0.67	3.81	2.42	1.4
ZrN	4.574	0.73	4.25	2.19	1.0

Table 2. Formation and migration energy of Al interstitial in TMN by DFT.

In experiment, rock salt TMN phase is found to be stable for a wide range of N stoichiometry *x* ($0.6<x<1.2$), and diffusion barriers properties can be tailored by selecting specific x values. In the following section, we will discuss the importance of non-stoichiometry on the performance of TMN diffusion barriers. In sub-stoichiometric TMN, N vacancy (N_{vac}) is the most prominent defects, while both N interstitial (N_{int}) and cation vacancy (TM_{vac}) can exist in hyper-stoichiometric samples due to the similar formation energies as shown in Table 3. As interstitial Al atoms hop around in TMN lattice, it may encounter N or TM vacancy and trapped at the vacancy site to form substitutional atom at N (Al_N) or TM (Al_{TM}) lattice site, or form stable interstitial complex with N interstitial (Al_{int}-N_{int}). The binding energies between Al interstitial and intrinsic point defects in TMN are listed in Table 4. When Al interstitial atom is trapped in vacancy site, it becomes essentially immobile unless either heated at extremely

high temperatures, or when there is another vacancy around. The migration energy of these trapped Al species is much higher than 4 eV.

TMN	N_{vac} (eV)	N_{int} (eV)	TM_{vac} (eV)	TM_{int} (eV)
TiN	4.237	0.67	3.81	2.42
ZrN	4.574	0.73	4.25	2.19

Table 3. Formation energy of point defects in TMN by DFT.

TMN	Al_{int}-N_{vac} (eV)	Al_{int}-N_{int} (eV)	Al_{int}-TM_{vac} (eV)
TiN	1.50	1.99	8.78
ZrN	3.37	1.32	8.24

Table 4. Binding energy between Al_{int} and N_{vac}/N_{int}/TM_{vac} in TMN by DFT.

In sub-stoichiometric samples, the trapped Al atom can attract nearby N vacancy and form a stable defect complex (Al_N-N_{vac}) in ZrN with positive bonding energy as shown in Table 5, while such defect complex is unstable in TiN. The migration of Al_N-N_{vac} defect complex requires at least two steps. In the first step, Al atom moves to N vacancy site and leaves behind a new vacancy. In the second step, a neighboring N atom moves to this new vacancy site. The migration barrier of the second step is much higher than the first step, therefore the rate-limiting step in the migration process. Since the migration energy of N vacancy is higher than that of Al interstitial, N vacancy is beneficial to slow the diffusion of Al atoms in ZrN.

TMN	Al_N-N_{vac} (eV)	Al_N-TM_{vac} (eV)
TiN	-0.16	0.00
ZrN	0.24	0.10

Table 5. Binding energy between trapped Al_N and N_{vac}/TM_{vac} in TMN by DFT.

In hyper-stoichiometric samples, the Al interstitial atom can attract a nearby N interstitial and form stable defect complex (Al_N-N_{int}) in both TiN and ZrN, as shown in Table 4. The migration Al_N-N_{int} complex requires three steps [18]. The migration energy of such complex is slightly higher than that of isolated Al interstitial. Therefore, non-stoichiometry is beneficial to slowing down the diffusion Al in TMN by trapping Al at N/TM lattice site or forming stable defect complex, especially for sub-stoichiometry samples.

4. Summary

We investigated the thermodynamic and kinetic stability of two transition metals and two transitional-metal nitrides as diffusion barriers for U-Mo/Al dispersion fuel. The reason to study transitional metals as diffusion barriers is due to their lower thermal expansion mismatch with respect to U-Mo alloy in comparison to ceramic TMNs. However, our DFT calculations show that Al can form stable intermetallic compounds with both Mo and Nb and therefore Mo and Nb are not thermodynamically stable barrier materials. Although ZrN and TiN are the most stable phase in the U-Mo-Al-TM-N system, they can reaction with Al at high temperature and form new compounds, AlN and $TMAl_3$. TiN is predicted to be thermodynamically more stable than ZrN when contacted with Al. The rate of such reaction is controlled by Al diffusion through TMN and newly formed AlN. A multilayer scheme TMN/AlN is proposed to avoid reactions between Al and TMNs diffusion barrier. To evaluate the kinetic stability of TMNs, we also study the defect formation and migration of Al in TiN and ZrN using nudged elastic band method. In pure TMN samples, the migration energy of Al interstitial in TiN is higher than that in ZrN. Al interstitial atom can be easily trapped by N or TM vacancy and becomes an idle atom unless additional N vacancy appears at its nearby site. Al interstitial atom can also attract close N interstitial and form stable defect. Overall, non-stoichiometry is beneficial to slowing down the diffusion of Al in TMNs, especially for sub-

stoichiometric samples. Our study indicates that TiN is a more superior diffusion barrier against Al than ZrN both thermodynamically and kinetically.

Acknowledgement
This work is sponsored by the U.S. Department of Energy, National Nuclear Safety Administration (NNSA), Office of Material Management and Minimization (NA-23) Reactor Conversion Program.

References

[1] M. K. Meyer *et al.*, Journal of Nuclear Materials **304**, 221 (2002).
[2] R. Jungwirth *et al.*, Journal of Nuclear Materials **434**, 296 (2013).
[3] S. Van den Berghe, W. Van Renterghem, and A. Leenaers, Journal of Nuclear Materials **375**, 340 (2008).
[4] J. M. Park *et al.*, Journal of Nuclear Materials **374**, 422 (2008).
[5] A. Leenaers, S. Van den Berghe, and C. Detavernier, Journal of Nuclear Materials **440**, 220 (2013).
[6] M. A. Nicolet, and M. Bartur, Journal of Vacuum Science & Technology **19**, 786 (1981).
[7] G. Kresse, and J. Furthmüller, Phys. Rev. B **54**, 11169 (1996).
[8] G. Kresse, and D. Joubert, Phys. Rev. B **59**, 1758 (1999).
[9] J. P. Perdew, K. Burke, and M. Ernzerhof, Phys. Rev. Lett. **77**, 3865 (1996).
[10] P. E. Blöchl, O. Jepsen, and O. K. Andersen, Phys. Rev. B **49**, 16223 (1994).
[11] J. C. Schuster, and J. Bauer, Journal of Solid State Chemistry **53**, 260 (1984).
[12] J. C. Schuster, J. Bauer, and J. Debuigne, Journal of Nuclear Materials **116**, 131 (1983).
[13] L. Krusin-Elbaum *et al.*, Thin Solid Films **104**, 81 (1983).
[14] H.-J. Lee *et al.*, Journal of Applied Physics **86**, 3096 (1999).
[15] M. Milosavljević *et al.*, Thin Solid Films **544**, 562 (2013).
[16] A. Leenaers, in RRFM20142014).
[17] L. Tsetseris, S. Logothetidis, and S. T. Pantelides, Applied Physics Letters **94**, 161903 (2009).
[18] L. Tsetseris, S. Logothetidis, and S. T. Pantelides, Surface and Coatings Technology **204**, 2089 (2010).

84 MEV XE IRRADIATION ON U-MO/AL DISPERSION FUEL

B. Ye, K. Mo, D. Yun, W. Mohamed, M. Pellin, J. Fortner, Y.S. Kim, G.L. Hofman, A.M. Yacout, T. Wiencek, L. Jamison
Argonne National Laboratory
9700 South Cass Ave, Argonne, IL 60439 USA

S. Bhattacharya
Department of Materials Science and Engineering, Northwestern University,
2220 Campus Dr. Evanston, IL 60208 USA

S. Van den Berghe, A. Leenaers
Nuclear Material Science Institute, SCK·CEN
Boeretang 200, 2400 Mol Belgium

ABSTRACT

Fuel samples containing ZrN-coated and uncoated U-Mo particles were irradiated with 84 MeV Xe ions up to various doses (1.8-2.9x10^{17} ions/cm^2). Several microstructure changes have been observed in the irradiated samples: (1) fuel-matrix-interaction (FMI) formed on the surface of uncoated U-Mo particles and the locations where ZrN coating layers were compromised; (2) SEM (scanning electron microscopy)-observable Xe gas bubbles distributed along grain/cell boundaries in U-Mo, and large bubbles (~ 200 nm in diameter) might form by interlinking small bubbles at the dose of 2.6x10^{17} ions/cm^2; (3) ZrN coating effectively eliminated FMI formation when the coating was intact. These observations are consistent with in-pile test results and will help understand U-Mo/Al dispersion fuel irradiation behavior in reactors.

1. Introduction

U-Mo fuels with very high uranium densities have been developed for use in high performance reactors in order to reduce the use of highly enriched uranium (HEU) fuel in the civil fuel cycle [1]. Undesired pillowing (plate swelling > 100%) of the fuel plate due to the formation of large pores filled with fission gas at the interface of the fuel-matrix-interaction (FMI) layer and the Al matrix has been observed in a number of in-pile tests [2]-[5]. One of the methods to improve the in-pile behavior of the low enriched U (LEU)-Mo/Al fuel is to apply a protective layer on the fuel particle surface to eliminate the interaction between the U-Mo particle and the Al matrix [6],[7]. ZrN is chosen as a suitable coating material, because it is metallurgically inert towards both the U-Mo particle and the Al matrix [7]-[9].

In order to investigate the effectiveness of the coating layer and the fission-product-driven fuel swelling behavior, a fission-fragment-energy Xe ion irradiation experiment was conducted at the Argonne Tandem Linac Accelerator System (ATLAS) at Argonne National Laboratory (ANL). In this out-of-pile experiment, U-Mo/Al dispersion fuel samples fabricated with uncoated U-Mo powder or ZrN-coated U-Mo powder were irradiated. The effectiveness of the ZrN coating was determined by comparing the behavior of these samples. In this study, Xe, a typical gaseous

fission product, is selected as the irradiation source to simulate in-pile irradiation effects. The advantages of using ion irradiation as a surrogate for in-reactor testing are rapid accumulation of damage under controllable conditions and easy accessibility, as handling of highly radioactive materials is not involved. This paper reports the unique set up of the irradiation and preliminary PIE results obtained.

2. Experimental

Two miniature dispersion fuel plates were fabricated at ANL for the ATLAS irradiation. One plate contained natural U-7Mo powder coated with a layer of 1 µm thick ZrN, and the other contained un-coated natural U-7Mo powder. The atomized natural U-7Mo powder was provided by Korea Atomic Energy Research Institute (KAERI), and the coating layer was applied by physical vapor deposition (PVD) at SCK·CEN [7]. For the ion irradiation experiment, small disks of 1.7 mm diameter were punched through the thickness of the fuel plates. One side of the cladding was removed using abrasive paper (with a final polish done with 5µm paper) to get access to the fueled zone. During irradiation, the polished surface was exposed to the ion beam.

A unique multi-specimen sample holder dedicated to ATLAS ion irradiation was designed and used in the irradiation. As shown in Figures 1(a) and 1(b), there are a total of 19 mini specimen holders (2 mm in diameter) within a 1 cm diameter area. Due to the Gaussian beam profile, the samples were exposed to four dose rates, depending on sample location (shown in Figure 1 (b) indicated with 4 different colors). Five thermocouples are connected to the stage through the backside, as seen in Figure 1(a), to monitor the sample temperatures across the sample stage during irradiation. This sample stage design significantly reduced the beam time required to complete the test material matrix.

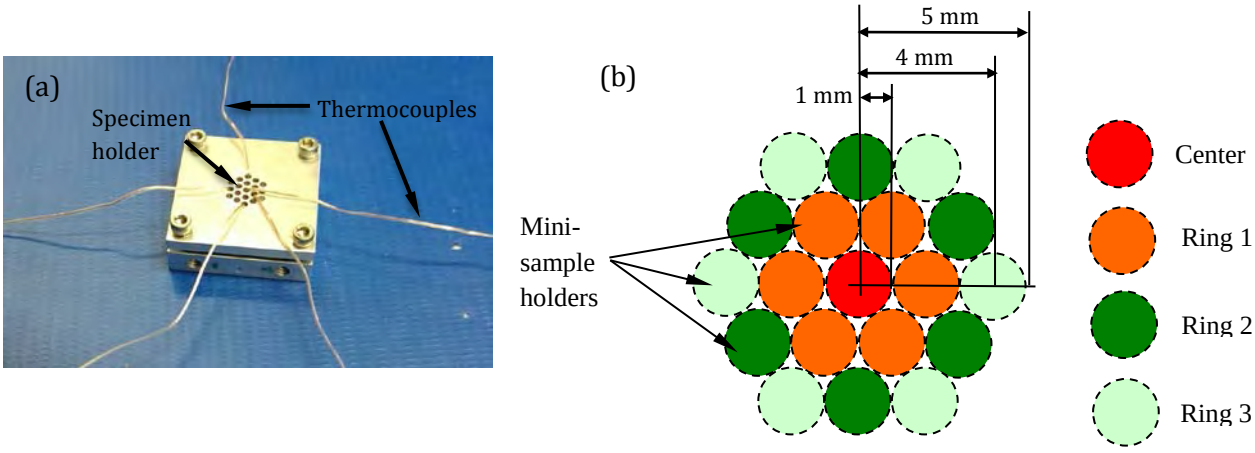

Fig 1. (a) multi-specimen sample holder dedicated for ATLAS irradiation, and (b) schematic drawing showing the loading arrangement of specimens in the sample holder (dose rate decreases from the center to Ring 3).

The irradiation was conducted with 84 MeV Xe^{26+} ions perpendicular to the sample stage surface. The accumulated dose received by each specimen was estimated based on the beam profile and the specimen location, and the calculated values are listed in Table 1. Note that all dpa (displacements per atom) values mentioned in this paper are the dpa at the peak damage

region in the irradiation depth direction. Figures 2(a) and 2(b) show the SRIM-calculated [10] ion distributions of 84 MeV Xe ions in U-7Mo and Al, respectively.

Table 1 Calculated irradiation parameters for each specimen

Location	Fraction of total current	Average dose rate (ions/cm^2/s)	Final dose (ions/cm^2)	Peak dpa
Center	0.031	9.2×10^{11}	2.9×10^{17}	1206
Ring 1	0.0276	8.2×10^{11}	2.6×10^{17}	1081
Ring 2	0.0221	6.6×10^{11}	2.1×10^{17}	873
Ring 3	0.0198	5.7×10^{11}	1.8×10^{17}	748

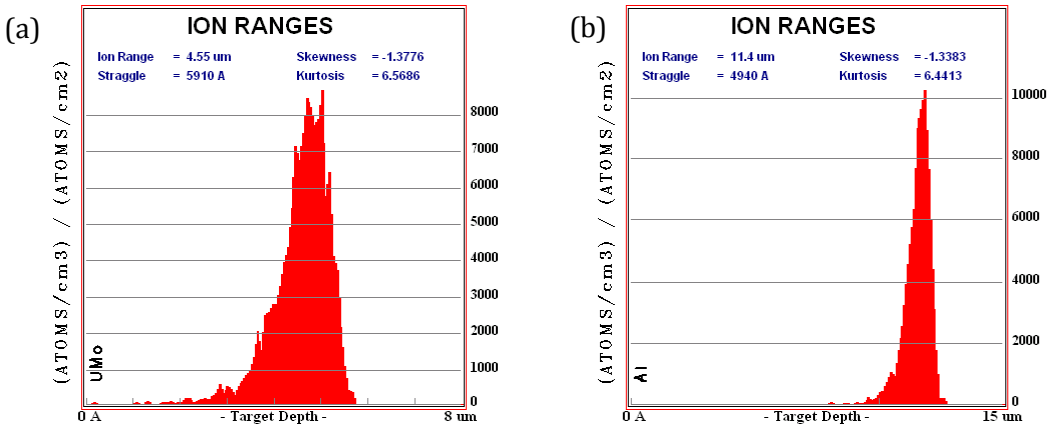

Fig 2. Ion distributions of 84 MeV Xe in (a) U-7Mo and (b) Al with calculated with SRIM-2008.

Following irradiation, both SEM and TEM were utilized for characterization. Both focused ion beam (FIB) milling and conventional mechanical grinding methods were utilized to prepare samples for microscopy. FIB milling was performed at Northwestern University with a FEI Helios Nanolab 600 dual-beam FIB/SEM, and conventional mechanical grinding was done at ANL. SEM observations were made either on the dual-beam FIB/SEM at Northwestern University or a Hitachi S3000N at ANL. The TEM characterization was performed with a Hitachi-9000 at the IVEM-Tandem facility at ANL.

3. Results

Post irradiation characterization reveals that FMI and gas bubble formed due to 84 MeV Xe irradiation. The details of these observations and the effectiveness of ZrN coating will be discussed in the following section.

3.1 FMI formation

3.1.1 Surface morphology

Figure 3 shows a typical irradiated sample surface observed with SEM. Each spherical fuel particle in Figure 3(a) is surrounded with a protruding phase. At higher magnification (Figure 3(b)), it can be clearly seen that the protruding phase covers the entire surface of small particles and piles up at the peripheral area of large particles. The width and the height of the protruding

phase on each particle are not uniform. Composition analyses on the protruding phase determined that it is U-Mo-Al interdiffusion (FMI) product.

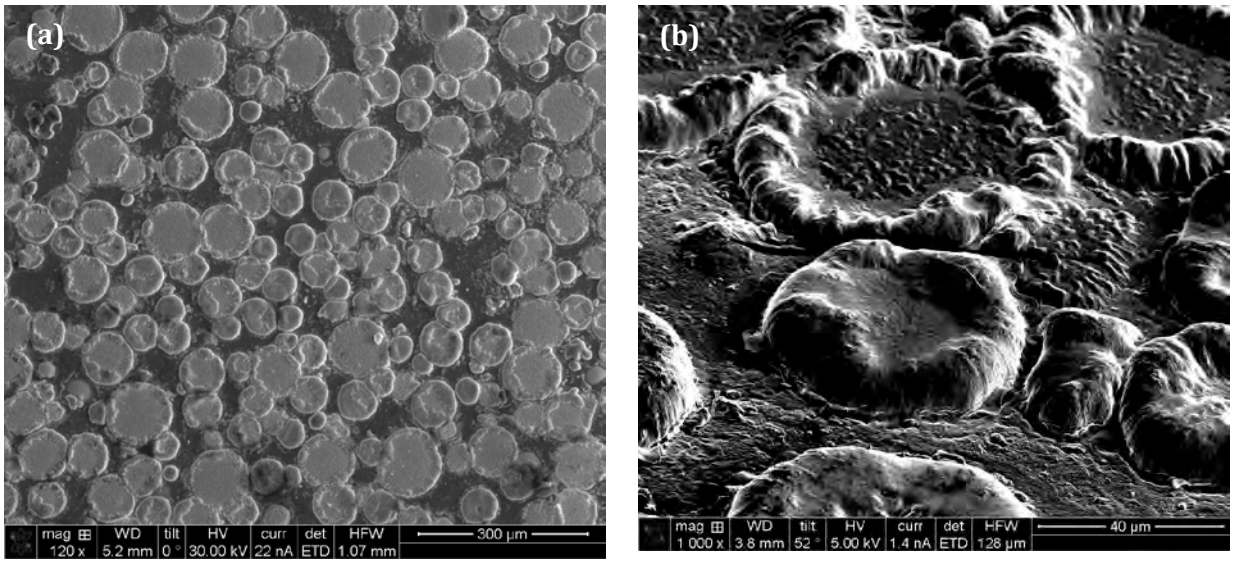

Fig 3. SEM images of the surface of the sample irradiated to 2.6×10^{17} ions/cm^2 in (a) lower magnification and (b) higher magnification.

3.1.2 Cross-section observation

Comparing the microstructure of the irradiated specimen (Figure 4(b)) to that of the as-fabricated sample (Figure 4(a)), substantial FMI growth (in light grey contrast) can be seen on the specimen surface exposed to the ion beam. The formation of FMI product is presumably induced by ion irradiation. Thermally-activated lattice diffusion can be excluded for the following two reasons: no FMI is found beyond the ion damage region, and a nearly uniform temperature distribution can be reasonably assumed across the entire sample due to the high thermal conductivity of the materials (λ_{Al}=225 W/(m·K), $\lambda_{U\text{-}Mo}$=14.2 W/(m·K) [11]) and relative flat beam profile due to defocused beam operated on the samples during irradiation.

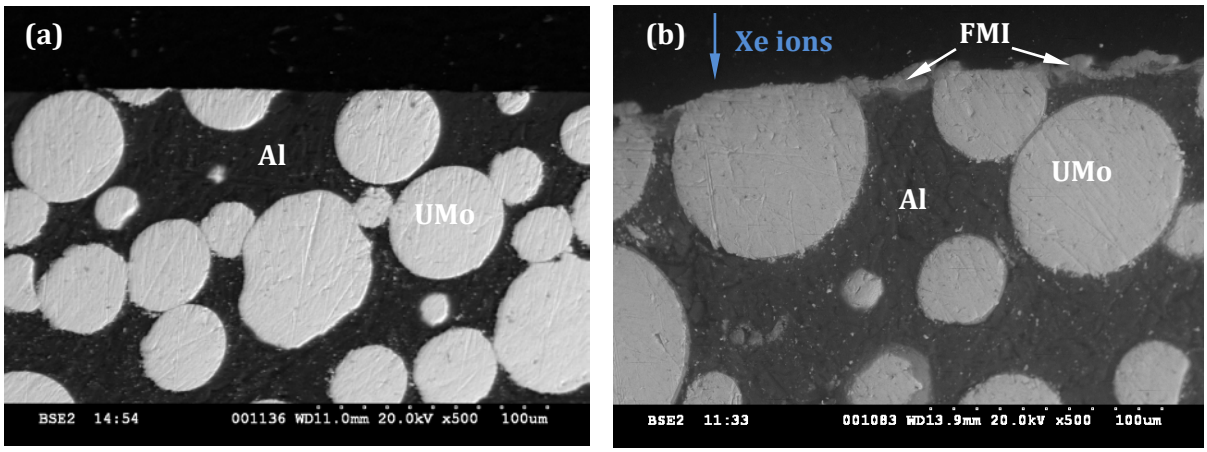

Fig 4. SEM images of (a) as-fabricated U-Mo/Al dispersion fuel and (b) irradiated with 84 MeV Xe to a dose of 2.9×10^{17} ions/cm^2. The specimens contain ZrN-coated U-7Mo.

3.1.3 Composition analyses

Energy dispersive X-ray (EDX) analyses were performed at several positions in each specimen to measure the composition of the FMI product. Representative results are summarized in Table 2, showing the atomic ratio of Al/(U+Mo) ranges between 2.5 and 4.7, similar to the FMI composition found in the FUTURE fuel plates [3].

Table 2. Measured composition of the FMI at several positions in various samples

Examined sample	at.% Al	at.% Mo	at.% U	X in (UMo)Al_x
Ring 1, ZrN-coated	77.8	3.9	18.3	3.5
Ring 1, ZrN-coated	78.7	4.0	17.3	3.7
Ring 1, ZrN-coated	85.6	2.0	9.8	7.3
Ring 1, uncoated	71.3	3.5	25.2	2.5
Ring 1, uncoated	82.4	2.4	15.2	4.7
Center, ZrN-coated	79.7	4.3	16.0	3.9

3.2 Xe gas bubble morphology

Figure 5 shows the Xe bubble distribution observed on a FIBed cross section of a U-Mo particle irradiated to a dose of 2.9×10^{17} ions/cm^2 (~1200 dpa). The bubbles formed in a range of 4-6 μm away from the surface (Figure 5(a)). It is evident in Figure 5(b) that the gas bubbles preferably reside along the grain/cell boundaries. As a result, the gas bubble density is far from uniform in the Xe deposition range. In some areas, large grain without the presence of SEM-observable fission gas bubbles (white arrow) can be found; but in other areas (dark arrow), the gas bubble density is so high that no clear grain boundaries can be identified. It is suspected that grain subdivision may have occurred in the densely bubble-populated regions; this will be explored with further TEM analyses.

Higher-magnification SEM micrographs of the areas of interest indicated in Figure 5(a) are presented in Figure 5(c) and (d). As depicted in Figure 5(c), bubbles in the U-Mo region vary in size, from tens of nanometers to hundreds of nanometers. The largest bubbles likely form at the expense of several small bubbles at a location where grain/cell boundaries intersect. Evidence of gas bubble interlinkage is clearly shown in Figure 5(c) (circled areas). PIE results on the samples irradiated to lower doses will help develop understanding of the bubble evolution process. In addition to the large bubbles, lines of small gas bubbles are present in the U-Mo region. These lines match the cell lines of the cellular structure formed during atomization of U-Mo particles.

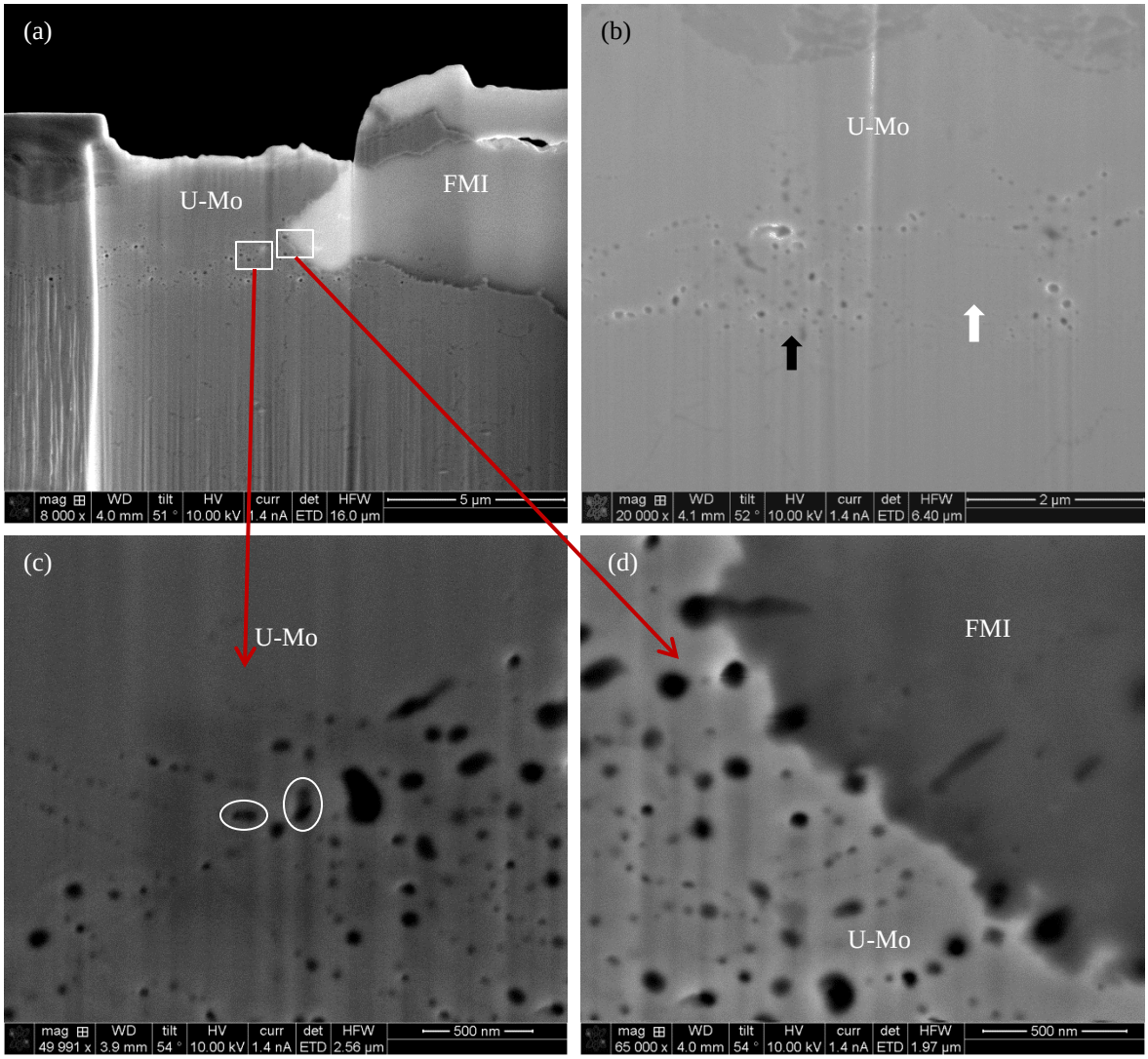

Fig 5. SEM micrographs of U-Mo fuel irradiated with 84 MeV Xe to a dose of 2.9×10^{17} ions/cm^2 (a) shows the Xe bubble distribution range; (b) shows bubble morphology in U-Mo fuel irradiated with 84 MeV Xe to a dose of 2.9×10^{17} ions/cm^2; higher magnification (c) in U-Mo and (d) at the U-Mo and FMI interface.

3.3 Effectiveness of ZrN coating

The evidence of ZrN as an effective diffusion barrier is presented in Figure 6. The SEM micrograph depicts the cross section of the sample irradiated to 2.9×10^{17} ions/cm^2 (~ 1200 dpa). For the U-Mo particle labeled as (A) in Figure 6, the ZrN coating layer is intact and no FMI products are observed within the ion penetration depth. In contrast, a considerable amount of FMI products have formed on the particle labeled as (B) in Figure 6 where the coating layer is absent due to either imperfect coating or fabrication damage. The absence of FMI for particle (A) also proves that no thermally-driven interdiffusion occurred during irradiation (~ 350°C, 88 hours) when the ZrN coating layer is present. These results demonstrate that a 1 µm thick ZrN

coating is sufficient to block the interaction between Al and U-Mo induced either by thermally driven diffusion at 350°C or by ion beam mixing. This observation is consistent with the results from ZrN-coated UMo/Al plate irradiated with 84 MeV I to a dose of 1×10^{17} ions/cm^2 [12].

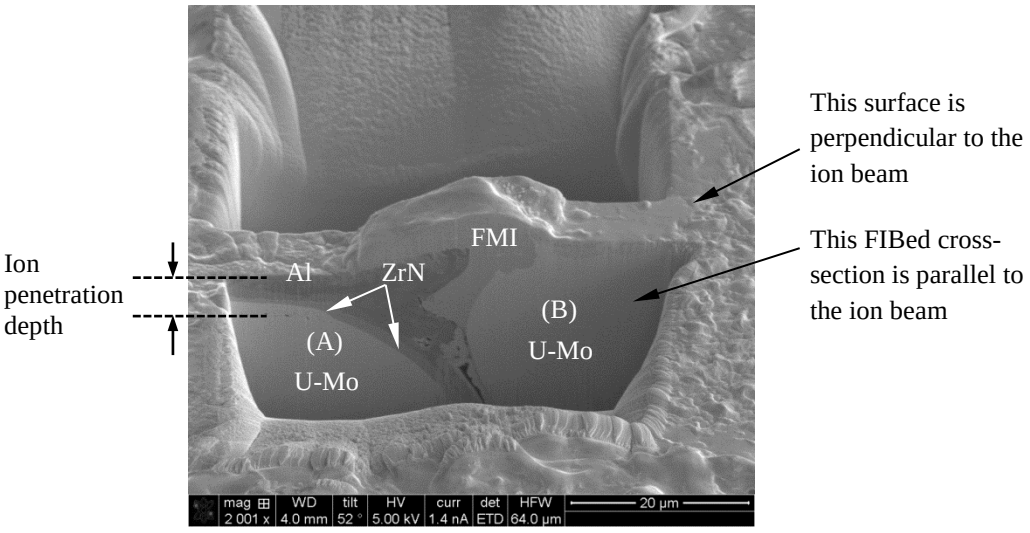

Fig 6. SEM image showing the cross section through the irradiated surface of the ZrN-coated U-7wt%Mo specimen irradiated with 84 MeV Xe to a dose of 2.9×10^{17} ions/cm^2.

4. Conclusion

Irradiation-induced FMI layer formation, ZrN coating effectiveness in preventing U-Mo-Al interdiffusion, and Xe gas bubble morphology were investigated by irradiating U-Mo/Al dispersion fuels with 84 MeV Xe ions. Characterization of the irradiated samples revealed that the FMI layer composition was in accord with reactor irradiation results. Gas bubble morphology was investigated in the sample irradiated to a dose of 2.9×10^{17} ions/cm^2 (~1200 dpa). The size of SEM-observable gas bubble in U-Mo ranged from tens to hundreds of nanometers. PIE results also demonstrated that an intact ZrN coating layer can effectively block the interdiffusion between the U-Mo particles and the Al matrix. Additional XRD and TEM analyses will be performed to reveal phase information of the FMI layer and to investigate the microstructure as a function of dose. The information obtained from this ion irradiation will help develop more complete understanding of the irradiation response of U-Mo/Al fuel and facilitate fuel system optimization.

Acknowledgements

This work was supported by the U.S. Department of Energy, National Nuclear Security Administration (NNSA), Office of Material Management and Minimization (NA-23) Reactor Conversion Program and the Department of Energy and Argonne strategic Laboratory Directed Research and Development (LDRD) program. The authors would like to thank KAERI for manufacturing the U-Mo powder and Mr. E. O'hare from ANL for fabricating the plates. This research used resources of ANL's ATLAS facility, which is a DOE Office of Science User

Facility. This work made use of the EPIC facility (NU*ANCE* Center-Northwestern University), which has received support from the MRSEC program (NSF DMR-1121262) at the Materials Research Center; the Nanoscale Science and Engineering Center (NSF EEC–0647560) at the International Institute for Nanotechnology; and the State of Illinois, through the International Institute for Nanotechnology.

This work is supported by the U.S. Department of Energy, Basic Energy Sciences, Office of Science, under contract # DE-AC02-06CH11357. The submitted manuscript has been created by UChicago Argonne, LLC, Operator of Argonne National Laboratory ("Argonne"). Argonne, a U.S. Department of Energy Office of Science laboratory, is operated under Contract No. DE-AC02-06CH11357. The U.S. Government retains for itself, and others acting on its behalf, a paid-up nonexclusive, irrevocable worldwide license in said article to reproduce, prepare derivative works, distribute copies to the public, and perform publicly and display publicly, by or on behalf of the Government.

Reference

[1] J.L. Snelgrove, G.L. Hofman, M.K. Meyer, C.L. Trybus and T.C. Wiencek, Nucl. Eng. Des. 178 (1997) 119-126.
[2] P. Lemoine, D.M. Wachs, in: Proceedings of the International Conference on Research Reactors: Safe Management and Effective Utilization, Sydney, Australia, 2007.
[3] A. Leenaers, S. Van den Berghe, E. Koonen, C. Jarousse, F. Huet, M. Trotabas, M. Boyard, S. Guillot, L. Sannen, M. Verwerft, J. Nucl. Mater. 335 (2004) 39-47.
[4] F. Huet, J. Noirot, V. Marelle, S. Dubois, P. Boulcourt, P. Sacristan, S. Naury, P. Lemoine, in: Trans. International Topical Meeting on Research Reactor Fuel Management (RRFM) 2005, Budapest, Hungary, 2005.
[5] V. Popov, M. Khmelevsky, V. Lukichev, O.A. Golosov, in: Proc. the 9th International Topical Meeting on Research Reactor Fuel Management (RRFM), Budapest, Hungary, 2005.
[6] G.A. Birzhevoy, V.V. Popov, O.A. Golosov, V.V. Shushlebin, V.A. Rychkov, M.S. Lyutikova, in: Trans. International Topical Meeting on Research Reactor Fuel Management (RRFM) 2007, Lyon, France, 2007.
[7] A. Leenaers, S. Van den Berghe, C. Detavernier, J. Nucl. Mater. 440 (2013) 220-228.
[8] S. Van den Berghe, A. Leenaers, E. Koonen, L. Sannen, Adv. Sci. Tech. 73 (2010) 78-90.
[9] H.-Y. Chiang, R. Jungwirth, T. Zweifel, W. Schmid, W. Petry, F. Kraus, in: Proc. Int. Meeting on Reduced Enrichment for Research and Test Reactors (RERTR), Santiago, Chile, 2011.
[10] J. Ziegler, SRIM, 2010. http://www.SRIM.org
[11] A.E. Dwight, J. Nucl. Mater. 2 (1960) 81-87.
[12] R. Jungwirth, T. Zweifel, H.-Y. Chiang, W. Petry, S. Van den Berghe, A. Leenaers, J. Nucl. Mater. 434 (2013) 296-302.

THE POTENTIAL FOR DIFFERENCES IN AS-FABRICATED MONOLITHIC FUEL PLATE MICROSTRUCTURE TO AFFECT FUEL PERFORMANCE

DENNIS D. KEISER, JR., JAN-FONG JUE, BRANDON MILLER, WALTER WILLIAMS, FRANCINE RICE, ADAM ROBINSON, BARRY RABIN, AND MITCH MEYER

Idaho National Laboratory
P. O. Box 1625, Idaho Falls, ID 83415-6188 U.S.A.

Corresponding Author Contact Information:
Dennis D. Keiser, Jr.
Idaho National Laboratory
P.O. Box 1625
Idaho Falls, ID, 83415-6146 U.S.A.
Phone: 1 (208) 533-7298
Fax: 1 (208) 533-7863
E-mail: Dennis.Keiser@inl.gov

For Publication in the Proceedings of the *Research Reactor Fuel Managment Conference*
(April 19-23, 2015 in Bucharest, Romania)
This manuscript has not been published elsewhere
and has not been submitted simultaneously for publication elsewhere.

THE POTENTIAL FOR DIFFERENCES IN AS-FABRICATED MONOLITHIC FUEL PLATE MICROSTRUCTURE TO AFFECT FUEL PERFORMANCE

DENNIS D. KEISER, JR., JAN-FONG JUE, BRANDON MILLER, WALTER WILLIAMS, FRANCINE RICE, ADAM ROBINSON, BARRY RABIN, AND MITCH MEYER

Nuclear Fuels and Materials Division, Idaho National Laboratory
P. O. Box 1625, Idaho Falls, Idaho 83403 USA

ABSTRACT

The starting microstructure of a monolithic fuel plate has the potential to impact the overall performance of the fuel plate during irradiation. To improve the understanding of the irradiation performance of different as-fabricated microstructures of monolithic fuel plates, microstructural analysis was performed using optical metallography (OM) and scanning electron microscopy (SEM) on archive fuel plates fabricated using different methods, and these microstructures have been compared with ones after irradiation. The data for irradiated fuel plates is primarily in the form of optical images, with some data from SEM analysis. By comparing the microstructures of as-fabricated and as-irradiated fuel plates, one can improve understanding of how specific features like chemical banding, grain size, impurity phases, etc. may impact the overall irradiation performance of monolithic fuel plates. This paper compares the as-fabricated microstructures for a small and larger-scale fuel plate from the RERTR-9B and AFIP6-MKII experiments with those that were observed after irradiation.

1. Introduction

The Material Mangement and Minimization program (known earlier as the Reduced Enrichment for Research Reactor program) is developing low-enriched uranium (LEU) fuel to reduce the demand of highly-enriched uranium (HEU) fuels currently used in research and test reactors throughout the world [1]. One fuel type being developed is a U-10Mo monolithic fuel, which is comprised of a U-10Mo fuel foil with a Zr diffusion barrier that is clad with AA6061. In order to support qualification of this fuel type, it is critical to understand changes in the as-fabricated fuel microstructure due to irradiation. The main regions of interest for monolithic fuel include the U-10Mo foil, the Zr diffusion barrier, and the interfaces between the Zr diffusion barrier and the cladding and the U-10Mo. Finally, an interface that exists between U-10Mo and the AA6061 cladding is of interest.

This paper describes the results of microstructural characterization that was performed on as-fabricated archive samples for AFIP-6MKII and L1P09T fuel plates, along with samples from the actual as-irradiated fuel plates. The samples were characterized using optical metallography (OM) and and in most cases scanning electron microscopy (SEM). This paper will investigate how the microstructure of the of as-fabricated fuel plates changed due to irradiation. Comments will be made about how certain features in as-fabricated monolithic fuel can impact fuel performance.

2. Experimental

2.1 Fabrication

The U-10Mo alloy fuel foil (at 58.85% U-235 enrichment) that was used to fabricate fuel plate L1P09T was produced with a Zr diffusion barrier using a hot co-rolling process [2].

During the rolling process, fifteen rolling passes were used and about 2 hours of exposure time to 650˚C. The final foil was sheared to a nominal size of 8.3 cm x 1.9 cm x 0.25 mm. The final mini-plate was produced using hot isotatic pressing [3] and had dimensions of 2.5 cm x 10.2 cm.

The U-10Mo fuel foil (at 40% U-235 enrichment) with a Zr diffusion barrier that was used to fabricate the AFIP-6MKII fuel plate was produced using both a hot and cold co-rolling process [4] Hot co-rolling was conducted at 650°C using 12 passes to obtain the targeted foil thickness of 635 µm. Thickness reduction by hot co-rolling was 84%. Post-hot-co-rolling annealing was performed at 650°C for 45 minutes. The total time experienced by this alloy at 650°C was estimated to be 125 minutes. Forty-four cold-co-rolling passes further reduced the foil thickness to 381 µm. The total cold-co-rolling thickness reduction was 40%. The final foil was targeted to have a 330 µm-thick U–10Mo fuel meat with a 25 µm-thick zirconium diffusion-barrier layer on each side. Fuel plate fabrication was performed by the Babcock and Wilcox Nuclear Operations Group (B&W NOG) using hot isostatic press (HIP) bonding. The bonding temperature, pressure and holding time were 560°C, 103MPa, and 95 minutes, respectively.

2.2 Irradiation Testing

Fuel plate L1P09T was irradiated in the RERTR-9B experiment. The test assembly was irradiated in the large-B position B-11 in the Advanced Test Reactor (ATR) in cycles 140A, 140B, and 141A for 46.5, 35.7, and 32.4 effective full-power days (EFPD), respectively [5]. There was a mid-cycle SCRAM during Cycle 140B for a duration of 8 days. In the reactor, the fuel plates were aligned vertically with the edge of each plate facing the core center. The associated neutron flux gradient, when combined with the higher enrichment of the plates (58% U-235) resulted in a very large fission gradient across the width of the RERTR-9B fuel plates [6]. The high (hot) side to low (cold) side fission density ratios for the different fuel plates were on the order of 1.5 to 2.5 times, across the 1.9 cm-wide fueled regions. This possibly resulted in non-uniform swelling and subsequent non-uniform stresses and strains within the plates. The L1P09T fuel plate reached an average fission density of 7.5 x 10^{21} fissions/cm^3.

Fuel plate AFIP-6 MKII was a larger fuel plate (114.3 cm long by 5.7 cm wide) than L1P09T, and it contained a 57.2 cm long foil comprised of U-10Mo alloy at 40% U-235 enrichment with Zr diffusion barrier. The enrichment was selected to achieve a surface heat flux of approximately 450-500 W/cm^2 [7]. The U-10Mo foil, Zr diffusion barrier, and overall fuel plate each had a nominal thickness of 330 µm, 25 µm, and 1.32 mm, respectively. In ATR, AFIP-6 MKII was irradiated during cycle151A in the ATR Center Flux Trap (CFT). Cycle 151A ran for 56.1 effective full power days (EFPDs). There was one mid-cycle SCRAM with a duration of three days. The fuel plate achieved an average and peak fission density of 3.96 x 10^{21} and 4.14 x 10^{21} fissions/cm^3, respectively.

2.3 Microstructural Characterization

Optical metallography (OM) and scanning electron microscopy (SEM) analyses were performed on samples from an as-fabricated hot co-rolled foil that served as an archive of what was irradiated in fuel plate L1P09T, and an actual fuel plate that served as an archive for AFIP-6 MKII. Microstructural analysis was performed using available instruments located in the Fuels and Applied Sciences Laboratory (FASB) and the Electron Micrsocopy Laboratory (EML).

Samples from the irradiated L1P09T and AFIP-6 MKII fuel plates were characterized in the Hot Fuel Examination Facility (HFEF) using OM analysis. This analysis was performed on a transverse cross-section taken at the midplane for each irradiated fuel plate. In addition, a

slow speed saw was used to slice two smaller samples from L1P09T that were then then shipped to EML for characterization using SEM and energy-dispersive spectroscopy (EDS) and wavelength dispersive spectroscopy (WDS). The two samples were produced from a 1-mm-thick transverse slice that was produced adjacent to the midplane of the fuel plate. The sample with the lowest radioactivity levels was selected first for characterization and these are the results discussed in this paper. Both secondary electron (SE) and backscattered electron (BSE) images were produced from the sample after it had been mounted and polished. Imaging was employed to evaluate the microstructure at the U-10Mo/Zr and Zr/AA6061 cladding interfaces, and the distribution of fission gas bubbles and solid fission product phases present in the U-10Mo fuel foil. Linescans and x-ray maps were generated using EDS and/or WDS.

3. Results

3.1 As-Fabricated Fuel Foil or Plate Characterization

3.1.1 AFIP-6MKII

Fig. 1(a) shows an optical image of the polished surface of a transverse cross section produced from the AFIP-6 MKII archive fuel plate. In the U-10Mo foil, areas of different contrast can be observed, along with dark precipitate phases. The Zr diffusion barrier exhibits some variation in thickness across the length of the sample, and only a few grains can be observed across the thickness. The BSE image in Fig. 1(b) confirms the variation in Zr thickness. Based on the linescan shown in Fig. 1(c), the contrast variation observed in the U-10Mo foil is due to varibility in Mo content. The darker regions contain higher levels of Mo. Since the regions with different Mo content are displayed as "bands" in the microstructure, the term "chemical banding" is commonly used to describe the heterogeneous Mo content in monolithic fuel. Besides the regions with different Mo contents, there are also areas where the original γ-(U,Mo) phase decomposed into a eutectoid structure (see Fig. 1(d)), in which α-U phase is likely present. The dark precipitates in the U-10Mo in many cases contain carbon, and when these phases are present at the U-10Mo/Zr interface they can impact the quality of bonding at the interface, as shown in Fig. 1 (e). During the sizing of the U-10Mo foil with Zr diffusion barrier, regions are generated around the edges where no Zr diffusion barrier is present. Fig. 1 (f) shows a region in the AFIP-6 MKII archive fuel plate where the U-10Mo foil has been deformed during the shearing process, and some interaction layers have developed at the interface with the cladding during fuel plate fabrication.

(a)

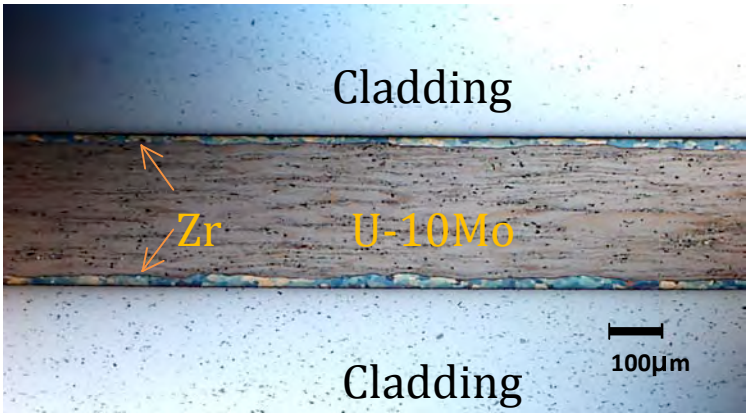

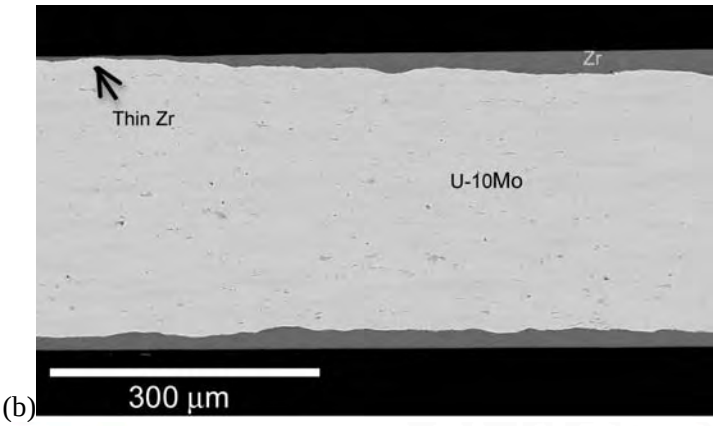

(b)

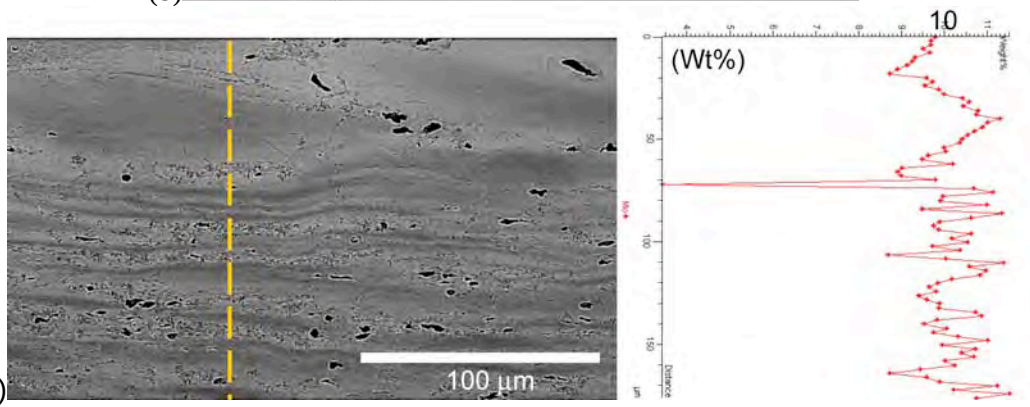

(c)

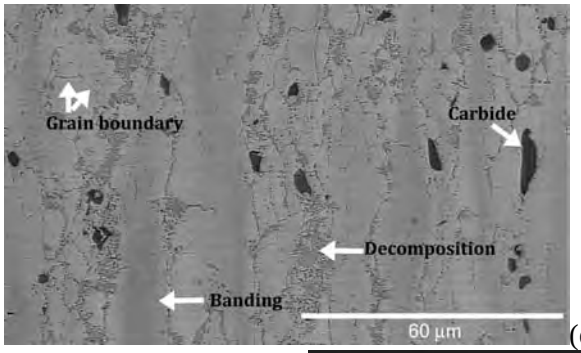

(d)

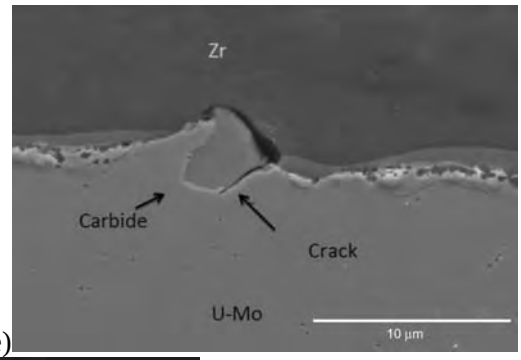

(e)

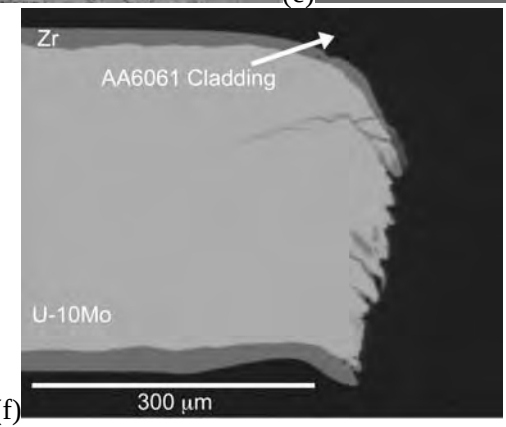

(f)

Figure 1. OM image (a) and BSE image (b) show the microstrructure observed for the archive AFIP-6 MKII fuel plate. In (b) a location where the Zr diffusion barrier is relatively thin is identified. (c) shows a higher magnification BSE image of the U-10Mo microstructure and the results of a Mo composition linescan taken along the line in the BSE image. The presence of decomposed γ-(U,Mo) phase, grain boundaries, and carbide precipitates are shown in the BSE image in (d). A carbide phase at the U-10Mo/Zr interface is shown in the BSE image in (e), and the microstructure of the sheared end of the U-10Mo foil is presented in (f).

3.1.2 L1P09T

Fig. 2(a) and 2(b) show an SE and BSE image of the polished surface of a transverse cross section produced from the L1P09T archive fuel foil. An interaction layer can be observed at the U-10Mo/Zr diffusion barrier interface, and in Fig. 2(a) some region of the interaction zone exhibits a unique topography. Like was the case for the AFIP-6 MKII archive fuel plate, great variability in the Mo content was observed in the U-10Mo foil. Fig. 2(c) shows the contrast variation that results from the heterogeneous Mo distribution, and Fig. 2(d) shows the results for a Mo linescan that was taken across the width of the fuel foil. Typically, the Mo concentration varied between 9 and 11 wt.%. To investigate the distribution of U, Mo, Zr, and oxygen, x-ray maps were generated at the U-10Mo/Zr interface (see Fig. 3). It was observed that an oxygen-rich phase could be present at the interface. To confirm this result, point-to-point compositional analysis was performed, and at the location depicted in Fig. 4 about 50 at.% oxygen was measured using EDS.

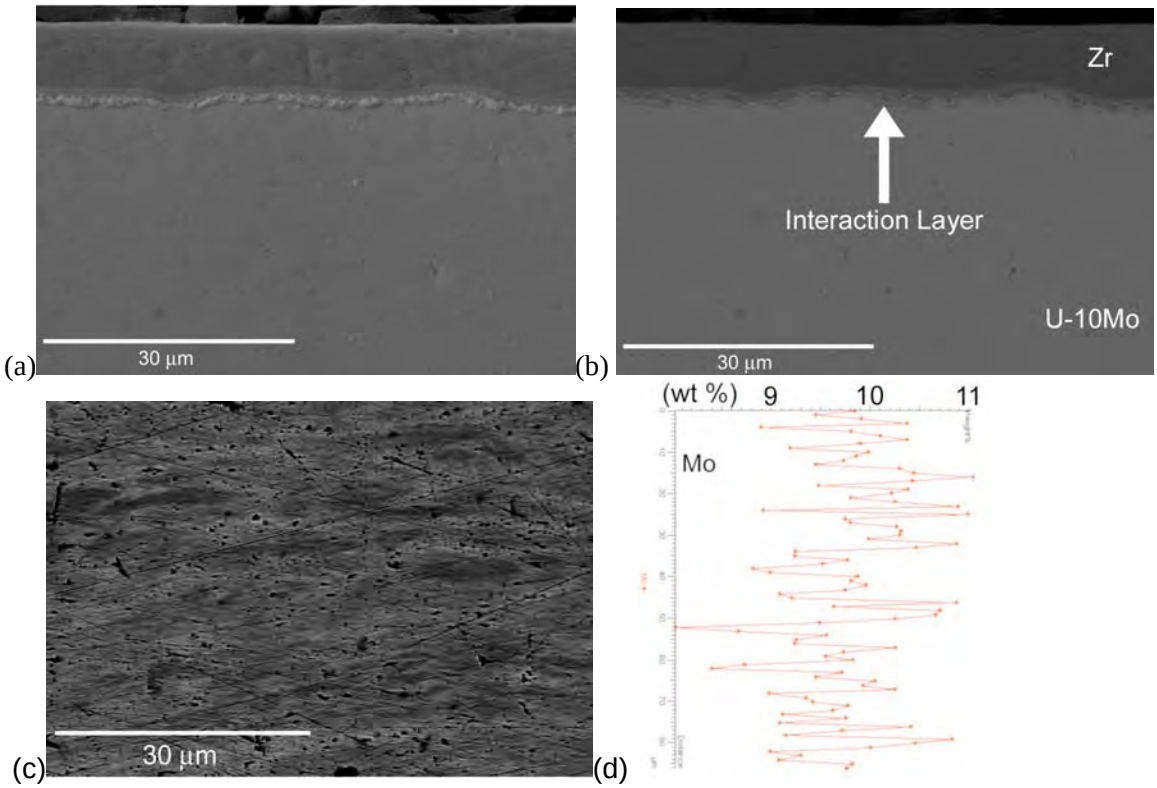

Figure 2. SE image (a) showing the microstructure that is revealed where a FIBINLO sample is generated from sample R3R050. The SE images in (b-d) show the uniform distribution of relatively large, faceted fission gas bubbles, and (b,c) shows a localized region without observable fission gas bubbles. (d) highlights solid fission product phases observed in some fission gas bubbles.

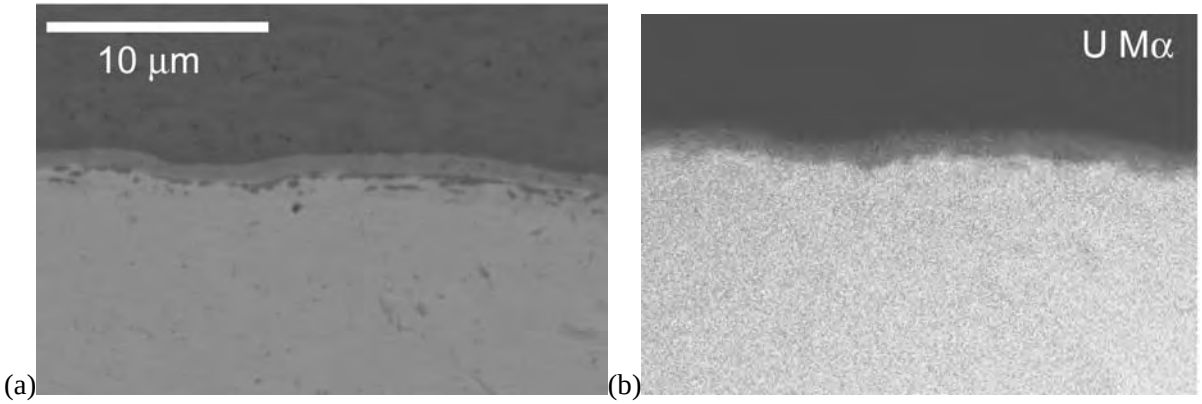

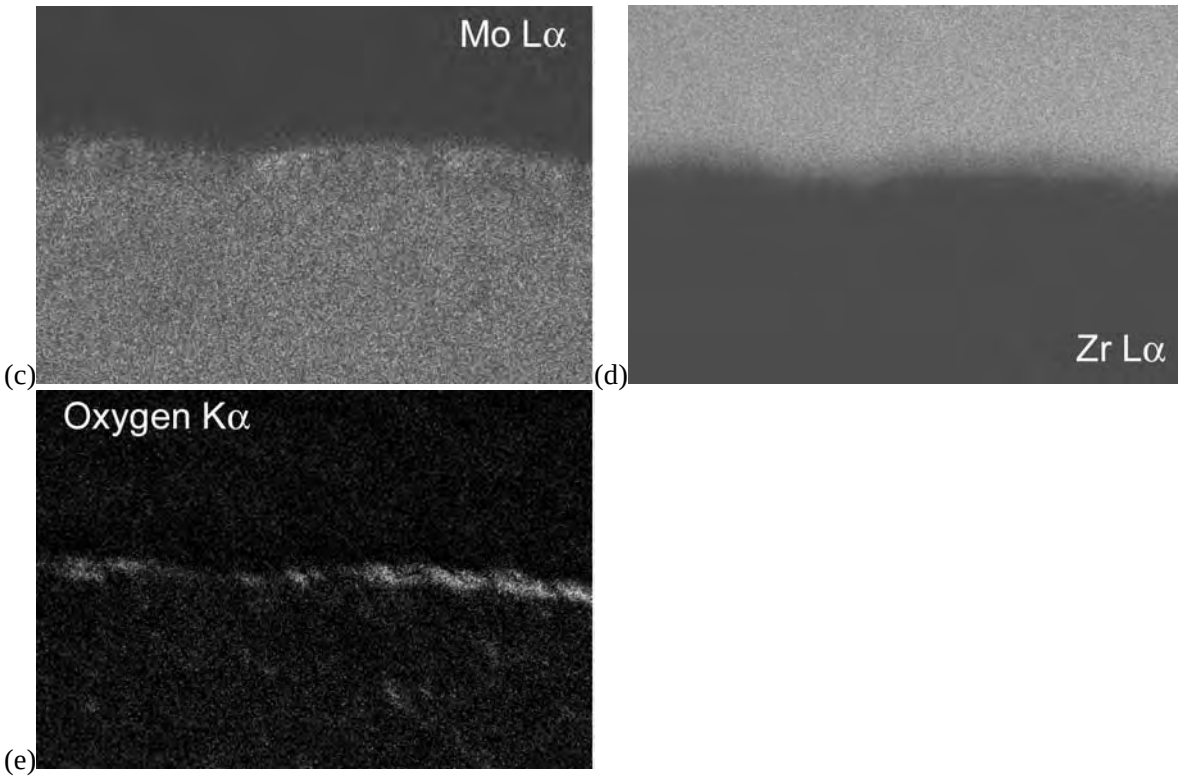

Figure 3. WDS x-ray maps for U, Mo, Zr, and oxygen.

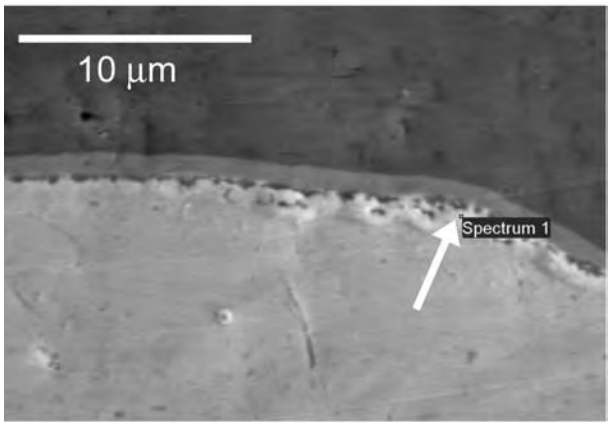

Figure 4. BSE image of a location (arrow) where point scan compositional analysis, using standardless EDS, was performed, and around 50 at.% oxygen was measured.

3.2 As-Irradiated Fuel Plate Characterization

3.2.1 Optical Metallography

3.2.1.1 AFIP-6 MKII

OM images of the microstructure observed for the irradiated AFIP-6 MKII fuel plate are presented in Fig. 5. No large pores, some dark precipitates, and Zr diffusion barrier with variable thickness can be observed in (a), and (b) shows regions in the micostructure without observable fission gas bubbles (arrows). Interaction layers at the U-10Mo/Zr, Zr/AA6061 cladding, and at the U-10Mo/AA6061 cladding interfaces are presented in c, d, and e, respectively. Fig. 5 (f) shows where precipitate phase are present at the U-10Mo/Zr interface, along with relatively large porosity and some cracks (arrows). These precipitates at the U-10Mo/Zr interface have impacted bonding of the fuel to the Zr, and may have served as stress concentration points, such that cracks in the fuel were produced.

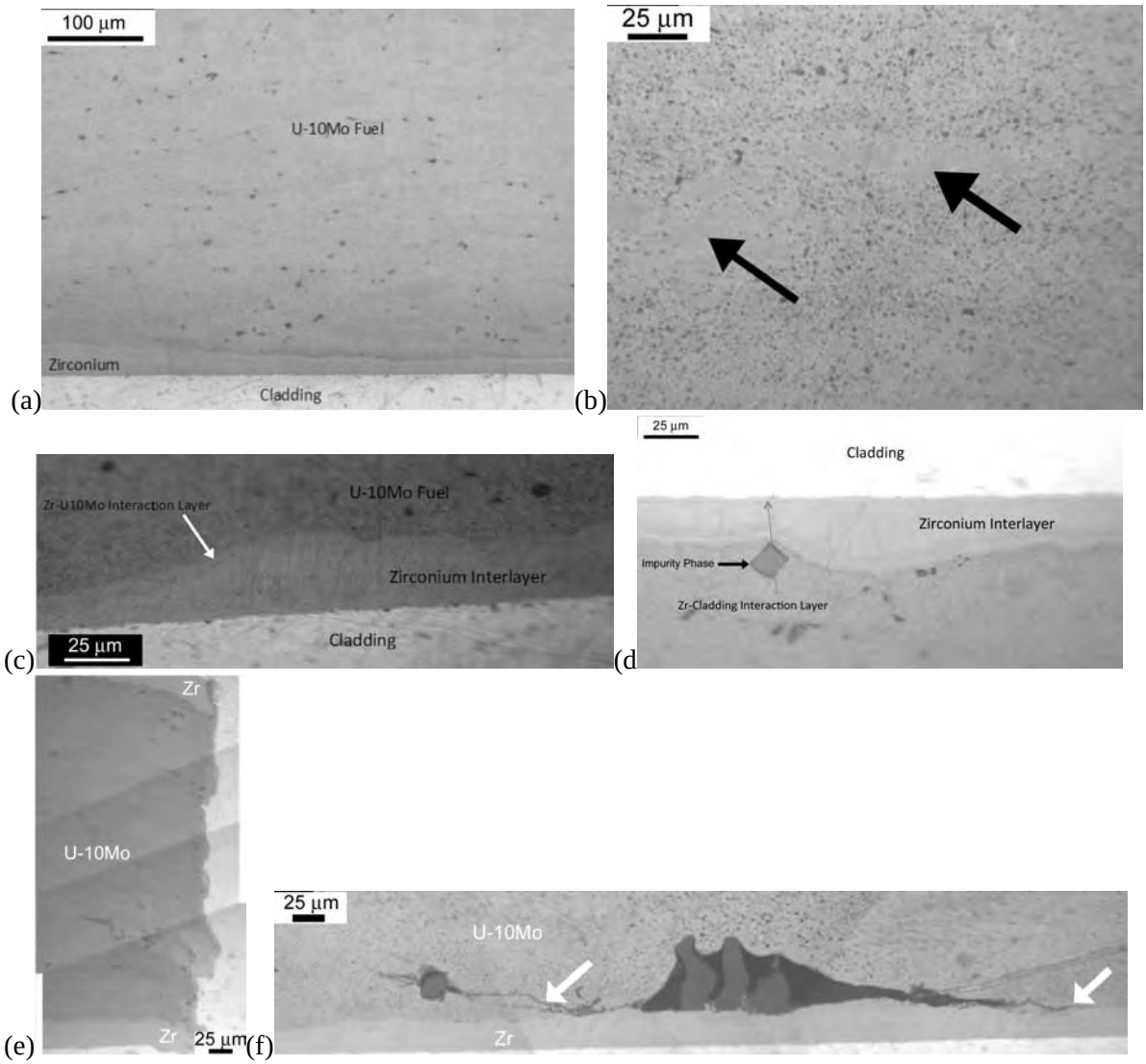

Figure 5. OM (a-f) images of the microstructure observed for the AFIP-6 MKII fuel plate. No large pores, some dark precipitates, and Zr diffusion barrier with variable thickness can be observed in (a), and (b) shows regions in the micostructure without observable fission gas bubbles (arrows). Interaction layers at the U-10Mo/Zr, Zr/AA6061 cladding, and at the U-10Mo/AA6061 cladding interfaces are presented in c, d, and e, respectively. (f) shows where precipitate phase are present at the U-10Mo/Zr interface, along with relatively large porosity and some cracks (arrows).

3.2.1.2 L1P09T

Since L1P09T was irradiated edge-on to the core, a neutron flux gradient was present across the width of the plate. OM images of the microstructure were generated across the fuel plate width to capture the regions of the microstructure irradiated to different fission densities. OM images taken at the center of the fuel plate width are presented in Figs. 6 (a) and 6 (b). OM images taken at the end of the fuel exposed to the highest fission density are presented in Figs. 6 (c-e). The highest levels of porosity in the U-10Mo are seen in the images taken at the high fission density side of the fuel, and the highest porosity levels are seen near the U-10Mo/Zr interface. In (d), a crack can be seen propagating through this region.

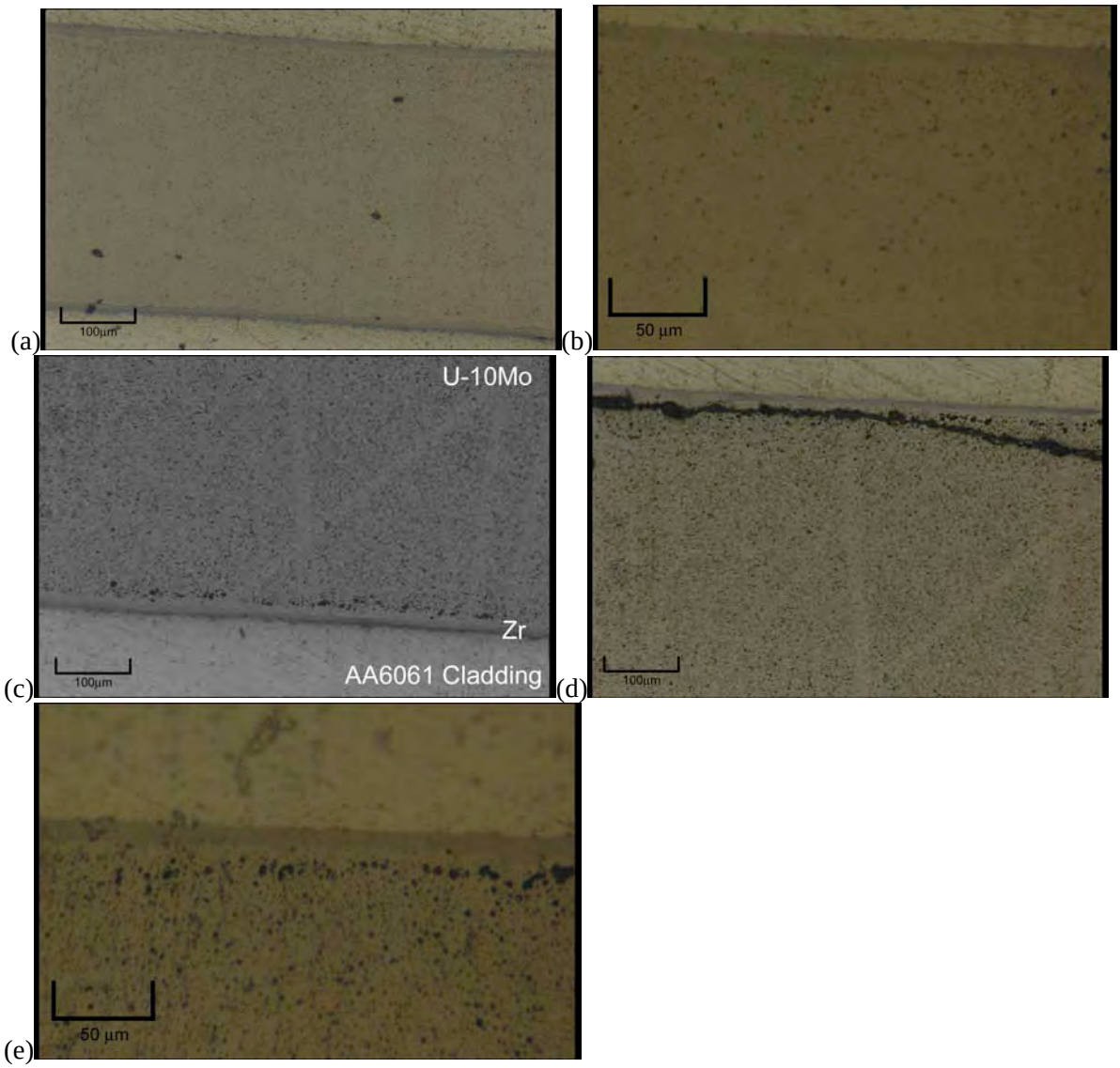

Figure 6. OM images at 200X (a) and 500X (b) of the microstructure observed at the medium fission density region of L1P09T and 200X images (c,d) and a 500X image (e) of the microstructure observed at the high fission density region of fuel plate L1P09T.

3.2.2 Scanning Electron Microscopy

BSE images of the polished surface of the sample taken from L1P09T are presented in Figs. 7 (a-c). Porosity is observed on the surface of the sample in the U-10Mo and not the Zr. A BSE image of a fracture surface that was present in the sample is shown in Fig. 7 (d). By comparing the fracture and polished surface, one can determine that smearing has probably occurred during sample preparation, making analysis of fission gas bubble size and distribution difficult. The arrow in Fig. 7 (c) highlights a region where a larger pore may have been filled in during sample preparation. In future analyses, a focused ion beam will be used to produce L1P09T samples for characterization, so that the problems associated with sample smearing can be eliminated. The relatively large pores observed in the fracture surface image (Fig. 7 (d)), confirms that L1P09T was irradiated to the high average fission density of 7.5 x 10^{21} fissions/cm^3. A compositional linescan was generated across the U-10Mo/Zr interface (see Fig. 8), and this linescan shows that when moving from the interface into the U-10Mo fuel the Mo concentration is still heterogeneously distributed after irradiation. Comparing to a similar linescan for as-fabricated fuel (Fig. 2 (d)), the Mo concentration has increased, probably due to the fact that U was consumed due to

fission and Mo fission product was produced during irradiation. The high Si concentration measured in the cladding is due to the Si-rich precipitates found in AA6061 cladding.

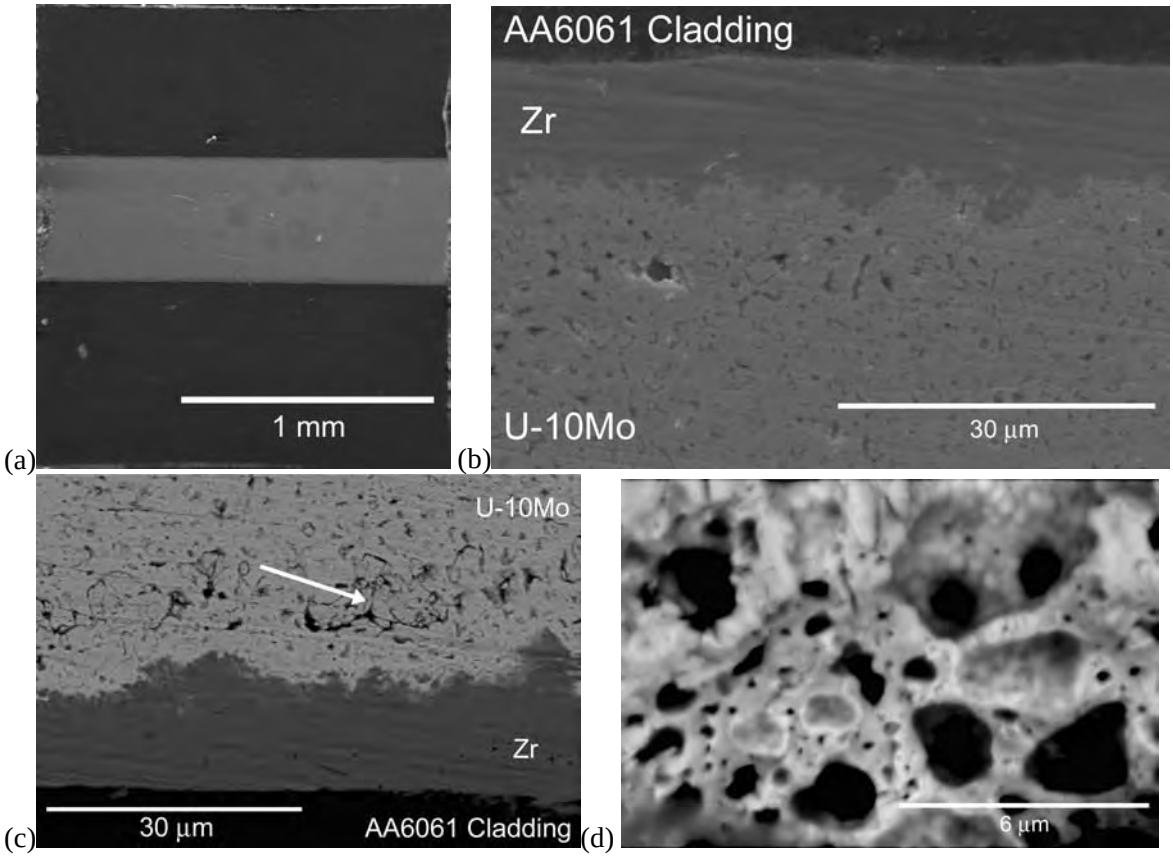

Figure 7. BSE images (a-c) of the microstructure observed for the polished sample surface, and (d) for a fracture surface observed at the end of the foil. The black regions in (d) are pores. The arrow in (c) indicates a region where large pores may have been present that were filled in with material during sample polishing.

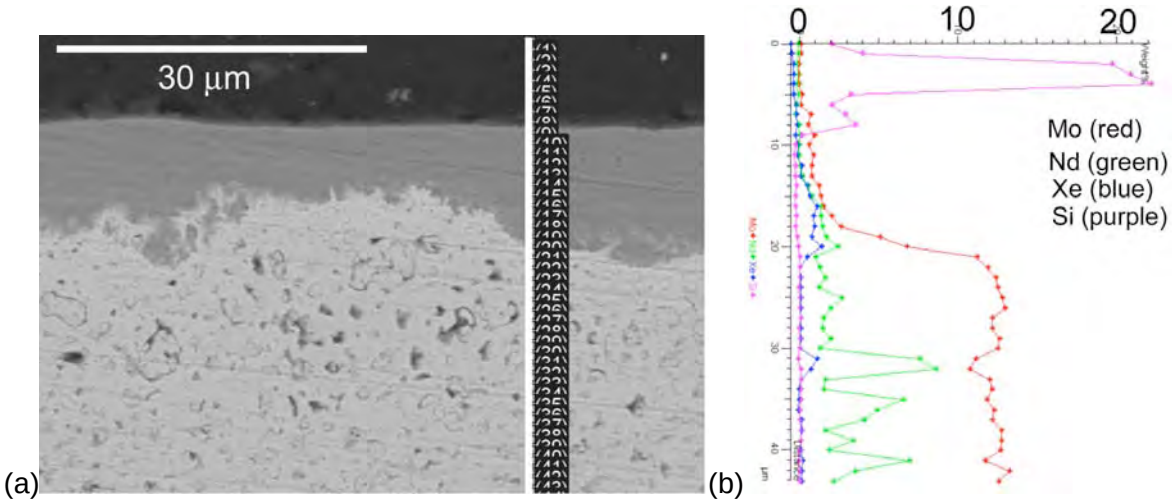

Figure 8. BSE image (a) showing the location where Mo, Nd, Xe, and Si EDS compositional linescans were produced across the Zr diffusion barrier. The results are shown in (b).

4. Discussion

Based on microstructural characterization of an as-fabricated foil, chemical banding, dark-contrast precipitates, regions of decomposed γ-(U,Mo) phase, and U-10Mo/Zr interaction layers existed in the L1P09T fuel plate after fabrication using hot co-rolling. Analysis of

samples from an AFIP-6 MKII archive fuel plate, which utilized hot co-rolling and cold co-rolling during foil fabrication, showed that in addition to these features, interaction layers were also present at the Zr/AA6061 cladding and U-10Mo/AA6061 cladding interfaces for as-fabricated fuel plates. These observed features agree well with what has been reported for as-fabricated monolithic fuel plates [8]. One difference between L1P09T and AFIP-6 MKII as-fabricated samples, is the chemical banding observed in the fuel foil. Comparing Figs 1 (c) and 2 (c), one can see that the characteristics of the chemical bands are different. The AFIP-6 MKII sample had larger chemical banding features, maybe a result of the use of hot and cold co-rolling used for producing the fuel foil.

For the AFIP-6 MKII fuel plate, many of the features observed in the as-fabricated fuel plate sample could also be resolved using OM for the fuel plate irradiated to an average fission density of 3.96 x 10^{21} fissions/cm^3. Things like chemical banding, precipitates, and interaction layers were all observable. In terms of how these features affected fuel performance, the fact that some banded areas had relatively few observable fission gas bubbles, suggested that local variation in Mo content can impact swelling behavior. With respect to the carbide phases, depending on where they were located in the microstructure, cracking and large porosity in the microstructure could result.

The microstructure of the higher fission density L1P09T fuel plate differed from AFIP-6 MKII in that, most of the U-10Mo foil microstructure was comprised of a uniform distribution of fission gas bubbles that were on the order of a few microns in size. Due to the high average fission density for this fuel plate (7.5 x 10^{21} fissions/cm^3), grain refinement of the U-10Mo has occurred, and it is expected that the microstructure would contain relatively large fission gas bubbles [9]. In OM images, the chemical banding that could be resolved for AFIP-6 MKII could not be resolved for L1P09T. Near the U-10Mo/Zr interface, relatively large fission gas bubbles that seemed to have some interlinkage could be observed in OM images taken at the high fission density side of the fuel plate. In typical as-fabricated fuel plate samples, this region of the fuel plate usually contains relatively low Mo concentrations [8]. Based on analyis of the L1P09T fuel foil archive, oxygen-rich phases were also present in this region. SEM analysis of the L1P09T sample showed that sample polishing resulted in smearing of the fission gas bubbles, but by having a fracture surface available for analysis it was possible to reveal the fact that the fission gas bubbles were actually larger than what could be seen on a polished surface. This agreed with what has been observed for U-7Mo dispersion fuel irradiated to high fission density, where similar smearing of fission gas bubbles was observed during sample polishing [10]. A Mo linescan for the irradiated sample showed that even though chemical banding could not be observed in optical images, the Mo concentration variability present after fabrication for L1P09T was still present after irradiation.

5. Summary

Based on the analysis of L1P09T and AFIP-6 MKII as-fabricated and as-irradiated samples, the starting microstructure of a monolithic fuel plate will impact how a monolithic fuel peforms during irradiation. Things like Mo distribution in the fuel foil, the size and distribution of precipitate phases, and the characteristics of interaction zones present at the different monolithic fuel interfaces will all play a role in determining how well the fuel performs.

Acknowledgments

This work was supported by the U.S. Department of Energy, Office of Nuclear Materials Threat Reduction (NA-212), National Nuclear Security Administration, under DOE-NE Idaho Operations Office Contract DE-AC07-05ID14517. Personnel in the Hot Fuel Examination Facility are recognized for their contributions in destructively examining fuel plates.

References

[1]. M. K. Meyer, et al., “Irradiation Performance of U-Mo Monolithic Fuel,” *Nucl. Energy and Tech.* 46 (2) (2014) 169-182.
[2]. G. Moore, et al., “Monolithic Fuel Fabrication Process Development at the Idaho National Laboratory,” *Proc. of the RERTR 2008 International Meeting on Reduced Enrichment for Research and Test Reactors,"* Washington, D. C., October 5-9, 2008.
[3]. Jan-Fong Jue, et al., “Fabrication of Monolithic RERTR Fuels by Hot Isostatic Pressing,” *Nuclear Technology* 172 (2010) 204-210.
[4]. Jan-Fong Jue, et al., "AFIP-6 MKII Characterization Summary Report," *Idaho National Laboratory Report*, INL/EXT-14-32457 (August 2014).
[5]. D. M. Perez, et al., "RERTR-9 Irradiation Summary Report," *Idaho National Laboratory Report*, INL/EXT-10-18421 (May 2011).
[6]. A. B. Robinson, et al., "US RERTR Fuel Development Post-Irradiation Examination Results," *Proc. of the RERTR 2008 International Meeting on Reduced Enrichment for Research and Test Reactors,"* Washington, D. C., October 5-9, 2008.
[7]. N. E. Woolstenhulme, "AFIP-6 MKII First Cycle Report," *Idaho National Laboratory Report*, INL/EXT-12-25170 (March 2012).
[8]. Jan-Fong Jue, et al., "Microstructural Characteristics of HIP-bonded Monolithic Nuclear Fuels with a Diffusion Barrier," *J. Nucl. Mater*. 448 (2014) 250-258.
[9]. J. Gan, et al., "TEM Characterization of U-7Mo/Al-2Si Dispersion Fuel Irradiated to Intermediate Fission Densities," *J. Nucl. Mater*. 424 (2012) 43-50.
[10]. D. D. Keiser, Jr., et al., "SEM and TEM Characterization of U-7Mo Irradiated to High Fission Density at Relatively High Power, High Temperature, and High Fission Rate," Proc. of the RERTR 2014 International Meeting on Reduced Enrichment for Research and Test Reactors*,"* Vienna, Austria, October 12-15, 2014.

FOUR-POINT BEND TESTING OF IRRADIATED MONOLITHIC U-10Mo FUEL

B. H. RABIN, W. R. LLOYD, J. L. SCHULTHESS, R. P. LIND,
K. M. WACHS, J. K. WRIGHT, B. J. FRICKEY, J. MAUPIN
Idaho National Laboratory
PO Box 1625, Idaho Falls, ID 83415 USA

ABSTRACT

This paper presents results of recently completed studies aimed at characterizing the mechanical properties of irradiated U-10Mo fuel in support of monolithic base fuel qualification. Mechanical properties were evaluated in four-point bending. Specimens were taken from fuel plates irradiated in the RERTR-12 and AFIP-6 Mk. II irradiation campaigns, and tests were conducted in the Hot Fuel Examination Facility (HFEF) at Idaho National Laboratory (INL). The monolithic fuel plates consist of a U-10Mo fuel meat covered with a Zr diffusion barrier layer fabricated by co-rolling, clad in 6061 Al using a hot isostatic press (HIP) bonding process. Specimens exhibited nominal (fresh) fuel meat thickness ranging from 0.25 mm to 0.64 mm, and fuel plate average burnup ranged from approximately 0.36E21 fissions/cm^3 to 6.2E21 fissions/cm^3. After sectioning the fuel plates, the 6061 Al cladding was removed by dissolution in concentrated NaOH. Pre- and post-dissolution dimensional inspections were conducted on test specimens to facilitate accurate analysis of bend test results. Four-point bend testing was conducted on the HFEF Remote Load Frame at a crosshead speed of 0.1 mm/min using custom-designed test fixtures and calibrated load cells. All specimens exhibited substantially linear elastic behavior and failed in a brittle manner. The influence of burnup on the observed bending modulus and the calculated fracture strength is discussed.

1. Introduction

The Office of Materials Management and Minimization (M^3) within the U.S. DOE/National Nuclear Security Administration (NNSA) is working to convert research reactors globally from highly-enriched uranium (HEU) fuel to low-enriched uranium (LEU) fuel. Of the 200 candidate research reactors, over 80 have been converted using LEU fuel developed in the 1980s. Additional reactor conversions using this fuel are currently underway. However, there is a small set of high-performance research reactors that require a new high-density LEU fuel for conversion, including five U.S. high-performance research reactors (USHPRRs) and one critical facility. A U-10Mo monolithic fuel system is being developed to meet this need, consisting of uranium-10 wt.% molybdenum alloy (U-10Mo), with thin zirconium (Zr) diffusion barrier interlayers, clad in 6061 aluminum (Al), as shown schematically in Figure 1.

The fuel meat is formed from a U-10Mo alloy, cast into a coupon, canned in a carbon steel picture-frame assembly, then hot- and cold-rolled to desired thickness. The zirconium interlayer is bonded to the U-10Mo alloy via co-rolling during the in-can hot rolling process. A detailed description of this process for plates tested is found in “RERTR-12 Fabrication Summary Report [1] and “AFIP-6 Mk II Fabrication Summary Report [2]. After rolling and de-canning, the foil is sized to nominal geometry, and aluminum cladding is bonded to the fuel meat using hot isostatic pressing (HIP).

One of the requirements for fuel qualification is ensuring mechanical integrity of the fuel is maintained under normal operating conditions and anticipated transients. It is also a requirement that the mechanical response of fuel plates to thermal hydraulic conditions and irradiation induced changes in the fuel are understood. Mechanical properties of the fuel constituents are also used as important inputs in fuel performance modeling. For these

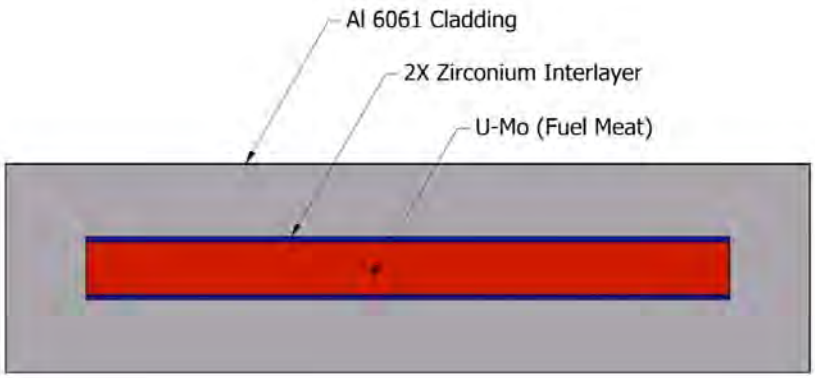

Figure 1. Schematic diagram of longitudinal cross-section of the base monolithic fuel plate.

reasons, efforts to characterize the mechanical properties of fresh and irradiated fuel are underway.

The measurement of mechanical properties in irradiated fuel is challenging and limited information exists in the literature. There are some early reports of the mechanical properties of irradiated U-Mo metallic fuels [3], however, the fuel fabrication techniques and irradiation conditions were notably different from current USHPRR fuels. In particular, the highest burnup of specimens examined in these early studies was on the order of 1 at.%, far below the nearly 100% burnup required for successful deployment of U-10Mo monolithic fuel in USHPRR conversions, and so is of limited use in current research.

This project had several goals, including developing necessary techniques, processes, equipment, and methods for mechanical property measurements on irradiated U-10Mo that are relevant for meeting USHPRR fuel qualification requirements, and then performing a representative series of properties measurements using available material from recently completed irradiation tests on U-10Mo monolithic fuel conducted in the Advanced Test Reactor (ATR) at Idaho National Laboratory (INL).

Limitations imposed by material thickness, available lengths, and current hot cell fabrication machining abilities mandated use of rectangular specimens tested in bending. The specimen thicknesses of 0.3 to 0.8 mm create undesirable high gradients in principal stress in the material thickness direction, but other constraints allowed no other specimen or test type option. To obtain more representative results, four-point bend loading was chosen to subject about half of the specimen length to constant maximum bending moment resulting in half the surface experiencing maximum bending stress, rather than three-point loading with maximum moment and stress only at the specimen centerline.

We report herein the results of bend tests conducted on thirty-six test specimens from ten different fuel test plates representing the RERTR-12 and AFIP-6 Mk II irradiation campaigns. The specimens tested had fission densities ranging from 0.36E21 to 6.2E21 fissions/cm^3. The resultant force and deflection data from each specimen were analyzed and stress at failure, strain at failure, and flexural stiffness were estimated.

2. Source Materials, Test Plate Fabrication, and Irradiation

The U-Mo monolithic fuel fabrication process is reported in detail in two INL reports [1, 2]. In general, vacuum arc melting of HEU source material, depleted uranium, and elemental Mo achieves alloying and down-blending to yield U-10Mo alloy having the desired U-235 enrichment. Cast alloy plates are cut and machined into coupons suitable for foil fabrication, which is accomplished via a combination of hot co-rolling within a steel can assembly for initial thickness reduction and application of the Zr diffusion barrier layer, followed by cold rolling to achieve the desired final fuel foil thickness. The fuel foil with the Zr coating is cut to size, and then encapsulated in 6061 aluminum cladding using hot isostatic press (HIP) processing. The fuel plates undergo final processing steps to achieve the desired

fuel plate geometry and cladding thickness, followed by appropriate quality assurance inspections prior to insertion in the reactor.

The RERTR-12 fuel plates were “mini-plates”, where the fuel zone within each plate was approximately 19 mm wide and 90 mm long, and total plate thickness was approximately 1.4 mm. Nominal thickness of the Zr-coated fresh fuel foil used in the RERTR-12 mini-plates was either 0.25, 0.50, or 0.64 mm. The AFIP-6 Mk II was a full-size fuel plate test with the fuel meat approximately 34 mm wide and 570 mm long, and total plate thickness including Al cladding was approximately 1.4 mm. The AFIP-6 Mk II fuel foil including the Zr coating had a nominal thickness of 0.35 mm prior to irradiation.

The finished fuel test plates were incorporated into experimental assemblies and irradiated in the ATR at INL. Details regarding the RERTR-12 and AFIP-6 Mk II irradiation test campaigns are reported elsewhere [4, 5]. The analyses used for determining the final fission density distributions within the plates are also reported elsewhere [6, 7]. Following completion of irradiation, the fuel plates were transferred to the Hot Fuel Examination Facility (HFEF) at INL for subsequent inspections, measurements, sectioning, and testing.

3. Test Specimen Preparation

All work with the irradiated fuel plates and specimens was completed inside the HFEF Main Cell under a dry argon atmosphere. All operations were performed remotely with master-slave manipulators, while viewing the work area through the leaded glass shield windows. This creates a challenging situation when handling very small and delicate test specimens. Extensive equipment and workflow preparations were necessary for successfully fabricating, handling, measuring and testing the precision specimens in this study. The experience, skill, care, and patience of the hot cell operators that performed this work were critical to the success of the program.

3.1. Test Plate Sectioning

Based on radiographic evaluation of fuel location within the cladding, the plates were cut with a low-speed diamond saw, according to pre-defined test plans and sectioning diagrams. The test specimens were oriented with specimen length (fixed by the original foil width) oriented parallel to the fuel plate width and specimen width oriented parallel to the fuel plate length, as shown in Figure 2. Three bend test specimens were sectioned from each of nine RERTR-12 mini-plates with a target width of 6.0 mm. The three specimens were located adjacent to each other and were centered at approximately 15, 21, and 27 mm from the end of the plate cladding. Six specimens were cut from adjacent locations near the mid-section of the AFIP-6 Mk II test plate in the same relative orientation used for the RERTR-12 sectioning, with a target width of 12.0 mm. An additional three specimens were cut from near the end of the AFIP-6 Mk II fuel zone towards the plate end with the identification marking. Referencing distance from the end of the fuel foil closest to the plate ID label, the specimen centerline positions were at approximately 315, 303, 291, 279, 267, 255, 40, 28, and 16 mm, corresponding to AFIP-6 Mk II specimens A, B, C, D, E, F, G, H, and J.

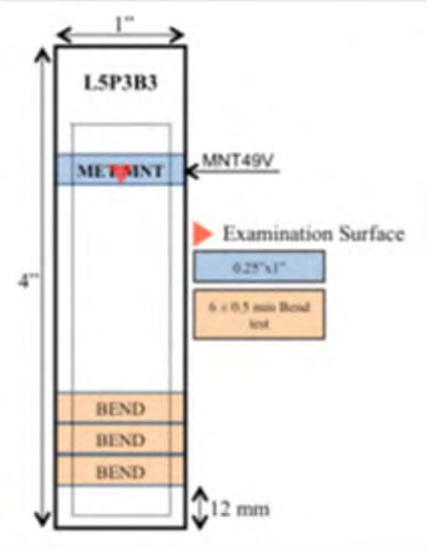

Figure 2. Diagram showing specimen sectioning orientation and locations in RERTR-12 test fuel plates.

3.2. Specimen Storage and Tracking

Following sectioning from the test plate, each specimen was immediately stored in a small screw-top aluminum container (KGT-type) with a unique identification number engraved on the outer surface. A material tracking database contains cross-reference data

associating the KGT number with individual specimen identification. The KGT number then references the complete fabrication, irradiation, and test plate location information for a particular specimen. Generally, no more than one specimen was removed from a KGT in any hot cell work area at any time, so individual specimen traceability was assured.

3.3. Dimensional Measuring Instruments and Specimen Measurements

Prior scoping tests on irradiated fuel suggested that, after cladding removal, the material is extremely fragile. The very small size of these specimens also demands very precise and accurate dimensional measurements to achieve confidence in calculated material properties. The difficulty of making such measurements with limited visibility and remote handling in the hot cell further complicates the problem. Two measuring instruments, shown in Figure 3, were designed, fabricated, qualified, and calibrated to make the specimen width and thickness measurements. Both instruments use high precision dial gauges with 0.0001 in. (2.5 µm) dial graduations and ±5 µm accuracy over the gauge measuring range of 1.25 mm. The instrument developed for measuring the specimen width dimensions required several moving components that provide dial gauge calibration and specimen positioning functionality. The final design provides necessary function but decreases the systematic accuracy to ±20 µm for any individual measurement. One percent of nominal width is accepted measurement accuracy for this type of specimen, and the instrument easily

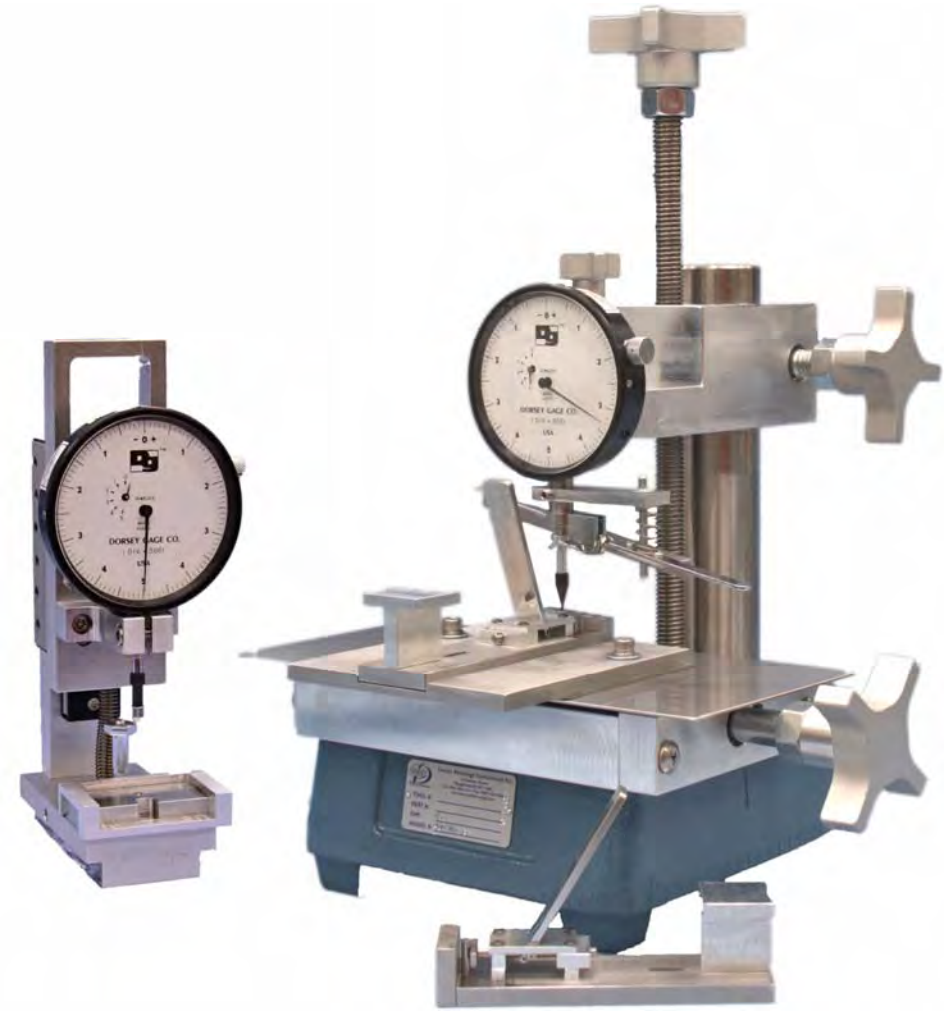

Figure 3. Test specimen thickness (left) and width (right) measuring instruments. The dial gauges are about 80 mm in diameter. Specimen holder for width measurement of RERTR specimens is installed on the measuring stand; the holder for the wider AFIP specimens is shown in front of the stand.

exceeded that requirement for the narrowest 6 mm wide specimens.

The specimen widths of 6 or 12 mm were much greater than the 1.25 mm gauge measuring range, so a stepped reference gauge block was incorporated into the specimen holder to offset the gauge zero reading to a known value. The specimen width then falls within the measuring range of the precision dial gauge. The zero reference value setting and gauge indication was checked and recorded before and after every specimen was measured. Width measurements were made at five equal-spaced locations along the length of the fuel specimen, and each location was independently re-measured at least three times to assure consistency. In all but two specimens, the width was measured prior to dissolving the aluminum cladding (see below) so the thin, delicate fuel material was better supported and protected from handling damage. The two specimens' width measurements performed after clad dissolution were handled very carefully to prevent damage.

The "bare" fuel materials (i.e. after cladding dissolution) were expected to have variations in thickness and possibly some curvature, owing to fuel swelling and dimension changes caused by irradiation. The thickness measuring instrument was designed with opposing spherical contact surfaces (see Figure 3 on left side, a hardened steel ball bearing protrudes about 0.25 mm above the platen surface) so local thickness measurements would be accurate and unaffected by minor specimen curvature. The instrument's dial gauge provided a direct thickness reading. A gauge calibration check was made using precision thickness gauges prior to measuring each specimen. A reference zero between the spherical contacts was measured and recorded before and after each specimen was measured. Instrument acceptance testing confirmed the accuracy of the individual thickness measurements is only limited by the accuracy of the dial gauge. Each bare fuel specimen was placed on the measuring support and three replicate measurements were made and recorded at each measurement location to confirm the thickness reading. RERTR-12 specimens were measured at nine locations using a 3-1-3-1-3 pattern and provided a good representation of thickness variation over the whole specimen. The AFIP-6 Mk II specimens were measured at 15 locations in a 3 x 5 grid. Specimen measurement locations are illustrated in Figure 4.

The measured thickness values were compared with thickness measurements made by other post-irradiation examination (PIE) methods (e.g. plate/oxide thickness, ultrasonic and radiographic); there was good general agreement between the various measurement methods.

3.4. Cladding Dissolution

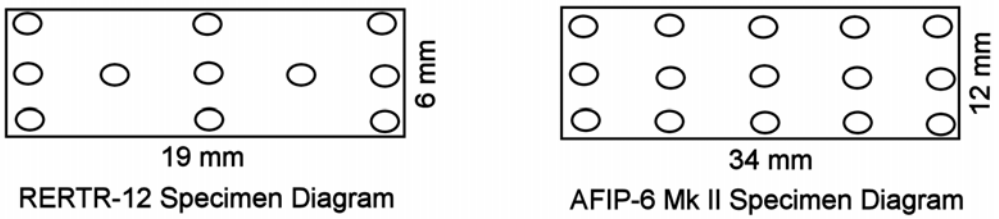

Figure 4. RERTR-12 and AFIP-6 Mk II specimen thickness measuring locations. Size and position of ellipses indicate zone of the individual thickness measurements.

The aluminum cladding was dissolved from specimens in a NaOH solution. The initial concentration was 6 M, but became more dilute as the aluminum cladding was dissolved. Periodic additions of more NaOH concentrate were made to the dissolution bath to maintain adequate dissolution rates.

A special tray made from stainless steel screen with multiple indexed specimen holder slots was built for the dissolution process, allowing cladding dissolution on up to six specimens simultaneously. Specimens were removed from the KGT - one at a time - and directly placed into a specific specimen holder position in the tray. Entries were made in a supplemental table for every specimen transfer to the tray including KGT number, tray slot index, and the relative orientation of the specimen in the slot, allowing orientation of the unmarked bare fuel relative to the original fuel plate to be maintained.

The dissolution process took between 4 and 18 hr. depending on solution concentration and cladding thickness. Once the dissolution reaction stopped, the specimen tray was removed from the NaOH and rinsed by immersion and mild agitation in a distilled water bath. One at a time, each bare specimen was removed from its slot and its orientation was re-marked with a permanent marker pen, and then returned to its respective KGT for storage.

The Zr coating on the U-10Mo is not removed in the aluminum dissolution process. The resultant “bare” fuel specimens are actually a composite structure with the relatively ductile Zr outer layer bonded to the surfaces of the U-10Mo. Owing to the co-rolling fabrication process, the thickness of the Zr layer is known to vary within a range of about 5 to 30 µm, even over small distances within an individual piece of fuel. Effects on test results due to the presence of this variable Zr layer are discussed later.

4. Mechanical Testing

The prepared and measured specimens in KGTs were transferred from the preparation area across the main cell to the mechanical testing workstation. Following testing, the broken specimen pieces were returned to their respective KGT, and transferred back to the storage location. Selected specimen pieces will undergo additional fractographic examinations in the future to better understand the fracture behavior.

4.1. Test Machine

A highly customized Instron 5869 electromechanical test machine was designed, built, and installed in the HFEF Main Cell. All control, signal conditioning, and motor power components were separated from the test frame and located outside of the hot cell. A sealed and shielded electrical feed-through connects the outside components to the test frame electrical components. All of the frame wiring and electromechanical components use radiation-resistant insulation and materials. The drive motor brushes are a special material that provides greatly improved service life in the dry argon environment.

A high-resolution analog resolver is attached to the drive motor output shaft and provides feedback for crosshead position. The data acquisition and processing of the resolver signal yields a crosshead displacement resolution of better than 0.05 µm, but the double-reduction toothed belt drive system attached to ball nut lead screws that move the machine crosshead suggest the relative accuracy of actual crosshead motion over a few millimeters of travel is probably on the order of a few microns.

Normal strain-gauge-type load cells constructed with radiation-resistant wiring provide force feedback signals. Different load cells with quick-connect attachments provide a wide range of accurate force measurements. The lowest capacity load cell has a 50 N full-scale capacity and was used for all AFIP-6 Mk II specimens and some of the RERTR-12 specimens. The remaining specimens were tested using a 500 N-capacity load cell. The compliance of each load cell is known, and was used to calculate load point displacements that are more accurate than the direct crosshead position information.

4.2. Bend Test Fixtures – Design, Features, and Use

The bend test fixtures were designed to meet various requirements of use in the hot cell for testing very thin specimens, and both fixtures use the same design, and have a nominal 2:1 load-to-support span ratio. The actual spans for RERTR-12 fixture are S1 = 16.02 and S2 = 7.95 mm (ratio 2.02); AFIP-6 Mk II fixure spans are S1 = 29.96 and S2 = 15.04 mm (ratio 1.99). The RERTR-12 bend test fixture is shown in Figure 5. The AFIP-6 Mk II test fixture is equivalent with support and load spans as provided above.

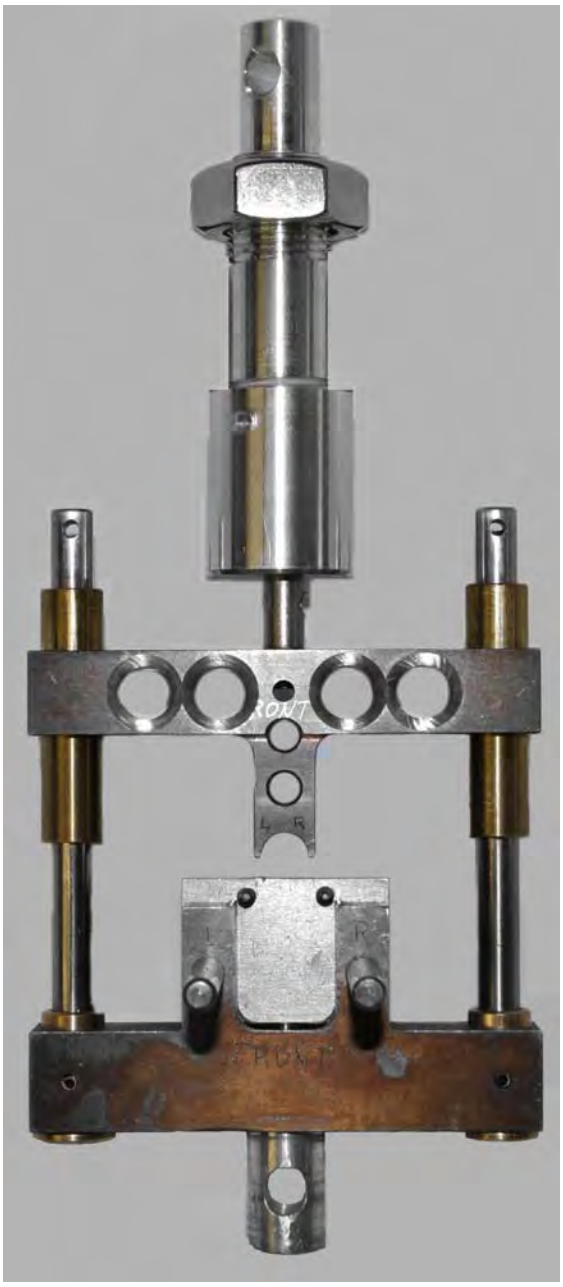

Figure 5. Bend test fixture used for RERTR-12 specimen tests. Top and bottom round clevis attachments are 12 mm dia.

Both fixtures have adjustable depth stop screws that align the specimen length normal to the support contact surfaces, and position the specimen so it is centered front-to-back on the supports. They also both have a removable specimen catch tray to retain the broken specimen pieces for return to the specimen KGT following test completion. Operational testing of the fixtures was performed in the hot cell mock-up shop prior to being placed in service inside the hot cell. The small size and very small overlap length on the specimen supports for the RERTR-12 specimens required a specimen installation guide be developed. Mock-up shop machinists designed, fabricated and tested a guide device and attachment method for the RERTR-12 fixture, allowing proper installation and alignment of specimens while minimizing the risk of specimen damage. The larger AFIP-6 bend test fixture did not require a specimen installation alignment device.

Friction force between the fixture crossheads and base guide columns was assessed prior to use inside the hot cell and was found to be less than 0.1 N for both fixtures over the functional range of testing motion. Specimen contacts on the fixtures were hard and polished to minimize any lateral friction forces as the specimens deform during testing. The small vertical deflection and resulting curvature of the specimen at the contact points causes minor change in support span and loading span during the test. Since contact forces are relatively low, the contact radii were kept small. The small radii minimize the span change with specimen deflection. The contact angles only change by a small amount up to failure, so the load application vectors never develop any significant horizontal component.

4.3. Test Procedures

Load cell calibration was verified daily with a calibrated 50 N check weight prior to any tests being performed. The operators carefully removed the selected test specimen from its KGT and observed the orientation marking. Consistent orientation of each specimen relative to the bend fixture was maintained, so specimen and fixture geometric asymmetries could be accounted for as necessary during subsequent data analysis. Special forceps were designed and built that allowed handling the small, delicate specimens with the bulky slave fingers. Care was always used so specimens were not tightly gripped or forced against any rigid surface, to prevent breaking or creating damage to the specimen prior to testing. Following specimen placement and alignment on the bend fixture, the specimen catch tray was

installed onto the fixture to capture and contain the broken specimen pieces for retrieval and return to their KGT.

Once the test set-up and specimen installation was confirmed, the machine crosshead was manually positioned to bring the fixture crosshead load points close to the test specimen surface. Visibility of small detail inside the hot cell is limited by window clarity. The load points were positioned within about 0.5 mm of specimen contact by visual observation with close-focus spotting scope or binoculars. After that, the crosshead was slowly lowered while the load cell readout was observed until the force appeared to slightly increase (see section 5.2 for discussion of noise in force signal). The crosshead position readout was then set to zero, and the Instron Bluehill software was commanded to execute a qualified test procedure to run the bend test at constant crosshead speed and collect the displacement, force, and elapsed time data. Data was acquired at 50 Hz or faster for all tests to ensure any small transient events were captured.

5. Data Analysis

The raw data files generated by the test system during a test require various processing prior to final analysis to determine specimen properties.

5.1. Displacement Data Corrections

The compliance of the load cells used for these tests was the dominant source of error between the resolver-indicated machine crosshead displacement and the actual load point contact displacement at the specimen. Each load cell compliance value was measured prior to its placement into the hot cell. The appropriate compliance value was used for each data set to convert the “machine crosshead displacement” into the specimen load point displacement. These corrected displacements are used in subsequent calculations of estimated specimen bending strains.

5.2. Force Data Processing and Correction

The custom Instron 5869 test system at the HFEF hot cell has an issue with electrical noise generated by the drive motor wiring creating anomalous force readings when the drive motor is running. There is an initial offset in the force reading when the motor power is applied and the offset magnitude is not consistent. Simultaneously, a somewhat cyclic noise signal with a fundamental period of about 1 sec is superimposed while the motor continues to run. The character of the cyclic noise signal is not uniform enough to numerically remove it from the data. However, the peak-valley amplitude of the noise signal is reasonably constant at about 0.15% of load cell full scale capacity. With this knowledge, we elected to use the local peak force values in each noise cycle to be representative of the specimen response during that cycle. This approach yields well over 100 data points for each specimen test providing a well-behaved force-deflection response curve.

The self-aligning bend fixture design causes a force plateau early in each test as the clearance (~0.08 mm) in the self-aligning slip joint is closed by machine crosshead movement. The force applied to the specimen during this plateau is equivalent to the fixture crosshead weight below the slip joint, 0.7 N for both fixtures. The specimen has no additional deflection during this plateau, so the plateau portion of data is removed and subsequent deflection data is offset to align with the pre-plateau data resulting in a smooth load-deflection curve. Due to the force offset occurring when the motor power is applied, a reliable force zero cannot be set prior to the start of a test. The indicated force levels at the force plateau and after specimen failure (while motor is running) were evaluated and the force data were offset as necessary to match the known force values. This results in a force at specimen failure accuracy of about 0.1 N.

5.3. Bending Strain Estimation

The bending strain for the test specimen can be estimated from the load-point deflection using various equations and assumptions. The load-deflection behavior of the specimens suggests predominantly elastic response up to the point of failure. This assumption ties the specimen surface strains to the corresponding local radius of curvature

during specimen deformation. The measured specimen deflections up to failure are relatively small with respect to the support span, justifying the assumption of small geometry change in estimated strain calculations. For this estimation, the average vertical dimension (thickness) of the specimen was used, and the deformed specimen geometry and bend fixture alignment were assumed to be symmetric. This allowed a closed-form equation for the specimen deformed shape. The specimen is subjected to constant bending moment within the load point span, leading to a part-circular deformed shape. The ratio of load point deflection to maximum deflection (at specimen center) can be determined from the elastic deflection equation for four-point bending. The specimen deformed shape defines a circular arc with a chord length equal to the loading span. This geometric form allows the radius of curvature to be calculated knowing the chord length (loading span) and the maximum chord-to-arc distance (calculated from the known load-point displacement and the ratio of load-point displacement to maximum displacement). The surface strain, ε, of the specimen in the constant moment region is then defined by the vertical depth (thickness, t) of the specimen, the loading span, S2, and the load-point deflection, v, as:

$$\varepsilon\ (\%) = 50 * t / (3 * v / 16 + S2^2 / (3 * v)) \quad (1)$$

The lower surface tensile strain at specimen failure for this series of tests can only be inferred from the available corrected specimen deflection value. The early portion of each specimen's calculated bend stress-strain response was nonlinear to varying amounts, with increasing instantaneous slope throughout. This early nonlinear behavior was not well replicated between various tests, and is attributable to slight curvature and/or warp of each specimen and the slight freedom of rotation of the fixture loading crosshead. As deflection increases, the specimen flattens since it is very thin relative to width and spans. Uniform contact across the full specimen width at each of the four radiused contact surfaces is eventually made. Such behavior creates the apparent stiffening response with increasing deflection, and the degree of curve or warp determines how much deflection is required before a true representative force-deflection response is indicated. The specimen flattening effects in the early portion of the response curve is significant when trying to estimate specimen surface strain at failure, but the small deviations in support span (decreasing) and load span (increasing) as specimen deflection increases have little influence on the force-deflection response, and is insignificant compared to the other factors.

To achieve relative consistency for specimen to specimen comparisons of bending strain at failure, the strain values for each specimen were offset to eliminate the early nonlinear effects of specimen flattening. A line fit to the stiffest linear portion of the stress-strain curve data was forced to pass through the bending stress-strain plot origin. The absolute magnitude of surface strain at failure may not be highly accurate using this approach, but the significant specimen flatness variability is effectively eliminated.

5.4. Bending Stress Calculation

Outer fiber bending stress is calculated using accepted elastic formulas, the applied force, bend fixture load and support span, specimen average thickness and width, using the same assumptions concerning specimen and loading geometry described in the previous section. The stresses calculated in this manner do not directly consider the effects of the bonded Zr layer (e.g. Zr thickness, thickness variation, slightly higher elastic modulus than U-10Mo, possible yielding of the Zr prior to failure, etc.). The resultant calculation assumes a linear through-thickness tensile stress distribution, with equal magnitude maximum stress on the top and bottom surfaces. These assumptions are appropriate until Zr coating mechanical properties and thickness distribution are better determined, allowing a more accurate estimation of stress in the U-10Mo at failure through numerical modeling that takes into account these complexities. Representative response curves, both uncorrected and processed, for one test is shown in Figure 6.

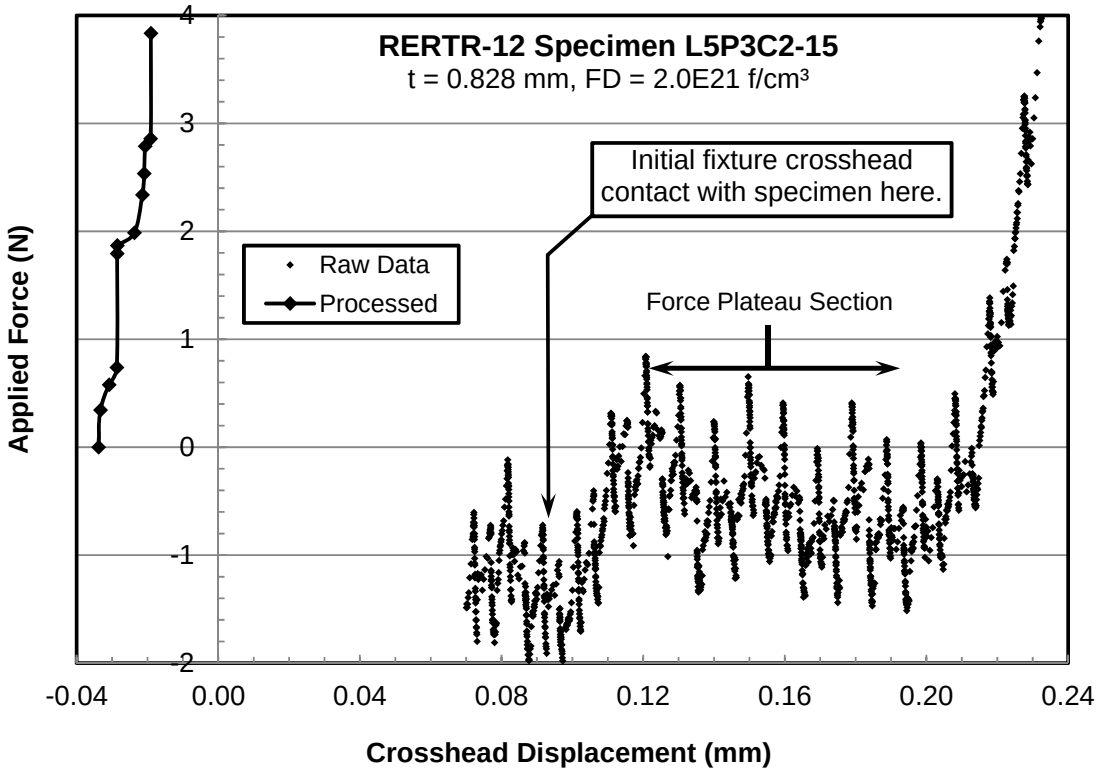

(a)

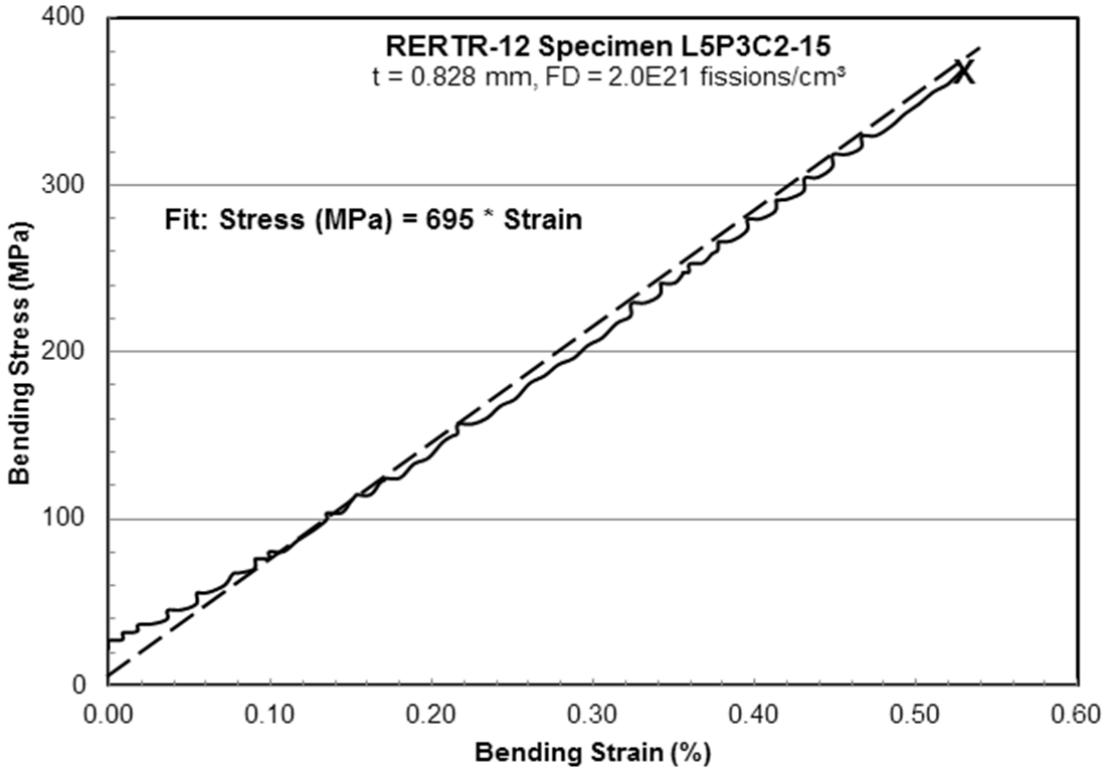

(b)

Figure 6. Test of L5P3C2-15. (a) Raw and processed force and deflection data from beginning part of test. (b) Processed stress-strain curve and line fit for flexural stiffness.

5.5. Flexural Stiffness Estimation

The slope of the stiffest linear portion of the stress-strain curve described in the strain calculation section above will be representative of flexural stiffness for the specific specimen it represents. Localized variations from the average in specimen width and thickness may perturb the estimated value, as will error in strain estimation and bending stress calculation. The flexural stiffness values reported from these tests should be interpreted with caution, as the unknown effects mentioned above and discussed later have not been considered in these estimated values. They are useful for qualitative comparison between specimens having different fission densities.

5.6. Specimen Fission Density Estimation

Large matrices of fission density values relative to planar position for each RERTR-12 test plate were created by neutronics analyses of the plate irradiation conditions including localized flux densities from the reactor and fuel burn-up within the plate. Through-foil information was also provided, but the plate surfaces were oriented approximately normal to the reactor flux, and the thin foil did not see much variation in estimated fission density through the thickness. As expected, the fission densities increased as the foil edges are approached, and the varying reactor flux density along the length of the test fuel plates created variation in average fission density with respect to the position along the plate length.

The spatial density of the fission density matrices provided about a 4 x 7 grid of fission density points covering each of the 27 test specimens. The specimen average fission density reported here was calculated as the numerical average of the 28 fission density values corresponding to the specimen location within the test plate. Distribution of fission density across the plate width (specimen length) for each specimen was also examined. Within a specimen, that distribution was nominally parabolic with the edge values higher than the minimum. Deviations from less than 2% to about 8% of the specimen average value were observed, and the distribution curves were typically not symmetric, i.e. the minimum value was not at the center of the specimen.

A preliminary single fission density value was provided by the neutronics analysts for each of the nine AFIP-6 Mk II specimens without explanatory details. The provided values are reported in the data below, and further analyses are still underway.

6. Results

Table 1 provides tabulated values of the measured and calculated properties and other information for each of the 36 specimens that were tested.

Table 1. Specimen information and calculated material properties, ordered by fission density.

Specimen ID	U-235 enrichment (%)	Avg. FD ($f/cm^3 x 10^{21}$)	t (mm)	W (mm)	Pmax (N)	Break Stress (MPa)	Break Strain (%)	Flexural Stiffness (MPa/%)
L1P786-15	70	6.2	0.422	6.114	22.2	246	0.43	566
L1P786-21	70	5.8	0.411	6.040	37.5	444	0.74	616
L1P786-27	70	5.6	0.414	6.081	21.8	253	0.46	551
6II-1-A	40	4.3	0.566	12.202	39.2	225	0.41	545
6II-1-B	40	4.3	0.613	10.402	34.8	199	0.48	419
6II-1-C	40	4.3	0.535	12.146	38.1	245	0.38	646
6II-1-D	40	4.3	0.531	11.959	46.5	309	0.48	654
6II-1-E	40	4.3	0.543	11.942	34.0	216	0.38	563
6II-1-F	40	4.2	0.535	12.158	34.7	223	0.35	634
6II-1-G	40	3.9	0.475	12.197	40.2	327	0.41	807
6II-1-H	40	3.9	0.467	11.928	38.6	332	0.39	857

Specimen ID	U-235 enrichment (%)	Avg. FD ($f/cm^3 x 10^{21}$)	t (mm)	W (mm)	Pmax (N)	Break Stress (MPa)	Break Strain (%)	Flexural Stiffness (MPa/%)
6II-1-J	40	4.3	0.466	12.005	37.1	318	0.38	834
L1P773-15	70	3.7	0.358	6.134	24.8	381	0.51	746
L1P773-21	70	3.5	0.349	6.276	22.5	356	0.46	770
L1P773-27	70	3.4	0.349	5.896	14.6	247	0.34	718
L5P3B1-15	30	3.8	0.768	5.767	166.8	593	0.80	729
L5P3B1-21	30	3.7	0.767	6.096	94.1	317	0.43	746
L5P3B1-27	30	3.7	0.771	6.029	94.0	317	0.45	715
L2P482-15	40	2.8	0.643	5.889	88.9	442	0.61	719
L2P482-21	40	2.7	0.635	6.012	48.3	243	0.35	671
L2P482-27	40	2.7	0.635	5.860	65.0	333	0.43	769
L5P3B3-15	30	2.7	0.743	5.939	84.0	310	0.41	751
L5P3B3-21	30	2.5	0.740	5.927	99.3	370	0.46	838
L5P3B3-27	30	2.4	0.746	5.977	122.3	446	0.58	775
L2P481-15	40	2.4	0.622	6.156	46.4	236	0.35	678
L2P481-21	40	2.3	0.614	5.888	75.3	410	0.52	794
L2P481-27	40	2.2	0.620	5.785	36.6	199	0.30	714
L1P461-15	40	2.1	0.313	5.881	16.0	335	0.40	867
L1P461-21	40	2.1	0.314	5.907	16.3	338	0.37	909
L1P461-27	40	2.0	0.310	5.768	21.4	467	0.46	1011
L5P3C2-15	30	2.0	0.829	5.719	120.8	373	0.53	707
L5P3C2-21	30	2.0	0.814	5.937	163.4	487	0.70	700
L5P3C2-27	30	2.0	0.824	6.009	157.7	467	0.75	625
L5P1B0-15	10	0.38	0.710	5.920	131.8	534	0.62	865
L5P1B0-21	10	0.36	0.708	5.974	107.1	432	0.50	871
L5P1B0-27	10	0.34	0.710	6.173	126.5	492	0.53	916

Graphical representations of specimen strength and stiffness with varying fission density are shown in Figures 7, 8, and 9. The AFIP-6 specimens appear in two distinct populations – the six center specimens, and the three end specimens - these are presented as two separate groups. Calculated bend stresses at failure are presented in Figure 7. Figure 8 shows the group average strength with ±1 standard deviation bars. Figure 9 presents the calculated flexural stiffness for each specimen relative to fission density.

7. Discussion

7.1. Ductility and Strength Loss in Irradiated Material

Room temperature tensile properties of unirradiated U-10Mo foil are: tensile yield from 1012 to 1108 MPa; ultimate tensile strength from 1014 to 1172 MPa; and ductility from 1.2% to 11.7%, depending on specimen orientation and thermal processing after rolling to final thickness [8]. Those foils had thicknesses similar to the foils tested in this study, and used similar rolling schedules. Those foils did not have the Zr diffusion barrier coating applied. As mentioned previously, all irradiated specimens tested in this study exhibited essentially elastic behavior up to the point of fracture, and failure occurred in a brittle manner, i.e. no measurable specimen ductility. Most significantly, the highest recorded strength for any irradiated specimen tested was under 600 MPa, indicating substantially reduced strength compared to unirradiated material.

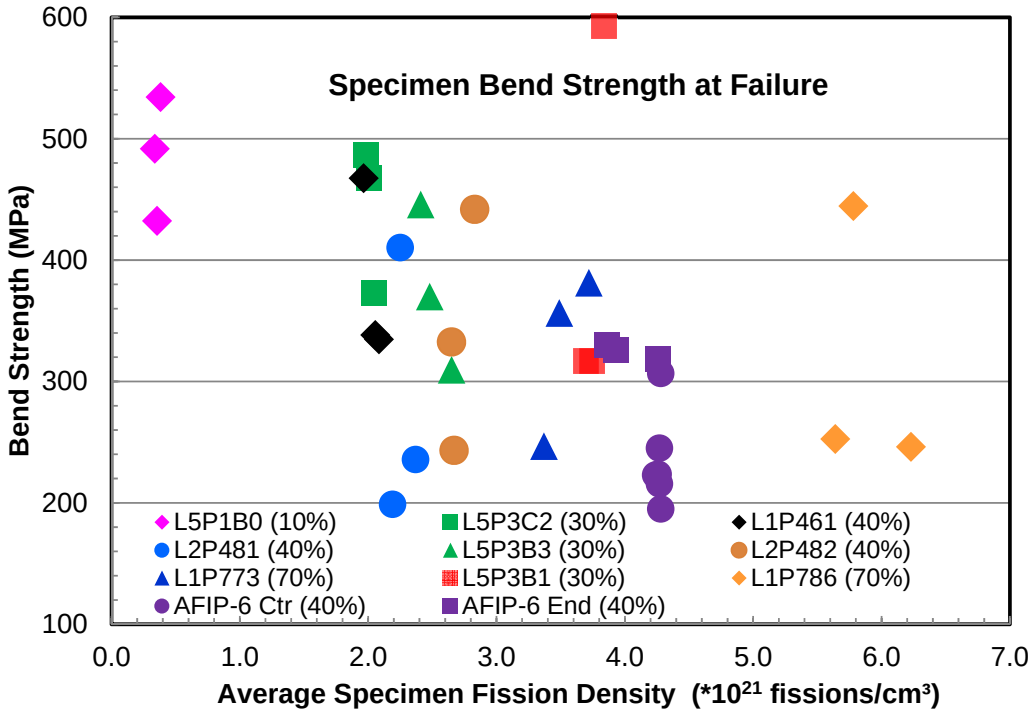

Figure 7. Calculated bend strength at failure as a function of specimen average fission density for all specimens tested. AFIP-6 specimens seem to be from two populations, so six center specimens and three end specimens are grouped separately.

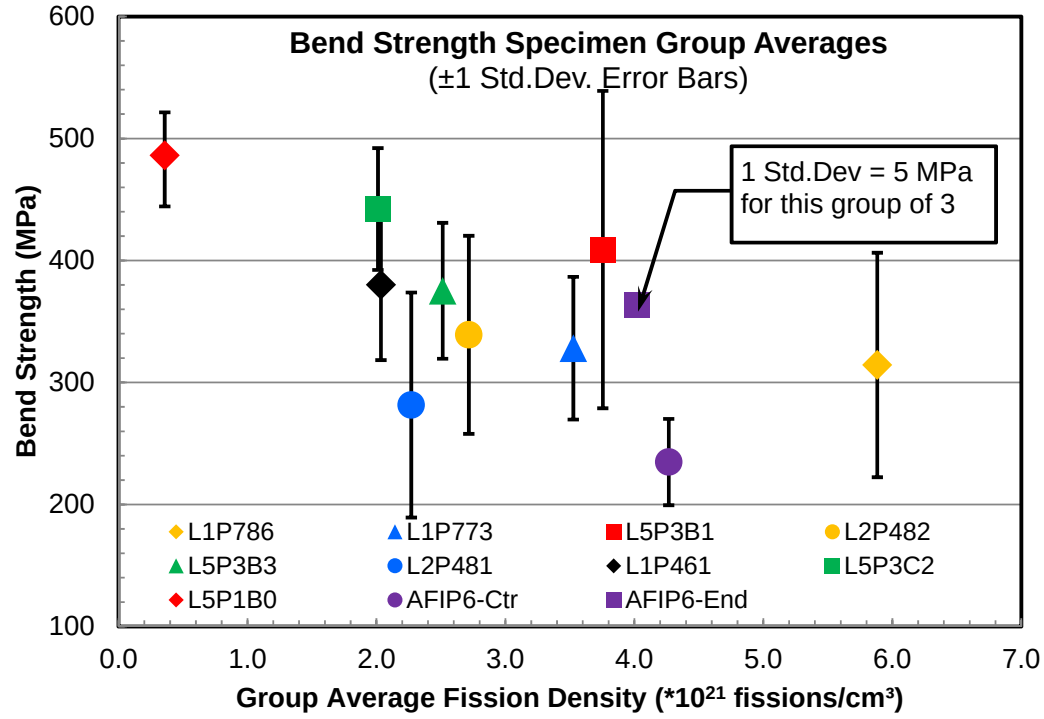

Figure 8. Mean failure bend strength and standard deviation for each specimen group tested. AFIP-6 specimens are divided into two groups – six specimens at plate center, and three specimens at plate end since they appear as separate populations.

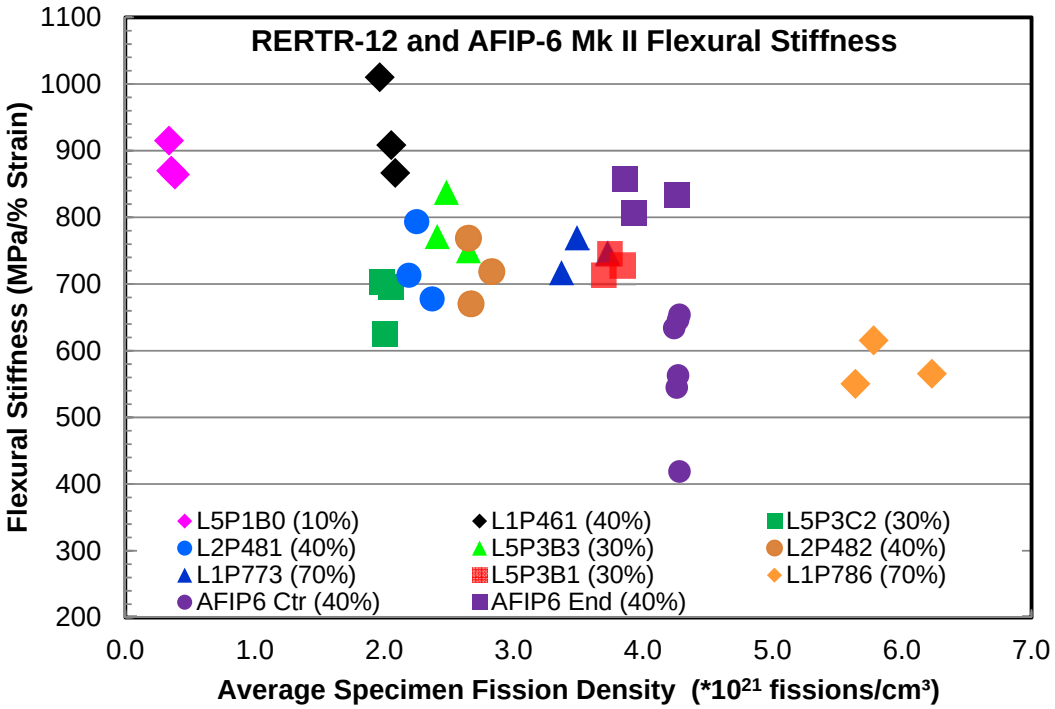

Figure 9. Calculated flexural stiffness as a function of specimen average fission density for all specimens tested. AFIP-6 specimens appear as two distinct populations – six center specimens and three end specimens, so are shown in separate groups

7.2. Bending Failure Strength and Fission Density Correlation

Figure 7 shows an apparent correlation of the measured bend stress at failure to the fission density, with bend stress at specimen fracture generally decreasing with increasing fission density. The L1P1B0 specimens had the lowest irradiated fission density range (0.34-0.38E21 fissions/cm^3) of all specimens tested. This fission density equates to approximately 4 to 5% of LEU burnup. These specimens had the highest bending strength values ranging from 490-530 MPa. Two specimens from plate L1P786 had the lowest bend strength values of 246 and 253 MPa, and the highest fission densities of 5.6 and 6.2E21 fissions/cm^3 respectively, representing approximately 73 and 79% of LEU burnup.

Two specimens had suspiciously high bend strength. L1P786-21 had 444 MPa bend strength at 5.8E21 fissions/cm^3 and L5P3B1-15 had 593 MPa bend strength at 3.8E21 fissions/cm^3 (see Table 1 and Figure 7). Plates L2P481 L2P482 had relatively large variation in strengths, but all values were within the general trend of the entire data set. Possible explanations and corrections to reduce the variation in calculated strengths are discussed below. Figure 8 presents the same data shown in Figure 7, but organized as specimen group mean and standard deviation (including the outlier values), as a function of the group average fission density. Comparing Figure 8 with Figure 7, it is interesting to note that, in general, the variability of strength within a particular specimen group (i.e. for a given fuel plate, or fuel plate region in the case of AFIP-6) was lower than the variability between average strength values for different groups. This suggests there may be systematic reasons for the observed strength differences between specimen groups of similar fission densities. For example, such behavior might be expected if there were differences in microstructure caused by fabrication variables, or differences in burnup profile, as might be expected from differences in irradiation conditions, between the different specimen groups. Investigations are underway to review as-run neutronic analyses and available fabrication records for potential explanations of these differences. A comparison with metallographic data generated during post-irradiation examination may also suggest if significant differences in irradiated microstructure were present.

7.3. Flexural Stiffness (Elastic Modulus) and Fission Density Correlation

The elastic modulus of the U-10Mo material is expected to decrease with increasing fission density due to gas bubble formation in the material. This is expected to be the dominant factor in reduction of elastic modulus as burn-up increases. The flexural stiffness provided in Table 1 and shown in Figure 9 is linearly proportional to material elastic modulus, given the assumptions in stress and strain calculations discussed earlier. The range of variation in the stiffness as percentage of maximum is similar to the range of bend strengths, but variability in specimen stiffness at given fission densities is generally smaller than the corresponding strength variation. The linear trend of stiffness to fission density supports this theory. Considering that flexural stiffness values calculated from the test data include assumptions in both specimen strain and bend stress calculations, and the stiffness variations tend to be less than corresponding strength variations support the conjecture that material strength is being influenced by additional factors beyond just fission density.

7.4. Sources of Data Variability

There are a number of possible sources for the observed variability in the calculated results. Differences in source materials, enrichments, fabrication process variables, microstructure, and irradiation conditions may have multi-variate effects that are not presently accounted for.

Reported bend strengths use a weighted average specimen thickness and width in order to apply closed form stress calculations, and all the specimens had some variations in thickness and width. The thickness variable has an inverse cubed relationship to calculated stress, the specimens are very thin, and the thickness variations can be a significant percentage of the average thickness. The calculated stresses reported are at the outer surface of the specimen. A first order estimate of surface bend stress range for each specimen could be bounded using maximum and minimum measured thickness and widths.

Reported surface bend strains also use the weighted average thickness, and the strain is a linear function of specimen thickness. The weighted average irradiated specimen thicknesses ranged from 310 to 829 µm. Individual specimen thickness variations were typically no more than 30 µm, but a few specimens had variations exceeding 90 µm. Most of this variation is expected to be the result of non-uniform radiation-induced swelling of the U-10Mo which can be significant at higher fission densities. The calculated strain error could be rather small to quite significant relative to flexural stiffness depending on the thickness distribution and magnitude relative the weighted average for that specimen.

Nominal specimen force-deflection response was linear to the point of failure for each test, indicating bulk elastic material response and no measurable ductility. The failure mode of the irradiated U-10Mo tested is therefore brittle, and likely has very low fracture resistance. Any material with these general characteristics have wider variations in measured strength due to significant effects of small defects, possibly undetectable, in the material. These effects are exacerbated by the small volume of stressed material in these specimens and presently unknown distribution of defect sizes and corresponding spatial defect distributions in the material. Such information, if available, can be used to determine a material strength distribution as a function of stressed volume.

The pure Zr coating on the U-10Mo surfaces is affected little by the irradiation, and has the following nominal properties: E = 94.5 GPa; Poisson's Ratio = 0.34; Yield Strength = 230 MPa; Ultimate Tensile Strength = 330 MPa; and Ductility = 32%. The elastic response limit of the material is in the range of 200 MPa and 0.20% strain. These properties are significant given the unknown variation in actual Zr thickness over the surfaces of each specimen tested. An earlier report [9] shows metallography of transverse fuel plate sections revealing Zr layer thickness variations. Localized Zr thickness variations over sub-millimeter distances from less than 5 to over 30 µm are seen, with a 15 to 25 µm range being more typical.

The Zr coating thickness potentially ranges from 20% of the specimen thickness for the thinnest specimens, to as little as 1% of specimen thickness for the thickest specimens, so thinner specimens are potentially affected more than the thicker ones. There is no

practical method to make non-destructive measurements of the Zr thickness with the required spatial resolution to completely account for its effects in the calculated test results. However, knowing its range of variation can be used to make bounded estimates of its effects.

Bending failure stress in the U-10Mo substrate would be proportionately reduced by the Zr thickness ratio from the calculated surface bend stress, assuming constant modulus throughout the specimen, no plastic deformation of the Zr, and uniform Zr thickness. The difference in modulus between the Zr (95 GPa) and U-10Mo (~85 GPa before irradiation, with reduction as fission densities increase), would increase the apparent stiffness of the U-10Mo substrate in the initial portions of the test. All specimen failures appeared brittle in nature, evidenced by nominal linearity of the force-deflection response up to the instant where the U-10Mo failed catastrophically. The effect of any Zr coating plasticity could not be separated from recorded force and deflection data as detectable non-linear response. This indicates the net effect of Zr plastic deformation combined with Zr thickness ratio was small relative to the bulk specimen response, and provides a basis for using a simplified correction method that does not account for the elastic-plastic behavior of the Zr coating. The unknown thickness distribution of the Zr coating for each specimen would still require statistical treatment, and even the simple correction to the measured strength and stiffness would result in upper and lower bounds determined by the risk tolerance associated with those values.

In a few cases, some very small load drops prior to final specimen failure were observed. It is possible that the ductile Zr coating was thick enough where a micro-crack initiation was arrested after small extension through energy absorption by plastic deformation of the bonded Zr coating. Continuing specimen deflection supplied more energy, resulting in more crack advance at later times in the test. At some point the Zr ultimate strength would be locally exceeded, and the absorbed energy was returned to the growing crack, leading to catastrophic failure of the specimen.

Information from specimen metallographic and fractographic studies now in progress may provide improved estimates of coating thickness and thickness variations, as well as failure initiation sites. Reanalysis of the existing data can then be undertaken to provide improved properties along with more accurate statistical distributions for use in fuel design and assessment models. Numerical modeling is ongoing to benchmark the calculated stress and strain values reported here. Sensitivity studies using numerical modeling should provide information on the expected variability in test results due to the sources of variability discussed above.

8. References

1. INL/LTD-14-33575, “RERTR-12 Fabrication Summary Report,” Idaho National Laboratory, 2014.
2. INL/LTD-12-27302, “AFIP-6 Mk II Fabrication Summary Report,” Idaho National Laboratory, 2012.
3. BMI-APDA-638, “Stress-Strain Properties of Uranium-10 w/o Molybdenum,” Battelle Memorial Institute, 1958.
4. INL/EXT-12-27085, “RERTR-12 Insertion 2 Irradiation Summary Report,” Idaho National Laboratory, 2012.
5. INL/EXT-12-26305, “AFIP-6 Mark II Irradiation Summary Report,” Idaho National Laboratory, 2012.
6. INL/ECAR-2016, “RERTR-12-5 Cycle 151B As-Run Physics Analysis Results for Use in Thermal and Oxide Growth Evaluations,” Idaho National Laboratory, 2012.
7. INL/ECAR-1941, “As-Run Neutronic Analysis for the AFIP-6 Mark II Experiment Irradiated in the Center Flux Trap of the ATR, Cycle 151,” Idaho National Laboratory, 2012.
8. INL/EXT-14-33639, “Elevated Temperature Tensile Tests on DU-10Mo Rolled Foils, Rev.1,” Idaho National Laboratory, 2015.
9. INL/EXT-14-32457, “AFIP-6 Mk II Characterization Summary Report,” Idaho National Laboratory, July 2014.

RRFM 2015 INTERNATIONAL MEETING ON
EUROPEAN RESEARCH REACTOR CONFERENCE

April 19 – 23, 2015
Bucharest, in Romania

UMo Fuel-Powder Production Process and Results

R. SCHENK, R. SCHAUER, W. PETRY, ,
Forschungs-Neutronenquelle Heinz Maier-Leibnitz (FRM II)
Technische Universität München (TUM), Lichtenbergstr. 1, 85747 Garching – Germany

B. STEPNIK, C. MOYROUD, M. GRASSE, C. COULLOMB, G. BOURDAT, C. JAROUSSE
AREVA NP
10, rue Juliette Récamier, F-69456 Lyon Cedex 06 – France

ABSTRACT

FRM II and AREVA have launched a common project for the construction and operation of an R&D UMo fuel powder production facility.
The project aims at providing feedstock atomized UMo fuel powder for future irradiation tests and at gathering know-how for industrial scale fuel-powder production by means of centrifugal atomization. Currently, the prototype facility consists of an induction furnace and an in-house designed rotating electrode process (REP) atomizer for casting and subsequent atomization of UMo electrodes, respectively.
After validation of atomizer operation with externally cast UMo electrodes in 2014, final objective of the prototype stage in early 2015 was to complete the production process by atomizing in-house cast UMo electrodes and characterizing the thereby produced powder.
The R&D project is complete. An R&D UMo atomization capacity is running in AREVA.
This paper presents and discusses obtained results and perspectives.

Utilisation of Research Reactors

NEUTRON SCATTERING IN VERY HIGH MAGNETIC FIELDS: THE NEW HYBRID MAGNET AT HELMHOLTZ-ZENTRUM BERLIN

P. SMEIBIDL, H. EHMLER, O. PROKHNENKO, B. LAKE
Helmholtz-Zentrum Berlin
Hahn-Meitner-Platz 1, 14109 Berlin – Germany

M. Bird
National High Magnetic Field Laboratory
1800 E. Paul Dirac Dr., Tallahassee, FL 32310-3706 - USA

ABSTRACT

At the Helmholtz-Zentrum Berlin (Germany), a dedicated facility for neutron scattering in high magnetic fields and low temperatures is close to completion: the High Field Magnet installed on the Extreme Environment Diffractometer. The new hybrid magnet, a 'first of its kind system' with horizontal field, will not only allow for novel experiments, it will be at the forefront of development in magnet technology itself. By combining a superconducting cable-in-conduit coil and a resistive coil, maximum fields between 26 - 31 T will be possible with cooling power between 4 and 8 MW for the resistive part. The 30° conical openings at both ends of the magnet are envisaged for neutron-scattering access. The Extreme Environment Diffractometer is a neutron instrument optimized to work with the High Field Magnet. It uses a band of incident neutron energies to compensate for the angular limitations imposed by the magnet and offers diffraction, small-angle neutron-scattering and in the future inelastic neutron-scattering in high magnetic fields. This paper gives an overview of the high field facility at the Helmholtz-Zentrum Berlin, its components and their present status.

1. Introduction.

Neutron-scattering is a powerful tool for studying structure and dynamics of matter over a wide range of length- and time-scales. The properties of the neutron, such as its electrical neutrality, magnetic moment, and quasi-random variation of the scattering power as a function of atomic number, makes it an ideal probe for many areas in modern physics, chemistry, and biology. Experimentalists can benefit from the high penetration depth of neutrons into most materials, neutron sensitivity to light elements, including hydrogen, sensitivity to magnetism etc.
Unfortunately, use of neutrons comes at a high price. For most neutron-scattering applications, neutrons are produced in large-scale research facilities by means of fission (in research reactors) and spallation (in accelerator-driven spallation neutron sources). Helmholtz-Zentrum Berlin (HZB), Berlin, Germany, operates the 10 MW research-reactor BER II [1]. The original 5 MW reactor was built in 1972 and commissioned in 1973. In 1991 it was upgraded to 10 MW. At the same time a cold neutron source was installed. The reactor is primarily used for neutron generation in thermal and cold energy ranges centred around 25 and 10 meV, respectively. A number of neutron instruments have been developed to tackle a variety of scientific applications (see Fig. 1a). The HZB neutron instrument suite includes instruments covering a broad range of experimental methods such as diffraction, small-angle scattering, reflectometry, imaging, and spectroscopy [2]. The special emphasis of the HZB is on neutron scattering under extreme conditions which include high pressures, high and low temperatures, and high magnetic fields and their combinations. In magnetic fields the HZB holds the world record of 17.4 T steady state (DC) field available for neutron experiments combined with temperatures as low as a few Kelvin (or 15 T at tens of mK). Neutron scattering in high magnetic fields led to a number of important discoveries such as Bose-Einstein condensation in magnetic materials and field-induced antiferromagnetic order in high temperature superconductors [3-4]. However, research of condensed matter systems is bringing up an increasing number of questions which require experiments combining

neutron scattering and magnetic fields above 17 T. In order to remain a world leading neutron facility, HZB started an ambitious project of extending the magnetic field-range to 25 T and beyond. One should mention that DC fields are essential for neutron scattering experiments. The pulsed magnets, which can reach fields above 30 T, have rather low duty cycle. Combined with relatively low neutron fluxes they significantly limit the number of possible experiments.
To reach high DC fields, a completely different magnet technology has to be used as compared to the 17 T superconducting magnets. This magnet technology is typically used at high magnetic field laboratories. Up to now it has never been used at neutron sources and, consequently, it is for the first time that such a magnet is built for neutron-scattering applications. To combine the magnet and the neutron instrument successfully, they have to be adapted to each other. For that purpose, the magnet has a geometry that is not fully optimal for achieving the highest fields while the neutron instrument has a special design that takes into account the limited angular access of the magnet.
In this contribution an overview of the HZB high-field facility for neutron scattering is given. Its main components are the High Field Magnet (HFM), the most powerful DC magnet for neutron-scattering in the world, and its neutron counterpart the Extreme Environment Diffractometer (EXED).

2. High Field Magnet

The HFM is a series-connected hybrid system with an outer superconducting coil and two inner resistive coils [5]. The total field of 26 T achieved with a 4 MW insert coil has the potential to be increased to 31 T with an upgrade in the power consumption to ~8 MW. The system is designed for the special geometric constraints of performing neutron-scattering experiments in a high field magnet. The main technical parameters are listed in Table 1.

Central Field	26 T (31) T
Bore	50 mm horizontal
Opening Angle	30°
Power Resistive Insert	4 MW (8 MW)
Field Homogeneity	< 0.5% (15 mm x 15 mm)
Operating Current	20 kA
Magnetic Field of Resistive Insert	13 T – 18 T (4 MW / 8 MW)
Magnetic Field of Superconducting Coil	13 T
Height	~ 5 m
Total Weight	~ 25 t
Cold Mass	~ 6 t

Table 1: Hybrid magnet system operating parameters

The inner resistive coil is the first to provide a conical bore at each end to allow neutron-scattering to detectors up to ±15° off the beam axis. The superconducting coil is a 13-Tesla, 600-mm cold bore coil consisting of Nb_3Sn cable-in-conduit conductor (CICC) and weights 5 ton (6 ton full cold mass including flanges, joints and piping). Design and fabrication of the superconducting cable-in-conduit coil and full cold-mass assembly was completed at the National High Magnetic Field Laboratory (MagLab), Tallahassee, USA. The cold-mass was then was transported to Criotec Impianti in Italy where the major components of the MagLab-designed cryostat were assembled around it with the magnet bore positioned vertically. After completion, assembled coil and cryostat were transported to a temporary “magnet assembly and testing” hall at the HZB (shown in Fig. 1a). It was rotated so that the magnet axis was

horizontal and the remaining parts of the cryostat including a supply turret were assembled. After magnet commissioning the system was moved to its final location in the neighbouring neutron guide-hall and installed on EXED.
A vertical section of the magnet system is shown in Fig. 1b. The inner resistive coil has a conically shaped inner bore to allow a conical scattering space. The resistive coils are series connected to a single superconducting coil made from Nb_3Sn CICC conductor. The entire magnet system has the bore horizontal so it can align with the neutron beam axis. In addition, the magnet system sits on an instrument table so it can rotate $\pm 15°$ for increased neutron scattering-angle. All cryogenic and electrical utilities port through an upper "turret" for interface with the supply systems. The thermal shields are cooled via the helium refrigerator down to nominally 50 K.

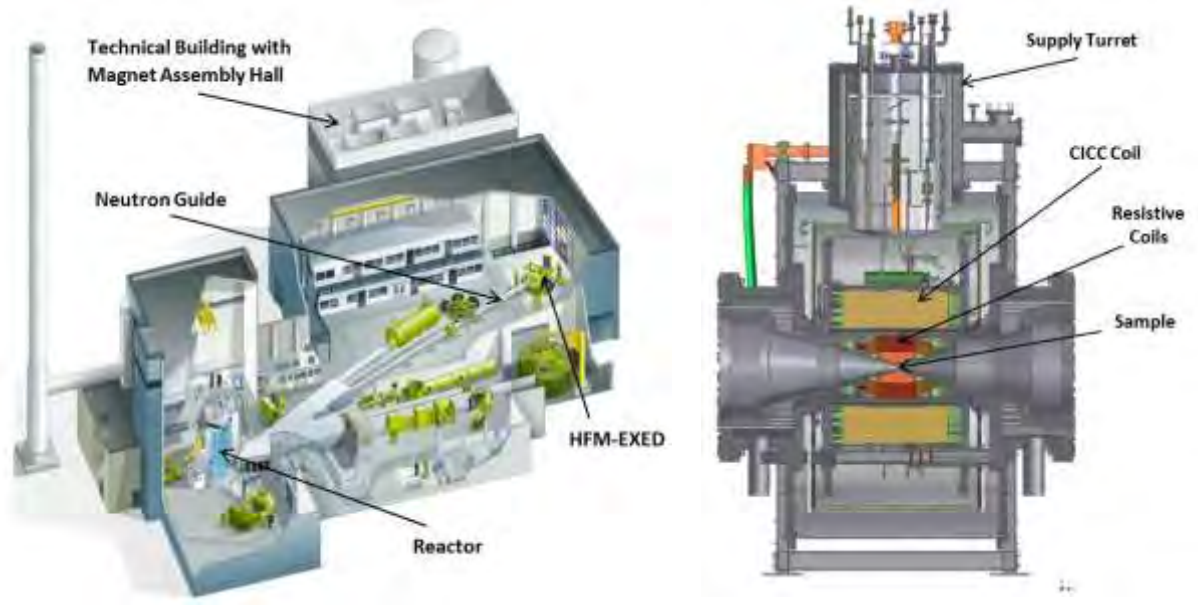

a) b)

Fig. 1. a) Reactor, neutron experimental halls and assembly-hall at the Helmholtz-Zentrum Berlin with the HFM and the EXED. b) Cross-section through HFM showing how the superconducting CICC coil with resistive insert coils are positioned in the cryostat. The cryogenic and electrical utilities enter through the upper supply turret.

A large part of the functional requirements of the cryostat stems from the electromagnetic interactions between the superconducting and resistive coils. Features are designed to accommodate potential axial and radial misalignments and axially offsetting forces created from a fault in the resistive coils.
The He-refrigerator system for the CICC coil and the 8 MW power supply as well as the high pressure water circulation required to cool the insert magnet which includes the necessary cooling towers and the water treatment plant were constructed using standardised industrial components. These are all located in the separate technical building for the HFM beside the neutron guide-hall (see Fig. 1a).
After 7.5 years of design and construction and after a series of commissioning activities of the technical infrastructure and the High Field Magnet, the system reached its maximum current of 20 kA and full field of 26.2 T for the first time on 16th Oct 2014.

3. Extreme Environment Diffractometer

The EXED shown in Fig. 2 is a dedicated neutron instrument optimized to work with the restrictions imposed by the magnet geometry [6-9]. To achieve that it utilizes polychromatic

(time-of-flight) technique which is fairly unusual for instruments on a continuous (reactor) source. Most of the instruments on reactor sources are monochromatic instruments exploiting a high time-averaged flux of the source. They use a single incident neutron wavelength while scanning over a range of scattering angles to cover the requested *d*-range according to the Bragg's law, $\lambda=2d\sin\theta$, where λ is the wavelength, *d* is the spacing between the lattice planes in the sample, and θ is the angle between the incoming beam and the lattice planes. This approach, however, would be ineffective for EXED in combination with HFM since θ is restricted to 2°-15° and 75°-85° by the magnet cones. Indeed, according to the Bragg's law, one cannot cover a reasonable range in *d* if λ is fixed and θ is limited. On the other hand, using a range of wavelengths instead can compensate for the limited θ. Fig. 3a visualizes this principle and compares *d*-coverage of monochromatic and TOF instruments.

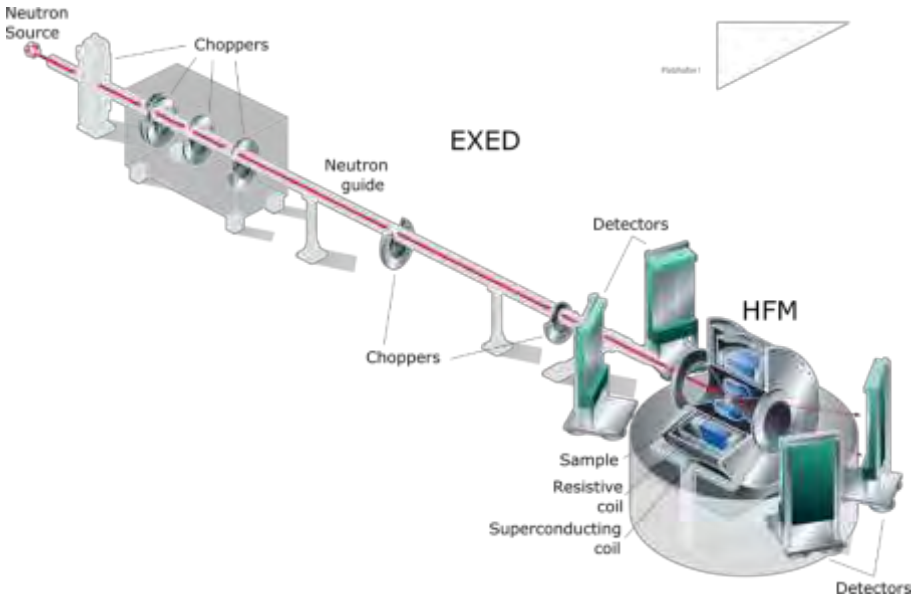

Fig. 2. Schematic layout of EXED showing the neutron source and main instrument components: the neutron guide, chopper cascade, and the HFM surrounded by detector banks. The picture is not to-scale, and the bispectral extraction system is not shown.

To have an access to broad wavelength range EXED is equipped with the so-called bispectral extraction system which allows neutrons from both thermal and cold moderators to enter the same neutron guide. The supermirror guide with a cross section 100x60 mm^2 (HxW) transfers the neutrons to the sample position located about 75 m away from the source (Fig. 2). Such a long distance is necessary to provide good wavelength resolution and low background conditions. Before reaching the sample the neutron beam in compressed spatially in both directions by a factor of two by means of an elliptically converging focusing guide section. For applications requiring low beam divergence, the focusing section can be replaced by a pin-hole collimation section with variable apertures. The resulting neutron spectrum at the sample position is shown in Fig. 3b. The data were obtained by a normalized ^{3}He neutron monitor and corrected for the chopper system duty cycle (see below). Maxima around 3 and below 2 Å represent contributions from cold and thermal sources, respectively.

In order to realize the TOF method on a continuous source, special mechanical devices called choppers are used (Fig. 2). They interrupt the neutron beam in a defined manner to provide bursts of neutrons. EXED has six choppers sharing the same vacuum with the neutron guide. Two of them – the 600 Hz Fermi chopper and the 200 Hz double disc chopper - located at 53.22 and 53.05 m away from the sample position are used for neutron pulse generation in a time range from a few μs up to more than one ms. Such a broad range

allows easy trading instrument resolution for intensity depending on the given scientific problem. The remaining four 120 Hz single disc chopper are necessary to select a bandwidth and eliminate the neutrons with undesired wavelengths that could otherwise leak through the system. The EXED chopper system parameters are such that the instrument can operate with the wavelength bands from 0.6 Å up to 14.4 Å centred at the region of interest.

a) b)

Fig. 3. a) Contour plot showing a *d*-spacing coverage as function of θ and λ. As the HFM limits θ to 2°-15° and 75°-85°, a thermal monochromatic instrument with λ = 1.8 Å will access only those *d*-values that appear under the vertical solid lines. A TOF instrument having access to wavelengths from 1 to 15 Å will cover the d-range in between horizontal dashed lines. b) Neutron flux measured on the EXED sample position.

For neutron detection EXED is equipped with 1/2" diameter position-sensitive ^{3}He detector tubes with ~50% efficiency for 1 Å neutrons. The effective length of the tubes is 0.9 m and position resolution is 1 %. These tubes are combined into 4 moveable detector banks with 48 tubes per bank. Two of these banks are positioned in backscattering and two in forward scattering to reflect the geometry of the magnet (Fig. 2). When the magnet rotates, the detector banks are shifted accordingly.

4. HFM-EXED operation

Finally, we turn to the most important question - what kind of experiments will become possible on EXED in combination with HFM? Since the magnet is permanently installed on one instrument, this instrument should be capable of doing several experimental techniques. This approach is contrary to the standard practice of neutron instruments which are usually optimized for one class of experiments only. In order to cope with a broad range of scientific tasks, EXED will operate in three modes: diffraction, small-angle neutron-scattering (SANS), and spectroscopy. The first two have been already commissioned while the spectroscopy is under construction. In diffraction-mode the instrument is suited for conventional crystallographic tasks, in particular studying static magnetic order in materials as a function of applied magnetic field. SANS-mode extends the accessible *d*-range beyond 500 Å enabling studies of matter in the nanoscale range such as e.g. vortex state in type-two superconductors. Finally, the spectroscopy-mode will make energy-resolved measurements on EXED possible. They will open a large area of research related to studying dynamics in materials with magnetic degrees of freedom.
Overall HFM-EXED has the ability to contribute to many areas of fundamental and applied research. Among them are current societal problems such as energy-related materials and energy storage and future information technologies. Understanding high temperature

superconductivity and the development of novel superconductors, along with other types of interesting and useful materials, remain in the focus of such research. Investigations of multifunctional materials for development of new technologies are necessary in order to establish the relationship between the lattice, spin and charge degrees of freedom. Experiments on various model materials that are not currently linked to applications constitute another important research branch. In these materials, novel quantum phenomena that are vital for the fundamental understanding of material properties will be studied.

5. Conclusions

In conclusion, the HFM-EXED facility is a unique combination of a high field hybrid magnet and a neutron-scattering instrument. It offers the highest static magnetic fields for neutron-scattering in the world. The field greatly exceeds those available elsewhere and is likely to do so for many years. Given this unique facility, HZB will concentrate on achieving cutting edge high-field neutron experiments until BER II research reactor stops operation in 2020.

References:

[1] See http://www.helmholtz-berlin.de/quellen/ber/index_en.html for reactor data
[2] See http://www.helmholtz-berlin.de/quellen/ber/instruments-neutrons/index_en.html for HZB instrument suite
[3] Ch. Rüegg, N. Cavadini, A. Furrer, H.-U. Güdel, K. Krämer, H. Mutka, A. Wildes, K. Habicht and P. Vorderwisch, Nature **423** (2003) 66
[4] B. Lake, H.M. Ronnow, N. B. Christensen, G. Aeppli, K. Lefmann, D. F. McMorrow, P. Vorderwisch, P. Smeibidl, N. Mangkorntong, T. Sasagawa, M. Nohara, H. Takagi & T. E. Mason Nature **415** (2002) 299
[5] M. D. Bird, T. Adkins, S. T. Bole, K. R. Cantrell, I. R. Dixon, A. V. Gavrilin, J. Lu, T. A. Painter, R. P. Walsh, H. W. Weijers, T. Xu, Y. Zhai, “The NHMFL hybrid magnet projects,” IEEE Trans. Appl. Supercond., vol. 19, pp. 1612-1616, 2009.
[6] J. Peters, K. Lieutenant, D. Clemens, and F. Mezei, Z. Kristallogr. 2006(Suppl. 23), 189–194.
[7] K. Lieutenant, J. Peters, and F. Mezei, J. Neutron Res. 14, 147–165 (2006).
[8] J. Peters, H-J. Bleif, G. Kali, L. Rosta, and F. Mezei, Physica B 385-386, 1019–1021 (2006).
[9] O. Prokhnenko, W-D. Stein, H-J. Bleif, M. Fromme, M. Bartkowiak, and Th. Wilpert, Rev. Sci. Instr. 86, 033102 (2015)

CHARACTERIZATION OF A *QUASI*-VERTICAL NEUTRON BEAM FROM THE BRAZILIAN TRIGA IPR-R1 REACTOR

A.S. LEAL, B. H. LEMOS
Centre for Development of Nuclear Technology (CDTN), Brazilian Nuclear Energy Commission (CNEN), Av. Antonio Carlos 6627 CAMPUS UFMG, CEP 31270-901 Belo Horizonte/Brazil

B.T. GUERRA
Federal University of Minas Gerais, Dept. of Nuclear Engineering Av. Antonio Carlos 6627 CAMPUS UFMG, CEP 31270-901, Belo Horizonte/Brazil

ABSTRACT

This work describes the experimental and calculated neutron flux from a proposed *quasi*-vertical beam from the TRIGA IPR-R1 Reactor's core. This beam was proposed as an alternative to evaluate the feasibility of installing a PGAA (Prompt Gamma Neutron Activation) facility at CDTN. The calculated, using the MCNP code, thermal and epithermal neutron flux and experimental results are presented and discussed. The results show that a thermal flux of 10^5 to 10^6 $cm^{-2}s^{-1}$ could allow some PGAA applications.

1. Introduction

1.1 The TRIGA IPR-R1 Reactor

The TRIGA IPR-R1 Mark-I, Fig. 1, is a pool type reactor installed at the Center of Development of Nuclear Technology (CDTN) in Belo Horizonte, Brazil since 1960. It is in operation since then at 100kW dedicated, mainly, to research, training, production of some radioisotopes and neutron activation analysis (NAA) [1-4]. A project to raise the power of operation to 250kW was concluded and the process of relicensing is under way. But, in spite of its long time of operation, like many others research reactors in the world, the TRIGA IPR-R1 Mark-I of the CDTN is largely sub-utilized. Less than 8% of its original fuel was burned during all the life of the reactor [5] !

In order to enhance the utilization of the reactor, a new project was launched in 2005. Since then several applications have been investigated involving the TRIGA reactor, such as, nanostructures and radiolabelled molecules focusing medical applications. In this context it has been also investigated the feasibility of enhancing the capacities of the NAA Laboratory with the installation of a new PGAA facility [6] .

The *quasi*-vertical beam, an aluminum tube from the core of the reactor till the floor's level, 6,5 meters above, see Fig. 2, was proposed as an alternative to run the PGAA using the TRIGA reactor. The tentative to extract neutron from the TRIGA's core started in the 80's, with a vertical beam tube s installed in the reactor, that time, to evaluate the potential of neutrongraphy investigations. This beam uses an aluminum tube with external diameter of 15,0 cm in top. During the operation, it is shifted from the pool´s wall to a position close to center of the reactor´s core. The idea of using the inclined tube is to avoid the heavy structure of the rack containing the shielding, the sample and the detector, be located directly over the reactor‘s pool, which would not be allowed for security reasons.

This work describes the MCNP (Monte Carlo N-Particle) model of the reactor and the proposed model for the beam. The preliminary results of the neutron flux measurements, experimental and

calculated are presented and discussed. One possible preliminary design for a future PGAA system at the TRIGA reactor is presented. An inclined, *quasi*-vertical tube of Al is the neutron guide from the core, located 6,0 meters from the reactor´s room level.

1.2 Proposed Design for the PGAA facility

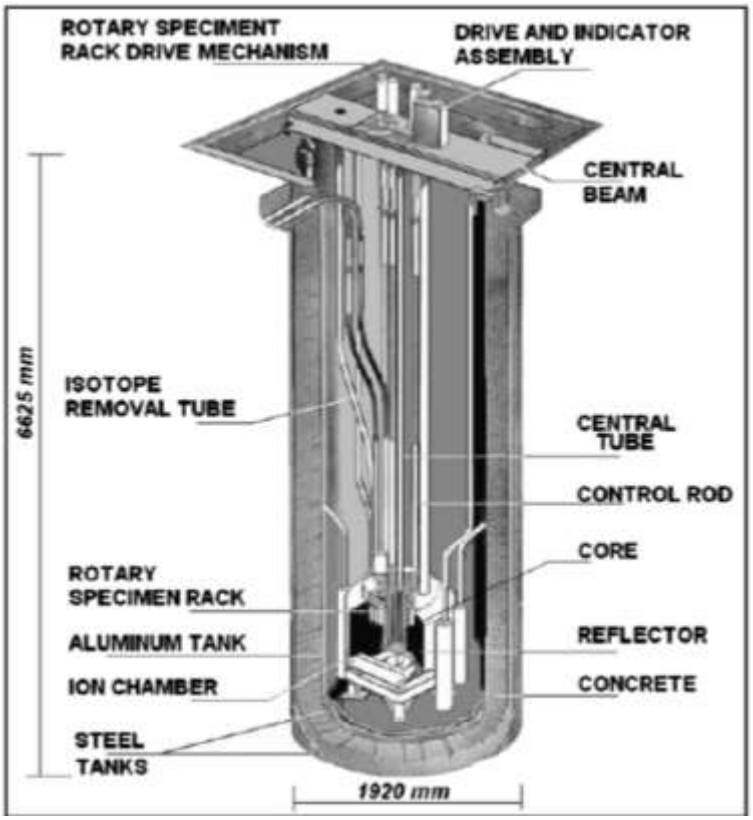

FIG 1. The TRIGA Mark 1 research reactor.

The initial calculations indicated that set the detector-sample-shielding system could be positioned at the height of approximately 2,0 meters from the floor. Figure 2 shows the preliminary design proposed model for a PGAA system at the TRIGA reactor. The inclined tube of Al is the neutron guide from the core to the reactor´s room level. The alternative of using the inclined tube is to avoid the heavy structure of the rack containing the shielding, the sample and the detector, be located directly over the reactor pool, which is not allowed for security reasons.

The basic design of m the system is illustrated in Figures 2 and 3. It is composed by the following main parts:

a) An aluminum guide tube with the diameter of 5 cm guides the neutrons from the top of the reflector in the core to the sample chamber;

b) The sample chamber, containing the sample holder and the detector, a 20–30% relative efficiency, HPGe detector covered with lead shielding leaving open just a small hole to the direction of the sample and the beam stop.

c) The shielding: borated paraffin is positioned around the tube externally from the wall and in the beam stop and lead box covering the sample holder.

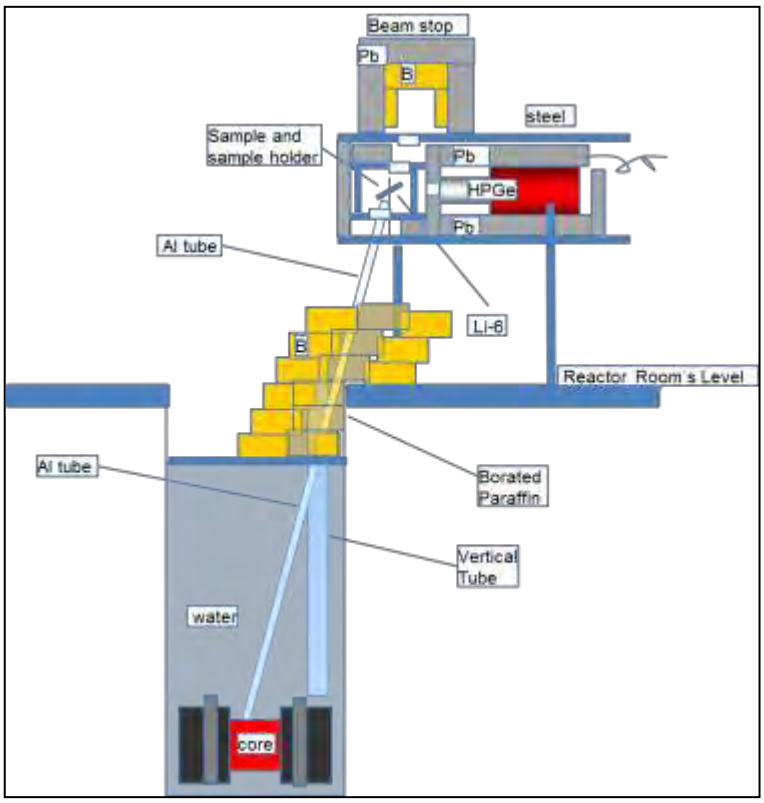

FIG 2. Preliminary no detailed model of the PGAA at the TRIGA Mark 1 reactor.

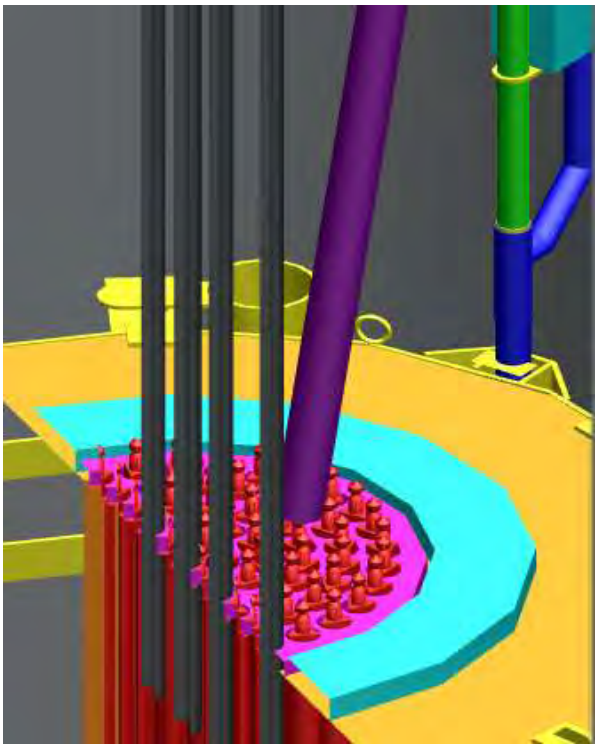

FIG 3. View from the core, top of fuel elements and the position of the neutron guide.

1.3 Computational Model

The code MCNP (Versions 5 and X) was used for evaluating the preliminary model of the system and to perform the calculations of the neutron flux in the inclined tube. The calculations reported in this paper were performed with version 5.1.40 of the code and with the ENDF/B-VII.0 cross section library (processed at the National Nuclear Data Centre at Brookhaven, obtained from the Radiation Safety Information Computational Centre at Oak Ridge), [7].

The thermal, (E < 0.625 eV), and epithermal (E < 100 keV) components of the neutron flux were calculated and compared with experimental results in order to validate and adjust the model of the system. Fast neutrons (E > 100 keV) were not investigated. The validation of the model using the flux measurements in vertical tube is a required preliminary step before the authorization for the experimental measurements using the inclined tube. In this work, the KCODE option of MCNP was set to 1.0 to 3.0 × 10^4 histories and 2500 to 3000 cycles were used. The software run in a Core Duo 2,5GHz processor with 50h of processing time, in average.

The performance of the MCNP model was validated comparing the results of the calculated and the experimental thermal neutron flux with measured in different positions of irradiation (3, 7 10, 20, 25 and 30) in the core of the reactor used for neutron activation analysis, Fig. 4.

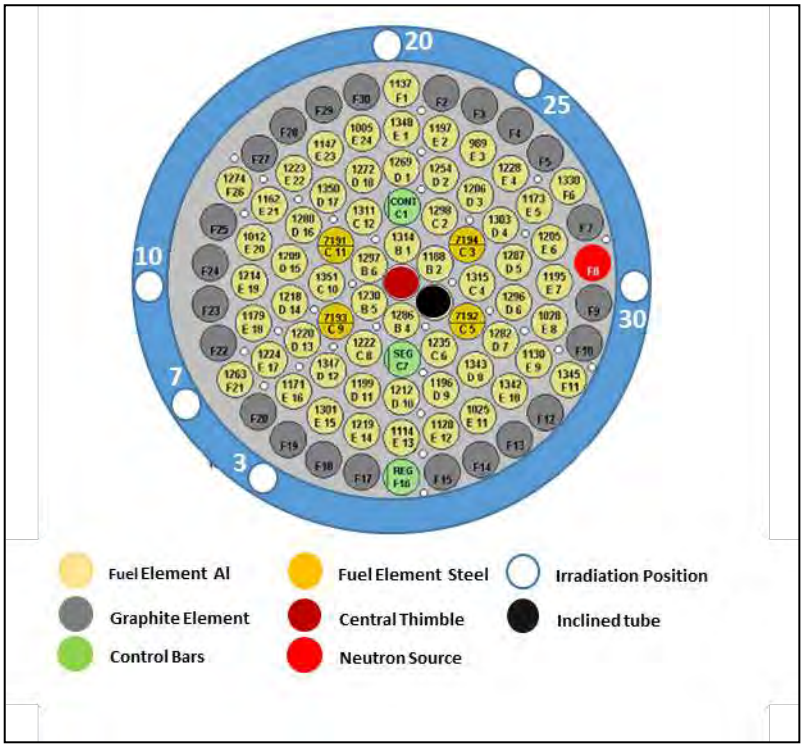

FIG 4. View from the core, top of fuel elements and the position of the inclined tube.

In order to visualize the behavior of the particles in the inclined tube and the geometry of the system beam-sample chamber, it was used the function *Particle Track* of the platform VISED of the MCNPX (Version X 24E-1), as it is illustrated in Fig. 9 [8]. The following parameters were used: number of particles to plot: 550 to 10.000, display: collision + tally, distance from the plot to plane: 100cm.

2. Experimental

2.1 Preparation of the Tube

Before to be inserted in the reactor´s pool, Figs. 5a and 5b, the aluminum tube was prepared as following: a ballast of 8,0 kg was fixed outside the at tube, approximately at its middle height, 2,6 meters height from the core. The weigh used was the minimum necessary for assuring no pressure over the head of the fuel elements in the core, Fig. 3. The ballast used was a set of cylindrical shells of type 304 stainless steel, connected by a sleeve outside the tube supported by an aluminum disc fixed to the tube by three screws in equidistant positions, Fig. 5b. On the disk, a support sleeve was also secured to the screw tube. As a safety factor, the whole system was tested and adjusted to support a load three times higher. In this position, the activation of the material was negligible.

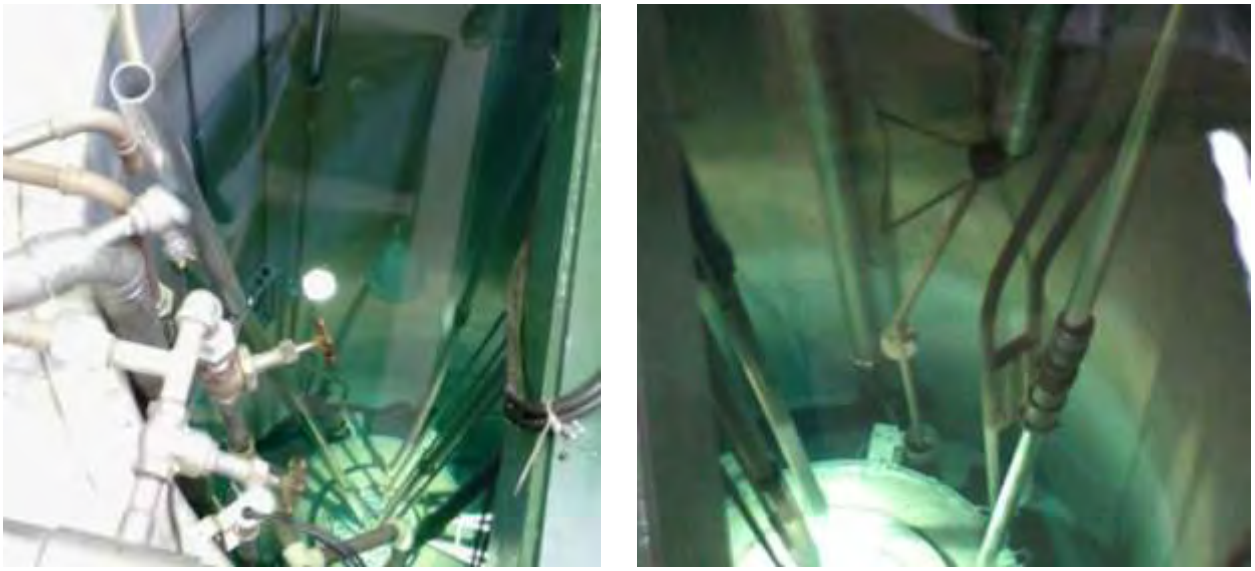

FIG 5. Views reactor´s pool. Inclined tube positioned over the core (right) and the ballast (left)

2.2 Measurement of the neutron flux

To determine the neutron flux in the inclined tube, disks of gold, (Au 100%), of 125 mg, 1.25 cm in diameter, and 0.06 mm height, bare and cadmium covered were used as flux monitors. Six monitors were inserted in the tube equally spaced in the 5,0 meters of the tube. The irradiation time was 4h, 8h, respectively, for bare, and cadmium covered samples. The reactor was operating at 100kW. The thermal and epithermal flux were determined from the gamma spectra of monitors using the formalism of Høgdahl convention. The gamma spectra of each sample was obtained using a system equipped with an HPGe detector GC 5019 and Genie 2000, v2.0 Spectroscopy software, provided by the Canberra Industries, Inc. The counting time was adjusted to provide a net peak area of, at least, 20,000 counts for the 411.8 keV peak from the ^{198}Au. Time counting varied according the position in the tube from 10 min to 15h [9, 10].

3. Results and Discussion

Fig. 6 illustrates the behavior of the experimental and calculated thermal neutron flux ϕ_{th}, with the vertical distance, Z(m), from the core to top of the reactor´s pool in the inclined tube. A good agreement was obtained between the experimental results and the MCNP model. It can be observed from the Fig. 6 that a thermal neutron flux of magnitude 10^5 could be obtained in the upper extremity of the tube. This result still must be confirmed experimentally but it suggests that, in principle, this design could be used for some PGAA applications. This scenario would be still more realistic with the possible future upgrade of the power reactor to 250 kW.

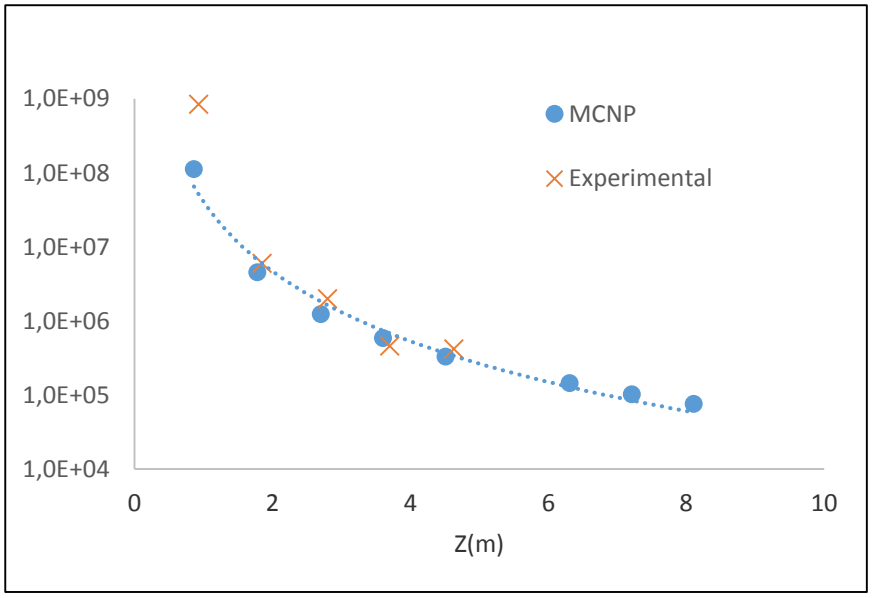

FIG 6. Experimental and calculated thermal neutron flux in the inclined beam of irradiation of the TRIGA Mark 1 reactor.

Table 1 shows the calculated, $\phi_{th(MCNP)}$, and experimental, $\phi_{th(EXP)}$ thermal fluxes in the inclined tube and the respective intrinsic MCNP error, $\Delta_{cod(\%)}$, and the relative calculated-experimental error, $\Delta_{exp.(\%)}$ with the vertical distance, Z(m), from the core of each point considered. The intrinsic relative error, Δ_{cod}, is lower than 10% for all the points calculated. The large relative, (Δ_{exp}), varying from 22 to 54% are due to the conjugated effects of the intrinsic code error and the several experimental uncertainties as the cadmium capsule, detector and counting efficiency and others. Additional experimental data are necessary to improve the accuracy of the measurements and to adjust the simulated the model for a better performance.

Table 1. Experimental, (EXP) and calculated (MCNP) thermal neutron flux, ϕ_{th}, ($cm^{-2}s^{-1}$), the relative, $\Phi_{th\ (EXP)}$, and intrinsic $\Phi_{th(MCNP)}$ errors in the inclined tube with the vertical distance Z(m) from the core.

Z(cm)	86	178	270	360	450	630	720	810
$\Phi_{th\ (EXP)}$	1.1×10^8	4.6×10^6	1.2×10^6	5.9×10^5	3.3×10^6	1.5×10^5	1.5×10^5	7.6×10^4
$\Phi_{th\ (MCNP)}$	1.7×10^8	6.0×10^6	2.0×10^6	4.6×10^5	4.2×10^5	--------	---------	--------
$\Delta_{exp(\%)}$	54	30	40	22	26	--------	---------	--------
$\Delta_{MCNP(\%)}$	9	10	2	3	3	2	2	2

Figure 7 shows a comparison of the results for the factor *f* (ϕ_{th}/ϕ_{epi}) for the calculated and experimental data from the inclined tube and two sets, (1) and (2),of experimental data thermal neutron flux obtained from the vertical tube, Fig. 2. The evaluation of f parameter is important to give an idea of the thermalization of the beam. Ideally, the neutron beam for PGAA applications must have energy lower than the thermal level [11]. It can be observed from the Fig. 7 that the neutron flux is more thermal for the same approximated vertical position, Z(m). These results give an idea about the behavior of the neutron flux in both experiments, but they cannot be compared directly due to the differences between the tubes, diameter and their relative position related to the core and geometry of each situation.

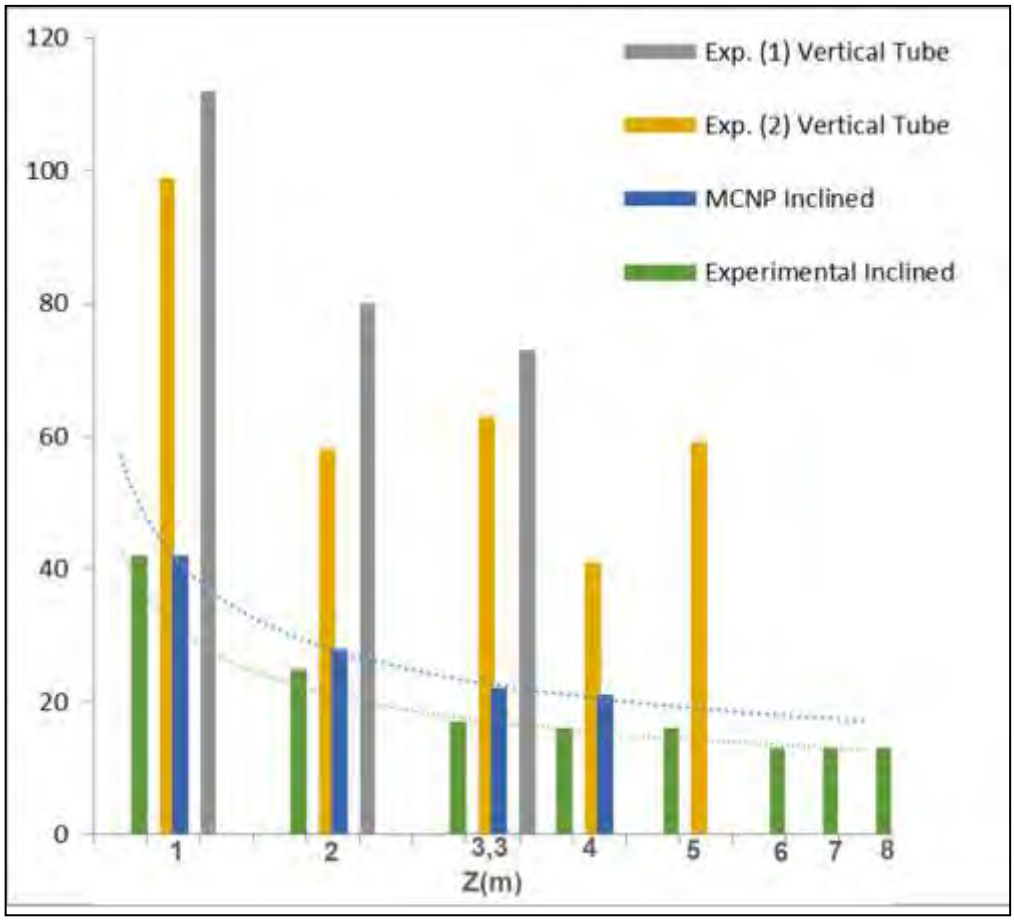

FIG 7. Experimental and calculated factor *f,* (thermal/epithermal) neutron flux in the vertical and inclined tubes of the TRIGA reactor.

Fig. 8 illustrates a frame of the population of the neutrons in the core of the reactor and across the incline tube. The box in the top of the tube is a simplified model of the set sample-detector-shielding. The function *particle track* of the VISED platform was used to illustrate the geometry of the system and to facilitate the identification of possible problems, such as the escaping of neutrons or photons in the reactor´s room. This graphical resource was very useful to demonstrate the safety of the preliminary experiments with the tube and how the system would work.

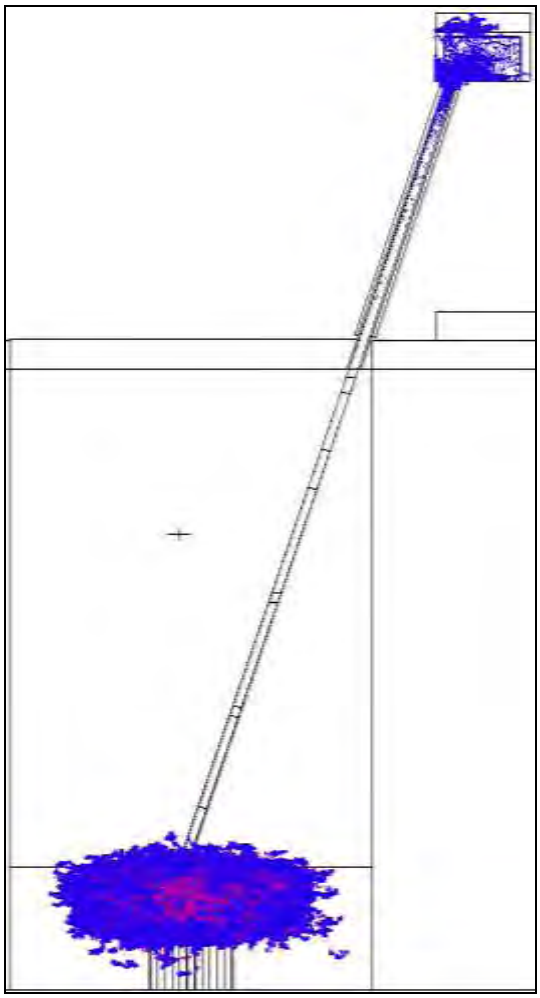

FIG 8. Picture of the “Particle Track” function obtained from the VISED platform of the MCNP code showing the core (bottom) the inclined tube and the model of sample-detector-shielding (up) of the TRIGA Mark 1 reactor.

4. Conclusion

The preliminary results, obtained from experimental data and the MCNP model for the proposed *quasi*-vertical neutron from the core of the TRIGA IPR 1 reactor, suggests that, in principle, the inclined tube could be used as a neutron guide for the PGAA facility. A more accurate definition about the feasibility of a future PGAA facility still requires a better characterization of both the thermal and epithermal neutron fluxes. The definition of power of operation of the TRIGA IPR-R1 is crucial for motivating these future investigations.

References

[1] D. M. Zangirolami, *MSc. Dissertation*: 100kW TRIGA IPR-R1 Neutron Flux Measurements, CDTN/Brazil, (2009)

[2] A. S. Leal, A.D. Carvalho Jr., F.M. Abrantes, M. A. B. C. Menezes, et.al., Production of the radioactive antitumoral cisplatin, *Applied Radiation and Isotopes*, 64, 178-181 (2006)

[3] A. S. Leal, K. Krambrock, L.G.M. Ribeiro, P. Vermaercke, L. Sneyers, Study of the neutron irradiation-induced colors in Brazilian topaz, *Nucl. Instr. Meth*. A: 580: 423-426 (2007)

[4] A. S. Leal, M. A. B. C. Menezes, R. Jacimovic, F. P. Sepe, T. C. B. Gomes, Investigation of the quality of the drug Enalapril commercilized by pharmacies of amnipulation in Belo Horizonte, Brazil*. J. Radioanal Nucl Chem DOI 10.1007/s10967-014-3073-6:* (2014)

[5] Dalle H., Simulatyion of the TRIGA IPR-R1 Reseacrh Reactor Using the MCNP, *PhD Thesis*, UNICAMP/Brazil (2005)

[6] A. S. Leal, R. Jacimovic, M.A.B.C. Menezes, B. T. Guerra, Proposed Design for the PGAA Facility at the TRIGA IPR-R1 Research Reactor*. SpringerPlus* 2:597, (2013)

[7] Briesmeiter. MCNP5 A General Monte Carlo N-Particle Transport Code Version. Los Alamos, LA/USA, (2005)

[8] Visual Editor Class Files (Version visedX_24J), (2013)

[9] De Corte F. The k0 standartization method. Ed Gent Weltenschappen (1987)

[10] S. Parry, Handbook of Neutron Activation Analysis. Viridian Publ. UK (2003)

[11] Molnar G.L Handbook of PGAA with Neutron Beams. Kluwer Acad. Pub. Netherlands (2004)

RECENT IRRADIATION TESTS FOR FUTURE NUCLEAR SYSTEM AT HANARO

MAN SOON CHO*, KEE NAM CHOO, SEONG WOO YANG, SANG JUN PARK

Korea Atomic Energy Research Institute
989-111 Daedeok-daero, Yuseong-gu, Daejeon, 305-600, The Republic of Korea
** mscho2@kaeri.re.kr, Tel : +82-42-868-8431, Fax : +82-42-863-6521*

ABSTRACT

The capsule at HANARO is a device that evaluates the irradiation effects of nuclear materials and fuels, which can reproduce the environment of nuclear power plants and accelerate to reach the EOL condition. As the integrity assessment and the extension of lifetime of NPP are recently considered as important issues in Korea, the requirements for irradiation tests are gradually being increased. The capacity and capability of irradiation tests at HANARO are becoming important because Korea strives to develop SFR and VHTR among the future nuclear system and to export the research reactors and to develop the fusion reactor technology. And also, U-Mo plate type fuel is being developed for use at the new Korean RR and use as LEU fuel for RERTR program. Recently, the irradiation tests of VHTR coated particle fuel and cladding material were conducted in the first half of 2014. In the end of this year, the fusion reactor materials called ARAA developed by some of KAERI's researchers, and mortar concrete material as well as Si and SiC etc. will be irradiated. In addition, SPND will be irradiated to verify the long-lived irradiation performance. And the tests of SFR fuel and PWR up-grade fuel will be conducted. In addition, the researches on the irradiation characteristics of super-conductor materials, Si and SiC etc. are being progressed as a part of fundamental research.

1. Introduction

HANARO has been operating as a platform for basic nuclear research in Korea and the functions of its systems have been improved continuously since its first criticality in February 1995. It is now being successfully utilized in such areas as fuel and material irradiation tests and neutron transmutation doping to meet industrial, academic, and research demands. Among the irradiation facilities, the capsule is the most useful device for coping with the various test requirements at HANARO. Most of irradiation testing using capsules have been performed under the condition of helium gas and at specimen temperatures of 300-500℃ within four reactor operation cycles at HANARO. There are 23 hexagonal and 8 circular flow tubes in the core and some circular flow tubes are located outside the core reflector region such as OR, IP, PTS, LH and NTD. Table 1 shows the maximum fast neutron fluxes calculated by the HANARO core analysis system in the CT, IR2, OR5 and IP5 irradiation holes. Because of the difference in fast neutron flux, the irradiation hole was selected according to the target fast neutron fluence. CT and OR5 irradiation holes were used for the irradiation test of nuclear materials owing to a high fast-neutron flux. The irradiation test for electromagnetic materials is conducted in IP and other irradiation holes with a high thermal-neutron flux.

Table 1. The maximum fast neutron fluxes of irradiation holes

Irradiation hole	Fast neutron flux (n/cm^2-sec)
CT	1.95×10^{14}
IR2	1.76×10^{14}
OR5	1.92×10^{13}
IP5	5.82×10^{10}

2. Irradiation devices at HANARO

The RPV materials of PWR are placed in the environment of coolant of about 300℃ during operation. As the reactors planned in the Gen-IV program will be operating under higher temperature and neutron flux, the temperature and flux at the requirement are gradually raising. The operating temperatures of the VHTR and SFR are expected to be about 1,000℃ and 550℃, respectively [1]. On the other hand, KAERI tries to develop and export new research reactors. Materials used for the reflectors are graphite, beryllium, and zircaloy. They are operating at the low temperature of less than 100℃. The requirements for irradiation temperature have been variously changed according to the environments of the specimens. The capsules at HANARO have been developed to meet the temperature requirements.

2.1 Standard material capsule

The standard capsule, which is usually called the instrumented material capsule, is shown in Figure 2. It is a cylindrical shaped stainless steel tube, and the main-body is about 60 mm in diameter and 870 mm in length. The main body has five stages of specimen holder which control temperatures independently. It includes the specimen, the specimen holder that plays a role of thermal media. It is filled with He gas. The temperatures of the specimens are adjusted by controlling He pressure between 0-760 torr during reactor operation. The standard capsule is mostly used for irradiation at temperatures of 250–400℃. It has an important role in the safety evaluation of the reactor core materials and the development of new materials through the irradiation tests.

Figure 1. Specimens, parts, and standard capsule

2.2 Irradiation capsule for the RR materials

Recently, KAERI is involved in the development of 2 research reactors, JRTR in Jordan and KJRR in Korea. So, the irradiation data of the core materials such as graphite, Be, Zircaloy-4 are required. The Irradiation of the reactor materials is required to be irradiated at temperature of less than 100°C. The concept of the capsule is the direct contact with the coolant to cool the temperature of specimen down. The capsule is formed the reactor coolant

to pass through the bottom hole, as shown in Figure 2. The configuration is different with the closed type of standard capsule in which He gas is filled. This capsule is called the low-temperature capsule.

The specimens are basically put in a tube 1 mm thick and made of stainless steel. The surfaces of the enclosed tubes and the external tube come in contact with the cooling water during the irradiation tests. This capsule is used for irradiation of the reflector material of the research reactor, such as graphite [2], beryllium, and zircaloy-4, because the research reactors are usually operating at low temperature (<100℃). The post-irradiation properties such as the growth, tensile strength, hardness, swelling, and thermal diffusivity will be investigated. The results will be utilized for an acquisition of the irradiation data necessary for the design of research reactors such as JRTR and Ki-jang.

Figure 2. Low-temperature capsule

The low temperature capsule was successfully tested for 4 cycles and transferred to a hot cell of IMEF. Figure 3 shows the variation of temperatures of the specimens during the irradion test at the CT Hole of HANARO.

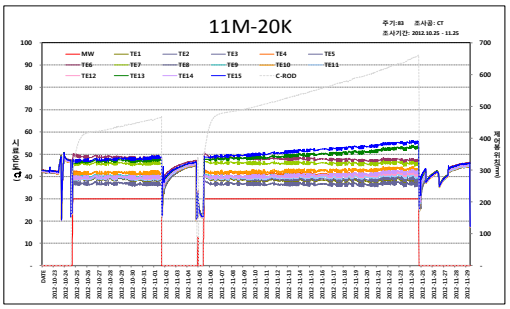

Fig. 3. Irradiation temperature of the low-temperature capsule

2.3 Irradiation capsule for future nuclear system

1. Capsule with solid thermal media

As future nuclear systems such as VHTR and SFR will be operating under conditions of high temperature and high neutron flux, a new type of irradiation capsule with double-layered thermal media composed of two kinds of materials, Al-Ti and Al-graphite, is being designed and fabricated, enabling it to be tested at higher temperature than a single thermal media capsule. Graphite and Ti materials combined with Al are used as the thermal media instead of Al in the standard capsule because Al might melt at high temperature. The high-temperature irradiation capsule has been developed as the concept with double thermal media, as shown in Figure 4. Because the Al thermal media used in a standard capsule might melt at high temperature, other materials enduring high temperature such as Ti or Zr would be used as the inner thermal media holding specimen. Recently, the first irradiation

test of the high-temperature capsule was conducted, in which the specimen temperature reached to 850℃. The irradiation test up to 1,000℃ will be conducted in the year 2016. In the first irradiation capsule, Ti and graphite were used as the inner thermal media, and Al was used as the outer thermal media. When the temperatures of the specimen were 850℃, the temperatures of the outer thermal media were lower than 550℃, and thus there was not much possibility of melting.

Figure 4. Structure of double thermal media

When the inner thermal media is Ti, and the outer is Al in the design of the double thermal media capsule, the analysis for temperatures when the specimen reaches 1,000℃ is important to evaluate the integrity of the components during irradiation. The temperature of the outer thermal media was calculated and reviewed to determine whether it would reach the melting of Al. When Ti/Al are used as inner/outer thermal media in a high temperature capsule, the temperature of outer thermal media reaches around 745℃, at which Al melts. Figure 5 shows the temperatures for various thermal media. According to the result, it would be better not to use Al as thermal media in a high-temperature irradiation capsule. Instead, Fe or Ni are recommended as the outer thermal media when a capsule will be used for high-temperature irradiation of up to 1,000℃ [3].

Figure 5. Temperatures of specimen and thermal media at each stage

2. Capsule using the liquid metal as thermal media

Since the irradiation tests for the future nuclear system SFR and VHTR will be conducted at relatively high temperature. it is desirable not to use aluminum as the thermal media of the high-temperature irradiation capsule due to the low melting point. As an alternative material of aluminum, the liquid metals such as NaK, LBE are being reviewed. NaK is a cooling medium of SFR, and thus it is desirable to conduct the irradiation test in the environment of NaK in order to study the irradiation features of SFR materials. However, it is highly reactive with water and may catch fire when exposed to air, so it must be handled with special precautions. It is not so desirable to use NaK at the irradiation test of capsule.

LBE is a eutectic alloy of lead and bismuth used as a coolant in some nuclear reactors, and is a proposed coolant for the lead-cooled fast reactor, part of the Gen-IV reactor initiative. LBE has significantly higher boiling points as compared to NaK, so it can be operated without risk of coolant boiling at higher temperature and improve thermal efficiency. Besides, it does not react easily with water or air, and has an excellent radiation shield

blocking gamma radiation. Even though LBE is more corrosive to steel than NaK, it is very advantageous to use LBE rather than NaK as the liquid thermal media in the capsule. Therefore, LBE is strongly recommended as a liquid thermal media for the high-temperature irradiation capsule instead of aluminum. In order to use LBE as a thermal media instead of NaK in the capsule, the effects of both materials exerted at the temperature of the specimens need be evaluated before using at the irradiation test. The overall shape of the capsule with the liquid metal thermal media is quite similar to the present standard material capsule except for using the liquid metal instead of aluminum as the thermal media.

The results of thermal analyses for the capsules with the solid and liquid thermal media, in which the solid thermal media is Al and the liquids are NaK and LBE, are shown in Figure 6. When NaK is used as the thermal media in the capsule, the specimen reaches the target temperature of 550 ℃ when G1, G2, T1 and T2 are 0.1, 1.0, 0.5 and 0.1 mm respectively. For the capsule with the same gaps and thicknesses, the temperature of specimen reaches 585 ℃ in case of Al thermal media, and 933 ℃ in case of LBE thermal media.

Figure 6. Temperature distribution of the capsules with 3 kinds of thermal media

This experiment was originally conducted to analyze the irradiation characteristics of SFR core materials. The SFR core materials will be placed under the atmosphere of NaK of 550 ℃. If it is the test in connection with the temperature distribution of specimen, the trend of the temperature distribution between NaK and LBE is similar, but the absolute temperatures will be adjusted according to the gap and He pressure. It does not have a great influence to the temperature distribution whatever liquid is used. Thus, the experiment to evaluate the temperature of the specimen may be as well conducted in LBE as in NaK.

3. Recent Utilization of Irradiation Capsules

As the integrity assessment and lifetime extension of an NPP are posing a big social issue around the world after the Fukushima accident, the irradiation data for structural materials and nuclear fuels for NPP are indispensable, and some are urgently required in Korea. Because the future nuclear energy systems are being developed as a method to obtain a new energy source worldwide, and Korea is participating in the development of an SFR and VHTR, the irradiation capabilities are emerging as an important issue. Recently, the irradiation tests for research reactor materials and RPV materials of power plants have been finished at HANARO. In addition, the irradiation tests for VHTR fuel and Zirlo fuel cladding material were conducted in the first half of the year. From the end of 2014, the fusion reactor materials, such as mortar concrete [4] and Si and SiC [5], will be irradiated. U-Mo fuel and SFR fuel, the up-grade of PWR fuel, are planned to be irradiated. The current status and future plan of the irradiation tests at HANARO are shown in Figure 7.

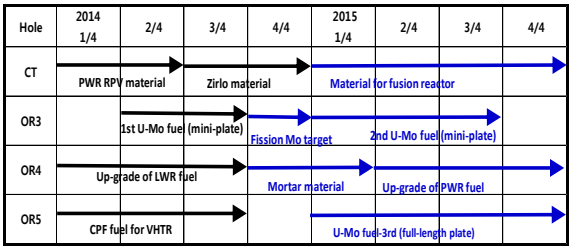

Figure 7. Plan of irradiation tests at HANARO

4. CONCLUSION

Korea is conducting R&D programs relevant to new nuclear systems including research reactors, future nuclear systems such as a VHTR, SFR and fusion reactor systems. In addition, research on the irradiation characteristics of super-conductor materials and new electronic materials is being conducted as a part of fundamental research. Irradiation tests at HANARO are mostly related to the R&D relevant to the ageing management and safety evaluation of an NPP and development of the future nuclear system and production of design data of a research reactor. The HANARO irradiation capsule system has been developed and actively utilized for the irradiation testing of fuels and materials. Although the irradiation tests up to the present have been performed usually at temperatures below 300℃, the various capsules for high- and low-temperature irradiation are being developed at HANARO with the irradiation requirements according to development of the Gen-IV nuclear system and the new research reactors

ACKNOWLEDGEMENTS

This work was supported by the National Research Foundation of Korea (NRF) grant funded by the Korea government (MSIP**) (**NRF-2013M2A8A 1035822**)**

REFERENCES

[1] J.Y. Park, “Possibility of Fusion Applications of Current Materials R＆D for GEN-IV Nuclear Energy System in KAERI”, Korea-Japan Blanket Workshop (2009).

[2] Y.M.Lee, et. al., “A study on the irradiated strength and stress evaluation of nuclear graphite material”, Nuclear Engineering and Design 269, 193-199 (2014)

[3] M. H. CHOI et al., “Temperature Evaluation of an Instrumented Capsule After Material Irradiation Tests in HANARO”, Journal of Nuclear Material, 362, 19-25 (2007)

[4] K. William, et. al., “A review of the effects of radiation on microstructure and properties of concrete used in nuclear power plants”, U.S. NRC, NUREG/CR-7171, 2013

[5] H.S. Jung, et. al., “Microwave losses of undoped n-type Silicon and undoped 4H-SiC single crystals at cryogenic temperatures” Electron Mater. Lett. Col 0. pp 1-9 (2014)

EXPERIMENTAL POSSIBILITIES OF RESEARCH FAST REACTOR BOR-60

V.V. KALYGIN, A.L. IZHUTOV, YU.M. KRASHENINNIKOV,
I.YU. ZHEMKOV, YU.V. NABOISHCHIKOV, A.V. VARIVTSEV
JSC "State Scientific Center Research Institute of Atomic Reactor"
Dimitrovgrad-10 433510 Russian Federation

INTRODUCTION

The BOR-60 fast neutron research reactor is one of the leading test facilities in Russia and worldwide in large-scale testing of a wide range of nuclear materials and items. The reactor has been operating safely and efficiently for more than 44 years. Along with the well-equipped material test laboratories and pilot fuel fabrication and reprocessing it has unique experimental capabilities to conduct comprehensive research in different areas.

The scientific results obtained in the reactor made it possible to show feasibility of structural materials, fuel pins and absorbers for the BN-350 and BN-600 fast reactors and for other reactor types. Below are the experimental capabilities and a short list of the conducted research.

1. Design features of the reactor

The reactor has a two-loop three-circuit heat removal process (Figure 1). Heat is recovered in sodium-air heat exchangers and sodium-water heat exchangers (steam generators) with power generation and heat transference via a heating unit to RIAR heating network. Heat and electrical power generation allows increasing the reactor economic efficiency [1, 2].

The vessel-type reactor is accommodated in a heavy concrete well. Under the well there is a monolithic concrete slab. There is external radiation shielding around the reactor in the well providing a decrease in radiation flux on the concrete to the established limits and biological shielding for the personnel.

The reactor has a vertical cylindrical vessel of variable cross-section made of welded cylindrical shells with conical junctions (Figure 2). The vessel has an elliptic bottom with an axial sleeve for the coolant inlet. The middle and bottom parts of the vessel are enclosed in a sealed safety jacket. The upper part of the jacket is intended to support the vessel. In the middle cylindrical part of the vessel there are two sleeves for the coolant outlet. The upper part of the vessel is a flange to mount a reactor core basket. Inside the cylindrical part of the vessel there are two cylindrical shells serving as a thermal shield intended to arrange a coolant flux from the reactor inlet to cool the vessel wall in the core.

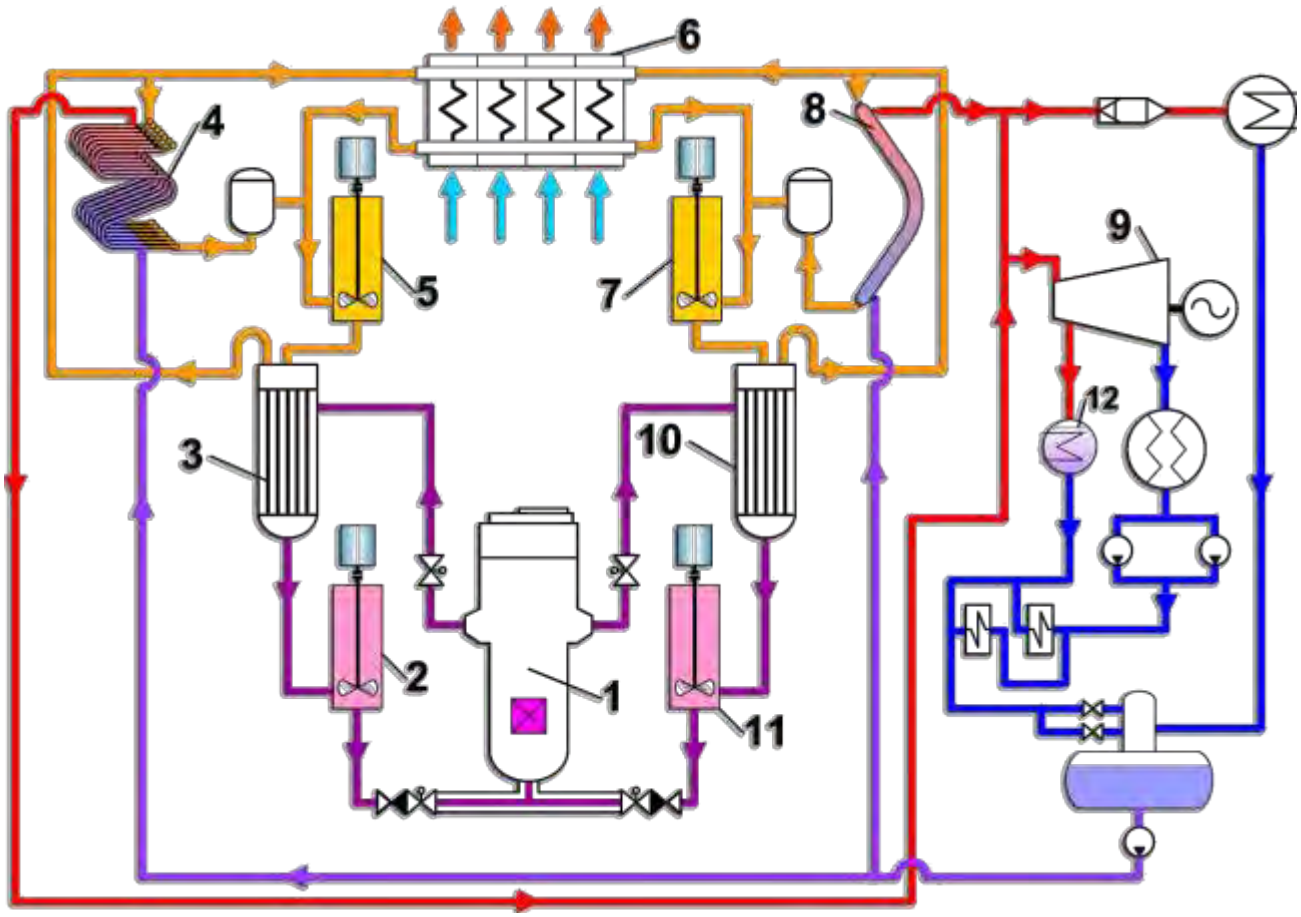

Fig 1. Simplified flow sheet of the BOR-60 reactor

1-reactor; 2, 5, 7, 11 – primary and secondary pumps, 10 – intermediate heat exchangers; 4, 8 – steam generators; 6 – air heat exchanger; 9 – turbine, 12 – heating unit.

The vessel is sealed on the top with two eccentric rotating plugs intended for refueling and biological shielding (small and large rotating plugs (SRP and LRP)). There are control rod driving mechanisms on the upper plate of the SRP. Inside the reactor vessel there is a basket to accommodate core FAs, blanket assemblies and rotating plugs. A pressure header flange is fastened to the basket lower end being one of the BOR-60 crucial points in terms of ensuring thermal and hydraulic irradiation conditions. It is intended to install core FAs, blanket assemblies, control rod sleeves as well as for hydraulic profiling of sodium flow rate through the FAs and blanket assemblies.

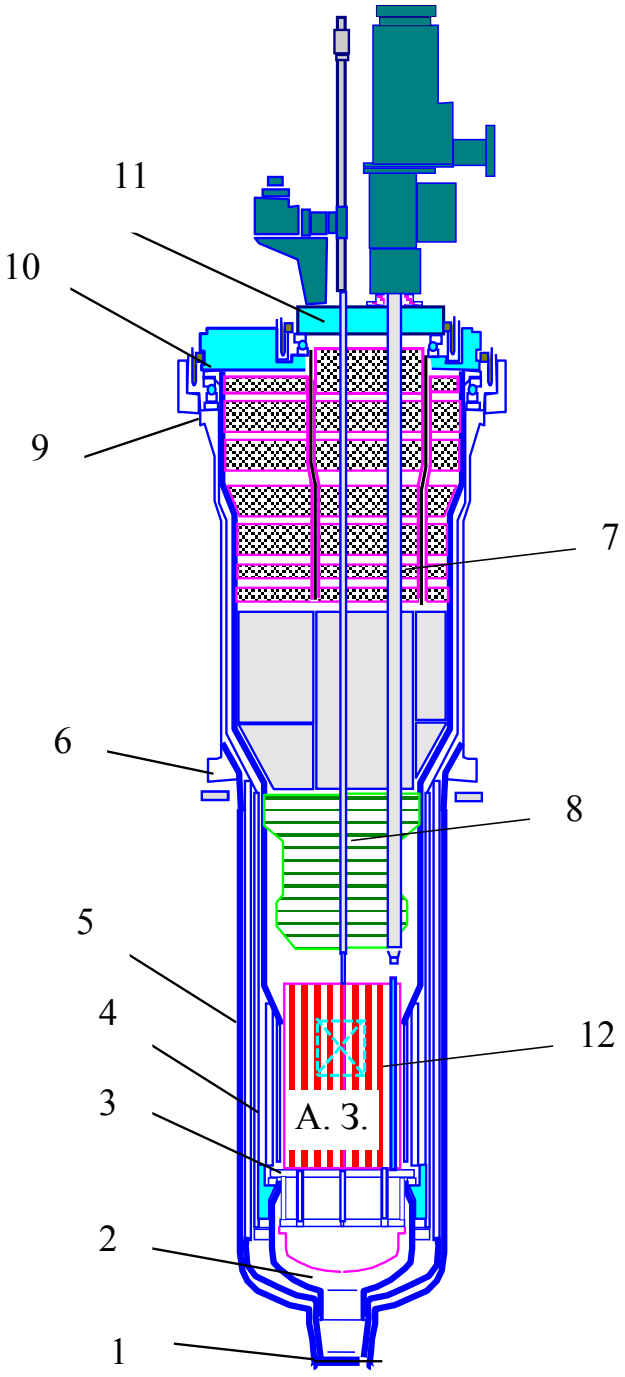

Fig 2. BOR-60 sectional view

1 – inlet sleeve, 2 – pressure collector, 3 – basket, 4 – thermal and neutron shielding of the reactor vessel, 5 – safety jacket, 6 – support flange, 7 – refueling channel, 8 – control rod driving mechanism, 9 – support flange, 10 – large rotating plug, 11 – small rotating plug, 12 – core assemblies and blanket assemblies

2. Reactor main parameters

The BOR-60 reactor main parameters are given in Table 1. In BOR-60 the assemblies are accommodated in a hexagonal grid, a total of 265 cells (Figure 3). There are up to 156 cells for the core FAs and 7 cells for control rods. The remaining cells are filled with blanket assemblies. Test fuel assemblies can be accommodated in any cells (except for the

cells with control and safety rods). The amount of FAs loaded in the reactor ranges from 75 to 130 depending on the burnup, core arrangement and fuel parameters [1].

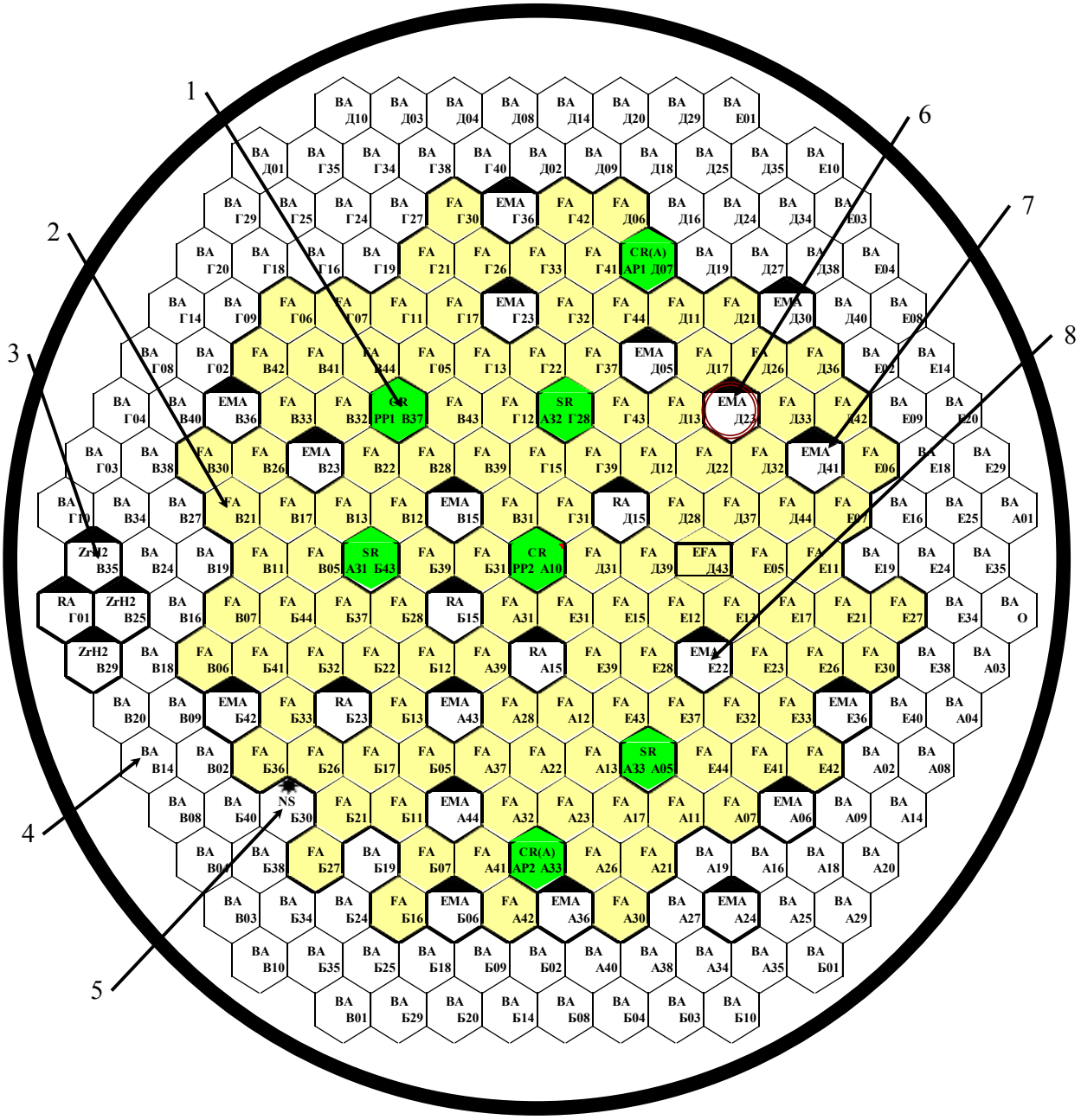

Fig 3. BOR-60 core arrangement

1 – control rod, 2 – FA, 3 – zirconium hydride, 4 – blanket assemblies, 5 – neutron source, 6 – instrumented cell (D23), 7 – material test assembly 8 – assembly for radionuclide accumulation

Parameter	Value
Thermal power, MW	up to 60
Electrical power, MW	up to 12
Heating output, Gcal/h	25
Sodium flow rate through the reactor, m^3/h	up to 1100

Sodium velocity in the core, m/s	up to 8
Coolant temperature, °C: reactor inlet reactor outlet	 300÷340 up to 540
Fuel	UO_2 or UO_2-PuO_2
Enrichment in ^{235}U,%	45÷90
Maximum Pu content,%	40
Peak volumetric power density in the core, kW/l	1100
Peak neutron flux density, $cm^{-2}s^{-1}$	$3.7x10^{15}$
Average neutron energy, MeV	up to 0.4
Neutron fluence per year, cm^{-2}	$3x10^{22}$
Damage dose accumulation rate, dpa/year	up to 25
Fuel burnup rate, %/year	up to 6
Power peaking factors: axial radial	 1.14 1.15

Tab 1: The main BOR-60 parameters

3 Main irradiation test parameters

3.1 In-pile tests

Due to a designed possibility to change over a wide range the core dimensions a large number of test assemblies may be loaded in different reactor cells. The neutron flux density (Fn) in some cells may vary by more than 3 times with the peak value of 3.7×10^{15} $cm^{-2}s^{-1}$ (at a thermal power of 60 MW and tight reactor loading). The above factors allow loading of different fuel compositions in the reactor and achieving almost any burnups. In doing so, up to 20 test rigs (TR) with structural materials can be accommodated in the core. The number of test FAs with advanced fuel compositions in the core and TRs with structural materials in the blanket is almost not specified.

A special thermometric channel is used for the instrumented irradiation tests. It allows placing the test rigs directly in the core with displaying the material irradiation conditions via 30-50 communication lines.

Figures 4–6 show the main neutronic parameters of the reactor at a power of 55 MW [3].

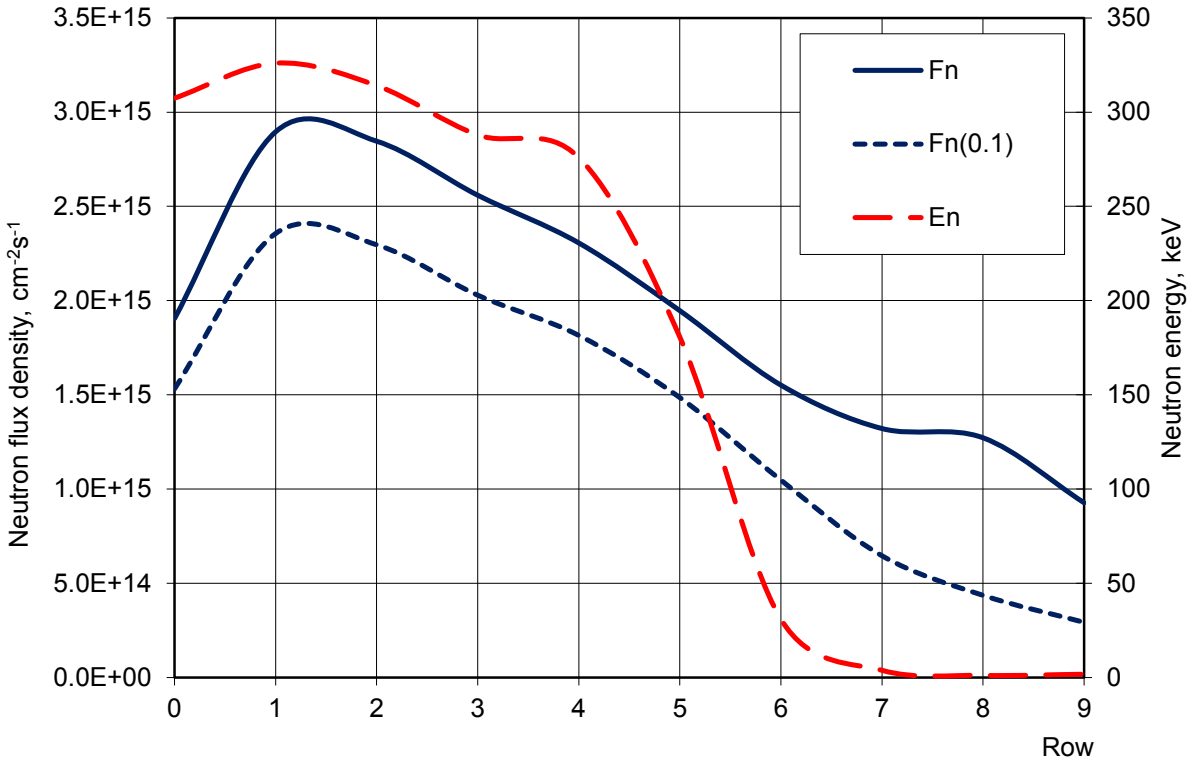

Fig 4. Radial distribution of the BOR-60 main neutronic parameters (average neutron energy (En), integral (Fn) and E>0.1 Mev neutron flux density (Fn(0.1))

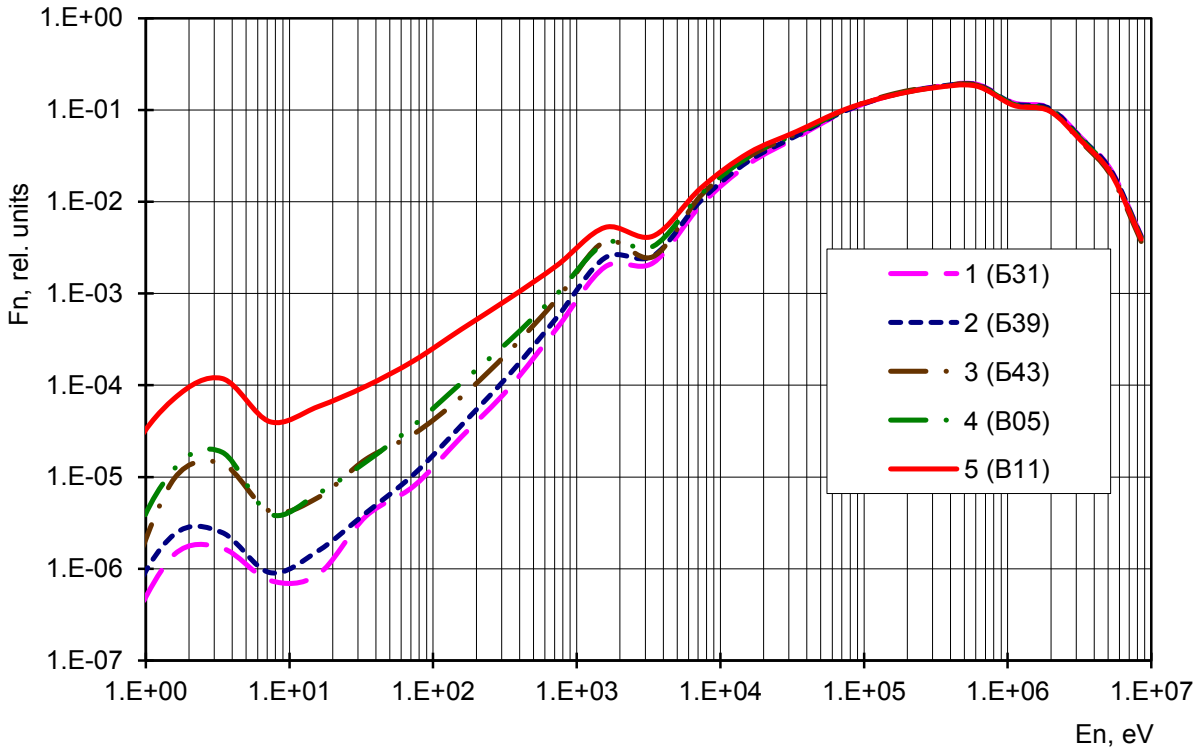

Fig 5. Neutron spectra in the BOR-60 core – row (cell name)

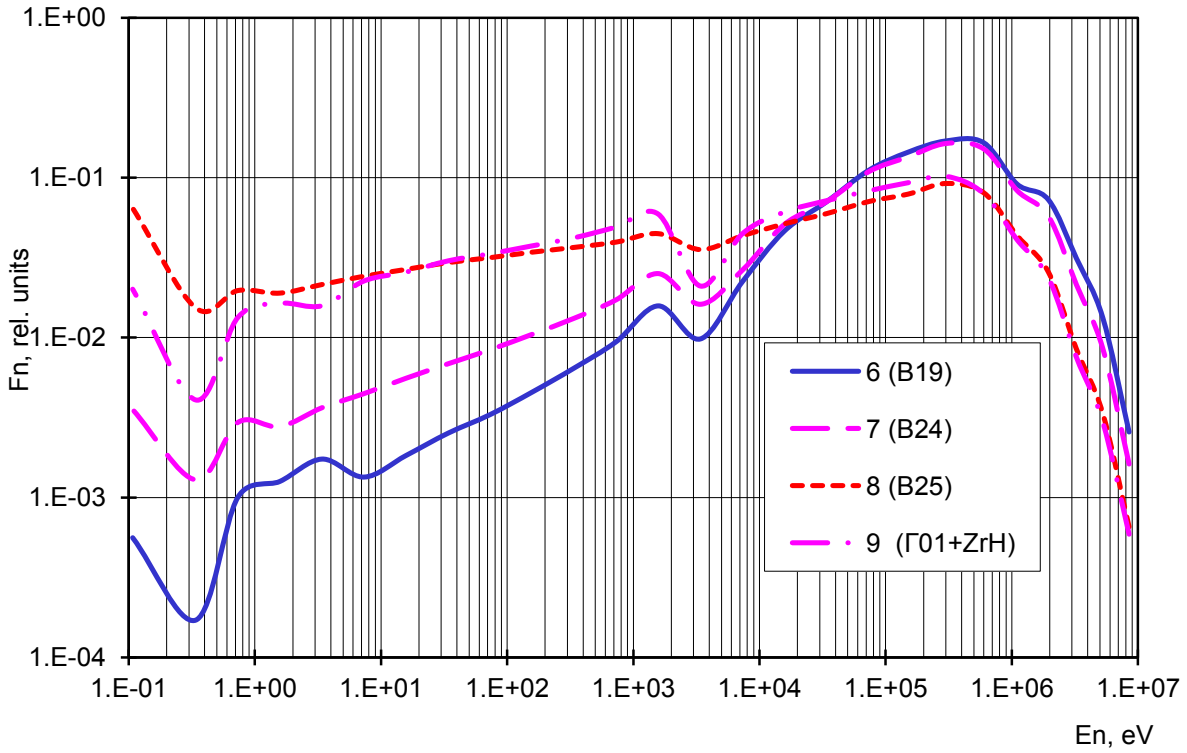

Fig 6. Neutron spectra in the BOR-60 blanket – row (cell name)

A test channel to perform instrumented irradiation tests is distanced at 196 mm from the core axis above fifth row cell D23 (Figure 3). The lower part of the test rig is a standard FA (a bottom nozzle and a hexagonal tube 44 mm width across flats). Table 2 presents the main D23 cell parameters.

Parameter	Value
Neutron flux density, $cm^{-2}s^{-1}$	$2x10^{15}$
Irradiation specific power density in structural materials (Z = 26÷30), W/g	4
Gamma radiation absorbed dose, Gy/s	$4.5x10^{3}$
Radiation density peaking factor along the core length (450 mm): neutrons gamma radiation	 1.13 1.25
Sodium flow rate, m^3/h: feeding from a high pressure chamber feeding from a low pressure chamber	 up to 8 up to 2

Tab 2: Irradiation conditions for materials and items in D23

It is a common practice to conduct short-term verification tests in the instrumented cell (D23) of BOR-60 to collect the information of interest. Then the irradiation is continued in the cell with the desired parameters. The parameters of different BOR-60 cells are given in Table 3.

Cell, row	E31, 1	A43, 3	D23, 5	D35, 8

Cell, row		E31, 1	A43, 3	D23, 5	D35, 8
Cell center radius with reference to the core center, mm		45	135	196	360
Neutron flux density, 10^{15} $cm^{-2}s^{-1}$: - E>0.0 Mev (F0) - E>0.1 Mev (F0.1)		 3.4 2.8	 3.1 2.5	 2.5 2.0	 1.2 0.6
Damage dose accumulation rate in steel (DPA), 10^{-6} dpa/s		1.4	1.3	1.0	0.2
K_z(core), rel. units	F0	1.15	1.16	1.15	1.12
	F0.1	1.17	1.17	1.17	1.15
	DPA	1.18	1.18	1.18	1.16
K_r(core central plain), rel. units	F0	1.00	1.05	1.09	1.13
	DPA	1.01	1.06	1.11	1.31
Neutron flux density fraction (E>0.1 MeV), rel. units		0.83	0.82	0.80	0.50
Average neutron energy, keV		350	320	250	40
Neutron fluence, 10^{22} cm^{-2}	E>0.0 MeV	5.5	5.0	4.1	1.9
	E>0.1 MeV	4.6	4.1	3.3	1.0
Damage dose in steel, dpa		24	21	17	4
1 year of irradiation - WT≈ 250 000 MW×h, Kz and Kr are axial and radial peaking factors.					

Tab 3: Neutronic parameters in different cells ($W_{reactor}$=55 MW)

3.2 Use of out-of-vessel equipment

The reactor is equipped with four horizontal channels and nine vertical channels accommodated beyond the reactor vessel. The channels are used mainly for irradiation of electrical materials and radiation doping of silicon (Figure 7)

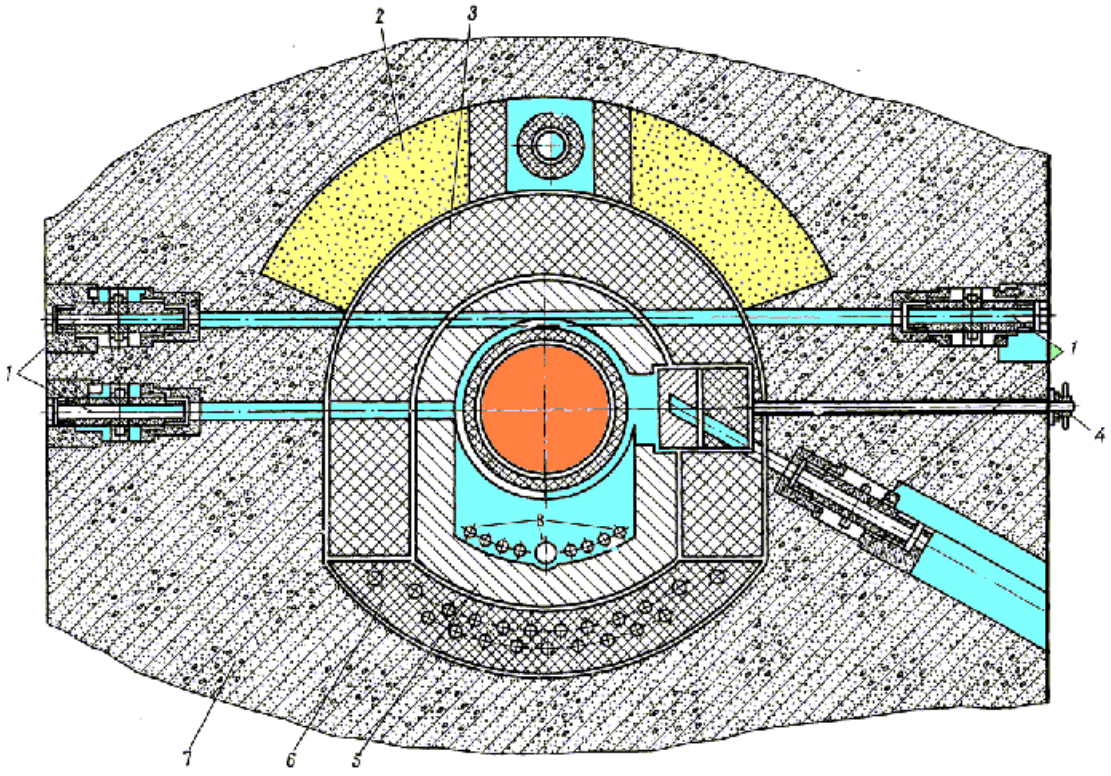

Fig 7. Layout of BOR-60 horizontal and vertical channels

1 – horizontal channel, 2 - sand, 3 – iron oxide, 4 – scatterer driver, 5 – cast iron, 6 - graphite, 7 - concrete, 8 – vertical channels

The Fn peak value in a vertical channel at a thermal power of 55 MW makes up $\approx 3.6\times10^{13}$ $cm^{-2}s^{-1}$, the fraction of Fn with energy higher 0.1 MeV amounts to ≈ 0.15÷0.25 rel. units, average neutron energy En ≈ 3 keV. When the vertical channel is surrounded by a moderator, the thermal neutron flux increases significantly (Figure 8).

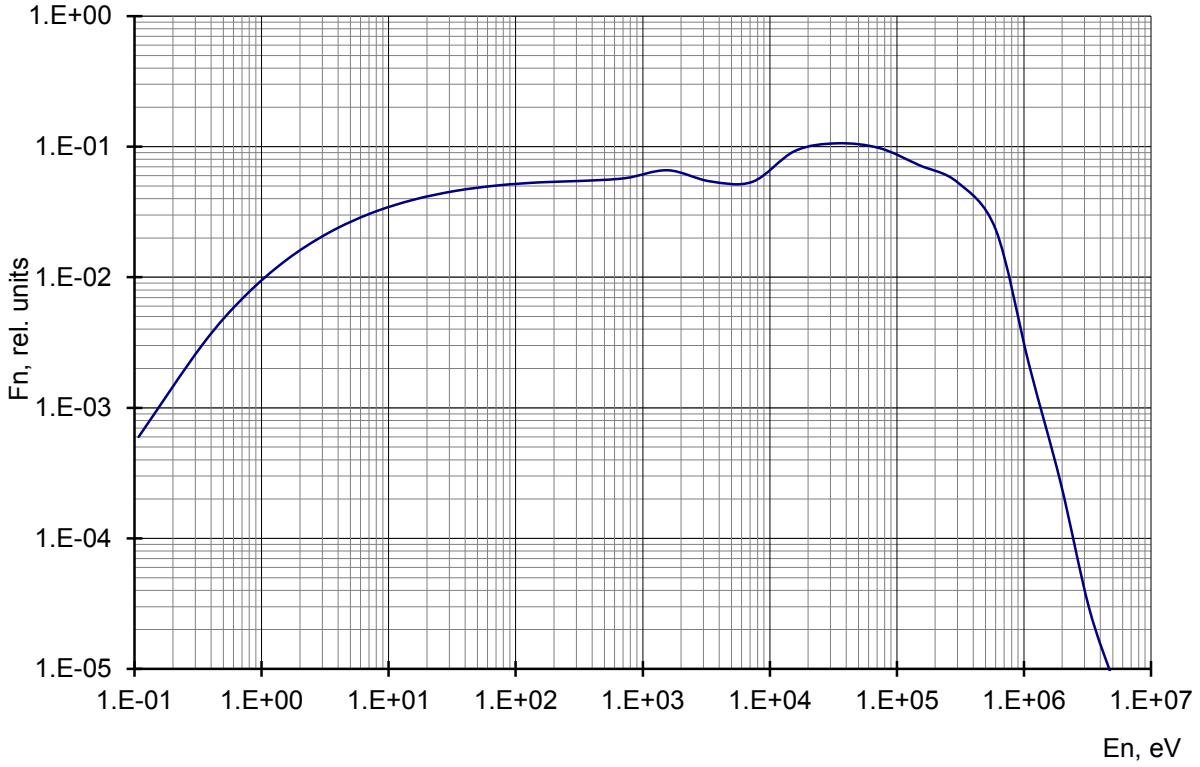

Fig 8. Neutron spectrum in the BOR-60 vertical channel

A possibility was considered of using a horizontal channel for medical purposes. In this context, its parameters were tested. The calculations showed that the main contribution to Fn at the horizontal channel outlet is made by neutrons 10 eV < En < 1.2 MeV (≈ 90 %). The calculated Fn values at the horizontal channel outlet make up $(0.84\div1.2)\times10^{10}$ $cm^{-2}s^{-1}$. Table 4 presents Fn and gamma quantum flux density (Fγ), and Figure 9 shows neutron spectra at the horizontal channel outlet.

Horizontal channel	Calculation		Test
	Fn, $cm^{-2}s^{-1}$	Fγ, $cm^{-2}s^{-1}$	Fn, $cm^{-2}s^{-1}$
Without a Pb shield, En>0 MeV	$(0.84\div1.2)\times10^{10}$	9.6×10^{8}	$(2.9\div3.4)\times10^{8}$
Without a Pb shield, En>1.2 MeV	$(6.2\div8.6)\times10^{7}$	-	$(5.7\div6.5)\times10^{7}$
With a Pb shield	3.6×10^{9}	2.9×10^{6}	-

Tab 4: Neutron and gamma quantum flux density at the BOR-60 horizontal channel outlet

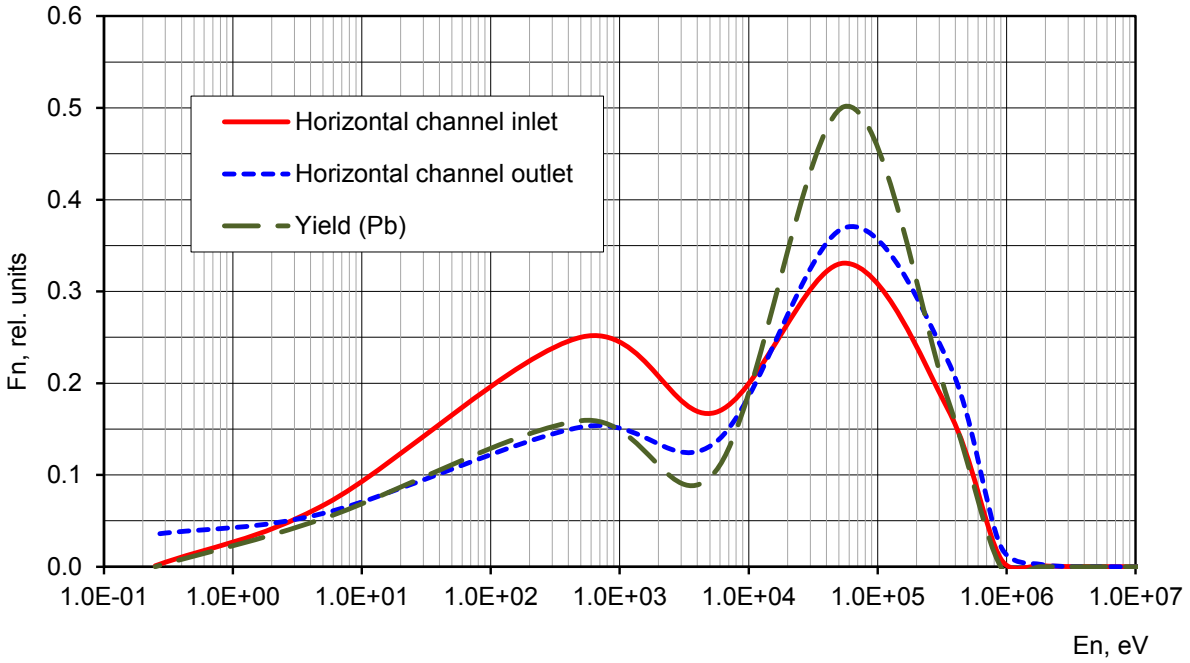

Fig 9. Neutron spectrum at the horizontal channel inlet/outlet

Following the test results it was concluded that the BOR-60 horizontal channel neutronic parameters are within the acceptable limits to conduct tests for the medical purposes.

4. Reactor operation schedule

In BOR-60 heat is removed by means of transference to a heating system, conversion into electrical power and air heat exchanger relief to atmosphere. Therefore, the reactor power may range 50÷55 MW depending on the season. Ongoing operation time (without outage) depends on the reactivity margin, test and irradiation programs usually not exceeding 90 days. In addition, verification tests are conducted to show feasibility of irradiation parameters of different items and materials. Such tests are conducted at the beginning or at the end of reactor life in relation to removing or installing test rigs in the D23 position.

Figure 10 shows an up-to-date standard reactor operation schedule during a year and an actual change in the reactor power. The average thermal output amounts to approximately 270 GWh per year. All specified outages are scheduled. Two long outages (45 days) are used for reloading fuel and test assemblies and repair and maintenance, 2 short outages (20 days) – for fuel additional loading or loading (unloading) of different non-fuel assemblies. During the reactor operation monitoring and recording of all the required parameters are done using process monitoring system and data processing system.

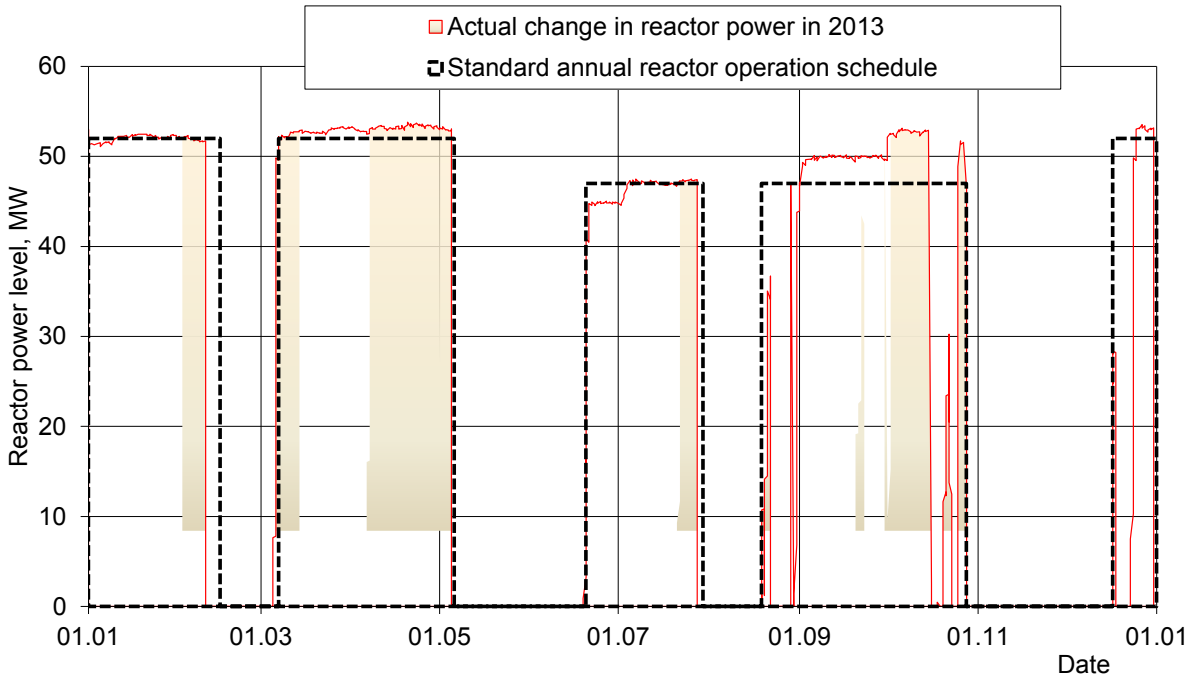

Fig 10. Comparison of the BOR-60 standard operation diagram and actual operation diagram

5. Calculations and methodological support of irradiation

Long-term testing of neutronics, thermal and hydraulic parameters, and dynamics of the reactor allowed creating a software package for online computations relative to reactor operation and tests.

From rich experience of testing the reactor parameters and based on a verified package of computer codes, methods were developed allowing rather precise control over the material irradiation modes and parameters in non-instrumented reactor positions.

Table 5 shows uncertainties in measuring the main parameters describing the irradiation mode of standard and test assemblies and rigs.

Parameter	Uncertainty
Thermal power	5
Sodium flow rate	4
Temperature of sodium and samples	5
Core FA power	6
Specific power density	6÷9
Neutron flux density	3
Neutron fluence	9
Damage dose	6
Irradiation heat rate	8÷12

Tab 5: Main irradiation parameter measurement uncertainty, %

6. Test methods and rigs

To irradiate a wide range of materials and items at different modes and parameters special test rigs are used including capsules, demountable material test assemblies,

independent instrumented channels, special instrumented FAs, etc. To solve the challenges of radiation material science in testing creep, resistance to corrosion and cladding and shroud materials, test rigs have been developed that allow testing of the samples at temperatures 320-1200^{o}C [1]. The benefits of these rigs include simplicity and a possibility of installing them almost in any core and blanket cell. The key challenge in developing such rigs is to create the required temperature modes for the samples. In doing so, heat insulating gaps are used as well as intense cooling or auxiliary heating due to irradiation power density or fuel fission. These rigs allow providing target altitudinal and azimuthal temperature irregularity.

Long-term strength and irradiation creep of cladding materials are tested using tube-shaped samples loaded with controllable internal pressure of inert gas. As a result, different advanced fuels and structural materials are tested under high thermal loads (100 kW/m), temperatures (1000^{o}C), burnups (33 %h.a.) and fluence (1.8×10^{23} cm^{-2} with E>0.1 MeV).

The lower range value of irradiation temperatures reliably provided in BOR-60 makes up 300-310^{o}C, which is by 40-80^{o}C lower compared to foreign fast reactors. This extends considerably the capabilities of irradiation tests conducted in the reactor through the inclusion of the tests of physical and mechanical parameters of zirconium alloys and VVER internal materials. If there is a necessity in intermediate unloading and testing of samples followed by their irradiation, a demountable assembly is used. Different capsules are widely used to irradiate samples in gas, sodium, potassium, lithium, lead, etc.

Similar rigs shaped as a standard FA are used in tests related to abnormal cases and feasibility of fast reactor safety. Serious anomalies and accidents may be studied using independent ampoule loops almost entirely accommodated in the reactor with the output of gas lines and gage signals. The loops have a two-circuit process with an independent sodium circuit. Depending on the design sodium can have natural or forced circulation using a centrifugal pump, electromagnetic pump or MHD pump [4]. In an ampoule loop with natural circulation tests were conducted related to an increase in cladding temperature up to 780^{o}C. In a loop with forced circulation a demonstration test was performed related to coolant flow rate blocking and fuel cladding melting. The gained experience allowed creating similar channels with liquid metal as a coolant to test advanced fast reactor fuel pin dummies. The information about different test rigs is presented in Table 6.

TR class and type	T, °C	Heater	Heater power, kW	Coolant flow rate, m^3/h	Way of maintaining temperature	Nuclear reactor type
untight refreshable: - with no heater - with a metal heater - with a fuel heater - based on a standard FA	 310-370 350-500 400-650 up to 650	 - tungsten nuclear fuel nuclear fuel	 20-50 50-200 up to 400	 2.5-3.5 0.2-1.0 1.0-4.0 3.0-4.0	 - - -	fast neutron
untight non-refreshable	500-700	radiation	-	-		
tight expansion gap: - stagnant liquid metal - inert gas temperature maintenance: - thermal resistance control - conic capsule - evaporating syphon	 400-1000 400-650 400-500 до 600 650-900	 own power density the same the same the same the same	 - - - - -	 1.0-4.0 1.0-4.0 - - -	 - - change in gas gap height and thickness boiling sodium tube	fast neutron, lead-cooled fast, lead-bismuth fast, VVER, RBMK, high-temperature gas-cooled, fusion
independent loop channels	300-1000	FA	up to 100	up to 3.0	change in coolant flow rate	fast neutron, lead-cooled fast, lead-bismuth fast, fusion

Tab 6: BOR-60 test rig parameters

7. Key trends of research

Since the reactor commissioning large-scale tests have been conducted using the abovementioned rigs with reference to irradiation of a wide range of reactor materials and fast reactor safety issues. Irradiation programs hold a special place in conducted research covering the following areas:

- large-scale tests of fuel pins and FAs to achieve burnup over 30% h.a. under stationary and transient modes;
- tests of different absorbing materials;
- irradiation tests of structural reactor materials;
- tests of electrical insulating, magnetic and heat-resistant materials for fusion reactors;
- tests related to radiation material science: determining the relationship of deformation, long-term strength and crack resistance at temperatures 330-1000°C to achieve 200 dpa;
- testing of transmutation process and burning long-lived radionuclides from spent fuel of different reactors;
- radiation doping of silicon for radioelectronics;

Over the reactor operating period a large-scale test of different fuel, structural materials of shrouds and fuel claddings has been conducted (Table 7).

Material		Type
Fuel	ceramics	UO_2, UO_2-PuO_2, (U,Pu)O_2, UC, UN, UPuN, UPuCN, PuO_2-MgO, ЯТ+Np,Am
	metal	U, UPu, UZr, UPuZrNb
	metal ceramics	U-PuO_2, UO_2-U, UN-U
	composite	(UPuZr)C, UO_2-NiCr
Absorbing	samples	B_4C, Ta, Hf, Dy, Sm, Gd, AlB_6, AlB_{12}, Eu_2O_3, HfH_x, Gd_2O_3, Dy_2O_3-HfO_2
	control rods	CrB_2, B_4C (^{10}B - 19÷80 %), Eu_2O_3, Eu_2O_3+ZrH_2
Structural	stainless steel	ОХ18Н9, Х18Н10Т, ЭП450, ЭП823 03Х16Н9М2, ЭП912, ЭИ847, ЭП172, ЧС68, ВХ24, ЭП302Ш, 09Г2С, АРМКО, SS316, ODS-(12,14,18)Cr, T91, T92, S421 (HT9), 15-15Ti, 800H, 14YWT, 800H, …
	nickel alloys	РЕ-16, Х20Н45М4Б, ВЦУ
	high-melting-point materials	V, W, Mo, Nb, WC, SiC/SiC
	zirconium alloys	Э110, Э635, Э125
	graphite, moderators	ГРП-2-125, МП6-6, ГР-280, АРВ, IG-11, ПГИ, ZrH_x
	neutron sources	Po-Be, Be, Sb-Be
Coolant	liquid metal	Na, Pb, Pb-Bi
Electrical	insulation	Al_2O_3, SiO_2, Si, mica
	cabling	КТМС, КНМС(Н)
	magnets	ЮНДК
Other	special ceramics	ГБ-7, ИФ-46, ЦТС, $LiNbO_3$
	biological shielding	concrete

Tab 7: Reactor materials tested in BOR-60

7.1 Testing of parameters and safety issues

Testing of dynamics, thermal and hydraulic parameters and accidents has shown that the reactor has inherent safety features preventing serious consequences of a range of beyond design basis accidents.

A large set of tests has been conducted with reference to sodium-cooled fast reactor safety including gas supply in the core, sodium boiling, flow rate blocking in a test FA with fuel failure, intercircuit leaking in steam generators, etc. A detailed study of different normal and abnormal cases in BOR-60 enabled testing and adapting methods and means of abnormality diagnostics which include acoustic imaging under sodium layer, calculation of reactivity balance as well as parametric, vibroacoustic and noise diagnostics. Several abnormalities have been detected: absorber failure, movement of a rod in a loose collet clamp, FA emergence in the core, etc. High performance of the systems was demonstrated in conducting tests in the reactor.

The analysis of the issues related to sodium process and irradiation parameters and properties of the reactor made it possible to develop a range of methods and means for monitoring and enhancement of radiation situation, reactor safety and sodium handling: three-channel cladding integrity monitoring system (gas and sodium activity, delayed neutrons); high-performance compact absorbers for sodium purification from caesium radionuclides; decontamination of equipment coming in contact with sodium and removal of non-draining sodium amount from equipment under repair or decommissioned equipment based on the innovative technologies; refreshment system of oxide cold traps which allows their operation without replacement with the new ones.

7.2 Large-scale tests of fuel pins and FAs

In 1981 the reactor core was converted to fuel pins with vibropac meats based on power plutonium. Getter introduction allowed solving the issue of physical and chemical fuel-to-cladding interaction and providing high average burnups (13÷15 % h.a.). On several test fuel pins the burnup achieved 32 % h.a. The positive results of large-scale tests with fuel pins containing vibropac U-Pu oxide fuel in BOR-60 to achieve a burnup of over 30% and 6 test FAs to achieve a burnup of 9.6% in the BN-600 reactor are a tangible basis for conducting large-scale tests in power fast neutron reactors to enhance their performance and safety [5].

Burning and transmutation of plutonium and minor actinides (MAs) are performed under the program on reprocessing of closed fuel cycle. Calculation and experimental research and analysis of isotopic composition of microcapsules (40 pcs) were performed using different sets of MAs irradiated in BOR-60. A range of work to determine a possibility and efficiency of BOR-60 operation as a MA burner was fulfilled. Different core arrangements of BOR-60 with MAs in fuel and single assemblies were considered. The efficiency of burning different actinides in BOR-60 was determined as well as their impact on the main neutronic parameters and safety of the reactor. The presence of MAs (up to 40%) in U-Pu nuclear fuel has almost no influence on the main BOR-60 neutronic parameters. The obtained calculation and experimental results may be used in adjustment of physical constants.

The obtained results related to different fuel compositions are a basis for developing a fuel cycle of advanced fast reactors of enhanced safety.

7.3 Testing of fuel, absorbing and structural materials

The implementation of all Russian projects on development and creation of advanced fast neutron reactors (BN, BREST, SVBR, MBIR) envisaged by Federal Target Program "Nuclear Power Technologies of Next Generation for 2010 – 2015 and up to 2020" [6] is associated with a large scope of tests in BOR-60. In addition, during the recent years there has been hard work done in terms of testing in support of foreign designs of fast neutron reactors under contracts signed with the customers from around the world.

7.4 Accumulation of isotopes for medical purposes

Based on the fast reactor physical parameters, parameters were tested related to accumulation of a range of commercial radionuclides generated as a result of threshold neutron reactions: ^{32}P, ^{33}P, ^{35}S, ^{89}Sr (reaction (n, p)) and ^{117m}Sn (reaction (n,n')). In addition, indices of ^{153}Gd accumulation were determined generated as a result of neutron radiation neutron capture reaction (n,γ) in the BOR-60 irradiation positions with a special heat-insulated neutron spectrum. At present, there is a batch production of strontium-89 using yttrium targets to produce "no-carrier strontium-89"chemical.

8. Plans on further reactor operation

The BOR-60 reactor has been operating for 44 years at the designed operating lifetime of 20 years. A decision on extending its operating lifetime was taken based on condition of its equipment and materials, strength analysis of sodium circuit equipment and pipelines important in terms of safety. A decision was taken on extending reactor operation up to 2020 with a prospective of extending its lifetime for a longer period.

There are long-term R&D programs funded under Federal Target Program "Nuclear Power Technologies of Next Generation" and international contracts. Therefore, BOR-60 has plenty orders for the next few years, and the tests will be conducted in this reactor up to its decommissioning.

By the end of BOR-60 operating lifetime Federal Target Program "Nuclear Power Technologies of Next Generation" envisages construction of a multipurpose research fast neutron reactor (MBIR). The MBIR reactor is intended to replace the BOR-60 reactor after its final shutdown [7] meeting the demands on conducting research under different projects related to fast neutron reactors. MBIR will have wider experimental capabilities. It will be located at the site of JSC "SSC RIAR" that will allow transferring the whole operation and research experience gained in BOR-60 within the shortest possible time.

Thus, long-term research programs launched in BOR-60 will be completed in the newly constructed MBIR reactor [8]. Moreover, such long-term programs are currently being implemented.

REFERENCES

1 RIAR Research Reactors and Their Experimental Capabilities. Edited by Tsykanov, V.A. Dimitrovgrad, 1991.

2 Korolkov, A.S., Gadzhiev, G.I., Efimov, V.N., et al. The BOR-60 Reactor Operating Experience, Nuclear Power, v.91, issue.5, p.363, 2001.
3 Zhemkov, I.Yu., Yakovleva, I.V., Ishunina, O.V. BOR-60 Neutronic Parameters. Dimitrovgrad, SSC RF RIAR, 2000. 40 p.
4 Gadzhiev, G.I., Efimov, V.N, Zhemkov, I.Yu., et al. Several Tests Performed in BOR-60, Nuclear Power, v.91, issue 5, p.369.
5 Maershin, A.A., Tsykanov, V.A., Golovanov, V.N. Development and Testing of Fast Reactor Fuel Pins with Vibropac Oxide Fuel, ibidem, p.378.
6 Nuclear Power Technologies of Next Generation for 2010 – 2015 and up to 2020: Federal Target Program [approved by Decree of the Government of the Russian Federation as of February 03, 2010. No.50].
7 Zhemkov, I.Yu., Tretyakov, I.T., Lopatkin, A.V., Poplavskii, V.M., et al. From BOR-60 to MBIR: Continuity and Development. Role of BOR-60 in the Nuclear Power Innovative Development: Proceedings of Scientific Technical Workshop, Dimitrovgrad, March 2, 2010. Dimitrovgrad, JSC “SSC RIAR”, 2010, 135 p.
8 Zhemkov, I.Yu., Izhutov, A.L., Novoselov, A.E., Poglyad, N.S., Svyatkin, M.N. Analysis of Possibility to Continue Irradiations Launched in BOR-60 in MBIR. X Russian Reactor Material Science Conference. Proceedings. Dimitrovgrad, JSC “SSC RIAR”, 2013, 551-558 pp.

OVERVIEW OF RESEARCH REACTOR UTILIZATION AND RELATED TECHNOLOGY DEVELOPMENT IN KAERI

I.C. LIM, C.H. LEE, B.S.SEONG, S.J. PARK, J.S.LEE, C.S. LEE

Research Reactor Utilization Department, Korea Atomic Energy Research Institute
989-111 Daedeok-daero, Yuseong-gu, Daejeon, 305-353, Korea

ABSTRACT

As the national center of user service as well as the core of research reactor utilization technology development in Korea, KAERI is operating the HANARO multi-purpose research reactor and conducting a project to build the Ki-Jang research reactor(KJRR). The utilization of HANARO has an emphasis in the basic research using neutron beam scattering instruments. The commissioning of four new neutron scattering instruments, Bio-C, Bio-D, Bio-REF and Cold-TAS, was completed in 2013 and they were opened for external users in 2014. Neutron activation analysis instruments using cold neutrons have widen the application of neutron activation technique. As an effort to promote the application of neutron scattering to the industrial development, an industrial user committee was established at the end of 2014. The development of fission Mo production technology is an essential part of researches for the Ki-Jang research reactor utilization. The evaluation of the developed technique under cold conditions was completed in 2014 and a trial irradiation and processing is being made. The neutron irradiation which has been applied mainly to the development and evaluation of materials or fuels for power reactor application is being applied to the development of super-conducting material and other industrial applications as well. When the Ki-Jang research reactor starts operation, the major applications of HANARO will be neutron beam research and material test and KJRR will serve for irradiation services including RI production and NTD.

1. Introduction

As the sole government funded nuclear research institute in Korea, KAERI is operating HANARO which is a 30MW multi-purpose research reactor. Since 2012, KAERI has been conducting a project to construct the Ki-Jang research reactor(KJRR) which will be used for RI production as well as NTD service. Tables 1 and 2 show the major characteristics of two reactors. When the KJRR becomes available, the role of HANARO will be concentrated to basic research activities and KJRR will serve mainly for irradiation services. To accomplish these roles, KAERI is expanding the utilization facilities of HANARO and developing the technologies required for the services using KJRR. This paper presents the status of utilization technology development for HANARO and KJRR.

2. Utilization of neutron beam in HANARO

Fig. 1 shows a plan view of reactor core and reflector region of HANARO. Even though HANARO is a multi-purpose research reactor, the most important utilization is the basic researches using neutron scattering instruments. Following the operation of cold neutron source from 2009, the installation of neutron scattering instruments has continued. The commissioning of four new neutron scattering instruments, Bio-C, Bio-D, Bio-REF and Cold-TAS, was completed in 2013 and they opened for the external users in 2014. The characteristics of these instruments are summarized in Figures 2 and 3. Now in HANARO, 7 thermal neutron instruments and 7 cold neutron instruments are available for the external users.

Reactor Type	Open-tank-in-pool
Thermal power	30 MW
Coolant/Reflector	Light water/Heavy water
Fuel Material	U_3Si in Al, 19.75% enriched
Absorber	Hafnium
Reactor Building	Confinement
Maximum Thermal Neutron Flux	$5x10^{14}$ n/cm^{2}s
Typical Thermal Neutron Flux at Beam Port Nose	$2x10^{14}$ n/cm^{2}s
Operation Cycle	28days@5weeks

Tab 1: Major Characteristics of HANARO

Project Period	April 2012~March 2018
Site	Ki-Jang Gun(Near to Busan)
Objective	RI production and research Neutron irradiation service
Thermal Power	15 MW
Fuel	U-Mo plate type fuel(LEU)
Fission Mo Target	U-Al plate type(LEU)
Coolant/Reflector	Light water/Be and graphite

Tab 2: Major Characteristics of KJRR

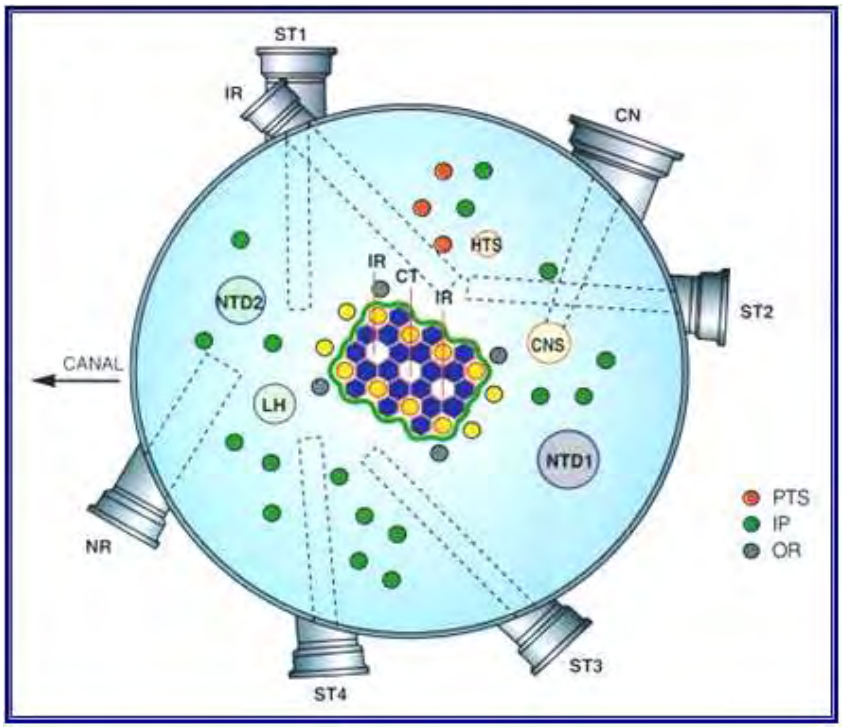

Fig. 1 Plan view of HANARO core and reflector region

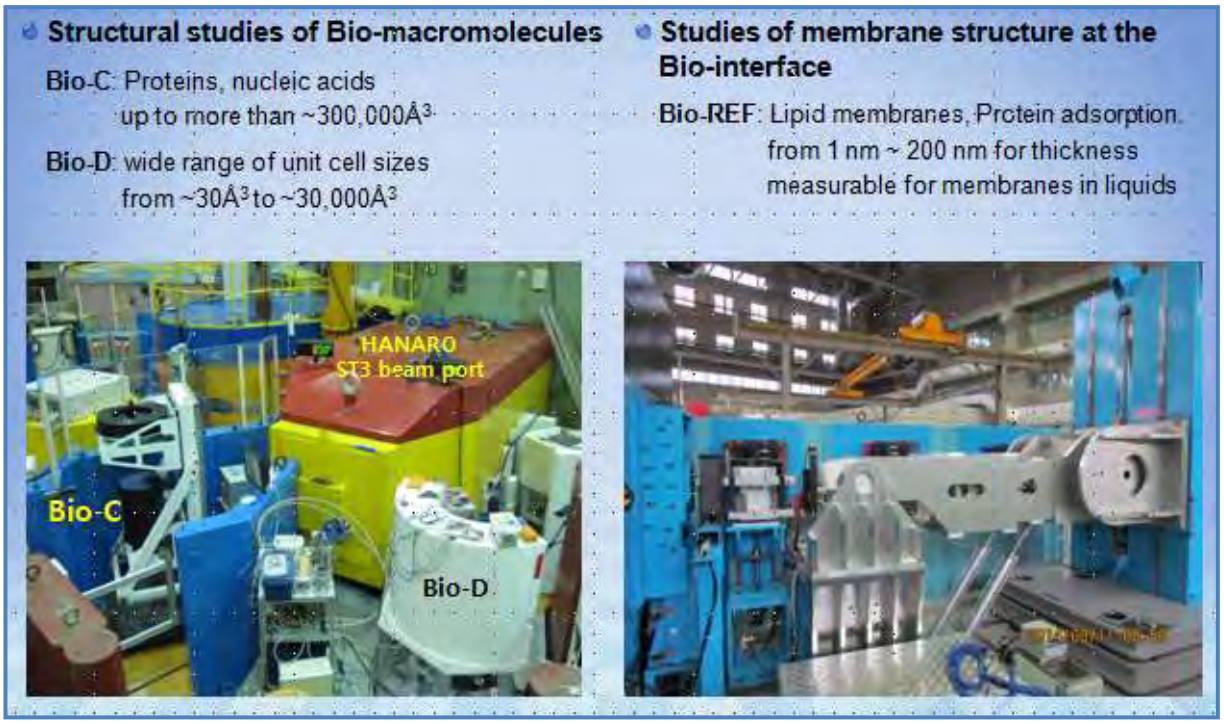

Fig. 2: View of neutron scattering instruments in HANARO

Fig. 3: View of Cold-TAS in HANARO

Neutron crystallography is a powerful technique for locating hydrogen atoms. For this reason, neutron diffraction is a complementary method to X-ray and NMR techniques. However, the big disadvantage of neutron crystallography is the relatively low flux of the available neutron beams and therefore a relatively lower through-put. The development of two types of neutron detectors was a big advance, especially for neutron protein crystallography: one is a neutron image plate(NIP) detector, and the other is a large-area curved 2-dimensional position sensitive detector(C-2DPSD). Bio-D is a single-crystal neutron diffractometer equipped with a large-area C-2DPSD developed by the collaboration of KAERI and Tohoku University, Japan. Bio-C

is a NIP-based diffractometer developed by the joint project of KAERI and KRIBB(Korea Research Institute of Bioscience and Biotechnology) [1].
Cold-TAS is a very compact but very powerful cold neutron triple axis spectrometer with polarized neutron capability for measurements of magnetic and nuclear inelastic scattering. The instrument has two exchangeable monochrometers (PG(002) and Heusler(111)), which enables focusing of the guide beam vertically. High monochromatic neutron flux at the sample position is from the pyrolytic graphite and polarized neutron beam from the heusler crystal monochrometers with neutron filters of PG, Be and BeO [2].
Bio-REF is a horizontal type neutron reflectometer that can measure liquid-solid and liquid-air interfaces, allowing the studies of bio-membranes and protein-membrane interactions. The Bio-REF at HANARO, which was developed through a collaborative project between HANARO and Sogang University, was built for the experiments in high q-ranges with the liquid-solid interface and those have air/water interfaces for the comprehensive investigation of biological application in addition to the classical depth profiling techniques for the polymeric thin films [2,3].
The introduction of these instruments enables the HANARO to be used for the basic researches in biology, low-energy dynamic of liquid and solid molecules as well as low dimensional magnetism.

3. Activation analysis using cold neutron

In 2014, CONAS(Cold Neutron Activation Station) in Fig. 4 was opened for the external users. CONAS is composed of PGAA(Prompt Gamma Activation Analysis), NIPS(Neutron Induced Pair Spectrometer) and NDP(Neutron Depth Profile).
PGAA based on the neutron capture reaction has been a complementary method to the conventional instrumental neutron activation analysis(INAA) as a nondestructive technique. A PGAA system was installed at the ST1 beam port of HANARO in 2001. Based on this achievement, the CN-PGAA was installed at the cold neutron guide CG2B. It is composed of an n-type HPGe and a BGO and is operated in single bare, Compton suppression and pair spectrometer modes [4]. The CN-NIPS is used for more quantitative measurements of miniscule amounts of atoms. The CN-NDP is an absolute depth profiling probe for some elements such as He, Li, B, O and N which are very important in industrial products including lithium ion batteries, semiconductors, glass and multilayered films. It measures charged particles emitted after neutron capture [5]. The installation of CONAS has enlarged the capability of activation analysis of HANARO.

Fig. 4: Cold Neutron Activation Station of HANARO

4. Fission Mo production technology development

The major application of the new research reactor, KJRR, is the production of Mo-99 which is the mother nucleus of Tc-99m. Fission Mo producers have used highly enriched uranium(HEU) targets so far. However, for non-proliferation reason, Mo-99 producers are asked to convert their HEU-based process to a process which uses low enriched uranium(LEU) targets. Therefore, KAERI is developing a LEU-based fission Mo production process which will be applied for the Mo-99 production in KJRR as depicted in Fig. 5. Even though there are many technical aspects to be resolved, the emphases are given on the development of a method to treat the aluminum waste and the methods to treat iodine. In KAERI's fission Mo process explained in Fig. 6, a plate-type LEU target with UAlx meat and aluminum cladding is used. Fabricated targets are assembled and transferred to the fission Mo production facility after irradiation in the reactor. Then, irradiated targets are dissolved in sodium hydroxide solution to extract Mo-99 in the solution. Other fission products including remaining uranium and actinides are removed from the solution. Medical-grade Mo-99 can be extracted after proper chemical treatments and multi-step separation and purification process. KAERI research team developed new technology to facilitate waste treatment by converting sludge-type waste, which is difficult to handle, into independent solid and liquid wastes [6]. After removal of radioactive iodine, Mo-99 can be extracted through the multi-step separation and purification process. Gaseous iodine is removed by copper oxide column installed in the off-gas treatment system. On the other hand, iodides remained in the alkaline dissolution is removed by silver-exchanged silica or silver-doped alumina [7].

The minimization of Xe release during the fission Mo-99 production process is an international issue and thus, KAERI has joined an IAEA CRP for the technical cooperation aiming the reduction of Xe release.

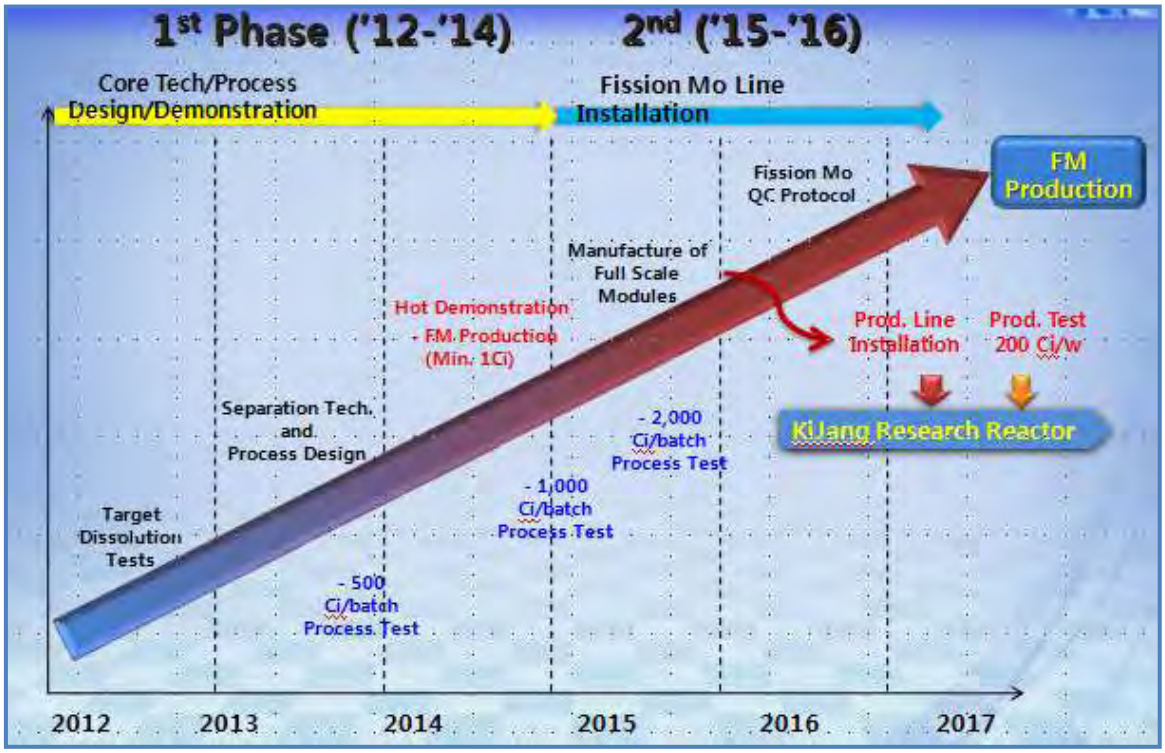

Fig. 5: Fission Mo production technology development plan in KAERI

5. Research on material irradiation

Efforts to improve the capabilities and instrumentation of the material irradiation facilities have been made at KAERI [8]. The irradiation facilities have been mostly utilized for the researches on commercial nuclear power reactors such as the ageing management and safety evaluation of the components. HANARO has recently supported national R&D

projects relevant to new nuclear systems including the System-integrated Modular Advanced Reactor (SMART), research reactors and future nuclear systems [9].

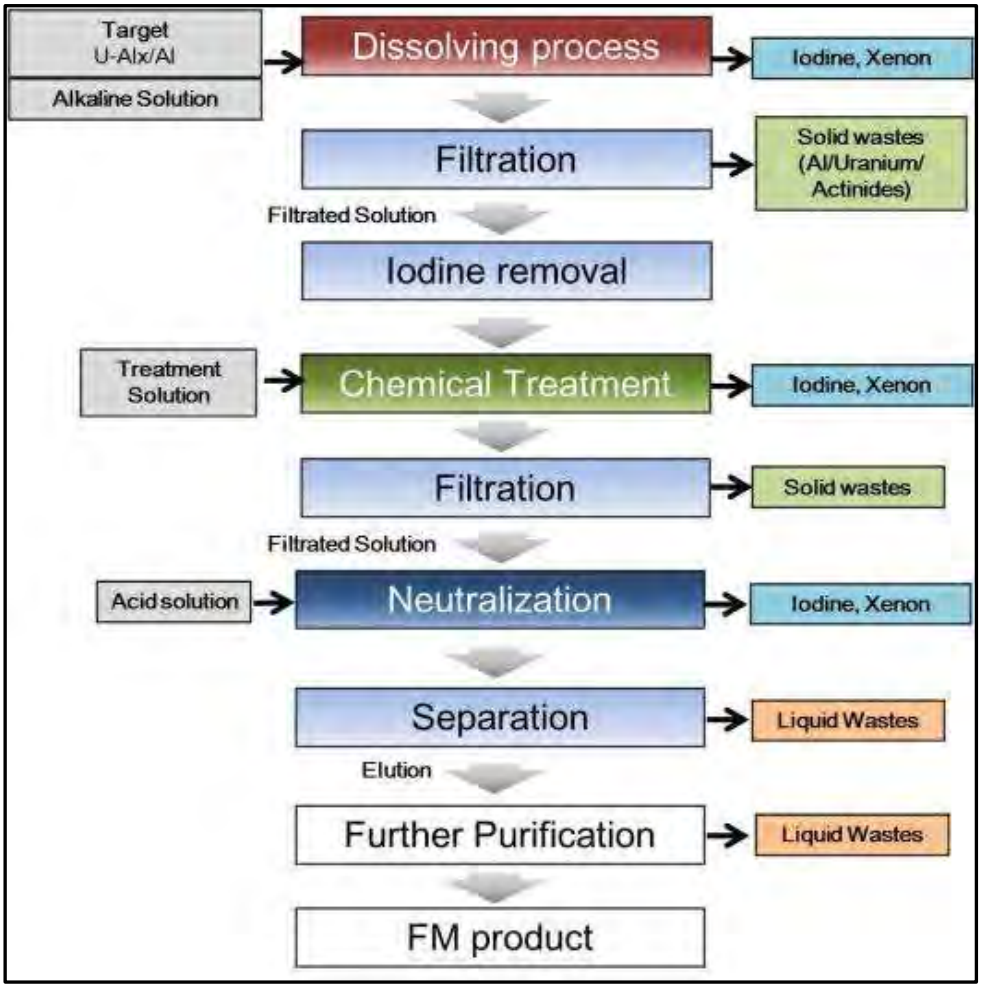

Fig. 6: Fission Mo production process being developed by KAERI

As neutron irradiation affects the structure of a material, radiation induced modification of materials has become a perspective method for the purposeful changes in material properties. Neutron interactions with matter occur as collisions, called scattering events creating defects, or as capture events called neutron transmutation. The electrical and magnetic properties of electronic materials are extremely dependent upon disorder in lattice structure. Neutron irradiation of these materials greatly increases this disorder through the creation of various defects. Some irradiation tests of electro-magnetic materials were also performed at HANARO for scientific researches [10].
KJRR is expected to have the capability to provide the neutron irradiation service for power semiconductor production in a large scale. This service includes not only NTD facility for ingot irradiation, but also fast neutron irradiation (FNI) facility for wafer irradiation. The fast neutron irradiation for a wafer is a promising technology for the efficiency gain and life extension of a power semiconductor. The FNI facility can be also utilized on the study of the separated effect of fast neutron irradiation on the properties of electro-magnetic materials. A research project related to this study was started in 2014.

6. Remarks

As the sole government funded national nuclear research institute, KAERI has continued its efforts for the development of research reactor systems as well as the development of technologies to use research reactors as a tool for basic research and one for industrial services. The project to construct a new research reactor which is call KJRR becomes a

motivation to expand the infra for utilization and to develop new technologies. KAERI is continuing the development of utilization technologies with a strong support from the Korean government.

References

[1] S.A. Kim and et al., “Bio-Diffractometers at HANARO”, Neutron News, 24:2, pp.33-35, 2013.

[2] S.J. Cho and et al., “Status of Cold Neutron Facilities at HANARO and a Thermal Neutron Guide Project of KAERI”, presented at IGORR 2014, Bariloche, Argentina, 2014.

[3] K.H. lee and et al., “Opportunities and Challenges of Neutron Science and Technology in Korea”, Nuclear Engineering and Technology, Vol.41, No.4, pp.521-530, 2009.

[4] G.M. Sun and et al., “A New Cold Neutron Prompt Gamma Activation System at HANARO Research Reactor”, submitted to NIM A, 2014.

[5] G.M. Sun and et al., “Development of Cold Neutron Activation Station at HANARO Cold Neutron Source”, KNS Spring Meeting, Jeju, Korea, May 17-18, 2012.

[6] S.K. Lee and et al., “LEU-based Fission Mo Process with Reduced Solid Wastes”, presented at the 8th ICI, Hyatt Regency Chicago, Aug. 24-29, 2014.

[7] S.S. Lee and et al., “Development of the adsorbent for the Gaseous Iodine Treatment for Applying to Fission Mo Production”, presented at the 8th ICI, Hyatt Regency Chicago, Aug. 24-29, 2014.

[8] B. G. Kim and et al., “Development Status of Irradiation Devices and Instrumentation for Material and Nuclear Fuel Irradiation Tests in HANARO,” Nucl. Eng. Technol., Vol. 42, No. 2, 2010, pp. 203- 210.

[9] M.S. Cho and et al., “Recent Irradiation Tests for Future Nuclear Systems at HANARO”, to be presented at RRFM 2015, Bucharest, Romania, April 19-123, 2015.

[10] C. J. Kim and et al., “Effects of Neutron Irradiation on Superconducting Critical Temperatures of in-situ processed MgB_2 Superconductors,” Progress in Superconductivity and Cryogenics, Vol. 16, No. 1, 2014, pp. 9-13.

RESEARCH REACTORS FOR REGIONAL NUCLEAR EDUCATION: EXPANDING THE EASTERN EUROPEAN RESEARCH REACTOR INITIATIVE MODEL

C. AMES, A. BORIO DI TIGLIOLE, E. BRADLEY, J. VYSHNIAUSKAS
Department of Nuclear Energy, International Atomic Energy Agency
Wagramer Street, 1220 Vienna - Austria

H. BOECK, M.VILLA
Atominstitut, Vienna University of Technology
Stadionallee 2, 1020 Vienna - Austria

L. SKLENKA
Department of Nuclear Reactor, Czech Technical University in Prague
V Holesovickach 2, 180 00 Prague 8 – Czech Republic

ABSTRACT

Making effective use of regional academic coalitions has been successful in Central and Eastern Europe, to the benefit not just of European states, but also to developing countries in other parts of the world. Education in peaceful applications of nuclear energy has developed significantly through the Eastern European Research Reactor Initiative (EERRI) Group Fellowship Training Programme, which bridges the gap between advanced academic institutions and IAEA Member States seeking to apply nuclear science and technology to achieve national development objectives.

The EERRI Group Fellowship Training Programme was developed in 2008 to educate young professionals with an existing basic academic background in physics or engineering in the safe operation, management and utilisation of research reactors. This course is unique for its practical nature and level of international collaboration. The course is academically supported by institutions in Austria, Slovenia, the Czech Republic and Hungary. The course runs approximately twice a year, at varying locations shared amongst the participating institutions. The EERRI Group Fellowship Training Programme has completed its ninth course, on which the presenter was an observer. The programme enhances not only individual competence amongst students, but also collaboration between the EERRI coalition and the institutions sponsoring the students.

This paper explores the statistics of countries and individuals who participated in the EERRI Group Fellowship Training Programme; the human resources challenges faced today by institutions and their governments in meeting nuclear education requirements; and how advantages of the EERRI Fellowship concept discussed in previous papers can be expanded to other regions, to enhance closer institutional cooperation and access to nuclear education for young scientists and engineers. In particular, this paper focuses on the flexibility of the EERRI Group Fellowship Programme concept via the use of multiple institutions in delivering nuclear education, and in the facilitation of institutional cooperation through such events as ‘train the trainer’ courses. Furthermore, nuclear education options in the Asia-Pacific region will be discussed in assessing the suitability of an EERRI Group Fellowship Training Programme concept in this region.

1. Introduction

1.1 The EERRI model

The Eastern European Research Reactor Initiative (EERRI) Group Fellowship Training Programme was developed in 2008, in response to an increasing demand for hands-on reactor physics education for graduates [1]. The course is primarily aimed at students with an academic background in physics or engineering, and from developing countries[1] with little or no nuclear experience [2]. However, there have also been a number of successful participants from countries with a developed nuclear science and technology research programme, including in some cases a nuclear power programme, who have benefitted from the course.

The programme is coordinated by the Atominstitut of the Vienna University of Technology, and always involves at least two other institutions from the Czech Republic, Slovenia, and/or Hungary.[2] The six-week programme is centred on the following topics [1]:

a) administrative and organisational topics including regulatory requirements, nuclear project planning, implementation and decommissioning;
b) reactor related topics including reactor physics and neutronics, nuclear power systems, fuel calculations and coding, instrument and control systems, and thermal-hydraulics;
c) radiation monitoring including dosimetry and radiation protection; and
d) a significant practical component including activities such as neutron activation analysis, control rod calibration, radiation dosimetry and fuel handling.

The EERRI Group Fellowship Programme provides hand-on training with at least three separate research reactors, particularly in neutronics. The success of the course is in its practical nature and variety of committed facilities, and is unique in its coalition involvement and international audience [3].[3]

Seven years since its inception, the EERRI model is on the verge of expanding to other regions. This may fill a gap in basic reactor physics and engineering education that is experienced not just by developing Member States planning their first nuclear build, but also amongst developed countries[4] with an established nuclear programme, including applications with a commercial component. The EERRI model relies on support from the IAEA, which receives financial support for the EERRI Group Fellowship by the US Department of State under the Peaceful Uses Initiative programme. However, this support is not sustainable beyond the establishment of the course. Long-term success depends on the commitment of a regional educational body to oversee the fundraising, implementation, refinement and continuation of its programme.

[1] For the purposes of this paper, a 'developing country' is defined as a country that has chosen to receive financial assistance from the associated IAEA Technical Cooperation Programme for the EERRI Group Fellowship Training Programme.

[2] The other participating institutions are: Jozef Stefan Institute (Ljubljana – Slovenia); KFKI Atomic Energy Research Institute (Budapest – Hungary); Budapest University of Technology and Economics (Budapest – Hungary); Czech Technical University Prague (Czech Republic); Research Centre Rez (Czech Republic)

[3] In addition to [3], informal sources to determine the unique nature of the course included liaison with experts on nuclear education from the IAEA, the Atominstitut in Vienna, the Czech Technical University Prague, and the University of New South Wales Australia.

[4] For the purposes of this paper, a 'developed' country is one which has chosen not to receive funding support from the IAEA Technical Cooperation Programme.

1.2 National benefits of the model

This course is of particular benefit to countries with little or no existing nuclear infrastructure, as it develops the basic human resources required to support the planning, analysis and evaluation of a future nuclear science and technology programme of national benefit [1]. Whilst the course was initially developed for this purpose, it has since been tailored to include states with an established research reactor programme, and for countries looking to embark on a nuclear power programme (NPP), through topics such as nuclear power systems, and use of research reactors for materials testing in support of nuclear power plant life extension [4].

The national capability of developed countries can also be enhanced by this model, where a research reactor or NPP exists, but there is no low power research reactor to provide practical neutronics education to students.[5] A number of countries have an NPP and full scope training simulator or programme, or have a medium or high power research reactor that is used primarily for commercial and research purposes (such as South Africa and Australia, respectively). In both cases, the country has advanced past the stage of an initial low power research reactor, and subsequently decommissioned, or never had a low power research reactor [5]. This creates a gap in reactor education for graduate physics and engineering students, who lack the opportunity to truly understand basic effects on reactivity through practical example. Therefore, practical education on a regional research reactor facility can assist in the preservation and continuation of a Member State's basic nuclear capability.

Rather than a coalition of host reactors supporting students from countries worldwide, the EERRI model can be adjusted by other coalitions so that a gap in education can be addressed at a regional, rather than global level. This could also provide a modest source of income for countries with a suitable low-power research reactor, and save costs on equivalent local training for a participant country in the same region.

1.3 Individual benefits of the model

This programme is aimed towards young professionals who have little nuclear experience, already possess a technical degree in engineering or science, and could be responsible for future peaceful nuclear activities in their country [1]. In practice, a number of more senior professionals, including senior reactor operators, have successfully completed the course.

The EERRI model particularly benefits individuals in enhancing their basic nuclear understanding. For a number of students, it is the first time they can operate a research reactor, directly experience the changes in reactivity from the manipulation of control rods, and to witness the effects of the negative temperature reactivity coefficient that is crucial to reactor safety. These experiments can only be performed on a research reactor at zero or low power. Furthermore, it is important that nuclear engineering designs are closely linked to quality assurance, and learning these concepts simultaneously enables the student to understand how reactor design impacts safety, security and safeguards. Due to this practical training, students gain a comprehensive and well-rounded understanding of neutronics and related engineering and management issues. So far, all EERRI participants have been from

[5] For the purposes of this paper, low power is defined as less than 1MW (not including pulse power).

developing Member States, however students from developed countries without a suitable research reactor for this type of education could also benefit greatly from a course based on the EERRI model.

2. Analysis of trends from previous EERRI Group Fellowship Training Programme

2.1 National level statistics on the EERRI Group Fellowship Training Programme

In total, there have been 66 EERRI fellows over nine courses, not including the nine students who are currently attending the tenth course. Greatest participation has come from the Western Asia (Middle East) region, which comprises 43% of all attendees. Figures 1 and 2 depict the nationality of students grouped into their regions [6], including the students currently attending the tenth course[6]:

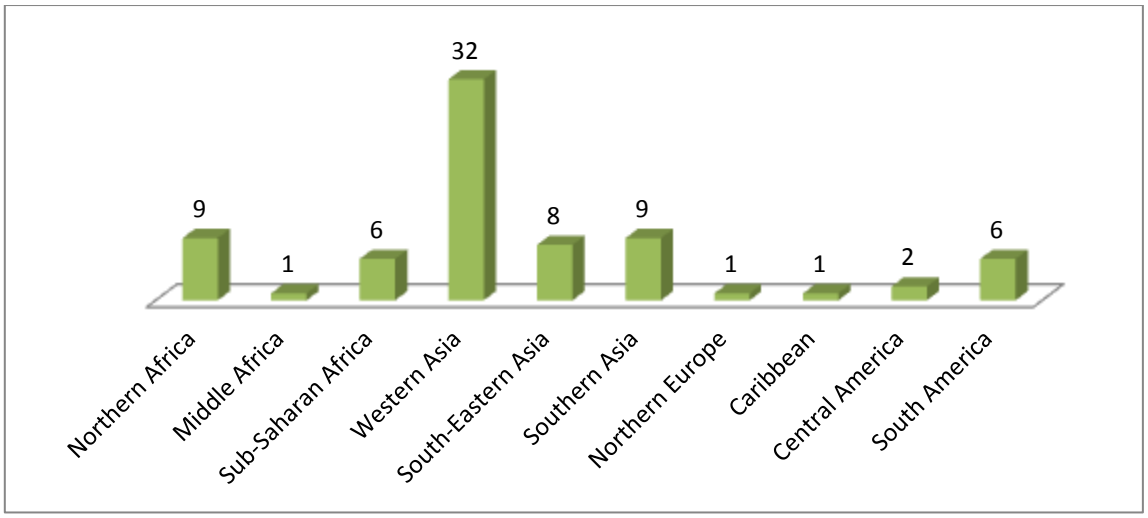

Fig 1. EERRI Group Fellowship participants by region

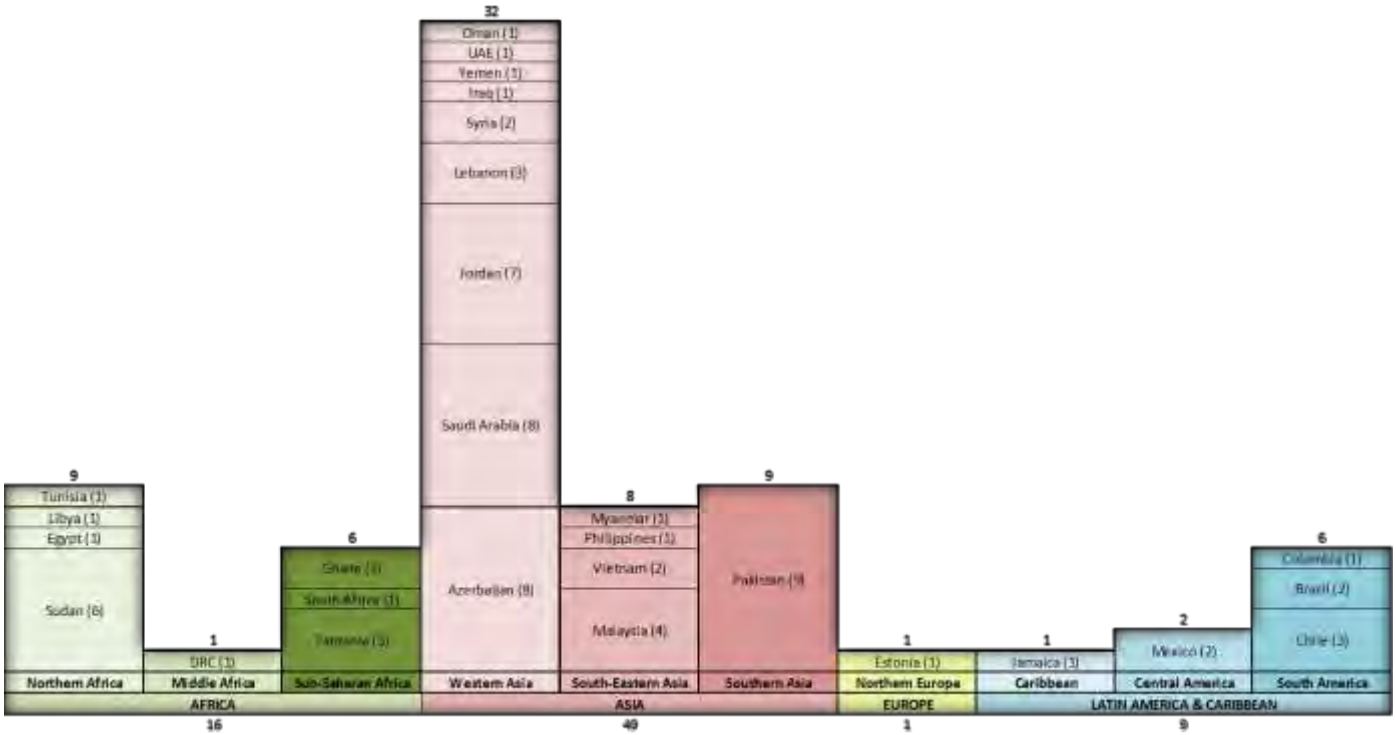

Fig 2: EERRI Group Fellowship attendees by nationality

[6] All participant data from spreadsheets from IAEA and Czech Technical University staff, and IAEA Technical Cooperation database (not publicly accessible).

The data represented in Figure 1 suggests that developing countries in further regions such as Latin America may have reduced representation due to travelling distances. It appears that many Member States represented on the course are considering a new build, planning a new build, or have an existing nuclear programme [5, 7]. The number of countries in the South East Asian region either considering or planning a new nuclear build appears to be approximately similar to the Western Asian region. This supports the idea that geographical proximity to the host reactor is important in fostering nuclear education capacity building.

Figure 3 represents the existing nuclear capabilities of countries participating in the EERRI Group Fellowship, proportional to the number of participants:

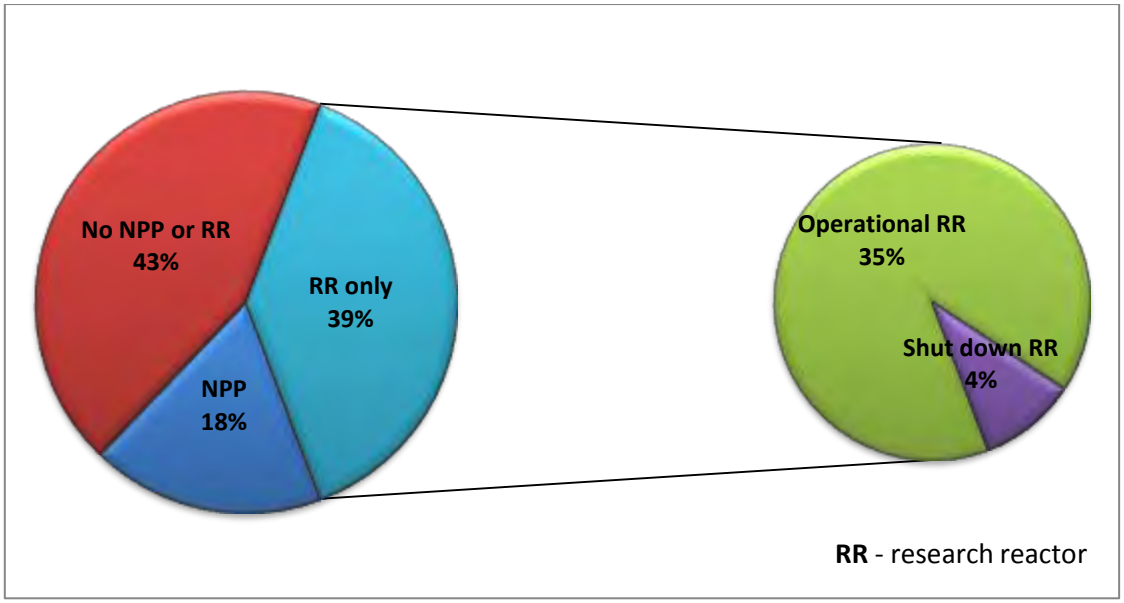

Fig 3. EERRI participants per national nuclear capability

Nearly one fifth of participants already have an NPP, which indicates the benefit of the EERRI Group Fellowship Programme to countries who have an established nuclear capability, but no reactor facility that is available and suitable to perform basic reactor experiments.

Figure 3 also demonstrates the relevance of the EERRI model to countries that are in the decommissioning process, where their existing nuclear capability is limited and access to decommissioning management information might not be readily accessible. This group constitutes only a small percentage of total course participants, but indicates a relatively inexpensive initial investment in educating a new generation workforce to reduce the economical and human resources risk for a particularly expensive and lengthy process.

2.2 Individual statistics on the EERRI Group Fellowship model

A general trend amongst EERRI participants is the tendency towards a more advanced academic and senior employment background, with over 40% having a master's level degree or higher at the time of application. Of those with no postgraduate education, 18% were already in senior level positions within their organisations, and a further 15% were already involved in reactor operations at their institution[7]. Figure 4 depicts the academic qualification levels of participants, and Figure 5 shows the employment fields of participants at the time of application.

[7] Participant data from IAEA Technical Cooperation internal database (not publicly accessible). An applicant was considered senior if the word 'principal,' 'chief,' 'head,' 'manager' or 'senior' was listed within the position title.

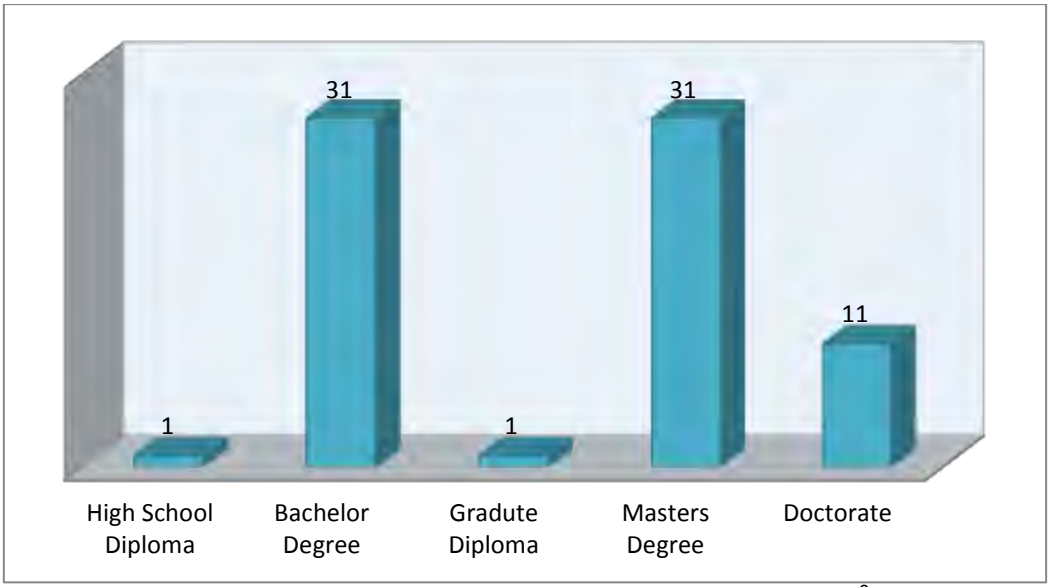

Fig 4: Academic qualifications of EERRI participants[8]

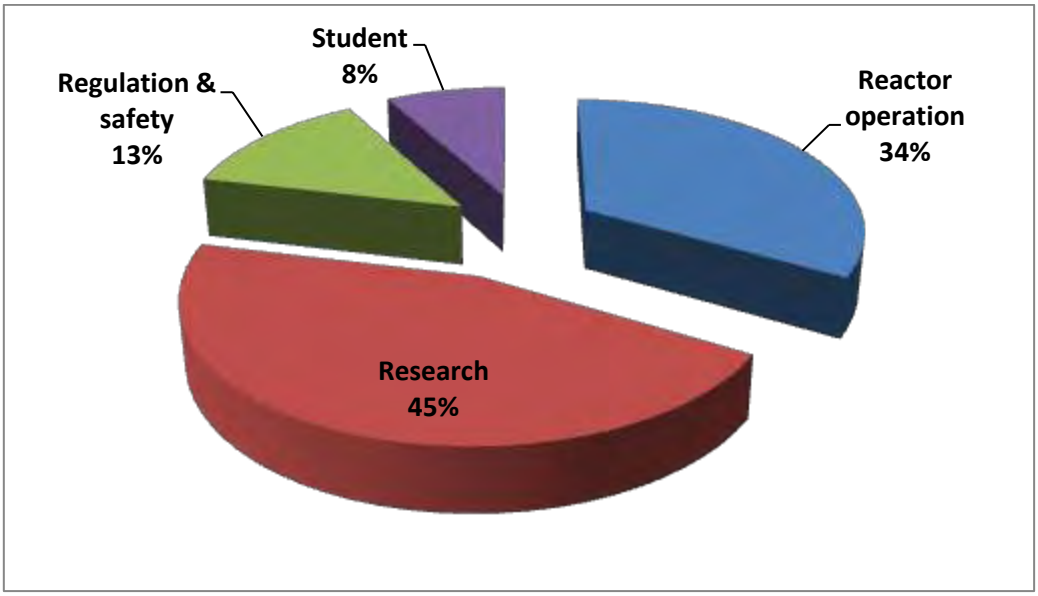

Fig 5: Employment fields of EERRI participants at the time of application

Figure 5 shows that only 8% of participants are university students, whereas over 45% identified employment with their national scientific body. In most cases, participants from a country with a research reactor were already employed by the research reactor institution, instead of postgraduate students at accompanying universities that might not have access to the research reactor to enhance their basic nuclear education. Encouraging Member States to nominate a greater proportion of university students would be beneficial. This type of applied course is also effective at augmenting university programmes in order to give students a practical understanding early in their career on the various considerations for research reactor operations and applications, and can better inform and shape their future career choice, thereby enhancing the workforce with a greater number of committed individuals.

3. Extension of the EERRI Group Fellowship to other regions

[8] A graduate diploma is generally a postgraduate qualification, taken following the completion of a bachelor's degree and allows progression to a master's degree.

3.1 National nuclear capacity building and programme sustainability

The EERRI Group Fellowship Programme is a unique example of research reactor networking that transfers knowledge and practical experience from one region to another. For example, KA CARE in Saudi Arabia has identified the benefit of knowledge exchange on the course to their national nuclear capability, and has begun funding their own places on the programme as they embark on their first nuclear build. This is essential to the sustainability of not just the capability of individual countries, but also the sustainability of the programme itself. However, there are currently not enough courses to meet the demand from Member States, which increases the need to expand the EERRI model to other regions.

Self-funding could also be explored by developed countries. Enhancing the accessibility of the EERRI course to students from developed countries, such as advertising programmes and including application forms on the relevant research reactor coalition website, could bring additional interest from countries in the region that may not benefit from an IAEA Technical Cooperation programme.

This programme is also effective in imparting training to instructors from other research reactor facilities outside the host region. The observation in paragraph 2.2 that more senior participants tend to be selected for the programme, suggests benefit in extension of the EERRI model to specifically cater for this group. A ‘train the trainer’ course may beneficial for more senior individuals who already have significant experience in research reactor operation, and could benefit a younger workforce through a greater number of skilled teachers.

Other research reactor coalitions are looking to apply a similar model to their own regions, the most recent being an upcoming course run jointly by Malaysia and Indonesia. Practical reactor physics courses have been raised in meetings of other research reactor coalitions, but they have not gained the requisite momentum to be conducted. Separately, a number of successful courses have been run in the past, with some continuing today, but have not included training on more than one reactor. Of note, the CEA ISIS reactor in France offers courses to international students and professionals on areas such as reactivity experiments, core loading, temperature effects, and the utilisation of research reactors, which covers similar topics to the EERRI course [8]. Additionally, the Baltic Research Reactor Network has previously offered one day experimental courses in Finland [9]. However, these examples are only of one reactor offering the training, and the EERRI model is greatly enhanced by delivering education at reactor locations with different capabilities, different teaching methods amongst staff, and the flexibility of different facilities to rotate the burden of limited time and resources. Of note, ISIS has since become a member of the EERRI Coalition, which may increase the number of facilities available on the course.

3.2. Applying the EERRI Group Fellowship model to the Asia-Pacific region

A recent extension of the EERRI model has resulted in the development of the ‘Nuclear School Experiments on Reactor Physics and Neutron Applications for the Asia-Pacific Region.’ The course is due to begin in late March 2015, and will run for two weeks. Like the EERRI Group Fellowship, it is a joint school run in cooperation with the IAEA by the Indonesian Nuclear Energy Agency (BATAN) and the Malaysian Nuclear Agency (MNA), at the TRIGA KARTINI reactor and the TRIGA PUSPATI reactor, respectively. The course is aimed towards countries in the region that already have a research reactor, or wish to develop nuclear competence as a first step in embarking on a new nuclear build (either a research reactor or NPP). The school is aimed at young professionals with basic nuclear experience, preferably with a technical degree in engineering or science, who intend to contribute to the national nuclear capability of their country. Like the EERRI programme, the school focuses on hands-on neutronics education, and research reactor operations and management [10].

As a number of countries in the South-East Asian region embark on a new nuclear build,

this course will alleviate the geographical distance and related higher costs to students from this region, by offering an alternative to the EERRI Group Fellowship course. The course has received technical and administrative support by the IAEA to help establish the course until it becomes self-sustainable.

Participant countries for the first course include Bangladesh, Indonesia, Malaysia, Vietnam, Thailand, Cambodia and Iraq. Nearly all course participants are young professionals in the early stages of their careers, or postgraduate students. It is anticipated that younger participants, rather than mid-career or senior reactor physics professionals, will gain more benefit in enhancing their fundamental knowledge and developing greater understanding of reactors and their requirements. This will also assist in motivating a new generation towards reactor physics and nuclear engineering.

Students from countries in the region that are economically developed but lack the capability to run equivalent practical training will also benefit from attending this type of course. For example, Australia is an economically developed country in the region that possesses a nuclear capability, however this capability consists of a 20 MW research reactor primarily used for commercial and research purposes, and is utilised too heavily in these areas to facilitate basic neutronics training. It is not economical for Australian universities to send a student to Europe for six weeks to conduct the EERRI Group Fellowship Programme, and the IAEA's Technical Cooperation mechanism is unable to fund students from developed countries. This shorter, closer and less expensive course could allow a small number of Australian students to gain practical experience in basic reactor physics and engineering, and reactor operations and management.

In addition to the training of students for this course, academic staff from the Czech Technical University in Prague (one of the EERRI training institutions), and the CEA's ISIS reactor in France, will attend a facility each to impart their teaching experience to local staff prior to and during the course. This IAEA-sponsored 'train the trainer' method will enhance the quality and sustainability of future courses in the region.

4. Conclusion

Key challenges remain for governments and their institutions to provide practical, fundamental and complete nuclear reactor physics and engineering education to a new generation entering the workforce. This is especially significant for countries that do not own a suitable research reactor, and are seeking education and training from overseas research reactor facilities in support of their nuclear capacity-building objectives. The success of the EERRI Group Fellowship Programme is largely based on both the motivation of the contributing staff from the host reactors, and the flexibility and variations in staff and research reactor facilities. Long term sustainability of coalition-based international programmes is a key challenge that requires planning and commitment. However, this involves a large financial burden, both to the IAEA who cannot permanently sustain these courses, and to the governments, institutions and students requiring this education. Additionally, the EERRI Group Fellowship Training Programme is currently only able to train approximately 20 students per year, which is outweighed by demand from applicant Member States.

Implementing regional research reactor courses will enable both developing and developed countries to benefit from suitable facilities nearby. This can be facilitated through the formation of a committed regional research reactor coalition, and by using experienced reactor training staff from other regions to guide and train teachers in the setup of their own regional courses. Furthermore, experienced reactor operators, such as many who have attended previous EERRI courses, could receive training and guidance on the teaching of students in their own regions as part of a coalition course. There are a number of research reactor coalitions currently in place over the world, and with further commitment, planning and training could successfully apply the approach established by EERRI and the Asia-Pacific network.

REFERENCES

1. H. Boeck, et al, 'Human Resources Development by the Eastern European Research Reactor Initiative (EERRI),' International Conference on Human Resources Development for Nuclear Power Programmes: Building and Sustaining Capacity, Vienna 12-16 May 2014.

2. L. Sklenka et al, 'EERRI Coalition as a Platform for Close Cooperation – an Enhanced Utilisation of Research Reactors in Central and Eastern Europe.' IAEA Technical Meeting, Vienna, 2012.

3. IAEA, Web Page on Research Reactor Section Utilization and Applications: http://www.iaea.org/OurWork/ST/NE/NEFW/Technical-Areas/RRS/Utilization-Applications.html.

4. L. Snoj et al, 'Eastern Europe Research Reactor Initiative Nuclear Education and Training Courses – Current Activities and Future Challenges,' PHYSOR Conference, Tennessee, USA, April 2012.

5. IAEA Research Reactor Database (RRDB): http://nucleus.iaea.org/RRDB.

6. United Nations Department of Economic and Social Affairs 'Classification of Countries by Major Area and Region of the World,' 2012 (to obtain definitions of regions)

7. IAEA Nuclear Technology Review 2015.

8. Working Document, Report of the IAEA Technical Meeting, 'F1-TM-42756, jointly with TC project RER1007 Research Reactor Coalitions: Concerted actions in the Mediterranean Region,' Istanbul, Turkey, 10 – 13 July 2012.

9. Report of the 3rd Coordination Meeting of the Baltic Research Reactor Network (BRRN), Stockholm, Sweden, 2-4 February 2011.

10. Nuclear School Experiments on Reactor Physics and Neutron Applications for the Asia-Pacific Region, Course Prospectus, IAEA, MNA and BATAN, February 2015.

11. Eastern European Research Reactor Initiative (EERRI) Coalition web page: www.eerri.org.

JULES HOROWITZ REACTOR: UPDATE OF THE EXPERIMENTAL CAPACITY

C. BLANDIN, J. ESTRADE, J. PIERRE, P. JAECKI, C. COLIN, T. DOUSSON, L. FERRY, C. GONNIER,

French Alternative Energies and Atomic Energy Commission (CEA[2])
CEA, DEN, DER, SRJH, F-13108 Saint-Paul-lez-Durance, France

ABSTRACT

The Jules Horowitz Reactor (JHR) is a high performance Material Testing Reactor under construction in southern France (CEA/Cadarache research centre), that will carry out experimental irradiations for Nuclear Power Plants (NPP) and fuel vendors, utilities, safety organizations and research institutes. Therefore CEA is developing a set of test devices that will be operational for the start-up of the reactor or few years later. These experimental hosting systems will have to fulfil experimental needs concerning current NPP technologies (GEN II-III) and future reactors (GEN IV) as well.

Experimental programs could be related to either fuel basis properties acquisition, mastering of margins or improvement of fuel products (clad and pellet), in term of performance, safety, maximum burn up, innovative materials or extension of validation domain of fuel performance codes.

Then the present paper describes the main experimental hosting systems currently under design:

- The MADISON device will be available at the JHR start up, and will allow testing the comparative behaviour of several instrumented fuel rods (from 1 up to 8 rods, of up to 60 cm fissile stack height) under NPP normal operating conditions (no clad failure expected).
- The ADELINE device will be available for the JHR start up, and will allow testing a single experimental rod up to its operating limits. The fuel rod will be tested under conditions that correspond to off-normal situations with possible occurrence of a clad failure. The first version so called ADELINE “power ramps” will focus on the clad failure occurrence during one of these abnormal situations.
- The LORELEI device will be available few years after the reactor start up and will allow testing a single rod under accidental situation that may lead to fuel damage. It will be able to reproduce all sequences of a LOCA-type transient, including the re-irradiation, the loss of coolant and the quenching phases, on a separate effect approach.

In-core and in reflector material test devices are presented as well, corresponding to large ranges of irradiation conditions, in terms of temperature, neutron flux and neutron spectra. A special attention focuses on the improvement of the thermal stability and gradients in the interest zones of irradiated samples. Some specific devices are described such as equipments designed to the qualification of reactor pressure vessel steels (OCCITANE test device), to the studies of creep-swelling of structural materials (MICA test device) or to the study of the stress corrosion cracking assisted by irradiation phenomena (CLOE test device: a corrosion loop with an accurate water chemistry monitoring for PWR or BWR requirement).

1. Introduction

The Jules Horowitz (JHR) Material Testing Reactor will be commissioned by the end of this decade as an international user’s facility on the CEA/Cadarache site. It will be dedicated to materials and fuel irradiations for the nuclear industry, utilities, TSO,

regulators, or research institutes. As an associated objective, the JHR will also contribute to secure the production of radioisotopes for medical applications. A detailed presentation of the project status is given in ref. [1].
The design of this facility allows a large flexibility in order to comply with a broad range of experimental requirements, regarding the type of samples (fuel or material), neutron flux and spectrum, type of coolants and thermohydraulics conditions (LWR, Gen IV,…), in accordance with the scientific objectives of the programs. These experimental tools are under development and some of them will be available at JHR start up.
After reminding the main characteristics of the reactor facility, the experimental capacity is described and a focus on the main test devices under development is given.

2. Main Characteristics of the JHR facility and experimental capacity

This facility is based on a 100 MW pool reactor compact core cooled by a slightly pressurized primary circuit. The core tank is located in the reactor pool.

2.1 A modern facility with a large area dedicated to experiments

The nuclear facility comprises a reactor building with all equipments dedicated to the reactor and experimental devices and an auxiliary building dedicated to tasks in support for reactor and experimental devices operation (see Figure 1).
The reactor building is designed to provide the largest experimental capacity possible with the largest flexibility. One half of this building is dedicated to the implementation of equipments in support to in-pile irradiations (for example, water loops). This corresponds to 700 m^2 over 3 floors for implementation of experimental cubicles and 490 m^2 over 3 floors for instrumentation and control equipments.

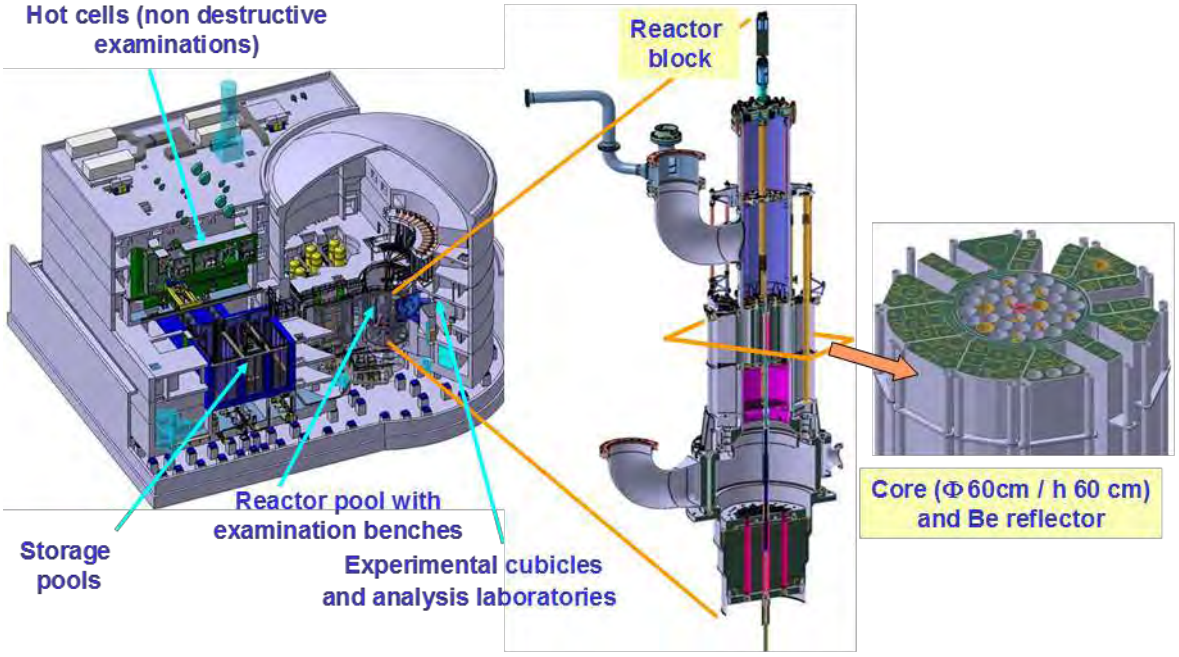

Figure 1: Views of the JHR facility and the reactor core

2.2 A powerful reactor with numerous irradiation sites and irradiation conditions

The design of the reactor (see Figure 2) provides irradiation sites situated inside the reactor core with the highest ageing rate (up to 16 dpa/year) and irradiation sites situated in the Beryllium reflector zone surrounding the reactor, with the highest thermal flux.

Numerous locations are implemented (up to 20 simultaneous experiments) with a large range of irradiation conditions:

- 7 in-core locations of small diameter (32 mm) with a high fast neutron flux (up to 5.5E14 $n.cm^{-2}.s^{-1}$ perturbed flux above 1 MeV)
- 3 in-core locations of large diameter (80 mm) with a high fast neutron flux (up to 4.E14 $n.cm^{-2}.s^{-1}$ perturbed flux above 1 MeV)
- 20 fixed positions (100 mm of diameter and one location with 200 mm) with a high thermal neutron flux (up to 3.5E14 $n.cm^{-2}.s^{-1}$ perturbed flux)
- 6 positions located on displacement devices located in water channels through the Beryllium reflector

A typical reactor cycle is expected to last 25 days, and CEA targets to operate the reactor 10 cycles per year.

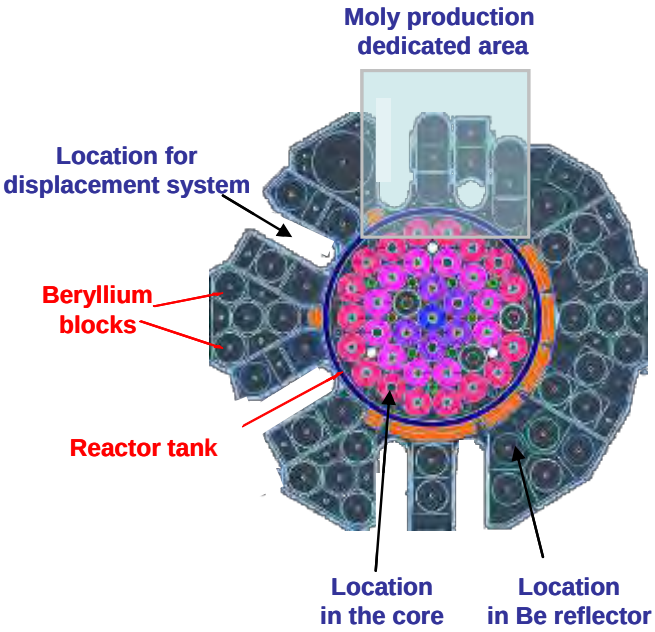

Figure 2: Views of the experimental locations

2.3 Non-destructive examination benches

The JHR experimental programs will also take advantage from Non-Destructive Examination (NDE) benches, present in the facility with the aim of significantly improving the scientific quality of the JHR irradiation process:

- A coupled gamma scanning-X tomography bench located in the reactor pool (adapted to welcome irradiation devices) (see details in ref. [3]) ;
- A neutron radiography bench (developed with EDF support) located in the reactor pool (see details in ref. [2]) ;
- A coupled gamma-X tomography bench, identical to the previous one and located in the storage pool of the Nuclear Auxiliary Building ;
- Non-destructive examinations in hot cells after extraction from the experimental devices (visual inspection, photography, metrology and Eddy Current testing).

These NDE stands can be used at several steps of the experimental program:

- For initial check of experimental load status by the irradiation phase (after transportation, assembly in JHR hot cell or insertion in the device) ;
- For adjustment of experimental protocol or control parameters after a first short irradiation run ;
- For a rapid examination of samples after an irradiation phase (e.g. geometrical changes after an off-normal transient, quantification of short half-life fission product distribution…) when the examination is performed in the reactor pool with limited handling ;
- For a delayed detailed examination of samples after the end of an irradiation program when the examination is performed in the storage pool, either for scientific data acquisition or for defining samples status before transportation.

3. Irradiation hosting systems available at the JHR start-up

3.1 MADISON test device

This test device will carry out irradiations of LWR fuel samples (60 cm fissile stack) when no clad failure is expected. Consequently, the experimental conditions correspond to normal operation of power reactors (steady states or slow transients that can take place in nuclear power plants) (ref. [4]).
This experimental device is made of an in-pile part (holding the fuel samples) fixed on a displacement system. This system allows on-line regulation of fuel linear power on the samples. Thanks to the high thermal neutron flux in the JHR reflector, this is possible to reach high linear power even on high burn-up samples (as an example, it is possible to reach 400 W/cm for a burn up of 80 GWd/t for a common UO2 fuel of initial enrichment 4.95%).
The in-pile part is connected to a water loop providing thermal-hydraulics conditions expected for a given experimental program. The water loop (implemented in a dedicated cubicle, see Figure 3) allows reproducing the thermal-hydraulics conditions of nuclear power plants (PWR, BWR or WWER technologies) in terms of water loop pressure (up to 160 bar) and temperature (up to 320°C). A specific chemical analysis system and a water treatment system allow a continuous regulation of chemical conditions.
In order to meet the large range of experimental needs expressed by the nuclear industry, the test section of the in-pile part has a large volume. This allows loading a large panel of sample holders from high embarking capacity (up to 8 samples) with low instrumentation to low embarking capacity (up to 1 sample), but highly instrumented.
The first irradiation rig version has a carrying capacity of 4 fresh or pre-irradiated samples (with a maximum of 2 sensors per sample) and is flexible enough to operate with 2 samples (highly instrumented).
For sample instrumentation, 5 tight high temperature and pressure connectors are implemented on the sample holder to allow the plug-in of specific instruments (see Figure 3).

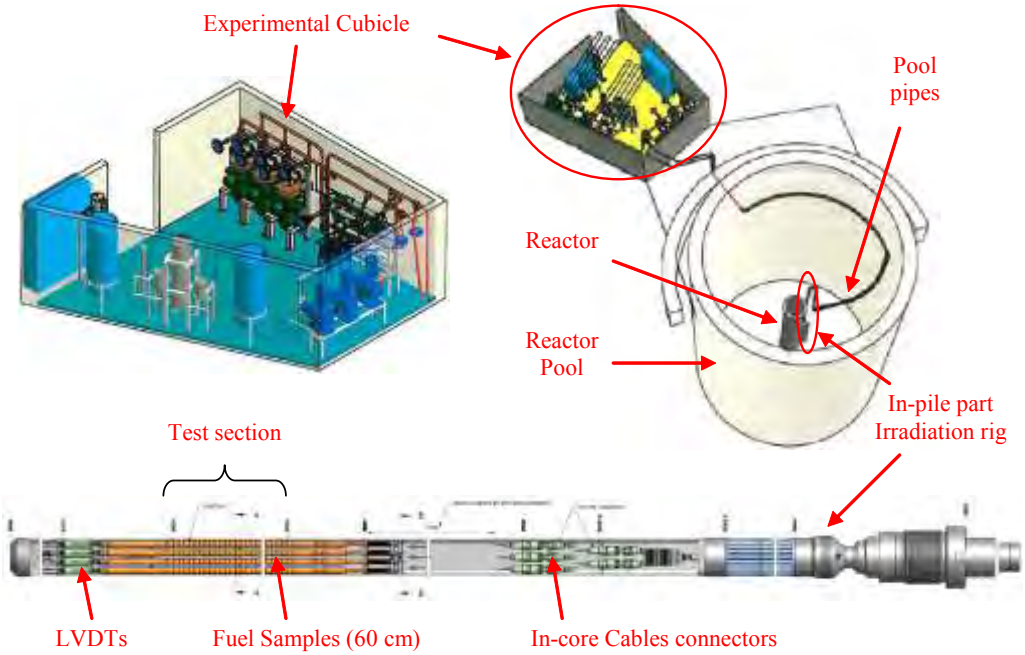

Figure 3: Views of the MADISON test device with focus on the water loop and on the first rig

The following instrumentation can be easily used in the first MADISON sample holder manufactured for the JHR start up: fuel central temperature, clad temperature, clad elongation, fuel stack elongation, fuel plenum pressure, fission gas release composition based on acoustic measurement device.

3.2 ADELINE test device

The ADELINE test device, developed with EDF support, is able to hold a single experimental fuel rod from all LWR technologies to reproduce various experimental irradiation scenarios where clad failure is either a risk or an experimental objective (ref. [4]). Similarly to the MADISON experimental device, this experiment is made of an in-pile part and an out-of-pile water loop (see Figure 4). Fresh or pre-irradiated fuel rods can be used to perform: power ramp tests, rod internal over-pressurization ("lift-off"), rod internal free volumes gas sweeping or power to melt approach margin mastering.
A first version is mainly dedicated to power ramps testing. In particular, the design of this device is optimized to provide a qualified thermal balance and a good accuracy on the clad failure instant and consequently a good knowledge of the linear power inducing the failure. A quantitative gamma spectrometry system allows quantifying the radiological source term released in the coolant since a rod fails.
Some enhancements are added in order to make on-line quantitative clad elongation measurement during power transients and to manage several successive experiments during one reactor cycle. In addition, this device can be easily upgraded in order to manage highly instrumented experiments with fuel and clad temperature measurement and fission gas release measurement by gas sweeping. In a longer term, a second version will be dedicated to the study of the long-term post-failure behaviour in normal conditions (failure evolution, secondary hydriding, release of fission products and of fissile material…), coupled with the fission product laboratory.

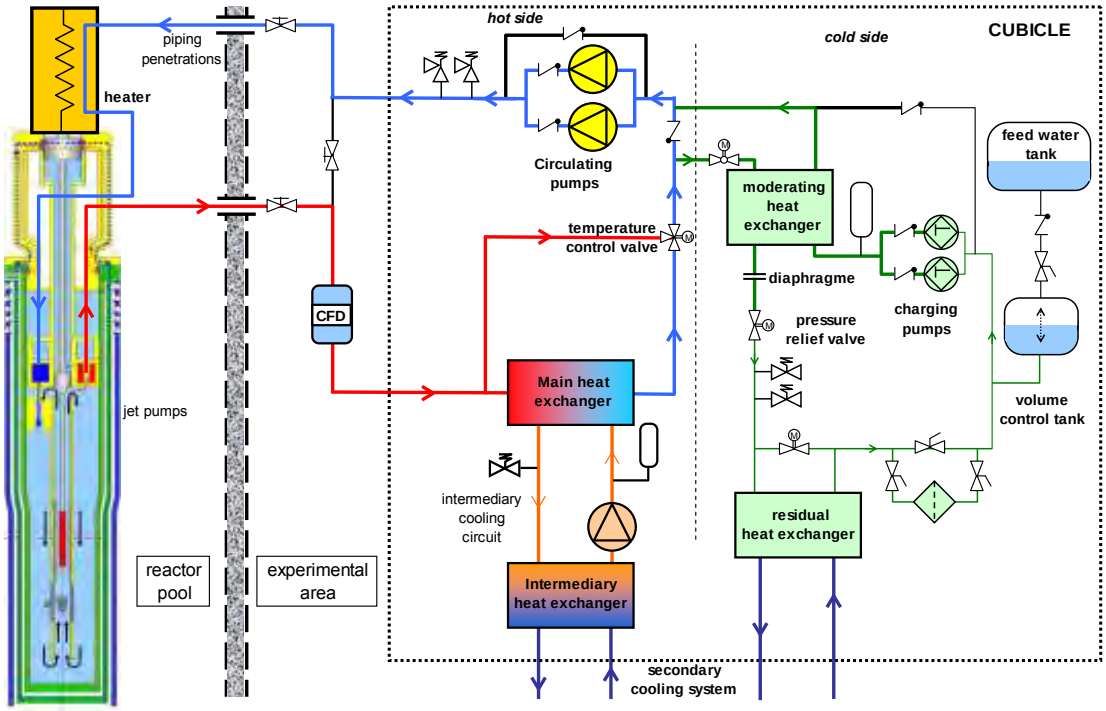

Figure 4: Schematic diagram of the ADELINE loop

A typical PWR power ramp sequence is made of the following phases (see Figure 5):

- A low power plateau (from 0.5 up to 7 days) with control of clad surface temperature at 330°C (±10 °C) while the sample linear heat rate is controlled between 50 and 250 W/cm, depending on customer's request ;
- A linear power ramp at a continuous rate ranging between 100 and 700 $W.cm^{-1}.min^{-1}$. During this phase, clad surface temperature is stable at saturation condition, as soon as the sample reaches 350 $W.cm^{-1}$ at its peak level ;
- A high power plateau that may last 24h at a linear heat rate up to 620 $W.cm^{-1}$ (at the sample peak level).

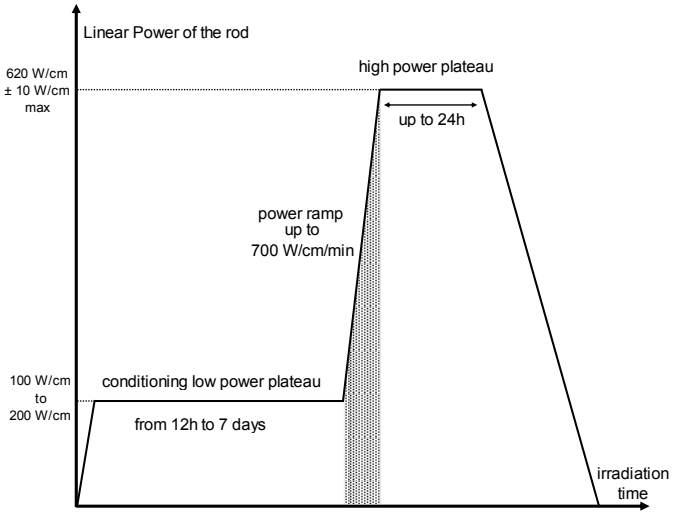

Figure 5: Standard power ramp test time history

3.3 MICA test device

The MICA test device is devoted to the irradiation of materials, such as fuel cladding materials or NPP internal structures materials. It consists of 2 concentric tubes delimiting a gas gap (see Figure 6), which is mainly used to adjust the temperature inside the internal tube (gap dimension, nature of the gas).
Electric heating elements are placed on the internal tube, embedded within an aluminium spray. This heating method ensures fine control of the samples temperature.
The MICA device has the same performances than the current CHOUCA test device widely used in OSIRIS reactor, i.e. irradiation of various geometries of samples in NaK (up to 450°C) or gas (up to 1000°C). These test devices are mainly designed for in core irradiations were fast flux can reach up to 16 dpa a year (at 100 MW).

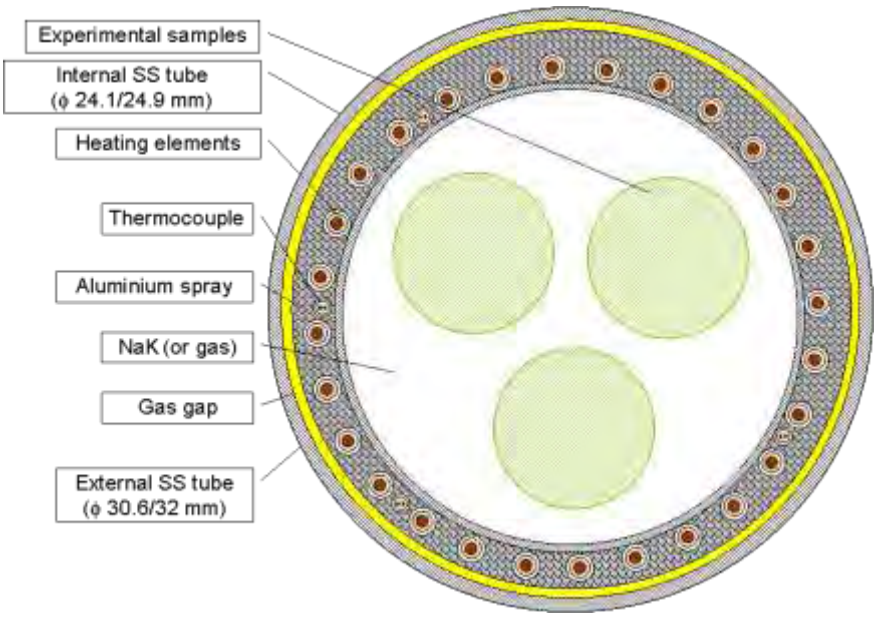

Figure 6: MICA test device cross-section.

4. Irradiation hosting systems available after the JHR start-up

4.1 CALIPSO test device

As the MICA hosting system, the CALIPSO test device (in-Core Advanced Loop for Irradiation in Potassium SOdium) is mainly dedicated to the irradiation of material samples immersed in NaK. Unlike MICA, NaK is not static within CALIPSO: a NaK flow is indeed induced with an innovative electromagnetic pump, implemented in upper in-pile part of CALIPSO (see Figure 7). This embedded thermohydraulic loop features mainly an electrical heater and a heat exchanger as well. CALIPSO meets the original need of a low temperature axial gradient (a maximum of 8 °C is the target) all along the samples stack, up to 450°C for a first step of development, and up to 600°C in a second phase. The setting of each parameter (power of heater, flow of the pump and efficiency of exchanger) will lead to a full control of the thermal conditions inside the test device and in particular in the sample location. Qualification tests with a regular scale CALIPSO model (and thus the innovative electromagnetic pump) have been successfully performed in 2014 using a dedicated experimental platform so called SOPRANO.

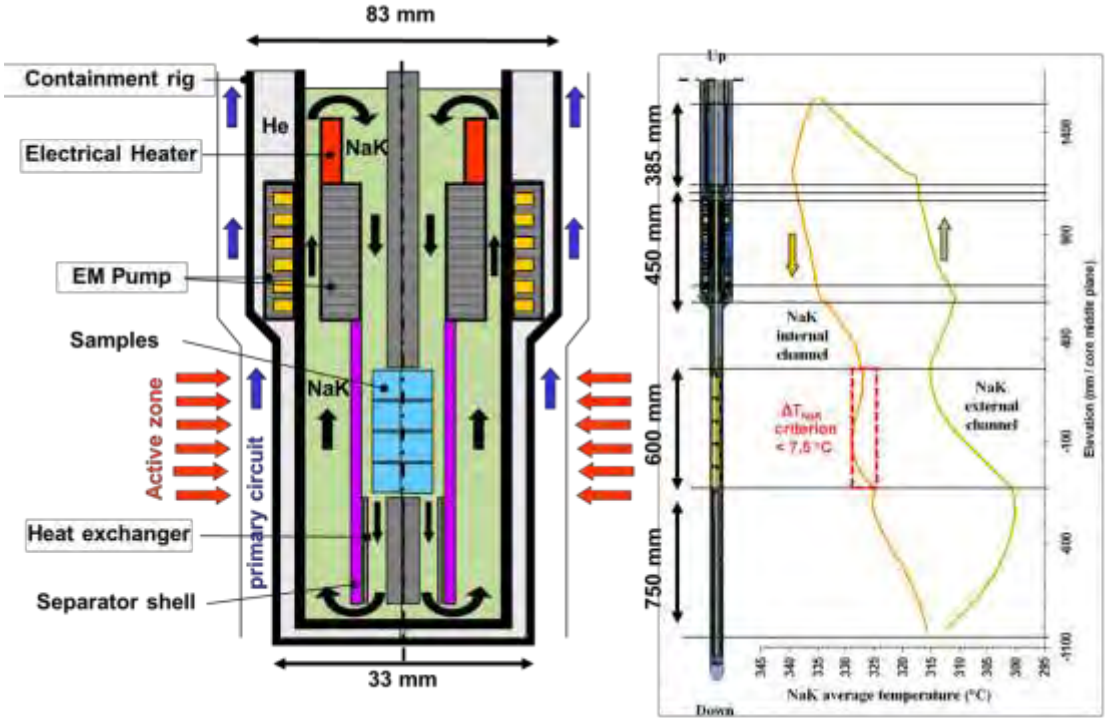

Figure 7: CALIPSO functional sketch

4.2 OCCITANE test device

In the field of pressure vessel steels of NPPs, irradiations are carried out to justify the safety of this 2nd containment barrier and to improve its lifetime. Then CEA is designing a hosting system so named OCCITANE (Out-of-Core Capsule for Irradiation Testing of Ageing by Neutrons), which will allows irradiations in an inert gas at least from 230 to 300°C. It will be implemented in the JHR reflector and reach damage rate around 100 mdpa/year (E >1 MeV). The associated instrumentation will include at least thermocouples and activation foils as close as possible to the samples. OCCITANE is based on IRMA device of OSIRIS. The ongoing design studies consist mainly in decreasing thermal gradient in the sample area (see Figure 8) and in integrating the capsule to the JHR environment.

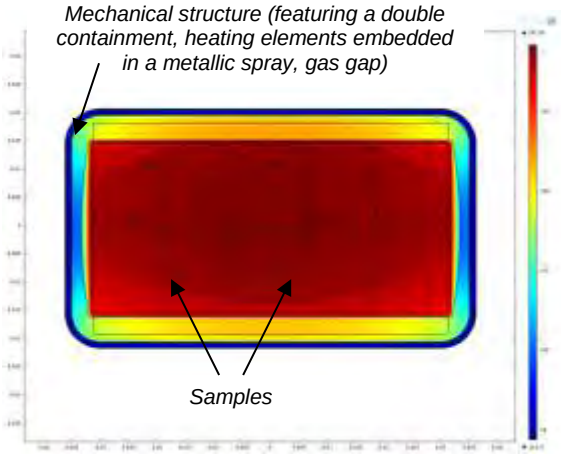

Figure 8: Calculated temperature map in the OCCITANE device (core mid-plane, 0.6 W/g)

4.3 CLOE test device

Due to ageing of the NPPs, stainless steel core components undergo increasing radiation doses, which enhance their susceptibility to local corrosion phenomena, known as irradiation-assisted stress corrosion cracking (IASCC). Cold laboratories can study and model SCC phenomena; but to really be representative of LWR environments, these studies require integral tests in MTR to take into account irradiation effects (radiation dose and flux). To answer to these industrial needs, DAE (India) and CEA have launched the design of a LWR corrosion loop (so-called CLOE), likely located in the JHR reflector, close to the tank. Then CLOE will reproduce as close as possible the nominal environment of LWR reactors, including well known and well controlled water chemistry and will allow to apply a mechanical loading of the specimens during the experiment (see Figure 9).

This test device will be made of a double wall pressure flask (cylindrical shape) containing an irradiation rig which will carry the samples and all measurement sensors for experimental and safety purpose. This in-pile part will be connected through under-water pipes to experimental components such as pumps, heat exchangers or water tanks located in an experimental cubicle (see Figure 10).

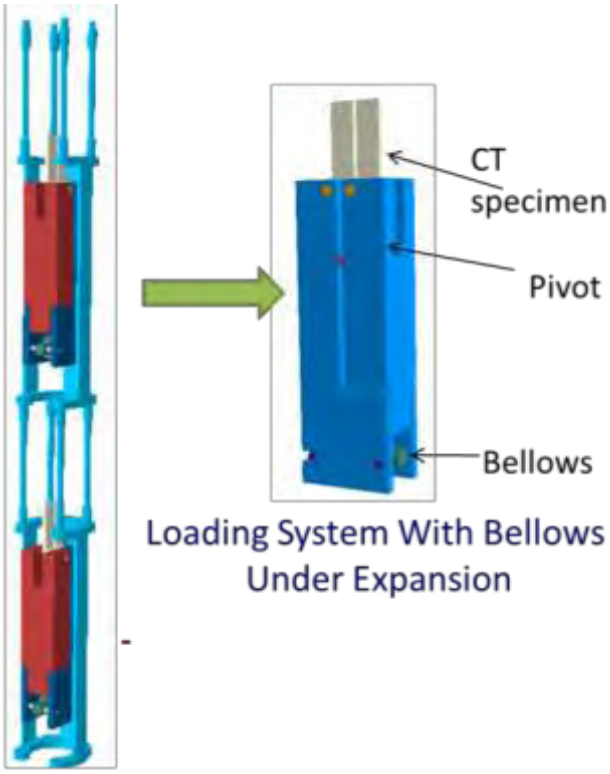

Figure 9: View of CLOE sample holder

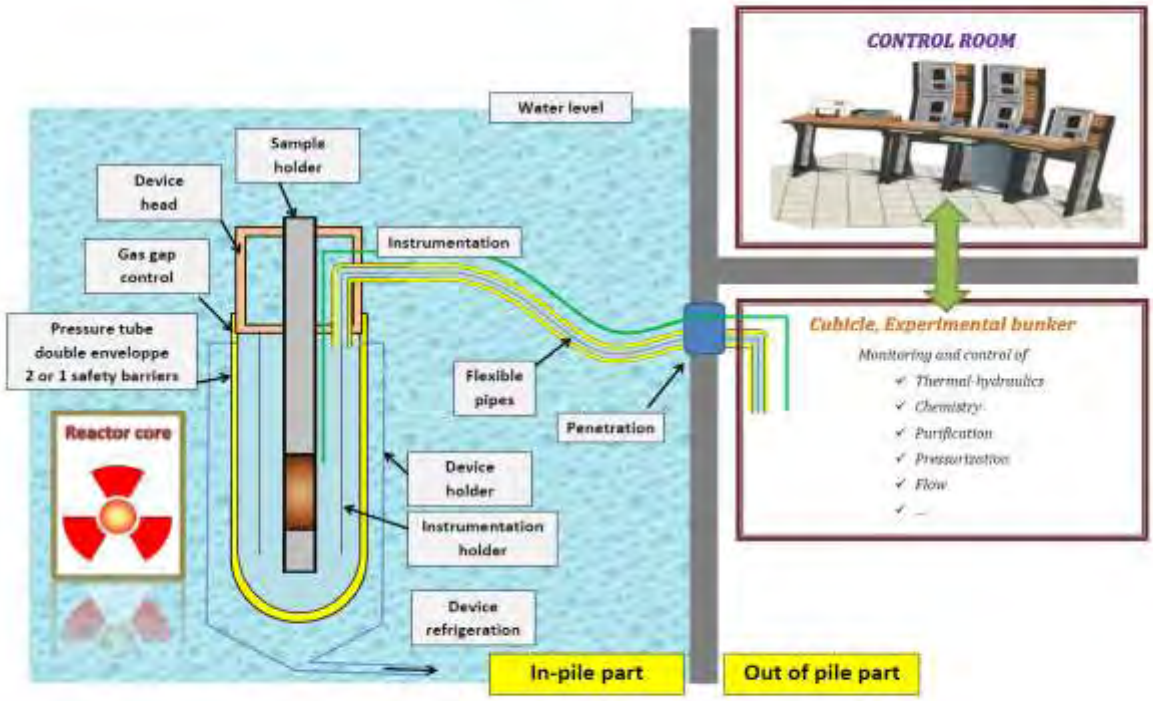

Figure 10: Architecture of the JHR Corrosion Loop (CLOE)

4.4 LORELEI test device

The purpose of LORELEI device is to investigate the behaviour (thermal-mechanical and radiological consequences) of LWR-type pre-irradiated fuel rods under “Loss Of Coolant Accident” conditions (ref. [4]). The thermal-hydraulic phenomena does not reproduce all phases of a realistic LOCA-type power reactor sequence (in particular the first clad temperature peak), but the thermal-mechanical conditions (clad temperature, clad over-pressure, steam environment) will be representative (see Figure 11).

This equipment consists in an integrated water capsule that can be operated as a thermo-siphon able to cool and re-irradiate a single pre-irradiated fuel sample, and to produce a short half-life Fission Product (FP) inventory. For the first version of the test device, the re-irradiation power is low and adapted to the production of a detectable short half-life FP inventory (versus long half-life radionuclides already present in the fuel material). Next version will allow reproducing thermal conditions representative of current LWR power reactors and performing a re-irradiation of samples at higher power in order to simulate the effects of the local peak power (“core hot spot”) and to produce a representative FP inventory and distribution at the accidental sequence start-up.

It is equipped with a gas injection able to rapidly empty the test device in order to simulate the dry-out phase of the fuel rod during LOCA transient. A neutron shielding can be used to flatten the axial neutron flux profile. An electrical heater implemented in the sample holder allows getting a homogeneous temperature azimuthal distribution and acts as a dynamic thermal insulation in order to get representative adiabatic conditions (initial heat-up rate depending on customer request and typically ranging from 10 up to 20°C/s).

The high temperature phase (up to about 1200°C) will be monitored by adjusting the rod nuclear power with the displacement system. During this phase, the electrical heater will be switched-off in order to increase heat losses and to prevent any temperature escalation (e.g. due to steam – zirconium reaction). At last, low temperature water can be re-injected in the device to simulate the quenching process.

This device, designed in collaboration with IAEC (Israel), allows investigating ballooning and burst of the fuel cladding (the inner pressure of the fuel rod can be monitored to that purpose), clad corrosion phenomena (oxidation and hydriding), thermal-mechanical behaviour, quenching, post-quench behaviour and fission product release. To that purpose, the device will be connected to a fission product laboratory.

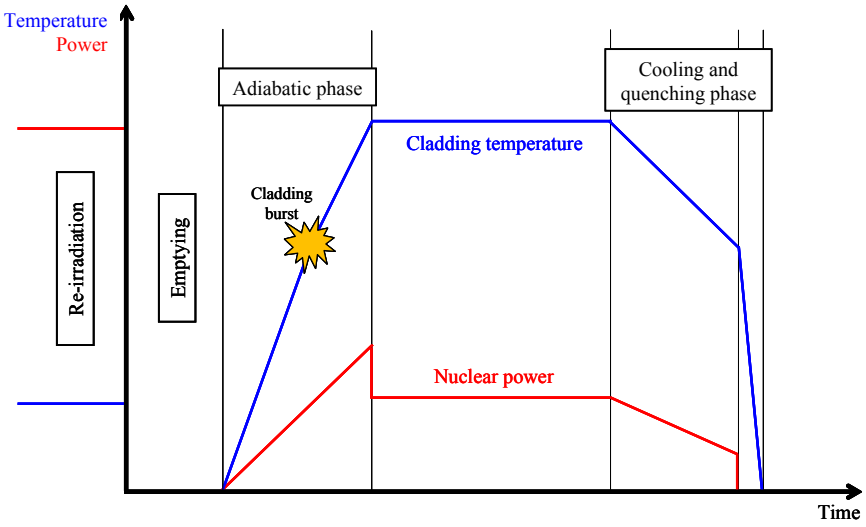

Figure 11: Phases of the LOCA sequence

5. Conclusion

The Jules Horowitz reactor is under construction at the CEA/Cadarache centre (France) with a target of commission by the end of this decade. Then JHR prepares to be a key infrastructure in the european and international research area for R&D in support to the use of nuclear energy during this century

This paper gives an overview of the JHR experimental irradiation capacity, and presents in particular the main material and fuel hosting systems currently under design and development. Some of them will be available at the JHR start-up: ADELINE, MADISON, MICA and NDE stands.

6. References

[1] G. Bignan et al., “The Jules Horowitz research Reactor: a new high performance Material Testing Reactor working as an international user facility”, International Group On Research Reactors (IGORR), 17-21 Nov., 2014, Bariloche, Argentina

[2] D. Parrat and al., “The future underwater neutron imaging system of the Jules Horowitz MTR: an equipment improving the scientific quality of irradiation programs”, International Group On Research Reactors (IGORR), 13-18 Oct., 2013, Daejeon, South Korea.

[3] C. Roure et al., “NDE development for the JHR material testing reactor”, ANIMMA, 23-27 June, 2013, Marseille, France.

[4] C. Blandin and al., “LWR Fuel irradiation hosting systems in the Jules Horowitz Reactor”. LWR Fuel Performance Meeting (LWRFP), 15-19 Sept. 2013, Charlotte, NC, USA

ACTIVITIES AT TRIGA RC-1 ENEA REASEARCH REACTOR

L. FALCONI, C. INNARELLA, M. PALOMBA, M. CARTA, M. SEPIELLI
Technical Unit for Nuclear Fission Technologies and Facilities, and Nuclear Material Management
ENEA
Via Anguillarese 301, 00123 S.Maria di Galeria (Rome) - Italy

ABSTRACT
TRIGA Mark II reactor of ENEA's Casaccia Research Center (in Italy named RC-1) reached its first criticality in 1960, with a maximum thermal power of 100 kW. In 1967 it was upgraded at the thermal power of 1 MW. Currently the core, fully reflected by graphite, contains 111 TRIGA fuel elements. The reactor is moderated by demineralized water, which serves also as first biological shield and coolant. Heat produced by the core is removed by natural convection. In this paper we describe the upgrade of the instrumentation, equipment and experimental devices, the implementation of a TRIGA RC-1 dynamic model and of a MCNP model for the evaluation of the fuel elements burnup. Since the first core configuration at the operating power of 1MW, labeled 38, a great amount of data regarding, among other things, critical configurations, measured flux and control rods calibration have been collected. To supply a more accurate database on the fuel element burnup values, and with the aim of integrate a TRIGA RC-1 internal procedure, based on the total power generated, computer codes such as MONTEBURNS and MCNP5 will be used in the next future. Moreover a dynamic model dedicated to the simulation of the reactor dynamic behavior is described: in particular the model simulates operational transients, alarm situations followed by scram or shut-down operational phases, criticality incidents and instantaneous water loss. The model is validated on experimental data regarding low and full power reactor tests, operation of the reactor in normal and incidental conditions, in this last case in accordance with TRIGA RC-1 SAR evaluations. Control rods calibration and Xenon reactivity data complete the validation of the model. Finally, considering operation and maintenance activities, the paper describes modernization of instrumentations in the control room and the installation of a new irradiation facility in the shielded tank.

1. TRIGA RC-1 Research reactor

RC-1 is a thermal pool reactor, based on the General Atomic TRIGA Mark II reactor design, operating at the thermal power of 1MW [1]. The core, in the current configuration loaded with 111 standard TRIGA fuel elements, is contained in an aluminium vessel, seven meters deep, filled with demineralised water. A cylindrical graphite structure around the core acts as lateral reflector of the reactor. The biological shield is provided by concrete with an average thickness of 2.2 meters. The water inside the vessel provides the first biological shield, neutron moderation and core cooling. Thermal power is removed from the core by natural convection, and exchanged with the environment through two thermohydraulic loops, coupled by two heat exchangers and two cooling towers. A horizontal section of the core, showing the graphite surrounding the core, a detail of the core with fuel elements, control rods and graphite dummies elements is provided in Fig 1.In Fig 2 the horizontal and vertical sections of the reactor are shown, together with a 3D section of the reactor showing the different neutron channels.

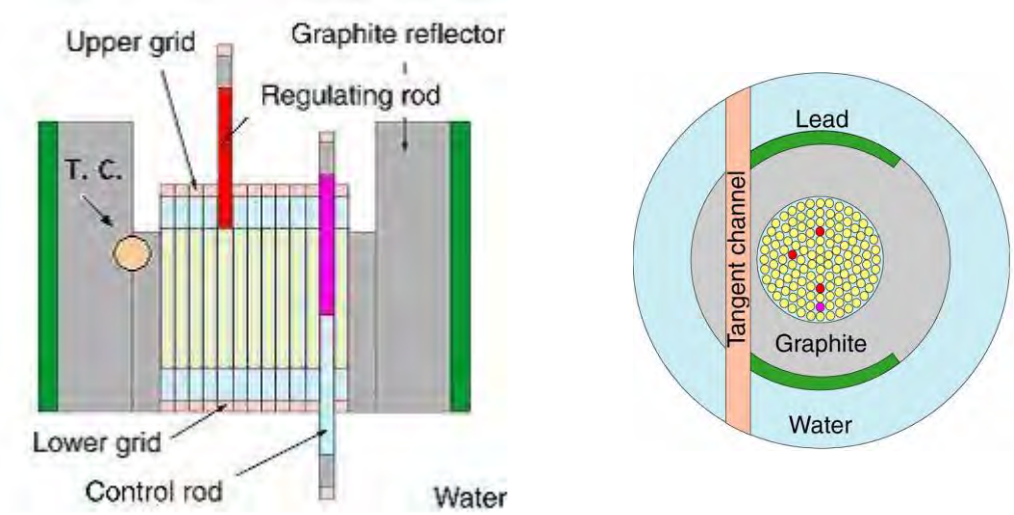

Fig 1 Vertical section of the core and a standard core loading configuration

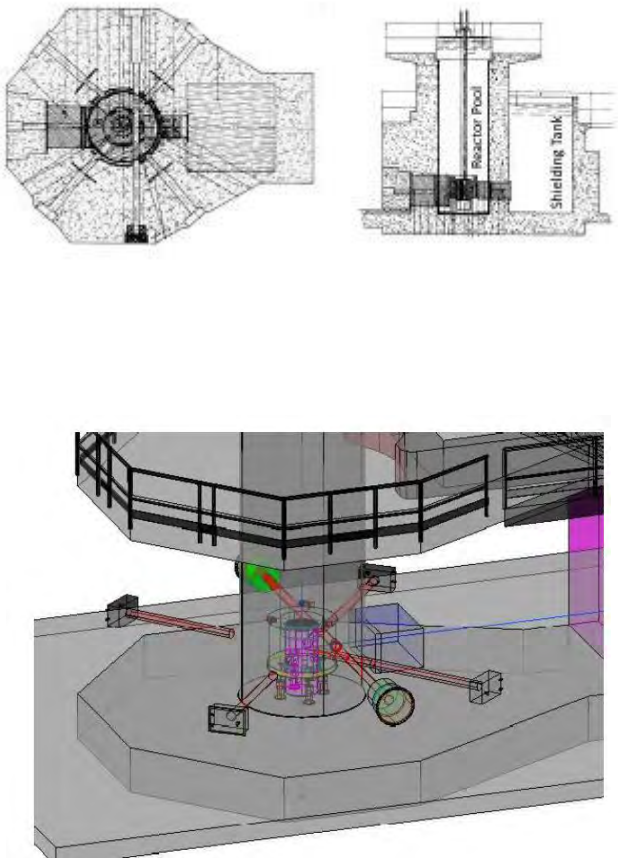

Fig 2 Horizontal and vertical sections of the reactor with neutron channels

The reactor is controlled by four boron carbide rods: three, stainless steel cladded, are *fuel followed* type (two shims and the safety rods) whereas the last, aluminium cladded, is the regulation rod.
The reactor is monitored by a starting channel, two wide range linear channels and one safety channel. One logarithmic channel operates between 10 W and 10 MW. Three X, γ

monitors, two monitors for α and β contamination, and one for gaseous contamination of the air extracted from reactor hall and radiochemical lab ensure a complete information about the radiological situation on the plant and relative laboratories.
In Fig 2 it's possible to identify the experimental channels used for the neutron extraction. Other irradiation facilities are the Lazy Susan, the pneumatic transfer system and the central thimble. In Tab 1 are summarized the neutron flux values available at different irradiation facilities at RC-1.[1][2]

Description	Neutron flux($ncm^{-2}s^{-1}$)
Lazy Susan	$2.00\ 10^{12}$
Pneumatic transfer system(rabbit)	$1.25\ 10^{13}$
Central channel	$2.68\ 10^{13}$
Thermal column collimator	$\sim 1\ 10^{6}$
Tangential piercing channel	$\sim 1\ 10^{8}$

Tab 1 Neutron flux available at RC-1 irradiation facilities

The RC-1 core, surrounded by a graphite reflector, consists of a lattice of TRIGA stainless steel standard fuel elements, graphite dummies elements, control and regulating rods. There are 127 channels on the upper grid plate available for these core components and the grid itself is divided into seven concentric rings. One channel houses the start-up source (Am-Be) while two fixed channels are available for irradiation (central channel and *rabbit*).
The TRIGA fuel elements, cylindrical shaped and stainless steel cladded (AISI 304 - thickness 0.5 mm),consist of a ternary alloy of H-Zr-U. The Uranium is 20% enriched in ^{235}U, and represents the 8.5%wt of the total fuel weight. Two graphite cylinders at the top and the bottom of the fuel rod ensure the upper and lower neutron reflection. The fuel element is provided externally with two fittings in order to allow the remote movements and the correct placements into the grid plates. Fig 3 shows some fuel elements details. [1][2]

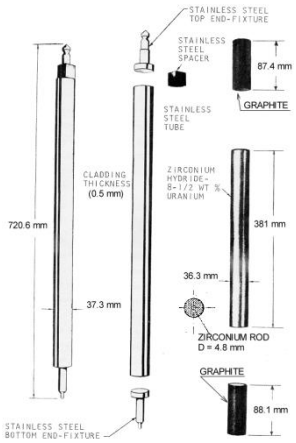

Fig 3 Fuel element details

The metallurgic alloy's stability is related to a variation of the total number of atoms less than 1%: The ternary mixture ensures that also in case of total burnup of ^{235}U present the total atom variation is 0.7%. Another feature regards the prescription that forces the removal of elements from the core if their burnup is higher than 35%: this is a condition linked to the U-ZR-H lattice properties. From the point of view of the utilization, the reactor is mainly utilized for training, flux measurements and irradiation of neutron detectors.

2. TRIGA RC-1 fuel burnup evaluation

One of the major problem regarding research reactors management is the fuel burnup evaluation, fundamental to predict future operation and refuelling process scheduling [11]. An exact knowledge of the fuel composition makes also possible a better and more efficient fuel utilization.
Since its first criticality, at the maximum thermal power of 1 MW, TRIGA RC-1 operation has been monitored and characterized so to collect a great amount of data, mainly through the execution of tests based on technical specifications for full power and low power operation. Fuel burnup has been calculated at each core configuration change, using the daily transcription on the log book of operation and assuming for each core ring specific values for the peak factors [4]. Each core configuration is defined by a suitable number of fuel elements to ensure the necessary reactivity excess. Since the first core configuration, labelled 38,a total of 22 configurations have been loaded into the core. The burnup of each fuel element has been characterized by U^{235} and U^{238}consumption,respect to the nominal isotopic composition provided by General Atomic, and Pu^{239} production. The energy production and the residual residence time for each fuel element has been calculated to verify the respect of the technical prescription about the maximum allowable fuel burnup level. In Tab. 2 are shown the original peak factors values. Moreover, the first configuration #38 has been deeply analyzed by several neutron flux measurements to ensure the full characterization of the core [4].

Ring	d(cm)	Azimuth φ(°)	Φ_{Max} n cm^{-2} s^{-1}	Φ_{Max}/Φ_{core}
B	4	202.5	2.19 10^{13}	1.95
C	8	202.5	1.83 10^{13}	1.63
D	12	157.5	1.53 10^{13}	1.37
E	16	157.5	1.4910^{13}	1.33
F	20	157.5	1.33 10^{13}	1.19
G	24	225	1.15 10^{13}	1.03
C4,C7,C10	8	180	1.39 10^{13}	1.24

Tab. 2 Evaluated peak factors for each ring and control rods positions (red positions in Fig.1)

It was assumed, for all the elaborations, that the mean flux inside the core was Φ_{core}= 1.12 10^{13} n cm^2 s^{-1}[4]. Successively, as a residual activity of the TRADE experiment [5], a further evaluation of the fuel burnup was necessary because of some errors found in the previous determination of the peak factors: as a consequence, fuel burnup was over estimated due to some wrong normalizations respect to the total energy production. Consequently, the original datasheets filled with the reactor operation data have been re-analysed using a more detailed mathematical fit of the experimental data, based on Bessel first kind and polynomial functions for the flux radial profiles, to obtain more accurate values for the peak factors in the various core positions. Tab. 3 shows the new peak factors values [3].

Ring	d(cm)	Azimuth φ(°)	Φ_{Max} n cm^{-2} s^{-1}	Φ_{Max}/Φ_{core}
B	4	202.5	2.10 10^{13}	1.87
C	8	202.5	1.80 10^{13}	1.61
D	12	157.5	1.52 10^{13}	1.35
E	16	157.5	1.45 10^{13}	1.29
F	20	157.5	1.27 10^{13}	1.13
G	24	225	1.15 10^{13}	1.03
C4,C7,C10	8	180	1.41 10^{13}	1.26

Tab.3 Evaluated new values for the peak factors

This procedure has generated new values for the burnup level in each fuel element for all the core configurations. Results confirm an overestimation of the previous fuel burnup level of about 5%.
A MCNP based model for the TRIGA RC-1 reactor core has been successively developed for the first configuration #38. The original fuel shipment documents by General Atomic have been used to generate their nominal isotopic composition. In Fig. 4 it's shown the implemented model. It has been validated for the configuration #38 by means of criticality calculations and control rods calibration. The comparison between experimental and calculated data for the safety rod calibration curve is shown in Fig. 5

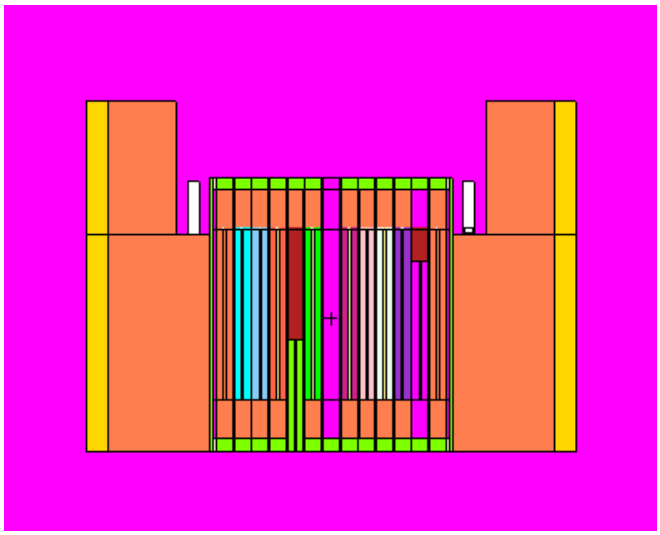

Fig. 4TRIGA RC-1 MCNP model (configuration #38)

In the next future this procedure will be iterated for all the TRIGA RC-1 configurations by changing the fuel composition by means of: a) data from re-evaluation [3] as described above; b) by means of MONTEBURNS code [6] calculations. Current MCNP results for the configuration #38 provide as reactivity value $\rho \pm \Delta\rho = -93 \pm 43$ pcm. The calibration curve for the safety control rod, shown in Fig. 5, indicates a good agreement between experimental and calculated data.

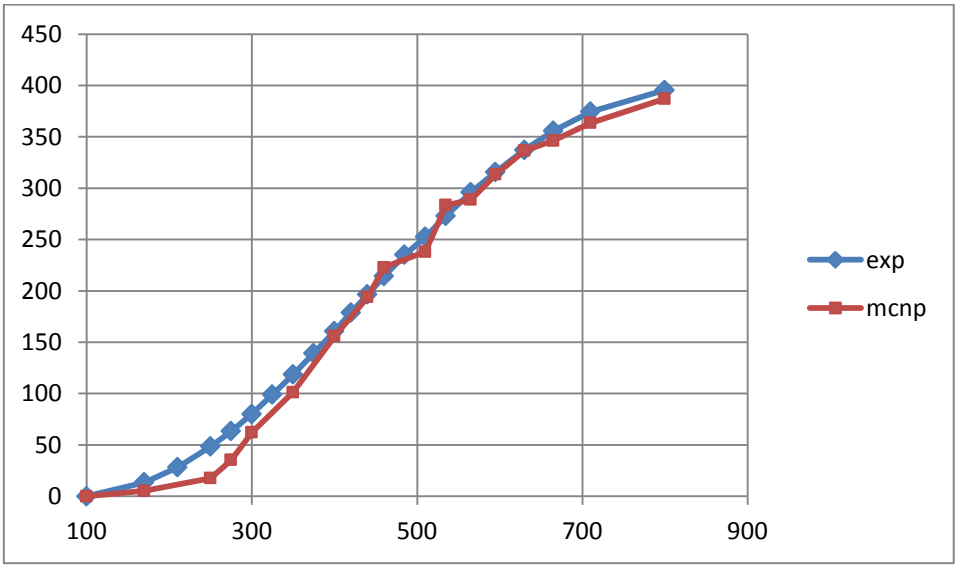

Fig. 5 Evaluated and experimental safety calibration curves

3. TRIGA RC-1 instrumentation modernization and a new facility for irradiation

TRIGA RC-1 consolle has never been refurbished during these years of operation, so nowadays the original one from General Atomic is still working. During about 50 years of operation, however, many instrumentations and corresponding chains of detection have been changed, upgraded or replaced because of components faults or ageing. Some recent instrumentation changes are: substitution of flow meters installed on the primary, purification and secondary circuits and substitution of the detection chains for the environmental monitoring regarding X and γ exposition. Furthermore, some upgrading have been implemented in the subsystem, located in a rack inside the control room, dedicated to the display of data regarding I^{131}, Ar^{41} and Kr^{85} levels, together with the corresponding HPGe detector, and α and β contamination of air extracted from both the reactor hall and the radiochemical laboratory.
It's to be underlined that all the modifications and upgrades on instrumentation and components were done by means of strict criteria compliance: precisely, changes were done in conformity with the licensing and/or authorization procedures issued by the regulation authorities. All the substitutions fulfil the current prescriptions for plant operation. A step-by-step process for substitutions was also adopted to dilute the costs. This strategy has been always applied for each substitution of plant components.
Since 1967 a calibrated flange was installed on each pipeline of the coolant circuit of TRIGA RC-1. In the control room, and in particular on the auxiliary consolle, an analogical indicator indicated the flow values. Due to ageing and difficulty in calibration procedure, during 2014 it was decided to replace the old sensors with new ones together with a digital display, while alarms and relative indicators have been remained unchanged. In particular, three new sensors were installed directly on pipelines. They work by means of ultrasound reflection on pipeline walls and the principle of difference in the transit time.

Fig. 6 Local Instrumentation for measures

Fig. 7 Sensor on the primary loop

The signal from each couple of sensors (Fig. 7) is displayed by local instrumentation (Fig. 6), and then transferred by a 4-20 mA loop to the remote instrumentation in the control room. A digital display, a SM1000 by ABB (Fig. 8), allows the operator to monitor continuously the values measured by the sensors. Optical and sound alarms, located in a panel close to the operator, provide information's about abnormal operation.

Fig. 8 Digital display with flows in the control room

In Tab. 4 are provided some details about the three independent loops of the cooling system.

	Temp (°C)	Pipeline extdiameter (mm)	Pipeline intdiameter (mm)	Thickness(mm)	Material	Design Flow (m^3/h)
Primary	43.00	127.00	115.00	6.00	Pal-Mo 3.5 UNI3575	~ 85
Secondary	30.00	219.10	207.30	5.90	Acciaio al C	~ 110
Purification	39.00	48.00	32.00	8.00	PVC	~ 2.5

Tab.4 Main features of the cooling circuit

Another upgrade concerned the environmental monitoring system for X, γ dose rate in the reactor hall and in the radiochemical laboratory. In this case, the instrumentation in case of failure had some problems due to spare parts retrieval. The upgrade of components was executed changing all the components of the detection chain: from sensors (operating range 1 μSv/h - 20 Sv/h) and local instrumentation located in the controlled zones(Fig.9), to the remote ones in the control room (Fig.10). The instrumentation measures the ambient equivalent dose rate H*(10). In the control room, signals and data are managed by a dedicated PC, and a digital panel allows to display the whole data from all the instruments. A particular attention has been dedicated to the interface: the aim was to optimize the HMI (Human Machine Interface) to increase operators knowledge about the plant status.

Fig. 9 Sensors in the reactor hall

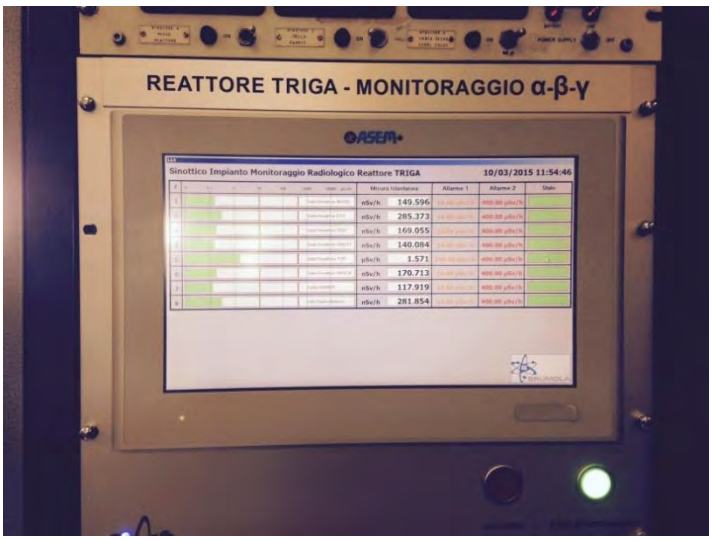

Fig. 10 Remote panel (X,γ) in the control room

Another upgrade was the modernization of the system dedicated to the monitoring of the air extracted from the controlled zone. The HPGe detector was changed together with the instrumentation in the control room dedicated to the signals elaboration and visualization. A PC and a touch screen panel have been installed, remaining unchanged all the subsystems for optical and acoustic alarms. Thanks to this upgrading the operator can monitor the entire γ spectrum and the signals from the different sensors, with colours highlighting thresholds and alarms (Fig. 11).

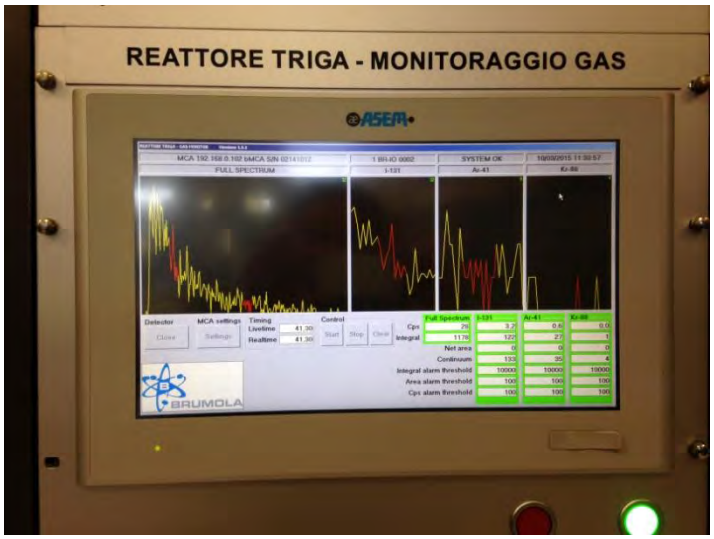

Fig. 11 Remote panel for gas monitoring

The changes above described have the final aim of increasing the reliability of the instrumentation, decreasing the occurrence of failures and to optimize the instrumentation maintenance.
Recently it has been implemented a new irradiation facility to be used into the shielding tank [7].The irradiation device (Fig. 12) is a cavity made by Plexiglas supported by a moving arm. The internal diameter is 170 mm and the available length is 330 mm. It is also equipped with a tube allowing to connect the cavity, by wires or cables, with the external of the pool. By means of the moving arm it is possible to place the cavity just in front of the thermalizing column.

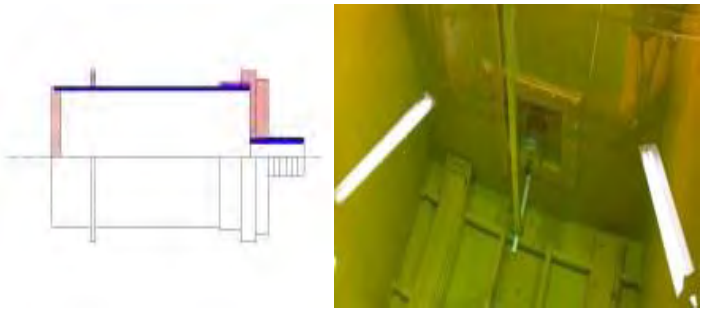

Fig. 12 Irradiation cavity: sketch and picture in the shielded tank

4. The dynamic model of TRIGA RC-1 research reactor

The goal of the model is to simulate the reactor dynamics for the following situations:

- operational transients, power changes, power regulation;
- steady, sinusoidal, pulsated states;
- alarm situations, with subsequent control rods scram and reactor shut-down;
- criticality incidents and instantaneous water loss (from reactor pool).

The dynamic model of TRIGA RC-1 [8][9], implemented by the MATLAB [10] platform, is based on the interaction of subcomponents modelling, i.e.:

- core thermohydraulics and neutronics;
- control rods movement;

- rods velocity control system;
- fuel Doppler coefficient;
- Xe and Sm poisoning;
- stable period behaviour;
- reactor protection system;
- thermodynamics of the heat exchange with the external environment.

The model is validated on experimental data regarding:

- tests @ 1 MW and one test with scram;
- tests at intermediate power and zero power (@ 20 watt)
- tests on increasing-decreasing power and power regulation;
- test on Xenon poisoning(after 15 days @1 MW);
- stable period measurements and comparison with Inhour curve.

As an example of the results obtained by the model, Tab. 5 shows the comparison between nominal and calculated data for some reactor parameters.

	Design value	Calculated
Power (MW)	1	1
Maximum thermal flux (n cm^2 s^{-1})	2.7 10^{13}	2.7 10^{13}
ΔT core (°C)	20	20
Core natural flow (m^3/h)	43	42.5
Primary flow (m^3/h)	80	80
Secondary flow (m^3/h)	182	182
ΔT primaryloop (°C)	-10.7	-10.4
ΔT secondaryloop (°C)	4.7	4.7

Tab. 5 Comparisons between nominal and calculated values

The dynamic model provides several output data; as an example, in Fig. 13 is shown the response of the reactor due to the insertion of 2$ of positive reactivity. It's in accordance with General Atomic evaluation of the same incidental situation [1].

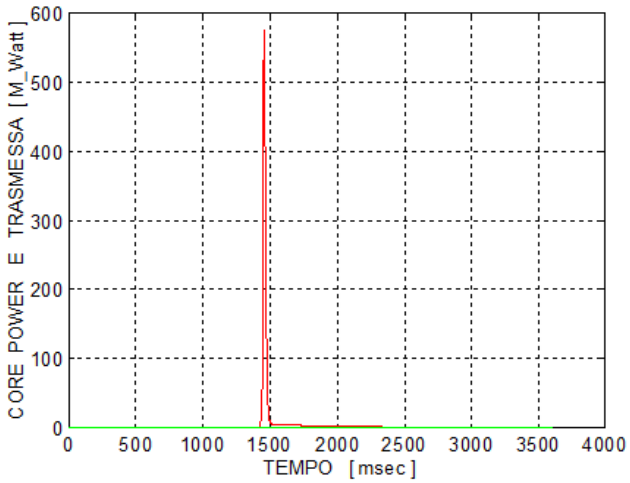

Fig. 13 TRIGA RC-1 dynamic model power response to 2$ reactivity insertion

5. Conclusions

The reactor TRIGA RC-1 continues to assure its role in the context of the Italian research activities and in particular it acts as a reference facility for Universities. The involvement in many activities and research projects is also made possible by the scheduled plan of interventions, oriented to modernization, upgrade and maintenance of systems and components, always executed taking into account, when possible, the optimization of the reactor shutdown periods. Also the activity in the field of modelling plays an important role, and both the modelling and the consolidated material irradiation activities make possible a full utilization of the facility.

6. References

[1] L. DI PALO, RC-1 Reattore 1MW – progetto definitivo e rapporto di sicurezza , CNEN Centro Studi Nucleari Casaccia , 1966 (Italian)
[2] Dipartimento FPN, ENEA , Manuale di Operazione del reattore RC-1 1MW, C.R. Casaccia (Italian)
[3] M.CARTA, Re-examination of the fuel burnup level of the TRIGA RC-1 Casaccia Reactor,ENEA Technical Report UTFISSM – P000 – 003 (2012)
[4] L. DI PALO, A. FESTINESI,G.FOCACCIA, Specifiche tecniche per l'esecuzione delle prove nucleari del reattore RC-1 a potenza nulla, CNEN, 1967(Italian)
[5] RUBBIA, C.et al., TRADE: a full experimental validation of the ADS concept in a European perspective, American Nuclear Society, Accelerator Applications Division, AccApp'03, Accelerator Applications in a Nuclear Renaissance, 1–5 June 2003, San Diego, California (2003).
[6] D. L. Poston, and H. R. Trellue, "User's Manual, Version 2.0 for MONTEBURNS Version 1.0," LA-UR-99-4999 (September 1999).
[7] M.PALOMBA, A.GROSSI, L.FALCONI, R.BOVE, M.SEPIELLI A new irradiation device at the thermalizing column of RC-1 TRIGA reactor, RRFM 2013 Saint Petersburg, Russia
[8] C.INNARELLA Il Modello Dinamico del Reattore Nucleare TRIGA-RC1dell'ENEA . Rapporto tecnico (Technical Report) PAR2011-ENEA-L1C4-010 , Settembre 2012 (Italian)
[9] C.INNARELLA Il Modello del Reattore Nucleare BWR4 di Caorso, Modello implementato su Calcolatore Analogico dell'ENEA. Rapporto tecnico(Technical Report) NRAF 1TP4B 84043 Dicembre 1984(Italian)
[10] http://it.mathworks.com/products/matlab/
[11] M. PALOMBA, R. ROSA The Management of TRIGA spent fuel ENEA RC-1 research Reactor - Management and Storage of Research Reactor Spent Nuclear Fuel – Proceedings of a Technical Meeting held inThurso, United Kingdom, 19–22 October 2009 - IAEA 2013

STATUS OF THE FLUORIDE SALT HIGH TEMPERATURE REACTOR MATERIALS IRRADIATION TESTS AT THE MIT RESEARCH REACTOR

David M. Carpenter, Michael Ames, Yakov Ostrovsky, Gordon Kohse, Lin-wen Hu
Nuclear Reactor Laboratory
Massachusetts Institute of Technology

Abstract – *The first irradiation test of structural materials and surrogate TRISO fuel particles in a molten, fluoride-based salt was completed successfully at the Massachusetts Institute of Technology Research Reactor (MITR). The irradiation test is part of an ongoing joint research program being conducted at MIT, the University of California-Berkeley (UCB), and the University of Wisconsin-Madison (UW). The objective of the overall research program is to develop a path forward to a commercially viable, fluoride-salt-cooled, high-temperature reactor (FHR). The baseline FHR concept combines a fluoride salt coolant called flibe (a mixture of LiF and BeF_2), with a graphite-matrix, coated-particle fuel. The objectives of the first FHR irradiation experiment at the MITR are: (1) to assess the corrosion and compatibility of 316 stainless steel, Hastelloy N®, SiC and SiC/SiC composites, and surrogate TRISO fuel particles in molten flibe, and (2) to examine the partitioning of tritium (produced when the flibe is subjected to neutron irradiation) among the various media in the experiment. This irradiation was performed with flibe temperature at 700°C which marks the first demonstration of flibe irradiation capability at the MITR. Initial results provide evidence of the high potential mobility of tritium in an FHR system consisting primarily of liquid flibe, graphite, and high-nickel alloys at high temperature. At the same time, a large percentage of the tritium that was predicted to have been generated in the salt was not detected in the gas phase, mirroring experience from the MSRE and indicating a potential for tritium control through tritium capture in solid components. Fast neutron activation products ^{16}N ($t_{1/2}$ = 7.1 s) and ^{19}O ($t_{1/2}$ = 26.9 s) were measured and shown to be significant radiation dose contribution in the gas phase. Post-irradiation examination of irradiated materials is ongoing and will attempt to identify if the tritium balance can be accounted for by tritium absorption in the salt, the specimens, and the capsule's structural materials. Measurements of the corrosion rates of SiC, SS316, and Hastelloy N coupons has shown that all three are susceptible to some corrosion in the salt, with higher rates when coupled with nuclear-grade graphite. In addition, surrogate TRISO particles exposed directly to flibe appear to have increased susceptibility to radial cracking after irradiation and salt freeze-melt cycling.*

I. INTRODUCTION

The Fluoride-Salt-Cooled High-Temperature Reactor (FHR) concept is the subject of an ongoing three-year U.S. Department of Energy-funded Integrated Research Project (IRP), which aims to develop the "path forward" to a salt-cooled test and commercial power reactor. This IRP is led by the Massachusetts Institute of Technology (MIT) in partnership with the University of California, Berkeley and the University of Wisconsin-Madison (UW).[1]

The FHR baseline concept is a fluoride-salt-cooled, graphite-moderated pebble-bed reactor with 600°C inlet and 700°C outlet coolant temperatures. The lithium-beryllium fluoride salt primary coolant (67%LiF-33%BeF_2), known as flibe, was chosen because of its favorable characteristics as a high-temperature, low-pressure heat transfer fluid that is optically transparent and has good neutronics properties.

The FHR concept is based on experience from the Molten Salt Reactor Experiment (MSRE), which operated at Oak Ridge National Laboratory (ORNL) between 1964 and 1969.[2] The MSRE used a fueled salt in its primary loop (ZrF_4-UF_4 was added to the flibe). In contrast, the FHR takes advantage of recent coated particle fuel

(TRISO) technology to provide compatibility between TRISO/graphite fuel compacts and the liquid flibe, isolate the fuel from the salt, and maintain a "clean" primary coolant.[3]

The combination of flibe coolant, TRISO compact fuel, and a graphite core structure allows the FHR to achieve a large thermal margin to core damage. The boiling point of the flibe is 1430°C, and the failure temperature of the graphite and TRISO particles is above 1600°C. With an outlet temperature of 700°C the FHR has a substantial temperature safety margin compared to existing light water power reactors.

Proposed materials for other structural components of the FHR design are 316 stainless steel (SS316), Hastelloy® N, carbon-fiber composites (CFCs), and silicon carbide fiber composites (SiC/SiC). Hastelloy N was developed specifically for use with liquid salt and has excellent corrosion resistance at the temperatures of interest, as was demonstrated in the MSRE. However, as a specialty metal Hastelloy N has limited commercial production and is not code-qualified as a vessel structural material for reactor operation at FHR conditions. Therefore this IRP is investigating the possible use of SS316 as a well-characterized and economical replacement. CFC and SiC/SiC materials have seen substantial development and improvement in quality in the last few decades, with increasing interest in their use in both fusion and fission reactor environments. In the FHR, these ceramics are being considered for the core barrel and as control element and instrumentation channel liners, which are structures in high-radiation areas that do not need to be as stringently code-qualified (e.g. are not classified as pressure vessels).

II. EXPERIMENT DESIGN

An irradiation test including the flibe and proposed FHR structural materials has been designed, built, and carried out at the MIT Nuclear Reactor Laboratory (MIT-NRL) utilizing the MIT Research Reactor (MITR). The purpose of this irradiation was threefold: (1) to demonstrate the ability to implement a flibe-bearing materials test at 700°C in the MITR; (2) to measure the transport and disposition of tritium produced in the flibe; and, (3) to evaluate the corrosion of TRISO and FHR structural materials exposed to flibe at 700°C during neutron irradiation.

The MIT test was carried out at the NRL in parallel with non-irradiated autoclave tests which took place at UW. The UW and NRL tests utilized an identical test matrix with the specimens and specimen holders sourced from the same materials and prepared at the same location. The main purpose of these initial parallel tests is to isolate the effects of irradiation damage and other irradiation-induced effects such as tritium generation on the test results and to help to determine what further irradiation experiments are required for initial FHR development. Furthermore, this irradiation represents the first attempt to irradiate significant amounts of flibe under active temperature control at the MITR.

II.A. MITR ICSA Facility

The MITR is a 6 MW, light water-cooled, heavy water-reflected tank-type research reactor. The MITR has a compact, HEU core with plate-type fuel in rhomboidal assemblies arranged in three concentric rings. Of the 27 in-core element positions, three (two in the central ring, one in the middle ring) are dedicated for in-core experimental facilities. The neutron flux available to experiments in-core is up to 3.6×10^{13} n/cm^2-s thermal and 1.2×10^{14} n/cm^2-s fast (E>0.1 MeV) when the reactor operates at full power, with a spectrum similar to that of a light-water reactor.

The MITR's primary coolant is light water at atmospheric pressure and an outlet temperature of about 50°C. The free space available in-core for a single experiment is approximately 5 cm in diameter and 56 cm in height. These constraints require the use of special facilities in order to achieve the desired test conditions. For this initial irradiation the target conditions are a constant 700°C exposure for 1000 hours under inert cover gas.

The irradiation utilized the In-Core Sample Assembly (ICSA) facility installed in one of the central-ring core positions. The ICSA is a general-purpose irradiation facility, which has been approved and demonstrated for capsule irradiations up to 900°C.[4] The ICSA outer thimble is a titanium tube with a 5 cm outer diameter and S-bend shape that extends from just below the reactor top shield lid, four meters down to the bottom of the core. The S-bend shape prevents direct radiation streaming up through the core tank. Connections at the top of the thimble and integral gas lines along its side allow for gasses to be continuously injected into the ICSA at the bottom of the core and exhausted from the top of the thimble. Experimental test components in the ICSA are contained in metal capsules that are inserted from the top of the ICSA. ICSA capsules are typically about 4.5 cm in diameter and 15 cm long. Several different capsules can be stacked within the in-core region.

Heating in the ICSA is accomplished passively, primarily utilizing gamma heating of high-Z materials. Heat is rejected from the system across the gap between the capsules and the thimble, and then into the MITR's primary coolant. Through careful design of the irradiation capsules and radial gas gaps, temperatures of up to 900°C are readily achievable. While the gross ICSA capsule temperature is controlled by reactor power and capsule design, fine control of temperature is achieved by varying the gas mixture in the thimble. To operate the ICSA at the lowest temperature, the thimble is filled with 100% helium; in order to increase temperature, neon (which has a lower thermal conductivity than helium) is added. The demonstrated temperature control range that can be

Fig. 1. Components of the experiment capsule prior to assembly. Left-to-right are the outer nickel capsule, the three sections of the graphite sample and flibe holder, and, top-to-bottom on the right, the bottom graphite support/spacer, the top cover plate, and the capsule lid (without thermocouples and gas lines).

achieved by varying the helium/neon mixture is about 450°C as demonstrated during ICSA testing at 5 MW, although this will vary somewhat depending on the absolute temperature and capsule geometry.

II.B. Capsule Design

The irradiation capsule for this experiment, components of which are shown in Figure 1, was designed to meet the experiment's thermal requirements, allow independent sampling of the capsule and thimble gases, and protect the ICSA from exposure to the salt or its corrosive byproducts. The outer capsule was constructed from Alloy 201 nickel except for the top threaded section and lid which are Inconel® 800H. These materials were chosen for their high-temperature strength and resistance to flibe and HF corrosion. HF may be produced from the flibe if it comes into contact with moisture or as a result of tritium generation (TF). These metals also provide a good susceptor for gamma heating of the capsule internals and are sufficiently resistant to neutron irradiation for the purposes of the 1000-hour test.

Inside the capsule is a three-section graphite sample holder, shown in the center of Figure 1, machined from IG-110U, a high-purity, isotropic graphite manufactured by Toyo Tanso. The graphite provides compatibility with the flibe, excellent thermal conductivity (providing a uniform temperature distribution), and is part of the test matrix for corrosion and tritium interactions. There are six vertical chambers machined into the graphite, 1 cm in diameter and 14.5 cm deep, where the salt and specimens reside. A nickel disk rests on top of the graphite and a thin nickel base plate supports the graphite above the bottom of the capsule. This arrangement is designed to produce a small vertical temperature gradient in the capsule, ensuring that the salt melts from the upper free surface downwards to prevent damage to the graphite holder from flibe expansion during the phase transition.

TABLE I

Specimen Test Matrix

Graphite Chamber	Liner	Specimens
A	none	2 Hastelloy N plates
B	none	2 SS316 plates
C	none	3 SiC/SiC, 1 SiC
D	none	~300 TRISO particles
E	SS316	2 SS316 plates
F	Hastelloy N	2 Hastelloy N plates

The capsule's lid has penetrations for two gas tubes and three nickel rods (all Inconel 600). The gas tubes allow the helium cover gas in the space above the flibe to be sampled and refreshed. The nickel rods were brazed into the lid and extend down into the graphite holder; their extra mass is used to assist with melting the flibe from the top down. Thermocouples run through two of these rods, and the thermocouple tips sit in the graphite at the half-height of the capsule between chambers. The lid threads into the lower capsule and seals it by compressing an Inconel 718 C-ring.

The specimen test matrix is given in Table I. Two of the chambers, E and F, were lined with metal – the flibe and specimens in these chambers are not exposed to graphite. All of the metallic specimens are rectangular coupons (25 mm x 6mm x 0.5 mm), which hang on wires made from the matching metal and are secured through small holes in the nickel disk above the graphite. The SiC and TRISO specimens sit freely at the bottom of their chambers.

Assembly of the capsule took place in three main steps. First, the capsule parts were manufactured from nickel and graphite, and the gas tubes, thermocouples, and nickel pins were brazed into the capsule lid.

Second, the loading of the flibe and specimens into the graphite chambers was performed inside an argon-filled glove box at UW using the same process and equipment used to load the flibe and specimens for the parallel UW autoclave test. Immediately prior to the loading the graphite sections and liners were heated at 800°C in an argon-10%-hydrogen atmosphere for 24 hours. This process removes oxygen and moisture that may be adsorbed on the surfaces of the components – such a surface preparation process is important for any equipment to be used with liquid flibe. After all of the specimens were placed in the graphite chambers, flibe was dripped slowly into each chamber directly from a heated storage container until the chamber's target mass was achieved. The flibe loadings in each chamber are given in Table II.

After loading the specimens and flibe into the chambers, the graphite was inserted into the nickel capsule, the capsule was closed with a temporary blank lid, and the closed capsule was then sealed into a secondary container for shipping back to MIT. All of sealing at UW was done inside an argon-filled glove box.

Final assembly took place at MIT. The capsule, with temporary lid, was placed in a circulating helium-filled glove box where the lid was removed. The full capsule was held at 250°C for five hours before the final lid (with thermocouples and gas lines) was sealed on. The capsule was then inserted into the ICSA tube in the reactor and immediately connected to gas lines for helium purging while cold.

A neutronics analysis of the ICSA experiment was performed using the MCNP-5.1.4 code and a 3D representation of the MITR core. This calculation predicted axial-average neutron fluxes of 2.35×10^{13} n/cm^2-s thermal and 1.16×10^{14} n/cm^2-s fast (E>0.1 MeV) in the salt chambers with the reactor at a power of 6 MW. Using this code the gamma heating rates of the graphite and nickel structural materials in the capsule and the titanium ICSA tube were also estimated. These data were fed into the ANSYS Fluent v13 computational fluid dynamics code for calculation of the temperature distribution inside the experiment. This process was used iteratively during the design phase to fine-tune the proper dimensions for the capsule wall in order to achieve the target 700°C in the salt chambers.

For the Fluent analysis, a 3D capsule model and a 13-inch high section of the ICSA tube was converted and meshed using the ANSYS meshing tools. This analysis modeled the flibe physically as a solid with the thermal properties of the liquid at 700°C. It also considered the gas flow in the outer ICSA tube, but not within the capsule (the capsule gas space was modeled as a heat sink, removing the small amount of energy calculated to be lost to the cold helium flowing at 50 cc/min). The initial analysis considered two extreme conditions for the outer ICSA thimble gas with the reactor operating at 5.9 MW: (1) 100% helium gas flow, and (2) 100% neon gas flow (both at 100 cc/min). In both cases the capsule internal gas remains pure helium. The simulation results are shown in Figure 3; the maximum predicted temperature in the sample chambers is 760°C with 100% helium and 1130°C with 100% neon.

TABLE II

Flibe Loading

Graphite Chamber	Flibe Mass (g)
A	21.3
B	21.2
C	21.2
D	21.2
E	18.2
F	18.1

II.C. Salt Preparation

The flibe salt used in the MIT irradiation and the UW autoclave test was procured from Oak Ridge National Laboratory. This salt is from the supply of flibe for the secondary coolant loop of the MSRE and has been in storage since that reactor's decommissioning. The flibe used in the primary and secondary systems of the MSRE was enriched in ^{7}Li because of the unfavorable ^{6}Li(n,α)^{3}H reaction, which has a large, 940 b thermal cross section. ^{6}Li, which is 7.5% abundant in natural lithium, is therefore both a neutron poison and a substantial source of tritium. To counter this, the MSRE utilized 99.995% ^{7}Li enriched flibe in its fueled primary loop, and 99.99% ^{7}Li enriched flibe in its clean secondary loop and flush systems.[5] However, even if ^{6}Li were removed entirely from the flibe, an equilibrium level of ^{6}Li will be reached due to generation from the ^{9}Be(n,α)^{6}He reaction, so flibe will always be a significant tritium generator. Smaller amounts of tritium are also produced in flibe by the ^{19}F(n,t)^{17}O and ^{7}Li(n,n+t)^{4}He reactions.

Flibe must be handled carefully and kept in a dry, inert environment as the salt will readily absorb moisture. It is a strong oxidizer, and will react with metal oxides (e.g. surface layers) to form metal fluorides. At elevated temperatures the salt will decompose in the presence of H_2O to form HF and BeO.[6] In turn, if the HF becomes hydrated, it will form hydrofluoric acid that can easily etch glass and steel surfaces.

The salt from the MSRE has been stored at ORNL in sealed steel containers for over 40 years. This, combined with our assessment that there may have been little or no chemical cleanup of the MSRE secondary system (metal corrosion product buildup was detected during reactor operation), presented the possibility of contamination of the MSRE flibe with various trace elements. It is likely this MIT irradiation represents the first time this enriched flibe has been analyzed, or irradiated, since the 1960's.

The flibe used in this experiment was transferred at ORNL into smaller stainless steel containers using a heated, sealed, and pressurized loading system, and then shipped to UW. At UW the salt was re-melted and extracted from the shipping container, and then purified to remove moisture and oxides and to reduce the presence of trace metals. In short, the flibe was first melted in the presence of metallic beryllium and sparged with argon and hydrogen gasses. Next, a 1:10 by volume mixture of hydrogen and hydrogen fluoride gas was bubbled through the liquid salt for 1.5 hours, followed by 24 hours of sparging with H_2. Samples of the flibe before and after this purification were sent to the MIT-NRL for neutron activation analysis (NAA). Although there was no explicit salt purity standard in place for this experiment, the

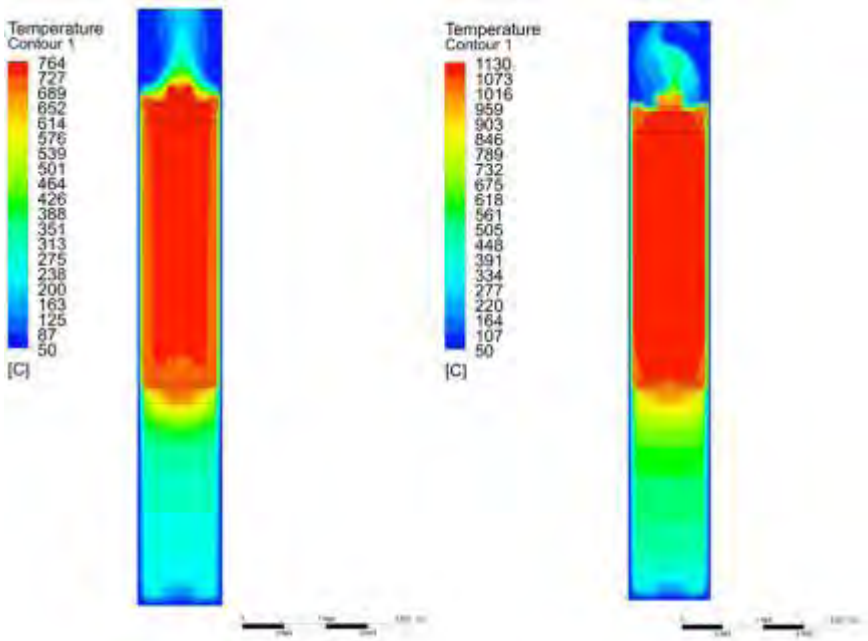

Fig. 2. Fluent calculation of experiment capsule with (left) 100% helium thimble gas, and (right) 100% neon thimble gas at 5.9 MW reactor power.

original impurity standards for the MSRE primary flibe were used as a point of reference. The NAA analysis found that the UW purification process did help to reduce the amount of trace metals in the flibe; however, levels of Al and Cr remained slightly above the MSRE impurity standard (173±19 ppm vs. 150 ppm Al and 36±1 ppm vs. 25 ppm Cr), and levels of manganese and nickel are still undetermined.[7]

Other than this initial purification and NAA, there was no active effort to control or monitor the redox potential of the flibe during the experiment. This was done in part because the optimum redox potential for the FHR had not yet been decided, but this also allowed design simplification for this initial demonstrative irradiation (and the parallel UW tests).

III. IRRADIATION EXPERIMENT

The ICSA and experiment capsule were installed in the MITR on September 10, 2013. A schematic of the ICSA gas system for this test is shown in Figure 4. The basic layout consists of three parallel gas supply systems regulated by mass flow controllers – one helium and one neon system to the ICSA thimble, and one helium system to the experiment capsule (the emergency helium system floods the thimble in the event of an over-temperature condition). The main helium gas flows are intended to be constant during the experiment; the neon mass flow into the thimble, however, is generally controlled manually or from a PID temperature controller that receives feedback from one of the two capsule thermocouples (TC 1). Because of the sensitivity of the flibe to contamination, an oxygen gettering furnace with a zirconium element is used on the helium supply gas to the capsule to help remove any traces of oxygen. Gas pressure is monitored at the inlet to the ICSA tube and capsule independently on the helium and neon lines, and controlled with a backpressure regulator at the outlet of the thimble and capsule. Helium and neon are supplied independently and mixed at the bottom of the ICSA thimble in order to decrease the response time between adjusting the neon flow rate and achieving a change in the gas mixture in the in-core section.

The outlet gas from either the thimble or the capsule can be directed through a train of instruments including a Dycor® LC Series residual gas analyzer (RGA), Overhoff Technology Corp. TASC tritium bubbler, and Omega Engineering Inc. PHE-4201 pH probe contained in a dedicated water bubbler. The exhaust gas is then directed through a charcoal filter before being mixed into the reactor building's ventilation system for monitoring and exhaust. The experiment exhaust line not being monitored by the instrument train runs directly into the charcoal filter.

After installation of the capsule into the ICSA thimble the gas system operated at ambient temperature and 100 cc/min helium gas flow through the thimble (100 kPa) and capsule (135 kPa) for three days in order to remove air and moisture before heating the capsule. Levels of both air (monitored as nitrogen) and water were evaluated using the RGA on the gas exhaust system.

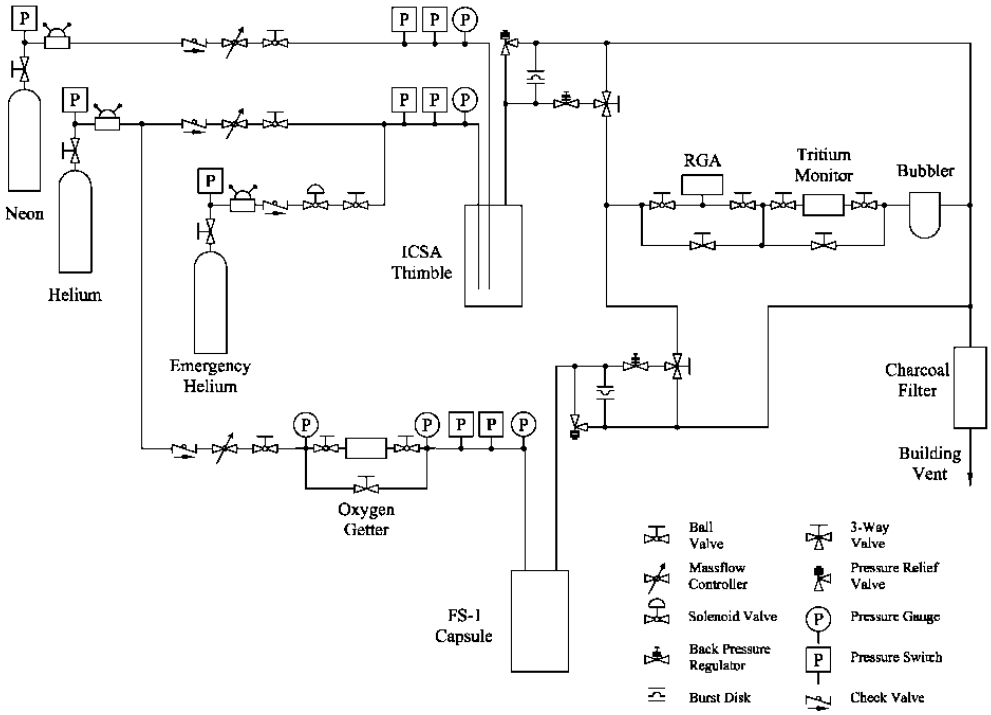

Fig. 3. Schematic layout of the ICSA gas system with the experiment capsule (labeled FS-1).

On September 13 the reactor was started and its power was raised in 500 kW steps with 20 minute stabilization periods up to a power of 2 MW, at which power the capsule temperature reached 290°C. The temperature was held there to allow any additional moisture to be evolved from the system.

While holding at 2 MW, a higher than expected level of radioactivity was observed near the capsule outlet tubing. Analysis of the radiation's gamma spectrum using a portable HPGe detector (Canberra Falcon 5000®) determined the primary contributors to be ^{16}N ($t_{1/2}$ = 7.1 s, primary E_γ = 6.129 MeV) and ^{19}O ($t_{1/2}$ = 26.9 s, primary E_γ = 197.1 keV and 1.357 MeV). These isotopes were being produced from fast neutron reactions on ^{19}F ((n,α) and (n,p), respectively) and were then escaping the flibe into the capsule cover gas. It was not clear if the rate at which these gases were being released at this time was controlled by reactions at the salt's free surface or by diffusion through the solid (though possibly porous) flibe. On September 16 reactor power was briefly lowered to 50 kW for adjustments to the capsule exhaust line. The length of exposed tubing in the capsule gas outlet line was reduced, a radiation monitor (GM tube) was placed immediately next to it, and a delay volume surrounded by 8 inches of lead shielding was installed.

It is interesting to note that the production of ^{16}N and ^{19}O in the flibe was not mentioned in the ORNL reports on their MSRE experience, likely because of both the short half-lives of these isotopes and the presence of many other highly radioactive fission products in the MSRE primary salt. In contrast, this experiment's salt contained few other radioisotopes. Also, the sweep gas transit time from the reactor core to the measurement location was on the order of one second. These isotopes were not detected in the ICSA thimble exhaust gas because: (1) they have no ready path into the thimble gas space, and (2) if they were present in-core, the transit time through the upper portions of the thimble is on the order of ten minutes. It should also be noted that while ^{16}N and ^{19}O isotopes are produced in water-cooled reactors (from neutron reactions with stable oxygen isotopes), on a curies per gram coolant basis, the production of ^{16}N is hundreds and of ^{19}O thousands of times higher in flibe than in H_2O (calculated using ORIGEN-S with the MITR neutron spectrum).

On September 17 reactor power was again increased in 500 kW steps. At 3.5 MW reactor power was held and the capsule temperature reached 425°C. Neon was then introduced into the ICSA thimble to slowly raise the capsule temperature through the flibe melting point (459°C). The ICSA gas system was held at 20 cc/min neon, 80 cc/min helium with the capsule at 470°C before reactor power was again increased in 500 kW steps. At 5.5 MW the capsule reached 640°C; helium flow was decreased and the neon flow was manually increased before regulation was turned over to the automatic PID controller. With a helium flow of 60 cc/min, the neon flow rate settled at 32 cc/min in order to hold the capsule temperature at 700°C.

As shown in Figure 4, the experiment ran without interruption and at constant reactor power for the next 1000 hours, with variations in the controlled neon flow rate of ±2 cc/min and temperature of ±1°C from one thermocouple and ±3°C from the second, noisier

thermocouple (this noise may be in part due to the first thermocouple being transmitted as a voltage and the second as a current loop).

Temperature, pressure, and flow rate data were monitored at 2 Hz by the data acquisition system, while RGA data was taken approximately once per minute and tritium samples were collected for 24 to 72 hours between exchanges.

While the reactor power remained constant, the capsule gas mass flow rate also remained constant. Only ^{16}N and ^{19}O were definitively measured in the capsule outlet gas (^{41}Ar was also detected in the gas, presumably due to activation of trace argon in the helium supply, but it was difficult to distinguish from low levels of ^{41}Ar normally present in the MITR containment building during reactor operation). The activity level of the capsule outlet gas, however, varied significantly as measured by the GM tube at the capsule gas outlet line. After rising during the reactor power increase to 2 MW, the activity peaked and then gradually decreased; it was reduced by a factor of 10 by the morning of September 16th. There were no substantial changes to the observed activity between the restart to 2.5 MW and reaching 5 MW despite passing through the flibe melting point. The activity increased sharply after reaching 5 MW, then decreased slowly over the next five hours after a similar increase at 5.5 MW. It then slowly increased over the following four days by a factor of three to its highest recorded value on September 21st (double the previous peak achieved at 5 MW). After this point it decreased linearly over time while the capsule gas was being monitored.

The mechanisms behind this variation in the release of the gaseous activation products is not clear, however it may be related to a second observed phenomenon. During the afternoon of September 24 the capsule pressure suddenly began rising, requiring a gradual decrease in the capsule inlet gas flow to stabilize the pressure. Within 16 hours of the first pressure rise, flow to the capsule had to be shut off completely to keep the inlet pressure from increasing. It is postulated that the capsule outlet gas line became constricted due to a buildup of some material from the capsule. The most likely source is volatilized BeF_2, which has a higher vapor pressure than LiF, and could preferentially condense on the walls of the colder 1.6 mm diameter outlet gas tube.[8] By momentarily redirecting the capsule inlet line from the helium supply to the charcoal filter vent to reduce the pressure in the capsule, it was demonstrated that ^{16}N and ^{19}O activity could be vented from the capsule, indicating that the inlet gas line was still communicating with the capsule internal gas space. From this point forward the capsule was held at 100 kPa with a static helium supply, however no further sampling of the capsule gas (RGA and tritium) was possible. After two weeks of operation in this mode the activation products were not observed during the attempted depressurization. Although this pressure testing continued twice weekly for

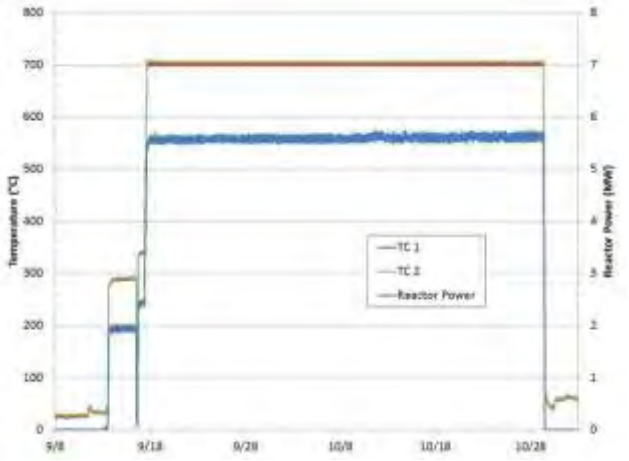

Fig. 4. Capsule temperature vs. reactor power over the irradiation. Differences in placement in the ion chambers used to record reactor power for the experiment result in readings slightly shifted from the official control value but respond more promptly to power changes.

the remainder of the experiment, it is assumed that at that point both the inlet and outlet lines had become constricted with the unknown material, and communication with the capsule internal gas space was not reestablished.

The experiment reached 1000 hours at temperature on the morning of October 29, and the reactor proceeded to reduce power in 500 kW steps with 10-minute stabilization periods at each step down to a reactor power of 2.5 MW. In a reverse of the startup procedure, with the capsule temperature starting at 500°C, neon flow was gradually reduced to zero.

IV. POST-IRRADIATION EXAMINATION

Following the irradiation, the nickel capsule was transferred to a shielded hot box for disassembly. The capsule lid was unscrewed, and the three graphite wedges were extracted and transferred to individual helium-purged containers. During the lid removal it was found that the graphite sections were unable to rotate, possibly due to larger-than anticipated swelling or deposition of volatiles, and therefore there was minor damage to the tops of the chambers above the frozen salt as the thermocouples and nickel pins were removed.

Each graphite section was then moved to a helium-filled glove where it was baked in a ventilated furnace at progressively higher temperatures to remove any moisture. After baking it was then heated above the salt melting point and the specimens extracted.

The specimens were allowed to cool, and then moved into a fume hood where they were immersed in clean water at room temperature for 6-12 hours to remove residual salt, air dried, and then weighed. This soaking, drying, and weighing process repeated until there was no longer any measurable weight change. The specimens were then

photographed with an optical microscope, scanned with profilometer, and surveyed with a gamma spectrometer. The TRISO particles were also mounted, sectioned, and then polished followed by additional photography.

V. RESULTS AND DISCUSSION

The irradiation experiment achieved 229.1 MWd (1000 hours) at 700°C, and 238.8 MWd total irradiation including operation below full power. The estimated total neutron fluence was 8.8×10^{19} n/cm^2 thermal and 4.4×10^{20} n/cm^2 fast (E>0.1 MeV). Final fluence determinations will be made through gamma spectroscopy of flux wires that were placed in the graphite sample holder.

The results of the tritium collection from the capsule and thimble exhaust gas are shown in Figure 5. The gas flow from the capsule or thimble was first mixed (at room temperature) with 50 cc/min of helium-1%-oxygen gas mixture and then bubbled through three 20 mL vials of deionized water. The gas was then passed through a high temperature catalyst before being bubbled through three additional 20 mL deionized water vials. The first set of vials collects any tritium in the gas stream that is in a water-soluble form, such as HTO, T_2O, or TF. The catalyst and oxygen supply are used to react any non-soluble species such as HT and T_2 to produce soluble species for capture in the remaining vials. At the end of each sampling period the six vials were replaced with new vials and fresh water. The collected vials were first counted on an HPGe detector, then samples were drawn from each vial, mixed with PerkinElmer® Opti-Fluor liquid scintillator and counted using a Packard® TRI-CARB 2900TR Liquid Scintillation Analyzer. This analysis was used to determine the gamma and tritium activity of each vial. No gamma activity was measured in any vial over the course of the experiment. The tritium activities were integrated over each sampling period.

During a given sampling round, the amount of tritium in each vial of the sampling train was consistently an order of magnitude higher than in the subsequent (downstream) vial. This indicates that the tritium was primarily collected in the first vials and was not breaking through the collection system. Some carryover of tritium is expected due to imperfect bubbling efficiency and evaporative losses into the dry helium, however the analysis showed on average 96%±3% of the tritium collected was contained in the first two vials of each set.

The original protocol for tritium collection during the experiment was to alternate the sampling between the capsule and thimble gas streams so that direct comparisons of tritium release at different stages of the irradiation could be made. However, after the obstruction of the capsule outlet line only the thimble gas was available for analysis. Tritium production in the salt from all sources was calculated using ORIGEN-S to be 2.63 mCi/MWd using cross sections generated from the MITR MCNP-5 full core

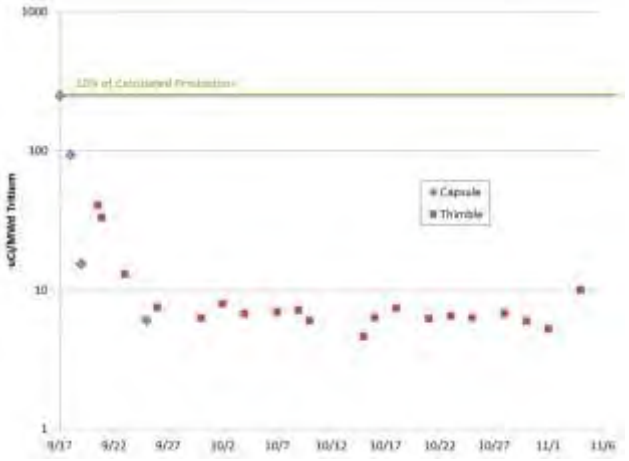

Fig. 5. Integrated tritium collected from the capsule and ICSA thimble exhaust gas. The final three points are taken during and after reactor shutdown but are adjusted for the equivalent time at 5.5 MW for direct comparison with the other data points.

model. 10% of this production rate is indicated by the line in Figure 5, aligning with the first measurement of tritium release from the capsule.

Although both capsule and ICSA thimble tritium levels decreased rapidly over the first week of irradiation, the thimble gas tritium release rates were consistently higher, indicating that the tritium diffused easily through the nickel capsule wall. The outside wall of the nickel is calculated to be about 50°C colder than the thermocouple, or ~650°C. At these temperatures metals are highly permeable to hydrogen, so such an effect is not unexpected compared to the smaller surface area available for axial diffusion of tritium from the salt chambers into the capsule cover gas stream.[9]

Future post-irradiation examination of the capsule and the material coupons will attempt to assess the total activity of tritium contained in the flibe and various materials and obtain a tritium balance for the experiment. Experience from the MSRE indicates that tritium, especially TF, will be preferentially adsorbed onto graphite.[5] The large amount of graphite in the MSRE therefore substantially reduced the amount of tritium released from the system. Tritium may also have been held up in the experiment gas sampling system due to adsorption on the tubing. This can be countered in future experiments by mixing hydrogen into the helium cover gas mixture, but this was not done in this initial irradiation test for simplicity, and to prevent altering the redox potential of the salt.

Investigation of the condition of the capsule gas space and gas lines will also potentially yield information concerning the cause of the gas line obstructions. Finally, the flibe and material coupons will be used to assess corrosion, transport of corrosion products, and other

material interactions with the liquid flibe environment under irradiation.

After cleaning and approximately one year of decay, the specimens' activities were measured with an ion chamber and a germanium spectrometer. The SiC specimens had a surface dose rate of ~10 mR/hr; this was primarily β-activity and therefore likely due to ^{14}C. The SS316 and Hastelloy specimens were approximately 100 mR/hr at 30 cm with contributions from ^{54}Mn, ^{58}Co, and ^{60}Co. These isotopes are all expected activation products based on the composition of each specimen.

The final specimen weights are given in Table 3 along with the calculated mass loss. It should be noted that the surface area for the SiC/SiC fiber composite specimens used the bulk geometric area, not accounting for roughness or porosity, and therefore is an overestimation of the material loss.

For the metallic specimens there are two apparent trends; first, the specimens exposed in a binary environment without graphite had less mass loss than those in the ternary environment. Second, in each environment the SS316 corrosion rate was higher than that of the Hastelloy N. The SiC specimens in general had lower mass loss than the metals with the exception of the HNLS composite. Again, the increased apparent mass loss of the composites may be due to their open porosity increasing the available surface area for salt interaction.

Optical examination of the specimens via macrophotography and scanning profilometry produced results that agreed qualitatively with the weight change measurements. As shown in Figures 6 and 7, the surface of the specimens from the un-lined chambers had increased roughness, indicating some acceleration of corrosion due to the presence of the graphite surface. This is significant because in a salt-cooled reactor with solid fuel there will be significant exposed surface areas of both graphite and metal in the primary system.

TABLE III

Specimen Mass Change after Irradiation

Specimen	Mass Change (mg/cm^2) ±0.01
N1 (Hastelloy, lined)	-0.23
N5 (Hastelloy, lined)	-0.28
N2 (Hastelloy, unlined)	-0.41
N6 (Hastelloy, unlined)	-0.42
S1 (SS316, lined)	-0.48
S5 (SS316, lined)	-0.54
S2 (SS316, unlined)	-2.09
S6 (SS316, unlined)	-2.08
CVD SiC 1	-0.10
CVD SiC 2	-0.09
SA3 SiC/SiC	-0.18
HNLS SiC/SiC	-1.23

The TRISO particles were found to have cracking in their outer pyrolytic carbon layer (OPyC) that was not observed in surveys of the as-received particles, or in preliminary results from the autoclave tests at UW. Additional testing of repeated freeze-thaw cycles of TRISO particles in flibe found that previously-irradiated particles were much more susceptible to OPyC cracking than un-irradiated particles, however additional testing on larger

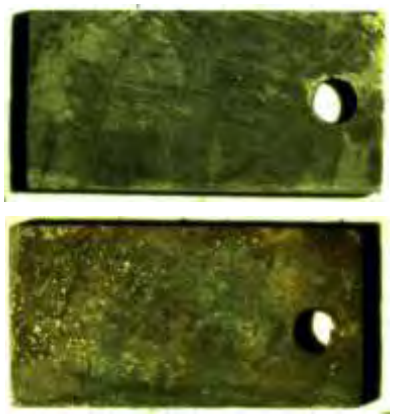

Fig. 6. Photographs of SS316 specimens after irradiation for lined (upper) and un-line (lower) chambers.

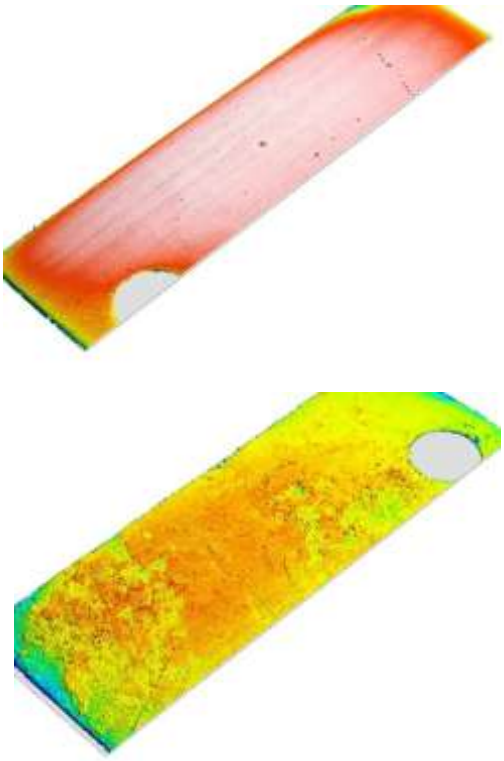

Fig. 7. Optical profilometry of the surface of irradiated SS316 specimens from lined (upper) and un-lined (lower) chambers.

batch sizes is required to definitively conclude that the irradiation sensitized the TRISOs to damage.

VI. CONCLUSIONS

A capsule containing fluorine-lithium-beryllium salt and a variety of material specimens was successfully irradiated in the core of the MIT Research Reactor for 1000 hours at 700°C. This irradiation marks the first demonstration of flibe irradiation capability at the MITR and the first irradiation experiment of the Fluoride Salt High-Temperature Reactor IRP.

Gas samples collected from the space above the flibe chambers and from around the sealed experiment capsule identified a steady release of tritium that is estimated to be only a few percent of the total tritium produced. Post-irradiation examinations will attempt to identify if the tritium balance can be accounted for by tritium absorption in the salt, the specimens, and the capsule's structural materials.

These initial results provide evidence of the high potential mobility of tritium in an FHR system consisting primarily of liquid flibe, graphite, and high-nickel alloys at high temperature. At the same time, a large percentage of the tritium that was predicted to have been generated in the salt was not detected in the gas phase, mirroring experience from the MSRE and indicating a potential for tritium control through tritium capture in solid components.

The data collected from this irradiation is immediately applicable to plans for future flibe irradiation experiments. In particular, there is increased confidence in the modeling and thermal control of the capsule with liquid flibe. In contrast, the gas handling system will need to be redesigned to prevent clogging of the gas sampling lines. Additionally, minimization of gas volumes must be balanced with personnel dose considerations due to the high activity and mobility of flibe activation products at any temperature. Future work on understanding tritium partitioning and the differences between nickel alloys and SS316 will help inform the evolution of the FHR conceptual design.

ACKNOWLEDGMENTS

Financial support for this work is provided by the U.S. Department of Energy through an Integrated Research Project grant. We would like to acknowledge the help of our colleagues at the MIT: Dr. Kaichao Sun, Dr. Charles Forsberg, John Stempien, Chris Haid, and the NRL staff; at UW: Dr. Mark Anderson, Dr. Guoping Cao, Brian Kelleher, and Guiqiu Zheng.

REFERENCES

1. C. FORSBERG, et. al., "Fluoride-Salt-Cooled High-Temperature Reactors (FHRs) for Base-Load and Peak Electricity, Grid Stabilization, and Process Heat," MIT-ANP-147, Massachusetts Institute of Technology (2013).

2. P.N. HAUBENREICH and J.R. ENGEL, "Experience with the Molten-Salt Reactor Experiment," *Nuclear Applications & Technology*, **8,** 118 (1970).

3. C. FORSBERG, "Fuel Geometry Options for Salt-Cooled Advanced High-Temperature Reactors," *Proceedings of ICAPP*, Nice, France, May 13-18 (2007).

4. S.J. KIM, Y. OSTROVSKY, L.W. HU, G. KOHSE, "Thermal Analysis of High Temperature Irradiation Modules in In-Core Sample Assembly," *Proceedings of the ANS Annual Meeting*, San Diego, June 13-17 (2010).

5. R.E. THOMA, "Chemical Aspects of MSRE Operations," *ORNL-TM-4658*, Oak Ridge National Laboratory (1971).

6. A.L. MATHEWS and C.F. BAES, "Oxide Chemistry and Thermodynamics of Molten Lithium Fluoride-Beryllium Fluoride by Equilibration with Gaseous Water-Hydrogen Fluoride Mixtures," *ORNL-TM-1129*, Oak Ridge National Laboratory (1965).

7. C. FORSBERG, "2013 Annual Report: High-Temperature Salt-Cooled Reactor for Power and Process Heat," *NEUP 11-3272 Quarterly and Annual Report*, October 20 (2013).

8. F.J. SMITH, L.M. FERRIS, and C.T. THOMPSON, "Liquid-Vapor Equilibria in LiF-BeF_2 and LiF-BeF_2-ThF_4 Systems," *ORNL-4415* (1969).

9. A. SUZUKI, T. TERAI, and S. TANAKA, "Tritium Release Behavior from Li2BeF4 Molten Salt by Permeation Through Structural Materials," *Fusion Engineering and Design* 51–52 (2000).

Innovative Methods in Research Reactor Analysis and Design

ESTIMATING BURNUP OF MTR FUEL USING THE LEAST SQUARE FITTING METHOD

LUAY M. ALAWNEH, SALIH ALKHAFAJI, KHALIFEH ABUSALEEM
Jordan Research and Training Reactor, Jordan Atomic Energy Commission
P. O. Box 70, Amman 11934, Jordan

CHANG JE PARK
Department of Nuclear Engineering, Sejong University
209 Neungdong-ro, Gwangjin-gu, Seoul 143-747, Republic of Korea

ABSTRACT

A simple and accurate model is proposed to calculate burnup based on the least square fitting method without additional depletion analysis. This was performed on plate type fuel assembly of research reactors based on the SCALE6 code sequences such as TRITON/NEWT and ORIGEN-ARP with some sensitivity analyses. One fuel assembly is modeled and its burnup is obtained for different power densities, enrichments, and fuel densities. Linear and non-linear polynomial fitting methods are used to provide a suitable formula for the burnup of the plate type fuel assembly as function of different parameters. This approach was applied to evaluate burnup of Jordan Research and Training Reactor (JRTR) and the results are compared to its Burnup results that were obtained using McCARD code. McCARD code is a Monte Carlo code which has burnup analysis capability that enables users to perform easy-to-use depletion computations with built-in subroutines for solving the depletion equations.

1. Introduction

In order to evaluate fuel performance and characteristics in the reactor, it is very important to estimate accurately fuel discharge burnup. Fuel burnup is defined as the amount of energy (usually heat) generated per metric ton of all uranium and plutonium isotopes contained in the fuel charged into a reactor [1]. And it is an important quantity for design and operation of reactors from a standpoint of safety as well as operability [2].

It is widely known that the uranium oxide fuel in normal commercial light water reactors approaches the 40 ~ 60 GWD/MTU. However, in the research reactor, the burnup is changeable due to different types of fuels such as U_3Si_2, U_3Si, U-Al, and U-Mo fuels. Generally, the metal fuels of research reactors provide higher burnup than the existing uranium oxide fuel of LWR. The discharge burnup is nearly 100 GWD/MTU, which is mainly resulting from higher power density in the research reactors. Therefore, it is important work to estimate accurately fuel burnup for safety analysis and fuel performance analysis.

In this study, linear and non-linear formulae for burnup of plate type fuel assemblies are suggested through the least square fitting method. This approach enables us to estimate burnup directly without following the detail fuel history including depletion analysis. Accurate burnup estimation is not an easy job due to several reasons such as the effect of fission products and

the power change caused by refueling and depletion. Mostly power density, uranium enrichment, and fuel density are key factors on burnup. The sensitivity of each factor has been investigated, and then their effects are combined into one fitted formula for each burnup step.

Several code systems were used to estimate discharge burnup such as SCALE6 [3] code system including TRITON/NEWT [4],[5], ORIGEN-ARP[6] and a Monte Carlo code such as McCARD[7].

The ORIGEN-ARP is a SCALE6 depletion analysis sequence used to perform point-depletion calculations with the ORIGEN-S[8] code using problem-dependent cross sections. The NEWT[5] computer code is a multigroup discrete-ordinates radiation transport code with flexible meshing capabilities that allow two-dimensional (2-D) neutron transport calculations using complex geometric models. The TRITON[4] is a SCALE control module that enables depletion calculations to be performed by coordinating iterative calls between cross-section processing codes, NEWT, and the ORIGEN-S point-depletion code. The McCARD[7] is a Monte Carlo (MC) neutron-photon transport simulation code. It is capable of performing the whole core neutronics calculations, the reactor fuel burnup analysis, the few group diffusion theory constant generation, sensitivity and uncertainty (S/U) analysis, and uncertainty propagation analysis.

2. Procedure of calculation

A crude formula is obtained to estimate burnup for plate type fuel assemblies based on different parameters such as power densities, enrichments and fuel densities. To obtain burnup formula, a sensitivity of each factor on burnup is carried out for various time steps where only a specific factor is changed and the others are maintained as constants.

As a first step, the TRITON/NEWT is used to generate burnup dependent cross section library for a plate type fuel assembly. Then the ORIGEN-ARP is used with the obtained to deplete fuel plate for several cycles. From the ORIGEN-ARP analysis the percentage burnup of U-235 is calculated cycle by cycle, and a schematic diagram for the analysis procedure is shown in Figure 1. The same approach is applied to various cases but using different fuels and time steps.

The percentage burnup is defined as

$$B = \left(\frac{\mathrm{n(0)-n(t)}}{\mathrm{n(0)}}\right) * 100\% \qquad \text{Eq.1}$$

where n(0) is the initial concentration of U-235 and n(t) is the U-235 concentration at time t.

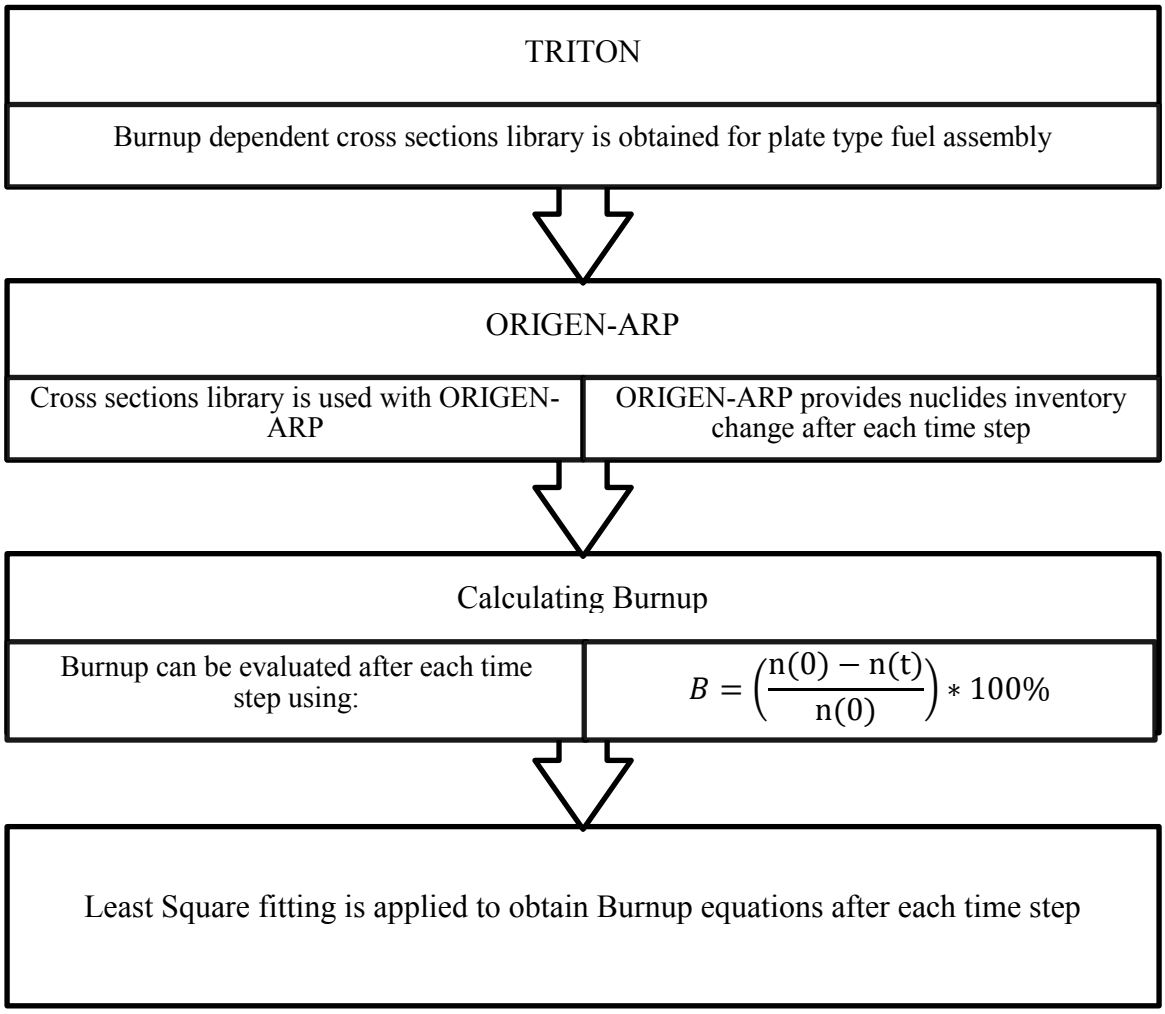

Figure 1 Procedure of the fitting method for burnup estimation

3. Application to JRTR

The JRTR core consists of 18 fuel assemblies with an enrichment of 19.75 wt%U-235 and 4 different fuel densities. Figure 2 shows the core configuration and the fuel density distribution in the core is shown in Figure 3. Each fuel assembly consists of 21 fuel plates of U_3Si_2 fuel.

All parameters of the fuel assembly are given in Table 1, which is a typical data for plate type fuel assembly. And a total of 27 TRITON/NEWT calculations are performed, in the first 9 inputs of the power densities are changed from 120 MW/MTU to 350 MW/MTU, while the enrichment and the fuel density are assumed to be constants. The power is chosen to be around 5MW, the enrichment is chosen to be 19.75 w% as in our problem specifications, the fuel density is chosen to be 5.5 g/cc which is almost the average of the fuel densities in the problem. In the next 9 inputs, the enrichment is changed the power density is chosen to be 240 MW/MTU which is the average the power densities. In the last 9 inputs, the fuel density is changed while the enrichment is constant. The fuel density range is from 3.8 g/cc to 7.2 g/cc which cover the whole range of density in the problem and the power density is also changed in accordance to maintain the same power level. After burning for one cycle, the fuel assemblies are shuffled a new assembly is loaded into the core at the fuel position of F17 and the one of F09 is discarded.

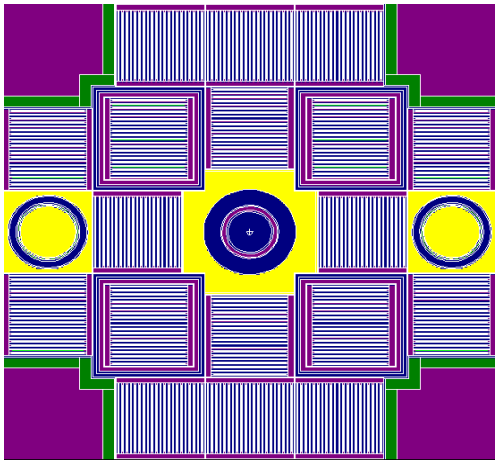

Figure 2 Configuration for JRTR core

Table 1 Properties of JRTR Fuel Assembly

Fuel Meat, Plate and Assembly	Data
Fuel meat thickness	0.51 mm
Fuel meat width	62.1 mm
Fuel meat length	640 mm
Cladding thickness	0.38 mm
Fuel plate thickness	1.27 mm
Fuel plate width	70.7 mm
Fuel plate length	680 mm
Coolant channel width	66.6 mm
Number of fuel plate/Fuel assembly	21
Fuel assembly width	76.2 mm
Material Property	**Data**
Fuel meat	U_3Si_2–Al
Uranium density in fuel meat	4.8 gU/cm3
Fuel meat density	4.2, 4.8, 5.9, 6.5 g/cm3
Cladding	Aluminum alloy
Cladding density	2.7 g/cm3

	F01 5.878	F02 6.543	F03 5.878	
F04 4.784	F05 4.784	F06 4.176	F07 4.784	F08 4.784
	F09 4.176		F10 4.176	
F11 4.784	F12 4.784	F13 4.176	F14 4.784	F15 4.784
ID Density (g/cm^3)	F16 5.878	F17 6.543	F18 5.878	

Figure 3 Fuel density distribution of the JRTR core

4. Results

In this test, three kinds of fitting models are tested such as the first order and the second order linear and the nonlinear fitting. And the burnup is estimated based on fuel assembly and 18 cycles are considered of which time step is assumed to constant as 40 days for the TRITON/NEW calculation.

The burnups of plate type fuel assembly are evaluated by using the fitted formulae and its results are compared with the McCARD results for 3 cycles. To provide a proper physics data such as power peaking factor, different cycle lengths are considered. The first cycle length is 87 days, the second cycle length is 34 days, and the third cycle length is 28 days. The burnup is evaluated by the equations after time step number 2 and 3 and an interpolation is made to get the burnup after the first cycle. The errors are evaluated based on McCARD results as a reference and Figures 4, 5 and 6 show the assembly wise burnup. All results of the fitting methods are comparable within 10%. The maximum errors for the first, the second order linear fitting and the nonlinear fitting are 9.6%, 6.9%, and 6.4%, respectively. The second order fitting gives better results than the first order case. The nonlinear approach is also a good alternative in this test.

	F01	F02	F03	
	9.60 9.02	8.60 8.14	9.70 9.08	
	6.08	5.32	6.34	
F04	F05	F06	F07	F08
12.70 12.00	13.20 12.20	16.50 15.00	13.30 12.24	13.00 12.26
5.51	7.61	9.11	7.96	5.73
	F09	CYC1	F10	
	17.10 15.60	1st order avg err.	17.20 15.75	
	8.78	7.13	8.46	
F11	F12	F13	F14	F15
12.60 11.88	13.00 11.90	16.10 14.56	13.00 11.95	12.80 12.10
5.68	8.49	9.57	8.05	5.49
	F16	F17	F18	
McCARD Equation	9.10 8.48	8.20 7.65	9.20 8.59	
Error%	6.82	6.70	6.58	

Figure 4 Estimated Burnup of the first order fitting for Cycle 1

	F01	F02	F03	
	9.60 9.29	8.60 8.36	9.70 9.36	
	3.24	2.78	3.55	
F04	F05	F06	F07	F08
12.70 12.37	13.20 12.56	16.50 15.42	13.30 12.61	13.00 12.62
2.57	4.83	6.55	5.21	2.91
	F09	CYC1	F10	
	17.10 16.01	2nd order avg err.	17.20 16.15	
	6.40	4.34	6.12	
F11	F12	F13	F14	F15
12.60 12.26	13.00 12.27	16.10 14.99	13.00 12.33	12.80 12.47
2.70	5.60	6.87	5.18	2.60
	F16	F17	F18	
McCARD Equation	9.10 8.77	8.20 7.88	9.20 8.88	
Error%	3.66	3.86	3.49	

Figure 5 Estimated Burnup of the second order fitting for Cycle 1

	F01	F02	F03	
	9.60 9.38	8.60 8.40	9.70 9.45	
	2.24	2.27	2.55	
F04	F05	F06	F07	F08
12.70 12.49	13.20 12.68	16.50 15.50	13.30 12.72	13.00 12.74
1.65	3.94	6.08	4.33	2.01
	F09	CYC1	F10	
	17.10 16.08	Non linear avg err.	17.20 16.22	
	5.95	3.56	5.67	
F11	F12	F13	F14	F15
12.60 12.38	13.00 12.39	16.10 15.07	13.00 12.44	12.80 12.58
1.78	4.71	6.38	4.28	1.69
	F16	F17	F18	
McCARD Equation	9.10 8.86	8.20 7.92	9.20 8.97	
Error%	2.65	3.39	2.48	

Figure 6 Estimated burnup of the nonlinear fitting for Cycle 1

After Cycle 1 the fuel assembly that is in position F09 is discharged, and all of the fuel assemblies are shuffled according to a specified scheme and a new fuel assembly is loaded at the position F17. The cycle length of Cycle 2 is 34 days and the burnup for three different cases are depicted in Figures 7, 8 and 9. The fitted results are acceptable within 10% compared with the McCARD results. The maximum errors are 8.8% for the first order equation, 8.4% for the second order equation and 9.2% for the nonlinear fitting approach.

	F01	F02	F03	
	11.90	11.50	13.00	
	11.83	10.94	12.04	
	0.55	4.91	7.36	
F04	F05	F06	F07	F08
17.30	17.70	22.10	18.00	13.20
16.69	16.90	21.32	16.58	13.27
3.53	4.50	3.53	7.89	0.52
	F09	CYC2	F10	
	23.30	1st order	22.80	
	21.81	avg err.	20.78	
	6.39	4.32	8.84	
F11	F12	F13	F14	F15
17.60	17.80	18.40	18.10	17.60
18.61	16.90	18.12	16.98	16.58
5.72	5.06	1.51	6.17	5.81
	F16	F17	F18	
McCARD	13.20	3.30	13.20	
Equation	12.83	3.32	12.92	
Error%	2.83	0.52	2.15	

Figure 7 Estimated burnup of the first order fitting for Cycle 2

	F01	F02	F03	
	11.90	11.50	13.00	
	12.04	11.22	12.40	
	1.19	2.42	4.61	
F04	F05	F06	F07	F08
17.30	17.70	22.10	18.00	13.20
17.21	17.42	21.95	17.11	13.47
0.49	1.56	0.68	4.95	2.03
	F09	CYC2	F10	
	23.30	2nd order	22.80	
	22.43	avg err.	21.43	
	3.75	2.65	6.02	
F11	F12	F13	F14	F15
17.60	17.80	18.40	18.10	17.60
19.09	17.42	18.51	17.50	17.11
8.44	2.14	0.62	3.31	2.80
	F16	F17	F18	
McCARD	13.20	3.30	13.20	
Equation	13.16	3.37	13.25	
Error%	0.30	2.03	0.37	

Figure 8 Estimated burnup of the second order fitting for Cycle 2 of 5 MW core

	F01	F02	F03	
	11.90	11.50	13.00	
	12.08	11.28	12.54	
	1.50	1.89	3.57	
F04	F05	F06	F07	F08
17.30	17.70	22.10	18.00	13.20
17.34	17.55	21.98	17.23	13.61
0.23	0.85	0.55	4.26	3.14
	F09	CYC2	F10	
	23.30	Non linear	22.80	
	22.45	avg err.	21.46	
	3.63	2.63	5.89	
F11	F12	F13	F14	F15
17.60	17.80	18.40	18.10	17.60
19.22	17.54	18.68	17.63	17.23
9.18	1.44	1.51	2.62	2.10
	F16	F17	F18	
McCARD	13.20	3.30	13.20	
Equation	13.30	3.39	13.39	
Error%	0.77	2.75	1.45	

Figure 9 Estimated burnup of the nonlinear fitting for Cycle 2

The cycle length of Cycle 3 is 28 days long and the burnup results of the equations are also compared with the McCARD results as shown in Figures 10, 11 and 12 for the first, the second order and the nonlinear equations, respectively. Similar accurate results are obtained and the maximum errors are 7.4%, 7.6% and 8.2% for first order, second order and nonlinear fitting approaches, respectively.

	F01	F02	F03	
	14.20	6.20	16.20	
	14.01	6.01	15.75	
	1.36	3.11	2.77	
F04	F05	F06	F07	F08
21.30	21.50	22.60	21.70	16.40
22.35	20.36	23.58	20.67	17.47
4.95	5.30	4.35	4.76	6.50
	F09	CYC3	F10	
	27.50	1st order	26.90	
	25.45	avg err.	25.92	
	7.44	4.01	3.63	
F11	F12	F13	F14	F15
16.20	21.90	22.00	21.50	21.00
15.31	20.86	22.05	20.72	20.39
5.48	4.75	0.24	3.61	2.92
	F16	F17	F18	
McCARD	15.90	2.80	14.50	
Equation	15.03	2.77	15.15	
Error%	5.45	1.01	4.51	

Figure 10 Estimated burnup of the first order fitting for Cycle 3

	F01	F02	F03	
	14.20	6.20	16.20	
	14.31	6.06	16.11	
	0.75	2.20	0.56	
F04	F05	F06	F07	F08
21.30	21.50	22.60	21.70	16.40
22.92	20.98	23.89	21.28	17.83
7.61	2.43	5.72	1.95	8.72
	F09	CYC3	F10	
	27.50	2nd order	26.90	
	26.23	avg err.	26.69	
	4.62	3.09	0.79	
F11	F12	F13	F14	F15
16.20	21.90	22.00	21.50	21.00
15.39	21.46	22.65	21.33	21.00
4.97	1.99	2.98	0.78	0.00
	F16	F17	F18	
McCARD	15.90	2.80	14.50	
Equation	15.41	2.77	15.31	
Error%	3.07	0.93	5.57	

Figure 11 Estimated burnup of the second order fitting for Cycle 3

	F01	F02	F03	
	14.20	6.20	16.20	
	14.40	6.12	16.28	
	1.42	1.31	0.50	
F04	F05	F06	F07	F08
21.30	21.50	22.60	21.70	16.40
23.05	21.10	24.15	21.40	18.01
8.20	1.87	6.87	1.39	9.83
	F09	CYC3	F10	
	27.50	Non linear	26.90	
	26.23	avg err.	26.68	
	4.63	3.02	0.80	
F11	F12	F13	F14	F15
16.20	21.90	22.00	21.50	21.00
15.60	21.59	22.79	21.45	21.12
3.68	1.44	3.58	0.22	0.58
	F16	F17	F18	
McCARD	15.90	2.80	14.50	
Equation	15.58	2.81	15.34	
Error%	2.03	0.23	5.77	

Figure 12 Estimated burnup of the nonlinear fitting for Cycle 3

5. Conclusions

In this paper, a least square fitting approach is proposed to estimate the fuel burnup for the plate type fuel assembly of the research reactor based on the SCALE6 calculation and some sensitivity analyses. Linear and nonlinear fitting methods are derived to obtain reliable results and they are applied to evaluate burnup of Jordan Research and Training Reactor. Three main

parameters are taken into consideration such as the power density, the uranium enrichment, and the fuel density. The maximum errors are below than 10% by comparing the results of the Monte Carlo code. When comparing the direct approach by using the Monte Carlo codes, the fitting approach is simple and acceptable, but it requires the preceding calculations to determine the coefficients. However, considering difficulties to estimate accurately burnup without enough information, the suggesting least square fitting is very challenging and it can be a good alternative to apply different new nuclear systems.

Acknowledgements

This work has been carried out under the auspices of the Jordan Research and Training Reactor Project being operated by Korea Atomic Energy Research Institute.

REFERENCES

[1]. Kulikowska, T., Szezesna, B., 1984.Fuel Management Module. FM-1; Fuel Burnup in Slow Neutron Fission Reactors, The VPI Program Package/Preliminary Version, Partially Supported by IAEA research contract No. 2841/RB.

[2]. Inoue, K., Tanuguchi, K., Murata, T., Mitsui, H., Doi, A., 1969.Burnup determination of nuclear fuel. Journal of Nuclear Science and Technology 17 (4), 830–842.

[3]. Bowman S. M., 2007. Overview of the SCALE Code System, American Nuclear Society 2007 Winter Meeting.

[4]. Dehart, M.D. 2009. TRITON: A Two-Dimensional Transport and Depletion Module for Characterization of Spent Nuclear Fuel, ORNL/TM-2005/39, Ver.6, Oak Ridge National Laboratory.

[5]. Dehart, M.D., 2005. NEWT: A New Transport Algorithm for Two-Dimensional Discrete Ordinate Analysis in Non-Orthogonal Geometry. ORNL/TM-2005/39, Version 6 Vol. II, Sect. F21 of SCALE: A Modular Code System for Performing Standardized Computer Analyses for Licensing Evaluation.

[6]. Gauld, I.C., Bowman, S. M., Horwedel, J. E., 2009. ORIGEN-ARP: Automatic Rapid Processing for Spent Fuel Depletion, Decay, and Source Term Analysis, ORNL/TM-2005/39, Ver6, Vol. I, Sect. D1.

[7]. Shim, H.J., Han, B.S., Jung, J.S., Park, H.J., Kim, C.H., McCARD, 2012.Monte Carlo Code for advanced reactor design and analysis. Nuclear Engineering and Technology 44, 161–176.

[8]. Gauld, I.C., Hermann, O.W., Westfall R.M., 2009. ORIGEN-S: SCALE System Module to Calculate Depletion, Actinide Transmutation, Fission Product Buildup and Decay, and Associated Radiation Source Terms, ORNL/TM-2005/39, Ver.6, Vol. II, Sect. F7.

[9]. Bratton Isaac John, 2012. Modeling and Validation of The Fuel Depletion and Burnup of the OSU Research Reactor Using MCNPX/Cinder'90, The Ohio State University.

[10]. Luay M. Alawneh, Mustafa K. Jaradat, Chang Je Park and Byunhchul Lee. "Burnup Estimation for Plate Type Fuel Assembly through Least Square Fitting Method", Annals of Nuclear Energy, 71 (2014) 37–45

[11]. Hussein, H. M., Amin, E. H., Sakr, A. M., 2011. Effect of Core Configurations on Burnup Calculations for MTR type Reactors, Proceedings of the 8th Conference on Nuclear and Particle Physics, Hurghada, Egypt.

[12]. Park C. J., Lee, B., 2012. Lattice Characteristics and Activity Analysis of U3Si2 AND UMo Plate Type Fuel Assemblies with SCALE6 Code," RERTR 2012 — 34nd International Meeting on Reduced Enrichment for Research and Test Reactors.

VALIDATION OF THE MCNP6 MODEL AT THE ATOMINSTITUT TRIGA REACTOR

M. CAGNAZZO, T.STUMMER, M.VILLA, H. BOECK

Atominstitut, Vienna University of Technology
Stadionallee 2, 1020 Wien, Austria

ABSTRACT

In order to calculate the reactor fuel burn-up and reactor critical parameters such as excess reactivity and shut-down margin, a primary requirement is to evaluate fluxes inside the fuel elements. For this purpose, a simulation model of the TRIGA Mark II research reactor at the Vienna University of Technology/Atominstitut (ATI) was developed by means of the Monte Carlo code MCNP6. This model allows to calculate the neutron flux in-core distribution and the energy spectrum in different in core positions, including inside the fuel elements.
The neutron flux distribution and the energy spectrum were measured in different core positions under a recent extensive measurements campaign performed at the TRIGA reactor Vienna. These data were used as benchmark to validate the simulation model of the reactor also with the purpose to extend the reliability of the results of the calculation to those regions where direct measurements cannot be performed (e.g. inside the fuel elements).
Aim of this work is to present the results of the MCNP6 reactor model against measured data.

1. Introduction

The core of the TRIGA Mark II research reactor at the Vienna University of Technology/Atominstitut has been fully refurbished with new fuel, slightly irradiated. In order to calculate the reactor fuel burn-up and reactor critical parameters (such as excess reactivity and shut-down margin) as well as to support future research activities, this new core configuration needs to be properly characterized, mainly evaluating fluxes inside the fuel elements.
The neutron flux distribution and the energy spectrum were measured in different core positions under a recent extensive measurements campaign performed at the TRIGA reactor in Vienna. The purpose of this work is to benchmark those results to validate the current reactor simulation model, implemented by means of the Monte Carlo code MCNP6 [1].

2. Facility description

The TRIGA (Training Research and Isotope production General Atomics) MARK II reactor [2] is a pool-type research reactor moderated and cooled by light water.
The TRIGA Mark II at the Atominstitut is licensed for 250 kW steady state and up to 250 MW pulse operation. Recently the reactor was converted from a highly heterogeneous core which included HEU (High Enriched Uranium) fuel elements to a full LEU (Low Enriched Uranium) core. As a result, the current core load consists out of 76 stainless steel clad zirconium-hydride fuel elements (8.5%-wt enriched 19.95%-wt in 235U), in a cylindrical geometry.
The TRIGA Mark II of ATI is equipped with various irradiation facilities inside and outside the reactor core. It incorporates facilities for neutron and gamma irradiation studies as well as for isotopes production, samples activation and students training.

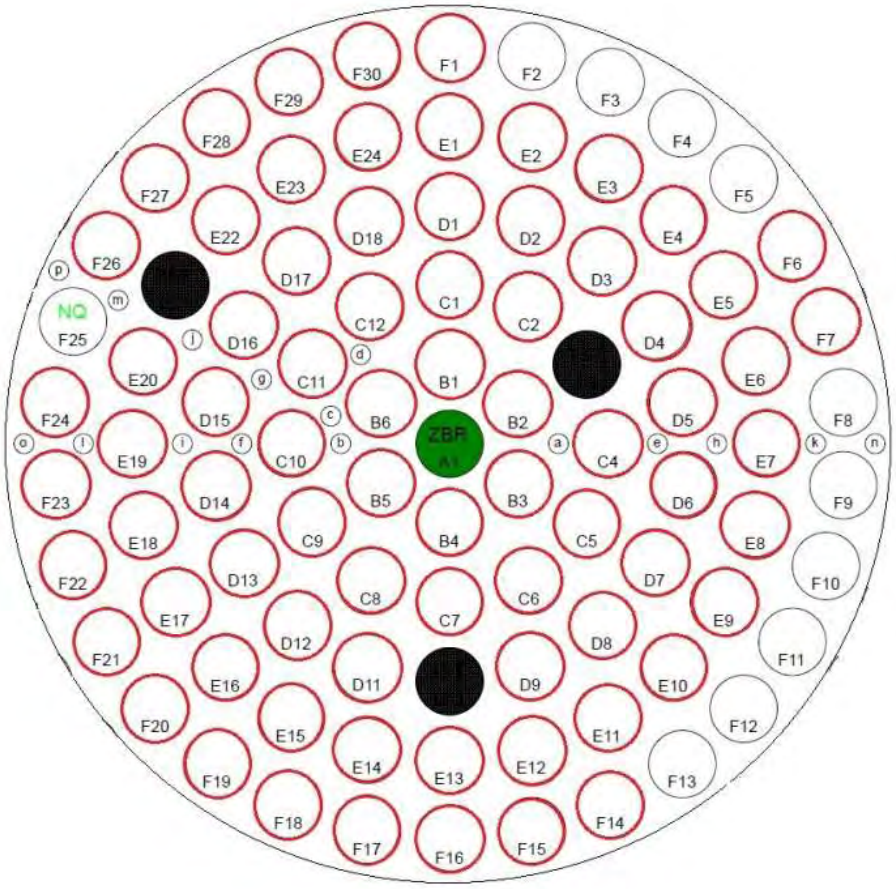

Figure 1: Current Core configuration with 76 Fuel Elements; ZBR indicates Central Irradiation Channel (CIR) and NQ the neutron source; the 3 control rods are represented in black color.

The reactor core is currently composed of 76 stainless steel clad FE(s), 3 control rods, one neutron source element and 8 dummy graphite elements in the F-ring (Figure 1). Besides three positions are dedicated to in-core irradiation facilities: the Central Irradiation Channel (CIR) and two pneumatic transfer systems (positions F08 and F11).
Two aluminium grid plates, at the top and bottom of reactor core respectively, constitute the support for the core. The top grid plate, of 49.5 cm in diameter and 1.9 cm in thickness, hosts 90 holes, each with diameter 3.82 cm, placed in five concentric rings to locate the core components (FE(s), source element, control rods etc.); while 91st central hole accommodates the CIR of diameter 3.81 cm.
The bottom grid plate supports the entire weight of the core and provides the exact spacing between core components. It is an aluminium plate of 40.7 cm in diameter and 1.9 cm in thickness. The central hole of 39.9 mm diameter serves as a clearance hole for the central thimble while the other ninety holes with 7.14 mm diameter provide alignment with the holes in the top plate.
Besides, 16 holes in the top grid plate (Figure1), each of 8 mm in diameter, are placed at various positions (*a,b,…p*) and permit the insertion and irradiation of foils into the core.

3. MCNP6.1 code and the reactor model

The MCNP (Monte Carlo N–Particle Transport Code) is one of the best known and most utilized Monte Carlo code in reactor physics. The last release version MCNP6.1 [1]

represent a general-purpose, continuous-energy, generalized-geometry, time dependent, Monte Carlo radiation-transport code designed to track many particle types over broad ranges of energies. MCNP6 is the merge result of the MCNP5 and MCNPX codes into a single product comprising all features of both. The code presents a set of new features that include the possibility to handle a multitude of particles and to include model physics options for energies above the cross-section table range, a material burnup feature, and delayed particle production. Expanded and new tally, source, and variance-reduction options are available as well as an improved plotting capability.
A simulation model of the TRIGA Mark II research reactor at the Atominstitut (ATI) was developed by means of MCNP6. The current model includes at the proper level of detail all the components that can affect the evaluation of the neutron flux in-core distribution and the energy spectrum in different in-core positions, including inside the fuel elements; as well as the reactor fuel burn-up and reactor critical parameters.
The reactor core horizontal section of model obtained by MCNP6 is shown in Figure 2, where the graphite reflector, the circular ring irradiation facility (Lazy Susan) surrounding the core inside the graphite reflector, the initial parts of thermal and thermalizing column are also displayed. The detail of the current reactor core (Figure 3) shows the different core component and their current location: the 76 cylindrical FE(s) (pink colored), including the visible central Zirconium rod; the neutron source (blue colored, in position F25); the control rods position (in yellow, as they are represented completely extracted); the instrumented FE (green colored); the graphite elements (purple colored); the water inside the core (yellow colored).
A vertical view of the reactor model including the graphite reflector is shown in Figure 4: main components of the FE(s) (such as fuel meat, central Zirconium rod, poison disks, axial graphite reflectors, Al-cladding) are visible.
The neutron source was simulated using the KCODE option with 10000 histories per cycle and 1050 cycles (the first 50 cycles were discarded). The initial spatial distribution of fission neutrons was entered by using the KSRC card with sets of location in the fuel elements.

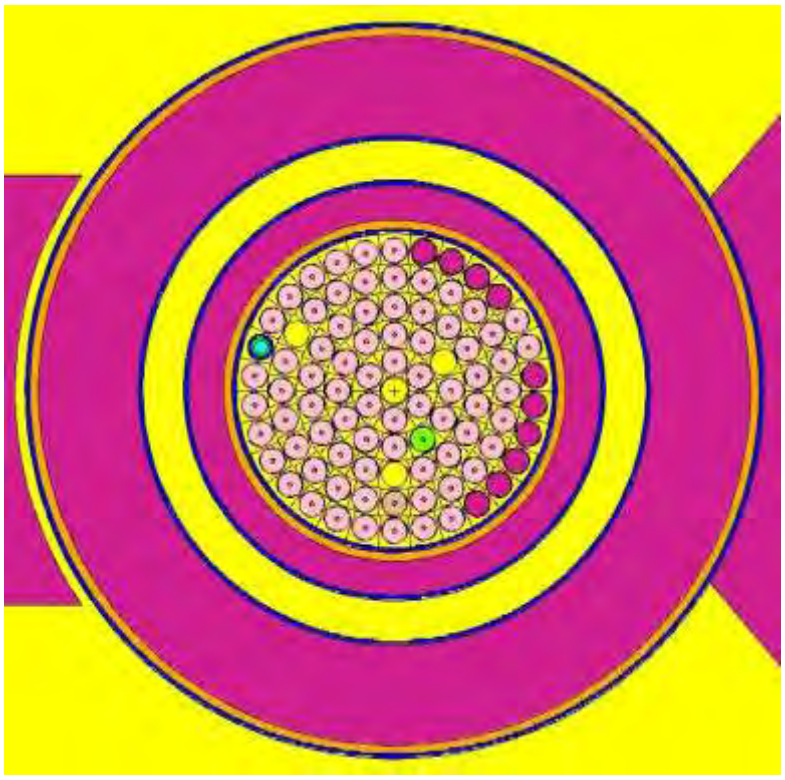

Figure 2: The horizontal section of the TRIGA reactor model as obtained by MCNP6

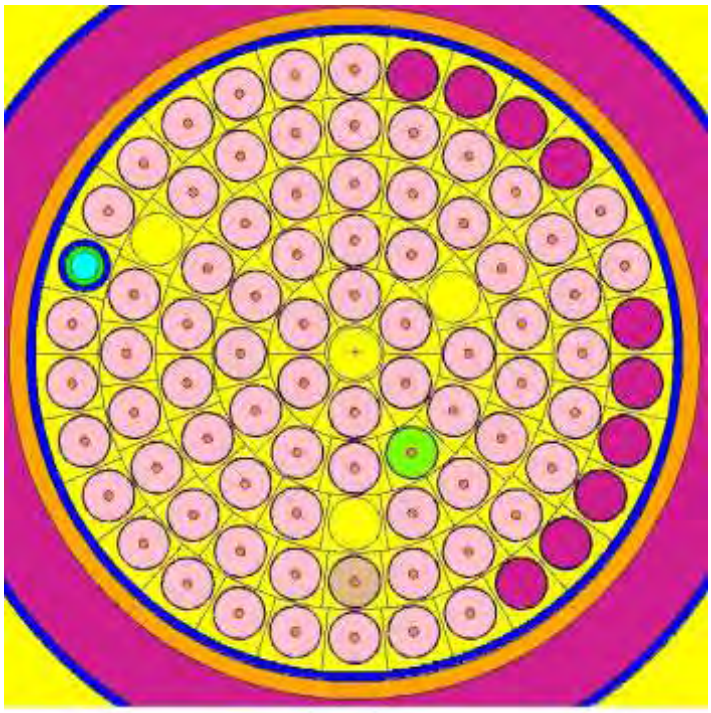

Figure 3: The horizontal section of the TRIGA core modeled by MCNP6.

4. Experimental determination of the in core neutron flux distribution

The in-core neutron flux distribution and energy spectrum measurements were performed applying a methodology based on a de-convolution technique of activated foils [3] [4] using SAND-II code [5]. The method allows to measure both slow and fast neutron components providing as result a neutron spectrum in 621 energy points in the range between 10^{-10} and 18 MeV. The deconvolution code as well as the selection of materials foils and irradiation characteristics are describe in the references [3] [4]. In the case of the measurements presented in this work, the absolute neutron flux was evaluated within an accuracy less than 10%.

The irradiation experimental facilities inside the reactor core for this measurement campaign were the Central Irradiation Channel (CIR) and a set of radial position defined by the holes in the core grid plates (§2).
The characterization of the neutron spectrum along the vertical axis was performed by measurements in 11 positions in the CIR. A proper sample holder was designed in order to determine very accurately each position: irradiation of different material foils were easily repeated at the same position. The locations of irradiation positions are shown by the markers in Figure 4 and the exact distances are reported in Table 1; distances are taken from the core equatorial position along the vertical axis (z=0). Position named Equatorial (EQ) corresponds to the core center; the two positions corresponding to the upper and lower end of a fuel element active part are named TOP (position 2) and BOTTOM (position 10) positions respectively. Two additional irradiation positions were added outside of the fuel element active part, in correspondence of the graphite axial reflector in the fuel element.
The characterization of the neutron spectrum along the radial direction was performed by irradiations in 3 of the available positions defined by the holes in the top grid plate (§2) at the equatorial level of the core (z=0). These selected positions (position *b, i, o*) are shown in Figure 1 and the radial distances from the center of the core (x=0) are listed in Table 1. Position 6 (EQ), i.e. core center position, is taken into account as 4th radial position.

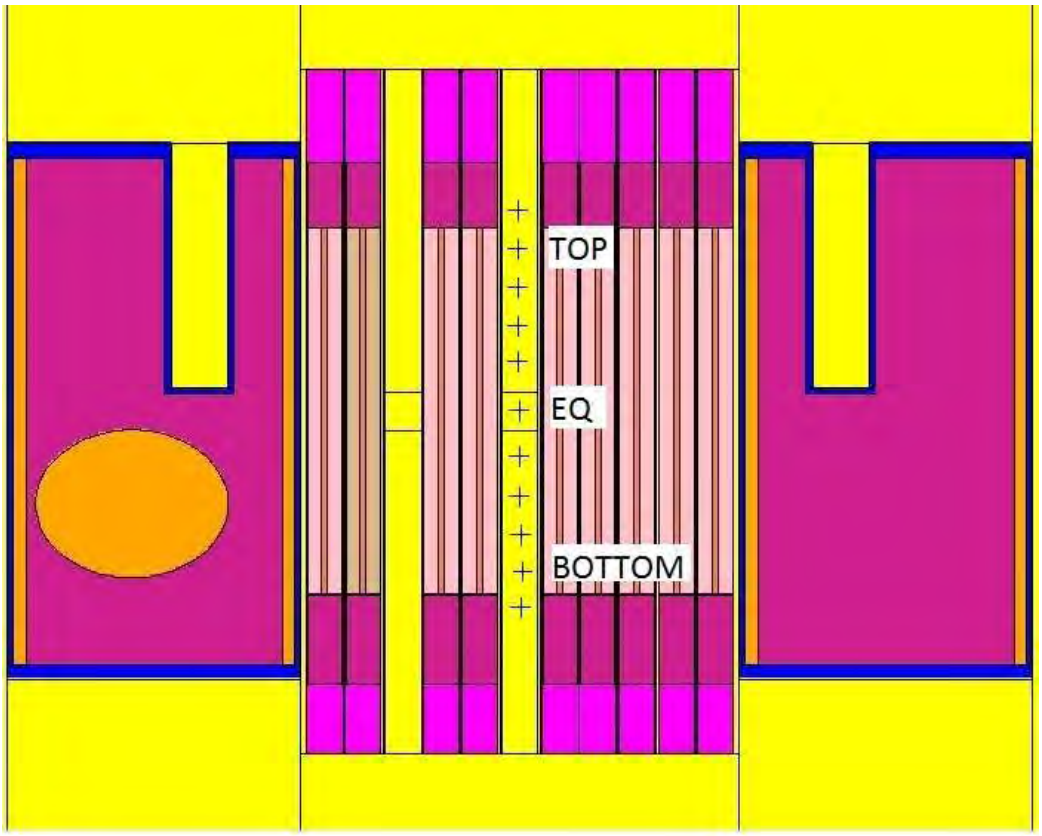

Figure 4: Vertical view of reactor core with indication of the irradiation positions (TOP, EQ, BOTTOM) in the CIR.

CIR Irradiation position	Vertical distance along Z axis (cm)
Position 1	20
Position 2 (TOP)	16
Position 3	12
Position 4	8
Position 5	4
Position 6 (EQ)	0
Position 7	-4
Position 8	-8
Position 9	-12
Position 10 (BOTTOM)	-16
Position 11	-20

RADIAL Irradiation position	Radial distance along X axis (cm)
Position 6 (EQ)	0
Position ***b***	-5
Position ***i***	-13.5
Position ***o***	-22

Table 1: In-core Irradiation positions for flux determination along vertical axis (Central Irradiation Channel, CIR) and along X axis (RADIAL Irradiation positions).

As results, the measurements provided differential fluxes for each irradiation position, distributed over 621 energy values in the range between 10^{-10} and 18 MeV: Figure 5 shows, as an example, the Differential Flux in 3 of the irradiation positions as obtained with this methodology.

As the results are given in the form of very detailed energy spectrum, it is possible to calculate integral flux values over desired energy intervals.

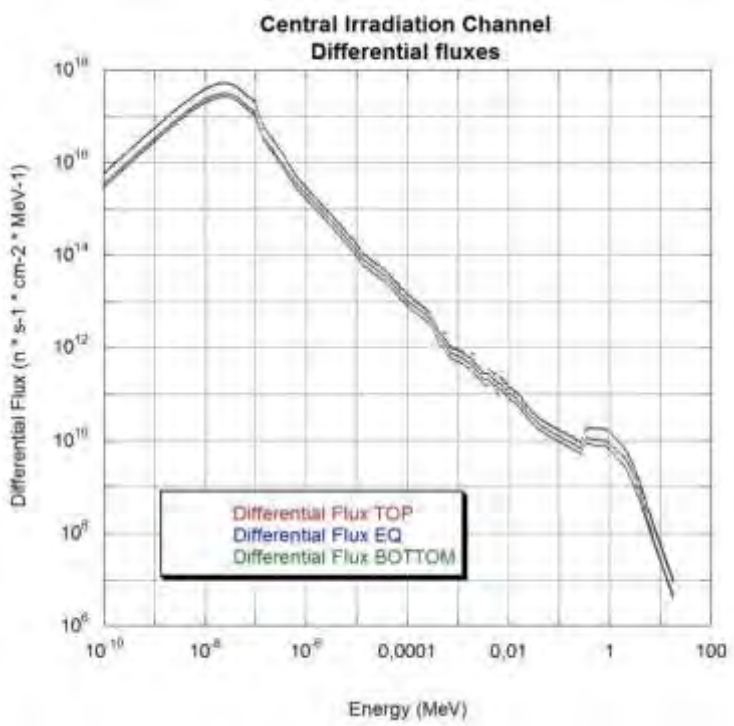

Figure 5: Measured Differential Flux in Central Irradiation Channel (Positions 2-EQ, 6-TOP, 10-BOTTOM).

5. Calculation and measurement results

The calculation performed with the current MCNP6 reactor model produced results in the form of integral neutron flux over 30 energy groups: the width of the energy groups was chosen to represent constant lethargy intervals. Dividing the integral value on each group by the width of the group, a differential flux distribution over 30 energy points was calculated.

As an example, the comparison between the calculated and measured differential flux over 30 energy points is provided in Figure 10 for the position corresponding to the center of the core (POS 6).

The total neutron fluxes along the vertical core direction (z axis) obtained both by means of MCNP6 simulation and through measurement campaign respectively are shown in Figure 6.

The values of the thermal component (E<0.69eV) of the fluxes along the vertical core direction obtained by MCNP6 simulation and measurement campaign are shown in Figure 7.

The neutron fluxes behavior along the core radial direction (x axis), is displayed in Figures 8 and Figure 9. Figures 8 compares the simulation and measured results for the total neutron flux; while Figure 9 shows simulation and measured results for the thermal neutron flux component (E<0.69eV).

All values reported are referred to the reactor power of 1 kW.

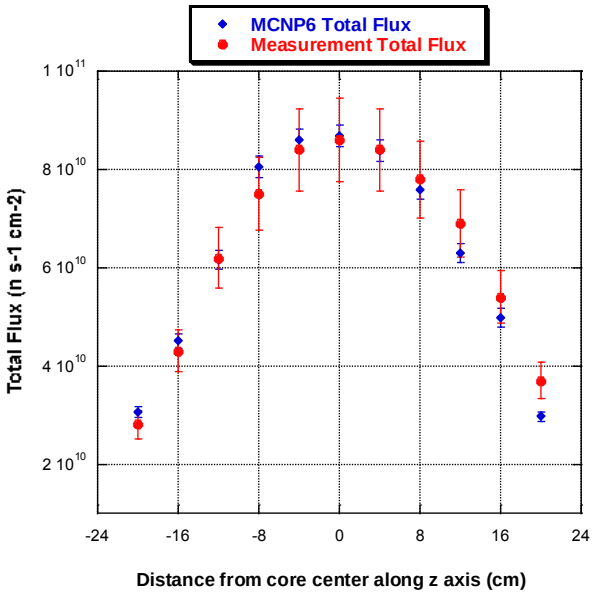

Figure 6: VERTICAL DIRECTION - Total neutron fluxes along the vertical core direction (z axis) obtained by means of MCNP6 simulation and through measurement.

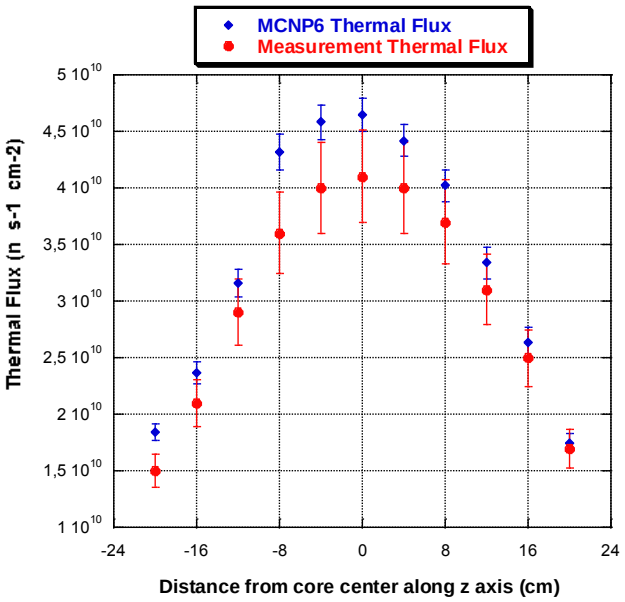

Figure 7: VERTICAL DIRECTION - Thermal neutron fluxes along the vertical core direction (z axis) obtained by means of MCNP6 simulation and through measurement.

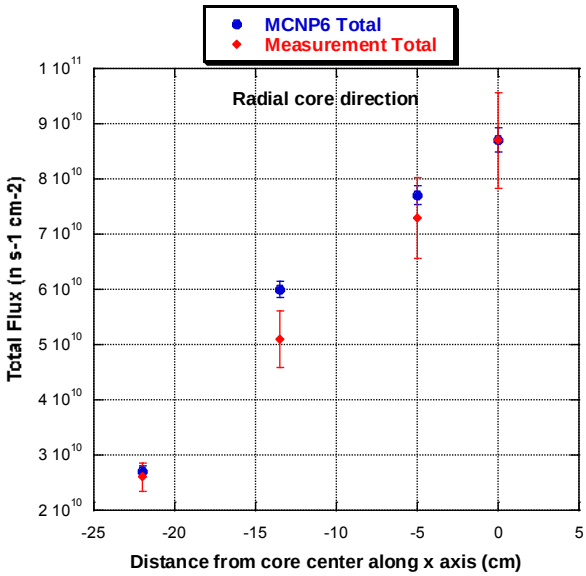

Figure 8: RADIAL DIRECTION - Total neutron fluxes along the radial core direction (x axis) obtained by means of MCNP6 simulation and through measurement.

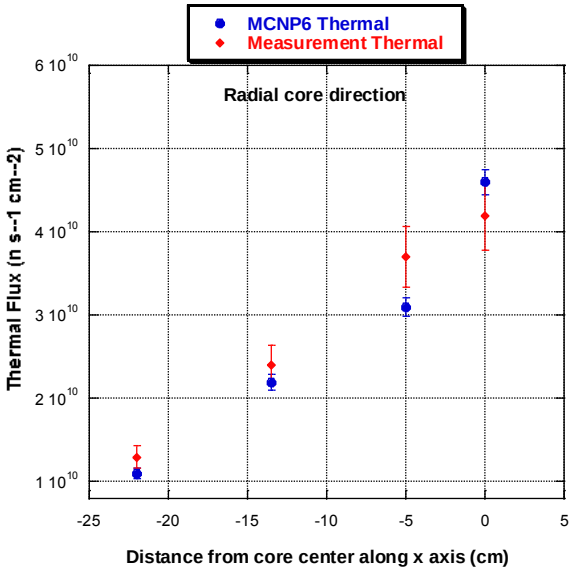

Figure 9: RADIAL DIRECTION - Thermal neutron fluxes along the radial core direction (x axis) obtained by means of MCNP6 simulation and through measurement.

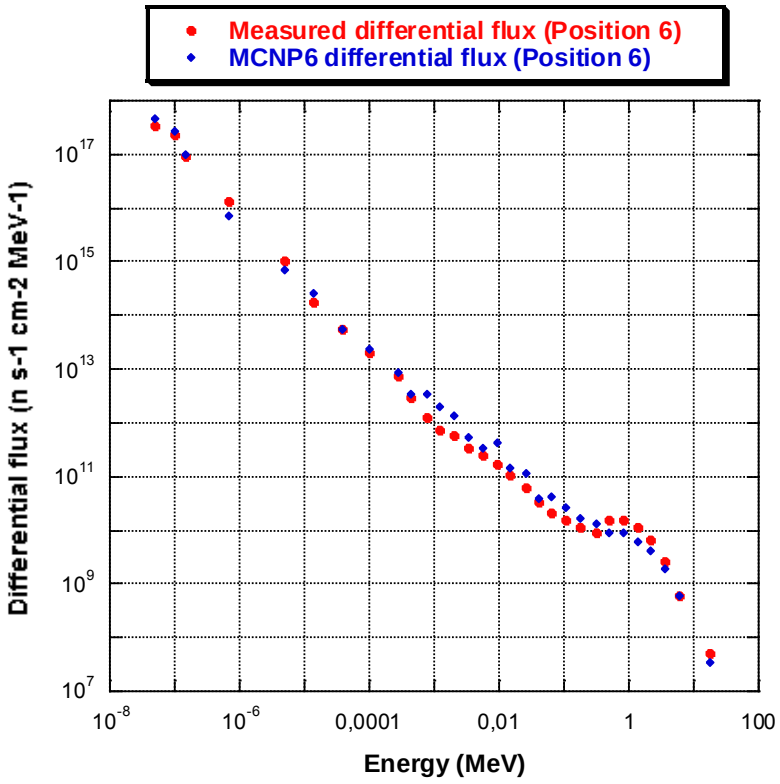

Figure 10: Comparison of measured and MCNP6 Differential Flux in Position 6 (Core Center).

6. Discussion and conclusions

The results of simulation and of the measurement show a fair agreement within the uncertainties.
The distribution of measured fluxes (total and thermal) along the vertical direction of the core shows a typical cosine behavior.
MCNP6 systematically overestimates the value of the thermal flux over the axial distribution: this could be explained by the fact that in the simulation the material are without impurities that may affect the absorption of neutrons, especially in the thermal region. However the same behavior is not reflected in the radial distribution of the thermal flux. Thus, the reason of this behavior needs to be further investigated.
The analysis of the fast component of the neutron fluxes was not performed and it is expected to be the addressed as a continuation of this research activity.
Additional irradiation positions outside of the core boundary are also planned to be characterized and will be used to extend the benchmark with Monte Carlo simulation.

7. References

[1] "MCNP6.1/MCNP5/MCNPX Monte Carlo N-Particle Transport Code System Including MCNP6.1,MCNP5-1.60, MCNPX-2.7.0 and Data Libraries", OAK RIDGE NATIONAL LABORATORY, August 2013;

[2] General Atomic (GA), March 1964, "TRIGA Mark II Reactor General Specifications and Description". General Atomic Company, U.S.A.;

[3] M.Cagnazzo et al., "Measurements of neutron flux distribution and energy spectrum in the horizontal beam tube at the TRIGA MARK II Vienna", RRFM 2014 European

Research Reactor Conference, 30 March - 3 April, Ljubljana (Slovenia) - ISBN 978-92-95064-20-1;

[4] M.Cagnazzo et al., “Measurements of the In-Core Neutron Flux Distribution and Energy Spectrum at the Triga Mark II Reactor of the Vienna University of Technology/Atominstitut”, Proceedings of the International Conference Nuclear Energy for New Europe (NENE), Portorož, Slovenia, September 8 -11, 2014 – ISBN 978-961-6207-37-9;

[5] CCC-112 SAND II Neutron Flux Spectra Determination by Multiple Foil Activation - Iterative Method, Oak Ridge national Laboratory, 1994.

BR2 REACTOR COUPLED MCNPX & MURE SIMULATIONS FOR THE SOLID EXPERIMENT (ANTINEUTRINO DETECTION)

L. GIOT, M. FALLOT
SUBATECH, Ecole des Mines de Nantes - CNRS/IN2P3 - Université de Nantes
4 rue Alfred Kastler, 44307 Nantes Cedex 3 – France

S. KALCHEVA, E. KOONEN
SCK.CEN, BR2 Reactor Department
Boeretang, 2400 Mol –Belgium

Corresponding author : lydie.giot@subatech.in2p3.fr

On behalf of the SoLid collaboration : Universiteit Antwerpen, Vrije Universiteit Brussel. Bristol University, Universiteit Gent, LAL, LPC Caen, University of Oxford, SCK-CEN Mol and SUBATECH .

Session: Innovative methods in reactor physics

ABSTRACT

Large quantities of antineutrinos are produced in a reactor due to beta decays of the fission products. The detection of these antineutrinos associated to reactor simulations could provide a method to assess both the thermal power and the evolution of the core fuel composition. One of the aims of the SoLid experiment located at the BR2 research reactor (SCK-CEN, Mol) is to investigate the ability of reactor monitoring with an antineutrino detector based on ^{6}LiF:ZnS and the use of such a detector for safeguards purpose. A detailed simulation of the BR2 reactor is needed to calculate the antineutrino spectrum emitted by the core for each cycle, i.e. for a given fuel loading map and operation history. A Monte-Carlo depletion code: MURE (MCNP Utility for Reactor Evolution) has been used for a few years in order to compute the antineutrino energy spectrum emitted by a PWR reactor but also research reactors. A detailed MCNPX/CINDER90 3-D simulation of the fission rates distribution in the BR2 core will be coupled with the MURE code. In this paper, the MURE code and the on-going developments for the BR2 simulation will be presented. The results of a benchmark performed between MURE and MCNPX/CINDER90 on the depletion calculation of a fuel assembly will also be discussed.

1. Introduction

The field of applied neutrino physics has shown new developments in the last decade. The idea that antineutrinos produced at reactors carry a direct image of the core that could be exploited for remote monitoring of nuclear power plants was first suggested in the late 1970s [1]. Large quantities of antineutrinos are produced in the reactor by beta decay of the fission products, with about 10^{21}antineutrinos/s emitted by a 1 GWe reactor core. The distribution of fission fragments produced by the fissile isotopes (^{235}U, ^{238}U, ^{239}Pu and ^{241}Pu) depends on the reactor power and on the neutron flux in the core. The energy released per fission and the average number of emitted antineutrinos and their mean energy also depend directly on the isotope undergoing fission, see Tab 1. Consequently, all differences in the fissioning process lead to variations in the associated antineutrino spectrum which will reflect the thermal power and composition of the core, opening several application possibilities such as burnup monitoring for fuel economy and safeguards. The proportionality between the antineutrino counting rate and the thermal power measured by the operators has been

demonstrated by two pioneering experiments performed at the Rovno power plant in the former USSR and at the Bugey power plant in France [1, 2], as well as the direct relationship between the antineutrino flux and energy spectrum as a function of the fuel content of the reactor core [3].

data per fission	^{235}U	^{238}U	^{239}Pu	^{241}Pu
released E (MeV)	201.7	205	210.0	212.4
$< N > \nu_e$	5.56	6.69	5.09	5.89
$< N > \nu_e$ with E>1.8 MeV	1.92	2.28	1.45	1.83
$< E_{\nu_e} >$ (MeV)	1.46	1.56	1.32	1.44

Tab 1 : Differences in the ^{235}U,^{238}U,^{239}Pu and ^{241}Pu fissions given in Reference [4] and a calculation of P. Huber and Th. Schwetz [5].

The International Atomic Energy Agency (IAEA) has expressed its interest in the potentialities of antineutrino detection as a new tool for reactor monitoring. Since IAEA disposes of only 250 inspectors and the number of nuclear facilities increases continuously, the diversity of the control means is mandatory for a rational utilization of the human efforts**.** IAEA is interested in the development of economic safeguards, promoting solutions able to provide a high degree of confidence regarding the detection of fissile material diversion and asked its member states to perform a sensitivity study on antineutrino detectors. Such a detector should be relatively small, portable, cheap, safe, and remotely controlled and sufficiently accurate to detect the diversion of a Significant Quantity (SQ) of nuclear material in a timely fashion (for instance, 8 kg of Pu in 3 months). These requirements constrain the sensitivity of the antineutrino probe. In a recent analysis [6], E. Christensen et al. were able to show that the application of antineutrino monitoring would have been able to provide timely information about plutonium production in the Democratic People's Republic of Korea, even given the actual, constrained and intermittent access by IAEA inspectors.

Worldwide effort concentrated on applied antineutrino physics has led to further investigations into the feasibility of using such detectors for safeguards purposes. An overview of the status of the development of a variety of compact antineutrino detectors for reactor monitoring is given in Reference [7]. The antineutrino measurement could be supplemented with the precise simulations of the reactor core. Following the declared core history, the proliferation scenario could be confirmed by comparing the reactor parameters extracted from the neutrino measurement with the ones predicted by simulations [8,9].

2. The SoLid experiment

The SoLid experiment aims to provide a significant contribution to the ability of reactor monitoring via a new approach using a highly segmented detector based on Lithium-6 [10,11]. SCK•CEN in Belgium has accepted to host the SoLid experiment closed to the BR2 research reactor and to provide support as the technological development and the potential for non-proliferation purpose is of particular interest as safeguards and a statutory task. The SoLid detector will be located on a radial distance at 5.5m from the BR2 core center. The experiment aims also at searching for active-to-sterile antineutrino oscillation at very short baseline and then to contribute to current research related to the existence of sterile neutrinos [12].

The SoLid technology for antineutrino detection is innovative compared with the classical approach based on liquid scintillator which generates problems related to safety, compactness and sensitivity to backgrounds [13]. The SoLid detector is a segmented detector (2.88t) divided in 10 modules (1,2m x 1,2m x 0,2m). Each module consists in 4 planes of 576 plastic scintillation PolyVinylToluene (PVT) cubes of size of (5×5×5) cm^3, each

cube being covered with one layer highly sensitive to thermal neutrons (^{6}LiF:ZnS(Ag)). The detector is read in (X,Y) by optical fibers coupled to Multi-Pixel Photon Counter MPPC. Antineutrino interacts with protons in the PVT cubes through the inverse beta-decay process: $\bar{\nu}_e + p \rightarrow e^+ + n$. A neutrino event is then defined by the time coincidence detection of a neutron and a positron. The outgoing neutron thermalises after a few elastic scatters and is eventually absorbed in the layer rich in Lithium-6 through the reaction: n + ^{6}Li → ^{3}H + α**.** The outgoing nuclei have sufficient kinetic energy to escape a few tens of microns in the mixture and excite the inorganic scintillator (ZnS). One of the first objectives of the SoLid collboration is the construction, installation and testing of a large scale prototype called SM1, close to the BR2 reactor at the end of 2014. The complete SoLid detector should be installed in 2016.

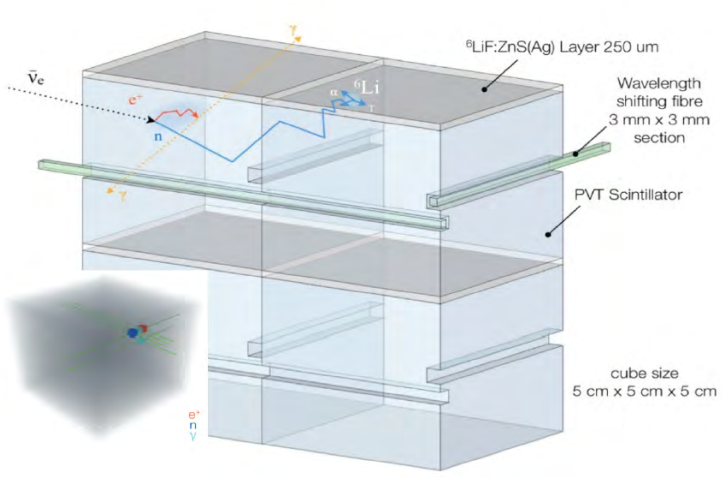

Fig 1 : Inverse Beta Decay interactions in the SoLid detector.

The antineutrino energy spectrum emitted by the BR2 core will be calculated for each cycle, i.e. for a given fuel loading map and operation history and provided as a reference for the antineutrino detection to the SoLid experiment.
This task relies actually on complementary expertises shared between :
- the SCK•CEN team which has a deep knowledge of the BR2 reactor and already developed a highly segmented 3D model of the reactor, using the Monte Carlo code MCNPX, described in section 3.
- the SUBATECH team which already developed and antineutrino spectrum calculations and power/research reactor simulations with the MURE code (MCNP Utility for Reactor Evolution) for previous antineutrino experiments, described in section 4.

In section 5, the first results of a benchmark performed between MURE and MCNPX/CINDER90 on the depletion calculation of a fuel element plus the on-going developments on reactor simulations for the SoLid experiment will be discussed.

3. The BR2 reactor and associated MCNPX modelling

The Belgian Material Test reactor (MTR) BR2 is a strongly heterogeneous high flux engineering test reactor operated by SCK•CEN at the Mol site in Belgium. This tank-in-pool reactor is cooled and moderated by light water in a compact HEU core (93% ^{235}U), positioned in and reflected by a beryllium matrix. The beryllium matrix is an assembly of a big number of irregular hexagonal prisms which are skew and form a twisted hyperbolic bundle around the central 200 mm channel H1 containing beryllium plugs. The reactor can be operated at the power level of 50-100 MW, currently about 120 full power days per year with a plan to increase the duty cycle to 150 days in 2016. The maximum admissible heat flux in the fuel plates of the standard BR2 fuel elements is 470 W/cm^2. The maximum neutron flux is

1.2×10^{15} $cm^{-2}.s^{-1}$ (E_n<0.5 eV) and 8.4×10^{14} $cm^{-2}.s^{-1}$ (E_n>0.1 MeV).

A 3-D model of the BR2 core was developed by the SCK•CEN team using the Monte Carlo transport code MCNPX [14]. The model is a complete 3-D description of BR2's one sheet hyperboloid reactor core composed of twisted and inclined reactor channels and represents each channel separately, with its individual position and inclination. The cross section at the mid-plane of the MCNPX model of the BR2 reactor core is depicted in Fig 2. The fuel assemblies, beryllium plugs, experimental devices or control rods loaded in the channels are modelled with the same level of details. The fuel region of each of the 6 fuel rings of every fuel element is axially divided into 10 material cells of 6 cm height and 2 extreme cells of 8.1 cm height. The MCNPX simulation can be coupled for the evolution part either to ORIGEN (included in the SCALE 4.4a system) or CINDER90 (included in MCNPX 2.7.0 code). The total number of material cells with varied fuel burn-up in the model is equal to 2304=12x6x32 in 32 fuel elements (without azimuth burn-up modelling). The credibility of the MCNPX model was for instance demonstrated by comparing code predictions with available experimental data, such as control rod worths, neutron fluxes, gamma heating and linear power. More details about modelling of the BR2 core, depletion and criticality calculations performed with MCNPX 2.7 can be found in Ref [15].

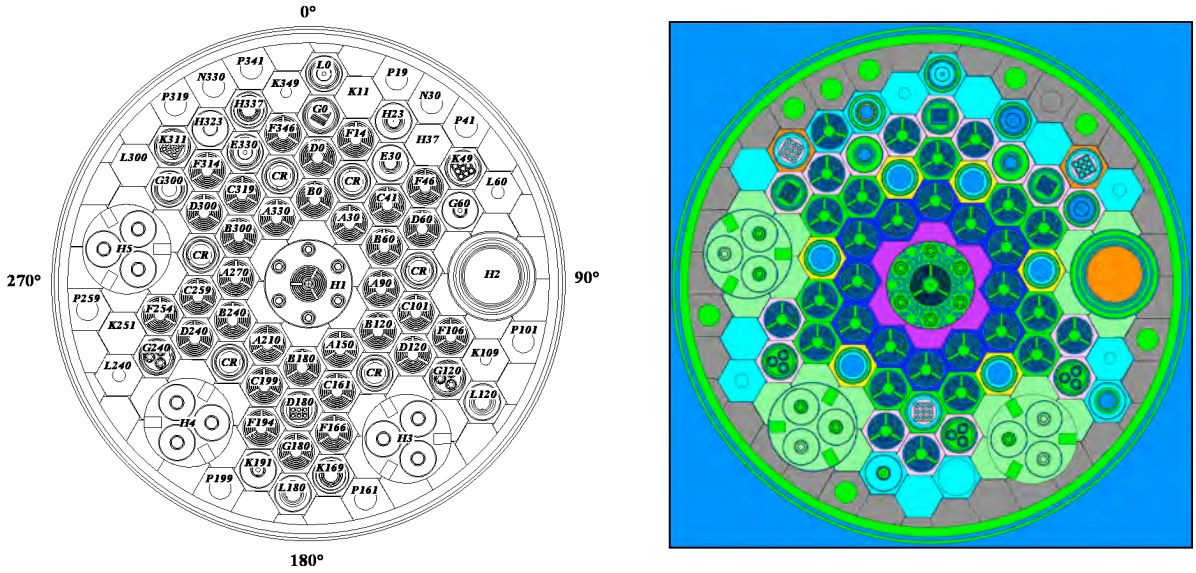

Fig 2. Cross sections at mid-plane of the BR2 reactor core (left) ; cross-section at mid-plane of the MCNPX BR2 reactor core model (right).

4. Antineutrino spectrum calculations and reactor simulations with MURE

In a reactor core, the number of antineutrinos produced over the time t_{run} is defined by :

$$N_{\bar{\nu}}(E) = \int_0^{t_{run}} \frac{P(t)}{\Sigma_k . \alpha_k(t) . E_k} \sum_k \alpha_k(t) . S_k(E) dt$$

The first term of the equation, accounting for the number of fissions occurring over the time, is the ratio of the thermal power (provided by the operators through measurements) over the average energy released per fission of the 4 isotopes (^{235}U, ^{238}U, ^{239}Pu and ^{241}Pu) present in the fuel. $\alpha_k(t)$ stands for the percentage of the total number of fissions undergone by the isotope *k*. The mean energy released per fission by each fissile isotope E_k is stored in nuclear databases. The second term represents the total antineutrino spectrum emitted by a reactor per fission. It is defined as the sum over the 4 isotopes of the fission fraction undergone by the k^{th} isotope times the antineutrino spectrum per fission of the same isotope $S_k(E)$ which can be calculated either using the conversion method or the summation method [16].

The conversion method is based on the measured β^- spectra of a fissile isotope at a given irradiation time and then is converted to $\bar{\nu}$. For ^{235}U and ^{239,241}Pu, the only β^- spectra are those from the ILL research reactor and were acquired after a quite short irradiation time in a quasi-pure thermal neutron flux, between 12 hours and 1.8 days depending on the isotopes. For antineutrino experiments, the irradiation time would be longer. Among the fission products, about 10% of them have a β^- decay half-life long enough to keep accumulating after several days. The increase in the $\bar{\nu}$ flux caused by the decay of these long-lived fission products has to be taken into account in the flux calculation with the conversion method, known as off equilibrium corrections.

The summation method computes the $\bar{\nu}$ spectrum emitted from a fissile isotope as the sum of the different contributions of all its fission products using the full information available per nucleus in nuclear databases. This method allows also to compute the off equilibrium corrections to be applied to the conversion method. In addition, the summation method is the only one allowing to predict antineutrino spectra associated to innovative fuels or reactor designs. This method is thus indispensable in the context of the study of proliferation scenarios with antineutrino detection.

In the frame of the following antineutrino experiments :
- Double Chooz which takes place in the Chooz nuclear power plant in France (EDF company), consisting of 2 pressurized water reactors (PWR N4 type) of nominal power 4.25 GW [16] ;
- and NUCIFER which takes place in the OSIRIS research reactor (CEA-Saclay), a light water reactor of open-core pool type and operated at a thermal power of 70 MW [13].

SUBATECH developed the needed reactor simulations with the MURE code [18,19] but also added new functions to MURE to analyze the beta decay properties of the fission products in order to compute the associated antineutrino energy spectrum.

Available at the NEA databank, the MURE (MCNP Utility for Reactor Evolution) code is a precision, open-source code, designed by CNRS/IN2P3 laboratories and written in C++ which automates the preparation, computation of successive MCNP (Monte Carlo N-Particle) calculations and solves the Bateman equations in between, using a Runge-Kutta method, for burnup purpose [20]. The MURE code is highly flexible to simulate reactors with a refuelling scheme, an operation history or a core geometry that does not follow the standards used in reactors dedicated to electricity production, and then can be used for safeguards scenarios with antineutrinos [8,9].

The evolution in time of the isotopic composition of the core is driven by the initial fuel composition, the input of the thermal power history, the considered geometry and control parameters of the core reactivity (e.g : boron concentration or controls rods history). It calculates the fission fractions α_k as a function of the reactor history and allows to follow up as a function of time all the fission products, which are needed for the summation method. The quality of the MURE simulations has been evaluated through various benchmarks, such as the Takahama benchmark [21]. MURE inventories of two assembly types used in the Chooz reactors were compared with those obtained with the DRAGON code and the APOLLO-2F code. In the latest case, the results were provided by the EDF Electricity Company [18]. In addition, an important work in the estimate of the systematic errors associated to the fission rates computed with MURE has also been performed for the Double Chooz experiment [18].

5. Reactor simulations for the SoLid experiment and first benchmark

The current strategy of the SoLid collaboration is to combine the work already performed by the SCK•CEN and SUBATECH. The BR2 team developed a 3D model of the reactor with MCNPX which can be coupled to CINDER90 and used as a starting point to produce the

fission rates. In addition to this highly segmented model, the MURE code will be used for the calculation of the emitted antineutrino energy spectrum. MURE will estimate the off equilibrium corrections needed for the conversion method spectra. Summation method spectra will also be calculated from the fission products inventory obtained with MURE. In addition, comparative studies will be perfomed to estimate the systematic errors between both codes. Other systematic errors associated to these simulations (thermal power, temperatures, loading burnups, nuclear data…) will be also determined and propagated.

As a first step, a depletion benchmark was performed between the MURE code and MCNPX coupled to CINDER90 for a single fuel element in an infinite lattice. Each of 6 fuel rings is embedded in an aluminium cladding, surrounded by water. No radial/axial discretization is considered for the fuel element included in an hexagonal beryllium prism with a mirror boundary condition. The geometry produced with MURE is shown in Fig 3.

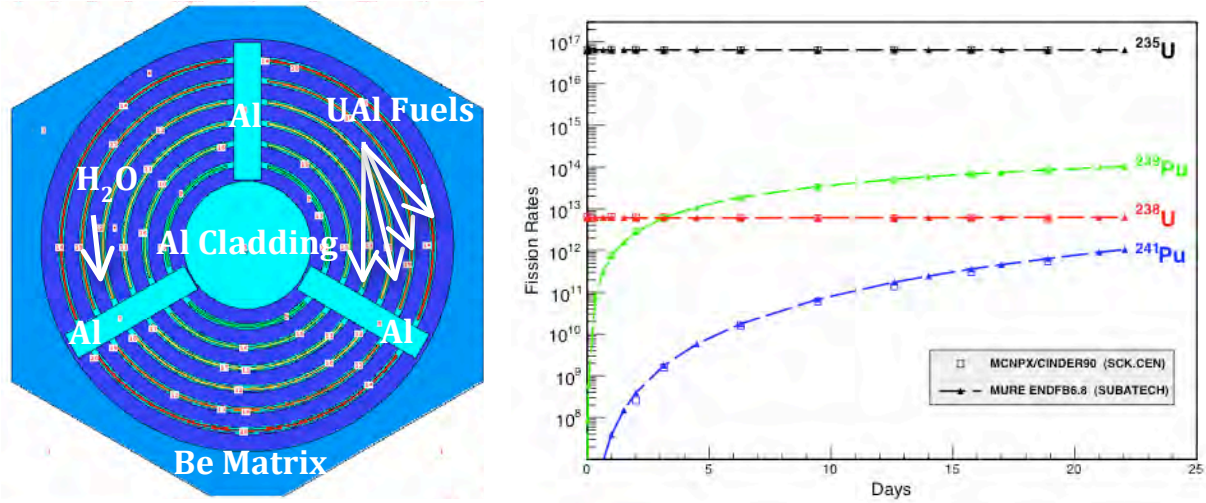

Fig 3. Fuel element geometry produced with MURE (left) ; comparison of fission rates for a fuel cycle (right).

A fuel cycle of 22 days is considered for the depletion calculation of this fresh fuel element (93% ^{235}U) with a constant power of 2 MW. The energies released per fission are taken from [22] for both codes. The input nuclear cross sections are respectively ENDF/B-VI.8 and ENDF/B-VII for the MURE and CINDER90 depletion calculations. The instantaneous fission rates for ^{235}U,^{238}U,^{239}Pu and ^{241}Pu are shown in Fig 3 as a function of time. The results are consistent between both codes. The fission rates are dominated by the contribution of the fission of ^{235}U (more than 99% due to the high enrichment of the fuel). The difference between both codes for the instantaneous fission rate of ^{235}U ranges from -1.5% to 2.7 % for the different depletion steps.

The next step is to perform the full core simulation for the last cycle of 2014. Studies will be done to determine the systematic errors associated to the BR2 simulations. To avoid the complete coding in a MURE format of the complex geometry of the BR2 core, the MCNPX input file of the SCK•CEN team will be directly read by MURE. For this purpose, a MURE module was developed and the adaptation to the considered fuel cycle and associated tests are on-going.

6. Summary

The SoLid experiment, installed at SCK-CEN BR2 research reactor in Mol, aims at validating a new technology to consolidate the use of antineutrinos as a safeguard tool with a detector using a composite scintillator based on ^{6}Li. A key ingredient in the success of the

experiment is the accurate calculation of the antineutrino spectrum emitted by the core. The principle of the calculation and the on-going work between the SCK•CEN and SUBATECH has been presented.

7. References

[1] L. A. Mikaelian, Proc. Int. Conf. Neutrino-77, Vol. 2, 383 (1978).
[2] Yu.V. Klimov et al., At. Energy 76, 123 (1994).
[3] V.A. Korovkin et al., At. Energy 65, 712 (1988).
[4] V. I. Kopeikin et al., Phys. Atom. Nucl. 60, 172 (1997).
[5] P. Huber, Th. Schwetz, arXiV :hep-ph/0407026v2 (2004).
[6] E. Christensen et al., arXiV: physics.ins-det/1312.1959v2 (2014).
[7] M. Fallot, Nuclear Data Sheets, Vol. 120, 137 (2014).
[8] T. Shiba et al., “Reactor Simulations for Safeguards with the MCNP Utility for Reactor Evolution Code”, Symposium on International Safeguards, October 2014, IAEAheadquarters, Vienna, (Austria), IAEA-CN-220/219.
[9] S. Cormon et al., Nuclear Data Sheets, Vol.120, 141 (2014).
[10] A. Vacheret et al., SoLid experiment proposal to the Institut Laue-Langevin PAC (2013).
[11] F. Yermia et al., Proceeding ICHEP, 2014.
[12] K. N. Abazajian et al., ”Light Sterile neutrino: a white paper”, arXiv:1204.5379.
[13] A. S. Cucoanes et al., Nuclear Data Sheets, Vol.120, 157 (2014).
[14] MCNPX, Version 2.7.0, LANL, LA-UR-11-02295. April, 2011.
[15] S. Kalcheva and E. Koonen, PHYSOR 2012 proceeding and references therein.
[16] M. Fallot et al., Phys. Rev. Lett. 109, 202504 (2012) and references therein.
[17] Y. Abe et al., Phys. Rev. Lett. 108, 131801 (2012).
[18] A. Onillon, Prediction of the Reactor Fission Rates and the Estimation of the Associated Uncertainties in the Frame of the Double Chooz Experiment, PhD Thesis, Ecole des Mines de Nantes (2014). Article in preparation.
[19] V.M. Bui, Beta decay of fission products for the non-proliferation and decay heat of nuclear reactors, PhD Thesis Ecole des Mines de Nantes (2012)..
[20] MURE, MCNP utility for reactor evolution (2009), O. Meplan. Tech. Rep. LPSC 0912 and IPNO-09-01 (2009).URL http://www.nea.fr/tools/abstract/detail/nea-1845.
[21] C. Jones et al., Phys. Rev D86, 012001 (2012).
[22] S. Kalcheva et al., Nucl. Tech., Vol.158, 36 (2007).

THERMAL HYDRAULIC AND NEUTRON KINETIC SIMULATION OF THE TRIGA IPR-R1 RESEARCH REACTOR USING RELAP5-PARCS COUPLED MODEL

P. A. L. REIS, C. PEREIRA, A. L. COSTA, J. GONZÁLEZ-MANTECÓN,
M. A. F. VELOSO, H. V. SOARES
Departamento de Engenharia Nuclear, Universidade Federal de Minas Gerais
Av. Antônio Carlos, 6627 – PCA1 – Anexo Engenharia – Pampulha
CEP 31270-901 Belo Horizonte, Brasil
Instituto Nacional de Ciências e Tecnologia de Reatores Nucleares Inovadores/CNPq, Brasil.

R. MIRÓ
Deparlamento de Ingenieria Quimica y Nuclear, Universidad Politécnica de Valencia
Camino de Vera, 14. 46022 Valencia, Spain

ABSTRACT

The computational advances observed in the last two decades have provided direct impact on the researches related to nuclear simulations which use several types of computer codes, including coupling between them, allowing also the analytical simulation and representing with very much accuracy the real behavior of nuclear plants. Studies of complex scenarios in nuclear reactors have been improved by the use of thermal hydraulic (TH) and neutron kinetics (NK) coupled system codes. This work presents a coupling methodology application between RELAP5 and PARCS system codes using as a model the research reactor TRIGA IPR-R1. Adequate cross sections for the PARCS code were supplied using the WIMSD5 code. Results of steady state and transient calculations using the 3D neutron modeling to the IPR-R1 are presented.

1. Introduction

Simulations of complex scenarios in NPPs have been improved by the utilization of coupled thermal-hydraulic (TH) and neutron kinetics (NK) system codes thanks also to development of the computer technology and new calculations methodology making possible to perform transport calculation schemes with accurate solutions. The TH and NK coupling technique consists in incorporating three-dimensional (3D) neutron modeling of the reactor core into system codes mainly to simulate transients that involve asymmetric core spatial power distributions and strong feedback effects between NK and TH [1].

The TH-NK coupling technique was initially developed and used to simulate the behavior of power reactors. However, several coupling methodologies are now being applied for research reactors [3]. In this way, this work presents the coupling methodology application between RELAP5 and PARCS codes using as a model the research reactor TRIGA IPR-R1. The cross sections were generated by WIMSD-5B code, using the compositions provided by a previous work [2]. These compositions represent the supposed core fuel state in November, 2004.

2. IPR-R1 TRIGA General Characteristics

TRIGA reactor is the most widely used non-power nuclear reactor in the world. General Atomic has sold 66 TRIGA reactors, which are in use or under construction at universities, government and industrial laboratories, and medical centers in 23 countries. The safety features of this fuel permit flexibility in siting, with minimal environmental effects [4].

The safety of the reactor would be guaranteed even if the engineered features were by-passed and the control rods, which contain the poison materials for shutting down an operating nuclear reactor, were rapidly removed.

The IPR-R1 is a reactor type TRIGA (Training, research, Isotope production, General Atomic), Mark-1 model, manufactured by General Atomic Company and installed at Nuclear Energy Development Center (CDTN) of Brazilian Nuclear Energy Commission (CNEN), in Belo Horizonte, Brazil. The reactor is housed in a 6.623 m deep pool with 1.92 m of internal diameter and filled with demineralized light water.

The water in the pool has function of cooling, secondary moderator and neutron reflector and it is able to assure an adequate radioactive shielding. The reactor cooling occurs predominantly by natural convection, with the circulation forces governed by the water density differences. The removal of the heat generated from the nuclear fissions is performed pumping the pool water through a heat exchanger. The core has a radial cylindrical configuration with six concentric rings (A, B, C, D, E, F) with 91 channels able to host either fuel rods or other components like control rods, reflectors and irradiator channels. There are 63 fuel elements constituted by a cylindrical metal cladding filled with a homogeneous mixture of zirconium hydride and Uranium 20% enriched in ^{235}U isotope [7]. There are 59 fuel elements covered with aluminum and 4 fuel elements with stainless steel. The main thermal hydraulic and kinetic characteristics of the IPR-R1 core are listed in [3]. IPR-R1 works at 100 kW but it will be briefly licensed to operate at 250 kW. The radial relative power distribution, represented in Figure 1, was calculated in a preceding work using the WIMSD4C and CITATION codes [2].

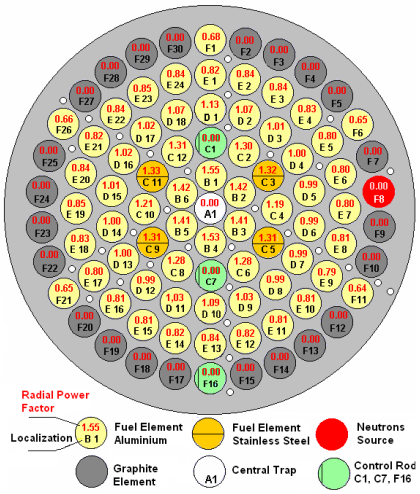

Fig 1. Radial relative power distribution

3. Coupling Between Thermal hydraulic and Neutronic Codes

The coupled system codes can model accurately not only reactivity-initiated accidents (RIA), but also typical reactor operational transients as turbine trip. These programs are often called “best-estimate” analysis tools and describe, in a more realistic way, the local core effects and coupled reactor core/plant dynamics interactions.

In this work, RELAP TH code and PARCS NK have been coupled. In the RELAP5-PARCS coupling calculation, PARCS [6, 16] makes use of the moderator temperature and density and of the fuel temperature calculated by RELAP5 [5] to evaluate the appropriate feedback effects in the neutron cross sections. Likewise, RELAP5 takes the space-dependent power calculated in PARCS and solves the heat conduction in the core heat structures. The

coupling process between RELAP5 and PARCS codes is done through a parallel virtual machine (PVM) environment, using an adequate association among thermal hydraulic and neutronic nodes. Figure 2 is the general scheme of the methodology used in this work for TH-NK coupling.

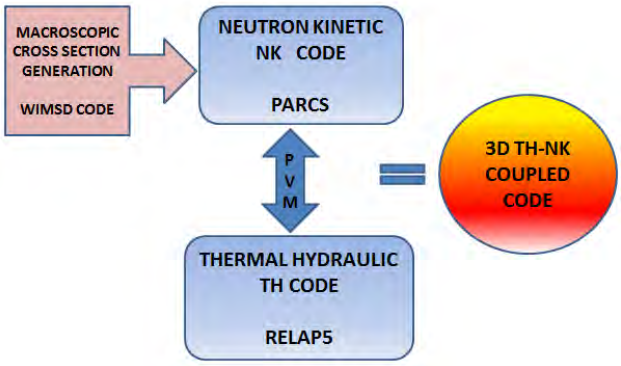

Fig 2. General scheme of the TH-NK coupling in this work

4. Thermal-Hydraulic Nodalization Description

The RELAP5 code was used to generate the IPR-R1 thermal hydraulic nodalization represented in a general way in Figure 3. The point kinetics model was used in RELAP5 simulations. The axial power distribution was calculated considering a cosine profile. The RELAP5 steady state calculations have been performed for models with 3, 7, 13 and 91 thermal hydraulic channels at 100 and 250 kW. The temperature values at the outlet of the TH channels at several positions were calculated and compared with the experimental available data [7]. Model verification was presented in preceding works [3, 8, 9, 11, 17]. In this present work, all TH calculations were performed considering the 3 TH channels model.

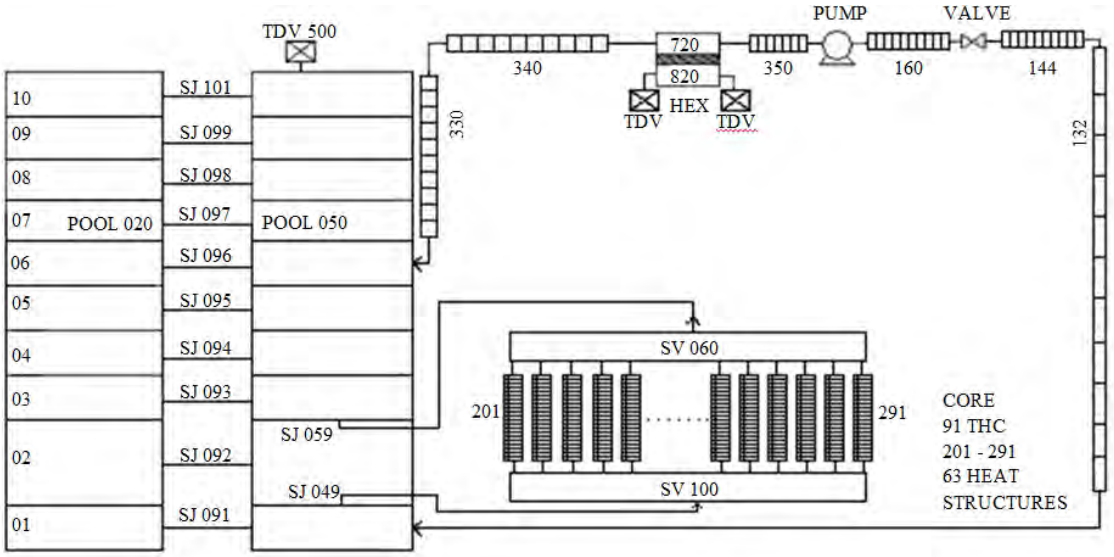

Fig 3. IPR-R1 reactor nodalization in the RELAP5 code for 91 TH channels

5. Macroscopic Cross Section Generation

The cross section libraries were generated by WIMSD5-B code (*Winfrith Improved Multigroup Scheme*) [13, 14] which is a general lattice cell program that uses transport theory to calculate flux as a function of energy and position in the cell.

In this work, geometry, position, composition and keeping the V_m/V_f ratio were considered when to define the cells (Fig. 4). As output, WIMSD-5B code provides the diffusion coefficient and the macroscopic cross sections that after will feed the code of neutronic analysis. The cross sections were calculated according to data of the IPR-R1 exposure in year 2004. The compositions were obtained from results of previous work using Monteburns code (MCNP-ORIGEN) and the available burn history of the TRIGA IPR-R1.

The cross section sets generated by WIMSD-5B code were included in the PARCS model. The tabular form of homogenized cross section libraries is organized in two energy groups. Data as the scattering, absorption, fission, cross sections, and diffusion coefficient were tabulated in PARCS. The assembly discontinuity factors (ADF) and corner discontinuity factors (CDF) were not considered. The WIMSD-5B code is a dimensionless code. The ADFs and CDFs factors were not directly provided in code output. The correction factors calculation will be done in future works.

WIMS code presents remarkable advances compared to other cell calculation codes in spite of some important isotopes missing in its nuclide table [14]. The user, while trying to construct fuel cells with no initial compositions will find insufficient decay chains and isotopes to cover the full range of nuclides that the fuel presents in the several stages of burning. In this work, when this was the case, those not found nuclides were replaced by those closest in relation to the cross section and decay behavior. Another problem was the lack of "upscattering" calculation by the code. This is an important factor in the evaluation of transient situations in the case of TRIGA type reactors (hydrogenated fuel).

As an initial study, to prepare the cross sections sets, ten compositions were considered in the model with six fuel compositions being: ring B of the core – fuel number 6, ring C (aluminum cladding) and ring C (stainless-steel cladding) – fuels number 4 and 5, respectively, rings D, E and F with fuel numbers of 3, 2 and 9, respectively. Number one represents the reflector composition. Numbers 7 and 10 represent, respectively, control rods and central thimble regions.

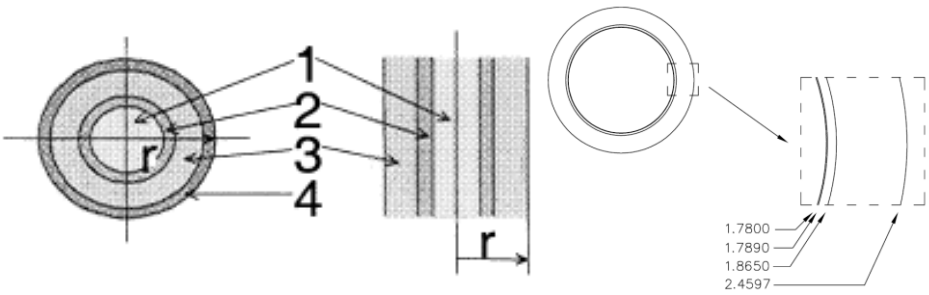

Fig 4. Left side: spatial model representing elementary cells (1) Fuel, (2) Cladding, (3) Coolant, (4) Moderator; Right side: cell example - ring B

The parameters used to calculate the macroscopic cross sections, such as coolant and fuel temperatures, should represent situations of steady state and accidents. Coolant temperature ranged from environment temperature to the water saturation temperature at the pressure of 1.5 bar, which corresponds to 384.0 K [11]. The fuel temperature was determined using the same criteria as in setting the coolant temperature. Room temperature was used as the lower limit, and 890.0 K as the upper limit. This last value corresponds to the temperature of fuel hydrogen dissociation. This represents a limiting safety factor of TRIGA IPR-R1 reactor.

6. PARCS Modelling

PARCS (*Pardue Advanced Reactor Core Simulator*) is a three-dimensional (3D) reactor core simulator which solves the time-dependent, two-group neutron diffusion equation to predict

the dynamic response of the reactor to external perturbations such as control rod movements or inlet coolant condition changes in reactor core [6].

To perform the IPR-R1 model, two energy groups were used and the core was modeled considering Cartesian geometry. The whole core has been simulated as a 3D model. The neutron kinetic modeling is shown in Figue 5 (left side), where the number 2 represents fuel region and the number 1 represents the reflector region. The input line “geo_dim” establishes a planar matrix 15 X 15 with 21 axial planes, where the first 4 and the last 4 planes are reflectors. As the core TRIGA geometry is cylindrical, the PARCS model was adapted to using a rectangular geometry. As an example, Fig. 5 (right side) shows the fuel compositions (2, 3, 4, 5, 6, 9), rod regions (7), the central thimble (10) and reflector regions (1) for the axial planar region 11. As there are 169 nodes for each plane and there are 21 axial planes, then the core has 3549 neutron kinetic nodes. Each one of the 63 fuel elements in the core was modeled representing 63 heat structures in the RELAP5 model and they were associated with three corresponding thermal hydrodynamic channels.

```
geo_dim  15  15  21  4  4
Rad_Conf
 0 0 0 1 1 1 1 1 1 1 1 0 0 0 0
 0 0 0 1 1 1 1 1 1 1 1 1 0 0 0
 0 0 1 1 1 1 2 1 1 1 1 1 0 0 0
 0 0 1 1 1 2 2 2 2 2 1 1 1 0 0
 0 1 1 1 2 2 2 2 2 2 2 1 1 0 0
 0 1 1 2 2 2 2 2 2 2 2 2 1 1 1 0
 1 1 1 2 2 2 2 2 2 2 2 2 1 1 1 0
 1 1 1 2 2 2 2 2 2 2 2 2 2 1 1 1
 0 1 1 1 2 2 2 2 2 2 2 2 2 1 1 1
 0 1 1 1 2 2 2 2 2 2 2 2 2 1 1 0
 0 0 1 1 2 2 2 2 2 2 2 2 1 1 1 0
 0 0 1 1 1 2 2 2 2 2 2 1 1 1 0 0
 0 0 0 1 1 1 1 1 2 1 1 1 1 0 0 0
 0 0 0 1 1 1 1 1 1 1 1 1 0 0 0 0
 0 0 0 0 1 1 1 1 1 1 1 1 0 0 0 0
!
```

```
Planar Region 11
                    1   1   1   1   1   1   1   1
                    1   1   1   1   1   1   1   1   1
                1   1   1   1   9   1   1   1   1   1
                1   1   1   2   2   2   2   2   1   1   1
            1   1   1   2   3   3   3   3   2   9   1   1
            1   1   9   2   3   4   7   4   3   2   1   1   1
        1   1   1   2   3   5   6   6   5   3   2   1   1   1
        1   1   1   2   3   4   6  10   6   4   3   2   1   1   1
            1   1   1   2   3   5   6   6   5   3   2   1   1   1
            1   1   1   2   3   4   7   4   3   2   9   1   1
                1   1   9   2   3   3   3   3   2   1   1   1
                1   1   1   2   2   2   2   2   1   1   1
                    1   1   1   1   1   7   1   1   1   1
                    1   1   1   1   1   1   1   1   1
                        1   1   1   1   1   1   1   1
```

Fig 5. Left side: IPR-R1 core representation using Cartesian geometry; Right side: Axial planar region 11 in the PARCS model

7. Results

In this work it was used the three channel thermal hydraulic nodalization to represent the reactor for the RELAP5. Stationary and transient situations were simulated, considering thermal hydraulic and neutronic calculations separately and TH-NK coupling.

7.1 PARCS Results

PARCS code was applied to simulate the IPR-R1 TRIGA for steady state calculation. The obtained value for k_{eff} was 1.021882, without control rods. Figure 6 shows the planar and axial assembly average relative power distribution calculated by PARCS.

```
Assembly Power Distribution

    #.####   box power

        1       2       3       4       5       6       7       8       9      10      11      12
 3                                                0.9216
 4                                        0.9811  0.9985  0.9914  0.9853  0.9737
 5                                0.9863  1.0952  1.1006  1.0956  1.0950  1.0022  0.9369
 6                        0.9399  1.0092  1.1041  1.0157  0.0000  1.0067  1.0980  0.9923
 7                        0.9888  1.0997  1.3256  1.3632  1.3521  1.3196  1.0981  0.9953
 8                        0.9784  1.0959  1.0133  1.3550  0.0000  1.3522  1.0086  1.0896  0.9720
 9                                0.9924  1.0921  1.3088  1.3373  1.3451  1.3066  1.0837  0.9748
10                                0.9813  1.0818  0.9883  0.0000  0.9903  1.0769  0.9853  0.9195
11                                0.9193  0.9786  1.0634  1.0577  1.0581  1.0551  0.9540
12                                        0.9437  0.9480  0.9450  0.9426  0.9335
13                                                                0.0000

   Maximum Pos.    Maximum Value
    (  7,  7 )    1.3632
```

Fig 6. Planar average relative power distribution calculated by PARCS

7.2 RELAP5 and PARCS/RELAP5 Coupled Results

The RELAP5 results are being presented with the RELAP5/PARCS coupled calculation for comparison.

7.2.1 Steady State

7.2.1.1 Neutron Kinetic Results

The coupled calculation was performed at 250 kW of power and presented expected behavior for the parameters as coolant temperature, pressure and mass flow rate for steady state simulation. The effective multiplication factor calculated was k_{eff} = 1.026693, slightly higher than the PARCS alone calculation. Such values were obtained considering control rods withdrawn and are in relative according with MCNP calculation of 1.02236 [21]. Figure 7 shows the fast and thermal neutron flux distribution obtained by PARCS out file in the center of the core (axial level 11).

Planar Flux at Plane 11

	1	2	3	4	5	6	7	8	9	10	11	12
3							8.712E+12 7.831E+12					
4						8.840E+12 7.871E+12	8.826E+12 8.018E+12	8.802E+12 7.958E+12	8.812E+12 7.905E+12	8.799E+12 7.807E+12		
5					8.880E+12 7.916E+12	8.894E+12 8.062E+12	8.826E+12 8.104E+12	8.719E+12 8.066E+12	8.804E+12 8.059E+12	8.834E+12 8.050E+12	8.760E+12 7.972E+12	
6				8.817E+12 7.999E+12	8.920E+12 8.111E+12	8.911E+12 8.131E+12	8.727E+12 8.156E+12	8.276E+12 8.094E+12	8.719E+12 8.077E+12	8.845E+12 8.083E+12	8.833E+12 7.969E+12	
7				8.874E+12 7.937E+12	8.947E+12 8.098E+12	8.979E+12 8.048E+12	8.727E+12 8.298E+12	8.512E+12 8.227E+12	8.801E+12 8.006E+12	8.864E+12 8.083E+12	8.858E+12 7.994E+12	
8				8.850E+12 7.849E+12	8.902E+12 8.069E+12	8.863E+12 8.135E+12	8.637E+12 8.246E+12	8.152E+12 8.157E+12	8.613E+12 8.228E+12	8.821E+12 8.095E+12	8.846E+12 8.021E+12	8.780E+12 7.797E+12
9					8.831E+12 7.969E+12	8.813E+12 8.037E+12	8.723E+12 7.937E+12	8.409E+12 8.132E+12	8.599E+12 8.182E+12	8.838E+12 7.926E+12	8.806E+12 7.975E+12	8.736E+12 7.822E+12
10					8.726E+12 7.876E+12	8.705E+12 7.959E+12	8.542E+12 7.921E+12	8.069E+12 7.902E+12	8.483E+12 7.939E+12	8.662E+12 7.919E+12	8.688E+12 7.910E+12	8.607E+12 7.818E+12
11					8.580E+12 7.816E+12	8.606E+12 7.851E+12	8.521E+12 7.813E+12	8.373E+12 7.768E+12	8.431E+12 7.769E+12	8.520E+12 7.748E+12	8.549E+12 7.643E+12	
12						8.491E+12 7.555E+12	8.427E+12 7.588E+12	8.307E+12 7.561E+12	8.206E+12 7.540E+12	8.310E+12 7.465E+12		
13									7.611E+12 7.180E+12			

Maximum Pos.	Maximum Value
(6, 7)	8.979E+12
(7, 7)	8.298E+12

Fig 7. Radial thermal and fast flux distribution in the center of the core (level 11) predicted by RELAP5-PARCS calculation

The calculated thermal flux by coupling methodology presented a value next to the available experimental and calculated data at 250 kW, as it is presented in Table I.

	Thermal neutron flux at 250 kW (x 10^{12} neutrons.cm^{-2}s^{-1})
PARCS/RELAP5	8.16
Experimental [18]	(9.0 ± 0.5)
Experimental [12]	(8.8 ± 0.5)
MCNP [2]	13.0
MCNP [21]	9.73

Tab 1: Calculated and experimental thermal fluxes in the central thimble at 250 kW

7.2.1.2 TH-NK Results

Figure 8 presents results of RELAP5 and RELAP5-PARCS calculations. The results are in good agreement being the value of outlet coolant temperature calculated by RELAP5 alone a

few overestimated in relation to RELAP5/PARCS calculation. Fig. 9 is the result of fuel, cladding and coolant calculation predicted by RELAP5-PARCS coupled calculation.

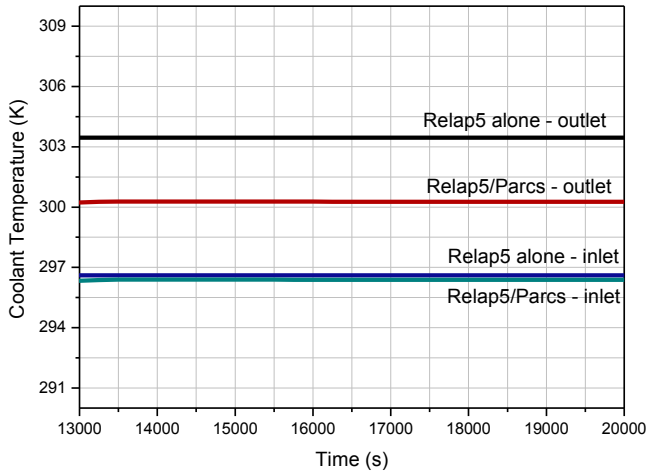

Fig 8. Comparison of coolant temperature at inlet and outlet of 201 TH channel, calculated with RELAP5 alone calculation and RELAP5-PARCS coupled in steady state.

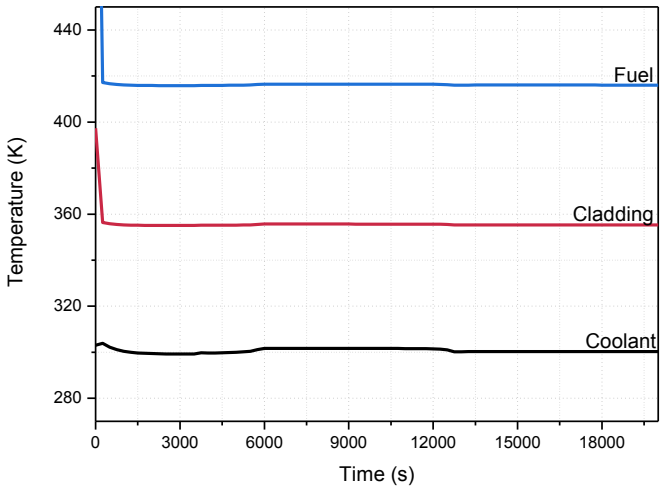

Fig 9. Fuel, cladding and coolant temperature – B1 rod and 201 TH channel, predicted by RELAP5-PARCS calculation

7.2.2 Transient Calculations

In this work three coupled transient simulations of loss of flow accident (LOFA) were studied. This type of accident is considered one of the more severe types for research reactors [15, 19].

The first considered event has been simulated closing the valve in the forced circulation part. It was initiated at 3000 s of calculation. After the beginning of the transient, the core temperature increases as consequence of no heat removal from the pool since the primary was off. Figure 10 shows the time temperature evolution for the channel 201 outlet, calculated by RELAP5 and RELAP5-PARCS coupled, both at 100 kW of power operation. Both curves presented approximately the same behavior in spite of the increasing of temperature in the coupled calculation was a few overestimated in comparison with the

RELAP5 alone. After the beginning of the transient, the coolant temperature increases with rates of 5.30 °C/h for coupled calculation and 4.70 °C/h for RELAP5 alone calculation. These results are both in good agreement with experimental available data (4.8 ± 0.2) ◦C/h [20].

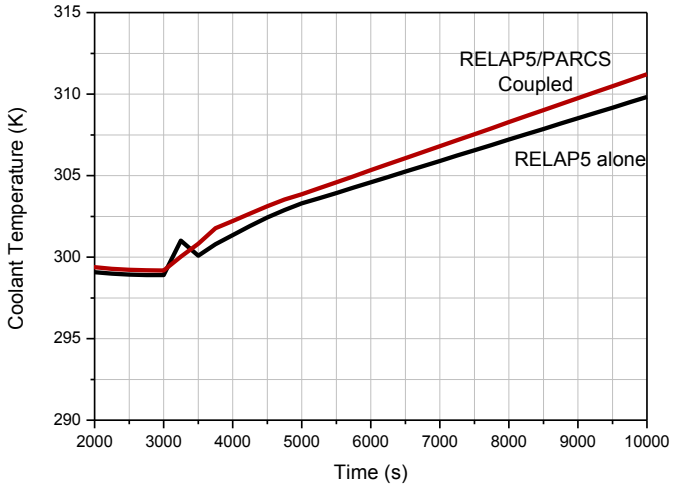

Fig 10. Fuel, cladding and coolant temperature – B1 rod and 201 TH channel

The second LOFA event considered was performed causing a inlet blockage of one of the thre TH core channels, by closing the valve number 401 indicated in Figure 11. The simulations were performed with both RELAP5 and RELAP5-PARCS coupled, at 250 kW of power operation.

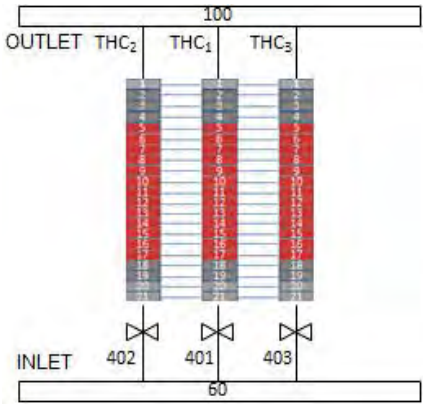

Fig 11. Core nodalization

Fig. 12 shows the behavior of the mass flow rate considering both calculations for channels 201 and 202 (THC_1 and THC_2, respectively, in the Figure 11). As it can be observed, both calculations presented the same behavior. The channels coolant outlet temperatures are illustred in Figure 13. RELAP5 alone and RELAP5-PARCS calculations presented the same tendency in spite of the coupled simulation takes more time to reach a new operation condition due the TH-NK calculation with feedback in the cross sections.

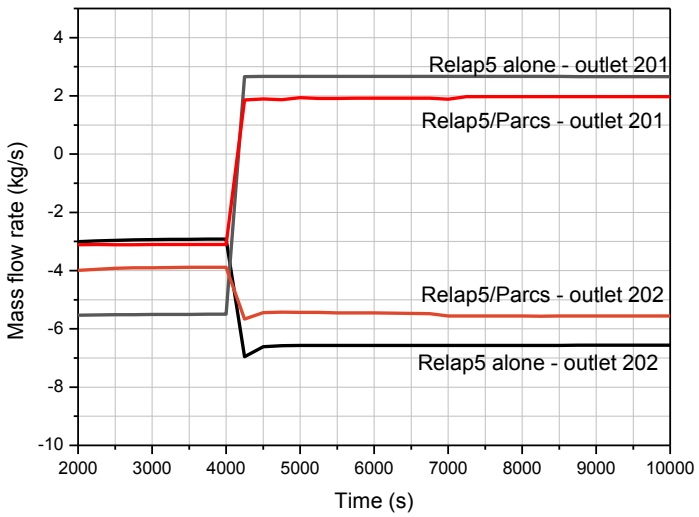

Fig 12. Outlet mass flow rate for channels 201 and 202 – RELAP5 alone and RELAP5-PARCS calculation

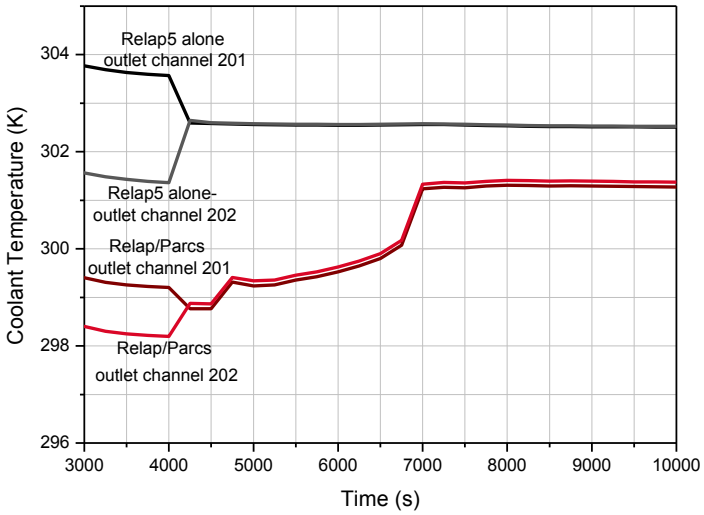

Fig 13. Outlet coolant temperatures for channels 201 and 202 – RELAP5 alone and RELAP5-PARCS calculation

In the third simulation another LOFA event considered was performed causing a blockage of the inlet of all TH channels, by closing the valves number 401, 402 and 403 (Figure 11). The simulations were also performed with both RELAP5 and RELAP5-PARCS coupled, at 250 kW of reactor power operation. Figure 14 shows the behavior of the coolant temperature at outlet of the channel 201, for RELAP5 and RELAP5-PARCS, at the right side and left side of the figure, respectively. Both calculations presented the same behavior. After the trip of the valves, the coolant temperature increases reaching the saturation temperature. Despite the increase of the coolant temperature more slow in the case of the coupled calculation shown at the right side of the Figure14, the insertion of negative reactivity, through of feedback in the macroscopic cross sections due the coolant temperature increase, was not enough to reproduce the behavior expected for type TRIGA reactors.

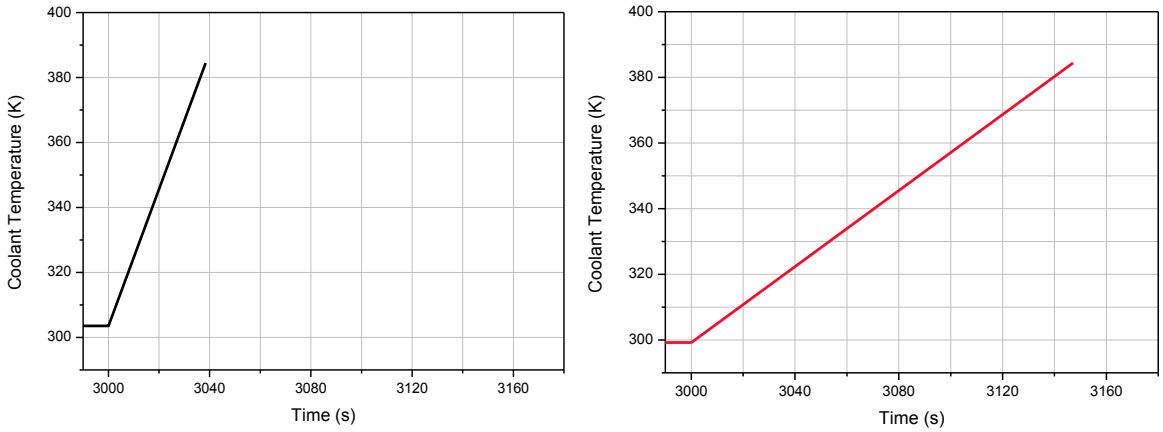

Fig 14 Coolant temperature at outlet of the channel 201, after the total core blockage for RELAP5 (left side) and RELAP5-PARCS (righ side) calculation

Acknowledgments

The authors are grateful to CAPES, CDTN/CNEN, FAPEMIG and CNPq for the support. Thanks also to Idaho National Laboratory for the permission to use the RELAP5-3D computer software.

References

[1] Costa, A. L. “BWR Instability Analysis by Coupled 3D Neutron-Kinetic and Thermal-Hydraulic Codes”, Doctor Thesis, Dipartimento di Ingegneria Meccanica, Nucleare e della Produzione, University of Pisa, Italy, 2007.

[2] Dalle, H. M. “Simulação do Reator TRIGA IPR-R1 Utilizando Métodos de Transporte por Monte Carlo”, Doctor Thesis, Faculdade de Engenharia Química da Universidade Estadual de Campinas, Brazil, 2005.

[3] Reis, P. A. L. “Estudos Neutrônicos e Termo-hidráulicos para o Desenvolvimento de uma Metodologia de Acoplamento entre Códigos Aplicada ao Reator de Pesquisa TRIGA IPR-R1”, Doctor Thesis, Universidade Federal de Minas Gerais, Brazil, 2013.

[4] General Atomics Company, http\\triga.ga.com/TRIGA ® Nuclear Reactors, 2015.

[5] US NRC, “RELAP5/MOD3.3 Code Manuals”, Idaho National Engineering Laboratory, NUREG/CR-5535, 2001.

[6] User Manual for the PARCS Neutronics Core Simulator - PARCS v2.7 U.S. NRC Core Neutronics Simulator User Manual, August, 2006.

[7] Veloso, M. A. F. “Análise Termofluidodinâmica de Reatores Nucleares de Pesquisa Refrigerados a Água em Regime de Convecção Natural”, Faculdade de Engenharia Química da Universidade Estadual de Campinas, Brazil, 2004.

[8] Reis, P. A. L. et al., “Assessment of a RELAP5 model for the IPR-R1 TRIGA research reactor”, Annals of Nuclear Energy, **37,** 1341-1350, 2010.

[9] Reis, P. A. L. “Avaliação Termo-hidráulica do Reator TRIGA IPR-R1 Utilizando o Código RELAP5”, Master Thesis, Universidade Federal de Minas Gerais, Brazil, 2009.

[10] Reis, P. A. L. et al., “Simulation of a TRIGA Reactor Core Blockage Using RELAP5 Code”, Science and Technology of Nuclear Installations, **v. 2015**, p. 1-10, 2015.

[11] Reis, P. A. L. et al., “Simulation of a Channel Blockage Transient in the IPR-R1 Research Reactor Using the RELAP5 Code”. In: European Research Reactor Conference, Rome. Transactions of RRFM 2011, Brussels: European Nuclear Society - ENS, 2011, 529-535, 2011.

[12] Souza, R. M. G. P. “Thermal Neutron Flux Measurements in the Irradiation Facilities of the IPR-R1 TRIGA Reactor”. In 3rd World TRIGA Users Conference, Aug 22 to 25, 2006, Belo Horizonte, Brazil 2006.

[13] Kulikowska, T. “Reactor Lattice Codes”, Institute of Atomic Energy, Swierk, Poland, Workshop on Nuclear Data and Nuclear Reactors: Physics, Design and Safety, Trieste, 13 March – 14 April, 2000.

[14] WIMSD-5B, 2007 - RSICC Computer Code Collection WIMSD-5B.12 – Deterministic Code System for Reactor-Lattice Calculations – Oak Ridge National Laboratory, 2007.

[15] Costa, A. L. et al., “Chapter 2: Safety Studies and General Simulations of Research Reactors Using Nuclear Codes” In: Nuclear Power - System Simulations and Operation. Ed. InTech, Rijeka, Croatia. ISBN: 978-953-307-506-8, Vol. 2, p. 21-42, 2011.

[16] Downar, T. et al., “PARCS v2.7 U.S. NRC Core Neutronics Simulator User Manual”, School of Nuclear Engineering Purdue University, 2006.

[17] Reis, P. A. L. et al., “Sensitivity analysis to a RELAP5 nodalization developed for a typical TRIGA research reactor”, Nuclear Engineering and Design, **242**, 300-306, 2012.

[18] Souza, R. M. G. P. SOUZA and Rezende, M. F. R., “Power Upgrading Tests of the TRIGA IPR-R1 Nuclear Reactor to 250 KW”, Proceedings of the 2nd World TRIGA Users Conference, Atominstitute,15-18 Sep 2004 Vienna, Austria, 2004.

[19] Suresh, Ch. S.Y et al., “Heat transfer from a totally blocked fuel subassembly of a liquid metal fast breeder reactor: Part I, Experimental investigation and Part II Numerical simulation”, Nuclear Engineering and Design, **235**, 885-912, 2005.

[20] Mesquita, A. Z. et al., “Thermal power calibrations of the IPR-R1 TRIGA nuclear reactor”, In: Proceedings of the 20th International Congress of Mechanical Engineering, COBEM 2009, November 15–20, Gramado RS, Brazil, 2009.

[21] Silva, C. A. M. et al., “Sensitivity Analysis of TRIGA IPR-R1 Reactor Models Using the MCNP Code”, International Journal of Nuclear Energy – **Vol. 2014**, Article ID 793934, 9 pages, 2014.

THERMAL-HYDRAULIC SIMULATION OF SINGLE PIN AND ASSEMBLY SECTOR GEOMETRIES FOR THE IVG.1M RESEARCH REACTOR

A.R. KRAUS, P.L. GARNER, N.A. HANAN
Nuclear Engineering Division, Argonne National Laboratory
9700 S. Cass Ave., Lemont, IL – USA

ABSTRACT

Thermal-hydraulic simulations have been performed for the highly-enriched uranium (HEU) design of the IVG.1M reactor at the Institute of Atomic Energy branch of the National Nuclear Center (NNC) in the Republic of Kazakhstan using computational fluid dynamics (CFD). This analysis is to aid in a study of the possible conversion of IVG.1M from HEU to low-enriched uranium (LEU). The reactor is water-cooled at elevated pressure and features "lozenge"-shape fuel pins that are twisted along their central axis and are in direct contact with each other. Steady-state simulations were performed for periodic sectors of two types of fuel assembly (FA) as well as for single pins in those FA. Simulations were performed for the actual twisted-pin geometry as well as a straight-pin approximation. These geometries were simulated for the operating conditions which correspond to a pin unit cell Reynolds number of only about 7500. Various Reynolds-Averaged Navier-Stokes (RANS) turbulence models yielded different temperature results, therefore some validation runs with a higher-fidelity Large Eddy Simulation (LES) code were performed given the lack of experimental data. These singled out the Realizable Two-Layer k-ε as the most accurate turbulence model for estimating cladding surface temperature. Single-pin results for the twisted-pin case, based on the average flow rate per pin and peak pin power, were conservative for peak clad surface temperature compared to the bundle results. The straight pin approach had many fewer mesh cells and gave more conservative peak temperatures compared to the twisted-pin case, but was more strongly influenced by boundary effects. The peak temperature pin was in a different location from the peak power pin in every case simulated. Future work will include simulations of the proposed LEU design.

1. Introduction

The geometries and flow conditions found in nuclear research reactors can present modeling and simulation challenges. The DOE/NNSA Reactor Conversion Program is tasked with investigating and applying analysis methods for research reactors. The overall goal is to convert reactors from HEU to LEU fuel to reduce proliferation concerns while striving to maintain the unique characteristics of each reactor, such as high neutron flux in a given area. Generally the HEU design must first be confidently modeled to ensure that the physical behavior of the reactor is well understood. This allows for establishment of appropriate analysis methods and generally also leads to a more sound LEU design.

The IVG.1M reactor at the NNC in Kazakhstan is one such reactor with exotic geometry. The core features annular assemblies containing twisted fuel pins in a roughly hexagonal lattice (Fig 1). There are two zones featuring different enrichments in each FA. The pins are in direct contact with one another and with the assembly can walls. There are cylindrical filler rods, made of E-110 Zr-Nb alloy, to maintain appropriate pin spacing at the assembly boundaries. Some

specifications for the fuel pins are provided in Tab 1. The fuel is a U-Zr alloy and the cladding is E-110 alloy [1]. Both fuel and clad are twisted together.

There are two different assembly types. One has 600 mm-length pins (termed the “600 mm” bundle), while the other has similar 600 mm pins but also 200 mm pins stacked above them (the “800 mm” bundle) which are separated from them by a metal grid and mesh screen. High-fidelity analysis was performed for the peak power assemblies for both FA types, based on one possible configuration used for the IVG.1M reactor. With the exception of the grid, there are no obstructions of the flow path for the entire fuel length of either FA.

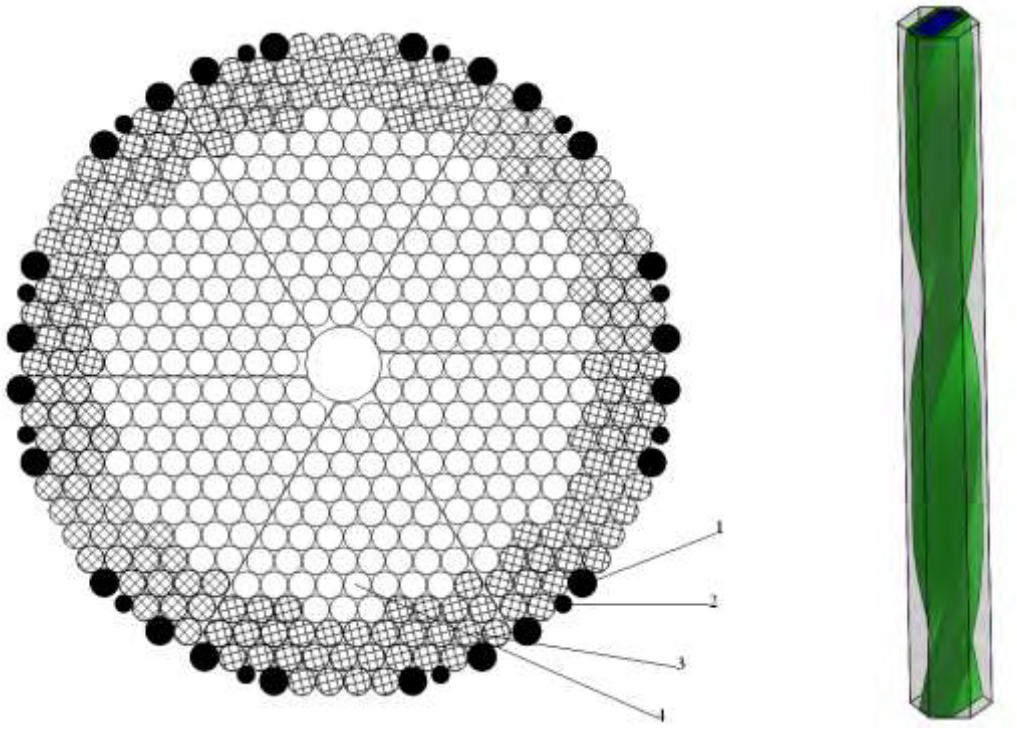

Fig 1. Fuel assembly layout (Left) featuring filler cylinders (1&2) and hexagonal fuel pin lattice with two enrichments (3&4). Note that the circular shape denoting the fuel elements is the projected area; the fuel elements are “lozenge” shape (Right). Here blue is fuel and green is cladding, with the remainder as coolant flow area.

Circumscribed circle diameter	2.8 mm
Blade width	1.5 mm
Helical pitch distance	30 mm
Cross-section of fuel core	1.0 mm x 2.3 mm
Length of fuel core	796 mm for 800 mm assembly; 598 mm for 600 mm assembly
Thickness of cladding	0.25 mm

Tab 1: Fuel pin dimensions.

The coolant for this reactor is water at a rated pressure of 0.8 MPa. The nominal flow rates for the 10 MW power level under investigation are 1.94 kg/s for the 600 mm FA and 2.1 kg/s for the 800 mm FA [2]. The inlet temperature for both cases was 328 K; this is the maximum allowed coolant inlet temperature. The power density, flow rate and pressure combination is such that boiling is not a likely concern during normal operation. For the 10 MW core power, the average

flow rate per pin is low enough that the pin-cell Reynolds number is only around 7500. Strong streamline curvature is anticipated due to the twisted pin geometry as well. These conditions can present challenges for standard RANS turbulence models. A further difficulty with modeling the reactor is that, to the authors' knowledge, there are no experimental data with which to compare simulation results. Thus multiple turbulence models should be tested and compared to provide a more confident final result. The pin orientations are not specified. Additionally, the pins are not strongly secured in the radial direction, and may shift or vibrate during operation. Given all of these uncertainties, it is important to reduce the physics modeling uncertainty to yield meaningful results for any future sensitivity studies.

2. Single-Pin Simulations

CFD was used to simulate the steady-state operating conditions for both FA configurations. The majority of simulations were performed using the commercial code STAR-CCM+ v8.04 from CD-Adapco [3]. The code is capable of solving many multi-physics problems and has undergone extensive testing and validation. STAR-CCM+ employs the finite-volume approach to solve the incompressible Navier-Stokes and energy equations. A suitable grid consisting of primarily polyhedral cells was generated within the code. A fine near-wall mesh is necessary due to the relatively high Prandtl number of water. The grid was based on multiple simulations; the final mesh density was that which showed negligible difference in peak temperature with refinement. The mesh count for a full-length 600 mm single twisted pin (fluid and solid regions) was 4.7 million cells, while the 1/6 600 mm sector consisted of 155 million cells.

2.1. 600 mm

Initial simulations in STAR-CCM+ focused on a full-length, 20-pitch twisted pin unit cell. The hexagonal sides of the cell were treated with periodic boundary conditions. An assumption of this approach is that all pins in the assembly have the same orientation. Since no information was available for the pin orientations, this was deemed a valid base geometry before testing the effect of perturbations by simulating a larger assembly section. The inlet was at the top and the outlet was at the bottom of the domain. A straight pin approximation was also investigated.

Data points from prior neutronics simulations were used to provide a power density shape for the pin. Fig 2 provides the peak pin power profiles for the 600 mm and 800 mm bundles. A polynomial fit to these data points allowed for incorporation of a power density profile with realistic axial variation. No radial variation of power density within a pin was assumed. The heat source was confined to the fuel region. Temperature-dependent fluid properties and constant solid properties were used.

A detailed turbulence modeling study of the single-pin was performed [4], of which only a cursory description is presented here. In STAR-CCM+, the RANS approach to turbulence modeling was used. Numerous formulations are available to model RANS turbulence, including the well-known k-ε model. The peak temperature spread for the cladding surface between a number of RANS models was roughly 6 K, or 15% of the total fluid temperature increase across the domain (40 K). This spread was deemed too large to arbitrarily select a turbulence model, particularly for assessing the impact of geometric perturbations. Given the lack of experimental data available, higher-fidelity calculations with an LES approach were performed using Nek5000 [5] to assist in model selection. Nek5000 is a massively-parallel, open-source CFD code developed at Argonne National Laboratory which employs the spectral element method.

Fig 3 displays streamlines for a single helical pitch. This clearly demonstrates the general twisting of the flow. The bulk flow runs parallel to the long edges of the pin, as expected. The streamlines also show that smaller secondary flow paths exist for which the flow separates from

the bulk in the area where the shorter pin edge is near the hexagon corner. This flow then rejoins the bulk further downstream. No large stagnation areas are present.

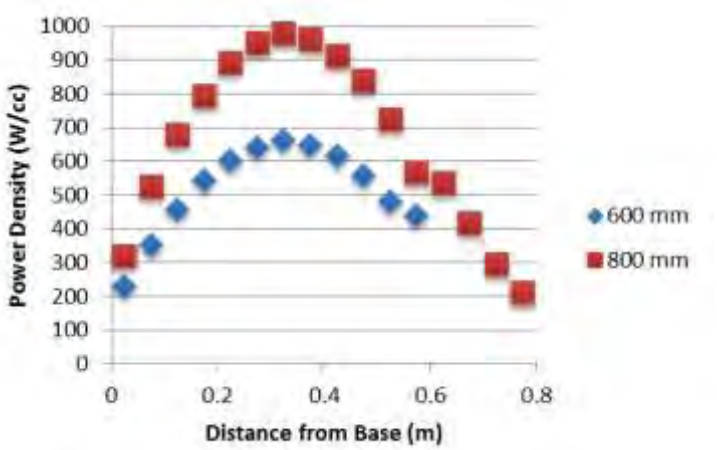

Fig 2. Radially-averaged axial power density profiles for the peak power pins in both the 600 mm and 800 mm bundles. The support grid is at 0.6 m.

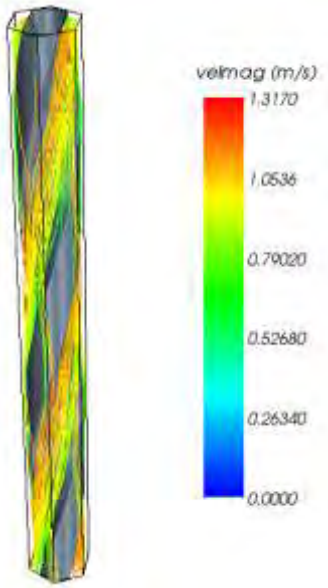

Fig 3. Velocity streamlines (non-dimensionalized by streamwise velocity) from the Realizable k-ε Two-layer model in STAR-CCM+ for single helical pitch. Note the presence of secondary flows near the cell corners.

Temperature profiles for some of the models near the peak location are compared in Fig 4. The temperature distribution in the fluid follows closely with the velocity distribution; the higher velocity areas generally have lower temperatures and vice-versa. The peak temperature from the LES run was roughly constant over time, indicating that any flow fluctuations had little effect on temperature. These results demonstrated that the Realizable k-ε Two-Layer model was most accurate at predicting surface temperature for these flow conditions. Peak cladding surface temperature for this model was 371.4 K. Results confirmed that the flow does indeed exhibit elevated turbulence, and heat transfer is enhanced over pure laminar simulation. For these reasons, the Realizable k-ε Two-Layer model was deemed most appropriate for these flow conditions and was used for all bundle calculations discussed below.

It is clear, as expected, that the twisting produces additional turbulence and enhances the heat transfer to the coolant. Thus the straight pin correspondingly has higher temperatures. Since its cross-sectional area is the same as the twisted pin and flow is similar for most of the pin length, this approximation may produce local hotspots that would not exist for the twisted pins. Hence the straight pin approximation should certainly be conservative with regard to the maximum temperature magnitude compared to the twisted pins.

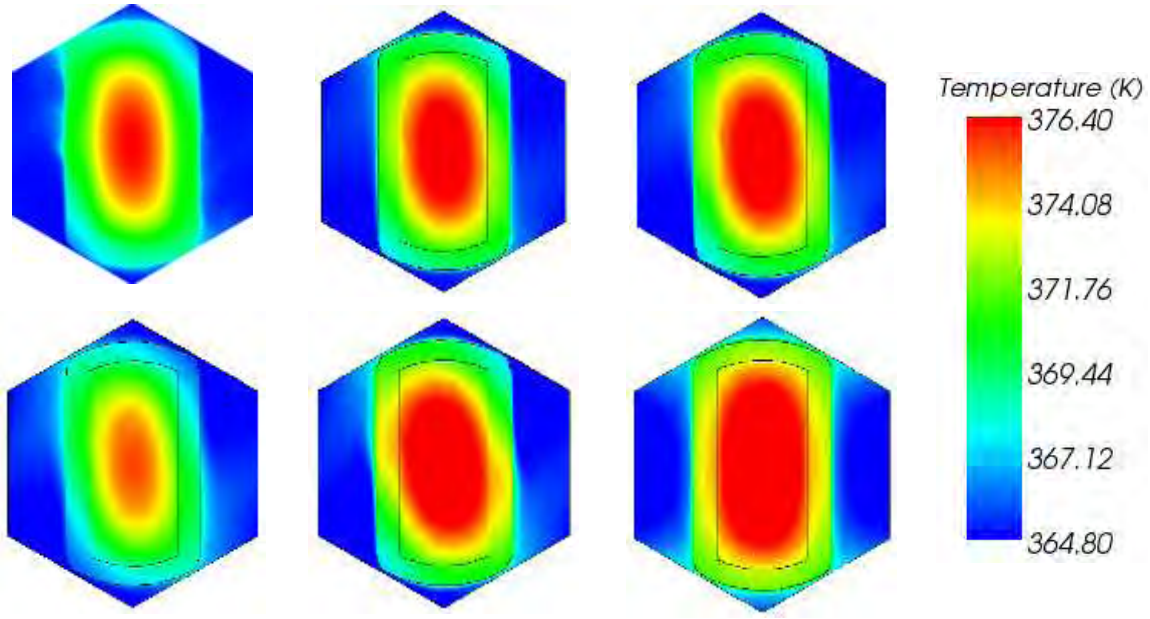

Fig 4. Temperature distribution at z = 0.075 m for the single twisted pin. Left to right, Top: LES, Realizable k-ε 2-layer, k-Ω SST. Bottom: V^2F All-y+, V^2F Low-y+, Straight-Pin Approximation with k-ε 2-layer. Min/Max are scaled to LES results.

There are some conservative assumptions for the single-pin models, however, notably that using a periodic boundary condition with the peak pin power implies that the surrounding pins also have the same power. This could cause an overestimate of temperature. The peak power pin (for both 600 mm and 800 mm cases) also lies at the outer edge of the assembly, where there is more flow area due to the spacing of the filler rods in that region. Thus extra cooling is available for the peak power pin compared to the interior unit cell approximation. Given the lack of experimental data, the relative influence of these factors can only be properly assessed by performing assembly sector simulations that incorporate the actual pin layout.

2.2. 800 mm (HEU Design)

The 800 mm pin assemblies feature the highest pin power density, and so are of greater concern for safety. For the 800 mm bundle, the grid warrants special treatment. To keep mesh count reasonable, the grid was modeled through a porous media approach. The goal was to provide an accurate estimate of the pressure drop while disrupting the flow that had developed prior to the grid, without detailed geometric modeling. To obtain appropriate loss coefficients for the porous media, a ¼-symmetric CFD model of the explicit grid geometry was built to test its hydrodynamic behavior. A trendline was drawn through the simulated pressure loss data points at multiple flow rates to obtain the loss coefficients for the porous media model. These loss coefficients were implemented only for the streamwise direction, and cross-flow directions had zero resistance in order to smooth out the flow.

Only the twisted pin case was run for the 800 mm simulations. The peak surface temperature for this case was 399.1 K. This is far below the saturation temperature of 443.6 K at the rated

pressure of 0.8 MPa. This demonstrates that there is a significant margin to boiling, even using the maximum allowed inlet coolant temperature and the normal coolant flow rate. The peak fuel temperature of 410.7 K is also hundreds of degrees below the melting point of the U-Zr alloy, supporting the assumption that the fuel temperature is of little safety concern during normal operation. It is important to note that these results are only based on one potential core configuration and one possible flow rate [2]. Thus these results provide relevant data for assessing the general behavior and flow patterns of this type of reactor core and power level, but may not necessarily be representative of the true typical operating conditions.

3. Assembly Sector Simulations

3.1. 600 mm

Methods for the FA sector simulations were largely similar to those for the single pin. The sector simulations were only run with STAR-CCM+ using the Realizable k-ε Two-Layer model, which was found to be the most appropriate from the single pin simulations. The sector was based on the 1/6 periodicity of the FA. The sector was roughly centered around the peak power pin in the bundle. In order to keep the sector boundaries periodic, the pins on each side must be aligned. This creates a different-shaped flow channel than for the interior pins (Fig 5), and could lead to noticeable boundary effects.

The 1/6-sector twisted pin simulations showed that the peak cladding surface temperature for the 600 mm FA of 370.4 K is less than that from the single pin analysis, suggesting that the single-pin analysis is conservative for the power distribution under consideration. This is largely due to the increased flow area around the peak power pin region. Fig 5 demonstrates that the velocity, and hence cooling, is increased in this region due to the non-uniformity of the spacing at the assembly outer edge. There is also little interaction between pin flow-fields, which is one reason that the differing orientation of the pins on the periodic boundaries with respect to the interior pins does not create any large temperature discrepancies. The peak temperature occurs near the middle of the sector (Fig 6), near the area where the pin enrichment changes. Note that for all temperature plots, the blue star corresponds to the peak *power* pin, while the red star corresponds to the peak *temperature* pin.

To test the effect of pin orientation, a simulation was performed with a randomized orientation for each of the pins in the domain. For the periodic boundary pins, one pin was randomized and the other was rotated 60° from that orientation in order to ensure that the periodic faces matched. Fig 6 shows that the pin orientation does not have significant influence on the peak temperature location or magnitude. The peak pin is in the same location and the magnitude is only different by about 0.1 K from the uniform orientation run, despite having a completely different cross-sectional flow area at a given plane. Thus the uniform orientation, whether true or simply an approximation, is a viable option for simulation and the pin orientation does not have a large effect on the peak temperature behavior.

Initial 1/6-sector simulations for the straight pin approximation were performed with pins in the same layout as those for the twisted case, but it became apparent that the boundaries and pin orientation played a more substantial role in determining the peak temperature than for the twisted pins. In Fig 7, the peak cladding temperature occurs at a periodic-boundary pin due to the pin orientation there. The short ends of the two boundary pins are in very close proximity for their entire length, and cooling is greatly reduced in that area. Thus despite having a significantly lower power density and being relatively far from the peak power pin, one of these pins has the peak temperature. Another simulation was run with a different orientation for the periodic-boundary pins; the peak temperature magnitude is similar but the pin location has changed, and was still near a periodic boundary.

To eliminate the effect of the periodic boundaries, full bundle simulations were then performed. This was possible only for the straight pins because the uniform cross-section allows for simpler and coarser mesh extrusion in the axial direction, reducing the number of mesh points to a practical level. While the periodic boundary influence was removed, it was found that the flow area difference due to the filler rod placement and pin orientation still had significant influence. Fig 8 displays how the smaller flow area for one of these pins contributed to it being the peak temperature pin. These consistent boundary issues suggest that the straight pin approximation should be used with care, particularly in regards to pin orientation.

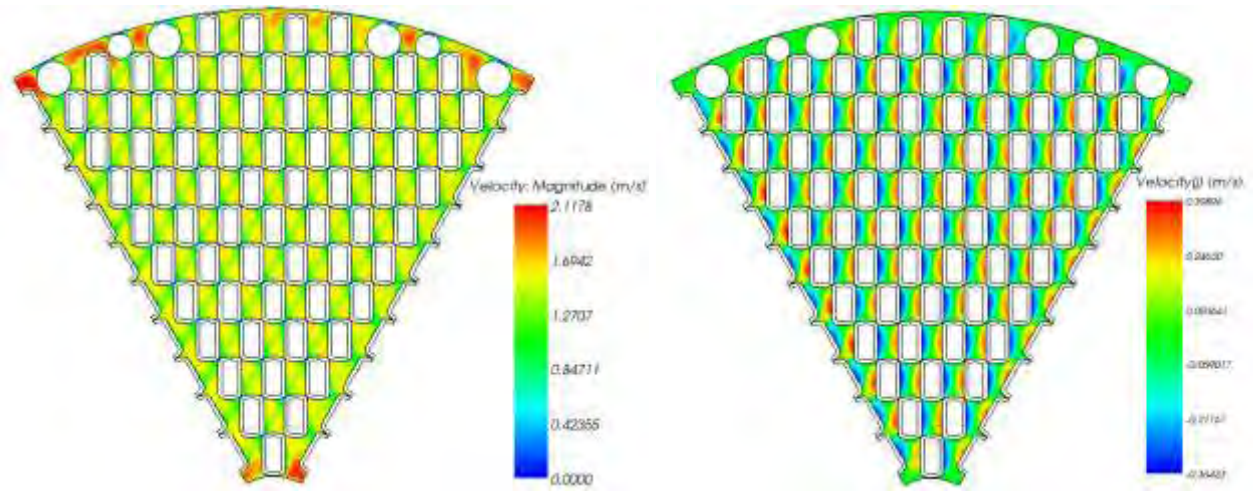

Fig 5. Velocity magnitude (Left) and J-component of velocity (Right, positive toward top of page) at the midplane for the 1/6-bundle twisted pin case.

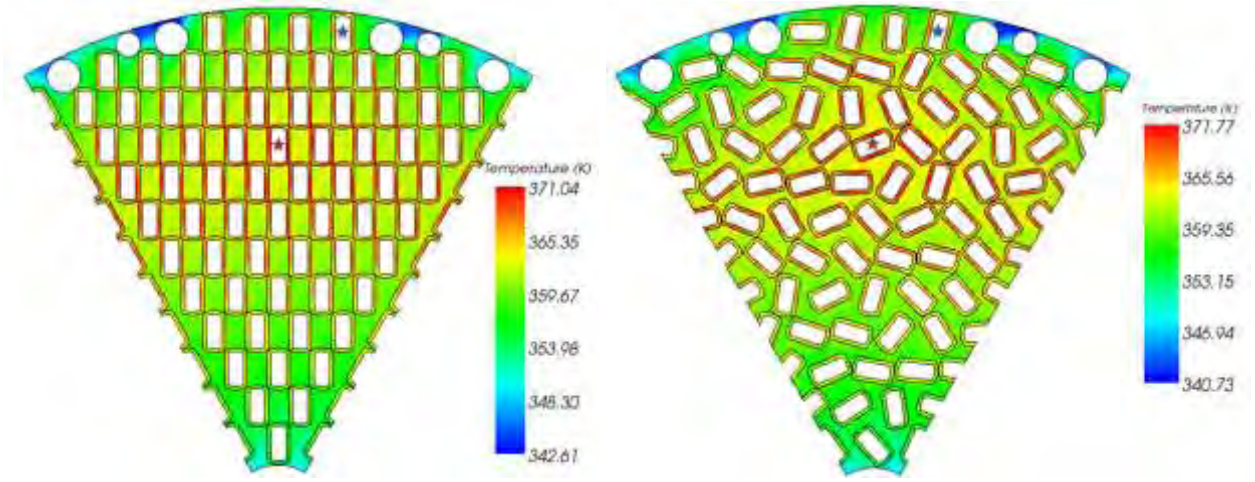

Fig 6. Temperature at z = 0.075 m for the 1/6-bundle twisted pin case for uniform (Left) and randomized (Right) pin orientations.

Tab 2 provides a summary of the peak temperatures for each of the twisted and straight pin 600 mm results. Again, the straight pin runs are more conservative than the twisted pin runs, as anticipated. Additionally, the single twisted pin is more conservative than the twisted pin bundle, which could potentially cut down simulation and meshing time if this is found to be true for further test cases. It should be stressed, however, that the single straight pin is not necessarily conservative with regard to the straight pin bundle. The boundary effects and orientation are much more important than for the twisted pin, meaning that the periodic unit cell for the straight pin is not an arbitrarily good representation of the peak temperature regions in the bundle.

It should be noted that although the straight pin approximation is not reliable for predicting the peak temperature location, this may not be of strong concern. The approximation is consistently conservative. The twisted pin results also demonstrate that a number of pins have maximum temperatures close to that of the peak pin, so the exact maximum location may not be crucial. Hence the straight pin approximation could still prove useful for some scenarios.

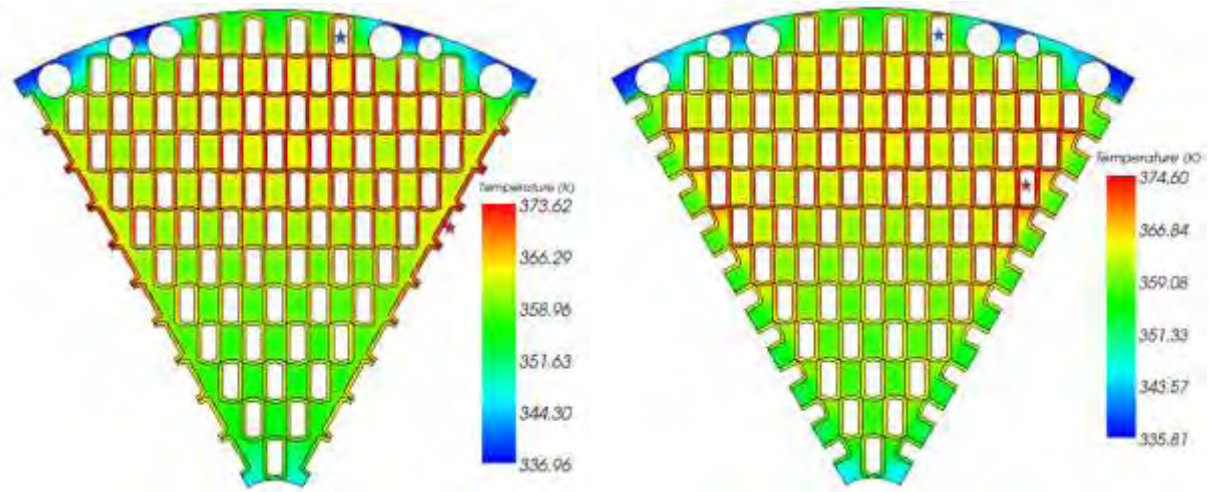

Fig 7. Temperature distribution for two different orientations of the 1/6-bundle straight pin case.

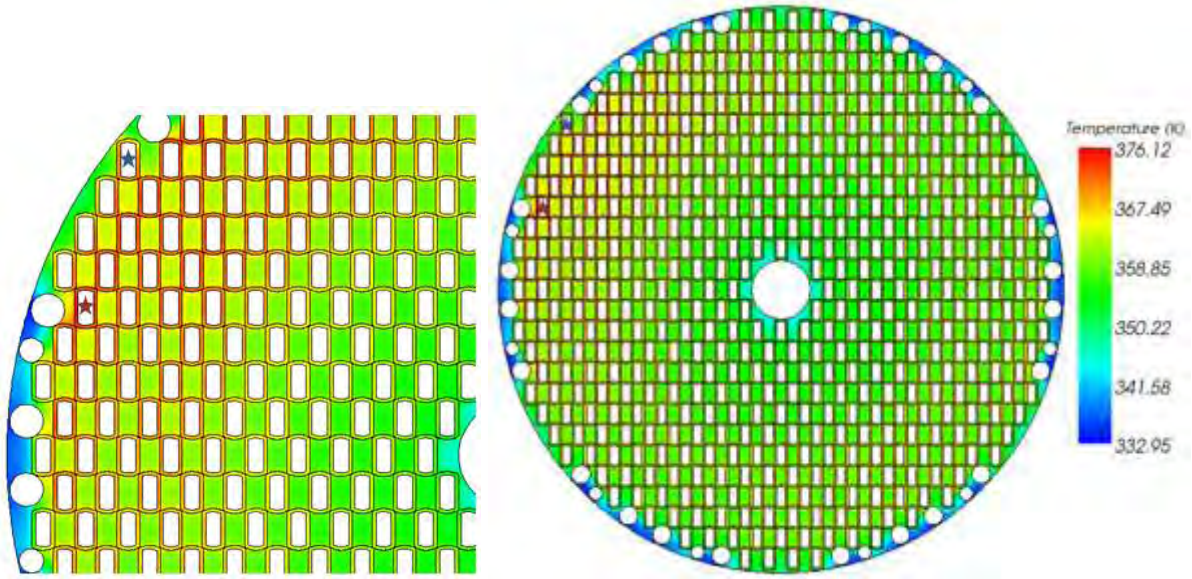

Fig 8. Temperature distribution for the full-bundle straight pin case (zoomed view on left).

	Single Pin Twisted	1/6-bundle Twisted Uniform	1/6-bundle Twisted Random	Single Pin Straight	1/6-bundle Straight Orientation 1	1/6-bundle Straight Orientation 2	Full Bundle Straight
Maximum clad surface temperature (K)	371.4	370.4	370.5	372.6	373.2	373.3	374.7

Tab 2: Summary of clad surface temperatures for each of the 600 mm geometries tested.

3.2 800 mm

The peak power pin for this FA was in a different position from that of the 600 mm FA, so the fluid domain was rotated 30 degrees azimuthally in order to keep this pin far from boundaries of the calculational domain. The base of each 200 mm pin (i.e. the part touching the grid) was assumed to be in alignment with the top of its corresponding 600 mm pin. The two pin types both have the same helical pitch.

The 800 mm pin bundle results corroborated many of the findings from the 600 mm runs. The peak temperature of 391.6 K was further from the single-pin peak than was found in the 600 mm case. This is due to the peak power pin in the 800 mm bundle being in a different location than that of the 600 mm bundle. This location has an even greater cooling area relative to the unit cell, and fewer fuel pins surrounding it. These extra factors are not accounted for in the single pin model. The peak temperature location (Fig 9) is actually very close to that in the 600 mm case. This is again roughly the area where enrichments change, and is an interior pin. This suggests that the single-pin model may again be a useful tool in reducing the simulation/meshing time while still obtaining relevant and slightly conservative results.

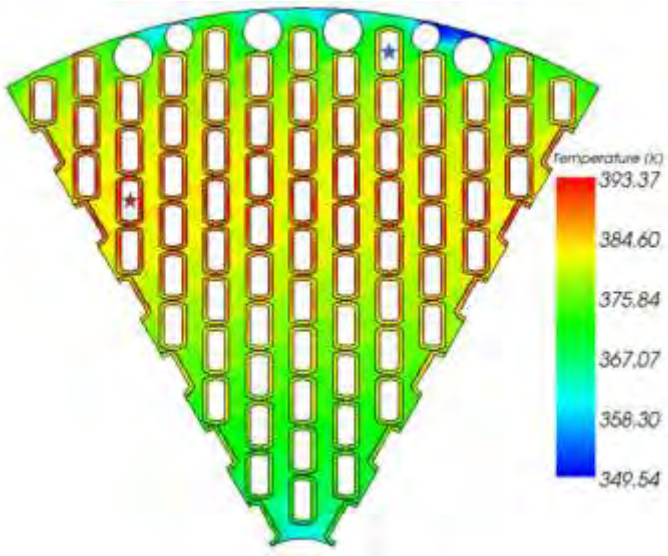

Fig 9. Temperature distribution at z = 0.075 m for the 800 mm 1/6-bundle twisted pin case.

4. CONCLUSIONS

In summary, the steady-state properties of the peak power assemblies have been characterized for one possible configuration of the IVG.1M reactor at the 10 MW power level. The peak temperatures for the cladding surface have sufficient margin to the boiling point at the rated pressure, and the peak fuel temperature is far below melting. Parametric studies on various simplifications, such as straight-pin approximations and pin orientations, do not show strong variability in peak temperature predictions.

The results have shown, as hoped, that the single-pin approximation is generally valid and conservative when based on the average flow rate and peak power. The twisted pin has the advantage of incorporating more realistic flow physics. Thus this approximation can likely be used to evaluate future cases much more quickly. Further work will include analysis of potential LEU core designs.

5. ACKNOWLEDGMENTS

The authors would like to thank Elia Merzari and Paul Fischer for performing the Nek5000 simulations and for their insights regarding the problem physics, and the Institute of Atomic Energy Branch of the National Nuclear Center of the Republic of Kazakhstan for the information provided. This work is sponsored by the U.S. Department of Energy, National Nuclear Safety Administration (NNSA), Office of Material Management and Minimization (NA-23) Reactor Conversion Program.

6. REFERENCES

1. A. D. Vurim, A. N. Kolbaenkov, V. S. Gnyrya, "Description of Reactor IVG.1M", Deliverable 2.1 under ANL-IAE Work Order 0J-30461-0002, Institute of Atomic Energy, Kurchatov, Kazakhstan (November 2010).

2. A.A. Kolodeshnikov, A.D. Vurim, V.A. Zuev, "HEU Core Characterization of IVG.1M Reactor", Deliverable 2.2 under ANL-IAE Work Order 0J-30461-0002, Institute of Atomic Energy, Kurchatov, Kazakhstan (December 2011).

3. "User Guide, STAR-CCM+ Version 8.04," CD-Adapco, Melville, NY, 2013.

4. Adam R. Kraus, Elia Merzari and Paul F. Fischer, "Turbulent Flow-Field Comparisons of RANS and LES for a Twisted Pin Lattice Geometry at Low Reynolds Number", *Proceedings of the ASME 2014 4th Joint US-European Fluids Engineering Division Summer Meeting and 11th International Conference on Nanochannels, Microchannels, and Minichannels* (FEDSM2014, Chicago, USA, August 3-7, 2014).

5. Paul F. Fischer, James W. Lottes and Stefan G. Kerkemeier, "Nek5000 Web Page", http://nek5000.mcs.anl.gov.

IAEA CRP ON "BENCHMARKS OF COMPUTATIONAL TOOLS AGAINST EXPERIMENTAL DATA ON FUEL BURNUP AND MATERIAL ACTIVATION FOR UTILIZATION, OPERATION AND SAFETY ANALYSIS OF RESEARCH REACTORS": UPDATE AFTER THE PROJECT KICK-OFF MEETING

W.B.KENNEDY[1], F.M. MARSHALL[2], D. RIDIKAS[3]
[1]Department of Nuclear Safety and Security
[2]Department of Nuclear Energy
[3]Department of Nuclear Sciences and Applications
International Atomic Energy Agency, Vienna International Centre, PO Box 100
1400 Vienna, Austria

ABSTRACT

The International Atomic Energy Agency (IAEA) initiated a new Coordinated Research Project (CRP) to collect available experimental data and benchmark the computational methods and tools used for fuel burnup calculations and material/target activation in utilization, operation, and safety analysis of research reactors (RRs). In a series of IAEA CRPs related to benchmarking exercises for RRs, this new CRP is a follow up to recently closed CRP1496 "Innovative Methods in RR Analysis: Benchmark against Experimental Data on Neutronics and Thermalhydraulic Computational Methods and Tools for Operation and Safety Analysis of RRs", jointly conducted and equally funded by the Division of Nuclear Installation Safety (NSNI), the Division of Nuclear Fuel Cycle and Waste Technology (NEFW) and the Division of Nuclear Applications (NAPC). The project was highly recommended by the partners involved in old CRP1496 and strongly supported by the Technical Working Group on Research Reactors (TWGRR) during its meetings in 2012 and 2013.

The benchmarks will be grouped into three categories. The first category, **multi-cycle core depletion analysis**, will focus on fuel depletion for the entire core, and include experiments which cannot be accurately modelled without performing neutronic and burnup analysis for multiple cycles of reactor operation. The second category, **target or sample activation and fuelled experiments**, will focus on the irradiation of in-core and ex-core samples, as well as experiments involving fissile materials. As opposed to the first category, the focus will be on experiments that can be modelled without analysis of full-core depletion. The option remains for some level of neutronic analysis if neutron fluxes within the samples are not provided as part of the benchmark specifications. The third category, **structural material activation**, will extend the activation analysis benchmark to structural materials that are irradiated during the utilization/operation of the reactor.

1. Introduction

With the progress in computer technology and numerical methods, the capabilities of computer codes have been substantially enhanced. The enhancement of these methods and tools allows for improved simulation of the complex processes taking place during the routine operation and transient conditions of research reactors. Correct application of these methods and codes is essential to improve design, operation/utilization, and safety aspects of research reactors (RRs) and associated experiments. However, the validation of computational codes is not an easy task. In order to demonstrate the capabilities of these computational methods and codes, it is necessary to benchmark them against experimental data, before assessing the validity of their application to the design, operation, utilization aspects and safety analysis of RRs.

The IAEA initiated a new Coordinated Research Project (CRP) to collect available experimental data and benchmark the computational methods and tools used for fuel burnup calculations and material/target activation in utilization, operation, and safety analysis of research reactors (RRs). In a series of IAEA CRPs related to benchmarking exercises for RRs, this new CRP is a follow up to recently closed CRP1496 “Innovative Methods in RR Analysis: Benchmark against Experimental Data on Neutronics and Thermalhydraulic Computational Methods and Tools for Operation and Safety Analysis of RRs”, jointly conducted and equally funded by the Division of Nuclear Installation Safety (NSNI), the Division of Nuclear Fuel Cycle and Waste Technology (NEFW) and the Division of Nuclear Applications (NAPC). More information on already finished CRP1496 can be found in References [1, 2, 3]. The new project was highly recommended by the partners involved in old CRP1496 and strongly supported by the Technical Working Group on Research Reactors (TWGRR) during its meetings in 2012 and 2013.

Per the approved CRP, the future benchmarks will be grouped into three categories. The first category, **multi-cycle core depletion analysis**, will focus on fuel depletion for the entire core, and include experiments which cannot be accurately modelled without performing neutronic and burnup analysis for multiple cycles of reactor operation. The second category, **target or sample activation and fuelled experiments**, will focus on the irradiation of in-core and ex-core samples, as well as experiments involving fissile materials. As opposed to the first category, the focus will be on experiments that can be modelled without analysis of full-core depletion. The option remains for some level of neutronic analysis if neutron fluxes within the samples are not provided as part of the benchmark specifications. The third category, **structural material activation**, will extend the activation analysis benchmark to structural materials that are irradiated during the utilization/operation of the reactor.

The following has already been achieved regarding the preparations for the project:

- A survey to gauge the availability of burn-up/activation data and use of different codes as well as potential participation in the CRP has already been carried out in 2013, yielding promising results, as 22 responders from 18 Member States indicated their interest in participating in the activity. Experience in a wealth of codes, broad coverage in RR types and power levels, as well as on-going irradiation/measurement activities were confirmed.
- A consultancy meeting was held in March 2014 to draft the design of this new CRP. The objectives of the meeting were to review the analysis of the preliminary survey, propose the structure of the burnup and activation database, draft the design of the new CRP, plan related follow up actions and prepare a meeting report with conclusions and recommendations.
- The finalized design of the CRP has been submitted by the Secretariat for approval and endorsed by the Committee for Coordinated Research Activities in June 2014. Right after, the call for submissions of research project proposals was distributed to the interested partners.

This paper will describe in more detail the scope and the structure of the new CRP, give additional information on the CRP partners, available experimental data, and provide the latest updates as a result of the project kick off meeting, scheduled just before the RRFM Conference.

2. Tentative structure of the CRP

As a result of the analysis of the extended survey carried out prior to the CRP, the future proposed benchmarks are grouped into three categories, each with its own set of objectives.

The first category, **multi-cycle core depletion analysis**, will focus on fuel depletion for the entire core, and include experiments which cannot be accurately modelled without performing neutronic and burnup analysis for multiple cycles of reactor operation. The objectives of this category are:

- Support validation of depletion and neutronics codes;
- Analyse the capability of codes and users to accurately predict full core burnup over multiple cycles of reactor operation.

The second category, **target or sample activation and fuelled experiments**, will focus on the irradiation of in-core and ex-core samples, as well as experiments involving fissile materials. As opposed to the first category, the focus will be on experiments that can be modelled without analysis of full-core depletion. The option remains for some level of neutronic analysis if neutron fluxes within the samples are not provided as part of the benchmark specifications. The objectives are:

- Support validation of activation and depletion codes and capabilities in the context of target/sample irradiation and fuel burnup;
- Assess the applicability and utilisation of isotopic evolution chains, cross-section libraries and user capabilities;
- If detailed neutronic modelling information is supplied, the focus extends to capability of the codes and models to reproduce detailed within-sample flux distribution and spectrum.

The third category, **structural material activation**, will extend the activation analysis benchmark to structural materials that are irradiated during the utilization/operation of the reactor. The objectives of this category are:

- Support validation of activation codes and capabilities in the context of structural activation for utilization, operational support, and/or decommissioning;
- Assess the applicability and utilisation of isotopic evolution chains, cross-section libraries, and user capabilities.

Successful fulfilment of these objectives will create a body of knowledge that will be useful for operating organizations, researchers, regulatory bodies, designers, and other interested parties involved in the safety, operation, and utilization of RRs. The results of the CRP will be especially useful for optimizing core management and experimental programmes without penalising safety.

3. Scope and Objectives of the CRP

The scope of this CRP is to collect available experimental data and benchmark the computational methods and tools used for fuel burnup calculations and material/target activation in utilization, operation, and safety analysis of RRs.

The overall objective of this CRP is to increase the knowledge and expertise of Member States in the area of numerical analysis to improve the design, operation, utilization, safety, and decommissioning of RRs. The results of the CRP, based on the new data base to be created by the end of the project, will be especially useful for optimizing core management and experimental programmes while maintaining safety. The CRP will also encourage cooperation and foster information exchange among the counterparts.

In order to meet the overall objective, the following specific objectives of the CRP were developed:

1. Collect experimental data, and, after thorough review, develop a comprehensive database of experimental results, measurements and associated facility specifications that is useful for supporting verification and validation of burnup and activation computer codes.
2. Perform benchmark studies of burnup and activation computer codes against experimental data, and develop a comprehensive report on the results.
3. Identify user effects on the results predicted by the computer codes and models.
4. Develop recommendations on open issues in the area of numerical analysis of research reactors for future research and development activities.

Potential participants (based on previous Member State interest) were invited to submit research contract/agreement proposals that cover the full scope of the CRP (i.e., data submission and performing benchmarking studies) or that cover a limited scope.

By January 2015, 20 Member States had submitted proposals and, of those, twelve were accepted to participate in the first phase of the CRP work – to collect the existing experimental data. These are Argentina, Australia, Austria, USA, Brazil, Egypt, Indonesia, Israel, Romania, South Africa, Slovenia, and Thailand. Also at the March 2014 consultancy meeting, a data submission checklist was developed to provide the participants a detailed description and scope of the benchmark data expected. This checklist was verified for completeness by potential data providers present at the meeting, and available to Member States in the call for proposals. The primary consideration for selection of the first set of participants was the availability of data to be provided.

The first Research Coordination Meeting (RCM) will be held in April 2015, with the objectives to have the participants present their data, and have the group agree on common format for data package submissions. The group will also review the data provided and ensure that there is good coverage of the various types of benchmarks and codes presented and included. The CRP work plan will be finalized for the first year, with recommendations for continuation of the work into the next two years. It is expected that a number of CRP partners will increase in the 2nd phase of the project as soon as the collected and verified experimental data become available for benchmarks.

The specific activities involved in completing this CRP will be three RCMs, and two publications. The first publication will be the database of the benchmark and experiment specifications, incorporating the feedback from the individual participants. The second publication will be the consolidated results obtained for all of the CRP activities, which will include any recommendations for further work in terms of new benchmark data, code development and research and development activities.

4. Conclusions

This CRP is expected to provide a valuable “next step” in the development of analytical tools available to research reactors, by improving the validity of the available modeling methods through benchmark against experimental data.

References

[1] IAEA CRP web page; activities related to closed CRP1496; last accessed in March 2015; http://www-naweb.iaea.org/napc/physics/research_reactors/crps/crp3/crp3.html

[2] IAEA Technical Reports Series No. 480, 'Research Reactor Benchmarking Database: Facility Specification and Experimental Data', IAEA, Vienna (2015); web access.

[3] IAEA TECDOC Series, ‘Results of the CRP on Benchmarks against Experimental Data of Neutronics and Thermal-Hydraulic Computational Methods and Tools for Operation and Safety Analysis of Research Reactors’, IAEA, Vienna (in preparation).

PROPAGATION OF UNCERTAINTY FROM FINE-GROUP CROSS-SECTION DATA THROUGH LATTICE PHYSICS CALCULATIONS FOR THE SAFARI-1 RESEARCH REACTOR

S.A. GROENEWALD, P.M. BOKOV
Radiation and Reactor Theory
Necsa, Building 1900, P.O. Box 582, Pretoria, 0001, South Africa

ABSTRACT

This work is a first attempt to perform uncertainty analysis for neutronics modelling of the SAFARI-1 research reactor. The uncertainty introduced in the neutron multiplication factor (k-inf) and few-group homogenised cross-sections due to the uncertainties present in fine-group nuclear cross-section data is investigated on a lattice physics level. A SAFARI-1 fuel element is modelled at different burnup states and in various environments, such as in an infinite fuel environment and adjacent to water, beryllium or a control assembly. The TSUNAMI code which forms part of the SCALE 6.1.2 code system is used in this study. TSUNAMI employs first order linear perturbation theory to calculate sensitivities and the sandwich rule to calculate uncertainties in output lattice physics parameters due to the uncertainties in input cross-section data. Results show that k-inf uncertainty is approximately 0.5% and the uncertainty in few-group homogenised macroscopic cross-sections is of the order of 1% for all studied cases. The contribution of individual cross-sections to the uncertainty in k-inf is also investigated.

1. Background

Lattice physics calculations are the first step in the deterministic approach to reactor modelling. Lattice physics calculations are used to produce few-group nodal parameters such as homogenised macroscopic cross-sections and diffusion coefficients. Such nodal parameters are generated for all materials (homogenised mixtures) that are present in the full core model of the reactor. As a second step these nodal parameters are used in full core diffusion calculations, where quantities such as the flux distribution in the reactor core, the neutron multiplication (k_{eff}) and power peaking factors are determined.

The cross-section data used by lattice physics codes are contained in evaluated nuclear data libraries created from experimental measurements and mathematical models. The nuclear data inherently carry uncertainties [1], which are usually characterised by the second moments (variances and covariances) of their joint probability distribution. The nuclear data uncertainties can be propagated through the calculational path, including lattice physics and core calculations. As a result, the uncertainty in reactor parameters of interest, such as k_{eff} or power distribution, due to uncertainties in the cross-section data can be obtained. Furthermore, the contribution of each individual source of uncertainty to the total uncertainty can be estimated, via a procedure known as sensitivity analysis. The uncertainty propagation and the sensitivity analysis are often performed together and are referred to as sensitivity and uncertainty (S/U) analysis.

Various methodologies can be applied to perform S/U analysis for the neutronic modelling of nuclear reactors. Methods based on stochastic sampling are among the most widely used approaches. In this approach many cross-section libraries (typically in the order of hundreds) are created by sampling cross-sections from nuclear data libraries, using pre-defined probability distributions. Reactor calculations are run with all the libraries and statistical analysis is performed on the output. This method is very general and allows for simultaneous uncertainty analyses of many reactor responses. However, it requires multiple evaluations of the model corresponding to each library which leads to a high computational cost.

Furthermore not all sampling methods allow for sensitivity analysis. Examples of codes that use this approach are XSUSA [2] and NUDUNA [3].

Another widely utilised approach to S/U analysis is to calculate sensitivity coefficients for responses using perturbation theory. Such sensitivity coefficients can be used in combination with covariance data to calculate the uncertainty in responses. While only two reactor calculations are required (a forward and adjoint calculation) in this method, its drawback is that S/U analysis can only be performed for one response at a time. Each response requires a new specification of the sensitivity coefficient. Examples of codes that use this approach are TSUNAMI [4] and CASMO-4 [5].

In this work we consider the SAFARI-1 research reactor for S/U analysis. SAFARI-1 is a 20 MW tank-in-pool type material testing reactor (MTR). The core grid holds a combination of fuel, control, several reflector types, irradiation facilities and structural materials. The size of the core is roughly 65 cm x 65 cm x 60 cm, with a fuel pitch of 7.71 cm x 8.1 cm. The core is fuelled with 26 flat-plate MTR type fuel assemblies. The fuel is a mixture of uranium-silicide and aluminium and the control rods have cadmium as the neutron absorber. It is operated at temperatures between 20°C and 60°C.

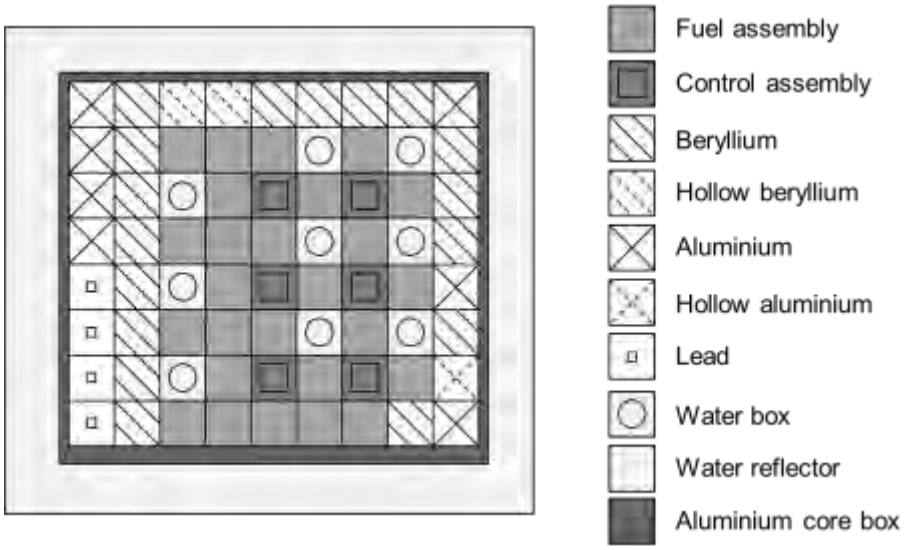

Fig 1. Schematic representation of a radial cut through the SAFARI-1 reactor

SAFARI-1 has a heterogeneous core layout (see Figure 1) where fuel elements neighbour various other elements including fuel, control rods, water and beryllium. This is a small core with a relatively high leakage compared to power reactors. Therefore the two energy group approach used to model power reactors is not sufficient. Instead SAFARI-1 is modelled in six energy groups in order to capture the correct neutron spectrum in and the leakage from the core. Furthermore, the fuel has a higher enrichment (19.75%) and is burnt much further (up to 60% ^{235}U depletion) than what is typical for power reactors.

A large number of S/U studies have been performed for power reactors, see for example references [2,6-8], but little work has been done on MTRs such as SAFARI-1. S/U analysis for neutronics modelling of the SAFARI-1 research reactor is the focus of this work. We follow the approach applied in the benchmark for uncertainty analysis in modelling of light water reactors [1], which is currently underway. This approach involves a successive propagation of uncertainties through the layers of the traditional nuclear reactor calculational path. The scope of this work is limited to analyses of lattice physics calculations. Propagation of uncertainties to full core calculations is left as future work.

Currently SAFARI-1 fuel cross-sections are prepared from an infinite fuel lattice calculation. From experience we know that this leads to large errors in the power calculations for assemblies adjacent to control rods and water. Generating nodal parameters for fuel in more representative colourseets could allow us to reduce the environmental error introduced in full-core calculations. However, changing the fuel environment in the lattice physics calculation will also change the uncertainty in the nodal parameters. In this work we will analyse a fuel element in different colourseets. This analysis will be performed for a fresh fuel element. The impact of nuclide composition changes induced by burnup is also studied by comparing results for a fresh and a depleted fuel element.

The following sections cover a description of the methodology and lattice physics models used. Results and a discussion thereof are presented and finally concluding remarks are given.

2. Methodology

This section describes the codes and method used to carry out S/U analyses as well as the models that were analysed.

2.1. Code description

We applied the SCALE 6.1.2 code system [9] to perform S/U analyses for lattice physics calculations. The 2D discrete ordinates transport code NEWT was used for forward and adjoint transport calculations on various lattice physics models. From these two solutions for the model, the sensitivity analysis code SAMS [4] calculates a sensitivity vector for a reactor response, using first order linear perturbation theory [10]. This vector quantity contains energy dependent sensitivity coefficients that describe the change in a response caused by a change in cross-section values. Furthermore SAMS calculates the relative standard deviation in this response, by applying the sandwich rule (see discussion below). This parameter describes the uncertainty in a response due to fine-group cross-section data uncertainties. The control module TSUNAMI-2D is used to coordinate S/U calculations in SCALE. The standard SCALE 238 group ENDF/B-VII.0 nuclear data library is used for transport calculations and covariance data are obtained from the SCALE 44 group covariance library [9].

A brief description of the S/U calculations done in SCALE is presented here. A more detailed discussion can be found in references [4,9]. Let $\boldsymbol{\alpha}$ be the vector containing neutron cross-sections for our model. Elements of this vector, $\alpha_{x,g}^{i}$, vary over all nuclides i, all reactions x for each nuclide and all energy groups g. Vector $\boldsymbol{\alpha}$ has N elements that correspond to the number of nuclide-reaction pairs times the number of energy groups. Let R be a calculated reactor parameter of interest (response) and the vector $\boldsymbol{S}$ of size N represent the sensitivity of this parameter due to cross-section covariance data. The elements of this sensitivity vector contain the fractional rate of change of the response R per fractional change in $\alpha_{x,g}^{i}$:

$$S_{R,\alpha_{x,g}^{i}} = \frac{\alpha_{x,g}^{i}}{R}\,\frac{\partial R}{\partial \alpha_{x,g}^{i}}. \tag{1}$$

The relative cross-section covariance data can be presented as the matrix $\boldsymbol{C}$ with elements defined as

$$C_{\alpha_{x,g}^{i},\alpha_{y,g'}^{j}} = \frac{\mathrm{Cov}\left(\alpha_{x,g}^{i}\,,\,\alpha_{y,g'}^{j}\right)}{\alpha_{x,g}^{i}\;\alpha_{y,g'}^{j}} \tag{2}$$

where $\mathrm{Cov}\left(\alpha_{x,g}^{i}\,,\,\alpha_{y,g'}^{j}\right)$ is the covariance between reactions x and y of nuclides i and j, for energy groups g and g'. This is an $N \times N$ symmetric matrix containing group-wise nuclide-

reaction uncertainties (variance) on the diagonal and shared uncertainties between two group-wise nuclide-reactions (covariance) for off-diagonal elements. Given the sensitivity vector and the covariance matrix, the uncertainty characterised by the variance in a response, σ_R^2, can be calculated using the formula which is often referred to as the sandwich rule [11]:

$$\sigma_R^2 = \boldsymbol{S}_R \, \boldsymbol{C} \, \boldsymbol{S}_R^T. \tag{3}$$

It is customary to present the uncertainty as percent relative standard deviation in the response R, which is calculated as

$$\text{rel. std. dev.}\,(R) \;=\; 100 \times \frac{\sigma_R}{R}. \tag{4}$$

Uncertainties reported in this work will be presented in terms of percent relative standard deviation. It is possible to isolate the contribution of two particular processes to the total variance by only considering a subset of the covariance matrix. The contribution due to nuclide-reactions α_x^i and α_y^j is given by

$$\sigma^2_{R,\alpha^{i,j}_{x,y}} = \sum_g S_{\alpha_x^i} \, C_{\alpha_x^i \alpha_y^j} \, S^T_{\alpha_y^j}, \tag{5}$$

where the summation is performed over all the energy groups. For the sake of consistency, results for contributions to the variance will also be given in percent relative standard deviation

$$\text{contribution} = 100 \times \frac{\sigma_{R,\alpha^{i,j}_{x,y}}}{R}. \tag{6}$$

2.2. Model description

Five models were created that represent SAFARI-1 fuel in typical core environments, as described in Table 1 and illustrated in Figure 2. These models can be used to study the environmental effect on nodal parameters for a fuel element. The first model is a single fresh fuel element in an infinite fuel environment. This model is currently used to calculate nodal parameters for the fuel in SAFARI-1. Three colourset models are included, where a fuel element is placed next to a reflector (water or beryllium) or a control rod. These are realistic colourseets found in the SAFARI-1 core.

Model	**Description**
Fresh fuel	A SAFARI-1 fuel element with reflective boundary conditions
Burnt fuel	A SAFARI-1 fuel element with a fuel composition representing a maximum burnup of 60% of ^{235}U. Reflective boundary conditions
Fuel-control	A 2-node model of a fresh fuel element adjacent to a control absorber. Reflective boundary conditions
Fuel-water	A 2-node model of a fresh fuel element adjacent to a water node. Reflective boundary conditions
Fuel-beryllium	A 2-node model of a fresh fuel element adjacent to a beryllium reflector node. Reflective boundary conditions

Tab 1: The calculational models used in the study

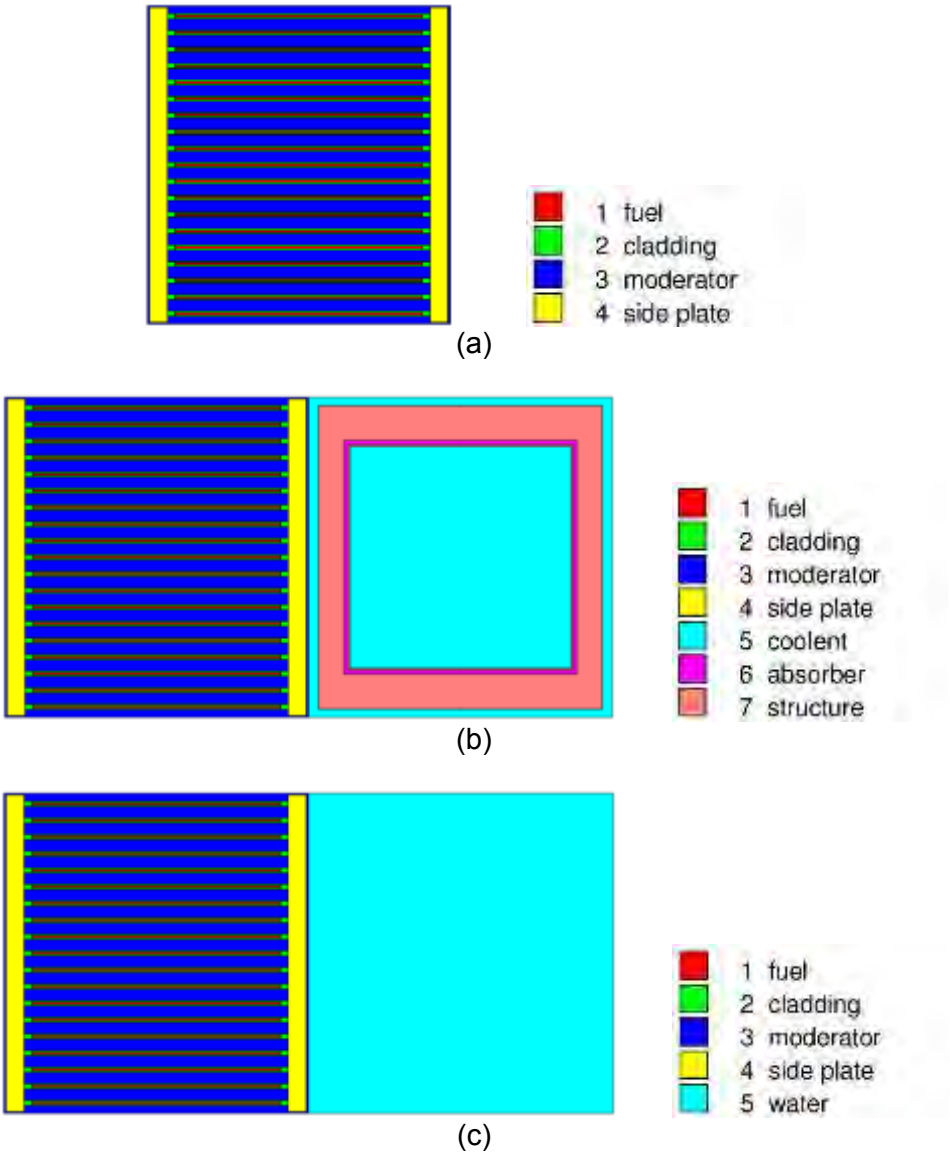

Fig 2. Representation of the calculational models used in the study: (a) standalone SAFARI-1 fuel element (fresh or burnt), (b) SAFARI-1 fuel element adjacent to a control absorber, (c) SAFARI-1 fuel element adjacent to a water (or beryllium) element

The last model is a fuel element burnt up to the safety limit of 60% of ^{235}U. The burnup calculations were performed with the nominal (average) values of nuclear data. We used the nuclide inventory of a burnt SAFARI-1 fuel element and created a second model with an infinite fuel environment. The material composition includes 35 of the most important fission products and actinides, namely isotopes of U, Np, Pu, Am, Cm, I, Xe, Ce, Pr, Nd, Pm and Sm.

Homogenised macroscopic cross-sections were calculated in 2 energy groups, as is usual in power reactor modelling, and in a 6-group structure that is currently used for modelling SAFARI-1. The thermal cut-off in the 2-group structure is at 0.625 eV and the upper energy boundaries for the 6-group structure are, in eV: 2.00×10^{7}, 8.20×10^{5}, 6.00×10^{3}, 4.00×10^{0}, 6.25×10^{-1} and 1.50×10^{-1}. Homogenised cross-sections are created for absorption (n,γ), fission (n,f), scattering and nu-fission reactions as well as for diffusion coefficients. Because of limitations in TSUNAMI, the diffusion coefficients are approximated as $D = 1/(3\Sigma_{\mathrm{t}})$, i.e. by using the total instead of the transport cross-section.

3. Results and discussion

We start our study with an analysis of the k_{inf} as an integral neutronic parameter and perform detailed S/U analyses on the various models under investigation. The main goal of this work is to determine the uncertainties in nodal parameters for different lattice physics models. However to analyse these nodal parameters in six energy groups for all models will be cumbersome. Instead we will continue the study with the industry standard of two energy groups.

The calculated values of the neutron multiplication factors (k_{inf}) for different models as well as their uncertainty due to cross-section covariance data (see Equations 3 and 4) are given in Table 2. The uncertainty in k_{inf} for the fresh fuel model has the lowest value, with a relative standard deviation of 0.411%. The burnt fuel element has a slightly higher uncertainty and all three colourset models have an even higher uncertainty in k_{inf}.

Model	k_{inf}	Rel.std.dev.(k_{inf}), %
Fresh fuel	1.65295	0.411
Burnt fuel	1.44125	0.439
Fuel-control	0.95773	0.479
Fuel-water	1.17595	0.488
Fuel-beryllium	1.67892	0.462

Tab 2: Uncertainty in k_{inf} for different models

The contributions from each nuclide-reaction pair to the relative standard deviation in k_{inf} (see Equations 5 and 6) are analysed next. The top 5 contributors to uncertainty for each model are presented in Table 3. The uncertainties presented in this table contribute up to 95% of the total uncertainty. This total uncertainty (column 3 in Table 2) can be obtained from all contributions, by adding the square of their positive values and subtracting the square of their negative values, then taking the square root. Only contributors with positive values appear in Table 3 because all negative values are too small to be included.

Contributor	Fresh fuel	Burnt fuel	Fuel-control	Fuel-water	Fuel-beryllium
^{235}U nubar	0.296	0.273	0.297	0.293	0.299
^{235}U (n,γ)	0.202	0.162	0.193	0.184	0.200
^{235}U (n,f) – ^{235}U (n,γ)	0.115	0.116	0.120	0.121	0.117
^{27}Al (n,γ)	0.111	0.142	0.113	0.093	0.122
^{235}U (n,f)	0.084	0.105	0.095	0.102	0.086
^{235}U chi	0.007	0.004	0.174	0.212	0.136
^{1}H (n,n)	0.010	0.010	0.122	0.145	0.024
^{135}Xe (n,γ)	–	0.162	–	–	–

Tab 3: Individual contributions to the uncertainty in k_{inf}, in percent relative standard deviation

The uncertainty of ^{235}U nubar (average number of neutrons released per fission) is the largest contributor to the total uncertainty of k_{inf} for all the models. The highest uncertainty is observed for the fuel-beryllium model, where the ^{235}U contribution is 0.299% relative standard deviation, which translates to 41.77% of the total variance in k_{inf}. The second largest contributing nuclide-reaction for all models is ^{235}U (n,γ), except for the fuel-water model, where ^{235}U chi (fission spectrum) is the second largest contributor.

In general, the fresh fuel, fuel-water and fuel-control calculations are the most sensitive to the same set of nuclear data uncertainties corresponding to ^{235}U, ^{27}Al and ^{1}H nuclides. The

models that contain the most water (i.e. the fuel-water and fuel-control) display a larger sensitivity to ^{1}H cross-sections. Only the elastic cross-section ^{1}H (n,n) is presented in Table 3 but the ^{1}H (n,γ) cross-section also has a small contribution to the uncertainty in k_{inf}. Also not indicated in this table, the fuel-beryllium model is sensitive to beryllium cross-section uncertainties. Contributions for ^{9}Be (n,2n), ^{9}Be (n,γ) and ^{9}Be (n,α) cross-sections are in the order of 0.09% relative standard deviation each. The addition of more water or beryllium can be responsible for the increase observed in the total uncertainty in k_{inf} for the colourset models.

In the case of a burnt fuel element, the ^{135}Xe (n,γ) cross-section is also a large contributor (0.162%) to the uncertainty. Not indicated in the table, ^{239}Pu nubar and ^{239}Pu (n,f) also contribute 0.08% and 0.03% relative standard deviation respectively. The uncertainty in k_{inf} is larger for the burnt fuel than for the fresh fuel model because covariance for fission products and actinides which are present in the burnt fuel also contribute to the total uncertainty.

Note that the most contributions to the k_{inf} uncertainty come from covariance data for a specific nuclide-reaction. Only one significant contribution comes from the covariance between two nuclide-reactions namely ^{235}U (n,f) and ^{235}U (n,γ).

We are also interested in the uncertainties in the nodal parameters that are generated with lattice physics calculations. Table 4 shows the 2-group homogenised macroscopic cross-sections for the standalone fresh fuel element model and the relative standard deviation in these values. We see that uncertainties are consistently larger for the fast than the thermal group cross-sections. The scattering cross-section from group 1 to 2 has the largest uncertainty of 0.949% relative standard deviation.

Cross-section	Energy group	Cross-section value	Rel.std.dev.(k_{inf}), %
Absorption	1	6.0119E-03	0.846
	2	1.0923E-01	0.232
Fission	1	2.2835E-03	0.691
	2	8.1136E-02	0.315
Scatter from 1 to	1	5.8583E-01	0.723
	2	2.7421E-02	0.949
Scatter from 2 to	1	4.8819E-04	0.270
	2	1.7422E+00	0.118
Diffusion coefficient	1	5.3828E-01	0.732
	2	1.7999E-01	0.109
Nu-fission	1	5.6356E-03	0.681
	2	1.9771E-01	0.442

Tab 4: Homogenised 2-group cross-sections and uncertainties for the fuel model

Similar uncertainty analysis of nodal parameters have been peformed for other models. Figure 3 shows the relative standard deviation in the homogenised fuel cross-sections for all five models investigated. These values show little dependence on the environment in which they are calculated. The exception to this is the fuel-beryllium model, for which some fast group uncertainties are up to 30% lower than for the other models. The largest values are observed for the uncertainties in the scattering cross-section from group 1 to 2 and in the group 1 absorption cross-sections. All uncertainties are less than 1% relative standard deviation. Once again we observe that the fast group uncertainties are larger than the thermal group ones for all models investigated.

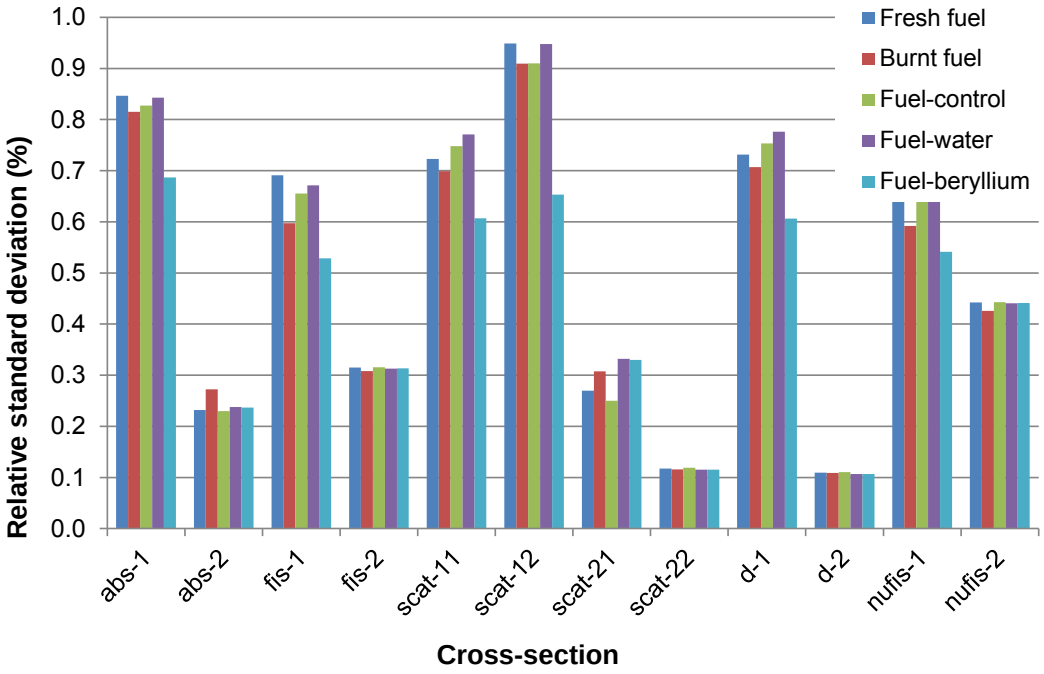

Fig 3. Uncertainty in 2-group homogenised macroscopic cross-sections

We can determine where in the energy range from 0.625 eV to 20 MeV the larger uncertainties lie by going to six broad groups instead of two. This information will be important in reactor calculations, which is done in six energy groups. Based on the observation that uncertainties are to a large extent independent of the fuel environment, we only consider the fuel model for this 6-group study. Tables 5 and 6 describe the uncertainty in 6-group homogenised macroscopic cross-sections for the fuel model, given as relative standard deviation.

Cross-section	Energy group					
	1	2	3	4	5	6
Absorption	1.874	3.967	0.488	0.387	0.285	0.261
Fission	0.647	0.437	0.275	0.466	0.362	0.329
Diffusion	1.006	0.462	0.153	0.119	0.110	0.101
Nu-fission	1.050	0.466	0.363	0.560	0.477	0.453

Tab 5: Uncertainty in 6-group homogenised macroscopic cross-sections for fuel, in percent relative standard deviation

Scattering from group	Scattering to group					
	1	2	3	4	5	6
1	0.861	1.970	1.882	1.890	2.117	2.463
2		0.470	0.518	0.521	0.521	0.521
3			0.158	0.159	0.160	0.160
4				0.146	0.100	0.101
5				0.188	0.126	0.110
6					0.108	0.109

Table 6: Uncertainty in 6-group homogenised scatter cross-sections for standalone fresh fuel, in percent relative standard deviation

The absorption cross-section for group 2 has the largest uncertainty of 3.967% relative standard deviation. Other large uncertainties from 1% to 2.5% are found in group 1 cross-

sections (Table 5) and scattering from group 1 to lower energy groups (Table 6). All other uncertainties are 0.521% or less. The largest relative standard deviations correspond to some of the smallest cross-section values, particularly the scatter cross-sections to thermal and epithermal groups and the group 2 absorption cross-section.

4. Conclusion

Fine group cross-section uncertainties have been propagated through lattice physics calculations, using the TSUNAMI-2D code, for several SAFARI-1 fuel element models. A fuel element in infinite fuel environment and three different colourseets as well as a burnt fuel element (also in infinite environment) have been modelled. Uncertainties in k_{inf} and homogenised macroscopic cross-sections due to fine-group cross-section covariance data have been calculated.

From uncertainty analyses of k_{inf}, we observed that nuclear data uncertainties cause approximately 0.45% standard deviation in the infinite multiplication factor for SAFARI-1 lattice physics models. The uncertainties for the colourset models and the burnt fuel model are slightly larger than for the standalone fresh fuel model. Sensitivity analysis has shown that the largest contributing cross-sections to the uncertainty are the average number of neutrons released per fission in ^{235}U, followed by the ^{235}U(n,γ) cross-sections and the ^{235}U fission spectrum. Cross-sections for non-fissionable materials such as beryllium, cadmium, aluminium and water contribute little to the total uncertainty in k_{inf}. The presence of fission products and actinides in depleted fuel contributes even less to the total uncertainty in k_{inf}.

Uncertainties in 2-group homogenised cross-sections for the fuel model are less than 1% relative standard deviation. There is little dependence on fuel burnup or the fuel environment. Fast group uncertainties are consistently larger than thermal group uncertainties. This was also observed in 6-group homogenised cross-sections for the fuel model, where all group 1 cross-sections, the group 2 absorption cross-section and down-scatter cross-sections from group 1 have the largest uncertainties.

It may be concluded that the uncertainty in k_{inf} increases (by approximately 16%) when fuel is modelled in a typical SAFARI-1 colourset environment. The uncertainty in the homogenised nodal parameters studied depends little on the environment, except in the fuel-beryllium model, where some uncertainties decrease. Due to shortcomings in the code used, diffusion coefficients were calculated approximately and discontinuity factors could not be calculated. It would be interesting to determine the uncertainties in discontinuity factors for various models, since this is a very important parameter affecting the accuracy of full-core calculations.

Sensitivity and uncertainty analysis were limited to lattice physics calculations for a SAFARI-1 fuel element. A similar study of other SAFARI-1 core components such as reflector and control elements will contribute to a better understanding of homogenised nodal parameter uncertainties due to cross-section covariance data. Finally, propagation of uncertainties to full core calculations is left as future work.

5. Acknowledgements

This study was financially supported by the National Research Foundation (NRF) of South Africa via the incentive funding Grant No. 70730. Any opinion, finding and conclusion or recommendation expressed in this material is that of the authors and the NRF does not accept any liability in this regard.

6. References

[1] K. Ivanov et al. “Benchmark for uncertainty analysis in modelling (UAM) for design, operation and safety analysis of LWRs”. Vol. I: Specifications and Support Data for Neutronics Cases (Phase I). NEW/NSC/DOC(2013)7. May 2013.

[2] W. Zwermann et al. “Uncertainty analysis with nuclear covariance data in reactor core calculations”. Journal of the Korean Physical Society, Vol. 59, No. 2, P. 1256 – 1259. August 2011.

[3] O. Buss, A. Hoefer and J. Neuber. “NUDUNA – Nuclear data uncertainty analysis”. Presentation at Nuclear Data Week Santa Fe. November 2010.

[4] B.T. Rearden et al. “Sensitivity and uncertainty analysis capabilities and data in SCALE”. Nuclear Technology, Vol. 174, p. 236 – 288. May 2011.

[5] M. Pusa. “Perturbation theory based sensitivity and uncertainty analysis with CASMO-4”. Science and Technology of Nuclear Installations, Vol. 2012, Article ID 157029. 2012.

[6] N. Garcia-Herranz, J. Garrido and O. Cabellos. “Sensitivity/Uncertainty analysis for BWR configurations of exercise I-2 of UAM benchmark”. PHYSOR 2014 – The Role of Reactor Physics Toward a Sustainable Future. Kyoto, Japan. September 28 – October 3, 2014.

[7] C.J. Díez et al. “Propagation of cross-section uncertainties in criticality calculations in the framework of UAM-phase I using MCNPX-2.7e and SCALE-6.1”. Science and Technology of Nuclear Installations, Vol. 2013, Article ID 380284. 2013.

[8] M. Hursin et al. “Pinpower uncertainty quantification of LWR-Proteus phase III experiments”. PHYSOR 2014 – The Role of Reactor Physics Toward a Sustainable Future. Kyoto, Japan. September 28 – October 3, 2014.

[9] C.V. Parks and US Nuclear Regulatory Commission. “SCALE: A modular code system for performing standardized computer analyses for licensing evaluation”. Oak Ridge National Laboratory, Oak Ridge, TN, version 6 edition, 2009. Available from Radiation Safety Information Computational Centre at Oak Ridge National Laboratory as CCC-750.

[10] W.M. Stacey. “Nuclear Reactor Analysis. John Wiley and Sons, Inc., New York. 1976.

[11] Y. Azmy and E. Sartori. “Nuclear Computational Science – A Century in Review”. Springer. 2010.

SAFETY ANALYSIS ON BRAZILIAN MULTIPURPOSE REACTOR USING THE RELAP5-3D CODE

H. V. SOARES, J. GONZÁLEZ-MANTÉCON, A. L. COSTA,
C. PEREIRA, P. A. L. REIS, M. A. F. VELOSO
Departamento de Engenharia Nuclear, Universidade Federal de Minas Gerais
Av. Antônio Carlos, 6627 – PCA1 – Anexo Engenharia – Pampulha
CEP 31270-901 Belo Horizonte, MG, Brasil
Instituto Nacional de Ciências e Tecnologia de Reatores Nucleares Inovadores/CNPq, Brasil.

I. D. ARONNE
Centro de Desenvolvimento da Tecnologia Nuclear/Comissão Nacional de Energia Nuclear – CDTN/CNEN, Av. Antônio Carlos, 6627, CEP 31270-901 Campus UFMG, Belo Horizonte, Brasil.

ABSTRACT

The Brazilian Multipurpose Reactor (*Reator Multipropósito Brasileiro* - RMB) is currently being projected and several analyses are being performed. It will be a 30 MW open pool multipurpose research reactor with a compact core using Materials Testing Reactor (MTR) fuel assembly with planar plates. RMB will be cooled by light water and moderated by beryllium and heavy water. This work presents the thermal hydraulic calculations of steady state operation of the RMB using a RELAP5 model and also a model of core using the multi-dimensional kinetic model in RELAP5-3D and PARCS code. The cross section was generated in the WIMSD-5B lattice code. The axial and radial relative power on the core was compared with three-dimensional CITATION diffusion code. The results showed good agreement with the reference.

1. Introduction

The Brazilian Nuclear Energy Commission *(Comissão Nacional de Energia Nuclear - CNEN)* is leading the project of the Brazilian Multipurpose Reactor (RMB) envisaged to be projected, constructed and operated to attend the present Brazilian need for a multipurpose neutron source, which will be able to supply the demand of radioisotopes, carry out material tests and develop scientific, commercial, and medical applications with the use of neutron beams. The RMB will have three main functions: radioisotope production (mainly molybdenum); fuel and material irradiation testing to support the Brazilian nuclear energy program. Moreover, it will provide neutron beams for scientific and applied research.

Among the different types of research nuclear reactors, the open pool reactors are the most common and the most used, because of their great versatility, easy operation and safety. The reactors Osiris in France, and mainly the Australian research reactor Opal (Open Pool Australian Lighwater Reactor) projected by Argentina and built in Australia are being used as initial references for the RMB project.

In the present work, a thermal-hydraulic nodalization for the RMB core using the RELAP5-3D and the most important components of the pool loop and core loop circuits are presented. A multi-dimensional neutron kinetics model of the RMB core was developed to RELAP5-3D and PARCS codes. The axial and radial relative power on the core was compared with three-dimensional CITATION diffusion code.

2. Brazilian Multipurpose Reactor

The RMB will be an open pool multipurpose research reactor using low enriched uranium fuel, with a neutron flux higher than 2 x 10^{14} n/(cm^2s). The reactor core will be compact using MTR fuel assembly type with planar plates and will be cooled and moderated by light water. Table 1 presents the main characteristics of RMB. Figure 1 shows the model of present concept of the RMB reactor [1] that was based in the Australian research reactor Opal [2]. The RMB pool is cylindrical with 12.8 m of high and 5.6 m of diameter.

Reactor	
Nominal Power	30 MW
Moderator and coolant	Light water
Reflector	H_2O, D_2O, Beryllium
Thermal and fast neutron flux in the core (higher than)	2.0 x 10^{14} neutrons.cm^{-2}.s^{-1}
Core	
Flow direction in core	Upwards
Control rods drive location	Below core
Grid array	5 x 5
Dimensions	0.51 x 0.55 x 0.815 m
Number of fuel and control elements	23 / 6
Absorbing material	Ag-In-Cd
Fuel assembly type	MTR (LEU)
Nuclear fuel	U_3 Si_2-Al enriched at 20%
Fuel density	4,8 gU/cm^3

Tab 1: General characteristics of RMB

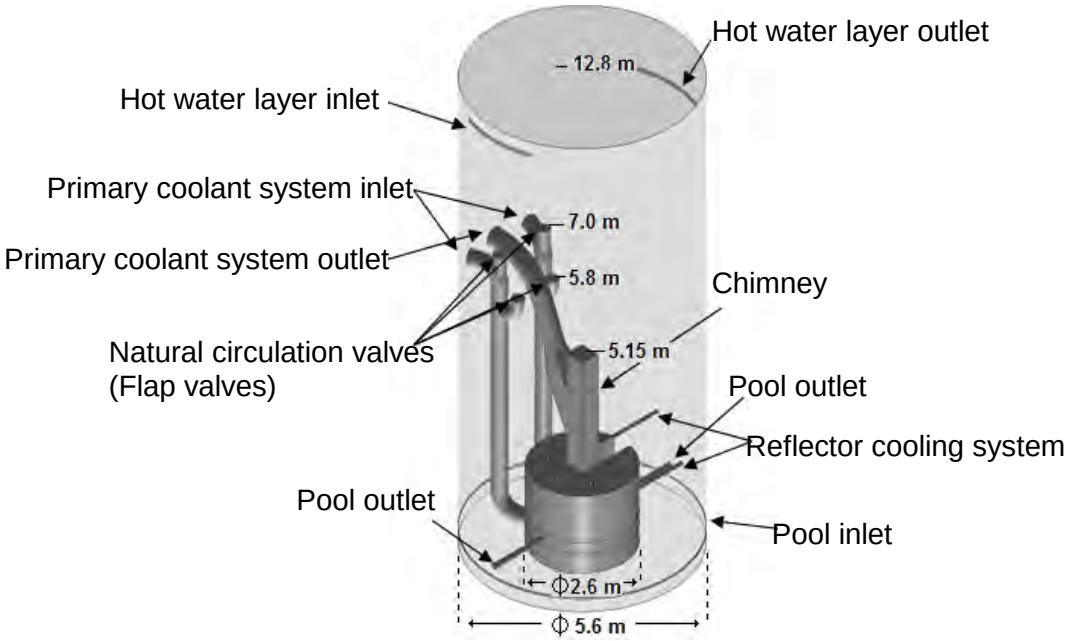

Fig 1. RMB present concept

A heavy water tank surrounds three quarters of the chimney in the core area working as a reflector and enabling the extraction of neutron beams and placement of materials for

irradiation. In the remaining quarter there is beryllium that also works as a reflector. The heavy water temperature will be controlled by a dedicated cooling system.

The whole core structure will be located within a square cross-section “core chimney” which constitutes part of the primary cooling circuit. The core will be cooled by a flow of demineralised light water moving upwards through the core. In normal operation, the coolant is pumped through the core and then through pipes to a heat exchanger before returning to the core inlet.

The core is constituted of 23 plate-type fuel assemblies, two experimental assemblies and two plate guide box. The box contains and protects six neutron-absorbing plates that can move upwards and downwards as shown in Figure 2 [3].

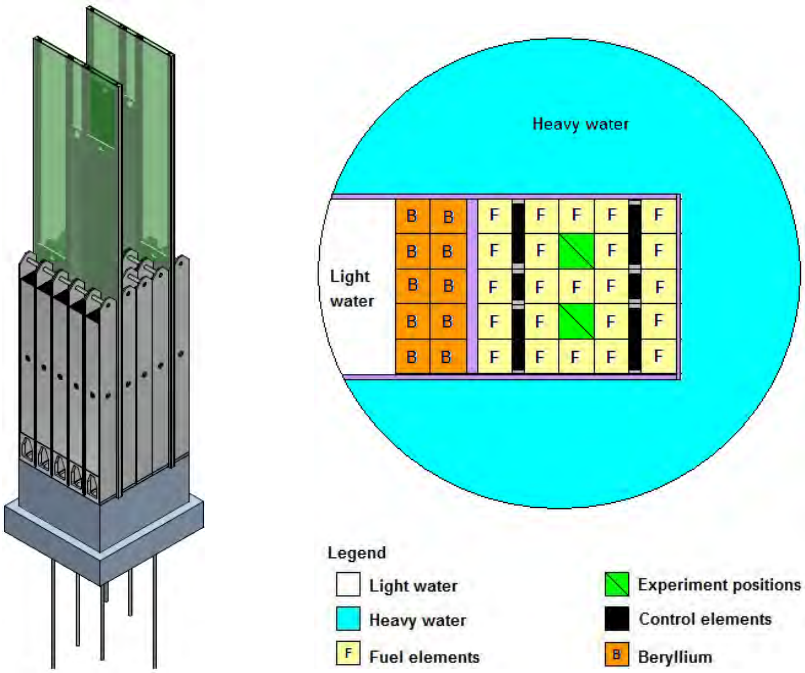

Fig 2. Representation of the RMB core (left) and its vicinity – upper view (right) [3]

The reactor cooling has four circuits: Hot Water Layer (HWL), Primary Cooling System (PCS), Reactor and Service Pools Cooling System (RSPCS) and Reflector Cooling System (RCS).

3. Thermal hydraulic model

Figure 3 shows the RELAP5-3D thermal-hydraulic nodalization developed to simulate the RMB and Table 2 shows the correspondence between the main plant components and their equivalent components in the RELAP5-3D nodalization scheme. The reactor pool was modelled using two pipe components (100 and 130) composed by twenty volumes each one. The heat generated by reactor in one side of the pool (100) leads to water circulation inside the pool through the cross junctions between the two pipes. The service pool was modelled using a pipe component (150) with twelve volumes. Volume 140 is a branch component that represents the upper pool surface, which is in contact with the atmosphere. Volume 190 is a time dependent volume that simulates the atmosphere on the top of pool surface.

The Reactor and Service Pools Cooling System (RSPCS) removes heat from the irradiation rigs in the reactor pool. The system comprises two pipes inside the pool, the long term pool cooling pipe (component 202) and a pipe (component 204). Components outside the pool are: a decay tank (components 222-226), a main pump (component 230), heat exchanger

(component 234 - primary side), a three-way valve (simulated by valves 209 and 211) and associated components. The position of the three-way valve defines which of the two lines is connected to the pumping equipment to perform forced circulation. The rigs cooling branch has a pipe (component 204) that extends from the irradiation rig plenum below the reflector vessel and passes through the reactor pool boundary at level +7.00 m inside the pool. From there, it is connected to the three-way valve and then to the decay tank.

The Primary Cooling System (PCS) comprises components 300 through 360 which are inside the pool and components 400 through 460 which are outside the reactor pool. Component 300 represent the core inlet lower plenum which conducts the light water to the core (components 311-335). The core has twenty five hydrodynamic channels with twenty three Heat Structure (HS) associated to it representing all fuel plates. The others two hydrodynamic channels there aren't HS, and represent the experiments positions. The heated water goes through the components 300 where it is mixed with a small downward flow coming from the pool through the chimney (component 346). The chimney flow corresponds about 10% of the total outlet flow of the PCS.

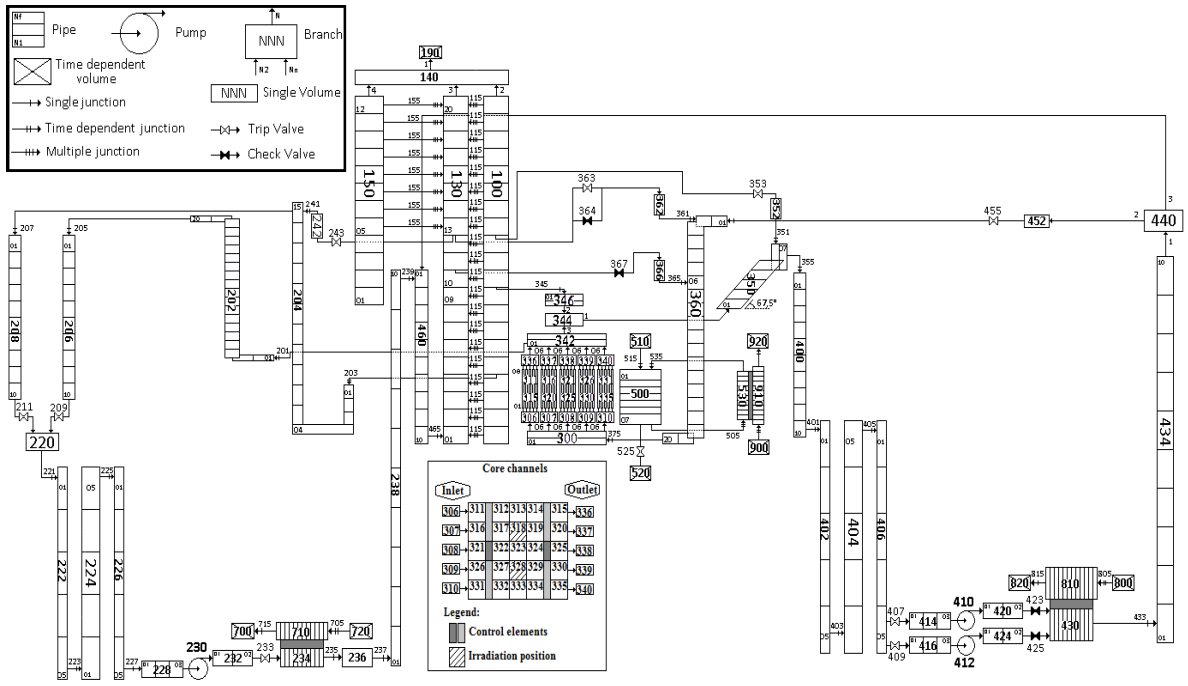

Fig 3. RMB nodalization for RELAP5-3D

In order to allow the establishment of natural circulation when the PCS pumps are not in operation three special flap valves are located in two lines returning to the pool, which are represented by the component 360. One set of valves is located at level +7.00 m and is represented by valves 363 and 364 and the other set, at level +5.80 m, is modeled by the valve 367. Both sets are above the upper edge of the chimney at level +5.15 m (component 340). Each set of these special valves is modeled by two valves, one trip valve and one check valve. Valve 363 is a trip valve and the components 364 and 367 are check valves. Both valve types behave as on/off switch. During a Loss of Coolant Accident (LOCA) the coolant goes out by rupture and the water level of the reactor pool drops until the upper flap valves, which will act as siphon breakers and will prevent the water level to decrease below +7.00 m. The lower flap valves will open, thus creating the natural circulation cooling flow path. Only one of the two valves is required to provide a flow sufficient to remove core decay heat.

The main components of PCS outside the pool are: a tank for nitrogen-16 decay (components 402-406), two parallel primary cooling pumps (components 410 and 412), the main heat exchanger (component 430 - primary side), valves (components 407, 409, 423 and 425), and pipe components.

The Reflector Coolant System, RCS, is composed by a heavy water tank (component 500) and its heat exchanger circuit (component 530 - primary side and component 910 - secondary side).

The area located on level -5.00 m (under the pool ground level) accommodates the pumps of the cooling systems, heat exchangers and associated components of both circuits PCS and RSPCS.

Component	**Identifier**
Reactor pool	100 and 130
Reactor Pool Cooling System (RPCS)	201-239
Reactor core	311-335
Reactor chimney	346
Primary Cooling System (PCS)	400-460
Heavy water tank	500
Reflector Cooling System (RCS)	500-530
Natural Convention Valves (Flap Valves)	364 and 367
Siphon breakers valves	243, 363 and 353
Pool atmosphere simulator	190
Decay tank of PCS	402-406
Decay tank of RPCS	222-226
Pumps of PCS	410 and 412
Pump of RPCS	230
Primary side heat exchanger of PCS	430
Secondary side heat exchanger of PCS	800-820
Primary side heat exchanger of RPCS	234
Secondary side heat exchanger of RPCS	700-720
Primary side heat exchanger of RCS	530
Secondary side heat exchanger of RCS	900-920

Tab 2: Main nodalization components and their input identifier number

4. Kinetic Model

In the present work, a 3D kinetic model was developed to represent the RMB core. The RELAP5-3D and PARCS codes were used to perform the modellings.

Figure 4 shows the RMB core. There are three different uranium densities to represent the RMB fuel elements. However, the kinetic modelling developed in this paper didn't take into account the presence of control rods from the geometric point of view, and then the core became square. The length of each radial mesh is 0.0817 m in both directions. There are five radial meshes in x and y directions and eight axial meshes in this present kinetic modelling. Table 3 shows the axial mesh lengths in thermal-hydraulic and kinetic modelling.

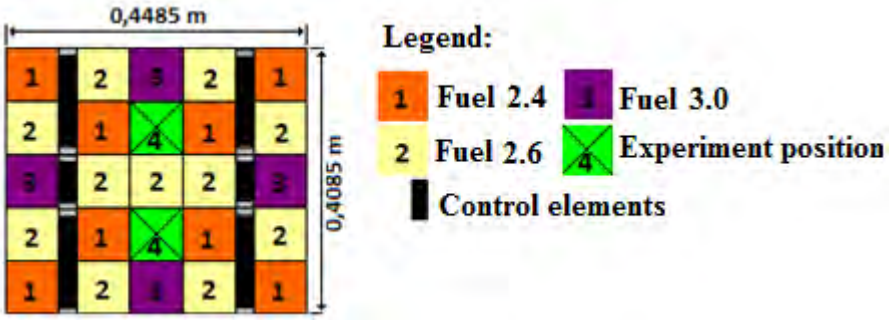

Fig 4. Upper view of RMB core

Axial meshes	Length (m)
1	0.135
2	0.0775
3	0.105
4	0.125
5	0.125
6	0.105
7	0.0775
8	0.135
Total (m)	0.885
Fuel element active length (m) (Axial meshes: 2+3+4+5+6+7)	0.615

Tab 3: Axial lengths to thermal-hydraulic and kinetic modelling

4.1 RELAP5-3D

The RELAP5-3D code is an outgrowth of the one-dimensional RELAP5 code developed at the Idaho National Laboratory (INL). The most prominent attribute that distinguishes RELAP-3D from its predecessors is the fully integrated, multi-dimensional thermal-hydraulic and kinetic modelling capability. The multi-dimensional neutron kinetics model in RELAP5-3D is based on the NESTLE code developed by Paul Turinsky and co-workers at North Carolina State University under an INL initiative. The NESTLE code solves the two or four group neutron diffusion equations in either Cartesian or hexagonal geometry using the Nodal Expansion Method (NEM) and the no-linear iteration technique [4].

4.2 PARCS

PARCS [5] is a three-dimensional (3D) reactor core simulator which solves the steady state and time dependent, multi-group neutron diffusion and SP3 transport equations in orthogonal and non-orthogonal geometries. The feedback effects are evaluated through a thermal hydraulic calculation modulus via a few group cross sections. A simple thermal hydraulic model is incorporated in the code for core temperature computation. Neutronically, the Coarse Mesh Finite Difference (CMFD) formulation is employed in PARCS to solve for the neutron fluxes at the homogenized nodes. The Analytic Nodal Method (ANM) is used to solve the two-node problems for accurate resolution of coupling between nodes in the core.

5. Cross Section Generation

To solve the neutron kinetics equations, the macroscopic cross section library for various materials in the core is set-up. For this purpose the WIMSD-5B lattice code is used [6]. In practice, the cells which may correspond to any region of the core (fueled and non-fueled)

are identified. When defining the unit cell dimensions, the principle of conservation of volume ratio of the different materials in the fuel assembly is considered. The fuel cell dimensions are calculated taking into account the fuel meat conservation criteria. The unit cell for Standard Fuel Element (SFE) is shown in Figure 5 (a). An extra region is added accounting for the remaining water and aluminum in the same proportions as in the physical fuel element; this region includes the aluminum in the plates beyond the width of the meat and the aluminum side plates, the water beyond the width of the meat, and the water channels surrounding the fuel element. In the particular case of Control Fuel Element (CFE), the super cell option of WIMS-D5 is used. The representative cell is modeled with 9 regions as shown in Figure 5 (b). The Tables 4 and 5 show the characteristics of the SFE and CFE, respectively.

The macroscopic cross-section data were generated by the WIMSD-5B code as function of fuel temperature and coolant temperature to Beginning of Life (BOL) core. Three fuel temperatures and three coolant temperatures were chosen in order to cover a large set of core conditions for normal and transient conditions. Tab 6. Presents values of isotopes concentration in U_3Si_2.

The WIMS-D5 with 69-group microscopic cross section (XS) library was run using the SLAB geometry option. The cell XS was generated for 69-Group and then collapsed to the desired number (2 and 4 energy groups).

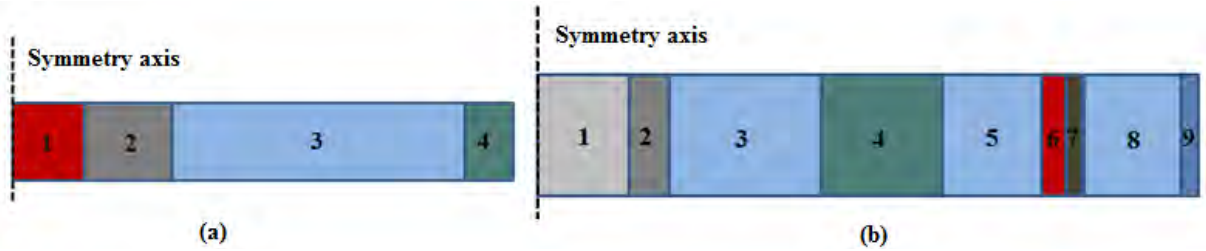

Fig 5. (a) Standard Fuel Element (SFE) unit cell and (b) Control Fuel Element (CFE) unit cell for WIMSD-5B lattice code

Type	Region	Length (cm)	Material	Isotope	Concentration (atoms/barn.cm)
Fuel	1	0.0305 (*)	U_3Si_2-Al	(**)	(**)
Cladding	2	0.037	Al	Al	6.02442×10^{-2}
Moderator/ Coolant	3	0.1225 (*)	H_2O	H O	6.67462×10^{-2} 3.33731×10^{-2}
Extra Region	4	0.02047 (*)	H_2O+Al	H O Al	2.26389×10^{-2} 1.13195×10^{-2} 3.98094×10^{-2}

(*) thickness half.
(**) available data in the Table 6 in function of the uranium density.

Tab 4: Standard Fuel Element (SFE) unit cell

Type	Region	Length (cm)	Material	Isotope	Concentration (atoms/barn.cm)
Absorber material	1	0.225 (*)	Ag-In-Cd	^{107}Ag ^{109}Ag In Cd	2.25711×10^{-2} 2.09773×10^{-2} 7.67108×10^{-3} 2.61208×10^{-3}
Cladding	2	0.1	SS-304	Mn Si Ni Cr Fe C Mo Co	1.37620×10^{-3} 6.38380×10^{-4} 7.67040×10^{-3} 1.58100×10^{-2} 5.54450×10^{-2} 1.05610×10^{-4} 7.94240×10^{-5} 1.63530×10^{-4}
Water	3	0.375	H_2O	H O	6.67462×10^{-2} 3.33731×10^{-2}
Rod guide	4	0.30	Al		6.02442×10^{-2}
Channel water between fuel plates	5	0.1225 (*)	H_2O	H O	6.67462×10^{-2} 3.33731×10^{-2}
Fuel	6	0.0305 (*)	U_3Si_2-Al	(**)	(**)
Cladding	7	0.037	Al	Al	6.02442×10^{-2}
Moderator/ Coolant	8	0.1225 (*)	H_2O	H O	6.67462×10^{-2} 3.33731×10^{-2}
Extra Region	9	0.02047 (*)	H_2O+Al	H O Al	2.26389×10^{-2} 1.13195×10^{-2} 3.98094×10^{-2}

(*) thickness half.
(**) available data in the Table 6 in function of the uranium density.

Tab 5: Control Fuel Element (CFE) unit cell

ρ(U) g/cm^3	Concentration (atoms/barn.cm)					U Mass ($\times 10^4$ g)
	U-234 ($\times 10^{-5}$)	U-235 ($\times 10^{-3}$)	U-238 ($\times 10^{-3}$)	Si ($\times 10^{-3}$)	Al ($\times 10^{-2}$)	
2.4	1.1405	1.1444	4.5802	3.8164	4.8209	3.2428
3.0	1.4257	1.4305	5.7253	4.7705	4.5196	4.0535
3.6	1.7108	1.7166	6.8703	5.7246	4.2183	4.8642

Tab 6: Isotopes concentration of U_3Si_2

6. Results and Discussions

The RMB reactor model was firstly verified for the RELAP5-MOD3.3 code [7, 8]. Then, the model has been adapted to be simulated in the RELAP5-3D code. The RELAP5-3D was run with nodal kinetic model reaching the steady state of the 30 MW power operation value. In the kinetic modelling, it was used the cross section to 2 and 4 neutron energy group options. However, PARCS code doesn't have the option of the 4 neutron energy groups and therefore, in this case, it was calculated only to 2 neutron energy groups (thermal and fast). The PARCS was run alone. Figure 6 shows the normalized average power in function of axial length to RMB core. The RELAP5-3D (2 and 4 neutron energy groups) and PARCS (2

neutron energy groups) were compared with 3D CITATION diffusion code (4 neutron energy groups) [1] and the results showed good agreement. Figure 7 shows the average relative planar power density of RMB core to steady state value. In both codes (RELAP5-3D and PARCS) the results showed good agreement, observing that the difference between 2 or 4 neutron energy groups is very little and the RELAP5-3D and PARCS codes calculation were very similar.

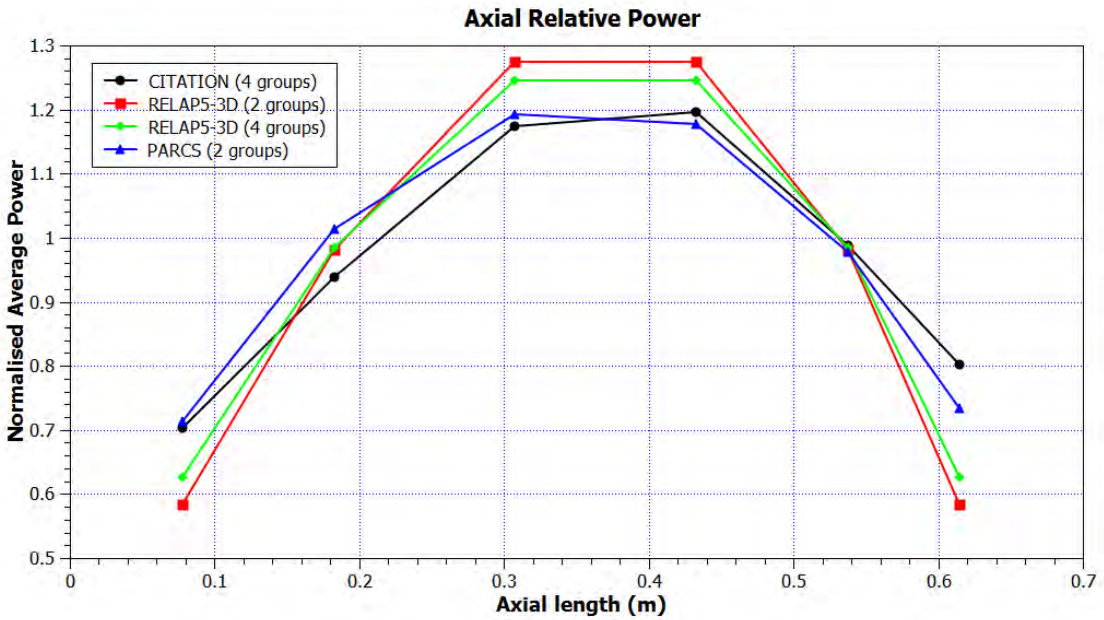

Fig 6. Comparison between axial normalised average power by CITATION, RELAP5-3D and PARCS

0.803 (1) 0.839 (2) 0.831 (3) 1.046 (4)	0.934 1.032 1.034 1.109	0.981 1.219 1.234 1.157	0.952 1.032 1.034 1.109	0.890 0.839 0.831 1.046
0.937 1.047 1.045 1.124	0.931 0.828 0.822 1.026	0.000 0.000 0.000 0.000	0.939 0.828 0.822 1.026	1.010 1.047 1.045 1.124
1.062 1.253 1.261 1.174	1.106 1.027 1.029 1.096	1.052 1.005 1.011 1.100	1.114 1.027 1.029 1.096	1.140 1.253 1.261 1.174
0.988 1.047 1.045 1.124	0.978 0.828 0.822 1.026	0.000 0.000 0.000 0.000	0.987 0.828 0.822 1.026	1.070 1.047 1.045 1.124
0.909 0.839 0.831 1.046	1.040 0.828 1.034 1.109	1.101 1.219 1.234 1.157	1.063 1.032 1.034 1.109	1.012 0.839 0.831 1.046

Fig 7. Average relative planar power density of RMB core (upper view) generated by codes (1) CITATION, (2) RELAP5-3D (2 groups), (3) RELAP5-3D (4 groups) e (4) PARCS (2 groups), respectively

7. Conclusions

The Brazilian Multipurpose Reactor (RMB) will have many functions with the main utilization for radioisotopes production to medical applications. Several characteristics of the OPAL reactor have been used in the initial project of the RMB. The development of the RMB is on the initial phase of theoretical calculations.

The thermal hydraulic model in RMB was presented in this work using RELAP5-3D code. After several tests, the steady state operation condition was reached at 30 MW with all thermal hydraulic parameters in stable behaviour.

The kinetic modelling was developed to represent the RMB core to RELAP5-3D and PARCS codes. The steady state was reached and the axial and planar relative power was compared between them and with 3D CITATION diffusion code. The results, as axial as radial, showed good agreement between the 3 codes used.

Acknowledgments

The authors are grateful to CAPES, CDTN/CNEN, FAPEMIG and CNPq for the support. Thanks also to Idaho National Laboratory for the permission to use the RELAP5-3D computer software.

References

[1] CNEN, Geração de seções de choque para o primeiro núcleo do Reator Multipropósito Brasileiro, Relatório técnico: RMB-10100-RD-003.00, Internal Document. CNEN, Brazil, 2010.

[2] ANSTO, Preliminary safety analysis report for ANSTO replacement research reactor facility, 2001.

[3] CNEN, Divisão de fabricação e projeto. Internal Document, CNEN, Brazil, 2012.

[4] The RELAP5-3D© Code Development Team, RELAP5-3D© Code Manual, INL, 2009.

[5] Joo, H. G. et al., PARCS: a Multi-dimensional two-group reactor kinetics code based on the non-linear analytic nodal method, PU/NE-98-26, Purdue University, 1998.

[6] Oak Ridge National Laboratory. WIMSD-5B.12 – Deterministic code system for reactor-lattice calculations, RSICC Computer Code Collection, 2007.

[7] Soares, H. V. et al., Analysis of Loss of Flow Events on Brazilian Multipurpose Reactor Using the Relap5 Code, International Journal of Nuclear Energy, Volume 2014, Article ID 186189, 12 pages, 2014.

[8] Soares, H. V., Avaliações de Segurança do Reator Multipropósito Brasileiro, Doctor Thesis, Universidade Federal de Minas Gerais, Belo Horizonte, Brasil, 2014.

A FULL CORE HOMOGENIZATION APPROACH USING SERPENT AS A CROSS SECTION GENERATION TOOL FOR THE OSCAR-4 CODE SYSTEM

B. ERASMUS, R.H. PRINSLOO, F.A. VAN HEERDEN, S.A. GROENEWALD, C. JACOBS
Radiation and Reactor Theory, Necsa, Building P-1900
P.O. Box 582, Pretoria 0001, South Africa

M. MASHAU
Department of Physics, University of Johannesburg, C1-Lab 140
P.O. Box 524, Auckland Park, 2006, South Africa

ABSTRACT

OSCAR-4 is a nodal diffusion based deterministic code system used for research reactor operational support. The system is used to perform routine core follow and reload calculations for each reactor cycle. In these small heterogeneous cores, typically encountered in research reactors, homogenization and equivalence theory play an important role. The effect of the environment in which an assembly's homogenized parameters are generated, has a large impact on the overall accuracy of the core simulation. Thus, generating few-group equivalence parameters, such as face discontinuity factors, in an infinite lattice or approximate colorset environment, is often not sufficient to capture the true assembly environment in the full core simulation. Currently, the OSCAR-4 system uses a low-order interface current, collision probability based lattice code, HEADE, to generate homogenized cross sections and discontinuity factors for the diffusion core simulator, MGRAC. HEADE suffers from some geometric limitations as well as the low-order coupling between cells in the geometry, limiting the code to small colorsets and resulting in the incorrect treatment of anisotropic effects in the lattice calculation. To overcome the shortcomings of HEADE, a link between the Monte Carlo code Serpent and the OSCAR-4 code system was developed. With this new development, Serpent can be used as a lattice code in the OSCAR-4 code system and without the geometric limitations present in HEADE, large colorsets or full core models can be used to generate equivalence parameters for the core simulator. In the work presented here, Serpent was used to produce few-group equivalence parameters for research reactor applications using 2D full core models. These homogenized parameters were then used in the core simulator to follow reactor operations and model various experiments such as control rod calibration experiments. The results of the calculations are compared to plant data obtained from experiments done during reactor operation.

1 Introduction

Deterministic reactor calculational code systems based on nodal diffusion theory, traditionally follow a two stage approach to simulating reactor cores. The first stage of the calculational scheme is homogenization on the assembly level, to produce spatially homogenized and energy condensed assembly cross sections for each reactor component through a transport calculation. In the second stage, the produced homogenized cross sections are used in a diffusion calculation to simulate the full reactor core. The aim of homogenization is to reduce the complexity of the problem by averaging the assembly cross sections, while preserving integral quantities from the transport calculation.

Diffusion theory, with homogenized cross sections alone, cannot preserve all integral quantities such as the reference transport reaction rates. To fully preserve the transport

reaction rates, additional homogenized parameters are required in the diffusion calculation. These requirements gave rise to the development of equivalence theory by Koebke [1] and subsequently Smith [2], where transport reaction rates can be preserved through assembly face discontinuity factors. In this approach, leakages and fluxes are calculated on the faces of the assembly in the transport calculation. An equivalent diffusion calculation of the problem is then performed, using the transport leakages in the diffusion calculation, to determine the diffusion flux.

One implication of this method is that the environment in which the transport calculation is performed should be a good approximation of the true environment in which the assembly will be in the full core calculation. This is because the equivalence parameters generated from the transport calculation, will only fully preserve the reaction rates of the environment in which the reference transport calculation was performed. Assembly level calculations are, however, typically performed in an infinite lattice environment for fuel assemblies and small colorset environments for non-fuel assemblies such as reflectors. Because of these approximate environments, the reference flux and leakages could differ significantly from the critical state that the assembly will be in during the core calculation.

To remedy this situation, approximations to the boundary conditions can be used such as albedos, or critical buckling can be used to adjust the multiplication factor in the reference problem to that of the core calculation [3]. Alternatively, the reference transport calculation may include more elements from the core environment of an assembly, to better approximate the assembly's true core environment. Recently calculational schemes have developed that follow the latter approach [4], including the use of Monte Carlo methods to generate homogenized parameters [5, 6, 7]. The use of Monte Carlo methods to generate homogenized parameters, eliminates the limitations and approximations encountered when deterministic transport is used in homogenization calculations. It is on the basis of the success of these schemes, that a link between the OSCAR-4 [8] code system and the Monte Carlo based code Serpent [9] was developed to generate homogenized assembly parameters in their reference core environments.

In this paper, the methodology of generating cross sections for assemblies in full core environments, using Serpent, is described. Results are given for two research reactor applications in the sections that follow, where the homogenized cross sections were used in the rest of the OSCAR-4 code system to simulate the reactor cores.

2 Tools

2.1 OSCAR-4

The OSCAR-4 code system follows the same two phase approach to reactor core simulations as described before. OSCAR-4 consists of transport codes, HEADE and STYX, which are used to perform the assembly homogenization calculations, a diffusion code, MGRAC, used to perform full core simulations and some utility codes to process the homogenized cross section library. HEADE is a collision probability based code which uses a low-order interface coupling between cells in the geometry. The code performs well when calculating homogenized parameters for assemblies where isotropic scattering dominates, but assemblies in which highly anisotropic effects are present, presents a challenge to its solution method. HEADE suffers from some geometric restrictions, limiting the code to the solution of single assembly problems or small colorset problems consisting of a few assemblies. STYX is a full collision probability code, but is limited to 24 group calculations. Compared to HEADE, STYX has more geometric flexibility, and is typically used to model control assemblies in more detail. HEADE uses the 172 group WIMS-E cross section library, while the 24 group library used by STYX, is generated from a spectrum calculation in HEADE, collapsing the material cross sections from 172 groups to 24 groups. To overcome

the limitations in HEADE and STYX, a link between the Monte Carlo based code Serpent and the OSCAR-4 code system was recently developed. This link allows Serpent to be used as a cross section generation tool for the diffusion code MGRAC, without the limitations present in HEADE. The core simulator, MGRAC, is a nodal diffusion code that uses an analytic nodal method to solve the diffusion equation.

2.2 Serpent

Serpent is a continuous-energy, Monte Carlo reactor physics burnup calculation code, which uses ACE format cross section libraries [9]. The code was created at VTT Technical Research Centre of Finland, and is currently still under development. A beta release of v2.1.15 was used to perform this study.

2.3 OSCAR-Serpent link

In order to connect Serpent to the rest of the OSCAR-4 code system, output is processed into the same file format used by the existing lattice code HEADE. A pre- and post-processor was developed for Serpent that eases the input creation and output processing. To help judge the convergence of the results, the post-processor prints a summary of the (statistical) relative error for all the quantities of interest, and performs a balance check in each node for which cross section sets are edited.

Serpent is responsible for calculating node averaged cross sections and surface averaged fluxes and net leakages. The diffusion to transport equivalence parameters (discontinuity factors) are calculated by a separate tool. Currently, the OSCAR-Serpent link cannot perform depletion and off-base calculations, so it is restricted to non-fuel components in the core. This restriction will be lifted in future versions.

3 Models

3.1 OSCAR-4 SAFARI-1 models

The SAFARI-1 reactor is a 20 MW tank-in-pool type MTR. An 8 x 9 core grid houses 26 fuel elements, 6 control rods, several in-core irradiation facilities and reflector elements. The size of the core is roughly 65 x 65 x 60 cm, with a fuel pitch of 7.71 x 8.1 cm. The core is fuelled with flat-plate MTR type low enriched uranium fuel assemblies and the control assemblies are follower-type, with a fuel element attached to the bottom of each cadmium absorber element. Figure 1 is a schematic representation of this reactor, with the control rods numbered as shown in the figure.

All cross sections for the *standard SAFARI-1 model* are generated with the HEADE transport code, with the exception of control rod cross sections, which are generated with both HEADE and STYX. All cross sections are homogenised by the standard flux-volume weighting method, however discontinuity factors are only generated for the fuel materials. The fuel is modelled in an infinite fuel environment. All other materials are modelled as 2-node problems consisting of a fuel element adjacent to the element for which cross sections are calculated. This core model has roughly 20 cm of water around the core, followed by a black boundary condition. The water region is divided into three water nodes, and the core box and first water node are homogenised together.

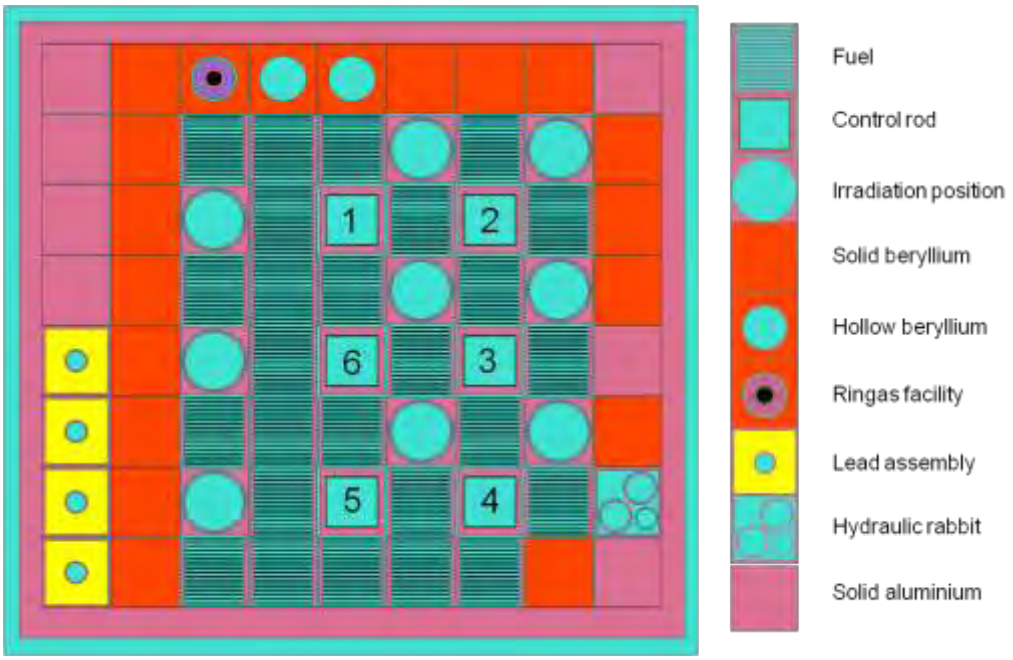

Fig 1. Schematic top view of the SAFARI-1 research reactor.

The construction of the *Serpent-based OSCAR-4 SAFARI-1 model* follows a particular philosophy associated with a developed OSCAR-Serpent link. This modelling approach entails, firstly, the development of a SAFARI-1 3D Serpent model based on the engineering description of the reactor. Thereafter, a selection of a relevant set of full-core 2D radial cuts of the SAFARI-1 core are taken from this 3D Serpent model, representing the various levels of axial heterogeneity present in the core. Nodal equivalence parameters are generated on a spatial grid in accordance with the full-core nodal diffusion model. In this case two 2D cuts, namely a core centre-line cut for an all rods in (ARI) case, and a centre-line cut for an all rods out (ARO) case are selected.

Full-core 2D Serpent calculations of each of these full-core 2D slices are performed, generating in the process the set of nodal equivalence parameters for each node (or core-grid component) present in the 2D cut. Given that the core-diffusion model of the SAFARI-1 core is designed on a 15 x 14 grid, 210 sets of nodal parameters are generated per 2D cut.
Construction of the 3D nodal diffusion model then proceeds by integrating the various 2D nodal equivalence parameter sets. The nodal diffusion model is constructed with 12 axial layers, with 8 layers in the fuel and 2 reflector nodes above and 2 reflector nodes below the active core and vacuum boundary conditions both radially and axially. A 3D model is constructed by combining cross sections from the two 2D cuts and axially constructing the 3D model with these building blocks. In particular:

- The ARO case is used as a base representative 2D cut, from which the majority of the core diffusion model is constructed as to retain the radial equivalence characteristics with the original Serpent transport calculation. However, the control rod absorber cross sections are taken from the ARI case, as these are not present in the ARO case.

- Fuel element and fuel follower element component models are taken from the HEADE models for each of these components, to replace the fuel element models from Serpent. This is done to allow microscopic burn-up and state dependent cross sections to be used for the fuel models, since these cannot as yet be generated through the OSCAR-Serpent link. The HEADE based fuel models are generated with reflective boundary conditions around the element, as this is still a reasonable approximation for fuel elements which move to different positions from cycle to cycle.

Note that the usage of an “infinite lattice environment” introduces an environmental error associated with the fuel models.

These sets of cross sections then allow for a complete 3D nodal diffusion model, which can be used to perform core reload, core follow and experimental comparison calculations. All the parameters generated for the diffusion models, are generated in six energy groups.

3.2 OSCAR-4 ETRR-2 models

ETRR-2 is a 22 Mega-Watt pool-type research reactor. It is fuelled with 29 low enriched uranium fuel assemblies, cooled and moderated with light water and reflected with beryllium. The reactor control mechanism consists of six control blades/rods made of a silver-indium-cadmium (AgInCd) alloy. The core has a central irradiation position and is surrounded with a core box containing the second shut down system -- chambers in the core box that can be filled with gadolinium (Gd). Figure 2 shows a top view of the reactor with the control rods inserted. The control rods are numbered 1 to 6 from top left to bottom right.

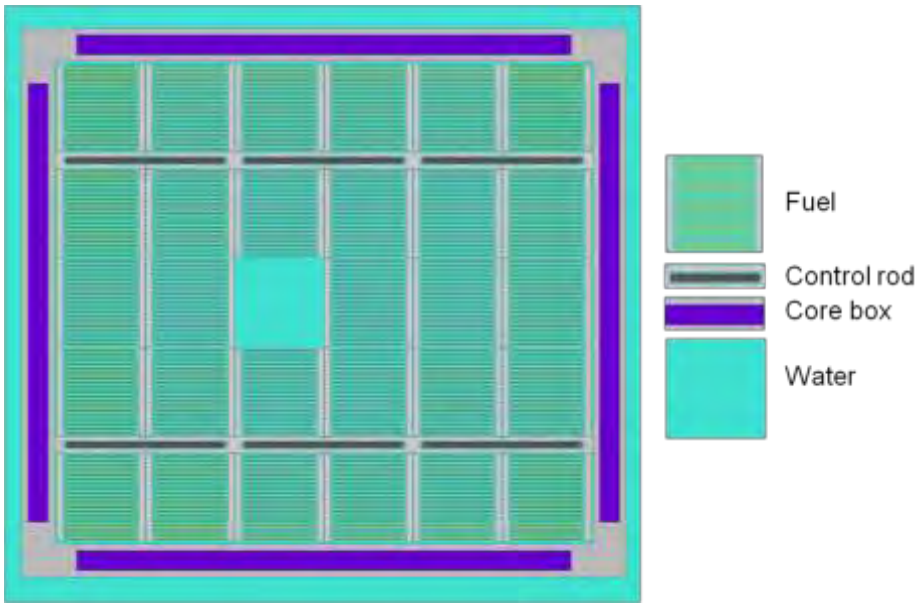

Fig 2. Schematic top view of the ETRR-2 research reactor.

Homogenized parameters for the *standard ETRR-2 model* are generated using HEADE only, with white boundary conditions for all configurations. Fuel assembly parameters are generated in an infinite lattice environment for the three different fuel types used during commissioning. Control rod parameters are generated from three-node colorset calculations, with two fuel assemblies on either side of a control rod. The central irradiation position and second shut down systems are modelled with a 3x3 colorset configuration and a 1x3 colorset configuration, respectively. In the 3x3 colorset, the irradiation position is surrounded with fuel assemblies and the 1x3 colorset calculation for the second shutdown system consists of a single fuel assembly, the core box structure and water outside of the core box.

In the *Serpent-based model*, a 2D full core calculation is performed with Serpent, to generate homogenized parameters for all non-fuel components including the central irradiation position, control rods, second shutdown system and the water reflector beyond the core box. Fuel assembly parameters for the three different start-up fuel types, are taken from the calculations performed for the *standard model*.

3.3 Serpent models

The *Serpent reference models* consist of fully detailed 3D models for both SAFARI-1 and ETRR-2, including all core component structures, core grid plate and assembly handling structures as well as ex-core structures, and is calculated using a high fidelity transport method. These models are used to perform the reference calculations to compare the *standard* and *Serpent-based models* to, for values that are not experimentally measured or available, such as core power distributions.

4 Results

4.1 SAFARI-1

Core follow calculations were performed for SAFARI-1 reactor operation during 2012 with the *Serpent reference model*, *standard model* as well as the *Serpent-based model*. Figure 3 shows the core multiplication factor calculated with all three models for core follow simulations for 2012.

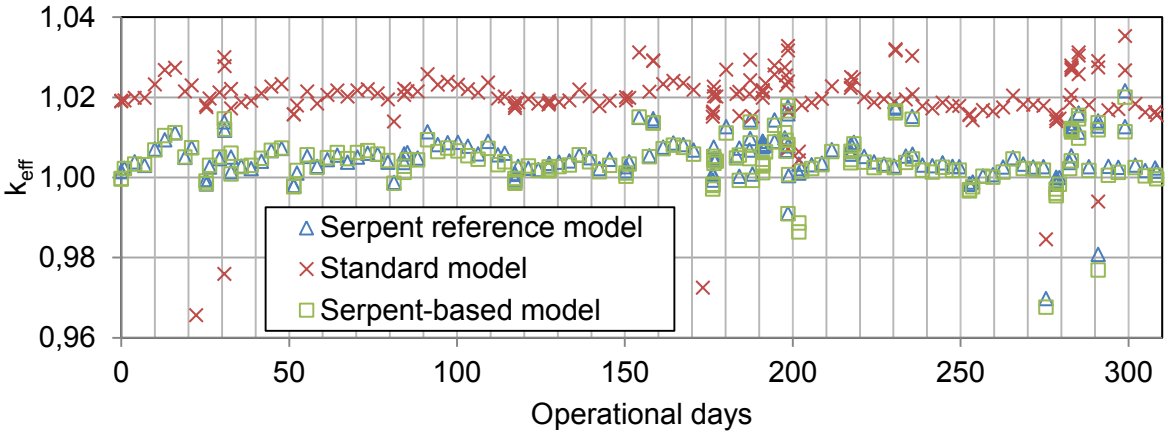

Fig 3. A comparison between the *Serpent reference model* and the *standard* and *Serpent-based models* core follow multiplication factor, for SAFARI-1 reactor operation during 2012.

For the 2012 operation period, the average multiplication factor calculated using the *Serpent reference model* is 1.00523 (std. dev. 509 pcm), while the same result calculated with the *standard model* is 1.01909 (std. dev. 630 pcm), and with the *Serpent-based model* is 1.00427 (std. dev. 523 pcm). These averages were obtained by filtering the core follow data to exclude shut- down and scram cases.

The core follow rod positions for all the models are generated from plant data which contain variations in rod position over time. The processing and averaging of the control rod positions from the plant data causes variations in the calculated multiplication factors. By subtracting the *Serpent reference* results from the *standard model* results and the *Serpent-based model* results, a better estimate of the variation in the multiplication factor can be found. This reduces the standard deviation of the *standard model* from 630 pcm to 286 pcm, and for the *Serpent-based model* the standard deviation is reduced from 523 pcm to 196 pcm.

To further investigate the differences between the *standard model* and the *Serpent-based model*, control rod calibration experiments were simulated over a two year period of operation (2012 – 2013). During this time seven control rod calibration experiments were performed, one experiment every three to four months. Figures 4, 5 and 6 show the control rod calibration curves for rods 2, 3 and 4 at the end of 2013.

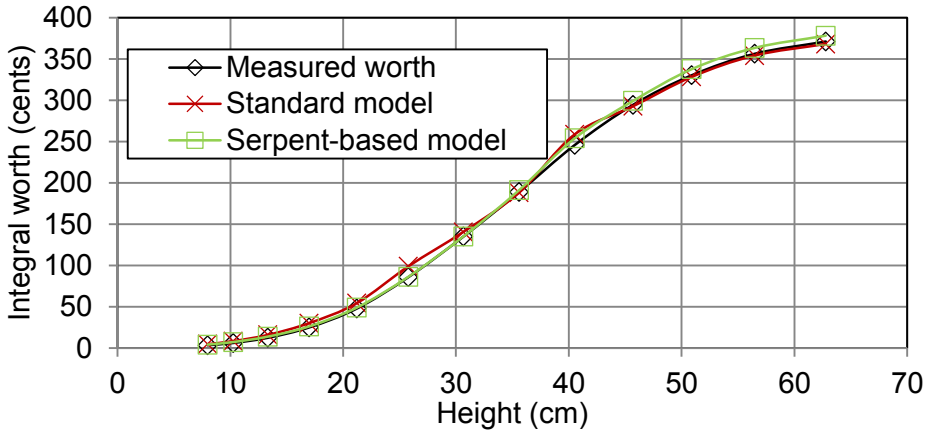

Fig 4. SAFARI-1 control rod 2 worth calculated using the *standard* and *Serpent-based models* compared to the measured worth.

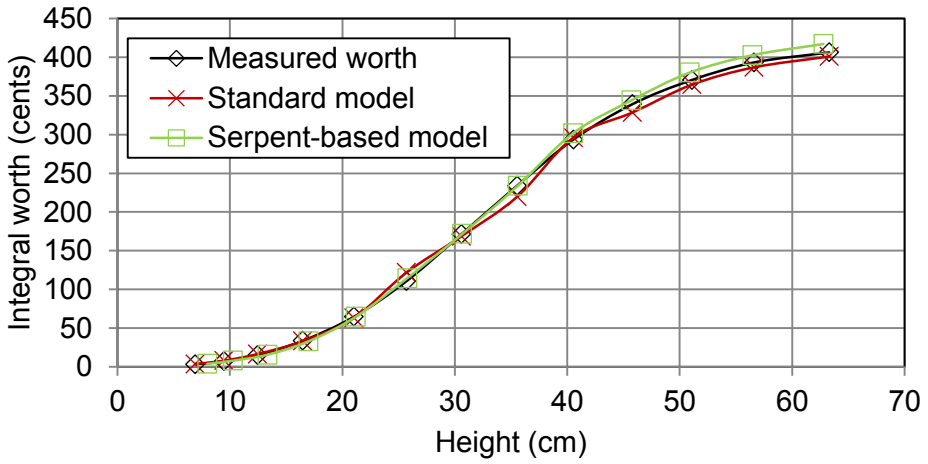

Fig 5. SAFARI-1 control rod 3 worth, calculated using the *standard* and *Serpent-based models* compared to the measured worth.

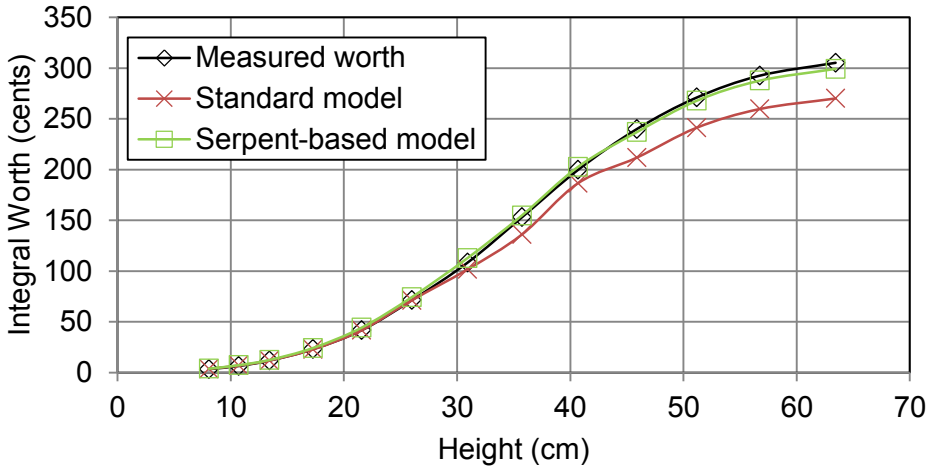

Fig 6. SAFARI-1 control rod 4 worth, calculated using the *standard* and *Serpent-based models* compared to the measured worth.

It is observed that the *standard model* underestimates the worth of the control rods 4 and 5, located at the south side of the core, when compared to the measured rod worth. The calculated worth of control rod 4 is shown in Figure 6 to illustrate the underestimation. This is due to the lack of equivalence parameters in the reflector nodes to the south of the core, where the fuel assemblies are adjacent to water nodes. As a result of this, the *standard model* does not account for the transport effects present at the fuel-water interface.

In comparison, the *Serpent-based model* predicts the worth of rod 4 (and rod 5) more accurately as compared to the measured worth, because the equivalence parameters present in the water nodes account for transport effects not captured in the *standard model*. Figure 6 shows the improvement in the predicted worth for control rod 4, compared to the measured worth.

Table 1 shows the measured total worth of all the control rods averaged over the two year operation period, and the average, maximum and standard deviation of the error for the *standard model* and the *Serpent-based model* compared to the measured worth. The table shows that the *Serpent-based model* improves the accuracy of the overall predicted control rod worth, with a lower average and maximum error as well as a lower standard deviation in the error.

Average measured worth (cents)	Standard model absolute error (cents)			Serpent-based model absolute error (cents)		
Average	Average	Maximum	Std. dev.	Average	Maximum	Std. dev.
2532.04	107.65	201.24	65.73	44.92	71.04	26.21

Tab 1: Comparison of error in SAFARI-1 control rod worth prediction, between the *standard* and *Serpent-based models*, over two years of reactor operation (2012--2013).

4.2 ETRR-2

The ETRR-2 reactor was chosen from the recently published IAEA research reactor benchmarks [10], as a test case alternative to the SAFARI-1 reactor. The ETRR-2 benchmark specification contains various commissioning core configurations and accompanying results for the experiments performed on those cores. In particular, core SU-29 was chosen from which the control rod calibration experiments were simulated and compared to the experimentally measured control rod worth. Table 2 contains a summary of the results for ETRR-2, comparing the standard and modified OSCAR-4 models, the Serpent reference model and the experimentally measured values.

Figure 7 shows a plot of the multiplication factor for each critical configuration during the control rod calibration of rod 5 (cases 1--12) and rod 6 (cases 13--18), calculated using the different models. The plot shows that the *Serpent-based model* has a smaller offset (from 1) than the *standard model*, and the variation in the calculated values is also lower as reported in Table 2. Assembly powers also show an improvement when compared to the *Serpent reference model*, with the maximum relative power error of 4.94% for the *standard model* decreased to 2.73% in the *Serpent-based model*.

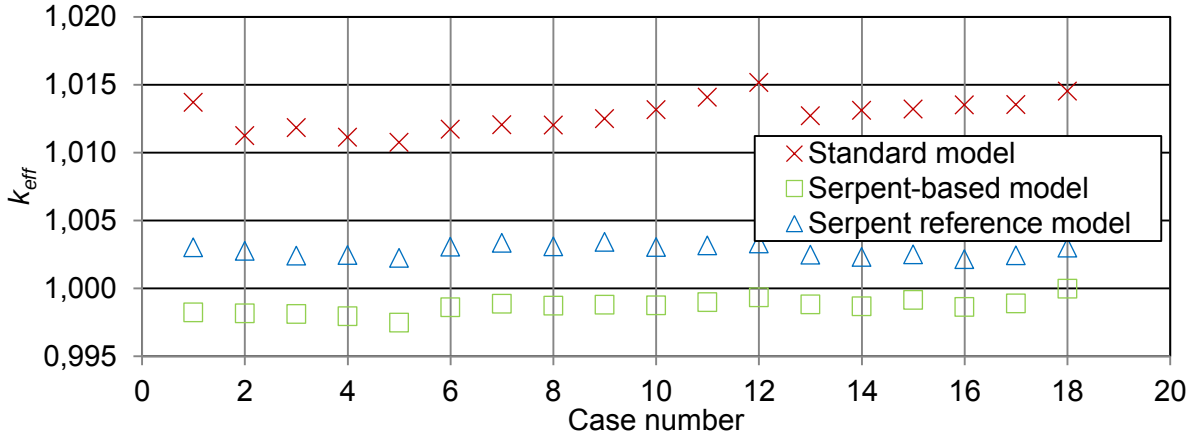

Fig 7. A comparison of ETRR-2 control rod calibration critical cases, between the *Serpent reference model* and the *standard* and *Serpent-based models*.

Model	Critical k_{eff} ± std. dev. (pcm)	Maximum power error (%)	Rod 5 worth ($)	Rod 6 worth ($)
Standard	1.01254 ± 128	4.94	3.28	0.95
Serpent-based	0.9985 ± 50	2.73	3.06	1.05
Serpent ref.	1.00294 ± 39	-	2.89	1.03
Experiment	-	-	2.17	0.86

Tab 2: Summary of the comparison between the standard, modified and Serpent models and experimentally measured quantities for the ETRR-2 research reactor.

Figures 8 and 9, show partial integral control rod worth curves for rod 5 and 6, comparing all the models and experimentally measured values. In both rod 5 and 6 the predicted control rod worth is higher than the measured values. Compared to the calculations done by Villarino et. al. [11], similar differences are obtained between the predicted control rod worth and the measured values. It is required to model the other commissioning cores with the current models to investigate these differences further. The calculated curves show that the rod worth, predicted by the *Serpent-based model*, is closer to those predicted by the *Serpent reference model* as compared to the *standard model*.

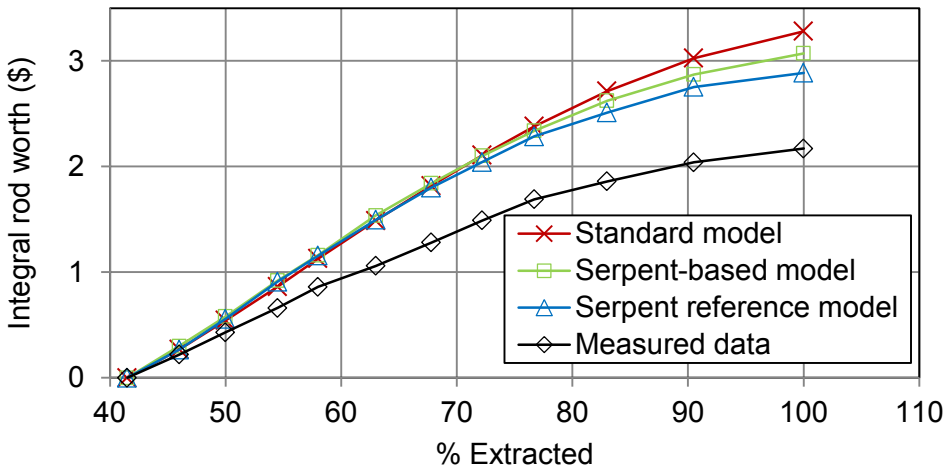

Fig 8. Comparison between calculated and measured integral control rod worth curves for ETRR-2 control rod 5 calibration.

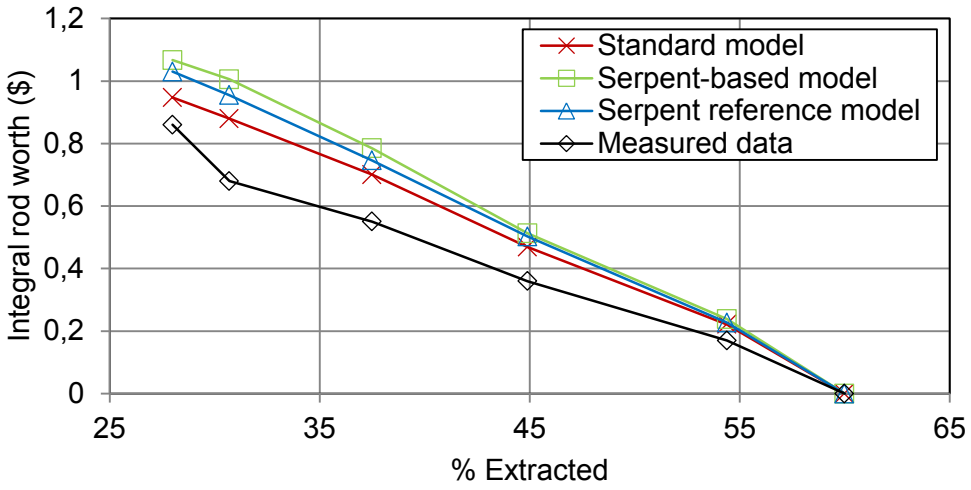

Fig 9. Comparison between calculated and measured integral control rod worth curves for ETRR-2 control rod 6 calibration.

5 Conclusions

A link was developed between Serpent and the OSCAR-4 system, and was used to generate homogenized assembly parameters for the core simulator MGRAC. This link allows the use of a high fidelity transport method to calculate radial equivalence parameters for assemblies in their true core environment, minimizing the environmental error in assembly parameters. With the ability to generate equivalence parameters from full 2D core calculations, important transport effects can be captured in the diffusion core simulation.

Results presented for the different modelling approaches show that the *Serpent-based model* improves the overall accuracy of the OSCAR-4 system for global parameters such as the multiplication factor, and for local parameters such as individual control rod worth in the case of SAFARI-1. Apart from the decreased offset in the multiplication factor, it can be seen from the core follow results that the predicted multiplication factor corresponds closely to that of the *Serpent reference model*, over the chosen period of operation.

In the case of ETRR-2, a similar improvement is seen in the calculated multiplication factor, and in the individual rod worth as compared to the reference Serpent calculation. Further investigation is required into the differences between the calculated values and the measured rod worth.

Benefits of the *Serpent-based model* include the use of different cross section libraries, such as different versions of the ENDF libraries in ACE format, for equivalence parameter generation, as the *standard model* currently only supports the use of the WIMS-E library.

6 References

[1] K. Koebke. A new approach to homogenization and group condensation. *IAEA-TECDOC–231*, 12:303–322, 1980.
[2] K.S. Smith. Assembly homogenization techniques for light water reactor analysis. *Progress in Nuclear Energy*, 17(3):303–335, 1986.
[3] R. Sanchez. Assembly homogenization techniques for core calculations. *Progress in Nuclear Energy*, 51:14–31, 2009.
[4] APOLLO2 year 2010. *Nucl. Eng. Tech.*, 42(5):474–499, 2010.

[5] E. Fridman and J. Leppänen. On the use of the Serpent Monte Carlo code for few-group cross section generation. *Annals of Nuclear Energy*, 38:1399–1405, 2011.
[6] H.J. Park, H.J. Shim, H.G. Joo, and C.H. Kim. Generation of Few-Group Diffusion Theory Constants by Monte Carlo Code McCARD. *Nucl. Sci. Eng.*, 172:66–77, 2012.
[7] E. Fridman and E. Shwageraus. Modeling of SFR cores with Serpent–DYN3D codes sequence. *Annals of Nuclear Energy*, 53:354–363, 2013.
[8] G. Stander, R.H. Prinsloo, E. Müller, and D.I. Tomašević. OSCAR-4 Code System Application to the SAFARI-1 Reactor. In *Proc. Conf. Reactor Physics, Nuclear Power: A Sustainable Resource, Interlaken Switzerland.* September 14–19, 2008.
[9] J. Leppänen. PSG2/Serpent – a continuous-energy monte carlo reactor physics burnup calculation code, 2012.
[10] IAEA research reactor innovative methods group (CRP). RR Benchmarking Database: Facility Specification & Experimental Data. In *IAEA Technical Report Series 480, IAEA Vienna*, 2014.
[11] E.A. Villarino, C. Lecot, and A. Enany. Comparison between experimental results and calculations during the commissioning of the ETRR2. In *Proc. Conf. Meeting of the Interanational Group On Research Reactors (IGORR), Bariloche Argentina.* October 26–29, 1999.

Neutronic Analysis of MTR Reactor Core using Monte Carlo Techniques

R. Khan[1*], R. Ali1, H. Boeck[2], T. Stummer[2]
1. DNE, Pakistan Institute of Engineering and Applied Sciences (PIEAS), Islamabad, Pakistan
2. Atominstitut, Vienna University of Technology, Vienna, Austria

ABSTRACT

The Pakistan Research Reactor –I (PARR) is a swimming pool type research reactor which operates since 1965. The initial core was loaded with 93% HEU fuel and started operation at 5 MW. Due to proliferation concerns, the HEU core was converted to a LEU core and the reactor power was upgraded to 9 MW in 1992 followed by a further uprating to 10 MW in 1998 using 19.99 % LEU Uranium Silicide (U3Si2-Al) fuel.

This paper presents a detailed three dimensional (3D) computer model of the reactor core and its validation against the reference results. For this purpose, the 3D Monte Carlo Computer code MCNP5 is used to simulate the fresh fuel loaded (so called first high power) reactor core. The simulated results of initial criticality, excess reactivity, shut down margin, control rod worth and flux density distribution are confirmed against the reference results. The comparison between simulated and reference results presents reasonably good agreement.

1 Introduction

There are two main kinds of the nuclear reactors being operated worldwide, power reactors and research reactors. Power reactors are used for the production of electricity; hence they have large cores with large thermal power output. They operate on the continuous basis till their refueling time so that electricity is provided continuously. On the other hand, research reactors are operated purely for the purpose of research, material testing and production of radioisotopes. Thus these reactors have small cores and they are operated intermittently. A nuclear reactor is operated by keeping it critical at all the times .i.e. the fission chain reactor proceeds at a constant neutron population rate and energy is releases at a uniform level [1]. For attaining this goal, mass of fissile material in the core is kept greater than the critical mass, which is the mass required to keep the system critical [2]. If a reactor core is loaded with mass equal to critical mass, first fission would render the system subcritical [2]. To avoid this situation, mass of fissile material in the core is always kept greater than the critical mass. With this greater mass, the reactor will become supercritical so to ensure that reactor remains critical for a fixed period of time .i.e. during core lifetime, neutron absorbing material is required [2].

With the excess reactivity present in the reactor core, it is necessary that appropriate safety margin is present. From neutronics point of view, this means that appropriate control absorbing material is present so that reactor can be shut down in the accidental case. From thermal hydraulics point of view, the neutron flux and power peaking should be within limits so that there is no hotspot in the core [3]. Therefore it is necessary that during the design phase of a reactor core, reliable analysis is made regarding neutronics of the core. Two methods widely used for the neutronics analysis are the deterministic method and the probabilistic method. In deterministic methods, neutron diffusion equation is solved to obtain the desired results, while in the probabilistic methods, actual neutron behavior is simulated.

This paper focuses the analysis of a MTR equilibrium core using probabilistic method. In this work,

Monte Carlo (MC) code MCNP5 is applied to develop a detailed computer model of the PARR-! Reactor core.

2 Deterministic vs Probabilistic Method

When compared with the deterministic methods, MC methods provide many advantages over the deterministic methods. The inaccuracies of diffusion equation and the imperfect modeling of the geometry, in the deterministic methods, give an upper hand to the stochastic MC method. The basic advantage of MC is the accurate and easy modelling of complex geometry. The approximations are few in MC as compared to the deterministic [4]. Deterministic methods require a simple geometry so that the method can converge and they use multi-group approximations for representing continuous energy neutron cross-sections. MC uses continuous energy cross-sections. The disadvantage of the MC method is that they provide an approximate solution to the problem, being statistical in nature. The solution is never exact and there is a small statistical error associated with it [4]. Probabilistic methods are also very time-consuming. Deterministic methods give an exact solution to an approximate model of the problem while MC methods give an approximate solution to an exact model of the problem [4]. An elaborate comparison between deterministic and MC methods is given by P. Vaz [5].

The concept of homogenization is used in deterministic codes. The heterogeneities in the reactor system are lost when the zones are homogenized. Homogenization refers to the concept where based on number densities and volume fractions, all of the materials in heterogeneous system are mixed together to form a uniform composition. Hence the local geometrical heterogeneities are lost, this is also counted as a major drawback of deterministic codes [6]. Geometry is exactly modeled in MC while it is approximated due to homogenization in deterministic method. Neutron energy treatment is also exact in MC due to usage of point cross-sections.

3 Materials Testing Reactor (MTR)

PARR – I is a swimming pool type Material Testing Reactor (MTR). The reactor core is moderated and cooled via demineralized water [7]. It achieved its first criticality in 1965 with 93% Highly Enriched Uranium (HEU) fuel. Later it was converted to Low Enriched Uranium (LEU) fuel with 19.99% enrichment of ^{235}U [8]. PARR-1 reactor utilizes the Uranium Silicide (U_3Si_2-Al) fuel. The core of PARR – I contains two types of Fuel Elements (FEs). One is the Standard Fuel Element (SFE) and the other is Control Fuel Element (CFE). SFE contains only fuel while CFE contains control absorber rod in addition to the fuel. Equilibrium core configuration of PARR – I is shown in Figure 1.

The core contains 29 SFEs and 5 CFEs. There are two flux irradiation sites present in the core locations C7 and C4. These sites are also called flux traps since thermal flux peaks in these locations. The flux value maximum at the location C7 as it is located at nearly centre of the core. The core also has two Fission Chambers at one end of the core. On one side of the core, nine GREs are present which act as neutron reflector. On the opposite face of the core, there is Graphite thermal column present as reflector.

Control absorber rod is rectangular in the direction parallel to fuel meat while it has semi-circular contours in direction perpendicular to fuel meat. Control absorber is made up of 80.5% natural Silver, 14.6% natural Indium and 4.9% natural cadmium [9].

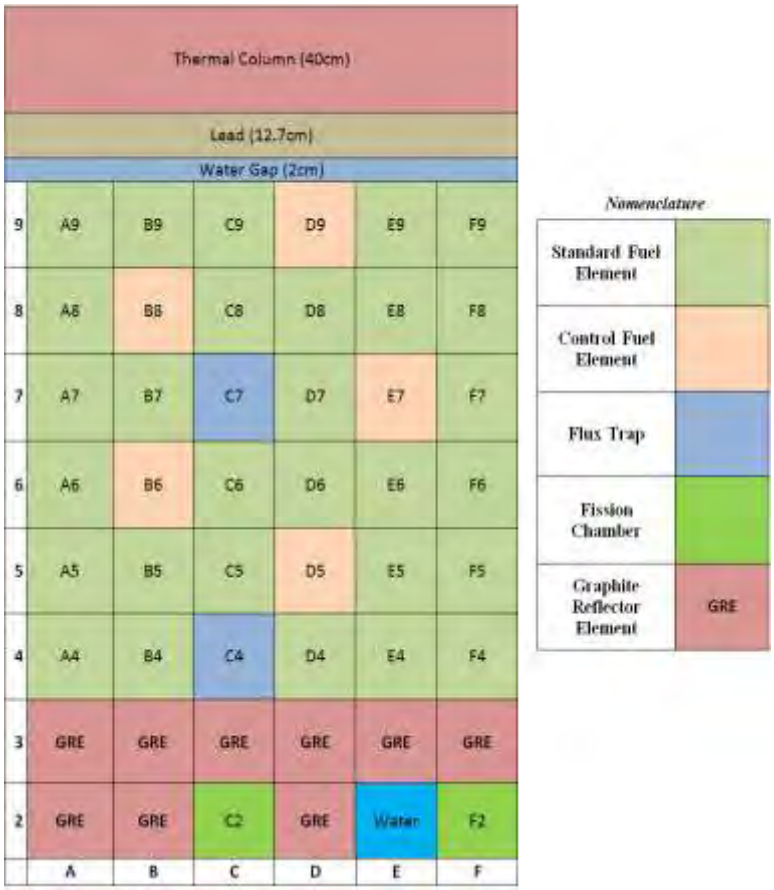

Figure 1: Equilibrium core configuration of PARR – I.

Table 1 lists the design parameters of PARR – I fuel.

Table 1: Description of PARR – I fuel parameters [8].

Parameter	Description
No. of Fuel Plates	
. Standard Fuel Element	23
. Control Fuel Element	13
Thickness of the Plates (*mm*):	
. Inner Plates	1.27
. Outer Plates	1.50
Fuel Meat Dimensions (*mm*):	
. Length	600
. Width	62.75
. Thickness	0.51
U^{235} Contents (*g*):	
. Standard Fuel Element	290
. Control Fuel Element	164
. Fuel Plate	12.61
Uranium density in Fuel Meat (*g/cc*)	3.325
U-235 density in Fuel Meat (*g/cc*)	0.657
Water Channel Thickness (*mm*)	2.10

4 Calculation Methodology

4.1.1 Monte Carlo N-Particle computer code

Monte **C**arlo **N**-**P**article (MCNP) is a general-purpose Monte Carlo based stochastic computer code. MCNP solves particle transport problem therefore it can be used for the transport neutron, photon, and electron separately, or coupled neutron/photon/electron transport [10]. Its capability to calculate eigenvalues for critical systems is exploited in this work. Rather than energy groups (as in deterministic techniques), MCNP uses a continuous energy concept with point-wise cross-section data [10]. The neutron energy ranges from 10-11 MeV to 20 MeV. MCNP has detailed tally capabilities e.g. neutron flux, fission energy, dose calculations can easily be performed [11].

The MCNP uses infinite surfaces for constructing 3D geometry of the system to be modeled.These surfaces then intersect and hence define the boundaries of finite volume elements called cells [12].

4.1.2 Coupling of Codes

Since MCNP5 only deals with static problems so WIMS/D4 is coupled with it to have a package that performs dynamic calculations. WIMS/D4 has the only purpose of providing the number densities for burnt fuel. Appropriate number densities are then picked up and used as input to the probabilistic code MCNP5.

4.1.3 MCNP Model of the PARR-1 Core

A detailed 3D MCNP model of the reactor core has been shown in the Figure 2. It includes 29 SFEs, 5 CFEs, two flux irradiation sites present in the core locations C7 and C4. The core also has two Fission Chambers at one end of the core. On one side of the core, nine GREs are present which act as neutron reflector.

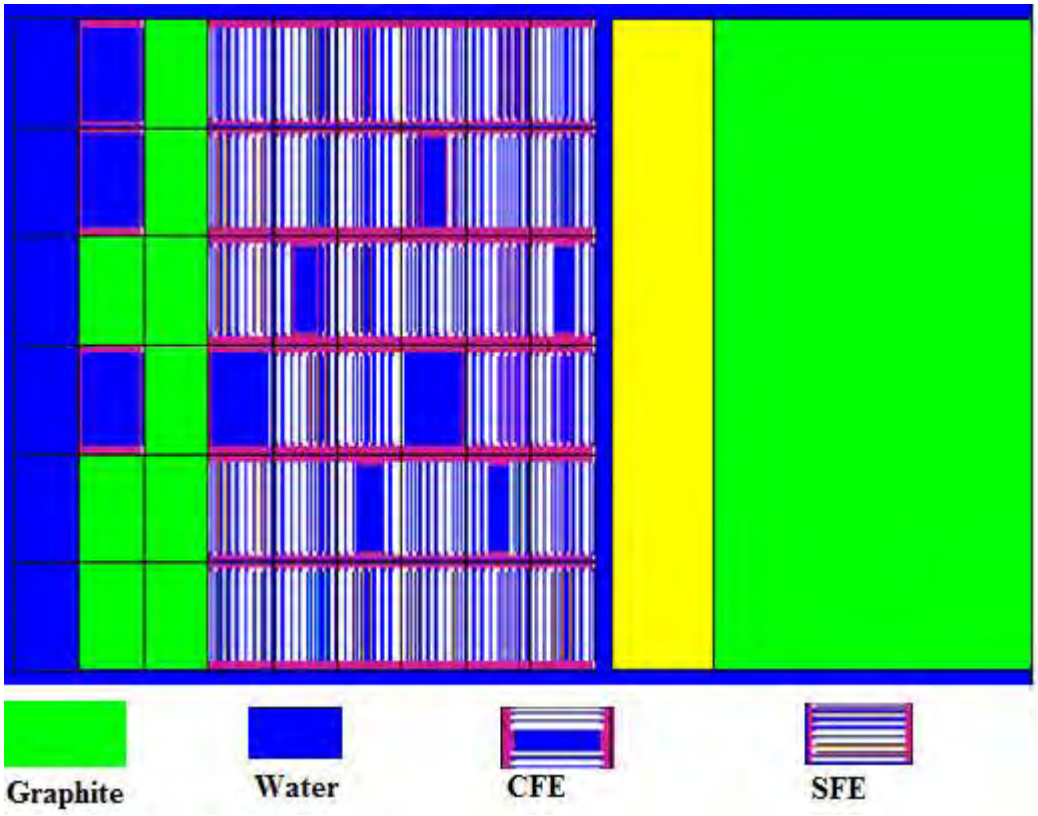

Figure 2: MCNP model of the PARR-1 reactor core.

5 Results and Discussion

The results for the equilibrium core include the calculations of excess reactivity, shutdown margin, combined control rod worth and neutron flux.

The results for these parameters using MCNP5 are given in Table 2. The standard deviation in the results of MCNP5 is also shown. Since MCNP5 is a probabilistic code therefore there is always a statistical fluctuation associated with the result. This statistical fluctuation is incorporated in standard deviation. The percent error in excess reactivity is 5.27% and it is on the positive side .i.e. value obtained by MCNP5 is over-estimated when compared to reported value [9]. For shutdown margin, percent error is 7.05% and it is on the negative side. For combined control rod worth, error stands to be 1.32%.

Table 2: Results calculated using MCNP5.

Parameters (pcm)	Reported [9]	MCNP5	Relative Error (%)
Shutdown margin	5760.00	5354.10 ± 19.98	-7.05
Excess Reactivity	5000.00	5263.56 ± 19.74	+5.27
Combined Worth	10760.00	10617.65 ± 28.09	-1.32

Now based on the previous results, with MCNP5 providing good results, the three-dimension total flux distribution is plotted. Figure 2 below shows the 3D distribution of neutron flux in the core. The X and Y co-ordinates in the Figure are according to the core configuration (shown in Figure 1). The flux peaks at the location C7 where inner irradiation site exists.

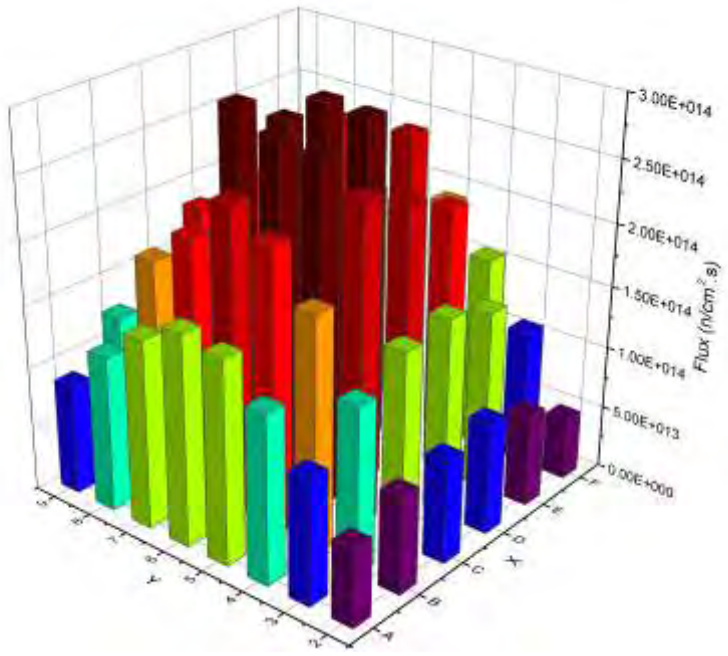

Figure 2: 3D flux distribution obtained using MCNP5.

6 Conclusions

In this work, neutronics study of the PARR – I is performed using probabilistic method. The developed model is verified against the available reported data. The parameters compared are excess reactivity, shut down margin, total control rod worth. The results conclude that the combination of lattice transport code WIMS/D4 and Monte Carlo computer code MCNP5 provides satisfactory results for further anayses. The confirmed model can be modified to other core configurations of the reactor.

7 References

[1] S. Glasstone and A. Sesonske, *Nuclear Reactor Engineering*. Canada: D. Van Nostrand Company, Inc., 1967.

[2] J. R. Lamarsh and A. J. Baratta, *Introduction to Nuclear Engineering*, 3rd ed. USA: Prentice Hall, Inc., 2001.

[3] J. J. Duderstadt and L. J. Hamilton, *Nuclear Reactor Analysis*. USA: John Wiley & Sons, Inc., 1976.

[4] H. Nifenecker and et al., *Accelerator Driven Subcritical Reactors*. Bristol, UK: Institute of Physics, 2003.

[5] P. Vaz, "Monte Carlo Methods and Techniques Status and Prospects for Future Evolution," *Applied Radiation and Isotopes,* vol. 68, pp. 536-541, 2010.

[6] H. Omar, K. Khattab, and N. Ghazi, "Neutron Energy Specta calculations in the Low Power Research Reactor," *Indian Journal of Pure and Applied Physics,* vol. 49, pp. 723-730, 2011.

[7] T. Hamid, "Reactor Kinetics Parameters as a Function of Fuel Burnup," PIEAS-445, Reactor Analysis Group, PIEAS 1999.

[8] R. Khan, T. Hamid, and S. Bakhtyar, "Feedback Reactivity Coefficients and their Coupling," *Nuclear Engineering and Design,* vol. 237, pp. 972-977, 2007.

[9] Nuclear Engineering Division, "Safety Analysis Report of Pakistan Research Reactor-1," Pinstech 2001.

[10] Los Alamos National Laboratory. (2010, 27 August, 2014). *A General Monte Carlo N-Particle (MCNP) Transport Code*. Available: https://mcnp.lanl.gov/

[11] X5 Monte Carlo Team, "A General Monte Carlo N-Particle Transport Code, Version 5," Los Alamos National Laboratory, USA 2003.

[12] X5 Monte Carlo Team, *"Criticality Calculations with MCNP5: A Primer"*. Los Alamos National Laboratory.

ASSESSMENT OF THE BURNOUT PHENOMENON IN THE SAFARI-1

M. BELAL and A.J. D'Arcy
South African nuclear energy corporation
Church street west, Pelindaba, Pretoria 0001 - South Africa

ABSTRACT

The analysis of transients for the SAFARI-1 research reactor is done using the RELAP5/SCDAPSIM Mod3.4 system code, while the analysis of critical phenomena associate with the Critical Heat Flux (CHF) is done using available correlations within the code, such as the AECL look-up tables, or from literature such as Sudo and Mishima correlations discussed and applied in this work.

In this paper a proposal is made on the application of the Sudo scheme of correlations to predict CHF conditions, supplemented by the AECL look-up tables. The application was used to evaluate the low flow burnout phenomenon that may occur during the beyond design loss of flow accident.

In applying the scheme and during the course of the transient, various validity and applicability checks were made on flow patterns and heat transfer conditions. These conditions (e.g. hot channel exit equilibrium quality, flow pattern, rate of variation of the channel inlet flow rate, and range of the experimental data) were selected on the basis of RELAP5/SCDAPSIM modelling of the experimental rig used by Sudo, observations made by the experimentalists, and our understanding of the CHF mechanism associate with the burnout phenomenon.

In the analysis, the hot channel of the SAFARI-1 model was adapted to resemble the test rig used by Sudo. The model provides adequate simulation of the phenomenon and means for editing the required conditions mentioned above.

Moreover, the paper discusses the development and validation of the above-mentioned models to adequately apply the Sudo scheme, and presents comparisons with an unbounded (i.e. no condition check) application that would conclude a challenging condition to the fuel, as opposed to this work that concludes no physical burnout and the fuel remains intact during the course of the transient.

1. INTRODUCTION

In this work a Beyond Design Basis Loss of Flow Accident (BDBA LOFA) for the SAFARI-1 research reactor was selected as a case study to discuss the application of the Critical Heat Flux (CHF) scheme proposed by Sudo and Kaminaga[1]. Moreover, this work makes an attempt to apply the scheme within the range of applicability, physical and experimental. The physical are that established on the basis of assumptions made in deriving the correlations and the experimental are the range of conditions or observations made during the experiment.

The selected case study is a BDBA scenario that contemplates the loss of offsite power to the primary pumps, accompanied by a loss of emergency power to the shutdown pump i.e. total loss of forced convection, additionally the failure of any of the control rods to insert and shutdown the reactor, and assuming operator actions that worsen the course of the transient.

Such BDBA accident scenarios are used as a concept to develop the emergency operating procedures and also for the emergency planning and preparedness. On one hand a best estimate plus uncertainties is conventionally used and on the other hand best estimate

analysis can be used to reveal phenomenon that is taking place to adequately establish the counter design or procedural provisions or actions to reduce the consequences, slowdown or eliminate the phenomenon.

The main objectives of this work are to identify model adequacy and aspects of future development for best estimate simulation of scenarios that may challenge the integrity of the fuel.

In section 2 we discuss the scheme and in section 3 we perform a pre-assessment of the BDBA LOFA transient to establish the region of interest for the comparison of RELAP5/SCDAPSIM Mod3.4[2] against the experiment. In section 4 we summaries the results of this comparison and validation. This validation assisted in establishing the adequate approach in applying the scheme and revealed aspects that should be considered for future development. These aspects are discussed in this paper.

2. THE CHF SCHEME PROPOSED BY SUDO

The CHF Scheme proposed by Sudo and shown in Figure 1 uses a dynamically set dimensionless mass flux that determines the correlation to be applied depending on the magnitude and flow direction. Figure 1 is divided into regions that depend on the dimensionless mass flux G*. The CHF in each region is respectively represented by equations 1 to 4 that is shown in the figure. When $G^*>G_1^*$ a difference in CHF is not observed between up-flow and down-flow and the CHF is well predicted by equation 4. When $G_2^*<G^*<G_1^*$ the CHF is predicted by equation 2 for down-flow and when $G_3^*<G^*<G_1^*$ the CHF is predicted by equation 1 with $\Delta T^*_{SUB,o}=0$ for up-flow. When $G^*<G_3^*$ for both up-flow and down-flow the mass flux is very low or the flow condition is a counter-current flow, the CHF is predicted by equation 3. Moreover in this figure the blue line refers to up-flow directions and the red lines refers to down-flow direction, while the green line refers to both up-flow and down-flow directions. The red dotted line represent the summation of Equ.2 and Equ.3 that is originally developed by Mishima[3] and modified for applications by Sudo.

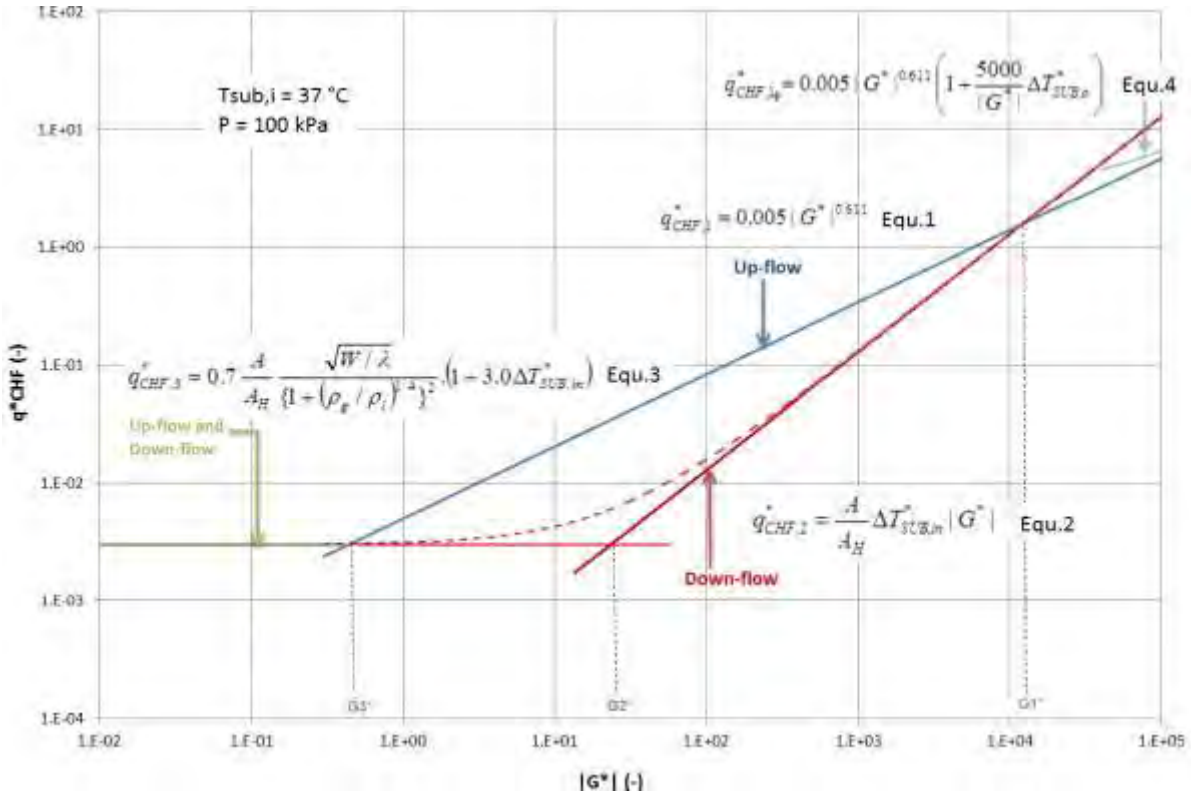

Figure 1 : Sudo and Kaminaga CHF Scheme

where:

A	:flow area of channel, m^2
A_H	:heated area of channel, m^2
q	: heat flux, W/m^2
q*	: dimensionless heat flux = q" / $h_{fg}\sqrt{[\lambda \rho_{g(}\rho_{l-} \rho_{g)g}]}$
W	:width of channel, m
G*	:dimensionless mass flux = G / $\sqrt{[\lambda \rho_{g(}\rho_{l-} \rho_{g)g}]}$
λ	:characteristic length
$\Delta T_{SUB,in}$	:sub-cooling for channel inlet, ˚C
$\Delta T^*_{SUB,in}$	dimensionless sub-cooling for channel inlet = $C_p \Delta T_{SUB,in}/h_{gf}$
$\Delta T^*_{SUB,o}$	:dimensionless sub-cooling for channel outlet
ρ_g, ρ_l	:vapour and liquid densities, kg/m^3
*C*p	: specific heat capacity, J/kg.K
h_{fg}	:latent heat of evaporation, J/kg

In the above correlations; Equ.1 and Equ.4 are correlated to the experimental data[1], Equ.2 was derived assuming zero exit equilibrium quality[3], and Equ.3 is derived from the heat and mass balance[3] in the heated section and the flooding condition by Wallis[4]; Moreover, the parameters that dominated the resultant value of CHF is the mass flux G* followed by the channel inlet sub-cooling $\Delta T^*_{SUB,in}$; while the values of channel configuration, namely, A, A_H and W, are apparently fixed for the configuration under evaluation as shown in Table 1 of section 4 below. All other parameters are evaluated at the saturation conditions at the channel inlet.

The dimensionless mass fluxes G_i^* (i=1..3) are the boundaries between the regions shown in Figure 1 and are calculated and defined as follows[1]:

$$G_1^* = \left(0.005 / (\frac{A}{A_H} \Delta T^*_{SUB,in}) \right)^{\frac{1}{0.389}}$$

$$G_2^* = \left[140 \frac{A}{A_H} \frac{\sqrt{W/\lambda}}{\{1+(\rho_g/\rho_l)^{1/4}\}^2} .(1+3.0\Delta T_{SUB,in}) \right]^{\frac{1}{0.611}}$$

$$G_3^* = 0.7 \frac{\sqrt{W/\lambda}}{\{1+(\rho_g/\rho_l)^{1/4}\}^2} \cdot \frac{1+3.0\Delta T^*_{SUB,in}}{\Delta T^*_{SUB,in}}$$

These dynamically calculated mass fluxes are compared with the actual mass flux in the hot plate channel, in terms of both magnitude and flow direction, to determine the applicable correlation (Equ. 1 to Equ. 4) to be used.

3. DBA and BDBA LOFA pre-ASSESSMENT

During the course of the DBA and BDBA LOFA the inlet sub-cooling varies between about 10°C and 80°C (80°C is the inlet sub-cooling during normal operation at 20 MW). Figure 2 is an extract of Figure 1 at the above inlet sub-cooling values where only the red and green lines are affected. The figure also superimposes the evolution of the hot channel dimensionless mass flux and heat flux during the course of the DBA and BDBA LOFA.

The main region of interest is highlighted when the mass flux G*(t) coincide with the heat flux q*(G*) that exceeds the predicted CHF (i.e. excess of CHF is mainly above the 10 °C inlet sub-cooling line which happen only in few instances during the transient as shown in Figure 3). This region of interest is used only for the comparison and validation of the RELAP5/SCDAPSIM model and to establish the adequate application of the scheme,

knowing the procedure and steady conditions used during the experiment when compared with the steep variations in the actual transient. Nevertheless in safety analysis the margin to acceptance criteria should be considered which may reduce the lines shown in the figure by this criterion.

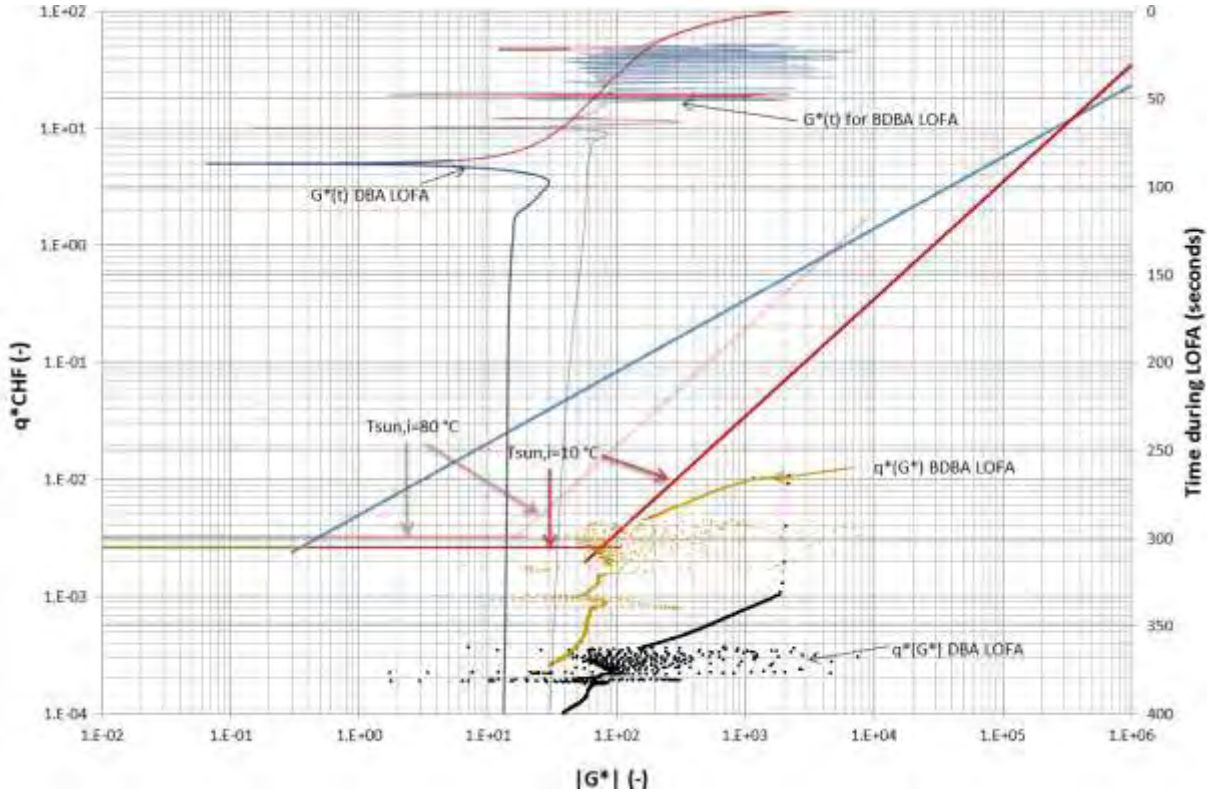

Figure 2: Extraction of CHF correlations of Figure 1 at 10°C and 80 °C of inlet sub-cooling, showing the DBA and BDBA LOFA actual dimensionless mass flux G*(t) and actual dimensionless heat flux q*(G*) and the region of interest.

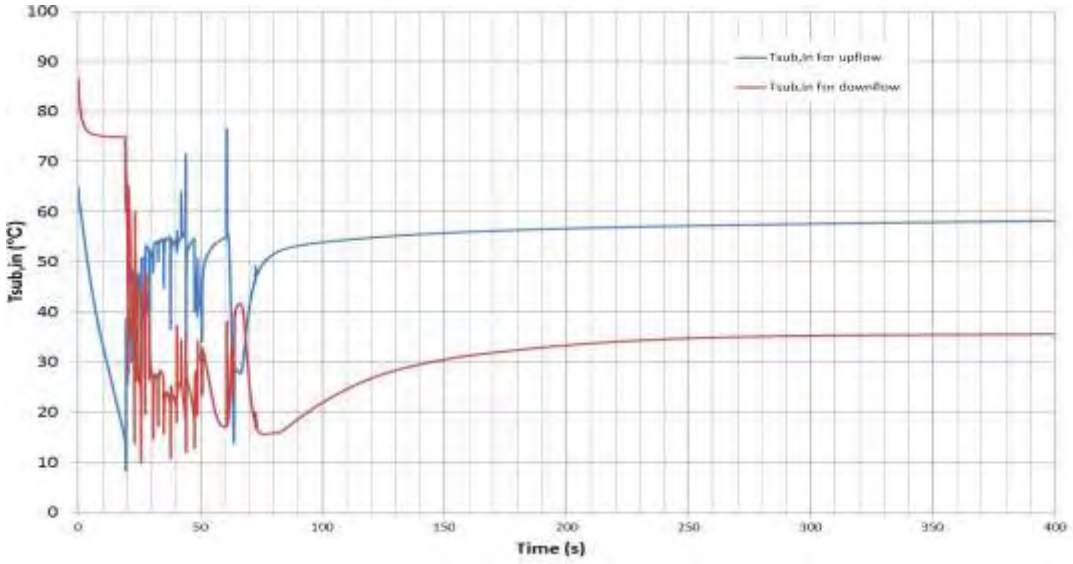

Figure 3: Inlet Sub-cooling during the BDBA LOFA for up-flow and down-flow

4. MODEL ASSESSMENT AND VALIDATION

The CHF and the application of the Sudo scheme does not depend only on the G* value and configuration but also on a set of CHF operating parameters that are correlated empirically in the range of parameters tested, and on the mechanism of the CHF observed[5]. The main CHF operating parameters are the flow pattern, the channel exit conditions and the range of the experimental data.

In order to establish the CHF operating parameters mentioned above and to validate the application of the scheme, a comparison is made between the experiment conducted by Sudo and Kaminaga and the behaviour of RELAP5/SCDAPSIM code system. Figure 4 shows the SAFARI-1 core nodalization (left) and the RELAP model of the hot channel that resembles Sudo and Kaminaga experiment (right). Table 1 presents the model parameters used for the comparisons and also the key parameters of the experiment. The validation was focused on the range of mass and heat fluxes that represent the region of interest identified in section 3 above.

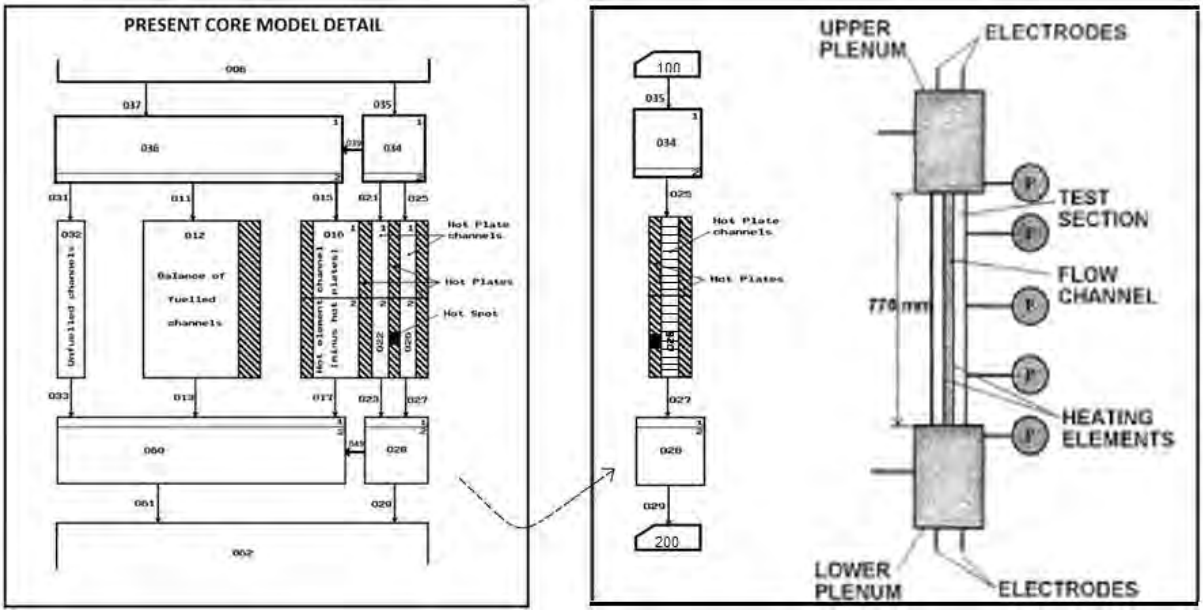

Figure 4: SAFARI-1 core nodalization (left) and RELAP model that resembles Sudo and Kaminaga experimental rig (right)

Table 1: Validation, Model and Operating Parameters

Model configration		
Flow channel width	(mm)	50
Flow channel length	(mm)	750
Water gap width	(mm)	2.25
Heated element width	(mm)	40
Heated element length	(mm)	750
Operating parameters		
Inlet subcooling	(°C)	37-39
Flow direcition	-	Upflow, downflow
Flow rate	(Kg/m^2s)	0 – 25,100
Heat input	(kW)	Up to 0.1MW
Pressure	kPa	100 – 120

034	Inlet plenum
026	Coolant channel
028	Outlet plenum
100, 200	Inlet subcooling and pressure controls

The procedure for comparison at each G* value was as follow:

1. Obtain the predicted CHF at cold condition (i.e. P=1Watt) and at the inlet sub-cooling and system pressure shown in table 1,
2. Assign power to the hot plate in steps (about 60 s each) until a sharp increase in the surface clad temperature is obtained,
3. Assess the RELAP behaviour as the condition approach the CHF and at the CHF.

In RELAP model that resembles the experiment; twenty axial nodes were made to compare with the thermocouples used in the experiment. This is due to the fact that at certain conditions, and specifically for non-uniform heat flux distribution, the CHF and the sharp temperature increase can take place away from the hot-spot. Moreover, the models and correlations that govern the energy and momentum closure relations and special flow process models were varied to identify aspects that affect the comparison. Amongst these models the interphase friction, wall drag and the Counter Current Flow Limitation (CCFL) model of Wallis affect the comparison within ±10%. The dominant closure relation that derives the comparison is the wall-to-fluid heat transfer (i.e. the transition between heat transfer mechanisms and the application of the corresponding heat transfer correlation).

Figure 4 is an extract of Figures 1 and 2 showing results of the comparisons. The initial comparison (red triangles) were performed using RELAP model without special adjustments. Figure 5 shows a case during one comparison run. In this case the CHF predicted by AECL look-up table[6] and by Sudo scheme is shown. According to Sudo scheme the transition to transition or film boiling should take place at 650 s (see black arrow in Figure 5) when the actual heat flux exceeds Sudo predicted CHF, while the AECL CHF, that is implemented in RELAP5/SCDAPSIM, is orders of magnitude higher.

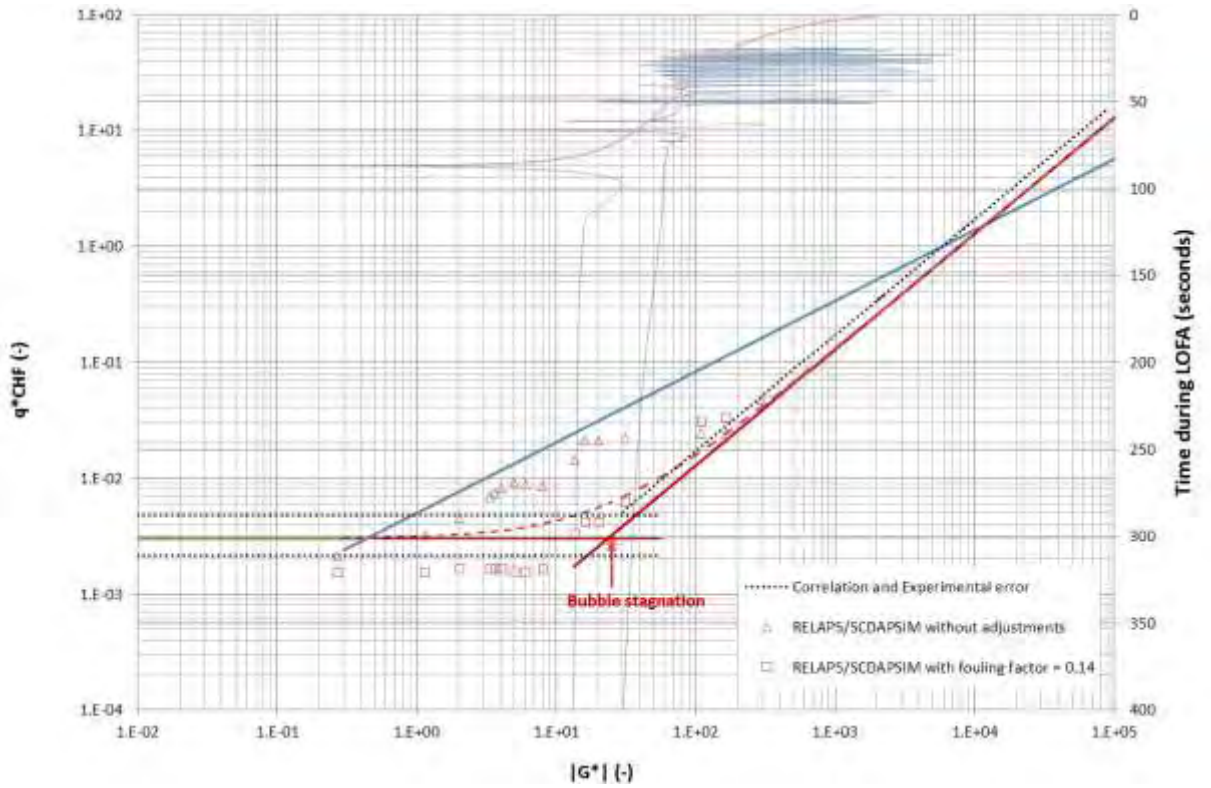

Figure 4: Comparison of Sudo and Kaminaga experiment and RELAP5/SCDAPSIM Mod 3.4 code.

As mentioned above that the dominante model that derive the comparison is the heat transfer logic while others provide ±10% variation, the adjuestment was done by selecting a

foulding factor of 0.14 that reduces the heat transfer coefficients and the CHF solution. This adjustment, even if not adequate, was reasonable to study the impact of the transition logic in the comparison. The results are presented in Figure 4 (red rectangulars) which show the same trend as in the Sudo scheme. A slightly higher fouling factor can bring the comparison within the experimental error however it was found unnessary at this stage.

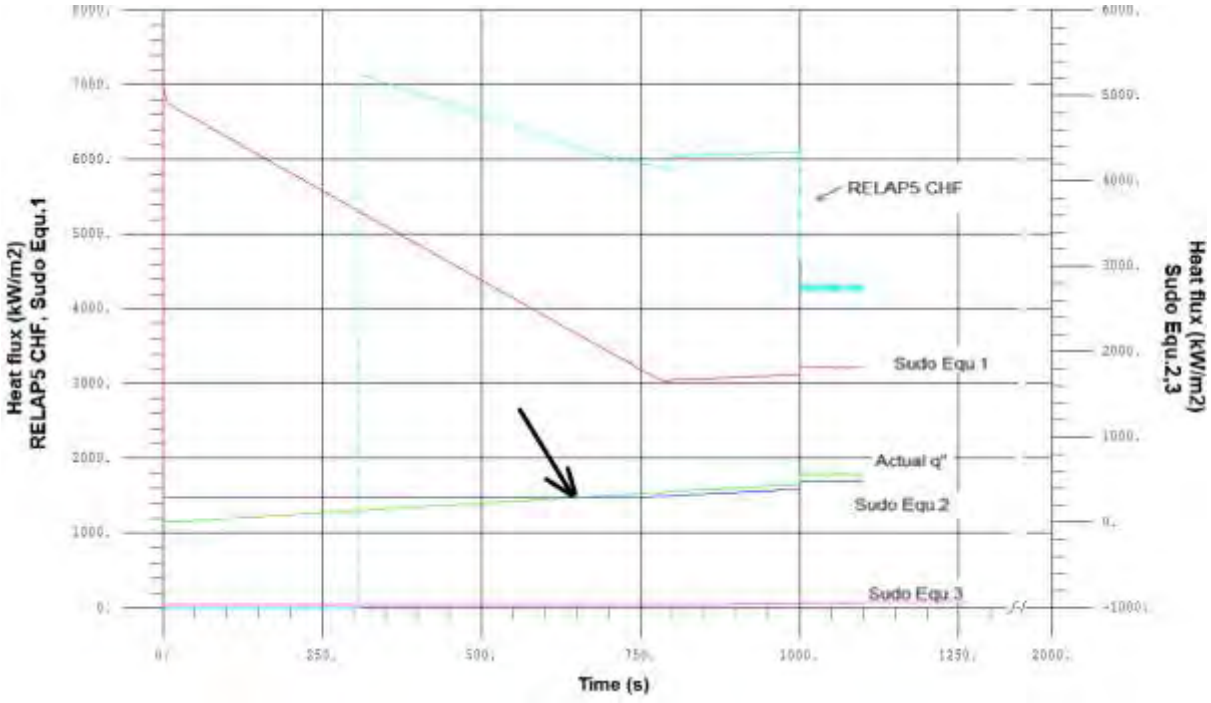

Figure 5: A sample of a comparison case showing the flow transition logic from nucleat boiling to transition or film boiling that depend on the CHF correlation implemented in the logic

The adjusted results were used to establish the conditions used to applying the Scheme and during the course of the transient. 0 shows the actual operating parameters stated by Sudo for equation 1 and 4[1], and by Mishima for equations 2 and 3[3], and the assumed operating parameters derived from the model validation and used in this analysis.

Table 2: Actual and conservatively assumed CHF operating parameters

Operating parameter	Actual	Assumed
$X_{e,o}$(-)	~<0	≥-0.02(1)
Flow pattern (-)	≥ANM	≥SLG (2)
Flow rate differential (kg/m^2.s /s)	~0	≤2.5e-03(3)
Mass flux (kg/m^2.s)	-600 to +480 -610 to +360	-600 to +480(4) -610 to +360(5)
Heat flux (MW/m2)	Up to 1.3	Up to 1.3(6)

(1) This criterion is applied to equation 2 since it was derived from the condition Xe=0 (the negative qualities refer to sub-cooled conditions). The '~<0' was recommended due to the presence of unheated side walls. The conservatively assumed equilibrium quality corresponds to about 10-15 °C exit sub-cooling.

(2) This criterion is applied to equation 3 and is based on the flow patter associated with the high quality flow burnout mechanism [1,3,5].

(3) This criterion is applied to equations 2 and 3 as noted by Mishima[3]: “The results are obtained for steady inlet-flow condition and may be valid also for a slow transient”. The assumed value is the maximum variation during the flow reversal as derived from DBA

LOFA. This criterion was also selected to study the influence of the timely behaviour required for the CHF condition to establish.

(4) The range of the experimental data for equations 1. Outside this range the AECL based DNBR is used.

(5) The range of the experimental data for equations 2 and 3. Outside this range the AECL based DNBR is used.

(6) The range of heat fluxes for equations 2 and 3. Outside this range the AECL based DNBR is used.

Figure 6 shows the Burnout Ratio (BOR) and the inline application of Sudo scheme (via RELAP control variables) when conditions of Table 2 is not applied while Figure 7 shows the BOR when conditions of Table 2 is applied. From Figure 7 it could be argued that the adequate application of Sudo Scheme within the range and conditions of the experiment shows sufficient margin to burnout and the fuel stay intact during the course of this transient.

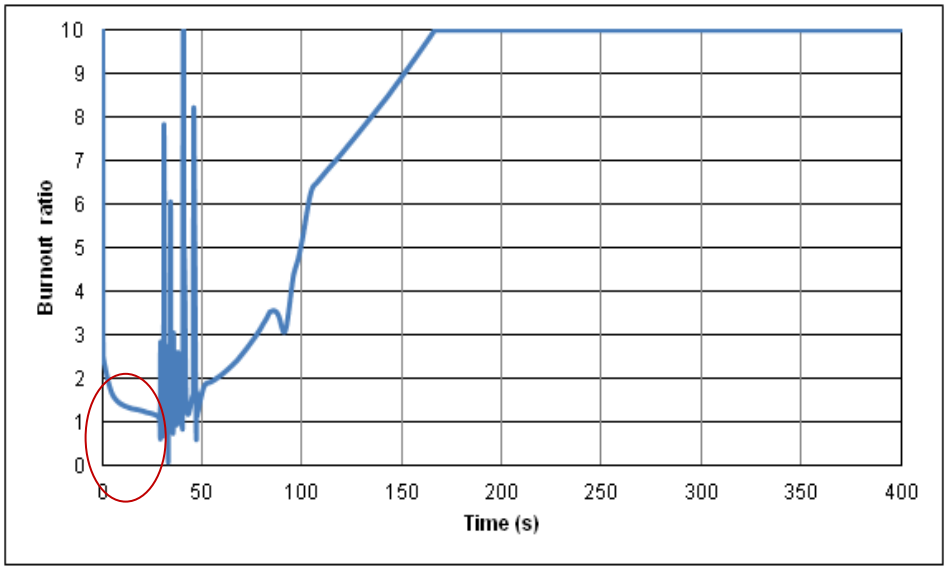

Figure 6: Burnout Ratio during the course of BDBA LOFA with unbounded application of Sudo Scheme

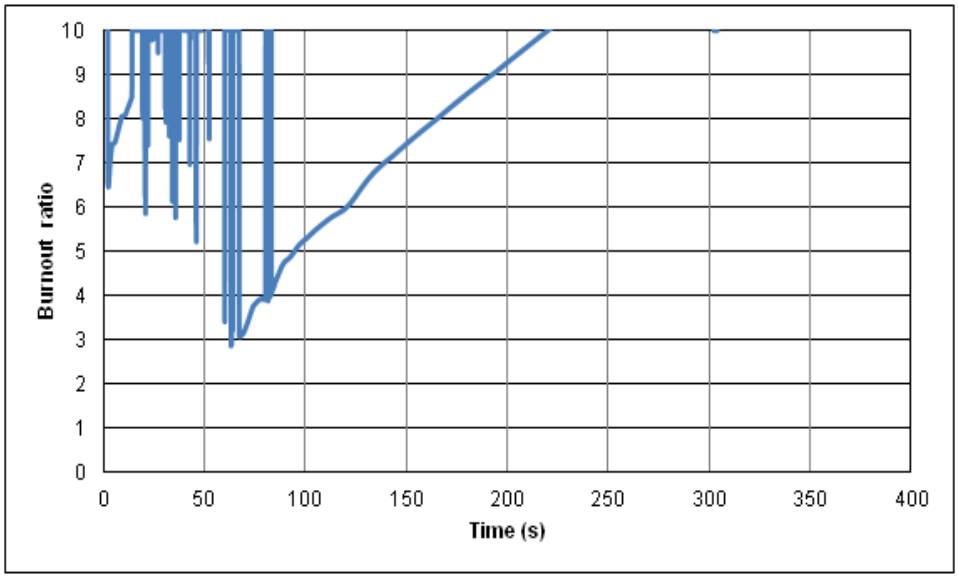

Figure 7: Burnout Ratio during the course of BDBA LOFA with a bounded application of Sudo Scheme

5. CONCLUSION

A detailed validation was performed of RELAP/SCDAPSIM Mod 3.4 against Sudo and Kaminaga experiment for the prediction of the CHF condition in a rectangular flow channel. This validation has identified the main drive of the comparison and the adequate application of the Scheme. The comparison was driven by the criteria used for the transition between heat transfer mechanisms to up to a factor of 5 while various models governing the two phase flow momentum and energy transfer vary the comparison with ±10%.

An adjustment was made to study the impact of the criteria used for the transition between heat transfer mechanisms which resulted in a better agreement with the experiment. The adjusted comparisons are used to establish the conditions of applicability of the Scheme.

The application of the Scheme, within the region of applicability, and during the course of beyond design basis loss of flow accident, showed a sufficient margin to burnout as opposed to deteriorating behaviour if the Scheme was applied outside its region of applicability.

6. REFERENCES

[1] M KAMINAGA, K YAMAMOTO and Y. SUDO, "Improvement of Critical Heat Flux Correlation for Research Reactors Using Plate-Type Fuel", Journal of Nuclear Science and Technology, Vol.35, No.12, p. 943-951, December 1998

[2] RELAP5/MOD3.3Beta Code Manual, "Models and Correlations", VOLUME IV, section 4.2.3.5, page 135.

[3] MISHIMA, K., "Boiling burnout at low flow rate and low pressure conditions, Dissertation Thesis", Kyoto Univ., (1984).

[4] Wallis, G.B.:”One-dimensional Tow-phase Flow”, (1969). McGraw Hill.

[5] L.S.TONG, Y. S. Tang, "Boiling Heat Transfer and Two-Phase Flow", 2nd Edition, para.5.2.3, 1997.

[6] D. C. Groeneveld, S. C. Cheng, and T. Doan, "1986 AECL-UO Critical Heat Flux Lookup Table", Heat Transfer Engineering, 7, 1-2, 1986, pp. 46-62.

LEU Fuel Fabrication & Conversion

FABRICATION OF PIN-TYPE MINI-ELEMENTS CONTAINING U-MO/MG DISPERSION FUEL FOR TEST IRRADIATION IN NRU

N. WANG[1], M. KULAKOV[2], AND S. HIBBINS[1]
[1]*Nuclear Fuel Fabrication Facility, Canadian Nuclear Laboratories, 286 Plant Rd., Chalk River, Ontario, Canada K0J 1J0*
[2]*Fuel Development Branch, Canadian Nuclear Laboratories, 286 Plant Rd., Chalk River, Ontario, Canada K0J 1J0*

ABSTRACT

Fabrication of pin-type mini-elements containing U-Mo/Mg dispersion fuel mini-elements was successfully carried out in the Nuclear Fuel Fabrication Facility at Canadian Nuclear Laboratories. The mini-elements contain U-7wt%Mo and U-10wt%Mo particles dispersed in a Mg matrix with a U loading of 4.5 g/cm^3 and will be irradiated in NRU up to 80 at% U-235 depletion at an element linear power up to 100 kW/m. This paper presents the U-Mo/Mg fuel design, fabrication processes, and pre-irradiation examination results.

1. Introduction

The early U-Mo fuel development work at Canadian Nuclear Laboratories (CNL) - formerly Atomic Energy of Canada Limited (AECL), Chalk River Laboratories (CRL) - was conducted based on the driver fuel design currently used in the National Research Universal (NRU) reactor. In the initial fuel design, U-Mo particles with a nominal U-235 enrichment of 19.75 wt% (i.e., low-enriched uranium - LEU) were dispersed in an Al matrix. Irradiation tests on the U-Mo/Al dispersion fuel showed unacceptable behaviours due to excessive interactions between the U-Mo fuel particles and the Al matrix [1-5]. New conceptual U-Mo fuel designs were proposed to solve the interaction problem [6-10].

At CNL/AECL, an irradiation experiment to conduct further tests on U-Mo based dispersion fuels with Mg as the failure-resistant matrix in NRU was proposed. The Mg matrix is not expected to have any metallurgical interactions with the U-Mo fuel particles. In the proposed irradiation experiment, pin-type mini-elements containing LEU-based U-7wt%Mo and U-10wt%Mo alloy fuel particles dispersed in Mg matrix with a U loading of 4.5 g/cm^3 in fuel meat (see Figure 1) will be tested in the NRU reactor up to 80 at% U-235 depletion at an element linear power up to 100 kW/m. The objectives of this irradiation experiment are to:

(1) Demonstrate the capability to fabricate the pin-type U-Mo/Mg dispersion fuel with a U loading up to 4.5 g/cm^3 in the Nuclear Fuel Fabrication Facility (NFFF) at CNL.
(2) Assess the irradiation behaviour of the proposed U-Mo/Mg dispersion fuel in NRU.

The U-Mo/Mg dispersion fuel fabrication process development and fuel fabrication campaign were conducted at CNL during the years of 2010~2014. The design parameters of the U-Mo/Mg mini-elements produced in this fuel fabrication campaign are given in Table 1. This paper presents the fabrication data of the U-Mo/Mg mini-elements and the results from pre-irradiation examinations.

2. Materials

The uranium metal (19.72 wt%U-235) lumps and molybdenum metal rods (99.95 % pure, 6.35 mm diameter) were used to fabricate the U-Mo alloys. Mg powder (<250 μm, >99.8% pure) was used as the matrix for the fuel cores. AA-1060 Aluminium was used for the cladding and end-plug materials.

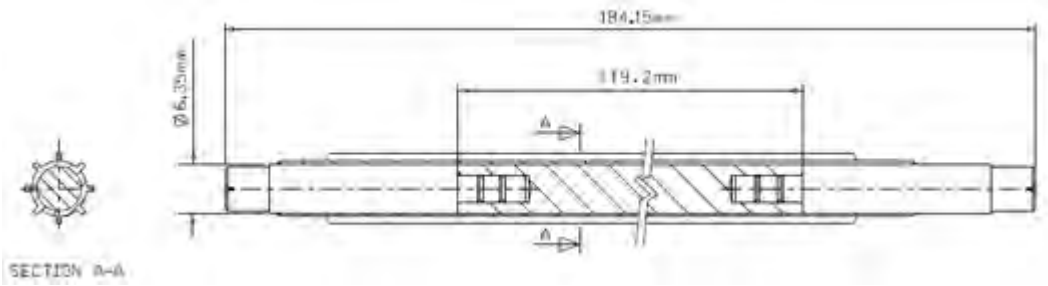

Figure 1: U-Mo/Mg fuel mini-element (The shaded area is the fuel core.)

Cladding	Material	AA-1060 Aluminium
	Outer Diameter (excluding fins)	7.87 mm
	Thickness	0.76 mm
	Fin Height/Thickness	1.02 mm/0.76 mm
Fuel Core	Material	U-7Mo + 20.7 wt%Mg U-10Mo + 19.8 wt%Mg
	Diameter	6.35 mm
	Length	119.2 mm
Endplug	Material	AA-1060 Aluminium

Table 1: Design parameters of U-Mo/Mg dispersion fuel mini-elements

3. Fuel Fabrication

3.1 Safety Aspects of Processing U-Mo/Mg

The Nuclear Fuel Fabrication Facility of CNL is a licensed Class 1B Nuclear Facility [11] as per the Canadian Nuclear Safety Commission Regulations. Since it was built in 1989, the Facility has been used mainly to manufacture NRU driver fuel (U_3Si/Al) and Mo-99 targets. Between 1995 and 2005, the facility also supplied HANARO driver fuel to Korea. Although fuel elements with an Al matrix have been fabricated in NFFF for many years and considerable experience has been gained in fabricating these fuels safely, use of Mg as the dispersion fuel matrix involves hazards different in nature and greater in magnitude than those associated with fabrication using Al.

As far as nuclear and radiation hazards are concerned, there is no difference between the Al-based and Mg-based fuels. However, Al and Mg have different physical, chemical, toxicological and combustion properties. Mg is more flammable than Al, particularly in the finely divided state. Once ignited, Mg can continue to burn in N_2, CO_2, and water. Burning of Mg in steam or water could release hydrogen. Fire protection in NFFF is mainly based on the isolation, elimination, or reduction of the important parameters including fuel, oxygen, and heat sources. To achieve this, ignition sources and combustible material present in the facility are minimized, inert gas is applied where pyrophoric materials are handled, and the facility is equipped with automatic fire detection and suppression systems. In addition, workstations where fuel materials with fine dimensions are handled or generated are provided with carbon microspheres. The other safety-related issues, such as the fuel thermal stability and the metallurgical interactions between Al and Mg, will be addressed in the following sections.

3.2 U-Mo Billet Casting and Heat Treatment

The U-7Mo and U-10Mo billets were cast using a vacuum-induction furnace. The U and Mo charges of both compositions were melted at above 1400°C in an argon atmosphere. The molten U-Mo alloys were then cast at about 1300°C and then allowed to cool to room temperature in the furnace. Figure 2 shows one of the as-cast LEU-Mo billets. The microstructures of the as-cast U-Mo billets were examined using a scanning electron microscope (SEM) in the backscattered electron imaging (BEI) mode. It is shown in Figure 2 that the U-Mo alloys solidified dendritically and the U-Mo dendrites are rich in Mo at the center (darker areas in the SEM BEI image) and rich in U around the periphery.

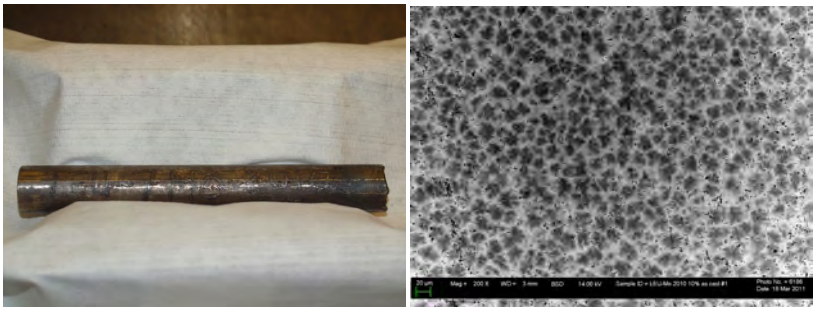

Figure 2: As-cast LEU-Mo billet (left) and its microstructure (BEI, right)

To homogenize the Mo distribution in U and obtain the desired single γ-U(Mo) phase, the as-cast U-Mo billets were heat-treated at 900±20 °C for 72±2 hrs under Ar protective atmosphere. A single metastable γ-U-Mo phase was obtained by directly quenching the U-Mo billets into cold water. X-ray diffraction analysis verified that both U-7Mo and U-10Mo billets, after the heat treatment, consisted of only the single γ-U(Mo) phase (see Figure 3).

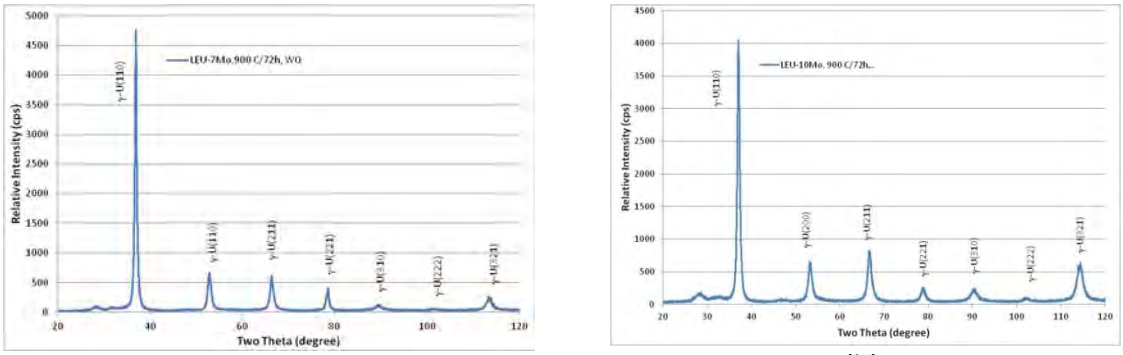

(a) (b)

Figure 3: X-ray diffraction spectra of heat-treated (a) U-7Mo and (b) U-10Mo billets

3.3 Pulverization of U-Mo Alloys

The heat-treated billets were machined into chips and then comminuted into U-Mo powders in a standard glovebox under Ar protective atmosphere. The particle sizes of the U-Mo powders used for this fuel fabrication campaign were less than 180 μm. Figure 4 shows SEM micrographs (secondary electron images - SEI) of the U-Mo powders with various particle sizes. It is seen that the U-Mo particle morphology changes from flaky to a more spherical shape as the particle size increases. No significant differences in the appearances of the U-7Mo and U-10Mo powders were noted. Chemical analysis indicated Fe and O are the major impurities in the U-Mo powders.

3.4 Preparation of Extrusion Billets

To meet the design U loading of 4.5 g/cm^3 in the fuel, the required U-Mo and Mg powders were weighed using a Mettler Toledo digital balance according to the specified core compositions (see Table 1). The weighed U-Mo and Mg powders were blended in a polyethylene bottle. Blended powders were then compacted into billets (typically 38.1 mm in diameter and 62~63 mm high) at ~170 MPa, which resulted in a compact ratio of ~80%.

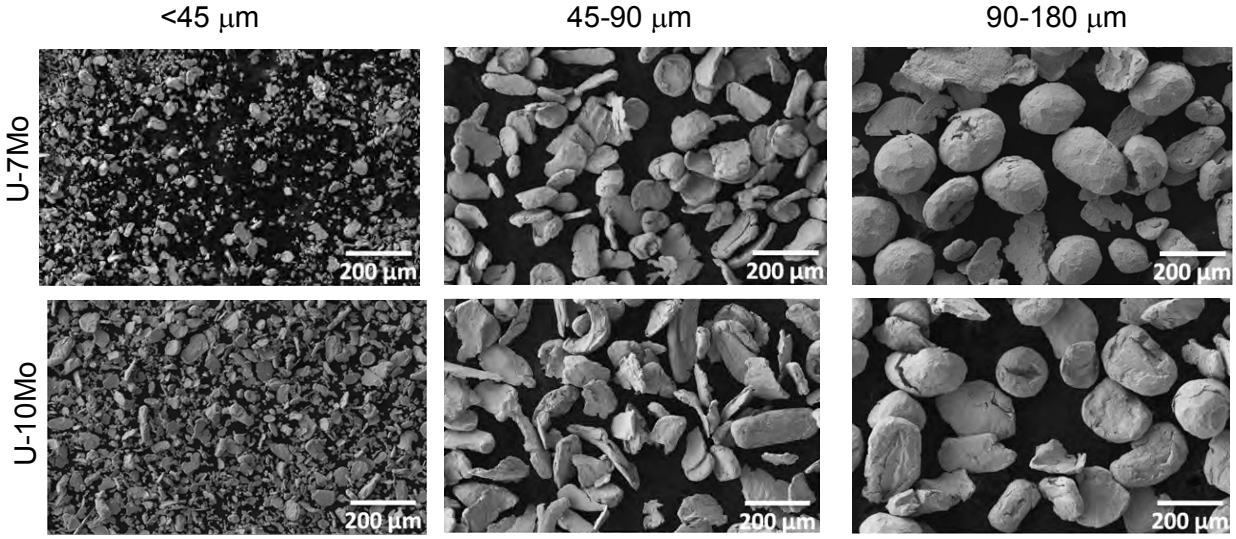

Figure 4: Secondary electron images of as-pulverized U-7Mo and U-10Mo powders

3.5 Fuel Core Extrusion

The compacted U-Mo/Mg billets were hot-extruded into U-Mo/Mg cores with a diameter slightly larger than the target diameter of ϕ6.35 mm. All the cores were extruded at a temperature ranging between 380 and 400 °C with a speed of 90 ft/min. To improve the homogeneity of the U-Mo particle distribution and the surface finish, the fuel cores were double-extruded. Figure 5 shows typical surface finishing of the as-extruded U-Mo/Mg fuel cores.

The specific densities of the cores were measured using the immersion technique. Based on the nominal core specific densities shown in Table 1, 96.05±8.67 % of the design density was achieved for U-7Mo/Mg cores and 98.75±2.48 % of the design density for U-10Mo/Mg.

3.6 Core Gamma Scanning

Gamma scanning was used to evaluate the axial U-235 linear distribution in the cores after being cold-drawn through a ϕ6.35 mm die and then straightened. Typical gamma counts as a function of the core length for the U-7Mo/Mg and U-10Mo/Mg cores are shown in Figure 6. The gamma scan indicated that the gamma counts variations (defined as ratio of the standard deviation to the average counts) were less than ~3 % within the cores, including 0.2~0.3 % noise of the gamma scanning system.

3.7 Core Machining, Cleaning and End Plugging

The cores were machined with Ar cooling as per the dimensions shown in Figure 1. The machined cores were cleaned with acetone and then methanol before the end plugs (AA-1060 Aluminium) were installed.

3.8 Cladding and Machining for Weld Preparation

The U-Mo/Mg cores were clad with AA-1060 Aluminium at 525 °C. The cladding extrusion speed and pressure were typically at 3 m/min and 180 tons, respectively. Although the cladding

extrusion temperature is higher than the Al-Mg eutectic temperature (~450 °C), the temperature at the Al-Mg interface was found to be no higher than 320 °C during the extrusion. An Al-Mg diffusion couple experiment has shown that the 525 °C cladding temperature will not cause any metallurgical interactions between the Al cladding and Mg matrix [12].

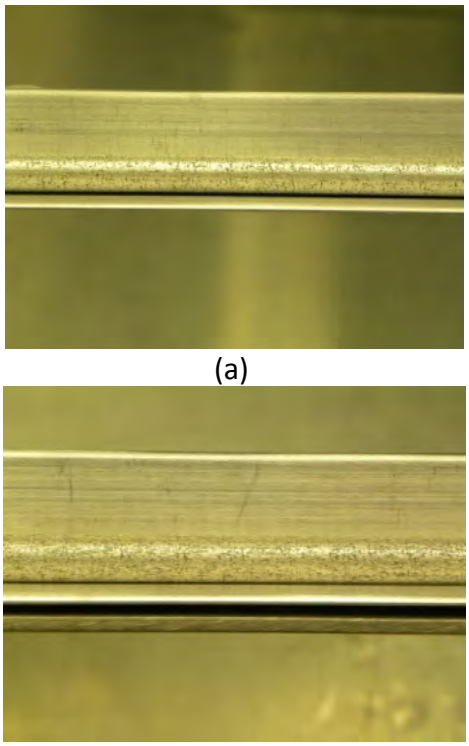

(a)

(b)

Figure 5: Typical surface finishing of the as-extruded LEU-Mo/Mg cores, (a) LEU-7Mo/Mg Core #65, and (b) LEU-10Mo/Mg Core #73

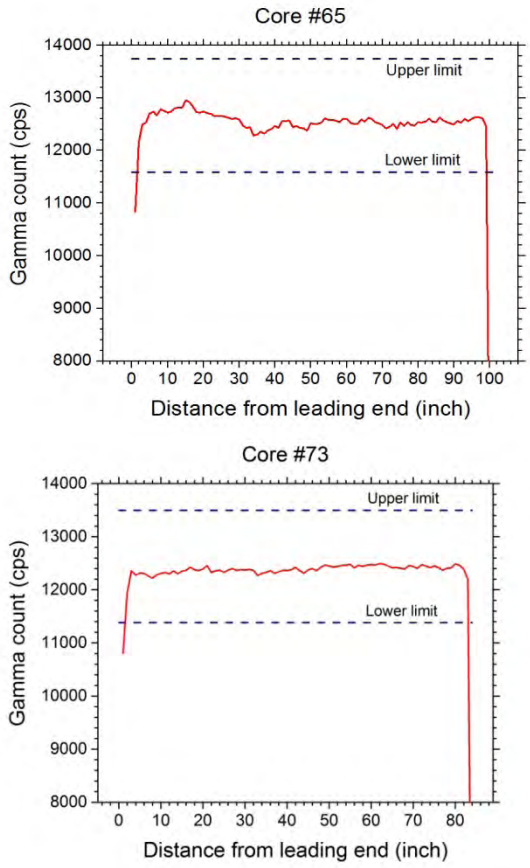

Figure 6: Typical gamma scan results of U-7Mo/Mg (top) and U-10Mo/Mg (bottom) cores

The concentricity of the cladding and the cores adjusted by fine-tuning the die and guide in the die block. The integrity of the cladding was inspected using the Eddy current scanning technique. The fin dimensions were inspected under a stereomicroscope with a digital micrometer. By changing the die design slightly, cladding with spiral fins can be extruded in the facility, which significantly improves the thermal hydraulic margins [13].
The fuel elements (fuel cores with cladding and end plugs) were prepared for final seal welds by machining to the dimensions shown in Figure 1.

3.9 End-plug Welding

An electron beam welder was used to weld the cladding to the end-plugs. The weld coverage was inspected using the real-time radiography. Figure 7(a) shows a typical RTR image. The root of the weld is clearly visible. The weld has a predominant columnar grain structure formed during solidification (see Figure 7(b)).

4. Microstructural Characterization of Fuel Elements

Figure 8 shows the microstructure of the extruded fuel cores. The U-Mo fuel particles (dark) are imbedded in the magnesium matrix (light). The fuel particles formed lines parallel to the

extrusion direction. The particles did not deform in the course of extrusion as their shape is similar to the original powder shown in Figure 4.
A transverse cross-section of a complete fuel element is shown in Figure 9(a). The width and height of the fins, as well as the cladding thickness conforms to the requirements. There is an intimate contact between the core, the end-plug and the cladding as can be seen from the longitudinal cross-section of the finished fuel element in Figure 9(b). No metallurgical interactions were observed at the interfaces.

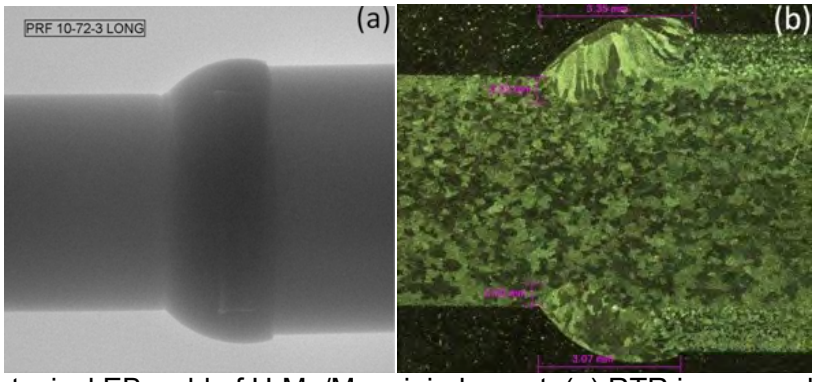

Figure 7: A typical EB weld of U-Mo/Mg mini-element: (a) RTR image and (b) optical microstructure

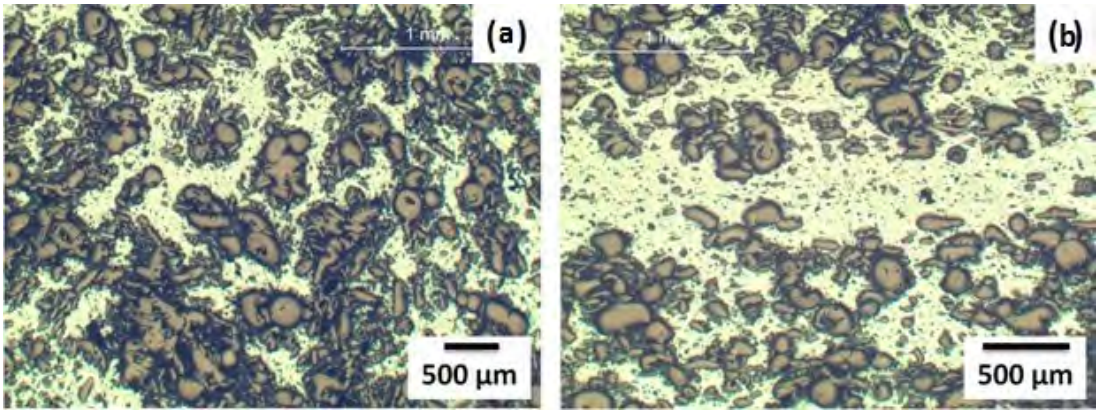

Figure 8: Micrographs of U-Mo/Mg cores, (a) transverse and (b) longitudinal cross-sections

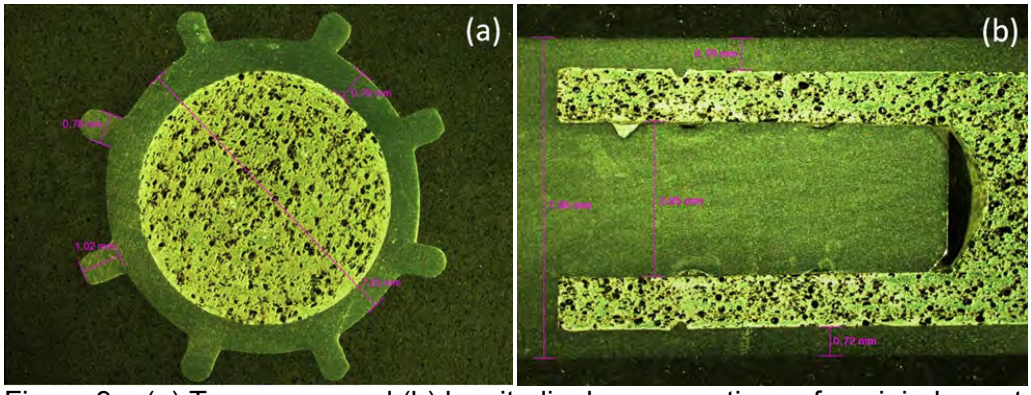

Figure 9: (a) Transverse and (b) longitudinal cross-sections of a mini-element

The XRD spectra collected from the transverse and longitudinal cross-sections of both U-7Mo/Mg and U-10Mo/Mg cores are shown in Figure 10 and Figure 11. In addition to γ-U(Mo), Mg and UO_2 (the three initial crystalline phases in the extrusion billets), the core extrusion process has led to a small portion of γ-U(Mo) decomposition into α-U(Mo). U_2Mo was not

identified in the spectra: one of the three strongest peaks at 38.1° 2-theta is clearly missing. Since the γ-U(Mo) phase in the U-10Mo is more stable than in the U-7Mo, the amount of decomposition products in the U-7Mo/Mg cores is noticeably higher than in the U-10Mo/Mg cores as indicated by the α-U(Mo) peak intensities.

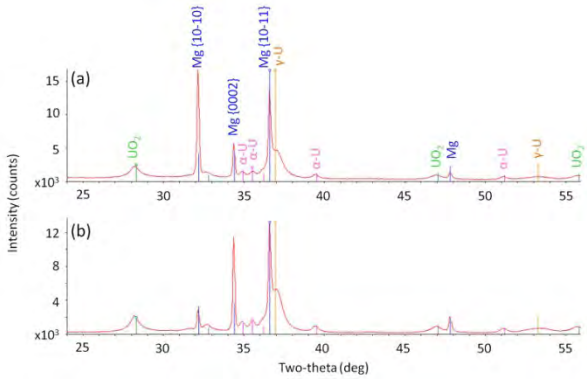

Figure 10: XRD spectra taken from a U-7Mo/Mg core in the (a) transverse and (b) longitudinal cross-sections.

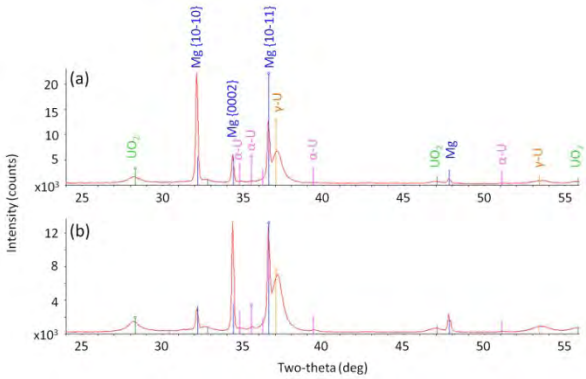

Figure 11 XRD Spectra taken from a U-10Mo/Mg core in the (a) transverse and (b) longitudinal cross-sections

It is also seen that the XRD intensities of the Mg {0002} and $\{10\bar{1}0\}$ peaks are significantly different between transverse and longitudinal cross-sections (see Figure 10 and Figure 11). Mg basal plane {0002} peaks are more intense for the longitudinal cross-sections, i.e. Mg basal planes are mostly parallel to the extrusion axis. More detailed analysis on the Mg texture was performed on the E3 spectrometer of the Canadian Neutron Beam Centre at CNL. Pole figures were obtained for the {0002}, $\{10\bar{1}0\}$, $\{10\bar{1}1\}$, $\{11\bar{2}0\}$ and $\{10\bar{1}2\}$ Mg reflections. The pole figures shown in Figure 12 (for basal and prism planes) have directions along the circumference corresponding to an arbitrary radial direction in the cylindrical samples. The centre of each pole figure corresponds to the axial or extrusion direction. The pole figures are reconstructed from the orientation distribution functions and the resolved fractions of basal poles (Kearns texture factor [14]) along the three pole figure axes are given in Table 2. It is seen that nearly 90% of the Mg basal plane poles are oriented mostly perpendicular to the extrusion axis.

Neutron diffraction (ND) was also used for detailed phase analyses. ND spectra (see Figure 13) were collected with a monochromatic (wavelength = 0.23712 nm) incident neutron beam and analyzed using the GSAS package. The α-U(Mo) peaks are stronger in the U-7Mo/Mg fuel core which further confirm the XRD results (see Figure 10 and Figure 11): γ-U(Mo) is more stable in U-10Mo than in U-7Mo. However, the α-U(Mo) peaks are significantly weaker than the γ-U(Mo) peaks, and the latter remains a dominant uranium phase in both materials. The amount of α-U(Mo) in the as-fabricated fuel is less than 5%. Lattice parameters of the γ-U(Mo) phase in U-7Mo and U-10Mo were obtained using the Rietveld refinement and found to be 3.426±0.002 and 3.412±0.002 A, respectively.

5. Conclusions

(a) Pin-type U-Mo/Mg dispersion fuel has been safely fabricated in the Nuclear Fuel Fabrication Facility at Canadian Nuclear Laboratories following the procedures presented in this paper. Quality assurance inspection shows that the U-Mo/Mg fuel elements meet the design requirements.

(b) A small amount (<5%) of γ-U(Mo) decomposition has occurred during the U-Mo/Mg fuel fabrication.

(c) There are no metallurgical interactions between Al cladding and Mg in the as-extruded U-Mo/Mg cores even though the Al cladding extrusion is done at 525 C above the Al-Mg eutectic temperature at ~450 C.

(d) The Mg in the as-extruded U-Mo/Mg cores is strongly textured with nearly 90% of its {0002} basal plane poles orientated in the direction perpendicular to the extrusion direction.

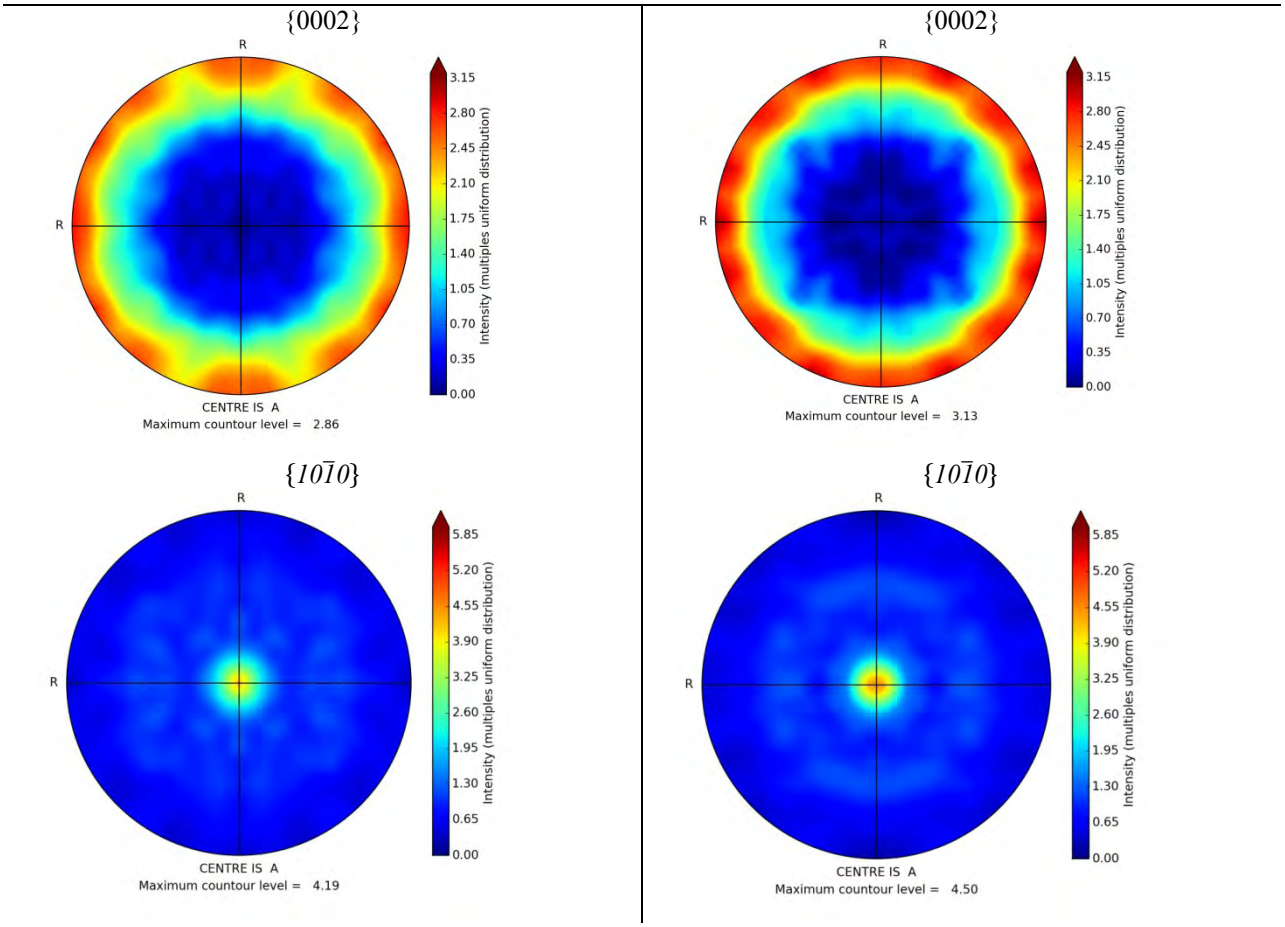

Figure 12 Pole Figures Measured from the U-Mo/Mg Fuel Cores (basal and prism planes)

Direction	U-7Mo/Mg (Core #65)	U-10Mo/Mg (Core #74)
Axial	0.12	0.11
Radial-1	0.43	0.44
Radial-2	0.45	0.45

Table 2: Resolved Fraction of Basal Pole (Kearns Texture Factor) of U-Mo/Mg Fuel Cores

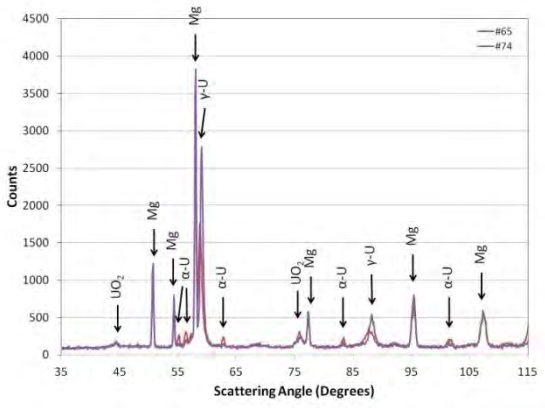

Figure 13 Neutron Diffraction Spectra of U-7Mo/Mg (#65) and U-10Mo/Mg (#74)

6. Acknowledgements

The authors would like to thank T. Shultz, R. Turgeon, J. Leppinen, M. Ryan, E. Yokale, K. Cleary, and R. Collins for U isotope and chemical analyses, Dr. M. Gharghouri for Mg texture analysis, R. Donaberger for ND phase analysis, A. Buyers for XRD, C. Mayhew and H. Rudzinski for SEM, A. Lockley for metallography, and L. Fu for engineering drawing support.

7. References

[1] D.F. Sears, “Development, Irradiation Testing and PIE of UMo Fuel at AECL”, The International Meeting on Reduced Enrichment for Research and Test Reactors (RERTR), 2004 November 7-12, Vienna, Austria.

[2] D. Sears, K. Conlon, J. Mason, A. Davidson, and C. Buchanan, "Post-irradiation Examination of Uranium-Molybdenum Dispersion Fuel Irradiated to High Burnup in NRU", Transaction of 10th International Topical Meeting on Research Reactor Fuel Management (RRFM), 2006 April 30 - May 4, Sofia, Bulgaria.

[3] G.L. Hofman, M.R. Finlay*, Y.S. Kim, “Post-Irradiation Analysis of Low Enriched U-Mo/Al Dispersions Fuel Miniplate Tests, RERTR 4 & 5”, The International Meeting on Reduced Enrichment for Research and Test Reactors (RERTR), Vienna, Austria, 2004 November 7-12.

[4] P. Lemoine, J.L. Snelgrove, N. Arkhangelsky, L. Alvrez, “UMo Dispersion Fuel Results and Status of Qualification Programs”, 8th international topic meeting on Research Reactor Fuel Management, Munich, Germany, 2004 March 21-24.

[5] J.M. Park, H.J. Ryu, Y.S. Lee, D.B. Lee, S.J. Oh, B.O. Yoo, Y.H. Jung, D.S. Sohn, and C.K. Kim, “An Investigation on the Irradiation Behavior of Atomized U-Mo/Al Dispersion Rod Fuels”, The International Meeting on Reduced Enrichment for Research and Test Reactors (RERTR), Vienna, Austria, 2004 November 7-12.

[6] T. C. Wiencek, I. G. Prokofiev, and D. J. McGann, “Development and Compatibility of Magnesium-Matrix Fuel Plates Clad with 6061 Aluminum Alloy”, 1998 International Meeting on Reduced Enrichment for Research and Test Reactors, October 18-23, 1998, São Paulo, Brazil.

[7] M.K. Meyer, J.L. Snelgrove, “Update on the Effort to Develop and Qualify New Low Enrichment Fuels”, Joint meeting of TRTR-2005 and IGORR-10, September 12-16, Gaithersburg, Maryland.

[8] M.K. Meyer, et al., “Progress in the RERTR Fuel Development Program”, Transaction of RRFM 2006, Sofia, Bulgaria, 2006 April 30 – May 3.

[9] D. Washs, et al., “Irradiation Testing of High Density U-Mo Fuels in the ATR”, Proceddings of RERTR 2005, Boston, Massachusetts, 2005 Nov. 6-10.

[10] Sven Van den Berghe, A. Leenaer and C. Detavernier, “SELENIUM Fuel: Surface Engineering of U(Mo) Particles to Optimise Fuel Performance”, Transaction of RRFM 2010, Marakech, Morocco, 2010 March 21-25.

[11] Canadian Nuclear Safety Commission, Nuclear Research and Test Establishment Site License, Chalk River Laboratories, License No. NRTEOL-01.00/2016 Expiry Date: 2016 October 31.

[12] L. Xiao and N. Wang, “Growth behavior of intermetallic compounds during reactive diffusion between aluminum alloy 1060 and magnesium at 573–673 K”, Journal of Nuclear Materials 456 (2015) 389–397.

[13] M.H.A. Piro and B.W. Leitch, “Conjugate heat transfer simulations of advanced research reactor fuel”, Nuclear Engineering and Design, 274 (2014) 30–43.

[14] J.J. Kearns, Thermal expansion and preferred orientation in Zircaloy, WAPD-TM-472, 1965.

UMO FOIL FABRICATION DEMONSTRATION LINE AT BABCOCK & WILCOX

R.E. JOHNSON, J.T. LOWELL, R.M. MAYFIELD,
D.W. NAVOLIO, J.M. WIGHT
Research Test Reactor & Development Engineering,
Babcock & Wilcox, Nuclear Operations Group
PO Box 785, Lynchburg, VA, 24504 - USA

ABSTRACT

The DOE NNSA Material Management and Minimization Conversion program has funded a project at Babcock & Wilcox (B&W) Nuclear Operations Group in Lynchburg, Virginia to demonstrate the fabrication of LEU high density UMo monolithic foils and plates with commercial-scale equipment. A review of the fabrication processes and equipment at laboratory-scale was conducted which led to a baseline commercial-scale process flow diagram, including the identification of new equipment and processes. Planning of project tasks included removal of decades old fuel powder fabrication equipment, installation of new utilities, safety evaluations for new equipment and processes, design and procurement of new equipment and tooling, as well as installation and testing of the new equipment. Planning included the review of existing equipment utilization, which led to the creation of a Memorandum Of Understanding between two DOE entities and B&W to use the INL hot roll mill. Significant resources among various departments were required to perform planning, engineering, decontamination, scrap removal and installation; additionally, constant oversight was required to ensure budget and schedule creep was kept to a minimum. Installation of new equipment is complete and depleted uranium testing has commenced. Initial results of surrogate and DU testing are presented. Discussion of future fabrication efforts for miniplate and full-size plate experiments utilizing the new fabrication line is also included.

1. Introduction

The U.S. Department of Energy (DOE)/ National Nuclear Security Administration (NNSA) manages the Conversion Program to reduce and eliminate weapons-usable nuclear material at civilian research reactors around the world. A focus of the Conversion Program is to convert research reactors currently utilizing highly enriched uranium (HEU) to low enriched uranium to remove the threat imposed by the continued use of HEU. A key component of the program is the conversion of six U.S. high performance research reactors to low enriched uranium (LEU). These reactors require a very high density fuel which has been developed at DOE national laboratories over the last 15 years. The baseline design for the fuel is a uranium-molybdenum alloy rolled as a solid fuel which is coated/bonded with a zirconium diffusion barrier layer. This fuel "foil" is then placed between two sheets of aluminum and then bonded together to create a fuel plate.

The Conversion Program maintains a comprehensive research and development project that includes the development and demonstration of the UMo foil and plate process at commercial-scale under the Fuel Fabrication Capability (FFC) Pillar. Specifically, the FFC is tasked to establish a cost-effective and efficient manufacturing process that can be implemented by a commercial entity through the transfer of technology from national laboratories to a commercial entity and the demonstration of the process on production-scale equipment at a commercial fabricator.

Babcock & Wilcox (B&W), Nuclear Operations Group in Lynchburg, Virginia, U.S.A. has been working closely with DOE on the Conversion Program for over 10 years. B&W was selected to demonstrate the baseline UMo process on commercial-scale equipment to provide FFC and the Conversion Program with necessary information to determine if the baseline process is in fact cost-effective and efficient or if alternatives and/or improvements must be implemented to ensure its objectives are met.

B&W has identified a baseline process at commercial-scale including the generation of equipment specifications for all new equipment for a UMo foil and plate demonstration facility. The equipment has been procured and is installed and demonstration of the process with depleted uranium (DU) on the new pilot line has commenced. A summary of those activities follows.

2. UMo Process & Equipment

2.1 UMo Process Review

The B&W UMo team performed a review of all processes and equipment that had been used to date to perform the fabrication of UMo foils and plates at various national laboratories. This led to the identification of a standard "baseline" process for the UMo foil/plate that was utilized in the selection of process equipment. The standard process is described in Figure 1.

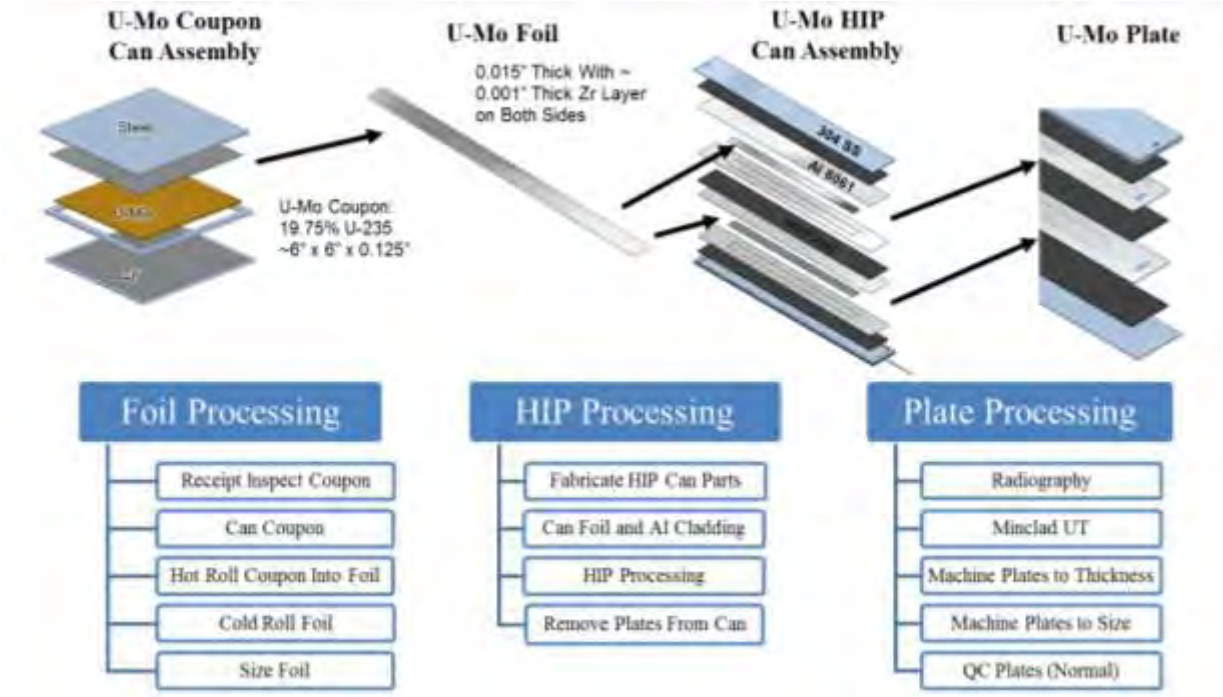

Fig. 1. UMo Baseline Process

A standard sized UMo coupon is received from the DOE Y-12 facility where it has been cast into a 3-plate book mold and machined to final size. This coupon is receipt inspected for size and surface defects. The coupon is then cleaned in a nitric acid bath prior to loading it into a rolling can. The mild steel hot rolling can is packed and seal welded in an argon glovebox to create an inert atmosphere during the hot rolling process. The rolling can frames and covers are sized to provide a minimal gap (< 0.38 mm) between the coupon and the edge of the frame. The frames and covers are cleaned with abrasive brushing techniques and a detergent wash. The inside surface of each cover of the can is also prepared by coating it with Neolube to act as a parting agent to ensure the foil is easily removed from the can after rolling. Next, a sheet of pure Zr (≥ 99.2%) is polished with diamond paste and tack welded to the cover. The UMo coupon is placed into the rolling can assembly; the edges of the assembly are then seal welded together inside an inert argon glovebox to capture the UMo coupon in the inert atmosphere.

The assembly is then hot rolled on a 2-high rolling mill at 650°C for a series of passes to an overall reduction of ~80%. The hot and cold rolling schedules are discussed in further detail in later paragraphs. When hot rolling is complete the foil is removed from the can by shearing off the welds on each side of the pack. The foil is cleaned with isopropyl alcohol and inspected for size and surface defects such as cracks, Zr tearing or Zr blisters. The foil is cold rolled to final thickness using a separate 4-high rolling mill. The foil is cut to size and is then ready to be placed into a HIP can.

The HIP can and aluminum sheets for cladding are prepared by mechanical and chemical cleaning prior to HIP can assembly. The time between cleaning of the Al 6061 and the assembly of the HIP can is kept to a minimum. Steel separator plates are also included inside the can to separate the aluminum from each fuel plate. The separator plates are coated with Neolube and baked out prior to assembly in the can. After multiple plates and foils have been assembled, the HIP can is seal welded in a vacuum atmosphere. The can is placed into a HIP at ~15 ksi and ~590°C for ~90 minutes to bond the Al to Al and the Al to the UMo foil. After the HIP cycle is complete, the welds on the HIP cans are mechanically removed, and the plates are carefully removed to

maintain identification. The plates then follow standard Al clad fuel plate processes and quality inspections to be sized to final dimensions and ensure quality control.

2.2 Equipment Identification

The identification of equipment for the demonstration line was created by generating a Work Breakdown Structure (WBS) for the process. For each WBS element of the process the equipment to be utilized, along with tooling and other necessary items were specified. A review of the B&W RTR facility and existing equipment utilization was made to determine what space was currently available and what could be made available based on removal of old equipment. This led to an equipment plan which included new equipment and the use of existing equipment for the UMo demonstration line. A list of the new equipment identified for the UMo foil process follows in Table 1. The list of existing equipment includes a hot roll mill and hot rolling furnace for UMo foil rolling and all equipment associated with fabricating the fuel plates. The existing hot roll mill furnace was identified as an interim measure because the process temperature was close to the max operating temperature; therefore, a new furnace was also planned for procurement.

New Equipment	Status
TIG Weld Glovebox	In-service
De-can Shear	In-service
Cold Rolling Mill	In-service
Slitter	In-service
Vacuum Anneal Furnace	Installed
Hot Roll Mill Furnace	Installed

Tab 1: New Equipment

The use of the existing Idaho National Laboratory hot rolling mill and companion furnace for UMo rolling necessitated the creation of a Memorandum Of Understanding (MOU) to formally document approval. Concerns were addressed, such as, the fabrication of a different set of rolls and the replacement of the rolls for hot rolling the mild steel pack. This replacement would eliminate the possibility of cross contamination of the steel to the standard aluminum product. The MOU also addressed upset conditions to the rolling mill and standard HEU product. The approval of the MOU between two DOE entities and B&W was attributed to extensive work and cooperation.

3. Demonstration Line Installation

3.1 Project Planning

Each part of the process and each new piece of equipment was documented in detail to identify the changes to the facility and the new uranium processes. Planning for the installation of the new foil demonstration line equipment included extensive reviews by various internal groups to address the impacts to the following:

- Nuclear criticality controls
- Nuclear material accountability
- Nuclear licensing
- Physical security
- Radiation and contamination protection
- Industrial health and safety
- Environmental regulations

Each group outlined various requirements which had to be addressed by the UMo engineering team. These requirements were used to create an integrated schedule for the preparation of the facility, the installation of the equipment, and the utilization of the facility to execute the initial development tasks.

For each piece of equipment, a new equipment specification was written and reviewed internally and externally to ensure technical requirements were met and, it would meet its intended function. Upon approval, the specifications were sent for quotes and proposals were reviewed and selected. Internal project management followed the procurement, fabrication, and testing of the equipment to ensure cost and schedules were monitored appropriately.

3.2 Facility & Equipment Preparation

A significant amount of space in the radiologically controlled area was necessary to accommodate the new equipment for rolling the UMo foils. This led to a plan to remove old glovebox lines which were obsolete or no longer in use. It also required the removal of other equipment and interior walls. The intent was to create a large single room where processing of the foils would not be inhibited by compartmentalized rooms. In addition, the overall HVAC system was required to be upgraded to allow for the significant increase in contamination hoods at each piece of new equipment. Demolition required a significant amount of waste drums and sea-land containers to dispose of the low level waste.

A majority of the new equipment also required an upgrade to the electrical service in the area. This upgrade was implemented such that additional equipment could be added to the service in the future, if required. Prior to shipping and installation, most of the new equipment required vendor acceptance testing. After shipment and installation, the new equipment went through detailed checks by engineering and safety staff to ensure the specification requirements were met and to identify any unintended safety issues.

4. UMo Process Demonstration

4.1 Surrogate Testing

Before processing of UMo material commenced, stainless steel surrogate material was processed through the equipment. The surrogate material served as a vehicle to verify the setup and operation of the equipment, allow for refinement of operating parameters and procedures, and finally to allow the operators to gain experience on the new equipment.

Prior to processing the stainless steel material, the rolls on the hot roll mill were changed to a dedicated set identified for the processing of UMo material. Stainless steel slugs, ~200 mm x 150 mm x 9.5 mm (LxWxT), were utilized to setup the hot roll mill and furnace. A time versus temperature study was performed to characterize the thermal properties of the stainless steel in the furnace. An infrared measuring device was used to track the heat up of the stainless steel slugs in the furnace and the heat loss as they were processed through the hot roll mill. The slugs were heated to 650°C. Unlike previous UMo processing at the national laboratories, where material is placed in a furnace for a preset time, the slugs were not processed through the hot roll mill until the target temperature was achieved. This resulted in a slightly longer heat up time as well as increasing the dwell time of the material in the furnace between passes through the mill. The slugs were processed through the mill to determine the maximum reduction that could be taken per pass. After several iterations a hot roll pass schedule was defined to target an 80% reduction for the canned surrogate material.

Stainless steel blanks the approximate size of the development UMo coupons, 150 mm x 100 mm x 3.2 mm, were canned in mild steel to simulate the proposed rolling process. Prior to canning, the stainless blanks, steel frames and covers were degreased and cleaned to remove any oils and residual surface debris. One side of each cover was coated with Neolube to act as a parting agent to aid with the decanning process. The steel cans and stainless blanks were assembled to form a rolling pack. The rolling packs were then sealed using a TIG weld. Twenty five rolling packs were prepared for rolling and separated into 5 lots of 5 rolling packs each.

After seal welding, the first lot of rolling packs was heated in a box furnace to 650°C. Once the target temperature was achieved the rolling packs were removed from the furnace and processed through the hot roll mill. The first lot was hot rolled using the pass schedule developed using the stainless steel slugs. The canned stainless steel reacted differently through the hot roll than the stainless steel slugs. The percent reduction per pass was reduced due to the softer steel can material. The dwell time of the packs in the furnace was also adjusted. Once the target hot roll reduction of 80% was achieved, the packs were allowed to air cool before decanning to remove the hot rolled foil.

The four remaining lots of surrogate rolling packs were processed individually to further refine the hot roll schedule. The percent reduction per pass in conjunction with furnace dwell times were adjusted until a consistent rolled pack was achieved. Once all surrogate steel packs were cooled, the hot rolled foils were removed by shearing the cans using a hydraulic shear. The hot rolled stainless foils were easily removed from the cans. The foils were flat and straight and exhibited consistent thickness and minimal camber.

The stainless foils were then cleaned and cold rolled to thicknesses ranging from 0.64 mm to 0.15 mm. The stainless steel foils cold rolled with minimal deflections, waviness, and camber. The thickness of the foils was also consistent. Final thickness was achieved using a combination of gap and force loadings on the cold roll mill. Each foil processed exhibited consistent and repeatable results.

4.2 Depleted Uranium Development

Prior to processing the depleted uranium (DU) material, a detailed development plan was established to identify usage of the material to ensure programmatic information is obtained and fabrication processing parameters are understood thoroughly. The plan was focused on generating information and demonstration of the process as needed to produce experiment specimens for the next irradiation experiment, MP-1.

The processing of the depleted UMo coupons occurred after the stainless steel surrogate foils following the same general process. The mild steel was cleaned using the same procedure as was employed for the stainless steel blanks. In addition to the mild steel, zirconium foil was polished using a water soluble diamond paste to remove any surface oxidation. Once the steel covers were coated with Neolube, the 0.25 mm thick sheet of zirconium was tacked to the cover over the area coated with Neolube. The pack covers and frames were then transported to the rolling pack assembly area.

The coupons were cleaned in a 30% nitric acid solution and deionized water to remove any surface oxidation. Before assembling the hot roll packs, the coupons were given a wipe using alcohol soaked lint free cloths. The cleaned coupons were then assembled into packs and seal welded in an argon atmosphere by TIG welding. The sealed hot roll packs were then transported to the hot roll area for rolling.

For hot roll, the initial lot was split into two groups of 5 coupons to minimize initial processing risk. The process parameters optimized on the stainless surrogates were

used for the initial lot of 10 coupons. This first lot was used to characterize the dwell time in the furnace as well as verify the hot roll pass schedule. The first DU lot (Lot #1) reacted slightly different than the canned stainless surrogate. The hot roll pass schedule was modified slightly to compensate for the change in the rolling characteristics of the DU. The final hot roll packs exhibited a consistent thickness across the pack which was flat and straight.

Before hot rolling the Lot #2, Lot #1 was decanned to evaluate the hot rolled foils (See Figure 2). The foils required a little more effort to decan due to the presence of the zirconium on the foil. Even though slightly more effort was needed, the foils were easily removed from the hot rolled packs. The foils exhibited a range of "orange-peel" historically seen on previous rolling efforts (See Figure 2). The first few foils showed some zirconium bonding to the steel covers on the leading edge of the pack. This was attributed to the aggressive rolling reduction schedule. A few of the foils also had some minor blistering of the zirconium. The blisters were concentrated mainly on the leading and trailing ends of the foil.

Fig 2: DUMo Foil After Decanning

Minor changes were made to the hot roll schedule for the DU lots #2 and #3 based on observations from Lot #1. The heat up and dwell times in the furnace were consistent. The per-pass reductions were reduced to better equalize them to achieve the target 80% reduction (See Table 2). Due to the slightly longer dwell times in the furnace, there was a more consistent ratio of can to UMo reduction. This translated to a pack reduction of 80% produced a UMo reduction of ~78-79%. The thickness of the foils after hot rolling for lots one through three averaged 0.76 mm.

Pass	Avg. Reduction (mm)	% Reduction	Furnace Dwell Time (min)
Pre Hot Roll Heat Up			60
1	1.68	16.3	20
2	2.01	23.3	20
3	1.80	27.1	20
4	1.30	26.6	20
5	0.79	22.3	20
6	0.46	17.0	20
Post Hot Roll Anneal			45

Tab 2: 80% Reduction Hot Roll Schedule

Before continuing to hot roll more DU material, Lot #1 was cold rolled. The hot rolled foils were cleaned using alcohol soaked lint free cloths. Once cleaned, the foils were measured for dimensions and mass before cold rolling. The foil thickness before cold roll averaged 0.76 mm with a standard deviation of 0.047 mm. A cold roll schedule using a combination of gap and force-feedback settings was used to reduce the thickness to ~0.5 mm. The DUMo foils did not reduce as easily as the stainless steel surrogate material. The stiffness of the foil inside the can resulted in less of a reduction per pass in the DUMo material when compared to the same reduction schedule used on the canned stainless steel material. Therefore, the pass schedule was adjusted slightly to reduce the per pass reduction in order to accommodate the DU foils. More foil-to-foil variation was observed in rolling the DUMo foils than the stainless foils. Variation was typical when compared to previous rolling efforts at the national laboratories. Foils exhibited waviness and camber during the rolling, but these were reduced as the foil thickness reduced. Any blisters on the foils were limited to the leading and trailing ends.

After hot roll, the foils from Lots #2 and #3 were decanned and evaluated for dimensions and mass. The hot rolled foils produced similar results as those obtained from the first DU lot. The foils were flat, straight, and the average thickness was 0.76 mm with a similar orange peel appearance. Again, there were a minimal amount of blisters on the ends of the foils. None of the foils had zirconium which stuck to the cover of the hot roll pack. The same cold roll schedule was repeated on Lot #2 and Lot #3 to achieve a final thickness of 0.5 mm. The foils in in these two lots were very similar in appearance to those in Lot #1.

The hot roll schedule was modified slightly for DU Lots #4 - #7 (See Table 3). For these lots the target hot roll reduction was 72%. The amount of hot work was reduced in order to allow more cold work into the foils to achieve a final foil thickness of 0.64 mm. An 80% hot roll reduction did not leave enough material to produce an adequate 0.64 mm foil. There were no issues hot rolling to a 72% reduction. When decanned, the hot rolled foils were on target with a thickness of ~1.0 mm. The surface appearance of the hot rolled foils was also consistent with the previous lots. As of this authoring, DU Lot #4 is currently being cold rolled to a target thickness of 0.64 mm. The cold rolled foils are behaving as the previous foils and are flat with some slight waviness when finished.

Pass	Avg. Reduction (mm)	% Reduction	Furnace Dwell Time (min)
Pre Hot Roll Heat Up			60
1	1.73	16.8	20
2	1.93	22.3	20
3	1.32	19.9	20
4	1.07	20.2	20
5	0.69	16.3	20
6	0.51	13.9	20
7	0.25	8.5	20
Post Hot Roll Anneal			45

Tab 3: 72% Reduction Hot Roll Schedule

4.3 Future Work

DU material processing will continue to be completed to gather fabrication information. Upon completion of DU work, LEU work will be performed to verify consistency between the two materials. Additionally, larger coupons, termed ingots (~90 mm x 225 mm x 5 mm, will be processed with an additional homogenization and hot/cold work prior to roll bonding the Zr onto the ingot. This work will be performed to demonstrate an optimized process to reduce internal defects, increase homogeneity of the U-Mo alloy, and to increase consistency and processing ingot-to-ingot. To reduce waviness of the foils prior to the HIP process, the foils will be subjected to a vacuum anneal. Finished foils will also be used to demonstrate the optimized HIP can and plate process.

5. Conclusions

Significant effort was made to plan and execute the removal of old equipment and the installation of new equipment to support the Conversion program. This work has produced a UMo foil demonstration line capable of producing a large quantity of foils at commercial-scale for full size research reactor fuel plates. The process and equipment are capable of producing consistent foils.

Several observations should be noted based on the stainless steel and DU rolling activities to date. The first is that stainless steel may be used as a setup for rolling, but it rolls more easily than the UMo. The second is the longer dwell times in the furnace allow the UMo to heat more, thus resulting in a more uniform reduction, relative to the steel can, during hot roll. The last observation is that each DUMo foil cold rolls slightly differently. It is believed that variations within the UMo coupon are a contributor to this affect, which may be improved with the optimized homogenization process. However, even with the variation in individual foils, we have been able to produce a consistent foil when the target thickness is achieved.

6. References

M.J. Nilles, J.M. Wight; “Babcock & Wilcox UMo Plate Fabrication Experience”; *Proceedings of the International Meeting on Reduced Enrichment for Research and Test Reactors*, Lisbon, Portugal, October 2010.

G.A. Moore & M.C. Marshall; “Co-Rolled U10Mo/Zirconium-Barrier-Layer Monolithic Fuel Foil Fabrication Process”; INL/EXT-10-17774; Idaho National Laboratory.

Dombrowski et al; “LANL Progress on U-Mo Fuel Fabrication Process Development”; *Proceedings of the International Meeting on Reduced Enrichment for Research and Test Reactors*, Vienna, Austria, October 2014.

Moore, Jue, Rabin, Nilles; “Full Size U-10Mo Monolithic Fuel Foil and Fuel Plate Fabrication-Technology Development”; *INL/CON-09-17519*; Idaho National Laboratory.

Hammon & Clarke “LANL experience rolling Zr-clad LEU10Mo foils for AFIP-7”, Los Alamos National Laboratory.

D.J. Senor & D. Burkes; “Fuel Fabrication Capability Research and Development Plan”, *PNNL-22528, Rev. 1;* Pacific Northwest National Laboratory.

“Specification for U-Mo Monolithic Foils”; *SPC-1167, Rev. 3*; Idaho National Laboratory.

Moly99 Production

THE ROLE OF THE IAEA IN SUPPORTING PRODUCTION OF Mo-99 AND/OR Tc-99m WITHOUT THE USE OF HEU

J. A. OSSO JUNIOR, M. VENKATESH, A. DUATTI
NAPC, IAEA
Vienna International Centre, PO Box 100, A-1400 Vienna, Austria

J. DIX, E. BRADLEY
NEFW, IAEA
Vienna International Centre, PO Box 100, A-1400 Vienna, Austria

ABSTRACT

Technetium-99m (Tc-99m) is the most widely used medical radioisotope, amounting to over 30 million studies per year and accounting for more than 80% of all procedures in diagnostic nuclear medicine. Apart from the ideal features of Tc-99m, its readily availability in a carrier free form from Mo-99/Tc-99m generators has been key advantage making it the 'work horse' of diagnostic nuclear medicine. Molybdenum-99 (Mo-99), the parent nuclide of Technetium-99m used in such generators, can be produced in several different ways, although the most prevalent is through the fission of high enriched uranium (HEU) targets. The supply of Mo-99 has been disrupted since 2007 for various reasons, although primarily stemming from the ageing fleet of reactors used in its production. The situation is expected to be precarious in the near future with possibilities of shortages when some of the key reactors producing Mo-99 cease operation, either permanently or for prolonged periods for maintenance and facility upgrades. Realising the need to support the Member States in mitigating the effects of a supply crisis of Mo-99/Tc-99m in the future, the IAEA has initiated a few activities that will be highlighted in this paper. The following three main on-going IAEA activities will be presented: (i) the Peaceful Uses Initiative project on "Supporting the Global Deployment of Mo-99 Production Capacity for Nuclear Medicine Applications without the Use of Highly Enriched Uranium (HEU)", aimed at assisting small-scale, national-level producers in setting up their production capability using low enriched uranium (LEU) fission or the Mo-98(n,γ)Mo-99 reaction; (ii) the HEU minimization project, aimed at the transition of Mo-99 production away from the use of HEU, and (iii) the Coordinated Research Project on "Accelerator-based Alternatives to Non-HEU Production of Mo-99/Tc-99m", aimed at the direct production of Tc-99m through the reaction Mo-100(p,2n)Tc-99m using cyclotrons. The outcomes of these projects thus far as well as the activities planned for the future will be discussed.

1. Introduction

1.1. Role of Tc-99m in Nuclear Medicine

While nuclear medicine applications encompass both diagnostic and therapeutic procedures, more than 90% of all nuclear medicine procedures are diagnostic imaging. The radionuclide Tc-99m plays a particularly dominant role in nuclear medicine as its radiopharmaceuticals are employed in more than 80% of all diagnostic procedures worldwide. Over 30 million procedures with Tc-99m radiopharmaceuticals are performed worldwide every year, with more than 50,000 procedures performed in the USA alone every day.

According to the report from OECD-NEA in 2014, the annual growth rate of Mo-99 in mature markets (North America, Europe, Japan and the Republic of Korea) is assumed to be 0.5%, and in emerging markets 5% [1].

Technetium-99m is an ideal medical radionuclide for the imaging technique Single Photon Emission Computed Tomography (SPECT) due to its appropriate physical decay characteristics, availability in the form of a radionuclide generator, and favourable chemistry.

Physical Decay Characteristics: Technetium-99m decays by isomeric transition to long-lived ground state Tc-99. During this decay, a low energy photon (140 keV) is emitted without the emission of particulate radiation. As a result of this and the short half-life of Tc-99m (6 hours), the radiation dose to both medical staff and patients is minimized while providing excellent imaging properties.

Radionuclide Generators: Molybdenum-99, the parent isotope of Tc-99m, has a half-life of 66 hours. As the half-life of Mo-99 is longer than that of Tc-99m, their activities reach an equilibrium state with time and it is possible separate Tc-99m at repeated intervals. The activity of Tc-99m reaches its maximum after 23 h of decay of Mo-99 enabling the medical institutions or centralized radiopharmacies to separate and use Tc-99m every day. Typically, hospitals use the generators for a week and some for 2 weeks. The most employed generator is the chromatographic based on alumina, that uses high specific activity Mo-99 and allow the elution of Tc-99m with a high radioactivity concentration, suitable for labelling the kits for the preparation of Tc-99m radiopharmaceuticals.

Favourable Chemistry and use in diagnostic nuclear medicine: The rich co-ordination chemistry of Tc, a transition metal element, enables Tc-99m to form complexes with a variety of molecules, which in turn permits easy labelling of different molecules in various kit formulations. More than 20 different kits can be labelled with Tc-99m and are routinely used [2, 3] to image various organs for structural as well as functional information. In particular, myocardial perfusion imaging (MPI) and scanning of bone metastatic invasion as a side effect of various primary cancers are among the most widespread applications.

1.2. Mo-99 Production Technologies and Impact on Supply

Although there are several ways of producing Mo-99 [4], the main route involves the neutron induced fission of U-235, which has a large cross-section (~584 barns for thermal neutrons) and a high Mo-99 production yield of 6.1%. This route produces Mo-99 with a high specific activity that is used in compact chromatographic Mo-99/Tc-99m generators based on alumina. Most Mo-99 production using this route is in multipurpose research reactors as they have operational schedules and space available for irradiating multiple targets at high neutron fluxes (10^{13}–10^{14} $n.cm^{-2}.s^{-1}$). While historically Mo-99 has been produced using high enriched uranium (HEU) targets, the Mo-99 community is currently in the process of transitioning to non-HEU based technologies.

Other Mo-99 production routes include:

- Fission of U-235 with neutrons produced in deuteron and proton accelerators through (d,n) and (p,n) reactions on heavy targets.
- Neutron activation of Mo-98 (i.e. Mo-98(n,γ)Mo-99). This reaction has a small cross-section (0.13 b for thermal neutrons) and produces Mo-99 with a low specific activity that is not suitable for use in the current chromatographic generators based on alumina. Further, the natural abundance of Mo-98 is ~24% and the use of enriched Mo-98 targets can increase the specific activity of Mo-99.
- Photo fission of Mo-100 (i.e. Mo-100(γ,n)Mo-99). The energetic photons used in this production scheme are obtained by irradiating heavy targets with electron beams produced by linear accelerators. The Mo-99 produced is of low specific activity.
- Direct production of Tc-99m in cyclotrons through the Mo-100(p,2n)Tc-99m reaction.

According to estimates made by the OECD-NEA [1], the weekly global demand for Mo-99 is approximately 10,000 6-day Ci[1], which is largely met by the fission of HEU targets in research reactors.
At present, there are five major producers of Mo-99: Nordion (Canada), the Institute for Radioelements (IRE) (Belgium), Covidien/Mallinckrodt (the Netherlands), NTP Radioisotopes (South Africa) and the Australian Nuclear Science and Technology Organisation (ANSTO) (Australia). The National Atomic Energy Commission (CNEA) in Argentina was the first Mo-99 producer to deploy LEU targets for small-scale, primarily national production (from 2002). Since 2010, both ANSTO and NTP Radioisotopes have been producing large scale quantities of Mo-99 using LEU targets.
Since 2007, the supply of Mo-99 has experienced disruptions for various reasons, primarily stemming from the ageing fleet of reactors. The situation is expected to be precarious in the near future with possibilities of shortages when some of the key reactors producing Mo-99 cease operation, either permanently or for prolonged periods for maintenance and facility upgrades.

1.3. Role of IAEA in supporting the production of Mo-99 and/or Tc-99m

Realising the need to support the Member States in mitigating the effects of a supply crisis of Mo-99/Tc-99m in the future, the IAEA has initiated the following activities:

(i) the Peaceful Uses Initiative project on "Supporting the Global Deployment of Mo-99 Production Capacity for Nuclear Medicine Applications without the Use of Highly Enriched Uranium (HEU)", aimed at assisting small-scale, national-level producers in setting up their production capability using low enriched uranium (LEU) fission or the Mo-98(n,γ)Mo-99 reaction;

(ii) (ii) the HEU minimization project, aimed at the transition of Mo-99 production away from the use of HEU, and

(iii) (iii) the Coordinated Research Project on "Accelerator-based Alternatives to Non-HEU Production of Mo-99/Tc-99m", aimed at the direct production of Tc-99m through the reaction Mo-100(p,2n)Tc-99m using cyclotrons.

2. Peaceful Uses Initiative project on "Supporting the Global Deployment of Mo-99 Production Capacity for Nuclear Medicine Applications without the Use of Highly Enriched Uranium (HEU)"

In 2005, the IAEA launched a coordinated research project (CRP) on "Developing Techniques for Small Scale Indigenous Molybdenum-99 Production Using LEU Fission or Neutron Activation." The aim of this CRP was to support interested Member States in adopting non-HEU technologies for the small-scale, national level production of Mo-99 through LEU fission or (n,γ) routes. The expected output of the CRP was that the Member States would acquire an understanding of the available technologies and be in a position to make a sound decision on whether to proceed with domestic production of Mo-99 or to look for alternative options to satisfy domestic demand. Fourteen Member States participated in this CRP, either as contract or agreement holders. During the CRP, which concluded in December 2011, four research coordination meetings (RCMs) and four workshops were hold. The four workshops covered the topics of operational aspects of Mo-99 production, LEU target fabrication, and waste management, which were of great practical help to participants. In January 2015, the IAEA published Technical Report Series No. 478, *Feasibility of Producing Molybdenum-99 on a Small Scale Using Fission of Low Enriched Uranium or Neutron Activation of Natural Molybdenum* [5], which summarizes the activities and results of this CRP.

[1] The activity of Mo-99 has traditionally been mentioned in Curies after decay correction for 6 days, to indicate the activity a user will get when the generator is shipped and arrives about 6 days later at the hospital radiopharmacy. Thus the actual production values are much (~4.5 times) larger.

This CRP and a 2013 IAEA Nuclear Energy Series publication: NF-T-5.4, 'Non-HEU Production Technologies for Molybdenum-99 and Technetium-99m' [4] served as the basis for the Peaceful Uses Initiative project on “Supporting the Global Deployment of Mo-99 Production Capacity for Nuclear Medicine Applications without the Use of Highly Enriched Uranium (HEU)”, which was initiated in 2013. The project is aimed at strengthening the supply of Tc-99m in developing countries by assisting small-scale, national level producers in setting up a production capability. This is achieved via (i) developing human resources and skills related to target irradiation and handling, radiochemical processing, Tc-99m generator production, supply logistics, and waste management and (ii) the direct, coordinated, multi-regional deployment of demonstrated, non-HEU based Mo-99 production technologies.

This project and supporting activities are being jointly managed by the IAEA’s Department of Nuclear Energy and Department of Nuclear Sciences and Applications. To achieve the objective, funding provided through the Peaceful Uses Initiative has been used for the following activities:

- *Detailed fact-finding missions to relevant facilities in participating Member States.* The purpose of the missions is to evaluate the status of the current available Mo-99/Tc-99m production infrastructure, taking into account the research reactor capabilities, radioisotope production facilities, waste management and overall logistics, including commercialization. Production infrastructure fact-finding missions were completed to Mexico, Morocco, Peru, Poland and Romania. Similar missions were conducted in Egypt (2010) and Malaysia (2011). The outputs came in the form of comprehensive mission reports, including recommended infrastructure improvements for various production options.
- *A training course on the practical aspects of the production of Mo-99 by the (n, γ) reaction.* This training course will take place in Mumbai, India in June 2015 and is intended to provide practical instruction on the (n,γ) production of Mo-99 to Member States that have previously participated in the fact-finding missions.

3. Activities supporting the transition from away from HEU

As part of the IAEA's continuing involvement to address security of supply as well as minimize the use of HEU in civilian applications, the IAEA has held a series of Technical Meetings on Conversion Planning for Molybdenum-99 Production Facilities since 2010. These meetings have provided a forum for representatives of the major Mo-99 producers and related stakeholders to identify issues associated with the conversion of existing isotope production facilities to LEU targets and to help develop a plan to address these challenges.

ANSTO (Australia) and NTP Radioisotopes (South Africa) continue to be the major suppliers of non-HEU Mo-99. In 2014, ANSTO broke ground on its new Mo-99 production facility, which is expected to increase production from 1,000 to 3,500 6-day curies of LEU-based Mo-99. NTP Radioisotopes is continuing to convert its processes to the exclusive use of LEU. IRE (Belgium) and Mallinckrodt (the Netherlands) have initiated efforts to support the conversion of their commercial-scale production processes from HEU to LEU. In February 2015, Canada announced that it would extend operations of the NRU until March 31, 2018 to support global medical isotope demand through any unexpected time of shortage.

Given the progress of the major Mo-99 producers in their conversion activities, it was recommended in the most recent IAEA meeting (February 2015) that the meeting as currently established has fulfilled its mission and that a forum dedicated to its specific discussion was no longer necessary. However, the participants stressed that there was continuing interest in addressing future activities that will assist the producers following their initial conversion. In line with this request, the IAEA is in the process of developing future meetings on global capabilities for targetry, including harmonization, optimization, and high-density aspects.

4. Coordinated Research Project on "Accelerator-based Alternatives to Non-HEU Production of Mo-99/Tc-99m"

An alternative procedure for producing the key radionuclide Tc-99m is to make use of medical cyclotrons commonly employed for the routine production of F-18 and C-11 radiopharmaceuticals for positron emission tomography (PET). An IAEA CRP on "Accelerator-based Alternatives to Non-HEU Production of Mo-99/Tc-99m" was launched in 2011 and will have its third and final meeting in June 2015 with the participation of representatives of 11 Member States. The aim of the CRP is to demonstrate the routine, reliable, commercial-scale production of Tc-99m via the Mo-100 (p,2n) reaction [6].

Recent technological improvements in cyclotron technology are opening the doors to the production of key medical radionuclides in higher yields, thus favouring their widespread clinical use. Available proton energies of commercial cyclotrons currently range from 6 MeV up to 70 MeV with the constant increase of proton current that can be as high as 750−800 μA. The availability of high currents has allowed for overcoming limitations in radionuclide production yields arising from low values of cross sections for proton interaction. This has stimulated important advancements of the technology for assembling solid targets that are able to efficiently dissipate the significant heat generated by high ion currents. With these new technological achievements, it will be possible to produce some crucial radionuclides in larger amounts and ensure their broader supply.

The studies performed so far under the CRP include building a high-efficiency target, finding the proper irradiation conditions (incident proton energy, target thickness and length of irradiation), implementing automated methods to extract and purify Tc-99m in the chemical form of pertechnetate, recycling of the enriched Mo-100 target, performing quality control of Tc-99m (in particular its radionuclidic purity), assessing the suitability of the technetium radioisotope for eventual human use, performing dosimetry calculations to estimate radiation dose to the patient from potential radionuclidic impurities, and comparing the image quality of standard Tc-99m-radiopharmaceuticals prepared using cyclotron-produced pertechnetate with commercial generator produced Tc-99m through animal imaging studies.

Most of the technical issues have been resolved and now the challenges relate to the regulatory approval, the distribution logistics and the supply of enriched Mo-100 for target preparation. Recently, one of the CRP participants, from TRIUMF, Canada, issued a press release stating the achievement of the production of 34 Ci of Tc-99m in one production and that clinical trials were initiated with cyclotron produced Tc-99m [7].

5. Conclusions

The IAEA, through a variety of activities continues to support actions aimed at securing a reliable, non-HEU supply of Mo-99 and/or Tc-99m. In addition to the efforts mentioned previously in this paper, the IAEA is pursuing new actions to assist in this goal. Upcoming activities include:

a- *A new CRP on "Sharing and Developing Protocols to Further Minimize Radioactive Gaseous Releases to the Environment in the Manufacture of Medical Radioisotopes, as Good Manufacturing Practice"*. The overall objective of this CRP is to formulate a roadmap to guide the international community of medical radioisotope produces on how to address and reduce the emission of radioactive gases resulting from medical isotope production, in particular Mo-99. This CRP was launched in December 2014 and the first Research and Coordination Meeting is expected to occur in August 2015.

b- *A Technical Meeting on "New Ways of Producing Tc-99m and Tc-99m Generators"*. This meeting is expected to discuss novel materials/technologies for preparation of Mo-99/Tc-99m generators using low specific activity Mo-99 and novel routes for producing Tc-99m other than the established ones and will take place in August 2015.

6. References

[1] – The Supply of Medical Radioisotopes, Medical Isotope Supply in the Future: Production Capacity and Demand Forecast for the 99Mo/99mTc Market, 2015-2020, April 2014; http://www.oecd-nea.org/med-radio/reports/sen-hlgmr2014-2.pdf

[2] – Technetium-99m Radiopharmaceuticals: Manufacture of Kits, IAEA TECHNICAL REPORTS SERIES No. 466, 2008; http://www-pub.iaea.org/MTCD/publications/PDF/trs466_web.pdf

[3] – Technetium-99m Radiopharmaceuticals: Status and Trends, IAEA RADIOISOTOPES AND RADIOPHARMACEUTICALS SERIES No. 1, 2009; http://www-pub.iaea.org/MTCD/publications/PDF/Pub1405_web.pdf

[4] – Non-HEU Production Technologies for Molybdenum-99 and Technetium-99m, IAEA NUCLEAR ENERGY SERIES No. NF-T-5.4, 2013; http://www-pub.iaea.org/MTCD/Publications/PDF/Pub1589_web.pdf

[5] – Feasibility of Producing Molybdenum-99 on a Small Scale Using Fission of Low Enriched Uranium or Neutron Activation of Natural Molybdenum, IAEA TECHNICAL REPORTS SERIES No. 478, 2015; http://www-pub.iaea.org/MTCD/Publications/PDF/trs478web-32777845.pdf

[6] – REPORT on the 2nd Research Coordination Meeting on “Accelerator-based Alternatives to Non-HEU Production of 99Mo/99mTc”, working material, 2013; http://www-naweb.iaea.org/napc/iachem/working_materials/TR-RCM2-Final-Report-Draft-oct-22nd.pdf

[7] – Canadian Team Demonstrates Solution to Medical Isotope Crisis, TRIUMF press release, January 05, 2015; http://www.triumf.ca/sites/default/files/2015-01-05_NR-ITAP-Milestone_vFINAL_0.pdf

U.S. DEPARTMENT OF ENERGY NATIONAL LABORATORY RESEARCH AND DEVELOPMENT ACTIVITIES DIRECTED TOWARD MINIMIZING THE USE OF HIGH ENRICHED URANIUM FOR MO-99 PRODUCTION AND DEVELOPING A DOMESTIC SUPPLY

G. F. VANDEGRIFT

Nuclear Engineering Division, Argonne National Laboratory
9700 S. Cass Avenue, Argonne, IL, USA 60439

U.S. DEPARTMENT OF ENERGY NATIONAL LABORATORY RESEARCH AND DEVELOPMENT ACTIVITIES DIRECTED TOWARD MINIMIZING THE USE OF HIGH ENRICHED URANIUM FOR MO-99 PRODUCTION AND DEVELOPING A DOMESTIC SUPPLY

G.F. VANDEGRIFT
Nuclear Engineering Division, Argonne National Laboratory
9700 S. Cass Avenue, Argonne, IL, USA 60439

ABSTRACT

The U.S. Department of Energy National Nuclear Security Administration's Convert program supports the conversion of domestic and international civilian research reactors and isotope production facilities from the use of high enriched uranium (HEU) to low enriched uranium (LEU) fuel and targets. The main technology components of the program are: (1) the development of advanced LEU fuels, (2) design and safety analysis for research reactor conversion, and (3) development of targets and processes for the production of ^{99}Mo without using HEU. This paper summarizes activities at the Department of Energy's national laboratories to provide technology (1) supporting international conversion from HEU for production of ^{99}Mo and (2) developing a domestic supply of Mo-99 without the use of HEU. For conversion, the high-density target program has developed an LEU-foil target and frontend processing to allow the use of this target in current processes that use HEU targets. For development of a domestic supply, the national-laboratories are performing R&D to assist in the development of production of Mo-99 using (1) the γ/n reaction on Mo-100 using an electron-linac-accelerator, (2) the n/γ reaction on Mo-98 using a nuclear reactor, and (3) fissioning of U-235 using a D/T-accelerator-driven sub-critical sulphate aqueous uranyl-sulphate target solution.

1. Introduction

As part of its nuclear non-proliferation mission, the U.S. Department of Energy (DOE) National Nuclear Security Administration's (NNSA) Office of Materials Management and Minimization (M^3) is working to develop a reliable supply of the critical medical isotope, molybdenum-99 (Mo-99), produced without the use of highly enriched uranium (HEU). This program is a critical part of M^3's global effort to reduce the risk posed by vulnerable nuclear and radiological materials located at civilian sites worldwide. M^3 works to develop and implement technologies to minimize and, to the extent possible, eliminate the civilian use of HEU, including in research reactors and isotope production facilities. This goal is accomplished through NNSA cooperation with international Mo-99 producers in the conversion of existing isotope production facilities to low enriched uranium (LEU) and with U.S. private-sector projects to accelerate the establishment of U.S. domestic Mo-99 production.

This paper discusses four M^3-directed development projects being performed in the DOE National Laboratories:

- Development of an LEU high-density target and frontend processing for use in converting current Mo-99 production from HEU to LEU targets.

- Technical assistance in the domestic production of fission-product Mo-99 by means of an accelerator-driven non-critical LEU-salt target solution
- Technical assistance in the domestic production of Mo-99 by means of neutron irradiation of enriched Mo-98 targets
- Technical assistance in the domestic production of Mo-99 by means of accelerator irradiation of enriched Mo-100 targets.

Each project will be discussed briefly below. Following that will be a write up describing each DOE Laboratory's role in development activities.

2. The Projects

2.1 Development of High Density Targets for Conversion from HEU to LEU

The annular LEU-foil target was first developed at Argonne and tested in cooperation with the Indonesian Badan Tenaga Atom Nasional (BATAN) and the Argentine Comisión Nacional de Energia Atómic—Argentina (CNEA) in the mid-1900s. In this effort, targets were produced at Argonne a few at a time for the specific use by the two partners. NNSA decided to broaden the scope of these activities to develop (1) a high-density LEU-foil target and frontend processes to allow the use of an LEU high-density target (HDT) for all Mo-99 purification processes currently being performed with HEU-target processing and (2) fabrication and irradiation of these targets to the point they could be considered for large-scale production. The HDT project was led by NNSA's Y-12 National Security Complex. Participating in the R&D were Argonne National Laboratory (Argonne), Oak Ridge National Laboratory (ORNL), the University of Missouri, the University of Missouri Research Reactor (MURR), and the Romanian Institute for Nuclear Research. Progress reports have been presented at Mo-99 Topical Meetings in 2013 and 2014.[1,2,3] Key logistical, coating, welding, and product qualification lessons were learned during this effort that will be invaluable to an organization wishing to utilize this target technology. In addition, the fabrication technology readiness (TRL) was raised to the point that it is mature enough to be handed off to a commercial organization. The experimental portion of this project was completed at the end of September 2014, but a compendium report is being compiled and will be published in the near future.

2.2 Accelerator-Driven Fission-Product Mo-99 Production

SHINE Medical Technologies is developing a system for producing Mo-99 by fissioning of U-235 in an LEU uranyl-sulphate solution.[4,5] The SHINE target solution (STS) is of non-critical geometry, and fissioning in the solution is initiated and sustained by a fast neutron stream from a D/T generator (a deuterium-ion beam impinged on a tritium-gas target). After approximately five days of operation, the accelerator will be shut down, and, after a cooling period, Mo will be recovered from the STS using a titania-based chromatographic column and then concentrated and purified. DOE National Laboratories are participating in all aspects of the development from innovations in the accelerator design, to purifying the spent tritium from the accelerator, to modelling the nucleonics of the target solutions, to understanding radiolytic gas generation and solution chemistry during irradiation, to assessing corrosion potential in the irradiation and processing equipment, to separating and purifying the Mo-99 product. Participants in this development are Argonne, LANL, ORNL, and Savannah River National Laboratory (SRNL).

2.3 Production of Mo-99 by Neutron Irradiation of Mo-98

NorthStar Medical Technologies is cooperating with MURR to produce Mo-99 from irradiating molybdenum disks in the central thimble of the reactor.[6,7] The NorthStar/MURR contract was put in place in March 2011, and they are close to beginning production, following FDA approval. Initial production will use natural Mo targets, but they are planning to move to enriched Mo-98 in the future. Because the Mo-99 produced has low specific activity, the key to NorthStar's business plan is the RadioGenix™ technology. This Tc-99m generator is unique in that it does not hold Mo-99 and elute Tc-99m as does a conventional generator.

Rather, the Mo-99 feed solution passes through the unit and technetium is adsorbed on the ABEC (Aqueous Biphasic Extraction Chromatography) column inside the unit.[8] The Mo feed solution is stored until the next milking, and the Tc-99m is eluted from the ABEC column in a small volume of saline solution. The Ci/mL of Tc-99m in the saline solution will be equivalent to that milked from a conventional generator. An important aspect of this technology is the recycle of enriched molybdenum; which is expensive and must be recovered for future irradiations. Only one DOE National Laboratory, Argonne, is cooperating with NorthStar in development activities.

2.4 Production of Mo-99 by Accelerator Irradiation of Mo-100

NorthStar Medical Technologies is developing the technology to produce Mo-99 by utilizing the γ/n photo-nuclear reaction on a Mo-100 enriched target for the production of Mo-99. In this approach, a high-power electron accelerator is used to produce the required flux of high energy photons through the bremsstrahlung process. Aside from the differences in the production method, development activities for target processing, Tc-99m generator, and molybdenum recycle parallel those for the Mo-98 approach. Three National Laboratories, Argonne, LANL, and ORNL are assisting in the development of this technology.

3. Roles of the DOE National Laboratories

The DOE National Laboratories have wide expertise in areas necessary for the development of these technologies. NNSA took advantage of specific expertise at each Laboratory to set up teams of experts for moving each of these technologies forward. Below are short summaries of the development activities for each of these Laboratories.

3.1 Argonne National Laboratory

Argonne has been involved in the Mo-99 Conversion program since 1986. It is currently involved in all four of these technology-development projects.

Its major role in the HDT project was developing and demonstrating the frontend processes and equipment for allowing incorporation of irradiated LEU foils into the commercial purification schemes whose feed is currently an alkaline solution from the digestion of HEU uranium-aluminium dispersion targets. Two methods were developed—one by dissolution of the uranium-metal foil in nitric acid followed by Mo recovery on a chromatographic column, which is stripped using a sodium hydroxide solution, and the second by electrochemical dissolution of uranium into a sodium bicarbonate solution followed by precipitation of uranium and alkaline-insoluble fission and adsorption products by CaO addition, which leaves the Mo in an alkaline solution.[9] It also fabricated LEU foils for targets for irradiation at MURR and the ORNL HFIR (High Flus Isotope Reactor).

Argonne has a wide set of activities directed toward development of accelerator-driven fission-product Mo-99 production.[10] Its major activity is performing mini-SHINE experiments; mini-SHINE is a pilot-scale demonstration of all aspects of the SHINE system. The major difference is that an electron linear accelerator is used to generate fast neutrons that cause fission in the uranyl-sulphate target solution. All Mo recovery and purification steps are performed in the mini-SHINE demonstration.[11] Other Argonne activities are: developing means to produce the SHINE target solution of the required composition; optimizing a clean-up procedure for the irradiated target solution; simulating the radiolytic bubble formation and thermal hydrodynamics of the SHINE target solution during irradiation by the electron linear accelerator of a 20-L “segment” of the SHINE target vessel; looking at radioactive compositions, waste volumes, and classification generated during SHINE processing; and developing an understanding of the effects of radiation on solution speciation and behaviour. More information on these activities can be found by reading a

series of papers presented at the 2013, 2014, and 2015 Mo-99 Topical Meetings and citations in these papers.[12]

Argonne development activities for production of Mo-99 by neutron irradiation of Mo-98 are in four major areas: (1) assisting in the set up and implementation of the Mo-product dispensing unit at MURR and performing a PAT (Process Analytical Technology) study for this unit to fulfil an Federal Drug Administration (FDA) requirement, (2) assisting in drafting manuals and other documentation for the Dispensing and RadioGenix™ units, (3) performing calculations to estimate dose rates on specific parts in the dispensing and RadioGenix™ units and irradiating these parts using a 3 MeV Van de Graaff generator, and (4) developing means to optimize the processing of enriched Mo disks and preparation of the generator feed solutions.

Argonne development activities for production of Mo-99 by irradiating Mo-100 targets using an electron accelerator are in four primary areas; an overview of the work was presented in June 2014.[13] The primary activity is irradiating Mo-100 targets at production-level energies and power densities using the electronic linear accelerator (linac) at energies up to 42 MeV. The irradiated Mo disks are then processed, and the resultant solution is tested on a NorthStar generator system. Argonne supports LANL on the production target design and shares responsibility with LANL on the design of production subsystems, which are then tested with the Argonne linac. Argonne cooperates with ORNL, who is optimizing means to prepare enriched-Mo disks of high density, by evaluating the rate of dissolution of disks prepared under a variety of conditions. Argonne has developed and is optimizing the method to recycle irradiated Mo that will provide high purity Mo in very high yield. The initial method developed was based on precipitating MoO_3 and multiple washes; which has been demonstrated successfully at full-scale. We are currently developing a recycle method that utilizes the extraction of MoO_2Cl_2 by tributyl phosphate that is showing very promising results.

3.2 Los Alamos National Laboratory

In partnership with several other National Laboratories, Los Alamos National Laboratory is providing engineering design and support to the two accelerator-driven technologies for SHINE Medical Technologies and NorthStar Medical Radioisotopes. A brief overview of the LANL support for both of these companies is given below.

LANL is supporting SHINE in several technical areas, including system simulation, thermal hydraulics modelling, uranium detection techniques, tritium-handling support, modelling a gas nozzle for SHINE's accelerator target, and fabricating a Zircaloy-clad Depleted Uranium (DU) for an accelerator target in one of the upcoming mini-SHINE experiments at Argonne. LANL has developed a dynamic system model to allow SHINE to predict the dynamic behaviour of their solution system.[14] LANL has also developed a system simulator based on this dynamic system model that can be used for operator training.[15] They have characterized the effects of the cooling system on the uranium solution through Computational Fluid Dynamic (CFD) modelling on a LANL computing cluster. Important behaviours include the natural circulation of the irradiated solution as well as the impact of radiolytic gas bubbles formed in the solution on these convection currents. Their modelling results have been compared to experimental results from a combined natural circulation with introduced bubbles experiment at the University of Wisconsin.[16] Uranium material control and accountability (MC&A) necessitates methods for accurate uranium analysis. To address this, LANL has developed a UV-Vis assay method that can be used to measure the uranium concentration of pH 1 uranium sulphate solutions to < 1 % of the actual concentration.[17,18] Working with SRNL, LANL has performed a requirements and technologies analysis and an engineering design justification study for the SHINE Tritium Purification System (TPS). They have also studied the performance of a tritium nozzle design for the SHINE accelerator target. The result is an understanding of the nozzle's performance in terms of important flow features that manifest themselves under different parametric profiles. For one of the upcoming mini-SHINE accelerator experiments at Argonne, LANL has been fabricating

several Zr-clad DU disks at the LANL Sigma facility for the mini-SHINE phase-2 photo-neutron production target.[19] The target, which was designed and will be built at Argonne, will contain ten 1.5 mm thick DU disks and twelve 5 mm thick DU disks.
LANL's support for the NorthStar accelerator project includes engineering and design support for a series of thermal and production tests being performed on a high-power electron accelerator at Argonne, as well as accelerator target design and other design support for the NorthStar ^{99}Mo production facility. To date, eight scaled target irradiations have been performed using the electron accelerator facility at Argonne. Six of these experiments have been tests to characterize the thermal performance of the accelerator target, and two have been production experiments using enriched ^{100}Mo targets. Because the high power electron beam is directly incident on the target in this design concept, the effective cooling of the target has been a significant area of research [20]. LANL has undertaken the primary design responsibility for the high-power target and target-cooling system.[21] Other target design subjects under investigation at LANL include maximizing the ^{99}Mo production rate in the target, evaluation of photonuclear cross section data,[22] and the quantification of other radioactive products produced in the target through photonuclear reactions. LANL is also designing several of the subsystems for the NorthStar production facility. These include an Optical Transition Radiation (OTR) system for imaging the beam spot on the target window, an Infrared (IR) camera system for monitoring the target window temperature during irradiation, a multichannel Beam-Current Monitoring (BCM) system for minimizing beam losses in the accelerator transport system, Beam Position Monitor (BCM) capacitive pickups for beam position monitoring within the beam transport system, a Supervisory Control and Data Acquisition (SCADA) system for these diagnostics in the production facility, a design of the beam transport system that reduces misalignments due to beam energy fluctuations,[23] and designs for the accelerator and target shielding.[24,25]

3.3 Oak Ridge National Laboratory

ORNL researchers are involved with three of the four projects—HDT development, accelerator production of fission product Mo-99, and photo-nuclear production of Mo-99 using Mo-100 targets.
For the HDT development work, ORNL developed plans and put together safety documentation for irradiating an LEU-foil target in HFIR (High Flux Isotope Reactor). They assisted Y-12 in developing a QA/QC plan for target fabrication and developed plans for demonstrating the frontend processes in their hot cells.
For SHINE development, ORNL is performing laboratory corrosion testing of candidate alloys representing the target solution vessel (Zr-4 and Zr-2.5Nb) and the process piping and balance-of-plant components (stainless steel types 316L, 304L, 2304, and 17-4 PH) in a variety of environments simulating the anticipated process conditions as well as relevant off-normal conditions expected to bound the range of possibilities.[26] The primary component of the test solutions is depleted uranyl sulphate, which is being examined in a range of concentrations. Other environmental variables include excess sulphuric acid concentration, addition of iodine species (a fission product), nitric acid additions (simulating oxidation resulting from radiolysis), and temperature. Tests include simple coupon immersions (and exposures within the vapour above solutions), galvanic coupling exposures, U-bends to consider stress-corrosion cracking, cavitation-erosion and rotating disk electrodes to examine velocity-related effects, and cyclic polarization to assess general passivity and sensitivity to localized corrosion. Using a more limited number of environmental variables, coupon exposures are also underway at the Gamma Irradiation Facility at HFIR. In these experiments, selected environments from the family of those listed above are loaded into approved containers with specimens of interest and placed within the flux trap of spent fuel cores in the reactor pool. In this manner, rather intense gamma irradiation at a process-relevant temperature can be utilized to generate radiolysis chemistry conditions in the test solutions (immersion and vapour space) to consider the potential effects of the formation of

various radicals within the aqueous environment during SHINE service conditions. The neutron irradiation performance of the same candidate alloys, with and without hydrogen charging, is being examined using miniature tensile specimens (commonly termed SS3s) in the as-received as well as irradiated conditions. Following exposure, mechanical tests at room temperature and study of microstructure evolution are underway to compare relative changes and sensitivity to relevant doses resulting from process service. Of primary concern is the tendency of neutron irradiation and hydrogen charging, as separate or combined effects, to embrittle many materials.
For the NorthStar process, ORNL is developing powder metallurgy approaches to fabricate high-density sintered Mo disks for irradiation targets.[27] The proposed targets are thin wafers, 29 mm in diameter with a thickness of 0.5 mm, with very stringent dimensional tolerances. Although tooling can be machined to very high tolerance levels, the operations of powder feed, pressing and sintering involve complicated mechanisms, each of which affects green density and shrinkage, and, therefore, the dimensions and shape of the final product. Combinations of powder morphology, lubricants and pressing technique have been explored to produce target disks with minimal variations in thickness and little or no distortion. In addition, sintering conditions that produce densities for optimum target dissolvability are being determined in cooperation with Argonne.

3.4 Savannah River National Laboratory

The Savannah River National Laboratory (SRNL) is supporting the development of the tritium supply and recycle system for the D/T accelerator approach for Mo-99 production.[28,29,30] The Savannah River Site is the US Tritium Center of Excellence. The steps of the tritium fuel cycle are common to many tritium applications. Tritium is used in many applications, including tritium-filled EXIT signs to fusion energy to defence programs applications. The tritium that is used in each of these applications requires common processing steps. Tritium (deuterium) supplied and received must be processed to remove impurities and condition waste gases for discharge. These processes are necessary to supply and recycle the tritium (and deuterium) gases, and are called the Tritium Purification System. Tritium gas is moved using vacuum pumping systems, impurities removed using various technologies, then the hydrogen isotopes are separated (as needed) and stored before reintroducing to the start of the process. Gas processing services such as service evacuation and supply gases are provided to recycle and retain as much tritium in the process as possible. Confinement and detritiation are provided to minimize tritium emissions to the worker and public/environment.
SRNL has provided initial design input for the tritium fuel cycle to support the D/T accelerator-driven Mo-99 production. A technology assessment was performed to identify candidate technologies. Further refinement of the requirements led to minimizing tritium inventory, and subsequently tritium emissions in the design of a Tritium Purification System. The scope of the work included initial development of a process control strategy, providing technical basis and operational strategy documents, and completing a hazard assessment summary. SRNL is continuing to evaluate design options, provide risk reduction testing of individual components, develop process control strategies, and provide consultation on tritium issues to further support the development of these efforts to produce Mo-99.
Consultation by SRNL subject matter experts in actinide chemistry and waste processing and packaging is also provided to the partner National Laboratories.

3.5 Y-12 National Security Complex

Y-12 led the activity to develop the high density target and processing and developed means for producing LEU foils and targets on a production scale. Various rolling techniques, coating technologies, and cladding methods were demonstrated and evaluated. Coatings included aluminium and nickel foil, nickel plating, and aluminium PVD. Cladding methods included 3 types of aluminium and TIG (GTAW) and electron beam welding techniques. They fabricated the targets for irradiation at HFIR and developed QA/QC

procedures in conjunction with ORNL. They contracted work performed at the University of Missouri where a variety of mechanical thermal hydraulic studies where performed for the fabrication and irradiation of LEU annular targets and investigated target modelling for safety and quality, as well as quality testing processes on the target. The MURR scope was to demonstrate target irradiations with a down-selected list of fission recoil barriers, and to measure fission gas release during target disassembly. Literature on metallic fuel targets indicated that the fission gas release was correlated with surface area exposed, as opposed to total fission product inventory, and the results of this experiment provided evidence that supports this conclusion. Several papers on this subject were presented at the Mo-99 Topical meetings.[12]

4. Acknowledgements

Work supported by the U.S. Department of Energy, National Nuclear Security Administration's (NNSA's) Office of Defence Nuclear Non-proliferation, under Contract DE-AC02-06CH11357.

There is a large team of personnel in the DOE sites that are responsible for the success of program. It did not make sense to add them all as authors, but their efforts need to be acknowledged.

- Argonne National Laboratory--Kurt Alford, James L. Bailey, Megan E. Bennett, Delbert L. Bowers, Michael A Brown, James P, Byrnes, Sergey D. Chemerisov, Jacqueline M. Copple, William L. Ebert, Artem V. Gelis, Donald G Graczyk, Roman Gromov, James J. Grudzinski, Lohman Hafenrichter, Andrew S. Hebden, Thad A. Heltemes, James L. , Jerden Jr, Charles D. Jonah, Michael Kalensky, John F. Krebs, Robert H. Lowers, Vakhtang Makarashvili, Bradley J. Micklich, Seema R, Naik, Candido Pereira, Kevin J. Quigley, David Rotsch, John F. Schneider, Martin J. Steindler, Dominique C. Stepinski, Peter Tkac Mathew J. Virgo, Kent E. Wardle, Kenneth A. Wesolowski, Thomas Wiencek, and Amanda J. Youker.
- Los Alamos National Laboratory--David J. Alexander, Scott A. Baily, Cynthia E. Buechler, Roy Copping, Gregory E. Dale, Dale A. Dalmas, David S. Decroix, Michael A. Holloway, Charles T. Kelsey IV, Robert H. Kimpland, Steve Klein, Iain May, Michael Mocko, Angela C. Naranjo, Arthur Nobile, Brett S. Okhuysen, Eric R. Olivas, Maria I. Peña, Sean D. Reilly, Heidi Reichert, Daniel Rios, Frank P. Romero, Craig M. Taylor, Robert M. Wheat, and Keith A. Woloshun.
- Oak Ridge National Laboratory—Chris Bryan, J. O. Kiggans Jr., Keith Leonard, Richard A. Lowden, Steven Pawel, and Steven Sherman.
- Savannah River National Laboratory-- Anita Poore, James E. Klein, Jason Wilson, Kenneth Karius, Sherrill (Ed) Wilcox, Roderick King, and Charles Mastromonico.
- Y-12 National Security Complex—John Creasy, Tom Hanlon, Barak Tjader, Elena Garlea, Jack Gooch, and Amy Demint.
- University of Missouri/MURR—Charles Allen, Ralph Butler, Gary Solbrekken, Leon Manson, David Robinson, Kyler Turner, Phillip Makarewicz, Srisharan Govindarajan, John Kendy, Jacob Harris, Amer Kravic, Annemarie Hoyer, Rafi Lasir, James Mooreland, and Andrew Gunn.

5. References

[1] J. Creasy, “UPDATE ON THE DEVELOPMENT, TESTING, AND MANUFACTURE OF HIGH DENSITY LEU-FOIL TARGETS AND PROCESSING FOR THE PRODUCTION OF MO-99,” 2013 Mo-99 Topical Meeting, April 1-4, 2013 Chicago, IL, USA, http://mo99.ne.anl.gov/2013/pdfs/Mo99%202013%20Web%20Presentations/S7-P2_Creasy.pdf

[2] M. Ciocanwscu and G.F. Vandegrift, “HIGH DENSITY LEU ANNULAR TARGET QUALIFICATION,” 2013 Mo-99 Topical Meeting, April 1-4, 2013 Chicago, IL, USA,

http://mo99.ne.anl.gov/2013/pdfs/Mo99%202013%20Web%20Papers/S7-P5_Ciocanescu_Paper.pdf
[3] J. Creasy, "UPDATE ON THE DEVELOPMENT, TESTING, AND MANUFACTURE OF HIGH DENSITY LEU-FOIL TARGETS AND PROCESSING FOR THE PRODUCTION OF MO-99," 2014 Mo-99 Topical Meeting, June 24-27, 2014, Washington D.C., USA, http://mo99.ne.anl.gov/2014/pdfs/presentations/S10P1%20Presentation%20Creasy.pdf .
[4] K. Pitas, "THE SHINE PATH TO A RELIABLE DOMESTIC SOURCE OF MO-99," 2014 Mo-99 Topical Meeting, June 24-27, 2014, Washington D.C., USA. http://mo99.ne.anl.gov/2014/pdfs/presentations/S10P2%20Presentation%20Pitas.pdf.
[5] Shine Medical Technologies' home page: http://shinemed.com/.
[6] J.T. Harvey, G.H. Isensee, S.D. Moffatt, and G.P. Messina, "NORTHSTAR PROGRESS TOWARDS DOMESTIC MO-99 PRODUCTION," 2014 Mo-99 Topical Meeting, June 24-27, 2014, Washington D.C., USA, http://mo99.ne.anl.gov/2014/pdfs/presentations/S8P3%20Presentation%20Harvey.pdf.
[7] NorthStar Medical Radioisotopes, LLC home page: http://www.northstarnm.com/.
[8] R.D. Rogers, A.H. Bond, S.T. Griffin, and E.P. Horwitz, "NEW TECHNOLOGIES FOR METAL ION SEPARATIONS: AQUEOUS BIPHASIC EXTRACTION CHROMATOGRAPHY (ABEC). PART I UPTAKE OF PERTECHNETATE, Solv. Extr. Ion Exch., 14(5), 919, 1996.
[9] M.A. Brown, J.L. Jerden Jr., A.V. Gelis, D.C. Stepinski, S. Wiedmeyer, A. Youker, A. Hebden, and G.F. Vandegrift, "DEVELOPMENT OF FRONTEND PROCESSING TO ALLOW USE OF HIGH-DENSITY LEU FOIL TARGETS IN CURRENT MO-99 PRODUCTION FACILITIES," 2014 Mo-99 Topical Meeting, June 24-27, 2014, Washington D.C., USA, http://mo99.ne.anl.gov/2014/pdfs/papers/S11P3%20Paper%20Brown.pdf.
[10] A.J. Youker, J.F. Krebs, M. Kalensky, P. Tkac, D. Rotsch, T. Heltemes, D.C. Stepinski, J.P. Byrnes, J.L. Jerden, W.L. Ebert, C. Pereira, M.J. Steindler, D.L. Bowers, S. Zaijing, S.D. Chemerisov, and G.F. Vandegrift, "Overview: Argonne Assistance in Developing SHINE Production of Mo-99," 2014 Mo-99 Topical Meeting, June 24-27, 2014, Washington D.C., USA, http://mo99.ne.anl.gov/2014/pdfs/papers/S10P3%20Paper%20Youker.pdf.
[11] D.A. Rotsch, A.J. Youker, P. Tkac, D.C. Stepinski, J.F. Krebs, V. Makarashvili, M. Kalensky, Z. Sun, T.A. Heltemes, J.F. Schneider, A.S. Hebden, J.P. Byrnes, L. Hafenrichter, K.A. Wesolowski, S.D. Chemerisov, G.F. Vandegrift, "Chemical Processing of mini-SHINE Target Solutions for Recovery and Purification of Mo-99;" 2014 Mo-99 Topical Meeting, June 24-27, 2014, Washington D.C., http://mo99.ne.anl.gov/2014/pdfs/papers/S9P8%20Paper%20Rotsch.pdf.
[12] Mo-99 Topical Meetings Website http://mo99.ne.anl.gov/2014/.
[13] S. Chemerisov, G.F. Vandegrift, G. Dale, P. Tkac, R. Gromov , V. Makarashvili, B. Micklich, C. Jonah, T. Heltemes, D. Rotsch, K.A. Woloshun, M. Holloway, F. Romero, and J. Harvey, "Overview of Argonne support for Mo-99 medical isotope production: NorthStar Medical Technologies," 2014 Mo-99 Topical Meeting, June 24-27, 2014, Washington D.C., http://mo99.ne.anl.gov/2014/pdfs/papers/S8P4%20Paper%20Chemerisov.pdf.
[14] S.K. Klein, , J.C Determan, L.J. Dowell, and M.M. Roybal, "Stand-Alone Dynamic System Simulation of Fissile Solution Systems," LA-UR-14-27033, Los Alamos National Laboratory (2014).
[15] S.K. Klein and C.M. Day, "Simulator for an Accelerator Driven Fissile Solution System - Notional Design," LA-UR-14-26996, Los Alamos National Laboratory (2014).
[16] C. Buechler, "SHINE SE Experiment Thermal Model Development," LA-UR-14-27981, Los Alamos National Laboratory (2014).
[17] I. May, S.D. Reilly, R. Copping, and D. Rios, "Uranium Measurement Control and Total Uranium Concentration Determination," LA-UR-14-25139,Los Alamos National Laboratory (2014).

[18] L.M. Colletti, I. May, and S.D. Reilly, “Uranium Concentration Measurement Technique Viability Analysis,” LA-UR-14-29709, Los Alamos National Laboratory (2014).
[19] D.J. Alexander, M.I. Pena, M.J. Dvornak, B. Aikin, B., J.D. Montalvo, P.A. Papin, D.A. Summa, S.D. Chemerisov, and J.L. Bailey, "Fabrication of Zircaloy-4-Clad Depleted-Uranium Targets for Production of Medical Isotopes", LA-UR-14-27951, Los Alamos National Laboratory (2014).
[20] G.E. Dale, S.D. Chemerisov, G.F. Vandegrift, K.A. Woloshun, C.T. Kelsey IV, P. Tkac, V. Makarashvili, C.D. Jonah, E.R. Olivas, M.A. Holloway, K.P. Hurtle, F.P. Romero, D.A. Dalmas, and J.T. Harvey, “Design and experimental activities supporting commercial U.S. electron accelerator production of Mo-99,” AIP Conf. Proc. 1525, 355 (2013)
[21] K.A> Woloshun ,A.C. Naranjo, and F.P. Romero, “Design and Thermal-Hydraulic Performance of a He-Cooled Target for the Production of Isotope Tc-99m,” LA-UR-14-29070, Los Alamos National Laboratory (2014).
[22] T. Kawano, “Evaluation of photo-induced reactions on 39,41K,” LA-UR-14-20531, Los Alamos National Laboratory (2014).
[23] K.A. Bishofberger, “Production Facility Beam Line Design Report,” LA-UR-14-28325, Los Alamos National Laboratory (2014).
[24] M. Mocko, “Local Target Shielding,” LA-UR-14-29061, Los Alamos National Laboratory (2014).
[25] M. Mocko, “Shielding design of Mo-99 production facility,” LA-UR-14-27486, Los Alamos National Laboratory (20140.
[26] S.J. Pawel, “*Corrosion Assessment of Candidate Materials for the SHINE Subcritical Assembly and Components – 2014 Report*,” Oak Ridge National Laboratory Technical Memorandum ORNL/TM-2014/556, October 2014.
[27] R.A. Lowden, J.O. Kiggans Jr., and C.D. Bryan, “Powder Metallurgy Fabrication of Molybdenum Accelerator Target Disks,” Oak Ridge National Laboratory Technical Memorandum ORNL/TM-2014/238, October 2014.
[28] E. Clark, "Normetex Pump Alternatives Study," SRNL-STI-2013-00325, Savannah River National Laboratory, Aiken, SC (2013).
[29] E. Clark, "Radiolytic Gas Production Rates of Polymers Exposed to Tritium Gas," SRNL-STI-2013-00506, Savannah River National Laboratory, Aiken, SC (2013).
[30] G. Morgan and B. Peters, "SHINE Vacuum Pump Test Verification," SRNL-STI-2013-00539, Savanah River National Laboratory, Aiken, SC (2013).

MO-99 PRODUCTION AT FRM II – STATUS OF THE PROJECT

C. MÜLLER, H. GERSTENBERG, A. RÖHRMOSER, A. KASTENMÜLLER, M. GIOURGES, G. HAAS, P. JÜTTNER
Technische Universität München, ZWE FRM II
Lichtenbergstraße1, 85748 Garching – Germany

ABSTRACT

FRM II is Germany's most recent and powerful research reactor. Due to the world-wide increasing need to produce the important medical isotopes Mo-99/Tc-99m it is foreseen to equip the reactor with a dedicated facility that allows the simultaneous irradiation of up to 16 plate-like LEU targets.

The irradiation facility is foreseen to be installed into a vertical thimble located in the heavy water moderator tank close to the reactor core. The entire facility will be subdivided into three major devices: target cooling system, target changing device and inert gas system. The location of the components within the reactor pool is defined, their design is completed and the detailed construction is underway. In order to gain experience with the future handling and to reduce the required time for non-nuclear commissioning two mock-ups are operated in a neighbouring laboratory. The expected output in Mo-99 activity and the corresponding heat production are taken from neutronic calculations. Thermo-hydraulic calculations are carried out now in detail. Major technical aspects of the irradiation facility and of target handling will be presented as well as the results of the calculations and safety considerations.

According to the present time schedule the facility will be installed into the FRM II reactor pool in 2017 and start production in 2018. The facility is supposed to contribute considerably to a reliable supply of the isotopes Mo-99/Tc-99m.

1. Introduction

Worldwide more than 30 million patients are diagnosed and treated per year with radioisotopes. The most common radioisotope used in diagnostics is technetium-99m (Tc-99m), which is accounting for roughly 80 percent of all nuclear medicine procedures [1]. Thus Tc-99m is by far the most widely used radioisotope in nuclear medicine. Its low gamma energy of 140 keV and its short half-life of only 6 hours make it an ideal probe for diagnostic imaging of many human organs.
The most applied way for production of Tc-99m requires the irradiation of uranium targets leading to the generation of molybdenum-99 (Mo-99) the mother isotope of Tc-99m which itself has a relatively short half-life of 66 h. Consequently neither Mo-99 nor Tc-99m can be stocked for weeks or longer.
At present, only five research reactors in Europe are equipped with facilities allowing the irradiation of uranium targets for the production of the medical isotopes mentioned above. In addition, all of these reactors are in operation since several decades and turned out to become vulnerable against malfunction. This situation induced a serious shortage for medical isotopes in 2008 and consequently a growing public awareness for the reliability of the Mo-99/Tc-99m supply chain.
To minimize the risk of a further shortage and to ensure continuity of Tc-99m production, it is foreseen to equip the Forschungs-Neutronenquelle Heinz Maier-Leibnitz (FRM II) with a dedicated facility to irradiate uranium targets for the production of Mo-99. After completing a feasibility study [2], the development and construction of such an irradiation facility started in 2010.

2. FRM II

The Forschungs-Neutronenquelle Heinz Maier-Leibnitz (FRM II) is a 20 MW heavy water moderated, light water cooled research reactor, being operated since 2005 by the Technische Universität München (TUM). The FRM II resides on the TUM research centre in Garching close to Munich.
The typical operational regime of FRM II is a reactor cycle of 60 days in a row and up to four cycles per year. Under typical conditions the reactor is operated 240 full power days per year.
The basic design feature of FRM II is a single cylindrical compact fuel assembly, representing the entire reactor core. One single control rod in the central hole of the fuel assembly is used to control the reactor power. The fuel assembly itself is mounted in the centre of a large cylindrical moderator tank, which has a diameter of 2.5 m. The moderator tank is as high as broad and contains about 11 m³ of heavy water (D_2O) for moderating fast neutrons and building a high thermal neutron flux density, due to the very low absorption of the D_2O. The whole installation is fitted in the reactor pool, which is filled with 700 m³ of light water.
One important design of FRM II is that the maximum of the thermal neutron flux density is located on outside the fuel assembly within the moderator tank. Eleven beam tubes, 10 horizontal and 1 inclined, are tangentially arranged around the core. Their tips are in immediate vicinity to the maximum flux of thermal neutrons or to one of the three secondary sources. By means of these installations it is possible to supply scientific experiments in the reactor building with neutrons of different energies.

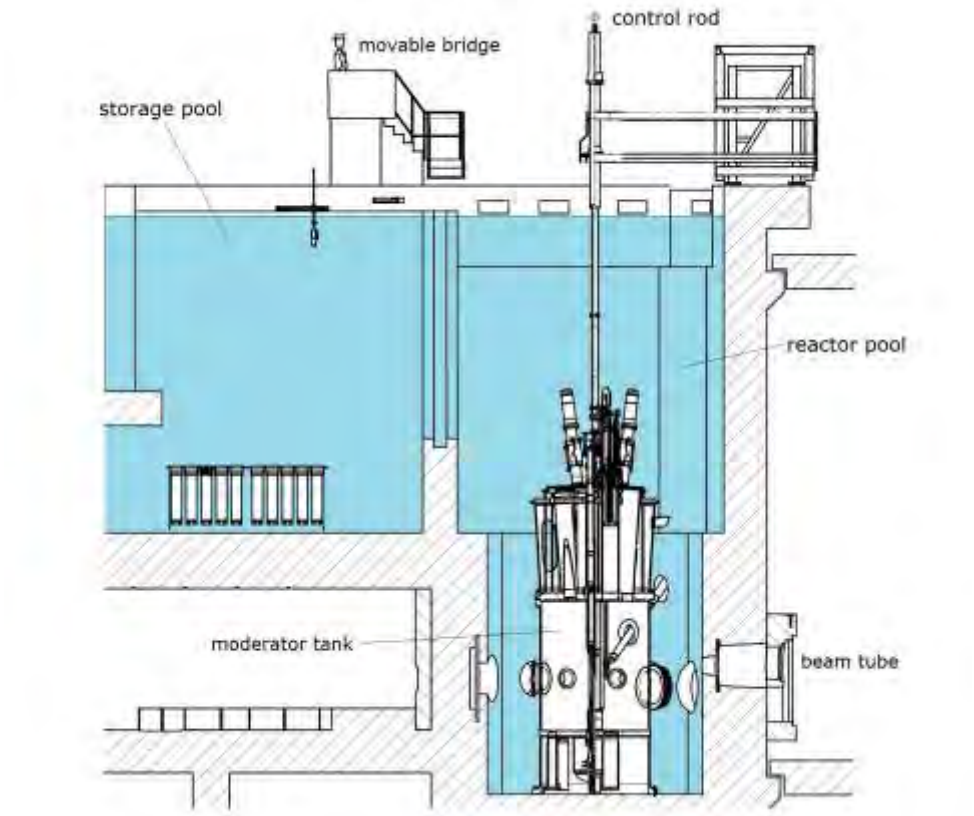

Figure 1: Cross-section through the reactor pool

Despite the fact that FRM II is clearly optimised for basic research by means of beam tube experiments it claims to be a multipurpose reactor offering already presently several irradiation facilities. Among others, these are a pneumatic rabbit system, a two channel hydraulic rabbit system and a silicon doping facility. A basic design feature of all of those facilities is an irradiation position which is geometrically located in a thimble or gas-filled tube

within the moderator tank. The irradiation channels are hermetically separated from the heavy water itself by a leak-tight flange connection between the thimble and the moderator tank top. Based on this design all of the irradiation channels are accessible from the top. Fortunately several spare flanges are still available on top of the moderator tank, by consequence it is sequentially to choose the same general design for the prospective Mo-99 production facility.

3. Design of the Mo-99 Production Facility

The production of Mo-99 requires a high thermal neutron flux of at least 1×10^{14} cm^{-2} s^{-1}. Therefore the irradiation of the uranium targets has to take place to the extent possible in the maximum flux of thermal neutrons. The exact irradiation position was examined and fixed in the context of a feasibility study [2]. Besides the need of a high neutron flux, the study also took boundary conditions into account, e.g. the influence on scientific experiments. As a result the Mo-99 production facility will be installed in a vertical thimble that was originally foreseen to be used for a fast rabbit irradiation system, which had never been built.
Initially it was planned to irradiate tubular targets containing highly enriched uranium (HEU). However, caused by to the restriction of the trade with HEU, the targets were modified to contain low enriched uranium (LEU) and the geometry was changed to plates. Due to this conversion of the targets, the design of the irradiation channels of the Mo-99 production facility has also been completely changed.

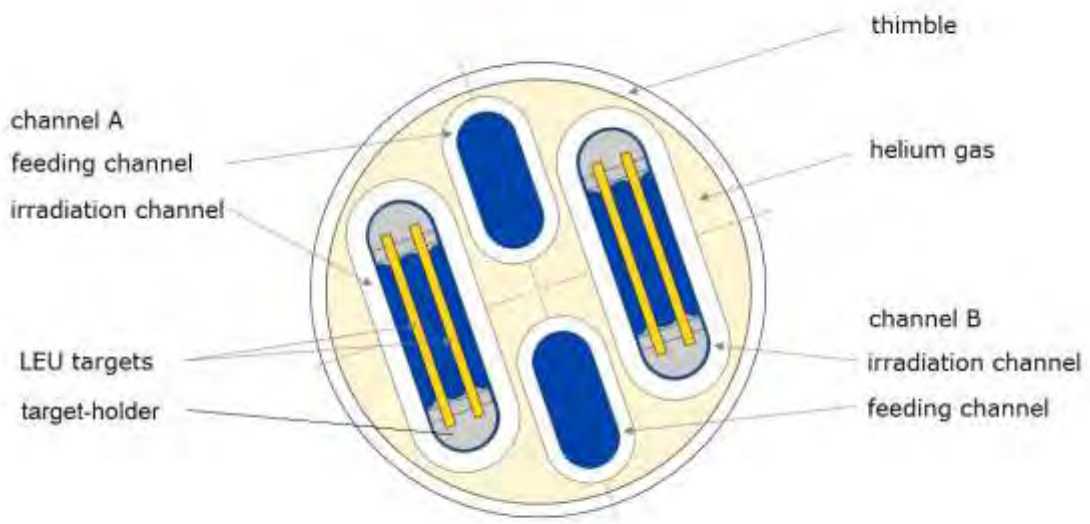

Figure 2: Top view of the thimble and the channels

As can be seen in figure 2, the thimble exhibits two identical irradiation channels, which are independently loadable and allow the simultaneous irradiation of 16 targets maximal. Up to eight targets are fixed in a target-holder that will be inserted into a channel A or B for irradiation. If an irradiation of less than 8 targets is desired, the empty positions will be filled up with aluminium-dummies. Consequently a target-holder will always be filled up with 8 geometrically identical items to provide a constant flow resistance for the cooling water stream.
There are two smaller channels, which are used to feed the irradiation channel with cooling water. These additional channels are arranged between the irradiation channels like it is shown in the figure 2.

In summary, the facility offers the possibility to irradiate up to 16 targets at the same time. The loading and unloading of targets, however, is restricted to the handling of one target-holder.

4. Description of major Systems

The Mo-99 production facility is composed of three functionally independent systems:

- a thimble with a helium gas protection system,
- a target cooling system and
- a target changing device.

Each system is built up of several components and is executing independent performances as a part of the entire facility.

Thimble with helium gas protection system

Following the decision to install the Mo-99 production facility at the position of the fast rabbit irradiation system, the existing thimble was replaced, because the length of the thimble didn't meet the best fitting irradiation position. In order to use the entire height of the fuel assembly and to irradiate as many targets as possible the new thimble has a length of five meters and shows a diameter of only nine centimetres.

The new thimble was mounted in February 2011 in a position 45 cm away from the fuel element (centre to centre), and as required close to the thermal neutron flux maximum. It is made of the durable and irradiation-resistant reactor material Zircaloy-4, a zircon alloy which offers high pressure resistance and long life time under neutron radiant exposures. The lower part of the thimble dives into the D_2O of the moderator tank while the upper part is in the supporting structure on top of the moderator tank.

In the future the thimble will contain the piping channel of the irradiation facility, shown in figure 2. The open space between the inner wall of the thimble and the cooling channels will be filled with helium as an inert protective gas. The pressure and the humidity of the helium gas will be permanently monitored. This feature will control the leak tightness of the thimble and of its installations as well.

Target cooling system

To dissipate the thermal output, generated in the targets, the installation of an additional cooling system is essential. In the framework of the feasibility study [2] various options were figured out to integrate the cooling circuit of the Mo-99 production facility into the existing cooling circuits of the reactor itself. Finally, the proposed design is based on an as far as possible independent cooling circuit which takes the water from the reactor pool, and after cooling the targets the water is fed back into the reactor pool, after passing a heat exchanger.

Three coolant pumps, one plate heat exchanger and connecting pipes with sieves, will be building the main components of the cooling circuit. The three pumps are located underwater within the reactor pool. Under standard irradiation conditions all pumps are in operation, however, only two of them are required to run simultaneously to ensure the necessary throughput of cooling water in the irradiation channels.

The pumps are foreseen to be battery buffered. In case of a power breakdown of the external power supply, it is secured that the targets are cooled until the afterheat is reduced sufficiently to allow unforced cooling by natural convection. The major advantage of this design is that no separate emergency cooling system will be required.

The heat load related to the simultaneous irradiation of 16 LEU targets is about 420 kW [3] while the reactor has a nominal power of 20 MW. For nominal operation at a water flow rate of 5 kg/s, a maximum local temperature of 122 °C for the cooling water was calculated. This temperature occurs in the region of the central targets and is far from the boiling temperature

of 180 °C at 10 bar water pressure. The average temperature of the cooling water is 60 °C at the outlet of the cooling water channel.
The availability of this cooling system is of particular importance for operating the irradiation facility. Due to its technical safety requirements, the system must be planned and designed procedurally in detail. A concept for adapting and adjusting the reactor cooling and integrating it into the existing control system is in progress. The bidding process for the pumps is set to begin in 2015.

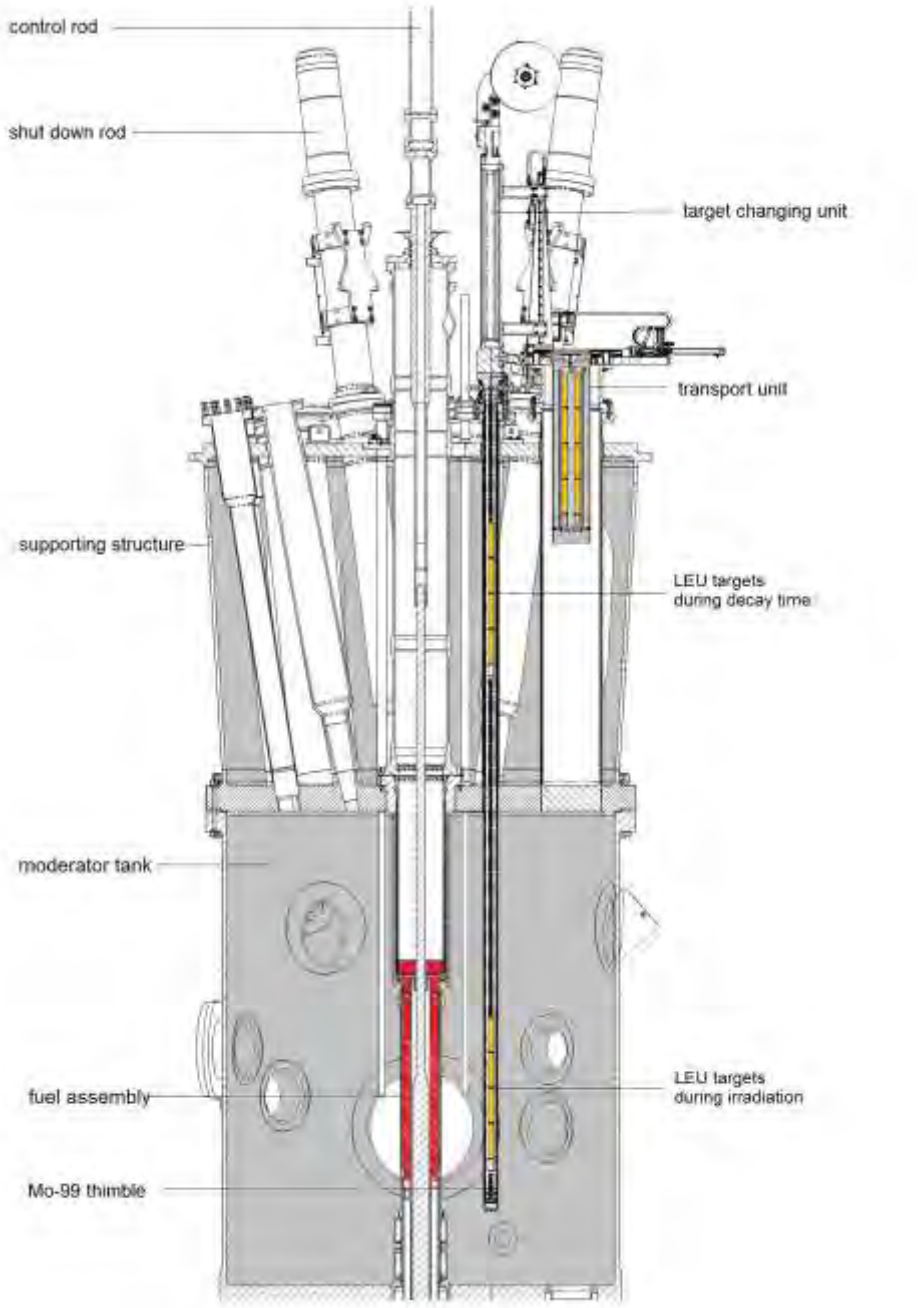

Figure 3: Schematic drawing of the future Mo-99 irradiation facility mounted on the moderator tank

Target changing device

Due to the main use of the FRM II as a research reactor, it is mandatory that the loading and unloading of targets will take place while the reactor is in operation. For this reason a target changing device for the Mo-99 production facility is developed which support an automatic change of targets.

The task of this device is the loading and unloading of targets between the irradiation channel and the transport unit. Therefore the device is consisting of two independently moveable units for channel A and B providing the required vertical and horizontal motions.
For the irradiation process the changing device places the targets inside the irradiation channel on the same vertical level with the fuel assembly (see figure 3). After the irradiation process is finished, the targets will be rised into the supporting structure above the D_2O level. This positon is defined as decay position for freshly irradiated targets, like it is illustrated in figure 3. Finally, after the necessary decay time has expired, the targets will be moved again into the transport unit and carried to the hot cell for loading into the transport container.
To implement this concept, the construction of two test stands on a 1:1 scale was realized; a replica of the cooling channel return flow as well as of the complete cooling channel unit with the two irradiation channels. These mock-ups serve to test and to optimize the technical construction, the manufacturability of the irradiation channels, and the handling steps of the target changing device. This step in the course of the project is of particular importance for the approval and the related evaluation of the concept by the nuclear experts, as the practical feasibility can be demonstrated and proven in advance and outside of the reactor.

5. Handling

In addition to the construction of the Mo-99 production facility, the handling of freshly irradiated targets and their transport within the FRM II has to be appraised.
Due to the comparatively short half-life of Mo-99 with 66 hours, it doesn't make sense to put the targets in storage at the FRM II. Consequently, after expiring of the minimum decay time the targets have to be loaded into the containers to be used for transport on public roads and shipped for further processing to the particular processors as quick as possible
This step of handling, putting the irradiated targets in the intended containers, will be done in the hot cell of FRM II. In consideration of radiation protection a dry packaging in the cell has the advantage that compared to an underwater loading the risk of contamination on the outer surface of the containers is considerably reduced.

The elaborated handling concept can be subdivided in three main steps:

- Firstly, the irradiated targets will be transferred underwater into the hot cell using a direct access from the reactor pool to a hatch in the floor.
- Secondly, the targets will be removed from the target-holder which had held them during irradiation and inserted into the transport container. The container is a type B (U) container which is provided by the processors.
- Thirdly, the containers will be moved to the truck lock at the ground-level of FRM II, where the transport cover for mechanic protection will be mounted.

The corresponding handling procedures are being developed, including various indispensable tools and equipment. As a first provision, the freight elevator to be used for the transport of the heavy transport containers within the reactor building has already been upgraded in 2013 to be able to transport up to 10 tons. Also a special floor-borne vehicle for the ground transportation of the heavy transport container was already purchased. This vehicle was evolved and delivered in 2014.

6. Neutronic Calculation

The present Mo-99 production facility has been introduced into the 3D-model for neutron transport calculations with the code MCNP [3] [4]. The model takes into account all relevant technical and experimental installations surrounding the fuel assembly in the moderator tank. For the purpose of Mo-99 production the model has been extended to include not only the thimble but also the inserted LEU targets as described above.

The thermal neutron flux density in the LEU targets and their geometrical profiles along the entire irradiation channels showed up to be rather structured (about 1.7×10^{14} cm^{-2} s^{-1} in target average). It is to be remarked that the flux at the target-holder structure is up to 3.5×10^{14} cm^{-2}/s.
The corresponding heat load resulting from the fission processes in the irradiated targets was determined to be equal to 420 kW for fresh targets provided that all 16 irradiation positions are taken. The xenon build up during the first day of irradiation will reduce the power by some percent. Taking into account this effect, the Mo-99 activity produced during irradiation is determined to sum up to 17 kCi right after a typical 156 hours irradiation run with the maximum number of targets, namely 16.
In addition to the neutron flux density and power production the neutronic calculations showed that the penalty caused by the target irradiation to the neighbouring beam tube experiments is marginal, in the majority of cases clearly below 1 %. The influence of the targets on the reactivity of the reactor core was calculated to be + 0.24 % for fresh targets in comparison to the target free facility.

7. Conclusion

Since the launch of the project in 2010 till now many intermediate steps were performed to reach the actual state. The design of the Mo-99 production facility is completed. Major technical aspects of the irradiation facility and of the target handling are developed and will be tested with two mock-ups.
The new thimble which will house the irradiation channels was installed in 2011 and the freight elevator was enhanced to be able to transport up to 10 tons in 2013.
The next step to be done shortly will be to initiate the approval procedure. According to the present time schedule the facility will be installed completely within the FRM II reactor pool in 2017 followed by the cold and hot commissioning in the same year. The facility is supposed to contribute considerably to a reliable supply of the isotopes Mo-99/Tc-99m starting from 2018.

8. References

[1] NEA (2011), The Supply of Medical Radioisotopes: The Path to Reliability, OECD, Paris, France

[2] H. Gerstenberg, C. Müller, I. Neuhaus, A. Röhrmoser, RRFM 2010, Marrakech, Morocco, 21 - 25 March 2010, Transaction pp 41 -45

[3] A. Röhrmoser, Nukleare Heizlast des FRM II Projekts zur Mo99-Isotopen-Erzeugung mit neuen LEU-Platten-Targets, Interner Bericht OPA 00481, 16.05.2014

[4] "MCNP - A General Monte Carlo N-Particle Transport Code, Version 5", LA-UR-03-1978 (4/2003,10/2005), X-5 Monte Carlo Team, Los Alamos National Laboratory

COATING OF LEU FOIL WITH ELECTRODEPOSITED NICKEL FOR 99Mo PRODUCTION

LUIS OLIVARES, JAIME LISBOA, JORGE MARIN, MARIO BARRERA
Nuclear Materials Department
Chilean Commission for Nuclear Energy - CCHEN
95 Amunategui St., Postal Code 6500687
Santiago – Chile

ABSTRACT

The manufacturing activities of fresh targets for 99Mo/99mTc radioisotope production are being developed at the Chilean Commission for Nuclear Energy - CCHEN since 2006. Chile was an active participant in an International Atomic Energy Agency (IAEA) Coordinated Research Project (CRP) to use targets based on the LEU-Modified Cintichem process to produce fission-product ^{99}Mo. In order to evaluate the possibilities for producing Technetium Generators from fission Mo in Chile, a local program, aimed to the development of technology for manufacturing and inspection of LEU annular targets to produce fission-product ^{99}Mo in Chile, was launched in 2007.

Seven years later, the development of the manufacturing technology for annular targets has been completed with satisfactory results. A closed semi-dourville mold design, integrally mounted with high alumina crucible allows the production of ingots with an acceptable surface quality, meanwhile the encapsulation technique with low carbon steel cladding is a very effective way to produce uranium foil. Written procedures have been established for annular target assembly, including controlling, adjusting and assembling of source materials and all internal components of the fresh target.

The standard methodologies include using a nickel envelope covering the LEU foil, as a barrier to avoid leaks of fission products. Nevertheless, an innovation developed at CCHEN considers replacing the nickel envelope by electrodeposited nickel coating on the uranium foil. The electrolytic process demonstrates to be a suitable process for the U-Ni system, obtaining a homogenous nickel deposit with good adhesion and free of porosity. The thickness measurement of the nickel deposit over a 135 microns (thickness) uranium foil, revealed an average value of 32.3 microns, with no surface porosity in the Ni deposit and without defects caused by the presence of hydrogen, which was minimized by the addition of a wetting agent that modified the surface tension between the substrate and the electrolyte. This paper presents and discusses the results and achievements of this development at CCHEN.

1. Introduction

Molybdenum-99 (^{99}Mo) is the most widely used medical isotope in the world, used approximately 40 million times worldwide every year in advanced highly accurate medical diagnoses. This material, which has a short 66-hour half-life, decays to another radioisotope – Technetium-99m (^{99m}Tc) – as it is packaged and shipped for use by physicians. It is the ^{99m}Tc, which is injected into patients to enable imaging techniques needed to diagnose cancer, heart disease and other ailments. ^{99}Mo is produced through irradiation of uranium targets in research reactor facilities, neutron activation of natural molybdenum, or molybdenum enriched in ^{98}Mo, [1] is another route of production. A third alternative for ^{99m}Tc production is the proton bombardment with the 22-MeV- of a Mo-100 target in medical cyclotrons.

^{99m}Tc has a very short half-life – only 6 hours – and it decays to nonradioactive materials and thus limits patient exposure. Because these materials have such short half-lives, they must be produced continuously. Disruptions in the supply chain of these medical isotopes can lead to cancellations or delays in important medical testing services. Unfortunately, supply reliability has declined over the past decade due to unexpected or extended shutdowns at a few of the ageing ^{99}Mo-producing research reactors and processing facilities. These shutdowns have created conditions for global supply shortages [2].

The supply chain of 99Mo is a sequence composed by:

1. Manufacturers of uranium targets (U-235): Molybdenum 99 (^{99}Mo) is produced in nuclear reactors utilizing either Highly Enriched Uranium 235 (HEU) or Low Enriched Uranium 235 (LEU) targets. These targets, either tubular or flat and of varying size, are fabricated as small from HEU or LEU and aluminium designed specific for each reactor.

2. Research Reactor Operators: HEU or LEU targets are placed in or near the core of the reactor. The location of targets within the nuclear reactor allows high neutron fluxes to surround the HEU / LEU. Fission reactions occur resulting in production of ^{99}Mo and a number of other isotopes.

3. ^{99}Mo processing facilities: after approximately six days in the reactor, fission produced ^{99}Mo has reached an optimum level. The targets are then removed and transferred to a processing facility where the targets are dissolved and chemically separated. ^{99}Mo facilities can only accept HEU/LEU targets from specific reactors for various reasons, including geographic location (proximity to the reactor), required technical specifications and regulatory authority approval. The finished product raw material ^{99}Mo is then isolated as radiochemical and shipped to the next stage in the process.

4. Manufacturing of ^{99}Mo/^{99m}Tc generators from ^{99}Mo: The radiochemical ^{99}Mo is transferred to a manufacturing facility in specialized transport containers via various overnight or same day shipping arrangements so it can be used to make ^{99}Mo/^{99m}Tc generators. Generator manufacturing is a health authority approved complex process. Finished product generators must meet all approved specifications as spelled out by the manufacturer's registered drug application as filed with the appropriate governing regulatory agency.

5. Pharmacies and Hospitals. Generators that meet the specific quality release criteria will move on to the distribution channel. Any of a variety of transportation methods may be necessary including air, ground, or a combination depending on customer location. The generators are then shipped for same or next day delivery to hospitals and radiopharmacies for elution and used to make diagnostic radiopharmaceuticals [3].

Based on this supply chain, at least the three first steps may be developed at CCHEN and in turn, the generators manufacture could be transferred to private companies.

Amongst other radioisotopes for nuclear medicine CCHEN produces ^{99m}Tc, ^{131}I, ^{192}Ir, ^{153}Sm in its research reactor RECH-1. In Chile, ^{mTc}99 is applied in more than 90% of the nuclear medicine studies (near 200,000 cases). In Santiago, ^{99m}Tc used is produced by neutron activation; nevertheless, in remote cities ^{99m}Tc of imported generators is used. With the purpose of supplying this radioisotope, CCHEN developed its own production of ^{99m}Tc generators using fission ^{99}Mo imported from Canada, production that lasted by two years. [4].

The 5 MW RECH-1 Research Reactor have a potential production capacity (weekly 6-day-Ci) of 250 Ci. Since 2007, a Technological Development Program is in progress at CCHEN that considers the production of ^{99}Mo based on the irradiation of annular targets containing a LEU uranium foil inside. Currently a feasibility studies is underway to provide irradiation services to produce fission-based ^{99}Mo. [5]

CCHEN's Nuclear Materials Department have joined efforts to overcome the development challenge for the annular targets manufacturing technology, including the design and manufacture of equipment, tooling and materials for the assembly and disassembly of the annular target after its irradiation in the reactor. The annular target comprises two concentric tubes made of Al-3003 AISI-SAE alloy, and between these tubes, into a properly machined annular region, a thin foil of metallic LEU is placed and encapsulated, on all its sides, by a Nickel (Ni) foil which acts as containment barrier for the fission products produced during the irradiation [6], [7].

The main difficulty after irradiation is the extraction of the uranium foil from the target into the hot cell. This is probably due, to the bonding between the uranium foil and the structural aluminium tubes, caused by the ions mixture produced by the fission products from the irradiated uranium foil. Therefore Ni is placed between the Al tubes and the uranium foil and used as a barrier to avoid the escape of fission products. The thickness of the barrier is selected according to the chosen recovery range of fission products. The maximum distance reached by the fission products is about 7 microns; however, to provide a safety range and a maximum of recovery, a layer with 15 microns thickness is selected.

This barrier should cover completely the uranium foil to avoid the possibility of localized bonding with the Al tube wall. This material should have a uniform thickness to ensure a proper fit during the assembly and has shown proper heat dissipation during irradiation [8]. Targets that use the Ni barrier have shown good behaviour under irradiation, considering the heat transfer and also to prevent bonding between the uranium foil and Al tube wall during irradiation, [9] [10]. The development of the manufacturing technologies for annular target at CCHEN was developed considering uranium foil with thickness about 120 microns wrapped with a Ni foil of 14 microns thickness.

The innovation studied and reported in this paper, suggested by G. Vandergrift [11], is the electroplating of Ni over the uranium foil. This Ni coating should be characterized to comply with the specifications for an effective barrier for fission products. The main goal for the use of electrodeposited Ni layer over the uranium foil is an attempt to solve certain technical and manufacturing details related to the use of thin Ni foils applied as an envelope for uranium foil to improve the quality and performance of the annular targets. This paper includes a summary of the results of manufacture, characterization and evaluation of targets at CCHEN [12], including the recent results of electrolytic deposition of Ni layers over U foils [13].

2. Experimental Methodology

The development of this programme started with the casting of a uranium metal ingot obtained by induction melting in a multipurpose furnace under inert atmosphere. In the melting process a high alumina crucible was used and the liquid metal was poured into a closed graphite mold, integrally mounted with the crucible in a semi – Durville assembly. The target manufacturing development was done either with foils manufactured at CCHEN and with NU or LEU foils received from KAERI-Korea in the frame of the IAEA Coordinated Research Project "Developing Techniques for Small Scale Indigenous Mo-99 Production using LEU Fission or Neutron Activation"

2.1 Uranium Foil Manufacturing

The uranium coupon must be protected from oxidation during the hot rolling process. For this purpose, cover and frame of low carbon steel was used as a sealing cladding. Considering that the aim of this stage is to obtain an uranium foil, the steel surfaces in contact with the uranium ingot were coated with an emulsion of yttrium oxide (Yttria) and ethanol, and thus preventing bonding and interaction between the uranium ingot and steel. Once applied this protective coating to the surfaces, the set was assembled and fixed by means of TIG

welding. Before the hot rolling process, the assembly was annealed for 1 hour at 630 ℃ in air. Thickness reductions of 5 % were applied in the first four rolling steps and the following reductions steps were done applying 10% reductions in each step, with intermediate annealing of 10 minutes between each reduction step.

During the hot rolling studies, the assemblies were removed from the furnace after reduction steps and radiographed for metrological control. The rolling deformation achieved values between 94 % and 96% of the total reduction in the thickness of the steel - uranium - steel assemblies. For cold rolling it was necessary to perform a surface cleaning to the uranium foils in order to remove the coating of yttrium oxide, and then the uranium foils were encapsulated into envelopes of 304 type stainless steel plates, primarily for protection of the rolls and to avoid its surface contamination with uranium. The reductions applied at this stage were below 3 % in each rolling step, reaching values between 7 % and 14 % of total reduction in thickness. Uranium foils were characterized mechanically by tensile tests according to ASTM E -345 standard for metal foil.

2.2 Assembly of Target

Before target assembly, the uranium foil was cleaned with nitric acid concentrated at 65%vol during seven minutes. The Ni foil was also cleaned using ethanol and acetone. The Uranium foil was wrapped by Ni envelope according to a written procedure.

2.3 Target expansion and welding

In the expansion process, just ethanol was used for lubrication, added by a hole located in the special tooling.

Before the welding of the target, the end of each tube, was machined a depth of 2 mm, finishing with an angle 0.5 x 45°, following a written procedure and drawings. The expansion operation is presented in figure 1.

Figure 1. Inner Tube Expansion in draw die and tooling

Immediately after the tubes machining and with the goal of improving the behaviour of the target during the welding operation, a degassing thermal treatment was applied. An annealing at 120℃ for 60 minutes was enough to eliminate the humidity, lubricant and organic material.

The TIG welding process was conducted using pulsed AC current and a gas mixture of Ar-5% He and the following parameters:

Current: Pulsed AC - 40 Amp – 120 Hz – TIG: HF

Welding electrode: Tungsten 2% Thorium, diameter 1/16”

Rotation speed: 3 rpm

2.4 Leak Test

The leak test was performed using a Varian He Leak Detector, Model 959 and an established inspection procedure. Besides, for the detection of big leaks, liquid nitrogen was used.

2.5 Electrolytic Nickel Coating

To perform the Ni electrodeposition a system composed of two cells containing the electrolyte one was used to heat the electrolyte and to control the solution pH, and the other to perform the electrodeposition. The heating of the solution was done by means of a coil in which hot water was circulated.

Stirring took place through recirculation of the solution between the two stainless steel cells. The anode, which corresponds to the positive electrode in which oxidation takes place, was built with 2 stainless steel baskets that contained nickel tablets, because if an anode that does not dissolve during the electrodeposition process is used, the nickel salts are converted into free sulphuric and hydrochloric acids, due to the effect of the electrolysis. In this case two phenomena take place: a decrease in pH because acidity increases, and a decreasing in salt concentration, both affecting the efficiency of the process. Uranium foil of approximately 100 x 50 x 0.12 mm was used as cathode. The electrodeposition system can be seen in Figure 2.

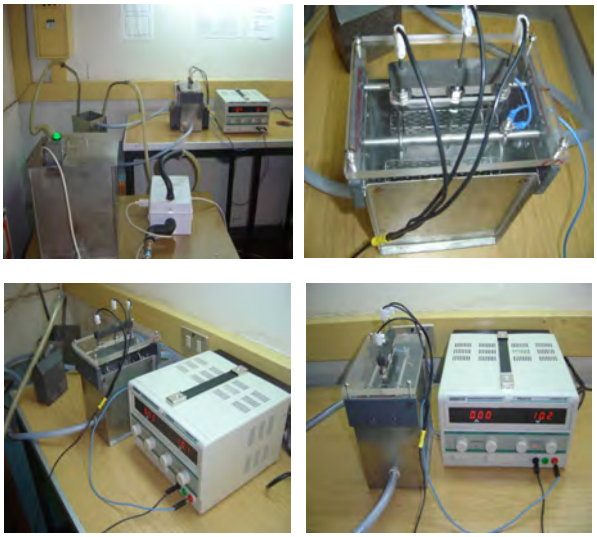

Figure 2. Electrodeposition system

The electrolyte was a solution with 250 g/L of nickel sulphate, 60 g/L of nickel chloride, and 40 g/L of boric acid in deionized water. The solution also contained 2 mL/L of Omega additive, which gives ductility and a semi-gloss appearance to the Ni deposit, and 4 mL/L of wetting agent to lower the surface tension of the Ni solution, thereby avoiding pore formation in the deposit. The Ni sulphate is the main source of Ni ions in this solution, while the nickel chloride contributes to dissolve the activated forms of Ni and the boric acid stabilizes the pH of the solution. The initial parameters used were those recommended for industrial electrodeposition, i.e., pH 4.0; temperature 40 ℃, approximate voltage 2.0 V.

The 100 x 50 x 0.12 mm uranium foil surface was cleaned with 65% HNO_3 during 10 minutes to remove the oxide layer, and the electrochemical experiments were performed immediately after. A Hewlett Packard power supply was used. Control of pH and temperature was made with an OAKTON pH/mV/℃ meter. Characterization of the deposits was performed by measuring the thickness with a film thickness meter, Karl Deutsch Leptoskop 2041 model, a

linear comparator, and the deposit was also characterized by optical microscopy, scanning electron microscopy and ultrasonic scanning.

3. Experimental Results

3.1 Uranium foil manufacturing

After hot and cold rolling of uranium coupons, framed into steel covers and frame, it was possible to obtain uranium foils with about 120 µm of thickness and a proper smooth surface for target preparation. Table 1 and 2 summarize the results for hot and cold rolling. Figure 3 shows the assembling of an uranium coupon into steel pack and final aspect of uranium foils after hot rolling.

Table 1. Results of hot rolling for NU foils

Foil identification	Starting Thickness (mm)	Length (mm)	Width (mm)	Final Thickness (mm)	Total Reduction (%)
FUN-10	3.11	20.97	58.48	2.069	33
		67.00	58.93	0.642	79
		125.73	59.60	0.339	89
FUN-11	3.33	20.05	50.57	2.260	32
		67.03	50.97	0.664	80
		123.97	51.68	0.355	89

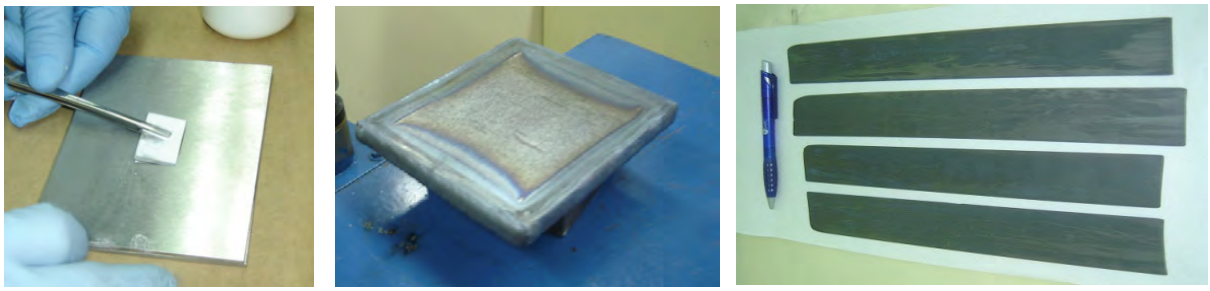

Figure 3. Hot rolling of uranium foil: packed of ingot into a steel frame and covers, and U foils at the end of hot rolling process

Table 2. Results of cold rolling for NU foils

Foil identification	Starting Thickness (mm	Length (mm)	Width (mm)	Final Thickness (mm)	Total Reduction (%)
FUN-10	0.339	100.58	60.5	0.121	96.11
FUN-11	0.355	102.33	52.6	0.124	96.28

3.2 Assembly of Target

Preliminary assembly tests conducted with steel and copper foil showed that the glue used, n-hexane and rubber cement was not suitable. Was necessary to try with different dilutions to find the appropriate concentrations obtain good bond, as well as the drying time to ensure the union of Ni and copper/steel foils.

The most important parameter for the assembly of the set was the air gap generated between the foil pack and the structural aluminium tubes. An acceptance gap range of 0.010 to 0.030 mm was established. Each assembled group was recorded on a proper form, which allowed calculating the mechanical requirements for the machining of the inner tube. However, it was necessary to measure the thickness of the foil and also the thickness of the foils assemblies Cu-Ni, Steel-Ni, UNAT-Ni or LEU-Ni, that is, the sum of the foil set. The total thickness value was used for calculating the final depth for the machining of the inner tube.

3.3 Expansion and welding of target

The results of target assembling with natural and LEU uranium foils are summarized in the Table 3, including the diameter of expansion die and final condition of expansion operation.

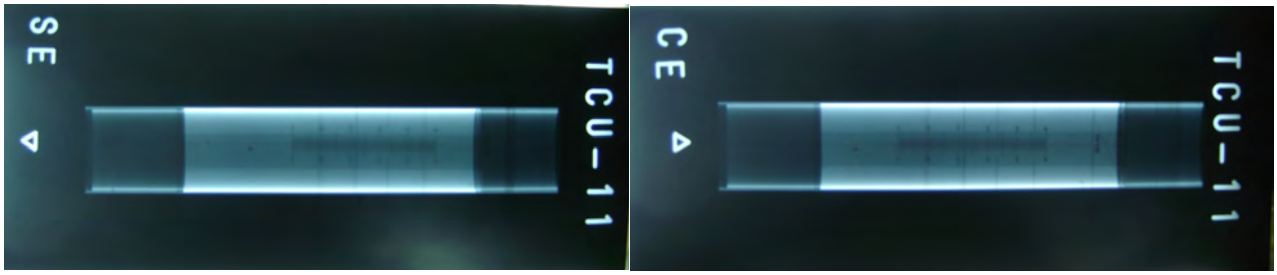

Figure 4. Radiographies of target before (left) and after (right) expansion

Table 3. Annular targets expanded with uranium foils, natural and LEU

Annular target identification	Uranium foil type	Air gap (mm)	Expansion die diameter (mm)	Final condition
TUN-51	Natural	0.009	26.34	Approved
TUN-52	Natural	0.028	26.34	Approved
TUN-53	Natural	0.007	26.37	Approved
TLEU-54	LEU	0.010	26.34	Approved
TLEU-55	LEU	0.008	26.29	Approved
TLEU-56	LEU	0.008	26.34	Approved

Welding

The first welded targets exhibited irregular welding cord and porosity. After degassing thermal treatment, the welding cord was improved with acceptable regularity and porosity.

The welding cord of six targets, three of them assembled with natural uranium foil and three with LEU were approved. In the figure 5 some pictures of these welding cords are presented.

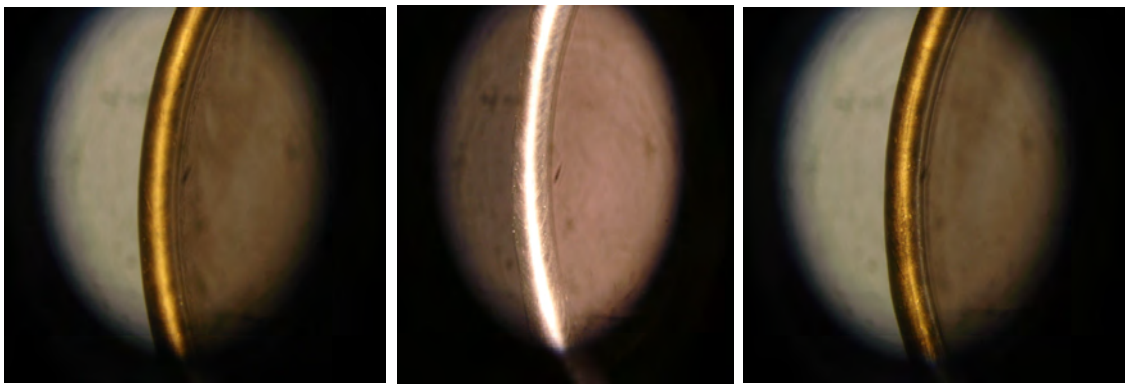

Figure 5. Welding cord of targets previously annealed for degassing**.**

3.4 Leak test

At the beginning some leaks were detected in targets assembled with natural uranium. After machining of both ends of the aluminium tubes and a degassing thermal treatment of the targets, they were welded with acceptable results and no leaks were observed.

3.5 Electrolytic Nickel Coating

Table 4 presents the results of the experiments carried out on natural uranium foil according to the sequence shown in Figure 6. The deposited mass approaches closely that foreseen by Faraday's law, but the thickness of the Ni deposit measured with the Leptoskop equipment differs from that calculated with Faraday's current and time, and this is attributed to the fact that even though uranium has very low electric conductivity compared to Ni, the method of measurement considers the substrate and coating as nonconducting and conducting. The Omega TM additive used actually improved substantially the appearance of the deposit, producing a cleaner and shinier surface, as shown in the last picture of Figure 6.

Table 4. Results of the electrodeposition of Ni on U

Foil id. UNAT	Current (Amp)	Time (min)	Mass deposited (1) (g)	Thickness (1) (µm)	Mass deposited (2) (g)	Thickness (2) (µm)
11.2	3.0	30	1.5	32.3	1.6	18.4
12.1	3.0	40	2.0	45.7	2.2	24.6
10.1	3.2	30	1.6	14.7	1.8	19.7
12.2	3.2	40	1.9	57.5	2.3	26.2
11.1	3.4	20	1.4	9.4	1.2	13.9
8	3.4	30	1.8	39.2	1.9	20.9
12.3	3.4	40	1.9	78.1	2.5	27.9

(1) Experimental measurements made with the Leptoskop; (2) Faraday's law calculations

Figure 6.- Sequence of the electrodeposition of Ni on U.

The superficial distribution of the thickness of the nickel coating for foil 11.2 is shown in Figure 7. The average value was 32.3 µm, from a sample population of 24 points for the 50 cm^2 area.

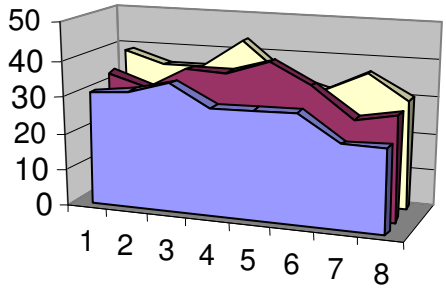

Thickness range (µm)	1	2	3	4	5	6	7	8
20-30	31.1	32.4	35.3	29.7	29.7	30.2	22.8	22.8
30-40	34.5	31.1	37.1	36.7	40.3	35	26.7	28.7
40-50	38.9	35.3	35.8	43.2	34.4	31.4	36.8	30.1

Figure 7.- Thickness distribution of Ni coating for 11.2 foil. Average value: 32.3 µm

Most of the values fit around the centre of the 30-40 µm range. The superficial distribution of the Ni deposit is quite homogeneous and the largest values are found in the bottom part of the foil, showing that the ion flow has an expected trajectory.

UT studies were made to determine the degree of adherence of the Ni deposits on U foil. Figure 8 left is an image of a linear C-scan of a sample, which shows a signal without discontinuity, which indicates qualitatively that there is good adherence of the coating.

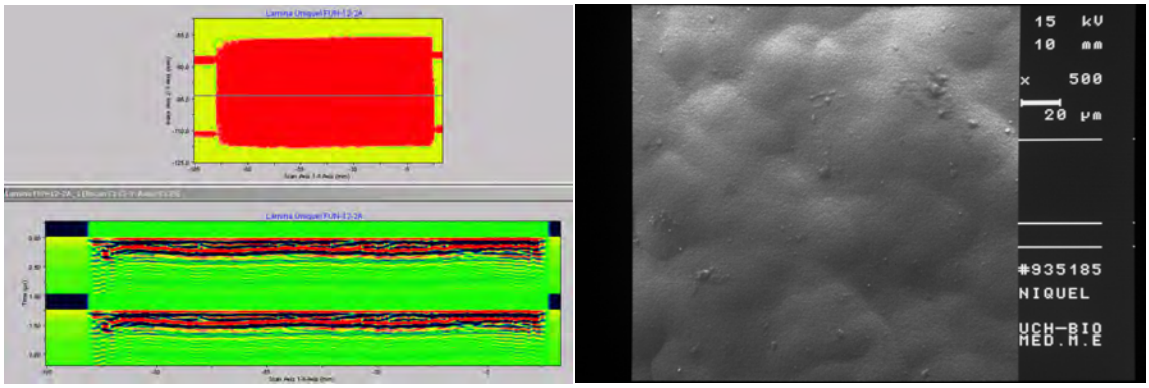

Figure 8. Left: UT view of the assembly of U-Ni and Right: SEM Ni coating surface

The orientation of the deposit follows the trajectory of the current flow, and therefore the grain size of the deposit is relatively small. The surface of the deposit is free of pores and is in layers with valleys and hills appearance, as seen in the micrograph of Figure 8 right, in agreement with what was found in the ultrasound C-scan signal of Figure 8 left. The addition of the wetting agent confirms the influence of a surfactant on the surface tension between the substrate and the electrolyte, and in this way minimizing the existence of defects caused by the presence of hydrogen.

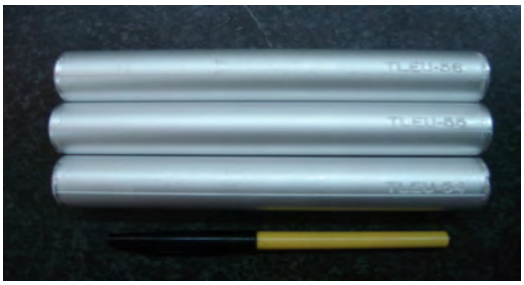

Figure 9. Picture of finished LEU annular targets for ^{99}Mo production

4. Discussions and Conclusions

- The closed semi-dourville mold design, integrally mounted with high alumina crucible allows the production of ingots with an acceptable surface quality.
- The encapsulation technique with low carbon steel cladding is a very effective way to produce uranium foil
- The electrolytic process demonstrates to be a suitable process for the U-Ni system, obtaining a homogenous nickel deposit with good adhesion and free of porosity.
- CCHEN is capable of offering and supply annular targets for Fission Mo production, manufactured according to technical specifications and special requirements of users.

5. References

[1] Technical reports series N° 478, Feasibility of Producing Molybdenum-99 on a Small Scale Using Fission of Low Enriched Uranium or Neutron Activation of Natural Molybdenum International Atomic Energy Agency - Vienna, 2015.
[2] The Supply of Medical Radioisotopes - Medical Isotope Supply in the Future: Production Capacity and Demand Forecast for the 99Mo/99mTc Market, 2015-2020OECD – NEA. Nuclear Development, NEA/SEN/HLGMR(2014)2 April 2014, www.oecd-nea.org
[3] http://www.mallinckrodt.com/Nuclear_Imaging/Global_99Mo_Supply_Chain.aspx
[4] Schrader, R. et al, 2007, “Progress in Chile in the Development of the fission 99Mo Production Using Cintichem”, 29th RERTR 2007 International Meeting on reduced Enrichment for Research and Test Reactors, Prague, Czech Republic.
[5] http:www.iaea.org/worldatom/rrdb/
[6] Schrader, R. et al, 2008, “Status of the Chilean Implementation of the modified Cintichem Process for Fission 99Mo Production Using LEU”, 30th RERTR 2008 International Meeting on reduced Enrichment for Research and Test Reactors, Washington D.C., USA.
[7] Lisboa, J., 2009, “Report Proyecto 99Mo fisión CCHEN – Preparación y ensamblado de prototipos de targets LEU”. Departamento Materiales Nucleares, CCHEN.
[8] Smaga, J.A., et al., 1997, “Electroplating Fission-Recoil Barriers onto LEU-Metal Foils for 99Mo-Production Targets”. Proc. of the 20th International Meeting on Reduced Enrichment for Research and Test Reactors, October 5-10 Jackson Hole, Wyoming, USA.
[9] Conner, C. et al., 1999, “Development of Annular Targets for 99Mo Production”. Proceedings of the 22nd, International Meeting on Reduced Enrichment for Research and Test Reactors, Budapest, Hungary.
[10] Conner, C. et al., 2000, “Production of 99Mo from LEU Target-Acid-Side Processing”. Proc. of the 23rd International Meeting on Reduced Enrichment for Research and Test Reactors, Las Vegas, Nevada, USA.
[11] G. F. Vandegrift, et. al, Converting Targets and Processes for Fission-Product ^{99}Mo from High- to Low-Enriched Uranium, Chapter for IAEA TECODOC, August 1997
[12] Lisboa, J., 2010, Report ID-PEC-DMN-CCHEN-01/2010, Fabricacion de Blancos Anulares LEU”. Departamento Materiales Nucleares, CCHEN.
[13] Jaime R, Lisboa, Jorge Marin, Mario E. Barrera, Gerardo Cifuentes, Manufacturing of Annular Targets Made of LEU Foil Coated with Electrodeposited Nickel, International Congress of Science and Technology of Metallurgy and Materials, SAM - CONAMET 2013, August 20 - 23, Iguazu, Misiones, Argentina.

STATUS AND FUTURE OF MO-99 SUPPLY

B. PONSARD
BR2 Reactor, SCK.CEN
Boeretang 200, B-2400 Mol – Belgium

ABSTRACT

The global supply of Mo-99 relies on a limited number of research reactors and processing facilities. Its production is essential as medical diagnostic imaging techniques using Tc-99m account for approximately 80% of all nuclear medicine procedures worldwide, i.e. 30 million patient doses per year. The short half-life's of Mo-99 (66 hours) and its daughter Tc-99m (6 hours) require a continuous supply of Mo-99/Tc-99m generators to hospitals or central radiopharmacies. Several severe disruptions have been experienced regularly over the past decade due to problems at different stages of the vulnerable Mo-99/Tc-99m supply chain: reactor outages, release of activity from processing facilities, recall of generators by manufacturers, … Currently, nine research reactors are involved in the production of Mo-99 at industrial scale: BR2 (Belgium), HFR (The Netherlands), OSIRIS (France), LVR-15 (Czech Republic), MARIA (Poland), NRU (Canada), SAFARI (South Africa), OPAL (Australia) and RA-3 (Argentina). They irradiate high and/or low enriched uranium targets for the production of about 95% of the available Mo-99 by six processing facilities: MALLINCKRODT (The Netherlands), IRE (Belgium), CNL/MDS NORDION (Canada), NTP (South Africa), ANSTO (Australia) and CNEA (Argentina). The coming period (2015 – 2020) will remain a serious challenge for AIPES (Association of Imaging Producers and Equipment Suppliers) in terms of coordination of research reactor operating schedules to ensure security of Tc-99m supply. Several parameters will indeed impact the supply chain very seriously, among which the definitive shutdown of the OSIRIS reactor (December 2015), the decision to cease Mo-99 production in the NRU reactor (October 2016), the scheduled refurbishment period of the BR2 reactor for the replacement of its beryllium matrix (February 2015 – June 2016), the transition period (2016 – 2017) to enable the conversion from HEU into LEU targets in research reactors and processing facilities, … Fortunately, the situation encouraged the industry to develop new projects and new production routes to increase existing production capacities. This paper summarizes the current status of Mo-99 supply and outlines the efforts made to achieve a reliable Tc-99m availability for nuclear medicine.

1. Introduction

The radioisotopes used for 'in vivo' diagnostic purposes are linked to specific chemical compounds to produce radiopharmaceuticals which allow the desired specific physiological processes to be examined (heart, thyroid, liver, kidney, blood flow, …), the detection of tumours (breast cancer, prostate cancer, …), bone scintigraphy, … They must emit gamma rays of sufficient energy to escape from the body so that they can be detected by a camera that will produce an image. Moreover, their half-life must be long enough to allow for logistic and preparations before imaging can occur, and short enough for it to decay during the imaging procedure and disappear soon after it is completed. Technetium-99m (Tc-99m), the daughter of Molybdenum-99 (Mo-99), is the most suitable radionuclide for SPECT (Single Photon Emission Computed Tomography) medical diagnostic imaging technique with a single 140 keV gamma-ray emission and a very convenient half-life of 6 hours. It is used in about 80% of all nuclear medicine procedures worldwide, representing yearly approximately 30 million examinations. According to the analysis performed by the OECD / NEA, there is good evidence that the Tc-99m demand for diagnostic imaging will continue to grow in the short to medium term. The related Mo-99 demand is estimated to grow at rates of respectively 0.5% per year for mature markets (Europe, North America, Japan, Republic of Korea) and 5% per year in emerging markets (South America, Africa, Asia) [1].

2. The Mo-99 global supply chain

Mo-99 is characterized by a half-life of 66 hours and is currently mainly produced in research reactors by fission of U-235 from high enriched uranium (HEU) and/or low enriched uranium (LEU) targets. There are only nine research reactors involved in this production on industrial scale: BR2 (Belgium), HFR (The Netherlands), OSIRIS (France), LVR-15 (Czech Republic), MARIA (Poland), NRU (Canada), SAFARI (South Africa), OPAL (Australia) and RA-3 (Argentina). Their weekly irradiation capacities are given in Table 1.

Reactors	Countries	Targets	Weekly irradiation capacities ['6-d' Ci]
BR2	Belgium	HEU	7.800
HFR	The Netherlands	HEU	4.680
NRU	Canada	HEU	4.680
SAFARI	South Africa	HEU/LEU	3.000
LVR-15	Czech Republic	HEU	2.800
OSIRIS	France	HEU	2.400
MARIA	Poland	HEU	2.200
OPAL	Australia	LEU	1.000
RA-3	Argentina	LEU	400

Table 1: Research reactors involved in the global Mo-99 production [1]

After an irradiation time of about 150 hours in a research reactor and a cooling period of 12 hours, the irradiated targets are loaded into shipment containers and sent to six processing facilities supplying about 95% of the bulk Mo-99 global needs: MALLINCKRODT (The Netherlands), IRE (Belgium), CNL/MDS NORDION (Canada), NTP (South Africa), ANSTO (Australia) and CNEA (Argentina). Their weekly processing capacities are given in Table 2.

Processors	Countries	Targets	Weekly processing capacities ['6-d' Ci]
CNL/MDS NORDION	Canada	HEU	4.680
MALLINCKRODT	The Netherlands	HEU	3.500
IRE	Belgium	HEU	3.500
NTP	South Africa	HEU/LEU	3.500
ANSTO	Australia	LEU	1.000
CNEA	Argentina	LEU	900

Table 2: Processors involved in the global Mo-99 production [1]

After dissolution of the irradiated targets, the extracted bulk Mo-99 is sent to Mo-99/Tc-99m generators manufacturers: MALLINCKRODT (The Netherlands and US), LANTHEUS MEDICAL IMAGING (US), GE-HEALTHCARE (UK), IBA-MOLECULAR (France), ... It is important to note that reactor irradiation capacities give only a partial view of the global Mo-99 availability and do not account for logistic issues related to targets and bulk Mo-99 shipments, ... Research reactors are not all linked to processing facilities on site which results in some regional constraints on processing capacities and in the loss of product through more decay during shipments. This is especially the case in Europe where irradiation capacities exceed processing capacities. Furthermore, processing facilities have to face some safety limitations in terms of number of targets processed per week according to potential fission gas release. For these reasons, the major risk in the Mo-99/Tc-99m supply chain in next future will be insufficient processing capacities rather than insufficient irradiation capacities. The geographical location of the main facilities currently involved in the Mo-99 global supply chain is illustrated in Fig. 1.

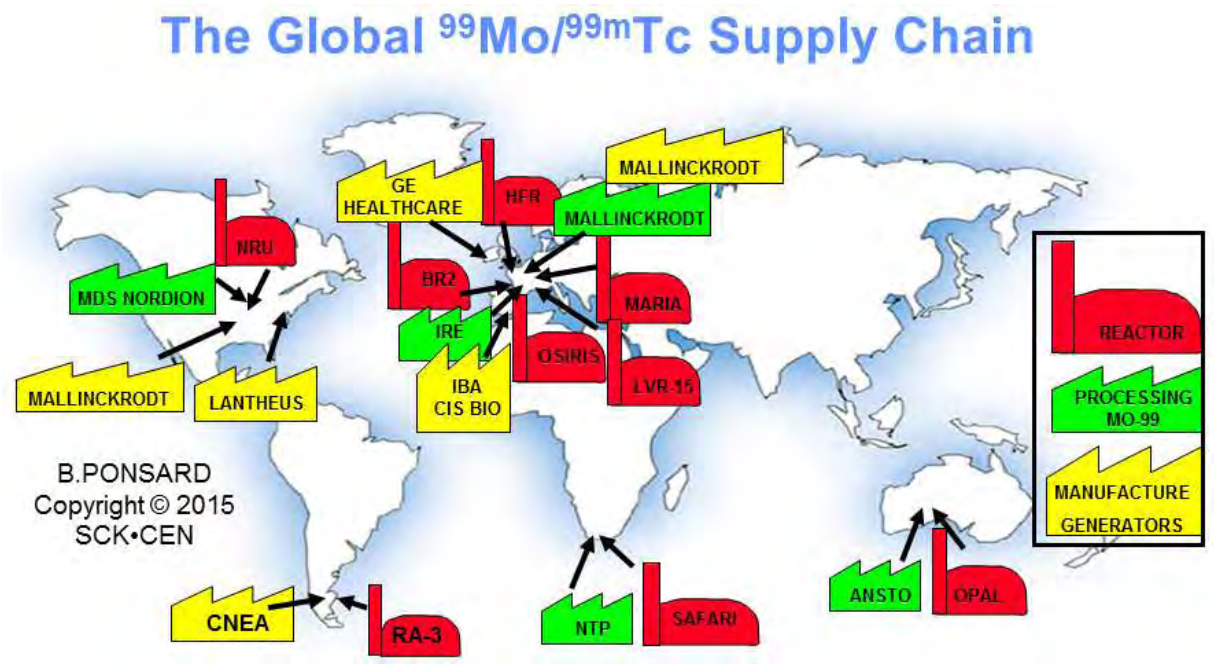

Fig. 1: Main facilities currently involved in the Mo-99 global supply chain

Finally, the Mo-99/Tc-99m generators are supplied to hospitals or central radiopharmacies as shown in Fig. 2 and can be used for only 1 week because of the loss of 1% of activity per hour. In normal circumstances, this strategy of supply allows the availability of Tc-99m every day, 365 days per year, on the basis of a weekly delivery of generators all around the world. Each partner in the supply chain must thus work very efficiently to avoid losing time so that the product can be delivered as quickly as possible, taking shipment constraints into account (by road, by air, …). Nevertheless, recurrent supply shortages have highlighted the vulnerability of centering production on a limited number of ageing reactors [2].

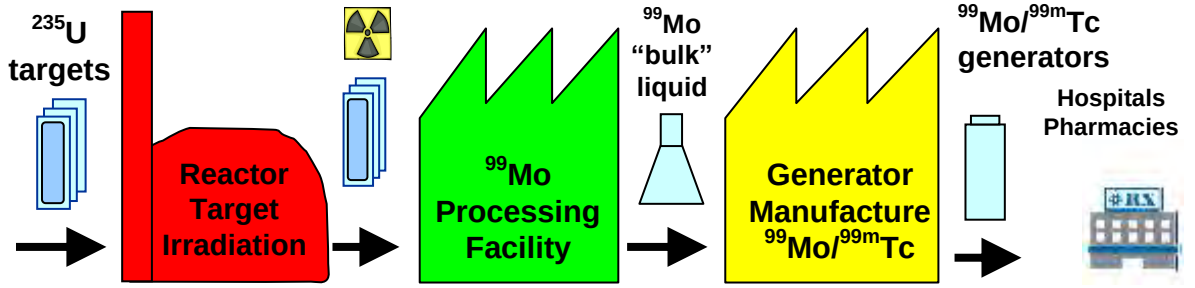

Fig. 2: The Mo-99 supply chain

3. The AIPES Reactors and Isotopes Working Group

The main actors (research reactors, processors, generator manufacturers) involved in the Mo-99 global supply chain are represented in the 'Reactors and Isotopes' Working Group of the Association of Imaging Producers and Equipment Suppliers (AIPES). They provide their best efforts to achieve optimal coordination of their operations to mitigate potential shortages in the Mo-99 global supply chain and to meet the current Mo-99 global demand of about 9.500 '6-d' Ci per week as reported at the last HLG-MR meeting held in Paris in February 2015. The FRM-II (Germany) research reactor is also represented within the AIPES 'Reactors and Isotopes' Working Group and aims to produce 1.600 '6-d' Ci per week from 2017 by the irradiation of LEU targets. The AIPES 'Reactors and Isotopes' Working Group plays a key role within the Mo-99 global chain in terms of coordination and communication. As shown in Fig. 3, the AIPES annual reactor schedule follows the operating periods of the main research reactors involved in the Mo-99 global supply chain. This schedule is updated each time an issue requires reactor rescheduling to mitigate Mo-99 shortage related to maintenance operations, unplanned reactor shutdowns, target manufacture, target shipment, issues at processor or generator manufacturer level, ...

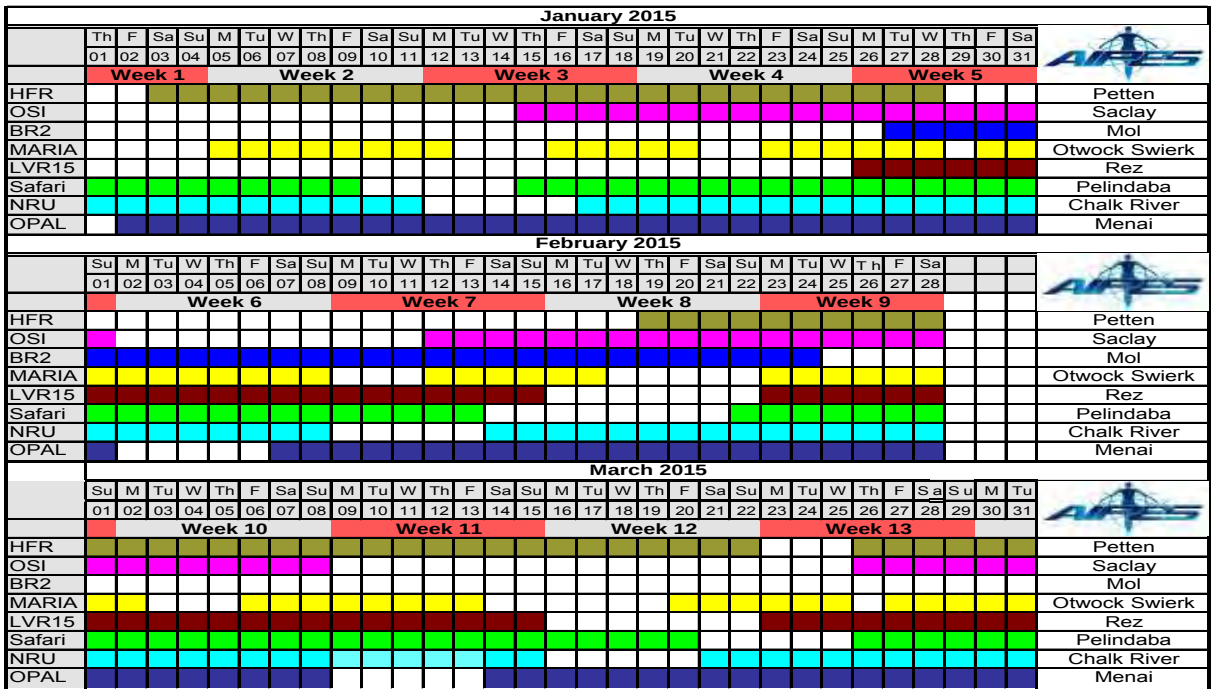

Fig. 3: AIPES reactor schedule (1st trimester 2015)

Several actions have been taken by the AIPES 'Reactors and Isotopes' Working Group in the past years to improve the Mo-99 production monitoring and provide suitable communication to stakeholders. As a result, there were no significant supply shortages in 2014 despite several reactor and processing facility events during this period.

The ERT (Emergency Response Team) has been created in 2012 within the AIPES 'Reactors and Isotopes' Working Group to follow production and supply issues – week by week – through conference calls if requested. This continuous follow-up allows to identify potential Mo-99 shortages and to define action plans with research reactors, processors and generator manufacturers, including support for ‘fresh’ and ‘irradiated’ targets shipments.

The "VERSAILLES Mo-99 MODEL" has been developed and validated by AIPES in 2014 based on data provided in the OECD / NEA report [1] and feedback delivered by the AIPES representatives (processors and generators manufacturers) for the years 2013 and 2014. This model follows the global Mo-99 maximum weekly reactor production capacity – week by week – and is a suitable tool to assist scheduling the reactor operating periods with respect to an optimal security of Mo-99 production.

Especially, the "VERSAILLES Mo-99 MODEL" will help to identify periods of increased risks for Mo-99 supply shortages and to define the optimal reactor operating periods taking into account the extended scheduled shutdown of the BR2 reactor for the replacement of its beryllium matrix (February 2015 – June 2016), the definitive shutdown of the OSIRIS reactor (December 2015), the decision to cease Mo-99 production in the NRU reactor (October 2016), the transition period (2016 – 2017) to enable the conversion from HEU into LEU targets in research reactors and processing facilities, the entrance of new Mo-99 (Tc-99m) production sources on the market, …

Fig. 4 illustrates the results of the AIPES "VERSAILLES Mo-99 MODEL" applied on the year 2015 during BR2's scheduled extended shutdown period for the replacement of its beryllium matrix. It appears that the supply of Mo-99 should be sufficient during this period subject to a reduced reserve capacity at reactor level and lesser flexibility for rescheduling in case unscheduled events would occur in the supply chain. It should also be noticed that a reactor production capacity below the 9.500 '6-d' Ci red line during a particular week does not means that the reduced Mo-99 production capacity would result into a severe Mo-99 shortage which would not be manageable by the supply chain and impact patient treatments seriously. However, the model is able to identify periods at risk which need to be further investigated at processor and generator manufacturer level. Suitable action plans can then be defined to mitigate the impact in the supply chain in case of necessity together with appropriate communication to stakeholders.

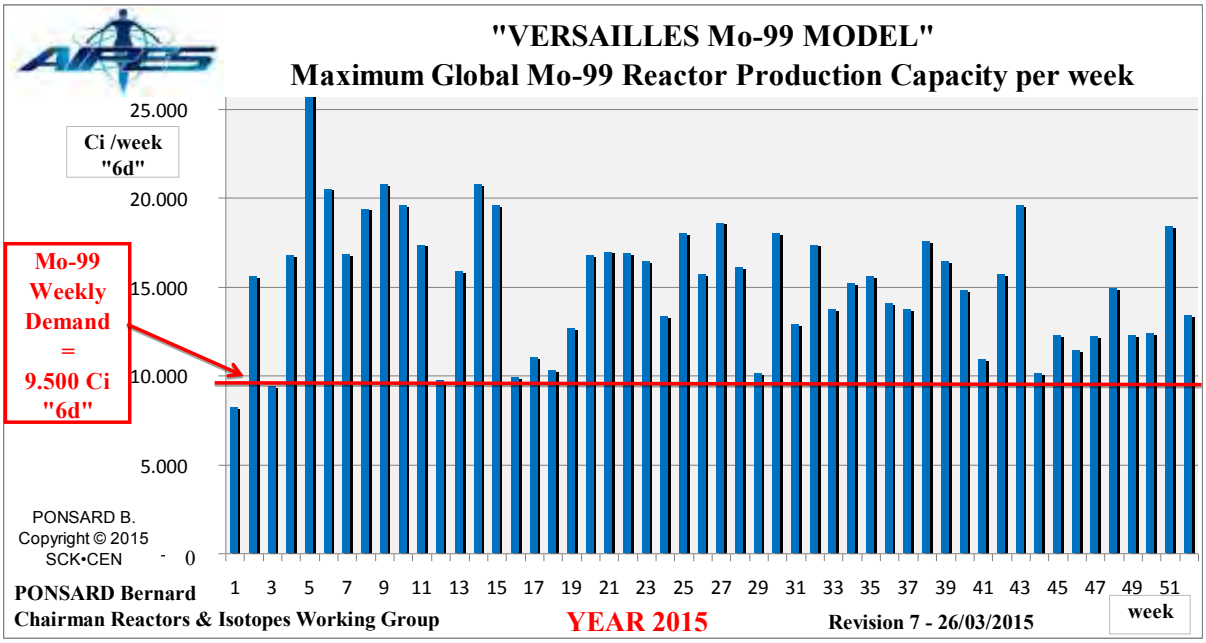

Fig. 4: AIPES "VERSAILLES Mo-99 MODEL" applied to 2015

4. Future Mo-99 supply

The recurrent supply shortages highlighted the vulnerability of centering production on a limited number of ageing reactors and encouraged the industry to develop new projects and new production routes to increase and diversify production capacities [1].

- Reactor Production Routes
  - Fission of solid LEU targets : $^{235}U(n,fission)^{99}Mo$
  - Fission of LEU in solution : $^{235}U(n,fission)^{99}Mo$
  - Neutron capture : $^{98}Mo(n,\gamma)^{99}Mo$

- Accelerator Production Routes
    - Photofission reaction : $^{238}U(\gamma,fission)^{99}Mo$
    - Photonuclear reaction : $^{100}Mo(\gamma,n)^{99}Mo$
    - Photoneutrons generated from e- beam for fission LEU in solution
    - D-T neutron generators to fission LEU in solution: $^{235}U(n,fission)^{99}Mo$
    - Spallation neutron source production (ADS) : $^{235}U(n,fission)^{99}Mo$
    - Direct Tc-99m production by cyclotron : $^{100}Mo(p,2n)^{99m}Tc$

The definitive shutdown of the OSIRIS (France) reactor at the end of 2015 and the decision taken by the Government of Canada to cease Mo-99 production at the NRU (Canada) reactor end of October 2016 will result in a reduction of about 30% of the global Mo-99 production capacity by the end of 2016.

Nevertheless, the Government of Canada has decided to support an extension of the NRU operations until March 31, 2018 after which point the reactor will be shut down definitively. NRU will remain fully operational to perform material testing programs and the production of radioisotopes other than Mo-99 such as Co-60 but not Xe-133 which is a fission product resulting from the dissolution of targets irradiated for Mo-99 production. However, it is Canada's intention to keep the NRU available between November 1, 2016 and March 31, 2018 as a back-up production capacity for Mo-99 in case of significant shortage on the market. CNL will maintain NRU and processing facilities on stand-by and work with key stakeholders to ensure appropriate response time to deal with emergency situations. In other words, Canada would consider calling upon the NRU to produce Mo-99 only as a last resort, should there be a global shortage that could not be mitigated through other means and that would have severe impact on patients. Canada is convinced that its decision to cease all routine production of Mo-99 from the NRU reactor from October 31, 2016 remains essential to the market entry of alternative sources to produce Mo-99 or Tc-99m directly and that the availability of new diversified production sources will ensure the long-term security of supply.

The restart of the BR2 reactor after refurbishment is scheduled in July 2016. Its operating regime could be upgraded from currently 5 up to 8 operating cycles per year depending on the economics, i.e. up to 200 operating days per year from 2017.

The first semester of 2016 – period during which the OSIRIS and BR2 reactors will not be in operation – could be at risk in terms of Mo-99 supply, especially in case the NRU reactor would require an extended maintenance in this timeframe. There are other potential reactor-based and non-reactor solutions for the secure supply of Mo-99 and Tc-99m in the medium to long-term future. As reported by the OECD / NEA [1], new irradiation projects are under development for global supply as can be seen in Table 3. However, there are many assumptions and uncertainties over whether projects will be operational within the period 2015 – 2020. If all these new projects would come on line as announced, there would be a massive overcapacity on the Mo-99 market in the coming years. Regarding processors, new projects are under development for global supply as reported by the OECD / NEA [1] and some are really welcome to increase security of supply. At processor level, ANSTO (Australia) is currently covering national Mo-99 needs by the dissolution of LEU targets irradiated in the OPAL reactor and is already FDA approved in the US. A new processing and waste facility is under construction and is expected to start in 2016 for the supply of 3.500 '6-d' Ci per week. During the period between July 2016 and December 2016, the return to service of the BR2 reactor and its increased production level would be sufficient to compensate the loss of irradiation capacity from the OSIRIS and NRU reactors subject to an appropriate scheduling of the available reactors and gradual conversion programs from HEU into LEU targets in the European research reactors and processing facilities at IRE (Belgium) and MALLINCKRODT (The Netherlands). The commissioning of the new processing capacity at ANSTO in 2016 is also essential to compensate for the loss of the processing capacity associated to the NRU reactor in Canada.

Reactors	Countries	Targets	Weekly irradiation capacities [6-day Ci]	Starting date
RIAR	Russia	HEU	1.200	2015
Karpov Institute	Russia	HEU	300	2015
NORTHSTAR/MURR	US	Mo-98	3.000	2015/17
MORGRIDGE/SHINE	US	LEU solution	3.000	2017
NORTHSTAR	US	LINAC	3.000	2018
FRM-II	Germany	LEU	1.600	2017
OPAL	Australia	LEU	2.600	2017
KOREA	Republic of Korea	LEU	2.000	2018
CHINA Advanced RR	China	LEU	1.000	2019
Brazil MRR	Brazil	LEU	1.000	2019
RA-10	Argentina	LEU	2.500	2019
JHR	France	LEU	3.200	2020

Table 3: New projects for Mo-99 and Tc-99m production – 'non exhaustive list' [1]

5. Conclusion

The definitive shutdown of the OSIRIS (France) reactor at the end of 2015 and the decision taken by the Government of Canada to cease routine Mo-99 production at the NRU (Canada) reactor from November 1, 2016 will result in a reduction of about 30% of the current global Mo-99 production capacity by the end of 2016. It should be also highlighted that the processing capacity associated to the NRU reactor will also be lost by November 1, 2016 for routine production. Fortunately, the BR2 reactor will come back into service in July 2016 for an operating period of at least 10 years and an increased operating regime subject to the economics. The commissioning of the new processing capacity at ANSTO in 2016 is also essential to compensate for the loss of the processing capacity associated to the NRU reactor in Canada. Furthermore, several new projects are expected to be commissioned in the period 2015 – 2020, including the conversion programs of targets from HEU into LEU in Europe, and will help to increase and diversify production capacities of Mo-99 and Tc-99m in future.

6. References

[1] OECD / NEA (2014) – The Supply of Medical Radioisotopes – Medical Isotope Supply in the Future: Production Capacity and Demand, Forecast for the Mo-99/Tc-99m Market, 2015-2020, NEA/SEN/HLGMR(2014)2, April 2014.

[2] B.PONSARD. "Mo-99 Supply Issues: Status Report and Lessons Learned", 14th International Topical Meeting on Research Reactor Fuel Management (RRFM 2010), Marrakech, Morocco, March 21-25, 2010. Published by the European Nuclear Society, ENS RRFM 2010 Transactions, ISBN 978-92-95064-10-2.

LEU Fuel Conversion

Conversion study for FRM II with backup fuel U_3Si_2

A. Röhrmoser
Forschungsneutronenquelle Heinz Maier-Leibnitz *(FRM II),*
Technische Universität München, D-85747 Garching , Germany

ABSTRACT

Conversion studies of the very compact core of FRM II are mainly based on the high uranium density UMo fuel of dispersive and also monolithic character and are kept on a conservative basis for exchange of reactor systems. A main constraint is to maintain the cycle time of the current fuel element and to stay rather marginal at losses in neutron flux levels.

Principal studies have shown that any conversion is still a big challenge for FRM II unless some change to the outer and inner geometry. Thus any realistic study must search for some gain in core volume to reach a lower enrichment value. First option is a somewhat prolonged fuel element with thicker fuel meat. And with further replacing the central channel (CC) tube by zircaloy material this would allow to reach 30% enrichment with an U7Mo fuel at density of 8gU/cc (RRFM 2012), as far as qualified.

A solution with the actual FRM II fuel U_3Si_2 at a density of 6 gU/cc would instead allow a decrease in enrichment to 35% at the same prolonged fuel element geometry. The n-flux loss would then lie somewhat better at about 6% for the mid plane BT-5 and also the average of BTs (again MOC). The user critical cold source (CS) would see only 4-5% loss in thermal flux, but users should obtain no loss in cold flux because of some regain of cold moderator caused by reduced heat load at the CS.

1 Introduction

FRM II has an obligation in its nuclear license for conversion of the reactor to lower enrichment. Principal as well as more realistic studies were performed for the conversion of the very compact core. The studies are mainly based on the high uranium density UMo fuel of dispersive and also monolithic character and are kept on a conservative basis without changes to major reactor systems like pumps and control or shut down rods. A main constraint at any conversion study is to fulfil the cycle time of the current reactor in order to avoid major penalties beside unavoidable losses in neutron flux levels.

The principal studies have shown that with an 8gU/cc UMo fuel an enrichment level of 50% is still a big challenge for FRM II unless some change to the outer geometry. Thus any realistic study must search for some gain in core volume to reach a lower enrichment value. The first option is a somewhat prolonged fuel element. The main reason for this prolongation is to regain reactivity lost due to the much higher U-238 content. But the most favorable measure would be an increase in the outer fuel radius, even if only in the mm range. This helps also very much to overcome higher heat loads for hot coolant stripes and could be achieved if the central channel (CC) tube could be replaced by zircaloy material. This would enable to reach 30% enrichment with U7Mo fuel at density of 8gU/cc through some optimizing at the plates with thicker fuel meat (RRFM 2012). The loss in thermal n-flux at beam tubes (BT) was calculated between 15% at the highest located BT-3 and 2% at low lying BT-7 for mid of the cycle (MOC). BT-5 in the core mid plane would lose 8% and the cold source (CS) 5% in thermal flux.

This work will show a geometrically similar conversion option with back-up fuel U_3Si_2 at 6 gU/cc, worked out parallel to the UMo solution [Frm12] in 2012. The results are all very similar to the UMo 30% enriched element but the thermal flux levels will be 2% better and less fuel would be required; the density lies somewhat above the qualified 4.8 gU/cc.

2 U_3Si_2 fuel

2.1 IRIS1, U_3Si_2-Schwelltests

Several experiments were examined in the past to clarify the swelling behavior of the ‚disperse U_3Si_2 in Al matrix' fuel und to qualify the fuel up to operational limits. At the IRIS1-fuel tests for the fuel element of FRM II plates of uranium density 3.0 g/cm³ (and also 1.5 g/cm³) [irrFrm2] were irradiated and investigated. The picture shows the measured swelling of the plates as a function of local fission density in the grains of the 3gU/cc fuel range.

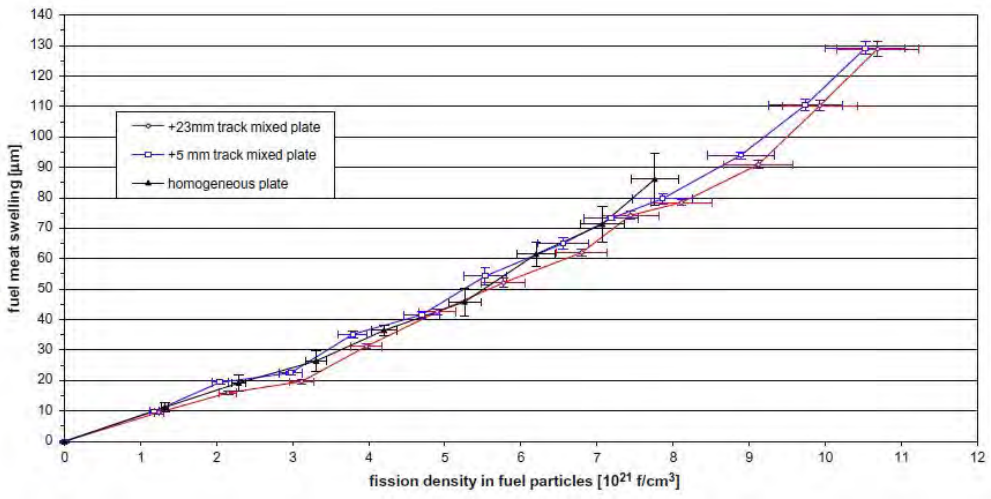

Fig. 1: Swelling of a 600 µm thick fuel layer at density 3g U/cm³ as a function of local fission density [irrFrm2] for several tracks along the IRIS1 plates. The measurements lie still 4mm to 5mm inside the fuel layer.

From the swelling measurements at the irradiated U_3Si_2 TUM-Platten IRIS1-Si it can be derived:

- the thickness of the plates increases rather linear with the local fission density (FD) up to high FD values
- stable binding in the plates up to very high FD in the fuel ($2.9 \cdot 10^{21}$ f/cm^3 or accordingly $1.08 \cdot 10^{22}$ f/cm^3 in the grains). The numbers are valid for the density of 3gU/cc and are scanned 4-5mm away from the exact border of the fuel layer, which will have higher FD.

2.2 Consequences for FRM II operation

The approval records for FRM II were focused on this experimentally covered area. It is mentioned, that this experimental limit ($2.9 \cdot 10^{21}$ f/cm^3 in the meat) is nowhere reached in the plates.

For the burnt fuel element there was calculated a form factor (FF_{fd}) of 1.9 in the zone with 3gU/cc. This FF was evaluated for a narrow radial area (outer burn up zones) in the plates corresponding to a stripe of 5mm width along the fuel meat. At cycle end with now 60 full power day (FPD) operation this means a FD of always below $2.0 \cdot 10^{21}$ f/cm^3 in the meat (or $7.5 \cdot 10^{21}$ f/cm^3 in den grains).

2.3 U_3Si_2 qualified

[NR1313] writes:
"One uranium silicide compound, U_3Si_2, has been found to perform extremely well under irradiation and can provide a uranium density of at least 4.8 g/cc."

The tests, mostly with mini plates, were done also with U densities up to nearly 6 gU/cc; the qualification limit is not due to worse irradiation behavior at higher density, but rather to fabrication issues, [NR1313]: "There is general agreement among the developers and fabricators of aluminum-matrix dispersion fuels that (production) yields of acceptable plates drop rapidly as dispersant loadings are increased beyond 43 to 45 vol%, or 4.8 to 5.1 gU/cc for U_3Si_2"

3 Calculational procedures and models

Topics for core conception are the start reactivity and the reactivity loss and, indivisible from these, the power and neutron flux distribution in and out of the fuel element during the whole operations cycle with one fuel element.

3.1 MonteBurns calculations

Most of the former complicated data preparation procedures and approximations of design calculations of the ‘80s can be bypassed today by use of 3d models and point data for cross sections. As computer power has exploded in the last 30 years and MonteCarlo (MC) methods for individual particle transport can be exploited intensively. In combination with a burn-up module, coupled codes allow a comparable tracing of flux and power profiles, covering the full core cycle. Several adaptations with respect to discrete energies and geometrical meshing are no more necessary. Furthermore, the capability to do burn-up calculations in 3d with real beam tubes in the moderator can be explored now, too. For this purpose, studies with the MCNP-ORIGEN2.2 coupled version of MonteBurns2 of LANL [MB2.2] were performed. This work will show mainly results obtained through this very powerful methodology, presented already for FRM II [Frm10]. There were used mainly ENDF/B-VI data sets for the studies.

3.2 MCNP models

In 2003, an extensive review of the former MCNP model was done. The core was depicted clearly heterogeneous. In the HW tank, 11 beam tubes, one cold and one hot source and multiple irradiation channels penetrating from the top, were updated to the ‘as-built’-situation [FrmMdl].

3.3 Burn up model

For the burn-up calculations, the MonteBurns code was modified to allow for 50 zones, meaning 8*6 (axial*radial) core zones and 2 burn-up zones for a boron ring in a 2d-cylindrical symmetry (r,z) model for principal comparison studies. Hereby all relevant operational aspects can be covered. To allow extra predictions, especially for flux levels at specific beam tubes, it can be finally run for preselected core geometries a real 3d-model. For this model, the modified code allows for three azimuthal zones or 5*3*3 (axial*radial*azimuthal) core zones +5 extra burn-up zones for a boron ring and some extra burnable inserts.

Incorporating a search mode for positioning of a movable structure like the CR, as done in the classical module sequence Mf2dAb, is less straight-forward choice here due to the stochastic manner of this system and computationally expensive. In this study the repositioning of the CR is done as expected for the time steps to be processed (very small deviations of the CR position are irrelevant here for calculating the burn up distribution).

3.4 Total uranium mass

At a 76 cm high active zone instead of actual 70 cm, one gains all together 45.3% in volume for the fuel. Taking into account the very high U density of 6.0gU/cc with U_3Si_2 instead of currently maximum 3.0gU/cc, the increase in uranium mass is nearly threefold, meaning that the fuel element would contain 24 kg uranium instead of 8.1kg now; a nice feature of this option would be the comparable amount of U-235 (scarcely more than now).

Geometry	**HEU / real**		**30% enr.,**	**gain in volume**	**35% enr.,**
fuel material	U_3Si_2		UMo		U_3Si_2
Enrichment	**93%**		**30%**		**35%**
uranium density [gU/cc]	3.0 and		8.0 and		6.0 and 3.0
inner radius of CC	6.5 cm		6.5 cm		=
outer radius of CC	11.45 cm		11.65cm	5.7 %	=
fuel free gap inside/outside	0.25 cm		0.25 cm		=
radius of reduced density	10.56 cm		10.8 cm		10.76 cm
active element height	70 cm		76 cm	8.6 %	=
meat thickness	0.6 mm		0.76 mm	26.7 %	=
cladding thickness	0.38 mm		0.30 mm		=
cooling channel (CC) thickness	2.2 mm		2.2 mm		=
number of plates	113		113		=
outer radius outer core tube	12.15 cm		12.35 cm		=
CCT inner radius	12.3 cm		12.45 cm		=
CCT outer radius	13.1 cm		13.1 cm		=
CCT material in calculation	AlMg3		Zirkaloy		=
volume 'meat'	2.960 l		4.302 l	45.3 %	
mass U-235	7.54 kg		9.51 kg		8.32 kg
mass uranium total	8.11 kg		31.7 kg		23.77 kg
Neutronics, all results by coupled MCNP					
cycle length at 20 MW thermal power after	60 days		60 days		60 days
k_{eff} BOC,	1.133		1.117		1.126
k_{eff} EOC, 3*5(*3) radial/axial(/az.) burn up zones core, dynamic CR and totally withdrawn at end	1.0076 ±0.0002		1.0070 ±0.0002		1.0062 ±0.0004
Fission density maximum (plate of 5mm*5mm), 60FPDs	$1.9\ 10^{21}$		$1.3\ 10^{21}$		$1.3\ 10^{21}$
Thermal hydraulics, calculation NBK					
pressure drop over element	5.3 bar		=		=
flow velocity of LW between plates	16 m/s		15.4 m/s		15.4 m/s
water temperature, fuel element inlet	38 °C		=		=
water temperature, fuel element outlet	54.3 °C		54.1 °C		54.1 °C
mass flow of LW through fuel element	274 kg/s		277½ kg/s		277½ kg/s
max. heat flux at plate surface (hot point)	370		336		333 W/cm^2
hot point at plate surface, **conservative heat transfer**	96.0°C		95.4°C		95.1°C
safety value, local voiding S_{onb} at minimum	2.48		2.575		2.615
(safety value S_{fi} against flow instability, channel average	4.24		4.4		=)

Table 1: Comparison of the basic data of current HEU fuel element with the proposal for a 30% (UMo) and 35% (U3Si2) enriched element for FRM II

4 Results for the reactor

It shall be again emphasized, that all results with a new fuel element must be directly compared with the actual values of the current HEU element.

4.1 Reactivities, safety

The radial dimensions of the core are totally unchanged from outside as well as from inside.

4.1.1 Control rod

The overall reactivity grasp and the differential reactivity of the CR are slightly lower than now. Consequently, the CR will use a greater span of its current driveway during normal operation.

First there is only an upper value for the moving speed of the CR, this should not have a new regulatory implication for reactor operation by the CR. And secondly there is the request, that the CR alone must keep any core situation very clearly below criticality and this is met even with the longer fuel element at unchanged CR system.

4.1.2 Shut down rod system

Any aspect of reactivity worth of the SRs during a 'scram' is very comparable to the current situation, and this is the case for comparison of the safety. The total reactivity grasp of the SRs in the final down position can be again slightly lower than now with a longer core.

4.2 Reactivities during operation cycle

The main result of the calculations procedure MB, which is described shortly above, can be seen in the necessity of an enrichment of only 35% to achieve the same burn up of 1200 MWDs in total for the extended core. Of course, the presented solution is not the result of a single guess but rather of a long series of optimisation steps not shown here. Especially the problem of too high local power values from former calculations with unchanged core geometry was the guide for finding a less enriched fuel element for FRM II that also solves the operational constraints like safety values against voiding in the cooling channels. This once more underlines the necessity of taking neutronic and thermal hydraulic factors into account at the same time.

4.3 Core cooling

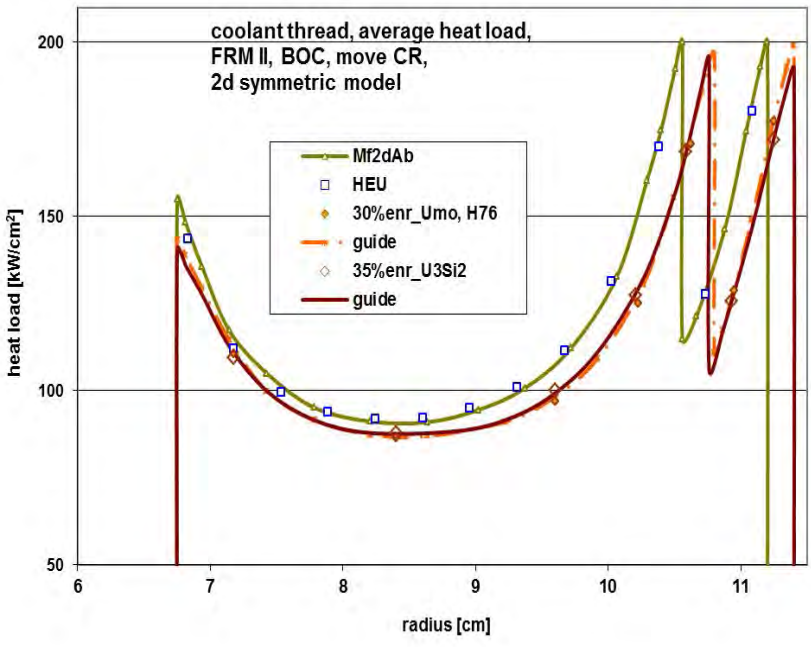

Fig. 2:
Heat load for coolant filaments over the radius in the coolant channels, calculated for the current HEU fuel and the 30% enriched case, both at BOL. The outer radius of the uranium zone was enlarged by 2 mm, gaining 6% in area for coolant flow at the active zone. The outer fuel zone with lower U density is of the same width in radius with U_3Si_2.

It is regarded a basic requirement for the safety of FRM II, that the hot streaming filament is always clearly inside the core at a deeply negative value for the local void-reactivity worth. Such a hot s tream filament must not be located at the outer edge of the cooling channel. Because of the cold stream filament at the edge, this is already very well guaranteed if the inner peak (speaking with Figure 2) has nearly the same height as the outer one, as it is the case with the current HEU fuel. For this purpose, the grading of the uranium density was, as with the U_3Si_2 HEU, located 6.4 mm inside of the outer radius (end of fuel zone).

Thermal hydraulic calculations were carried out using the in-house developed code NBK [THnbk], which is tailored especially for the involute shaped plates and channels of the fuel element. Starting from Fig. 3, it might appear that the hot stream filament is still located at the outer edge of the plate. However, NBK calculations using 30 stream filaments show that the hot filament is located further inside, near the density jump (compare Fig. 4). The reason for this is the lateral heat transport in the plates into the direction of the cold stream filaments. Conservative thermal hydraulical assumptions like 'no mixing of the coolant filaments' were used, together with a moderate choice for the convective heat transfer correlation identical in both NBK calculations. It was shown that modern CFD codes like Ansys CFX predict lower cladding surface temperatures and therefore even higher safety margins. However, experimental validation for CFX with the narrow channels is still missing.

The operation conditions were taken nominal with 20MW and 5.3 bar pressure loss over the element. As a result the absolute values of total heat load at the radial maxima are now comparable to the actual HEU case.

If we assume the same outer pressurizing conditions with the existing primary pumps, some small differences in values like the local pressure at the hot points appear with the NBK calculation, the overall water throughput being nearly untouched (s. Table 1). The only clear difference that arises is a general lower flow velocity with a prolonged fuel element in the primary coolant circuit (here 15,4 m/s instead of 16 m/s at nominal conditions between the fuel plates)[&]. The hot spots in temperature are calculated to be very similar with a maximum value of 95°C at the plate surface.

Fig. 3:
Calculated safety factor S_{onb} against local voiding in comparison of the current HEU case to the studies with longer and lower enriched element. It is always shown S_{onb} for the hot stream filament 23 in this thermohydraulic NBK calculation with 30 filaments in total. Some conservative assumptions as for the convective heat transfer correlation at nominal operation conditions (20MW, 5.3 bar pressure loss) were the same in both cases. NBK was fed with the most unfortunate power distribution at BOC, calculated with the 3d-MCNP model at reactor start with a fresh fuel element.

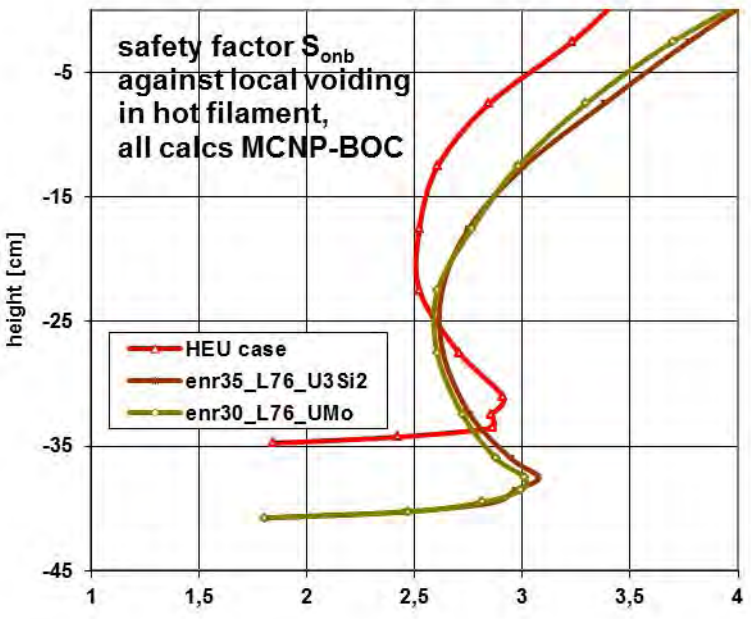

[&] We are aware, that any relicensing will be addressed by any flow changes, what may hinder a simple replacement of the current fuel element by the one discussed here.

Although differences in local flow conditions and the most unfortunate power distributions at BOC are supposed for both cases, the safety factor S_{onb} against local voiding is again comparable to the actual case, being 2.63 for the 35% enriched element instead of 2.46 for the HEU case under nominal operational conditions. Assuming more severe off-normal conditions, the safety factor S_{onb} gain appears even clearer. The lower values S_{onb} at the end are not the relevant ones for the overall assessment of the reactor, because of their very small axial extent of a few mm and the missing axial heat flow in the plates, which is not calculated in NBK. The very narrow peaks are flattened when scaling to local heat flux and safety values. Extra calculations, which utilize the 3D heat transfer in the cladding, confirm this.

Concerning the safety value S_{fi} against flow instability after Forgan/Whittle, the 35% enriched element of this study (as well as the 30% enriched UMo case) shows some preference - bearing in mind possible limitations when assuming the same outer pressurizing conditions.

4.4 Fission densities

The fission densities in a 45% increased fuel volume are 31% lower in average and are as well lower for any maximum (s. table). The distribution has a tendency towards more homogeneity than in the more compact case with HEU. The maximum fission density is now found at the outer edge of the high density region at a height 10 cm below fuel element mid plane with a value of $1.3 \cdot 10^{21}$ f/cm^{-3}. For the U_3Si_2 fuel density of 6gU/cc this means a maximum FD value in the meat of not more than $2.5 \cdot 10^{21}$ and a very low value in Fig. 1 and even for the low density region in the outer fuel stripe (here 3gU/cc as in figure 1) with a maximum FD value of only $1.1 \cdot 10^{21}$ f/cm^{-3} the value in the grain is nowhere more than 4×10^{21} f/cm^{-3}. Hence the fuel swelling shouldn't bear a real problem for this low fuel burn up.

5 Results for the users

With the new procedure based on 3d-calculations of the core and its surrounding the relative flux output at different beam tubes can now be calculated directly and it shows up that the flux losses will be very dependent on the beam or irradiation tube of regard. But beforehand a general discussion of the flux losses is appropriate.

5.1 Flux loss in the HW tank in general

The following results are in comparison to the actual HEU case as a function of radius, averaged over the full height of ±35 cm around the core mid plane and therefore including the complete area in the HW tank that is relevant for nearly all user installations of FRM II. They are shown in Fig. 5 for mid of cycle (MOC).

- The thermal flux values are most important since thermal neutrons are most relevant for the experiments carried out at FRM II. While it is true that, in fact, a huge number of experiments utilize cold neutrons with 3 or 4 times slower velocities, those come from the cold neutron source (CNS) and represent just a remoderated fraction of Φ_{th} down to the cold flux Φ_c.
  This (averaged) loss in Φ_{th} in comparison to the actual HEU case is about 8% at a typical beam nose position at radius 30 cm, it decreases down to 7% till the radius 50 cm and finally to 6% till the HW tank wall.
- The fast flux Φ_s amounts to a rather constant level of 91% of the HEU value outside the core. This is mainly because of the more distributed neutron source term due to the extended fuel element. Further away from the core, Φ_s looses more and more. At a radius of 50cm Φ_s is then 85% in relative value and 80% at greater radius, but there the flux is already a very clean thermal one.
- The loss for the intermediate flux lies rather in between the values for the thermal and the fast flux.

The loss in fast flux is not a restriction for the neutron source, the loss in Φ_s is at any radius higher than the loss in thermal flux. For beam tube applications this is not a disadvantage, instead the opposite could be problematic. In general, it can be stated that the situation with disturbance by fast neutrons for thermal beam tubes will not become worse with the clearly lower enriched fuel element.

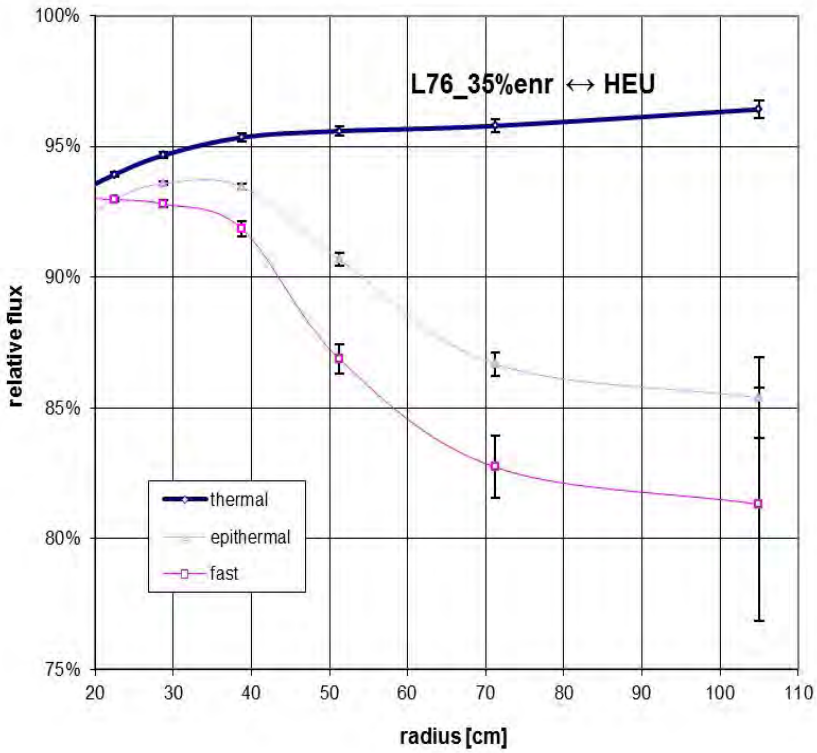

Fig. 4:
Calculated relative loss on neutron flux in the HW tank of FRM II as a function of radius averaged over the full height of ±35 cm around the core mid plane. Both calculations was done with the 3d-MCNP model for the mid of cycle (MOC) situation after a burn up of 30 days with 3d burn up model of MB (MonteBurns); the MOC situation is the best snap-shot moment to show an average loss over a full cycle.

5.2 Thermal beam tubes

The vertical location of the thermal beam tubes is rather distributed at FRM II. For comparison we regard the beam tubes BT-3 at a height 30cm above core mid plane (CMP), beam tube BT-5 at CMP and 20 cm below CMP, the beam tubes BT-7 and BT-8. Because of the in average lowered position of the fuel element in the core, different values of loss in thermal output for the thermal beam tubes are found, meaning a smaller loss for the low lying tubes and a higher loss for the top tube BT-3 (see Fig. 6).

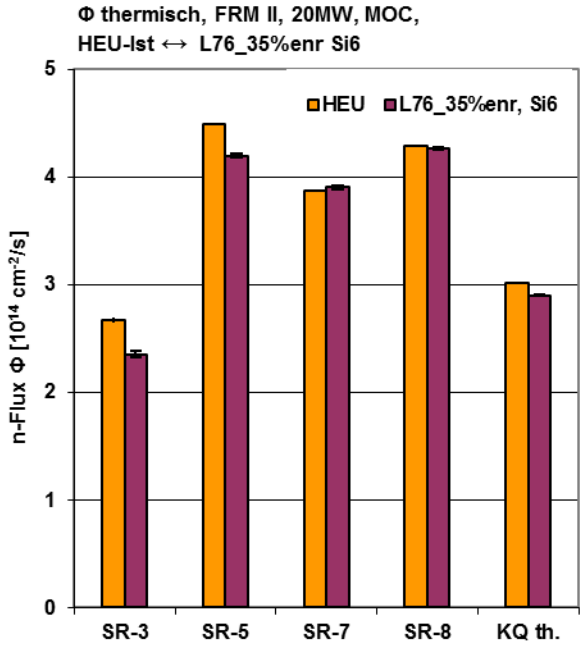

Fig. 5:
Calculated thermal flux at the thermal beam tubes of FRM II, calculated with the 3d-MCNP models for the mid of cycle (MOC) situation after a burn up of 30 days with 3d burn up model of MB (MonteBurns); the MOC situation gives the best snap-shot for the typical loss over a full cycle for the HEU as well as the 35% enriched case of this study.

The most far-reaching consequences from a decline of the thermal neutron flux have experiments which are scarce in neutrons from their discriminating nature, i.e. those who are taking only an extremely low part of the neutron phase space arriving at the sample. These are mainly the three axis spectrometers (TAS). At FRM II, those TAS instruments with thermal neutrons are located at the beam tubes BT-5 and BT-7. Losses of 6½% and 0% are calculated for them with the new core situation. On the other side there is a high loss of about 12% at BT-3, where the strain scanning instrument STRESS-SPEC is located. And it is one of the most popular and overbooked instruments. The low lying beam tube BT-8 provides neutrons for two diffractometers; like BT-7, they both would see no loss because of the low position in the HW tank.

5.3 Cold source beam tubes

Of real interest is also the situation for the flux at the cold neutron source (CNS), which provides neutrons for 19 out of a total of 30 instruments. At the radius of 40 cm of the CNS the loss in thermal flux will be about 4,5% (cmp. fig.1). The exact value is also 4% loss in thermal flux in the same amount of D_2 in the CNS.

The CNS radial position in the HW tank is again something unchangeable for FRM II, but the high heat load of the CNS, resulting from the close neighbourhood to the core, can be reduced by moving the fission power somewhat away from the CNS. This is the case for the core of this study, which is now extended to the bottom away from the CNS. The very detailed study on the different contributions to the heat load of the CNS of mostly neutronic/photonic and promt β-decay character gave a reduction in heat load in comparison to the actual HEU case of 14% at the same fill state of the CNS. This could be a great advantage, if the lower or cooling heat load for the CNS would lead to a better fill state with D_2. The possible flux gain under actual cooling conditions was studied in 2014 at FRM II. It showed up, that at 80% heat load (16 MW reactor power instead of nominal 20 MW in the test) we see not 80% cold flux at the remote guide positions but a regain of about 4-5% in relative flux. Transforming the current CNS situation of FRM II to the 35% enriched fuel element of this study at FP 20 MW, this would mean in summary no loss for the very pronounced cold neutron usage at FRM II with this 35% enriched fuel element option.

5.4 Hot beam tube

Some extra regard needs the case for the hot neutrons of also low lying beam tube BT-9. The heat load from the core is more distributed over the core height due to the extension. But it is also more to the bottom now, what could compensate and help to achieve the same hot temperature at the hot source and hot neutron flux for the diffractometers at beam tube BT-9.

5.5 Irradiation positions

A comparison of the situation at the different irradiation positions at FRM II can be obtained the same way as for the beam tubes using the 3d model discussed before.

Although such an analysis was not performed in detail for this work, it can be stated, that because of the tendency to suffer of higher location in the HW tank, the loss for most positions will be comparable to the high lying beam tube BT-3. However, one of the most important irradiation locations is the remote silicon doping facility. It will suffer only 6% loss. A loss of this magnitude is at the border of what could be understood as "marginal", but seems inevitable with a fuel element with reduced enrichment for FRM II. Another facility that shall become important in the future for irradiations at FRM II is the irradiation of LEU targets for the production of Mo-99 for medical use. It is located in a beam tube that was prolonged to the bottom of the HW tank during the shut-down period in 2011 for this purpose. This target irradiation will have only a very marginal loss with the 35% enriched fuel element of this study.

SUMMARY

A physical and technical evaluation was presented for a 35% enriched fuel element for FRM II based on dispersive fuel U3Si at a maximum density of 6gU/cc. The study was kept on a conservative embedding regarding the current physical situation of the reactor with no changes necessary to major operational systems like control (CR) and shut down (SR) rods.

The geometry is identical to a proposed solution with 30% enriched UMo fuel at density 8gU/cc. The fuel element was extended 6 cm to the bottom and the inner diameter of the element and the outer diameter of the central channel tube were kept in the study.

Again all safety values of the reactor should be met at a comparable level to the current HEU fuel element. Especially for the cooling aspects, some geometric changes had to be introduced, as far as the very restricted outer dimensions for a new element could allow. Finally safety criteria for the coolant flow are found comparable to the actual case.

The relative flux output at different beam tubes was calculated. The expected losses are very dependent on the beam or irradiation tube of regard, between 0% and 12% at thermal beam tubes and at irradiation channels. The results are thus slightly better than for the comparable UMo fuel case.

Nevertheless the major question that remains is about the licensing for the new fuel element with respect to the extended core. Such legal aspects might well turn out to be show-stopper. Any final solution for FRM II with a new and clearly reduced enrichment will need to be further investigated for licensing with more tools than done in this conversion study, regarding also transient behaviour of the reactor.

ACKNOWLEDGEMENT

This work has been supported by a combined grant (FRM0911) from the Bundesministerium für Bildung und Forschung (BMBF) and the Bayerisches Staatsministerium für Wissenschaft, Forschung und Kunst (StMWFK).

REFERENCES

[Frm12] "Extended studies of FRM II core conversion with UMo dispersive fuel at a prolonged fuel element", International Topical Meeting on Research Reactor Fuel Management, RRFM 2012, Prag, A. Röhrmoser, W. Petry, H. Breitkreutz

[irrFrm2] "Test Irradiations of Full Sized U_3Si_2-Al Fuel Plates up to Very High Fission Densities", K. Böning, W. Petry, 2008, Journal of Nuclear Materials

[NR1313] "Safety Evaluation Report related to the Evaluation of Low-Enriched.'Uranium Silicide-Aluminum Dispersion Fuel for Use in Non-Power Reactors", NUREG1313, US NRC, July 1988

[MB2.2] "MonteBurns (2), an Automated Multi Step Monte Carlo Burnup Code System", LA-UR-99-4999, Los Alamos National Laboratory, distributed by RSICC or NEA

[Frm10] "FRM II, New burn up calculations", Lisboa, Portugal, RERTR meeting 2010, A. Röhrmoser

[FrmMdl] "Core Model of new German Neutron source FRM II", Nuclear Engineering and Design, June 2010, A. Röhrmoser

[THnbk] "Fuel plate temperatures during operation of FRM II" , 14th International Topical Meeting on Research Reactor Fuel Management, A. Röhrmoser, RRFM 2009, Vienna

REPLACEMENT FUEL FOR THE VIENNA AUSTRIA TRIGA RESEARCH REACTOR

DALE LUKE & ALAN ROBB
*CH2M*WG Idaho (CWI), LLC*
1580 Sawtelle St., Idaho Falls, Idaho - USA

ABSTRACT

Since 1998 the Idaho Nuclear Technical and Engineering Center (INTEC) located at the Idaho National Laboratory (INL) has been receiving used Training, Research, Isotopes, General Atomics (TRIGA) nuclear fuel from foreign and domestic research reactors. The returns program is a part of the, "Atoms for Peace" program wherein the United States (U.S.) provided nuclear technology to foreign nations for peaceful applications. As a part of this program when the fuel was expended the agreement was to return the U.S.-origin fuel back to the U.S. for storage and ultimate disposition.

Over the years, 1998 through 2012, the INL has received many TRIGA elements from foreign and domestic research reactors with very low burn-up. A fair amount of the inventory of TRIGA fuel stored at the INL is only lightly irradiated and has significant remaining life. Since the production line for TRIGA fuel was anticipated to be down for a few years, it was suggested that perhaps Austria would find it cost effective to "harvest" a core's worth of TRIGA fuel for their continued future operations. This option also facilitated the "conversion" from using any high enriched uranium (HEU) TRIGA to low enriched uranium (LEU) fuel at the Vienna, Austria University of Technology (TU Wien).

In late 2011 personnel from the TU Wien research reactor and Austrian Ministry personnel came to the United States and met with key U.S. Department of Energy (DOE) and CH2M-Washington Group Idaho (CWI) personnel to discuss the feasibility of retrieval and shipment of used TRIGA fuel to their facility. DOE and CWI gave the Austrian delegation a tour of the INTEC fuel storage facility and explained the capabilities of that facility. The Austrian delegation then presented their proposal with a request for 77 of the low burn-up stainless steel clad, 20% enriched TRIGA fuel from the INTEC storage facility.

The proposal was accepted and INTEC/CWI harvested and shipped fuel to Austria and the HEU fuel, along with other high burnup TRIGA LEU fuel, was shipped from Austria (TU Wien) to the INL. This conversion and relocation of spent nuclear fuel (SNF) from Austria to the INL supported U.S. nuclear weapons non-proliferation goals and the consolidation of the DOE's inventory of SNF. This presentation describes the process, preparations, and work efforts that were accomplished which allowed the successful shipment of lightly irradiated TRIGA fuel to Austria and the return shipment of SNF to the INL from Austria.

1. INTRODUCTION

This paper describes the process of "harvesting" lightly irradiated TRIGA research reactor fuel in Idaho for the TU Wien Mark II TRIGA Research Reactor in Vienna, Austria (Fig. 1).

The TU Wien Research Reactor went critical in March 7, 1962 and is the only operating reactor in Austria. It operates at a steady state power of 250 kW, with a pulsing capability up to 250 mW.

Figure 1. TU Wien Mark II TRIGA Research Reactor

The reactor has and is still being used for the following:

- ✓ Development of safeguards instrumentation
- ✓ Calibration of nuclear instrumentation
- ✓ Training for IAEA junior inspectors
- ✓ Support and testing for IAEA member states

2. THE IDEA FOR "HARVESTING" LIGHTLY IRRADIATED TRIGA FUEL

At a previous research reactors conference it was announced that the TRIGA fuel fabrication line was going to be down and new elements may not be available for several years.

At about this same time, Reed College (Portland, Oregon, USA) was in dire need of new fuel to enable them to continue operation due to fuel burnup and condition of the aluminum-clad fuel. The Univ. of Arizona (Tucson, Arizona, USA) was shutting down and had a nearly a core's worth of fairly low burnup stainless steel-clad TRIGA fuel that could be utilized for years to come. Reed College coordinated the transfer of the fuel from Arizona to their location and then planned the return of their spent (mostly aluminum-clad) fuel to the Idaho Nuclear Technical Engineering Center (INTEC) in Idaho. The swap was a success and the reactor at Reed has been in full operation and will continue to operate for many years to come.

CH2M*WG Idaho (CWI) personnel identified INTEC as a source of used TRIGA fuel elements with low burnup that could potentially be re-used. Most of these elements were shipped to Idaho from research reactors that have discontinued operations.

The idea of "harvesting" fuel from the fuel storage facility in Idaho was picked up by the US Department of Energy (US-DOE) program responsible for assisting in the conversion of high enriched uranium (HEU) fuels used in research reactors and discussed in meetings with Austria as an option to replace their HEU TRIGA fuel elements.

Austria liked the idea a lot and decided to ask for enough elements (77) to replace their HEU elements and almost a core's worth of much greater burnup, mostly Al-clad TRIGA elements.

Using information from fuel storage data, CWI personnel identified low burnup fuel elements that could be candidates for future use in TRIGA research reactors. Some of these elements were "prime" streamlined SS-clad TRIGA elements (Fig. 2) with very low burnup.

Figure 2. Picture of a Standard "Streamlined" TRIGA Element

3. MAKING PLANS

In December of 2011 Austria sent over a delegation of personnel from the reactor facility and the Austrian ministry to meet with DOE and CWI to discuss the possibility of a "harvesting" lightly irradiated TRIGA fuel and sending their higher burnup fuel to Idaho. The delegation was given a tour of the storage facility and the discussions led into what capability the storage facility had and the feasibility of doing such work.

CWI personnel, with seed money and directions from US-DOE, developed a detailed cost estimate and project plan.

DOE and Austria agreed to the terms (Austria paid for the elements, the work to harvest them, and the transport) and the work started to make the exchange. The cost savings over procuring new elements was significant.

Austria reviewed the fuel element data and identified 88 'prime' elements that they were interested in from the inventory (of which 77 were selected for shipment).

Austria identified 91 of their 'well used' elements that were to be returned to the U.S. These included the remaining HEU TRIGA elements that were returned to the U.S. for storage.

The NAC-LWT cask was chosen to ship the lightly used elements to Austria. The cask was unloaded and used to return the used elements to the U.S.

A preliminary meeting was held in Austria at the TU Wien reactor facility with CWI personnel to discuss the workings of the fuel exchange and to begin the preparations of required documentation, which proved to be extremely useful to work out potential problems and to:

- Evaluate facility equipment and fuel storage configuration needs;
- Discuss and determine the logistics of the fuel exams and loading (big “Ah Ha” moment: Austria realized they needed to determine where to store elements until their elements were loaded to ship to Idaho, criticality safety issue, etc.)
- Determine extent of documentation needed (RSD, etc.) and begin preps
- Determine work schedules, training and entry into work areas at Austria and Idaho

4. EXAMINATION OF TRGIA FUEL AT TU WEIN AND SHIPMENT TO IDAHO

Fuel examination equipment was packaged and sent ahead of CWI personnel to Austria in preparation for the fuel exam at the research reactor facility. CWI personnel traveled to Austria in June 2012 to perform a detailed visual examination.

A total of 91 TRIGA elements were examined at Austria. Ten elements had damaged cladding and were required to be placed in sealed failed fuel cans for shipment and storage. Nine of the elements were classified as failed fuel (failed fuel is any element that exhibits the following: greater than hairline cracks, pinholes, or “suspect“). These elements are required to be placed in a sealed failed fuel can for transport and storage. One element, stored in their hot cell, had no cladding at all (was bagged with ID number for purposes of material and configuration control) (Fig. 3).

Figure 3. TRIGA Element with no Cladding

During loading of the NAC-LWT baskets, the element that had no cladding was transferred to a sealed failed fuel can in preparation for loading into the cask. After the fuel was placed in the can the lid was put on, torqued and leak tested for integrity. The can was then transferred to the pool where it was lowered into the awaiting NAC basket.

Note element pieces in the can (Fig. 4).

Figure 4. NAC Sealed Failed Fuel Can with TRIGA Fuel Pieces Being Loaded

The photo below (Fig. 5) shows one of the actual elements that was examined at the reactor facility and was subsequently identified as needing to be placed in a sealed failed fuel can prior to cask loading. (You can see completely through the other side of this “hole”).

A total of 6 sealed failed fuel cans were used.

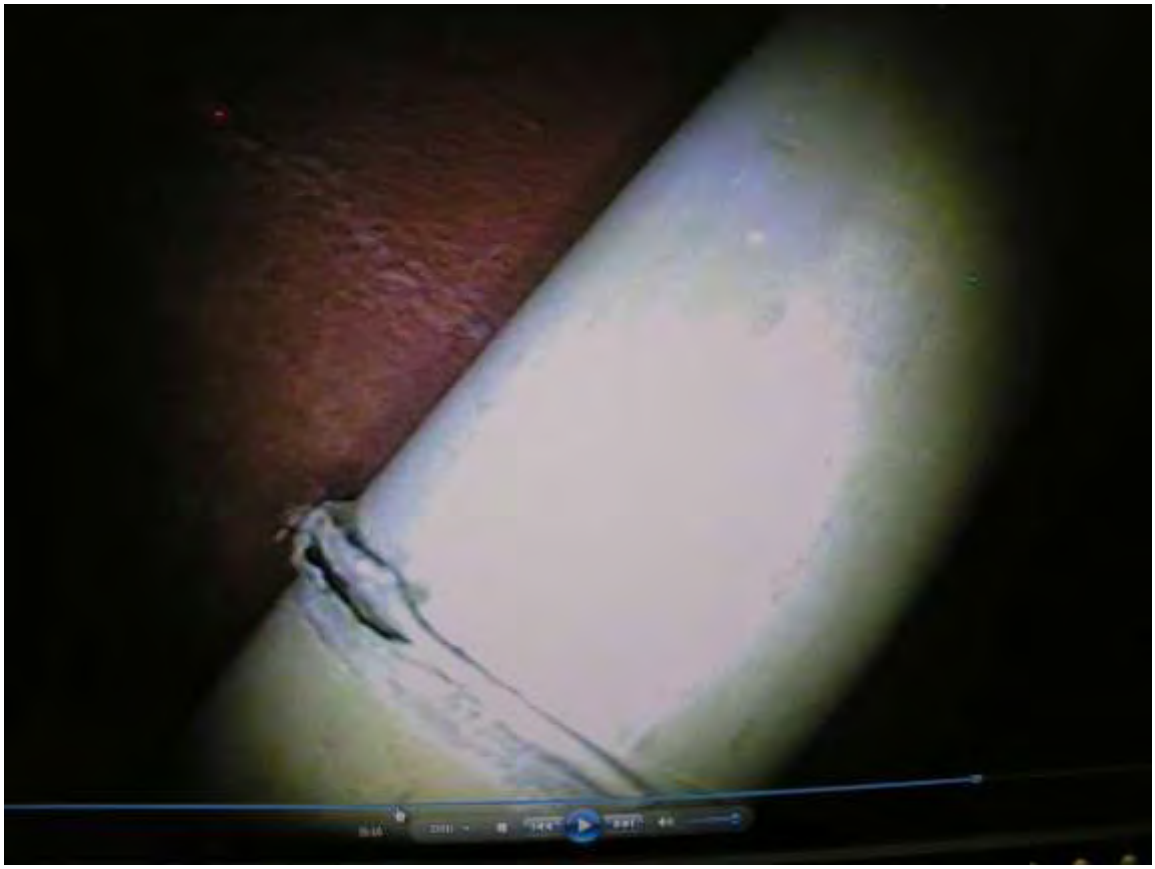

Figure 5. Al-Clad TRIGA Element with Cladding Breached

Austria identified 91 of their 'well used' elements that were to be returned to the U.S. These included the remaining HEU TRIGA elements that were returned to the U.S. for storage.

The NAC-LWT cask was chosen to ship the lightly used elements to Austria. The cask was unloaded and used to return the used elements to the U.S.

Figure 6. NAC-LWT Cask Used for Shipments of TRIGA Fuel

5. HARVESTING TRIGA FUEL AT INTEC

In September 2013, Austrian reactor personnel traveled to the U.S. to participate in the fuel examination and loading of the chosen elements in preparation for shipment to Austria.

Three Austrian research reactor personnel traveled to Idaho to perform fuel inspections and witness the loading of baskets in which the TRIGA elements were shipped to Austria.

Figure 7. Robert Bergmann, Andreas Musilek, & Mario Villa from Austria

From a pool of 88 pre-selected TRIGA elements, 79 elements were inspected by placing each element into a specially made examination stand that was placed in the fuel handling cave. The stand had a scale to allow any anomalies to be documented as to where they were and a bracket for holding an AMP-200 radiation monitor to determine radiation levels of the elements.

The three delegates from Austria, through remote cameras/monitors and working with CWI fuel inspectors, evaluated the elements for acceptance or rejection. Two of the elements were rejected because of indications of damage to the cladding.

75 of the elements were previously used at the Musashi, Japan research reactor and 2 elements were previously used at the Cornell University research reactor. Therefore, 77 elements were selected and sent to Austria from Idaho.

Overall, the process went fairly smoothly, though we did have some problems resulting from aging in-cell equipment and working out a few minor bugs associated with new processes, procedures, and equipment.

Both Austria and Idaho were very pleased with how things worked out so well. In the future the process should be even smoother and less costly now that the process and procedures have been developed and proven.

6. FUTURE OPPORTUNITIES FOR HARVESTING TRIGA ELEMENTS FROM INTEC

Table 1 is a summary of the data we have compiled about intact stainless steel-clad TRIGA fuel elements stored at INTEC. More detailed information is available for each element, though we are certainly dependent on the information that was provided by the research reactor that sent this fuel to Idaho.

There are two styles of SS-clad "regular" TRIGA elements. One is the "standard" element and the other is the "streamlined" element. Either style can typically be used in regular TRIGA research reactors. They are shown in the blue boxes in the table.

The other "type" of TRIGA SS-clad elements are the "conversion" (conversion of older MTR-type research reactors, like Texas A&M, Univ. of Wisconsin, and Washington State) or "cluster" elements that are bundled into assemblies of up to four elements. These elements are shown in the green boxes in the table.

	Burnup (%)										
Intact SS TRIGA Elements	**0 - 5**	**5 - 10**	**10 - 15**	**15 - 20**	**20 - 25**	**25 - 30**	**30 - 35**	**35 - 40**	**40 - 45**	**45 - 50**	**> 50**
SS - Std (8.5/20)	42	112	194	67	73	52	96	9	3	0	8
Cum	42	154	348	415	488	540	636	645	648	648	656
SS - Streamlined (8.5/20)	28	17	8	2	0	0	0	0	0	0	0
Cum	28	45	53	55	55	55	55	55	55	55	55
SS - Total (8.5/20)	70	129	202	69	73	52	96	9	3	0	8
Cum	70	199	401	470	543	595	691	700	703	703	711
SS - Conversion (8.5/20)	29	112	37	29	0	0	2	0	0	0	0
Cum	29	141	178	207	207	207	209	209	209	209	209

Table 1. Intact SS TRIGA Elements Available for Harvest from INTEC

Idaho stores the TRIGA fuel in dry storage and so little if any degradation of the fuel cladding is expected.

We have tried to ascertain what the acceptable burnup level is to be able to effectively re-use the TRIGA fuel. Mr. James Sterbentz at Idaho, who has extensively modeled TRIGA fuel, gave us a preliminary value. He said that fuel with even up to 20% or higher burnup could probably be effectively re-used, providing significant life expectancy to make it worthwhile for consideration of re-use (dependent on cost of recovery, of course).

Further input from the research reactor community, however, to exploit your expertise in relation to TRIGA fuel performance at higher burnup levels is needed. Also, needed is information on whether time out of reactor significantly impacts the performance of the fuel.

7. CONCLUSION

Both Austria and Idaho were very pleased with how things worked out so well. In the future the process of “harvesting” and swapping fuel elements should be even smoother and less costly now that the process and procedures have been developed to pave the way for future activities.

If there is interest in this process, it is probably best to contact Mr. Jeff Galan and or Mr. Ron Ramsey of the US-DOE.

Physics Experimental Study for Prototype MNSR with LEU core

Li-Yiguo Peng-Dan Wu- Xiaobo Hong-Jingyan, Lu-Jin, Zhang-Yongbao
Liu-Xinling, Hao-Qian, Zhang-Jinhua.

China Institute of Atomic Energy, Beijing,102413,P.O.Box 275-75,China

Abstract: $MNSR_S$(Miniature Neutron Source Reactor) are low power research reactors designed and manufactured by China Institute of Atomic Energy (CIAE). $MNSR_S$ are mainly used for NAA, training and teaching, testing of nuclear instrumentation. The first MNSR, the prototype MNSR, was put into operation in 1984, later, eight other $MNSR_S$ had been built both at home and abroad. For $MNSR_S$, highly enriched uranium(~ 90%) is used as the fuel material.

Prototype MNSR has the fuel （UAl_4）with ^{235}U of 90.3% enrichment，Al alloy as cladding, metal Be as reflectors and light water as moderator and coolant.

Without changing the core dimensions of the Prototype MNSR，but substituting the HEU fuel with LEU fuel and Al cladding with Zircaloydding, the critical mass, the control rod worth, top Be reflector worth and neutron flux distribution are measured, the final loading of fuel elements are determented. The experiment was done on the Zero Power Experiment equipment of MNSR.

1 Description of equipment

The reactor with thermal power 27kW is an under-moderated reactor of pool-tank type, and UO_2 with enrichment of 12.5% as fuel, light water as coolant and moderator, and metallic beryllium as reflector. The fission heat produced by the reactor is removed by the natural convection. Fig. 1 shows the diagram of the experimental equipment.

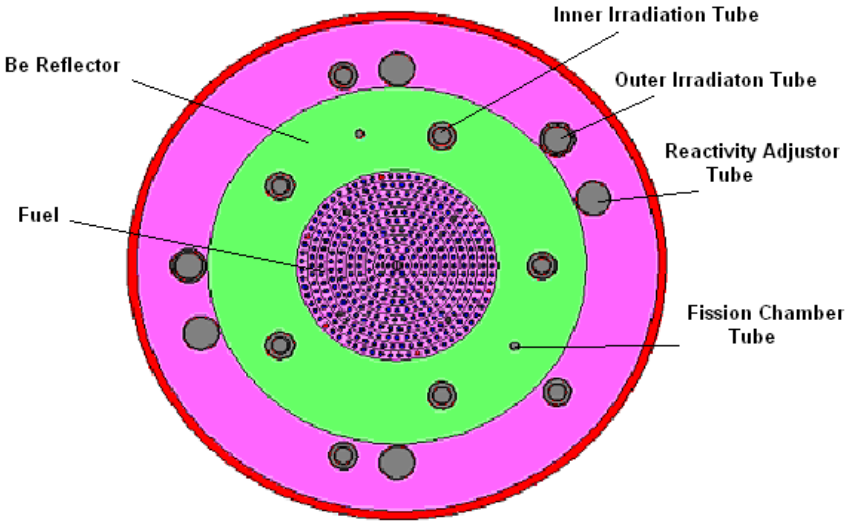

Fig.1 The diagram of the experimental equipment

One central control rod is in the center of reactor core.

1.1 Reactor

The upper and lower grid plates are linked by five tie rods, ten rows of 411 lattices are concentrically arranged, the central lattice is reserved for central control rod. While the five tie rods are uniformly arranged at the eighth row. The rest lattices are for fuel element and dummy elements (see Fig.2).

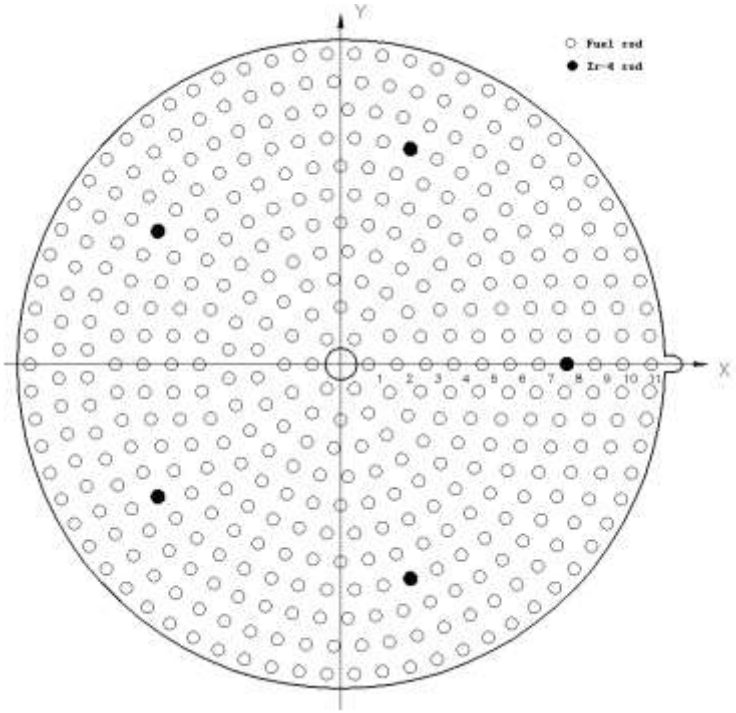

Fig.2 The fuel arrangement

The UO_2 is used as the fuel meat with density 10.6g/cm^3, ^{235}U enrichment is 12.5%, the

dimension is 4.0mm×250mm. The cladding material is Zr-4 alloy with wall thickness of 0.45mm and 270mm in length（10mm end plug at up end, 9 mm end plug at lower end, 1mm Helium gas between the up end and fuel meat ）

The central control rod : 1）Guide tube：inner dia. 9mm，outer dia. 12mm，length：278mm；2）Meat：Cd tube outer dia. 4.5mm，inner dia. 2.5mm, length 290mm；inside Cd tube：Al rod Φ 2.5×290（mm）; 3) Outside Cd tube S.S tube outer dia. 6.0mm，wall thickness：0.5mm , total length：450mm。

The fuel Cage：1）Dia：240mm，heiqht：278mm; 2）Top core plate：Zr-4 alloy thickness：3.5mm, lower core plate：Zr-4 alloy thickness：5mm.

1.2 Side Be reflector

The dimension：inner dia. 242mm，outer dia. 440mm, height：260mm

1.3 Bottom Be reflector

The dimension：dia. 340mm，thickness：50mm，central hole of 20mm in diameter.

1.4 Top Be reflector

The Al alloy tray for Top Be reflector：inner dia.：268mm, outer dia.：274mm，height：145mm，bottom thickness：2mm.

The dimension of top Be reflectors：dia.: 264mm, hole dia.: 40mm，total thickness：109.5mm（1.5，3.0，6.0 and 12.0mm）.

1.5 Irradiation and guide Tubes

1）Inner irradiation sites：5 sites are uniformly and vertically arranged in the side Be reflector at the radius of 170mm；the irradiation tube（rabbit tube）inserts into the irradiation site to the depth of 190.0mm，Outer thimble of the irradiation tube：outer dia.32.0mm，inner dia 29.0mm；inner thimble：outer dia.22.0mm，inner dia.19.0mm.

2）Outer irradiation sites（outside the side Be）: 5 sites are uniformly and vertically arranged outside the side Be reflector at the radius of 250mm，insertion depth is 190.0mm. Outer thimble：outer dia. 42.0mm, inner dia. 39.0mm；inner thimble：outer dia.34.0mm, inner dia.31.0mm

3) The four ionization chamber tubes are arranged in the same circle with the radius of 255mm. The outer diameter of the tube is 56.0mm，The inner diameter is 52.0mm.

2 Zero power experimental results

The experiment was done in the MNSR zero power equipment, some parameters were measured.

2.1 Critical mass

Two ways of extrapolation and insertion were used for the measurement of critical mass. The results are 356.9 fuel elements, the fuel elements in the outermost circle are not uniformly arranged.

2.2 Worth of the central control rod

The worth was measured by the period method. Insert a part of the rod in the reactor, measured the worth by the same method again. Do it Alternately, the total worth of the rod was measured finally(see Fig.3). The total worths of the central control rod of the experiment are 7.5 mk .

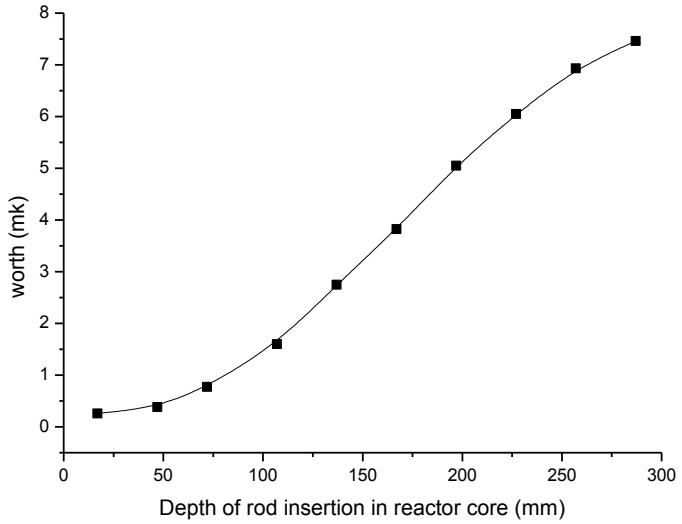

Fig.3 Central control rod worth

2.3 Worth of the top Beryllium reflectors

By the period method, the worth was also measured. Add the piece of top Be, measured the worth; and then, take out the fuel element from the reactor core, add the top Be, measured the worth again; Do it Alternately, the total worth of the rod was measured finally(see Fig.4). The total worths of the top Be reflectors by the experiment measurement is 16.2mk.

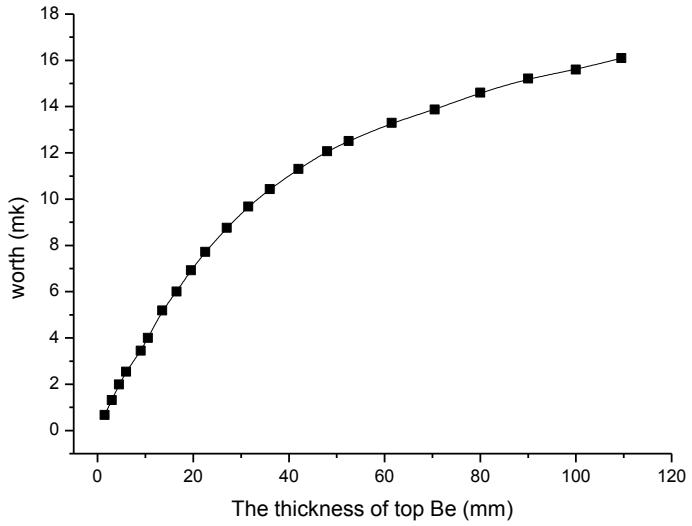

Fig.4 Top Be worth

2.4 Relative neutron flux distribution

Using the Mn activation method, the neutron flux distribution in the reactor core was measured.

The Mn foils were put in the height of 125mm from the up surface of the lower plate at the different position in the radial direction, the Mn foils were put between the 5^{th} circle and 6^{th} circle at different position for the measurement of axis neutron flux. the activity was measured by γ spectrum equipment. See Fig.5, Fig.6.

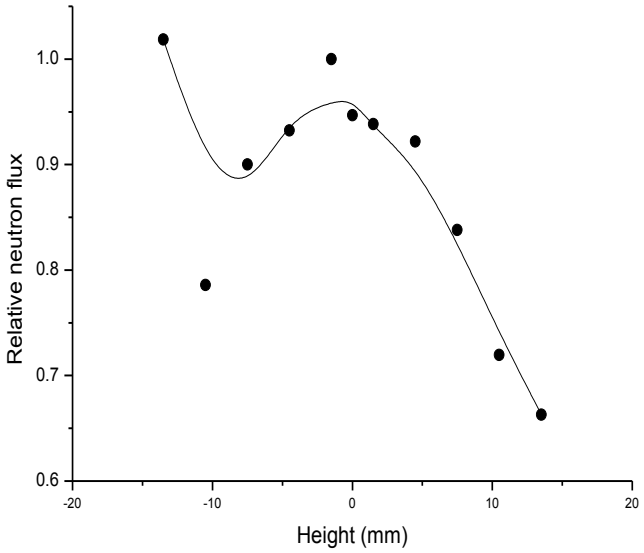

Fig.5 Radial Neutron flux distribution in the reactor core

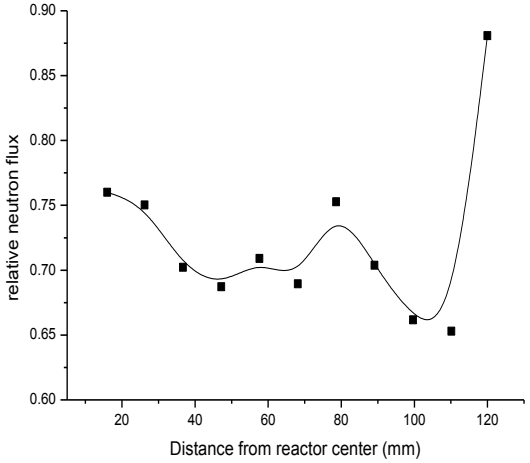

Fig.6 Axial Neutron flux distribution in the reactor core

2.5 Worth of fission chambers and their tubes

By the period method, first, the reactivity of the core was measured, and then, put the two fission chambers and their tubes into the holes of fission chamber in the side Be respectively, the reactivity of the core was measured again. The worth of two fission chamber and their tubes was measured by the reactivity difference of two values. The measuring worth is -0.131mk.

2.6. Worth of Fuel

By the period method, first, the reactivity of the core was measured, and then, take out one fuel element from the 1st circle in the core, and then, Measuring the reactivity of the core again, The worth of one fuel element in the 1st circle was measured by the reactivity difference of two values. Do it Alternately, the worth of the fuel element in the 2^{nd} – 11^{th} circle was measured finally(see

Fig.7).

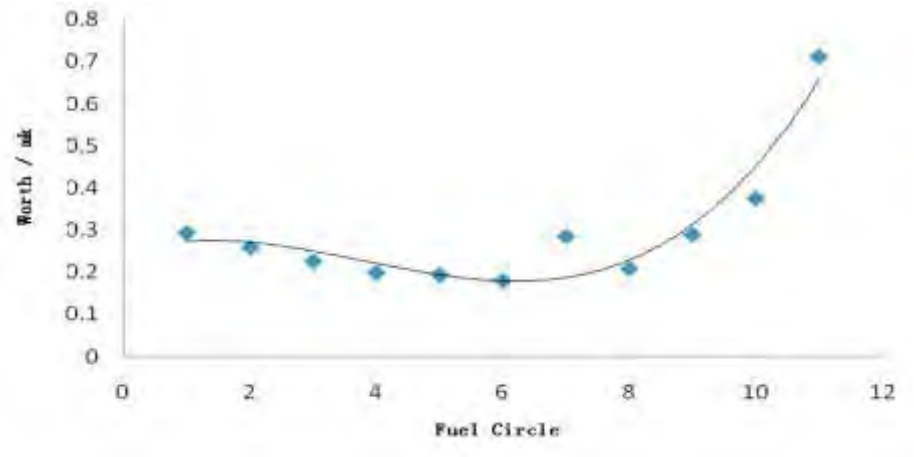

Fig.7 Worth distribution of fuel element

2.7 Worth of Inner irradiation tubes

By the period method, first, the reactivity of the core was measured, and then, put the two inner irradiation tubes into the holes in the side Be respectively, the reactivity of the core was measured again. The worth of two inner irradiation tubes was measured by the reactivity difference of two values. The measuring worth is -0.74mk.

2.8 . Worth of outer irradiation tubes

By the period method, first, the reactivity of the core was measured, and then, put the two outer irradiation tubes into the holes outside the side Be respectively, the reactivity of the core was measured again. The worth of two outer irradiation tubes was measured by the reactivity difference of two values. The measuring worth is -0.29mk.

3 Final loading

At the initial state of Prototype MNSR with LEU core, there are five inner tubes in reactor core, five outer tubes in reactor core, two reactivity regulator tubes, two fission chambers and their tubes and Lower part of control rod in reactor core, there is no top Be tray and top Be shim. Their worths should be considered for the final loading. The worth of five Inner tubes in reactor core is -1.85mk, the worth of five outer tubes in reactor core is - 0.71mk, the worth of two reactivity regulator tubes is -0.28mk, the worth of two fission chambers and their tubes is -0.13mk, the worth of lower part of control rod is -0.23mk, and the worth of top Be tray is - 0.25mk, the total worth is -3.45mk.

The initial excess reactivity of the prototype MNSR is 4.0mk, the average worth of one fuel element at outmost circle is 1.06mk, so the final loading at the initial state of reactor is 365 fuel elements, the rest lattices will be filled by dummy elements.Fig.8 shows the arrangement of the fuel elements.

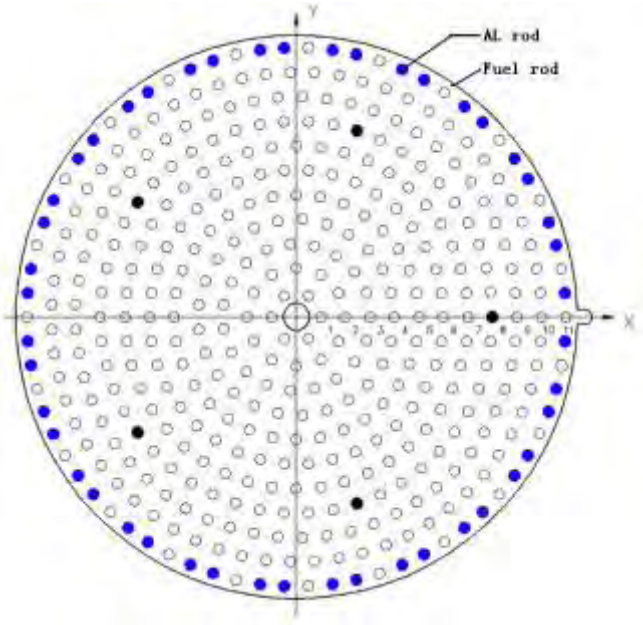

Fig. 8 The arrangement of the fuel elements.

Safety and Security of Research Reactors

ENHANCEMENT OF SAFETY REQUIREMENTS FOR RESEARCH REACTOR FACILITIES IN THE LIGHT OF THE ACCIDENT AT THE FUKUSHIMA DAIICHI NUCLEAR POWER PLANT

D.N. POLIAKOV
Research Reactor Safety Division, SEC NRS,
Malaya Krasnoselskaya, 2/8, build. 5, 107140 Moscow, Russia

ABSTRACT

Review of the Fukushima Daiichi accident has been performed by Russian experts along with the nuclear community and its results demonstrated necessity of enhancement of regulations in the area of research reactor safety [1, 2]. The first evaluation of specific areas of such improvement was conducted by SEC NRS experts in 2012 as a part of joint activities with the State Corporation "Rosatom" on review of the results of additional safety assessments of Russian research reactors under extreme external hazards ("stress tests"). Based on the review results it was concluded that the improvement of existing regulations and development of the new ones should relate to the following issues: research reactor emergency power supply; usage of values of the parameters characterizing external factors as a signals activating research reactor emergency shutdown; requirements to the list of beyond design basis accidents which should be considered within the safety assessment report; methods of analysis of beyond design basis accidents; model structure and content of the emergency response plan. Currently, improvement is being performed as changes in the regulations being in force. Specific improvements of regulations are described in this paper.

1. Introduction

Analysis of the events at the "Fukushima Daiichi" nuclear power plant began almost immediately after the first press reports. The first actions have been associated with the analysis of the consequences and possible impact of the accident on the environment. The next actions have been associated with assessment of the accident to determine causes of the accident and prevent its recurrence at other nuclear facilities [1, 2, 3] including research reactors (RR). Russian regulator Rostehnadzor decided to perform additional safety assessments of research reactors based on the preliminary results of the analysis of the event in Japan and international activities. Rostehnadzor developed "Program of Additional Safety Assessment of Research Reactors, Including Critical and Subcritical Assemblies (Stress Tests) in Russian Federation" [4] in 2011.

The main objectives of this Stress Test Program included assessments of:

- Possible changes in the set of external events (natural and human induced) affecting research reactor in the site and possible changes of values of external event parameters;
- RR ability to stay safe at the external events with parameters identified in the RR project;
- RRr safety at the external events with parameters exceeded values identified in the RR project;
- Efficiency and adequacy of technical resources and organizational measure indented to withstand design extended external events.

This Stress Test Program was sent to the government authorities responsible for utilization of RRs. Stress tests were conducted by operating organizations and their results were sent to the government authorities, which, in their turn, submitted the reports with the results of

stress tests to Rostehnadzor. Review of the stress tests results was performed by the SEC NRS experts. SEC NRS is the Rostehnadzor technical support organization.

The review was implemented in two stages. RR stress test results considered at the first stage in 2012 are given in Table 1.

RR	Thermal power, MWt	Operating Organization	RR Commissioning
VK-50	Up to 200	RIAR	1965
MIR.M1	100	RIAR	1975
SM-3	100	RIAR	1961/1993
BOR-60	60	RIAR	1969
IVV-2M	15	INM	1976
RBT-10/2	10	RIAR	1984
RBT-6	6	RIAR	1976

Tab. 1: RR considered at the first stage of stress test review

It should be noted that RRs considered at the first stage were characterized by such features as high thermal power and high density in the site (for RIAR). RR stress test reports considered at the second stage in 2014 are given in Table 2. Considered critical assemblies are not included in the Table.

RR	Thermal power, MWt	Operating Organization	RR Commissioning
PIK	100 / 0.0001	PNPI	Construction/2013
VVR-M	18	PNPI	1959
IR-8	8	KI	1981
IRT-T	6	TPU	1967/2005
IRT	2,5	MEPhI	1967
IBR-2	2	JINR	1984/2010
OR	0.3	KI	1989
Gamma	0.08	KI	1981
Argus	0.05	KI	1981
U-3	0,05	Krylov Centre	1964/1990
F-1	0.024	KI	1946
Gidra	0.001	KI	1972
MR	-	KI	Decommissioning, 1993

Tab. 2: RR stress test reports considered at the second stage of stress test review (considered critical facilities are not included in the Table)

Stress test results for storages of fresh and spent fuel, and radwaste storages were reviewed along with the safety assessments for RR.

The main objectives of the RR stress test review were:

- Review of safety assessments for RRs under extreme external events (natural and human induced) and their combinations performed by operating organizations;
- Development of recommendations on improvement of potential safety deficiency;
- Development of recommendations on improvement of safety regulations.

Review of the RR stress test results was performed on the basis of existing RR safety regulations. Despite the fact that for each RR some remarks on stress test procedure or the results were made, in general, the review demonstrated that:

– Available technical and organizational measures to protect RR from extreme external events with parameter values specified in the design meet the requirements of regulatory documents;

– In the accidents considered in the stress test reports evacuation is not require.

2. Enhancement of Safety Requirements for Research Reactor Facilities

Analysis of adequacy of safety requirements being in force was performed simultaneously with the review of RR stress test results. Recommendations on improvement of existing regulations and on developing the new ones were developed. The following issues were determined for the further activities:

– Emergency power supplies;

– Usage of maximum values of external factor parameters as a trigger for RR shutdown systems;

– Requirements to the list of design extended conditions to be analyzed in SAR;

– Methodology of beyond design basis accident analysis (taking into account the simultaneous effects of several external factors on all nuclear and radiation hazardous facilities located in the site);

– Standard instruction on personnel actions in beyond design basis accidents including those caused by extreme external events;

– Content of the action plan to protect personnel in the case of an accident at nuclear research facilities.

Realization of the developed recommendations is going to be implemented as through the development of new regulatory documents, and by improvement of the regulations being in force. The general long-term plan on enhancement of the system of federal rules and regulations in the area of nuclear and radiation safety [5] was developed by SECNRS. This plan includes documents on RR nuclear and radiation safety. For example it is planned to develop new document entitled "Requirements to RR Emergency Power Supplies". Currently, actions are taking on improvement of the federal level regulatory document "Rules on RR Nuclear Safety" (NP-009-04) and "Requirements to the Content of RR SAR " (NP-049-03).

Within the improvement of the "Rules on RR Nuclear Safety" the following provisions taking into account lessons of the accident at the "Fukushima Daiichi" nuclear power plant were included:

– RR design documents (project) should include analysis of the response of systems important to safety to external events (natural and human induced) taking into account combination of external events along with the impact of other research reactor facilities located in the site (if they are available);

– RR design documents (project) should include a list of the groups of beyond design basis accidents including RR blackout, the loss of the ultimate heat sink, and airplane crash;

– Redundant and emergency power supplies should be included in the RR hardware;

– Emergency power supply should ensure:

a. Operation of at least two reactor power control channels and monitoring of control rod position;

b. Temperature monitoring in the reactor core and spent fuel storage facility;

c. Operation of systems and components used for emergency core cooling;

d. Shutdown of the RR and control of its cooling from the supplementary control room in the case of failure of the main control room.

It should be noted that, in accordance with Russian federal level regulatory document NP-064-05 [6]: "Maximum values of hydrometeorological, geological and engineering-geological processes and phenomena should be determined on a time interval equal to 10,000 years and in the design basis should be considered human induced factors, for which the

frequency of their implementation is equal to or more than 10^{-6} 1/year". In view of the lessons of the accident at the "Fukushima Daiichi" it is proposed to perform analysis of some accidents regardless of their frequency as beyond design basis accidents. The draft revision of regulatory document “Requirements to the Content of SAR” prescribes to analyze the following groups of beyond design basis accidents;

– Accidents involving unauthorized insertion of positive reactivity due to the superposition of a number of human errors or hardware failures causing core damage and fuel melting;

– Accident in which initial event of design basis accidents is accompanied by a complete failure of reactor safety system and accompanied by failure of any one element of confining system or human error in controlling of this system;

– Loss of off-site power accompanied by failure of any one element of confining system or human error in controlling of this system;

– RR blackout including emergency power supplies;

– Loss of coolant accompanied by failure of any one element of confining system or human error in controlling of this system;

– Loss of ultimate heat sink;

– Accident caused by the simultaneous effect of several external factors of maximum values;

– Accident caused by the personnel failure to implement emergency measures during the initial events of design basis accidents.

3. Summery

Lessons of the accident at the "Fukushima Daiichi" nuclear power plant were taken into account within development of the long-term plan on enhancement of the system of federal rules and regulations in the area of nuclear and radiation safety up to 2023 [5]. The results of RR stress test review did not lead to a radical change in RR safety provisions, generally these results are being realized in RR accident regulations.

4. References

1. IAEA Action Plan on Nuclear Safety, GOV/2011/59-GC(55)/14, Board of Governors, General Conference, 8 September 2011.

2. Lankin M.Y., Khamaza A.A., Sharafutdinov R.B., Miroshnichenko M.I. Some Aspects of Nuclear Power Plant Safety (Lessons of Accident at the Fukushima Daiichi NPP) // Nuclear and Radiation Safety. 2012. № 1(63).

3. Action Programme of Russian Authorities and Organizations Concerned in Implementation of the IAEA Action Plan. Moscow. 2012, http://www.gosnadzor.ru/activity/international/post-Fukushima/action_programme.

4. The Regulatory Implications of the Fukushima-Dai-Ichi NPP’s Accident to Russian Research Reactors. Alexander Sapozhnikov. European Research Reactor Conference Transactions. St. Petersburg, Russia 21-25 April 2013.

5. Concept of Improvement of Safety Regulation and Standardization in the Field of Nuclear Energy // Nuclear and Radiation Safety. 2014. № 1(71).

6. Accounting of External Natural and Man-Induced Impacts on Nuclear Facilities. NP-064-05 // Nuclear and Radiation Safety. 2006. № 3(40).

SEISMIC IMPACT ON MARIA RESEARCH REACTOR REACTIVITY AND POWER CHANGES

M. LIPKA
Reactor Measurement and Analysis Group, Research Reactor Technology Division,
National Centre for Nuclear Research
ul. Andrzeja Sołtana 7 05-400 Otwock, Poland

ABSTRACT

The goal of the research was to investigate the possible impact of earthquakes on the change of reactivity and therefore power of the MARIA research reactor in Otwock – Świerk. The reactivity changes could be caused by potentially occurring vertical and horizontal oscillations of control rods that can that can happen during the earthquake.
The issues related to the earthquake hazard on the territory of Poland were checked and described. While there is no seismic code in Poland, the hazards were compared to the international guidelines, and on their basis the calculations of the reactivity and power changes were performed.
For the purpose of calculations, with the measurements of the actual vibrations of the reactor, a calculation model with vibrations transfer function obtained by Fourier transformation and control rods vertical and horizontal movements based upon simple Newtonian mechanics was developed and used to determine the possible scale of the threat.
Data used for the calculations of control rods movement and solving the problem of reactivity and power changes were actual waveforms of earthquakes registered in Poland, scaled up to the peak ground acceleration (PGA) value recommended for the calculations of the earthquakes' impact on nuclear reactors by the International Atomic Energy Agency (IAEA).

1. Introduction

The aim of the assignment was to assess the possible reactivity and power changes of the reactor, that can occur due to vertical oscillations of reactor control rods, during an earthquake. Their movements cause the reactivity and power changes. Those changes, if big enough, can possibly lead to the instability or even damage of the nuclear reactor.

Poland is generally considered to be the aseismic zone, with Peak Ground Acceleration (PGA) lower than 160 cm/s^2. The MARIA reactor is situated in even safer area, with predicted max. PGA = 50 cm/s^2.[1] Because of the low earthquake risk, there is no existing seismic code in Poland. For this reason, for calculations, the values recommended by International Atomic Energy Agency (IAEA) were taken. The IAEA recommends the for aseismic zones calculations the value PGA = 0.1 g [2], where g=9.81 m/s^2.

2. Methodology

Initially, the waveforms of ground displacement in three directions, obtained from the Institute of Geophysics, Polish Academy of Sciences, were differentiated twice to get ground accelerations as the result. For this purpose, the central differencing scheme was used. The next step was to strenghten the derived accelerations to PGA=0.1 g in the potentially most damaging direction (vertical), and the other two directions proportionally. Then by Runge-Kutta fourth-order method they were integrated twice to get dislocations of ground constrained to reactor foundations. After the integration, the results had large systematic error caused by the high sensitivity of accelerometers, that were used to obtain the waveforms. To get correct values, certain correction scheme, taken from [3] and [7] was introduced.

After those steps, the data were appropriate to be used in the numerical simulation of an earthquake impact on the MARIA reactor reactivity and power changes. It is vital to say,

that due to many possible uncertainties, the conservative approach was used at all of the steps, so the results show worst case scenario.

It was assumed that in MARIA reactor the control rods can move in the two ways: vertically or horizontally along with the trolley that carries control rods moving mechanism, as shown in the Figure 1.

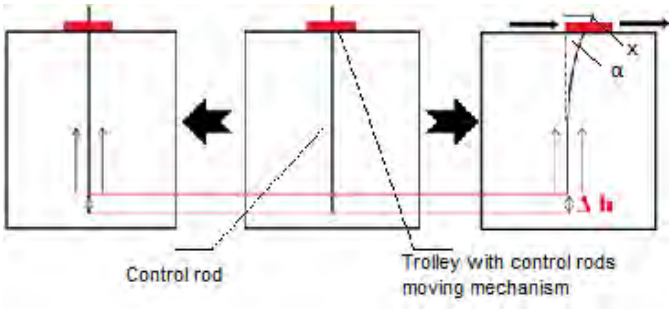

Figure 1: Control rods possible movement

The locations of reactor elements valid in the calculations are shortly presented in the Figure 2. The significant numbers are summarized in the table 1.

Parameter	Value
Distance between reactor core and the trolley (L)	7000 [mm]
Single control rod length (H)	1100 [mm]
Control rods total reactivity weight	8 [$]

Table 1: MARIA reactor significant construction details.

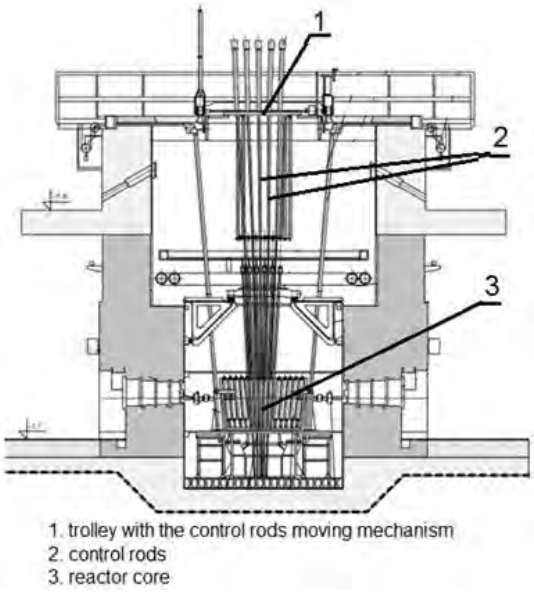

Figure 2: MARIA reactor significant elements location [5]

The vertical motion was described by a simple Newtonian correlation as the combination of motion of a material point and elastic collision. During an earthquake, there are two possibilities of control rods displacement in relation to the reactor core:

1. When the movement of the reactor corpse caused by an earthquake is changing its direction from "up" to "down". In that case the control rods have initial velocity caused by inertia force. If that velocity is higher than negative velocity vector caused by gravity force, control rods can move along the reactor core as described in the equations shown below in equations (1) and (2).

$$V_p(t) = V_p(t - \Delta t) + g \cdot t \quad (1)$$
$$S_p(t) = S_p(t - \Delta t) + V_p(t) \cdot t \quad (2)$$

With boundary condition:

$$S_p(t) > S_k(t) \quad (3)$$

2. After the situation described in the previous case, the control rod is eventually going down and hitting the reactor corpse. The elastic collision happens. The equations (1) and (2) are also valid in this case, but with different boundary conditions (4) and (5)

$$S_p(t) \leq S_k(t) \quad (4)$$
$$S_p(t - \Delta t) < S_p(t) \quad (5)$$

The control rod can also change its position in the reactor core by retraction caused by horizontal movement of the trolley that contains control rods mechanism. The trolley can move freely along rails and due to construction constraints +- perpendicularly to them, as shown in Figure 1.

To determine the possible trolley movement caused by foundations movement, the vibration transfer function was determined. Initially the accelerations of reactor foundations and trolley were measured. Then the time series was transformed into frequency series, using Fast Fourier Transform algorithm (FFT).

Then the vibration transfer function was obtained by division of Trolley and Foundation Fourier Transformations (6)

$$\hat{a}_w(\xi) = \hat{a}_k(\xi) \cdot A(\xi) \quad (6)$$

For the range 0 - 50 Hz the function shown below was obtained and approximated by 7th grade polynomial (7)

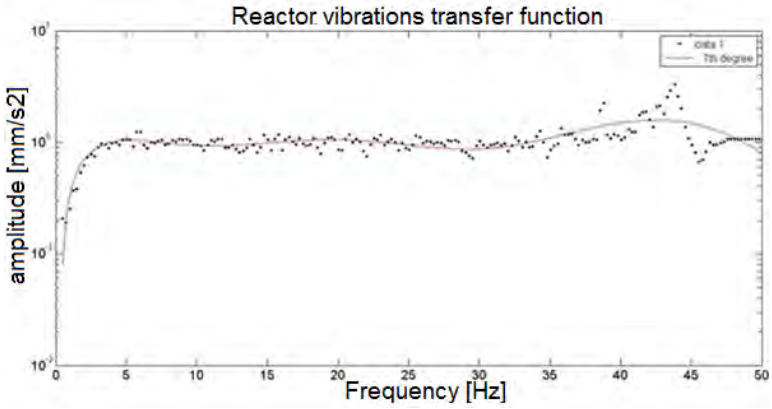

Figure 3: MARIA reactor vibrations transfer function

$$A_x(\xi) = a_7 \cdot \xi^7 + a_6 \cdot \xi^6 + a_5 \cdot \xi^5 + a_4 \cdot \xi^4 + a_3 \cdot \xi^3 + a_2 \cdot \xi^2 + a_1 \cdot \xi + a_0 \quad (7)$$

where:

$a_7 = 1.367 \cdot 10^{-9}$
$a_6 = -2.538 \cdot 10^{-7}$
$a_5 = 1.863 \cdot 10^{-5}$
$a_4 = -0.0006906$

$a_3 = 0.01371$
$a_2 = -0.1427$
$a_1 = 0.7006$
$a_o = -0.2365$

After obtaining reactor vibrations transfer function, determining of control rods movement was possible.

The waveforms of accelerations were transformed into frequency spectrum using FFT and multiplied by transfer function (7). Then the Inverse Fast Fourier Transform was used. Finally the trolley absolute accelerations were obtained

Then the data were integrated twice using Runge-Kutta 4th order algorithm, and the correction scheme taken from [3] was applied.

Displacement of the reactor corpse was subtracted from the displacement movement of the trolley, thereby obtaining a displacement of the trolley relative to the foundations. From these values the total length of displacement vector for each time step was calculated as shown in (8)

$$S_h = \sqrt{S_x^2 + S_y^2} \tag{8}$$

To calculate how horizontal displacement of the trolley (stretching from the core) changes control rods immersion into core, simple trigonometric functions (9) were used

$$\Delta h = L - L \cdot \cos(\alpha) = L \cdot (1 - \cos \alpha) \tag{9}$$

With known vertical displacement of the control rods in relation to the reactor core, their impact on reactivity changes can be calculated. As it can be seen from the reactivity S-curve (Pic. 4.), the biggest change in reactivity occur when the rod is depressed halfway in the core. Therefore in accordance with accepted principle of conservative approach, this situation was assumed for the purposes of the model, and described by the correlation (10).

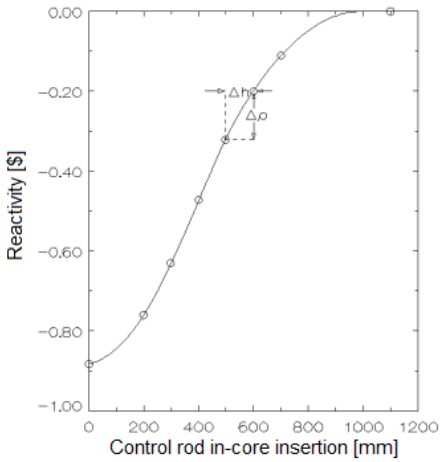

Figure 4:Control rod reactivity weight as a function of its insertion [6]

Due to impossibility of measuring individual control rods vibrations transfer function, all of the control rods were treated as one with total reactivity weight of 8$

$$\frac{d\rho}{dh} = \frac{2\rho_{max}}{H} \tag{10}$$

Calculated reactivity changes were used to derive reactor power changes, with Point Reactor Kinetic equations (11-15) derived from [4]. The existence of fifteen delayed neutron groups was assumed. Runge - Kutta fourth order algorithm was used for integration. The nuclear reactor kinetics parameters values are summarized in the Table 2.

$$\frac{dn}{dt} = \frac{\rho - 1}{} \beta_{ef} \cdot n + \sum_{i=1}^{15} \lambda_i C_i \tag{11}$$

$$\frac{dC_i}{dt} = \frac{\gamma^d \beta_i}{} \cdot n - \lambda_i C_i \;\; i = 1,2, \ldots\ldots, 15 \tag{12}$$

With initial conditions:

$$n(0) = n_0 \tag{13}$$

$$C_i(0) = \frac{\beta_{ef}}{ef} \frac{\beta_i}{\lambda_i} n_0 \tag{14}$$

$$n_0 = 1 \tag{15}$$

Nr	$\beta_i \cdot 10^3$	$\lambda_i [1/s]$	Nr	$\beta_i \cdot 10^6$	$\lambda_i [1/s]$
1	0.243	0.0127	7	20.7	2,265 E-2
2	1.363	0.0317	8	36.6	8,886 E-3
3	1.203	0.015	9	18.5	3,610 E-3
4	2.605	0.311	10	36.8	7,453 E-4
5	0.819	1.4	11	3.66	2,674 E-4
6	0.167	3.87	12	32.0	6,191 E-5
			13	2.60	1,591 E-5
			14	0.38	2,478 E-6
			15	0.57	6,098 E-7

Table 2: MARIA reactor kinetics parameters values - delayed neutrons groups [6]

After the final integration of Point Kinetics Equation, the reactor power fluctuations caused by an earthquake based control rods vibrations were The results of the whole calculation are presented and discussed in the next chapter.

3. Results

Results of the calculations, briefly described in the *Methodology* section, were summarized in the set of charts (Figures 5 – 9), showing time related changes of the most important parameters. Maximal values were gathered in Table 3.

Parameter	Value
PGA	0.1 g
trolley vertical displacement	0 mm
trolley horizontal displacement x-axis	13 mm
trolley horizontal displacement y-axis	10 mm
control rod vertical displacement	0,016 mm
reactivity change	$2{,}29 \cdot 10^{-4}$ \$
power change	0,065%

Table 3**:** Extreme values of the results obtained from the numerical calculations.

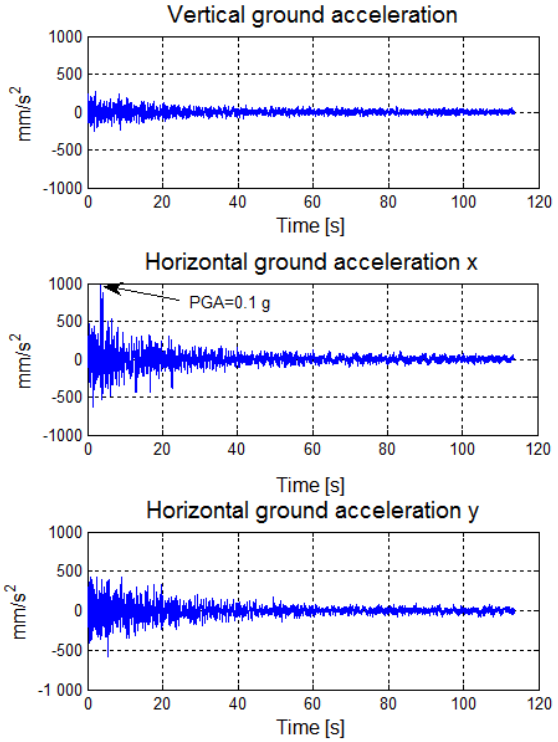

Figure 5: Three dimensions of the earthquake based ground acceleration

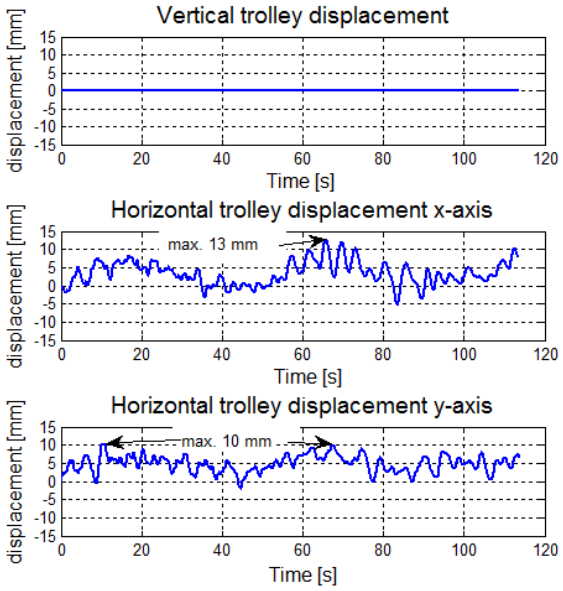

Figure 6: Trolley displacements in relation to the reactor foundations

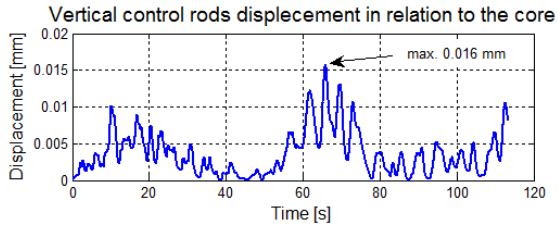

Figure 7: Control rods vertical displacement in relation to the core

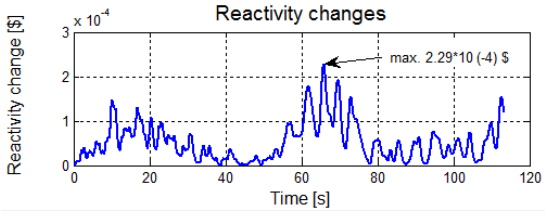

Figure 8: Reactivity changes

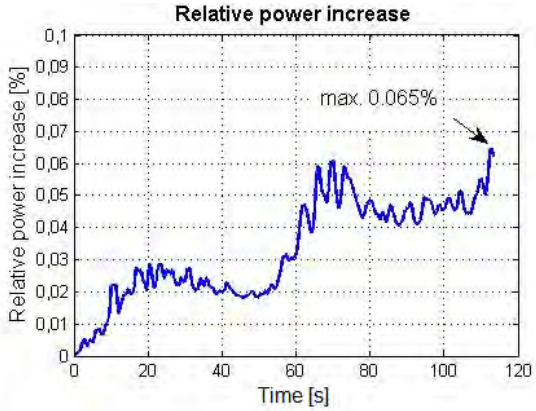

Figure 9: Relative power increase

4. Conclusions

The obtained results show reactivity and power fluctuations of the MARIA nuclear reactor caused by the earthquake based control rods movement. Calculation was carried out on the basis of the real earthquake time series registered in Belsk Seismic Monitoring Station, Poland (Kaliningrad 2004 earthquake).

Despite the high values of ground acceleration adopted for the calculation, PGA = 0.1g, vertical movements of control rods in relation to the core, and the resulting changes of reactivity and nuclear reactor power were vanishingly small. That is because of the vibrations damping by the reactor foundations. In the Figure 3 it can be seen that for earthquake frequency lower than c.a. 5 Hz, ground motion can be damped even by an order of magnitude.

Changes of the reactor reactivity and power are within the range of noise and are impossible to measure during normal operation of the reactor and definitely will not cause deviations from the normal operation regime.
To sum up it is also worth mentioning that those fluctuations are within the range of natural noise of the reactor, which are of the order of +- 1%.

REFERENCES

1. B. Guterch, *Sejsmiczność Polski w świetle danych historycznych*, Przegląd Geologiczny,, vol. 57, nr 6 2009.
2. *Seismic Hazards in Site Evaluation for Nuclear Installations*, No. SSG-9, IAEA, Vienna, 2010
3. N. Zhinguo, L. Tonghun, H. Shaowei, *The Synthesis and Correction of Simulated Earthquake Wave*, The 14th World Conference on Earthquake Engineering, China, Bejing, October 12-17 2008
4. M. Kiełkiewicz, *Teoria Reaktorów Jądrowych*, Oficyna Wydawnicza Politechniki Warszawskiej, Warszawa, 1987.
5. K. Pytel et al, *Eksploatacyjny Raport Bezpieczeństwa Reaktora MARIA*, Świerk, 2009
6. K. Pytel, Pomiary *Reaktywności w reaktorze MARIA*, Narodowe Centrum Badań Jądrowych, Świerk, 2011
7. P.K. Malhora, *Smooth Spectra of Horizontal and Vertical Ground Motions,* Bulletin of Seismological Society of America vol. 96, 2006, pp.506-508

NOMENCLATURE

t	time
Δt	time step
g	gravity acceleration
V_p	control rod velocity
S_p	control rod displacement
S_k	reactor foundation displacement
$\hat{a}_w(\xi)$	Fourier transform of the trolley accelerations
$\hat{a}_k(\xi)$	Fourier transform of the reactor corpse accelerations
$A(\xi)$	reactor's vibration transfer function
S_h	total vertical displacement vector of the trolley
S_x	x-axis trolley displacement vector
S_y	x-axis trolley displacement vector
Δh	control rod immersion from the core
L	core - trolley distance
ρ	reactivity
H	control rod length
n	relative reactor power
	effective lifetime of an neutron generation
β_{ef}	effective fraction of delayed neutrons
λ_i	delayed neutrons decay constant
C_i	the power of delayed neutrons corresponding to the i-th group
γ^d	neutrons efficiency
β_i	fraction of the i-group delayed neutrons
n_0	relative reactor power at the begining of calculation

A SAFETY ANALYSIS REPORT FOR THE CONVERSION OF THE NIST RESEARCH REACTOR

D.J. DIAMOND, J.S. BAEK, A.L. HANSON, L.-Y. CHENG, A. CUADRA, N.R. BROWN

Nuclear Science and Technology Department, Brookhaven National Laboratory
33 North Renaissance Road, Upton, NY 11973-5000 USA

ABSTRACT

The National Institute of Standards and Technology (NIST) operates a 20 MW research reactor for neutron-based research. The heavy-water moderated and cooled reactor is fueled with high-enriched uranium (HEU). A programme to convert the reactor to low-enriched uranium (LEU) fuel using a high density U-Mo alloy (rather than the current HEU dispersion fuel) has led to a new fuel element design. The new design minimizes changes to the fuel elements and maintains the current optimum fuel cycle length, but incurs a penalty to researchers because the additional ^{238}U in the core reduces the neutron flux that goes into the beam tubes. As part of the development programme, a Preliminary Safety Analysis Report (PSAR) was submitted to the U.S. Nuclear Regulatory Commission (NRC) for their review. It follows the format and content recommended by the NRC and emphasizes the impact of the conversion. Hence, it focuses on the nuclear and thermal-hydraulic design of the core, the analysis of accidents, and the calculational methodology used. The operational requirements on shutdown margin, reactivity feedback, critical heat flux ratio, and onset of flow instability ratio are shown to be satisfied in the document. The accidents considered are those due to reactivity insertion, loss of flow, loss of coolant, low power operation with natural circulation cooling, misloaded fuel elements, experiment malfunctions, external events, loss of normal power, and flow blockage of one fuel element. The accidents take into account worst-case assumptions expected to lead to the most severe consequences. The conclusions of the safety analysis are that the proposed LEU core will operate in a manner similar to the current HEU core and that there is sufficient safety margin to assure that no unacceptable consequences are possible and/or that no regulatory requirements are violated.

1. INTRODUCTION

The NIST Center for Neutron Research (NCNR) is a reactor-laboratory complex at the National Institute of Standards and Technology (NIST) outside of Washington, D.C. The heart of this facility is the NIST research reactor (aka NBSR); a heavy water moderated and cooled reactor operating at 20 MW. It provides users with thermal and cold neutron beams to carry out diverse world-class research. It is fueled with high-enriched uranium (HEU) fuel elements. A U.S. Global Threat Reduction Initiative (GTRI) programme (now under a new name) has been underway to convert this reactor, and similar reactors in the U.S., to low-enriched uranium (LEU) fuel. This programme includes the qualification of the proposed fuel, the development of the fabrication techniques for the fuel, and the development of the Safety Analysis Reports (SARs) that would need to be submitted to the U.S. Nuclear Regulatory Commission (NRC) and approved before conversion.

The conversion preliminary SAR [1] was submitted to the NRC in December 2014. The report follows the recommended format and content from the NRC codified in NUREG-1537, "Guidelines for Preparing and Reviewing Applications for the Licensing of Non-power Reactors," [2, 3] Chapter 18, "Highly Enriched to Low-Enriched Uranium Conversions." The emphasis in any conversion SAR is to explain the differences between the LEU and HEU cores and to show the acceptability of the new design; there is no need to repeat information regarding the current reactor that will not change upon conversion. Hence, as seen in the report, the bulk of the SAR is devoted to Chapter 4, Reactor Description, and Chapter 13, Safety Analysis.

2. DESCRIPTION OF REACTOR

The NBSR is a heavy water (D_2O) cooled, moderated, and reflected, tank-type reactor that operates at a design power of 20 MW. It is cooled by forced circulation upward through two concentric plenums within the reactor core. There is no pulsing capability in the NBSR. There are thirty fuel elements on a triangular pitch and each one is split axially into two sections with a gap between the two at the vertical mid-plane of the core. This gap allows beam tubes to be pointed directly at the mid-plane of the core so that thermal neutrons can escape for use in thermal and cold neutron scattering research while minimizing contamination from fast neutrons and gamma rays. Each (upper or lower) half-element encapsulates seventeen curved fuel plates in the materials test reactor (MTR) geometry. The control elements within the NBSR consist of four semaphore-type shim safety arms and a single automatic regulating rod. Fig Error**! No text of specified style in document.**. shows a drawing of the vessel internals including the reactor core.

The NBSR is operated for 38.5-day cycles. At the end of each cycle four fuel elements are removed from the core. The remaining 26 fuel elements are moved to new positions and four fresh, unirradiated fuel elements are inserted into the core. Fourteen of the thirty fuel elements are in the core for seven cycles and sixteen fuel elements remain for eight cycles.

The large volume and spacing within the core provides very flexible capabilities for thermal neutron irradiation. Insertion of eight radial beam tubes and two cold neutron sources into the plane of the fuel gap (see Items 4 and 15 in Figure 1. allows high intensity, low energy beams of neutrons to be extracted. A pneumatic rabbit system provides researchers with the ability to automatically inject samples into the core region of the reactor while thimbles provide for manual sample loading.

In normal operation the NBSR is cooled by forced convection of the D_2O coolant; for accidents, there are emergency cooling sources. A large D_2O inner reserve tank (IRT) and a D_2O hold-up pan ensure adequate coolant supply in the event of a piping rupture. The IRT (Item 11 in Fig Error**! No text of specified style in document.**.) is located in the top reflector and is drained through two non-isolable pipes at the bottom of the tank. These pipes feed a flow distributor that routes emergency cooling to the individual fuel elements. A hold up pan (Item 20 in Fig Error**! No text of specified style in document.**.) keeps the bottom half of the individual fuel elements immersed in coolant at all times.

There are several D_2O reflectors in the NBSR. During refueling the top reflector is drained to slightly above the top of the top grid plate. This level is maintained by the low-level overflow pipe that is concentric with the overflow pipe. During abnormal operation, a third overflow pipe, concentric with the fuel transfer chute, serves as a moderator dump to drop the D_2O level to just above the active core for emergency shutdown.

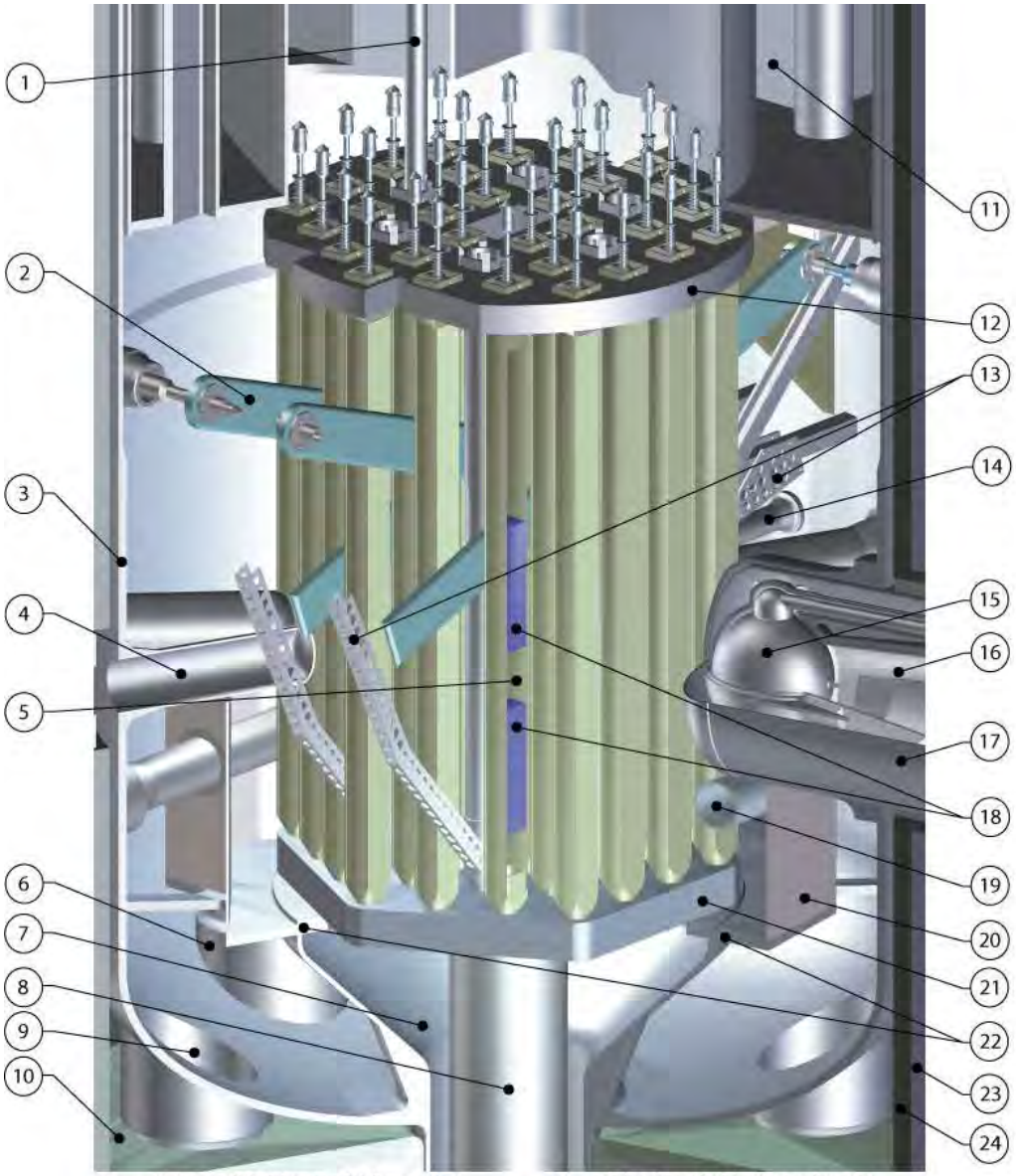

Fig **Error! No text of specified style in document.**. NBSR Vessel Internals and Reactor Core

A complete description of the NBSR reactor and support facility is provided in the current SAR [4]. *The only changes that will be made in the NBSR reactor because of the conversion are the changes in the fuel meat composition within the fuel plates, the thickness of the fuel meat and the aluminum cladding, and the introduction of a zirconium layer between the clad and the fuel meat.* The external dimensions of the fuel plates remain the same as does the design of the fuel elements and other structures within the vessel.

3. NUCLEAR DESIGN

To design the LEU fuel elements and assess the neutronic characteristics of the converted core, a three-dimensional model was developed to be used with the well-known Monte Carlo code MCNP [5]. This was an adaptation of the model previously developed for the existing core [6]. MCNPX v.2.7.0 [7] was utilized to take advantage of its burnup capability. The ENDF/B-VII cross section library was used for the analysis.

The analyses performed have been shown to be valid by satisfying the constraints imposed, namely, that with the measured shim arm positions at the startup and end of a fuel cycle the code gives a multiplication constant (k_{eff}) of unity, within an acceptable uncertainty (<0.01). In addition, the shim arm worth at startup (SU) is calculated to be 24.9%Δk/k for the HEU core, whereas the measured value obtained from data over many cycles is 25.2%Δk/k with an estimated uncertainty of ±10%.

A horizontal cross-section of the NBSR core at the mid-plane is shown in Figure 2. The major geometric features incorporated in the model include:

- a triangular-pitch array of 30 fuel elements, six vertical thimbles, the moderator dump line, and the fuel transfer chute
- all 1020 fuel plates with explicit cladding, and D_2O-filled coolant channels, positioned in hexahedral repeated structures for the upper and lower halves of the core
- sixty fuel material specifications that represent the upper- and lower-half of each individual fuel element
- the four shim arms, which can be positioned anywhere between the fully withdrawn and fully inserted (SCRAM) positions, and the regulating rod,
- nine radial beam tubes, two tangential beam tubes, the vertical beam tube, and the four in-core pneumatic 'rabbit' tubes
- the large cryogenic beam port, the large liquid hydrogen cold neutron source (CNS), and the small CNS located in beam tube 9
- the reactor vessel, D_2O moderator, and the core reflector
- layers of lead and iron outside of the vessel, comprising the thermal shield, and a layer of concrete, for part of the biological shield
- a portion of the D_2O tank, providing neutronic coupling with the graphite in the thermal column.

The model was originally used to determine the ^{235}U loading needed in the LEU equilibrium core [8]. It was then used to determine the following parameters which were compared with the corresponding parameters for the HEU core.

- Excess reactivity
- Differential shim arm worth and shutdown margin
- Regulating rod worth
- Reactivity coefficients for moderator temperature and different void locations
- Reactivity worth of flooding of different beam tubes and dumping of moderator
- Power distributions in all fuel plates
- Delayed neutron parameters and neutron lifetime.

For all parameters the values for the LEU core were within Technical Specifications and close to those values obtained for the HEU core.

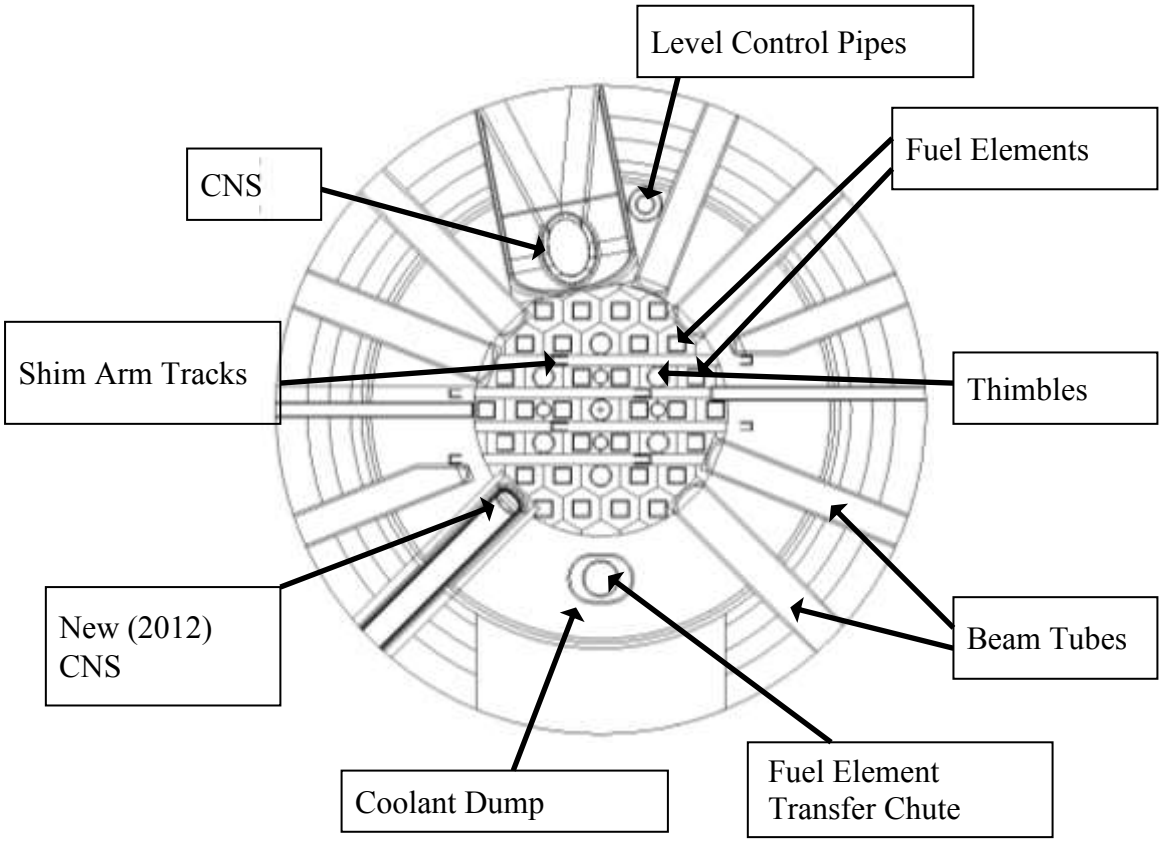

Fig 2. MCNP Model Planar View at Core Mid-Plane

4. THERMAL-HYDRAULIC DESIGN

The design basis of the thermal-hydraulic design of the NBSR is that there shall be no fuel damage resulting in the release of fission products during normal operation and any credible accident. The criterion chosen was that the heat transfer to the primary coolant shall not exceed critical heat flux (CHF) conditions, including any excursive instability; the latter being defined by “onset of flow instability” (OFI). This would preclude blistering and the potential for fuel damage.

In order to determine how close the reactor operates to CHF or OFI a statistical methodology [9, 10] is first used to determine acceptable limits. Cumulative distribution functions are obtained for critical heat flux ratio (CHFR), and onset of flow instability ratio (OFIR). The correlation used for CHF is one from Sudo-Kaminaga [11] and the correlation for OFI is that of Saha-Zuber [12]. These correlations are discussed in [13] along with their application.

The statistical methodology provides the ratios which have a specific probability of precluding the limit (CHF or OFI). The results at the 95% and 99.9% probability level are shown in column 2 in Table 1 along with the ratios calculated at steady state at two statepoints. The results show the large margin to the limits.

Tab 1. Steady State Thermal-Hydraulic Parameters

	Limit 95%/99.9%	HEU	LEU
CHFR SU	1.39/1.78	4.03	4.12
CHFR EOC	1.39/1.78	3.99	3.96
OFIR SU	1.40/1.83	5.50	5.61
OFIR EOC	1.40/1.83	6.17	6.15

5. ACCIDENT ANALYSIS

The health and safety of the public and workers are protected in the event of an accident as a result of the facility design features, the Technical Specifications (e.g., Limiting Safety System Settings (LSSS), and Limiting Conditions for Operation (LCOs)), and the well-qualified and trained staff of the NCNR. The accident scenarios that need to be considered for the equilibrium core with LEU fuel are identical to those considered in the SAR [4] for the NBSR with HEU fuel; namely,

- reactivity insertion accidents
- loss-of-flow accidents
- loss-of-coolant accidents (LOCAs)
- natural circulation cooling at low power operation
- complete flow blockage in one fuel element
- misloaded fuel elements
- experiment malfunctions
- external events
- loss of off-site power

The analyses take into account worst-case credible assumptions expected to lead to the most severe consequences and bound all possible events. The progression of each accident is analyzed to the extent necessary to determine the degree of potential hazard and results are compared to acceptance criteria based on whether the accident is considered credible or not. The complete flow blockage in one fuel element is not considered credible and is treated as the “maximum hypothetical accident (MHA).”

In general, accidents are analyzed at two points in the fuel cycle: startup (SU, which is at the beginning of a cycle before equilibrium xenon has built into the core) and end-of-cycle (EOC). At SU there are four fresh fuel elements in the core and the short-lived fission product poisons such as ^{135}Xe have decayed away during the refueling period since the previous cycle. The power peaking is highest at this statepoint making it the limiting state-point for some events. However, some events are most limiting at EOC because differential shim arm worth is lowest when the shim arms are inserted from the fully withdrawn (EOC) position.

The majority of accidents addressed are non-LOCA events [14, 15] and are based on a methodology that uses the systems analysis code RELAP5 [16]. The RELAP5 model, shown in Figure 3., includes the primary piping from vessel inlet to outlet, primary and shutdown pumps and their flow paths, heat exchanger, fuel elements, flow channels for the six inner and twenty-four outer fuel elements, and special items like the hold-up pan and the inner reserve tank. The heat structures simulating the fuel plates are represented by the red color. The numbers after “H” are heat structure node numbers and “-1” and “-2” associate the heat structures with hydraulic flow channels in the lower and upper fuel elements, respectively.

Most initial conditions (e.g., flows and temperatures) were assumed to be at their most limiting values or at the LSSSs. The NBSR reactor protection system logic was modeled and initiated a reactor trip, upon reaching a setpoint and after the appropriate instrumentation response delay. Fuel and clad temperatures are calculated to assure that no fuel damage can take place. In addition, the CHFR and OFIR are evaluated as supplementary parameters indicative of a potential threat to the integrity of fuel elements.

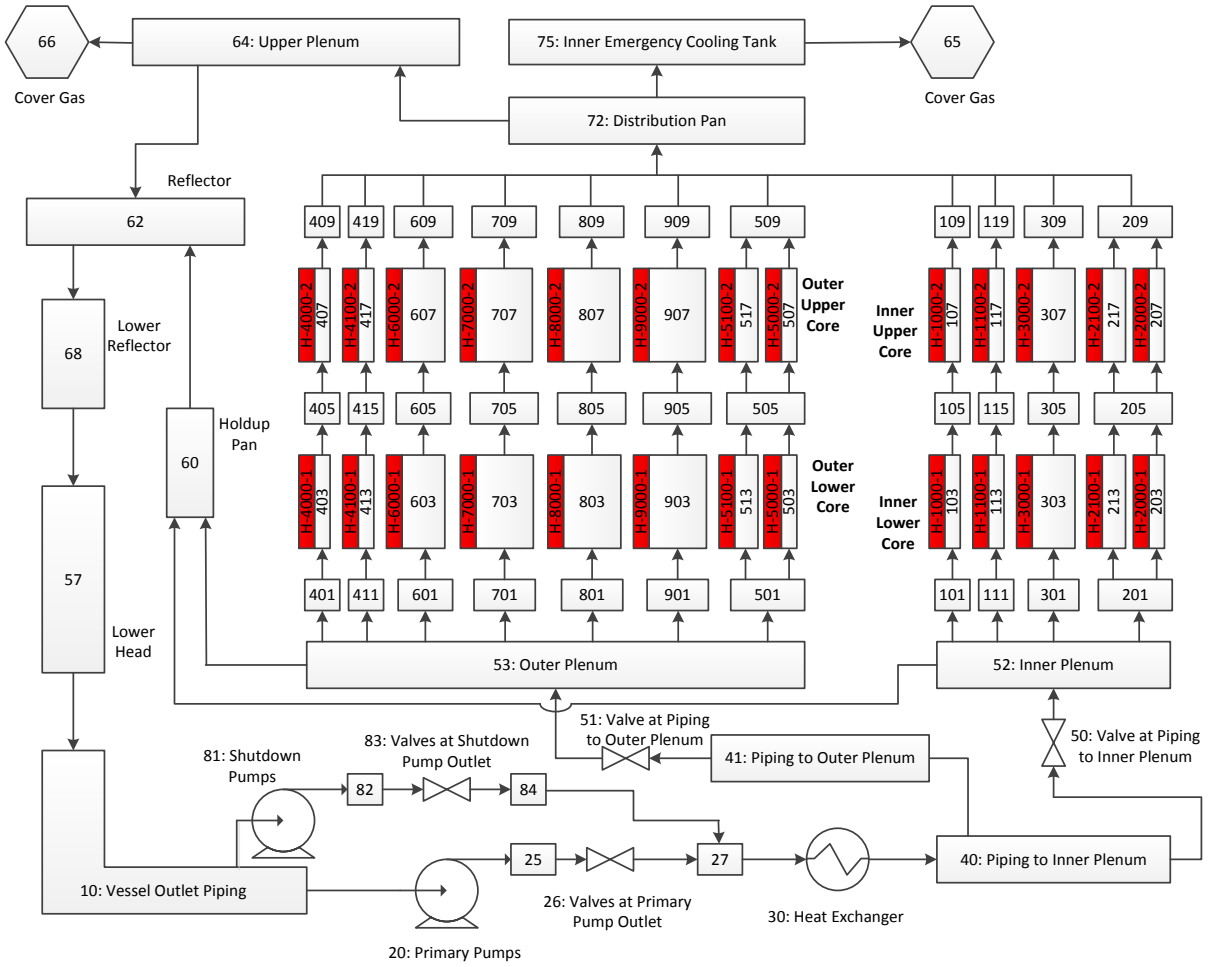

Fig 3. Nodal Diagram of RELAP5 Model

The RELAP5 model was the basis for a similar model using the TRACE systems analysis code [17] to calculate the draining of coolant during a LOCA. The TRACE analysis is combined with heat conduction analysis for a fuel element using the three dimensional heat conduction code HEATING7.3 [18] to determine the time dependent peak clad temperature during the accident.

The acceptance criterion for all credible accidents is given by the NRC as no loss of fuel integrity [2]. A clad temperature of 582°C, the solidus temperature, would certainly cause the release of fission products. However, at the much lower temperature where blistering is possible fuel integrity might be challenged. Hence, herein, the blister temperature is considered as the acceptance criterion. The current NBSR Technical Specification Safety Limit (i.e., for HEU fuel), which is 450°C, is the minimum blister temperature for aluminum clad dispersion fuel [19]. It is used as a conservative surrogate to preclude the release of fission products and act as the acceptance criterion for HEU accidents.

For the proposed LEU fuel (U10Mo alloy foil), the information available regarding blister temperature is still being interpreted. For U10Mo fuel the blister threshold has been

determined experimentally as a function of fission density but many more tests are yet to be completed. For the LEU reactor, the maximum fission density is conservatively estimated to be 7.2×10^{21} fissions/cm^3 [20], occurring at the bottom of upper section fuel plates near the mid-plane gap at EOC. The isothermal blister threshold based on the experimental data [21] is 380±55ºC at this fission density. However, the measured fission density is an average over the experimental plate and not the fission density in the locale of the observed blisters, which would be higher. This means that the value cited above may be a conservative estimate of the blister temperature. Also, the fact that the blister temperature is not a single value but depends on burnup (and hence, location in the fuel element) means that 380ºC is a conservative estimate for a large fraction of the fuel at lower fission density. Nevertheless, in the absence of more information, it is used for LEU fuel as the acceptance criterion for credible accidents.

This acceptance criterion does not apply to any non-credible accident such as the MHA wherein, even without a known cause, it is assumed that there is complete flow blockage of one fuel element and fission products are released. This event is analyzed to see if radiation dose limits as specified in the Code of Federal Regulations are exceeded [3].

6. CONCLUDING REMARKS

The analyses done for the conversion SAR show that the LEU core will have similar behavior to the current HEU core and no credible accident will lead to fuel damage. These analyses support the bases for the Technical Specifications as do the thermal-hydraulic limits based on CHFR, OFIR and peak clad temperature. The results show that the LSSS determined for routine operation are adequate to provide assurance that the Safety Limit will not be exceeded during any credible accident.

The MHA is not considered credible but would lead to fuel damage if it occurred. Nevertheless, the resultant radiological consequences are well within the statutory limits which apply to Test Reactors. Therefore, operation of the NBSR will present no undue hazard to any member of the general public or to the NCNR staff.

The SAR is now awaiting review at the NRC. This review will provide feedback to the conversion programme and help expedite actual conversion when the fuel is qualified and capable of being manufactured.

7. REFERENCES

1. D. J. Diamond, J. S. Baek, A. L. Hanson, L.-Y. Cheng, N. Brown, and A. Cuadra, “Conversion Preliminary Safety Analysis Report for the NIST Research Reactor,” BNL-107265-2015-IR, Brookhaven National Laboratory, December 30, 2014.

2. NRC, “Guidelines for Preparing and Reviewing Applications for the Licensing of Non-Power Reactors; Format and Content,” NUREG/CR-1537, Part 1, U.S. Nuclear Regulatory Commission (NRC), February 1996.

3. NRC, “Guidelines for Preparing and Reviewing Applications for the Licensing of Non-Power Reactors; Standard Review Plan and Acceptance Criteria,” NUREG/CR-1537, Part 2, U.S. Nuclear Regulatory Commission (NRC), February 1996.

4. NIST, “Safety Analysis Report (SAR) for License Renewal for the National Institute of Standards and Technology Reactor - NBSR; NBSR 14, Rev 4," National Institute of Standards and Technology (NIST), 2010.

5. LANL, "MCNP — A General Monte Carlo N-Particle Transport Code, Version 5 Volume I: Overview and Theory (LA-UR-03-1987)," Los Alamos National Laboratory (LANL), 2008.

6. A. Hanson, and D. Diamond, "A Neutronics Methodology for the NIST Research Reactor Based on MCNPX," in *19th International Conference on Nuclear Engineering (ICONE19)*, Chiba, Japan, May 16-19, 2011.

7. D.B. Pelowitz, "MCNPX User's Manual Version 2.7.0," Los Alamos National Laboratory, 2011.

8. A.L. Hanson, and D.J. Diamond, "Calculation of Design Parameters for an Equilibrium LEU Core in the NBSR," Technical Report, Brookhaven National Laboratory, September 29, 2011.

9. L-Y. Cheng, et al., "Physics and Safety Analysis for the NIST Research Reactor," BNL-NIST-0803, Rev. 1, Brookhaven National Laboratory, April 2004.

10. A. Cuadra, and L-Y. Cheng, "Statistical Hot Channel Analysis for the NBSR," BNL-105288-2014-IR, Brookhaven National Laboratory, May 27, 2011.

11. M. Kaminaga, K. Yamamoto, and Y. Sudo, "Improvement of Critical Heat Flux Correlation for Research Reactors using Plate-Type Fuel*," J. Nucl. Sci. Technol. 35[12],* 943-951, 1998.

12. P. Saha and N. Zuber, "Point of Net Vapor Generation and Vapor Void Fraction in Subcooled Boiling," Proc. 5th Int. Heat Transfer Conf., Vol. IV, p. 175, Tokyo, Japan, September 3-7, 1974.

13. J.S. Baek, L.-Y. Cheng, A.L. Hanson, A. Cuadra, N.R. Brown, and D.J. Diamond, "Accident Analysis for the NIST Research Reactor Before and After Fuel Conversion – Revision 2," BNL-98524-2014-IR-R2, Brookhaven National Laboratory, July 22, 2014.

14. J.S. Baek, A. Cuadra, L.-Y. Cheng, A.L. Hanson, N.R. Brown, and D.J. Diamond, "Analysis of Reactivity Insertion Accidents for the NIST Research Reactor Before and After Fuel Conversion," *Nucl. Tech., 185,* p.1, January 2014.

15. J.S. Baek, A. Cuadra, L.-Y. Cheng, A.L. Hanson, N.R. Brown, and D.J. Diamond, "Analysis of Loss–of-Flow Accidents for the NIST Research Reactor with Fuel Conversion from HEU to LEU," *Nucl. Tech., 189,* p.1, January 2015.

16. ISL, "RELAP5/MOD3.3 Code Manual," NUREG/CR-5535/Rev1, Information Systems Laboratories, Inc., December 2001.

17. NRC, "TRACE V5.0 Theory Manual," U.S. Nuclear Regulatory Commission (NRC), June 4, 2010.

18. ORNL, "Multidimensional, Finite-Difference Heat Conduction Analysis Code System, Versions 7.2i and 7.3," RSICC Code Package PSR-199, Oak Ridge National Laboratory (ORNL), August 2007.

19. NIST, "Technical Specifications for the NIST Test Reactor (NBSR)," Appendix A to License No. TR-5, National Institute of Standards and Technology (NIST), 2010.

20. N.R. Brown, J.S. Baek, A.L. Hanson, A. Cuadra, L-Y. Cheng, and D.J. Diamond, “Irradiation Experiment Conceptual Design Parameters for NBSR Fuel Conversion,” BNL-99897-2014-IR-R2, Brookhaven National Laboratory, April 30, 2014.

21. INL, Discussions at the High Performance Research Reactor Working Group Meeting in Pasco, WA, Idaho National Laboratory (INL), July 2014.

ACKNOWLEDGMENTS

This work was supported by the National Nuclear Security Administration and the NIST Center for Neutron Research (NCNR). The authors appreciate the information obtained from, and the review by, Sean O’Kelly, Robert Williams, and Michael Rowe at the NCNR.

LESSONS LEARNED FROM HIGHLY ENRICHED URANIUM SOLIDIFICATION AND SHIPMENT PROJECT

G. L. PFENNIGWERTH
Y-12 National Security Complex
Oak Ridge, TN, USA

TRENT ANDES-Presenter
Y-12 National Security Complex
Oak Ridge, TN, USA

ANTONIO PROIETTI, FERNANDA DI GASBARRO, LUCIA BONAVIGO
SOGIN (Societa' Gestione Impianti Nucleari)
Rome, Italy

ABSTRACT

The Global Threat Reduction Initiative (GTRI) Gap Program supports the removal or disposition of excess WMD-usable nuclear and radiological materials from civilian sites worldwide. This paper summarizes actions taken and lessons learned to convert highly enriched uranium materials to a form suitable for removal from the Italian EUREX (**E**nriched **Ur**anium **Ex**traction) site near Saluggia, Italy. The source material was HEU dissolved in aqueous solution stored in cylindrical polyethylene safe bottles. Solid materials can be directly packaged for shipment; however the liquid solutions of uranyl nitrate were unsuitable for shipment since there was not an approved shipping container for liquids. The solutions were processed to a solid form suitable for shipment using a precipitation and furnace treatment method. This processing was performed by SOGIN (Societa' Gestione Impianti Nucleari) at the EUREX site using methods and procedures developed in collaboration with subject matter experts at the Y-12 National Security Complex. The solidification process was validated for the Italian Regulatory Authority (ISPRA) initially using available low enriched uranium (LEU) solutions before the highly enriched uranium (HEU) solutions were processed. The resulting uranium oxide (U_3O_8) was packaged and shipped to the U.S.

1. Introduction

The purpose of the highly enriched uranium (HEU) solidification project was to process HEU solution (uranyl nitrate) to a solid form suitable for shipment. The uranyl nitrate was left in storage after processing experiments in the 1970s. The process was previously discussed in a paper presented in 2013. The processing facility had not operated in an experimental production mode for a number of years and was undergoing clean-out and decommissioning. The solidification process involved batch precipitation of the solution using ammonium hydroxide to form ammonium diuranate (ADU), filtration, calcination to triuranium octoxide (U_3O_8) and product sampling. The precipitation/calcination process resemble a production process in scale and complexity more than it resembled typical decommissioning activities. The processing campaign required procurement of new equipment, restoration of three laboratories, procedure preparation, training and reviews/approvals from the Regulatory Authority. This paper describes some of the lessons learned from the uranyl nitrate solidification project.

2. Materials and Process

The uranyl nitrate was stored in a number of polyethylene safe-by-shape bottles and had been re-packaged in the late 1980s which was the last time the containers had been closely inspected. The solution was relatively pure as the result of solvent extraction processing prior to storage, but it had been characterized in order to meet 1980's standards for storage and was therefore not well characterized for shipping nowadays, in particular for fission and daughter product contents. There were also two smaller bottles of LEU uranyl nitrate that were used to prove in the process prior to processing the HEU uranyl nitrate. While not quite a "cold" test, the material did reduce the risks associated with the first test operations of the process and equipment.

The solidification process was manually performed on a laboratory scale using laboratory glassware and small laboratory furnaces. The ammonium diuranate precipitation process is a simple one-step process that uses reagent grade ammonium hydroxide to precipitate the uranium at a slight elevated temperature on a hot plate with a magnetic stirrer yielding a bright yellow precipitate. The precipitate was then filtered using a vacuum-assited Buechner funnel onto circular filter ashless papers. The loaded filters were then collected into several ceramic calcination capsules/crucibles, loaded into the furnace and heated. The furnace heating cycle allowed drying of the solid and removal of residual ammonia under a nitrogen purge followed by heating to 750^{o}C in air to convert the ADU to U_3O_8. The product oxide was then tumbled to break up the lumps, sampled and packaged.

Fig 1 Equipment used for ADU precipitation in exhaust hood

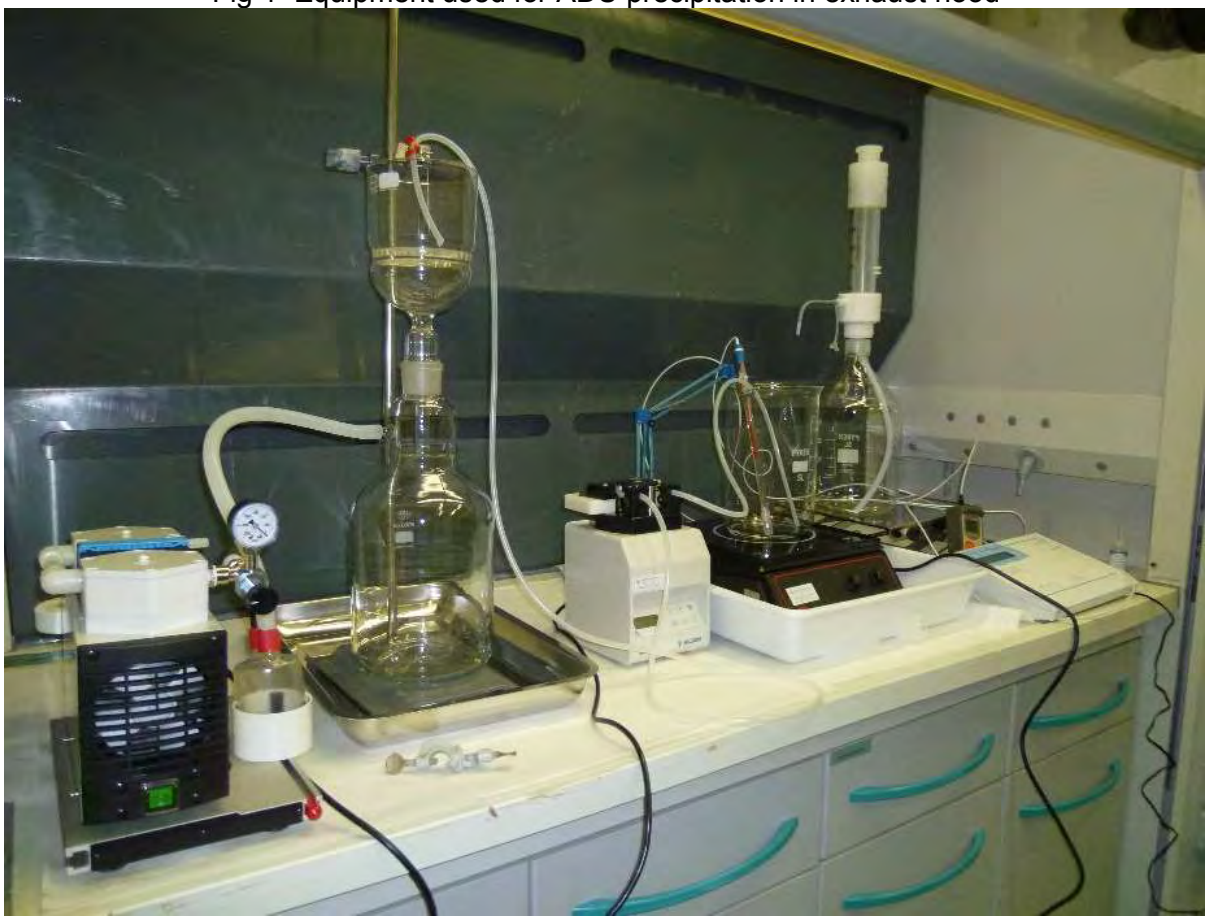

Two adjacent laboratories were retrofitted to accommodate the required ventilation hoods and process equipment. Another laboratory was updated and a new inductively-coupled

plasma mass spectrometer (ICP-MS) installed and calibrated for analytical characterization of the feeds and products.

Fig 2 Ammonium diuranate (ADU) precipitation product after filtration

Fig. 3 Crucibles loaded with ammonium diurninate (ADU) filter cakes inside the chamber of the calcination furnace prior to firing.

Two crews of laboratory technicians, radiological control technicians, supervisors and support staff were assigned to the project and trained on the safety requirements, process and equipment operation.

This processing was performed by SOGIN (Società Gestione Impianti Nucleari) personnel at the EUREX site using methods and procedural outlines provided by subject matter experts at the Y-12 National Security Complex. All final procedures, health, safety and nuclear criticality safety requirements were written and approved by SOGIN engineers and the Italian Regulatory Authority ISPRA. The solidification process was validated for ISPRA initially

using available low enriched uranium (LEU) solutions before the highly enriched uranium (HEU) solutions were processed.

3. Process Objectives and Requirements

The objective of the process was to convert HEU solution that could not be readily shipped into a form that could be shipped under the package certifications of existing shipping containers. Several processes were studied, but the ADU precipitation process was chosen since it yielded a stable, dry, powdered oxide product that met the package certification requirements. It was also desired that the process result in as complete a conversion as possible to minimize losses to waste.

Fig 4. Two crucibles containing calcined U_3O_8 product prior to blending.

In addition to packaging and shipment requirements there were receiver acceptance criteria that had to be met. The process history of these solutions indicated that the uranium had been irradiated in a reactor, but had undergone solvent extraction separation to remove fission and daughter products as well as transuranic isotopes. The receiving facility limited the radiological dose and constituents to levels that were close to fresh EU. Analysis was necessary to confirm that the U_3O_8 product met all of these criteria prior to packaging and shipment.

4. Lessons Learned from the Solidification Project

A number of lessons were learned and observations made, both positive and some requiring correction, during the course of the preparations, execution, and completion of the solidification project. For ease of assimilation these lessons and observations have been

categorized into a number of topical areas. The topical areas and details of the lessons learned and observations follow:

4.1. Preparation and Approval

Direct historical knowledge of personnel about this legacy material was limited due to personnel turn-over since the time of last use. Records indicate that the uranyl nitrate solutions were re-packaged into the current bottles in 1989.

Close involvement and development of constructive working relationships with the management, technical, and operating personnel at both the EUREX facility and SOGIN central staff greatly facilitated the resolution of issues and convergence on suitable methods and requirements. This required a significant investment of time on the part of the lead engineers, but paid dividends in terms of product quality and the final delivery schedule.

A detailed feasibility study was prepared that provided the process description, operating procedure, material and equipment requirements, safety analysis outline, suggested radiological control and criticality safety requirements. This helped bring the facility management and technical staff quickly up to speed on the proposed activity and requirements. This document and procedural outline were directly used in the preparation of approval documentation and operating procedures.

4.2. Procedures and Safety Requirements

The SOGIN engineers expressed a concern over the potential for hydrogen gas formation during the calcination operation (attributed to decomposition of the ammonia to nitrogen and hydrogen). This required alteration of the originally proposed heating cycle to include a drying and decomposition phase under nitrogen purge. After holding at a suitably high temperature to complete the potential decomposition and purging of gasses, the nitrogen purge was removed to allow introduction of air to complete the ADU conversion to U_3O_8. In normal practice within the US, the drying and decomposition has routinely been performed using only an air purge without incident for decades of operation in multiple facilities and sites.

The criticality safety analysis for the solidification process was performed by the SOGIN Rome office. Several observations were made during early walk-downs of the facilities and equipment prior to operations concerning spacing, good practices, and waste water connections that resulted in a few recommendations. SOGIN engineers concurred with the recommendations.

The plant internal operational procedures did not allow to use any laboratory glassware in with this kind of solutions and the use of stainless steel containers was expected due to the potential for glass breakage and injury. After explaining that visual observation of the precipitation process was very important, and after specific exemption authorization to internal procedures, Pyrex laboratory glassware was approved for use. No glassware was broken during the five months of daily operations.

The Italian regulatory authority (ISPRA) was very involved in the safety- and accountancy-related details of the operation and necessitated generation of information and data, through LEU operations to satisfy uncertainties due to unfamiliarity with the technology, materials and risk-averse philosophy.

ISPRA required the LEU completion of the entire solidification process using LEU (~20% U-235 enrichment) solution in each of the laboratories before the authorization the HEU material processing. The LEU demonstration was successfully performed and a report of the demonstration was submitted to ISPRA. HEU operations were then approved about a week later.

4.3. Facilities and Equipment

Calcination furnace heating cycle programming required multiple visits by the vendor representative to adjust the heating program. A heat rate software clamp provided in the as-delivered vendor setup was initially limiting how fast the furnace was heating and would have taken too long to cycle the furnace. The issue was resolved and both furnaces performed well throughout the remainder of the campaign.

The calcination process resulted in full conversion of the ADU and resulted in a friable, dry oxide product. Analysis of the moisture content of the product was less that 0.1% after calcining to 750^{o}C which was well below the 2% maximum moisture limit imposed for the ES-3100 shipping container. The volume of the oxide product was greater than expected due to the low density and fluffiness of the product and required mixing of source batches in the interim storage cans due to the limited number of cans available for use.

Local ingenuity resulted in several improvements to the process. An improved stainless steel separable Buechner funnel was designed and fabricated that enabled easier and more quantitative transfer of the thick ADU filter caked from the bottom of the deep funnel to the calcination crucible. Another example was the design and procurement of the interim storage cans that were used to blend and house the oxide product prior to convenience can loading for shipment.

Fig 5. Locally designed and fabricated separable Buechner filtration funnel.

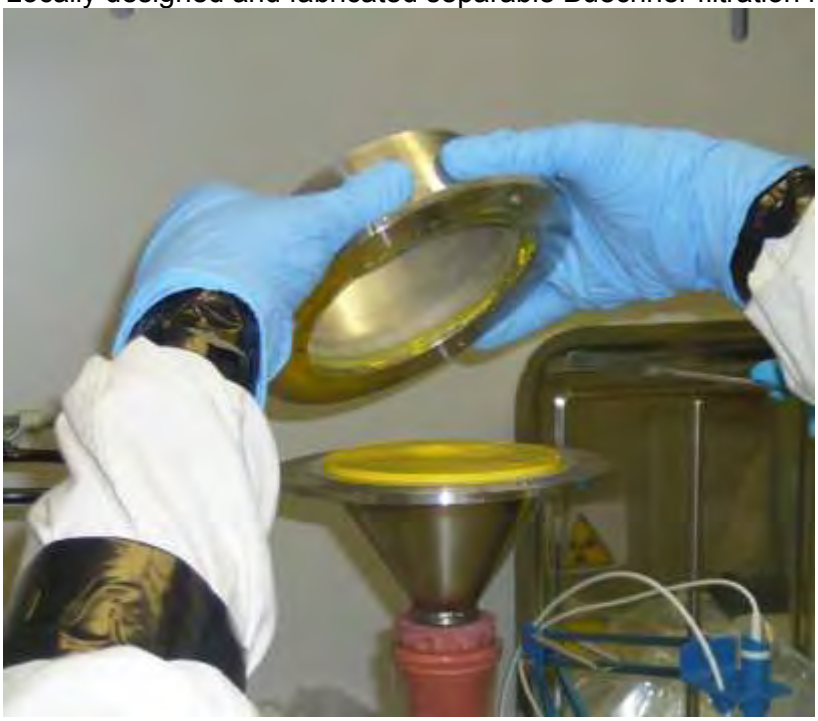

A final rotary rod mill/blending operation for the oxide product was recommended to homogenize the product oxide before sampling, but local management felt that it would

increase the opportunity for airborne contamination/exposure during the extra oxide transfer step, so the blending was performed in the smaller diameter interim storage cans.

4.4. Execution and Schedule

The technical aspects of the solidification process performed as desired. The precipitation process was quick and quantitative. Filtration was sufficient once appropriate vacuum settings (low) were employed. Uranium losses to waste via the process filtrate were small (2-15 ppm) as expected. . Radiation protection local procedures, which include fastidious cleanliness on the part of the operating technicians to keep the hoods clean and through numerous glove changes, may lead to losses to laboratory waste (gloves, wipes, etc.) greater than expected. Nevertheless, HEU total loss of mass remained under the 0.7%, an acceptable percentage.

The ability to be flexible and adaptive to unanticipated conditions is important to permit the tasks to proceed. Application of sound professional judgment and adherence to the project, procedural and regulatory requirements supplemented by full and open communications are necessary. Deviations should be documented (photographs are very helpful).

It is important to be observant of fissile material handling practices and not to assume that the general training requirements for the local personnel are as broad or comprehensive as those required in an operating production facility. Many of the operators were familiar with safe handling of waste and low-level concentrations of radioactive material, but were less familiar with the special handling requirements for larger quantities of fissile material. Additional operator training for nuclear criticality safety was developed to address process-specific requirements and practices for the HEU processing operations. Assistance was provided to the SOGIN nuclear engineer in the preparation of a suitable training module that was both task-specific and mirrored US training materials.

Initially the proposed conceptual time line for the solidification process required 64 days (approximately 3 months) to complete, but SOGIN responded with a time line that required 200 working days to complete. The difference was due to running three shifts per day versus one, the need for no concurrent (wet and dry) operations and additional contingency days for process turn-around. Concurrent operations would not have required simultaneous fissile material handling since the calcination furnace operation would require at least two shifts to complete the heat-up and cool-down cycle. This would have allowed the execution of the wet operations while the furnace was cycling, but serial operations were performed until late in the timeline until ISPRA approval for concurrent operations. Two laboratories were ultimately set up and placed in operation to meet the production schedule. The conceptual time line was revised to reflect a 100 day completion. Each laboratory was operated only during the day shift 6 days a week. Evening/night shifts were not used due to the limited availability of the technical, medical staff that was required to be on site during chemical operations. Operating one laboratory around the clock with appropriate staffing could have more effectively utilized the initial operating equipment suite.

Scale calibration is important to validate weight data. Using available weight standards, a calibration curve was prepared during the days of operation that was subsequently used to correct scale biases that would have affected accountability measurements. This is particularly important when SNM is manipulated in a manner more complex than simple container transfers or when SNM is converted between chemical forms to account for processing losses.

Numerous photographs were taken at various stages of the processing, packaging, and shipping container loading using SOGIN-owned and controlled digital cameras. This permitted both the US team and SOGIN the freedom to photograph essentially anything since SOGIN would retain the camera and photographs and review them prior to release. All relevant photographs requested were released to the US to document the solidification activities. The photographs were useful to document the equipment, methods, materials, colors, and activities involved in this complex operation.

4.5. Chemical and Isotopic Analysis for Product Acceptance Requirements

It is important to determine, document and communicate all of the acceptance criteria, especially the radiological characteristics, prior to engaging on a processing campaign. Units of measurement, methods of data acquisition, and calculations for new or different materials must be clarified to ensure that the materials are well characterized, well understood and meet all of the acceptance criteria.

Early draft preparation of the scrap declarations allowed iteration of the documents between the generating and receiving sites to acquire the necessary information and reinforce the need for data collection to fill out the forms.

Indigenous analytical laboratory equipment, techniques, standards, accuracy, and reporting may not be available to support US receiving organization measurement requirements or may require technical assistance or even re-analysis of samples in the US. SOGIN/EUREX did not initially have an instrument for uranium isotope, Pu, and TRU analysis. A newly procured inductively-coupled plasma mass spectrometer (ICP-MS) was calibrated and used to characterize the UNH and oxide product materials.

Fig 6. New inductively-coupled mass spectrometer (IPC/MS) installation

Detailed involvement in calculations performed at indigenous laboratories is necessary to ensure accurate reporting of results. Technicians' and engineers' skills may be not be well exercised or they may be unfamiliar with the required methods. US SME cross-checks of material balance and laboratory analysis calculations revealed some errors that were corrected to resolve apparent discrepancies in mass balance that were then solved.

As mentioned above, the inadequate blending accomplished in the interim storage cans was a significant source of sampling error due to undesirable variability in sampling the material and analysis sample preparation issues caused by the large lumps of oxide product from mixed batches of source material.

Samples that were representative of the material in each of the shipping cans were collected and packaged for shipment to the US to permit validation of the analytical results without opening the shipping cans upon arrival in the US. The samples were packaged in plastic vials in a separate shipping can to facilitate handling.

4.6. Personnel and Training

The availability of qualified indigenous personnel necessary to perform the operations may be limited. This may require adjustment of the processing schedule and/or requests for additional personnel from other functional areas or even other sites. In this case, additional personnel were brought in from another facility to fully staff the operation.

The care and attention to detail was evident in the way the operating technicians performed the operations. They were also very open to constructive suggestions that improved quantitative transfers of the uranium materials and minimized losses to waste.

4.7. Packaging and Shipment

In past removal projects, the indigenous staff only had authority over the operations up to the point of shipping container loading with final shipping container loading governed by US/GTRI procedures. Full cognizance and approval was required by both ISPRA and SOGIN throughout the entire container loading process, including oversight of leak testing of the shipping containers. Even if the cask loading activities were performed under DOE Y-12 responsibility, the Italian Regulatory Authority required that the container loading procedures be written in Italian in the local format and that the loading activities be tracked according to those procedures by plant supervisor. Minor unanticipated events occurred during the aggressive project time line, were promptly solved with the agreement of the Regulatory Authority (ISPRA). Careful inspection of items provided in the ES-3100 “toolbox” is necessary prior to shipment to ensure that all of the toolbox items are present and meet their intended use expectations. During preparation for packaging of the RANA fuel element (Material Test Reactor plate type) it was discovered that the aluminum tape provided in the toolbox was not useable. A work-around was implemented that used the stainless steel zip-ties that were included in the toolbox.

5. Summary and Conclusions

Successful international projects that involve complex material handling, processing and shipment activities require considerable planning and care in execution. Collaboration, participation and communication are essential to ensure that physical facilities and equipment are prepared properly, procedures are clearly written, personnel are available, trained and qualified and that materials are properly characterized to meet both shipping and receiver organization acceptance criteria. Specific lessons learned were collected as a result of this successful conversion of highly enriched uranium in solution form to a solid form suitable for shipment and storage.

Back-end of Fuel Cycle

6 YEARS OPERATION OF THE NCS 45 PACKAGE FOR IRRADIATED FUEL RODS

PIERRE LEFEBVRE, FRANZ HILBERT

Nuclear Cargo + Service GmbH (DAHER-NCS)
Design and Technology Department, Service irradiated materials unit
Rodenbacher Chaussee 6, 63457 Hanau-Germany

ABSTRACT

The type B(U)F-96 packaging NCS 45, which is until now mostly dedicated to the transport of irradiated fuel rods (defect and/or intact), was approved in the country of origin “Germany” end of 2008, some seven years after the application for package approval.

The presentation at hand will show the “highlights” of the first 6 years of operation in nuclear power plants and in hot cells and the flexibility of the NCS 45 for adaptation to any nuclear facility.

The first step after approval was its validation in further countries. In some countries the validation process is a relatively fast and administrative process, whereas in other countries, extensive reviews are carried out. The presentation will give a short summary of procedures and questions asked.

The next step was, in parallel, the analysis of each site specific interfaces and requirements in order to receive the NCS 45 cask (it concerns for example the development of a specific earthquake safety frame for loading pool and a basket with specific rolling system to handle it easily in hot cells), and the introduction of the packaging into the operations handbooks of the respective nuclear sites. In general, a site specific handling instruction comprising a detailed step by step plan must be written by DAHER-NCS, checked by the nuclear site and – at least in Germany – double checked by the supervising expert organization of the nuclear site. The presentation will show schematically the evolution of the handling procedure of the licensed package in respect of the site specific handling procedures.

DAHER-NCS has developed and qualified a new technology which makes it possible to encapsulate defect fuel rods (uranium, MOX, high burn-up etc.) by using a “underwater brazing device”. This technical evolution is already included as a content in the package approval Rev.2 of the NCS 45.

Finally, the presentation will give a summary of the transports carried out so far, the short- term planned transports as well as the future needs and developments such as NCS15 (1,5 m usable inner length).

1. Introduction

1.1 Design of NCS45

The packaging NCS 45 is primarily designed for the transport of irradiated fuel rods for Post Irradiation Examinations (PIE) between Nuclear Power Plants (NNPs) and Hotlabs. The main design principles are:

- **Safety:**
  The package NCS 45 was designed and tested according to the IAEA 96-Regulations and is licensed as a type B(U)F-96 package.

- **Quality:**
  QA measures during design, manufacturing and operation comply with the high requirements of the German Competent Authority. Independent witnessing by an expert assigned by the Authority is mandatory in Germany.
- **Easy to use:**
  The packaging NCS 45 was designed for loading and unloading under water in a NPP's pool and in dry conditions attached to a Hot Cell. The orientation of the packaging during loading/unloading can be vertical or horizontal. Tools which come with the package allow handling in all worldwide relevant nuclear facilities.
- **Easy to transport:**
  The NCS 45 is transported in a tailor-made 22' IP-2 container for easy tie-down to transport means and transfer between transport means and facilities. The gross weight of the transport unit consisting of package, container and truck is well below 40 tons.

Fig. 1 shows the main design features. The packaging body is a sandwich design of stainless steel sheet encasing a thick layer of lead. On both sides the packaging body is closed by bolted plugs which accommodate on one end the rotary plug mechanism and on the other end the push plug mechanism. These plugs are only removed for maintenance purposes and allow easy access in case of necessary repairs. For loading and unloading only small lids need to be operated which can be handled manually.

The packaging is equipped with two trunnions on each end which are designed and licensed for vertical handling (two trunnions) and horizontal handling (four trunnions) in nuclear facilities. Shock absorbers are attached to each end of the packaging during transport to ensure the ability to withstand accident conditions of transport.

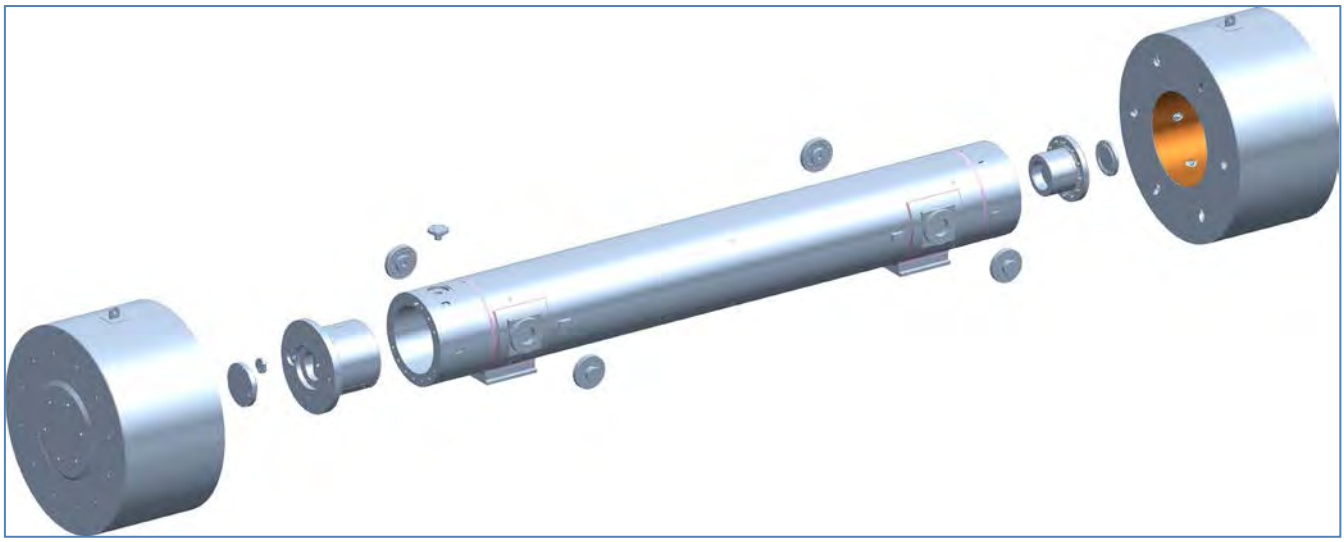

Fig 1: The NCS 45 packaging design

1.2 Licensing of the NCS45 packaging

The country of origin for the certificate of packaging approval is Germany. The first license was issued by the German Competent Authority end of 2008. Currently, Rev. 2 of the certificate is valid and will expire in August 2015. Rev.3, which should include a specific customer quiver in addition to the already approved contents given in Rev. 2, is planned to be obtained at the latest in August 2015.

The content description of Rev. 0 of the certificate comprised mainly UOX fuel in a rather general specification. It allowed enrichment up to 7 wt.% U-235, burn-up values up to 120 GWd/MgU and cooling times as short as 120 days. With Rev. 1 only a geometrical variation of fuel with 7 wt.% enrichment in U-235 was added to enable the transport of rather old fuel of the German Otto Hahn research vessel from Germany to France. Rev. 2 extended the content description to MOX fuel with the same burn-up and cooling time values as for UOX fuel. The encapsulation technology to encapsulate fuel rods under water patented by DAHER-NCS [3] was also included in Rev. 2 of the approval.

Rev. 0/1 of the certificate was validated in Denmark, France, Spain, Sweden, Switzerland, UK and USA. Rev. 2 is validated in Denmark, France, Spain, Sweden, Switzerland. Revalidations of Rev. 2 in UK and the USA were not applied for because of economic reasons. Whilst the validations in Denmark, Spain, Sweden, Switzerland and UK went rather smoothly, the validation processes in France and the USA took a lot of effort to come to a successful completion.

Although the Competent Authority in France had been informed from an early stage about all relevant issues of the licensing procedure in Germany and contributed to the drop trial/test program, during the validation procedure many requests for additional information were raised. These requests for additional information were not only restricted to the criticality safety proof but also to all other safety aspects of the type B(U) package design for fissile material. The validation procedure could be completed after more than one year; however, only a partial validation covering about 50% of the content description of the original certificate could be achieved. It should be mentioned here that France and Germany are both ADR Member States and RAM transport is hence regulated by the same dangerous goods code.

Validation of the NCS 45 certificate of package approval in the USA required considerable effort because all European and International standards used for materials, manufacturing and safety analysis had to be translated to US standards. Furthermore, some concepts used for the specification of the content in the German certificate were at that time not considered to be adequate by the US Competent Authority. E. g., the source term based formula specified in the German certificate for the proof that the dose rate limits are met had to be replaced by a definite specification of no. of fuel rods, burn-up and cooling time. As result, the content description in the US validation is to a large extent different to the one given in the German original certificate.

1.3 Site specific procedures and cold trials/tests

In order to be able to use the NCS 45 packaging in nuclear facilities following steps were necessary

- Development of site specific handling procedures.
- Adaptation of handling tools to comply with site specific requirements.
- Acceptance of the safety case by the site authority.
- Cold trial/test.
- Acceptance of the cold trial/test by the site authority.

Development of site specific handling procedures

The handling procedure referenced in the German certificate of package approval specifies a framework of handling steps required to ensure that the package complies with the requirements of the certificate. In the site specific handling procedures this framework is completed with the handling steps and provisions required to ensure safe handling and

operation inside the nuclear facility. Tab. 1 shows schematically the evolution of the package specific step by step plan into a site specific step by step plan.

An important part of the site specific handling procedure is the definition of responsibilities and interfaces between the different parties present during handling. The document is as well used to document the execution of the individual steps by each of the responsible functional units named for the respective step and to record items for possible improvements.

Step by step handling instruction			
Package specific		**Site specific**	
Step no.	**Description**	**Step no.**	**Description**
X	Drying of the cavity of the packaging according to procedure no. 4711	Y	Connect vacuum pump type 123 to connection A of the packaging and connect the air outlet to the site ventilation system
		Y + 1	Start the pump and set up a vacuum of not less than ZZ hPa
		Y + 2	Check the dryness of the cavity according to checklist procedure no. 4711
		Y + 3	Disconnect the vacuum pump type 123 and check the interfaces for contamination

Tab 1: Evolution of the packaging specific to sites specific handling instructions (example)

Adaptation of handling tools to comply with site specific requirements

The NCS 45 packaging comes with a comprehensive set of handling tools which interface with the nuclear facility

- Handling tools for horizontal lifting.
- Tie-bar with telescopic tabs for handling in the fuel assembly pool.
- Gripper for handling of the baskets.
- Support plates and earthquake fixations.
- Transport and tilting frames.

Fig 2: The NCS 45 equipped with its earthquake safety equipment in a NPP (2015)

Fig 3: The NCS 45 with its earthquake safety equipment, tilting frames and telescopic tabs in a NPP (2015)

The interface between the lifting tools and the facility is rather simple – the crane hook – so that rarely adaptations are necessary. Adaptations of the gripper are necessary if non-standard baskets are to be used. The safety of the support plates and the earthquake fixations must be checked against the design earthquake spectra of the facility and, if necessary, adapted. And finally, transport and tilting frames must be fitted to internal transport means and handling positions of the facility.

Acceptance of the safety case by the site authority

In Germany, all nuclear sites are regulated by the ministry of environment of the respective federal state where the site is located. Independent expert organizations (e. g. TUEV) are assigned by the ministry to give expert advice concerning the operation of the facilities. The safety case consisting of the handling procedures, safety proof of the tools, loading plan and related documents must be submitted to the expert organization responsible for the respective site and must be released by this expert organization before the cold trial/test can be carried out.

Cold trial/test

In general, a cold trial/test is required in all nuclear facilities before the NCS 45 can be handled and loaded with fuel. The cold trial/test is supposed to prove that the site specific handling procedure covers all necessary steps and that all responsibilities and interfaces are specified. For that, the complete step by step plan is processed except for the loading of fuel into the packaging. The documentation of inconsistencies and/or possibilities for improvement is used to amend the handling procedure accordingly.

Acceptance of cold trial/test by the site authority

The last step of the qualification of the NCS 45 for the use in a nuclear facility is the acceptance of the handling procedures and of the cold trial/test by the expert organization responsible for the respective site and the regulator.

2. Overview about 6 years of operation

NCS 45 packaging series no. 1 was commissioned in 08/2009, series no. 2 in 08/2011. Fig. 4 shows the number of fuel transports, cold trials/tests in the years 2009-2014.

In the first three years of operation, only one fuel transport from Germany to France was carried out, but cold trial/test in 6 different nuclear facilities were performed. In 2012 and 2013 fuel transports increased considerably and cold trials/tests were carried out in 5 further nuclear facilities.

Despite the nuclear crisis, which took place the last years,

- 4 transports of normal, defect and/or high burn up fuel rods between 1 NPP and 1 hotlab and between 2 hotlabs have been performed in 2014,
- 2015 and 2016 scheduled transports campaigns have been prepared
- And feasibility studies have been done.

It clearly stresses that the NCS45 packaging is a worldwide recognized and easy transport solution for NPPs and hotlabs.

In 2012 and 2014 the first 3 years periodical recertifications of, respectively, the NCS 45 series no. 1 and series no. 2 were carried out successfully. The recertification consisted of visual inspections, dye penetration tests of welding seams, dimensional checks of bolts and threads and leakage tests. There were no deviations from the requirements of the certificate of package approval.

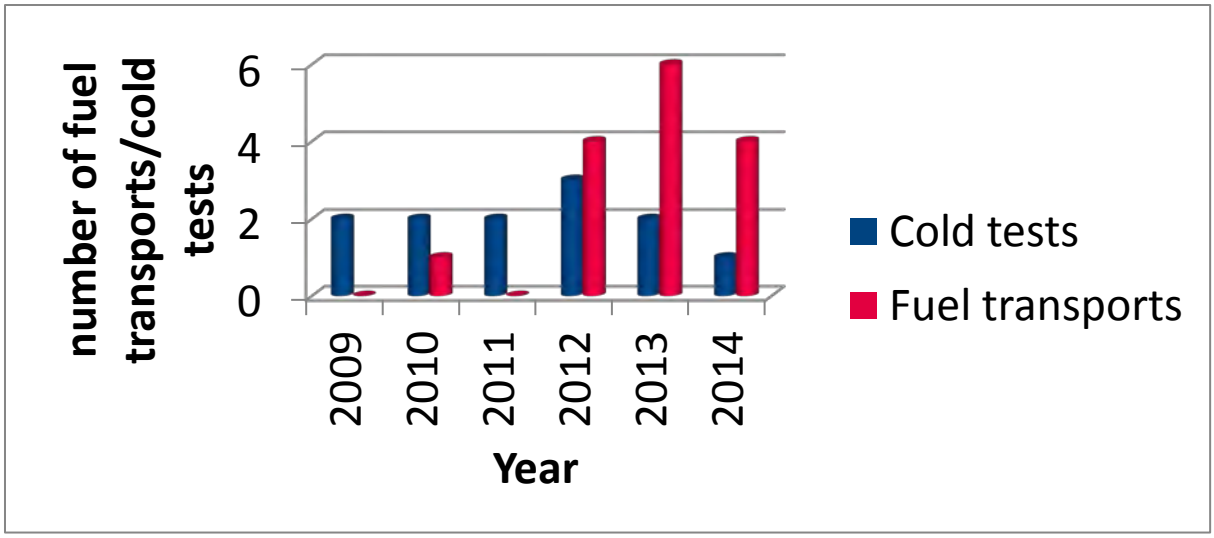

Fig 4: Number of fuel transports and cold trial/trials/tests with the NCS 45 in the years 2009-2014

3. Underwater Brazing Equipment

To investigate a fuel rods with high and very high burn-up or a larger number[1] of defective fuel rods it is necessary to transport these rods, for example to a hotlab. Because of the unknown conditions of the fuel rods, they have to be encapsulated in leak tight conditions for a safe transport. Currently this encapsulation process is possible in dry conditions (in a hot cell) by a welding process, but there was no solution to produce such a capsule under water several years ago.

During the last four years the development of an Underwater Brazing Equipment (UBE) was undertaken by DAHER-NCS. Based on the positive results of the smaller model successfully used for the qualification tests, a full size prototype was designed and manufactured. This prototype was tested in dry conditions as well as under water. The brazed capsules show reproducible results for both conditions and independent of the dimensions. The correctness of the brazing is controlled by temperature and power measurements during the brazing, conducted with visual controls with underwater cameras. After the brazing an integral helium leakage test is carried out on the capsule in a special testing chamber, which is part of the UBE. Helium leakage rates which are well below the requirements for the transport can easily be achieved.

The design of the UBE allows very flexible and different ways how to place the UBE in the pool of a nuclear facility. The following figures show different options how to put the UBE in the pool. The first solution used for the operation test in a pool was a hanging construction fixed at the balustrade of the pool. This solution allows the operation in conditions that are independent of the floor of the pool. Furthermore it has advantages concerning the tipping, buckling or earth quake aspects. So it is possible to use a light construction in this way.

The second solution was developed for a NPP in Germany, where the last qualification cold handling trial is scheduled in 2015. Here the UBE is put on the ground. Four independent feet allow the adjustment in case of unevenness of the floor. This rack has to be designed stronger (meaning it has a bigger mass) due to mechanical aspects but allows a very quick positioning of the UBE in the plant. Furthermore it has advantages regarding the flexibility of the positioning in the pool. Just an area of approximately 1.5 x 1.5 m is required, but no wall of the pool, special attachment points etc.

[1] The NCS 45 package is licensed to carry small quantities of defective fuel rods without encapsulation!

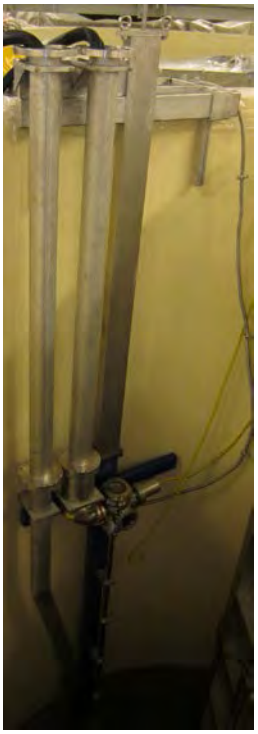

Fig 5: UBE hanging at wall of pool (before filling with water)

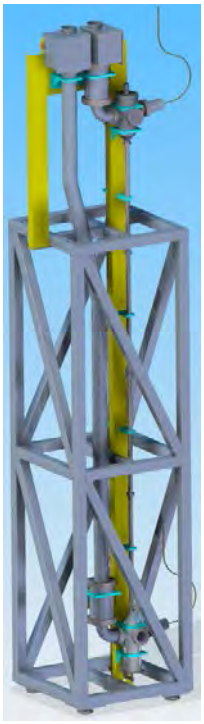

Fig 6: UBE in standing rack will be used for cold handling trial in 2015

4. Conclusion

NCS 45 type B(U)F package

In the 6 years of operation the NCS 45 package proved to be a safe and reliable transport solution for the transport of irradiated standard, defect and/or high burn up fuel rods.

In 2015, the 6 years periodical recertification of the NCS45 series no. 1, which includes the same controls as for the 3 years periodical recertifications and additional over-load tests on the trunnions, will be performed.

Considering DAHER-NCS huge experience with loading, unloading and handling casks in hotlabs (R52, NCS45), the 9 different contents already accepted in the agreement of the NCS45 cask and the hotlabs' increasing needs to transport small amounts of radioactive materials around the world DAHER-NCS can propose a shorter version of the NCS45: the NCS 15 which has an inside cavity's length of 1,5m.

Due to the fact that the safety report already exists for the NCS 45 version and that all the BAM (Federal Institute for Materials Research and Testing) released handling instructions are applicable for packagings which are structurally identical but with different usable lengths, the NCS 15 cask can be at customer disposition relatively fast (between 1 and 2 years).

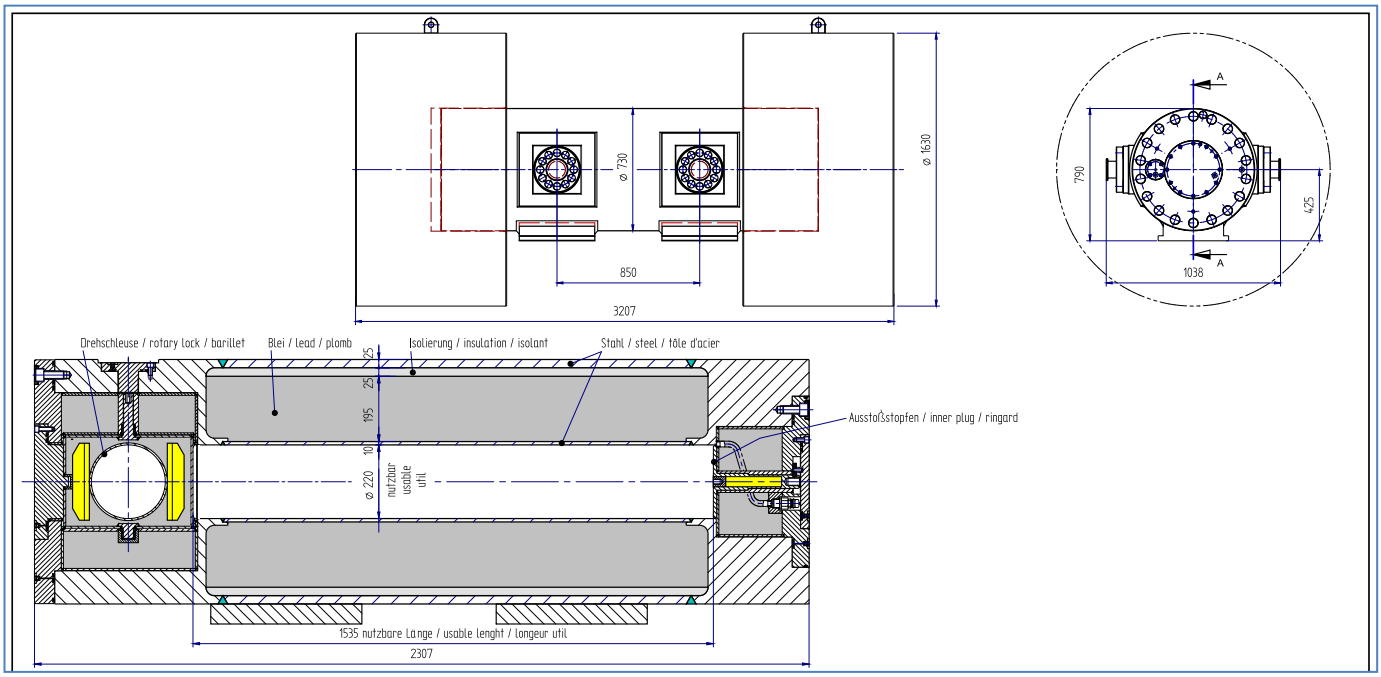

Fig 7: Drawing of the NCS 15 cask

Underwater Brazing Equipment

The development of the UBE should be finished this year. The next milestone will be the first operation in a German NPP. The corresponding cold handling trial is scheduled for summer this year, the first capsulation of fuel rods should follow during 2015 in the same power plant and the fuel rods will be transported to a hotlab in Sweden.

As soon as the final cold trials are finished and the results released by the BAM the following quantities of fuel rods will be first encapsulated and transported with the NCS 45 in Germany.

- 20 “standard” defective fuel rods
- 2 “MOX” defective fuel rods
- 10 high burn-up fuel rods

Thanks to the combination of DAHER-NCS long know-how on the challenging transport of standard and defective fuel rods and the 2 following main advantages of the UBE, which are:

- the removal of all the water present between the fuel rod and the internal diameter of the capsule thanks to its specific drying process,
- and the modularity and the robustness of the UBE to work under water in any type of reactor pools,

DAHER-NCS is, on the one hand, already studying the possibility to adapt the UBE in order to detect the presence of water in a defective fuel rod and dry it and, on the other hand, is discussing with different NPPs to adapt the UBE in order to perform different types of inspections on potential defective fuel rods like, for example, the measurement of the free volume in the plenum.

DAHER-NCS is in position to propose a solid approach for drying trials on defined representative defect fuel rods using the existing UBE (with some adaptations); the trials will:

1. First demonstrate the capacity of the adapted UBE to detect and dry dummy defective fuel rods.
2. Then to define a maximum quantity of water that remains in the defective fuel rod.
3. In parallel the demonstration that the over canning can withstand the effects of radiolysis of the maximum remaining water after the drying process.
4. The demonstration that the modified UBE will ensure a qualified brazing encapsulation of the dried fuel rods.

References

[1] W. Bergmann, F. Hilbert, The NCS 45 Cask Family: an Updated Design Replaces an Old Design – Lessons Learned during Design, Trial/testing and Licensing, PATRAM 2004

[2] F. Hilbert, W.Bergmann, 5 years operation of the NCS 45 package for irradiated fuel rods, PATRAM 2013

[3] S. Stanke, F. Hilbert, Encapsulation of Fuel Rods for Transport, PATRAM 2010

[4] T.Breuer, F.Hilbert, Qualification of the DAHER-NCS fuel rod encapsulation Process for transport and storage, PATRAM 2013.

COATINGS TO PROTECT SPENT ALUMINIUM-CLAD RESEARCH REACTOR FUEL DURING WET STORAGE

S.M.C.FERNANDES, O.V.CORREA, J.A.DE SOUZA, L.V.RAMANATHAN,
Materials Science and Technology Center,
Instituto de Pesquisas Energéticas e Nucleares- IPEN
Av. Prof. Lineu Prestes 2242, Cidade Universitaria
05508-000 São Paulo. Brazil.

R. A. ANTUNES
Engineering, Modelling and Applied Social Sciences Center (CECS),
Federal University of ABC, 09210-170, Santo André-SP, Brazil.

M.C.L. DE OLIVEIRA,
Electrocell Ind. Com. Equip. Elet. LTDA, CIETEC, 05508-000 São Paulo-SP, Brazil.

ABSTRACT

Pitting corrosion of the aluminium cladding of spent research reactor (RR) fuels in wet storage has been reported and attributed to synergistic influence of certain water parameters. Hence, use of conversion coatings to protect spent Al-clad RR fuel during long term wet storage was proposed. The objective was to develop a coating using a conventional chemical process as opposed to an electrochemical process due to constraints related to the shape of the fuel and its high radioactivity. In this context hydrotalcite (HTC) and boehmite were considered. This paper presents: (a) preparation of boehmite and hydrotalcite (HTC) coatings from different baths followed by post-coating treatments; (b) corrosion behavior of coated AA 6061 alloy; (c) results of field studies in which uncoated and coated AA 6061 alloy coupons and plates, the latter assembled as a dummy fuel element, were exposed to the IEA-R1 reactor spent fuel basin for periods of up to 14 months. The laboratory tests revealed marked increase in corrosion resistance of HTC coated specimens. In field tests the HTC coated coupons and plates did not reveal any pits. The mechanism of corrosion protection is presented.

1. Introduction

In most countries spent aluminum-clad fuels from research reactors (RRs) are stored in light water filled pools or basins for decades. Despite water quality management programs at the fuel storage sites, pitting corrosion has been reported to be the main form of degradation and this could lead to cladding failure, release of fissile material and radioactive contamination of the storage facilities. The pitting corrosion of the fuel cladding has been attributed to synergism in the effect of some basin water parameters on corrosion of aluminum and its alloys. [1, 2] Hence some form of corrosion protection of spent RR fuel was considered imperative for safe long term wet storage. Conversion coatings are widely used to control the corrosion of a variety of metallic materials in many industries and rare earth compounds have been used to inhibit aqueous corrosion of aluminium alloys. [3] Chemical treatments have been proposed to form

rare earth based conversion coatings on Al alloys. [4-6] The shape of the RR fuel and the radioactivity of spent fuels preclude electrochemical surface treatments. Therefore chemical surface treatment to form a coating is the only option and the use of conversion coatings to protect spent Al-clad RR fuel was proposed in 2007. The results of preliminary laboratory and field investigations carried out at IPEN in Brazil revealed that cerium hydroxide coatings increased the corrosion resistance of Al alloys. [7, 8] These investigations were extended to include boehmite, hydrotalcite (HTC), cerium modified boehmite and cerium modified HTC coatings on Al alloy surfaces. HTC is lithium aluminium-nitrate-hydroxide hydrate and it forms on Al alloys immersed in an appropriate alkaline lithium salt solution. [9-11] The HTC coating imparted marked improvements in pitting corrosion resistance. [12, 13] Further studies were carried out recently to obtain HTC coatings from baths at different temperatures followed by post-treatments.

This paper presents: (a) the preparation and characterization of hydrotalcite coatings from different baths followed by post-coating treatments; (b) the effect of duration of both HTC formation and cerium treatment on corrosion behavior of HTC coated AA 6061 alloy in NaCl; (c) results of field studies in which uncoated, boehmite and HTC coated AA 6061alloy coupons and full size plates were exposed to the IEA-R1 reactor spent fuel basin for different duration.

2. Methods and materials

Aluminium alloy AA 6061 specimens (2 x 2 x 0.2 cm) for the laboratory tests and coupons (10 cm in diameter and 0.3 cm thick) as well as plates (62.4 cm x 7.0 cm) for the field tests were treated to coat their surfaces with either boehmite or HTC, with or without incorporation of cerium in the coating, by immersion in solutions and under conditions shown in Table 1.

Tab 1: Solutions and conditions used to prepare coatings on Al alloys.

Solution	Purpose	Composition of solution and conditions
1	Degrease	25 g/L Na_2SiO_3; 25 g/L Na_2CO_3; 65 °C; 2 min.
2	Deoxidize	10% HNO_3; 3% $NaBrO_3$; 55 °C; 3 min.
3	Form boehmite	Deionized water; 97-100 °C; 5 min.
4	Incorporate Ce in boehmite	0.1% $CeCl_3$; 97 °C; pH 4; 5 min.
5	Form HT-HTC	6.9g/L $LiNO_3$; 28.3 g/L KNO_3; 2.4 g/L LiOH; 0.06 g/L $NaAlO_2$; 98 °C; pH 12; 10 min.
6	Form LT-HTC	0.1M Li_2CO_3; LiOH; Al; pH 12; 15 min; R.T.
7	Incorporate Ce in HTC	10 g/L Ce $(NO_3)_3$; 30% H_2O_2; R.T.; 5 min.
8	Sealing	$MgC_4H_6O_4$; 82 °C; 15 min.

- HT-high temperature; LT-low temperature

The coatings were examined in a field emission scanning electron microscope. The corrosion behavior of uncoated and coated specimens was determined from laboratory tests. In these tests, anodic potentiodynamic polarization measurements were carried out with a conventional 3-electrode arrangement in 0.01 M NaCl, using a saturated calomel reference electrode and a platinum counter electrode. The potential was scanned from - 0.3 V to + 0.5 V at 0.167 mV/s. The effect of duration of both HTC formation and cerium treatment was also examined.

The field test procedure consisted of: (a) preparing uncoated and coated coupons and plates; (b) stacking of the coupons in racks (Figure 1 a); (c) assembling the plates to form a full size dummy fuel element (Figure 1 b); (d) immersion of the racks and the dummy fuel elements in the spent fuel section of the IEA-R1 reactor in IPEN, Brazil, for

different duration; (e) removal of the racks or dummy fuel elements, rinsing and decontamination; (f) disassembly and examination of the coupons and plates with an optical microscope. [1]

(a) (b)

Fig 1. Photographs of: (a) coupons stacked in a rack; (b) plates assembled to form dummy fuel elements.

3. Results and discussion

3.1 Laboratory tests

The morphology of HTC formed from solutions 5 and 6 are shown in Figure 2. The surfaces revealed intersecting blade like HTC crystallites that formed a layer across the surface. The coatings also formed inside the pits and recesses that resulted during pre-treatment of the substrate as shown in Figure 3. Typical HT-HTC coating thickness after 10 minutes of immersion was ~2 μm. A layer of amorphous or nanocrystalline lithium aluminate forms below the outer layer and this was confirmed from the broadened x-ray diffraction peaks. (9)

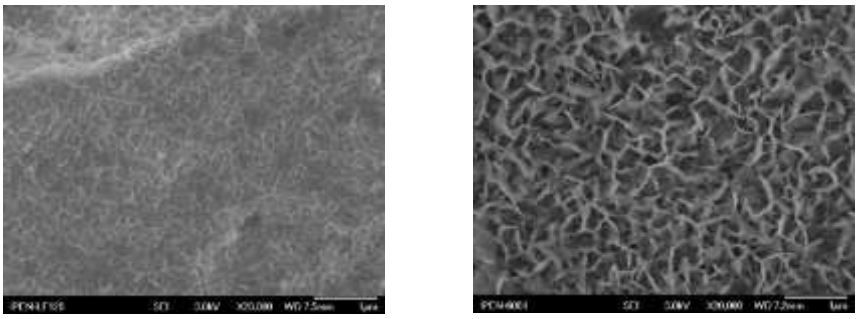

(a) (b)

Fig 2. Scanning electron micrographs of: (a) LT-HTC (b) HT-HTC

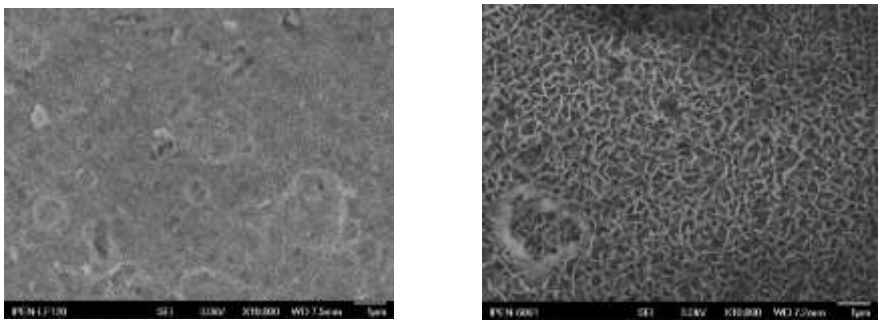

(a) (b)

Fig 3. Scanning electron micrographs revealing HTC formation within pits and crevices: (a) LT-HTC; (b) HT-HTC.

Tab 2: The corrosion potential E_{corr} and corrosion current i_{corr} as determined from the electrochemical polarization curves.

Specimen	i_{corr} ($\mu A.cm^{-2}$)	E_{corr} (V)
Uncoated	1.56	-1.23
Boehmite coated	0.32	-0.54
Boehmite + Ce (S4)	1.75	-0.59
Boehmite + Ce (S7)	1.69	-0.58
HT-HTC	0.35	-0.90
HT-HTC + Ce (S7)	0.26	-0.69
LT-HTC	0.77	-0.62
LT-HTC + Ce (S 7)	0.71	-0.60
HT-HTC + sealed	0.13	-0.63
LT-HTC + sealed	0.99	-0.61

- S4 and S7 are solutions 4 and 7 in Table 1.

The anodic polarization curves of the different specimens in 0.01 M NaCl solution at room temperature were plotted and data extracted from these curves are in Table 2. It is evident that specimens with any type of coating, with or without post treatments were more corrosion resistant as indicated by the shift in their open circuit potentials (OCP) or E_{corr} to more anodic values. The corrosion current densities i_{corr} of the coated specimens were significantly lower than that of the uncoated specimen indicating marked increase in protection rendered by the coatings. The corrosion behavior of boehmite coated specimen deteriorated with incorporation of Ce, due in part to partial corrosion of the boehmite during the Ce treatment and formation of discontinuities. The incorporation of Ce in the HT-HTC or LT-HTC coating reduced its i_{corr}. Sealing improved corrosion resistance of the HT-HTC coating whereas it decreased that of LT-HTC.

Tab 3: Effect of duration of HT-HTC formation on electrochemical parameters of uncoated and coated AA 6061 in 0.01 M NaCl.

Specimen condition	i_{corr} ($\mu A.cm^{-2}$)	E_{corr} (V)
Untreated	1.56	-0.79
HT-HTC (20')	0.35	-0.58
HT-HTC (30')	0.78	-0.57
HT-HTC (60')	0.93	-0.58

Tab 4: Effect of duration of LT-HTC formation on electrochemical parameters of uncoated and coated AA 6061 in 0.01 M NaCl.

Specimen condition	i_{corr} ($\mu A.cm^{-2}$)	E_{corr} (V)
Untreated	1.56	-0.79
LT-HTC (20')	0.77	-0.59
LT-HTC (30')	0.46	-0.59
LT-HTC (60')	0.72	-0.60

The effect of duration of treatment in the solutions to form LT-HTC and HT-HTC on electrochemical parameters revealed that the E_{corr} remained unchanged but the I_{corr} increased slightly with increase in duration of HT-HTC treatment and without any significant change in the duration of LT-HTC treatment, as shown in Tables 3 and 4.

The corrosion current density of specimens coated with HT-HTC and further treated to incorporate Ce did not vary significantly with increase in duration of treatment in S4 as shown in Table 5. However i_{corr} of specimens coated with LT-HTC and further treated in S7 to incorporate Ce showed a decrease with increase in time of treatment. Overall the i_{corr} of the cerium incorporated HT-HTC coated specimens was significantly lower, compared with specimens that were coated with cerium incorporated LT-HTC.

Tab 5: The electrochemical parameters of specimens coated with cerium incorporated HT-HTC and LT-HTC. Effect of duration of cerium treatment in solutions S4 and S7 of Table 1.

Surface condition	i_{corr} ($\mu A.cm^{-2}$)	E_{corr} (V)
HT-HTC + Ce (S4 - 5 min.)	0.26	-0.60
HT-HTC + Ce (S4 - 10 min)	0.12	-0.59
HT-HTC + Ce (S4 - 15 min)	0.37	-0.59
LT-HTC + Ce (S7 - 5 min)	0.96	-0.58
LT-HTC + Ce (S7 - 10 min)	0.78	-0.56
LT-HTC + Ce (S7 - 15 min)	0.71	-0.58

3.2. Coupons and plates exposed to IEA-R1 reactor spent fuel section.

Examination of the coupons after exposure to the spent fuel section was done with an optical microscope. The top surface of the untreated coupons revealed more pits compared to the bottom facing surface of the same coupon, indicating the influence of settled solids on the top surfaces. The main features of the coupons exposed for 3 and 5 months to IEA-R1 spent fuel basin, compared with those prior to exposure are summarized in Table 6. After 3 months of exposure the LT-HTC coated coupon revealed no pits but after 5 months, it revealed pits even with post treatments. The HT-HTC coated coupons did not reveal any pits even after 5 months exposure. On the basis of these observations the full-size plates were coated with HT-HTC and not LT-HTC.

Tab 6: Coupon surface features compared to those observed prior to exposure to the IEA-R1 research reactor spent fuel section.

Coating	Surface features after exposure for	
	3 months	5 months
None	Many pits	Stained + one pit
Boehmite	No difference	Many tiny pits
Boehmite + Ce	No difference	Few pits
HT-HTC	No difference	No difference
HT-HTC + Ce	No difference	No difference
HT-HTC + sealed	No difference	No difference
HT-HTC + Ce + sealed	No difference	No difference
LT-HTC	No difference	Dark + some pits
LT-HTC + Ce	No difference	Dark + some pits
LT-HTC + sealed	No difference	Very dark + one pit
LT-HTC + Ce + sealed	No difference	Very dark, two pits

(a) (b)

Fig 4. Photographs of full-size plate surfaces. (a) Boehmite coated and (b) HTC coated. The plates above the identification mark were exposed for 8 months and the plates below, for 14 months.

Figure 4 shows photographs of the uncoated and coated plates exposed to the IEA-R1 reactor spent fuel section. The plates stained to different extent, depending on the duration of exposure and the nature of surface treatment. The HTC coated plates were stained very dark compared with the boehmite coated and the uncoated plates. These plates however did not reveal pits. All these plates were examined visually and with an optical microscope and the main surface features are summarized in Table 7.

Tab 7: Surface features on untreated and treated AA 6061 plates exposed to the IEA-R1 reactor's spent fuel section for 8 and 14 months.

Surface treatment	Plate surface features			
	After 8 months		After 14 months	
	Side - A	Side - B	Side - A	Side - B
Untreated	11 pits surface dark.	5 pits, surface dark.	10 pits, surface dark.	No pits, surface dark.
Boehmite	No pits, surface very dark.	1 pit, surface very dark.	4 pits, stained.	6 pits, stained.
Boehmite + Ce	No pits, surface white.	7 pits, dark stain in center.	No pits, Grey stain.	No pits, stained.
Boehmite + Ce + sealed	No pits, surface oxide layer.	5 pits, dark stain in center	1 pit, surface stained.	4 pits, surface stained.
HTC	**No pits**, dark surface.	**No pits**, dark surface.	**No pits**, very dark surface.	**No pits**, dark surface.
HTC + Ce	8 pits at lower end.	8 pits at lower end.	**No pits**, stained.	**No pits**, stained.
HTC + Ce + sealed	**No pits**.	**No pits**.	**No pits**.	**No pits**.

The uncoated plate exposed for 14 months was more stained than that exposed for 8 months. The boehmite coated plates, with or without cerium treatment and/or sealing, were stained to the same extent after 8 and 14 months. The HTC coated plates

exposed for 8 and 14 months were heavily stained. The HTC + Ce coated plates did not reveal stains after 8 months but were slightly stained after 14 months. The plates that were HTC coated, cerium treated and sealed did not reveal any stains or pits after 8 and 14 months, indicating marked increase in the corrosion resistance imparted by the HTC coating followed by cerium incorporation and sealing.

4. General discussion

The laboratory and field tests have indicated a marked increase in corrosion resistance of Al alloys coated with HT-HTC. The corrosion resistance was further enhanced by cerium incorporation in the coating. Cerium was chosen to enhance corrosion protection as it is the only rare earth (besides europium) that can involve a change in oxidation state and form a water insoluble hydroxide/oxide on Al. The faint yellow coating obtained upon immersion of the HTC coated plate in the cerium solution is constituted of an insoluble cerium hydroxide/oxide. [3, 14, 15] Progressive loss of the yellow color with time has been observed and attributed to the hydroxide transforming to oxide [16], or surface degradation of the surface peroxide containing species. Sealing of the coatings with magnesium acetate improved the pitting corrosion resistance of specimens coated with HT and LT-HTC. In the context of eventually protecting spent Al-clad RR fuels during long term wet storage, the coating process for irradiated fuels would be facilitated if treatments were to be carried out at room temperature. At present the extent to which LT-HTC imparts protection is lower than that imparted by HT-HTC and attempts are in progress to increase the LT-HTC layer thickness to increase its protection efficiency. Nonetheless, protecting spent fuel with cerium incorporated HTC coatings is the obvious choice. The HTC layer imparts pitting corrosion protection by acting as a physical barrier between the solution and the surface. The higher corrosion resistance of the Al surface with cerium in the HTC coating could be also attributed to coarsening of the HTC crystallites during cerium treatment at 98 °C and also during the long term exposure to the spent fuel basin, which is akin to a hydrothermal treatment. The mechanism by which the cerium in the HTC imparts protection is considered to be ‘active corrosion protection’, analogous to chromium coatings. According to this mechanism, the lower solubility of $CeO_2.2H_2O$ allows the formation of $Ce(OH)_2^{2+}$ ions in solution which then diffuse to defects in the coating that have exposed bare metal. When in contact with the bare metal, these ions reduce to Ce^{3+} and precipitate as $Ce(OH)_3$ and thus seal the layer. Basically, this involves release of Ce ions from the coating, transport of Ce ions through the solution and its action at defect sites to stifle corrosion. It has been speculated that if a Ce^{4+} bearing inorganic coating contacts a solution, soluble Ce^{4+} is released into the solution. When these ions encounter reducing conditions, like those associated with exposed bare metal at coating defects, it reduces to Ce^{3+}, which forms an insoluble hydroxide and precipitates. The precipitated cerium hydroxide at the defect then stifles further corrosion. Another reason that can be attributed for the increased protection given by the HT-HTC +Ce compared with that given by LT-HTC + Ce is the availability of more cerium in the former, caused by treatment in a high temperature solution as opposed to treatment of LT-HTC coated specimen in a room temperature cerium solution.

5. Conclusions

1. Hydrotalcite (HTC) coatings on AA 6061 alloy were prepared from nitrate baths at 98 °C and carbonate baths at room temperature.
2. HT-HTC coating increased pitting resistance of the alloy more than LT-HTC coating
3. Cerium incorporation in the HT-HTC and boehmite coating increased pitting resistance of the alloy.
4. The corrosion resistance of HT-HTC coated specimens did not increase with increase in duration of HTC formation or cerium treatment.

5. Sealing of LT-HTC coatings increased pitting corrosion resistance of the alloy.
6. Coupons and full size plates coated with HT-HTC and exposed to the IEA-R1 reactor spent fuel section for periods of up to 14 months did not reveal any pits, indicating marked potential for use of HT-HTC as a protective coating on spent RR fuel during long term wet storage.

6. References

1. Corrosion of Research Reactor Aluminium Clad Spent Fuel in Water", IAEA - TRS 418, 2003.
2. L.V. Ramanathan, R. Haddad, P. Adelfang and I. Ritchie, Corrosion of Spent Aluminium-clad Research Reactor Fuel – Synergism in the Role of Storage Basin Water Parameters, Proceedings of 12th International topical meeting on Research Reactor Fuel Management (RRFM), Hamburg, Germany, 2008.
3. B.R.W. Hinton, D.R. Arnott and N.E. Ryan, Mater. Forum 9, 162, 1986.
4. D.R. Arnott, N.E. Ryan, B.R.W. Hinton, B.A. Sexton and A.E. Hughes, Appl. Surf. Sci., 22/23, 236, 1985.
5. M. Dabalà, L. Armelao, A. Buchberger and I. Calliari. Appl. Surf. Sci., 172, 132, 2001.
6. A.E. Hughes, S.G. Hardin, K.W. Wittel, P. R. Miller, in the Proceedings of the NACE meeting: Corrosion/2000, Research topical Symposium: Surface Conversion of Aluminum and Aluminum alloys for Corrosion Protection, Orlando, USA, 2000.
7. S.M.C.Fernandes, O.V.Correa, J.A.de Souza and L.V.Ramanathan, Lanthanide based conversion coatings for long term wet storage of aluminium-clad spent fuel, Proceedings of 14th International topical meeting on Research Reactor Fuel Management, Marrakech, Morroco, 2010.
8. S.M.C. Fernandes, O.V. Correa, J.A.de Souza and L.V. Ramanathan, A coating to protect spent aluminium-clad research reactor fuel assemblies during extended wet storage, Proceedings of 13th International Topical meeting on Research Reactor Fuel Management, Rome, Italy, 2011.
9. R.G.Buchheit, M.D.Bode and G.E.Soner, Corrosion, 50, 3, 205, 1994.
10. C.A.Drewien, M.O.Eatough, T.R.tallant, C.R.Hills and R.G.Buchheit, J.Mater. Res., 11, 1507, 1996.
11. W. Zhang and R.G.Buchheit, Corrosion, vol.58, 7, 591, 2002.
12. S.M.C. Fernandes, O.V. Correa, J.A.de Souza and L.V. Ramanathan, Coatings for increased corrosion resistance of aluminium-clad spent fuel in wet storage, Transactions of European Research Reactor conference, (RRFM), Prague, Czech Republic, 2012.
13. S.M.C. Fernandes, O.V. Correa, J.A.de Souza, R.A. Antunes, M.C.L. Oliveira and L.V. Ramanathan, Conversion coatings to protect Al-clad spent fuel in wet storage, Transactions of European Research Reactor Conference, Saint Petersburg, Russian Federation, 2013.
14. D.R.Arnott, B.R.W Hinton and N.E.Ryan, Mat. Performance, 26 (8), 42, 1987.
15. D.R.Arnott, B.R.W Hinton and N.E.Ryan, Corrosion, 45 (1), 12, 1989.
16. F.H.Scholes, C.Soste, A.E.Hughes, S.G.hardin, P.R.Curtis, Appl. Surf. Sci., 253, (4), 1770, 2006.

IAEA CRP ON "OPTIONS AND TECHNOLOGIES FOR MANAGING THE BACK END OF THE RESEARCH REACTOR NUCLEAR FUEL CYCLE" CURRENT STATUS

F.M. MARSHALL, C. AMES, S. GOUZY-PORTAIX, S.J. MAYER
Department of Nuclear Energy
International Atomic Energy Agency, Vienna International Centre, P.O. Box 100
1400 Vienna, Austria

ABSTRACT

The International Atomic Energy Agency (IAEA) initiated a Coordinated Research Project (CRP) to review and summarise the options and technologies available for managing the back end of the research reactor (RR) nuclear fuel cycle, and to raise awareness among project participants on the irrevocable waste management responsibilities associated with the operation of a RR, in particular as pertaining to RR spent nuclear fuel (SNF). The focus of this CRP is on matching SNF management options to the capabilities of countries with RRs, and on informing Member States about the competences needed to effectively manage RRSNF. The need for a comprehensive methodology for RRSNF management decisions has been highlighted in several prior IAEA workshops and reports. The work to be performed will focus on three areas. First, past work will be reviewed to identify a comprehensive set of short and long term fuel management strategies for RRs. Then, economic, technological, and infrastructural requirements for implementing each strategy will be defined. Finally, any specific needs for future developments, for example pertaining to safe and sustainable disposal options adapted for the resulting, comparatively small inventories of intermediate or high-level waste, will be specified.

IAEA hosted a meeting in July 2014 to discuss the CRP, specifically to develop the preliminary structure of the cost model, identify the data that need to be collected from participating countries, and determine how some of the qualitative information can be represented in a quantitative model that compares diverse technologies. The primary end result of the project is expected to be an IAEA Technical Report Series document and the software for cost analysis. Additional outputs are contributing country reports presenting individual spent fuel strategies, and regional workshops to ensure that Member States are aware of the information developed via this CRP.

1. Introduction

The International Atomic Energy Agency (IAEA) maintains information about research reactors (RRs) in the RR Database (RRDB). According to the RRDB, there are currently 284 RRs operational, temporarily shut down, under construction, or planned. For each of these reactors, there should be a strategy for managing the spent nuclear fuel (SNF), either at the final decommissioning, or on an ongoing basis during the operating life of the facility. For most of these reactors, however, there has not been a strategy developed, in many cases because the ultimate disposal options are not known or fully understood. Additionally, according to the RRDB, there are 481 RRs that are shut down and/or decommissioned that still have fuel stored at the facility, typically in wet pool storage, many of them with no specific plan for ultimate treatment or disposal of the fuel. In order to assist Member States (MS) in their strategy development and spent fuel management decisions, IAEA has initiated a Coordinated Research Project (CRP). The CRP participants will collect information about the RR spent fuel management options, and raise awareness to RR owner and managing organizations about their irrevocable waste management responsibilities associated with RR operation.

Presently many countries lack an effective long term policy for managing the back end of the RR nuclear fuel cycle. A methodical review of technology options and policy issues for RRSNF management is needed. The review should focus on matching options to available skill sets, resource levels, and other country-specific factors. It should be especially sensitive to the unique position of countries that are building, planning to build, or have recently completed their first or only research reactor.

One of the challenges with RR spent fuel strategy is the diversity, as well as the small quantity, of the RR spent fuel. The range of RR designs, coolant types, and core geometries is accompanied by wide variation in the type, size, design and composition of RR fuel. Plates or cylinders of uranium-aluminum alloy (U-Al) clad with pure aluminum are very common, as are pins of steel-clad U-ZrH, although U_3Si_2-Al - uranium silicide dispersed in aluminum - is more common in low enriched uranium (LEU) fuel. The RRDB shows that the research reactors' power outputs span seven orders of magnitude, ranging from 1×10^{-5} MW to greater than 100 MW. According to the RRDB, the combined total thermal power of all the existing RRs amounts to just over 3000 MW. This is approximately the same thermal power output as that of one commercial nuclear power plant, out of the more than 450 worldwide. Since research reactors are rarely operated at the 90% full power uptime typical of commercial power plants, even this comparison overstates the size of the world research reactor spent fuel inventory. Although detailed data are not universally available, there is also wide variation in spent fuel burn-up histories, mass inventories, and isotopic compositions.

Security is another area where the range of reactor locations and fuel types creates unique conditions and requirements. In the late 1970s the Reduced Enrichment for Research and Test Reactors (RERTR) program was launched with the objective of exchanging high enriched uranium (HEU) fuel, with LEU fuel enriched to below 20%. This program and related international initiatives have succeeded in removing most of the HEU from the operating RR fleet. Even so, any viable RRSNF management strategy must provide robust physical security as well as material control and accounting, as defined in the IAEA Nuclear Material Accounting Handbook [1].

The importance of the RRSNF management challenge has been highlighted in past IAEA-sponsored reports and workshops. For instance, a 2004-2006 study addressed spent fuel management options for RRs in Latin America [2]. A 2006 workshop [3] surveyed national perspectives on one RRSNF back end option, return to country of origin, specifically the USA. In 2009, the IAEA published an extended summary and account of the experience obtained from the completion of international projects on return of SNF to the Russian Federation from RRs in Uzbekistan, Czech Republic, Latvia, Bulgaria, and Hungary [4]. These resources provide an excellent foundation for informing a dialogue with stakeholder nations.

2. Tentative Structure of the CRP

The overall objective of this CRP is to define, characterize, and disseminate information about a range of developed long-tern strategies for managing the back end of the RR nuclear fuel cycle. Included in the information to be collected is cost data for each of the RRSNF management options, to be used with a cost model to enable a MS to understand fully the commitment of the spent fuel management option chosen. A publication will be issued to ensure that CRP findings are available to all MSs with RRs.

This CRP will specifically seek to include MSs who are responsible for the management of RRSNF, as well as those who are currently planning and building new RRs. It is important to recognize that economic and human resources, existing infrastructure, and geography will

play key roles in identifying the strategies that are optimum for each country. For that reason, this CRP will emphasize concerns specific to countries that *do not* possess commercial nuclear energy infrastructures. The key product of this work will be the compilation and evaluation of RRSNF management options, taking into account safety and security requirements, technologies, and human and economic resource requirements with respect to the constraints faced by these countries.

IAEA hosted a meeting in July 2014 to discuss the CRP, specifically to develop the preliminary structure of the cost model, identify the data that needs to be collected from participating countries, and determine how some of the qualitative information can be represented in a quantitative model that compares diverse technologies. Nine consultants, representing seven countries, participated in this meeting. A cost model is being prepared that will seek to capture all elements of the RR fuel cycle back end, including (but not limited to) spent fuel management activities at the reactor facility; interim storage prior to any shipping activities; shipping to interim or final storage; spent fuel treatment and conditioning for reprocessing or for storage and direct disposal; spent fuel reprocessing; waste shipments; preparation of final storage facility; and transportation to the disposal location. Many MSs were directly encouraged to participate in this CRP, although any MS may submit a proposal, and 13 proposals have been submitted thus far. Of those, 12 have been tentatively selected for participation. Participating MSs are expected to share both their RRSNF management expertise and cost data with the CRP group. Some of the CRP participant MSs have commercial nuclear power programs and some have mature RRSNF management strategies, while some participants have no appreciable experience with RRSNF management and are seeking to develop their national strategies.

3. CRP Scope and Objectives

This CRP will review, summarize, and identify the costs associated with the developed options and technologies available for managing RRSNF. This project will achieve two key objectives. First, past work will be leveraged to identify and define a comprehensive set of strategies for managing RRSNF. Single-country strategies will be analysed by using a standard approach and compared to potential take-back regional and multinational options, including commercially available or otherwise agreed nuclear fuel management services. Second, a costing model will be developed to enable participating MSs to determine the most economical and responsible means of RRSNF management for their situation. The focus will be on matching feasible options to the capabilities of countries with RRs. Country specific case studies will be developed. Three research coordination meetings (RCMs) and up to two workshops are planned in order to disseminate information about the RRSNF management strategies to MSs.

Research tasks to achieve the CRP objectives will include:

- Development of a standard approach to assess and analyse individual RRSNF management options. This methodology will consider the amount of RRSNF, the costs involved, identification and characterization of the broad classes of short and long term RRSNF management strategies (e.g., ongoing at-reactor or away-from-reactor storage, processing/separation, disposal, take-back to country of origin and other cooperative multinational options), and identification of the economic and human resource requirements associated with each technology and RRSNF management strategy.
- Quantitative assessment of the RRSNF management options for all participant countries in the CRP.
- Quantitative comparison of national RRSNF management approaches versus regional or multinational arrangements for commercially available or otherwise agreed back-end services.

- Evaluation of available cost data with the model to understand the actual cost implications of the various options presented.
- Examination of the value of RR coalitions in strengthening the negotiating power of the coalition compared to a single RR (i.e. increase of the economic scale because of the larger number of spent fuel, reducing transportation costs, safety and security costs and in general overhead costs).
- The results will be published as an IAEA Technical Report Series document and will be made available to the research reactor community.
- Each participating MS will prepare a report about their individual country's RRSNF strategy.
- Regional workshops to help disseminate the information developed via this CRP.

The standard costing model will be developed as a tool to assist in the planning for a costing methodology for RRSNF management. The proposed topics to include in the systematic structure of typical activities of the RR fuel cycle for principal activities are listed below:

- Preparation of RRSNF options
- Fuel management activities at the reactor
- Long term interim storage activities
- Fuel return programs involving other countries
- Fuel reprocessing
- Fuel conditioning
- Disposal of fuel and/or radioactive waste
- Fuel transportation and packaging
- Management and support activities

For each of these activities, CRP participants will seek to define the associated costs to use with the standard cost model.

Because so many RRs currently have SNF stored at their facilities, it will be important for the CRP participants to consider the fuel condition and determination of the SNF isotopic inventories. There are various tools and methods for this determination, and MSs are at liberty to select the most appropriate one for their use. Other modeling & simulation requirements may arise in connection with evaluating containers for storing RRSNF, potential reprocessing technologies, disposal environments, or additional engineered systems.

Additionally, the following criteria for assessing RRSNF management strategies will need to be considered. Broadly speaking, these criteria measure the sustainability of the strategies in terms of suitability of the strategy relating to other national and regional interests and priorities:

- Political
- Environmental
- Public and Stakeholder Acceptance
- Regulatory
- Security and Safeguards
- Third Party

While the cost model will not include a quantitative methodology for directly evaluating these sustainability criteria, the accompanying report will provide some guidance for MSs on how to include these criteria in their RRSNF management strategy decisions. The criteria can be thought of as representing the risk that a given strategy becomes much more expensive, or even impossible, to carry out. These criteria can also be considered as representing strengths contributing to the sustainability of the strategy.

As part of the preliminary costing tool development, it has been identified that further research is required on the following areas to improve the financial accuracy of the model:

- Sensitivity analysis
- Currency conversion (such as determining the correct from which to conduct the conversion, whilst still obtaining an acceptable result)
- Inflation factors (how to apply the model some years after its creation to economies that inflate at different rates)
- Divergence estimates (determination of the likelihood of divergence from the cost and the magnitude of the divergence)

A larger IAEA decommissioning costing project, Data Analysis and Collection for Costing of Research Reactor Decommissioning (DACCORD) [5], which focuses on developing a cost estimation process for the entire process of RR decommissioning, is exploring these issues through economics professionals in the commercial sector, however, to date, these issues have only been identified with no acceptable solutions yet.

4. Conclusions

Accomplishing the activities defined above will greatly contribute to the implementation of long term RRSNF management strategies in accordance with the unique constraints and conditions faced by the dozens of countries that possess RR, many without a corresponding nuclear energy programme. Upon completion of the work, the IAEA will elaborate and disseminate a comprehensive review of possible RRSNF management options, highlighting some key fuel cycle technologies. This should enable sustainable RRSNF management, including options and technologies for its reprocessing, storage, and ultimate disposal. Through the IAEA Technical Report Series, the CRP will make available information to the RR community, facilitating the ability of a MS to make informed decisions about the RRSNF management strategies for their individual country or RR.

5. References

1. IAEA Nuclear Material Accounting Handbook, http://www-pub.iaea.org/MTCD/publications/PDF/svs_015_web.pdf.
2. *Spent Fuel Management Options for Research Reactors in Latin America*, IAEA TECDOC 1508, 2006.
3. *Return of Research Reactor Spent Fuel to the Country of Origin: Requirements for Technical and Administrative Preparations and National Experiences*, IAEA TECDOC 1593, 2008.
4. *Experience of Shipping Russian-origin Research Reactor Spent Fuel to the Russian Federation*, IAEA TECDOC 1632, 2009.
5. Data Analysis and Collection for Costing of Research Reactor Decommissioning (DACCORD Terms of Reference http://www.iaea.org/OurWork/ST/NE/NEFW/WTS-Networks/IDN/idnfiles/DACCORD_TM_2012/DACCORD_ToR.pdf

STATUS ON SILICIDE FUEL REPROCESSING AT AREVA LA HAGUE

J.F. VALERY, X. DOMINGO, P. LANDAU
AREVA NC
1 place Jean Millier, 92084 Paris La Défense Cedex - France

C. ALAMEDA-ANGULO
AREVA E&P
1 Rue des Hérons, 78180 Montigny-le-Bretonneux - France

C. PECHARD
AREVA NC La Hague
50440 Beaumont-Hague - France

V. LALOY
AREVA TN
1 Rue des Hérons, 78180 Montigny-le-Bretonneux - France

ABSTRACT

Silicide fuels are widely used in Research Reactors in order to meet both with international policies on Uranium enrichment and with technological issues on fission densities in-core. For many years AREVA has been developing solutions for RRSF management, especially reprocessing, and will soon be able to reprocess silicide fuels at its La Hague site.
This paper covers the following:

- overview of the past studies (R&D and industrial preliminary studies) and of the next steps for industrial reprocessing,
- range of fuels for which reprocessing at La Hague will be available,
- identification of the necessary steps to be taken in a reprocessing project.

1. Introduction

After completion of the Research Reactor Spent (RRSF) management programs created under the Global Treat Reduction Initiative (GTRI) umbrella, major part of research reactors operating with highly enriched fuel and new reactors operating with low enriched fuel will use silicide-type fuel (U_3Si_2). The “take-back” option of GTRI programs will cease for RRSF irradiated after May 2016 [1], leaving no sustainable back-end option to research reactor operators who previously planned to benefit from GTRI programs until shutting down of their facilities.
Since 1990’s AREVA has proposed sustainable and responsible solutions for RRSF management, including reprocessing at its La Hague[1] plant for aluminium-type fuels (UAl).
In order to make U_3Si_2 fuel users benefit from reprocessing solutions, AREVA is currently finalizing the silicide fuel reprocessing industrialisation at La Hague plant.
This article will update the reader on the planning for silicide fuel reprocessing solution availability, and on how to prepare to include reprocessing in research reactor’s back-end strategy.

[1] The AREVA La Hague plant is located in North-West of France, in the Normandy region, next to Cherbourg.

2. Reminder on the process

Reprocessing of RRSF at AREVA La Hague is based on the PUREX process for both UAl and U_3Si_2 spent fuels. In both cases the main reprocessing steps are dissolution of the RRSF, mix with dissolution solution from Light Water Reactor (LWR) spent fuels (for aluminium management), liquid/liquid extraction and separation of U and Pu from Fission Products (FP) solutions and vitrification of the FP solutions after concentration.

However, for silicide spent fuels, a new step has to be added considering their high silicon content in the fuel meat. Indeed, this Si content leads to a high Si concentration in the dissolution solution which is not compliant with the PUREX liquid/liquid extraction process.

In order to meet the PUREX requirements the Si has to be separated from the dissolution and managed through a dedicated process flow.

This additional process step will be performed thanks to the existing centrifugation equipment commonly used to separate the fines[2] during reprocessing operations for LWR spent fuels. Consequently, the separated silicon will be managed through the fines line and will be vitrified mixed with FP solutions at the end of the reprocessing operations: the vitrification step.

The following diagram reminds the whole reprocessing steps for U_3Si_2 RRSF including the new step of silicon separation.

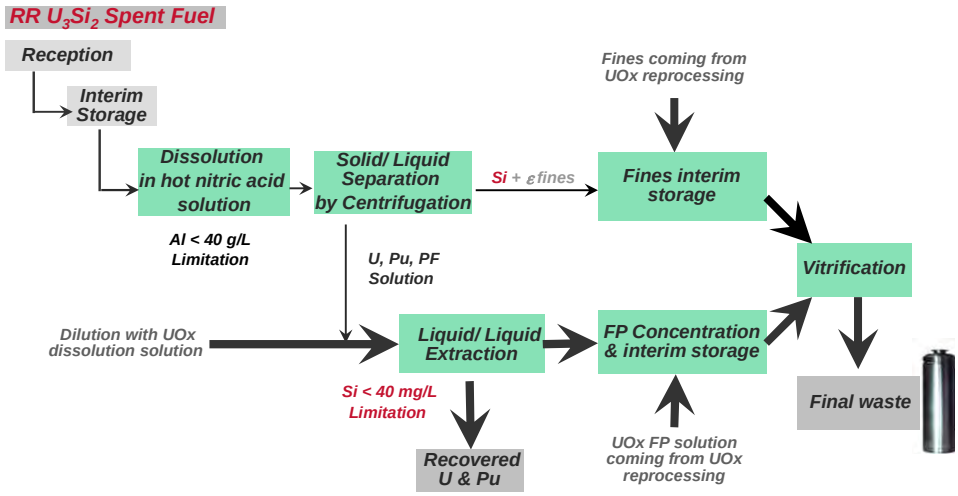

Fig.1: Process diagram for Silicide fuels reprocessing in AREVA NC LA Hague plant

3. Update on ongoing actions and planning for industrial commissioning

3.1. Past R&D and studies

In order to be able to reprocess silicide fuels at the AREVA La Hague reprocessing plant, an important R&D program has been carried out by AREVA and the CEA [2]. The main goals of this R&D program were to characterise the behaviour of silicon from U_3Si_2 during dissolution and to qualify the separation process of the silicon and the behaviour of the resulting silicon concentrated solution through the fines flow in the process. This R&D program was completed end of 2013

[2] The fines are small metallic parts mainly issued from LWR SF cladding shearing during reprocessing operations

In 2014 AREVA focused on the industrial qualification program in order to:

- take into account the process parameters coming from the R&D in the technical documents describing the industrial operating conditions for RRSF reprocessing,
- refine the reprocessing rhythm and annual capacity of reprocessing for silicide fuels,
- assess the impact of flows coming from silicide fuels dissolution on the whole AREVA La Hague processing activities.

The industrial feasibility and preliminary studies have been completed mid-2014. Operating ranges were successfully extended for the silicon separation step by centrifugation and the related management of silicon through the fines line, which will allow AREVA to offer more attractive reprocessing solutions to its customers. Based on their results, AREVA has moved from preliminary studies to the detailed studies phase during summer 2014. Considering this timeline, AREVA expects to file its U_3Si_2 reprocessing application to the French Safety Authority (FSA)[3] around mid-2015.

All the results and qualified operating ranges were taken into account in the current process book dedicated to U_3Si_2 reprocessing operations.

3.2. Current status

Since the detailed studies phase started, AREVA has finalized the main part of technical documents in order to perform U_3Si_2 reprocessing in its La Hague plant.

This first batch of documentation includes all the required documents for the main process steps (dissolution & silicon separation). For instance unit description technical notes, process flow diagrams, chemical flow sheets, instrumentation process & automatism data sheets and process malfunction analyses have been successfully completed. Studies to assess the impact of reference U_3Si_2 reprocessing operations on the whole AREVA La Hague plant activities (extraction, vitrification…) have been also performed and have concluded that this new qualified U_3Si_2 reprocessing fits with the whole plant operating & safety referential, even if the new Si flow does impact some other operations.

Currently, the final studies phase is dedicated to finalize:

- detailed command and control systems studies considering that U_3Si_2 reprocessing operations will be performed thanks to the same existing industrial equipments used to process UAl or LWR spent fuels. These studies will lead to the final command and control programs which will be used at industrial scale,
- the whole safety studies and the related U_3Si_2 reprocessing authorisation file (RPS) with the aim of considering operating ranges as wide as possible, and consistent with the reference U_3Si_2 spent fuel.

The studies completion is consistent with AREVA aim to apply to French Safety Authority for the U_3Si_2 process authorisation file by mid-2015.

[3] As for a major part of nuclear installations and sites worldwide, new processes or adaptations to existing processes are to be licensed by the competent Safety Authorities before the operations begin.

3.3. Planning overview

The following timeline summarizes the current tentative planning that will conduct to industrial reprocessing of silicide fuel at AREVA La Hague plant.

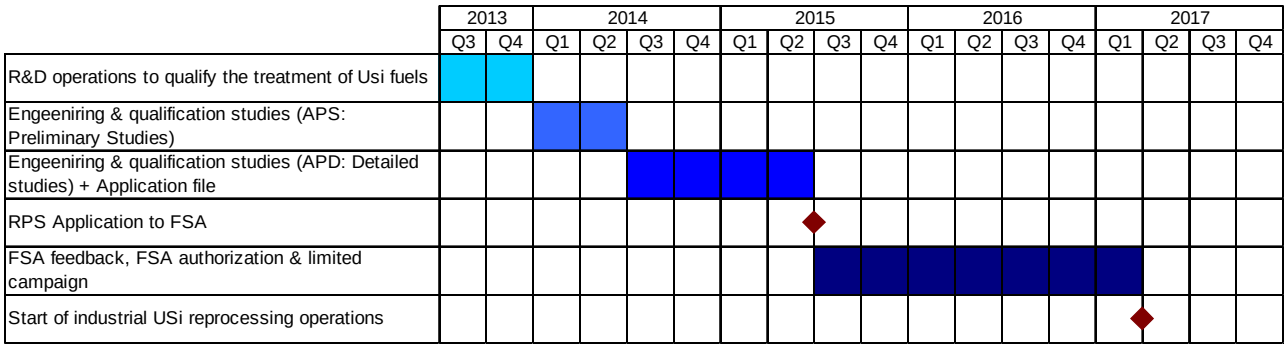

Fig.2: Tentative timeline of the industrial qualification program prior to process authorization

4. Fuel Characteristics consistent with the qualified process

4.1. General case

Considering the basic key steps of silicide fuel reprocessing operations (silicide dissolution, silicon separation, silicon management…), any type of silicide spent fuels can theoretically be reprocessed by AREVA thanks to the reference qualified process described in the process book.

However, all the studies performed by AREVA are based on a reference silicide fuel to be reprocessed in La Hague plant. This allows AREVA to define operating conditions ranges linked to fuel characteristics ranges. These ranges are described in the application file (RPS) to be submitted to the French Safety Authority (ASN) in order to get the authorization for reprocessing silicide fuels in the AREVA La Hague plant as mentioned above.
In any case, reprocessing of other silicide RRSF than the reference one will be subject to specific authorization to be delivered after a dedicated application by AREVA to FSA.

This situation leads to two cases:

- 1/ If the RRSF **is consistent** with all the acceptance and operating ranges described in the current application file (for reference silicide fuel), the considered RRSF reprocessing application file will be a light dedicated one according to the current reference fuel application file,
- 2/ If the RRSF **is not consistent** with all the acceptance and operating ranges described in the current application file, it will be necessary to perform additional studies in order to assess the impact of its characteristics deviations on the reprocessing operations and its related cost in comparison with the reference fuel. If needed, an update of the reference process will have to be performed prior to the preparation of the dedicated application file for this spent fuel.

4.2. Relevant criteria for reprocessing scenarios assessment

To perform a reprocessing scenario assessment, AREVA needs to obtain relevant information about the RRSF in order to:

- assess the reprocessing rhythm, annual reprocessing capacity and associated reprocessing costs for the RRSF,

- perform dedicated studies depending on RRSF specificities and/or if the characteristics deviation compared with the reference silicide fuel are significant, even if the core process operations are similar (centrifugation to separate the Si prior to U & Pu extraction). One these preliminary studies are completed, it will be possible to assess the reprocessing rhythm, annual capacity and reprocessing costs for such silicide fuels.

The first criteria are the geometrical characteristics of the spent fuel (diameter, length). Indeed, the current process consists in dissolving the SF in a dissolution pit that imposes some constraints on the SF to be reprocessed (maximum acceptable diameter and length). If the fuels size is not consistent with this “physical entrance” range, additional operations will have to be considered such as prior cutting operations for instance. Detailed characteristics (such as, but not limited to plates thickness,…) are also useful to perform the capacity assessment.

The other important characteristics for the reprocessing assessment are linked to the chemical composition of the spent fuel. Basically, the type of Al alloy (cladding and fuel meat matrix) is a key parameter for the capacity assessment as it is linked to the dissolution kinetics. It can be a key point for additional study especially if the type of alloy is not included in the considered alloy range of the process book or if it includes a chemical element which can have a strong impact on downstream reprocessing operations (extraction, concentration or vitrification).
Standard chemical weight ratios for RR spent fuels (such as $U_{initial}$/Al or Si/Al) are very important to assess the reprocessing rhythm and especially the silicon ratio in case of U_3Si_2 SF. The amount of silicon to be separated from the dissolution solution has an impact on the dissolution/centrifugation stage (number of operations and reprocessing rate) and leads to dilution of “usual” reprocessing flows with consequences on the fission products concentration capacity and on the vitrification rate. Regarding Al total mass, possibilities of upstream cropping operations in order to reduce the total mass to be reprocessed can be taken into account in a scenario assessment as an optimisation.

The content of minor elements (ex. magnesium, molybdenum, cadmium…) is also helpful for reprocessing scenarios assessment considering the fact that such minor elements can have an impact on the reprocessing rhythm. Such elements can have a link with corrosion phenomena, deposition formation, management of releases in the environment, vitrified residue specification… ; that is why it is necessary for AREVA to get the RRSF chemical composition as detailed as possible.

Obviously, other common information such as burn-up, cooling time, initial and post irradiation composition, integrity (leakage)… are useful for the scenario assessment, for the comparison with the reference ranges given in the current U_3Si_2 process book, and more generally with all the reprocessing steps at La Hague, from receipt of the RRSF to final waste production.

4.3. Requested information

The following table presents the basic data information requested to start an assessment of possible reprocessing scenarios This list has to be considered as a starting point for exchanges with AREVA on RRSF reprocessing, and can be updated according to the SF characteristics, or after first exchanges between AREVA and the RR operator.

Basic information Datasheet								
Reactor Name - type of fuel (standard, control, USi, UAl, …)								Comment
1	Burn-up rate (average and max)	average			max			
2	Cooling time (min and max)	min			max			
3	De-activation date							
4	Amount of cycle							
5	Spent fuel integrity (any leaking, disassembled fuel?)							
6	Do sipping tests have been conducted? If yes, can you please give procedure and results?							
7	α and $\beta\gamma$ spectra							
8	Total α and $\beta\gamma$ activity per FA (Bq/FA)							
9	Thermal power							
10	Contents of U and Pu post-irradiation	U (g)			Pu (g)			
11	Initial/Post irradiation enrichment of U and Pu	Enrich.	Initial	U_{tot} (mass)				
				U^{235}/U				
			Post	U_{tot} (mass)				
				U^{235}/U				
12	Si and Al content	Before cutting	Al (g)					
			Si (g)					
		After cutting	Al (g)					
			Si (g)					
13	Structure, cladding, fuel meat matrix & spacer material	Structure						
		Cladding						
		Fuel meat matrix						
		Spacer						
14	Other items in assembly (including materials, quantities, dimension (mm) and weights (g))							
15	Presence and detailed weight percentage of any other minor elements (Mg, Mo, B, Se, Cd…)							
16	Do you have any possibility to cut pieces (head or foot) on site? If yes, could you please describe parts that can be cut?							
17	Exhaustive fuel specifications and drawings	Circular section, length, thickness… (FA, plates) Before and after cropping if any						
18	Total mass for each fuel element (g) (before and after cutting)							
19	Any useful information regarding the fabrication process specificities							
20	Amount of element to be transported/treated / mid-long term inventory planning							
21	Absorbed dose at 1m from surface of the spent fuels							

Table 1: Basic data information needed for U_3Si_2 reprocessing scenarios assessment by AREVA.

5. Performing reprocessing scenario assessment with AREVA

Along with the reprocessing feasibility assessment and associated cost estimations, some other activities are to be looked at in order to set up a reprocessing project for silicide RRSF. These necessary activities are to be conducted in order to plan the transportation part, intergovernmental exchanges between the reactor's country and France, final waste management, and to set-up the overall project schedule.

5.1. Transportation

Transportation of silicide-type RRSF does not differs from transportation of aluminium-type fuels. In that regard, AREVA has already acquired a worldwide experience in RRSF transportation (among others silicide-type), including the provision of several types of transport casks & baskets using multimodal transportation.

In order to assess transportation scenarios, RR operators have to select casks and transportation modes that meet their operational, regulatory and governmental constraints. The transportation of the RRSF needs also to be plan early enough within reprocessing scenarios assessment.

5.1.1. Site preparation and interfaces with selected transportation casks

Transportation cask selection is key in the overall reprocessing project timeframe. The type of cask will have direct impacts on the transportation frequency, possible modifications of RRSF storage and handling procedures at reactor site, possible modifications of RRSF receipt facilities and handling procedures at the AREVA La Hague plant.

The following criteria are to be reviewed in order to prepare a reprocessing project and to assess the possible options for transportation:

- Compliance with local (RR country), France, and applicable international regulations and technical requirements. The competent Safety Authorities will have to review the cask safety files and provide agreements for transportation of each specific RRSF content.
- Capacity, i.e. amount of RRSF per cask, is also a key factor in order to reduce the amount of transports to be performed and the transportation frequency during RR lifetime. Along with public acceptance, the cost for transportation will directly be impacted by this parameter.
- Compatibility with RR site and handling procedures. Several criteria such as the cask weight, cranes and floors capacities, handling tools and procedures are to be looked at in order to identify the range of RRSF transportation casks that suits with the constraints of each reactor site. In some cases, adaptations of RR site may be needed in order to allow selected transportation cask usage. AREVA can provide, when applicable, complementary and flexible transfer systems in order to simplify loading of RRSF in transportation casks.
- Compatibility with the AREVA La Hague site and its handling procedures. RRSF unloading operations are performed under-water in the NPH pool at La Hague. This facility has been designed for flexible operations and can consequently adapt to several RRSF transportation cask designs. Nevertheless, safety studies and adaptation of equipments can be required to unload new cask designs.

5.1.2. Transportation of RRSF

Before effective transportation, the transportation licensing phases are to be completed.
For France, two agreements are to be granted by ASN:

- Transportation license, for transportation of the cask with the relevant RRSF content on French territory.
- License for receipt, unloading and reprocessing at La Hague, after required safety reviews.

For several RRSF transportation casks, these licenses are already available and consequently need to be slightly adapted for each RRSF specific content.
In the RR country, the same kind of transportation licences is necessary.

Transportation modes also have a strong influence on a reprocessing project.
As La Hague is located by the sea, next to the Cherbourg harbour, designed for receipt and unloading of nuclear-material dimensioned-ships, both maritime and road transportation can be considered.
For European RR, the road transportation mode is often selected. It may raise some additional licensing costs (for the countries the truck drives through).
For overseas RR, the transportation casks capacities and availability in the project time-frame become major issues in order to reduce project uncertainties and associated costs.

The casks availability, the long-lasting technology and safety of the cask design are to be considered during scenario assessment.

5.2. Intergovernmental framework

According to European Directive[4] and French law[5], the introduction on French territory of spent nuclear fuels for a reprocessing purposes has to be framed by an intergovernmental agreement (IGA) between France and the SF country of origin. This agreement settles “a forecasted schedule for reception and processing of the material and, if any, the later planned use of the material separated during reprocessing”. Article L542-2 of the French Environmental Code specifies also that disposal in France of radioactive waste from abroad is forbidden, including waste resulting from RRSF reprocessing.

The above-mentioned IGA is to encompass the following items:

- Project description:
  - Material owner,
  - Main stakes for the owner,
  - Location of the nuclear material,
  - Legal status and origin of the material,
  - Material owner country presentation,
  - Planned contractual structure for material reprocessing,
    After RRSF reprocessing, the valuable material can be managed by AREVA in order to be re-used in civilian purposes (new LWR or MOX fuels).
  - Planned scope of collaboration between the parties,

- Acceptability of reprocessing:
  - Type and characteristics of material to be reprocessed: design, total mass, mass of oxide and heavy metals, rate of combustion, cooling, initial enrichment,...
  - Material transportation scheme (cask and transportation procedures),

[4] Council Directive 2011/70/EURATOM of 19 July 2011 establishing a Community framework for the responsible and safe management of spent fuel and radioactive waste: http://eur-lex.europa.eu/LexUriServ/LexUriServ.do?uri=OJ:L:2011:199:0048:0056:EN:PDF

[5] French Environmental Code resulting from the law of June 28, 2006 on the sustainable management of radioactive materials and waste, and application decree no. 2008-209 of March 3, 2008 on procedures applicable to the reprocessing and recycling of foreign spent fuel and radioactive waste specifies certain conditions

- Schedule:
  - Quantities to be reprocessed and timing,
  - Period of delivery of RRSF from the customer to AREVA La Hague,
  - Period of reprocessing,
  - Period of waste return,
  - Use /reuse of the recovered material,
  - Deadline for the last return of waste,
  - Destination of waste.

From AREVA's experience on conducting this IGA process, between six months and two years are necessary to get the final agreement from all parties, starting from the official discussion between the countries. Consequently, this whole process has to be well included in RRSF reprocessing overall project.

A commercial transportation and reprocessing contract between AREVA and a RR owner can be concluded before the end of the IGA process. Nevertheless, the IGA conclusion will be necessary in order to start transportation of nuclear material.

5.3. Final waste management

Another application of French law[5] concerns the final waste calculation method.
In order to comply with this regulation, AREVA applies a material accountancy system including a unique activity unit for waste (UAR, *Unité d'Activité de Résidu*) and a unique mass unit for waste (UMR, *Unité de Masse de Résidu*).

This system allows AREVA to calculate the amount and type of waste to be sent back to its customers. This system called EXPER (*EXPEdition des Résidus*) has been approved by decree, and has been implemented since October 2008 for all new RRSF reprocessing operations.

In the case of silicide-type RRSF reprocessing, if all the material is dissolved, the only remaining waste corresponds to the UAR system, based on the Nd quantities imported in France in the RRSF.

The UAR system implies two possible types of vitrified residues: CSD-V (*Conteneur Standard de Déchets Vitrifiés*) and CSD-U (*Conteneur Standard de Déchets U)*.
The CSD-V concentration in FP is highly superior to the CSD-U one. The thermal power is consequently higher in CSD-V than is CSD-U.
According to each country regulation, CSD-V and CSD-U can be considered respectively as HLW and ILW.

AREVA proposes to study the conditions under which the final waste can be managed with the RR operators and their regulatory bodies.
Two different examples can be underlined for final waste management:

- Belgium
  After reprocessing of BR2 RRSF, CSD-Vs have been jointly sent back to Belgium with residues from Belgian utilities SF reprocessing. As the LWR SF reprocessing results in much higher volumes of CSD-V than RRSF reprocessing, the residues return was almost insignificant for the BR2 operator (SCK)
- Australia
  Australia does not operate any Nuclear Power Plant. Australia does not have any HLW to take manage. The CSD-U was consequently the best option for Australia as it is managed as ILW and does not need large investments for long term management (in comparison with final HLW disposal).

AREVA proposes to adapt the final waste responsible and sustainable management to each country regulations and specificities.

5.4. Overall project schedule

The overall silicide RRSF reprocessing project can be separated in two major phases: the preparation phase, and the execution phase.
Depending on RR operators' needs and on the AREVA-RR operator partnership, commercial contracts and commitments can be concluded for the overall project, or separately for each phase.

5.4.1. Preparation phase

The preparation phase is mainly composed of the above-mentioned steps (see paragraphs 4 and 5).

The following timeline can be considered in a silicide RRSF reprocessing project preparation:
- Confirmation of reprocessing feasibility and cost estimation: 3 to 18 months
- Transportation preparation : 3 to 24 months
- Intergovernmental Agreement and related exchanges: 6 to 24 months

These timelines are to be adapted for every single case with regards to all aspects of the reprocessing project. Of course, all these activities can be run in parallel in order to shorten the preparation period.

Even if the IGA finalization is a mandatory milestone between preparation and execution phases, it is reminded that a commercial contract for execution phase can be signed by the parties before IGA signature.

5.4.2. Execution phase

The execution phase starts with RRSF evacuation from RR site, transportation to the AREVA La Hague plant, unloading and interim storage of RRSF in AREVA La Hague SF pools.
Depending on the AREVA operational constraints and IGA-bound timelines, reprocessing operations can be performed directly, or several years after receipt at La Hague.
After reprocessing, the final waste is stored for cooling.
As the final waste quantities are very low after RRSF reprocessing, the residues return can be optimized for the entire RR-reprocessed inventory in order to perform as less transportations as possible for a dedicated country, for example by mutualizing it with other transportations.
The residues are sent back conditioned and packaged in compliance with the country of destination's waste management policy: in dual-purpose casks for transportation and long-term storage or in transportation casks for transfer to a storage/disposal facility.

This overall timeline is described in the Fig.3 bellow and is 10 to 40 years long depending on the reprocessing scenarios and the concluded IGA.

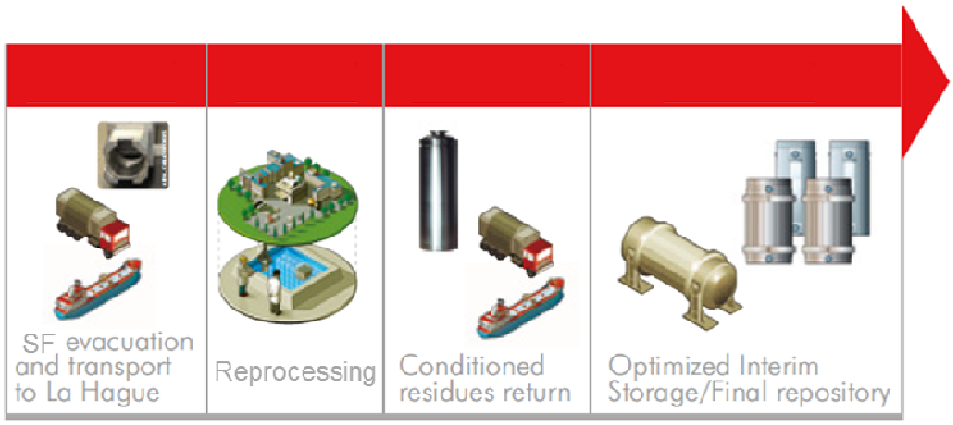

Fig.3: Timeline of the reprocessing project execution phase

6. Conclusion

In order to provide its customers with sustainable, cost-effective and responsible RRSF management solutions, AREVA has been developing silicide-fuel reprocessing at its La Hague plant. This new back-end solution will be available as from 2017 for U_3Si_2 RRSF types, after verification of the corresponding operating conditions, available capacities and associated costs, on a case-by case basis.
AREVA is ready to support RR operators in their back-end strategy definition for silicide fuels as of today.
The first transportations will be possible starting 2017, after Safety authorities authorizations for reprocessing and transportation, and after IGA finalization between France and the corresponding countries.

7. Reference

[1] "Global Threat Reduction Initiative"
C.E. Messick, J.J. Galan
RRFM2014, Ljubljana, March 30th – April 3rd 2014, Transactions, p. 274-279

[2] "Status of silicide fuels reprocessing at La Hague plant"
C. Eysseric, A. Juvenelle, N. Reynier-Tronche, JP. Feraud, T. Randriamanantena, D. Ode, B. Lorrain, J.F. Valery, X.Domingo
RRFM2014, Ljubljana, March 30th – April 3rd 2014, Transactions, p. 298-307

REMOVAL OF FRESH HEU TRIGA FUEL

T.E. HANLON, B.E. WILHOIT, & T.C. ANDES
Y-12 National Security Complex, Nuclear Nonproliferation and Global Security Programs
P.O. Box 2009 Oak Ridge, Tennessee 37831-8112 U.S.A.

Abstract
Y-12 has removed 51 unirradiated Training, Research, Isotope production, General Atomics (TRIGA) fuel elements containing highly enriched uranium (HEU) from domestic and international research reactor facilities since 2007. The removals were performed in support of the National Nuclear Security Administration's Global Threat Reduction Initiative (GTRI). The fuel elements were removed from South Korea, Mexico, and several U.S. Universities (Oregon State, Washington State, and Wisconsin) and transported to the Y-12 National Security Complex (Y-12) for storage and recovery. In 2006, the U.S. Department of Energy's ES-3100 Type B shipping package was certified for use and the allowable contents included TRIGA type fuel via air transport. For each removal project, the ES-3100 shipping package was utilized. The process of removal included cropping/canning the fuel elements, loading the cans, sealing/leak testing each ES-3100, and transporting to Y-12. As of March 2012, all unirradiated U.S. Origin HEU TRIGA fuel has been removed by GTRI. This paper will provide basic details of those removal projects and the processes by which they were executed.

1. Introduction
The TRIGA (Training, Research, Isotope production, General Atomics) reactor has been one of the most popular research reactor designs with a history stretching back to the first operational model built in 1958. The TRIGA reactor has an installation base of 65 reactors in 24 countries on five continents. The well-known TRIGA fuel element was patented in 1960 and was available in a Highly Enriched Uranium (HEU) version until 1979 [1,2]. The popularity of the TRIGA type fuel and the world-wide dispersal of the HEU version of the fuel created an unintended proliferation threat. The mitigation of the threat created by the wide distribution of these materials has been a goal of the National Nuclear Security Administrations Global Threat Reduction Initiative (GTRI). To that end, since 2007 the Y-12 National Security Complex has removed 51 unirradiated TRIGA fuel elements containing HEU. As of March 2012, all unirradiated HEU TRIGA fuel has been removed by GTRI.

Removal of these materials would not have been possible without a shipping container approved to accept full and partial HEU research reactor fuel elements. The U.S. Department of Transportation (DOT) specification 6M container was the work-horse for bulk HEU shipping for the Department of Energy (DOE) and many others for well over 20 years. However, the DOT 6 M container was terminated for shipping radioactive materials in 2008, because it was not a performance based package. In response to this situation, the DOE developed the ES-3100 type B shipping container [3]. The ES-3100 shipping container is a general purpose fissile material container designed to accommodate many forms of HEU and other special nuclear materials in bulk quantities for ground and air transportation. Among the approved contents for the ES-3100 shipping container is $UZrH_2$ TRIGA research reactor fuel components.

While the ES-3100 shipping container is approved for the shipment of $UZrH_2$ fuels, the Certificate of Compliance (CoC) requires size reduction (cropping) of TRIGA type fuel elements and placement into metal cans (maximum of 3 fuel elements per can and ES-3100) prior to packing and shipping. The typical dimensions of the fuel meat section of all types of TRIGA fuel elements is 38cm (15 in) tall, not including graphite reflectors or boron carbide poison, or top and bottom fittings [4]. The inner height of the ES-3100 containment vessel is 78.7cm (31in). The CoC requirement for size reducing TRIGA fuel and the need to optimize the packing configuration to minimize the number of ES-3100 containers necessitated the development of a fuel cropping procedure.

Lastly, the packed materials needed to be shipped. The ES-3100 being approved for both land and air transport provided great flexibility in this regard. Depending on the requirements of the individual TRIGA materials and the removal site, an appropriate and compliant shipping method was employed.

2. ES-3100

The U.S. Department of Transportation (DOT) specification 6M container had been the work-horse for bulk HEU shipping containers for the Department of Energy (DOE) and many others for well over 20 years. However, termination of the DOT 6M drum for shipping radioactive materials in 2008 left a void for transporting bulk HEU materials. In response to this need the DOE developed the ES-3100 type B shipping container (shown in Figure 1).

Figure 1: ES-3100 Shipping Container.

The ES-3100 shipping container uses a patented insulation technology and a neutron absorber to achieve high fissile material cargo loadings. The container has an outer diameter of 48.3cm (19in) and height of 109.2cm (43in). The inner containment vessel is 12.7cm (5in) in diameter by 78.7cm (31in) in height. It has a maximum shipping weight of 190.5kg (420lbs) [5].

Among the approved contents for the ES-3100 shipping container is nearly every unirradiated uranium form common to the nuclear industry (solid or broken metal and alloys, metal powder, oxides, compounds, and research reactor fuel elements or components) and of particular note the $UZrH_2$ TRIGA research reactor fuel components. $UZrH_2$ TRIGA fuels composed of highly enriched uranium can be packed into an ES-3100 with a U235 limit of 0.408Kg per package without need of neutron absorbing spacer cans.

3. Fuel Cropping and Packing

The TRIGA fuel element presents a unique packaging challenge not found in more routine bulk HEU materials packaging. In more standard operations pieces of broken metal or bulk uranium oxides are canned, sealed, and packed. Research reactor fuel elements require greater preparative work for size reduction. The TRIGA fuel presented the particular challenge of being a cylindrical fuel of $UZrH_2$. Unlike plate-type fuels such as MTR where the fuel meat is exposed and can be visibly identified prior size reduction, the TRIGA fuel required a detailed study of the fuel construction diagrams to develop the procedures and establish the best practices of size reduction. Adding to the challenge was the fact the fuel sections shift approximately 0.64 cm (0.25in) when held in an upright position.

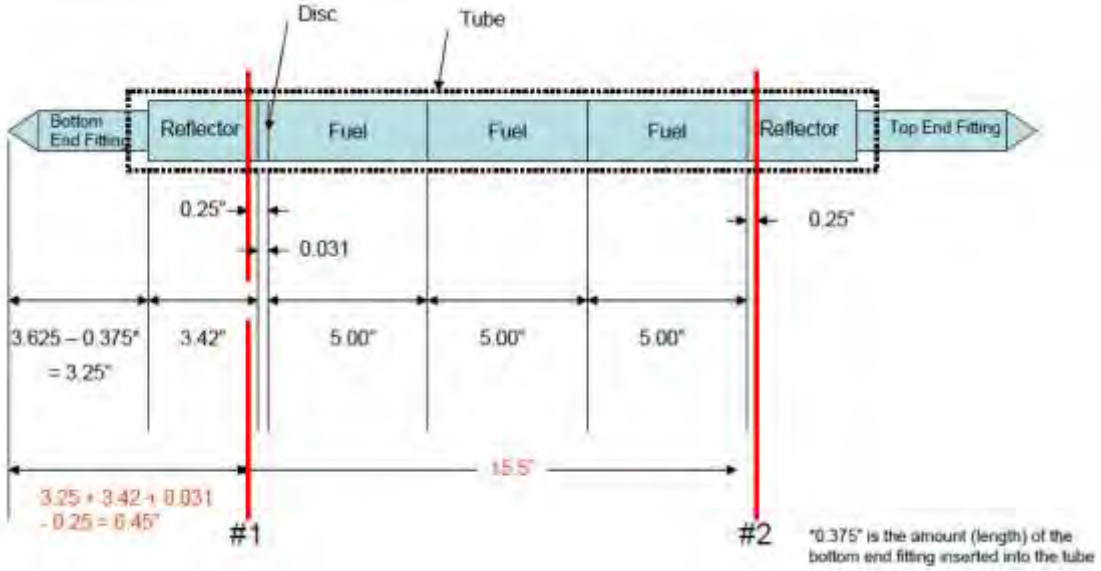

Figure 2: Schematic of standard TRIGA fuel element with cropping locations noted as #1 and #2.

In order to meet the requirements for comfortably fitting the TRIGA fuel elements into the ES-3100 shipping container a size reduction procedure was developed for the various types of TRIGA fuel elements which are commonly used (standard fuel element, fuel follower control rod, and instrumented fuel element). A schematic of the procedure for a standard element can be seen in Figure 2 and a Fuel Follower Control Rod diagram with cropping regions emphasized can be seen in Figure 3.

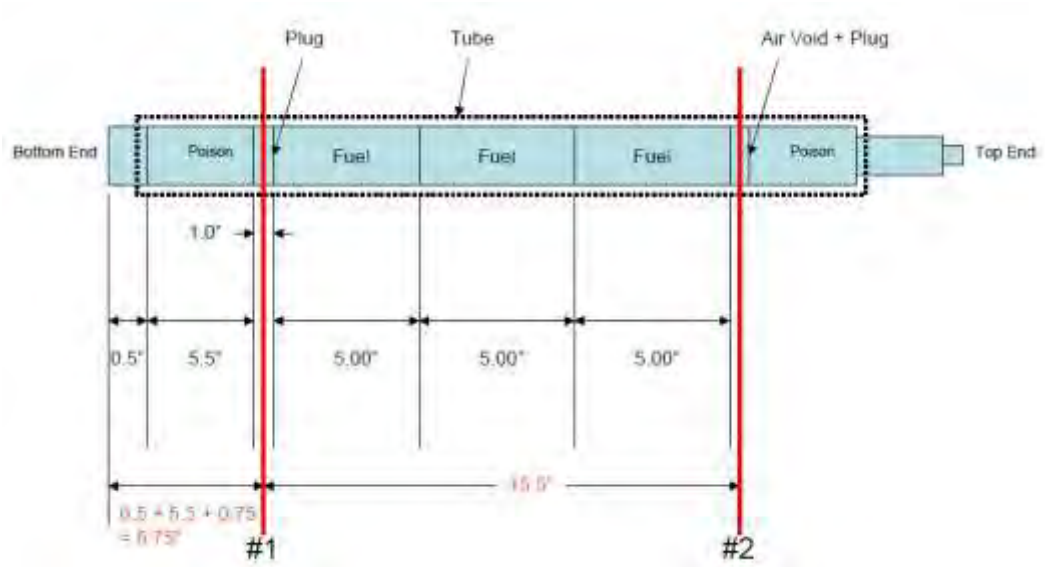

Figure 3: TRIGA Fuel Follower Control Rod schematic showing region to be cropped.

In order to remove the non-fissile elements from the fuel rod a standard industrial pipe cutter was employed to cut the cladding just above the location of the HEU fuel; as shown in Figure 4. Once the non-fuel section was separated from the fuel-bearing section the remaining graphite reflector or boron carbide poison was removed and the ends crimped (if needed) to prevent the fuel pellets from falling from the tube; as shown in Figure 5. This procedure was performed on both ends of the fuel so that only the fuel-bearing portion of the fuel was left.

Figure 4: Cropping Fuel Follower Control Rod element and removing non-fissile parts with industrial pipe cutter.

Figure 5: Cropped Standard fuel element with visible fuel section and central zirconium rod.

Cropped TRIGA fuel elements were then gathered in groups of up to three, wrapped in plastic bags and loaded into 10.8cm (4.25in) by 40.6cm (16in) tin coated carbon steel cans; shown in Figures 6 and 7. The canned fuel elements were then packed into the ES-3100 shipping container with an empty 10.8cm (4.25in) by 22.2cm or 12.4cm (8.75in or 4.875in) tin coated carbon steel can and stainless steel pads placed on top to prevent excessive shifting during transportation.

Figure 6: Bundle of cropped TRIGA fuel elements bound and being packed in plastic bags.

Figure 7: Bagged bundle of cropped TRIGA fuel elements being packed into 40.6cm (16-inch) tall carbon steel can.

4. Shipping/Transportation

The packed ES-3100 shipping containers are collected in groups of four on metal pallets as shown in Figure 8. The four ES-3100 shipping containers are strapped together as well as to the metal pallet. This assembly can then be loaded into the chosen shipping vehicle.

Figure 8: Palletized full ES-3100 shipping containers being transferred on a forklift.

Figure 9: Palletized and loaded ES-3100 shipping containers being loaded for land transportation in South Korea.

The removal of the TRIGA fuels from international sites was greatly helped by the use of air transportation and the 2006 approval of the ES-3100 shipping container for air transport. The use of aircraft affords greater security of materials custody by reducing the amount of time the HEU fuels are in transport.

Figure 10: Palletized and loaded ES-3100 shipping containers ready for shipment by air.

Conclusion:

Since 2007, both domestically and internationally, the Y-12 National Security Complex removed 51 unirradiated TRIGA fuel elements containing highly enriched uranium (HEU) for disposition. These removals were performed in support of the National Nuclear Security Administration's (NNSA) Global Threat Reduction Initiative (GTRI). The fuel elements were removed from South Korea, Mexico, and several U.S. Universities. For each shipment, the ES-3100 shipping package was utilized. The process of removal included cropping/canning the fuel elements, loading the cans, sealing/leak testing each ES-3100, and transport. In the cases of South Korea and Mexico, the shipments were made by air transport; a benefit of using the ES-3100 shipping container. As of March 2012, all unirradiated U.S. Origin HEU TRIGA fuel has been safely and securely transported to the Y-12 National Security Complex for final disposition under Peaceful Use activities (downblend to LEU).

References:

[1] D.M. Fouquet, J. Razvi, & W.L. Whittemore. Nuclear News. November 2003, 46-56.

[2] M.T. Simnad. Nuc. Eng. & Des. 64 (1981) 403-422.

[3] J.G. Arbital & K.E. Sanders. PVP2009 (2009) 117-124.

[4] W.P. Wallace et al. U.S. Patent 3,119,747. Jan. 28, 1964.

[5] “Safety Analysis Report, Model ES-3100 Package with Bulk HEU Contents” Y/LF-717, Rev. 4. March 3, 2011.

HANDLING THE TYPE C PACKAGE TUK-145/C DURING SPENT FUEL REMOVAL FROM DNRI RESEARCH REACTOR, VIETNAM

S. Kashkirov, S. Komarov, A. Ivashchenko
Sosny R&D Company

Nguyen Nhi Dien
DNRI, Vietnam

Stanley D. Moses
ORNL, USA

ABSTRACT

In 1963, the U.S. General Atomics constructed the TRIGA Mark II research reactor in Dalat Nuclear Research Institute. In 1983, the reactor was reconstructed to the Soviet Union design named IVV-9 reactor, which has used highly enriched uranium (HEU) VVR-M2 fuel assemblies. In 2013, under the Russian Research Reactor Fuel Return (RRRFR) Program the HEU spent fuel assemblies (SFAs) were removed to Russia for reprocessing.

The transportation was carried out by air involving a Type C package for the first time. Such a package for research reactor spent fuel (TUK-145/C) was developed in Russia on the basis of the SKODA VPVR/M cask; it satisfies all Russian, Vietnamese and international (IAEA) safety requirements. A procedure for "dry" loading of spent fuel assemblies into the SKODA VPVR/M cask through its top using a transfer cask and a support plate was developed for the first time ever.

The paper describes the work on preparation and implementation of the spent fuel removal.

INTRODUCTION

Dalat is located in the south of the Socialist Republic of Vietnam, 1500 km from Hanoi and 300 km from Ho Chi Minh City. This is the home place for Dalat Nuclear Research Institute (DNRI). The Dalat Nuclear Research Reactor (DNRR) is a pool-type 500-kW research reactor with a light water moderator and coolant consuming the Russian fuel VVR-M2.

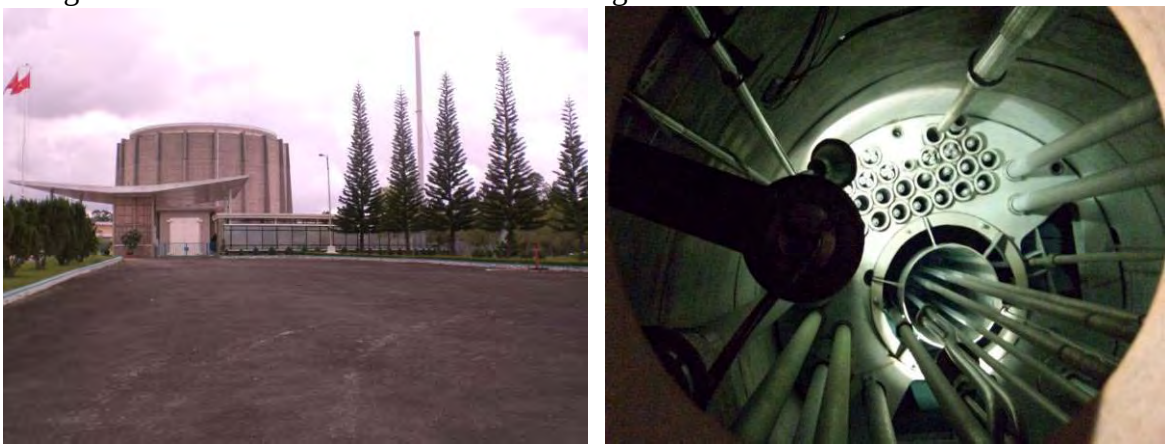

a – outside view b – reactor pool

Fig. 1. DNRR reactor

In 2007, low enriched uranium (LEU) assemblies were supplied to DNRI and non-irradiated VVR-M2 highly enriched uranium (HEU) fuel assemblies were removed from DNRI to the Russian Federation for reprocessing within the framework of the RRRFR Program. Then the DNRI specialists started gradual replacement of the HEU VVR-M2 for LEU fuel assemblies in

the reactor core. In October, 2011, 106 irradiated HEU fuel assemblies were reloaded from the reactor pool into the spent fuel storage pool.

a – HEU SFAs in the storage pool b – LEU VVR-M2 FAs

Fig. 2. VVR-M2 fuel rods

Spent nuclear fuel has never been removed from Dalat Nuclear Research Institute before, the institute infrastructure was not fitted out for spent fuel loading into transfer and shipping casks. So, the consignor's site was explored, the scope of activities for the infrastructure modernization was determined and the data was collected for further development of the procedure and equipment for reloading the SFAs from the storage pool to the SKODA VPVR/M shipping cask.

MODERNIZATION OF FACILITY INFRASTRUCTURE

Following the requirements to the facility infrastructure, the areas for loading the spent fuel into the transfer and shipping casks were provided with the main power supply and a backup system powered by a diesel generator. Enhancements were made to the polar crane in the reactor hall, and a jib crane was additionally installed to shorten the fuel loading time and to ensure safety of the operations. The equipment, developed and fabricated in Russia, was shipped to the Institute by sea in ISO containers. A horizontal ground was prepared for handling them there. A 16-ton capacity forklift was procured to deliver the SKODA VPVR/M cask to the reactor hall.

a – unloading the equipment b – delivering SKODAVPVR/M cask to the reactor hall

Fig. 3. Handling the equipment and SKODAVPVR/M cask

It was decided that the SFAs would be transported to the Russian Federation by air. All SFAs needed to be loaded in one SKODA VPVR/M cask. A procedure for reloading the DNRI research reactor spent fuel from the storage pool into the shipping cask was developed by the

specialists of Sosny R&D Company. An unique feature of the procedure was top loading of the spent fuel assemblies into the SKODA VPVR/M cask instead of usual bottom loading. For this purpose, a special transfer cask and ancillary equipment were used, which had been developed and fabricated particularly for this procedure. This was needed since it was impossible to install a SKODA VPVR/M cask directly above the pool, because it was located 4 meters above the floor level, and the crane in the reactor hall was limitted to 5 tons in its capacity.
Preliminary investigations and the data provided by DNRI enabled the Sosny experts to design the equipment with due regard to the peculiarities of the facility. In total, 27 types and 72 pieces of equipment and tools were fabricated; the designs of 10 of them were very sophisticated. Each ready-made piece of the equipment was subject to strength and performance tests at the fabricator's facility.
There are three groups of equipment and tools developed:

- for loading the SFAs into the transfer cask;
- for loading the SFAs into the shipping cask;
- for loading the shipping cask into an aircraft for air shipment.

Nuclear and radiation safety of reloading the SFAs into the shipping cask as well as mechanical strength of the equipment and tools were analyzed. Safe reloading of VVR-M2 SFAs into the SKODA VPVR/M cask was provided by the developed operation safety instruction.
On completion of fabrication, all equipment units were delivered to the experimental site in Dimitrovgrad, Russia, which had the structure approximated to the parameters of the DNRI spent fuel storage pool. The equipment was installed and its performance tests were carried out.

Fig. 4. Equipment installation at UJV

Then the equipment was packed and delivered to UJV, Rez a.s., the Czech Republic, by road. Once installed at UJV, the VVR-M2 loading equipment was tested for compatibility with the SKODA VPVR/M cask. During the tests a support plate with an adaptor and positioners were installed onto the SKODA VPVR/M cask; the load units were transferred from the dry storage pool in the SKODA basket using a transfer cask.
The transfer cask with the load unit was installed on the adaptor with its plug having been removed, and the load unit was put into the SKODA VPVR/M cask basket using an electric winch. After removing the transfer cask, the plug was remotely installed in the adapter cell with a hook rod.

Fig. 5. Compatibility tests of VVR-M2 loading equipment and SKODA VPVR/M cask

After the tests, the equipment was re-packed, loaded into the ISO containers and delivered to the Slovenian seaport of Koper by trucks; from there, it was sent to the seaport of Cai Mep, Vietnam, aboard an Aspol-Baltic vessel *Mikhail Dudin*. The underway time was about 30 days. The ISO containers with the equipment were delivered to Dalat Nuclear Research Institute by trucks.

At DNRI, the delivered equipment was unpacked, installed, adjusted and calibrated. Then the DNRI personnel training started with demonstration of video lessons with comments. After that the personnel learned all positions of the equipment, its purpose, composition and principle of operation. The next stage was practicing the use of the equipment and tools for handling mockup VVR-M2 SFAs. The personnel also learned the structure of the SKODA VPVR/M cask.

Loading the VVR-M2 SFAs into the shipping cask followed the training. The operations took 4 working days. Once the spent fuel was loaded, the lid with the metallic o-ring seals was installed, the cask was evacuated, and a leak test was performed. The IAEA Safeguards experts supervised all the operations.

Fig. 6. Practicing in loading VVR-M2 SFAs into the shipping cask

The forklift moved the dried SKODA VPVR/M cask containing 106 VVR-M2 spent fuel assemblies out of the reactor hall and placed it near the tilter. A truck crane installed the cask in the tilter to put on the lower shock absorber. After that, the SKODA cask was transferred into a special ISO container, where the upper shock absorber was put on it; then, the cask was tied down.

Fig. 7. Installing the SKODA VPVR/M cask in the tilter, loading into ISO container

Then the equipment was packed, loaded into the ISO containers and prepared for shipment to UJV, Rez a.s.

Fig. 8. Packing the equipment and loading into ISO containers.

On June 30, 2013, 4 ISO containers with the equipment and tools started in the vehicle convoy from Dalat to Bien Hoa Airport. On July 1, 2013, an ISO container with the SKODA VPVR/M package was convoyed from Dalat to Bien Hoa Airport too. The convoy was escorted by the police and the military.

Fig. 9. Delivering the equipment from Dalat to Bien Hoa Airport

On July 1, 2013, an *AN-124-100* aircraft delivered the energy absorbing container to Bien Hoa Airport. The handling equipment was deployed on the ground at the aircraft, and the SKODA VPVR/M cask and the energy absorbing container were joined together to build up the TUK-

145/C package. The TUK-145/C package was pulled into the aircraft with a winch, and the handling equipment was put into the ISO containers.

Fig. 10. Building up the TUK-145/C package and loading it into the aircraft

In the morning of July 3, 2013, the *AN-124-100* aircraft left Bien Hoa Airport for Koltsovo Airport (Yekaterinburg, Russia). The flight provided for a refueling stop-over at the airport of Vladivostok.

CONCLUSION

The HEU SFAs have been prepared for removal for three years. Meanwhile, a new procedure for loading the SFAs into the SKODA VPVR/M cask using a load unit was developed and the corresponding equipment was fabricated. Safe operation of the equipment was assured by strength, radiation and nuclear safety analysis, series of tests, as well as theoretical and practical training of the personnel.

Removal of the HEU SFAs from DNRI was the first air shipment with a TUK-145/C package certified for compliance with IAEA regulations for Type C package.

Effective cooperation of American, Vietnamese, Czech, Russian and IAEA specialists ensured the project success.

The technologies developed and the experience gained are useful for removal of the spent fuel from other research reactor facilities.

AVAILABLE REPROCESSING AND RECYCLING SERVICES FOR RESEARCH REACTOR SPENT NUCLEAR FUEL (A NEW IAEA REPORT)

S. TOZSER, F. MARSHALL, P. ADELFANG, E. BRADLEY
International Atomic Energy Agency,
PO Box 100, 1400 Vienna – Austria

M. BUDU
SOSNY Research and Development Company,
11 Derbenyovskaya Naberezhnaya, 115114 Moscow – Russian Federation

M. CHIGUER
AREVA
1 Place Jean Miller, 92084 Paris La Défense – France

ABSTRACT

International activities in the back end of the research reactor (RR) fuel cycle have so far been dominated by the programmes of acceptance of highly-enriched uranium (HEU) spent nuclear fuel (SNF) by the country where it was originally enriched. These programmes will soon have achieved their goals and the HEU take-back programmes will cease. However, the needs of the nuclear community dictate that the majority of the research reactors continue to operate using low enriched uranium (LEU) fuel in order to meet the varied mission objectives. As a result, inventories of LEU SNF will continue to be created and the back end solution of RR SNF remains a critical issue. In view of this fact, the IAEA, based on the experience gained during the decade of international cooperation in supporting the objectives of the HEU take-back programmes, drew up a report presenting available reprocessing and recycling services for RR SNF. This paper gives an overview of the report which will address all aspects of reprocessing and recycling services for RR SNF, including an overview of solutions, decision making support, service suppliers, conditions (prerequisites, options, etc.), services offered by the managerial and logistics support providers with a focus on available transport packages and applicable transport modes.

1. Introduction

IAEA, NEA and OECD continue to support the nuclear community in developing geological repositories. Therefore, a wide range of publications addressing specific safety requirements, international conferences proceedings, joint research reports, guidelines etc. on this subject is available.

The new IAEA report presented here [1] addresses the available mature options for the management of the back end RR fuel cycle (Fig. 1). Thus emphasis is made on reprocessing and recycling, including an overview of solutions, considerations of decision, regulatory requirements, fuel management service suppliers' conditions (prerequisites, options, etc.), services of the managerial and logistics support providers, and licensed transport packages and applicable transport modes.

Industrial entities in two countries, France and Russia, offer international SNF management services on a commercial basis. These services can provide the basis for viable RR SNF management options, depending upon their scope, technical compatibility, cost and accessibility.

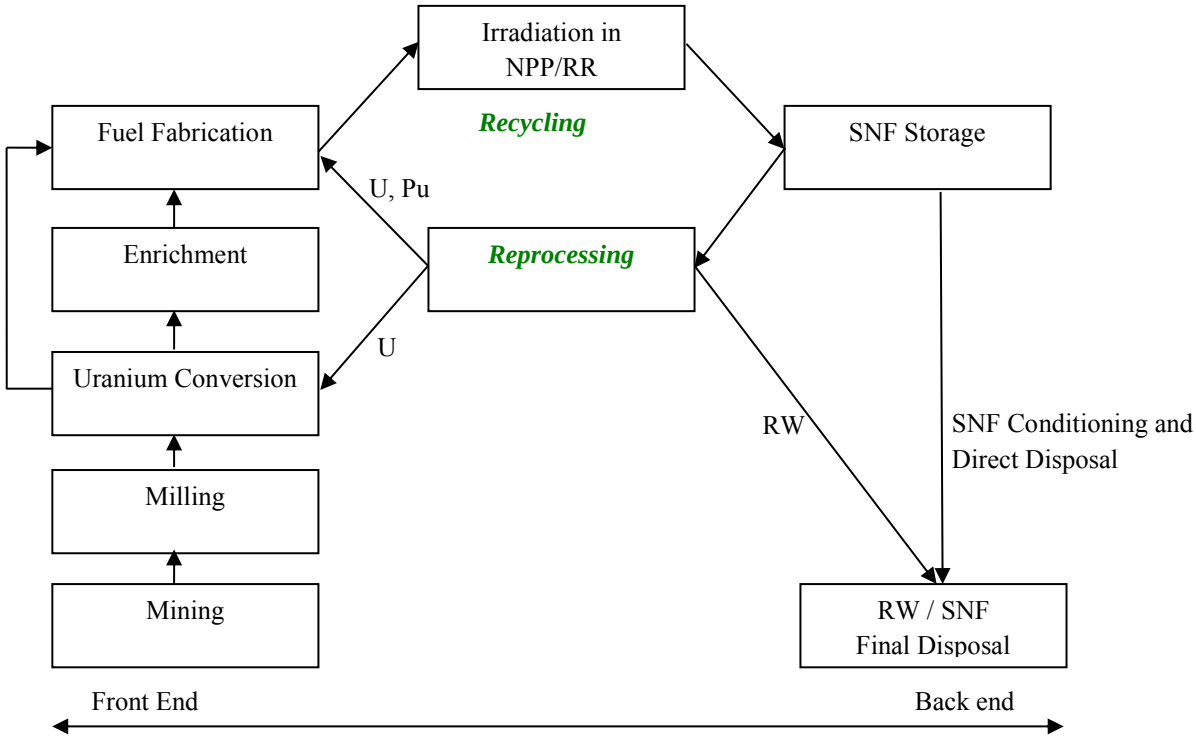

Fig 1. Nuclear fuel cycle

This paper summarizes the collection of information included in the IAEA report “Available reprocessing and recycling services for RR SNF” and presents the status of this publication.

2. Content of the IAEA Technical Report on Available Reprocessing and Recycling Services for RR SNF

The present document includes four chapters and three Appendixes.

Chapter 1 (the Introduction) outlines an overview of the back end nuclear fuel cycle solutions and considerations of decision. Chapter 2 presents the country specific reprocessing service description. Currently, only France and the Russian Federation offer RR SNF reprocessing services, which are addressed in this chapter. First of all the legislative background with the possible options for reprocessing are described in this chapter. Special attention is paid to the licensing procedures. The description of reprocessing facilities includes applied technology, environmental aspects, and time frame of a project realisation. Chapter 3 presents managerial and logistics support services and service providers. It considers examples of available transport packages, equipment and accessories, and transport modes. Based on experience, selection criteria, engineering, contracting and licensing support, and examples of a cost distribution for implementation projects, and of completed RR SNF shipments are also included. Chapter 4 presents conclusions, drawn during the preparation of this publication.

The Appendixes contain specific technical information about packages and equipment for RR SNF handling, as well as a service description template (SD) that outlines considerations to guide RR SNF disposition strategy based on reprocessing.

3. Overview of Included Information

3.1. RR SNF Management in France

The reprocessing process as performed at the AREVA La Hague facility [2] is summarized in Fig 2. The RR fuel reprocessing technology of the La Hague facility includes the following steps:

A - The reception and cooling step: once the fuel is received at La Hague facility, it is placed in interim storage pools for cooling. This cooling or deactivation substantially decreases the radioactivity of the fission products.

B - The reprocessing (treatment) step: after shearing the fuel is introduced into the existing dissolver through a pit specially designed for RR spent fuel. The dissolution is accomplished in a hot nitric acid solution. At this step, the process is limited by the aluminium concentration to 35-40g aluminium/L, to manage the risk of precipitation into aluminium nitrate. The resulting solution is then blended with the solution coming from the dissolution of the UOx fuel (power reactor fuel). Uranium and plutonium are extracted from the solution by a liquid-liquid extraction process. Several extraction cycles in pulsed columns, mixer-settler banks, or centrifugal extractors are necessary to meet the end-product specifications. At the end of these cycles, the following solutions are generated:

- a solution specifically containing the uranium;
- a solution specifically containing the plutonium;

a solution containing the fission products and the minor actinides.

C - The vitrification and storage step: the fission products and the minor actinides solution is then vitrified, i.e. conditioned into a stable, homogeneous and durable glass matrix, and encased in a standard canister, “Vitrified Universal Canister” (UC-V)[1]. The UC-Vs are then stored in a specific storage facility at La Hague site for cooling.

D - Following a cooling storage period, the UC-Vs are returned to the customer country for interim storage prior to final disposal.

In order to comply with the customer country’s regulations and technical constraints, the waste can also be conditioned by other means.

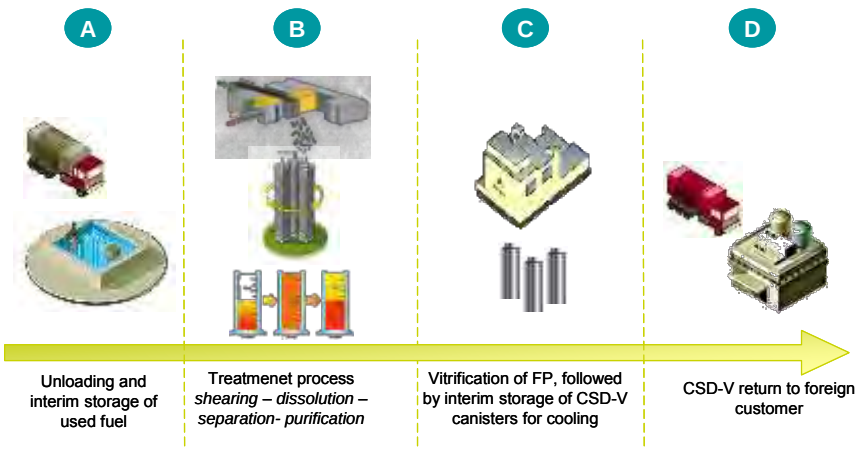

[1] Conteneur Standard de Déchets Vitrifiés (CSD-V)

Fig 2. Schematic view of the research reactor fuel treatment process

The AREVA reprocessing plant of La Hague has reception and reprocessing authorization for a wide range of known RR SNF. An extension of this authorization shall be obtained if the plant plans to receive new types of RR SNF.

Based on the past activities and experience in reprocessing various type of research and fast reactor spent fuel, AREVA has decided to launch the project of a new Polyvalent Fuel Treatment Facility (TCP[2]) at La Hague site. TCP will address various fuel specificities at the shearing and dissolution steps in order to answer varied customers' needs without hampering current La Hague reprocessing plant capacity. The new facility will substantially expand the reprocessing spectrum services of the La Hague plant.

AREVA is also conducting reprocessing qualification at La Hague plant for silicide RR SNF (U_3Si_2), with a similar process as for U-Al fuel adapted to the specific characteristics of silicide. The R&D program has already showed positive results and the solution is currently being qualified at an industrial-scale.

3.2. French International Agreements and Licensing Summary

Along with the usual customer-supplier commercial and industrial relationship, the inter-governmental discussions for Intergovernmental Agreements (IGA) between the Governments of France and the corresponding country are to be very well considered in the whole project time frame. Fig 3 bellow shows the typical schedule and main steps to be followed from first discussions and exchanges about a RR SNF management solution up to the effective contract signature.

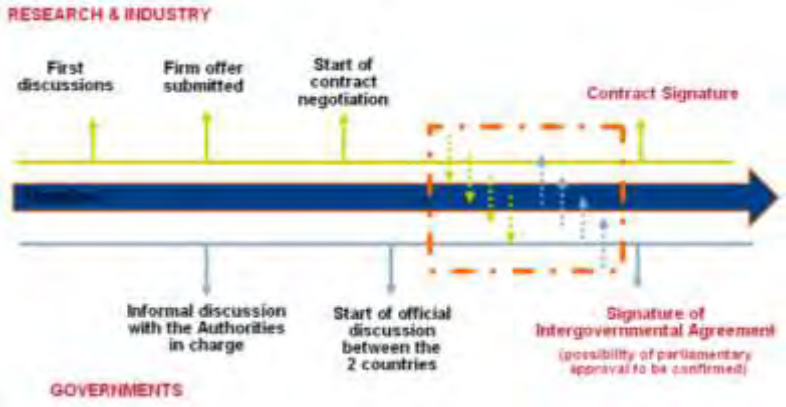

Fig 3. Typical schedule for a new RR spent fuel reprocessing contract

The IGA application requires three groups of information. Each of these is to be clearly developed in the final agreement:

– Project description: information on the material owner or related contractor (if different from the material owner), introduction of the main stakes for the owner or related contractor, location of the nuclear material, legal status and origin of the material, , the planned contractual structure for material treatment and recycling, the planned scope of collaboration between the parties;

[2] Traitement des Combustibles Particuliers

- Acceptability of reprocessing: type and characteristics of material to be reprocessed (design, total mass, mass of oxide and heavy metals, burn-up rate, cooling, initial enrichment, etc.), the material transportation (cask and transportation procedures to be realized);
- Schedule: quantities to be reprocessed and timing, period of delivery of SNF from the customer to AREVA La Hague facility, periods of treatment, period of waste return, use/reuse of the recycled material, deadline for last return of waste, destination of waste.

The French approval certificates of AREVA transportation casks are regularly renewed in order for this equipment to be available for all RR SNF removal projects. Agreement extensions have to be obtained for each type of RR SNF to be transported in these casks. When needed, specific baskets can be designed and manufactured for RR SNF transportation.

Two main authorizations issued by the French Nuclear Safety Authority (ASN) [3] are necessary in order to implement a reprocessing solution in France: transportation authorization and reception-reprocessing authorization at La Hague plant.

3.3. RR SNF Management in Russia

At present, in Russia functions one reprocessing facility – FSUE Mayak PA reprocessing plant RT-1, situated in Ozersk of the Chelyabinsk Region [4]. The main distinctive feature of the plant RT-1 is a wide range of reprocessed fuel. SNF of power reactors (VVER-440 and BN-600), naval propulsion reactors, commercial-scale reactors and research reactors is reprocessed here [5]. The distinctive features of the plant RT-1 technology are:

- Three multipurpose process lines allow not only reprocessing different fuel types on each of them, but also implementing joint reprocessing of different SFAs.
- Extraction of neptunium during SNF reprocessing is aimed at its separated storage and fabrication of radioisotopic products.
- Commercial output of regenerated uranium with targeted ^{235}U enrichment by means of mixing the uranium resulted from reprocessing different SNF.
- Separation of different elements from residual SNF solutions for fabrication of radioisotopic products (caesium, strontium, promethium, krypton, etc.).

The SNF delivered to the plant is placed into a cooling pool (Fig.4), where more than three meters of water above the fuel make a reliable biological shielding. The duration of RR fuel interim storage is up to 2 years before reprocessing. Safety of the SNF interim storage is ensured by highly efficient pool water purification system and radiation monitoring systems. The first stage of SNF reprocessing is to cut the SFAs and load the fragments into a batch-type dissolver, where the fuel is dissolved in nitric acid solution. Then the nitric-acid solution of fuel composition is clarified by filtering and after that is reprocessed by the PUREX process. The PUREX process allows to extract and separate the valuable elements (uranium, plutonium, neptunium). The targeted products of SNF reprocessing are:

- Uranyl nitrate melt, obtained from evaporation of nitric-acid solution of uranium;
- Triuranium octoxide, obtained from precipitation by ammonia and subsequent roasting of the precipitate;

- Plutonium dioxide, obtained from precipitation by oxalate and subsequent roasting of the precipitate.

Beside the mentioned targeted products, krypton (^{85}Kr), strontium (^{90}Sr), caesium (^{137}Cs), americium (^{241}Am), promethium (^{147}Pr) and other radionuclides are separated from the spent fuel [6].

Fig 4. General view of the SNF pool at FSUE Mayak PA

The FSUE Mayak PA directions of further development include extension of the reprocessed SNF domain from 2017 by U-Be, U-Zr, uranium metal, plutonium fuels and materials, SNF from molten salt RR and other spent nuclear fuels.

Development and implementation of optimizing process design solutions is aimed at minimizing the operating costs and volumes of liquid radioactive waste during SNF reprocessing. This includes a number of new processes making part of the SNF reprocessing cycle, the implementation of which is anticipated to result in a three-fold decrease of operational medium-level (ILW) radioactive waste (RW). New RW processing facilities (a cementation complex, a high-level waste (HLW) vitrification complex, a solid RW management complex) are planned for construction and commissioning between 2015 and 2020. Simultaneous upgrades to the existing equipment and asset replacement are in the plan, too. The developed concept of the new multi-functional vitrification complex will allow the solidification of all types of liquid HLW in borosilicate or alumophosphate glass using detachable single-use fusion crucibles. Thus, the solidification of operational HLW resulted from reprocessing Russian and foreign SNF, return of the RW to foreign SNF suppliers, and clearing the storage tanks from the accumulated waste will be ensured [7].

3.4. Russian International Agreements and Licensing Summary

The main provisions of the Federal Law No. 7-FL “On Environmental Protection” dated 10 January 2002 are as follows:

- The SNF import is permitted for interim storage and/or reprocessing.

- The project shall undergo a state ecological expertise [3] during which a general decrease of the radiation effects and enhancement of environmental safety, resulted from implementation of the project shall be justified.
- The basis for the import are international contracts of the Russian Federation.
- The Law gives preference to the option of returning the radioactive waste resulting from reprocessing to the country of origin of the RR SNF.
- The RR SNF imports are subject to the yearly limits approved by the Government of the Russian Federation.

In compliance with the Government Decree no. 418, dated 11 July 2003 the following project preparation procedure has been formed:

(1) Conclusion of a government-to-government agreement with the foreign country on cooperation in SNF import (both of Russian and foreign origin) into the Russian Federation. In a number of cases, Russia already has an acting agreement. The international contract should contain provisions for the destiny of radioactive waste resulted after SNF reprocessing. Two options are possible: RW re-turn to the export country, or permanent disposition in the Russian Federation.

(2) Elaboration of the documentation for an SNF import Unified Project in compliance with the established requirements, including:

- Draft Foreign Trade Contract (FTC);
- Special ecological programme (programmes) (SEP);
- Materials to justify general decrease of the risks of radiation impact and enhancement of environmental safety as result of the Unified Project implementation, as well as the timeframe of interim technological storage of spent fuel assemblies and reprocessing products, stipulated by the FTC;
- Other materials to be submitted to the state ecological expertise, including the conclusion of the Russian Federal Service for Environmental, Technological and Nuclear Supervision (Rostechnadzor) and the Ministry of Public Health of the Russian Federation.

An import/export license is required for nuclear commodities and technologies, including RR SNF or RW resulted from reprocessing. Federal Centre for Nuclear and Radiation Safety (FCNRS) is authorized by the Government of the Russian Federation to sign FTCs for SNF imports, and also prepares applications, and obtains import licenses for SNF.

The Russian regulations for the safe transport of radioactive material (RM) establish the following approvals:

- Package design approval;
- Shipment approval.

[3] Measure in the field of ecological expertise organized and implemented by the federal or regional executive body in conformity to the procedure established by the Federal Law “On ecological expertise” No. 174-FZ from 23.11.1995 and other regulatory acts of the Russian Federation. The ecological expertise means establishing the conformity of the documentation justifying the economic or other activity envisioned by the object of the ecological expertise to the ecological requirements established by technical procedures and regulations in the field of environmental protection, with the purpose to prevent the negative impact of such activities to the environment.

The Special Transports Unit of Rosatom's Nuclear and Radiation Safety and Organization of Licensing and Approval Activities Department coordinates the preparation of all commercial RM package design and shipment certificates.

3.5. Managerial and Logistics Support

During the preparation of this technical report and by the time of its publication the IAEA made sustained efforts to encourage all potential suppliers to send relevant contributions. The entire Chapter 3 contains information received from various French, Russian, Czech and German suppliers who provided services for RR SNF shipments to France and Russia, and who could offer their contribution to this technical report by the time of its publication, as well as by the courtesy of Savannah River National Laboratory. Packages, equipment, and services from any other suppliers may be accepted in France and Russia provided that the relevant certificates and licenses are obtained.

A brief description of required support equipment, as well as examples of engineering support for project preparation and implementation are addressed in the IAEA technical report. A summary of available RR SNF packages presented in the IAEA technical report is included in Table 1.

TABLE 1. SUMMARY OF AVAILABLE RR SNF PACKAGES

Package	Service Provider	Countries	Mode of Transport	Appendix I Ref.
TUK-19	Sosny R&D Company	Russia, Kazakhstan, Latvia, Libya, Poland, Romania, Serbia, Uzbekistan	Road, Railway, Water, Air	I.1
TUK-145/C	Sosny R&D Company	Russia, Vietnam, Hungary, Uzbekistan	Road, Railway, Water, Air	I.6
ŠKODA VPVR/M	ÚJV Řež Sosny R&D Company	Russia, Belarus, Bulgaria, Czech Republic, Hungary, Poland, Serbia and Ukraine	Road, Railway, Water	I.2
Castor MTR2	DAHER – NCS, Sosny R&D Company	Russia, Germany	Road, Railway, Water	I.3
TUK-128 (TUK-135)	Sosny R&D Company, FSUE Mayak PA	Russia	Road, Railway	I.4
TUK-32	Sosny R&D Company, FSUE Mayak PA	Russia	Railway	I.5
TN™MTR-68, 44, RHF	AREVA TN	France, Denmark, Portugal, Italy, Venezuela, Australia, Belgium, USA	Road, Railway, Water	I.7
TN™MTR-52, 52S, 52SV2	AREVA TN	France, Denmark, Portugal, Australia, USA	Road, Railway, Water	I.7
TN-LC	AREVA TN	France, USA	Road, Railway, Water	I.8
TN®17/2	AREVA TN	France, Netherlands, Italy, Sweden, Belgium	Road, Railway, Water	I.9
NAC-LWT	NAC International	USA, EU, South America, Asia countries	Road, Railway, Water	I.10

The principal characteristics of available transport modes (Table 2) are described in detail, along with a summary of transport selection and shipment coalitions considerations, and applicable international conventions and agreements.

TABLE 2. AVAILABLE TRANSPORT MODES

Shipment by air	Most suitable in case of SNF small amounts; in case of long distances from the RR's site; if there are transit countries to cross; if maximal physical protection must be provided; implies highest cost-per-unit; demands more labour- and time-consuming safety analysis.

Shipment by water	Most suitable in case of SNF large amounts; in case of long distances from the RR's site; if there are any sea ports in the export country; special regulations apply for inland waterways.
Shipment by railway	Most suitable for states that share common borders with the reprocessing country; implies lowest cost-per-unit.
Shipment by road	Often the only possible mode for SNF shipment over short distances (from the RR's site to the railway station, the airport, the seaport, from the railway terminal to the sea terminal, from the airport to the reprocessing plant); for safety reasons not applicable for SNF shipment over long distances.

Experience shown that engineering support is required during SNF preparation and shipment different stages:

(1) Decision preparatory phase: preparation of feasibility studies, selection of route, transport modes and packages, support in forming RR coalitions for cost and schedule optimization, development and licensing of new packages and transport means etc.

(2) Contracting support: allows implementation of turnkey solutions providing project management of subcontractors, interface with authorities, schedule control, work implementation coordination etc.

(3) Licensing support: according to [8] RR SNF is transported in Type B(U)F or C packages (for fissile materials) that require multilateral approval of certificates for package design and shipment, therefore engineering support is provided during licensing in the country of the RR, reprocessing plant as well as in transit countries.

(4) Support for the RR facility preparation: during SNF inspection and acceptance by the reprocessing facility, development of spent fuel assemblies' loading technology in transport packages, RR facility modifications for allowing the transport package handling, failed fuel repackaging etc.

(5) Shipment support: carriers licensing, contracting and coordination, SNF loading in transport packages, preparation of shipment documents, technical escort of the shipment, interface between the RR, reprocessing plant, carriers and different authorities during shipment etc.

(6) Post shipment activities support: support during preparation, licensing and shipment of the RW resulted from reprocessing back to the SNF originator country.

During many years of international cooperation lead by IAEA [9], US and Russian Governments for the implementation of the HEU take-back programmes, as well as of RR SNF commercial reprocessing and recycling services provided by France and Russia, worldwide service providers have worked together and developed experience in all above mentioned stages of SNF preparation and shipment.

AREVA TN has several decades of experience in the international transport of spent fuel by road, rail and sea, can rely on the collaboration of companies in the AREVA group and can offer efficient, reliable and safe solutions. AREVA TN's main activity is to design, manufacture and deploy package systems for nuclear material for both nuclear power plants and research reactors. AREVA TN has extensive experience under the U.S. Foreign Research Reactor Fuel Return Program with the transport of irradiated research reactor fuel elements (TRIGA, MTR, DIDO, etc.) to the Idaho National Laboratory and Savannah River Site in the USA from Japan, Denmark, Austria, Netherlands, Portugal, Taiwan, and Indonesia, shipments of LEU and HEU from the DOE/NNSA Y-12 site in Oak Ridge to France, and of fresh MTR and TRIGA fuel elements and radioisotope production targets from France to numerous countries, including the USA, Australia, Indonesia, The Netherlands,

Sweden, Norway, Japan and South Africa. AREVA TN also transported nuclear fuel to AREVA's La Hague reprocessing plant from Australia, France, and Belgium. AREVA TN also has significant experience transporting irradiated targets, irradiated fuel pins, and irradiated hardware to hot cells and other research facilitates using the smaller TN-106 cask.
Beside its reprocessing and recycling activities, AREVA also provides comprehensive solutions for SNF management such as engineering work in developing waste storage and disposal equipment and facilities.

Sosny R&D Company's main activities are focused on research and development in the field of nuclear energy. Sosny R&D Company took part in the implementation of the RRRFR Programme in the framework of which re-search reactor fresh and spent fuel of Russian origin was returned to the Russian Federation from Belarus, Bulgaria, Czech Republic, Germany, Hungary, Kazakhstan, Latvia, Libya, Poland, Romania, Serbia, Ukraine, Uzbekistan and Vietnam. The role of the Sosny R&D Company in the programme is to develop technologies and equipment for SNF loading in packages, provide training services for the RR operators on handling Russian packages and equipment, prepare regulatory documents including safety assessments. In support for SNF shipments organization projects Sosny R&D Company provided many technical solutions:

- Foreign package certification in the Russian Federation (Czech ŠKODA VPVR/M in 2005, German CASTOR MTR2 in 2010) and FSUE Mayak PA technology adaptation for handling new packages;
- Development of an overpack for the Russian TUK-19 package shipment by any conveyance, including air;
- Vessel modernization for RR SNF shipments;
- Development of transfer casks for SFA loading in TUK-19 and ŠKODA VPVR/M packages;
- Development and delivery of equipment, safety assessment and licensing for new fuel reprocessing technologies at FSUE Mayak PA;
- Creation of the type C package TUK-145/C for shipments by any conveyances including air of radioactive materials with no restrictions on the radioactivity content.

Different other contractors have proven international experience in different stages of RR SNF preparation and shipment:

- Czech Republic: ÚJV Řež, a. s. (SKODA VPVR/M package services), SKODA a.s. (package development) and DMS s.r.o. (Class 7 dangerous goods shipment on public road);
- Germany: DAHER – NCS (package and shipment services);
- Russia: J/S ASPOL-Baltic Corporation (SNF sea shipments) and Volga-Dnepr Airlines (fresh and spent nuclear fuel air shipments);
- USA: Edlow International (radioactive materials transport), Holtec International (spent fuel management); NAC International (spent fuel transport packages and services).

The IAEA technical report also contains a summary of US- and Russian-origin HEU RR SNF take-back programmes, IAEA involvement in these programmes, and examples of LEU RR SNF shipments for reprocessing.

5. Preparation Status and Conclusions

The preparation and editorial phase of the IAEA Technical Report “Available Reprocessing and Recycling Options for Research Reactor Spent Nuclear Fuel” ended, and is now following the publication procedure within the IAEA.

The upcoming IAEA Technical Report “Available Reprocessing and Recycling Options for Research Reactor Spent Nuclear Fuel” offers a comprehensive description of services available, at the time of writing, for reprocessing and recycling RR SNF. The presented existing experience, service providers available to develop feasibility studies and available technologies that can serve as models form a complete knowledge basis for the assessment of the potential project technical specificities, risks, time frame, and budget estimations at the initial phase of planning and decision-making.

REFERENCES

[1] DRAFT Technical Report “Available Reprocessing and Recycling Options for Research Reactor Spent Nuclear Fuel”, IAEA, 2015.

[2] B.Stepnik, M.Grasse, D.Geslin, C.Jarousse, A.Tribout-Maurizi, F. Lefort-Mary, “AREVA involvement in UMo fuel manufacturing and research test reactor fuel treatment”, RRFM-2012, Prague, 2012.

[3] FRENCH NUCLEAR SAFETY AUTHORITY, About ASN (2014), http://www.french-nuclear-safety.fr/ASN/About-ASN

[4] FSUE Mayak PA, About the facility (2014) (in Russian), http://www.po-mayak.ru/wps/wcm/connect/mayak/site/About/.

[5] V. Savkin, “Reprocessing of research reactor spent nuclear fuel at the PA “Mayak”, Workshop on “Technical and Administrative Preparations for Shipment of Russian-Origin Research Reactor Spent Fuel to the Russian Federation”, Rez, 2008.

[6] D. Kolupaev, “Handling SNF at FSUE “Mayak” PA”, paper presented at the meeting on SNF removal from Germany to Russia, Berlin, 2009.

[7] K. Ivanov, “Plans of SNF reprocessing until 2030 at FSUE Mayak PA”, IAEA Contact Expert Group Workshop: Economic Aspects of Spent Fuel Management: Reprocessing and Direct Disposal, Stockholm, 2011.

[8] IAEA Regulations for Safe Transport of Radioactive Materials, SSR-6, Vienna, 2012.

[9] Tozser, P. Adelfang, E Bradley: (IAEA): “A Decade of IAEA Cooperation with the RRRFR Programme”, PATRAM-2013, 18-23 August 2013, San Francisco, USA.

AREVA TN TRANSPORTS AND LOGISTICS ACTIVITIES - FLEET OF TRANSPORT CASKS FOR INTERNATIONAL SHIPMENTS IN SUPPORT OF RESEARCH REACTOR AND LABORATORIES

Nicolas GUIBERT, Jay THOMAS
AREVA TN Americas
7135 Minstrel Way, Suite 300, Columbia, MD 21045 - USA

Vanessa LALOY
AREVA TN Europe
1 rue des Hérons 78 1280 Montigny le Bretonneux - FRANCE

ABSTRACT

AREVA TN operates a comprehensive fleet of certified packages for a wide spectrum of radioactive material shipments worldwide. Some of AREVA's certified packages, such as the TN®106 or the TN®MTR are dedicated to the shipments of irradiated material or used fuel from research reactors. The TN®106 has been used recently in the US for the first time and paved the way to other potential shipments.

In order to respond to emerging shipment needs and to support future US domestic and international reactors, AREVA TN is constantly innovating with new package developments. The new TN®-'Long Cask' (TN®-LC) offers a specific and customized solution for unconventional research reactor and laboratory irradiated fuel shipments. It will be available to support US domestic and international shipments by September 2015.

AREVA TN has access to other types of casks used for various types of needs, ranging from the medical isotopes transport packages to fresh and spent fuel transport casks. This consistent fleet of transport packages along with AREVA TN transport and logistics activities is supporting the safe transports of a broad range of nuclear and radioactive material across many countries.

AREVA TN handles nearly 3 000 shipments of radioactive material annually; and, with the TN®-LC, TN®-MTR, TN®-106 and the Flying Pig, now expects to expand its used fuel transport capabilities in the US and in the diverse worldwide market.

1. Introduction

AREVA TN, which provides Nuclear Logistics Operations for AREVA, has a unique and solid expertise in the shipment of radioactive and nuclear material. AREVA TN is the world's leading designer of used fuel and high level waste (HLW) casks, for transport and/or storage. Anticipating regulatory changes, AREVA TN has its own licensing department which works closely with international organizations and with more than 30 Safety Authorities throughout the world. AREVA TN has developed and licensed more than 40 different cask designs over the years for used fuel and for HLW. With AREVA TN having locations around the world, like AREVA TN-Europe, AREVA TN-Americas, and AREVA TN-Asia, transport operations are performed seamlessly.

AREVA TN, in cooperation with the CEA (French Atomic Commission) operates a comprehensive fleet of certified packages for a wide spectrum of radioactive material shipments worldwide. Some of AREVA TN's certified packages, such as the TN®-LC or the TN®-MTR are dedicated to the shipments of irradiated nuclear materials or used nuclear fuel from research reactors. Others, like the TN®106 and the 'Flying Pig', have unique features that better support research programs and activities performed in hot cell facilities. In order to better support the ever changing demands of the research reactor and nuclear research programs community, AREVA TN is constantly looking to improve the capabilities of its existing fleet of packages while evaluating new, innovative designs. The TN®-LC and the Flying Pig represent two of these new package designs. Each of these casks is described in this paper.

2. Fleet of Packages for Irradiated Nuclear Materials

TN®-MTR

The TN®-MTR (Material Test Reactor) cask has been the work horse of AREVA's used fuel packages for research reactors. Since its deployment in 1999, more than 200 shipments using TN-MTRs have been conducted. The TN-MTR has successfully transported used nuclear fuel from reactors within France, and from Denmark, Portugal, Indonesia, Australia and Belgium. It is authorized for unloading operations at La Hague, in France and the Savannah River Site in the United States.

With six different basket configurations (with capacities to transport from 4 to a market leading 68 fuel assemblies) available and a broad safety analysis, the TN®-MTR is capable of transporting a wide variety of MTR type fuel assemblies. For facilities with sufficient crane capacity (23.4 mt) over their fuel pools, the TN®-MTR can be easily and quickly loaded underwater, removed from the pool and dried, and prepared for shipment. The use of the dry transfer system helps to accommodate fuel loading in smaller facilities.

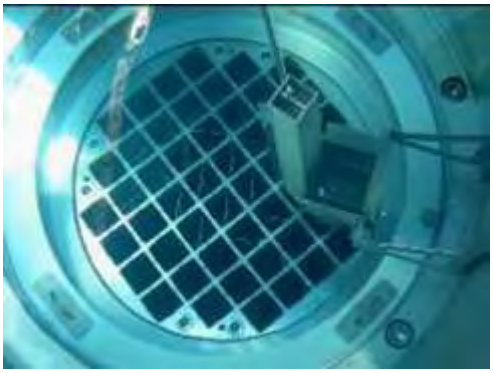

Figure 1: TN-MTR wet loading at Research Reactor site
© AREVA

Figure 2: Transfer system for loading TN-MTR at Research Reactor site
© AREVA

	Loaded	Empty
Mass	21,750 kg	18,950 kg
With shock absorber	23,400 kg	20,600 kg
	Length	**Diameter**
Cavity	1,080 mm	960 mm
Overall	2,008 mm	2,080 mm

TN-LC

The newly designed and soon to be deployed TN®-LC is a U.S. Nuclear Regulatory Commission (NRC) certified transport package designed with the increased capacity to transport various types of fuel pins and assemblies, including commercial fuel assemblies (BWR, PWR), rods or pins (EPR™, MOX, PWR, BWR), and research reactor assemblies such as NRU/NRX, TRIGA elements, and MTR fuel assemblies. AREVA TN is very excited to have this cask enter the market in September 2015.

With four different internal basket arrangements, the TN®-LC can also accommodate a variety of assembly types in a number of configurations.

- MTR basket: Each basket has a capacity of 9 fuel assemblies. With six tiers per basket, the MTR capacity is 54 assemblies.

- TRIGA basket: This basket is available in different lengths to accommodate intact TRIGA elements of different sizes including TRIGA Fuel Follower Control rods. The basket has a capacity of 36 fuel elements and using five tiers, gives a capacity of 180 fuel elements.

- NRU/NRX basket: This configuration consists of two baskets each with a capacity of 13 NRU or NRX assemblies for a total capacity of 26.

- 1FA basket: This basket can accommodate one intact full length fuel PWR or BWR assembly or pin cans that can accommodate up to (25) intact PWR, BWR, EPR™ or MOX fuel rods.

Other baskets can also be designed to accommodate other transportation needs.

The TN®-LC has the capability of transporting full length commercial high burn-up fuel rods in support of Post Irradiation Experiments (PIE). The significant length of the cavity gives sufficient room for the irradiation growth that can be of importance for fuels with high burn-up. To add capacity in the future, AREVA TN is working on revising the safety analysis to include the transport of damaged, failed, or sectioned pins and rods.

With its 25 ton weight, the TN®-LC complies with most commercial or research reactor site weight restrictions. The TN®-LC is designed to be loaded or unloaded in the vertical or horizontal position and can be operated in wet or dry conditions, in fuel pools or hot cells. A dry transfer system is being developed allowing operation in sites with weight restrictions and shallow pools.

Figure 3: TN-LC Cask Body
© AREVA

Figure 4: TN-LC Cask with Impact Limiters
© AREVA

	Loaded	Empty
Mass	24,500 kg	18,950 kg
	Length	**Diameter**
Cavity	4,636 mm	457 mm
Overall	5,017 mm	1,130 mm

TN®106

The TN®106 cask entered the market in 2002 as a versatile medium sized cask offering excellent support to the research community. It is certified in France as a Type B(U)F package authorized for transport by road, sea and rail. It has proven to be a dependable cask, with a history of over 200 shipments since it was deployed. The TN®106 has been used in France, Great Britain, Sweden, Switzerland, Belgium, Germany, and Norway. Recently, it was used to transport irradiated experimental fuel pins from France to the Idaho National Laboratory in the United States.

The cask can be loaded and unloaded underwater. But, it's most prominent feature is the revolving plug which allows for efficient operations with hot cells. The authorized contents are:

- UO_2 fuels, rods and pins, powder
- MTR fuel Elements
- MOX fuel rods
- Fast neutron reactor fuel rods
- Non fissile solid radioactive materials

Figure 5: TN-106 Cask on its transport frame
© AREVA

	Loaded	**Empty**
Mass	9,100 kg / 9, 700 kg	9,700 kg / 10, 300 kg
With shock absorbers	11,600 kg / 12, 300 kg	11,100 kg / 11, 700 kg
	Length	**Diameter**
Cavity	2,200 /2,400 mm	203 mm
Overall	3,624/ 3,824 mm	1,458 mm

The 'Flying Pig'

Over the past years, the demand for a cost-effective and flexible solution to transport small quantities of irradiated material for research purposes has been continuously increasing. However, there was no small and inexpensive transport cask available on the market to carry out this task.

In an effort to optimize cooperation between worldwide hot labs, some hot lab operators, assisted by members of industry, authorities, and transport organizations, started to refocus their attention on the international transfer of research radioactive material. During the past few years, the main design principles were optimized to meet hot lab specifications. Designs also incorporated improvements based on valuable feedback on past experiences with existing casks. AREVA TN was selected by hot lab operators to design and license this new cask.

The Flying Pig is based on the concept of the TN®106, thus taking advantage of an existing and established design.

- The TN®106 is known to hot lab users, thus the easiest way to guarantee good operability
- The TN®106 is also known to the respective authorities:
  - The French Competent Authority (FCA) has issued a certificate
  - The United States Competent Authority has issued a DOT validation

The cask will be certified as a Type B(U) package. It will be transportable by **air**, road, rail, and sea. The package will be authorized to transport small quantities of irradiated fuel or structural materials in solid form (fissile excepted or fissile limited according to §674 AIEA2012). The physical form of the material can be clad and unclad fuel, powder, or solid, mounted pellets, and pin segments. Chemical compositions include metal, oxide, carbide, and nitride forms or mixtures. As with the TN®106, the package can be unloaded and loaded wet or dry and houses a rotating plug for hot cell operations. Thus, the Flying Pig will be equipped with a component allowing direct interface with the "La Calhène" system.

The design process is currently planned to be completed in 2016. Performed in parallel, fabrication of the cask and receipt of the French Competent Authority approval will be completed by 2017. Afterwards, the Flying Pig can be used in countries that signed the ADR regulation. For the U.S., the DOT validation will be issued approximately six months later.

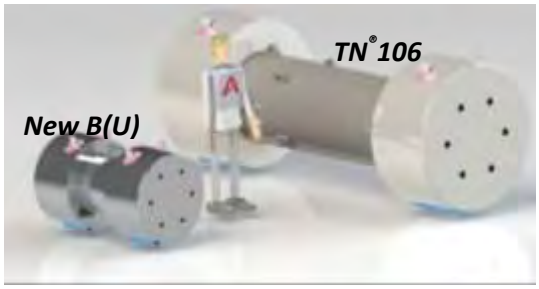

Figure 6: Flying Pig next to TN®106
© AREVA

Figure 7: Flying Pig (exploded view)
© AREVA

Mass (With shock absorbers)	~ 2,500 kg	
	Length	**Diameter**
Cavity	300 mm	150 mm
Overall	1,500 mm	900 mm

3. About AREVA

AREVA is the world leader in the back end of the nuclear fuel cycle with more than 48,000 employees around the world. As part of the AREVA Group, AREVA TN offers innovative solutions for the transportation and storage of nuclear materials for nuclear power plants and research reactors around the world. AREVA operates the largest fleet of transportation casks in the world and organizes more than 3,000 multi-model shipments of nuclear material each year; more than 70 shipments are in progress at any given time.

4. About AREVA TN

AREVA TN is present at all stages of the nuclear fuel cycle. With its expertise, AREVA TN oversees and manages nuclear transports throughout the world, at a very high level of safety. The benefits of this experience and global footprint are shared by AREVA TN's wide panel of international customers.

DESCRIPTION OF THE PROCESS FOR FUTURE RETURNS OF IRRADIATED TRIGA FUEL FROM RESEARCH REACTORS TO IDAHO

DALE LUKE & ALAN ROBB
*CH2M*WG Idaho (CWI), LLC*
1580 Sawtelle St., Idaho Falls, Idaho - USA

ABSTRACT

The returns program is a part of the, “Atoms for Peace” program wherein the United States (U.S.) provided nuclear technology to foreign nations and domestic research reactors for peaceful applications. As a part of this program when the fuel was expended the agreement was to return the U.S.-origin fuel back to the U.S. for storage and ultimate disposition.

The U.S. Department of Energy (DOE) reviewed many options for consolidation of SNF at select facilities in 1995. The results of that review were presented in an Environmental Impact Statement that identified the INL as the temporary storage location for DOE-owned non-aluminum clad fuels currently stored at DOE, domestic, and foreign locations. All TRIGA fuel (which includes all types of cladding) was slated to be sent to the INL. This relocation of non-aluminum SNF to the INL supports U.S. nuclear weapons non-proliferation goals.

This presentation will describe the requirements and practices associated with preparing and shipping irradiated TRIGA fuel to the U.S. DOE facility in Idaho for consolidation and storage from foreign and domestic research reactors.

This information is expected to be very useful as many research reactors may be evaluating the options of continued operations vice having to shut down and dispose of the TRIGA fuel in light of the probability of ending the returns program by the year 2019.

1. INTRODUCTION

This paper describes the process for future returns of irradiated TRIGA fuel from research reactors to Idaho fuel storage facilities (Fig. 1). This paper defines the requirements for documentation of the irradiated fuel to ship to Idaho, typically defined as the “Appendix A” information that is part of the shipping contract between the research reactor and DOE.

Figure 1. Idaho Nuclear Technology Engineering Center (INTEC)

2. BACKGROUND

This information is anticipated to be very useful as many research reactors may be evaluating the options of continued operations vice having to shut down and dispose of the TRIGA fuel in light of the probability of ending the U.S.-origin Removal Program by May 12, 2019. If the option to return the fuel is taken or is being considered, irradiation of the fuel elements needs to cease by May 12, 2016.

No change to this authorization is anticipated or expected at this time.

3. APPENDIX A INFORMATION (DATA) FOR THE SHIPPING CONTRACT

Three forms are used for the Appendix A information (data) for the shipping contract.

- Fuel and Packaging Required Shippers Data (F&P RSD) – Form 434.28 (Includes Forms 434.28, 434.28A, & 434.28B)
- Proposed Shipment Contents RSD (PSC RSD) – Form 434.30
- Shipment Contents RSD (SC RSD) – Form 434.31

This paper will walk us through these forms – why, what and when the data is needed.

4. WHY DATA IS NEEDED

The used / spent nuclear fuel that comes to Idaho is planned to go to a national repository, therefore much of the required shippers data is needed to support disposition of the fuel to the national repository.

The fuel is stored in a dry storage facility that has safety limits that must be met, so adequate fuel data is needed to support those limits.

Materials control and accountability (MC&A) requirements must be met to ship and receive fuel from research reactors.

5. F&P RSD FORM (FORM 434.28)

The form shown below (page 1) in Figure 2 is part of the Fuel and Packaging (F&P) Required Shippers Data (RSD) form (Form 434.28).

Page 1 of the F&P RSD asks for needed shipper & shipment identification information – mostly to assist in materials control & accountability (MC&A). Checkboxes are provided to simplify filling in the form. The Information on this form is typical for Appendix A to the shipping contract.

Much like page 1, subsequent pages require the shippers to provide data about:

- The reactor – reactor name; initial criticality date; shutdown date; typical core; rated power; significant events in operations; etc.
- Spent nuclear fuel data – fuel type (e.g., TRIGA); total number of elements to be shipped; description of the fuel, including how identified and any changes to the fuel; condition of the fuel unit and cladding integrity; etc.
- Spent nuclear fuel packaging data – identify and describe the fuel handling units (FHUs) (e.g., cans, baskets, buckets) to be shipped; details of the FHUs, including how identified, materials of construction, etc.; describe the loading process and resultant weight and condition of FHUs

Figure 2. F&P RSD Form (Form 434.28)

Revision Number:

Description	Shipper Summary **NOTE:** If items do not apply, mark as N/A.	References (list reference number from Form 434.28B)
I. SHIPPER AND SHIPMENT IDENTIFICATION INFORMATION		
1. Shipper Information[1]		
a. Shipper Reporting Identification Symbol (RIS):[2]		N/A
b. Shipping Facility Name:		N/A
c. Shipping Facility Address:		N/A
d. Shipping Facility Point of Contact (name of authorized person for shipper):		N/A
e. Shipping Facility Point of Contact Telephone Number:		N/A
2. License number:[3]	☐ N/A	N/A
3. Transfer authority – contract, NM draft or order number (foreign shipments only):[4]	☐ N/A	N/A
4. U.S. port of entry (foreign shipments only):	☐ N/A	N/A
5. IAEA batch identification number (International Atomic Energy Agency [IAEA] protocol or signatory facilities or domestic facilities subject to IAEA inspection and inventory requirements only):[5]	☐ N/A	N/A
6. Ownership of accountable nuclear material:[6]		N/A
7. Shipping Agent Information (entity ensuring fuel arrives at the INL)[7]		
a. Shipping agent name:		N/A
b. Shipping agent address:		N/A
c. Name of authorized person for shipping agent and Phone number:		N/A

- Transportation package (shipping cask) data – identify the transportation package to be used; identify the certificate of competent authority (or equivalent); identify the current safety analysis report for transportation for the cask; and other pertinent information (if applicable)
- Hoisting and rigging fixtures – provide drawings, reports, approvals of design, etc. if additional or different hoisting and rigging fixtures are required
- Environmental safety and health – provide documentation that demonstrates proper evaluation of the shipping container and FHUs, if applicable
- Quality assurance (QA) – provide documentation that the shippers QA program has been approved for any additional or different equipment used for the shipment

6. F&P RSD (FORM 434.28A) – FUEL ELEMENT DATA

Detailed fuel element data is provided on an Excel spreadsheet (Form 434.28A) and includes:

- Fuel Unit Identification Number
- Fuel Drawing Number
- Total U, U-235, U-238 (All Pre-Irradiation)
- Total U, U-235, U-238, Total Pu, Pu-239, Pu-240, Pu-241 (All Post Irradiation)
- Date Element Loaded in Core
- Date Element Removed from Core
- Element Burnup (MW-days)
- Element Burnup (% U-235)
- Element Decay Heat (Watts)
- Element Radiation Dose Rate at 1 Meter in Air (R/hr)

This Table Results from Modeling of Fuel Data (Usually from Logs)

7. F&P RSD (FORM 434.28B) – REFERENCES

References for the data provided by the shipper are listed on Form 434.28B. Copies are requested from the shipper for certain references (see Figure 3).

Figure 3. F&P RSD Form 434.28B - References

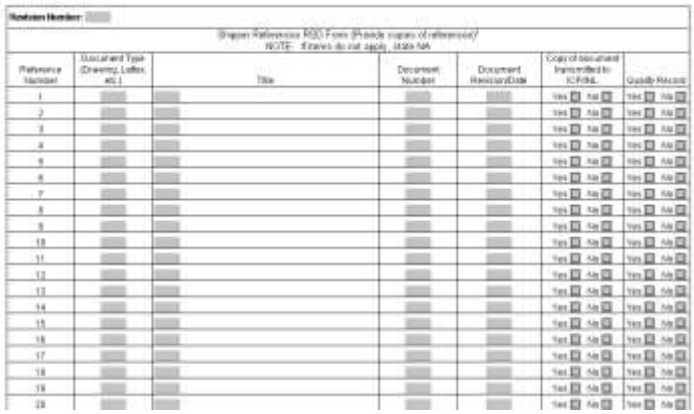

8. PROPOSED SHIPMENT CONTENTS (PSC) RSD FORM (FORM 434.30)

The Primary Purpose of This Form is to Address Proposed Loading of the FHUs Used for Shipment.

Figure 4. PSC RSD Form (Form 434.30)

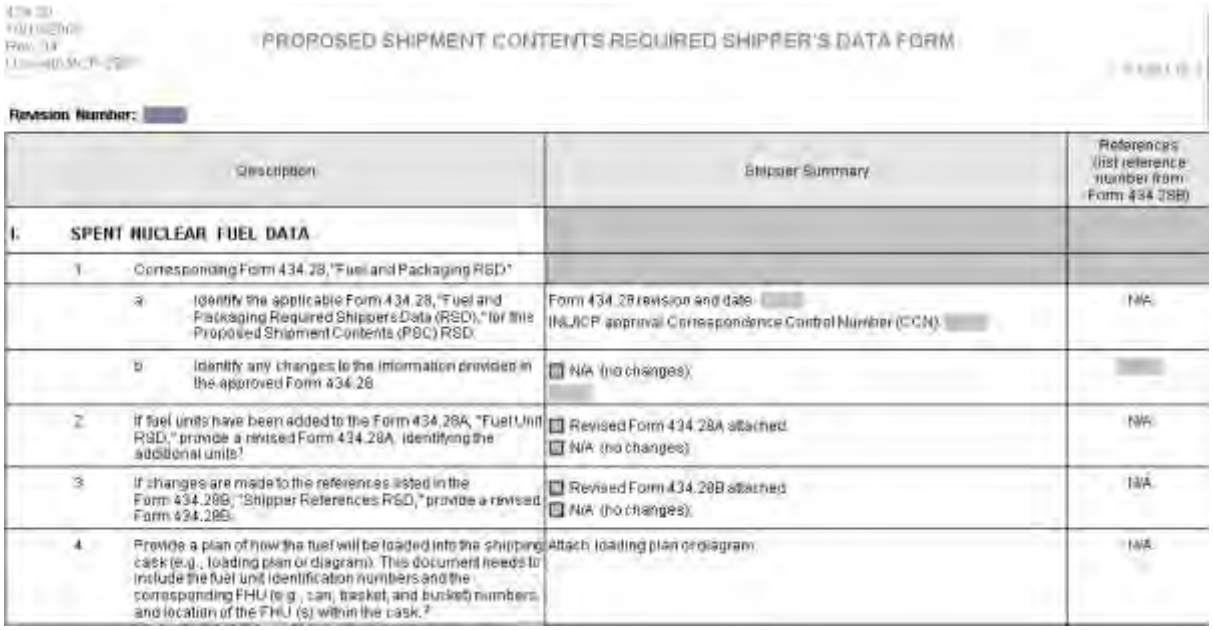

PROPOSED SHIPMENT CONTENTS REQUIRED SHIPPER'S DATA FORM

Revision Number:

	Description		Shipper Summary	References (list reference number from Form 434.28B)
I.	SPENT NUCLEAR FUEL DATA			
1	Corresponding Form 434.28, "Fuel and Packaging RSD"			
	a	Identify the applicable Form 434.28, "Fuel and Packaging Required Shippers Data (RSD)," for this Proposed Shipment Contents (PSC) RSD.	Form 434.28 revision and date: INL/ICP approval Correspondence Control Number (CCN):	N/A
	b	Identify any changes to the information provided in the approved Form 434.28.	☐ N/A (no changes):	
2	If fuel units have been added to the Form 434.28A, "Fuel Unit RSD," provide a revised Form 434.28A identifying the additional units?		☐ Revised Form 434.28A attached ☐ N/A (no changes)	N/A
3	If changes are made to the references listed in the Form 434.28B, "Shipper References RSD," provide a revised Form 434.28B.		☐ Revised Form 434.28B attached ☐ N/A (no changes)	N/A
4	Provide a plan of how the fuel will be loaded into the shipping cask (e.g., loading plan or diagram). This document needs to include the fuel unit identification numbers and the corresponding FHU (e.g., can, basket, and bucket) numbers and location of the FHU (s) within the cask.*		Attach loading plan or diagram	N/A

The form is used to address any changes to the F&P RSD Forms (434.28, 434.28A, or 434.28B) that may have occurred. Loading sheets are attached (Fig. 5) to show proposed loading of the FHUs and the cask. If needed, information is supplied on shipper supplied equipment. Lastly, data is provided on the shipping package (cask) that is expected to be used.

The form shown above is typical of the one used for the NAC-LWT cask. It contains: the fuel ID number; can number; and the location of each element in the FHU. Witnesses are required by MC&A.

Figure 5. Loading Sheets (Typical) for Shipping TRIGA Fuel to Idaho

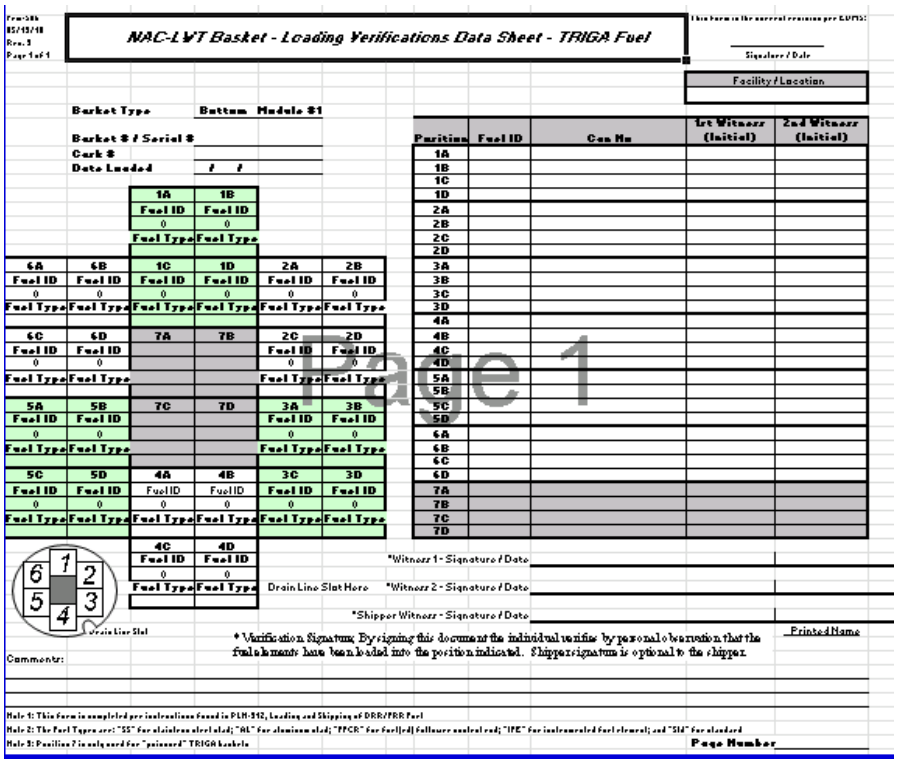

NAC-LWT Basket - Loading Verifications Data Sheet - TRIGA Fuel

Facility / Location

Basket Type: Bottom Module #1

Basket # / Serial #:

Cask #:

Date Loaded: / /

Position	Fuel ID	Can No	1st Witness (Initial)	2nd Witness (Initial)
1A				
1B				
1C				
1D				
2A				
2B				
2C				
2D				
3A				
3B				
3C				
3D				
4A				
4B				
4C				
4D				
5A				
5B				
5C				
5D				
6A				
6B				
6C				
6D				
7A				
7B				
7C				
7D				

Page 1

*Witness 1 - Signature / Date

*Witness 2 - Signature / Date

*Shipper Witness - Signature / Date

Printed Name

Drain Line Slot Here

* Verification Signature: By signing this document the individual verifies by personal observation that the fuel elements have been loaded into the position indicated. Shipper signature is optional to the shipper.

Comments:

Page Number

9. SHIPMENT CONTENTS (SC) RSD FORM (FORM 434.31)

This form is completed at time of loading of the elements into cans, basket/buckets, and the cask. Again, the form (Fig. 6) is used to address any changes to the F&P RSD Forms (434.28, 434.28A, or 434.28B) that may have occurred. The DOE/NRC Form F-741 (MC&A) is referenced, listing its number, and the tamper indicating device installed on the cask is identified by number. Any damage during loading to the FHUs or packaging is documented.

Loading sheets are attached to show actual loading of the FHUs and the cask to show location of each fuel unit within the shipping package (Attachment 1). Details are furnished of any tests performed prior to shipment, including leak or pressure tests for the FHUs and/or shipping cask, etc. (Attachment 2). Document the details of the transportation package (cask), including cask model number; cask and container serial numbers; transport vehicle(s); carrier identification; gross weight of loaded shipment package; etc. Provide the radiological surveys of the transportation package, including internal and external radiation and contamination levels (Attachment 3).

10. TIMING FOR THE RETURNS PROCESS / RSD SUBMITTALS

CWI likes to perform an initial site visit / assessment 12-18 months prior to proposed shipment date (usually with DOE). During visit, discuss:

- Decisions/information that affect planning for shipment/receipt
- Number and type of elements to be shipped
- Preliminary fuel condition (what is known about elements?)
- Approximate range of fuel “burnup”
- Fuel condition determination (logistics and timing of a fuel examination)
- Receiving and storing examination equipment at shipper’s facility
- Fuel and packaging data needs
- How to provide copies of required shippers data documentation / forms

Figure 6. SC RSD Form (Form 434.31)

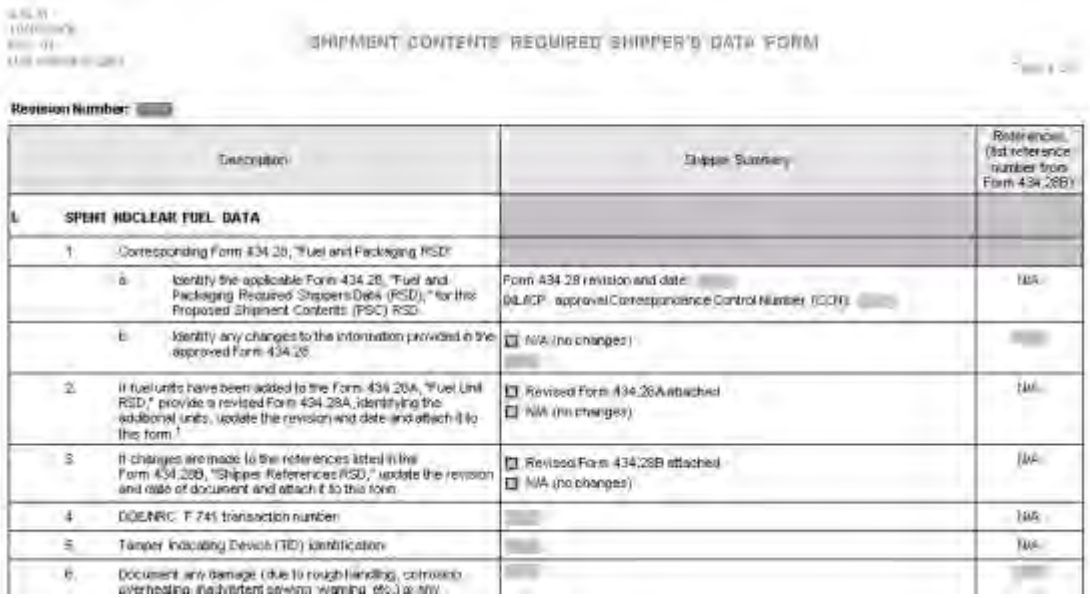

SHIPMENT CONTENTS REQUIRED SHIPPER'S DATA FORM

Revision Number:

	Description	Shipper Summary	Reference (list reference number from Form 434.28B)
I.	SPENT NUCLEAR FUEL DATA		
1.	Corresponding Form 434.28, "Fuel and Packaging RSD"		
a.	Identify the applicable Form 434.28, "Fuel and Packaging Required Shippers Data (RSD)," for this Proposed Shipment Contents (PSC) RSD.	Form 434.28 revision and date: DE-NCP approval Correspondence Control Number (CCN):	N/A
b.	Identify any changes to the information provided in the approved Form 434.28.	☐ N/A (no changes)	
2.	If fuel units have been added to the Form 434.28A, "Fuel Unit RSD," provide a revised Form 434.28A, identifying the additional units, update the revision and date, and attach it to this form.	☐ Revised Form 434.28A attached ☐ N/A (no changes)	N/A
3.	If changes are made to the references listed in the Form 434.28B, "Shipper References RSD," update the revision and date of document and attach it to this form.	☐ Revised Form 434.28B attached ☐ N/A (no changes)	N/A
4.	DOE/NRC F 741 transaction number		N/A
5.	Tamper Indicating Device (TID) identification		N/A
6.	Document any damage (due to rough handling, corrosion, overheating, inadvertent sawing, warping, etc.) or any		

- Shipper's capability for modeling fuel (ORIGEN or other)
- Potential casks to use for shipment
- Fuel loading logistics
- How to assist research reactor personnel to begin filling out forms
- Exchange of facility and contact information
- What to expect during inspection of the fuel and where to place the inspection equipment to best support the fuel handlers

A preliminary F&P RSD (Forms 434.28, 434.28A, & 434.28B) should be completed prior to the fuel examination. Extra time can be allocated by CWI to assist in completing the F&P RSD forms during the visit for the fuel examination (exam should occur approximately 8-12 months prior to planned shipment). The F&P RSD forms should be complete approximately 6-9 months prior to shipment so CWI can prepare necessary analyses and preparations to receive the fuel. The PSC RSD should follow immediately behind the completion of the F&P RSD and be completed approximately 6 months prior to shipment so timely preparations, including shipment of baskets/cans to the research reactor, can be made. The SC RSD is prepared at time of fuel loading for shipment. CWI personnel will be present to help answer questions and assist where possible.

Removal of Legacy Plutonium Materials from Italy

F. DI GASBARRO, A. PROIETTI
Sogin S.p.A.
Rome, Italy

K.A. DUNN, E.R. HACKNEY, N.C. IYER
Savannah River National Laboratory
Aiken, SC USA

S.L. DICKERSON
U.S. Department of Energy – National Nuclear Security Administration
Washington, D.C USA

ABSTRACT

Research and pilot scale fuel cycle facilities were operated in Italy until the 1970s to demonstrate the reprocessing of irradiated nuclear fuels and to develop the technology for the mixed oxide fuel with the intent to gain technical and economic data for a full-scale plant. The separated plutonium materials from these activities have been safely and securely stored in several nuclear facilities within Italy for several decades and managed by Sogin, S.p.A. The plutonium and mixed oxide materials had heterogeneous characteristics in terms of isotopic composition, physical and chemical state. Sogin, Italy and the U.S Department of Energy – National Nuclear Security Administration (DOE-NNSA) collaborated in a project to stabilize the legacy plutonium materials stored in Italy and repackage them for safe transport. This paper will provide an overview of the joint project that culminated with the removal of legacy separated plutonium materials from Italy to the U.S prior to the 2014 Nuclear Security Summit. The packaging and removal of the plutonium materials required design, construction, regulatory approval and start-up of a new plutonium glove box line in Italy to thermally stabilize and package the materials for transport. The key project activities will be described including the isotopic characterization of the plutonium materials, development of the packaging process, development of the necessary glove box infrastructure for the packaging operations, procedure development and training of the personnel, validation of the 9975 plutonium package certificate by the Italian regulatory authorities and execution of the package operations. The plutonium material was packaged and sealed in accordance with IAEA safeguards prior to the transport to the U.S. The Prime Minister of Italy and the President of the United States announced successful completion of this project at the 2014 Nuclear Security Summit.

1. Introduction

Fuel cycle facilities were operated in Italy until the 1970s to demonstrate the reprocessing of irradiated nuclear fuels and for the pilot scale production of mixed oxide (MOX) fuel in order to gain technical and economic data for a full-scale plant. The pilot scale reprocessing facilities separated plutonium materials from research and test reactors including the Material Test Reactor (MTR) type spent fuel. The separated plutonium materials including mixed oxide materials were stored at the EUREX plant (Enriched Uranium Extraction) of Saluggia Research Center, Vercelli, Italy and IPU plant (Impianto Plutonio) of Casaccia Research Center, Rome, Italy. Since 2003, Sogin S.p.A (Sogin) has managed these plants with the mission to perform the decommissioning of the facilities in order to achieve “green field” status. The first step in decommissioning is the removal of the separated plutonium materials. Sogin has worked with the U.S. Department of Energy (DOE) – National Nuclear Security Administration’s (NNSA) to repackage the legacy plutonium materials for transport to the U.S. This paper will highlight the joint project with DOE-NNSA to characterize, package, and remove the plutonium materials.

The DOE 9975 Type B radioactive materials (RAM) package was selected for the transport of the plutonium materials. Removal of the plutonium materials from Italy initially required consolidation of the materials within Italy i.e. transport of materials from the EUREX plant to the IPU plant for the stabilization treatment activities. Furthermore, it required Sogin to design and construct a new glovebox facility at the IPU plant to facilitate the characterization, thermal treatment and packaging of the materials for maritime transport and to comply with U.S DOE requirements. These activities culminated in the removal of the excess plutonium material from Italy as announced by the Prime Minister of Italy and the President of the U.S.A at the 2014 Nuclear Security Summit. The key elements of this joint project will be described in this paper.

2. Consolidation of Plutonium Materials within Italy

The consolidation of plutonium materials within Italy in as-is condition was an initial step in the project. Since the 9975 package was selected to transport the materials from the EUREX plant to the IPU plant, a special certificate amendment had to be obtained through the appropriate regulators in the U.S and validated by the Italian Regulatory Authority (ISPRA).

The plutonium material at EUREX plant was stored in a shielded plastic bottle within a plastic bag at the EUREX plant (Figure 2.1 – referred to as the EUREX bottle).

Figure 2.1 Condition of the EUREX bottle containing plutonium materials shipped as-is

Plutonium and plutonium/uranium mixed oxides stored within plastic bottles generate radiolytic gases. These gases can, at times, become flammable. The 9975 SARP precludes the shipment of flammable gases by restricting the amount of oxygen available for combustion or by keeping the hydrogen within the 9975 below the lower flammability limit (LFL) for hydrogen-oxygen mixtures by restricting the shipping period. Thus, there are only two considerations for hydrogen gas accumulations i.e the pressure within the primary containment vessel (PCV) needs to be below a safety limit threshold and the hydrogen needs to be below the LFL. The technical basis for the certificate amendment required extensive modelling to assess potential for radiolytic gas generation during handling and transport. Conditions and transport windows were established such that the PCV gases remain non-flammable and the overall pressure remains well below the baseline of the safety limits.

Once a certificate amendment was approved special inspection and packaging protocols were developed to implement the conditions of the package certificate amendment. The moisture content was estimated to be under the transport limits considering the calcination treatment performed at EUREX. The condition of each bag and bottle was non-destructively examined (Figure 2.2) to preclude presence of gas and/or water inside the bag. Potential embrittlement or degradation swelling or ballooning of the bottle was also assessed.

Figure 2.1 Non-destructive examination of EUREX bottles

The EUREX bottles were found to be in a very good condition and as seen in Figure 2.1, the bag is adhering to the bottles indicating absence of gas (hydrogen) build up inside the bag. Each EUREX bottle was packaged in a 9975 Type B package per the requirements of the package certificate of compliance and the competent authority certificate validated by ISPRA. 9975 packages were staged in cargo restraint transporter (CRT) and transported in two isocontainers from the EUREX plant to the IPU plant for subsequent treatment and packaging activities.

3. Stabilization and Packaging Operations

The plutonium material inventory at the IPU plant along with the EUREX plant plutonium inventory transferred to the IPU plant had to packaged to comply with the U.S DOE receiving facility requirements including demonstration of moisture content to be <0.5 wt%. The characterization, thermal stabilization, packaging and transport of plutonium materials present unique handling challenges due to its inherent radioactivity and pyrophoricity. The handling of plutonium material required design, construction and installation of specially engineered gloveboxes at the IPU plant. Furthermore, the materials had to be thermally stabilized at 950^{o}C for 2 hours to ensure moisture content of <0.5wt%, a key DOE requirement.

The key activities at the IPU plant in order to meet DOE and transport requirements included: (i) identification of a location for the new plutonium glovebox facility (ii) procurement and installation of alpha glove boxes and associated analytical equipment; (iii) qualification of the furnace within the glovebox and associated analytical equipment, iv) submission and approval of a safety basis for the new plutonium facility within an existing plant, (v) recruitment and training of operators and staff and vi) facility startup and regulatory approvals for radioactive operations.

Figure 3.1 New plutonium glove box system installed at IPU plant

Figure 3.1 shows a view of the new plutonium glovebox line installed at the IPU plant. The containers containing the plutonium materials inventory from the IPU and EUREX plant were opened in the gloveboxes, the material mixed to get homogenous mixtures and thermally treated in a furnace at 950^{o}C for 2 hours. Upon cool down, representative samples were analysed using a thermogravimetric analyser to ensure that the moisture content of the mixture was less than 0.5 wt%. The material was further mixed and packaged into a slip-lid and screw-lid container set (Figure 3.2). The material in the container was subjected to ISOCS[1] gamma spectroscopy analysis in order to characterize the isotopics of the material.

Figure 3.2 Slip-lid/Screw-lid container set with the plutonium material

The slip-lid/screw-lid container set was loaded into the primary containment vessel (PCV) of the 9975 shipping package (Figure 3.3) and packaged to meet the conditions established in the the Certificate Of Compliance (COC) for the 9975 package (Ref.1). The results of the ISOCS analyses and the accountancy information validated that the composition of the proposed contents of the Sogin plutonium bearing materials fell well within the limits of the Content Envelopes in the package certificate.

Figure 3.3 Plutonium container loaded into the PCV of the 9975 package

[1] ISOCS - In-Situ Object Counting Systems

4. Safety and Safeguards

All the activities were performed in compliance with the highest standards in terms of safety and security. The 9975 packages guaranteed the protection of the people, property and environment from the effects of radiation during the transport of radioactive material assuring the containment of the radioactive contents, the control of external radiation levels, the prevention of criticality and the prevention of damage caused by heat.

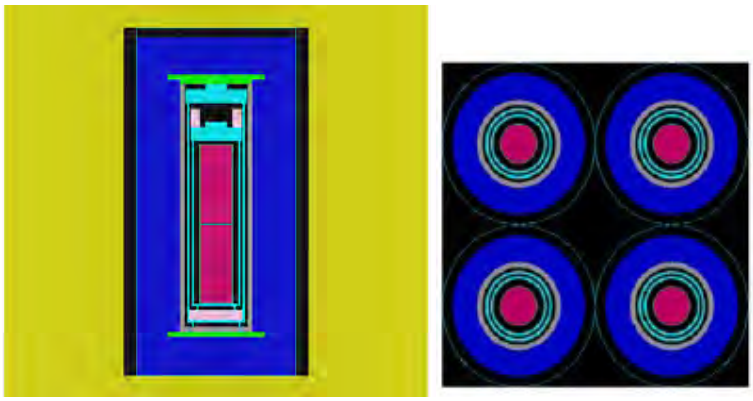

Figure 4.1 Criticality Modeling of the 9975 package

The 9975 package used for the shipment, containing fissile, was designed and constructed and its contents so limited that under the specified conditions, the package would have been subcritical. The updated safety analysis report for packaging (SARP) and associated certificate amendments to accommodate the transfer of materials within Italy did not affect the structural integrity of the components of the 9975 shipping package. Bounding gas space volume assumptions were not challenged by this new content configuration. Detonation loads were precluded by ensuring the absence of flammable atmospheres within any gas space of the primary containment vessel.

The 9975 SARP precludes the presence of flammable gases by restricting the amount of oxygen available for combustion or by keeping the hydrogen within the 9975 below the lower flammability limit (LFL) for hydrogen-oxygen mixtures by restricting the shipping period. The package procedure adopted ensured that the oxygen content in the package is below the LFL and was fully validated in laboratory experiments.

The packages were sealed to meet IAEA, Italian regulatory authority and DOE-NNSA protocols. Security considerations consistent with the IAEA and international requirements for Category 1 materials packaging and transport was implemented.

5.0 Transport Operations

The 9975 Type B packages were loaded into the CRT (cargo restraint transporter) pallets and tied down with dedicated slings (Figure 5.1). The CRT pallets were fixed to special anchorage system designed, constructed and installed in the ISO containers specifically to fasten the CRT pallets to the ISO container (Figure 5.2). The anchorage systems were designed to satisfy ADR[2] and IMDG[3] regulations, tested with the dynamic load required by the maritime transport regulation.

All the transport activities were executed in compliance with the highest security standards and regulations. Highest level of information security was maintained and information compartmentalized and disseminated on a need-to-know basis. All the information exchanged in the framework of the transport project was classified according to the appropriate security standards. Use of an INF3-class vessel assured the security during the maritime transport.

[2] European Agreement concerning the International Carriage of Dangerous Goods by Road
[3] International Maritime Dangerous Goods Code

Figure 5.1 – 9975 package being lifted into the CRT

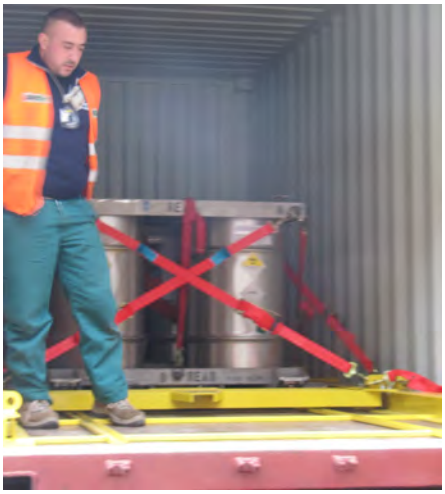

Figure 5.2 9975 packages loaded into the ISO container and anchored with special systems

Figure 5.3 - Land transport with ISO containers

6. Conclusion

The successful completion of the transport project by Sogin and DOE-NNSA was possible due to the active and continuous collaboration with the operators, commercial partners and authorities involved. Teamwork was essential during all the phases of the project to assure the effective coordination with the stakeholders. Comprehensive planning of all phases of the project

complemented by frequent conference calls and meetings between Sogin and U.S. DOE was a key element for the successful conclusion of the project. Many important lessons learned were acquired especially about the organization and management of all the activities connected to the packaging, receipt at the treatment facility packages palletisation, port activities and the transport itself. In particular a strong collaboration between Sogin, DOE-NNSA, the Italian Ministries (Ministry of Industry and International Trade, Ministry of Interior and Ministry of Foreign Affairs), the Italian Regulatory Authority (ISPRA), Euratom, IAEA, the Italian transport company Mit Nucleare and the maritime transport company INS enabled prompt resolution of emerging issues and ensured a successful project outcome within the scheduled transport window.

7.0 References

1. Competent Authority Certificate for 9975/B(M)F-96 Revision 2 (based on the Certificate Of Compliance (COC) for Radioactive Materials Package (DOE F 5882.1) Revision 9)

Decommissioning and dismantling of research reactors and waste management

THE DISMANTLING OF THE MONTECUCCOLINO RB3 RESEARCH REACTOR: RADIOLOGICAL CHARACTERISATION OF MATERIALS FOR FREE RELEASE

M. CAPONE, N. CHERUBINI, A. COMPAGNO, A. DODARO
ENEA, C.R. Casaccia
Via Anguillarese 301, 00123 S.Maria di Galeria, Rome – Italy

F. ROCCHI
ENEA, C.R. "E. Clementel"
Via Martiri Monte Sole 4, 40129 Bologna – Italy

ABSTRACT

The research reactor RB3, located at the CR ENEA Montecuccolino, Bologna, was a typical "zero power" critical facility, moderated by heavy water, used for research purposes. Its construction dates back to the '60s by the CEA of Saclay and it worked for 19 years.
The purposes for which the reactor had been set up were the evaluation of the reactivity managed by control and shutdown rods for nuclear power plants like CIRENE.
Since December 2012 ENEA started the decommissioning of RB3, aiming to the green field status (no radiation protection requirements).
The activity is performed by different ENEA departments, each one involved for its peculiar characteristics. The ENEA Casaccia Nuclear Materials Characterization Laboratory has been involved in the radiological characterization activities of different types of materials derived from the dismantling (metal, concrete, plastic, etc.).
The main part of the radiological characterization has been carried out on site using the mobile gamma spectrometry system ISOCS (In Situ Object Counting System), while a scaling factors verification was made with destructive analyses.
The measurement system is based on a ISOCS characterization via Monte Carlo transport code assessment of the detector/shield/collimator assembly. The objective of this characterization is to provide a database consisting of the detector response to a large number of different measurement configurations. The ISOXSW software automatically determines the relationship between the radioactive source geometry, the measured count rate and the amount of radioactive material present using the ISOCS characterized detector data.
The user phase of the efficiency computation allows accurate efficiency calibrations to be performed rapidly for a wide variety of sample shapes, sizes, densities and distances between the sample and the detector.
Before the radiological characterization, an intense research activity was carried out in order to:
• estimate the level of accuracy of the software for the calculation of the efficiency of detection in this particular experimental configuration;
• quantify the measurement uncertainties related to the deviations of the actual situation from the chosen one from the ISOCS template database;
• define correction factors providing a basis for conservative measuring results, i.e.: guarantee the overestimation of any activity eventually present in batches of materials.
These objectives were pursued using experimental measurements with radiation sources of known activity and using the simulation code MCNP5.
After the qualification step, the characterization was carried out resulting in a maximization of free released materials.

1. Introduction

The research reactor RB3 was a "zero power" critical facility moderated by heavy water, used for research purposes.

Constructively, the reactor was of the pool type, with 60 fuel elements arranged in a square form with a pitch of 27 cm.
The main container was a cylindrical aluminium tank, diameter 290 cm and height 430 cm, surmounted by a steel structure for the support of the fuel elements and closed by a rotating stainless steel lid.
The reactor core was placed at the bottom of the tank surrounded by heavy water with moderator and reflector function and with a plenum of about 3 meters in height interposed between the free surface of the moderator and the support structures. The average volume of the core was about 5.4 m^3. Laterally and below, the core was surrounded by graphite blocks, as reflector function for neutrons.
The purposes for which the reactor had been set up were the evaluation of the reactivity managed by control and shutdown rods for nuclear power plants like CIRENE.
At the end of the nineties ENEA decided to ask for dismantling authorization aiming at returning as green field (without radiological constraints) the premises that housed the reactor.
After several years and many interactions with the Regulatory Authority, the decommissioning plan was approved and operational activities began in 2012.
The activity was performed by different ENEA departments, each one involved for its peculiar characteristics. The ENEA Nuclear Materials Characterization Laboratory, the Radioprotection Institute and the Reactor Safety and the Fuel Cycle Laboratory, have been involved in the radiological characterization of all materials coming from the dismantling, while the Infrastructure Unit of Montecuccolino Research Center took care of all the dismantling operation.
The activities described in this paper are focused on the characterizations carried out by the Nuclear Materials Characterization Laboratory using the mobile gamma spectrometry system ISOCS (In Situ Object Counting System) for free release purposes, while beta characterization and scaling factors verification were made in laboratory with destructive analyses.

2. Radiological characterization procedures

The decommissioning of the research reactor RB3 involves management of potentially radioactive materials for which a destination has to be chosen, in our case two options were investigated: free release and treatment as radioactive waste. To achieve the objectives of proper classification of materials from dismantling, a robust characterization program has been planned and implemented covering all the components and structures of the reactor.
To define the sampling criteria and plan the radiological characterization activities, the international guidance “Radiation Protection 122” was followed, even if the free release limits imposed by the Control Authority were slightly lower and the characterization of all items intended to release was required.
The first step was to classify the materials depending on the reactor history and their position inside the reactor as follows:
“A” category (activated and contaminated): materials which have been in contact with potentially contaminated fluids and subjected to significant neutron flux;
“B” category (contaminated but not activated): materials which have been in contact with potentially contaminated fluids but not subjected to significant neutron flux;
“C” category (activated but not contaminated): materials subjected to significant neutron flux but never in contact with potentially contaminated fluids;
“D” category (not activated or contaminated): so called exempt materials.

Within each category four homogeneous groups of materials based on composition have been identified:

- metals: iron, copper, aluminium, and steel;
- barytes concrete;
- other: paper, plastics, asbestos and fiberglass;
- cast iron.

The radiological characterization performed consisted in a series of measurements made with different objectives:

a) elemental analysis on samples from the tank (hyper pure aluminium) and other metals (mainly steel) in order to find impurities and elements that could have been activated during the operation of the reactor;
b) α, β and γ destructive measurements on samples taken from different materials belonging to the each group to verify the homogeneity and the category;
c) gamma spectrometry measurement on each batch of material to verify the fulfillment of release conditions.

Following RP122, our metric unit for each homogeneous group was a volume of 1 m^3 and this was considered homogeneous with regard to the internal distribution of radioactivity. Examples of metric unit are given in Figure 1.

Fig 1: Homogeneous groups of materials: metals, barytes concrete, other (paper, plastics, asbestos and fiberglass), cast iron

2.1 Elemental characterization

As previously mentioned, the elemental analysis was carried out to identify the elements present in the potentially activated materials subjected to neutron flux: ICP-MS analysis were performed on samples taken from metal materials belonging to category A and C.
The ICP-MS method is a technique generally used for the '"trace analysis" (<ppb, μg/L). The detection limits are typically in the range pg/L-μg/L.
The technique is based on measurement of ions produced by a plasma of Ar inductively coupled to an appropriate radio frequency. The analytes present in the solution are atomized in the form of aerosols and transported in the plasma torch where, due to the high temperature, they ionize. Then they are extracted from the plasma by means of a high-vacuum interface and separated according to their mass-charge ratio m/z by a quadrupole system.
The elemental characterization of the chemical elements in samples of liquid or solid in general needs an appropriate sample preparation with acid or microwave digestion.
The final concentration C_x for each element X is expressed by the following formulas:

$$C_X\ (mg/kg) = \frac{S_X \cdot d \cdot V}{M}$$

where
S_x = concentration of element X in the mineralized solution (mg/l);
d = dilution factor;
V = total volume of the solution mineralized (l);
M = weight of dry sample (g).

2.2 Beta Characterization

The radiometric technique used for the determination and quantification of the β activity concentrations of ^{63}Ni and ^{55}Fe radionuclides was the liquid scintillation by means of the Liquid Scintillation Counting System Hidex 300 SL: this system, using three photomultipliers placed at 120° to each other, implements the TDCR technology (Triple to Double Coincidence Ratio). This technology has the advantage of assessing the counting efficiency of the detection system without any radioactive calibration source.

The mineralization of the samples has been made with microwave mineralization in two different mixtures of acids depending on the matrix to be solubilized (steel and aluminium).
After acid microwave digestion, hydroxide precipitation was used to separate ^{55}Fe and ^{63}Ni from the matrix elements. Ion Exchange Chromatography was used to separate ^{55}Fe and ^{63}Ni from the interfering radionuclides as well as from each other.
The separated ^{63}Ni was further purified by extraction chromatography using Ni-DMG cartridges. The purified ^{63}Ni and ^{55}Fe were then measured by liquid scintillation counting (Fig. 2).

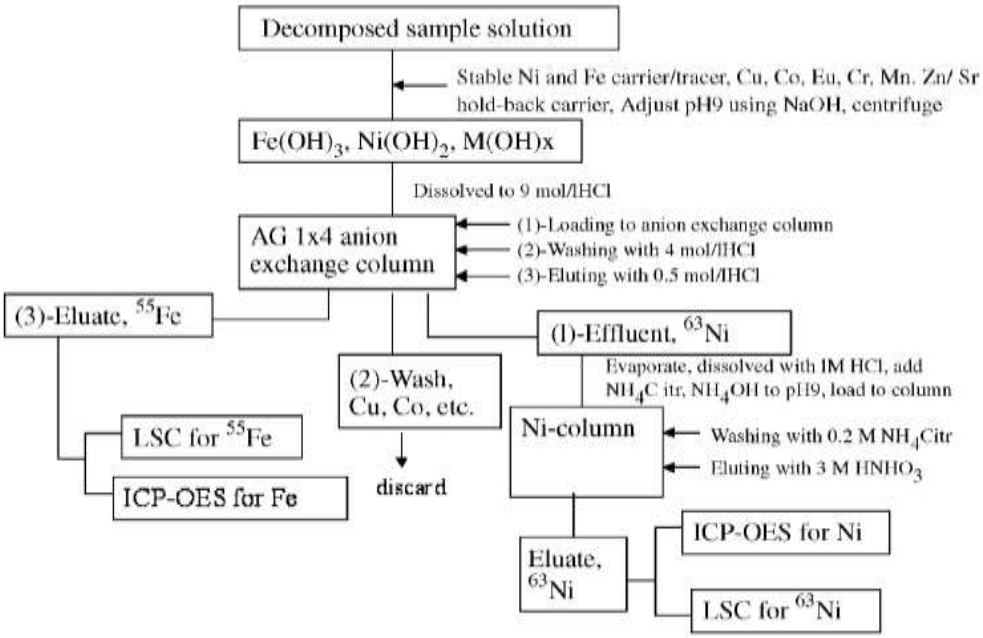

Fig. 2: Chemical procedure for the separation of ^{63}Ni and ^{55}Fe from other radionuclides and from each other

The formulas for the calculation of the concentration of activity (A), Decision Threshold (DT) and Minimum Detectable Activity (MDA) are the following:

$$A_X\ (Bq/g) = \frac{CPM_X - CPM_B}{60 \cdot M \cdot Eff_X \cdot Y_X}$$

$$DT \quad (Bq/g) = k_{1-\alpha} \cdot \frac{1}{Eff_X \cdot M} \cdot \sqrt{\frac{CPM_B}{T_X} + \frac{CPM_B}{t_B}}$$

$$MDA\ (Bq/g) = \frac{2.71 + 4.65 \cdot \sqrt{C_B}}{Eff_X \cdot M \cdot T}$$

where
CPM_X = counting rate of the sample (counts/min);
CPM_B = counting rate of blank sample (counts/min);
M = weight of the solid sample (g);
EFF_X = counting efficiency (coinciding with the parameter TDCR);
Y_X = chemical yield (%);
$k_{1-\alpha}$ = 1.65 (with α=β=0.05);
T_X = counting time of the sample (min);
t_B = counting time of the blank sample (min);
T = total counting time (min).

2.3 Gamma Characterization

The In Situ Object Counting System (ISOCS) developed by Canberra, Inc. is the portable, in-situ gamma spectroscopy system used by the ENEA-Casaccia Laboratory to identify radioactive isotopes and to determine the amount of radioactive material.
The ISOCS system operates with a characterized Germanium detector with portable cryostat; a cart support for holding the detector, lead shielding and collimators; an InSpector portable spectroscopy analyzer; a portable computer with Genie-PC software; and the ISOXSW in situ calibration software. The detector is a BEGe (Broad Energy Germanium) detector (active volume: diameter 60 mm and 25 mm thickness) whose response to a series of point sources surrounding it has been characterized using a Monte Carlo code. The system has been equipped with a shielding package of 50 mm lead shield assemblies and collimators of 90° to minimize interfering or background radiation and limit the field of view of the detector.
The software ISOXSW automatically determines the relationship between the geometry of the sample, the measured counting rate, and the amount of radioactive material present.
The configuration of measurement and the chemical and physical characteristics of the samples produced from the dismantling of the reactor RB3 have been reproduced, with the maximum possible precision, with the template "Simple Box".
The sample to be measured has been in fact geometrically delimited by the lateral surface and the base of a wooden cube having an internal volume equal to 1 m^3, which have been included within the materials to be characterized.
This template is a rectangular box containing radioactive materials uniformly distributed on one or two layers with the corresponding concentrations.
The software GENIE 2k allows the identification of the peaks and provides the activity (A) and the statistical uncertainty of measurement. In case of absence of peaks the system allows the evaluation of the Decision Threshold (DT, considered as the limit for radioactivity absence in the sample) and the Minimum Detectable Activity (MDA, proportional to the Detection Limit) both expressed in units of activity (Bq).

2.4 Validation of gamma characterization procedure and uncertainty estimation

The ISOCS system estimates the measurement efficiency according to the description of the experimental configuration provided by the operator. Naturally the efficiency estimation is accurate only if the geometry description given by user is close to reality: in order to minimize the inaccuracy due to non-uniform distribution of activity in the sample and to guarantee overestimation of the measured activity, the measurement procedures were validated using both Monte Carlo simulations and experimental measurements with non-radioactive samples having inside, in different positions, reference calibration sources.
The objectives of the procedure were:

- estimate the level of software accuracy in the calculation of the detection efficiency in particular experimental situation;
- quantify the measurement uncertainties related to deviations of the real situation from that schematized in ISOCS templates;
- define correction factors providing a basis for conservative measuring results, that is likely to overestimate any activity present in batches of materials to an extent.

These objectives were pursued using experimental measurements with known activity radiation sources and/or using the MCNP5 code.
The procedure validation and uncertainty estimation can be summarized as follows:

- ✓ each measurement configuration was simulated with MCNP5;
- ✓ simulation results were confirmed with reference calibration sources;
- ✓ correction factors were calculated to take into account the non-homogeneity of matrix and the eventual presence of non-identified hot spots.

2.4.1 Uncertainty associated with the calculation of the efficiency through ISOCS.
This component of uncertainty is mainly due to the differences between the ISOCS template and the real experimental configuration: in particular, the non-homogeneity of the matrix

means that, even in case of known distribution of the activity, there is a variance between the true and the measured value not attributable exclusively to the statistical measurement.
The evaluation of this component of uncertainty was performed in modes dependent on the sample matrix.
An experimental approach was followed when the sample matrix can be considered homogeneous.
If the sample was characterized by density up to 0.5 g/cm^3, a series of measurements with sealed sources of known activity positioned inside the sample were performed.
For each reference matrix measurements in 12 different positions (Figure 3) with ^{60}Co and ^{137}Cs sources were carried out; for each radionuclide and for each reference matrix the parameter

$$\delta = \sqrt{\frac{\sum(A_i - A_R)^2}{N}};$$

was calculated where
A_i: measured activity in different positions;
A_R: certified activity for the sealed source;
N: number of measurements.

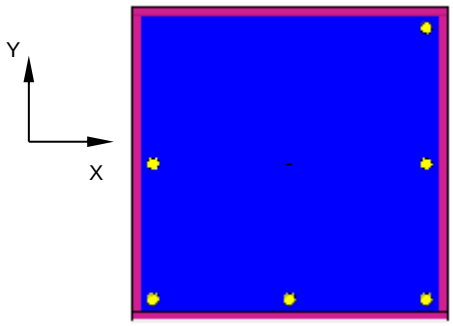

Fig 3: Horizontal section of the “light” sample, showing the positions of the sources of known activity used to evaluate the uncertainty of calibration.

For the barites concrete sample matrix, due to the high density (1.84 g/cm^3), the measurements carried out in order to calculate the δ parameter used only 6 different positions (Figure 4) with ^{60}Co known sources.

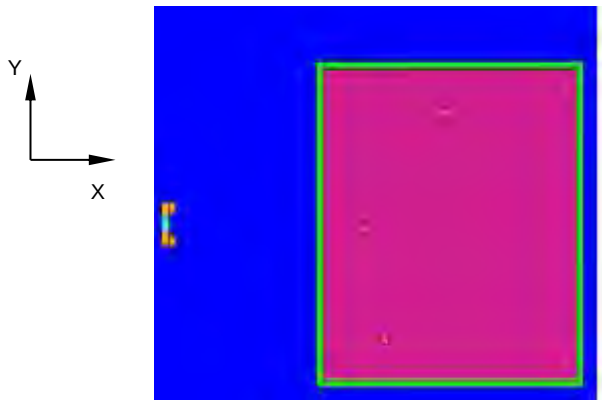

Fig 4: Horizontal section of the concrete sample, showing the positions of the sources of known activity used to evaluate the uncertainty of calibration

For the samples constituted by panels of cast iron, the particular geometry of the sample is not comparable to a simple box: consequently an equivalent homogeneous material was introduced, "iron apparent", characterized by the apparent density of the complex iron-air mixture. In this case the component of uncertainty was calculated evaluating, by means of MCNP5 simulation, the percentage difference between the detection efficiency at ^{60}Co energies both in the real configuration (cast iron) and in the ISOCS template ("iron apparent") (Figure 5).

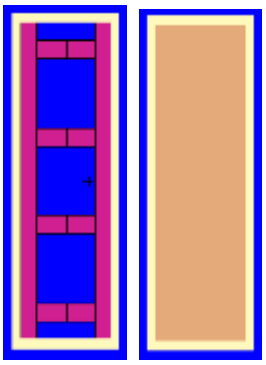

Fig 5: Horizontal section of the cast iron sample (left) and “iron apparent” template (right)

2.4.2 Uncertainty due to the non-uniformity of the distribution of activity within the sample.
The response of the measurement system to a non-uniform distribution activity depends mainly on three contributions; the position of possible hot spots, the density of the material constituting the matrix and the energy of the emitted radiation.
To minimize the errors in the estimation of the efficiency due to the position of eventual hot spots, in the measurement procedures has been included also the research of hot spots: in case of hot spot recognition, the sample is positioned in order to have the hot spot as close as possible to the detector to ensure an overestimation of the measured activity.
To do that, it has to be possible to detect the hot spot with certainty, or at least establish a range of positions in which the hot spot is recognizable: with this purpose with a series of Monte Carlo simulations for each kind of samples were carried out.
The goal of the simulations was to derive the minimum distance from the center, both horizontally and vertically, which allows to recognize the presence of a hot spot using a monitor of dose equivalent rate available at the reactor RB3.

2.4.3 Gamma activity calculation inside the sample.
The peculiar method of calibration of ISOCS system makes it necessary the application of correction factors to the formulas generally used in gamma spectrometry which become:

$$A = \frac{C_N}{\varepsilon T y} FC$$

$$DT = \frac{k\sqrt{2B}}{\varepsilon T y} FC$$

$$MDA = \left(\frac{k^2}{\varepsilon\, T\, y} + 2DT\right) FC$$

where

$$FC = \begin{cases} sample\ \ \rho_{app} < 0.4\,\frac{g}{cm^3} & \begin{cases} 1 & hot\ spot\ recognizable \\ f(\rho_{app}, E_i) & no\ \ hot\ spot\ recognizable \end{cases} \\ sample\ barytes\ concrete & \begin{cases} 1 & hot\ spot\ recognizable \\ \begin{cases} 52.3 & for\ E_i = 1173.2\ keV \\ 49.4 & for\ E_i = 1332.5\ keV \end{cases} & no\ hot\ spot\ recognizable \end{cases} \\ sample\ cast\ iron\ \ \left(\rho_{app} \approx 4\,\frac{g}{cm^3}\right) & \begin{cases} \begin{cases} 30\ (1173.2\ keV) \\ 22\ (1332.5\ keV) \end{cases} & hot\ spot\ recognizable \\ \begin{cases} 46\ (1173.2\ keV) \\ 33\ (1332.5\ keV) \end{cases} & hot\ spot\ recognizable \end{cases} \end{cases}$$

$$f(\rho_{app}, E_i) = \begin{cases} 1.1788e^{4.1031\rho_{app}} & forr\ E_i = 661.6\ keV\ \ (^{137}Cs) \\ 1.3059e^{2.9559\rho_{app}} & for\ E_i = 1173.2\ keV\ \ (^{60}Co) \\ 1.3073e^{2.7328\rho_{app}} & for\ E_i = 1332.5\ keV\ \ (^{60}Co) \end{cases}$$

ρ_{app}: apparent density;
C_N: net area;
ε: detection efficiency (expressed in s^{-1} Bq^{-1});
T: measurement time (s);
y: yield of emission of the line in question.
$k = k_{(1-\alpha)} = k_{(1-\beta)}$: is the (1-$\alpha$) percentile (or (1-$\beta$) percentile) of the normal distribution (if $\alpha=\beta$ = 0.05 then k = 1.645);
B: background counts.

3. Results

The Nuclear Materials Characterization Laboratory has performed elemental characterization of the steel shield and the aluminium tank, beta and gamma characterization on each batch of material belonging "A" (activated and contaminated), "C" (activated but not contaminated) and "D" (not activated or contaminated) categories.
As foreseen from the decommissioning plan, some "A" and "B" category materials, which have been in contact with the heavy water like the tank or the hydraulic system, have been analysed by the Radioprotection Institute because potentially contaminated by ^{3}H.

3.1 Elemental characterization

The elemental analysis was carried out to identify the elements present in the potentially activated materials subjected to neutron flux: the steel shield and the aluminium tank.
In Table 1 the final concentration C_x for each element founded in the steel shield is reported:

Shield	Fe	Ni	Cr	Mn	Zn	Co	Ti	V
C_X (%)	76.3	0.49	17.1	1.64	0.59	0.09	1.12	0.95
Uncertainty	±0.1	±0.01	±0.3	±0.01	±0.01	±0.02	±0.01	±0.01

Tab 1: Concentrantions of the main elements in a sample of steel shield from RB3 reactor determinated by ICP-MS Agilent 7700 Series X

In Table 2 the final concentration C_x for each element founded in the aluminium tank is reported:

Tank	Al	Si	Fe	Mn	Mg	Cr	Ti	Ni
C_X (%)	99.0	0.20	0.10	0.150	0.15	0.03	0.010	0.076
Uncertainty	±0.9	±0.01	±0.01	±0.004	±0.01	±0.01	±0.002	±0.004

Tab 2: Concentrations of Al and other impurities in a sample of Al-Tank from RB3 reactor evalueted by ICP-MS technique

The results indicate that the aluminium of the tank was virtually pure while, in the steel of the shield, apart from Fe, Ni and Co, it is unlikely that some activation products are still present.

3.2 Beta characterization

As the ^{60}Co activity concentrations were measured on all materials to be released, the liquid scintillation was used for the determination and quantification of the β activity concentrations of ^{63}Ni and ^{55}Fe radionuclides.
The measured activity concentrations of ^{55}Fe and ^{63}Ni were always below the Decision Threshold (DT), making it unnecessary the scaling factors verification.
In Table 3 the range of estimated DT and MDA for each material analyzed are reported:

Material	meas. performed	Radionuclide	DT (Bq/g)	MDA (Bq/g)
Steel	53	^{55}Fe	0.005÷0.018	0.008÷0.020
		^{63}Ni	0.004÷0.020	0.006÷0.022
Aluminium	5	^{55}Fe	0.005÷0.006	0.007÷0.008
		^{63}Ni	0.002÷0.004	0.003÷0.006
Iron cast	10	^{55}Fe	0.008÷0.010	0.009÷0.011
		^{63}Ni	0.007÷0.010	0.010÷0.012

Tab 3: Beta characterization of ^{55}Fe and ^{63}Ni

3.3 Gamma characterization

Regarding the materials belonging to category “D” (exempt, almost everything outside the biological shield), the measured activity concentration of ^{137}Cs and ^{60}Co were all below the Decision Threshold (DT).
In Table 4 the range of estimated DT and MDA for this category are reported with reference to each homogeneous group.

Material	volume (m^3)	mass (kg)	meas. performed	^{60}Co		^{137}Cs	
				DT (mBq/g)	MDA (mBq/g)	DT (mBq/g)	MDA (mBq/g)
Metals	108	24047	136	1.6 – 7.3	4.2- 15.8	3.8 – 15.8	8.7 – 33.4
Concrete	1	444	1	56.1	114.2	22.6	46.8
Other	38	5865	40	2.8 – 13.7	6.4 – 29.9	4.7 – 19	10 – 40

Tab 4: Gamma characterization for “D” category materials.

In Table 5 the range of measured activity concentrations as far as the estimation of DT and MDA is reported for “A” and “C” category (potentially activated, almost everything within the biological shield) materials, with reference to each homogeneous group.

Material	volume (m^3)	mass (kg)	meas. performed	^{60}Co		
				activity concentration (mBq/g)	DT (mBq/g)	MDA (mBq/g)
Metals	105	43652	129	5.3 - 28.9	3.4 - 17	7.6 - 37.3
Concrete	17	26202	27	<DT	28.0 - 38.7	59.3 - 81.0
Cast iron	4	12712	43	40.3 - 207.8	21.2 - 65.5	48.6 – 141.3

Tab 5: Gamma characterization for “A” and “C” category materials.

4. Conclusions

Up to now the dismantling activities of RB3 reactor allowed the removal of all the materials inside the reactor building and biological shield. The result of the radiological characterisations performed allowed the release of about 100 tons of materials without any radiological constraint.
The last step is the verification of the contamination levels of the floor and the walls of the building, now in progress, in order to fulfil the prescriptions given by the Regulatory Authority return as “green field” the premises that housed the reactor.

5. References

1. Radiation Protection 122 “Practical use of the concepts of clearance and exemption”, Directorate General Environment, 2000.

2. Radiation Protection 89 “Recommended radiological protection criteria for the recycling of metals from the dismantling of nuclear installations”, Directorate General Environment, 1998.
3. ISO 11929-1:2000 “Determination of the detection limit and decision threshold for ionizing radiation measurements Part 3 Fundamentals and application to counting measurements with high resolution gamma spectrometry without the influence of sampling treatment.”
4. EPA Reference Method 6020A (EPA 2007) – Inductively Coupled Plasma-Mass Spectrometry.
5. EPA Reference Method 200.8 – Determination of Trace Elements in Waters and Wastes by Inductively Coupled Plasma-Mass Spectrometry.
6. AGILENT ICP-MS 7700 X Series User’s Manual
7. Eichrom Tecnologies Inc., Analytical Procedures NIW01 for Ni-63 e FEW01 for Fe-55.
8. LSC HIDEX 300 SL User’s Manual
9. ISOCS Calibration Software User’s Manual, V4.0 9231013D, Canberra Industries, Inc., USA 2002.
10. J. F. Briesmeister, Ed, ”MCNP – A general purpose Monte Carlo code for neutron and photon transport”, Los Alamos National Lab. – Report LA – 13709 – Manual Version 4C (April 2000).

THE DECOMMISSIONING PROGRAM OF THE RESEARCH REACTOR RTS-1 "G. GALILEI - ITALY"

ALESSANDRO DODARO
Board Chairman, NUCLECO SpA
Via Anguillarese, 301 – 00123 Roma

LEONARDO BALDASSARRE
Radiation Protection Expert, NUCLECO SpA
Via Anguillarese, 301 – 00123 Roma

MASSIMILIANO RUSSO
Radiation Protection Expert, CISAM Interforce Center for Studies and Military Applications
Via Bigattiera lato monte, 10 – 56122 S. Piero a Grado (PI)

EMILIO CIMINI
Responsible for reactor, CISAM Interforce Center for Studies and Military Applications
Via Bigattiera lato monte, 10 – 56122 S. Piero a Grado (PI)

ABSTRACT

The Reactor "G. Galilei" RTS-1 is a nuclear research reactor of the Ministry of Defense located in Pisa - Italy at the Interforce Center for Studies and Military Applications (CISAM). Nucleco is a qualified and specialized operator in the field of radioactive waste management, remediation and decontamination of nuclear sites and industrial areas. A part of Nucleco activities are carried out in decommissioning of nuclear power plants and nuclear fuel cycle facilities throughout the country.
The "G. Galilei" RTS-1 is a pool type reactor, light water moderated and cooled, fed with uranium enriched to 90%, and able to function to the power of 5 MW_{th}. RTS-1 has reached its first criticality on April 4, 1963 and remained in operation until April 7, 1980 (shutdown). Since the early '80s began decommissioning operations aimed at achieving the Unconditional Release of the site, interspersed with phases of Passive Protective Case.

This paper describes the strategy for decommissioning the reactor primary circuit of the "Galileo Galilei" RTS-1, including heat exchangers and tank decay; dismantling and conditioning system for collecting radioactive liquid effluents; dismantling and conditioning the drain circuit of the pool water and hot effluents. The decommissioning activities have been designed by CISAM experts and will be performed by Nucleco SpA, with particular emphasis on aspects of decontamination, treatment and conditioning of radioactive waste products.
In all the materials that have been subjected to neutron flux during the life of operation of the Plant, residual radioactivity is present: in particular it is located, as well as in the structural elements of the core, in all the components surrounding it and up to a certain depth of the biological shield, and the facilities irradiated in experiments. At the end of the system was calculated to be present total activity, excluding fuel, of the order of 10^{16} Bq. At 30 years from arrest (2010), these activities were reduced to about $5x10^{11}$ Bq. The main radionuclides of interest in radiation protection are: ^{60}Co, ^{3}H, ^{90}Sr, ^{137}Cs, ^{235}U, ^{238}U, ^{238}Pu, ^{239}Pu, ^{240}Pu, ^{241}Am. Surface contamination of the accessible areas of installations which contained liquid contaminants (underpool, demineralization active, primary pump room) is near equal to 1.6 Bq / cm2, while in the hot labs (average cell activity and chemical laboratories) the maximum value is equal to about 0.5 Bq / cm^2. The inaccessible surfaces

(inside walls of the pool, reservoirs and primary circuit), have an average contamination of 4.5 Bq / cm^2.

The decommissioning activities, began in 2008 with the dismantling of the secondary circuit, continued in 2010 with the removal and conditioning of the control rods and other highly radioactive material present in the reactor pool. These activities restarted in September 2013 until July 2014, with the dismantling of all plant components still present in the pool and with the treatment of liquid effluents.
The next planned activities in order to obtain the unconditional release of the site will cover:
• Dismantling and conditioning of active purification system and ion exchange resins, and in particular:

- radiological and chemical characterization of the resins;
- removal of the resins;
- decommissioning of the exchange resins system;
- conditioning in standard containers which meet the requirements of a national repository, and granting at CISAM GRRD temporary storage.

• Dismantling of the primary circuit including the heat exchangers and the decay reservoir, conditioning of waste products;
• Dismantling of the collector of radioactive liquid effluents and conditioning of waste products;
• Dismantling of the draining circuit of the pool water and hot discharges and conditioning of waste products;
• Conditioning of the waste stored inside the shelter near the reactor.

All the above activities will be carried out trying to minimize the volume of radioactive waste to be delivered to the national repository by implementing proper decontamination procedures and radiometric control for the unconditional release of dismantled materials and conditioning of radioactive waste products. The strategy developed by the experts of the Interforce Center for Studies and Military Applications (CISAM) along with the know-how of Nucleco SpA provide a useful example for the definition of technical and management procedures for decommissioning of research reactors with an optimal radwaste management.

1. INTRODUCTION

The reactor "RTS-1 Galileo Galilei" is a pool type research reactor, which belongs to the family of highly enriched uranium (90%) heterogeneous reactors, light water moderated and cooled.
It was commissioned by the Ministry of Defence in 1958 and was built by Vitro Italy (on project of Babcock & Wilcox) between 1960 and 1963. The first criticality was on April 4th, 1963 and worked for 17 year. On March 7th 1980, the reactor was shut down.
The plant is located on the site of the Interforce Center for Military Applications Studies (CISAM) in San Piero a Grado (Pisa).

2. RTS-1 Galileo Galilei REACTOR

The general layout of the buildings is shown in Figure 1. The main structures are the following:
1. Reactor Building;
2. Secondary circuit premises (including the building of the secondary circuit pumps and cooling towers);
3. Collecting and storage tank for pool water;
4. Power supply building;
5. "Shelter" for activated materials and / or contaminated;
6. Box 1 for obsolete materials;

7. Box 2 for contaminated materials;
8. Laboratories outside fromReactor Building.

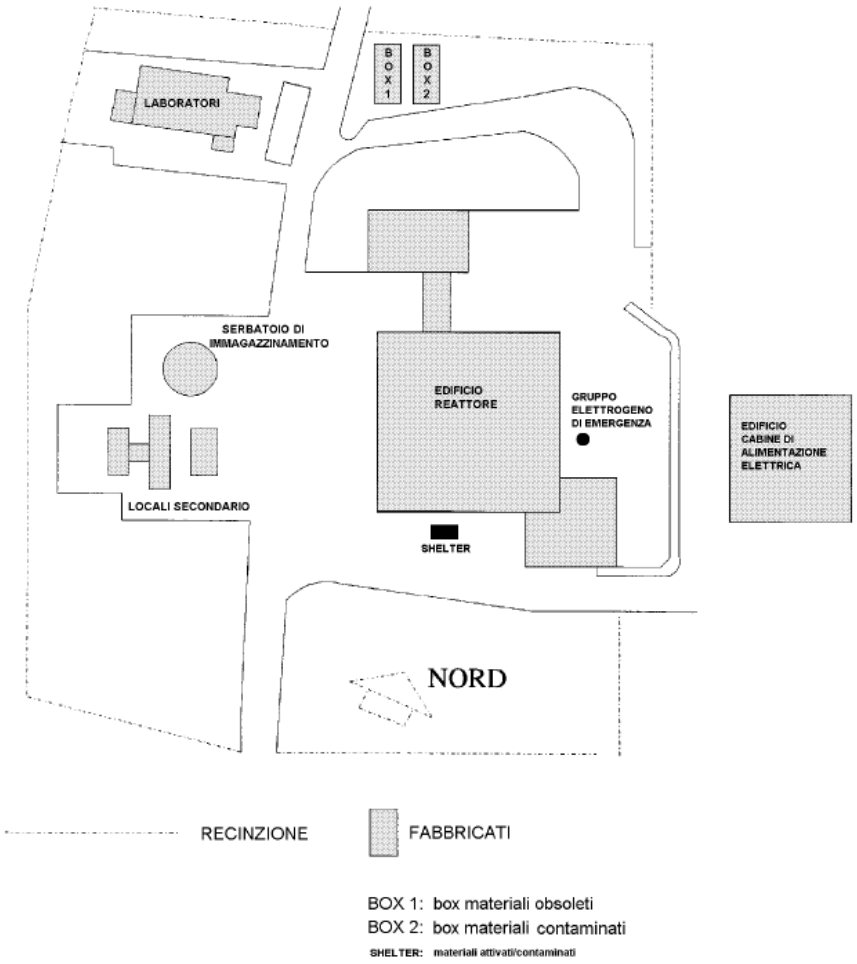

Figure 1. General layout of RTS-1

The reactor building is constituted by a two-story building, surface 40x40 m, surmounted by a 18 m in height and 24 m in diameter cylinder and a structure, limited to the west side of the cylinder, with a radiation facilities.

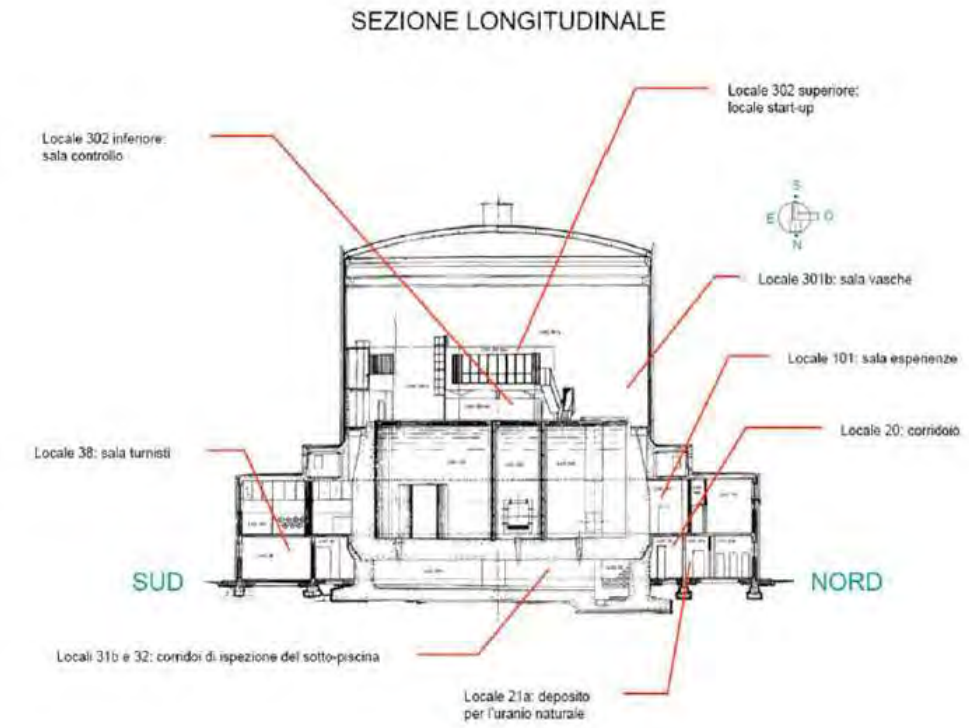

At the center of the building, close to the cylinder, is located the reactor pool , 20 m long, 3.5-6 m wide and 9 m deep.
The premises of Reactor Building relevant for the current phase of decommissioning are as follows:

On the ground floor:

- inspection corridors under pool (rooms 31 and 32);
- active purification room (30);
- liquid effluents collection tank (room 29 below);
- pumps, primary circuit and heat exchangers room (28),
- irradiation channel services (rooms 27a, 27b);
- natural uranium storage area (room 21);
- intermediate activity cell (room 36);
- demineralization plant (room 25);
- air conditioning plant (room 2);
- control panels (room 1);
- compressed air plant (room 19).

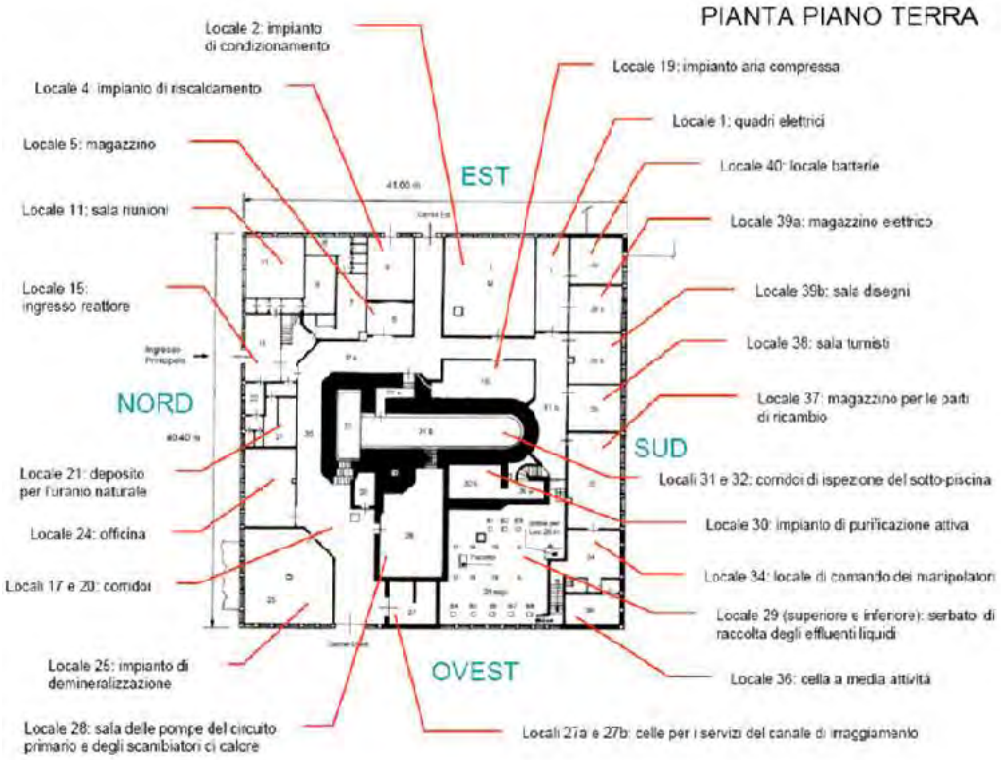

On the first floor:

- experiences room (room 101);
- irradiation channel services (rooms 120 and 114);
- irradiation channel (cell 1-room 117, cell 2-room 118, cell 3-room 119);
- gamma cell (room 116);
- Chemistry lab (room 104);
- measurements lab (room 102);
- warehouses.

At the intermediate level:

- fans (room 209a);
- prefilters (room 209b);
- preheating of pool water (room 202).

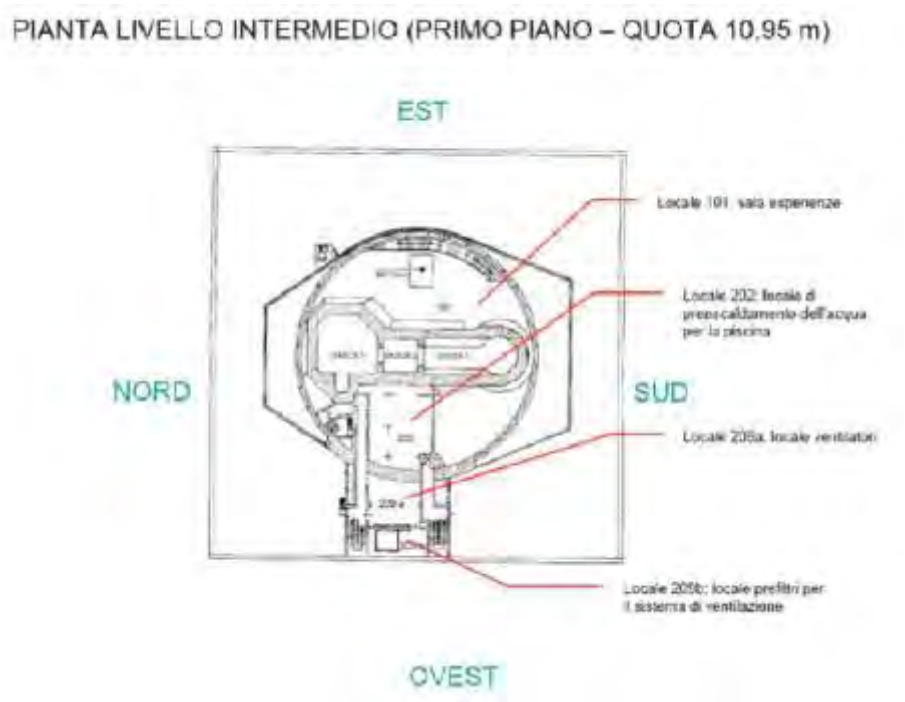

On the second floor:

- tanks (room 301).

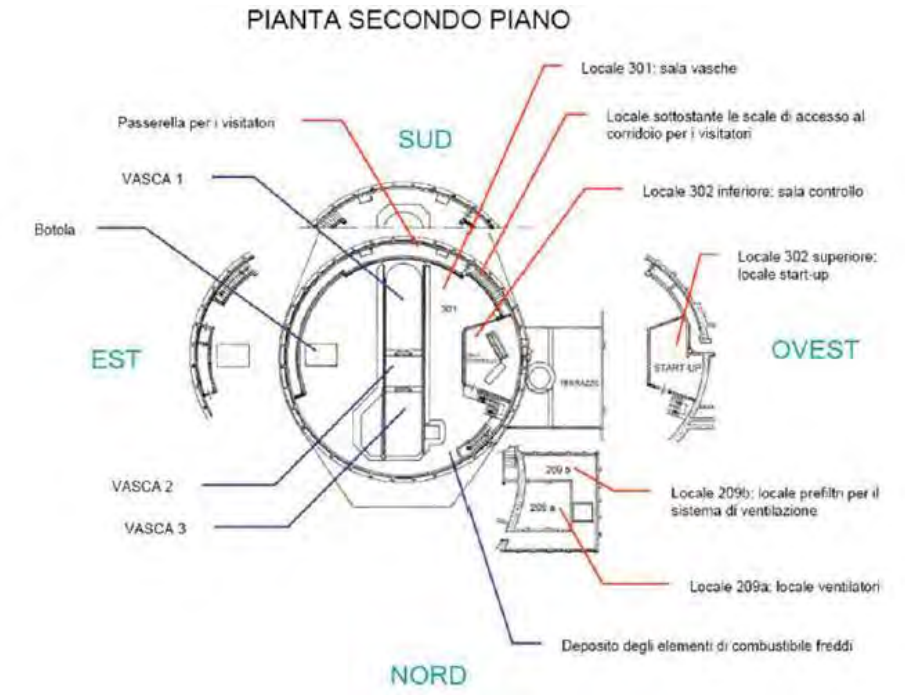

3. DECOMMISSIONING STRATEGY OF PRIMARY CIRCUIT

This paper describes the decommissioning strategy of the primary circuit of the reactor "G. Galilei" RTS-1, including heat exchangers and decay tank, the dismantling and conditioning of the radioactive liquid effluents collection plant; the dismantling and conditioning of the pool water and hot effluent discharge draining circuit.
Decommissioning activities have been designed by the CISAM experts and will be performed by Nucleco SpA with particular regard to the aspects of decontamination, treatment and conditioning of radioactive waste produced.
Nucleco is a qualified and specialized operator in the field of radioactive waste management and site remediation with several years' experience in decontamination activities of nuclear and industrial sites. Part of the Nucleco activities are carried out under the decommissioning program of nuclear power plants and fuel cycle circuit in the national territory.
As part of the decommissioning of the primary circuit of the reactor "G. Galilei" RTS-1, NUCLECO should first provide a technical-management program indicating the organization of activities, the materials flows at each stage and for each area (areas of dismantling, temporary storage, Materials Management area, radiological monitoring and outdoor storage areas) and a detailed timetable of activities.
The Operational Plan will analyze in detail the planned activities and will evaluate the sequential logic of all phases of operation, in order to optimize the decommissioning programme and start the future final phase aimed at obtaining the unconditional release of the civil structures of the reactor building, in full compliance with all applicable radiation safety procedures.
NUCLECO will then define in detail the techniques for disassembly, cutting and demolition that will be used, the preliminary treatment of radioactive waste produced, their decontamination and their packaging, the storage as well as the characterization of all materials (waste management plan).
First of all, NUCLECO will define the physical limits of the spool (defined as the system or part of it, resulting from decommissioning activities, characterized by an appropriate size allowing the disposal in a suitable store, identified and radiologically classified following the decommissioning plan), with the description of the type and size of material. The size of each spool must be:

- for materials releasable without radiological constraints, not exceeding 1m x 1m x 1m;
- for materials activated and / or contaminated, adapted to the respective packaging in containers of cylindrical CC220 / 440/500 complying the standard UNICEN 203, in order to guarantee a complete radiological characterization followed by a correct labeling.

Then NUCLECO will define the procedures for the radiological characterization of systems / structures / components (SSC) to be dismantled and will perform the experimental measurements.
Subsequently the pathways for materials handling will be defined and the areas of temporary storage of the spools will be identified: hot area (used as a temporary storage of the contaminated materials coming from the measurement area), cold area (used as a temporary storage of the not-contaminated materials coming from measurement area) and transfer area (used for the radiological monitoring of the materials coming from dismantling operations).
After the planning activities, NUCLECO will perform the activities indicated in the operational sequence :

- dismantling and conditioning of purification plant and ion exchange resins;

- dismantling and conditioning of the whole primary circuit including the heat exchangers and the decay tank;
- dismantling and conditioning of the radioactive liquid effluents collection plant;
- dismantling and conditioning of the pool water and hot effluent discharge draining circuit;
- Conditioning of the materials stored inside the shelter close to the reactor.

The ion exchange resins to be conditioned have a the volume of about 1500 liters, with a total activity estimated at 1,4E + 09 Bq.
NUCLECO will ensure the complete removal of the resins contained in the columns of the purification plant and, subsequently, the conditioning in special standard containers type CC220 / 440/500 and their assignment at the temporary storage of GRRD CISAM.
All liquids arising from the removal of resins, will be properly treated and incorporated into the cement matrix.
The procedure for the treatment of resins consists of the following steps:

- radiological and chemical characterization of resins, activated carbon and gravel;
- resins' saturation, if the saturation has not been achieved during their previous use;
- removal of resins (mixed with water) through sludge pump and transfer of the remaining water in containers ;
- removal of activated carbon and transfer to appropriate containers;
- removal of coarse gravel from the bottom of the carbon filters and transfer to containers.

The cutting activities of ferrous materials, when possible, will be performed with the "knurl tube cutter" technology for stainless steel with a maximum thickness up to 40 mm and for tubes with outer diameter up to 350 mm.
This technology guarantees the production negligible quantities of secondary products and is applicable on most of the expected components to be dismantled.
The above activities will be carried out trying to minimize the volume of radioactive waste to be temporary stored at GRRD CISAM, implementing proper decontamination procedures and radiometric control for the unconditional release of dismantled materials, allowing an appropriate conditioning of radioactive waste products.
Based on the operating procedures for the radiological characterization of the resulting materials and their labeling, as defined in detail in the operational plan, NUCLECO will:

- store in the proper area (cold or hot depending on the case), the resulting material and perform radiological characterization and related labeling of all spools resulting from dismantling;
- separate materials not activated and / or contaminated, on the basis of their type (ferrous, light alloy, inert, hazardous) and origin.

The materials will be characterized in order to verify the possibility of unconditional release.

4. RADIOLOGICAL CHARACTERIZATION AIMED TO FREE RELEASE

4.1 Reference framework

The Basic Safety Standards suggests the levels of exemption (Exemption Level), which are defined in a more restrictive sense in national law. The unconditional clearance levels (Clearance Level) are also suggested in the publications Radiation Protection (RP): in particular, the RP 89 offers specific levels of removal (Specific Clearance Level) for metals.
The definition of clearance levels, whether they are general or specific, guarantees the radiological non-relevance of materials removed without additional controls: the same RP 122 Part I states that the materials removed should not be subjected to further examination,

otherwise it would contradict the principle of Unconditional Removal that prescribes the release of materials from the regulatory system (Clearance = release from regulatory requirements). The Italian legislation on radioprotection (Article 154 paragraph 3 bis of Legislative Decree 230/95 and subsequent modifications and additions) states that "... the removal from installations subject to authorization ... of materials containing radioactive substances intended to be disposed of, recycled or reused .... is subject to specific requirements to be included in the authorization... The clearance levels ... take into account the guidelines, recommendations, and technical guidance provided by the European Union".
An operative indication on the methods and procedures for radiological control with the purpose of unconditional release is provided by the UNI 11458:2012, and it outlines strategies for the measurement of low levels of radioactivity in solid materials from nuclear facility.

4.2 Equipment used

For the unconditional release of materials from nuclear power plants is necessary to perform measurements of surface contamination and concentration of activity on a number of samples as described in the following.
For surface contamination's measurements it will be used the portable contamination monitor Berthold LB 124. It has a detection surface of 170 cm^2 equipped with a scintillation detector ZnS for measurement of "total alpha" and " total beta / gamma". For the determination of the concentration of activity will be used a system based on high-resolution gamma spectrometry. It is constituted by an HPGe detector and a hardware unit with a MCA (multichannel analyzer) that operates associated to a computer equipped by a dedicated software, which controls the entire flow of information from the MCA to the computer. The calculation of the activity will be determined by factor of proportionality between the activity and net counts rates obtained from the spectrum output multichannel analyzer MCA, using the calibration models Gamma Vision.
Combining the data response characteristic of the detector with the measuring geometry and the chemical, physical and geometrical characteristics of the object analyzed, the software is able to determine the efficiency curve.
The specifications of the measuring system are listed below:
• coaxial HPGe detector Detector System
• energy range: 50-3000 keV / 5-1500 keV
• relative efficiency: 50% - 55%
• resolution: 1.9 to 1332 keV; Peak / Compton: 66:1

4.3 Characterization Plan

All materials will be divided into homogeneous waste streams. For each of them an appropriate plan of radiological characterization will be drawn up.
For the unconditional release of materials, will be verified that the condition of maximum concentration levels of mass and surface contamination for the radionuclides listed in the document "Proposal for a definition of the limits of release for solid materials from the dismantling of the reactor and the RTS-1 decontamination of equipment or complex subject to prior clearance under the Legislative Decree no. 230/95 and Delegate Decrees (Prime Ministerial Decree 183/05) and subsequent amendments and additions " will be satisfied.
The condition to be fulfilled in the case of more than one radionuclide is the following:

$$\sum_i \frac{C_i}{C_{li}} < 1$$

being C_i the concentration of the i^{th}-radionuclide and C_{li} the appropriate limit value.

The verification of condition "Surface" recalled in Table 1 will be carried out on 100% of the areas to be investigated.
The determination of surface contamination of radionuclides emitting alpha and beta emitters will be carried out in terms of concentration "gross alpha", "beta total" and "gamma total" using portable instrumentation described in paragraph 3. Not being able to discriminate the contribution of each radionuclide listed in the above mentioned document ", will be adopted the most restrictive level among those present in the table. The instrumental data will be corrected conservatively for the efficiency of the most difficult to detect radionuclide and for the extension of the sensitive area.
In order to estimate the concentration of activity it will be used the system based of high-resolution gamma spectrometry previously described. Measurements of activity concentration will be performed on a sample representative of the whole material to be removed. For the determination of the scaling factors between radionuclides easily detectable (Easy To Measure ETM) and hard to detect radionuclides (Hard To Measure HTM) will be defined the appropriate carriers of radionuclides on the basis of historical information of the operation of the reactor RTS-1 that can be derived in the literature and / or on the basis of experimental determinations using destructive measurements on representative samples of the materials to be analyzed.

4.4 Representativeness of the sample

The measurement of the concentration of activity will be conducted on a sample of material representative of the whole material to be released. The representativeness of the sample is assured by compliance with the requirements defined in the UNI 11458:2012.
In particular, the following assumptions will be considered:

- Probability of error of the first type (the material has a radioactivity which does not exceed the levels of removal, but it is not considered removable) α = 0.05 ;
- Probability of error of the second type (the material has a radioactivity exceeding the levels of removal, but it is considered removable) β= 0.05 ;
- C_{LR} (clearance levels) of 0.1 Bq / g for ^{137}Cs and ^{60}Co;
- C_0 (estimated value of residual activity in the material) considered 0.05 Bq / g for ^{137}Cs and ^{60}Co;
- σ_m standard deviation of the measure, conservatively assumed equal to 20 % of the C_{LR}.
- σ_s standard deviation of the spatial distribution of radioactivity considered equal to σ_m;

The sampling strategy used was the one fixed in the sampling plan, i.e. a number of analysis points determined by the Noether's formula:

$$N = \frac{(Z_{1-\alpha} + Z_{1-\beta})^2}{4 \times (p - 0{,}5)^2}$$

Where $Z_{1-\alpha} = Z_{1-\beta}$ = 1,645 (percentile of the normal distribution);

$$p = \frac{1}{\sqrt{2\pi}} \int_{-\infty}^{\frac{\Delta}{\sigma}} e^{-x^2} dx$$

with

$\Delta = C_{LR} - C_0$
x = value of the size in measure
$\sigma = \sqrt{\sigma_s^2 + \sigma_m^2}$ total standard deviation

With the above mentioned assumptions, the number of samples to be analysed is equal to N = 13, but, conservatively, will be analyzed N = 15 samples for each matrix of homogeneous material coming from the site, and belonging to the specific waste stream.

5. CONCLUSIONS

All materials characterized that will result activated and / or contaminated will be subject to subsequent treatment, conditioning and temporary storage at the Temporary storage area of GRRD, otherwise they will disposed in accordance with the provisions of current legislation on conventional, special and / or dangerous wastes.

The strategy developed by the experts of the Center for Military Applications Interforces Studies together with the know-how of Nucleco SpA provide a useful example for the definition of technical and management procedures for decommissioning of research reactors with an optimized radioactive wastes management.

DECOMMISSIONING THE IFIN-HH VVR-S NUCLEAR RESEARCH REACTOR DISMANTLING THE PRIMARY COOLING CIRCUIT

M.DRAGUSIN, A.ZORLIU, R.DEJU, C.A.DRAGOLICI, I.MINCU, D.STANGA, D.GURAU, C.MUSTATA, C.PETRAN, I.STOIAN

Reactor Decommissioning Department, National Institute for R&D in Physics and Nuclear Engineering – Horia Hulubei (IFIN-HH)

30 Reactorului Street; RO 77125, Magurele, Ilfov-Romania

ABSTRACT

The nuclear research reactor VVR-S from IFIN-HH, 2 MW thermal power, was in operation during 1957-1997. Was in permanent shutdown for preparation the decommissioning from 2002. No any incidents in operation during of the 40 years. The all nuclear spent fuel assemblies both highly enriched uranium and low enriched uranium types were repatriated in the Russian Federation since December 2012. From 2013 started the decommissioning the research reactor based of the immediate dismantling strategy. The end use of the nuclear facility will be reutilisation the building in nuclear field-research-development-innovation in material science, fundamental, experimental and applied in nuclear physics. In this paper will be presented the works executed in order to dismantle the primary circuit of the research reactor, the techniques, methods and technologies used, the material management resulted from dismantling activities, radioactive waste management – handling, segmentation, technical specifications for package prepared to send for treatment, conditioning in the Radioactive Waste Treatment Plant form IFIN-HH for storage or disposal in the National Repository for Radioactive Waste. The methods and equipment used for free release of the materials resulted in order to demonstrate complying with the clearance level will be presented. Radiation protection, nuclear and radiological safety, industrial safety, environmental protection aspects will be highlighted.

1. Introduction.

IFIN-HH Nuclear Research Reactor is a Russian VVR-S Type. A 2MW thermal power research reactor with thermal neutrons, moderately, cooled and reflected with distilled water, filled up with 10% enriched uranium in the beginning of operation. In 1980 the fuel type was changed to 36% enrichment in U235 isotope that was used till the end of operation. The main purpose of this reactor was the research and the production of radioisotopes for diagnosis and therapy in nuclear medicine.

The operation of the research reactor started on 1957 July 29th and was shut down in 1997 December 30th, when a preservation license for the reactor was issued by CNCAN.
During the 40 years of operation, the energy produced was 9.51 GWd and the utilization factor was 65 % (~9510 days of effective operation) with an average thermal power of 1 MW.

Romanian Government Decision 418/25.04.2002 decided the “Permanent shut down of the VVR-S Nuclear Reactor from “National Institute for Research and Development in Physics and Nuclear Engineering Horia Hulubei” (IFIN –HH)” and, stated that IFIN-HH, in its position of both user and operator of the Nuclear Research Reactor, will complete the decommissioning objective.

The Feasibility Study for “Decommissioning of VVR-S Nuclear Reactor, Repatriation of EK-10 Spent Nuclear Fuel and Modernizing of Nuclear Waste Treatment Plant Installations”,

code: IFIN-VVRS-STDR-SF/MT Rev.1, November 2008 was approved by Ministry of Education, Research and Innovation.

The Governmental Decision HG 898/2009 August 20th has approved the technical and economic indicators of the investment "Decommissioning of the VVR-S Nuclear Research Reactor, Repatriation of EK-10 Spent Nuclear Fuel and Modernizing of Nuclear Waste Treatment Plant Installations". This decision represents the financial source for financing the decommissioning project.

Following this decision the IFIN-HH Reactor Decommissioning Department started to work on the preparation of the necessary documents for getting all the necessary licenses and agreements from the National Institutes involved in nuclear field: CNCAN, Nuclear Agency, Agency for Environmental Protection, Health and so on.

Picture 1. IFIN-HH VVR-S NUCLEAR REASEARCH REACTOR

2. Decommissioning Plan, Decommissioning Strategy, Decommissioning Phases.

The Decommissioning Plan was issued to comply with the content of the IAEA Safety Reports Series No.45 and the Feasibility Study "Decommissioning of VVR-S Nuclear Reactor, Repatriation of EK-10 Spent Nuclear Fuel and Modernizing of Nuclear Waste Treatment Plant Installations".

The selection of the decommissioning strategy within the framework of the laws and regulations in force (which protect the public interest) is the responsibility and privilege granted to the owner of the facility (who is protecting his own interests). In case of VVR-S NR, the owner's interests (Romanian State) coincide with the public interest so that the determining factors for the selection of the decommissioning method are socio-economic, political and overall safety type at local, national and European scale.

Taken into account all the qualitative and quantitative assessments done, the financial and technical point of view and the results of the radiological characterization of the plant (max activity of 20 to 30 Ci) and the radioactive waste inventory and considering that 10 years have already passed since the reactor was shut down, the immediate dismantling strategy option was chosen for the Decommissioning Project.

Duration of the decommissioning project is 11 years and will be implemented in three phases:

- Phase one, three years: 2010 - 2012 (finalized)
- Phase two, one year and 10 months: 2013 - October 2014 (finalized)

- Phase three, 6 years and 2 months: November 2014 - December 2020

After a series of revisions under the IAEA Technical Cooperation Project ROM-29-04 with the participation of an International Mission of Experts from IAEA the Research Reactor Decommissioning Plan Revision 9 /May 2008 was approved by CNCAN.

Picture 2. The reactor hall before the beginning of decommissioning activities

3. Pre decommissioning activities.

3.1. Documentation issued

- Radiological Characterization Report
- Detailed Decommissioning Plan
- Environmental Protection license
- CNCAN license for decommissioning.
- Sanitary license

3.2. Field of the Works

- Cleaning the rooms and laboratory in the reactor building
- Removal the radiological wastes from the reactor preservation channels
- Removal of the research equipment from the reactor hall
- Repatriation of the high enriched spent fuel S-36 type to Russian Federation in 2009
- Radiological characterization works; drilling for samples in the reactor shield, walls and floor.

3.3. International Projects

The following projects with DOE/USA, IAEA and PHARE were a great help for the Reactor Decommissioning Department (RDD) to finish a lot of pre decommissioning tasks like: issue a Decommissioning Plan, repatriation of the S-36 spent fuel, issue the Radiological Characterization Report and provide the RDD with some equipment for decommissioning activities.

3.3.1. Project BOA 3J-00201 with funds from ANL-DOE/USA:
Preparation of documents:

- Preliminary Radiological Characterization Plan for VVR-S Nuclear Reactor
- Radiological Characterization Plan for VVR-S Nuclear Reactor (approved by CNCAN)
- Radiological Characterization Report (approved by CNCAN)
- Preliminary Cleanup Plan for VVR-S Nuclear Reactor
- Training course in the decommissioning field attended and graduated by all DDR staff in 2005-2006 (approved by CNCAN).
- Purchase of equipment for radiological measurements, radiation protection and industrial safety

3.3.2. TCP ROM-04-029 with funds from IAEA Vienna: technical assistance for preparation of the Decommissioning Plan for VVR-S Nuclear Reactor, purchase of equipment for radiological measurements, radiation protection, industrial safety, Clean-up activities and some dry decontamination works (blasting, scarifying, cutting, drilling/coring, air filtration, etc.), training for people involved in the decommissioning activities.

3.3.3. Under the Global Reduction Threats Initiative (GTRI) was implemented the Russian Research Reactor Fuel Return project (RRRFR) with funds and technical assistance from DOE/USA for the return of the S 36 highly enriched fuel:preparation of documents associated to the fuel return process (studies, calculations, technical documents, procedures, instructions, agreements, etc.), works for the characterization of the S-36 spent nuclear fuel, special arrangements for the technological area in the controlled area of the Reactor Hall, purchase of equipment for radiological measurements, radiation protection and industrial safety, upgrading the physical protection system, return of the S-36 highly enriched spent nuclear fuel to Russian Federation, completed in 2009.

3.3.4. PHARE-2006/018-411.03.04 and PHARE-2006/018-411.03.05: equipping Radioactive Waste Treatment Plant facility with a liquid radioactive effluent treatment plant, radiological monitoring and material characterization system pursuant to the requirements for the Nuclear Reactor decommissioning, area monitoring system in the technological areas pursuant to the requirements for the Nuclear Reactor decommissioning, equipment for intervention in radiological emergency situations, training for the use/operation of the aforementioned equipment.

3.4. Activities performed with internal funds (co-financing)

3.4.1. HG 700/2005: preparation of the documents for the safety management of the radioactive waste arising from cleanup of Nuclear Reactor, purchase of containers for the safety management of the radioactive waste resulted from cleanup of Nuclear Reactor, purchase of equipment for: radiological measurements, radiation protection and industrial safety, cleanup activities.

3.4.2. Funds allocated by the Ministry of Education, Research and Youth.(HG 898/2009) for decommissioning the VVR-S Research Reactor, repatriation of SNF EK-10 and up-grading the Radioactive Waste Treatment Plant from IFIN-HH for period 2010-2020.

4. Decommissioning Activities in Phase 1.

The following activities have been already completed:

- Interruption and isolation of all electrical circuits for the control of the reactivity: ionizing chambers, control rods, emergency rods.
- Dismantling of some electro-mechanical components for the reactor control
- Rehabilitation of some rooms in the reactor building basement and preparing them to serve as airlock, decontamination rooms/shower rooms, locker rooms for the workers who enter/exit the reactor hall for/after performing decommissioning activities.
- Rehabilitation of the rooms and former laboratories in the reactor building
- Rehabilitation of the building No. 18 in the nearby of the reactor to be used as a characterization laboratory for the radioactive wastes resulted from decommissioning.
- Construction of a temporary storage for radioactive wastes and materials resulted from decommissioning activities.
- Acquisition of equipment and tools for decommissioning.
- Repatriation of the low enriched spent fuel EK-10 type to Russian Federation, December 2012.
- Drainage of the primary cooling circuit

Phase 1 was finalized at the end of 2012.

5. Decommissioning Activities in Phase 2.

In phase 2 of decommissioning a lot of systems, equipment and structures have been dismantled, taken to the cutting shop for size reduction and treated as radioactive wastes.

5.1. The secondary cooling circuit was dismantled.

Since this system was not contaminated nor activated the works were done as for a usual industrial structure. A wall structure, the biological protection between rooms 30 and 31 had to be demolished in order to gain access to all components of the circuit. There were no significant problems encountered.

5.2. The cooling pound near the reactor was drained and the contaminated water transported to the Waste Treatment Plant. Also a small room in the basement with a lot of I&C components that measured the level, temperature and flow of the water in the reactor vessels was dismantled.

5.3. Internal components from the reactor have been dismantled

Works started with the dismantling of the reactor leads and plugs. They were measured from dosimetry point of view to detect any contamination and finally were free released.

The I&C components from the reactor core were dismantled: ionizing chambers, control rods, emergency rods, associated guiding channels and cables and were treated as radioactive wastes. They were cut and dropped in 220 l drums and sent to the Waste Treatment Plant. A difficult job was done to remove the stainless steel rod belonging to the automatic regulator which was highly activated – 10 mSv/h. Although a remote control tool – Brokk 50 - was used to cut the rod, the operator couldn't stay to close to the rod to maneuver it for the cutting operation without taken a high dose. To solve the problem, the mechanical department has adapted a tool that was driven by the crane with the activated rod above a led shielded drum where the shares of the Brokk machine cut the rod into small pieces that fall in the drum. All operation have been remotely driven from the sealed room situated on the top of the reactor hall.

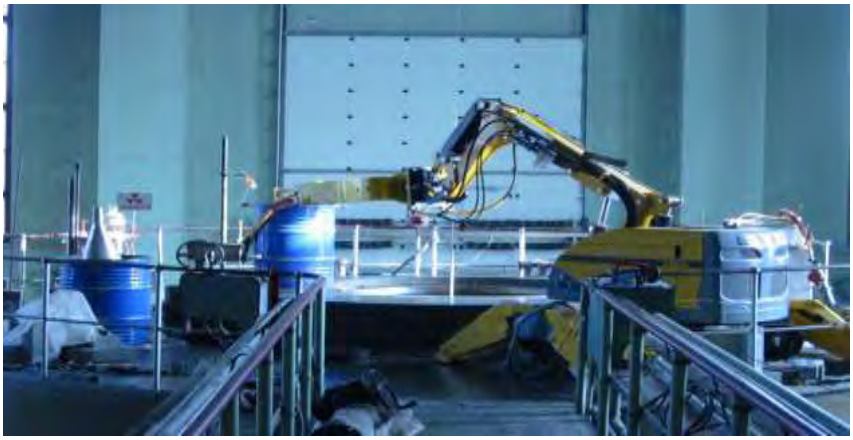

Picture 3. Using the Brokk 50 on the top of
Reactor for cutting the activated control rods

Picture 4. Remotely operation for cutting
the activated control rod in a shielded drum

After removal the I&C components the other internals have been successfully removed: the reactor separator, diaphragms, washers, tubes and channels used for irradiation of materials during research activities.

5.4. The dismantling of the primary cooling circuit.

The route of the primary cooling circuit encloses the reactor, circulating pumps, heat exchangers, and connecting pipes. The equipment of the primary circuit is mounted in the pump room (room 31 in the basement of the reactor hall). The handling of each valve is made from two adjacent corridors to the pump room (rooms 32 and 33). Three pumps out of five were providing the necessary flow and pressure of cooling agent to operate the reactor at a nominal power.

The heat evacuation from the primary circuit is made through 2 heat exchangers, with « u » type pipes, having a heat exchange surface of 95 m^2. Upwards and downwards of the heat exchangers, on the cooling pipes there are mounted two fittings that are manually and remotely driven, allowing the isolation of the exchangers in case of intervention (only by closing the primary circuit).

The dismantling of the primary cooling circuit started in the basement room 31 with the dismantling of the 5 pumps and motor pumps. All component have been measured by the

dosimetry operator and segregated in contaminated and non-contaminated parts. Also it is worth to mention that parts of the primary circuit pipes are made of aluminum and other of stainless steel. Each had its own approach for threatening according to the approved procedure. Some components have been decontaminated locally with special gels, other have been treated as radioactive waste and the rest which are big components were temporary deposited in order to be transported to the Waste Treatment Plant for size reduction. Next, started the work on demolishing the heat exchangers and dismantling the pipes. As shown in the following pictures special tools have been used to dismantle and cut these pipes.

Picture 5. Pipe cutting machine using a turning chisel system – Proma MCA 6

Picture 6. Workers in the pumps room are cutting pipes connection to the heat exchanger from the primary cooling circuit using a Reciprocating Electric/Pneumatic Band Saw - Bosch

Picture 7. Cutting the 108 mm pipe with Semi-Automatic Cutting Horizontal Band Sawing Machine - Proma BMSY 440

Picture 8. Cutting the fuel assembly rack with Holmatro Mobile Electro-hydraulic Scissors – CU 4030 C GP

Picture 9. Using the plasma torch for cutting heavy metal structures

The dismantled pipes according to their size were cut in the reactor hall or taken in the cutting shop to be cut with a different tool.

In the reactor hall was installed a cutting shop for activated and contaminated structures and components. This ModuCon Enclosure Assembly is made of UPVC material, easy to wash

and decontaminate. It comprise an air lock, a working room and a decontamination room with shower and is provided with a HEPA filtration system.

Picture 10. The cutting shop

6. Decommissioning Activities in Phase 3.

Phase 3 started with the decommissioning of the **de-aerator system** of the primary circuit. This auxiliary system had the purpose to eliminate the gas of the primary circuit, formed during the reactor operation and their discharge in the ventilation system. This circuit is mounted in the room of the main circuit pumps and in the closed chamber of the de-aerator. The operators work on demolishing the wall where the de-aerator is mounted. The work is hard because the heavy concrete contains a lot of metal components in its structure. Workers are using drilling machine to drill a few holes and then a diamond chain saw to cut concrete pieces. After the whole wall will be down the work will start on dismantling the de-aerator vessel and the associated pipes.

The other activities foreseen for this phase are the following: dismantling the reactor vessels, dismantling the cooling pond, demolishing the reactor block, decontamination the hot cells. The final statement in the decommissioning of the VVR-S Research Reactor will be the removal of the installation from the Regulatory Body (CNCAN) control and reutilization the building in fundamental and applied nuclear physics with particle accelerated.

7. Radioactive Waste Treatment

The radioactive wastes generated by VVR-S reactor decommissioning process are classified as follows: activated radioactive waste, contaminated radioactive waste, secondary waste resulted from decommissioning activities.

According to CNCAN Order 156/2005 classification of all radioactive waste generated from the activities can be included in the class of Low and Intermediate Level Waste, subdivided as follows: Exempt waste, Very low level waste (VLLW), Short lived waste (LILW-SL), Long lived waste (LILW-LL)

All the solid radioactive wastes resulted from the decommissioning activities are loaded in 220 l and 420 l drums and then transported to the Waste Treatment Plant situated about 200 m close to the reactor building. Both type of drums 220 l and 420 l are licensed by CNCAN. After the treatment and conditioning of wastes, the measurements and all the necessary controls are done, packages with wastes are transported by a special truck to DNDR Baita Bihor.

Picture 11. Stainless steel 220 l drum

Picture 12. 40 l drum “ecolRad50”

The Waste Treatment Plant is part of Department for Radioactive Waste Management (DMDR). DMDR is licensed for collecting, treatment, conditioning and temporary storage of radioactive waste resulted from research, medicine, education, industry using nuclear techniques or technologies, others than those which would result from the nuclear fuel cycle, for controlled release to the environment or disposal at National Repository for Radioactive Waste (DNDR) Baita-Bihor. The National Disposal facility was adapted in a former uranium mine in the central-western part of the Bihor Mountains in west of the country. Two galleries at a depth of 840 m were selected. DNDR has the license for the final disposal of conditioned radioactive wastes resulted from VVR-S reactor decommissioning.

The Waste Treatment Plant and the DNDR were modernized in Phase 1 according to the Feasibility study in order to be ready to receive the wastes generated from the decommissioning activities.

The liquid wastes resulted from the drainage of the primary cooling circuit, the cooling pond and other sources were collected in a 30 m^3 buffer tank near the reactor building. From this tank the liquid wastes were transported to the Waste Treatment Plant in one of the 300 m^3 storage tank.

In the decommissioning process will also be generated special long life radioactive waste which cannot be disposed in DNDR-Baita-Bihor. These are aluminum and graphite radioactive wastes for which treatment and conditioning technologies are not yet available. The aluminum waste will result from the reactor vessels and the graphite from the thermal column.

For these type of waste it was decided to be intermediary stored in the former storage for the spent nuclear fuel. The storage building contains 4 pools made of aluminum. Those pools will be drained, decontaminated and rehabilitated in order to deposit the graphite and the aluminum wastes. The storage fulfills all the necessary condition required for a waste storage. All the systems: physical protection, I&C, video surveillance, lifting installation, power supply and ventilation are perfect functional.

The thermal column is made of 6 independent discs containing the activated graphite. The discs can be dismantled one by one, will be transported to the Intermediary Storage and deposited in one of the 4 pools. After the reactor vessel will be reduced in size, the aluminum waste will be filled in the 220 l drums and then transported and deposited in the Intermediate Storage until will be available and validated technology for treatment and conditioning for disposal.

LEGAL AND CONTRACTUAL FRAMEWORK FOR SPENT FUEL BACK-END MANAGEMENT IN CONNECTION TO THE DECOMMISSIONING OF THE FINNISH TRIGA FIR 1

I. AUTERINEN
VTT Technical Research Centre of Finland
Otakaari 3, FI-02044 VTT, Espoo – Finland

ABSTRACT

VTT Technical Research Centre of Finland as the licensee of the government owned FiR 1 TRIGA research reactor has decided to close down the FiR 1 reactor as soon as it is technically and legally possible. An environmental impact assessment of the decommissioning has been conducted as a prerequisite for the application to the government for shutting down of the reactor.

For the spent fuel back-end preparations are made for the US-DOE Foreign Research Reactor Spent Nuclear Fuel Acceptance Program. The legal framework for this has been complicated by the fact that VTT became beginning of year 2015 a limited company owned by the government. The ownership of the reactor was transferred to the company. This caused issues in relation to nuclear liability and international agreements which were hold by the Finnish State. Already in the past Finnish government has stated that it will take full responsibility of all the decommissioning costs of the reactor. Solutions how this will be facilitated are discussed.

The contractual framework of the US-DOE Foreign Research Reactor Spent Nuclear Fuel Acceptance Program with associated transports arrangements is discussed from the customer point of view.

1. Introduction

FiR 1 -reactor is a TRIGA Mark II type research reactor manufactured by General Atomics (San Diego, CA, USA). The purchasing contract between General Atomics and the government of Finland was signed May 30th 1960. The reactor was purchased through an agreement between the International Atomic Energy Agency (IAEA) and the government of Finland for assistance by the agency to Finland in establishing a research reactor project [1]. IAEA and the Government of the United States of America had on 11 May 1959 concluded an Agreement for Co-operation arrangements to transfer and export material, equipment or facilities for a Member of the Agency in connection with an Agency project. The fuel for the reactor was purchased through Supply Agreements between the IAEA, the Government of Finland and the Government of the United States of America. The first agreement entered into force on 30 December 1960 and the fourth on 27 November 1969 [2]. The last fuel delivery arrived at the reactor January 4th 1971. All fuel is 20% enriched uranium.

The IAEA project relating to the FiR 1 reactor constituted the prototype of those relating to the simultaneous provision of a small research reactor and of the fissionable material (fuel and fission counters) therefor from the United States to another Agency Member. [3, 4].

Boron Neutron Capture Therapy (BNCT) has dominated the utilization of the reactor since late 1990's. Also radioisotope production, as well as education and training have played an important role until recently [5]. The operating licence of the reactor was extended for the period 2011 to 2023 by the government of Finland in December 2011.

In June 2012 VTT Technical Research Centre of Finland as the licensee of the government owned research reactor decided to close down the reactor as soon as it is technically and legislatively possible [6]. An environmental impact assessment of the decommissioning has been conducted as a prerequisite for the application to the government for shutting down of the reactor [7].

VTT became beginning of year 2015 a limited company owned by the government. The ownership of the reactor was transferred to the company. This caused issues in relation to nuclear liability and international agreements which currently are hold by the Finnish State. In the past Finnish government has stated that it will take full responsibility of the nuclear liability and all the decommissioning costs of the reactor. Solutions for this have been discussed between VTT and the government.

For the spent fuel back-end preparations are made for the US-DOE Foreign Research Reactor Spent Nuclear Fuel Acceptance Program. The contractual framework for this has been complicated by the change in the legal status of VTT and the uncertainties in US Department of Energy capabilities to receive spent TRIGA fuel to the storage facility in Idaho.

2. Main findings on spent fuel management in the environmental impact assessment

According to the Finnish Decree on Environmental Impact Assessment Procedure (713/2006) [8] nuclear power plants and other nuclear reactors, including the demolition or decommissioning of these plants and reactors, require an environmental impact assessment (EIA). The EIA coordinating authority is the Ministry of Employment and the Economy (MEE). The assessment is a prerequisite for the project to receive required permits.

VTT submitted its final EIA report to the coordinating authority in October 2014 [9]. MEE requested statements on the assessment report from various government and municipal authorities and the nuclear energy companies. The report was also open for public opinion in a public hearing and on the website of MEE [10]. The MEE got 16 statements from authorities, research institutes, and companies. Two position papers were also received End of February 2015 MEE issued its statement on the environmental impact assessment report [11].

The Ministry noted that VTT's report meets the content requirements of EIA legislation and it has been handled in the manner required by the legislation. The MEE also noticed that its earlier statement on the EIA programme had been taken into consideration in the assessment. In the statements delivered to the MEE, the EIA programme has been seen to be mainly pertinent and comprehensive. The shortcomings that were noted must be rectified later in the project as the planning moves forward.

The MEE statement noted that for getting the licence to decommission the research reactor, VTT is required to supply authorities with reports demonstrating, among other things, the safety of the decommissioning, under the Nuclear Energy Act and Decree. For the decommissioning effort a separate plan must be drafted according to guidelines set in the Nuclear Energy Act. VTT must also fix the shortcomings and errors for documents required for the licence procedure and must take into consideration matters that have emerged in the EIA procedure in other respects as well. MEE informed that under current plans, the research reactor is to be shut down in 2016. The dismantling work is expected to take from two to three years in total.

The Ministry of the Environment stated that the report was insufficient to assess whether the requirements under section 7 (b) of the nuclear energy decree are met. It states that the treatment, storage and emplacement of spent nuclear fuel generated from operating a research reactor in Finland in a manner intended as permanent outside Finland can be justified for safety reasons, or for a significant financial or another cogent reason. MEE was of the opinion that this issue will be dealt with in the final decommissioning plan.

3. Change in the legal status of the licence holder

VTT became beginning of year 2015 a limited company owned by the government. The ownership and the operating licence of the reactor were transferred to the company. That meant that all the obligations of the licence holder as stipulated in the Nuclear Energy Act (990/1987) were transferred to VTT Ltd.

According to the Finnish Nuclear Liability Act (484/1972, 28§) government does not have to take insurance for nuclear liability. So VTT as a government office did not have a nuclear liability insurance and the government would have stood for the compensations in case of a nuclear liability incidence. Through an agreement between MEE and VTT Ltd this situation could have continued but MEE decided VTT has to buy insurance from a commercial insurance pool.

Finland has a National Nuclear Waste Management Fund as stipulated by the Nuclear energy Act, Chapter 7 Financial provision for the cost of nuclear waste management. Funds for implementing the financial provision of nuclear waste disposal are in the fund, independent of the State budget but controlled and administered by the Ministry of Employment and the Economy. The share of FiR 1 is currently 9,7 M€. The ownership of this share in the fund was transferred to VTT Ltd. As the Finnish government has stated that it will take full responsibility of all the decommissioning costs of the reactor independent of the role and position of VTT it has covered the cost of the increased deposit in the fund. However it is still unclear how the government would cover decommissioning costs which VTT could not recover from the fund. This would occur if VTT has direct costs due to decommissioning at the same time when the required deposit in the fund is increasing due to estimated cost increases in the future phases of the decommissioning.

The Finnish solution for the administration of a decommissioning of a *de facto* government research reactor differs from the models adopted in the other Nordic countries. In Sweden a separate company SVAFO Ltd [12] was established to be responsible for coordinating and managing historic waste - primarily from government research activities - under the so-called 'Studsvik Act' of 1988/89. Its operations are financed by the Swedish Nuclear Waste Fund to which owners of the nuclear utilities pay fees, like in Finland too. In Denmark Danish Decommissioning (DD) [13] was established in 2003 as an institution under the Ministry of Science, Technology and Innovation. DD is responsible for decommissioning, i.e. dismantle, the nuclear facilities formerly attached to Risoe DTU - National Laboratory for Sustainable Energy.

4. US-DOE Idaho site as spent fuel back-end solution for FiR 1

The delivery of the TRIGA fuel from the US to Finland was part of the ‘Atoms for Peace’ program announced by US President Eisenhower in UN in 1953. At that time the handling of fuel after it has been used in FiR 1 was not an issue and nothing is mentioned about this in the contracts. Only the reprocessing of molybdenum producing targets was dealt with.

US DOE started to accept spent nuclear fuel from domestic and foreign research reactors in a program which was described in the DOE Federal Register Notice entitled "Spent Fuel: Chemical Processing and Conversion" [14], which was published in January 1968. This Notice was subsequently amended nine times and the policy expired after 25 years on December 31, 1992 for LEU fuels. This service was based on the idea of reprocessing of spent fuel; but it included also TRIGA-fuel although no reprocessing was developed for that. Without further elaboration DOE stated:

> In lieu of processing uranium-zirconium hydride fuel types, DOE will agree to provide disposition services for such fuels. In this case, no compensation for recovered uranium will be made. Research reactor operators may prefer to write off the value of uranium contained in the fuel and accept this service. Additional information concerning DOE's disposition service may be obtained from the Manager, Idaho Operations Office, U.S. Department of Energy, 785 DOE Place, Idaho Falls, Idaho 83402.

In November 1993 also FiR 1 received a letter from DOE Office of Arms Control and Nonproliferation stating that DOE was evaluating its proposal on renewal of its policy to receive the spent nuclear fuel that the United States has furnished to foreign research reactors and requested "Information Regarding Spent Nuclear Fuel Originating in the United States and Irradiated in Foreign Research Reactors." This information allowed DOE to evaluate environmental, economic, safety, and nuclear nonproliferation aspects of the proposed policy renewal.

In 1996 a new policy started with the Record of Decision (ROD) on a Proposed Nuclear Weapons Nonproliferation Policy Concerning Foreign Research Reactor Spent Nuclear Fuel [15]. Under this policy DOE planned to accept for thirteen years aluminum-based and TRIGA spent fuel assemblies that completed their irradiation within ten years after the ROD became effective. The motivation for this ten year period was to allow reactor operators, their governments and international organizations time to address solutions for managing their spent fuel after DOE’s Spent Fuel Acceptance Policy expires. DOE stated that it did not intend to renew this policy. In December 2004 DOE extended the program with 10 years [16]. After the basic decision (ROD) in 1996 the TRIGA fuel issue has not been separately discussed in the subsequent RODs, but for the price of the service. In summer 2014 TRIGA reactor operators received a letter from DOE National Nuclear Security Administration stating that the United States is not planning to extend or renew the program to allow for returns after May 12, 2019 [17].

European Union regulation [18] notices that some Member States have already participated and intend to participate further in the US-Russian driven programme, called the Global Threat Reduction Initiative, by shipping the spent fuel of research reactors to the United States of America and to the Russian Federation. Article 2 of the directive allows shipment of spent fuel of research reactors to a country where research reactor fuels are supplied or manufactured, taking into account applicable international agreements. There is no time limit in this directive.

4.1 TRIGA and DOE Idaho spent fuel facility – unique US technologies and capabilities

All together 69 TRIGA reactors have been constructed or converted to. All TRIGA fuel fabricated until now is US origin. All TRIGA RR, worldwide, are now operating with less than 20% enriched fuel. The uranium-zirconium-hydride fuel is chemically very stable and therefore there is no reprocessing process developed for it. Thus spent TRIGA fuel does not actually form a non-proliferation risk but merely a radiological risk and a potential material for a dirty bomb.

The DOE INL storage facility has served and is continuing to serve 32 US domestic TRIGA reactors, 17 university reactors and 15 non-university reactors [19]. From the university reactors 12 are under the United States domestic research reactor infrastructure TRIGA reactor fuel support [20]. Also the spent fuel from the Vienna TRIGA will arrive there sometime around 2025 [21]. It would be of great value to the global TRIGA community to keep this service by the dedicated TRIGA SNF storage available to all TRIGAs. Less than one third of the projected amount of TRIGA SNF from foreign RR has been received to the storage facility in Idaho [22]. As the DOE TRIGA SNF storage facility in Idaho is serving the needs of 32 US TRIGA reactors and - at least – one foreign reactor, equal treatment of the customers of this US technology would indicate that also the remaining 19 non-domestic TRIGAs should have access to this service till the end of their lifetime. And the technical lifetime of the TRIGAs now in operation is certainly beyond May 2016.

4.2 Problematic issues

Shipments of spent nuclear fuel into the State of Idaho are restricted, and tied to completion of various INL environmental restoration and radioactive waste management activities that are important to the State of Idaho in accordance with specific provisions of the settlement agreement between DOE and the State of Idaho [19].

Spent nuclear fuel shipments to Idaho have been banned by the state since Jan. 1, 2013, as a consequence for DOE missing a nuclear waste clean-up deadline in the 1995 Settlement Agreement [23]. The missed 2012 deadline remains out of compliance because of ongoing problems with a treatment facility — the Integrated Waste Treatment Unit, at DOE's desert site. The plant, built after a 2005 request from DOE to change how it would treat sodium-bearing waste stored in out-of-compliance underground tanks, has cost more than $500 million and is still undergoing testing.

Another Settlement Agreement milestone, which requires an average of 2,000 cubic meters of transuranic waste to leave Idaho per year, also recently was violated because of the temporary closure of a New Mexico waste repository. A barrel buried at the Waste Isolation Pilot Project burst open in February, causing a fire and extensive damage that closed the plant, stopping shipments from Idaho and other DOE sites. DOE has not said when the plant will reopen.

It seems that DOE will be able to receive spent TRIGA fuel at the earliest in 2017.

DOE has constructed into the return program a three year period between the last use of the fuel and the last date of arrival to US. According to DOE the additional three years in the shipping period were included to provide time for the radiation levels of the last spent fuel discharged during the 10 year policy period to decay enough to allow its transportation, to provide time for logistics in arranging for shipment of the last spent fuel discharged, and to allow for potential shipping delays.

In practise the fuel has cooled down for shipment already in one month, waiting longer than that will not make a difference. This waiting period will unnecessarily prolong the decommissioning process as demolition work cannot be started before all spent fuel has been transported away. If the schedule of the ROD is followed and the reactor shut down before May 2016 the reactor will stay untouched for at least a year, maybe several, waiting for opening of the Idaho site for receiving the spent fuel. The customers of the reactor, users of technical radioisotopes, university researchers and nuclear education courses, would rather continue to exploit the reactor during that time.

Once the shipments are again possible DOE and its sole supplier for transport services could consider offering a joint service with a combined, single contract and DOE taking title of the SNF already at the sending research reactor, as mandated in the ROD 2008 [24], allowing also easier combination of shipments.

5. Conclusions

All TRIGA research reactors, worldwide, are now operating with Low Enriched Uranium (LEU) fuel. There are no means available for reprocessing the chemically very stable uranium-zirconium-hydride fuel and therefore there is no way to extract nuclear weapons material from it. Thus spent TRIGA fuel does not actually form a non-proliferation risk.

Operating TRIGA reactors should not be considered as nonproliferation risk but as inherently safe sources of neutrons and tools for education and training. By offering a safe storage for spent TRIGA fuel not used any more by the reactors United States Department of Energy can reduce the radiological risk and potential for a dirty bomb.

.

References

1. INFCIRC/24, IAEA 24 January 1961.
2. INFCIRC/24/Add. 2, 3, 4 , IAEA 25 July 1966, 12 January 1968, 5 February 1970.
3. SZASZ, P.C., The Law and Practices of the International Atomic Energy Agency, IAEA Legal Series no 7, Vienna 1970, pp. 411–423.
4. INFCIRC/40, IAEA 23 October 1962 MATERIALS DELIVERED BY MEMBER STATES.
5. Auterinen I, Salmenhaara S.E.J, The 250 kW FiR 1 TRIGA Research Reactor - International Role in Boron Neutron Capture Therapy (BNCT) and Regional Role in Isotope Production, Education and Training, Research Reactors: Safe Management and Effective Utilization - Proceedings of an international conference held in Sydney, Australia, 5-9 November 2007, Proceedings of an International Conference organized by the International Atomic Energy Agency (IAEA), IAEA-CN-156, 2008. http://www-pub.iaea.org/MTCD/publications/PDF/P1360_ICRR_2007_CD/datasets/I.H.%20Auterinen.html
6. Auterinen I, Rapid shutdown and decommissioning of the Finnish TRIGA FiR 1 – decisions and preparations, RRFM2013 transactions, pp. 354-359. http://www.euronuclear.org/meetings/rrfm2013/transactions/RRFM2013-transactions.pdf
7. Auterinen I, Viitanen T, Räty A, Häkkinen S, Kotiluoto P, Preparations for the decommissioning of the Finnish TRIGA FiR 1 – spent fuel back-end management and distribution of the unspent fuel, RRFM2014-A0084, RRFM2014 transactions p.269. http://www.euronuclear.org/meetings/rrfm2014/transactions/RRFM2014-transactions.pdf
8. Act (468/1994) and Decree (713/2006) on Environmental Impact Assessment Procedure. http://www.ymparisto.fi/download.asp?contentid=84193&lan=en
9. Decommissioning of the FiR 1 Research Reactor, Environmental Impact Assessment Report, VTT and Pöyry PLC, October 2014. https://www.tem.fi/files/41245/FiR_1_YVA_selostus_FINAL_ALL_21102014_pieni_resoluutio_(2).pdf (in Finnish).
10. https://www.tem.fi/files/41514/Lausuntopyynto_5.11.2014.pdf
11. Ministry of Employment and the Economy (MEE), Statement on the environmental impact assessment report of the decommissioning of the FiR 1 Research Reactor. https://www.tem.fi/files/42360/TEM_lausunto_25022015.pdf
12. http://www.svafo.se/

13. http://www.dekom.dk/english.aspx
14. 1986 and 1987 Federal Register Notices that provide "Receipt and Financial Settlement Provisions for Nuclear Research Reactor Fuels", http://www.rertr.anl.gov/REFDOCS/FR51.html
15. Record of Decision for the Final Environmental Impact Statement on a Proposed Nuclear Weapons Nonproliferation Policy Concerning Foreign Research Reactor Spent Nuclear Fuel, Federal Register / Vol. 61, No. 97 / Friday, May 17, 1996 / Notices.
16. Revision of the Record of Decision for a Nuclear Weapons Nonproliferation Policy Concerning Foreign Research Reactor Spent Nuclear Fuel, Federal Register /Vol. 69, No. 230 /Wednesday, December 1, 2004 /Notices.
17. Letter to TRIGA operators via *Embassy of the United States of America* from Sarah Dickerson, Director of Removal Operations, Global Threat Reduction Initiative, National Nuclear Security Administration, summer 2014.
18. COUNCIL DIRECTIVE 2011/70/EURATOM of 19 July 2011 establishing a Community framework for the responsible and safe management of spent fuel and radioactive waste.
19. Wade J, The U.S. Department of Energy/Idaho National Laboratory's Research Reactor Spent Nuclear Fuel acceptance programme, in RETURN OF RESEARCH REACTOR SPENT FUEL TO THE COUNTRY OF ORIGIN: REQUIREMENTS FOR TECHNICAL AND ADMINISTRATIVE PREPARATIONS AND NATIONAL EXPERIENCES, IAEA, VIENNA, 2008, IAEA-TECDOC-1593.
20. Morrell D, United States Domestic Research Reactor Infrastructure TRIGA Reactor Fuel Support, Joint RRFM 2011 / World TRIGA Users Conference, March 2011, INL/CON-10-20313, PREPRINT
21. Supplement Analysis on the Transfer and Return of Low-Enriched Uranium Fuel Elements from the Idaho National Laboratory to the Research Reactor in Vienna, Austria, May2012, Prepared by the Department of Energy's Idaho Operations Office, DOE/EIS-0218F-SA-05.
22. Supplement analysis for the foreign research reactor spent nuclear fuel acceptance program, November 2004, DOE/EIS-0218-SA-3.
23. Ramseth L, Spent nuclear fuel could once again be headed to Idaho National Laboratory, Idaho Falls Post Register, January 14, 2015, http://www.idahostatesman.com/2015/01/14/3590694_spent-nuclear-fuel-could-once.html?rh=1#storylink=cpy
24. Revised Record of Decision for the Environmental Impact Statement on a Proposed Nuclear Weapons Nonproliferation Policy Concerning Foreign Research Reactor Spent Nuclear Fuel, Federal Register / Vol. 73, No. 165 / Monday, August 25, 2008 / Notices.

SAFETY REGULATION OF DECOMMISSIONING OF NUCLEAR RESEARCH FACILITIES IN RUSSIA

ALEXANDER SAPOZHNIKOV
Department for Safety Regulation of Nuclear Power Plants and Nuclear Research Facilities,
Federal Environmental, Industrial and Nuclear Supervision Service of Russia,
Taganskaya, 34, 109147 Moscow, Russia
F.Sapozhnikov@gosnadzor.ru

ABSTRACT

The report presents information on safety regulation of decommissioning of Nuclear Research Facilities (NRFs)[1] in the Russian Federation including the issues of release of the sites from regulatory control. The challenges, faced by the regulatory bodies in these activities and the efforts taken for strengthening regulatory system in the decommissioning area are discussed.

1. Introduction

Holistic solution of problems concerning safe decommissioning of nuclear and radiation hazardous facilities (NRHF)[2] along with the relevant problems of safe management of spent fuel (SF) and radioactive waste (RW) is of vital importance not only in view of ensuring nuclear and radiation safety in the use of atomic energy, but is also considered as a major prerequisite of developing the nuclear industry on the whole.

The decommissioning of NRHF should be carried out in accordance with the provisions of the Joint Convention on the safety of spent fuel management and on the safety of radioactive waste management [1], and should be aimed at achieving the highest level of safety that can reasonably be achieved, taking into account economic and social factors.

This report informs of the most significant recent results in implementation of the programmme on decommissioning of NRFs in the Russian Federation. It also considers the tasks regarding to regulation of safety and release of sites from the regulatory control, set in accordance with the IAEA standard on decommissioning [2] and the Fundamentals of state policy of nuclear and radiation safety in the Russian Federation for the period up to 2025 [3].

2. Development of the national system of decommissioning of nuclear facilities in the Russian Federation

In the Russian Federation the problems arising with RW, SF, contaminated areas, research institutions and industrial nuclear facilities (“nuclear legacy”) have been accumulated within more than 50 years since the beginning of the Soviet Nuclear Programme at the end of 1940s because of their lower priority at that period.

[1] NRF – nuclear facility including research nuclear reactors (RR), critical (CA) and subcritical (SCA) nuclear assembles, and related complex of premises, structures, systems, elements, experimental facilities, and personnel that are in boundary of territory (NRF site) defined by the design for utilization of neutrons and ionizing radiation for research purposes.

[2] Nuclear and Radiation Hazardous Facilities (NRHF) - hereinafter referred as nuclear installations, radiation sources, storage facilities of nuclear materials and radioactive substance and storage facilities of radioactive waste.

Currently this has been changed, and the strategy of management of RW and SF generated during operation and decommissioning of NRHF is based on approaches adopted in the international practice [4, 5], that cover also liquation of the "nuclear legacy" components.

This progressive strategy underlies the Federal Law "On Radioactive Waste Management" and is used in the Federal Target Program "Provision Nuclear and Radiation Safety for 2008 and the period up to 2015" (FTP NRS) [6], in which about 80% of funds are allocated for decommissioning of NRHF and associated activities with RW and SF.

FTP NRS is one of the main tools for implementation of the state policy in the sphere of nuclear and radiation safety (NRS). To date, a great deal of work in the area of decommissioning, removal of SF from the sites, reprocessing of RW and implementation of new technologies has been performed in the framework of the FTP NRS [7, 8].

The FTP NRS arrangements have provided formation of the main elements of the national system for adequate planning, organization and management of decommissioning activities. These cover:

- Legislative and regulatory framework;
- Policy framework and managerial mechanisms (empowered authorities assigned; specialized organizations established; the responsibilities defined, including establishment of special state company responsible for long term storage and disposal of RW - National Operator);
- Strategy of decommissioning (timescale and stages);
- Funding mechanisms.

The result of evaluation of nuclear legacy in Russia is given in Table 1 [9].

Shutdown (or planning to shutdown)						
Type of NRHF	Num-ber	before 2008	2008-2015	2016-2025	2026-2035	After 2035
Nuclear facilities	331	37	31	73	25	165
Storages Radwaste	1253	290	68	120	61	714
Radiation sources	479	24	41	34	25	355
Contaminated buildings and structures	44	9	4	8	11	12
Contaminated territories	22	-	-	-	-	-
The sites of peaceful nuclear explosions	81	-	-	-	-	-
Total	2210	360	144	235	122	1246

Tab 1: The result of evaluation of nuclear legacy in Russia

According to table 1, 31 nuclear installations should be decommissioned in the period 2008-2015, and 73 nuclear facilities are planned to be decommissioned during the next 10 years.

The works initiated by the FTP NRS for 2008-2015 will be logically continued through development of the FTP "Provision of Nuclear and Radiation Safety for 2016-2020 and for

period up to 2025" (FTP NRS-2). It is planned that the FTP NRS-2 will provide for resolving of not less than 20 % of problems concerning SF, RW, and decommissioning of NRHF.

Currently there are following decommissioning strategies applied to NRFs and other nuclear facilities:

- Liquidation (immediate or deferred dismantling);
- Step-by-step dismantling;
- Postponed decision with regard to the end state.

The requirements to decommissioning activities for the whole period of decommissioning (from setting the decommissioning programme to the end state of the facility) are determined by the decommissioning project and take into account the decontamination criteria at the site. General criteria on achieving an acceptable level of site radiation can be derived from the basic dose limits, set in the Norms of radiation safety (NRB-99/2009) [10]. Depending on the end state of the site the two main dose limits are in use:

- 20 mSv/year for the personnel (group A-nuclear professionals);
- 1 mSv/year for population (citizens, industrial workers).

The criteria for clearance of decontaminated materials are established by the Sanitary Rules of radioactive waste management (SPORO-2002) as a level of residual contamination (specific activity), which is given for the major radionuclides [11]. In case of unknown radionuclide composition the residual specific activity should be less than:

- 100 kBq/kg for beta emitters;
- 10 kBq/kg for alpha emitters;
- 1 kBq/kg for transuranic radionuclides.

Gamma-contaminated materials with unknown radionuclide composition are cleared from regulatory control if the absorbed dose at their surface (0,1 m) does not exceed 0,001 mGy/h above the background.

In line with the requirements of Sanitary rules of radiation safety (OSPORB-99/2010) [12] the decommissioning works at radiation facility or its separate parts must be carried out in accordance with the project that should also include rehabilitation of released premises and territories.

Financial aspects of decommissioning are defined by the Governmental orders of the Russian Federation № 68 [13] and № 576 [14], which oblige the organizations – owners of NRHFs to do annual deductions in the special funds. The deducted funds are covered by the cost of production or service and are cleared from the taxation. In line with Federal Act № 317 (Article 20) the State Corporation "Rosatom" creates special reserve funds, which are also dedicated for financing the decommissioning works [15].

3. State of legislative and regulatory framework for NRHF decommissioning

Among the set of federal laws in the area there are the three fundamentals on the use of atomic energy:

- Federal Law "On the Use of Atomic Energy" № 170-FZ dated 21.11.1995;
- Federal Law "On Radioactive Waste Management" № 190-FZ dated 11.07.2011;
- Federal Law "On Radiation Safety of Population" № 3-FZ dated 09.01.1996.

At the same time a special legislation on regulation of decommissioning activity does not exist. The legislation does not define a concept of "decommissioning" and does not contain provisions regarding procedures of decommissioning and order of full or partial release of the site from regulatory control. Instead, the Federal Law "On the Use of Atomic Energy"

№ 170-FZ defines that the arrangements and procedures for NRHF decommissioning should be specified in the Federal regulations with regard to each specific type NRHF. At present a number of such regulations have been put in force:

- Safety rules for decommissioning of Nuclear Power Plants, NP-012-99;
- Safety rules for decommissioning of Nuclear Research Facilities, NP-028-01;
- Safety rules for decommissioning of ships and other crafts with nuclear installations and radiation sources, NP-037-11;
- Safety rules for decommissioning of production nuclear facilities, NP-007-98;
- Safety rules for decommissioning of nuclear installations of nuclear fuel cycle, NP-057-04;
- General Safety Provisions for Radiation Sources, NP-038-11;
- Sanitary rules for liquidation, conservation and conversion of facilities for mining and processing of radioactive ores, SP LKP-91;
- Safety ensuring for decommissioning (closure) of tailings, RB-078-12.

The regulations NP-012-99 and NP-028-01 define “decommissioning” as activity which is performed after removal of nuclear materials from the site and aimed at achievement of the end state of the nuclear facility and its site. This approach is in line with the current state of economic and social factors in the Russian Federation and allows being flexible with regard to the process of decommissioning of nuclear facilities: setting a mode of the end state, establishing end state criteria, identifying stages of work implementation.

This may be compared with the term “decommissioning” in the IAEA safety standard “Decommissioning of Facilities, General Safety Requirements” [2], that refers to the administrative and technical actions taken to allow full or partial clearance of the facility from the regulatory controls. In strategy aspect it clearly specifies that only release of NRHF from the regulatory control makes it possible to conclude that the NRHF has been fully decommissioned.

In this regard the work on the harmonization of the legislative and regulatory framework on decommissioning of NRHF in the Russian Federation is continuing with due account to the IAEA recommendations including the recommendation on setting safety criteria for release of the sites from regulatory control, made by the Integrated Regulatory Review Service (IRRS) Mission to the Russian Federation [16].

It should be noted that in case the functioning of the NRHF is terminated, but decommissioning has not been started and a decommissioning plan, other supporting documents are not available (transition period), this NRHF is regulated by the same safety regulations as the similar facilities in operation, taking into account graded approach.

4. Decommissioning of NRFs

In spite of the fact that the decommissioning activity in the Russian Federation is focused mainly on achieving safety state of nuclear facilities and treatment of SF and RW, essential experience has been gained in resolving the numerous problems in decommissioning of a variety of nuclear facilities. For example, over the last five years, 2010 – 2014, the end state has been reached, and the authorization for decommissioning accordingly terminated, at the following ten NRFs and one storage point of SF NRF:

- Critical assembles: “Strela” (2010), «BR-1» (2011), RF-GS (2012), Federal state unitary enterprise “State Scientific Center of the Russian Federation - Institute for Physics and Power Engineering A.I. Leypunsky» (“FEI”);
- Critical assemble № 3 (2012), Joint-Stock Company “TVEL”;
- Subcritical assemble (2012) – Sankt-Petersburg Institute of Mechanical Engineering “LMZ-VTUZ”;

- Subcritical assemble SO-2M (2012), Joint-Stock Company “The Basic Institute of Chemical Technologies” (VNIIHT);
- Research reactor RBT-10/1 (2014), State Scientific Center “Scientific Institute of Atomic Reactors” (NIIAR);
- Research reactors VVRL-02 и VVRL-03, (2011), point of storage SF, (2014), Federal state unitary enterprise “Research Institute of Scientific Instruments” (NIIP).

Table 2 below gives data on those facilities which have been brought to the end state and acceptable radiation conditions, defined in the decommissioning project. The authorizations for decommissioning of these facilities were terminated in 2014 accordingly.

Nuclear facility, location	Specifics/year of putting in operation	License for decommissioning /cancellation	End state
RBT-10/1, State Scientific Center “Scientific Institute of Atomic Reactors, Dimitrovgrad	Pool, water-water, 10 MW , a single pool with RBT-10/2 /1983	2008/ 02.08.2014	Partial dismantling, improving technological capabilities of RBT-10/2
Storage of spent fuel (SF) buildings 60,100, Research Institute of Scientific Instruments, Moscow region	Bld. 100 - SF of space nuclear power facility WWR-L-02 and solution pulse RR IIN-3M; Bld. 60 – SF of space nuclear power facility «Yenisey» / 1974	2009/ 04.04.2014	Radiation - technology object

Tab 2: NRFs and Storages of SF, which decommissioning was completed due to achieving the end state in 2014

A complex of research reactors RBT-10 comprises two similar in design pool-type thermal neutron reactors RBT-10/1 and RBT-10/2 that utilize a high flux reactor SM-3 spent fuel assemblies as fuel. The two reactors share a building, pool, ventilation and special sewage systems, central vault, maintenance room, casings, water purification system, feeding and coolant filling system. The reactors were commissioned step-by-step: 1982 – power startup of RBT-10/1, 1983 – RBT-10/2. The reactor RBT-10/1 was decommissioned, and resulting from this the cooling system, the safety and technology capabilities of the reactor RBT-10/2 were improved.

The information on NRFs that were licensed for decommissioning or final shutdown mode of operation (transition period, the authorization for activities) is shown in table 3.

Attention may be paid to the special approach concerning the end state of the research reactor F-1 (the first physical reactor in Eurasia).and the research reactor AM (the First in the world NPP).

The research reactor F-1 was launched by I.V. Kurchatov on 25 December, 1946. It is uranium-graphite reactor without forced cooling, with nominal power 24 KW. The reactor is assembled with graphite units. The core graphite has cells filled with metal uranium units of natural isotope composition.

№	NRF, Location	Type/Power, MW	Startup/ Shutdown	End state
	Decommissioning			
1	ARBUS-ACT-1, Dimitrovgrad	Tank, organic/12	1963/1988	RAW storage in reactor pit
2	TVR, Moscow	Tank, channel, heavy water/2,5	1949/1986	green field
3	MR, Moscow	Pool, channel, multiloop /water-beryllium mod./50	1964/1992	Radiation technology objects (RTO)?
4	AM, Obninsk	First–in-the word NPP, U-graphite, channel/10	1954/2002	Museum, finishing D&D after 2080
	Final Shutdown			
1	BR-10, Obninsk	Tank, fast/liquid metal/8	1959/2002	Dismantling 2053-2058, RTO?
2	F-1, Moscow	the first physical reactor in Eurasia U-graphite/0,024	1946/2014	Museum

Tab 3: NRFs that are licensed in decommissioning or in final shutdown mode of operation (transition period)

The reactor F-1 used as reference neutron source for metrological certification and study of performances of neutron flux measuring means for NPPs and other nuclear and physical plants. It was recognized as a national cultural and scientific heritage of Russia by certificate of 15 May 2001. The decision on final shutdown and use of the facility F-1 as a museum, preserving the original configuration of the basic systems, was made on 18 March 2014. The review of documents for licensing reactor F-1 in final shutdown mode of operation is planned to be completed in 2015 (preparatory phase for decommissioning).

The nuclear facility AM was put into operation in 1954, June 27, in Obninsk as the First NPP in the world with electrical power 5 MW (hereinafter used as a research reactor AM). This first NPP in the world demonstrated the possibility of using nuclear energy for generation electricity and heat supply. The reactor AM is water-graphite, thermal neutron reactor with design power 30 MW. The power operation of the reactor AM was stopped on 29 April, 2002. It was recognized as a national cultural and scientific heritage of the Russian Federation by certificate of 07 December, 2004. There is a decision on creation a memorial museum and educational center on the basis of the First NPP in the world in Obninsk, approved by the order of the President of the Russian Federation of 09 April, 2004. The decommissioning strategy of the reactor AM includes four stages: preparation for decommissioning (years 2002 - 2010); preparation for long preservation under supervision and containment (years 2010 -2015); long preservation under supervision (years 2015-2080); finishing (after 2080). License for decommissioning of AM was issued on 30 April 2010.

The experience of implementation of national decommissioning programme of the Russian Federation brought out the following scientific and technological challenges in decommissioning of nuclear facilities:

- handling with irradiated graphite;
- removal of impurities from liquid metal coolant and its conversion into safe solid phase of radioactive waste;
- treatment of high-level radioactive heavy water;
- reprocessing of non-standard spent fuel including soluble fuel.

Resolving the outlined challenges has a practical importance and will contribute to decommissioning of other NRHFs, including nuclear power plants and production reactors.

5. Decommissioning issues at stages of sitting, design and commissioning of NRFs

Currently, the regulation “Ensuring safety in decommissioning of nuclear facilities. General provisions” (NP-091-14) has been put in force. It defines that the concept of decommissioning should be developed and updated at stages of sitting, design and commissioning of NRHFs as part of the design documentation and Safety Analysis Report (SAR). The experience on preparing and updating the NRF decommissioning concept, decommissioning procedures, and release of facility and/or site from regulatory control is systemized in the draft "Safety rules for decommissioning of Nuclear Research Facilities” that was developed instead of NP-028-01. The draft contains requirements to a content of a database on decommissioning, a content and structure of the programme of comprehensive engineering and radiation survey, structure and a content of the Principle programme of decommissioning (decommissioning Plan), structure and a content of the SAR of decommissioning, design documentation for decommissioning, final inspection and release of NRF and the site from regulatory control. The draft contains specific requirements to the certain stages of the NRF life cycle including:

Sitting:

- The analysis of the site characteristics, as well as of external natural and technogenic impacts, should take into account possible decommissioning actions, including removal of SF and operational RW from the site, storage (disposal) of RW and the end points of the waste;
- Performing background survey of the site, including radiological conditions, which results should be used for justification of planned end state of the NRF site;

Design:

- Materials used for equipment manufacture, structures and radiation protection should satisfy in reliability and lifetime and should have the lowest level of induced activation in operation conditions.
- The activation indicators (irradiation specimens) should be installed to determine a radiation load on the vessel and internals of the reactor core, equipment and building structure.
- Concrete structures in hazardous radiation indoors should be covered by waterproof low absorption materials allowing their decontamination.
- A service life for non-renewable buildings construction, structures and equipment should cover the period of the NRF operation and its decommissioning.
- Preliminary technical solutions and estimates should be performed regarding the following: set of systems and equipment necessary to perform work on decommissioning of the NRF; technologies appropriate for the dismantling and decontamination; amount (volume) and activity of RW from decommissioning; radiation situation on the site of NRF after termination of the NRF functioning.

Commissioning:

- Systematization of data on the chemical composition of materials should be performed to evaluate their induced activity during the NRF operation.

The above mentioned requirements are applied to the projects of the new NRFs being under construction:

- Complex of nuclear research reactor PIK, National Research Centre "Kurchatov Institute" B.P. Konstantinov Petersburg Nuclear Physics Institute, Gatchina;
- Multipurpose Fast Research Reactor (MBIR), State Scientific Center – Research Institute of Atomic Reactors, Dimitrovgrad.

In case the NRF has been in stage of operation, the operating organization, should, if appropriate: (a) update the presented project concept of the NRF decommissioning with regard to preparatory works; (b) complement decommissioning database, and (c) take measures to provide financial resources for safe decommissioning.

Participation of countries in the International Decommissioning Network (IDN) can facilitate early planning of the decommissioning of various nuclear facilities and, as a result, provide for reducing the financial burden associated with the decommissioning process [17].

6. Summary and Conclusions

The experience of the Russian Federation in safety regulation of decommissioning of various nuclear facilities, in particular nuclear research facilities, is important for international cooperation in this area and contributes to achieving the global safety regime.

Resolving the scientific and technical challenges of NRF decommissioning has a practical importance and will contribute to decommissioning of other NRHFs, including nuclear power plants and production reactors.

Elimination of the nuclear legacy in the Russian Federation is planned and realized within the framework of the Federal Target Programme "Provision of Nuclear and Radiation Safety", which is generally based on the strategy of step-by-step dismantling and deferred decisions with regard to the end state.

Establishing of the uniform procedures for decommissioning of various nuclear facilities has the highest priority in improvement of the legislative and regulatory framework concerning strengthening safety of nuclear and radiation facilities in the Russian Federation. It is based on the two major strategies: liquidation of the facility (immediate, deferred); and creation of radioactive waste repository on the facility site.

The existing legislative and regulatory framework of the Russian Federation provides for the safety of NRHF decommissioning, NRHF release from the regulatory control and meeting provisions of the Joint Convention.

7. References

[1] JOINT CONVENTION on the safety of spent fuel management and the safety of radioactive waste management (ratified by Federal law of 04.11.2005 № 139-FZ), articles 7, 9, 22, 24, 25, 26.
[2] INTERNATIONAL ATOMIC ENERGY AGENCY, Decommissioning of Facilities, General Safety Requirements Part 6, IAEA Safety Standards Series No. GSR Part 6, IAEA, Vienna (2014).
[3] Fundamentals of state policy of nuclear and radiation safety in the Russian Federation for the period up to 2025 and further period, approved by order of the President of Russian

Federation on 1 March, 2012, № Pr-539, access on 3 January 2015 (in Russian) http://www.garant.ru/products/ipo/prime/doc/70190228/ (in Russian).
[4] INTERNATIONAL ATOMIC ENERGY AGENCY, Disposal of Radioactive Waste, IAEA Safety Standards Series No. SSR-5, IAEA, Vienna (2011).
[5] INTERNATIONAL ATOMIC ENERGY AGENCY, Predisposal Management of Radioactive Waste, IAEA Safety Standards Series No. GSR Part 5, IAEA, Vienna (2009).
[6] Federal Target Program "Provision of Nuclear and Radiation Safety for 2008 and for the period up to 2015" (FTP NRS), fcp-radbez.ru (in Russian).
[7] S.V. Mikheykin "Main principles of organization of decommissioning activities for legacy sites", INTERNATIONAL ATOMIC ENERGY AGENCY, Planning, Management and Organizational Aspects of the Decommissioning of Nuclear Facilities, IAEA-TECDOC-1702, IAEA, Vienna (2013), pp.113-148.
[8] A.F. Nechaev, A.A. Akatov "The needs for and the basic elements of an integrated approach to planning, organization and management of decommissioning activities in the Russian Federation", INTERNATIONAL ATOMIC ENERGY AGENCY, Planning, Management and Organizational Aspects of the Decommissioning of Nuclear Facilities, IAEA-TECDOC-1702, IAEA, Vienna (2013), pp. 149-176.
[9] Abramov A., Dorofeev A., Komarov E. and other Concerning the evaluation of nuclear legacy volume in the nuclear industry and other facilities of nuclear energy peaceful use in Russia, SECNRS, Nuclear and Radiation Safety, № 3 (73), 2014, c.1-11
[10] Radiation safety standard 2.6.1.2523-09 "Norms of radiation safety (NRB-99/2009), http://docs.cntd.ru/document/902170553 (in Russian).
[11] Sanitary Rules of radioactive waste management, SP 2.6.6.1168-02 (SPORO-2002), http://base.garant.ru/4178777/ (in Russian).
[12] Sanitary rules of radiation safety СП 2.6.1.2612-10 (OSPORB-99/2010), paras 3.6.2., 3.6.4. http://base.garant.ru/12177986/ (in Russian).
[13] Rules of deductions by enterprises and organizations operating particularly dangerous radiation and nuclear hazardous facilities (nuclear power plants), funds for the creation of provisions to ensure the safety of nuclear power plants at all stages of their life cycle and development, approved by decree of Government of Russian Federation from 30 January 2002, № 68 (In Russian).
[14] Rules of deductions by organizations operating particularly dangerous radiation and nuclear hazardous facilities (excluding nuclear power plants), funds for the creation of provisions to ensure the safety of mentioned plants and facilities at all stages of their life cycle and development, approved by decree of Government of Russian Federation from 29 September, 2005, № 576 (In Russian).
[15] The Federal Law "About the State Corporation on Atomic Energy Rosatom", № 317 from 1 December, 2007, http://docs.cntd.ru/document/902074550
[16] Action plan following the results of the IAEA extended post-mission "Integrated Regulatory Review in the Russian Federation" in November 2013, approved by Rostechnadzor's order from 22 December, 2014, № 593 (In Russian)
[17] The International Decommissioning Network (IDN) web page http://www.iaea.org/OurWork/ST/NE/NEFW/WTS-Networks/IDN/proceedings.html

Research Reactor Operation and Maintenance

NEW CORE CONFIGURATIONS FOR THE IPEN/CNEN-SP IEA-R1 RESEARCH REACTOR USING HIGHER DENSITY FUELS

THIAGO GARCIA JOAO, PEDRO CARLOS R. ROSSI AND ANTONIO T. E SILVA
Nuclear Engineering Center, IPEN/CNEN-SP
Av. Lineu Prestes 2242 - Cidade Universitaria - CEP: 05508-000 - Sao Paulo – SP - BRAZIL

ABSTRACT

This study was performed considering prospective candidates for the IEA-R1 research reactor core. Some neutronic calculations were developed in order to pick up a new core configuration and push forward the thermal-hydraulic and safety analysis. The current IEA-R1 core configuration is a 5x5 (5MW) using U_3O_8-Al and U_3Si_2-Al as fuels, containing, respectively, 2.3 gU/cm^3 and 3.0 gU/cm^3. The new core configuration will be smaller for several reasons (e.g., better fuel utilization and neutron fluxes). In order to achieve such a smaller arrangement, the U-fuel density has to be increased. In the current study, configurations with 4.8gU/cm^3 U_3Si_2-Al fuels were tested using the software MCNP and a set of new core configurations for the IPEN/CNEN-SP research reactor has been created and discussed.

1. INTRODUCTION

This study was proposed in order to change the current IEA-R1 research reactor core configuration (5x5), through neutronic and thermal-hydraulic (TH) calculations, establishing a set of new prospective candidates. The neutronic analysis of nine different core configurations was performed, starting from 3x3 up to higher ones, calculating the multiplication factor (K_{eff}) for the clean core and the power density profile using the code *MCNP5* [1]. The composition of the fuel and control elements is LEU U_3Si_2-Al (4.8gU/cm^3, 42,5% of U_3Si_2 in the volume). The power density was calculated for each fuel plate in order to find out the hottest one. Thus, a steady-state thermal-hydraulic analysis took place to calculate the temperature profile at the hottest fuel plate per configuration. The *nodal method* combined with the *Engineering Equation Solver* (EES) program [2] was used and the TH margins were checked. In summary, the main target of this study is to reach new smaller core configurations for the IEA-R1 research reactor, once this study has already been performed for other research reactors, providing better neutron fluxes and fuel utilization.

2. THE IEA-R1 RESEARCH REACTOR

The IEA-R1 research reactor core is composed of LEU (19.9% in U^{235}) U_3O_8-Al and U_3Si_2-Al fuels containing, respectively, 2.3 gU/cm^3 (33% of U_3O_8 in volume) and 3.0 gU/cm^3 (26% of U_3Si_2 in volume). It's a pool-type reactor and has light water as coolant [3]. In 2007, the IEA-R1 heat exchanger was replaced, alloying, reliably, a power increase from 3MW up to 5 MW. The current IEA-R1 core arrangement has 20 fuel elements (FE), each one with 18 fuel plates; 4 control elements (CE), containing 12 fuel plates and 2 control rods; 1 beryllium irradiator (BI) and graphite (GR) and beryllium (BR) reflectors surrounding the core. The IEA-R1 current core configuration is depicted in Fig 1. The control rods are composed of Ag-In-Cd alloy.

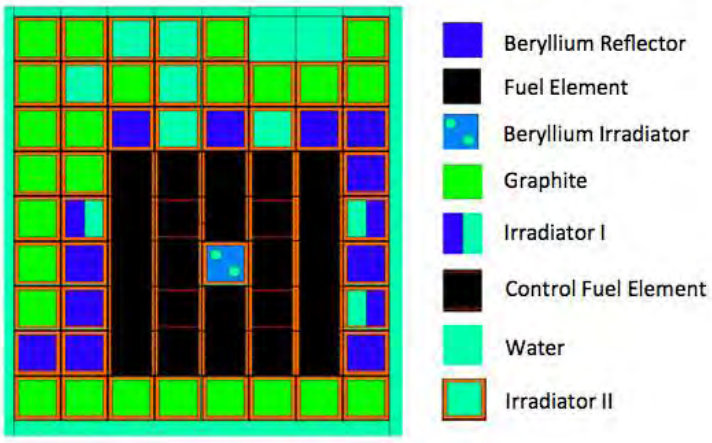

Fig 1. The current IEA-R1 core configuration (5x5) top view (MCNP)

This configuration was changed into others, changing the U-fuel density to 4.8gU/cm^3 (using only U_3Si_2-Al), allowing arrangements with less fuel elements (FE).

3. NEW CORE CONFIGURATIONS

3.1 Neutronic Analysis

New configurations were tested starting from 3x3 as shown in from Fig 2 to Fig 4. The simulations were performed with *MCNP5*, using the Mont Carlo approach to solve the real *transport equation* [4]. The code NJOY [5] was also applied to upgrade the cross section library (ENDF/B-VII) also considering the temperature effects. Further information is found in Table 1. Check the Fig. 1 in order to identify, properly, each element in the next pictures.

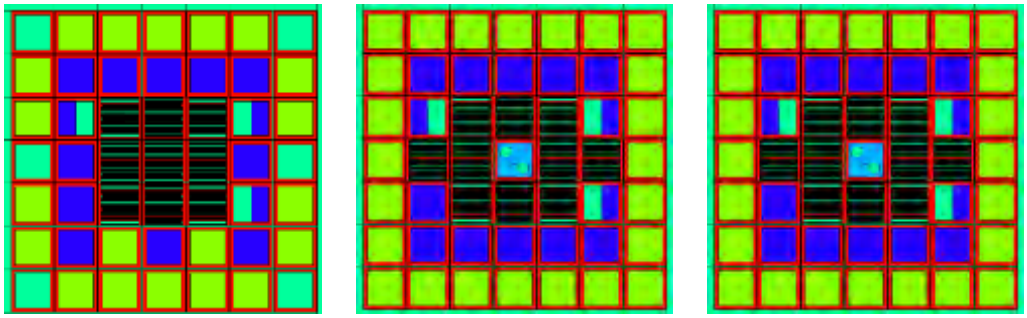

Fig 2. Configuration 5: 5FE+4CE - Configuration 6: 6FE+4C - Configuration 7: 7FE+2CE

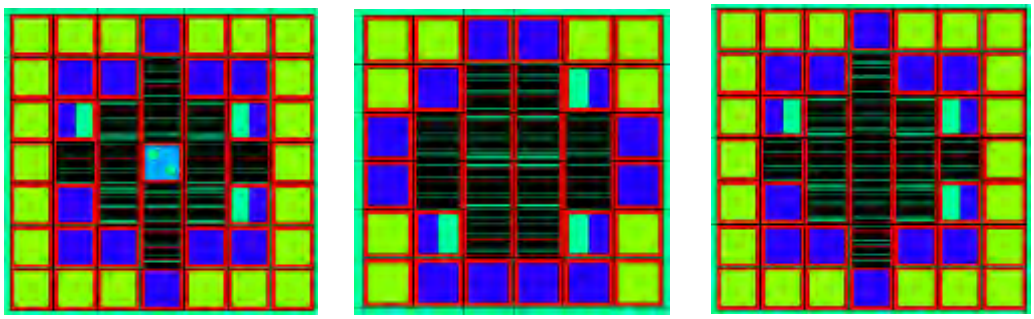

Fig 3. Configuration 8: 8FE+4CE - Configuration 8*: 8FE+4CE - Configuration 9: 9FE+4CE

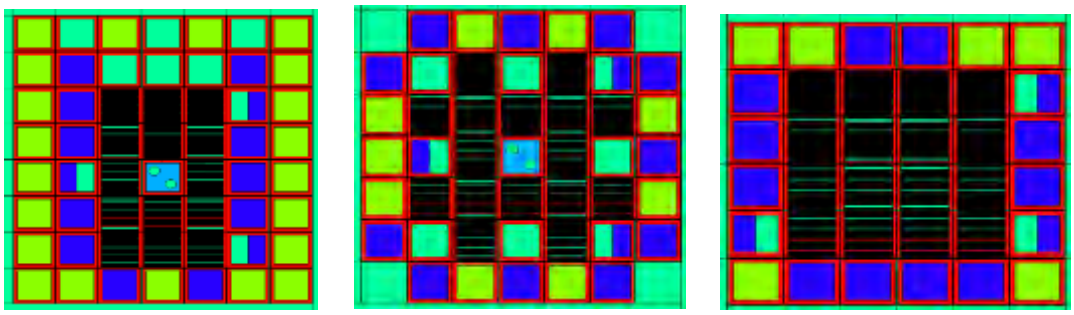

Fig 4. Configuration 10: 10FE+4CE - Configuration 12: 12FE+4CE - Configuration 12*: 12FE+4CE.

It's important to mention that all parameters in the Table 1 were calculated for clean and "ideal" cores, meaning that there was no impurities in the fuel, only the main components: U_3Si_2-Al and Al (cladding). Depending on the core, impurity levels may change considerably the multiplication factor (K_{eff}) and the neutron flux profile.

	All control rods withdrawn				All control rods Within				
		S. Dev.				S. Dev.			
Core	K_{eff}	MCNP	pcm	ρ_{ex}	Keff	MCNP	pcm	ρ_{SM}	$\Delta\rho$
5	1.00312	0.00030	29.81	311.03	0.79186	0.00031	49.44	-26284.95	-25973.92
6	1.01671	0.00033	31.92	1643.54	0.79282	0.00031	49.32	-26132.04	-24488.50
7	1.03063	0.00032	30.13	2971.97	0.88447	0.00029	37.07	-13062.06	-10090.09
8	1.06388	0.00031	27.39	6004.44	0.84794	0.00031	43.12	-17932.87	-11928.44
8*	1.08691	0.00031	26.24	7996.06	0.84976	0.00029	40.16	-17680.29	-9684.22
9	1.09327	0.00034	28.45	8531.29	0.89129	0.00030	37.76	-12196.93	-3665.64
10	1.09849	0.00029	24.03	8965.94	0.88789	0.00031	39.32	-12626.56	-3660.62
12	1.11973	0.00034	27.12	10692.76	0.91097	0.00032	38.56	-9773.10	919.66
12*	1.15367	0.00030	22.54	13320.10	0.95053	0.00031	34.31	-5204.46	8115.64

Table 1: Clean Core Multiplication Factor (k_{eff}), Excess of Reactivity (ρ_{ex}), Shutdown Margin (ρ_{SM}) and Total Control Element Worth ($\Delta\rho=\rho_{ex}+\rho_{SM}$).

Fig 5 shows the multiplication factor variation with the core configuration and Fig 6, the core-average power density per arrangement.

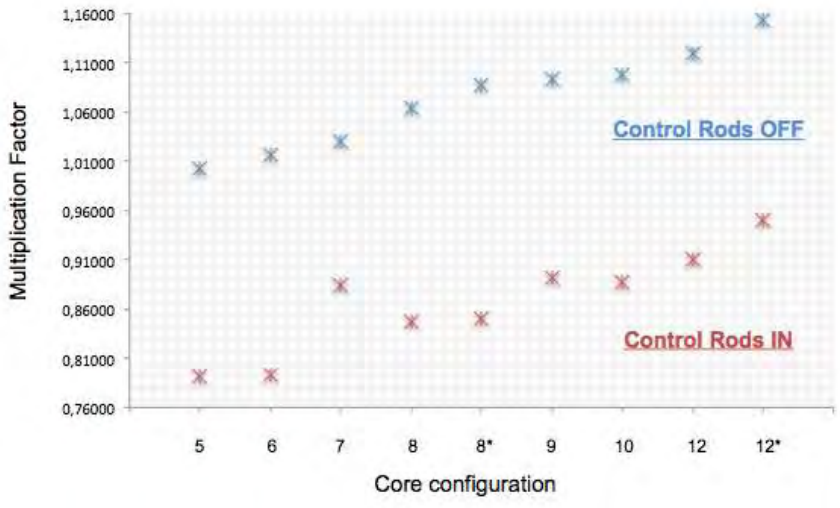

Fig 5. Multiplication Factor Variation vs. Core Configuration

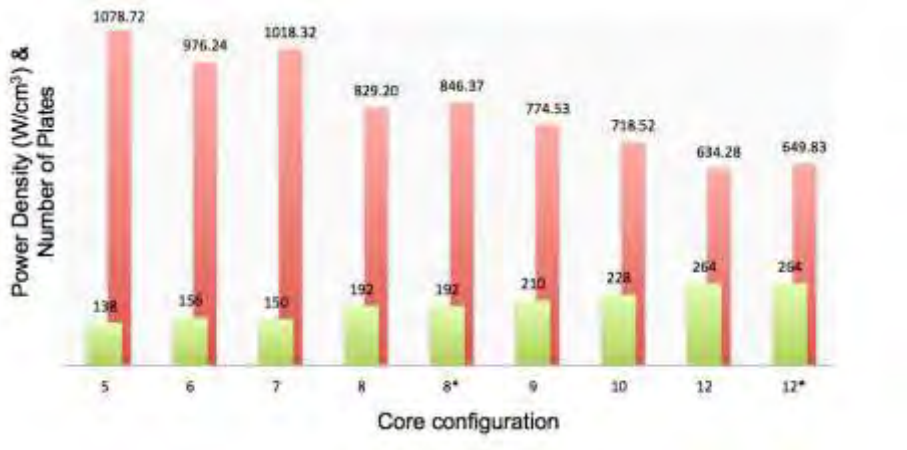

Fig 6. Core-Average Power Density per Configuration

For each new configuration, the hottest plate, the one in which the higher average power density appears, was found and the axial power density profile (in 21 nodes) was calculated in order to determine the temperature distribution and the TH margins. The hottest fuel plate average power density for each configuration is depicted in Table 2. Fig 7 shows the axial peaking factor (local power density/core-average power density) profile for each hottest fuel plate per arrangement.

Core	Average Power Density [W/cm^3]
5	1447.88
6	1438.41
7	1458.56
8	1281.14
8*	1508.53
9	1113.84
10	1179.19
12	1056.64
12*	1259.23

Table 2: Average Power Density in the Hottest Fuel plate per configuration.

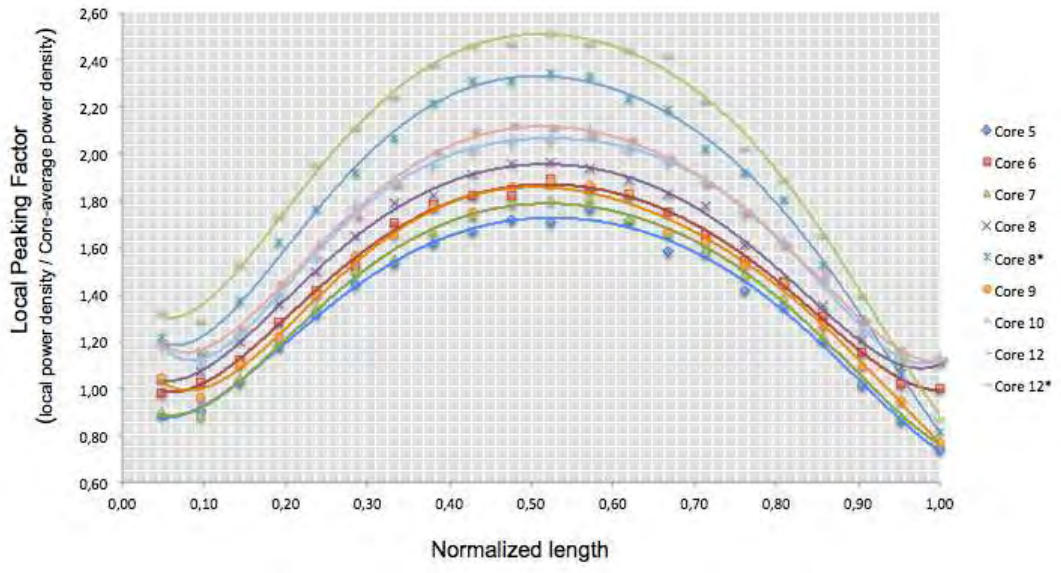

Fig 7. Local Peaking Factor vs. Hottest Fuel Plate Axial Normalized length

3.2 Thermal-Hydraulic Analysis

In this section, it's presented the temperature profile in the hottest fuel plate for each new configuration, as well as the verification of the Thermal-Hydraulic (TH) margins, both considering a stead-state behaviour. The study was performed using the *Engineering Equation Solver* program along with the *nodal method*. The distribution of nodes was created as follows: 1 node in the fuel (central position); 1 node at the interface between the fuel and the cladding|; 1 node at the interface between the cladding and the coolant; 1 node in the coolant region (bulk). In principle, the number of axial nodes is variable, but in this study it was fixed in 21 nodes. In the next analysis, it will be considered only the node distribution in the hottest fuel plate, in order to check the maximum temperature as a function of the coolant flow and to verify the TH margins, once all other plates will have lower temperatures and then, automatically, will satisfy these criteria. Remember that all control rods are withdrawn in this study. The main difference when the control rods are partly within is that the neutron flux will be flattened into the bottom also decreasing the multiplication factor. However, once the searching for the worst-case scenario is been the main target, all control rods should be withdrawn. Table 3 shows the minimum and maximum values for the MDNBR (minimum ratio of the critical to actual heat flux found in the core) and FIR (ratio of the heat flux that induces flux instability and the local heat flux) per core configuration per specified coolant flow (the ones in which the temperature at the cladding/coolant interface is always under 90 degrees Celsius, avoiding the Al Corrosion) in the fuel (FE) or control (CE) element under analysis. The configurations 12 and 12* were not taken into account for the temperature profile calculation, once both present no good results in the neutronic analysis (Check Table 1).

	Maximum MDNBR		Minimum MDNBR			
	Labuntsov	Mirshak	Labuntsov	Mirshak	FIR	Coolant Flow (m^3/h)
Core 5	15	15	5	5	9	60 (FE)
Core 6	16	16	5	5	9	55 (FE)
Core 7	12	13	4	4	5	35 (CE)
Core 8	17	18	6	6	9	45 (FE)
Core 8*	13	15	4	5	6	30 (CE)
Core 9	17	18	6	6	8	40 (FE)
Core 10	13	14	6	6	8	35 (FE)
Core 12	13	15	6	7	7	30 (FE)
Core 12*	11	14	5	6	5	20 (CE)

Table 3: Maximum and Minimum values for the MDNBR, using both Labuntsov and Mirshak [7] approach, and FIR.

The temperature vs. coolant flow, and the axial temperature profile for the cores 5, 6, 7, 8, 8*, 9 and 10 are depicted below from the Fig. 8 to 14. The temperatures for each core configuration were calculated using the coolant flow value presented in Table 3. Table 4 shows the fuel element geometry information along with the operating pressure and initial coolant temperature.

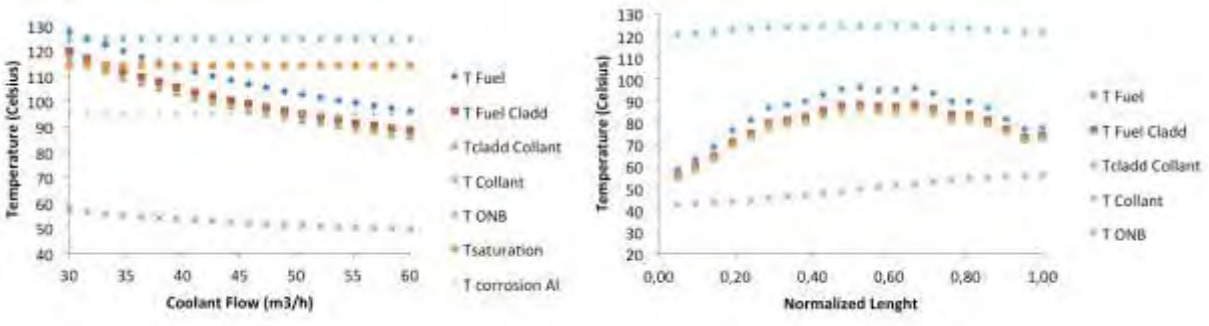

Fig 8. Core 5 - Temperature Distributions

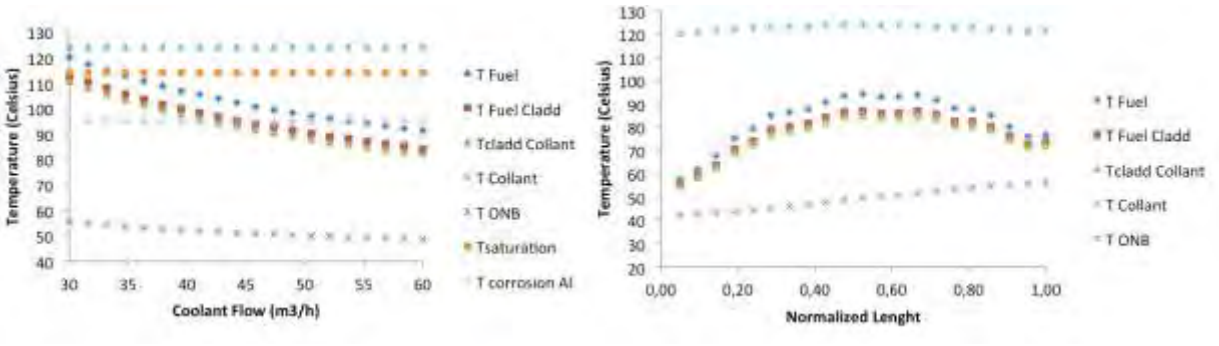

Fig 9. Core 6 - Temperature Distributions

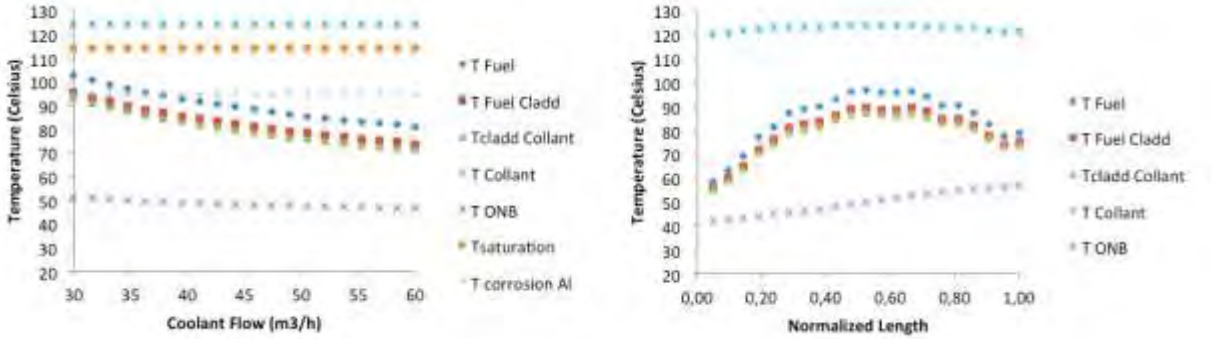

Fig 10. Core 7 - Temperature Distributions

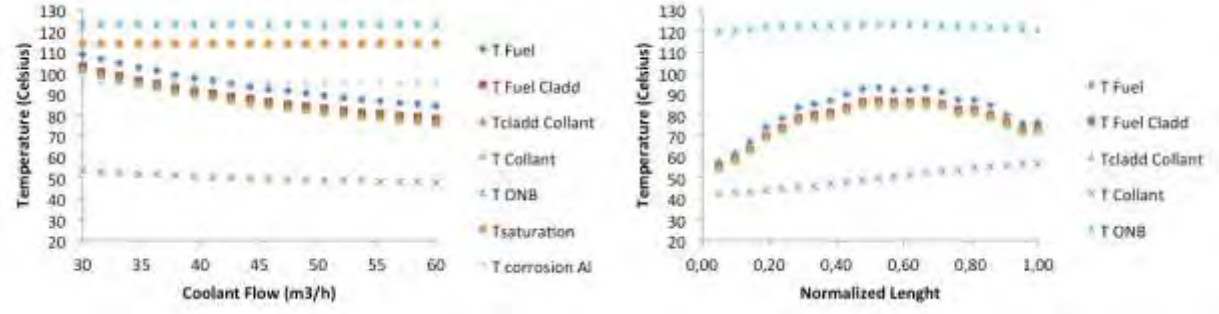

Fig 11. Core 8 - Temperature Distributions

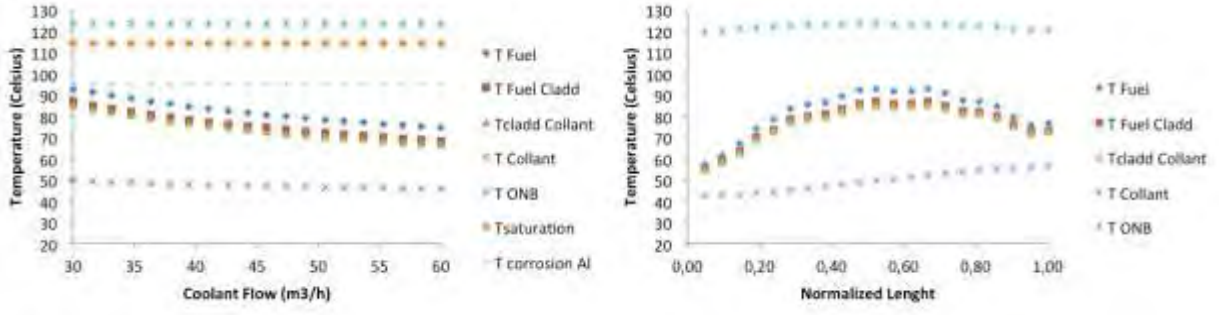

Fig 12. Core 8* - Temperature Distributions

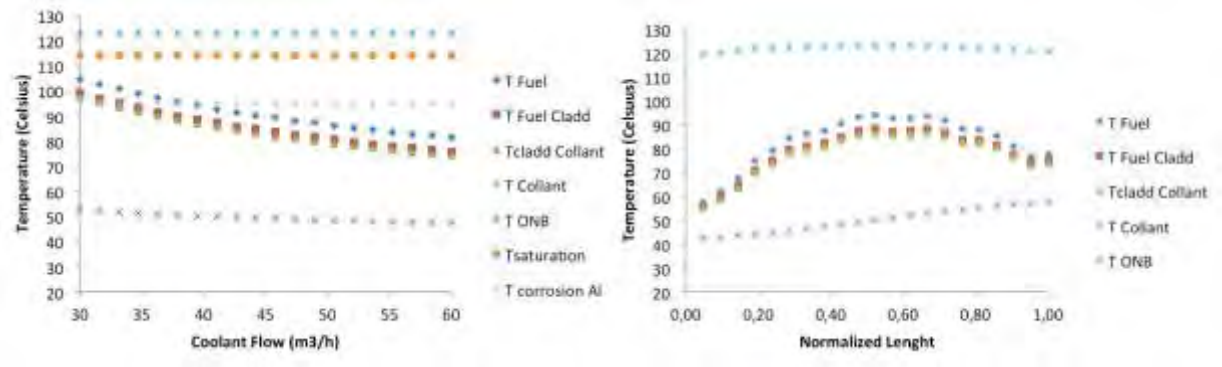

Fig 13. Core 9 - Temperature Distributions

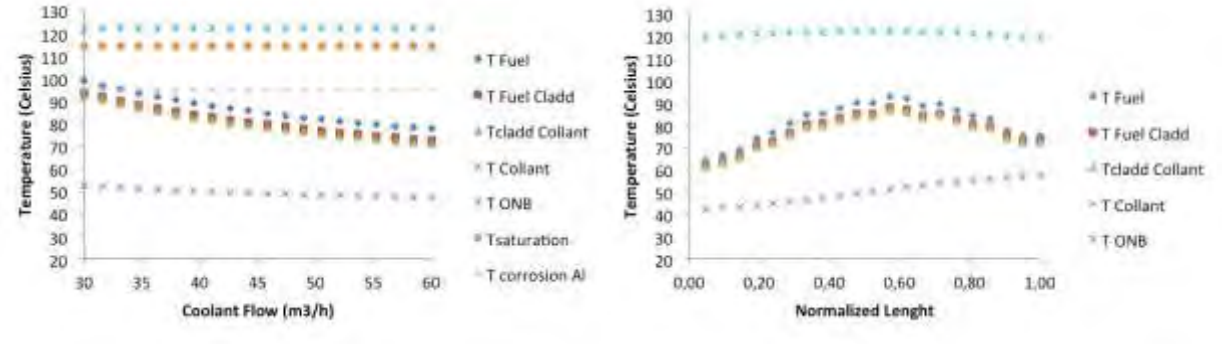

Fig 14. Core 10 - Temperature Distributions

Cooling channel width	67.1 mm
Fuel plate active width	62.0 mm
Channel thickness	2.89 mm
Fuel plate thickness	1.52 mm
Fuel thickness	0.80 mm
Cladding thickness	0.38 mm
Plate total height	625 mm
Plate active height	600 mm
Coolant	light water (42°C)
Operating pressure	1.6 bar

Table 4: IEA-R1 Fuel Element Geometry, Operating Pressure and Initial Coolant Temperature

4. CONCLUSIONS

Among nine different new core configurations for the IEA-R1 research reactor presented in this study, seven of them are good enough to replace the current core of this Brazilian research reactor. The neutronic calculation shows that the core 12 and 12* are week from the control rods safety point of view (Table 1), but they could be useful if the number of control rods increase. The thermal-hydraulic analysis ensures that no TH margins are exceeded and also depicts that, from a steady-state analysis point of view, no high temperatures are reached and calibrating the main pump one can control the critical temperature that induces corrosion in the aluminium (~95 degrees Celsius). The next step of this study will be the safety analysis of each new core, along with the *burnup* calculation and at the very end, choose the best configuration depending on the desired characteristics.

5. ACKNOWLEGMENT

The authors acknowledge support from the Sao Paulo Research Foundation (FAPESP), an independent public foundation with the mission to foster research and the scientific and technological development of the State of Sao Paulo. Grant #011/17090-7, Sao Paulo Research Foundation (FAPESP). The conclusions and ideas presented in this study reflect the authors' opinions only and do not necessarily reflect the FAPESP's point of view.

6. REFERENCES

1- "MCNP – A General Monte Carlo N-Particle Transport Code, Version 5", Los Alamos National Laboratory, April 24 2003 (Revised 10/3/05);
2- "EES - Engineering Equation Solver for Microsoft Windows Operating Systems", F-Chart Software, 1992-2014 by S.A. Klein;
3- "IEA-R1 Safety Analysis Report, Version 2011", Nuclear Engineering Center, IPEN/CNEN-SP;
4- John R. Lamarsh-Anthony John Baratta "Introduction to nuclear engineering", Upper Saddle River, NJ-Prentice Hall-2001-3rd Ed;
5- NJOY 2012 User Manual LA-UR-12-27079;
6- Y. komori, M.Kaminaga et al, "Safety Criterion for Burnout of the Plate-Type Fuel in Pressurized Conditions", JAERI-M 92-028;

EFFECT OF THERMAL GRADIENT ON IN REACTOR OXIDATION OF MTR FUEL PLATES

D. Valdez Tordoya and R. Haddad
Corrosion Department, CNEA-CAC
Av. Gral. Paz 1499, B1650KNA San Martín (Bs. As.) – Argentina

ABSTRACT

Aluminium oxide is a poor thermal conductor. It interferes with the cooling process as it grows during Research Reactors operation. This factor has to be taken into account in the design process of high flux reactors, because oxidation excess may affect fuel performance by causing the plate's surface to spall, generating blisters, dimensional changes and even intergranular perforation. The oxidation mechanism is not well understood, being strongly influenced by water chemistry, mainly its pH, water flow, heat flux and thermal gradient, among other variables. In oxidation tests in static autoclaves at water reactor temperature the oxide layers produced are much thinner than those generated during reactor operation. It is possible that the process controlling temperature be the aluminium plate temperature instead that of the bulk water. Or, a temperature gradient -associated with heat transfer- is needed to accelerate the reaction.

This paper describes the efforts carried out to study the effect of heat transfer on oxidation, through experiments performed in similar conditions, some in isothermal systems, using an autoclave, and some others in a device capable to produce thermal transfer through the plates. In both approaches the hydrodynamic conditions and other parameters have been set up in such a way that the results can be compared. For instance, the exposure temperature in the autoclave is not the reactor bulk water temperature, but the value measured with a thermocouple inserted inside the aluminium plate during the heat transfer test, a much more demanding condition. The water flow in the fuel channel was simulated in the autoclave by means of a rotating sample, where the tangential velocity is similar to the one of the coolant. If the oxidation would progress similarly in both conditions, then it could be possible to develop a full oxide growth correlation with simple autoclave tests, a much more accessible tool than the one needed to simulate a reactor fuel channel with heat transfer. Tests at different times were carried out, ranging from one week to two months, in both systems. In all cases, the oxide obtained in thermal transfer conditions is thicker than the one produced in autoclave, up to an order of magnitude for longer times, indicating a strong influence of the thermal gradient on oxidation mechanism. These results are discussed considering the migration of reacting species under temperature gradients, the effect of hydrodynamics in the formation of the diffusion layer and other factors.

1. Introduction

Efforts have been carried out in the past to evaluate the degree of oxidation of MTR aluminium fuel plates during operation of Research or Production Reactors [1], [2], [3], [4]. Several correlations have been derived, which are valid in the same parameters range of the experiments used to develop them. One of the main variables to adjust in the fitting equations is the pH of water. In open pool reactors water pH is not controlled and can normally vary between 5.5 and 7, depending on the carbonation rate, temperature and other factors [5]. Figure 1 shows how the oxide thickness may grow in time according to the various estimations, including -for one of them- the calculations for pH 5 and 7. The difference reaches about an order of magnitude after about 2 months of irradiation. Particularly, the pH 7 curve reaches the safety limit (estimated in around 30 to 50 μm) long before this period is completed. When oxide films grow above this value, deterioration of the fuel plates may be expected, in the form of oxide peeling, blistering, deformation and intergranular corrosion.

It follows that a reliable prediction base is needed to evaluate fuel performance in specific reactors, such as the 30 MW RA10 or RMB. It is also a need to investigate the oxidation

mechanism, in order to understand the influence of the many parameters involved, such as pH, water flow, heat flux and thermal gradient, among other variables.

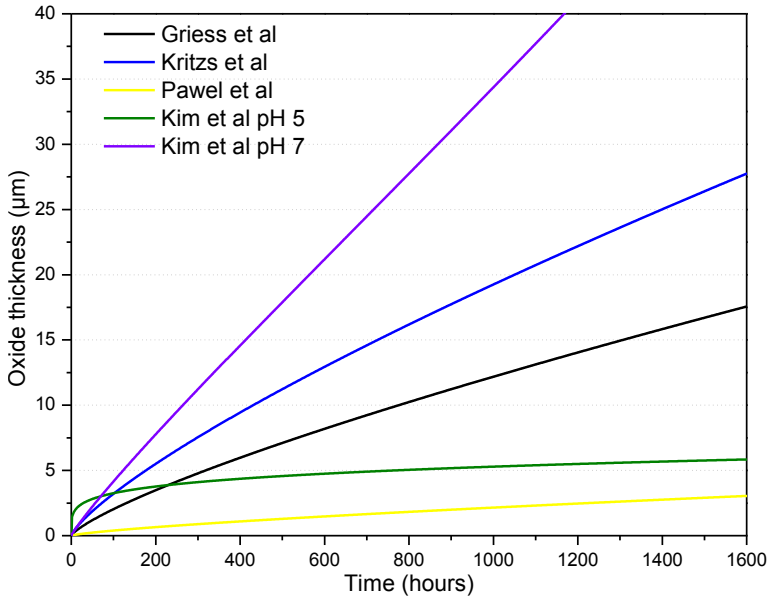

Figure 1: Oxide thickness predicted by various models for the same heat transfer conditions: heat flux 2 MW/cm^2, plate temperature 104 ºC and coolant speed 8 m/sec.

Being oxidation a diffusion controlled process, it is expected that the temperature should play an important role in the kinetics. It is not clear, though, which would be the adequate point to measure it, because during heat transfer there is a temperature profile established through the various interfaces, as depicted in Figure 2.

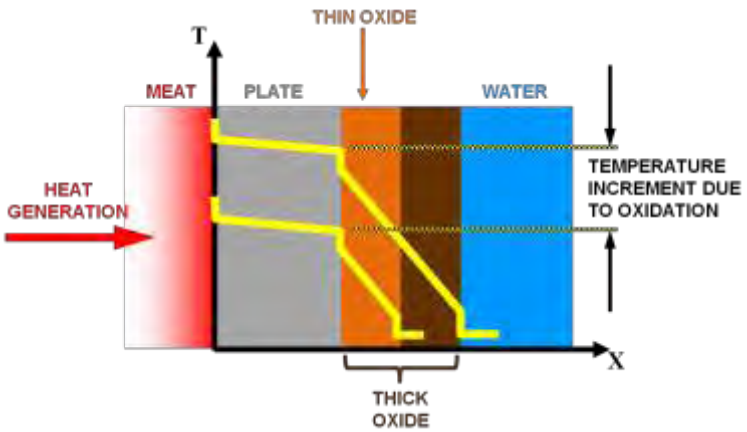

Figure 2: Temperature profile across the thickness of the fuel plate.

Moreover, attempts to simulate the in reactor oxidation through exposition of aluminium to water in static autoclaves yielded much lower film thicknesses than those produced during reactor operation [6]; these discrepancies may not be ascribed only to the irradiation [7], but may make evident the effect of the temperature gradient itself [8]. This point is studied in this work by comparing the oxidation rate in experiments carried out both with and without heat transfer.

2. Experimental approach

In order to study the effect of temperature gradients on aluminium oxidation, two types of experiments were carried out. In one of them, a device simulating a fuel channel was used [9], in which heat is transferred at a controlled rate from a hot source to aluminium plates refrigerated by circulating water. This is achieved by a double loop, with a hot fluid circulating

in the primary circuit and reactor-like water through the secondary. The heat is exchanged through a 10 x 4 cm window at the centre of two parallel aluminium plates in the channel, as depicted in Figure 3.

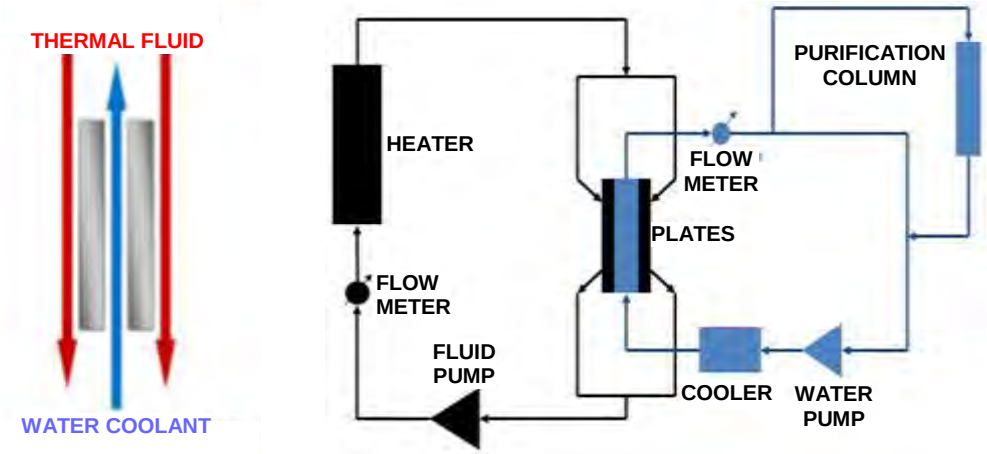

Figure 3: Schematic diagram of the simulated fuel channel (LEFT) and the heat transfer double circuit (RIGHT).

In this installation several parameters can be monitored and/or controlled; among them, hot side temperature, water inlet and outlet temperatures, plate temperature (in the bulk of the aluminium plate at about 0.5 mm from the aluminium-oxide interface) and coolant speed. More information on this installation can be found in [9].

The experimental conditions in all the tests performed in this installation were as follows:

- Heat flux density: 3 MW/m^2
- Coolant velocity: 6 m/s
- Coolant mass flow: 2 m^3/h
- Refrigerant inlet temperature to the channel: 50 °C
- Water temperature difference between inlet and outlet: 4 °C
- Coolant conductivity: < 1μS/cm
- Thermal fluid flow: 24.5 m3/h
- Thermal fluid temperature: 200 ºC
- Initial plate temperature: 100 ºC

All these parameters remained constant in time, with the exception of plate temperature, which increases as the oxide grows, due to its thermal insulating capability.

The other experimental method consisted in exposing a cylindrical aluminium rotating sheet to hot water inside an autoclave (Figures 4 and 5); in this case there is no heat transfer through the metal. To perform the comparison, the initial temperature in this case was set to the same plate temperature measured in the simulated fuel channel, updating its value on a daily basis as the fuel plate heats up; the speed of rotation was established in 1420 rpm for a 3 cm radius sample, so to get a tangential velocity of 4.5 m/sec, as close as possible to the speed of water in contact with the aluminium plate in the heat transfer test. Oxidation reaction is at least favoured in the autoclave test with respect to the other, because the maximum process temperature is taken as the controlling one and the water is significantly hotter than the coolant channel temperature (100 ºC as compared with 50 ºC in the channel).

If the autoclave test would yield values similar to those of the heat transfer experiment, this would indicate that the controlling temperature is that of the plate. In this case, this approach would make for a much simpler experimental arrangement in order to obtain data values in all reactor operating conditions.

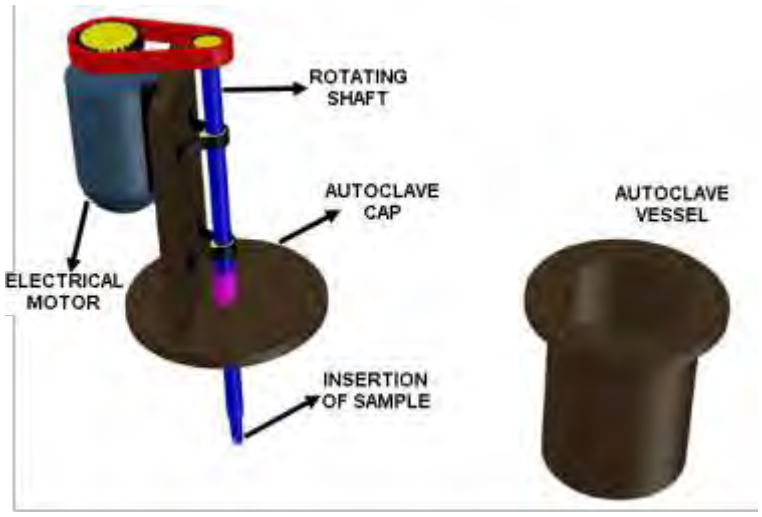

Figure 4: Drawing depicting the rotating autoclave system.

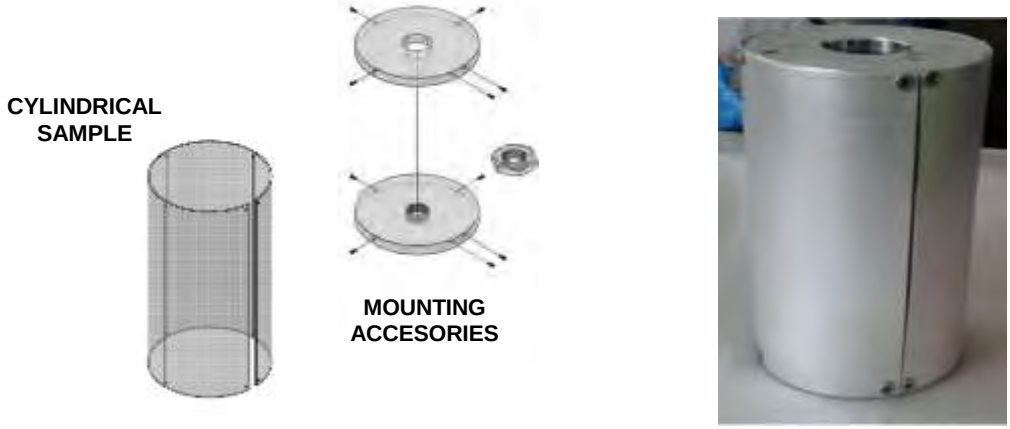

Figure 5: Mounting scheme of rotating sample (LEFT) and assembled specimen (RIGHT).

Both the plates and the cylinders were manufactured using aluminium alloy AA 6061 with the same thermomechanical and surface finishing condition used to make fuel plates. The final treatment includes a pickling with sodium hydroxide at 70°C, subsequent neutralization and rinsing. After tests completion, oxide layer thicknesses were measured by means of Eddy Current technique, using a Fisher DualScope MP40E-S equipment.

3. Results

Three tests were carried out in the two systems described, lasting 96, 600 and 1200 hours.

3.1. Heat transfer tests

The plate temperature in the tests with transfer of heat increased continuously from the initial value, set to 100 ºC, as can be seen in Figure 6. This is an indication of the growing oxide. This behaviour is taken as a reference for the autoclave test.

Figure 7 shows the oxide profile in the three cases, together with the surface appearance of the aluminium plates after the runs. As it can be seen, the peak thickness inside the heat transfer window increases with exposure time: 3.5 to 4 µm for the 96 hours test, about 24 µm after 600 hours and 28 µm for 1200 hours.

3.2. Autoclave tests

Figure 8 shows the oxide profiles obtained in the three autoclave tests. The oxide thickness is almost the same in all of them. The difference observed for different exposure times barely exceeds the determination error, which is ±1 µm. The values obtained are 2, 4 and 3 µm for

96, 600 and 1200 exposure hours, respectively. In the 1200 hours test there was a water leak which was detected on disassembling the device at the end of the experiment. This situation may have altered the result; for this reason, this particular test shall be repeated in the future and a question mark is drawn on the graph.

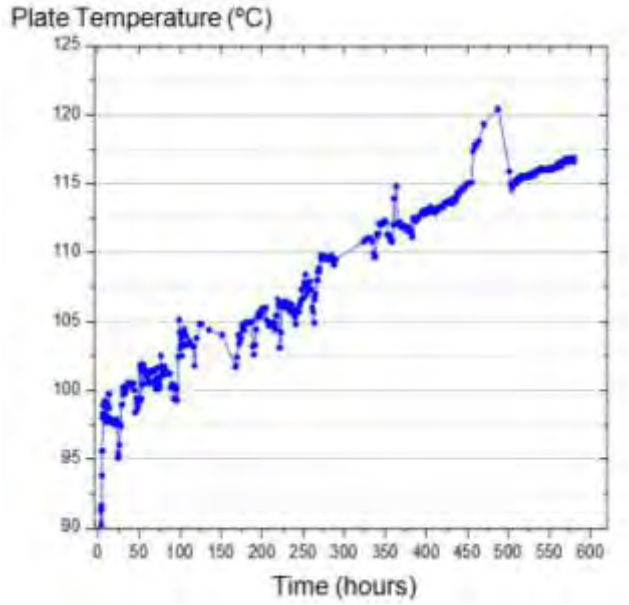

Figure 6: Evolution of Plate Temperature throughout the 600 hours test with heat transfer.

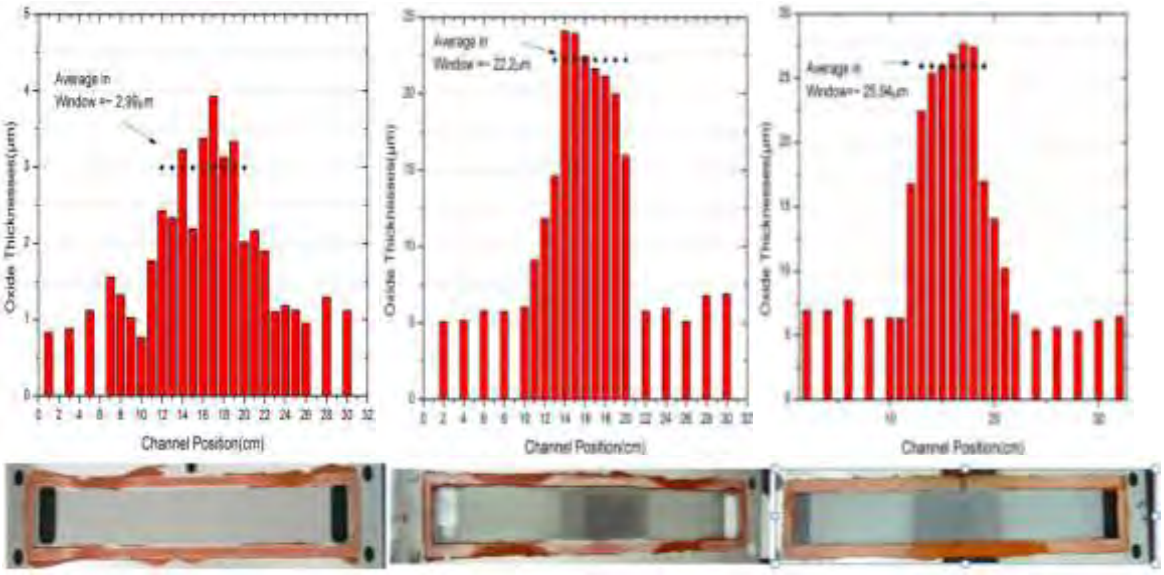

Figure 7: Histograms (above) of oxide profile and surface appearance (below).
From left to right: 96, 600 and 1200 hours. Heat transfer tests.

4. Discussion

All the results are plotted and compared in Figure 9. As can be clearly seen, in both approaches a parabolic-like evolution is obtained, i.e. the oxide grows at a decreasing rate. Films grown in autoclave are about one order of magnitude thinner than those generated in the double loop. This indicates that the temperature is not the main factor affecting oxidation, but it seems that the temperature gradient plays a more important role. Moreover, being the water in the autoclave at a higher temperature than in the simulated fuel channel, the diffusion layer is thinner, what should give place to an increment in the oxidation kinetics, which is a diffusion process. The fact that this is not the case adds more sustentation to the idea that the whole process is driven by the temperature gradient.

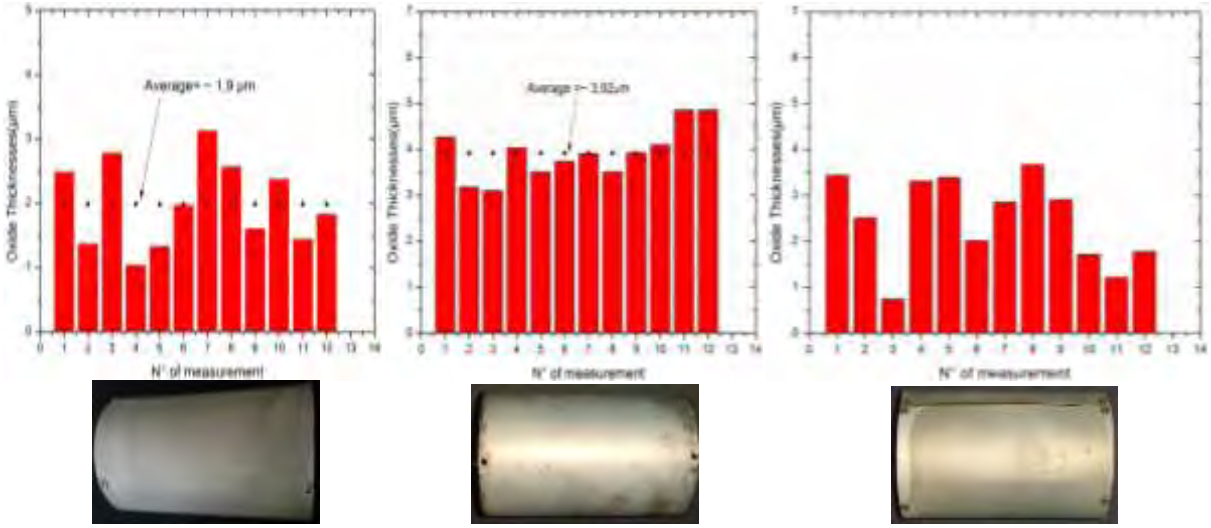

Figure 8: Histograms (above) of oxide profile and surface appearance (below). From left to right: 96, 600 and 1200 hours. Autoclave tests.

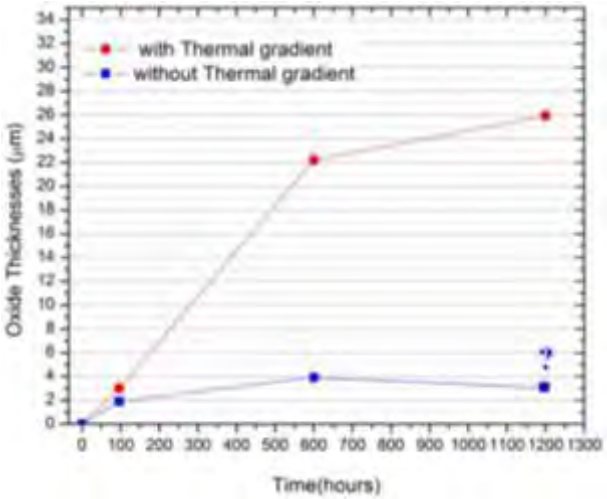

Figure 9: Comparison of oxide thickness obtained for different exposure times, with and without heat transfer.

5. Conclusions

In tests performed at the same plate temperature, aluminium alloy oxidise at a rate one order of magnitude higher in heat transfer conditions than without heat transfer.

The temperature gradient through the aluminium plate seems to be more relevant to oxidation than the bare temperature.

6. Acknowledgements

The authors wish to acknowledge to the crew members who maintained continuous attention to the experimental installations through the day and night during the full period of testing: R. Amoruso, R. Fort, C. Lafont, L. Lemos, J. Migliori, F. Rodríguez, G. Sapia and L. Vela. Special thanks to the late J. Falcone(†).

This work is strongly supported by the Project RA10 of CNEA.

7. Referencies

[1] J. C. Griess et al., "Effect of heat flux on the corrosion of Aluminium by water. Part IV", ORNL-3541 (1964).

[2] R. S. Ondrejcin, "Evaluation of Mark 22 cladding", Savannah River Laboratory DPST-83-324 (1983).
[3] S. J. Pawel et al., "Influence of coolant pH on corrosion of 6061 Aluminium under reactor heat transfer conditions", report ORNL/TM-13083 (1995).
[4] Yeon Soo Kim et al, “Prediction Model for Oxide Thickness on Aluminium Alloy Cladding During Irradiation.”, 25th Int. Meeting on RERTR, Chicago (Illinois), October 5-10 (2003).
[5] "Good Practices for Water Quality Management in Research Reactors and Spent Fuel Storage Facilities", IAEA Nuclear Energy Series, NP-T-5.2 (2011).
[6] Matthieu Wintergerst, "Étude de la corrosion uniforme d'un alliage d'aluminium utilisé comme gainage du combustible nucléaire du réacteur expérimental Jules Horowitz", Thesis presented at Université Paris-Sud 11, France, January 3rd, 2006 (in French).
[7] R.S. Lillard *, D.L. Pile 1, D.P. Butt, "The corrosion of materials in water irradiated by 800 MeV protons", Journal of Nuclear Materials 278 (2000) 277-289.
[8] D. Valdez Tordoya, "Oxidación de placas combustibles de aluminio de combustibles MTR en condiciones de transferencia térmica", CNEA internal report, June 2013 (in Spanish).
[9] A. Burkart, R. Haddad, C. Lafont and R. Amoruso, "Experimental Simulation of Al fuel plate oxidation",Transactions of RRFM 2009, ENS ed., pp. 105-109 (2009).

SAFARI-1 POOL LINER LEAKS

B.J. STEYNBERG
SAFARI-1 Research Reactor, Necsa, Pelindaba,
Pretoria, South Africa

ABSTRACT

SAFARI-1 is a 20 MW tank-in-pool light water cooled, light water moderated, and beryllium reflected research reactor which first reached criticality on 18 March 1965. The aluminium pool liner has developed a leak in the 1980s. These leaks were repaired in 1989 during a lengthy shutdown which allowed for the pool to be drained and for adequate decay of the core structures to access the problem areas. Following the repair, the leak was acceptable until it required further repairs in 2003. The high utilisation of the reactor no longer allowed a lengthy shutdown, and methods were develop to pinpoint the location of the leaks and to repair it during normal shutdowns without draining the pool. By forcing reverse flow of a dye through the leak paths, the positions of the leaks were determined. The leaks were then repaired by painting an epoxy resin onto the leaking areas. A monitoring system was put into place to monitor and trend the leak rates. It became necessary to repair the leaks approximately every three years, following the same methodology. The pool liner leak issue at SAFARI-1 therefore appears to have been brought completely under control and, while a small leak reappears every three years or so, the method of eliminating it is very well established and successful.

1 Introduction

SAFARI-1 is a 20 MW_{th} tank-in-pool Oakridge design type nuclear research reactor, owned and operated by the South African Nuclear Energy Corporation (Necsa) and it is located at Pelindaba, 30 km west of Pretoria. SAFARI-1 is an acronym for **S**outh **A**frica **F**undamental **A**tomic **R**esearch **I**nstallation Number **1** and is South Africa's only nuclear research reactor.

SAFARI-1 went critical the first time at 18:33 on 18th March 1965, and celebrated its 50th anniversary in 2015. SAFARI-1 provides products and services both locally and internationally to various industrial and institutional sectors, proving that nuclear technology does indeed offer many beneficial applications.

In 1998 SAFARI-1 was awarded the prestigious ISO 9001 certificate for compliance to international quality standards. At the time it was the second nuclear reactor in the world to receive this award. The ISO 9001 accreditation recognizes the ability of SAFARI-1 to operate within the international standards of design and production in providing quality products and services to industry and community.

SAFARI-1 has subsequently also received the ISO 14001 Environmental Management (2003) and OHSAS 18001 Occupational Health and Safety Management System (2011) certification. SAFARI-1 utilises an overall Integrated Management System which not only encompasses environmental controls but also includes operational safety, product quality radiological and conventional safety and security systems which ensure that a good safety culture is established.

The operating and utilisation of SAFARI-1 over the last 50 years is well represented by its power history graph (refer to Fig. 1).

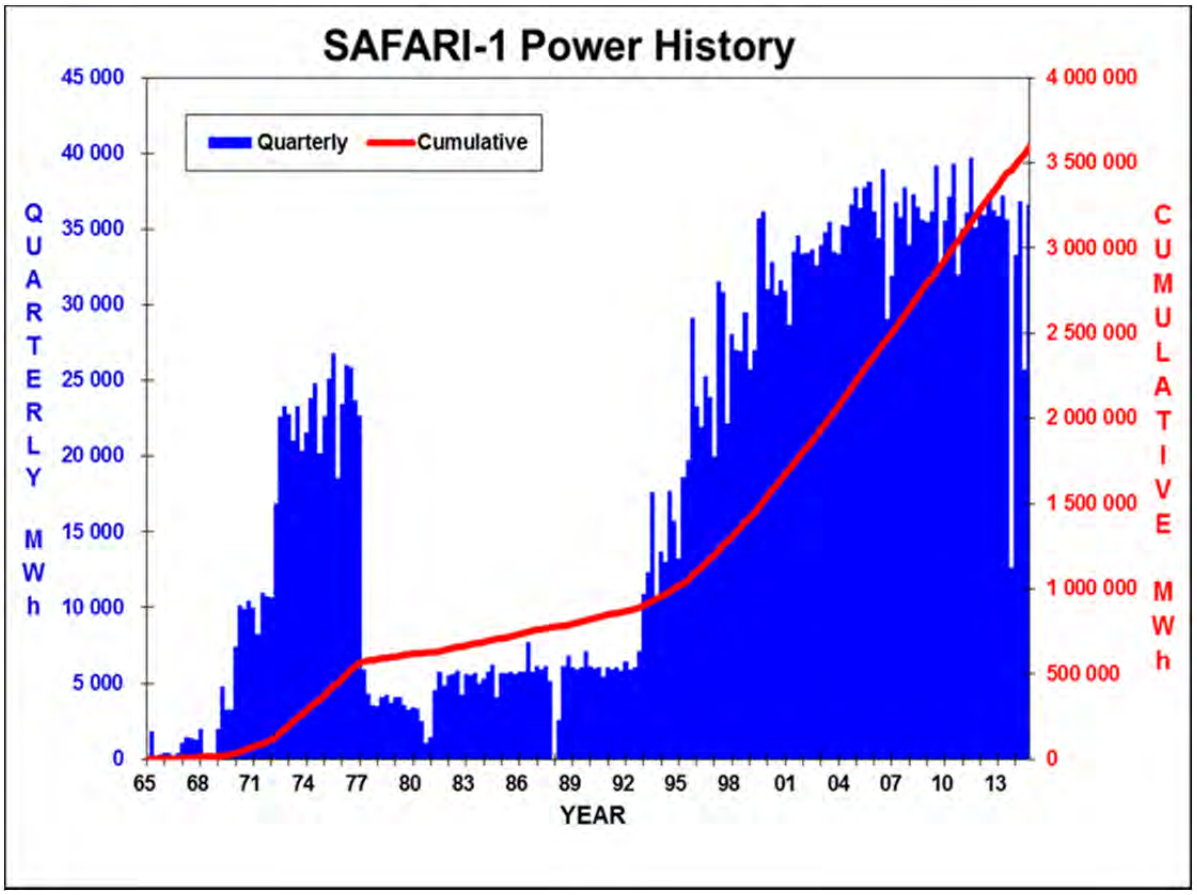

Fig. 1 – SAFARI-1 Power History

2 Initial repairs – 1988

During the early 1980's a leak in the aluminium reactor pool liner was detected via the dedicated drain pipe (refer to Fig. 2). In 1988 SAFARI-1 was shut down for approximately six months to affect the repairs. Water in the reactor pool was drained and the necessary radiological shielding was installed in place prior to the refurbishment.

Aluminium samples at various positions in the pool liner were removed, i.e. disks of approximately 50 mm were cut out of the pool liner for metallurgical analysis and evaluation. Results showed that no abnormalities with respect to corrosion were present in the aluminium test pieces. These areas were patched and repaired at a later date.

Visual inspection of the pool aluminium liner revealed cracks at the number 4 and 6 beam ports and the east and west, top and bottom through-tube penetrations. Holes were drilled in selected crack ends to limit their propagation. All cracks were eventually TIG welded closed. Furthermore, aluminium patch plates in the form of a split collar were machined to fit around the beam port and through-tube penetrations. These were welded in position to strengthen the penetrations area. Dye penetrant tests were done on all pool liner welds to check their integrity. Finally the reactor systems were restored to normal operating conditions in preparation of start-up.

Approximately two months following the repairs, a leak in the reactor pool was again detected via the leak pipe. A follow up programme was subsequently initiated to find the new leak in the pool system.

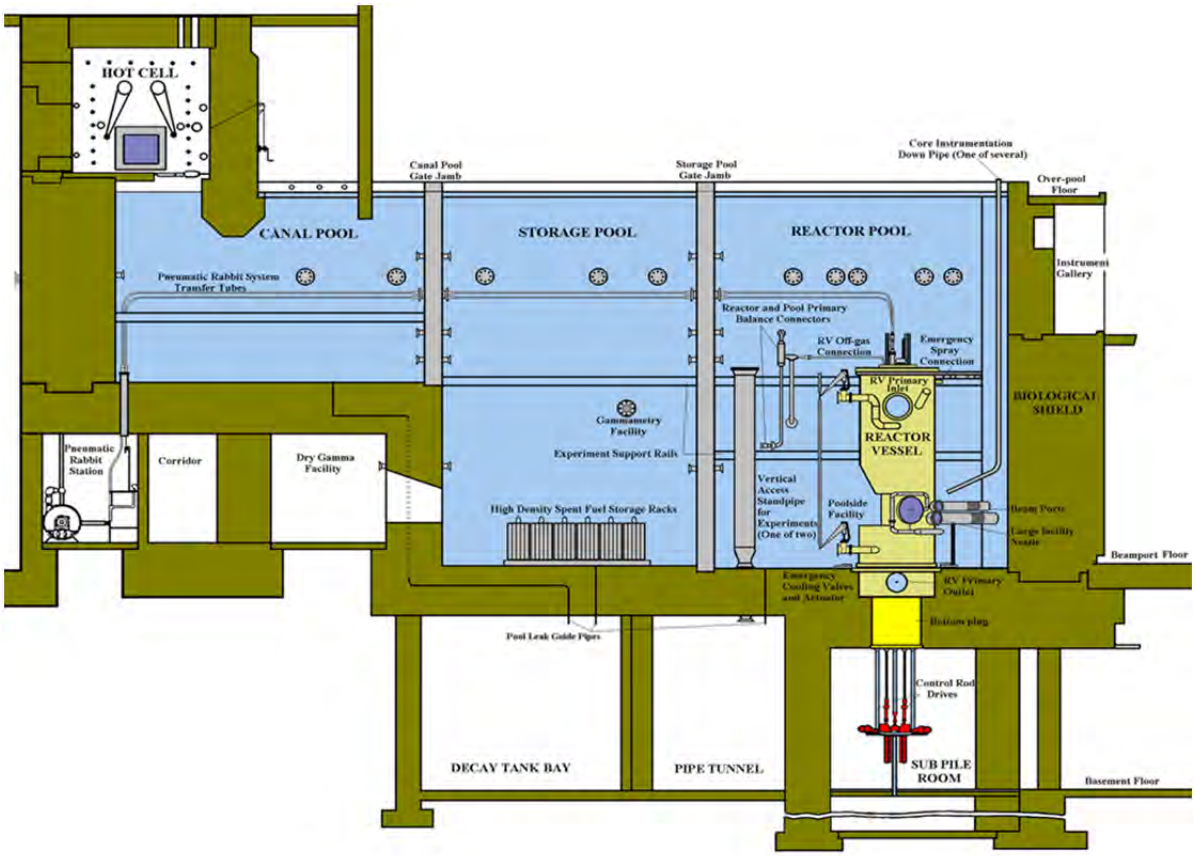

Fig. 2 – Cross Section through SAFARI-1 Pool Structure

Over the years since these first repairs continued attention was given to the pool leaks and numerous repair operations were carried out and recorded in internal reports [1 & 2]. All the leaks detected over time were in the heat-affected zones next to welds.

3 Follow-up actions after the 1988 repairs

A number of steps were taken over an extended period to trace the source of the water leak in the pool liner, include the following:

- ***Ultrasonic evaluation of pool liner****:* A competent authority was contracted to evaluate the pool liner floor thickness, using ultrasonic measurements. Comparisons were made to determine if thinning caused by corrosion had taken place during the course of time (1995 and 1998).
- ***Fluorescein dye tests:*** This entailed introducing a fluorescein dye into the reactor pool via the back flow through the leak drain pipes. With the use of ultraviolet electric lights, the position of numerous leaks in the liner could be identified (1995).
- ***Visual inspection:*** The pool liner plates and component penetration welds were visually inspected using an underwater camera and a periscope (1995 to 2003).
- ***Radioisotope spiking:*** The pool water was spiked with radioisotopes to determine the location of the leaks not identified by the fluorescein dye tests (2000).
- ***Evaluation of the biological shielding***: Another competent authority was contracted to determine the condition of the steel reinforcing and the concrete structure of the biological shield in general (2000 to 2002).

3.1 Ultrasonic evaluation of pool liner (1995 and 1998)

In October 1995, a competent authority was contracted to evaluate the reactor pool floor liner thickness and to determine if thinning had taken place due to corrosion of the aluminium. From the ultrasonic test results it was concluded that there was no change in the thickness compared to the original dimension as constructed. The examination of the liner was repeated in December 1998. Again the final conclusion was that there was no evidence of change in the liner thickness.

3.2 Fluorescein dye tests (1995)

A fluorescein dye test on the reactor pool system was undertaken. This entailed the mixing of a solution of fluorescein dye with water in a drum container fitted with a valve at its lower end. The drum container was then connected to the reactor pool leak drain pipe via an extended polyethylene tube. By raising the drum plus the contents via the overhead crane and opening the valve, the fluorescein dye flowed back via the pool leak drain pipe and through the cracks or defects into the reactor pool. With the aid of an ultraviolet lighting system within the pool, defect areas could now be identified. Observations made during the test revealed evidence of leaks around both primary coolant inlet pipes to the reactor vessel on the pool liner penetrations. Furthermore, the leak on the stand pipe mounting flanges was confirmed prior to the fitting of the dedicated mechanical seals.

A caution, with hindsight, is not to be too hasty to obtain a result from this test (by raising the drum higher to increase the hydrostatic head), as too strong a reverse flow at a leak site may flush accumulated deposits out of the cracks in question and result in a large increase in the leak flow rate after the test equipment has been removed. A further caution is to be aware that applying even a small excessive differential pressure the wrong way across the pool liner can result in a significant force on the liner that could separate it from the concrete walls of the pool and damage the liner permanently. Hence it is recommended to have a hydrostatic head of not more than about 1 meter, and a lot of patience while waiting for the result.

3.3 Visual inspections

3.3.1 Welds on Stand Pipes (1995 and 2003)

Two stand pipes are installed in each comer on the north side of the reactor pool to provide access between the reactor and the pipe tunnel for loop type of irradiation rigs. Visual inspection has confirmed that weld cracking has occurred in specific areas between the stand pipe mounting flange and the pool floor liner. The fluorescein dye test also confirmed that this was indeed a fact and that corrective actions should be implemented. A mechanical flange designed to compress a neoprene seal in position around the stand pipe defective weld area via jacking bolts, was designed and manufactured. Both stand pipes were fitted with this type of mechanical seal. Flow measurements indicated that limited success was achieved in stemming the leak rate. The fittings were a permanent installation as the welds could not be repaired unless the reactor pool is completely drained. At time of installation it was, however, envisaged that, due to the expected deterioration caused by gamma radiation, the neoprene seal would have to be renewed from time to time.

When the pool leak rates did not reduce as expected it was assumed that the mechanical seals fitted to the two standpipes had failed, and that the neoprene rubber which physically seals the cracks had deteriorated due to gamma radiation damage. In an effort to reduce the water leak, it was thus decided to renew the neoprene rubber on both the east and west standpipe mechanical seals. The west standpipe mechanical seal was replaced in June 2003 during a reactor scheduled maintenance shutdown period. After removal, inspection of the mechanical seal showed a clear imprint of the weld crack profile formed by a deposit of aluminium oxide on the neoprene rubber. A major crack in the weld was identified to be on the west side of the

standpipe. Evidence of smaller cracks in the liner is also to be seen on the neoprene rubber around the east side of the standpipe. In general, the neoprene seal was found to be in good condition and there was no evidence that hardening had taken place over the period of time due to the gamma radiation. Following the replacement of the mechanical seal on the west standpipe, no significant change was recorded in the pool leak rate.

The mechanical seal fitted to the east standpipe was replaced in July 2003, again during a scheduled reactor maintenance shutdown period. Again, the neoprene seal was found to be in good condition and there was no evidence that hardening had taken place due to the gamma radiation. The neoprene was however renewed. No significant improvement in the pool leak rate was recorded following the replacement of the mechanical seal on the east standpipe.

A decision was then taken by to remove the standpipe top flanges. It was reasoned that the buoyancy in the standpipe when filled with air induced tension in the weld arrangement at the base causing the cracks to open. In July 2003, the top flanges were duly removed and replaced by aluminium expanded metal gratings. The fitting of the aluminium gratings prevent foreign objects from inadvertently falling down into the standpipes while at the same time allow a water flow to take place under convection conditions. Again, no change in the water leak rate was measured following these modifications.

Fluorescein dye tests indicated a large crack in the weld area around the base of the east standpipe. So, obviously, the mechanical seal was not fully effective in this instance. An alternative sealing mechanism was developed, following the success with the use of the epoxy resin sealant elsewhere in the pool (see section 3.3.4 below). For the repairs, the reactor pool level was lowered to the reactor vessel top and the mechanical seal removed from the base of the standpipes. Epoxy was liberally applied under water around the defective weld area and allowed to flow into the crack in the pool liner, without reinstalling the mechanical seal following these repairs. The water leak rate dropped dramatically following the repairs in this region.

3.3.2 Welds in Pool Gate Jamb (1996)

To facilitate the visual inspection of the pool gate jamb welds, both the top and bottom gates between the reactor and storage pools were removed and placed in storage. With the aid of an underwater camera and a periscope, the gate jamb was inspected. Observations made showed that certain welds on the floor section of the gate jamb appeared decidedly suspect. In an attempt to seal the suspect weld area, aluminium spacer pieces were placed under the lower gate. The seal that forms an integral part of the gate was thus raised to opposite the suspect weld area, effectively sealing the water leak path in the gate jamb. Indications on the flow rate monitoring system showed that the leak rate have been reduced and is acceptably small. This modification is considered as a temporary solution until a more permanent solution is needed and can be implemented.

3.3.3 Pool Liner (1998)

With the aid of a dedicated underwater camera and a periscope, the pool liner welds were visually inspected for physical defects paying particular attention to the liner penetrations and the heat affected welds around these penetrations. Generally the aluminium plate welds were observed to be in good condition. It must however be noted that due to the construction, not all the welds are accessible for inspection.

3.3.4 Primary Coolant Water Inlet Penetrations (1998 and 2003)

The leaks identified with the fluorescein dye test in the primary coolant water inlet penetrations were confirmed with visual inspections. An initial attempt was made to seal the weld cracks around the reactor inlet coolant pipe penetrations through the liner by applying a conventional

silicone sealant to the area. These repairs were not too successful as the silicone sealant deteriorated within a short period of time due to gamma radiation damage emanating from the reactor core and from the spent fuel in the storage pool.

Since the operational commitments of the reactor in 2003 no longer permitted a lengthy shut down, means to identify and repair the leaks during normal shutdowns were developed. An European company specialising in the development and marketing of ceramic epoxy resins for sealing applications was approached for advice on a sealant that could be utilised for the pool repairs as required. Subsequently, an epoxy was developed together with them which met the specification necessary for the SAFARI-1, that is, it must be able to be applied and cure underwater, have acceptable bonding properties in demineralised water, and to be resistant to radiation damage. The epoxy was duly tested under radiation conditions, etc. and found to meet the requirements.

In July 2003, the water level in the reactor pool was lowered to below the primary coolant inlet pipes. The old silicone sealant was removed and the pool liner wire brushed around the weld area in preparation for the epoxy coating. A single coat of epoxy was applied to the defective area by means of a paintbrush to the weld areas around the coolant inlet pipes and the pool liner. Subsequent fluorescein dye tests confirmed that this solution was successful in stopping those leaks.

3.3.5 Repairs to the east through-tube penetration

The position of the leak on the east through-tube penetration as identified during the fluorescein dye test was positively identified on the top flange aluminium patch that was welded in position during the major repairs in 1989 on the east through-tube liner penetration. The crack obviously propagated during the period following the 1989 repairs. To seal the crack, the reactor pool water level was lowered to the vessel top. A profiled aluminium plate was coated with a thick layer of epoxy and then pushed under water firmly against the area of the crack thus smearing the epoxy onto the defective area. The plate was held in position for approximately five minutes prior to it being removed. Fluorescein dye tests later performed showed that the repairs to the defective area were successful. In this instance, a definite reduction in the water leak rate was recorded.

3.4 Radioisotope spiking (2000)

A series of tests was done by using radioisotopes as a tracer. The logic applied was to release two radioisotopes, in this instance ^{24}Na and ^{99m}Tc, at different positions in the pool water system with all pumps switched off. By taking water samples at the leak points for activity analysis, it is reasoned that the isotope that is first detected in the sample is the closest to the leak in the pool. By repeating a series of tests and by the process of elimination, the approximate area of the leak can be identified. These tests were repeated as no final conclusion has been reached on the position of the leak at the first attempt of these tests. In the end these radioisotope tests were considered as ineffective to determine the position of the pool leaks.

3.5 Evaluation of biological shielding (2000 to 2002)

Water seepage through the concrete biological shielding has taken place over a period of time, especially on the eastern side of the beam port floor. A competent authority was contracted to evaluate the condition of the concrete structure in general. In their report they concluded that the concrete was basically sound and that there was no evidence of corrosion of the steel reinforcing. They had, however, recommended that the concrete be hermetically sealed to eliminate seepage and subsequently stabilise the situation. The logic of this action was to stop the flow of water through cavities in the concrete thereby halting any leaching that might occur, and to force the water flow to follow the designed path to the leak drain pipe.

Contractors specialising in the sealing of concrete were appointed to seal the biological shielding around the reactor on the beam port floor, i.e. the worst affected areas. These repairs were implemented in phases commencing with the area from north of the east through-tube to the south of beam port number 4. The plaster cement was removed (chipped off) to a height of approximately two meters above floor level before sealing the concrete. Furthermore, a resin compound was pumped under pressure into the cavities between the beam port access port steel plates and the concrete to prevent corrosion of the steel structure. Finally the concrete biological shield walls were re-plastered.

4 Leak rate monitoring

A system was designed, built and installed to measure the water leak rates from the pools. Essentially the apparatus consists of small tipping buckets based on a design to measure precipitation. Water leakage from five areas, namely, reactor pool, storage pool, canal pool, sub-pile room and seepage through the biological shielding on the east side of the beam port floor are measured and recorded on the Scada system. A gutter, used for the catchment of water leaking through the concrete, was mounted around the perimeter of the biological shielding to divert the water to the measuring apparatus installed in the reactor hall basement. Measurements made with respect to radionuclides show that the water is non-radioactive. However, it is finally diverted to flow into the active waste drains.

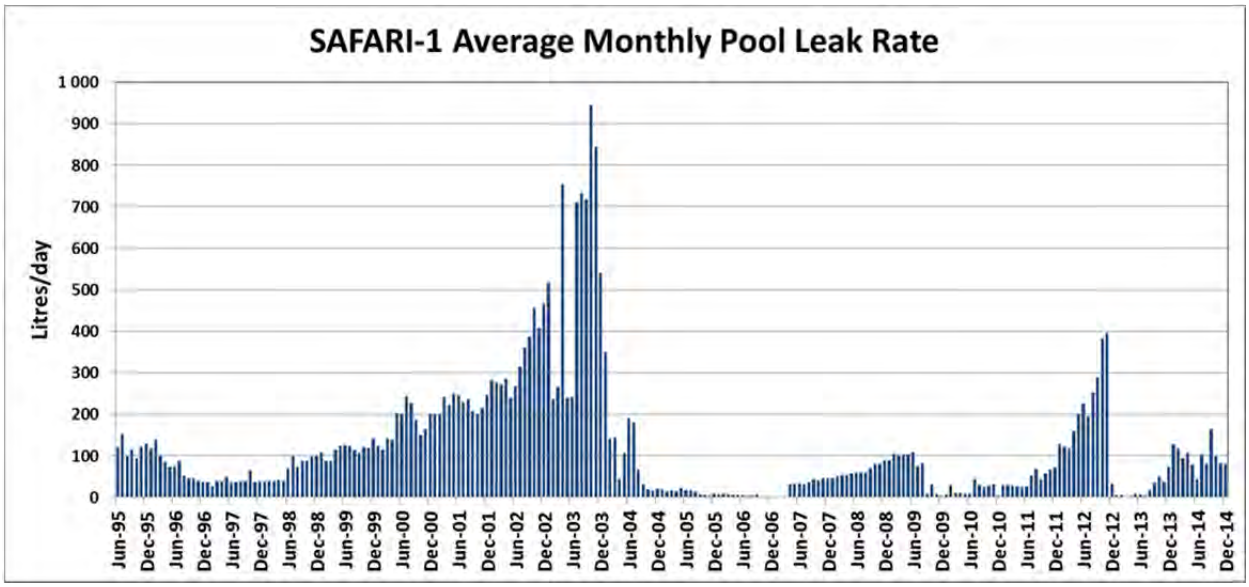

Fig. 3 – SAFARI-1 Average Monthly Pool Leak Rate

SAFARI-1 had a cooperation agreement with the HFR Petten and Studsvik reactors where operation learning was shared on an annual basis. This allowed the SAFARI-1 pool leak to be compared with the pool leak at Studsvik R-2 prior to their final shutdown. Since 1995, the leak rate at SAFARI-1 has been accurately monitored and recorded (refer to Fig 3). It can be seen from this graph that (except for the period from October 2002 to November 2003 when the leak rate peaked at one stage on 945 litres per day) the leak rate varied between very low and about 400 litres per day. At Studsvik R-2 the pool leak was on average 4320 litres per day. The SAFARI-1 pool leak is thus on average less than 10% of the historical Studsvik leak.

A comparison was also made between the SAFARI-1 pool leak rate and the normal evaporation rate of the pool system over a twenty four hour period. These results are as follows:

- Average measured leak rate of pool system 220 litres per day
- Pool evaporation rate as measured June 1999 (winter) 289 litres per day
- Pool evaporation rate as measured January 2001 (summer) 555 litres per day

From the above results, it can clearly be seen that the pool system leak rate is approximately equal to the winter evaporation rate, and about half of the summer evaporation rate.

The leak rates are continuously monitored on a data logging system and manually verified on a weekly basis. This is important for two reasons, first for knowing that the designed leak channels in the pool liner and biological shield are open and secondly that no water is built up in the biological shield that could lead to corrosion of entombed structures.

5 Pool leak ageing management

The repairs which were carried out in 2003 effectively stopped all the leaks. The estimated life-time of the epoxy resin at the time, based on the radiation resistance testing, was 3 years. In 2006 a small leak reappeared and by 2009 had increased to about 100 litres per day. It was determined that the through-tube penetrations, the closest of the sites to the core, were the first to start leaking in 2006, followed by the reactor inlet penetrations in 2009. The life expectancy of the epoxy resin was therefore verified in actual service. Inspection of the sites where the resin has degraded showed that it is possible to brush it off by hand with a stainless steel brush on an extension, dispersing a powdery cloud of the material into the pool water and leaving a bare aluminium surface. The degraded epoxy was removed and fresh epoxy coatings were applied to the tangential through-tube and reactor inlet penetrations in 2009 and again to the tangential through-tube penetrations in 2012. The stand pipe applications in the pool floor liner, which experience very little radiation dose, were confirmed in 2014 to be still hard and sound and have lasted more than 10 years, providing further confirmation that the degradation of the epoxy is due to radiation rather than to its constant emersion in water.

Recognising that the pool leak repairs would need to be maintained, a maintenance schedule was developed and refined over the last decade. During such maintenance activity, the old epoxy is brushed with a hard brush until no more of the old epoxy comes free during brushing. New epoxy is then applied under water in a similar manner as the original application of the epoxy. As can be expected, the required frequency of maintenance of these repairs is proportional to the amount of radiation exposure received by the repairs (and inversely proportional to the distance from the reactor core). The following maintenance frequencies were developed:

- Through-tube penetrations — Every 3 years
- Primary coolant water inlet penetrations — Every 5 years
- Stand pipe penetrations — Longer than 10 years

The leak at the pool gate jamb had been confirmed to be a very small leak and at this stage it is only monitored and no active maintenance work is performed to fix this leak.

Although these above maintenance frequencies for the pool leak repairs are included on the maintenance schedules, the daily monitoring of the pool leak rates are also used to decide when repairs are needed again.

6 Regulatory reporting

The regulatory body has been fully informed and involved in all aspects relating to the pool leaks and the repair attempts in 2002 and 2003. In 2002, the dramatic increase in the leak rate was reported to the regulator as a Level 3 Nuclear Occurrence (lowest level on a scale of 3). Plans to locate the problem, to develop a solution and to implement an enhanced interim monitoring program on the leak were also communicated to the regulator as they were developed. Tests of the leakage water were conducted to verify that it was in fact pool systems water and not reactor primary water. All information from these tests and from the monitoring program was submitted

monthly to the regulator while the repair was being developed. On completion of the repair and confirmation that all leakage had stopped and remained stopped for several months, the Nuclear Occurrence was closed-out in collaboration with and in agreement with the regulator.

Subsequent re-appearance of the leak and actions taken to eliminate it are not separately reported to the regulator each time, but are contained in the routine maintenance plans communicated to the regulator for each outage, for their information.

7 Conclusions

The chance of developing pool leaks over a period of time is common for reactors of a similar design and age of SAFARI-1, and the pool leak problems encountered at SAFARI-1 are not unusual. However, earnest attempts were made to address the situation, namely, to trace the sources and rectify the leaks.

By the periodic application of a specially developed epoxy resin to the leaking areas, and by the constant monitoring of the leak rates, the risk of a major pool leak had been effectively managed. Since the epoxy resin can be applied and cured under water, it is not necessary to drain the pool for these repairs, and thus excessive downtimes are avoided.

The pool liner leaks at SAFARI-1 therefore appears to have been brought completely under control and, while small leaks reappear on a periodic basis, the method of eliminating it is very well established and successful.

8 References

1. RR-VLG-02/01 (00) Status Report on SAFARI-1 Pool Leak, January 2002.

2. RR-VLG-04/12 (00) Pool Leak Repairs Up To August 2004, September 2004.

MANUFACTURING CONDITIONS OF FRENCH REACTOR PRESSURE VESSEL STEELS TO AVOID THE OCCURRENCE OF HYDROGEN FLAKES

D. BUISINE, F. CHAMPIGNY, J.M. FRUND, C. MILLER
Electricité de France, Direction Production Ingénierie, CEIDRE
2, rue Ampère, 93206 Saint-Denis Cedex 01 - FRANCE

T. BERGER, P. JOLY
Areva NP
Tour Areva, 92084 Paris La Défense Cedex - FRANCE

ABSTRACT

The formation of hydrogen flakes in Reactor Pressure Vessels (RPV's) forgings is a well known phenomenon that can affect forging components during manufacturing. Following recent data from Belgium, it has been the object of important assessments during the last 3 years. We will present in this paper elements pertaining to the RPV's of the French nuclear fleet.

A thorough review of fabrication processes and specifically of ultrasonic examination of forgings, including the oldest ones has demonstrated that the risk of leaving undetected hydrogen flakes in RPV's forgings is not a problem in French RPVs. The French Regulator also clearly shared this position point in 1985.

Parts with defects were once again observed at the beginning of 2012 but the defects were attributed to errors in hydrogen measurement at the steel maker shop. Those hydrogen induced defects were detected at an early manufacturing stage (before quality heat treatment) by ultrasonic examination, and the concerned parts were consequently rejected through the normal quality control process.

1. Introduction

In June 2012, a first in-service inspection was carried out on the core shells of the Doel 3 RPV (Belgium) in addition to the regular requirements in the ASME Code Section XI. The ultrasonic technique used - introduced and qualified in France since 2005 for underclad cracks detection - identified flaw indications in the base metal.

Similar inspections were conducted in September 2012 on the Tihange 2 unit, which reactor pressure vessel is of identical design and construction. Flaw indications were detected as well, but to a lesser extent.

Looking at their shape, orientation and location in the zones of suspected macro-segregations, the most likely origin of these indications relates the hydrogen flaking to the manufacturing process of the original forgings [1].

There is a consensus in current literature that three factors are necessary in order to create hydrogen flaking: a sufficient amount of hydrogen at a rather low temperature, tensile stresses and a sensitive microstructure.

Differences in hydrogen solubility play a major role for explaining how hydrogen can concentrate in some areas of the forgings at low temperature: Hydrogen is much more soluble in a γ structure (face cubic centered) such as austenite than in an α structure (body cubic centered) such as ferrite. As the material cools down after forging, the austenite to ferrite transformation occurs first in the zones of negative segregation and in segregation-free zones. This leads to an increased hydrogen concentration in the zones of positive segregation which are still in an austenitic state. If no precaution is taken to remove this excess hydrogen, flaking will occur at ambient temperature around microstructural traps formed by the discontinuities in the material where hydrogen concentrates.

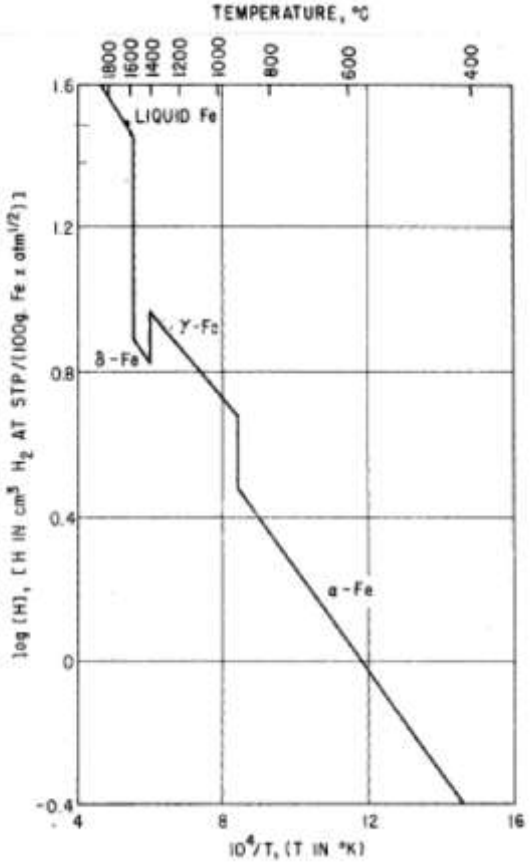

Figure 1: Hydrogen solubility

The preventive measures applied during the manufacturing process to limit the risk of hydrogen flaking consist therefore in limiting the hydrogen concentration at the ingot pouring stage at the steel maker's shop, and applying a heat treatment to extract hydrogen from the forgings after the end of forging operations at the forge master'shop. The final step to assure that the parts are free of hydrogen flakes are acceptance tests of the base material including appropriate ultrasonic testing.

2. Manufacturing History of the Vessels

Regarding the manufacturing history of the forgings of the french NPP fleet, a few parts were affected by hydrogen flaking. They were all rejected after non destructive examinations conducted at the time of manufacturing (12 RPV and SG forgings between 1983 and 1985 and more recently 2 SG shells in 2011 and 2012).

In 1985 and 1986, a thorough review of the construction files has been performed and discussed with the national regulator. This analysis confirmed the acceptability of all RPV core shells manufactured before 1985 and led to implement the following precautions:

- Having a low residual hydrogen content before the cooling down to ambient temperature after the end of forging,

- Limiting the cooling down temperature after the end of forging to $\theta \geq 300°C$ (and later 200°C) and this temperature was held for a time as a function of the thickness of the part in order to ensure a complete transformation of the structure in ferritic phase,

- Performing of a dehydrogenation heat treatment at 650°C during a time function of the thickness of the part and the initial hydrogen content,

- Improving the ultrasonic inspection method.

The reoccurrence of hydrogen flaking in lower SG shells in 2011 and 2012 can be considered as accidental as these precautions were occasionally not completely fulfilled.

Since 2012, further to the Doel 3 and Tihange 2 operational feedback, an additional review of the End of Manufacturing Reports has been performed for core shells of French RPVs.

It was devoted to reviewing the preventive actions performed to detect flakes at inspection and allowed retrieving the results of the ultrasonic tests mandated for all forgings by the CPFC and RCC-M codes [2] [3].

All the parts were controlled at 100% and the results are in accordance with the requirements.

The suitability of the ultrasonic examination has then been demonstrated on a reference material: a forged shell mentioned above, identified as VB395, meant for a 1,300 MW plant steam generator, and rejected in 2012 because of hydrogen flaking.

The thickness of the VB395 forged shell is comparable to the Doel 3 and Tihange 2 RPV shells (maximum 264 mm), though it has a slightly smaller internal diameter (3,564 mm). The forged shell showed a large number of hydrogen flakes (~5,000) distributed in the center part of the forging and homogeneously distributed on the ¾ height.

Ultrasonic testings have been performed on a block (200 x 175 mm) of VB395 forged shell containing flakes in agreement with the early procedure used to apply CPFC code, then with procedure which was later used in application of the RCC-M code and finally with the ASME code procedure which had been used for acceptance tests of Doel 3 and Tihange 2 RPV forgings [4].

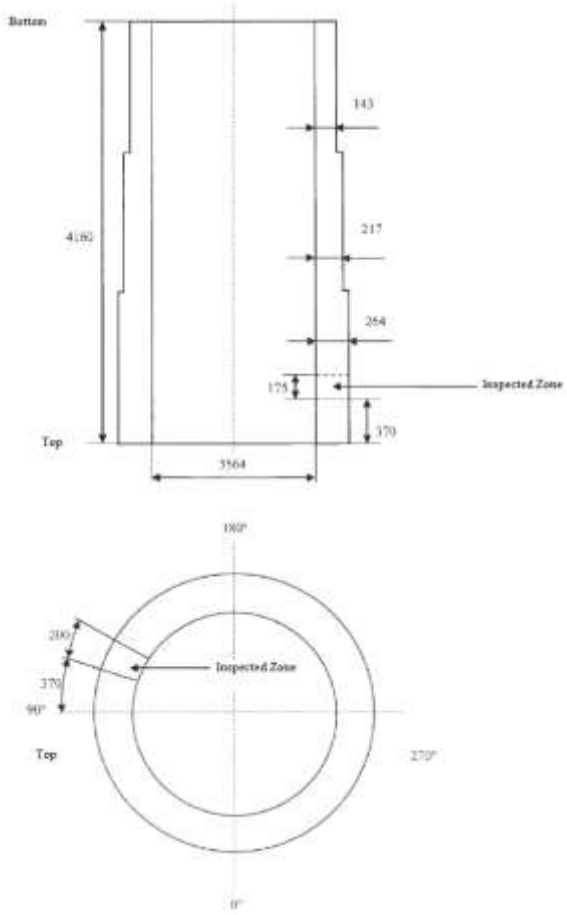

Figure 2: Inspected area on the VB395

The results are presented hereafter.

Inspection Procedure	Results	
	Recordable Indications	Unacceptable Indications
ASME	50	1
CPFC	43	26
RCC-M	47	47

Figure 3: Ultrasonic testing results on the VB395 shell

They confirm that the ultrasonic examination mandated by the CPFC and RCC-M has been well appropriate to detect flaking and to reject the affected parts since the earliest procedures and demonstrate that the phenomenon observed at Doel 3 and Tihange 2, of leaving undetected defects due to flaking, could not happen in the core shells used to manufacture the French 58 RPVs.

3. In-service Inspection

An additional review has been conducted on the recorded in-service inspection data obtained with the current process "Zone De Coeur" devoted to detect underclad cracks from seven to twenty-five millimeters (i.e. the first millimeters of the base metal) in depth from the inner

surface on the core area of the 900MWe and 1300MWe French RPVs. These in-service inspection are carried out on the whole core zone each ten year outage.

Figure 1 -Core area inspection

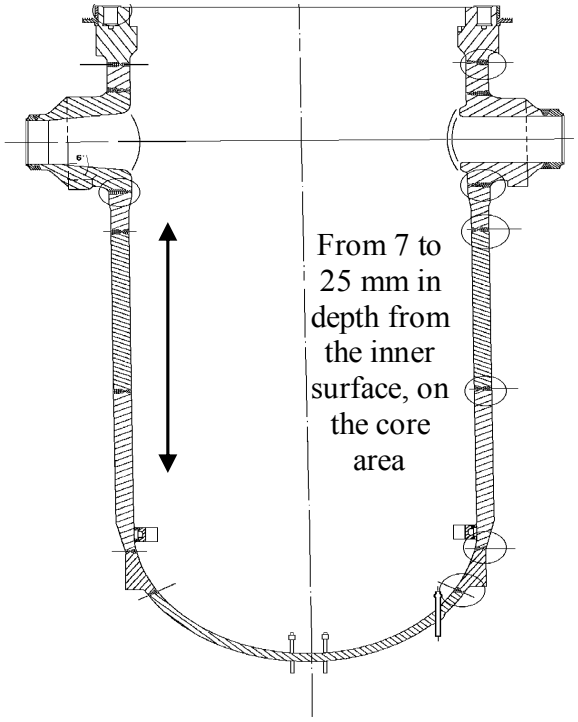

Figure 4: Core Area Inspection

The “ZDC” process guaranteeing the detection, localization and characterization of any flaw of 5 mm high x 25 mm long with an accuracy of ± 2 mm. For more details concerning the robot, the NDE process and the qualification phase see ref [5].

The method used here to ensure the absence of flaking on French RPVs consists in analyzing the data gathered by the 0° longitudinal wave’s transducers used for synchronization during ZDC control. These transducers are normally dedicated to clad thickness measurement and clad bonding but their ability to detect hydrogen induced cracks was justified up to an 80mm depth.

The review was conducted by:

- Analyzing available records from previous in-service inspections: 40 vessels were concerned by this analysis,

- Making use of the current 2013-2014 in-service inspections: 8 vessels were concerned by this control,

For 34 of these 48 RPVs there was no indication found. The few indications detected in the 14 remaining vessels (max. 17 indication per RPV) are non significant, very small (smaller than the diameter of the transducer focal spot) and their amplitude is very low compared to the sensitivity of the transducer at equivalent depth.

In agreement with the request of the national regulator, a new NDE process - adapted from the one used for inspecting shell’s circular welds - was also developed to inspect full thickness of the under-cladding vessel core. The aim was to ensure the absence of flaw indications with parallel orientation to the inner and outer skin of vessel core. 6 vessels were concerned by

this control called "Virole Epaisseur Complète" and there was no indication found.

Finally, none of the results obtained on the 54 RPVs of the 900MWe and 1300MWe plants has highlighted defects similar to those observed at Doel 3 and Tihange 2.

4. Conclusion

In 2012, during in-service inspections of the core shells, conducted for the first time in two Belgium reactor pressure vessels (Doel 3 and Tihange 2), several thousands of flaw indications were detected. Looking at their shape, orientation and location in the zones of suspected macro-segregations, these indications were unambiguously assigned to the manufacturing process of the original forgings.

Further to this operational feedback, EDF and AREVA have reviewed, for the RPV core shells of the French NPP fleet, the preventive manufacturing measures taken to avoid the presence of hydrogen flakes. The results of the ultrasonic testings, mandated for all forgings by the CPFC and RCC-M codes, have been retrieved from the end of manufacturing reports. They demonstrate that the phenomenon observed at Doel 3 and Tihange 2 did not happen in the core shells used to manufacture the 58 French RPVs.

An additional review has been performed using the results of the In-Service Inspection conducted with the current process qualified since 2005 and used on the EDF RPV core zone to detect underclad planar defects. The numerous records have thereby been analyzed to check the absence of flakes up to a 80 mm depth.

To confirm the results of the manufacturing inspection, 12 shells from 6 RPV have been fully inspected during their 10 year visit. The internal constitution of the forgings is confirmed, using 0° longitudinal wave's transducers adapted to detect flakes in the thru-whole extent during plant operation. No defect similar to those observed at Doel 3 and Tihange 2 was detected in the core zone forgings of the controlled RPVs.

All these investigations are in good agreement with the WENRA recommendation [6].

References

[1] Pressure Vessel Doel 3 & Tihange 2, *www.fanc.fgov.be*

[2] Cahier des Prescriptions de Fabrication et de Contrôle (C.P.F.C) – Edition Janvier 1974.

[3] Règles de Conception et de Construction des Materiels Mecaniques des Ilots Nucleaires REP (RCC-M) – Edition 2007, Addenda 2008 et 2009.

[4] ASME Code Section III – Rules for Construction of Nuclear Facility Components - Edition 1973.

[5] K. Zamoum, T. Pasquier, F. Lasserre, "French Reactor Pressure Vessels – Non-destructive examination of the core area – Detection performance demonstration of the ZDC process", 5th International Conference on NDE in Relation to Structural Integrity for nuclear and pressurized compnents, 2006.

[6] WENRA Recommendation in connection with flaw indications found in Belgium reactors, 2013, *www.wenra.org.*

MODERNISATION OF I&C SYSTEMS IN NUCLEAR RESEARCH REACTORS

A. AVILA
Instrumentation & Control Department, INVAP S.E.
Colón 4050 2° Piso – 5000-Córdoba - Argentina

ABSTRACT

The Instrumentation and Control (I&C) systems have an important role in the safe operation of Research Reactors. The modernisation of the I&C systems, usually is driven by a major reason such as equipment ageing, increasing of failure rate of components, the obsolescence of the systems, the unavailability of spare parts or the noncompliance with updated safety standards. The replacement of the I&C systems permits to implement state of the art technology improving safety, operation and maintenance of reactors and associated facilities.
This paper presents ways to replace partially or totally the I&C systems adapting the new systems to the existing reactor and separating the safety systems from the non-safety systems.
The replacement of the Reactor Protection System (RPS) presents a flexible and compact design. As a safety system, the components are environmentally and seismically qualified under a qualification process. The replacement of the Reactor Control and Monitoring System (RCMS) allows the operators to interact with the plant in a simple and versatile way with the benefit of a SCADA software system. The replacement of the reactor control console presents improvements in HMI and human factors while the new design preserves the visual appearance and the operability of the original console implementing new and modern concepts.

1 Introduction

The term "modernisation" is used in this report to represent the three types of changes in I&C systems and components. These are the replacement of old systems and components, the upgrading of old systems and components, and the implementation of new systems and components.
The benefits of a modernisation in I&C systems are unquestioned even though the licensing process shown to be a thorough process.

2 Causes of I&C Modernisation

2.1 Need to update Safety Systems

As the requirements may have been changed from the requirements in force when the plant was built, it is necessary to establish the new licensing requirements for the modernisation.
The general requirements, usually issued by the licensing body or authority of the country, are established to improve the safety of the plant and to be able to modify the plant so that it can meet current safety standards.

2.2 Need to Increase the supervision and automation

When the installation of new digital I&C equipment is planned, a change of the balance between automation and human actions should be considered. Due to technical and operational factors, it

may be desirable to increase the level of automation to improve safety and plant availability and also for maintenance. This can be done in an easier and more cost-effective manner than before due to the capabilities of modern supervision technology.
The advance in control and information technology makes possible to present information to operators in the control room in better and more friendly ways. This feature has a direct improving efficiency in the operator's actions and responses during the operation of the plant.

2.3 Equipment Ageing

The degradation of the performance or dependability of I&C equipment with time is understood by ageing. This degradation is due to physical mechanisms inherent to component materials and linked to the I&C equipment design, assembly and functional characteristics. It is influenced by the stresses from the equipment environment and from the equipment operation.
Some examples of stress factors, ageing mechanisms, and ageing effects are given as follows:
High temperature environments, High humidity environments or contact with water or chemicals, Vibration and mechanical shock, exposure to radiation, Wear-out of semiconductor components, Operation of electronic components above specified maximum supply voltage, repeated maintenance operations entailing the withdrawal/reinsertion of electronic cards.
It is important to address the I&C ageing issues in terms of plant life management and license renewal not only for normal operation but also, and more importantly, for the response of the safety systems during and after the design basis events.
At the end of the I&C equipment's lifetime the failure rate of the component and hence the I&C equipment or system becomes greater ("bathtub" reliability curve). The reliability is no longer statistically predictable and hence the equipment becomes undependable.
Equipment is qualified to operate for a limited period of time. After this period expired, the manufacturer does not assure that the equipment is able to operate under the design basis conditions. Therefore, the degraded parts of the equipment or the complete equipment must be replaced.

2.4 Equipment Obsolescence

Obsolescence of the systems components most of the times makes very difficult and expensive to get spare parts. The growing obsolescence problem with I&C systems is a significant contributing factor to increasing costs for plant operation and maintenance and decreasing continually the plant availability.
Rapid pace in the evolution of electronic technology is a significant factor in I&C equipment obsolescence. The inability to obtain spare parts and supplier support is a major problem.

3 Modernisation of I&C Systems

3.1 General Context

The general context diagram of I&C systems is presented in the Fig 1. The reactor plant variables are measured by nucleonics, process and ionizing radiation instrumentation. The signals are connected to the Reactor Protection System (RPS), a safety system that performs the protective actions; and the Reactor Control and Monitoring System (RCMS), a safety-related system that implements the reactor control and provides the visualisation of the reactor variables to the reactor operators.

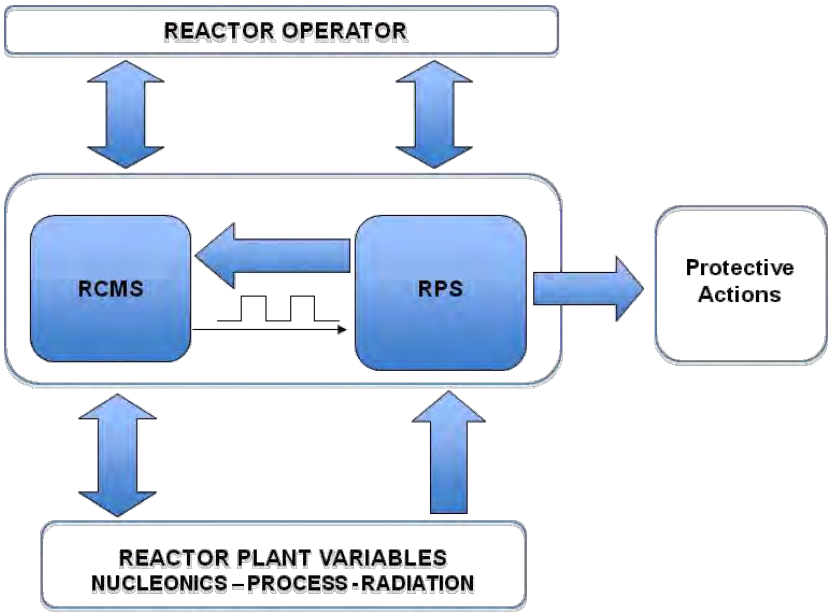

Fig 1: I&C Context Diagram

3.2 Safety Functions

The safety function required to be implemented in a reactor and which are accomplished by the safety systems are:

1. Shutting down the reactor and maintaining it in a safe shutdown condition for all operational states or accident conditions;
2. Providing for adequate removal of heat from the core after shutdown, including in accident conditions;
3. Containing radioactive material so as to minimize its release to the environment.

Typically the RPS is responsible to accomplish the first safety function but, depending on the plant design, it could be designed that the RPS need to satisfy second and/or third safety function too.

3.3 Separation and Independence of Safety Systems

It is a mandatory requirement that the Safety Systems shall be separated and independent of other reactor systems. In particular the RPS shall be separated and independent from the other Instrumentation & Control systems.
It is important to verify that all components of the instrumentation loops, such as sensors/transmitters, wiring, logic panels and console, which are part of the safety systems comply with the separation and independence criteria.
Some existing plants do not comply with separation and independence criteria for safety variables. Therefore, the modernisation of I&C systems is the opportunity to provide a new design that complies with the current codes and standards.

3.4 Nuclear Qualified Equipment

Nowadays, the tendency at nuclear research reactors is to qualify the equipment belonging to safety systems as nuclear class equipment. Standards IEEE Std 323-2003 and IEEE Std 344-2004

IEEE can be applied in order to determine the qualification process considering only those relevant parts of both standards that are applicable to research reactor.

3.5 Nucleonics Instrumentation

The following neutron flux measurement channels (a, b, c, d) and gamma measurement channel (e) can be used to replace the existing instrumentation:

a) Start-up Channel: 5 measurement decades. Used at start-up range.
b) Compensated Ionisation Chamber Channel: 7 measurement decades. Used at power range.
c) Campbell processing Fission Chamber Channel: 10 measurement decades. Used at start-up and power range.
d) Self-Powered Neutron Detectors: used at power range
e) Nitrogen 16 gamma Channel: used at power range for global core power measurement.

3.6 Reactor Protection System (RPS)

3.6.1 RPS Architecture

For small reactors that have to be modernised with cost-effective systems, it is recommended to install a hardwired system based on discrete electronics and relays.
For large reactors that require increasing the number of safety variables, it is recommended to install a safety PLC software based system already qualified in nuclear research reactors.
The RPS architecture should be flexible to allow be adapted to the existing reactor safety instrumentation and safety logic. An architecture based on two, three or four independent measurement channels can be implemented.
The following figure shows the architecture implemented with three measurement channels using a two out of three (2oo3) voting logic for each safety variable.

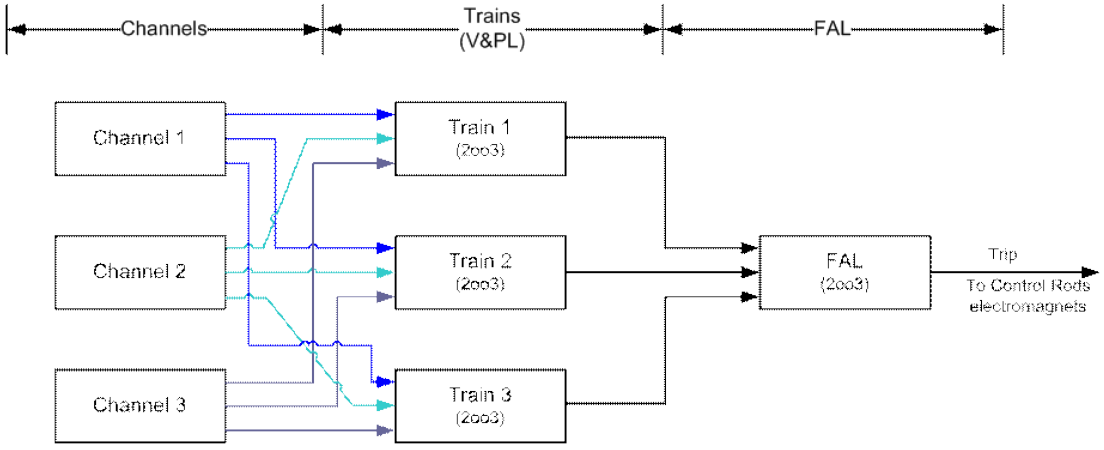

Fig 2: Example of 2oo3 RPS Architecture

In our experience, the flexibility of the RPS Architecture allows to find the appropriate configuration for the reactor requirements. The already modernised reactors show a solution of the combination of a dual redundant architecture with triple redundant architecture.

3.6.2 RPS Hardwired Modules

The standardised hardwired design architecture presents generic modules implemented on NIM standard that allow easy maintenance and thus having less types of spare parts.

Example1, Fig 3 –Generic Logic Module: multipurpose modules designed to implement any combinational logic. They were designed to be used in safety systems for nuclear applications.
Example2, Fig 4 - Indicator modules: LCD display modules designed and tested for console applications.
This technology presents a compact and modular design that allows to the system to be installed in the plant using less space than the old system and allowing easy maintenance and the possibility to expand or modify the system in the future.

Fig 3: RPS Generic Logic Module

Fig 4: RPS indicators

3.7 Reactor Control and Monitoring System (RCMS)

The main functions of the RCMS are:

- Reactor supervision
- Process control
- Reactivity control by the Control Rod Drive system
- Limitation Logic – Defence in Depth Criterion
- Reactor State Transition Logic
- Data acquisition & recording
- Alarms annunciation

3.7.1 RCMS Architecture

The modernisation of the RCMS is potentially the most visible change in the I&C systems.
This modernisation allows increasing the automatic and manual actions to provide new operational features to the reactor and the overall plant.
Modern systems present all information efficiently to operators in a user-friendly manner. New alarms and limitation functions can be added to maintain the reactor parameters within operational limits without reaching safety limits.
The architecture of a modern RCMS is usually divided in three levels: Supervision – control - field.
The communication between the three levels is provided by the field network and the control network, in that way there are savings in costs and space compared to the standard point to point philosophy where signals are wired individually. Fig 5 shows the architecture of a RCMS based on a Distributed Control System (DCS) used in the OPAL reactor. Fig. 6 shows the architecture of a RCMS based on a Programmable Logic Controller (PLC) architecture used at the Romanian 14MW TRIGA reactor.

Plant variables are stored in historic data recordings which allow trending visualisation. Historic data also allow operation and maintenance staff to keep historic values that can be used in for future analysis.
The Supervision Units run the SCADA application that allow operators to supervise and command the reactor using mimics that shows the reactor process schematically. Fig 7 shows an example of a process screen.

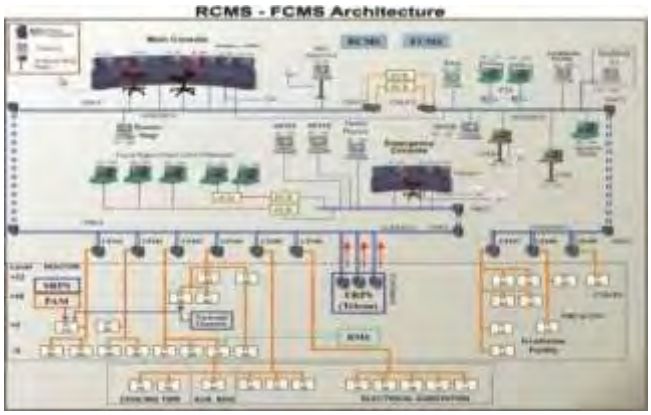

Fig 5: RCMS architecture of OPAL reactor based on DCS (Australia)

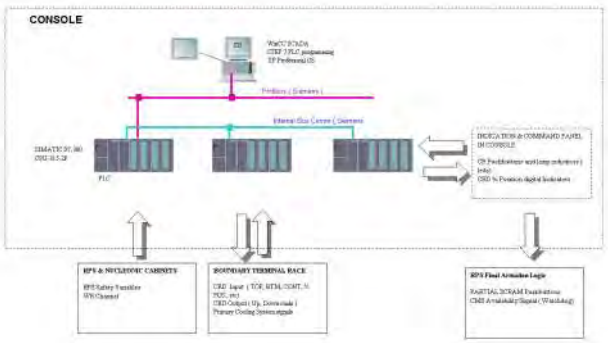

Fig 6: ICN Triga RCMS architecture based on PLC (Romania)

3.7.2 Human Machine Interface (HMI)

The extensive data, information processing, and display capabilities of modern technology support the ability to improve considerably the HMI. This includes the effective use of Video Display Units (VDU) and large overview screens in the Control Room, the presentation of complex conditions by means of specialised graphs and diagrams, and the rapid access to information that supports the more safe and efficient operation of the plant. These improved HMI capabilities reduce the potential for human error and support improved productivity and enhanced safety.
The main variables of the reactor such as neutron flux, reactor power, position of control rods, are shown on dedicated screens.
It is highly recommendable that the reactor staff is involved in the modernisation project in an early stage particularly to verify that new HMI satisfies their needs and is consistent with existing procedures and equipment.

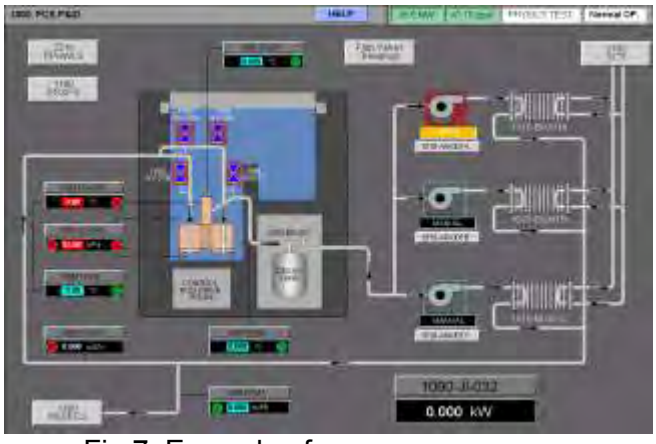

Fig 7: Example of a process screen

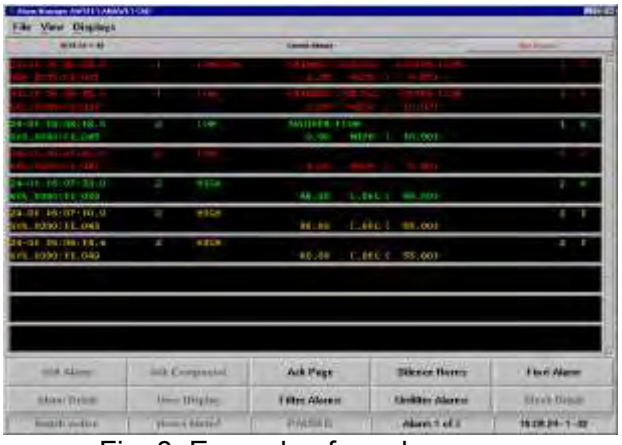

Fig. 8: Example of an alarm page

The HMI defines color codes in order to easily visualise the status of a reactor process variables and alarms: Fig. 8 shows the alarm page where reactor alarms are shown ordered by date and time.

3.7.3 Interface RPS to RCMS

As presented in Fig. 1 there is a one way communication, from RPS to RCMS. The communication uses galvanic isolation.
The data transferred from RPS usually are:

- RPS input signals
- Trip Unit signals
- Voting & Protective Logic signals
- Safety system settings
- RPS status

3.8 Control Room and Console

If the desired control room layout requires major modifications, it is recommended to plan a global replacement of the panels during a suitable outage in order to install newer technology that will allow further incremental implementations. For that condition, the easier solution is to plan the entire migration process by taking into account the availability needed of essential functions during the outage.

Fig.9: Console for 14MW TRIGA Research Reactor (Romania)

Fig 10: New Console for 10MW reactor at Tajoura (Libia)

Regardless of the scope of the modernisation project, it is necessary to assess the potential problems of operating old and new systems in parallel. Sometimes major parts of the old control room equipment are left unchanged and the new systems are implemented in the middle of old equipment.
In such cases, special care to harmonise the old and the new systems should be exercised. Control room changes should always be considered carefully to make sure that new problems are not introduced when the operators have to transfer from a familiar to an unfamiliar system, which in addition may contribute to potential human errors.

An example of this case is the modernization of the 14Mw TRIGA Research Reactor at Pitesti, Romania. Here, the console of the steady state reactor was replaced by a new console which design is very similar to the original console.
The actual trend in new or major I&C modernization is the use of modern concept and design that takes into account the overall human engineering factors.

4 Conclusions

The nuclear reactors look forward for extended future operation and licensing renewal and they will inevitably continue the replacement of their ageing and obsolete equipment or they will need to adapt the I&C to current safety standards and an efficient plant operation.
On the other hand, the technology development of the I&C has been very fast over the last years.
For that reason, the use of modern technology in the research reactors offers the opportunity to enhance safety, to increase productivity, to reduce operation and maintenance costs and to support plant staff in the performance of their jobs. Modem technology can be used to improve availability, improve reliability and increase productivity of the plant. Proper use of this technology can not only reduce the potential for human errors, but can also support improved human performance.
A careful planning of the I&C life cycle should consider the modernization of the I&C equipment or systems taking advantages of modern architectures and technologies in the area of instrumentation, RPS and RCMS to provide a safe, reliable and cost-effective operation of the reactor keeping as low as possible the impact in the plant layout and enhancing the reactor operability while maintaining the human factors in the console.

5 References

1. IAEA, Safety of Research Reactors, Safety Requirements, IAEA Safety Standard Series No., NS-R-4, IAEA, Vienna (2005)

2. IAEA, Safety in the Utilization and Modernisation of Research Reactors, Specific Safety Guide, IAEA Safety Standard Series No. SSG-24, IAEA, Vienna (2012)

3. IAEA-TECDOC-1402 Management of life cycle and ageing at nuclear power plants: Improved I&C maintenance

4. IAEA-TECDOC-1016 Modernization of instrumentation and control in nuclear power plants

5. IAEA-TECDOC-1389 Managing modernization of nuclear power plant instrumentation and control systems

6. IAEA TECDOC 973 Research Reactor Instrumentation and Control Technology

7. IEEE Std 323-2003 IEEE Standard for Qualifying Class 1E Equipment for Nuclear Power Generating Stations

8. IEEE Std 344-2004 IEEE Recommended Practice for Seismic Qualification of Class 1E Equipment for Nuclear Power Generating Stations

New Research Reactor Projects

OYSTER Reactor Upgrade Project:
Cold neutrons for cool science

A.E. MOLAG, C.N.J. KAAIJK
Reactor Institute Delft, Delft University of Technology
Mekelweg, 2629JB Delft – The Netherlands

ABSTRACT

The Reactor Institute Delft (RID) of Delft University of Technology (TU Delft) is a knowledge centre on nuclear topics, and it operates a 2 MW research reactor, its irradiation facilities and laboratories and its neutron- and positron instruments. Our research program is focussed on health and sustainable energy. The institute accommodates resident and visiting scientists and other users from a variety of (scientific) disciplines, educates students, professionals and scientists, and serves as an independent source of information for society on radiation- and nuclear-related issues.
On January 20, 2012, the RID was awarded 38 million EUR by the Dutch government for the OYSTER project ("Optimized Yield - for Science, Technology and Education - of Radiation"). OYSTER was designed to expand the capabilities of the research reactor at the RID for the sake of the broader Dutch and international research communities. It consists of a cold neutron source, modernization of several reactor systems and several new experimental facilities. In this contribution we will present the new research possibilities after realization of Oyster, technical details about the cold neutron source and new experiments and the current status of the project with regards to licensing and engineering.
The consortium KHC, consisting of KAERI, Hyundai Engineering and Hyundai Engineering & Construction, was selected for the execution of the reactor related work packages of the OYSTER project in June 2014 after a "competitive dialogue" European tender procedure.
The Request For Proposal (RFP) of our institute requested an increase in cold neutron flux of a factor 30 at wavelength 0,5 nm (3 meV) and a factor 45 at 1 nm (0,8 meV). Currently the KHC consortium is working on the basic engineering of the changes to the reactor.
The reactor institute and external experts are preparing the required documentation for obtaining a new operational license. These documents include a new safety analysis report and an environmental assessment report, all of which have to comply with new legislation currently in preparation by the Dutch government, the Dutch Safety Requirements.
The installation phase of the in pool facilities including the cold neutron source will commence in the summer of 2017 and the end of the commissioning phase is planned in the first quarter of 2018. The construction of new experimental facilities, which will greatly benefit from the cold neutron flux started in 2012. The first new experimental facility to become operational for end-users in 2015 is the neutron powder diffractometer PEARL.

1. Introduction

The 2 MW open pool research reactor of the Delft University of Technology (TU Delft) has been in operation since 1963. It is a powerful research tool around which the TU Delft developed and strengthened research and educational programs. The Reactor Institute Delft [1] (RID) is a knowledge centre on nuclear topics, operating the reactor, irradiation facilities, and neutron- and positron instruments. In conjunction with the scientific Department of Radiation Science and Technology [2] (RST) of the Faculty of Applied Sciences, RID accommodates resident and visiting scientists from a variety of scientific disciplines, educates students, professionals and scientists, and serves as an independent source of information for society on radiation- and nuclear-related issues. Over the years, the scientists around the reactor have gained a strong reputation in developing and using new and often unique instruments, irradiation facilities and methods. The RID is one of the few IAEA Collaborating Centres worldwide[3].

The Oyster program provides the institute the opportunity to further develop and expand the potential of the research reactor. OYSTER stands for “Optimized Yield -for Science, Technology and Education- of Radiation”, and is co-funded by the Dutch government, the TU Delft and a number of commercial parties, all of whom are gratefully acknowledged. OYSTER aims to improve and expand the infrastructure around the reactor to better address current and future educational, scientific and societal questions. OYSTER was granted in January 2012 [4] and spans a ten-year period for new research and education on reactor-based radioisotope production, neutron activation analysis, positron annihilation spectroscopy, neutron scattering and imaging. The innovative facilities and instruments that will be built as part of OYSTER will be accessible to scientists from academia and industry and will thus become useful tools in developing materials and technologies that are better and/or more sustainable than current ones.

2. Project Aims

- To further develop RID/RST as a coordinating centre for the application of neutron, positron and radionuclide science and techniques, radiation detection and reactor technology, thereby supporting and uniting the Dutch scientific community.
- To create a home base for neutron scattering and mobilize the scientific community to secure Dutch collaboration with major international neutron sources.
- To establish RID/RST as a knowledge centre and training institute in Europe, and thus a coordinating partner in European research networks.
- To stimulate ground-breaking innovations in the field of neutron, positron and radiochemistry science.
- To sustain RID/RST leading role in the use and knowledge of world-class instruments such as continuous positron beams, high resolution Larmor diffraction, the development of new routes for radioisotope production and the ISO 17025 accredited laboratory for Instrumental Neutron Activation Analysis.
- To contribute to the development of the European Spallation Source (ESS). The ESS is a multi-disciplinary research centre based on the world’s most powerful neutron source, currently under construction in Sweden [5].

3. OYSTER scope

The Oyster project is scheduled to run till 2023. The technical part of the realization of the OYSTER project has been divided in three work packages, to be executed in parallel in order to get as many as possible of the new scientific instruments and facilities operational at the close-out of the project. An external project manager is in charge of the project.

The main items of the scope are the following:

- The installation of a liquid hydrogen Cold Neutron Source (CNS) of the thermosiphon type. The CNS related activities have been divided in two work packages. Work package one “Reactor Modifications” encompasses the installation of the near-core part of the cold neutron source. Work package two “Utilities” consisting of the installation of support systems for the CNS outside the reactor building.
- Work package three. Design and construction of new research instruments and new irradiation facilities.
- A financial contribution to the operational costs of the institute till 2023

A reactor power upgrade from 2 to 3 MW was removed from the original scope due to budget and neutron efficiency constraints.

5. Tender process

The tender was issued for work package 1 and 2 under the European competitive dialogue regime [6]. Work package 3 is carried out by RID and RST staff, so a formal tender was not required for this work package. For this process the Reactor Institute Delft wrote a goal oriented specification (Request For Proposal document) which provided several objective criteria and a minimum of technical details. As an example a requirement on cold neutron flux gain was put in the RFP document without requiring a specific type of CNS. This ensured that manufacturers from all over the world had an equal opportunity to obtain the contract. Three selected manufacturers were asked to deliver a basic design according to the requirements in the RFP. These designs were to be rated according to a scoring table that was part of the original RFP document.
During the process a continuous dialogue took place between the suppliers and the Reactor Institute. This helped the RID to further clarify and improve the scope by benefiting from the knowledge present in all suppliers. According to the EU competitive dialogue transparency criteria information and questions from any party were shared with all competing parties. The goal of this dialogue was to obtain a better final design through the application of supplier knowledge than initially could have been imagined by the institute.
As a result of this approach our original ideas on how to realize OYSTER were transformed into a better specification for the project through an updated RFP document. In addition this approach offers an increased flexibility for necessary modifications of the basic design.
Flexibility was needed when new Dutch nuclear legislation, the Dutch Safety Requirements (DSR), was unexpectedly announced during the project. The DSR project is a modernization of Dutch nuclear law based on the latest IAEA standards, the lessons learned from the Fukushima accident and on the WENRA safety reference levels. This had a significant impact on the project due to more strict safety requirements that created a need for additional defence in depth layers and safety barriers. Each of the three parties was invited to present a case about five selected DSR items.
A careful rating of the three competing basic designs according to all items of the scoring table of the RFP document was carried out. The KAERI, Hyundai Engineering, Hyundai Construction (KHC) basic design proposal scored the highest number of points of the three competing parties and KHC was therefore awarded the OYSTER contract in June 2014.
The official contract was signed in November 2014 by the President of Delft Technical University, representing Delft Technical University, and the President of KAERI, representing the KHC consortium, in the presence of the King of the Netherlands and the President of South Korea. The signing of the contract also marked the start of the basic design phase.

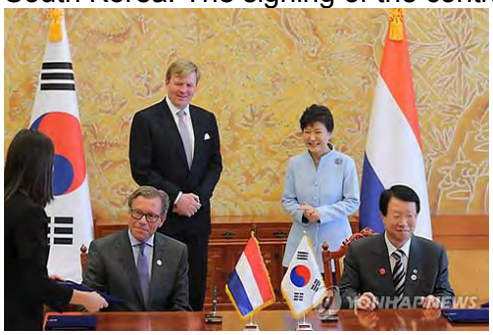

Figure 1 Signing of the OYSTER contract

6. Time line

The project was officially started in January 2013 after government funding had been announced in January 2012. Installation of the cold neutron source is scheduled to start in the summer of 2017. The start-up of the reactor after the installation of the CNS is foreseen for the first quarter of 2018. Modified and new experiments and irradiation facilities will be installed between now and during the whole OYSTER project.
As part of the OYSTER project a complete new nuclear operations license is required. In order to obtain the license a new Safety Analysis Report (SAR), based on the latest IAEA standard [7] and the new Dutch Safety Requirements, an environmental assessment report and an updated decommissioning plan will be written. The SAR will be completed in the beginning of 2016.

7. Cold Neutron Source: Thermosiphon

The new cold source is of the thermosiphon type and is similar to the one in the HANARO reactor in South Korea, operated by KAERI. The effect of a cold neutron source is to shift the peak in the neutron energy spectrum towards lower energies. This is increases the neutron flux at a wavelength that is interesting for many scientific experiments. As a result RID will be able to install new experiments that optimally benefit from the increased cold neutron flux. The cold moderator cell filled with hydrogen will be installed on the face of beamtube R2 next to the reactor core.

A thermosiphon operates in a natural circulation mode that is driven by hydrogen density differences. The heat generated by the irradiation of the cold moderator is removed by a thermosiphon cooling loop into a vertical insert, which contains at its top a heat-exchanger/condenser. Liquid hydrogen in the moderator cell boils due to neutron moderation and gamma heating. Hydrogen gas from boiling rises to reach a condenser cooled by cold helium. The heat exchanger liquefies and cools the rising gaseous hydrogen flow, which then flows back down to the moderator cell by gravity. During reactor operation there is a balance between the amount of evaporated hydrogen in the moderator cell and the amount of condensed hydrogen in the heat exchanger. A natural circulation flow occurs in the hydrogen loop. Natural circulation eliminates the need for moving parts inside the loop which is one of the advantages of this type of CNS. The design conditions for the moderator cell are a temperature of 23 K and pressure of 2 bar.

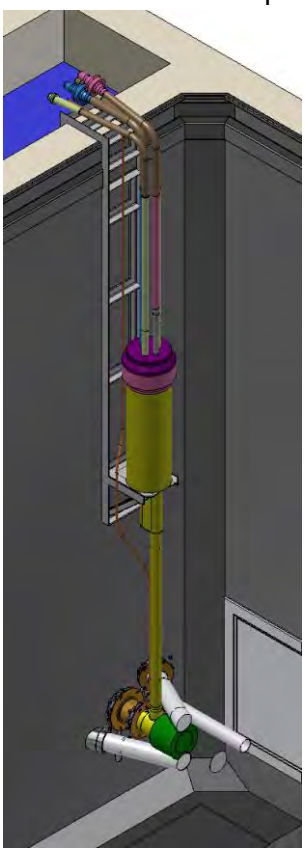

Figure 2 Three-dimensional view of in pool assembly of CNS (figure courtesy of KAERI)

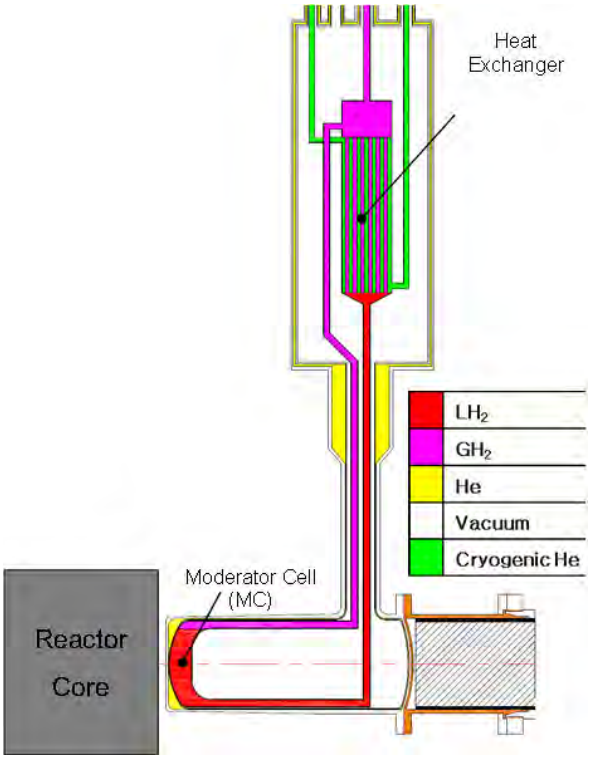

Figure 3 Schematic view of cold neutron source in pool assembly (figure courtesy of KAERI)

An important safety feature of the CNS is a triple barrier for the cold hydrogen loop. The aluminium moderator cell is surrounded by a vacuum layer that is surrounded by a helium gas system. The pressure of the helium gas blanket will be monitored as a means of leak detection.

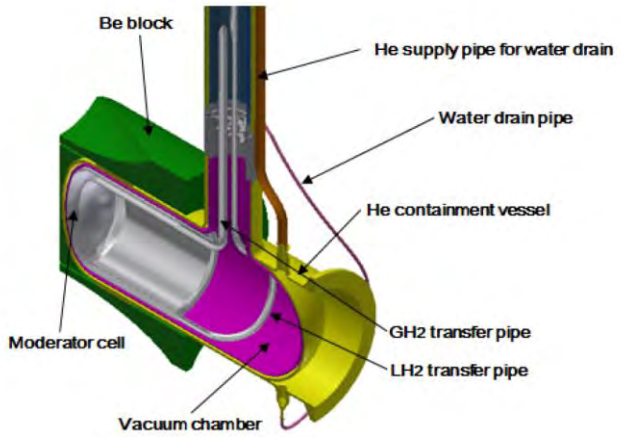

Figure 4 CNS moderator cell (figure courtesy of KAERI)

A beryllium block will placed around the moderator cell. This material acts as a neutron reflector and helps to optimize and orient the cold neutron flux along beamtube R2 towards our experimental hall. The helium hydrogen heat exchanger will be placed in the reactor pool (under water). The hydrogen systems including the hydrogen buffer tank will be placed inside the reactor hall.

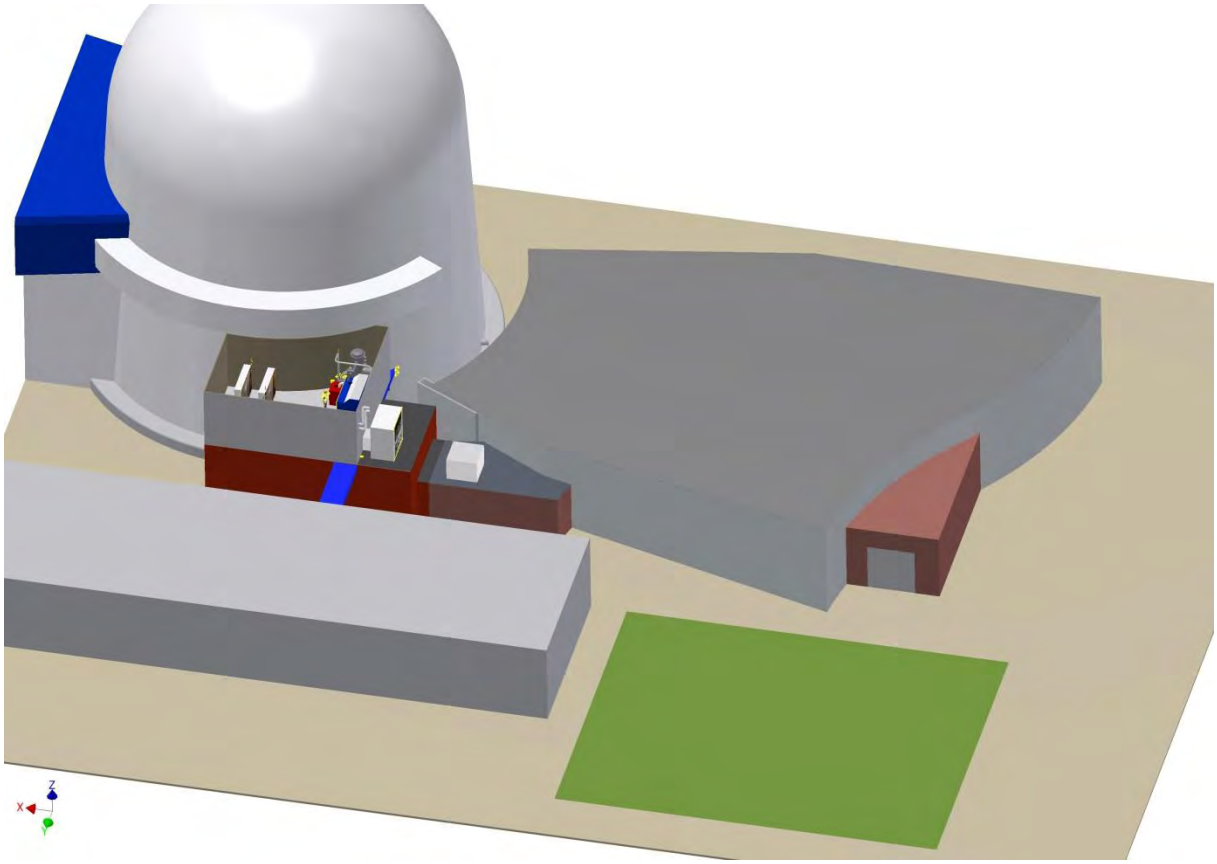

Figure 5 Reactor hall, CNS utilities building, experimental hall

A utilities building housing the other CNS support systems: helium cooling machines, helium buffer tank and vacuum support systems will be built directly next to the reactor hall. This location is necessary in order to minimize transport losses and heat-in-leak since there is insufficient space in the reactor hall.

8. New experimental facilities

During the OYSTER period we aim to realize improvements to existing instruments as well as installing new instruments.

- ROG – upgrade and relocation of the time-of-flight neutron reflectometer to a cold beam line
- PEARL – a new neutron powder diffractometer that is expected to become operational in 2015.
- SANS – relocation, installation and testing of small-angle neutron scattering instrument obtained from Helmholtz-Zentrum Geesthacht, Germany
- SESANS – upgrade of spin-echo labelled SANS, a unique Delft instrument
- FISH – a new multi-purpose neutron imaging facility
- NDP – neutron depth profiling spectrometer
- POSH – intense positron beam
- PALS – positron annihilation lifetime spectroscopy, using positrons from POSH
- 2D-ACAR – upgrade of thin-film 2-dimensional angular correlation of annihilation radiation spectrometer, using positrons by POSH
- Mossbauer spectroscopy – a new in beam Mossbauer facility

9. Irradiation Facilities

The irradiation facilities of the RID reactor allow materials to be irradiated with neutrons or other types of radiation in a well-controlled environment. They are used for research on and with radionuclides and for analytical purposes such as Neutron Activation Analysis (NAA). For each specific purpose there is a dedicated irradiation facility. Optimal irradiation conditions can be selected (e.g. samples shielded from γ-rays, cooled, irradiated by thermal or epithermal neutrons, short- or long irradiations), mostly depending on characteristics such as the radionuclide of interest and the nuclear reactions required. The irradiation facilities will mostly benefit health related research at the institute. Examples include the research in to novel production methods of radionuclides such as holmium-166 microspheres [8] and alternative production methods of molybdenum-99 [9]. Details of the new irradiation facilities are not yet available, since the near-core and in-core facilities depend on the layout of the definitive cold source design.

10. Conclusion

After realization of the cold neutron source in 2018 the Reactor Institute Delft will have an excellent infrastructure to serve as international research centre for neutron and radiation related research. The renewed nuclear operations license will be based on state of the art analyses. The decommissioning plan will be updated to include all changes to the reactor. The cold neutron source, new instruments and irradiation facilities will benefit users from the scientific community in health, materials and energy research. The expected gain in cold neutron flux will enable experiments and research at the Delft reactor which previously required access to an international higher flux reactor. Through OYSTER the Reactor Institute Delft is better equipped to participate in large national and international research collaborations

11. References

[1] Reactor Institute Delft, Delft University of Technology, http://www.rid.tudelft.nl

[2] Radiation Science and Technology, Delft University of Technology, http://www.tnw.tudelft.nl/over-faculteit/afdelingen/radiation-science-technology/

[3] IAEA collaborating centres Europe, http://www-naweb.iaea.org/na/cc-europe.html

[4] Press release Dutch ministry of Education, Culture and Science http://www.rijksoverheid.nl/ministeries/ocw/nieuws/2012/01/20/forse-investering-in-toponderzoek-tu-delft.html

[5] The European Spallation Source (ESS), http://europeanspallationsource.se/

[6] EXPLANATORY NOTE – COMPETITIVE DIALOGUE – CLASSIC DIRECTIVE, European Commission, Directorate General Internal Market and Services http://ec.europa.eu/internal_market/publicprocurement/docs/explan-notes/classic-dir-dialogue_en.pdf

[7] Safety Assessment for Research Reactors and Preparation of the Safety Analysis Report, IAEA SSG-20, 2012

[8] Thijssen, L, Schaart, DR , De Vries, DJ, Morgenstern, A, Bruchertseifer, F & Denkova, AG (2012). Polymersomes as nano-carriers to retain harmful recoil nuclides in alpha radionuclide therapy: a feasibility study. *Radiochimica Acta: international journal for chemical aspects of nuclear science and technology, 100*, 473-481.

[9] Wolterbeek, HT , Kloosterman, JL , Lathouwers, D , Rohde, M, Winkelman, A, Frima, L & Wols, F (2014). What is wise in the production of 99Mo? A comparison of eight possible production routes. *Journal of Radioanalytical and Nuclear Chemistry: an international journal dealing with all aspects and applications of nuclear chemistry, 302-2*, 773-779.

THE JULES HOROWITZ REACTOR: A NEW HIGH PERFORMANCE MTR (MATERIAL TESTING REACTOR) WORKING AS AN INTERNATIONAL USER FACILITY IN SUPPORT TO NUCLEAR INDUSTRY, PUBLIC BODIES AND RESEARCH INSTITUTES

J.ESTRADE; G. BIGNAN; X.BRAVO
French Atomic Energy and Alternatives Energies Commission
Cadarache and Saclay Research Centres
France

Corresponding author: Jerome.estrade@cea.fr

ABSTRACT

The Jules Horowitz Reactor (JHR) is a new Material Testing Reactor (MTR) currently under construction at CEA Cadarache research center in the south of France. It will represent a major research infrastructure for scientific studies dealing with material and fuel behavior under irradiation (and is consequently identified for this purpose within various European road maps and forums; ESFRI, SNETP…). The reactor will also contribute to medical Isotope production.
The reactor will perform R&D programs for the optimization of the present generation of Nuclear Power Plans (NPPs), support the development of the next generation of NPPs (mainly LWRs) and also offer irradiation capabilities for future reactor materials and fuels.
JHR is fully optimized for testing material and fuel under irradiation, in normal and non-normal conditions:

- with modern irradiation loops producing the operational condition of the different power reactor technologies,
- with major innovative embarked in-pile instrumentation and out-pile analysis to perform high-quality R&D experiments,
- with high thermal and fast flux capacity to address existing and future NPP needs.

JHR is designed, built and will be operated as an international user-facility open to international collaboration. This results in several aspects:

- a partnership with the funding organizations gathered within an international consortium,
- setting-up of an international scientific community around JHR through seminars, working groups to optimize the experimental capacity versus future R&D needs.
- preparation of the first JHR International Program potentially open to non-members of the JHR consortium.

It will answer needs expressed by the scientific community (R&D institutes, TSO…) and the industrial companies (utilities, fuel vendors…).
Consequently, the JHR facility will become a major scientific hub for cutting edge research and material investigations (multilateral support to complete cost effective studies avoiding fragmentation of scientific effort, access to developing countries to such state of the art research reactor facilities, supra national approach….).
This paper gives an up-to-date status of the construction and of the developments performed to build the future experimental capacity and also provides focus on proposed operating rules of JHR as an International user facility on research reactors.

1. Introduction

European Material Testing Reactors (MTR) have provided an essential support for nuclear power programs over the last 50 years within the European Community.

However, the large majority of these Material Test Reactors (MTRs) will be more than 50 years old this decade, leading to the increasing probability of some shutdowns for various reasons (life-limiting factors, heavy maintenance constraints, possible new regulatory requirements…). Such a situation cannot be sustained in the long term [1].
On the other hand, associated with hot laboratories for the post irradiation examinations, MTRs remain key structuring research facilities for the European Research Area in the field of nuclear fission energy.
MTRs address the development and the qualification of materials and fuels under irradiation with sizes and environment conditions relevant for nuclear power plants in order to optimize and demonstrate safe operations of existing power reactors as well as to support future reactor design:

- Nuclear plants will follow a long-term trend driven by the plant life extension and management, reinforcement of the safety, waste and resource management, flexibility and economic improvement.
- In parallel to extending performance and safety for existing and power plants to come, R&D programs are taking place in order to assess and develop new reactor concepts (Generation IV reactors) that meet sustainability purposes.
- In addition, for most European countries, keeping competences alive is a strategic cross-cutting issue; developing and operating a new and up-to-date research reactor appears to be an effective way to train a new generation of scientists and engineers.

This analysis was already made by a thematic network of Euratom 5th FP, involving experts and industry representatives, in order to answer the question from the European Commission on the need for a new Material Testing Reactor (MTR) in Europe [2].
Consequently, and in its specific position of new MTR under construction in Europe, the JHR research infrastructure has been identified on the ESFRI Roadmap since 2008.

2. Highlights of the JHR project

JHR will offer modern irradiation experimental capabilities to study material & fuel behavior under irradiation. JHR will be a flexible experimental infrastructure to meet industrial and public needs within the European Union related to present and future Nuclear Power Reactors.
JHR is designed to provide high neutron flux (notably twice as large as the maximum available today in the currently operating French MTR OSIRIS, and at the best standards worldwide), to run highly instrumented experiments, to support advanced modelling giving prediction beyond experimental points, and to operate experimental devices giving environment conditions (pressure, temperature, flux, coolant chemistry, …) relevant for water power reactors (PWRs, BWRs, VVERs), but also in support of non-water reactors R&D (Sodium cooled fast reactors…).
These objectives require representative tests of structural materials and fuel components as well as in-depth investigations with “separate effects” experiments coupled with advanced modelling.
For example, the JHR design accommodates improved on-line monitoring capabilities such as a fission product laboratory directly coupled to the experimental fuel sample under irradiation.
As a modern research infrastructure, JHR will contribute to the development of expertise and know-how, and to the training of the next generation of scientists and operators with a positive impact on nuclear safety, competitiveness and social acceptance. The JHR is designed mainly to meet these technical objectives.
As an associated objective, the JHR will also contribute to secure the production of radioisotopes for medical applications.

JHR, as a future international User Facility, is funded and steered by an international consortium gathering industry (Utilities, fuel vendors…) and public bodies (R&D centers, TSO, Regulator…). The generic model of JHR consortium is the following:

- CEA remains the owner and the nuclear operator of the nuclear facility with all liabilities,

- JHR Consortium Members are the owners of Guaranteed Access Rights to the experimental capacities in proportion to their financial commitment to the construction and with a proportional voting right in the Consortium Governing Board,
- A Member can use totally or partly his access rights for implementing proprietary programs with full property of results and/or for participating to the Joint International Programs open to non-members
- JHR consortium membership is open to new members until completion of the reactor.

CEA is encouraged by the consortium to enlarge JHR membership and, as of mid-2014, the present members list of JHR consortium is the following:
CEA (France), EDF (France), AREVA (France), European Commission-JRC, SCK-CEN (Belgium), UJV (Czech Republic), VTT(Finland), CIEMAT(Spain), Vattenfall (Sweden), DAE(India), IAEC (Israel), NNL (UK).
There also exists an implementing agreement between CEA and JAEA (Japan) with a view to access to JHR.

A more extensive and in-depth JHR facility description including development of the first experimental capacity can be found in the proceedings and presentations of recent RRFM and IGORR conferences (see for examples ref [3], [4], [5] and [6]).

3. JHR general description

As a short description, the JHR layout is as follows:

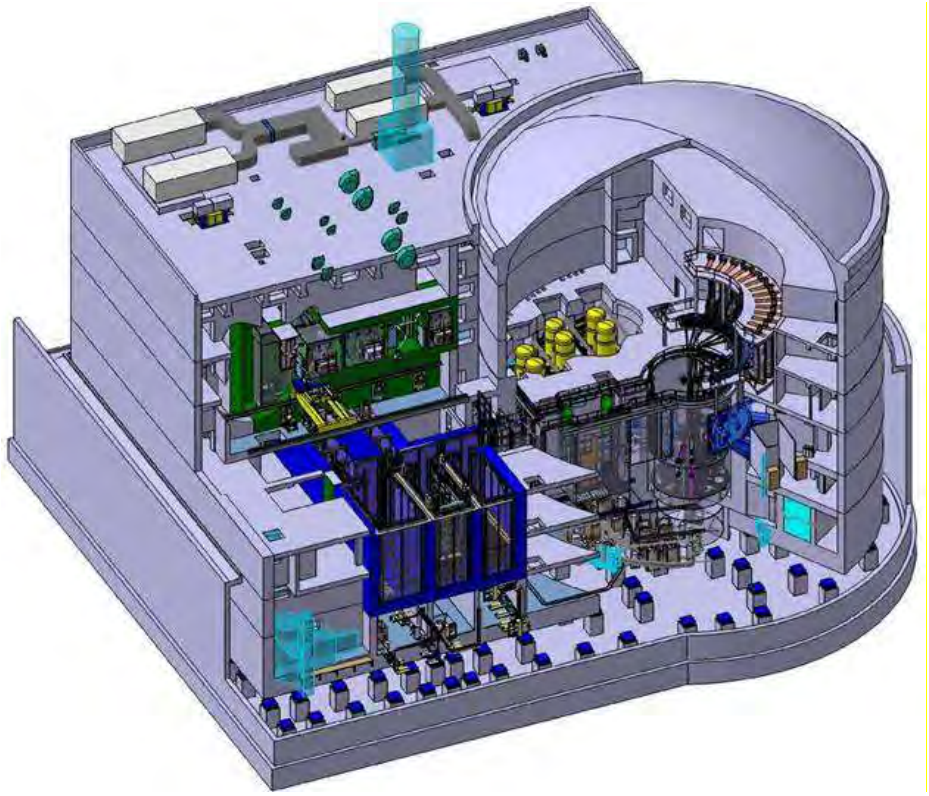

The nuclear unit of JHR consists in a reactor building and a nuclear auxiliary building.
The reactor building is made in pre-constraint concrete with a diameter of 37 m. The nuclear auxiliary building consists in 3 storage pools for spent fuels, irradiated experimental devices and in 4 hot cells for preparation, conditioning of experiments and non-destructive examinations on irradiated samples. A transfer channel between the reactor building and the nuclear auxiliary building allows the underwater transfer of spent fuels and experimental devices between the two buildings.

In support to the nuclear island, one can quote the following:

- 1 support building for cooling
- 1 support building for the fluids and ventilation
- 2 emergency diesel generators buildings
- 1 building for assembly and test of experimental devices before entering the nuclear island (“cold workshop”)

4. JHR update status

Construction is currently under progress at CEA Cadarache Centre. Engineering studies were devoted to AREVA group subsidiary AREVA-TA, which ensures the supervision of the construction site, and which is also in charge of providing key reactor components. More than twenty other suppliers in the fields of civil works, mechanics, heating, ventilation, air-conditioning, electric components… contribute to the construction of the facility.

Some illustrations of undergoing construction activities are hereby provided.

December 2013: Reactor dome installation

April 2014: Reactor pool internal structures

General view of Reactor Building and Auxiliary unit building (Fall-2014)

Figure 1: some views of the building site

Regarding the construction work currently underway, apart from anticipated work (civil works, cranes, manufacturing of the main reactor pumps), the main electro-mechanical contracts were started from year 2011 on.

Current status on construction site is more than 80% progress of civil works and increasing contribution of electro-mechanical tasks is going-on (recent highlights: polar crane tests and installation of the support structure for the pools liner).

Next important milestones will be the installation of main circuits components (for the reactor building), and the completion of the hot cells complex structure (for the nuclear auxiliaries building).

Operation of the new JHR facility is planned for the end of the decade.

5. JHR Safety

As a new-built facility, JHR incorporates safety analysis right from the design phase, based on a modern reference system and methodologies; these can be related to those used in contemporary projects such as the EPR GEN3 NPPs under construction, but adapted to the characteristics and situation of a research reactor project.
The JHR Safety approach was presented in detail at the IAEA General Conference on Research Reactors in Rabat last November 2011.Some examples of incorporating safety from the design phase can be found in reference [7].
Following the Fukushima-Daichi Accident (March 2011), the French Regulator (Autorité de Sûreté Nucléaire-ASN) also asked CEA to perform complementary safety assessments to meet objectives under extreme situations exceeding licensing basis (with focus on “cliff-edge” effect prevention).
The complementary safety assessments basically confirmed the sound design bases of the newly built JHR. A few selected needs for extra equipment were also identified, and, as an answer to French nuclear regulator requirements, CEA proposed a set of “hardened core” measures including for example:

- an ultimate recirculation pump on the reactor main cooling circuit
- pipes and valves for ultimate pool water supply from outside the containment building,
- ultimate valve actuation on some ventilation lines
- dedicated sensors to independently measure pressure and radio-activity level in the containment building,
- specific ultimate power set for the above-mentioned equipments.

This set of “hardened core” measures was assessed by the technical support of the French Regulator (ASN) and reviewed in April 2013 by its standing advisory committee.

6. Developing a modern experimental capacity

JHR is designed as a High Performance MTR (thermal power up to 100 MW) with the capacity to perform about 20 experiments at the same time. Characteristics (at full 100 MW capacity) are as follows:

- thermal neutrons flux in reflector: up to 5.5 E14 n/cm².s
- fast neutron flux in the core: up to 5.5 E14 n/cm².s for E > 1 MeV and/or up to 5 E15 n/cm².s for E> 0.1 MeV
- material ageing: up to 16 dpa/y
- 6 displacement systems to adjust fissile power and perform power transients

- power transients for fuel limit to clad failure studies: up to 600 W/cm.

At nominal operation JHR is to operate with 10 cycles a year (representing about 260 EFPD-Equivalent Full Power Days)

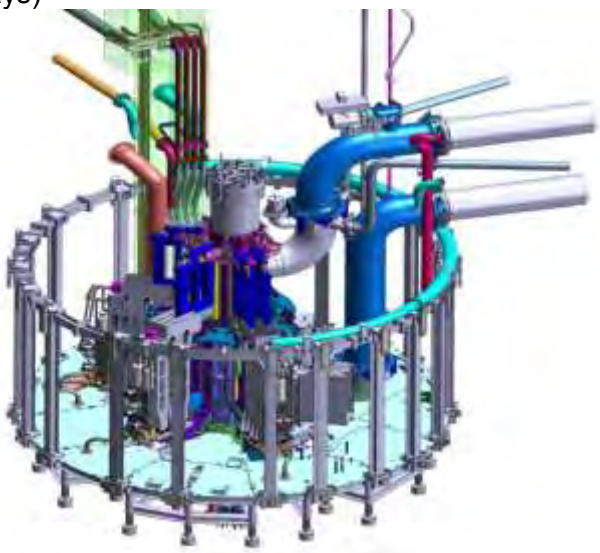

Figure 2: schematic view of JHR core and reflector where will be located experimental loops

CEA with its partners is preparing the first experimental capacities by developing some modern experimental devices for fuel and material behavior studies under irradiation such as the following:

- the MADISON loop (*in relationship with HRP-Halden*) for fuel investigation under normal situation (for PWR,BWR and VVER conditions): the ADELINE loop for power transient studies allowing clad failure for up-to-limit situations (*with support from EDF*):
- the LORELEI loop for safety LOCA (Loss Of Coolant Accident) studies for accidental scenarios (*in collaboration with IAEC-Israel*): the MICA capsules-CALIPSO loop for material investigation under high fast neutron flux and high dpa rate:
- the MELODIE device for on-line bi-axial constraint analysis on material (*in collaboration with VTT-Finland*):
- the CLOE loop for material corrosion studies under constraint (*in collaboration with DAE India*):

Apart from MICA capsules (under design optimization phase), other devices have entered or are well into detailed design phase with an objective to go for manufacturing beyond detailed design.

The MELODIE device has already been manufactured and will undergo qualification tests in OSIRIS MTR by 2015.

Compared to the existing experimental capacities worldwide, a great effort is ongoing to improve the performance of such loops and to develop new devices with innovative concepts by:

- better monitoring and follow-up of the irradiation conditions,
- having a lot of on-line instrumentation to address key parameters (fast and thermal neutron fluxes, gamma heating, temperature, fission gas release for fuel investigation, material elongation…),

- having up-to-date post-irradiation exams either directly within JHR nuclear building (for non-destructive assay) or in Cadarache Hot Laboratory (for NDA and DA) or in Consortium Members Hot Laboratory.

7. JHR as an International User-Facility through International Joint Programs and /or Academic Support

Parallel to the construction of the reactor, the preparation of an international community around JHR is continuing. This is an important topic because, as already indicated, building and gathering a strong international community in support to MTR experiments is a key-issue for the R&D in nuclear energy field.

Building international joint programs: According to the consortium agreement, JHR is aimed to become a user reactor at international level (cf achievements of the OECD/Halden Reactor Project) with multinational project and proprietary experiments. As anticipated preparatory actions, the JHR consortium has set-up a yearly scientific seminar and three working groups (Fuel, Material and Technology) to identify R&D topics of common interests and to prepare the first international joint programs addressing fuel and material issues that are key for operating plants and future NPP (mainly focused on LWR).

This yearly seminar (the 4th seminar was held last April 2014)-gathering about 80 participants- is a unique opportunity for the future end-users to share and discuss progress on the latest developments on JHR experimental capacities. The main outputs of such seminars allows to identify scientific needs leading to proposal of future R&D programs with precise requirements regarding the management of irradiation conditions and the performances associated to the instrumentation of the experimental devices.
The priorities given by the participants for future programs (Fuel behavior investigation under normal, incidental and accidental conditions –Material behavior such as Reactor Pressure Vessel, Internals studies under irradiation) give confidence on the well-designed experimental capacity described above in §5.

Academic opportunities / training

The JHR experiment team at Cadarache is already welcoming scientists, engineers (called Secondees) from various organizations/institutes who are integrated within the team for a limited period of time (typically one year) for various topics such as physics studies for the development of the experimental devices (neutron physic, thermo-hydraulic…) and/or for support to the future operator (Safety Analysis, I-C&C…).
This Secondment program is an important topic for countries willing to invest in nuclear technology helping them to create and sustain key competences.

In fact, between the academic training and the “commercial training linked to a product” there is a need to set up a framework for nuclear education “in the field” using modern High-Performance infrastructures dedicated to the training of future senior scientists, engineers…for the benefit of decision-makers in countries wishing to develop nuclear energy. The JHR Secondee Program is giving nuclear education “in the field” that offers direct experience of working in nuclear facilities and provides training opportunities that fill the gap between academic education and commercial-product specific training. This is fully compliant with the recent IAEA initiative on establishing labialized ICERR

(International Centre based on Research Reactors) in order to rationalize the research reactors fleet worldwide and to harmonize Operation and Safety.

8 Conclusions

The JHR construction is continuing, in accordance with plan to start operation by the end of this decade. Beyond construction activity, the facility – especially regarding the experimental capacity – is already open (and will be more and more so in the future) to international collaboration: As some examples we can quote some outputs of the working groups who identified R&D topics of common interest such as:

- LWR fuel testing up to limits and in incidental conditions (fuel element thermal-mechanical behavior, fuel to cladding chemical interaction, fission gas and volatile fission products release and associated source term, transient swelling)
- Dose accumulation in low alloyed steels for reactor pressure vessel and new cladding studies for accident tolerance.

Typically, such R&D programs could be managed through international joint programs open to non-Members of the JHR consortium.

To summarize, JHR prepares to be a key infrastructure in the European and International Research Area for R&D in support to the use of nuclear energy during this century.

References

[1] The Green Paper, “Towards a European Energy Security Strategy”, published by the European Commission in November 2000

[2] FEUNMARR, Future European Union Needs in Material Research Reactors, 5th FP thematic network, Nov. 2001 – Oct 2002

[3] “The Jules Horowitz Reactor Project: a new High Performances European and international Material Testing Reactor for the 21st century”- G. Bignan, D.Iracane
Nuclear Energy International publication (NEI-Dec 2008)

[4] “Sustaining Material Testing Capacity in France: From OSIRIS to JHR”
G. Bignan, D. Iracane, S. Loubière, C. Blandin CEA (France) IGORR 2009 Conference (Beijing)

[5] “The Jules Horowitz Reactor: A new European MTR open to International collaboration” Gilles Bignan et al, IGORR 2010 (Knoxville TN –ORNL- September 2010)

[6] “The Jules Horowitz Reactor: A new European MTR (Material Testing Reactor) open to International collaboration: Description and Status”
G.Bignan, J.Estrade –IGORR 2013 –Daejeong Korea (October 2013)

[7] The Jules Horowitz Reactor: A new European MTR (Material Testing Reactor) open to International collaboration: Update Description and focus on the modern safety approach.
G. Bignan et al –IAEA International Conference on Research Reactors: Safe Management and Effective Utilization (Rabat- November 2011)

THE TUNISIAN SUBCRITICAL ASSEMBLY PROJECT: PRELIMINARY MONTE CARLO RESULTS OF A FIRST PROPOSAL CORE DESIGN

W. DRIDI, I. ROMDHANI AND A. BEN ISMAÏL

National Center of Nuclear Sciences and Technology, Sidi-Thabet Technopark 2020 Ariana Tunisia.

ABSTRACT

The National Center of Nuclear Sciences and Technology of Tunisia has decided to build a subcritical assembly as its first nuclear facility, in order to strengthen its technical capabilities with a facility that is dedicated for education, training, and research in the field of nuclear reactor physics.
The subcritical assembly will be extremely useful for carrying out research projects in order to provide scientists with a basic understanding of the main concepts relevant to nuclear reactors. Studies related to site selection and technical characteristics of the facility are currently in progress and almost finalized.
The Tunisian subcritical assembly will be uranium fueled, light water moderated, and reflected. The reactor will be driven by a plutonium-beryllium or americium-beryllium neutron source. The core consists of few hundred of LEU fuel rods, loaded into a water-filled vessel in a square lattice. Fuel rods are based on PWR fuel structural pattern type, made of uranium dioxide (UO2) with less than 4wt% 235U enrichment in zirconium alloy (Zr-4) cladding.
Design and optimization were performed using the MCNP transport code [1]. The resulting computed effective multiplication factor (keff) was around 0.95.
This paper presents a first design proposal, modeling, and core analysis (neutron flux distributions and multiplication factor) of the assembly.
We will also present the current status of the project aiming to implement a subcritical assembly in CNSTN.

1. Introduction

The implementation of the Tunisian subcritical assembly is considered as one of the basic steps for the Tunisian's efforts to develop national nuclear infrastructure and to introduce nuclear power as part of its energy mix. Tunisia announced its intention to pursue a nuclear power program joining more than 60 newcomer countries that expressed their interest or declared their intention to develop a nuclear power program for the first time.

In the absence of reactors or any other nuclear facility essential for education, training, and experimental research of its engineering students, Tunisia chose to implement a subcritical reactor as its first nuclear facility. The subcritical reactor will be the main experimental laboratory in order to provide students a hands-on experience in nuclear reactor engineering fundamentals.

The project of implementing the Tunisian subcritical assembly started in 2012. The project studies are currently focused on the finalization of the feasibility study and the bidding

specifications. The design, construction and commissioning phases of the project are expected for the next two years (2016-2017) [2].
This paper presents an overview of the study results already achieved under this Tunisia's first nuclear facility project.
The aim of this study is to perform (as a first step of a main project), Monte Carlo validations and calculations for particular cases of subcritical assemblies that already exist in the world. Some notable cases of subcritical assemblies of subcritical assemblies are today operating in Delft University [3], Pavia University [4] and JUST University [5]. Validating our Monte Carlo model by using, as a reference, one of these facilities is a very important step to design our future assembly.

2. Motivation

Low cost and short construction time in addition to the relative simplicity and accessibility were the main driving force for the design and construction of the subcritical assembly, thus providing timely training for students.

The reactor simple construction (fuel and moderator) in an open tank makes it, one of the most effective tools for educating and training nuclear engineering students, allowing them to change core configuration, work very close to reactor core, observe and see every part of the reactor, and obtain a clear physical picture of the basic features of a reactor in a way that is impossible in power or research reactors.

The inherently safe subcritical design enables nuclear engineering students to gain first-hand practical experience on the applied physics of the fission process and of a nuclear reactor, neutron balance, with minimal training and radiation exposure and without any risk of criticality accident.

3. Facility description

The Subcritical Assembly is low enriched uranium fueled, light water moderated and reflected, small nuclear reactor facility, designed for the purpose of education, training, and experimental research.
The assembly is designed to never reach criticality; while being capable of sustaining nuclear chain reaction in the presence of an extraneous neutron source generally driven by a pneumatic control drive. Criticality safety is maintained at all times by its design with a large reactivity margin compared to a critical system and is verified by performing criticality calculations and core analysis, making it inherently safe to be operated by students and trainees. Parts of the subcritical assembly are easily accessible for demonstration, inspection, and experimental purposes.

3.1. Design Criteria [6]

The projected design criteria of the Tunisian Subcritical Assembly are as follows :

(1) Effective multiplication factor (Keff) less or equal to 0.90.
(2) Fuel enrichment less than 4% wt ^{235}U.
(3) Neutron emission rate higher than 1×10^{6} n/s, for the neutron source made with plutonium-beryllium (Pu-Be) or americium-beryllium (Am-Be).

4. Description of Model configuration

4. 1 Experiment Tank

The reactor Tank or vessel is made with stainless steel, 1.2 m outer diameter and 1.3 m height. The thickness of the tank is 20 cm.

4.2 Fuel Rods and Support Plate

The reactor core consists of 313 LEU fuel rods, loaded into a water-filled vessel in a square lattice expanding 20 cm in radius and 55 cm in height.

The fuel rods are positioned in the reactor core by two grids that hold the rods in place. The upper grid plate is made of acrylic Plexiglas and the lower grid plate is made of aluminum alloy. The grid is 70 cm in diameter and is fixed to the reactor vessel with joint poles. The support plate was penetrated by a few holes 1.2 cm in diameter for control and safety rods. The number of these holes varied for different lattice pitches and temperatures.

4.3 Neutron Source

We have chosen in our design an extraneous neutron source; a plutonium beryllium (Pu-Be) source was selected because of its long half-life, high neutron yield, and low gamma-ray intensity. The Pu-Be source has an activity of 0.8 Ci and a neutron intensity of 1.1×10^6 n/s.

The figure 1 presents the energy spectrum of the neutron source.

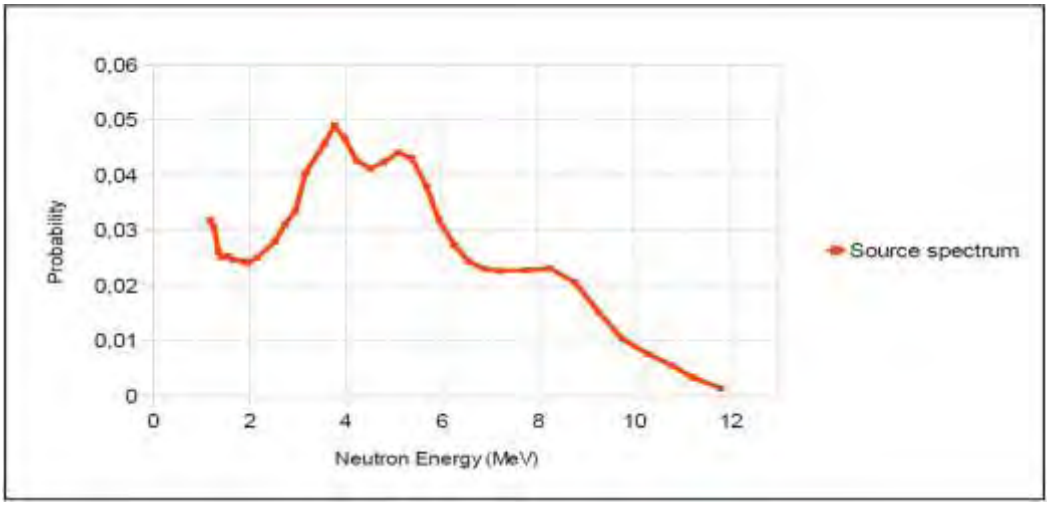

Figure 1: Normalized Plutonium-Beryllium Neutron source energy Spectrum [7]

4.4 Water Moderator / Reflector

The water in the vessel is high deionized distilled light water, which serves both as a moderator and reflector.
The reactor vessel is enveloping the nuclear core with a water layer of as shown in the *x-z* view of the reactor in Figure 3. The top water surface for the assembly was always no less than 20 cm above the top of the fuel region of the rods. The top water surface was always 30 cm above the fuel. The thickness of the bottom water reflector is about 42 cm.

The thick water layer not only serves as a reflector that scatters neutrons back into the reactor core but also as an effective shielding against neutrons leaking out of the system, thus reducing radiation around the reactor; in fact the calculated escape probability of any neutron is found to be less than 0.1%.

5. Descriptions of Material Data [8]

5.1 UO2 Fuel rods

There are 313 fuel rods of PWR fuel structural pattern type. These certificates give the weight of uranium dioxide, weight of uranium, and its enrichment. For pellet fabrication, uranium of enrichments (3.4 wt.%) was used.

The average weight of uranium dioxide in the rod was determined by averaging of the data for all existing rods. It was found to be 216.173 g.
The average oxygen content of the uranium dioxide in approximately half of all fuel rods was equal to 12.27 wt.%

Table 1: The subcritical assembly design characteristics parameters.

Item	**Design parameter**
Total number of fuel rods	313
Fuel element height (mm)	550
Fuel element (including clad) D (mm)	10
UO_2 Fuel diameter (mm)	8.26
Active height (mm)	430
Number of pellets per element	43
Fuel material	UO_2
235U enrichment (wt%)	3.4
Cladding material	Zr-4

Five insulator pellets made of aluminum trioxide are added to the fuel rod: four below the fuel pellets and one above the fuel pellets that is held down by a spring; the fuel rod is plugged at both ends with upper and lower caps. Atom densities of isotopes in the fuel rod materials are listed in Table 2.

Table 2: Uranium dioxide Composition.

Element	Wt (%)	Atom mass g/mol	Atom Density $(barn\text{-}cm)^{-1}$
U235	3.4	235.043	8.06236E-04
U234	0.054	234.04	1.2859E-06
U238	96.5946	238.05	2.26159E-02
O	-	15.99943	4.6847 E-02
Total			7.02704219E-02

Density is 10.5 g/cm^3

5.2 Zirconium alloy

The fuel rod can was made of zirconium alloy 110. Its composition is given in Table 3.

The cladding tube is made of zirconium alloy (Zr-4). Fuel specifications and design parameters are listed in Table 1.

Table 3: Zirconium Alloy Composition.

Element	wt (%)	Atom mass g/mol	Atom Density (barn-cm)$^{-1}$
Zirconium	98.23	91.2242	4.254E-02
Tin	0.45	118.7107	4.825E-04
Chromium	0.1	51.99616	7.5975E-05
Iron	0.21	55.8452	1.4855E-04
Hafnium	0.01	178.492	2.2132E-06

Density is 6.56 g/cm^3

5.3 Stainless Steel

The support plate, both lattice plates, and upper plate were fabricated from stainless steel *SSS 304 L*. The composition of this steel is presented in Table 4.

Table 4: Stainless Steel Composition.

Element	wt(%)	Atom mass (g/mol)	Atom density (barn-cm)$^{-1}$
Manganese	2 %	54.9380499	1.76E-03
Nickel,	10 %	58.69342	8.2388E-03
Chromium	18 %	51.99616	1.674E-02
Iron	70 %	55.8452	6.06E-02

Density is 8.03 g/cm^3

6. Modeling and Optimization

Calculational model consist of square-pitched zirconium-clad fuel rods immersed in water.

This facility was modeled based on actual design parameters. Criticality and reactor physics calculations are performed using the MCNP5 Monte Carlo code [1], which has been verified and approved by the nuclear community worldwide. The MCNP-5 code is based on pure transport theory.

The simulation model of the assembly uses continuous energy neutron ENDF/B-VI cross section data libraries and was developed as a nuclear analysis computational tool to calculate nuclear parameters and verify the design using the most recent version of MCNP5 version 1.51. The reactor model as shown in the *x-z* view of the reactor in Figure 2.

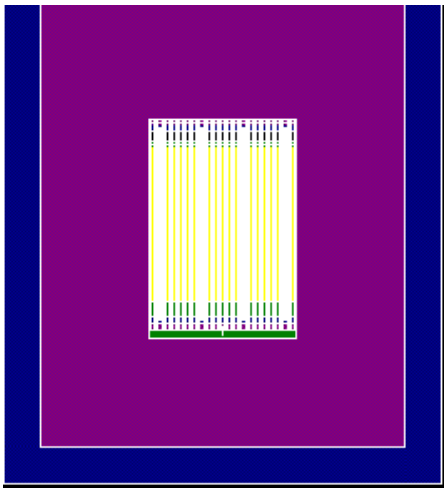

Figure 2: MCNP modeling *x-z* view of the reactor, showing the core in the water filled vessel.

The MCNP code explicitly models the fuel pellets, clad, fuel elements loading arrangement, grid plates, water moderator/reflector, and the vessel tank; an *x-y* view of the reactor core at mid-plane, showing fuel rods (blue) arrangement surrounded by the water (purple) moderator/reflector, is shown in Figure 3.

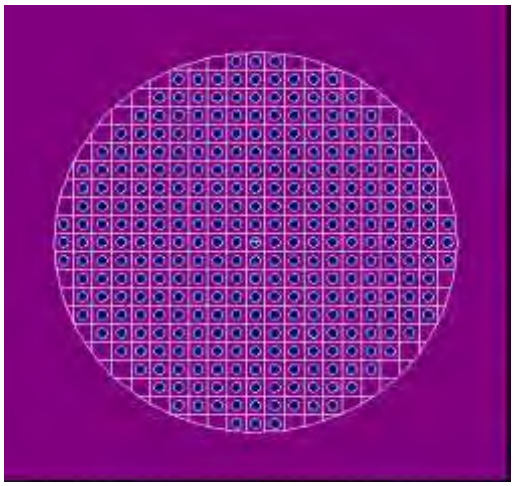

Figure 3: MCNP modeling *x-y* view of the reactor at mid-plane, showing fuel rods (blue) arrangement surrounded by water (green) moderator/reflector.

6.1. Optimum Moderator to Fuel Ratio

The assembly is designed with the optimum moderator to fuel ratio, so that the reactor is operated in the best moderated condition. Fuel loading pattern with the optimum moderator-to fuel ratio was obtained using MCNP5 code; the effective multiplication factor as a function of the lattice pitch was calculated and is shown in Figure 4. The optimum value of 19.1 mm is chosen for the fuel lattice pitch.

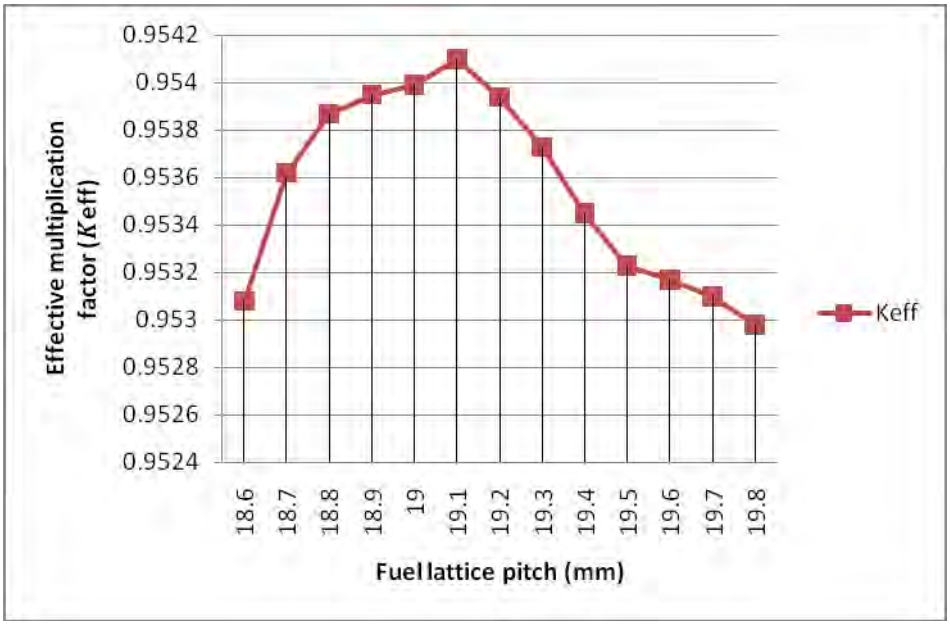

Figure 4: The effective multiplication factor (Keff) versus fuel pitch.

6.2. Criticality Calculations

Criticality calculations were performed using Monte Carlo code MCNP5 version 1.51 [1] and the nuclear data library ENDF/BVI; the code was installed and tested by running the MCNP criticality validation suite of 31 international benchmark experiments and comparing results.
The effective multiplication coefficient Keff was calculated by running a total of 550 cycles with 5000 neutrons per cycle, totaling 2,750,310 fission neutron source histories. The final estimated combined (collision/absorption/tracklength) Keff is 0.95410 ± 0.00049.
The average number of fission neutrons produced per neutron absorbed was calculated to be 0.9546. The majority of neutrons did not cause fission and were absorbed in capture reactions accounting for 60.85% of neutrons; only 39.04% of neutrons caused fission producing on average 2.442 neutrons per fission. 92.9% of all fissions were caused by thermal neutrons of energy <0.625 eV; criticality calculation results are listed in Table 5.

Table 5: Effective multiplication factor (Keff): Comparison between JUST and CNSTN results

K-code results (2.5 millions de particules histories) MCNP5	JUST	CNSTN
Effective multiplication factor (k_{eff})	0.95923 ± 4.4 10^{-4}	0.95410 ±4.9 10^{-4}
The average number of neutrons produced per fission	2.446	2.442
Prompt removal lifetime (sec.)	9.5452E-05	9.1880E-05
The average fission neutrons produced per neutron absorbed (capture + fission) in all cells with fission	1,7087	1.7080
The average fission neutrons produced per neutron absorbed (capture + fission) in all the geometry cells	0.9595	0.95463

The average neutron energy causing fission	---	8.7312E-05 eV
Percentage of fissions caused by neutrons in the thermal neutron range (<0.625 eV)	93.01%	92.89%
Percentage of fissions caused by neutrons in the intermediate neutron range 0.625 eV - 100 KeV	---	4.12%
Percentage of fissions caused by neutrons in the fast neutron range >100 KeV	---	2.99%
Fraction of Neutrons escape the reactor	0.08%	0.104%
Fraction of Neutrons captured	60.72%	60.853%
Fraction of Neutrons induced in fission	39.19%	39.044%

6.3 k_{eff} as function of ^{235}U enrichment

Some series of calculations were performed by changing the weight percentage of U235 and is presented in figure 5.

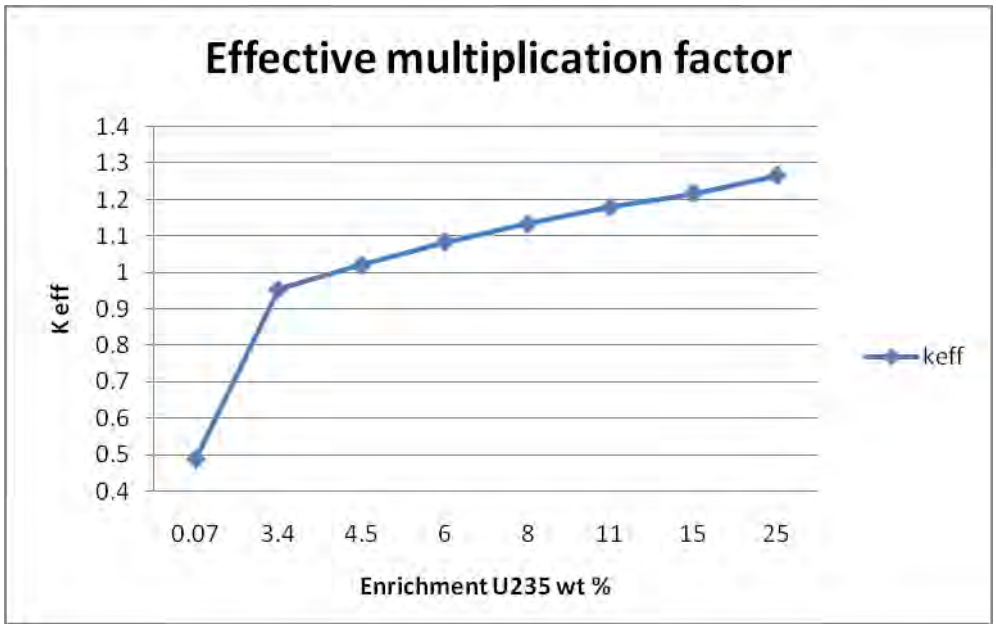

Figure 5: The effective multiplication factor (Keff) versus the enrichment

6.4 3D neutron flux distribution

Simulation results for the total average neutron flux (per neutron source) were like Gaussian function. The distribution is centered in the middle where the neutron source was placed in the bottom of the core. The 3D neutron flux distribution is presented in figure 6 [9].

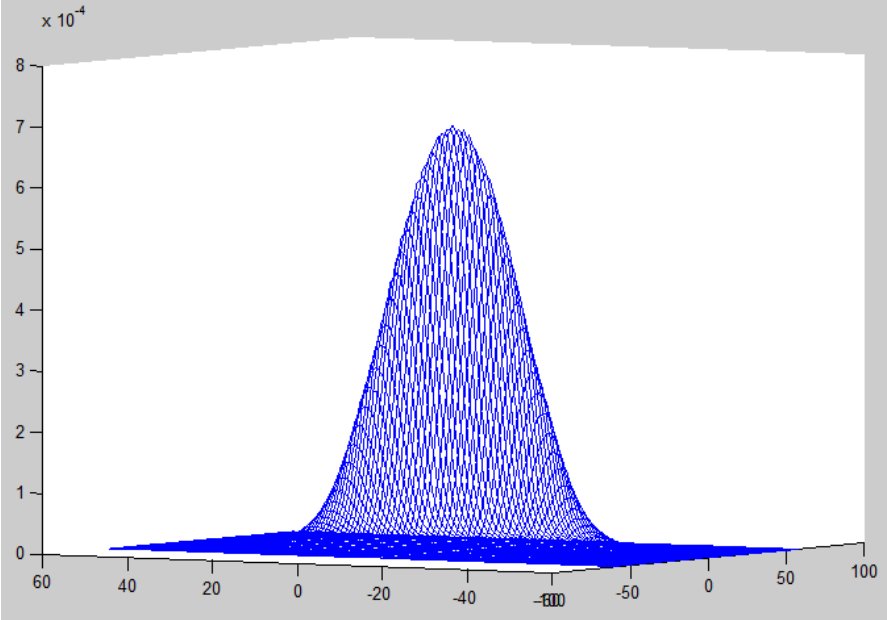

Figure 6: The total 3D neutron flux Distribution

7. Conclusions

Important efforts, regarding the installation of the subcritical assembly, which is the first facility with nuclear material in the country, continue to be exerted. As the subcritical assembly project is planned as a preparatory step for installation based on the IAEA safety standards and guidelines, in the development and implementation of this project, is applied.
The implementation of the subcritical assembly project will be conducted according to the IAEA safety standards and guidelines. However, a safety committee within CNSTN, independent from the project management, is being implemented, in order to perform independent safety reviews and assessments of the project phases and activities important to safety.
On the other hand, efforts are also exerted to ensure the technical criteria by some benchmarks models using Monte Carlo calculation like this study to reproducing the Jordan subcritical assembly.

Acknowledgments

This paper was developed under (TC Project TUN1009/02/01) ‘‘Installing a subcritical assembly in the National Centre for Nuclear Sciences and technology, for education and training in the field of reactor physics’’.

References

[1] X-5MONTE CARLO TEAM, “MCNP—a general Monte Carlo N-particle transport code, version 5”, LA-CP-03-0245, LANL, 2003.

[2] A. BEN ISMAÏL et al., “Research reactor projects in Tunisia: case of the Tunisian subcritical assembly project”, RRFM 2014, Slovenia.

[3] D. Alloni et al, “Neutron flux characterization of the SM1 sub-critical multiplying complex of the Pavia University” Progress in Nuclear Energy 67 (2013) 98-103.

[4] J.L. Kloosterman, “Description of the Delphi subcritical assembly at Delft University of Technology”. Delft, (2003).

[5] N. Xoubi, “Design, Development and Installation of Jordan Subcritical Assembly”, Hindawi Publishing Corporation Science and Technology of Nuclear Installations Volume 2013, Article ID 197502, 5 pages.

[6] IAEA technical consultancy meeting report, “on the review of the preparation of the technical requirements for the bidding process for a sub-critical assembly in Tunisia”, Vienna, 19-21 february 2014.

[7] M. Edwad Anderson and William H. Bond, Amsterdam, “Neutron Spectrum of a Plutonium-Beryllium source”, JR. Nuclear Physics; North-Holland Publishing Co, 43 (1963) 330-338.

[8] I. ROMDHANI, “Modélisation et simulation par le code Monte Carlo MCNP pour la détermination des paramètres neutroniques réacteur-assemblage nucléaire sous-critique au CNSTN”, Master thesis, Faculty of sciences of Tunis, University of Tunis El Manar/ CNSTN, 2014.

[9] W. DRIDI et al, “Neutron flux distribution in a Subcritical Assembly using MCNP Monte Carlo code”, the 11th National conference of Physics research, 20-23 December 2014. Sousse. Tunisia.

IAEA INTEGRATED RESEARCH REACTOR INFRASTRUCTURE ASSESSMENT (IRRIA) MISSION

A. BORIO DI TIGLIOLE[(1)]*, E. BRADLEY[(1)],
A. SHOKR[(2)], D. RIDIKAS[(3)],

(1) Research Reactor Section, NEFW-NE
(2) Research Reactor Safety Section, NSNI-NS
(3) Physics Section, NAPC-NA
International Atomic Energy Agency
Vienna International Centre, PO Box 100, Vienna, AUSTRIA

*Corresponding author: A.Borio@iaea.org

ABSTRACT

A research reactor project is a major undertaking that requires the development and implementation of an adequate national nuclear infrastructure. According to the IAEA Milestones approach for a research reactor project (IAEA Nuclear Energy Series No. NP-T-5.1), 19 infrastructure issues should be addressed in each phase of the project.

To develop a holistic approach for the evaluation of the status of the national nuclear infrastructure the IAEA is preparing a new publication with the title “Assessment of the National Nuclear Infrastructure to Support a New Research Reactor Project”. This publication is meant to be used by a Member State wishing to self-assess its own progress in the development of the national nuclear infrastructure and as a basis for an IAEA review service under development, namely the IAEA Integrated Research Reactor Infrastructure Assessment (IRRIA) mission.

The IRRIA mission will be coordinated and led by the IAEA (in the frame of the cross-cutting activities on research reactors) and conducted by a team of international experts who have experience in different aspects of developing and deploying relevant infrastructure for a research reactor project. The mission will provide Member State involved organizations with an opportunity to have in depth discussions with international experts about experiences, good practices and lessons learned in different countries. The results of the mission are expected to help the Member State to develop an Integrated Work Plan to address identified gaps, and implement actions to close them (with the assistance of the IAEA, if desired) which, in turn, will help with the development of the necessary national infrastructure to support a new RR project.

1. Introduction

A research reactor (RR) project is a major undertaking that requires the development and implementation of an adequate national nuclear infrastructure. According to the International Atomic Energy Agency (IAEA) Milestones approach for a RR project [1], 19 infrastructure issues should be addressed in each of the three phases of the project (pre-project phase, project formulation phase and project implementation phase). These infrastructure issues cross cut RR related activities managed across the IAEA by many Sections in the three technical Departments as well as the Department of Safeguards and the Office of Legal Affairs. Therefore, it is believed that Member States needs will be best

served through integrated and coordinated efforts supported by the different groups within the IAEA.

To develop a holistic approach for the evaluation of the status of the national nuclear infrastructure the IAEA is preparing a new publication with the title “Assessment of the National Nuclear Infrastructure to Support a New Research Reactor Project”. The main aims of the evaluation process are:

1) To allow all 19 infrastructure issues to be assessed in an equal and consistent manner;

2) To bring the results together in order to develop an Integrated Work Plan (IWP) for moving into a subsequent phase of the RR project;

3) To enhance national competence through participation in a detailed and comprehensive evaluation.

This publication is meant to be used by a Member State wishing to self-assess its own progress in the development of the national nuclear infrastructure and as a basis for an IAEA review service under development, namely the IAEA Integrated Research Reactor Infrastructure Assessment (IRRIA) mission (see §.3).

However, besides the IRRIA mission, a Member State is likely to request other already well-established and technical area-specific IAEA review services to assist on specific issues of infrastructure development. These specific-issue focused services are organized and delivered by the IAEA Departments, Divisions or Sections responsible for the particular issue and are not looking into the overall status of RR infrastructure.

The IAEA will also continue to provide assistance for human resources development of the Member States establishing their first RR, and to facilitate sharing experience and knowledge among Member States through its programmatic activities including expert mission services, technical meetings, training courses and workshops addressing relevant technical and safety topics.

2. Assessment of the national nuclear infrastructure to support a new research reactor project

To continue the process of facilitating the successful development of new RR projects, in conjunction with other IAEA existing standards, publications and services, the IAEA has developed a publication on “Assessment of the National Nuclear Infrastructure to Support a New Research Reactor Project”. Scope of this publication is to provide guidance to Member States in determining their national nuclear infrastructure status and to identify gaps and future development needs. It is essential that teams and individuals involved in developing the RR infrastructure read and fully assimilate the contents of the Research Reactor Milestones publication [1] before considering this evaluation approach. In the areas of safety, security and safeguards, the framework for an evaluation of infrastructure development is well established and based on the fulfilment of Member State obligations to international safety, security and safeguards conventions. Therefore, they are not elaborated further in this publication but emphasis is provided when appropriate.

The publication consists of three main sections and one annex. Section 1 is an introductory section including background, objectives, scope, users, structure and use of the publication. Section 2 summarizes the project phases and milestones associated with a new research reactor; it also describes the steps of the evaluation approach. Section 3 provides the detailed bases for evaluation of each of the 19 infrastructure issues for phase 1 and phase 2 of project development. Annex I provides guidance for preparing and conducting an IRRIA and follow-up missions. A comprehensive bibliography providing information and guidance on each of the infrastructure issues is also included in the document as well as some pre-designed templates for recording the available data and analysing results of the evaluation.

This publication deliberately addresses the assessment of the two initial phases of a new RR project as described in the Research Reactor Milestones publication for three key reasons:

a) It is important in any major programme to invest wisely and effectively during the initial preparatory stages;
b) Several Member States requesting guidance and support from the IAEA are in these initial phases of their RR projects;
c) Assistance for the evaluation of the status of a number of the infrastructure issues during phase 3 (construction and commissioning) and beyond (operation) of a RR is already provided by several well-established IAEA services, assessment tools and methodologies (some of them could be partially applicable also in phase 1 and phase 2).

During the evaluation process, it is necessary to review progress across all 19 infrastructure issues because each of them is essential, and because there are significant relationships between them. For example, the human and financial resources which are required to support each of the infrastructure issues need to be fully integrated. It is for this reason that the evaluation approach described in this publication addresses the 19 issues in equal and consistent manner. Some of these issues, particularly related to safety, security and safeguards, already have detailed assessment methodologies developed by the IAEA. These principally address activities in phase 3 but can be adapted to review the status of activities in earlier phases. The results of the evaluation process include the evidence to demonstrate that:

a) All of the work required in each phase of the project has been adequately completed;
b) The plans for the following phase of the project are well defined, comprehensive and realistic.

In general, the scale of the typical RR project requires infrastructure of the same scope, but to a lesser extent than would be the case for a nuclear power programme. Thus, a graded approach [2] should be used, i.e. the nuclear infrastructure elements should be tailored to the needs of the RR project. Through appropriate consideration of all of the key issues, the infrastructure implementation for the RR project can be simplified whilst maintaining the required high standards of nuclear safety and appropriate effectiveness of nuclear security. A risk informed analyses of the characteristics, uses and associated facilities of a RR influence the scale of the required infrastructure.

This publication can be used either by a Member State wishing to evaluate its own progress (self-assessment) or as the basis for evaluation in the framework of IRRIA missions. The scope of the publication also includes planning and conducting IRRIA missions. In the case where a Member State is planning to embark on both a new RR project and a nuclear

power programme, the scope of the publication is also to identify means of coordination of services provided by the IAEA for related infrastructure assessment.

This publication is meant to be primarily oriented to Member States developing their first research reactor; however, it could be also used for the re-assessment of the national infrastructure in case of a subsequent reactor in a country, in particular considering a RR of higher power. The guidance provided by this publication will apply to RRs of all types and sizes, including critical and sub-critical assemblies, with proper use of a graded approach proportional to the potential hazards of the project [2].

3. IRRIA missions overview

3.1 What the IRRIA mission is

The IRRIA mission is a holistic, IAEA coordinated peer review conducted by a team of international experts who have direct experience in specialized RR infrastructure areas. The team is led by a senior IAEA staff member experienced in providing integrated support to RR infrastructure development. The team comprises both designated IAEA staff from various disciplines and organizational units, and international experts recruited from Member States and selected by the IAEA in consultation with the host Member State.

The major objective of an IRRIA mission is to assist the Member State in determining its RR infrastructure status and to identify further development needs; hence, the performance of a Member State self-evaluation is emphasized. An IRRIA mission is intended to build upon the Member State self-evaluation in order to determine areas where further work would be beneficial. While an IRRIA mission aims to perform an independent and objective review, it is not intended to be an external audit of the RR national infrastructure. An IRRIA mission is geared to helping the Member State to identify areas for further action and assistance, including that from the IAEA. The review uses knowledge already obtained by the IAEA and the recommendations of previous missions, and avoids duplicating work carried out previously by the IAEA. The mission's detailed scope and the work plan are specifically defined and adjusted to meet the needs of the requesting Member State. In specific, a graded approach should be adopted in the application of the requirements for the RR project [2], including for the development of the national supporting infrastructure, based on the complexity and hazard of the project itself. The review scope is adjusted to the degree of development of the different RR infrastructure issues but is focused on evaluating, as much as is realistic in a limited period of time, all parts of the national research reactor infrastructure.

3.2 What an IRRIA mission is not

It is relevant to note that the IRRIA mission is not:

- An audit or an inspection against established requirements;
- An endorsement of the Member State self-evaluation;
- An assessment of detail or verification of what has really been done or achieved;
- A confirmation of the effectiveness of the Member State processes/actions.

For example, the IRRIA mission can evaluate whether some RR site prospecting activities were performed and criteria established. However, an assessment of the appropriateness of the prospecting performed and the adequacy of the criteria adopted is a matter for RR

site specialists, and an appropriate IAEA review service is needed to cover these technical aspects in detail. The same logic applies to all the other issues.

3.3 Timing of IRRIA mission

The timing of the IRRIA mission needs to be agreed with the Member State, considering the pace of the Member State infrastructure development, the completion of the Member State self-evaluation report and the added value of the IRRIA mission in covering all the 19 issues. IRRIA missions can be requested at any time during the development of the RR infrastructure. They will typically be expected to be arranged in the following sequence: 1) initial, 2) follow-up and 3) prior to invitation of bids for the RR.

4. IRRIA mission request and implementation process

The first step is accomplished with an official governmental request from the Member State to the IAEA that is conveyed through the Department of Technical Cooperation, unless a relevant Technical Cooperation project does not yet exist. In this latter case, the request should be conveyed through the Deputy Director General of the Department of Nuclear Energy.

A short preparatory meeting may be arranged at an appropriate time in advance of the mission, preferably in the host Member State. This preparatory meeting is named “pre-IRRIA mission”. The purpose includes clearly defining, with the host counterpart, the IRRIA mission specific scope, work plan and logistical arrangements. This is also used to identify and collect available advance material. It is the opportunity to identify representatives from the Member State’s most relevant institutions and to establish the expectations for the availability of appropriate specialists from them.

The IRRIA mission focuses on evaluating the fulfilment of the conditions for the corresponding infrastructure development phase. Reviewers seek to acquire information for identification of possible gaps in infrastructure issues through:

- Review of written material;
- Discussion with counterpart’s representatives;
- Review of the response to previous missions;
- Direct observations;
- Visits to organizations and facilities;
- Discussion between team members.

The IRRIA mission concludes with the exit meeting. This consists of a presentation of the main results by the team, which can be followed by a discussion with the key representatives from the host Member State on possible ways to address the points that have been raised.

The Deputy Director General, Head of Nuclear Energy, formally delivers the IRRIA mission report to the host Member State through the official channels. The IAEA restricts initial distribution of the report to the authorities concerned, the contributors to the report and the responsible IAEA staff. The IRRIA mission report is not made publicly available unless the host Member State specifically requests otherwise. However, in the interest of openness, countries are encouraged to make their report public.

Using the results from the IRRIA final report, the host Member State is expected to develop an IWP to specify the actions to be taken to develop and improve the national nuclear infrastructure further by addressing recommendations and suggestions from the mission report.

5. REFERENCES

[1] INTERNATIONAL ATOMIC ENERGY AGENCY, Specific Consideration and Milestones for a RR Project, Nuclear Energy Series No. NP-T-5.1, IAEA, Vienna (2012).

[2] INTERNATIONAL ATOMIC ENERGY AGENCY, Use of a Graded Approach in the Application of the Safety Requirements for Research Reactors, Safety Standards Series No. SSG-22, IAEA, Vienna (2012).

BUILDING CAPABILITIES FOR NEW REACTORS

Gabriel Lazaro Pavel, Ghitescu Petre
University "Politehnica" of Bucharest
313 Splaiul Independentei Street, Sector 6
ZIP Code, 060042, Bucharest, Romania
gabriel.pavel@gmail.com, ppghites@hotmail.com

Fosca di Gabriele
Dep. of Materials for Energy,Centrum vyzkumu Rez s.r.o.
Hlavní 130,ZIP Code 250 68,
Husinec-Řež, Czech Republic
fosca.di_gabriele@cvrez.cz,

Climate change issues together with security of supply are the main issues addressed by the European Union as future key elements for development. This positions the nuclear energy as a recommended option when comparing to other sources of energy. Generation IV (Gen IV) reactors seem to be the innovative solution that addresses the security of supply at a competitive cost of energy, also tackling the main issue of the nowadays nuclear industry, nuclear waste. Currently, at European level there are several nuclear Gen IV reactor ongoing projects.
The development of new types of reactors requires huge scientific, financial and organizational efforts. It should be based on international cooperation in order to accomplish a proper build-up of competences and suitable research facilities as support. Romania assumed the responsibility of building on its territory of the first of a kind Gen IV demonstrator called ALFRED (Advanced Lead Fast Reactor European Demonstrator). Building of ALFRED observes the best practices formulated by the IAEA and other international organizations, integrated in the Romanian regulatory frame.
The ARCADIA project was conceived to provide support for the realization of ALFRED and it focuses on the identification of the primary needs, mainly to what concerns E&T, supporting Infrastructures, and Regulatory aspects. FALCON is a consortium established at international level, which deals with the technical and organizational needs concerning R&D issues. Exhaustive research of the required expertise and of the experimental needs must be carried out.
Technical competences of future personnel must be based on brand new educational and skill capacities. In the long term, ALFRED achievement should take into account the E&T needs, capability of the E&T system to prepare and provide the expected human resources with expertise in the management and implementation of complex and innovative projects. As hosting country, Romanian educational system will have to fulfil most of the requirements for personnel training prior to ALFRED being set into operation. These needs must tackle issues related to: existing and projected expertise, topics to be introduced into existing curricula or development of a new curriculum, exchange of pilot courses and curricula, multilateral and bilateral cooperation with experienced countries, eventually mutual recognition and accreditation.

1. Introduction

Nuclear power is today considered to have one of the lowest CO2 emitting footprints among other energy producing technologies. Climate change is considered to be the biggest challenge of our recent history. European Union (EU) tackles this challenge with a series of initiatives that are intended to diminish this problem whilst keeping in the same time a satisfying energy mix, security of supply, well-being of citizens and a safe environment.

Nuclear power production units have a major advantage in this challenge being one of the least greenhouse gas emitters among other technologies. Nuclear industry is under continuous development aiming at overcoming its own issues. Generation IV (Gen IV) reactors are considered to be the result of years of accumulated experience in designing and operating nuclear power plants combined with nowadays necessities and desideratum. They are intended to provide energy at a competitive cost while keeping waste to a minimum.

Several Gen IV technologies are supported by the EU and all of them are the result of international cooperation. Long before these technologies will become commercially available, proper build-up of competences and suitable research facilities as support must be developed. Development of Gen IV reactors must be based on the identification of the principal technical and organizational needs for what concerns R&D, on the identification of required expertise and experimental needs.

Personnel knowledge, skills and attitudes have to be the result of a proper educational system and R&D facilities, capable of providing necessary competence. Any successful project must consider the E&T needs, capability of the E&T system to prepare the expected human resources and experience.

2. Context

Regarding climate change issues, EU Energy Policy is based on several major objectives: reduction of emissions of greenhouse gases by an average of 20% at the level of 2020, reduction of energy losses in the sectors considered to be the main contributors for greenhouse gas emissions i.e. transport and power production industry. On 19 December 2011, European Commission (EC) adopted the Energy Roadmap 2050[1], a document tackling this challenge, which presents a set of measures aiming to reduce by the end of 2050 the greenhouse gas emissions up to 80-95% below 1990 levels. The content of the document addresses the technical challenges raised by this objective while providing in the same time, security of the energy supply. Roadmap 2050 became the framework document for the long-term development of the European energy policy, focusing on the member-states good industrial competitiveness and a functional society based on the well-being of citizens. These desiderates can be obtained with a proper and reliable power supply at competitive costs and with high efficiency. Well-being of citizens (from energy supply point of view) is related to: having a clean source of energy, supply of energy to be safe and secure and to protect the environment as much as possible. Energy demand forecasts foresee a continuous increase in energy demand. In order to be able to have an answer to this challenge the financial effort it is estimated to be of approximately 1 000 billion Euros. This figure includes replacement of production units that are becoming obsolete and other improvements to power production facilities in order to make them complying with newer rules when it comes to environmental pollution. In November 2000 EC published the document entitled “Green Paper on the security of energy supply”[2], the pillar of “Energy Roadmap 2050” One important conclusion of the document is that the EU energy dependency on external sources is very high. More than 50% of crude matter needed is provided from imports. One major conclusion is that if the EU doesn't manage to improve energy sector in the next years, its dependency on primary sources of energy will increase to more than 70 %. One key aspect is that the imports will come from regions threatened by instability. Afterwards several initiatives were developed, focused on sustainable development (promotion of renewable energy sources and other sources with reduced carbon footprint, etc.), competitiveness and security in the power supply (reducing imports, energy mix diversification, etc.).

3. Analysis of new reactors in Europe

New Gen IV reactors started getting strong support in early 2000 when Generation IV International Forum (GIF) meetings began.

Several technologies gained trust and start being supported: GFR-Gas Fast Reactors, SFR-Sodium Fast Reactors, LFR-Lead Fast Reactors, MSR-Molten Salt Reactors, SCWR-Super Critical Water Reactors, VHTR-Very High Temperature Reactors.

Following the “roadmap” to a cleaner environment the European Union started supporting the realization of several types of reactors as Gas, Lead and Sodium Fast Reactors. These fourth generation reactors must fulfil four main objectives: sustainability; cost-effectiveness, to be safe and reliable and proliferation resistant.

The ALLEGRO project is a Gas Fast Reactor Demonstrator which undergoes a preparatory phase that is supposed to last from 2010 until 2020. The Gen IV GF Reactor intends to combine the benefits of fast spectrum with high temperature, using helium as coolant. High temperature of coolant allows high efficiencies to be obtained.The project has several open issues but some conceptual characteristics are worth to notice:

- Self-generation of Pu in the core (breeding ratio ~ 1),
- Reducing the proliferation risk,
- Limited mass of Pu in the core,
- Ability to transmute long-lived nuclear actinides,
- Favourable economics owing to a high thermal efficiency,
- etc.

ALLEGRO reactor aims to be the first ever built GFR demonstrator capable to prove the viability of the technology:

- Core behaviour and control, fuel and the fuel elements,
- Specific safety systems,
- Helium purification etc.

The SFR prototype ASTRID is a Sodium-cooled Fast Reactor project led by CEA, also supported by the French Government in cooperation with industrial partners. It is foreseen to be built within 2015-2020 time frame, close to the old Phénix reactor at the Marcoule site as it is considered to have the most mature technology. The proposed objective for ASTRID is to achieve a safety level equivalent to that of a 3rd generation PWR, and also to fulfil some other requirements, such as: economic competitiveness, improved core behaviour, safety-attention to the reaction with sodium, resistance to internal and external hazards etc. The aim is to demonstrate that after a few years of operation, ASTRID will be able to have an availability factor comparable to that of the current fleet of reactors in service (i.e. approximately 80% of availability).

MYRRHA (Multipurpose Hybrid Research Reactor for High-tech Applications) is designed to be a 50-100 MWth flexible multi-purpose fast spectrum irradiation facility. MYRRHA is capable to operate both in sub-critical and critical mode as an Accelerator Driven System (ADS), capable to demonstrate the ADS technology and the efficient burn-up of Minor Actinides in subcritical mode. It contains also a proton accelerator of 600 MeV, a spallation target and a multiplying core with MOX fuel, cooled by liquid lead-bismuth. The concept it is currently under development by the SCK Cen, the Belgian Nuclear Research Centre in Mol. MYRRHA will be able also to function as a critical flexible fast spectrum irradiation facility, which will contribute to the development of LFR technology. It is foreseen to be fully functional around year 2023.

Another initiative is the European Lead Cooled Fast Reactor ELFR, which lead to the proposal of an Advanced Lead Fast Reactor European Demonstrator-ALFRED. This is a 300 MWt reactor, intended to be built in Romania, near Pitesti site. Pure lead is used as primary coolant and it is foreseen to have a 40% thermal efficiency. The FALCON consortium has been set-up in order to ensure the development of the demonstrator. The aim of the

consortium is to constitute a pan-European network of organizations interested in the LFR technology development having as ending point ALFRED construction and safe operation. The members of the consortium are ANSALDO NUCLEAR and ENEA, from Italy, ICN from Romania and CVR from Czech Republic.

The main challenges of the FALCON Consortium and ALFRED are:

- Be able to develop a safe and operational configuration for ALFRED;
- Funding of the project;
- Be able to quantify the facilities capable of supporting lead technology;
- Show the safety features and obtain licensing,
- Be able to build competences and attract young generations by shaping proper E&T programs.

4. Existing infrastructure

The development of Gen IV nuclear program must be backed-up by a good national strategy and support. One other key factor is the existence of suitable research laboratories supported by good personnel that perform thorough research in the field. This brings expertize and support in designing, engineering and operation. The educational component is aimed to provide sustainable and qualified workforce to keep the initiative sustainable for further developments.

Intensive work [3] has been carried out around Europe to identify the existing and needed infrastructure as support for these reactors. Several facilities have been identified and considered to be able to have a future impact on the development of these reactors.

For SFR: the SUSEN project (CVR) aiming at studying heat and mass transfer in cover gas, aerosols behaviour, instrumentation, slab geometry, Brayton cycle energy conversion system, SC-CO2 technology development; KIT Platform (KIT Karlsruhe) aiming at studying 2D slab pool model of SFR on heat exchanger, flow sensors, scaled heat transfer, test of full length 19 rod bundle, test of natural convection, etc.; Liquid Metal Platform (ENEA Brasimone) tests aimed to characterize physical effects induced by sodium-water interaction in the intermediate loop; AMPERE Platform (IPUL) aimed at studying the materials in extreme conditions, qualification of innovative heat exchangers, test of EM pumps and their calibration, tests and calibration of instrumentation; Na School (ESML-CEA) aimed at providing training to Na facilities; DRESDYN Platform, aimed to provide basic studies on Na boiling and gas entrainment, tests for new instrumentations and measurement techniques; CHEOPS Platform (CEA) aimed at providing qualification of ASTRID SGU,fuel handling, fuel assemblies, detection systems; PAPIRUS Platform (CEA Cadarache) includes some facilities that will be refurbished so as to be able to provide support; PLINIUS-Na platform (CEA)-capability to study interaction Na-corium Molten-corium, capability for study of debris formation, code validation; PLATEAU platform and ATHENA Platform, both supported by CEA.

For GFR several issues were identified: high temperature materials behaviour, thermal hydraulics, qualification of components, severe accidents material testing facilities. All these issues can be addressed by different facilities across Europe. The SUSEN projects is one of the main supporting structure, as it is providing experimental loops for the technology validation (materials, gas chemistry, instrumentation, thermo-hydraulics, in-pile feasibility,…).

The LFR technology is also supported by different facilities and platforms across Europe. The number of these facilities is greater than 30 and other are under development. These facilities include: COMPLOT (Partially funded by Belgium); HELENA (Partially funded by Italy); NACIE; CIRCE; E-SCAPE (Partially funded by Belgium); DEMOCRITOS (Partially

funded by Belgium); ATHENA (Partially funded by Italy); RHAPTER; Lilliputter-2 (Partially funded by Belgium); TELEMAT (Germany); Electra (Sweden); CRAFT (Partially funded by Belgium); LIMITS 3,4,5 (Partially funded by Belgium); HELIOS III; MYCENE, etc. Moreover, the SUSEN project (CVR) is also devoting a large part of its facilities to the support of the LFR technology.

5. Existing knowledge

For decades E&T institutions and R&D facilities in Romania succeeded to provide the necessary and properly qualified workforce for the national nuclear industry. The Cernavoda Nuclear Power Plant (NPP) needs for personnel have been fulfilled by these institutions. ALFRED demonstrative reactor, a 4-th generation type that is planned to be built in Romania can be considered as a successor of 19 years of safe operation for the Cernavoda NPP.

Development of a strong and efficient personnel training system must be based on a good cooperation between all involved entities acting as support, namely education and training networks existing at national level, extended to regional and international ones. These networks are to be constituted by: universities, research facilities, training centres, etc. The leading entity for the development of ALFRED reactor is the Institute for Nuclear Research in Pitesti. The ARCADIA project was the first step in order to support the identification of primary needs for the ALFRED. One of the major objectives of ARCADIA is to determine the existing national, regional and international supporting structures for defining needed competences.

In Romania there are Universities offering a partial nuclear curriculum such as University of Pitesti, University *Ovidius* Constanta, University *Babes-Bolyai* in Cluj, University of *Bucharest* and University *Politehnica* of Bucharest (UPB) that provides a complete nuclear E&T program (e.g.) at bachelor, master and doctoral level. UPB curriculum is adapted to Bologna scheme, meaning that in the first 3 years of study a student will receive only general information about nuclear field. In the last year of study a person receives specific courses, such like: Nuclear Processes, Radioprotection and Dosimetry, Reactor Theory (Diffusion Theory), Nuclear Materials, Reactor Engineering, Nuclear Power Plants, Nuclear Equipment and Installations, NPP Control and Instrumentation, Nuclear Safety, Radwaste Management, Numerical Methods, Reactor Physics Experiments. With MSc level deep analysis courses are implemented. These courses tackle more or less the same topics but adapted to advanced nuclear reactors (Advanced NPPs- Gen. 3+ and 4; Nuclear Reactor Advanced Physics (Transport Theory) and Codes, Nuclear Materials for Advanced Reactors; Modelling and Simulation of Dynamics of Nuclear Installations; Codes used in Radioprotection; PSA/codes; Codes used in Thermal-hydraulics; etc.).

This analysis should stress that at present time there is no expertise available regarding Gen IV reactors. No curriculum and courses, no students, no plans, no laboratories and even worse, no learning capacity and competence.

Well trained personnel is obtained in due time. Developing an existing nuclear program or starting a completely new nuclear program can be made also after a certain amount of time. Upgrading the existing nuclear E&T curricula or building a new one takes skilled trainers. Having skilled trainers takes also a certain amount of time. Skilled trainers can only be obtained based on a good cooperation between universities, training centres and

research organization. **Knowledge transfer takes time and personnel.** Other key factors for success are the exchange of pilot courses and curricula and multilateral and bilateral cooperation with experienced countries.

But all these developments must be furtherly improved so that the Universities curricula can satisfy the knowledge requirements for the personnel that will have to work Gen IV reactor types.

It should undoubtedly be a priority the formation of international schemes, where the present knowledge, concentrated in several countries, could be opened to other Members States which are making commitments towards GenIV. In fact, the existing infrastructures should be considered key training points, where to base and develop further the knowledge and experience of the scientific community in the EU. However, while education of trainers may present some challenges, the reverse approach could be proposed as a valid alternative. In fact, training of young scientists is among the programs of most countries with relevant infrastructures. The young scientists would, afterwards, take back to his/her country the experience gained and create and develop a working group, as a nucleus containing the bases for the further development and exchange of experience.

6. Conclusions

Knowledge transfer takes time.

Safe operation of new generation reactors can only be achieved by trained personnel.

Several facilities [4] are already built as support for future Gen IV reactors but much more are needed. Although huge amount of work has already been deployed, in order to meet all requirements (safety, economic, availability, efficiency and others) for future reactors a lot needs to be done in the future.

Trained human resources need skilled trainers. Skilled trainers are also formed in a certain period of time. Skilled trainers can be obtained only by good cooperation between Universities, training centres and R&D facilities. Such networking between all these entities must be made on national, regional and international level. This type of networking aimed at improving the existing expertise or developing new ones represent a trusted base for international cross linking.

References

[1] http://ec.europa.eu/news/energy/111219_en.htm, as of 01.03.2015

[2]http://europa.eu/legislation_summaries/energy/external_dimension_enlargement/l27037_en.htm , as of 01.03.2015

[3] http://cordis.europa.eu/fp7/euratom-fission/docs/03-p-agostini-adriana_en.pdf, as of 12.03.2015

[4] ftp://ftp.cordis.europa.eu/pub/fp7/euratom-fission/docs/adriana-final-report_en.pdf, as of 12.03.2015

Acknowledgements

The work has been partially funded by the Sectoral Operational Programme Human Resources Development 2007-2013 of the Ministry of European Funds through the Financial Agreement POSDRU/159/1.5/S/134398.

The work has been partially funded by the EC through FP7 Program, Theme: Fission, Widening involvement in the Fission, Safetyand Radiation Protection Programme, Grant Agreement no. 605116.

The authors would also like to aknowledge the support by the SUSEN Project CZ.1.05/2.1.00/03.0108 realized in the framework of the European Regional Development Fund (ERDF).

NEUTRONIC DESIGN OF THE COQUI REACTOR

D. FERRARO
Nuclear Engineering Department, INVAP S.E.
Esmeralda 356 – P.B. C1035ABH, C.A.B.A, Buenos Aires, Argentina - dferraro@invap.com.ar
F. BOSCHETTI, E. VILLARINO, F. SARDELLA
Nuclear Engineering Department, INVAP S.E.
Av. Cmte Luis Piedrabuena 4950, R8403CPV S.C. de Bariloche, Rio Negro, Argentina

ABSTRACT

The Reactor unit of the Coquí Medical Radioisotope Production Facility (MIPF) is an open-pool type reactor designed by INVAP S.E. (Argentina) to Coquí Pharmaceuticals (USA) to be built in Alachua, Florida (USA). This Reactor design has a nominal fission power up to 10 MW, and it is specially developed to ^{99}Mo production by fission in mini-plates.

Several Research Reactor designs are capable to produce large amounts of ^{99}Mo, but Coquí Reactor will be specially designed for such unique purpose. Accordingly, the overall design is held considering the interfaces and main aspects of the Radio Isotope Production Plant, in order to create a commercially scalable and reliable supply of medical diagnostic radioisotopes scheme.

The plant is aimed to produce 7000 6-Day Ci per week of ^{99}Mo through fission in LEU mini-plates, using a compact core of MTR type LEU fuels. The key approach on this project is the use of already proven technology from the several reactors designed and commissioned by INVAP, as well as the experience gained in the construction of Radio Isotope plants around the world.

The present work describes the neutronic calculation process and the current state of the design, including the main aspects of the design criteria and the design philosophy applied in order to reach the stated ^{99}Mo production goals in a reliable scheme with safety as a priority.

1. Introduction

Nuclear Medicine Diagnosis techniques using radioactive tracers represent one of the most powerful tools available to perform a quick and accurate diagnosis of several patient's diseases. In such techniques the most frequent radioisotope used is ^{99}Tc (obtained from ^{99}Mo decay) accounting for 80% of all nuclear medicine procedures worldwide.

Nowadays most of the world's supply of ^{99}Mo comes from only five reactors, all of them more than 40 years old. As far as the global demand for such Radio Isotope is expected to be increased, the global concern to ensure a reliable and economic viable production of large amounts of ^{99}Mo is stated. As an example, in 2014 the *Joint Declaration on the Security of Supply of Medical Radioisotopes* (ref. [1]), which seeks mainly to ensure the ^{99}Mo supply for the following decades, has been adhered formally by more than a dozen of nuclear developed countries.

In order to face this global challenge, last November 2014, Coquí RadioPharmaceuticals Corp., a USA medical isotope company working to become the first U.S. commercial producer of ^{99}Mo, has signed a contract with INVAP (Argentina) to design a Medical Isotope Production Facility (MIPF) to be built in Alachua, Florida (USA). The global design of such facility is based on the wide experience of INVAP on the design, construction and commissioning of research Reactors on the one hand (refs. [2] and [3]) and ^{99}Mo turn-key production facilities using LEU fission techniques on the other hand (sized from the well proven LEU techniques developed by the Argentine National Atomic Commission - CNEA, ref. [4]).

The present work describes the up-to date preliminary neutronic design of the Coqui Reactor (where the ^{99}Mo is to be produced through fission in LEU miniplates). The overall design

process and tools used by INVAP, together with the preliminary main Reactor neutronic parameters are presented and discussed.

2. General Description of COQUI Reactor

The Medical Isotope Production Facility (MIPF) design is an integrated facility that includes two Reactor Units (one operating reactor unit, and a back-up unit), a Radio Isotope Plant and a set of specifically designed transfer and processing hot cells.

Each Coquí Reactor unit is an open-pool type reactor specifically designed to produce large amounts of ^{99}Mo. The overall design is held considering the interfaces and main aspects of the Radio Isotope Production Plant, in order to create a commercially scalable and reliable supply of medical diagnostic radioisotopes scheme.

The reactor unit Design is based on already proven technology used in other Reactor Designs held by INVAP, selecting the most suitable technology for this particular case. The main characteristics for the up to date reactor design are presented in Table 1.

Table 1 Main characteristics of Coqui Reactor Design components

Component	Description
Reactor Type	MTR – compact core
Reactor Thermal Power	<10MW
Fuel Assembly (FA)	MTR parallel plate type - LEU silicide + Al cladding
Core Coolant	Light water
Reflector	Beryllium Blocks
Molybdenum production devices (Moly)	Fission miniplates - LEU U-Al + Al cladding
Reflectors and Moly Coolant	Light water
Shutdown System	Hafnium Plates Control Rods (CR) placed in Control Rod Guides

3. Design Requirements

As for all INVAP reactors, the design philosophy for Coqui reactor unit is developed considering the following key aspects:

- Overall design considering Safety as priority.
- Selection of components based on proven technologies as far as possible.
- Follow best-international practices and experience.
- Include INVAP experience in similar facilities to obtain a reliable and economically profitable design.

Accordingly, both Safety and Performance Requirements are stated that should be solved from the neutronic point of view.

3.1. Safety Requirements

Safety Requirements arise from the combination of applicable Regulations (ref. [5]), using as support the knowledge from international best practices and the cumulative INVAP´s experience on Reactor Design Process. The main safety requirements applied to neutronic design are summarized in Table 2 .

Table 2 Main Safety Requirements of Coqui Reactor

Parameter	***Value***
Shutdown Margin (SDM)	> 3000 pcm
Shutdown Margin with single failure (SDM-1)	>1000 pcm
Overall power coefficient	Negative
Reactivity Worth of movable devices	< 1 β

3.2. Performance Requirements

Performance Requirements play a key role to obtain a reliable and economically profitable design. The combination of production requirements together with the cumulative INVAP´s experience on Reactor Designs are used to define the main performance requirements applied to neutronic design, which are summarized in Table 3.

Table 3 Main Performance Requirements of Coqui Reactor

Parameter	***Value/description***
^{99}Mo Production	7000 6-Day Ci per week
Irradiation characteristics	Fission in U-Al LEU mini-plates.
Production Management	7 days irradiation scheme
Operational Related aspects	Reliable & continuous operation

4. Neutron Design Process and Tools

For the last three decades, INVAP´s Neutronic design team has developed a wide range of reactor designs successfully [2]. The basis of such success is the employment of a design and calculation methodology that deals with the whole design process in order to obtain accurate results, starting from the nuclear cross section data up to the calculation tools, the calculation procedures, the review process and the qualification of the nuclear analyst involved.

4.1. INVAP Neutronic Design Process

INVAP's design methodology (ref. [6]) is an integrated approach to Neutronic Design. A scheme of such methodology applied for Coqui Reactor Design is presented on Figure 1.
The overall process is based on the following key concepts:

- *Consider Safety as priority*: Using the requirements of the regulatory body of the country where the reactor will be built, supporting the criteria with the Argentine regulatory body requirements (if applicable), the IAEA safety guidelines or recommendations and INVAP´s own experience.
- *Custom designed reactor:* All the operational design criteria are taken into account and all project specific engineering data are collected in a database.
- *Minimize risk using proven technology:* When a novel design is needed experiments or mock-ups are used to adequately verify the design.
- *Qualified methods, tools and procedures:* New versions of the codes are in continuous development. A dynamic improvement and maintenance process is adopted to keep up with modern reactors evolving requirements (always maintaining a proper verification and validation stage).
- *Design held by well trained nuclear analysts:* The design teams are continuously trained or re-trained to properly develop a solid understanding of each reactor design. This allows the analysts to prepare accurate models.

Figure 1 INVAP´s Neutronic Design Flowchart

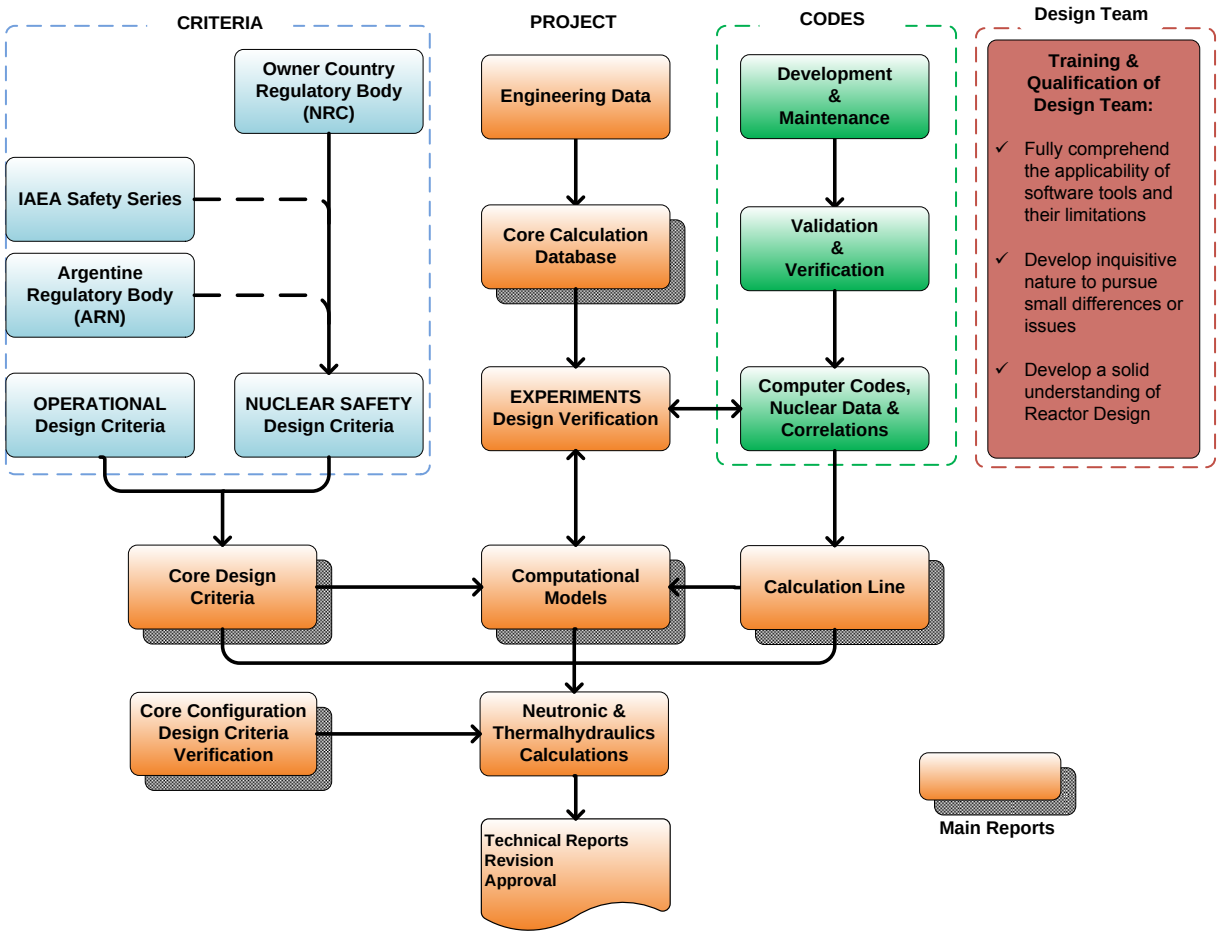

4.2. INVAP Neutronic Calculation Line

INVAP´s Neutronic Calculation line (ref. [7]) is composed by a combination of own-developed codes and utilities together with diverse Nuclear Data and well-known third-party codes. These codes, data and utilities are integrated in a practical and error-minimizing scheme, as it is shown in Figure 2.

Some of the most relevant characteristics of this calculation line are:

- The integration between deterministic and stochastic codes.
- The capability to perform calculations with macroscopic or microscopic cross section data.
- The capability to perform thermal-hydraulic analysis for coupled neutronic/thermal-hydraulic calculations. This is a key feature for the calculation of power feedback coefficients, thermal-hydraulic margins to critical phenomena and the growth of oxide layer, which is a limiting factor for high performance MTR fuel assemblies.

Figure 2 INVAP´s Neutronic Calculation Line

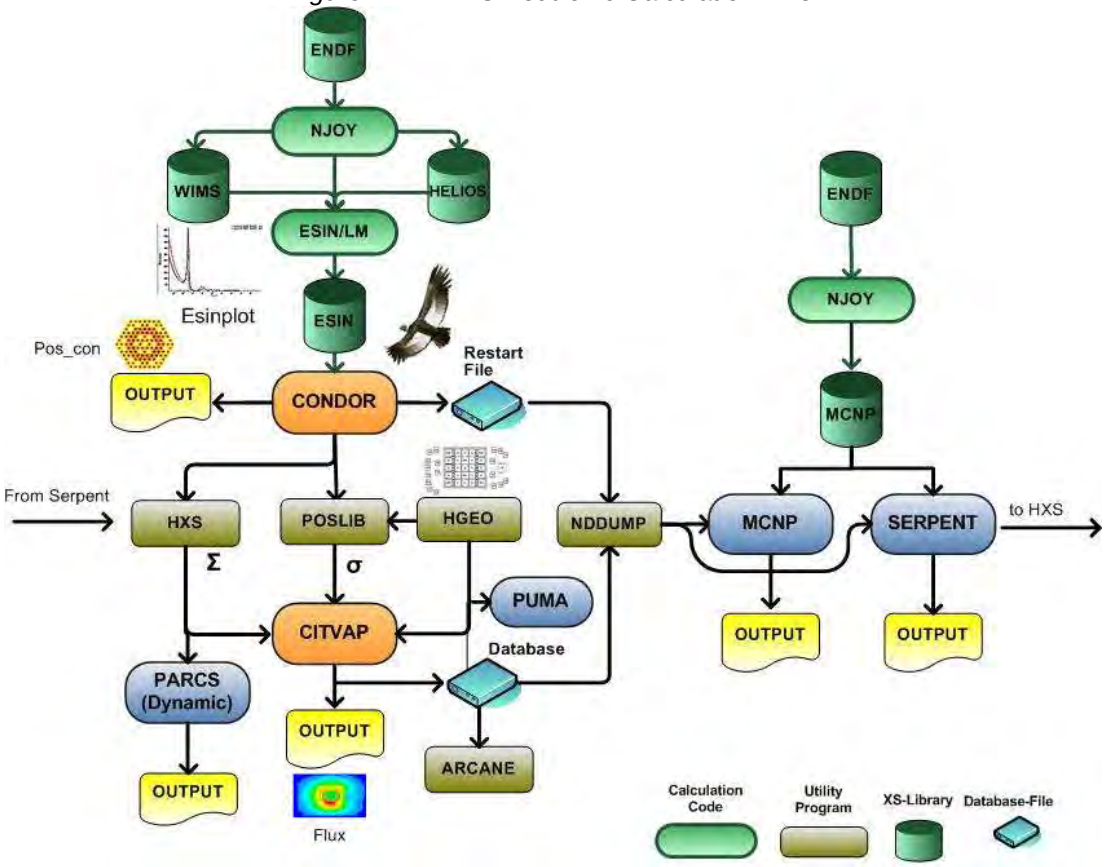

This calculation line is in constant actualization and validation and has been used by INVAP and several of its customers for the design, optimization and follow-up of several reactors all around the world obtaining optimal results in diverse reactors such as RA-6, RA-8, RA-10 (RR, Argentina), RMB (RR, Brazil), NUR (RR, Algeria), ETRR2 (RR, Egypt), OPAL (RR, Australia), CAREM, CNA-II (NPP, Argentina), and several others.
These codes are also used by nuclear engineering students, master's and doctoral thesis students of the Balseiro Institute (Argentina), performing a large number of calculations for different reactor types such as MTR, PWR, BWR, PHWR, TRIGA, FBR and Homogeneous reactors.

5. Main aspects of Neutron Modeling of COQUI Reactor Unit

The overall Neutronic modeling and design of Coqui Reactor Unit is carried out using both deterministic and stochastic Models. The deterministic calculation models are used to obtain main core design parameters, such as equilibrium core characteristics, while stochastic models are used primarily to obtain detailed flux calculations, to perform alternate criticality and kinetic parameters calculations and to carry out heat deposition calculations.

5.1. Deterministic modeling: Cell and Core models

The deterministic Neutronic modeling of Coqui Reactor is carried out using the cell and core approach of Figure 2. Thus, CONDOR (2-D cell HRM code) and CITVAP (3-D core finite differences diffusion code) models are developed. All components are modeled at cell level in CONDOR using 1-D or 2-D approach in order to obtain condensed and homogenized few-group cross sections to be used in further 3-D CITVAP calculations. As an example, the preliminary CONDOR cell model for the FA is presented in Figure 3.

Figure 3 Preliminary CONDOR model for FA.

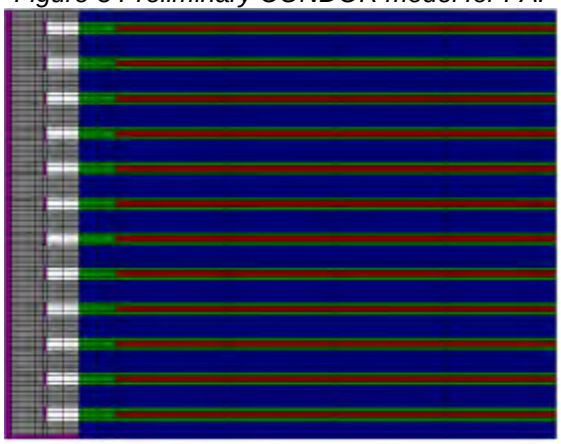

5.2. Stochastic modeling: Full core models

A preliminary full 3-D MCNP5 Stochastic model is developed to obtain detailed flux calculations, alternate checks for reactivity and kinetic parameters calculations and to perform nuclear heat depositions calculations. In order to model the reactor characteristics considering the diverse reactor burnup states, the burned core compositions obtained from CONDOR-CITVAP are included in MCNP models using NDDUMP program, as it is shown in the calculation line described in Figure 2.

6. Estimation of main neutron parameters

Main neutronic parameters are estimated using the models presented in last section. Thus, parameters such as excess reactivity, cycle time, shutdown margins (SDM) are calculated in order to analyze main neutronic design characteristics of Coqui Reactor. These results represent the preliminary values estimated for the up to date Coqui Reactor neutronic design. The main results obtained with the CONDOR-CITVAP models are presented in Table 4, and compared with the Safety Requirements from Table 2.

Table 4 Main neutron parameters of Coqui Reactor preliminary design

Parameter	***Obtained value (preliminary)***	***Requirement***
Reactor Power [MW]	~ 9.6	< 10
FA consumed per cycle	1	-
Cycle Time [FPD]	~21	-
Excess Reactivity (BOC/EOC) at Hot Full Power state (HZP) [pcm]	~2700/~1000	-
Shutdown Margin (SDM) [pcm]	~ 8900	> 3000 pcm
Shutdown Margin with single failure [pcm]	~ 4000	> 1000 pcm
Overall power coefficient	< 0	Negative
Reactivity Worth of movable devices	~ 0.6β	< 1β

To guarantee the performance requirements, a neutronic optimization procedure is applied. Main neutron flux characteristics are presented in Table 5. Additionally, thermal neutron (E<0.625eV) flux maps for BOC obtained from MCNP5 models are shown in Figure 4.

Table 5 Main neutron flux characteristics of Coqui Reactor preliminary design

Component	***Average neutron thermal flux (preliminary) [n/cm2s]***
Core	~9.6E+13
Molybdenum production facilities	~1.5E+14

Figure 4 Preliminary thermal flux profile, obtained from MCNP5 model

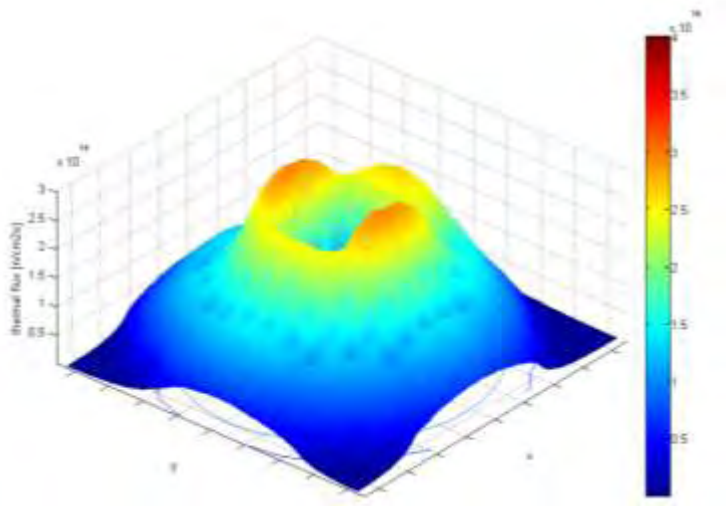

Finally, the estimated weekly production of the preliminary design for Coqui Reactor is obtained using the masses, power, irradiation times, cooling times and overall efficiencies of production process (ref. [8]). Accordingly, the estimated performance characteristics are presented in Table 6.

Table 6 Main performance parameters of Coqui Reactor preliminary design

Parameter	***Obtained value (preliminary)***	***Requirement***
Irradiation Days	***7***	-
Week production [6-day Ci ^{99}Mo]	~7000	7000

7. Conclusions

The Coquí Reactor unit is an open-pool type reactor designed by INVAP (Argentina) to Coquí Pharmaceuticals (USA) to be built in Alachua, Florida (USA) specially to produce ^{99}Mo RadioIsotope. The main characteristics of the proposed design, together with the philosophy (ref. [6]) and the calculations tools (ref. [7]) used by INVAP in the neutronic design are presented. The application of this design scheme, using as key aspects the "*safety as priority*" and "*proven technology*" concepts allowed INVAP design successfully similar facilities (refs. [2], [3] and [8]).

The preliminary neutronic design process was presented, together with the estimation of main neutronic parameters related to safety and performance, showing that all limits and constrains are satisfied in order to obtain a safe, reliable and commercially scalable design to satisfy the required production of ^{99}Mo radioisotope.

8. References

[1] OECD/NEA Joint Declaration on the Security of Supply of Medical Radioisotopes - 17 December 2014 - C(2014)133 - C/M(2014)13

[2] INVAP´s Research Reactor Designs – Eduardo Villarino and Alicia Doval - Science and Technology of Nuclear Installations - Volume 2011 (2011), Article ID 490391, 6 pages

[3] Juan Pablo Ordoñez – Argentina "Status update of INVAP activities in Research Reactor Design & Construction" on the Proceedings of the IGORR 2014/IAEA technical Meeting – 17-21 November 2014 Bariloche, Argentina

[4] F. Molli, C. Maneiro, J. Merino, D. Boock, E. Brandt and A. Alaniz, INVAP "Use of the ETTR-2 Reactor for the Production Of RadioIsotopes in Egypt" – Proceedings of the 6th

International Symposium on Material Testing Reactors, Bariloche, Río Negro, Argentina October 28-31, 2013.
[5] United States Nuclear Regulatory Commission, Office of Nuclear Reactor Regulation, Division of Reactor Program management “Guidelines for Preparing and Reviewing Applications for the Licensing of Non-Power Reactors " – NUREG 1537 – Part 1 & Part 2 – February 1996
[6] Eduardo Villarino – INVAP "Neutronic Calculation Methodology For Research Reactors" on the Proceedings of the IGORR 2014/IAEA technical Meeting – 17-21 November 2014 Bariloche, Argentina.
[7] E. Villarino, I. Mochi, I, P. Sartorio; “INVAP Neutronic Calculation Line”, Mecánica Computacional Vol. XXXIII, pages from 3217 to 3226; Asociación Argentina de Mecánica Computacional.
[8] Daniel Hergenreder – INVAP "Irradiation Requirements for Radioisotope Production" on the Proceedings of the IGORR 2014/IAEA technical Meeting – 17-21 November 2014 Bariloche, Argentina.

DESIGNS OF MEDICAL ISOTOPE PRODUCTION FACILITIES

C. M. MAZUFRI
Nuclear Project Division, INVAP S.E.
Av. Cmte Luis Piedrabuena 4950, R8403CPV S.C. de Bariloche, Rio Negro, Argentina

ABSTRACT

Since the supply of medical isotopes temporarily declined over the past decade due to unexpected shutdowns at the few and aged Mo-99-producing research reactor, the need for a continuous and reliable production was established as a high priority short-term objective in different countries. During the last four years, INVAP has been involved in the design of two new nuclear reactor facilities to address the medical isotopes production, the RA10 in Argentina and the RMB in Brazil, both multipurpose research reactors using the Australian OPAL reactor, designed and built by INVAP, as a reference reactor.
Recently, INVAP has also signed with Coquí RadioPharmaceuticals Corp., a medical isotopes company, a new contract to design a Medical Isotope Production Facility to be built in Alachua, Florida.
This work describes the general features of these three projects intended to overcome the present fragile supply chain of Molybdenum 99.

1 Introduction

INVAP has designed, constructed, commissioned and supported the licensing of several research reactors and the associated facilities for more than 35 years. In the particular case of the reactors used to produce medical isotopes, with the support of the National Atomic Energy Commission of Argentina (CNEA), production facilities using a successful tailoring of LEU based production technologies of Molybdenum 99 and other radioisotopes were supplied. Among other projects, two important facilities for production of Molybdenum 99 (Mo-99) have been successfully completed by INVAP in the past years. One project involved the supply on a turnkey mode of a Radioisotope Processing Plant and associated installations for the use of the Egyptian Test and Research Reactor ETRR II, devoted to cover the Egypt needs of radiopharmaceuticals. The other significant project was developed in Australia where INVAP was selected by ANSTO to retrofit with a completely new process its existing infrastructure of operating hot cells in Lucas Heights.
This large experience in nuclear development has allowed INVAP to be contracted to develop new projects, like the design of two new nuclear reactor facilities, the RA10 in Argentina and the RMB in Brazil, both multipurpose research reactors using the Australian OPAL reactor, designed and built by INVAP, as a reference reactor. Additionally, INVAP has recently signed with Coquí RadioPharmaceuticals Corp., a medical isotopes company, a new contract to design a Medical Isotope Production Facility to be built in the United States.
In the next sections, the main characteristics of these new reactors projects to produce Mo-99 based on the LEU technology are described.

2 RA10 Multipurpose Research Reactor

During 2011, the National Atomic Energy Commission of Argentina (CNEA) began implementing the design, construction and commissioning of the multipurpose research reactor RA-10, primarily to increase the production of radioisotopes for diagnosis and treatment in order to support the local and regional demand. This new reactor to be constructed in Ezeiza Atomic Center (Buenos Aires Province) will provide a replacement for

the RA-3 reactor (1967), and will also add technological development in the field of fuels and nuclear materials.
Under contract with CNEA, INVAP has completed the basic engineering and at present the detailed design is being developed and completed. The following is a summary of the main characteristics of the reactor [1].

2.1 RA-10 REACTOR

The reactor is a 30 MW open-pool facility. The core is a square array with 19 LEU MTR fuel assemblies and 6 in-core irradiation facilities. The core is contained inside an open pool of demineralized water that provides both cooling and shielding. Reactivity control is performed by 6 control plates placed inside guide boxes, constituting also the first shutdown system. A heavy water reflector tank surrounds the core and provides a space with high thermal neutron flux for the irradiation facilities and a liquid deuterium Cold Neutron Source, also performing a diverse and independent shutdown system by means of its drainage.
A chimney rises above the core to guide the primary flow towards the pump while a closure flow entering the top of the chimney prevents active particles from reaching the surface of the pool. Under shutdown condition the core is cooled by natural circulation of the water inside the reactor pool. A set of out-of-core irradiation positions, positioned in the reflector vessel region, are independently cooled by means of the pools cooling system. A scheme of the RA-10 reactor pool is presented in Fig 1.

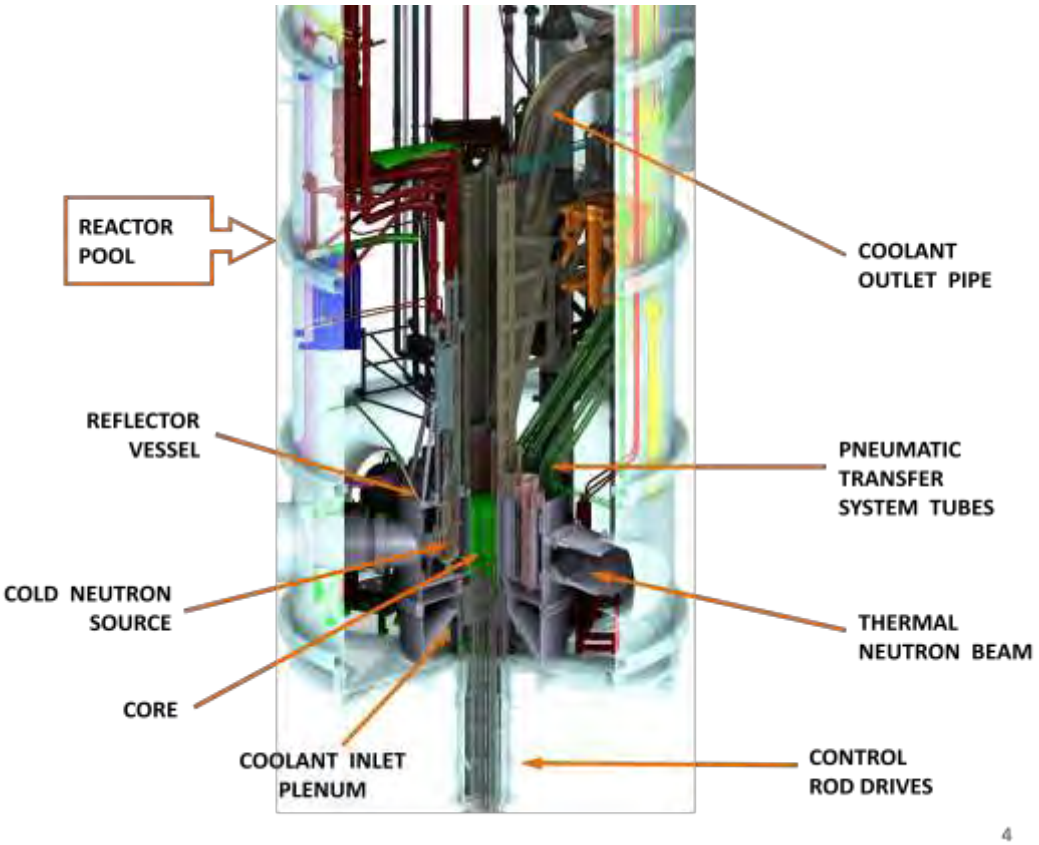

Fig 1. RA10 Reactor Pool

2.2 IRRADIATION FACILITIES FOR MOLYBDENUM PRODUCTION

The facility is designed with the capacity to produce up to 4000 Ci of Mo-99 per irradiation position at the end of irradiation. LEU plates targets used to obtain Mo-99, are irradiated

inside special rigs which are manually loaded into 10 irradiation positions (up to 8 targets each one) of the Reflector Vessel as shown in the Fig 2.

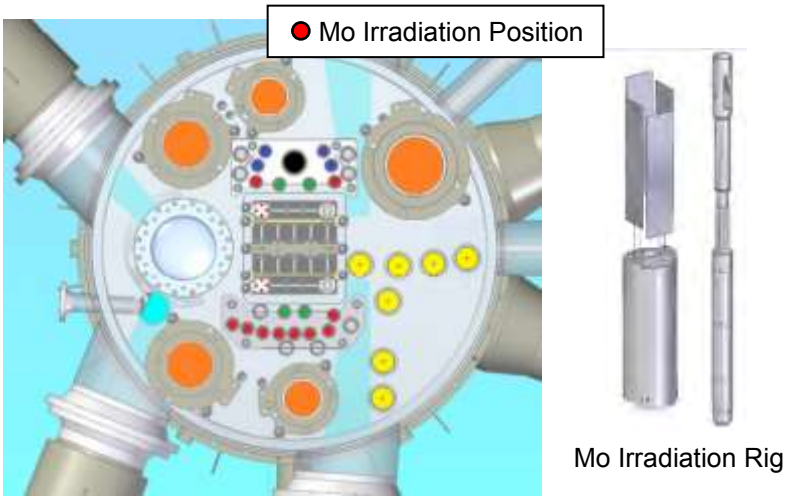

Fig 2. RA10 Core Irradiation Positions and Rigs

After 5 days in the position, irradiated rigs are manually moved to the Service Pool for partial decay before they are transferred to one of the Hot Cells located in the upper level by means of the Elevator, as shown in Fig 3

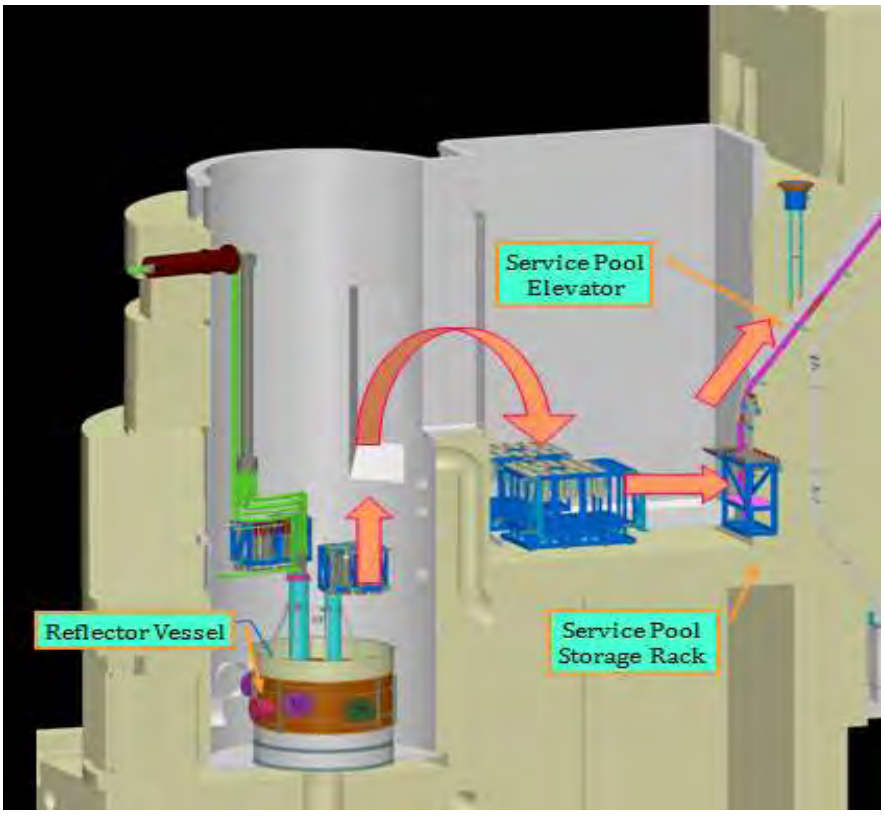

Fig 3. RA10 Molybdenum rigs transfer

The rigs are then disassembled and the irradiated targets are then sent to the Transfer Hot Cell by a shaft as presented in Fig 4.

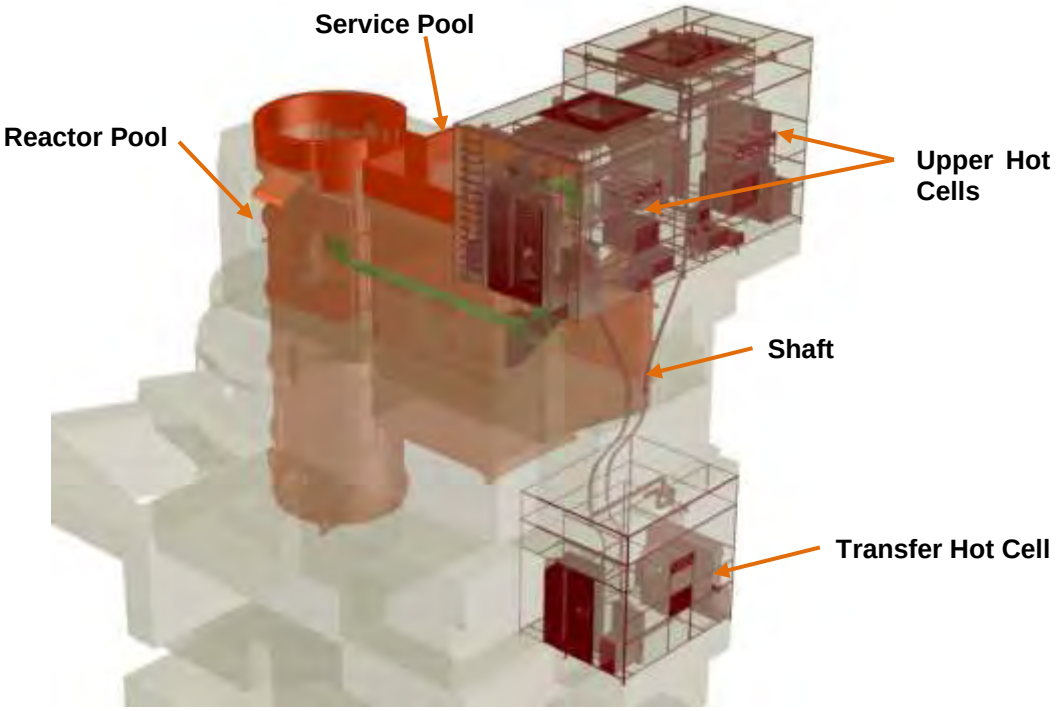

Fig 4. RA10 Hot Cells for Molybdenum targets transfer

In the Transfer Hot Cell, the targets are transferred to casks which allow their transport to the Radioisotope Production Facility. This facility is located in a separate building.
The Radioisotope Production Facility is based on a LEU UAlx target, successfully developed by CNEA in 2002 making Argentina a pioneering country in the matter.

3 Brazilian Multipurpose Reactor

In May 2013, the National Nuclear Energy Commission of Brazil (CNEN) signed with INVAP a contract to develop the basic engineering of the Brazilian Multipurpose Reactor (RMB). The RMB will be one of the main facilities of a high-tech centre to be developed in Iperó in the state of Sao Paulo. The Reactor Facility is being developed to be used for different purposes, using proven technology tailored to the specific requirements stated by CNEN. As in the case of RA-10, the facility design addresses the following objectives:

- Provide relevant radioisotope production and irradiation facilities;
- Provide a Neutron Activation Analysis Facility,
- Provide tuned facilities to conduct advanced scientific and industry neutron research

The following is a summary of the main characteristics of the reactor, extracted from [2] and [3].

3.1 RMB Reactor

The RMB configuration is based on a 30 MW open pool design with 23 LEU MTR fuel assemblies and 2 in-core irradiation facilities, reflected by a heavy water tank and beryllium blocks providing space for both, in and out-of-core irradiation positions and a liquid deuterium Cold Neutron Source. The reactivity control system and shutdown system features similar characteristics to OPAL and RA-10 reactors, as well as the cooling systems. A scheme of the RMB reactor pool is presented in Fig 5.

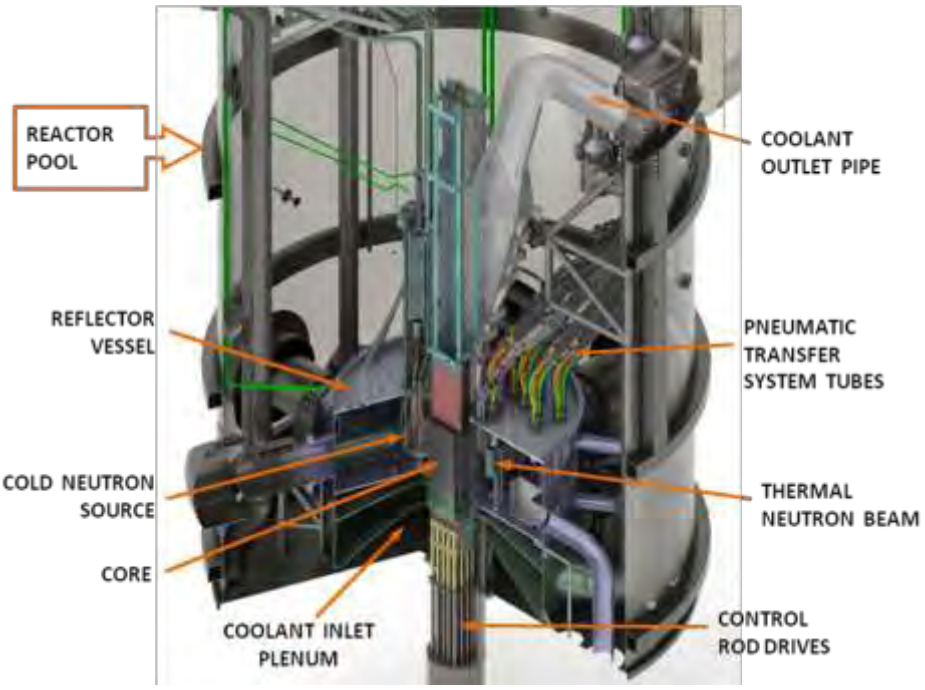

Fig 5. RMB - Reactor Pool

3.2 IRRADIATION FACILITIES FOR MOLYBDENUM PRODUCTION

The facility is designed with the capacity to produce up to 3000 Ci of Mo-99 per irradiation position at the end of irradiation. LEU UAlx plate targets used to obtain Mo-99, are irradiated inside special rigs which are manually loaded in up to 11 production irradiation positions of the Reflector Vessel, as shown in Fig 6.

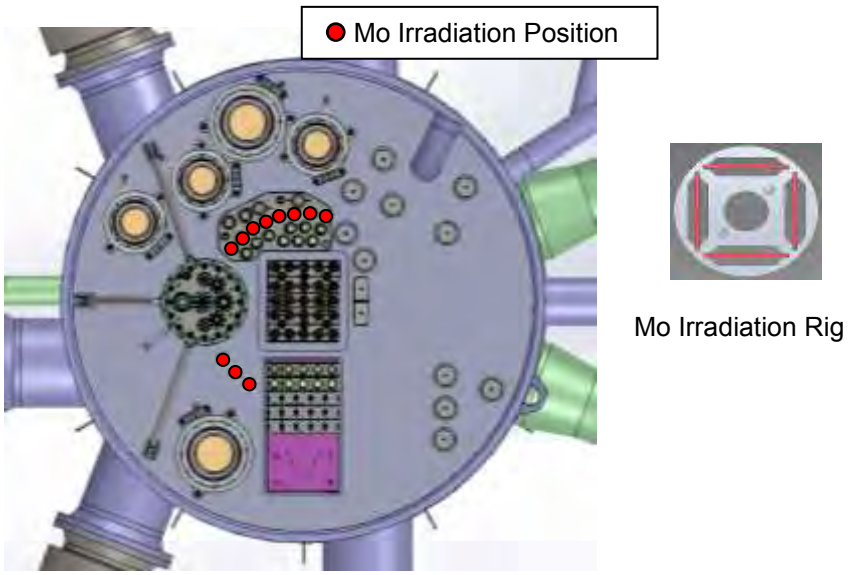

Fig 6. RMB - Core Irradiation Positions and Rigs

After 7 days in the position, irradiated rigs are then manually moved to the In-Confinement Service Pool for partial decay before they are transferred to the Molybdenum Hot Cell by means of an elevator. Then the plates are sent to the Transfer Hot Cell by a shaft.

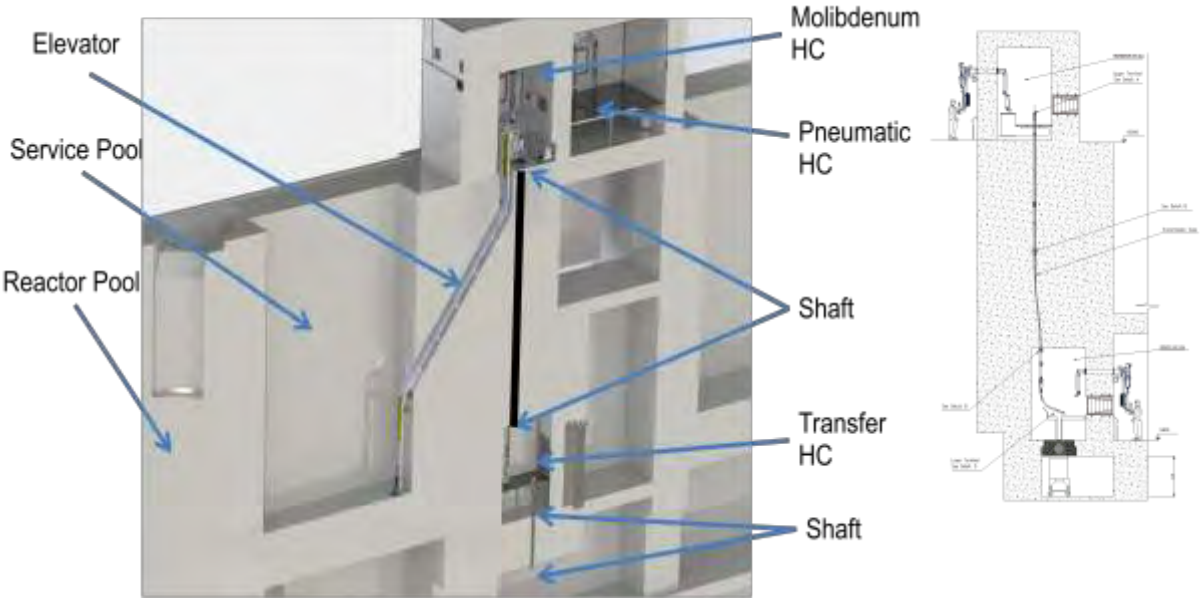

Fig 7. RMB - Molybdenum Hot Cells for targets transfer

In the Transfer Hot Cell, the targets are transferred to casks which allow their transport to the Radioisotope Production Facility, located in a separate building.
For this project, CNEN is developing the radiochemical process and Radioisotope Production Plant.

4 Medical Isotope Production Facility

In November 2014 INVAP has signed a contract with Coquí RadioPharmaceuticals Corp., a medical isotope company working to become the first U.S. commercial producer of Mo-99, to design its Medical Isotope Production Facility (MIPF) in Alachua, Florida. MIPF is an industrial facility dedicated to the production of radioisotopes Mo-99 and Iodine 131 (I-131).
The MIPF is designed in order to meet the regulatory requirements of the United States Nuclear Regulatory Commission (NRC). The Mo-99 will meet the purity requirements of the US Pharmacopoeia as well as the requirements of the major radiopharmaceutical companies that operate today in the United States market, based on the requirements INVAP understands they have today.
The Medical Isotope Production Facility (MIPF) encompasses two non-power Reactors, one Radioisotope Production Plant (RPP), and one Waste Conditioning & Temporary Storage Plant (WCP), together with the on-site services required.
The whole complex is intended to sustain, with high availability, an average production of 7000 Ci (six days calibration) per week (with the reactors each having the capability to produce a total capacity of 7000 Ci per week) of Mo-99 and 1200 Ci (end of process) per week of I-131 as a byproduct of Mo-99. Fig 8 shows a cross section view of the preliminary design of the facility

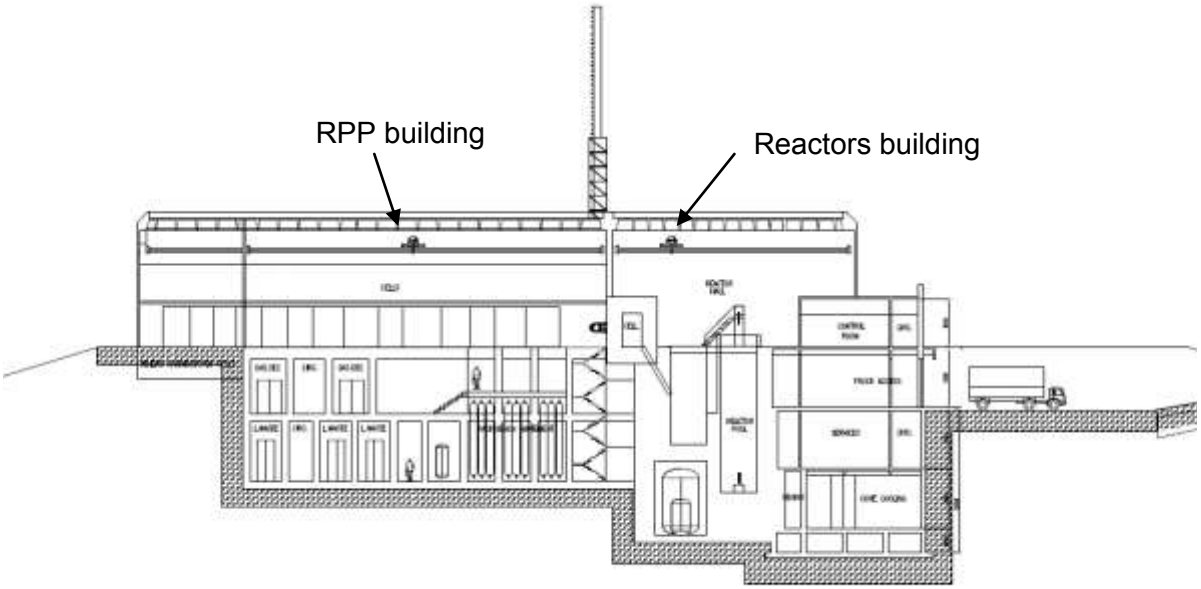

Fig 8. Cross section view of the preliminary MIPF

4.1 REACTORS

Both non-Power Reactors are identical regarding the core, shutdown system, cooling systems, reactor protection system and safety systems. Fig 9 shows the arrangement of the reactors. Highlights of the design of one of the reactors follows:

- **Reactor type and power:** The reactors design is based on the well proven open pool-type reactor concept with plate type fuel. The reactor core will be placed at the bottom of a stainless steel reactor pool filled with demineralized water. The core will feature MTR LEU (i.e. U_3Si_2 with U enrichment below 20%) fuel assemblies with aluminium cladding in a fixed core configuration. The total power level will be below 10 MW as required by 10 CFR 171.5 [3], optimized to ensure the radioisotope production goals whilst minimizing the fuel consumption rate.
- **Core design:** The reactor core will feature several fuel assemblies in a compact arrangement. The core will be surrounded by blocks of beryllium that will serve as neutron reflectors enhancing the neutronic performance of the core. The LEU UAlx targets for Mo-99 production will be located outside the core in the reflector.
- **Reactor control and shutdown:** The reactor will be controlled by displacing vertically a set of neutron absorbent plates. The reactor will include an automatic shutdown system. This automatic shutdown system will be triggered by the Reactor Protection System based on a redundant voting logic over relevant reactor signals.
- **Reactor cooling:** The power released by the fission process in the reactor fuel and the Mo-99 production targets will be removed by a forced flow of demineralized water through the cooling channels available in the fuel assemblies and target holders. The core flow will be provided by the Primary Coolant System and the flow in the targets by the Reactor Pool Coolant System, both built in stainless steel. The Primary Coolant System will transfer the thermal power received at the core through a heat exchanger towards a Secondary Coolant System that will reject the power to the atmosphere by means of Cooling Towers.

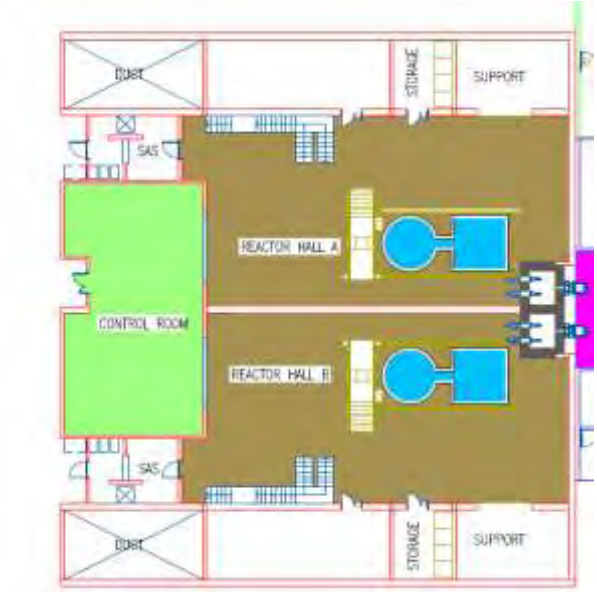

Fig 9. Overview of the MIPF reactors

4.2 RADIOISOTOPE PRODUCTION PLANT

The Coqui-MIPF will include an integrated Radioisotope Production Plant (RPP). The plant will be able to produce Mo-99 and I-131, and will be integrated with the reactor, in a way that the irradiated targets can be transferred directly from the service pool to the reactor cells which have a direct access to the Radioisotope Production Plant.

The Radioisotope Production Plant is designed and constructed to accomplish the good manufacturing practices and the international standards for the production of radioisotopes, in order to obtain products according to international pharmacopeia quality requirements and standards.

The RPP features two separated areas with three identical production lines. Each production line is composed of shielded hot cells housing the chemical processing and purification equipment that form the several stages required to extract and refine the Mo-99 and I-131.

The Mo-99 process encompasses the dissolution of the irradiated targets, the filtering and purification of the solution, separation of the Mo-99, followed by a final purification stage. Finally the material is prepared and bulk loaded into shielded transport casks to be shipped to the clients.

To deliver 7000 six-day Ci the RPP will be running several batches per week using 3 of the available lines. In case of unavailability of one of the two hot corridors (i.e. decontamination activities or maintenance) the RPP can continue delivering the average production. Additional shielded hot cells are dedicated to the conditioning of the radioactive wastes.

The arrays of shielded hot cells are designed in compliance with applicable ALARA and dose limits regulations.

Dedicated ventilation systems service the active areas and the shielded hot cells with appropriate air intake, recirculation, filtering, delay and exhaust features. A ventilation stack (shared with the reactors) is provided with a dedicated radiation monitoring system.

All the techniques and equipment for the quality control of the produced radioisotopes are available in the plant. The quality control laboratory has the needed equipment to perform the quality control of the products, including radiochemical, chemical, and biochemical control to assure the products meet the specifications for medical use.

A preliminary layout of the RPP is shown in Fig 10.

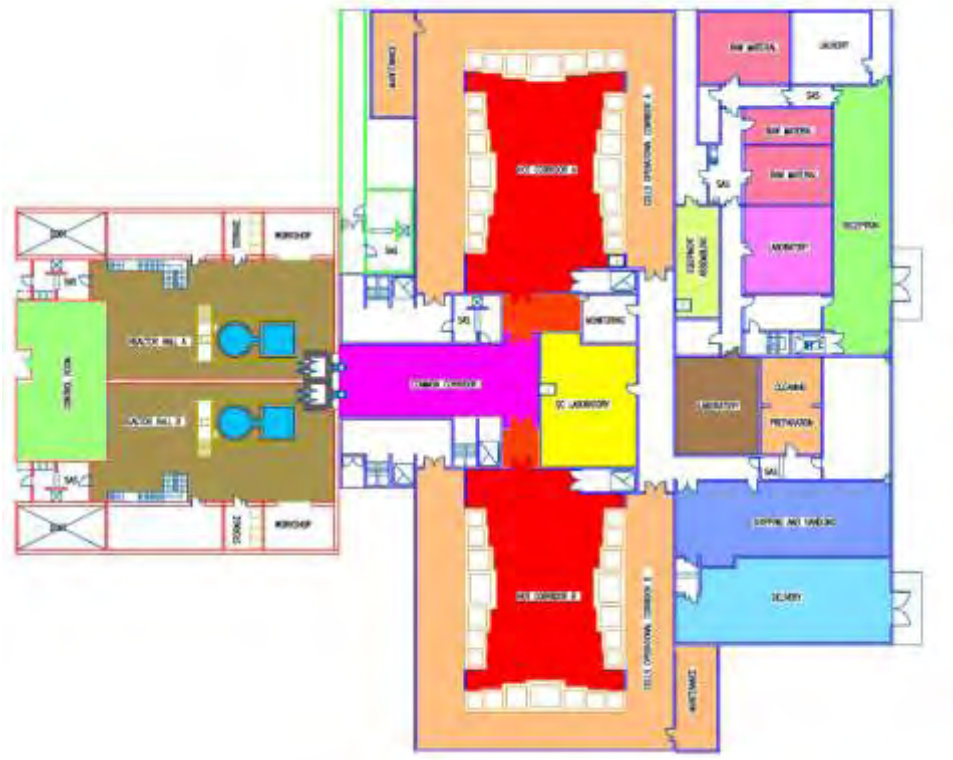

Fig 10. Preliminary Layout of MIPF

All the wastes generated by the reactors and the RPP will be managed in compliance with existing regulations and taking into account their specific characteristics (i.e. whether they are solid, liquids or gases; their nuclide composition, radioactivity level and their chemical composition). The dedicated WCP is set next to and integrated with the reactors and the RPP.

5 Summary and Remarks

As a recognized technological company with more than 35 years in nuclear development, INVAP is presently focused on projects related essentially to the design, construction and commissioning of reactors and irradiation facilities, radiochemical process plant, waste management, and integral regulatory support to our customers.
The present work is only a brief summary of the main projects related to the nuclear research reactors designed by INVAP to produce Mo-99 based on the LEU technology developed by CNEA. All these projects will play a central role to cover the international supply needs of radiopharmaceuticals in the near future, to overcome the present fragile Mo-99 supply chain.

6 References

[1] Herman Blaumann - “Argentina Advance in the RA-10 Project”, IGORR 2014, S. C. De Bariloche - Argentina, November 2014
[2] José Perrotta - “The new Brazilian Multipurpose Research Reactor”, IGORR 2014 S. C. De Bariloche - Argentina, November 2014.
[3] Claudio Mazufri – “The RMB Research Reactor Project”, IGORR 2014 S. C. De Bariloche - Argentina, November 2014.
[4] Code of Federal Regulation 10CFR171.5 Title 10 – Energy; Chapter I -- Nuclear Regulatory Commission; Part 171 - Annual Fees for Reactor Licenses and Fuel Cycle Licenses and Materials Licenses, Including Holders of Certificates of Compliance, Registrations, and Quality Assurance Program Approvals and Government Agencies Licensed by the NRC
[5] Diego Ferraro – “Neutronic Design Of The Coquí Reactor”, RRFM 2015, Bucharest, Romania, April 2015


RRFM
EUROPEAN RESEARCH REACTOR CONFERENCE 2015
ROMANIA
Bucharest
19 - 23 April 2015

Poster

MULTI-CHANNEL THERMAL HYDRAULIC ANALYSIS OF PLATE TYPE RESEARCH REACTOR

MOHAMMAD ALBATI, ASHRAF ALFANDI, KHALIFEH ABUSALEEM, SALIH ALKHAFAJI

Jordan Atomic Energy Commission (JAEC), Amman 11934, Jordan.

The University of Jordan, Amman 11942, Jordan

DAESEONG JO

Korea Atomic Energy Research Institute, 1045 Daeduk-daero, Dukjin-dong, Yuseong-gu, Daejeon, 305-353, Republic of Korea

ABSTRACT

An introduction of the multi-channel systems is introduced. The geometry of the multi-channel systems is described. The basic conditions used in the multi-channel analysis are introduced. The methodology of the multi-channels analysis is explained. An explanation of the different iterations used in the analysis is described. A description of the methodology used in the calculation of the temperature profiles of a multi-plate system is introduced. A multi-channels Thermal hydraulic analysis code is developed using the MATLAB programing software. A verification of the mass and energy conservation equation models and the basic conditions applied to the multi-channel analysis is conducted through the run of multiple test cases. The code is used to calculate the mass flow distribution and the temperature profile radially and axially for the China Advanced Research Reactor (CARR). The code results are validated against the results of (Tian et al., 2005). The developed code is applied to a 5 MW MTR reactor and the results for the mass flow distributions and temperature profiles are validated against the PLTEMP V3.7 code. A conclusion and suggestion for future work is introduced.

Keywords: TMAP, COOLOD-N2, thermal margin, forced convection, natural convection, research reactor

1.0 Introduction

Research reactors are nuclear reactors that are used primarily as a neutron source. These neutrons are utilized for many applications such as neutron transmutation doping (NTD), radioisotope production, material testing, and research and education. Research reactors are used all around the world. There are around 764 research reactors around the world from which 246 are operational, 5 under construction, and 8 planned .Research reactors are simpler than power reactors and operate at lower pressure and temperatures than power reactors. Although the fuel needed in the research reactor is less than power reactor, the uranium enrichment is much higher and in these days is limited to 20 percent enrichment as stated by the U.S. Department of energy in its program that was initiated to develop the means to convert research reactor from the use of highly enriched uranium to the low enriched uranium. This program was then called the Reduced Enrichment Research and Test Reactor (RERTR) project. There are many types of Fuel that are used in research reactors such as MTR type, TRIGA type, VVR, and many others. The most common type of fuel is MTR type. Almost 25% of the operational reactors around the world (65 research reactors) use the MTR type fuel, which constitutes the largest percent of the different fuel types used in research reactors (IAEA, 2009). The thermal power generated in research reactors have a very wide range starting from almost Zero power to the highest power of 250 MW in the ATR reactor in the United States (IAEA, 2009). The research reactor produces neutrons by uranium fission process. Each fission process produces about 200 MeV of energy. Most of This energy is carried out by fission products as kinetic energy and the rest goes as neutron or radiation energy. This energy is transferred to a heat form generated in the fuel and then transferred through cladding to the coolant. In the design process of research reactors, many limitations control the way of design. One of the most important steps in the design of research reactors is to ensure their safety against nuclear and thermal hydraulics margins. The insurance of reactor safety against these limits is very important to prevent any failure in the fuel plate that can lead to a release of radioactive materials into the environment. These limitations are divided into nuclear limitations and thermal limitations. The nuclear limitations includes reactivity control, power density, etc. the thermal limitations includes fuel, cladding, and coolant temperatures, along with many safety limiting parameters such as Onset of Nucleate Boiling (ONB), Onset of Flow Instability (OFI), and Departure from Nucleate Boiling (DNB). In general, computer codes are used to evaluate the thermal hydraulic margins of research reactors, but unfortunately most of the developed and commercialized codes are originally designed for power reactors such as RELAP and RETRAN. Although more recent versions of these codes include modifications capable of simulating the operational conditions of research reactors, the use of these codes requires a lot of effort in the input preparation and program simulation. For this reason, many attempts had been made to develop simpler thermal hydraulics codes to design, license, and evaluate the performance of research reactors under various conditions. For example, JAERI (Japan Atomic Energy Research Institute) developed COOLOD-N2, which was applied to evaluate the steady state thermal hydraulic analyses for JRR-3. In 2011, KAERI (Korea Atomic Energy Research Institute) developed a computer code, TMAP, to evaluate the thermal hydraulic margins of a plate type fuel research reactor. Although there are many computer codes, they cannot be directly applied to a newly designed research reactor owing to the unique features of the research reactor or the different methodology adopted by the regulatory body. Most of these designed thermal hydraulic codes are used for single channel analysis, in which the mass flow rate and heat flux are provided as input parameters. In single channel codes, it is assumed that the heat generated in a fuel plate is distributed equally to the two adjacent channels. This assumption may not be true for the case where different cooling conditions exist on the two sides of the fuel plate. In some cases, the mass flow distribution and the heat distribution between the different types of flow paths in the reactor should be calculated rather than assumed.

Most of these are designed for single channel analysis, in which the mass flow rate and heat flux are provided as input parameters. The following study is conducted to develop a thermal hydraulic code that is capable of calculating the mass flow distribution between different flow paths in parallel with each other and connected to a shared upper and lower plenum. The code is also capable of calculating the coolant, cladding, and fuel temperature profiles radially and axially.

2.0 Geometry model

The geometry of the parallel coolant mass flow paths are shown in Figure II-1. The system is composed of (***np***) number of parallel flow paths that is connected only at the upper and lower plenums. It is assumed that each flow path is composed of different axial regions. Each axial region in a flow path has its own, geometry and properties. There are two main types of flow paths which are:

1. Heated flow paths (Fuel assemblies).
2. Un-heated flow paths (different types of bypasses).

In the heated flow paths there is a parallel fuel plates, and so more calculation efforts are needed to obtain the mass flow distribution in the flow channels parallel to the fuel plates. Figure II-2 shows the geometrical model for single fuel assembly which is considered as single flow path in the system shown in Figure II-1. The fuel assembly is composed of different axial regions. Each region has its own shape and dimensions. Axial Regions are numbered from ***J=1*** to ***J=nr*** including the region between fuel plates. The pressure drop in the fuel assembly is the sum of the pressure drops in each of the axial regions.

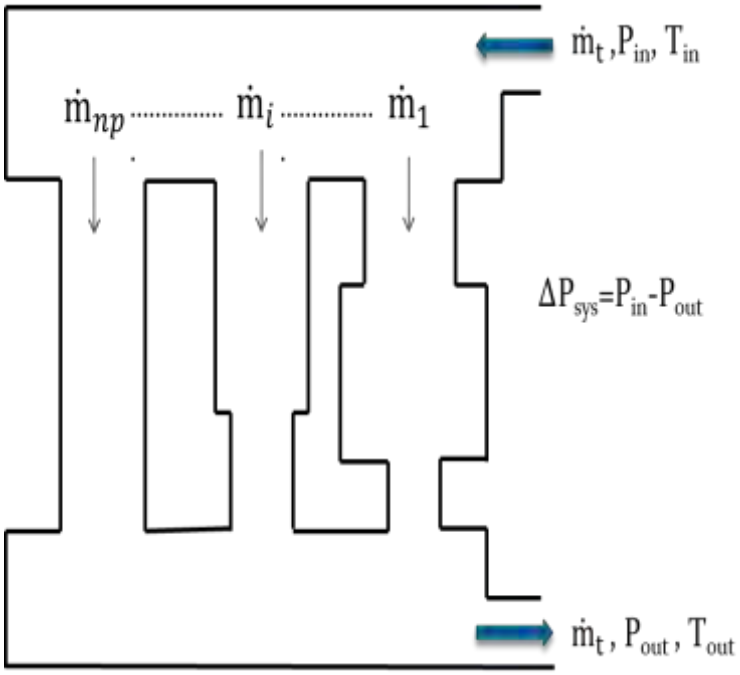

Figure 1: Parallel flow paths system.

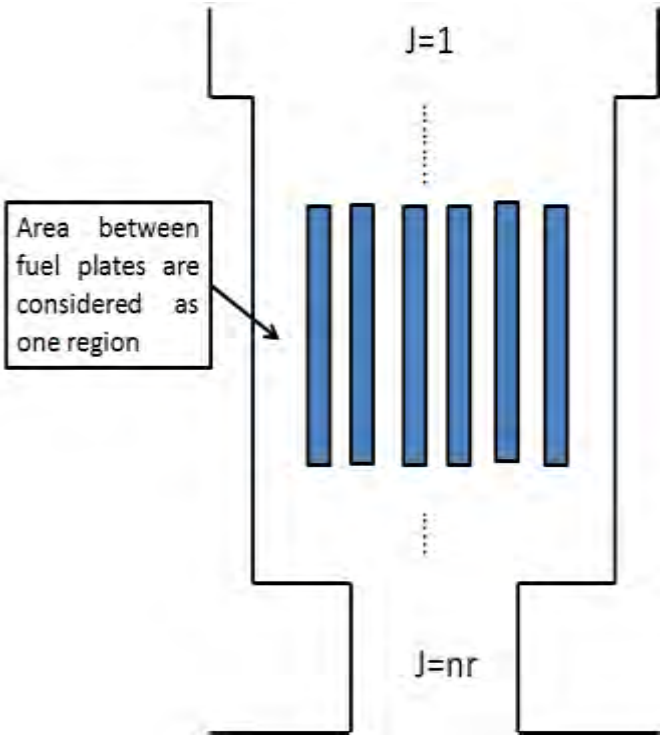

Figure 2: Assembly geometry.

3.0 Governing equations:

In this section, the general governing equations for mass, momentum, and energy are introduced. The assumptions used in the derivation of the final version of these equations are described.

3.1 Mass conservation equation:

The mass conservation equation (continuity equation) is

$$\frac{\partial \rho}{\partial t} + \frac{\partial}{\partial z}(G) = 0$$

Where ρ is the coolant density in *kg/m*^{3}, G is the coolant mass flux in *kg/m*^{2}*.s*, t is time in *s*, and *z* is the axial location in *m*. Assuming steady state conditions, the equation reduces to

$$\frac{\partial}{\partial z}(G) = 0$$

Integrating along the axial length of the channel and multiply by the constant flow area yields

$$G * A_{flow} = Constant$$

This constant is the mass flow where $G * A_{flow} = \dot{m}$.

3.2 Momentum equation

The momentum equation is

$$\frac{\partial G}{\partial t}+\frac{\partial}{\partial z}\left(\frac{G^2}{\rho}\right)=-\frac{\partial p}{\partial z}-\frac{f\,G\,|G|}{2D_h\rho}-\rho g\cos\theta$$

Where G is the coolant mass flux in *kg/m².s*, t is the time in *s*, z is the axial location in *m*, ρ is the coolant density in *kg/m³*, p is the pressure in *kg/m.s²* (*Pascal*), f is the dimensionless friction factor, D_h is the hydraulic diameter in *m*, g is the gravity acceleration in *m/s²*, θ is the angle from the vertical position ($\theta = 0$) for vertical channels. Assuming steady state condition yields to

$$\frac{\partial}{\partial z}\left(\frac{G^2}{\rho}\right)=-\frac{\partial p}{\partial z}-\frac{f\,G\,|G|}{2D_h\rho}-\rho g\cos\theta$$

Assuming a vertical channel (θ=0) of length L, and integrating yields to the total pressure drop in the channel as

$$\Delta p=\int_0^L \rho g\,dz+\int_0^L\left(\frac{f\,G\,|G|}{2D_h\rho}\right)dz+\sum\left(\frac{K\,G\,|G|}{2\rho}\right)dz+G^2\left(\frac{1}{\rho(L)}-\frac{1}{\rho(0)}\right)$$

3.3 Energy equation

The energy equation used in the analysis is

$$\dot{m}C_p\frac{dT}{dz}=q''*P_h$$

Where $\dot{m}$ is the mass flow rate in *kg/s*, C_p is the specific heat of coolant in *kJ/kg.°C*, T is the temperature in *°C*, *z* is the axial length in *m*, q'' is the heat flux in *kW* ,and P_h is the heated perimeter in *m*.

4.0 Analysis methodology:

4.1 Multi-Channels basic applied condition:

In this section, a description of the two main conditions that should be satisfied in the analyses of Multi-channel systems is described. These two conditions are used in the multi-channel thermal hydraulic codes to obtain the mass flow distribution in the system. The two conditions are:

1. Equal pressure drop in all flow paths.
2. Conservation of the total mass flow rate.

Pressure drop condition

Since the parallel flow paths are connected to the shared upper and lower plenums, they all share the same coolant pressures at the inlet and outlet. This means that all the flow paths shares the same amount of pressure drop given as

$$\Delta P_1=\Delta P_2=\Delta P_3=\ldots..=\Delta P_i=\cdots..=\Delta P_N=P_{in}-P_{out}$$

Where ΔP_i is the total pressure drop through the i-th flow path, P_{in} is the inlet pressure to the system (shared for all flow paths), P_{out} is the outlet pressure to the system (shared for all flow paths).

Conservation of the total mass flow rate

The total mass flow rate is equal to the summation of all the flow rates in the different flow paths. This provides us with

$$\dot{m}_t = \sum_i \dot{m}_i$$

Where $\dot{m}_t$ is the total mass flow rate in the system in *kg/s* and $\dot{m}_i$ is the mass flow rate in the i-th flow path in *kg/s*.

4.2 Calculation methodology:

The calculation methodology of the thermal hydraulic analysis is summarized by the following three main functions:

1. Iteration on pressure drop.
2. Iteration on mass flow (subroutine FLOW).
3. Solution of the multi-plate temperature profile.

Each of the previous main functions is explained separately.

4.2.1 Iteration on pressure drop

In this section the solution procedure to obtain the mass flow distribution is described. The inputs needed for the calculations are the total mass flow rate, the inlet pressure and temperature to the system, the geometry of all the flow paths, and the heat generation in each flow path. The unknowns are:

1. The mass flow rates distribution in the system.
2. Pressure drop through the system.

The known parameters are:

1. Total mass flow rate.
2. Inlet pressure and temperature to the system.
3. Geometry of all flow paths.
4. Heat generation in each fuel plate.

Iteration on the pressure drop in the system is the main body of calculation procedure, and it is the outer iteration of the calculation code.

4.2.2 Iteration mass flow rate (subroutine FLOW)

The subroutine **FLOW** is used to calculate the mass flow in a single flow path for a given pressure drop. The known variables are:

1. Pressure drop in the flow path (from the pressure drop iteration).
2. Geometry of the flow path.
3. Heating condition of the flow path.

The unknown variable is the mass flow rate in the flow path. There are two procedures used in subroutine flow depending on the heating condition of the flow path:

1. Procedure for the un-heated flow path (different types of bypasses).
2. Procedure for the heated flow path (fuel assemblies).

4.2.3 Multi-plate temperature profile solution:

In The single channel thermal hydraulic analysis, it is always assumed that the heat is distributed symmetrically from the fuel plate to the two adjacent channels and that the maximum fuel temperature is located in the middle of fuel plate thickness. This assumption is valid only for the case where exact cooling conditions are applied to the two sides of the fuel plate. In some cases the cooling conditions from the two sides differ from each other. This happens if a different channels thickness and so different mass flow rates exists on both sides of the fuel plate. In this analysis, it is assumed that each channel have different flow area and wetted perimeter and also it is assumed that each fuel plate have different dimensions, thicknesses, and heat generation rates. First, a differentiation of the heat and energy transfer equations is conducted on a system composed of only two plates and 3 channels. Then the solution is extended to a system composed of N plates separated by N+1 Channels. The description of the solution requires a large amount of explanation and derivation so it was dismissed in this paper.

5.0 Results:

The China Advanced Research Reactor (CARR) is located at the china institute of atomic energy. It is multi-purposes research reactor used for neutron scattering measurements, radioisotope production, neutron transmutation doping, etc. the CARR is a tank in pool reactor with nuclear power of 60 MW. Slightly pressurized light water is used as the primary coolant. The top of the reactor core is located 16 m below the surface of the pool. The core is about 0.85 m in height and 0.451 m in diameter. Under the normal operation of CARR, the coolant is pumped to flow through the cold leg, downward through the active core, then through the decay tank, the hot leg, the heat exchanger, and re-circulated to the main pump (Tian et al., 2005).
In 2005, a thermal hydraulic study is conducted on the CARR by (Tian et al., 2005). In the study, the whole reactor core is analysed to find the mass flow distribution in reactor assemblies, and the temperature profile of coolant, cladding, and fuel in each fuel element. In the following sections, the CARR reactor is analysed using the developed Multi-Channel Code. And the results are compared and verified against the results shown by (Tian et al., 2005).

Design parameters of CARR:

The main design parameters of CARR are shown in Table 1. The core is composed of 17 standard fuel assemblies and 4 follower fuel assemblies. Each standard fuel assembly is composed of 20 fuel plates separated by 21 coolant channels. All the standard fuel assemblies have the same geometry. All the fuel plates in the standard fuel assembly have the same shape and geometry. The channels in the assemblies vary in thicknesses and are symmetrical around the centre channel. The channels thickness variations are shown in Figure 3 (Xian et. al) below. As can be seen, there are 5 different channel thicknesses. In the code, the channels are numbered from left to right starting from 1 to 21 as shown in Figure 4. The geometry of fuel plates and coolant channels are summarized in Table 2

Table 5: Main design parameters of CARR.

Design parameters	Input
Core diameter (m)	0.399
Core height (m)	0.85
Elevation of reactor pool water surface (m)	13.2
Core inlet temperature (^{o}C)	35
Core inlet pressure	0.89
Core nuclear power (MW)	60
Core thermal power (MW)	56.4
Mass flow rate in primary loop (kg/s)	600
Number of standard fuel assembly	17
Number of follower fuel assembly	4
Type of fuel elements	Plate

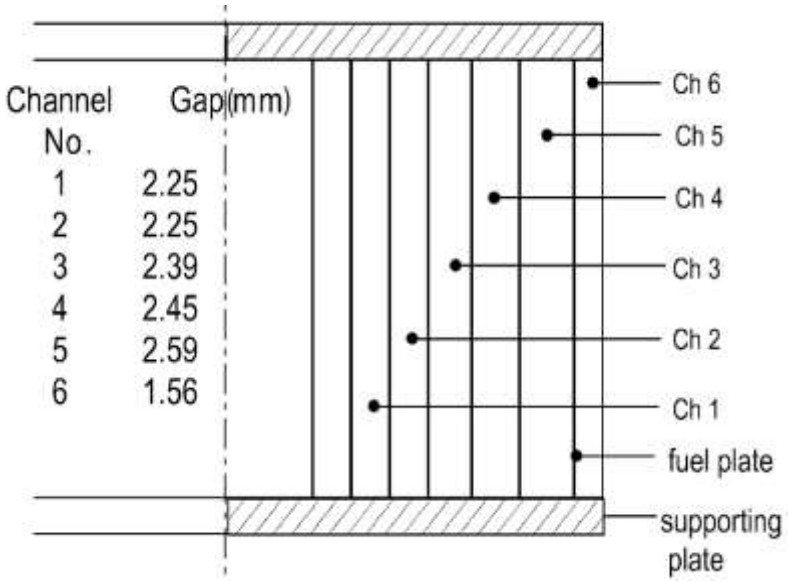

Figure 3: Detailed structure of CARR standard assembly.

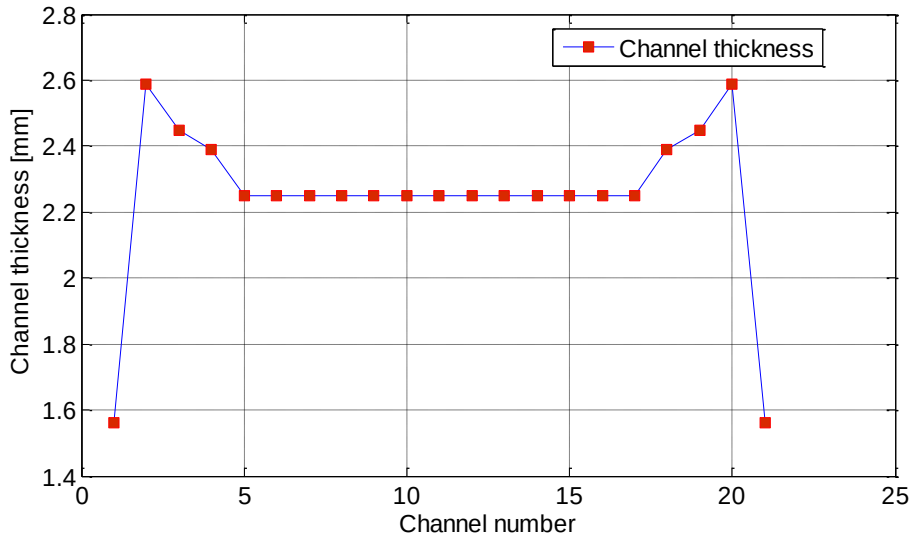

Figure 4: Channels thickness variation of the standard fuel assembly.

Table 2: Fuel plate and coolant channels geometries.

Geometry parameter	Input
Fuel plate	
Fuel thickness[mm]	0.6
Fuel width [mm]	61.6
Fuel length [mm]	850
Cladding thickness [mm]	0.38
Fuel thermal conductivity [W/m.oC]	32
Cladding thermal conductivity	180
Coolant Channel	
Channel width [mm]	71
Channel thickness [mm]	Figure 4
Channel length [mm]	880

The power distribution in the fuel assemblies is represented by the radial power peaking factor distribution that is shown in Figure 5. The power generated in one assembly is assumed to be distributed equally between the different fuel plates in the assembly. The axial length of the active core is divided into 17 control volumes. Each control volume has its axial weighted power factor. The axial weighted power distribution used in the analysis is shown in Figure 6.

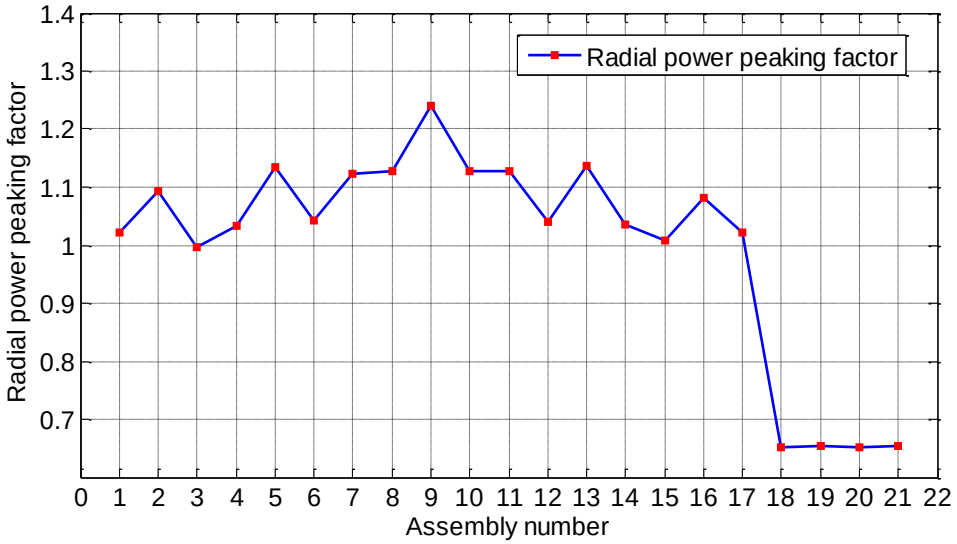

Figure 5: Radial power peaking factor distribution.

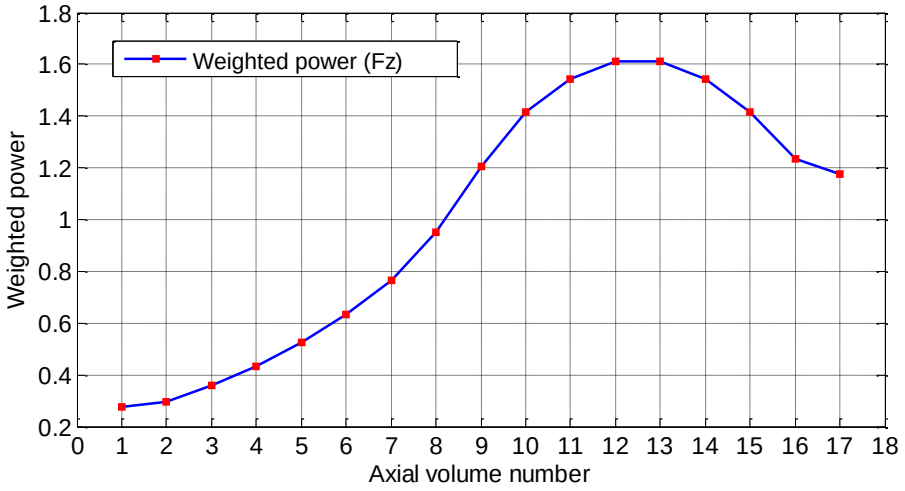

Figure 6: Axial weighted power distribution.

The results of thermal hydraulic analysis of CARR show a good agreement between the developed code and the results published by (Tian et al., 2005). The mass flow distribution in the standard fuel assemblies is shown in Figure 7. The results shows a good agreement with a maximum relative error of 0.3% which could be neglected. As can be seen from Figure 7, the assembly mass flow rates distribution follows the same trend in both results. The assembly with the highest power generation requires more mass flow rate in order to keep the same pressure drop. This phenomenon is studied in detail and the reason is found to be the effect of temperature on the density and viscosity of water. As it is already described the pressure drop is calculated using The Equation below

$$\Delta \mathrm{P}_{friction} = \frac{1}{2}\rho V^2 \frac{fL}{D_h}$$

The friction factor used is calculated as

$$f = 0.316 Re^{-0.25}$$

Where Re is given by

$$Re = \frac{\rho V D}{\mu}$$

And the velocity V is given by

$$V = \frac{\dot{m}}{\rho A}$$

This gives the following equation for pressure drop

$$\Delta P_{friction} = \left(\frac{0.316}{2}\right)\left(\frac{{D_h}^{-1.25} L}{A^{1.75}}\right)\left(\frac{\mu^{0.25}}{\rho}\right)\dot{m}$$

The first and second terms on the right hand side are independent of heat flux, and only the third term in parentheses is to be studied. The change in μ , ρ, and $\frac{\mu^{0.25}}{\rho}$ with temperature is shown in Figures 7, 8, and 9 respectively. As can be seen from Figures 7 to 9, the effect of increasing the heat flux is to decrease the value of ($\mu^{0.25}/\rho$), which in turn decreases the frictional pressure drop and so the total pressure drop.

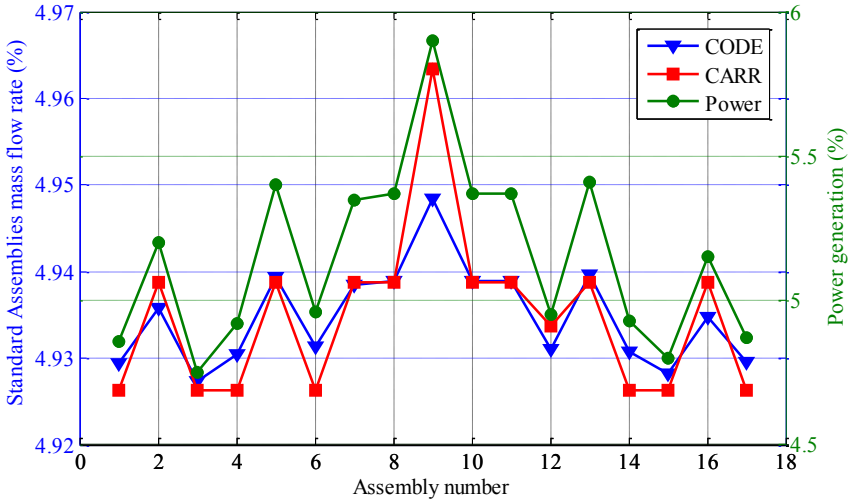

Figure 7: Assemblies Mass flow rate distribution.

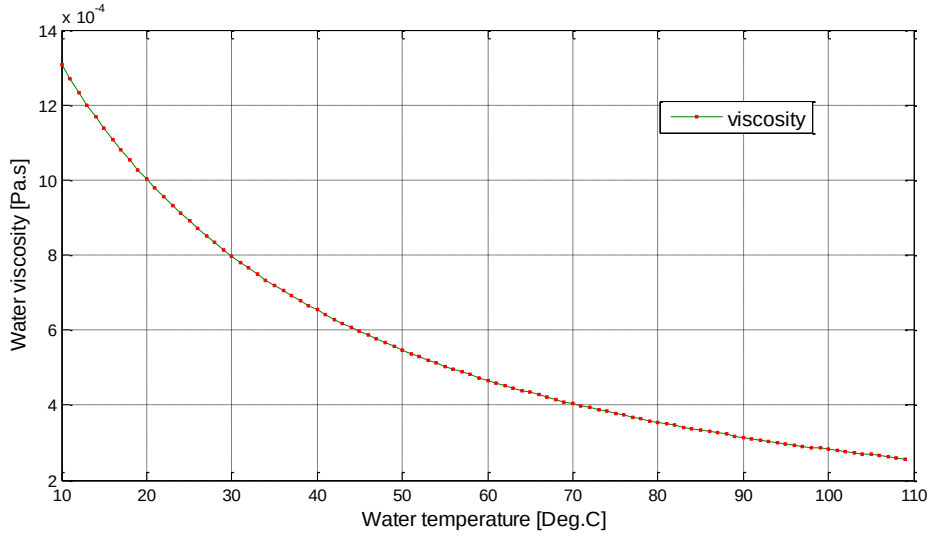

Figure 5-1: The change in water viscosity μ with temperature under a fixed pressure of 0.17 MPa.

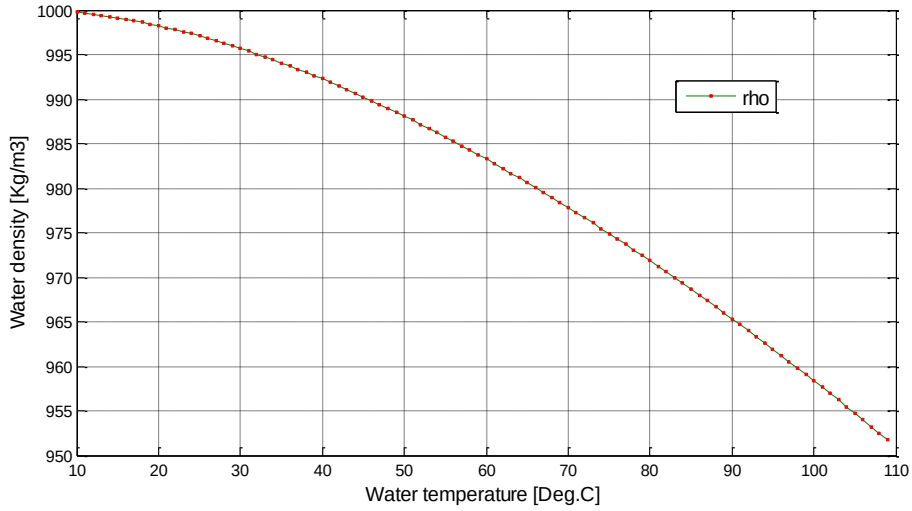

Figure 8: The change in water density $\boldsymbol{\rho}$ with temperature under a fixed pressure of 0.17 MPa.

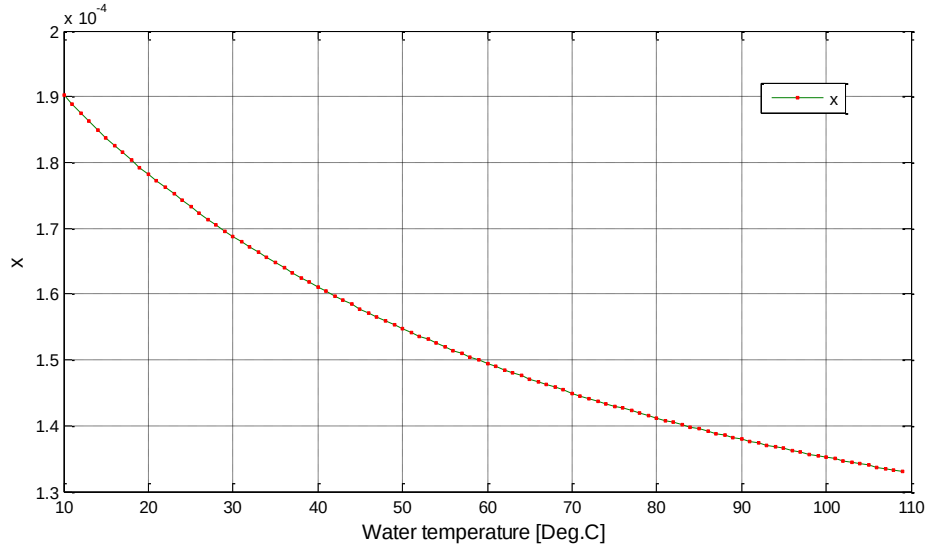

Figure 9: The change in $\boldsymbol{x = \frac{\mu^{0.25}}{\rho}}$ with temperature under a fixed pressure of 0.17 MPa.

The channels mass flow distribution is shown in Figure 10 below. As can be seen, the results show a good agreement. The maximum error in the channels flow rates is calculated to be 3.7%.

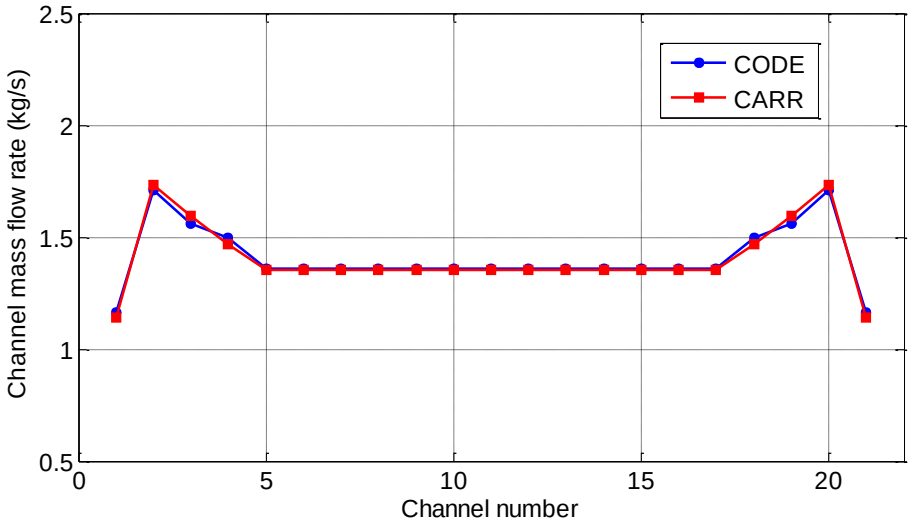

Figure 10: Channels mass flow distribution in the hot assembly (Assembly No.9).

The axial coolant temperature profiles in Channels types numbered from 1 to 6 are shown in Figure 11 below. Figure 12 shows the zoom out view for channels 1 and 2. The coolant channels outlet temperatures for all the 21 channels (numbered 1 to 21 starting from left to right) of the hot assembly in CARR reactor are shown in Figure 13. The maximum difference is 0.7 °C.

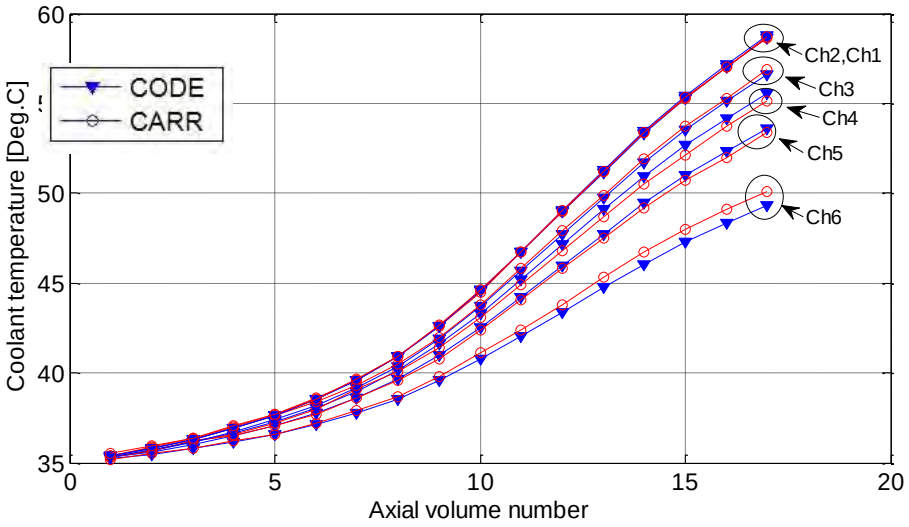

Figure 11: Axial coolant temperature profile along the hot assembly for channels 1 to 6.

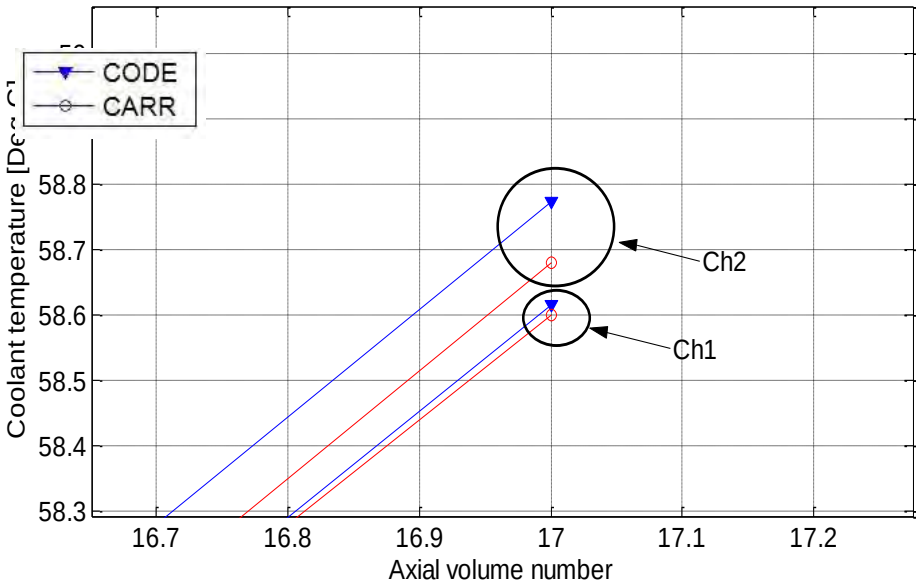

Figure 12: Zoom out of Figure III-11 around channels 1 and 2.

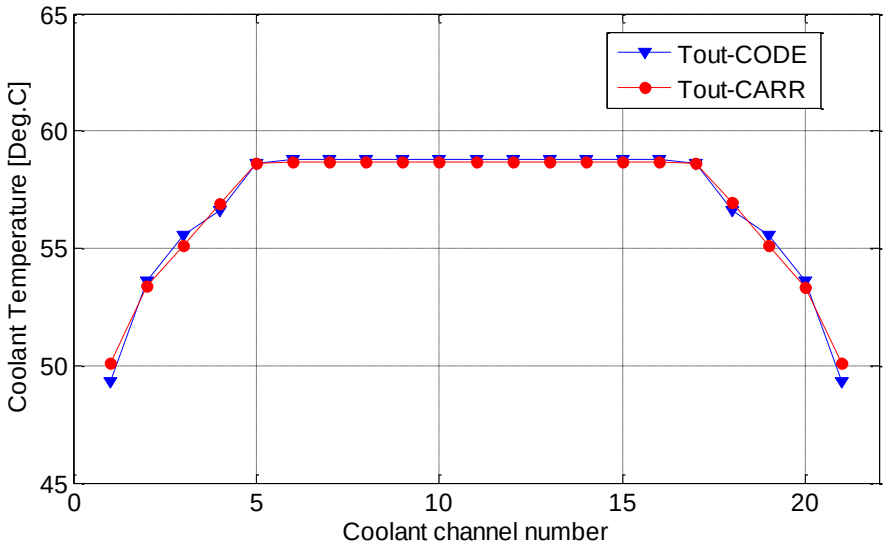

Figure 13: Channels coolant outlet temperatures in the hot assembly in CARR.

As can be seen from Figures 10 to 13, the mass flow rates and coolant temperature shows a very good agreement.

Development of performance analysis code for research reactor fuel

G.Y. JEONG, D-S. SOHN

UNIST, 50 UNIST-gil, Eonyang-eup, Uljoo-gun, Ulsan 689-798 – Republic of Korea

Kyu Hong Lee, Jong Man Park

Korea Atomic Energy Research Institute, 989-111 Daedeokdaero, Yuseong, Daejeon 305-353,– Republic of Korea

ABSTRACT

Thermo-mechanical code dedicated to the modeling of U-Mo dispersion fuel plates is being under development in Korea to satisfy a demand for advanced performance analysis and safe assessment of the plates. The major physical phenomena during irradiation are considered in the code such that interaction layer formation by fuel-matrix interdiffusion, fission induced swelling of fuel particle, mass relocation by fission induced stress, and pore formation at the interface between the reaction product and Al matrix.
The framework of performance analysis code for U-Mo dispersion fuel has been established with newly updated models.

1. INTRODUCTION

The need to develop an advanced performance and safety analysis code for research reactor fuel grows in Korea. A performance analysis modeling applicable to research reactor fuel is being developed with available models describing fuel performance phenomena observed from in-pile tests. We established the calculation algorithm and scheme to best predict fuel performance using radio-thermo-mechanically coupled system to consider fuel swelling, interaction layer growth, pore formation in the fuel meat, and creep fuel deformation and mass relocation.

In this paper, we present a general structure of the performance analysis code for typical research reactor fuel and advanced features such as a model to predict fuel failure induced by combination of breakaway swelling and pore growth in the fuel meat.

2. CODE FRAMEWORK

Accurate prediction of fuel temperature and states of stresses induced by fission is essential for research reactor fuel performance code. It is necessary to employ proper and sufficient models that are applicable evaluate in-pile behaviors such as a dimensional change, stress-strain variation, and material degradation by fission and neutron irradiation.

Drastic microstructure changes in the dispersion fuel meat have been observed and investigated including interaction layer (IL) formation by fuel-Al matrix interdiffusion, fuel-Al

matrix consumption, and large pore formation, particularly at the interface of IL and Al matrix. It is necessary to take into consideration of the coupling between thermal and mechanical response to predict those microstructure variation of the meat.

In this section, a general fuel performance model implemented in the code such as temperature calculation, stress-strain analysis, fission induced swelling are described.

2.1. PERFORMANCE MODEL

The coupling among thermal, mechanical, and irradiation-related performance issues is critical to fuel performance modeling. Typical operation temperature for U-Mo/Al dispersion fuel meat for plate type is below 200 ^{o}C, but it is dependent on fuel meat thermal conductivity which is influenced by fuel meat morphology and material composition. Particularly, fuel meat thermal conductivity degradation is mostly influenced by Al matrix depletion by IL growth since it is believed that IL has poor thermal conductivity.

The variation of fuel meat morphology is induced by three major phenomena : fuel swelling, IL formation, and pore formation. Details of models implemented in the code are described in the following subsection.

2.1.1. FUEL SWELLING

U-Mo fuel swelling is dependent on Mo content. An empirical correlation for U-10Mo fuel swelling was documented by Kim [1]. U-10 wt% Mo fuel swelling is given as a function of fission density (FD) as follows :

$$\begin{aligned} (\frac{\Delta V}{V_0})_f &= 5.0 f_d && f_d \le 3\times10^{21}\,\text{fission/cm}^3 \\ (\frac{\Delta V}{V_0})_f &= 15 + 6.3(f_d - 3) + 0.33(f_d - 3)^2 && f_d \ge 3\times10^{21}\,\text{fission/cm}^3 \end{aligned} \quad (1)$$

where f_d is in 10^{21} fission/cm^3.

The correlation for U-7 wt% Mo fuel swelling is also expressed as a function of FD as follows [2]:

$$\begin{aligned} (\frac{\Delta V}{V_0})_f &= 5.0 f_d && f_d \le 2\times10^{21}\,\text{fission/cm}^3 \\ (\frac{\Delta V}{V_0})_f &= 10 + 6.7(f_d - 2) + 0.58(f_d - 2)^2 && f_d \ge 2\times10^{21}\,\text{fission/cm}^3 \end{aligned} \quad (2)$$

where f_d is in 10^{21} fission/cm^3.

Compared to the U-10Mo fuel, the fuel swelling model for U-7Mo gives higher swelling rate since grain subdivision is assumed to occur at lower FD due to lower Mo content.

2.1.2. INTERACTION LAYER

IL growth is believed to cause an increase in meat volume. A time-dependent volume fraction of IL in meat needs to be modeled to evaluate volume expansion by IL growth.
IL growth models by using in-pile test data have been reported [3],[4]. The available IL growth model for in-pile tests is given as a modified Arrhenius equation, in which the fission rate is multiplied to account for fission-enhanced diffusion:

$$Y_0^2 = 2.6\times10^{-8}\sqrt{\dot{f}}\exp(-\frac{3850}{T})t \qquad (3)$$

where Y_0 is IL thickness for pure Al matrix in μm, $\dot{f}$ the fission rate in fission/cm^3-sec, T the temperature in K, and t the irradiation time in second.

The addition of Si in the Al matrix reduced IL thickness growth. It is also known that IL growth is dependent on the Mo content in the fuel. Additional factors to consider Si and Mo effects on IL growth are multiplied to Eq.(3) as follows:

$$Y^2 = Y_0^2 f_{Si} f_{Mo} \qquad (4)$$

where Y is IL thickness for Si-added Al matrix in μm f_{Si} is the reduction factor by Si addition into the matrix and f_{Mo} the Mo content factor on IL growth. Detailed explanation on these additional factors can be found in [4].

2.1.3. PORE FORMATION

Pores are formed in dispersion fuel; 1) pores within fuel particles, 2) pores in interaction layers (ILs), 3) pores at the interfaces (Fuel-IL, IL-Al). The pores contain fission gases. Pores in the ILs, specifically at IL-Al interfaces, tend to be larger than those in the fuel particles. Pore formation degrades fuel performance and integrity and has a potential to cause fuel failure.

Mechanism of pore formation, particularly at the interface between IL and Al matrix has been studied by different authors **Error! Reference source not found.**,[7]. It is assumed that the large pore formation is initiated with as-fabricated pores in the meat and fission gases released to those pores is a driving force of pore growth.

The advanced code is desired to have capability to predict fuel failure caused by pore formation and growth. To fulfil this, pore formation mechanism needs to be investigated further.

2.1.4. MASS RELOCATION

The mass transport of the meat in the dispersion fuel plate observed at the meat end region where fission density is highest along the width of the plates, has been studied [5],[6]. It is believed that the stresses caused by fission induced fuel swelling, and chemical volume expansion by interaction layer growth were mitigated by the creep deformation of a continuous phase which surrounds fuel particles.

The following equation was employed for the creep rate of the U-Mo fuel particles as:

$$\dot{\varepsilon}_c = A_c \sigma \dot{f} \tag{5}$$

where $\dot{\varepsilon}_c$ is the equivalent creep rate in s^{-1}, A_c the creep rate constant in cm^3/MPa, and $\dot{f}$ the fission rate in fission/cm^3-sec.

Recently updated modelling for mechanical deformation of fuel particles and meat swelling caused by fission-induced creep is considered in the developed code.

2.2. CODE STRUCTURE

Finite element analysis will be employed to calculate the temperature distribution in the fuel meat and cladding region. A fuel plate sectioned in length direction is shown in Fig. 1. Typical plate length is longer than any other dimension, so that it is assumed that heat conduction in the length direction is negligible. It also allows strain out of plane to be constant or zero, which is plane strain condition.

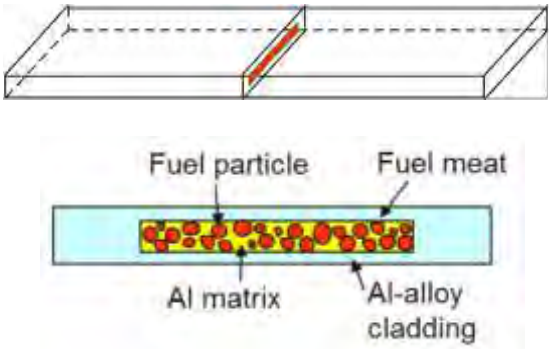

Fig. 1 A schematic of dispersion fuel plate and cross section at axial mid-plane.

The temperature distribution throughout the fuel meat and cladding in 3-dimension is calculated at each node. The models used in the temperature calculations assume a transversally symmetrical fuel plate surrounded by coolant.

User supplied conditions such as coolant information including coolant inlet temperature, coolant flow velocity, and coolant mass will be used to determine boundary conditions. User supplied fission rate will be used to calculate temperature distribution from the coolant to the meat centerline. A film temperature rise from the bulk coolant to cladding surface is calculated by finding film heat transfer coefficient for a given coolant and geometry. The temperature at the interface between clad and meat is calculated by using Fourier's law. The temperature rise to the meat centerline is determined by solving heat conduction equation for fuel particle, Al matrix, and IL with heterogeneously.

The modeled governing equations for temperature distribution calculation is given as follows:

$$-\nabla \cdot (k_{fuel}(\mathrm{T})\nabla T) = q'''$$
$$q''_{\mathrm{meat}} = -k_{clad}\nabla T \qquad (6)$$
$$q''_{clad} = h_c(T_{c,o} - T_{coolant})$$

Where q''' is the power density in the meat, k the thermal conductivities, q''_{meat} the total heat flux from the meat, q''_{clad} the heat flux from the cladding surface, $T_{c,o}$ the cladding outer surface, and $T_{coolant}$ the bulk coolant temperature.

With assumption on strain condition as mentioned, meat and cladding deformation calculation will be performed after obtaining temperature distribution. An accurate calculation of stresses in the meat and the cladding is needed to accurately calculate the strain and evaluate a potential of large pore formation and fuel failure.

Strain caused by irradiation can be obtained by solving the mechanical equilibrium equation as follows:

$$\sigma + \rho(\mathrm{T})f''' = 0 \qquad (7)$$

where ρ is the density, f''' is volumetric forces induced by fission, and σ the stress tensor.

Fig. 2 shows the overall structure of the new code system. Each performance model will be classified in several modules. Mechanical response prediction for each plate component will be performed with prescribed condition from previous thermal analysis.

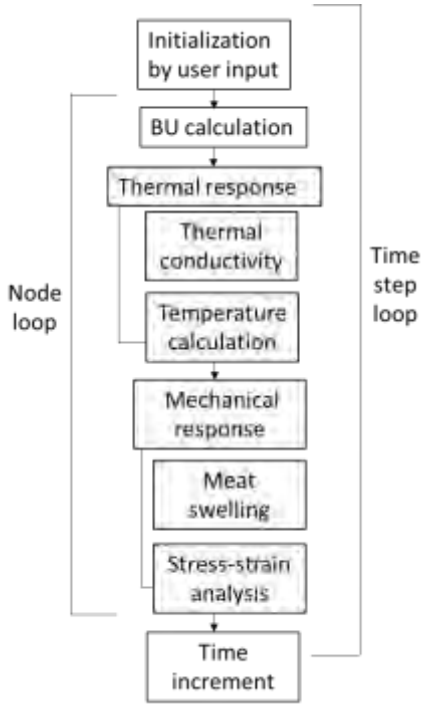

Fig. 2 Overall structure of research reactor fuel performance code.

3. CONCLUSION

Thermo-mechanical code dedicated to the modeling of U-Mo dispersion fuel plates is being under development in Korea to satisfy a demand for advanced performance analysis and safe assessment of the plates. The major physical phenomena during irradiation are considered in the code such that interaction layer formation by fuel-matrix interdiffusion, fission induced swelling of fuel particle, mass relocation by fission induced stress, and pore formation at the interface between the reaction product and Al matrix.

The framework of performance analysis code for U-Mo dispersion fuel has been established with newly updated models with studies on advanced fuel performance modeling.

ACKNOWLEDGMENTS

We would like to acknowledge helpful discussion and kind consultation by Yeon Soo Kim. UNIST was supported by the National Research Foundation of Korea (NRF) grant funded by the Korean government (Ministry of Education, Science and Technology) (No. 2011-0031771), and in part by National Nuclear R&D Program sponsored by Ministry of Science, ICT and Future Planning. (NRF-2013M2A8A1041241) for the KAERI contribution.

REFERENCES

[1] Yeon Soo Kim, G.L. Hofman, J. Nucl. Mater., 419 (2011) 291.
[2] Yeon Soo Kim, G.Y. Jeong, G.L. Hofman, J. Nucl. Mater., submitted (2015).
[3] D.M. Wachs, D.E. Burkes, S.L. Hayes, W. Skerjanc, G.L.Hofman, Yeon Soo Kim, H.J. Ryu, Proc. Int. Meeting on Reduced Enrichment for Research and Test Reactors (RERTR), Cape Town, South Africa, Oct.29 - Nov. 2, 2006.
[4] Yeon Soo Kim, G.L. Hofman, H.J. Ryu, J.M. Park, A.B. Robinson, D.M. Wachs, Nucl. Eng. Technol., 45 (2013) 827.
[5] Yeon Soo Kim, G.L. Hofman, J.S. Cheon, J. Nucl. Mater., 436 (2013) 14.
[6] G.Y. Jeong, Yeon Soo Kim, D-S. Sohn, J. Nucl. Mater., submitted (2015).
[7] A. M. Tentner, A. Bergeron, Y. S. Kim, G. L. Hofman, J. G. Stevens, S. Van den Berghe, V. Kuzminov, Proc. Int. Meeting on Reduced Enrichment for Research and Test Reactors (RERTR), Vienna, Austria, Oct.12 - 15, 2014.
[8] A. Leenaers, S. Van den Berghe, E. Koonen, V. Kuzminov, C. Detavernier, J. Nucl. Mater. 458 (2015) 380.

EVALUATION OF PERFORMED EXPERIMENTS ON FAST MULTIPLYING SYSTEMS WITH HEU FUEL FOR RECEIVING BENCHMARK DATA ON CRITICALITY

S.N.SIKORIN, S.G.MANDZIK, S.A. POLAZAU, A.V. KUZMIN,
Y.V.DAMARAD, I.S. SOLTAN

The Joint Institute for Power and Nuclear Research – Sosny,
99 Academic Krasin Street, 220109 Minsk - Republic of Belarus

ABSTRACT

Benchmark criticality experiments of fast heterogeneous configurations with HEU fuel were performed using "Giacint" critical facility of the Joint Institute for Power and Nuclear Research – Sosny of the National Academy of Sciences of Belarus. The critical assemblies' cores have consisted from fuel assemblies of without a jacket. Fuel assemblies contain 19 fuel rods of two types. The first one is metallic U (90% U-235); the second one is UO_2 (36% U-235). The active area length is 500 mm. The clad material is stainless steel. Three types of fuel assemblies with different content fuel rods were used. Side radial reflector: an inner layer – Be, an outer layer – stainless steel. The top and bottom axial reflectors – stainless steel. The analysis of the experimental results obtained from these benchmark experiments by developing detailed calculation models and performing simulations for the different experiments is presented. The sensitivity of the obtained results for the material specifications and the modeling details were examined. The analyses used the MCNP and MCU computer programs. This paper presents and compares the analytical model details, the obtained experimental and analytical results.

1. Introduction

This paper presents the experimental and analytical parameters of criticality of the uranium-containing fast neutron multiplication systems with a core based on fuel assemblies with 36% and 90% U-235 fuel rods. The experiments were performed using the "Giacint" critical facility of the Joint Institute for Power and Nuclear Research – Sosny (JIPNR-Sosny) of the National Academy of Sciences of Belarus [1]. The experimental results were analyzed in order to estimate whether they can be used as benchmark criticality data.

2. Fast critical assemblies

The fast critical assemblies represent a lattice (35.7 mm pitch) of fuel assemblies with fuel rods based on metal uranium and uranium dioxide, 90% and 36% enrichment by U-235, respectively, with a beryllium-steel reflector (Fig 1). The critical assemblies included the core, the side reflector, the top and bottom axial reflectors and the control and protection system (CPS) rods.
The cores of critical assemblies, comprising fuel assemblies, are surrounded by several rows of beryllium and steel reflector units. These elements of the critical assemblies are placed on the stainless-steel support grid. The neutron detectors are attached on special poles around the critical assemblies.
The support grid of the critical assemblies is placed on the frame and represents a stainless-steel cylinder, 950 mm in diameter and 40 mm in thickness. The support grid has 18.2 mm diameter holes drilled in the hexagonal lattice with the 35.7 pitch; the holes receive the shanks of the fuel assemblies and the side reflector units.

Fig 1. The fast critical assembly

The fuel assemblies (Fig 2) represent assemblies without a casing and comprises 19 fuel rods. There are three types the fuel assemblies: type 1 — 16 fuel rods type 2 and 3 fuel rods type 1; type 2 — 19 fuel rods type 2; type 3 — 19 fuel rods type 1 (Fig 3). The fuel rods are arranged around the hexagonal grid with the 8 mm pitch and are fixed by means of the end parts. The fuel assemblies have dimensions for the 34.8 mm wrench, with the total length 1047 mm (the active part in 500 mm long, the top shank of the fuel rod is 60 mm, the top shank of the fuel rod is 60 mm, the top end parts of the assembly are 216 mm, and the bottom end parts of the cassette are 211 mm). All top and bottom end parts of the fuel assemblies are made from stainless steel.

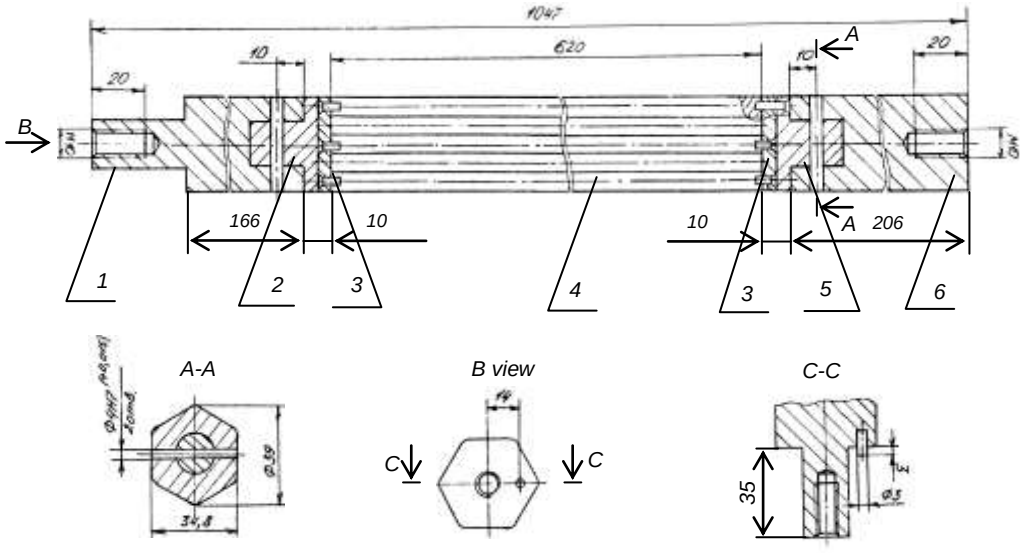

Fig 2. Fuel assembly:
1, 2 – bottom end parts, 3 – tube plate, 4 – fuel rods, 5, 6 – top end parts

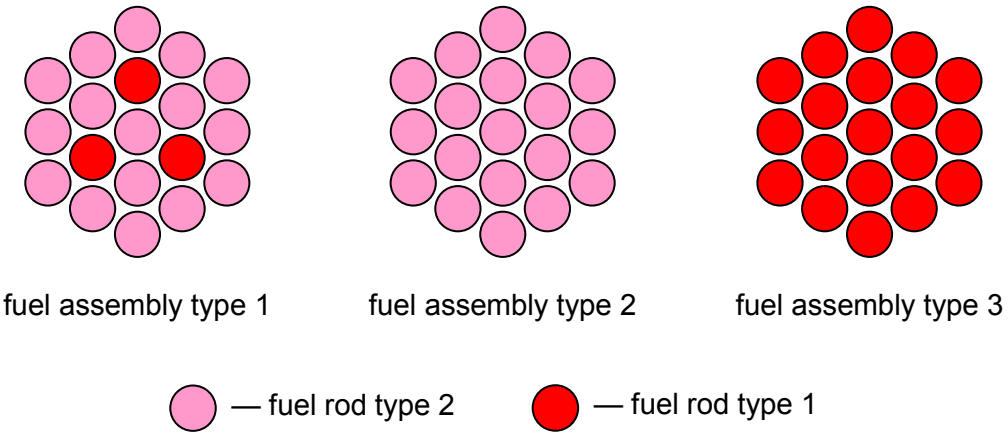

Fig 3. Layout of fuel rods in the fuel assemblies

The type 1 fuel rod (Fig 4) comprises a fuel core, a clad and end parts. The fuel rod cladding is from stainless steel with the outer diameter 7 mm and the wall 0.2 mm thick. The fuel core comprises tablets, 6.4 mm in diameter and 5 mm in height, made from metal uranium 18.9 g/cm3. The U-235 enrichment is 90%. The total core height is 500 mm. The U-235 weight in the fuel rod is 259.8 g. The top shank of the fuel rod is made from stainless steel with the 60 mm length and 6.6 mm diameter. The bottom end part of the fuel rod comprises the bottom shank 10 mm long and 6.6 mm in diameter and the bushing 50 mm long with the 6.6 mm diameter. The fuel rod is sealed, with the total length 620 mm.
The type 2 fuel rod (Fig 4) has the same structure as type 1 fuel rod, but with a different fuel core, comprising tablets with the 6.4 mm diameter and the 4-7 mm height, made from uranium dioxide 9.8 g/cm^3. The enrichment by U-235 is 36%. The total fuel core height is 500 mm. The 90% U-235 weight in the fuel rods is 49.1 g.

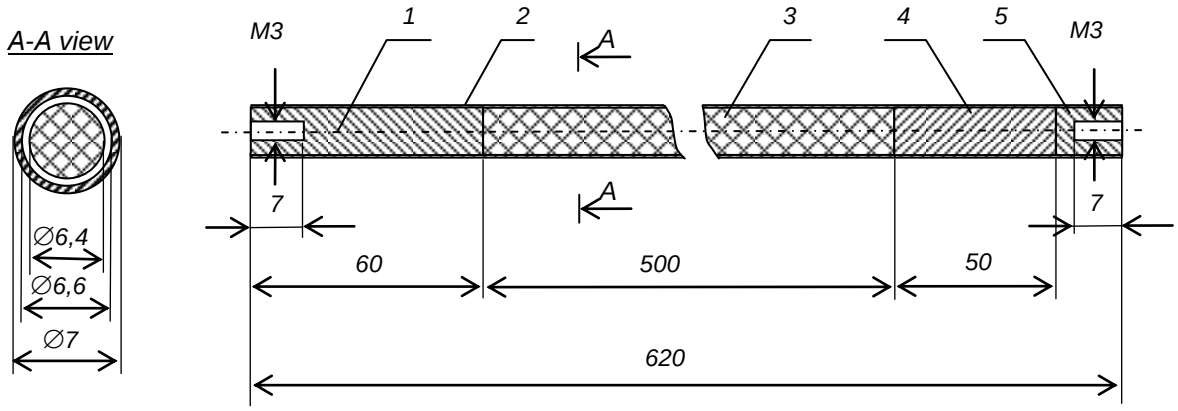

Fig 4. Fuel rod type 1 (type 2):
1 – upper end part; 2 – cladding; 3 – fuel core; 4, 5 – lower end part

The side reflector of the critical assemblies is several rows of the beryllium and stainless steel reflector units. The bottom axial reflector of the critical assemblies comprises bottom plugs of the fuel rods, bottom end parts of the fuel assemblies and the support plate. The top axial reflector of the critical assembly comprises top ends parts of the fuel rods and top end parts of the fuel assemblies.

The beryllium reflector unit (Fig 5) represents a hexagonal prism beryllium prism for the 34.8 mm wrench, 972 mm long. The bottom part of the unit bears a stainless steel shank, representing a seating surface when loaded into the critical assembly. The top part of the unit bears a stainless steel head for the 34.8 mm wrench, 40 mm long. The total length of the beryllium reflector unit is 1047 mm.
The steel reflector unit (Fig 6) is made from stainless steel, representing a hexagonal prism for the 34.8 mm wrench, 1047 mm long. The bottom part of the unit bears a shank, representing a seating surface when the critical assembly is installed on the support plate.

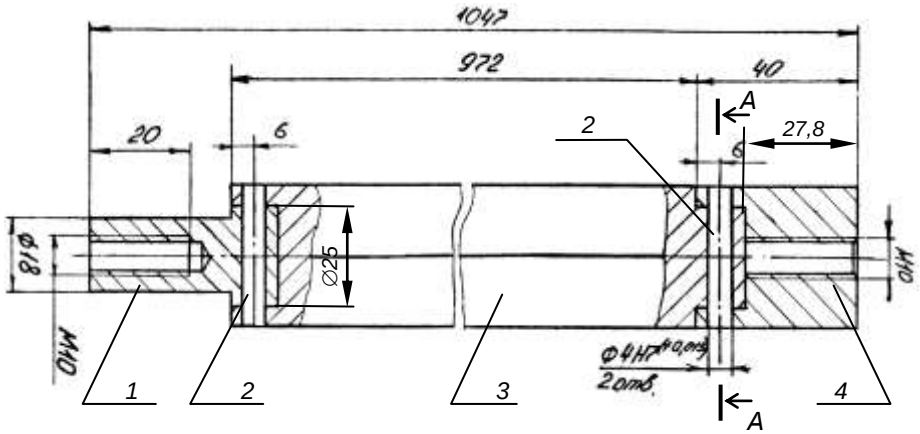

Fig 5. Beryllium reflector unit:
1 – bottom end part; 2 – pin; 3 – beryllium prism; 4 – top end part

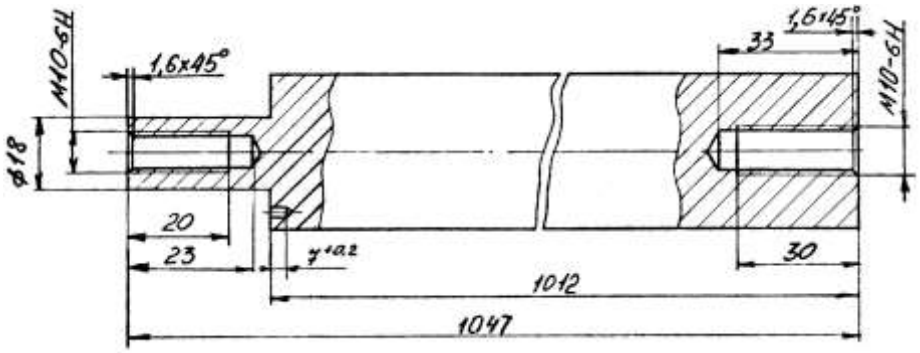

Fig 6. Steel reflector unit

The control and protection system of this critical assembly included three rods for emergency protection (EP), three rods for manual regulation (MR) and three rods of compensating reactivity (CR).

3. Neutron physical parameters of the critical assemblies

Figures 7 – 10 represent loading charts of the fast critical assemblies. The core and reflector compositions of the fast critical assemblies are presented in Tab 1.

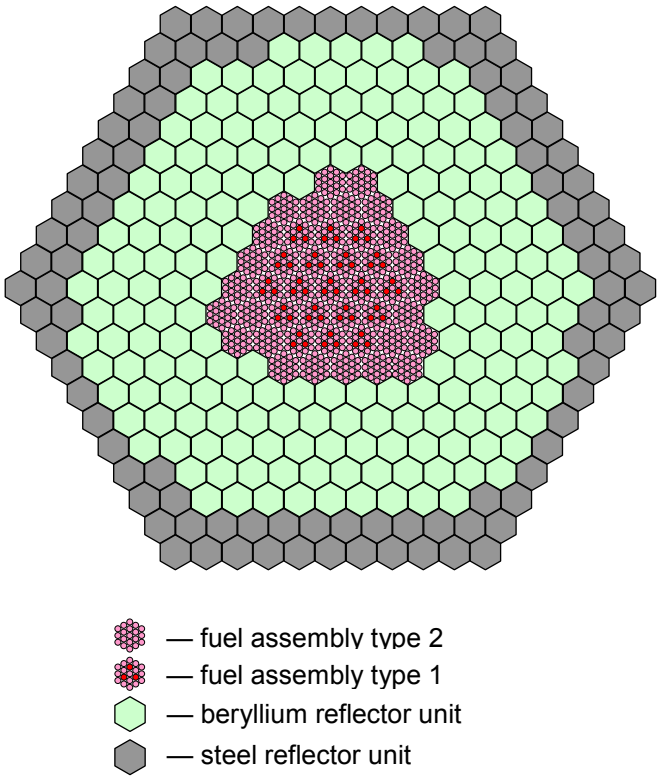

Fig 7. Loading chart of the critical assembly type 1

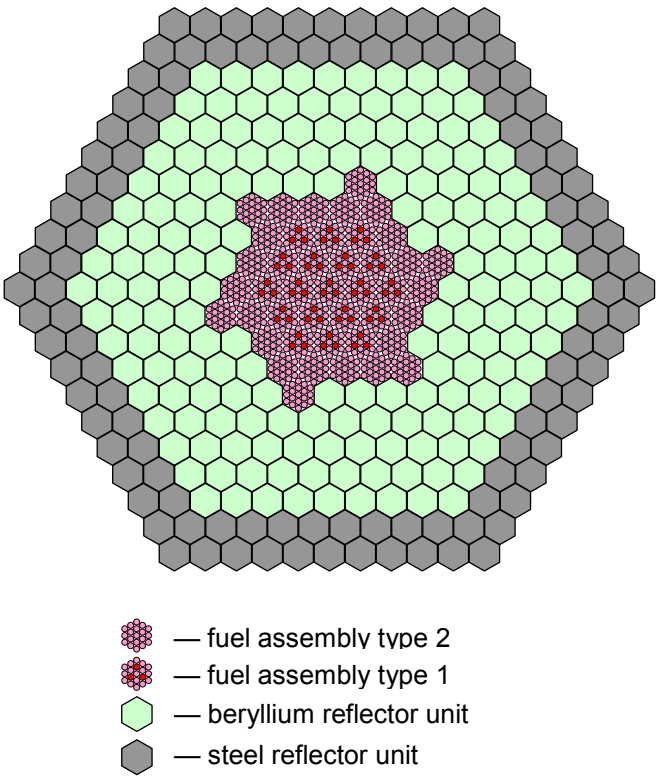

Fig 8. Loading chart of the critical assembly type 2

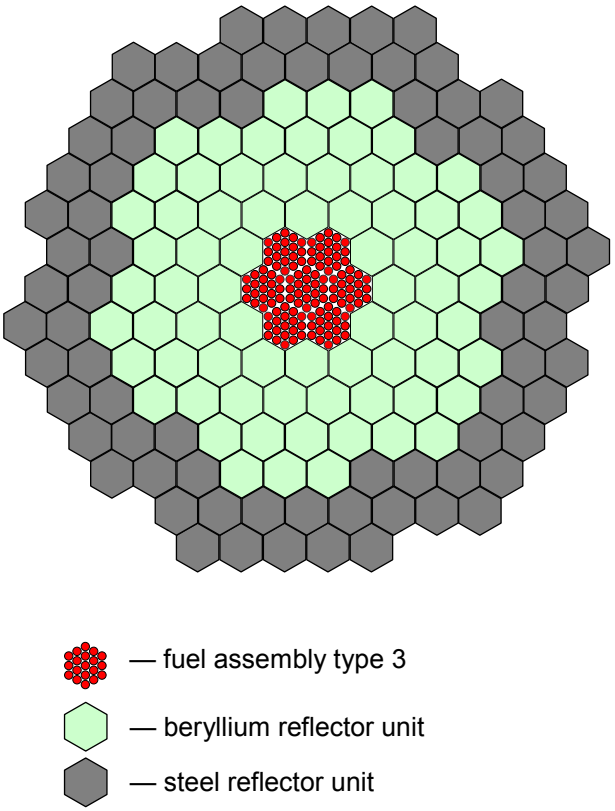

Fig 9. Loading chart of the critical assembly type 3

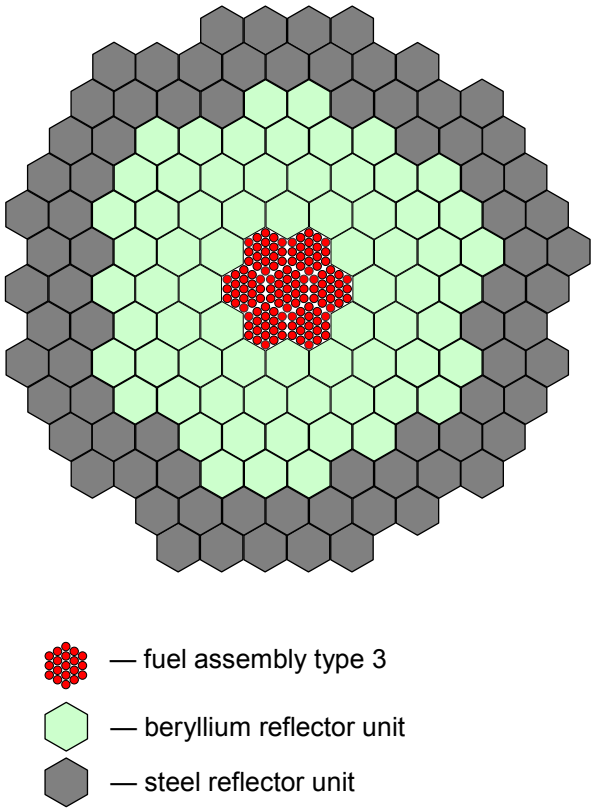

Fig 10. Loading chart of the critical assembly type 4

The critical assembly	The fuel assembly, pcs			Beryllium reflector unit, pcs	Steel reflector unit, pcs
	type 1	type 2	type 3		
Type 1	19	24	—	189	99
Type 2	19	24	—	174	114
Type 3	—	—	7	72	78
Type 4	—	—	7	69	78

Tab 1: The core and reflector compositions of the fast critical assemblies

The neutron physical characteristics of the critical assemblies are measured by the experimental unit “Reactivity Meter”, using the inverted solution of reactor kinetic equation [2, 3]. In order to exclude spatial effects of reactivity, the measurements were made using three ionization chambers, arranged at every 120° behind the side reflector of the critical assembly.

For estimating the results of the critical experiments we calculated the effective neutron multiplication coefficient K_{eff} of the fast critical assemblies. The calculations were made by the Monte Carlo method using the MCNP-4C [4] and MCU-PD [5] computation codes. The experimental data and the calculation results are presented in Tab. 2.

The critical assembly	Reactivity measurement result *, β_{eff}	K_{eff} calculation result		β_{eff} calculation result
		MCNP-4C	MCU-PD	MCU-PD
Type 1	0,43 ± 0,02	1,00447 ±0,00012	1,00349 ±0,00037	0,007454 ±0,000003
Type 2	-0,09 ± 0,01	1,00176 ±0,00017	1,00059 ±0,00043	0,007467 ±0,000003
Type 3	0,60 ± 0,02	1,00310 ±0,00022	1,00130 ±0,00050	0,007227 ±0,000003
Type 4	0,03 ± 0,01	0,99860 ±0,00022	0,99764 ±0,00036	0,007227 ±0,000003

* – total error of experimental results for the given confidence probability 0,68.

Tab 2: The experimental data and the calculation results of the fast critical assemblies

4. Conclusions

Analysis of the experimental data (including data on the composition and sizes of the critical assembly components) and of the calculated K_{eff} allows a conclusion that the results of criticality experiments obtained on this assembly can be used as benchmark data.

5. References

[1] Sikorin S., Hryharovich T. Research Nuclear Installations in Republic of Belarus / Enhancing Use and Safety of Research Reactors through Networking, Coalitions and Shared Best Practices, IAEA, Vienna, Austria, 10-14 February 2014. — CD.

[2] S.A. Polazau, S.N. Sikorin, "Digital reactimeter on the basis of the microcomputer and apparatus «CAMAC»", Proceedings of the Academy of Sciences of Belarus, Power engineering physical series, № 4, pp. 87-92, 1987.

[3] G.I. Buznitsky, A.I. Golovach, F.A. Grinevich, V.V. Luk'yanets, N.M. Sidoruk, S.N. Sikorin "An analogous meter for measuring nuclear reactor reactivity", Proceedings of the Academy of Sciences of Belarus, Power engineering physical series, № 1, pp.22-27, 1992.

[4] "MCNP – A General Monte Carlo N-Particle Transport Code, Version 4C," Ed. J. F. Briesmeister, Report LNL, LA-13709-M, 2000.

[5] Application Description and User's Manual for MCU-PD program: report №36-10/30-11 / NRC "KURCHATOV INSTITUTE" . — Moscow, 2011. — 569 p.

JRTR INITIAL CRITICALITY CALCULATIONS AND NUCLEAR COMMISSIONING TESTS

MUSTAFA K. JARADAT, S. ALKHAFAJI, K. ABU SALEEM
Research Reactor Project, Jordan Atomic Energy Commission
P. O. Box 70, Amman 11934, Jordan

CHANG JE PARK
Sejong University, 209 Neungdong-ro, Gwangjin-gu, Seoul, Republic of Korea
And Reactor Core Design Division, Korea Atomic Energy Research Institute
1045 Daeduk-Daero, Yuseong-Gu, Daejeon, 305-353, Korea

ABSTRACT

The Jordan Research and Training Reactor (JRTR) is a multi-purpose open-tank in pool type reactor under construction with nominal power of 5 MW. The core consists of 18 fuel assemblies with low enriched uranium (LEU) of ^{235}U enrichment of 19.75%. During the commissioning of JRTR many tests will be performed. In this work the initial criticality and fuel loading pattern are simulated using Monte Carlo code McCARD. One fuel loading scheme had been chosen based on lowest amount of fuel loaded into the core and the smallest number of fuel assemblies loaded. Also the control rods worth calculation using swap method have been modeled for a fully loaded core. These calculations should be compared with measured results during commissioning tests of JRTR.

1. Introduction

Jordan Research and Training Reactor (JRTR) is a multi-purpose open-tank-in-pool type reactor under construction with nominal power of 5 MW. The JRTR core consists of standard and special MTR fuel assemblies. A standard fuel assembly is a plate-type, a total of 21 fuel plates with aluminum-clad constitute. The fuel for the core is low enriched uranium (LEU) with a ^{235}U enrichment of 19.75 weight %. Each fuel plate is composed of a fuel meat with surrounding aluminum cladding. The fuel meat is made of fine and homogeneous dispersion of U_3Si_2 particles in a continuous aluminum matrix with a uranium density of 4.8 g U/cm^3.
The JRTR core configuration contains 18 fuel assemblies with four control absorber rods and two second shutdown rods. The control absorber rod is a square tube with the neutron absorbing material made of Hafnium, while for the second shutdown rods B4C powder is used as the neutron absorbing material. The core has a central flux trap, four beam ports, and several irradiation holes. The reactor is light water moderated and cooled and reflected with beryllium and heavy water. [1]

2. Initial Core Description

The initial core configuration is determined based on the following strategies: the initial core should be similar to the equilibrium core; the excess reactivity should be enough for a good

fuel economy, the reactor controllability should be maintained, the power peaking factor should be as low as possible, the transition from the initial core to the equilibrium core should be easy, and the number of fuel types should be minimized.
The initial core is configured using fuel assemblies of different densities. Fuel assemblies are fully loaded at the appropriate locations in view of the controllability of reactivity worth in the core and the safety margin. Figures 1 and 2 depict the core configuration and the initial fuel loading with 4 different densities of 4.176, 4.784, 5.878, and 6.543 g/cm^3. Table 1 lists the major parameters of the fuel and core. [1]

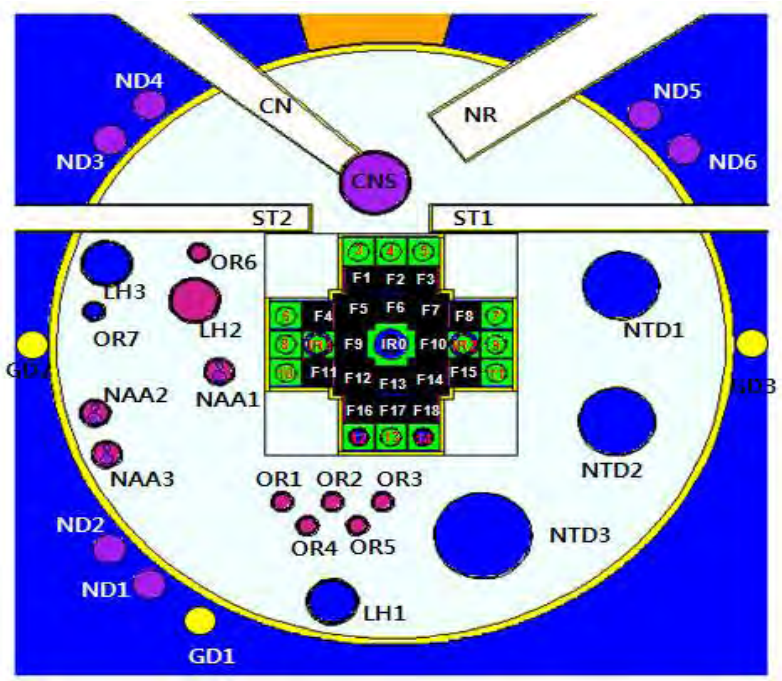

Fig.1 Plan View of the JRTR Core

	F01 4.0 5.878	F02 4.8 6.543	F03 4.0 5.878	
F04 2.6 4.784	F05 2.6 4.784	F06 1.9 4.176	F07 2.6 4.784	F08 2.6 4.784
	F09 1.9 4.176		F10 1.9 4.176	
F11 2.6 4.784	F12 2.6 4.784	F13 1.9 4.176	F14 2.6 4.784	F15 2.6 4.784
ID gU/cc Density (g/cm^3)	F16 4.0 5.878	F17 4.8 6.543	F18 4.0 5.878	

Fig.2 Initial Fuel Loading of JRTR

Table (1) Major Parameters of the Core, Fuel Assembly and Fuel Plate

Reactor Core	Data
Number of fuel assembly sites	18
Number of irradiation sites in the Be reflector	12
Number of control absorber rods	4 (Hf)
Number of second shutdown rods	2 (enriched B_4C)
Number of beam tubes	4
Reactor power	5 MW
Fuel Meat, Plate and Assembly	Data
Fuel meat thickness	0.51 mm
Cladding thickness	0.38 mm
Fuel plate thickness	1.27 mm
Fuel plate width	70.7 mm
Fuel plate length	680 mm
Coolant channel thickness	2.35 mm
Number of fuel plate/Fuel assembly	21
Fuel assembly width	76.2 mm
Fuel assembly height	1015 mm
Material Property	Data
Fuel meat	U_3Si_2–Al
Uranium density in fuel meat	4.8 gU/cm^3
Fuel meat density	6.543 g/cm^3
Cladding	AG3NE (aluminum alloy)
Cladding density	2.7 g/cm^3

3. JRTR Commissioning Tests

The commissioning of JRTR is required to demonstrate that the requirements and intents of the design as stated in the safety analysis report can be met. The commissioning activities should include adequate testing and inspection of structures, systems and components based on the importance of reactor safety. A graded approach for testing should be properly established in advance from the planning stage. The tests have to be arranged in functional groups and in a logical sequence and to be conducted with written procedures. The commissioning tests and stages are divided into few different sequences as follows;

a) Stage A for pre-fuel loading tests.
b) Stage B for fuel loading tests, initial criticality tests and low power tests.
c) Stage C for power ascension and power tests. [2]

In stage B neutronics tests must be carried out following the test procedures, so simulation results of these tests must be provided in advance. Some of these tests are:

a) Fuel loading and approach to the first criticality of JRTR
b) Configuration of operation core
c) Tests and experiments at zero-power
d) Test and experiments at each power level.

In this work the initial criticality of the JRTR core and control absorber rods worth were investigated using McCARD code. McCARD is a Monte Carlo Code for Advanced Reactor Design & Analysis. It was developed in the Department of Nuclear Engineering of Seoul National University since 1998. McCARD is a Monte Carlo (MC) neutron-photon transport simulation code designed exclusively for neutronics analyses of various nuclear reactors and fuel systems. McCARD estimates of neutronic design parameters of a nuclear reactor or fuel

system such as effective multiplication factor (k_{eff}), neutron flux and current fission power, etc. by using continuous-energy cross section libraries and detailed geometrical data of the system. [3]

4. Results of JRTR Fuel Loading and Initial Criticality:

Fuel loading, removal of the absorber or addition of the moderator during the approach to criticality necessitates calculations or estimates to predict changes in core reactivity, and periodic measurements of subcritical multiplication to determine subsequent safe increments of reactivity.

For fuel loading to reach first criticality of the core the fuel assemblies are loaded into the core one by one until the core approach criticality. After adding each fuel assembly the multiplication factor must be checked before adding the next one. When the core reaches critical state the control rods should be inserted into the core before adding fuel assembly until the core is fully loaded and the control rods are at the critical position. So the fuel loading pattern should be defined in advance before starting real fuel loading into the core to avoid approaching any super critical state.

Criticality calculations using McCARD were performed to determine fuel loading scheme to approach to criticality. For fuel loading 20 core configurations were simulated for the first criticality but four configurations were suggested for fuel loading of JRTR core as shown in figure (3) because they can make the reactor critical without control rods.

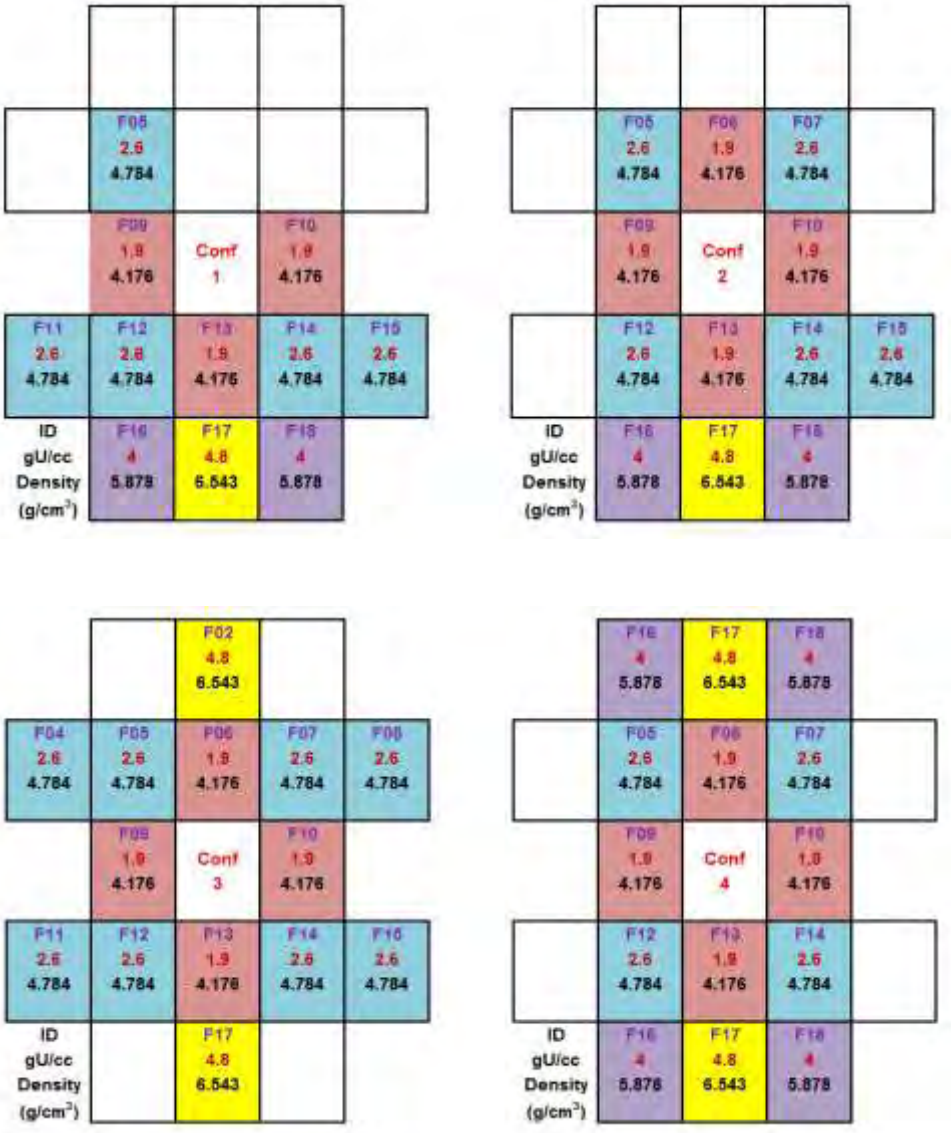

Fig.3 JRTR core fuel loading configurations

Since the fuel assemblies for the initial core have different densities and hence they have different uranium content, one of the four configurations will be chosen for JRTR first criticality based on the following criteria:

1. The minimum number of fuel assemblies loaded into the core.
2. The lowest mass of uranium loaded into the core.
3. The uniformity of the fuel assemblies' distribution into the core.

The differences between the suggested configurations are shown in table (2) based on number of FA, Uranium mass and Uniformity of FA distribution. Configuration 1 has the lowest number of fuel assemblies to reach criticality which is 11 but the fuel assemblies' distribution in non-uniform while Configurations 3 and 4 have higher uranium content and higher number of fuel assemblies but they have uniform fuel assemblies. Configuration 3 is chosen to be followed for JRTR initial criticality because it has smaller uranium content than configuration 4 although they have the same number of fuel assemblies.

Table (2) Differences between suggested JRTR core configurations for initial loading

Core Configuration	Number of FA	k-eff	Total Uranium Mass (kg)	Total U-235 Mass (kg)	FA Distribution
1	11	0.99962	16.09	3.18	Non-Uniform
2	12	0.99319	17.24	3.41	Non-Uniform
3	14	0.99687	19.86	3.92	Uniform
4	14	1.00863	21.50	4.25	Uniform

The core pattern and fuel assemblies order in the core is shown in figure (4) for critical and fully loaded core. During approach to criticality dummy fuel assemblies are used to fill empty fuel assembly spaces in the core to maintain uniform flow distribution.

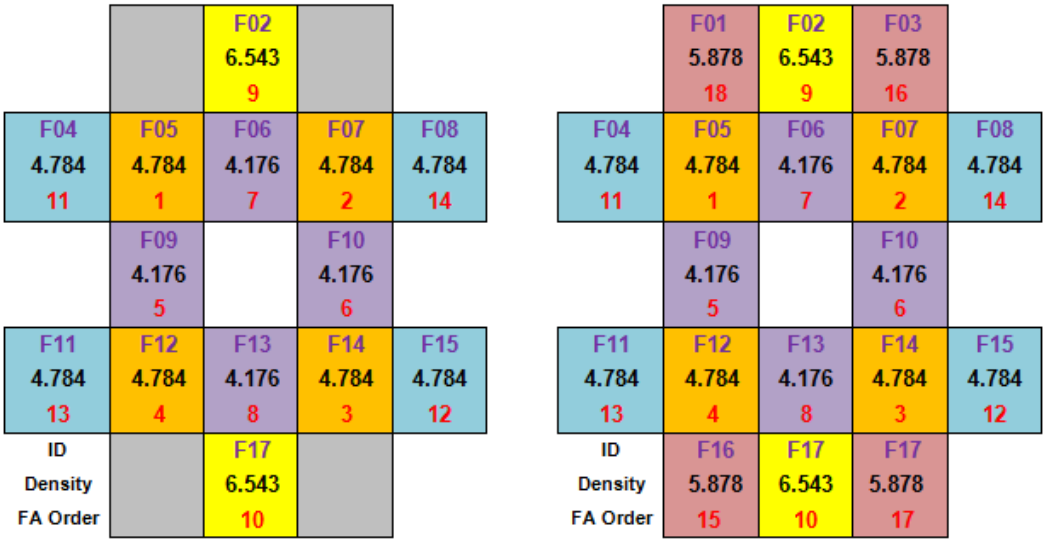

Fig.4 Fuel loading pattern for initial criticality

During fuel loading neutron count rates must be recorded and inverse of multiplication must be calculated to determine the critical mass of the core. The inverse of multiplication method $(1/M)$ method $n = S\Lambda/\rho$ is used to determine the critical mass using the following formula:

$$M = n_m/n_o = 1/(1 - k_{eff})$$

Where *M* is the subcritical multiplication factor; the reciprocal of the multiplication is plotted against the mass of the fuel in figure (5).

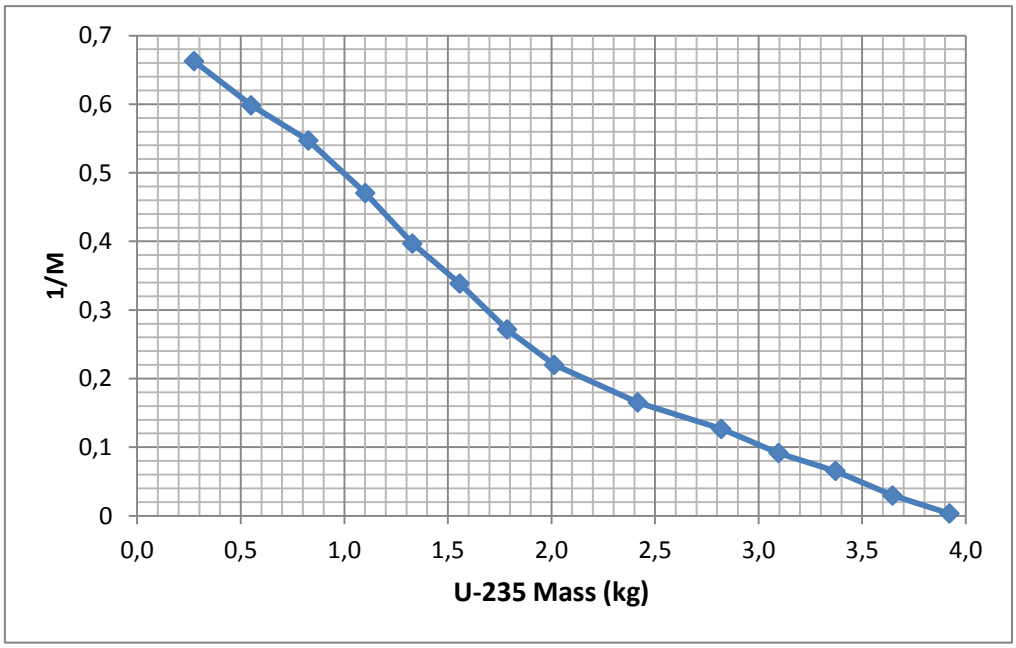

Fig.5 Fuel mass with inverse of multiplications

It can be found by interpolation that the critical mass of the core is about 4 kg of U-235 for this configuration with 14 fuel assembly loaded into the core. Table (3) shows the results of the inverse of multiplications with control rod positions for critical state. As shown in the table the control rods needed to be inserted to avoid super criticality as the core approaching criticality.

Table (3) Inverse of multiplications with control rod positions

Number of FAs Loaded	Assembly ID	Mass of U-235 in The Core	k_{eff}	1/M	Control Rod Position (cm)
1	FA05	0.275	0.33747	0.66253	ARO
2	FA07	0.551	0.40159	0.59841	ARO
3	FA14	0.826	0.44285	0.54715	ARO
4	FA12	1.102	0.48944	0.47056	ARO
5	FA09	1.330	0.60317	0.39683	ARO
6	FA10	1.558	0.66157	0.33843	ARO
7	FA06	1.786	0.72840	0.2716	ARO
8	FA13	2.014	0.78001	0.21999	ARO
9	FA02	2.417	0.83496	0.16504	ARO
10	FA17	2.821	0.87331	0.12669	ARO

11	FA04	3.096	0.90861	0.09139	ARO
12	FA15	3.372	0.93477	0.06523	ARO
13	FA11	3.647	0.97042	0.02958	ARO
14	FA08	3.922	0.99687	0.00313	ARO
15	FA16	4.279	1.00198	___	53 (22.1% In)
16	FA03	4.635	0.99976	___	45 (33.8% In)
17	FA18	4.992	0.99977	___	39 (42.6% In)
18	FA01	5.348	0.99949	___	36 (47.1% In)

5. Results of JRTR Control Rods Worth:

The other test is calculating the CARs worth using rod swap method to determine the worth of each control rod separately when all fuel assemblies are loaded into the core. In this test one control rod is fully withdrawn and one control rod is fully inserted and the other two control rods are at critical position. Then to calculate the CAR worth the test starts by inserting the pre-calibrated CAR which is already out of the core and recording the reactivity while the fully inserted rod is withdrawn until the reactor become critical and recording the reactivity. This procedure continues until the fully inserted rod becomes fully withdrawn. Finally the worth of this rod can be calculated. By exchange of positive and negative reactivity the nuclear reactor is kept at a relatively constant power. Figure (6) shows the positions of the CAR and the rod swap technique.

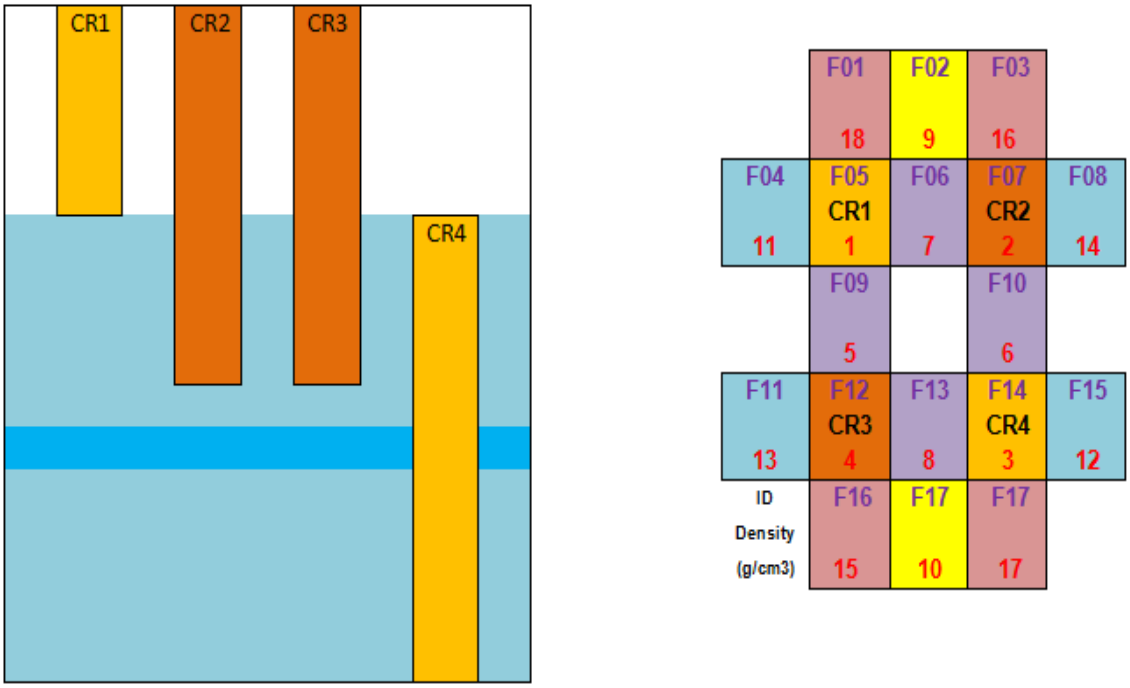

Fig.6 Control rod swapping method to calculate the control rods worth

McCARD simulation for CAR4 worth calculations using rod swapping method is shown in figure (7) for CAR4 integral worth and figure (8) CAR4 deferential worth.

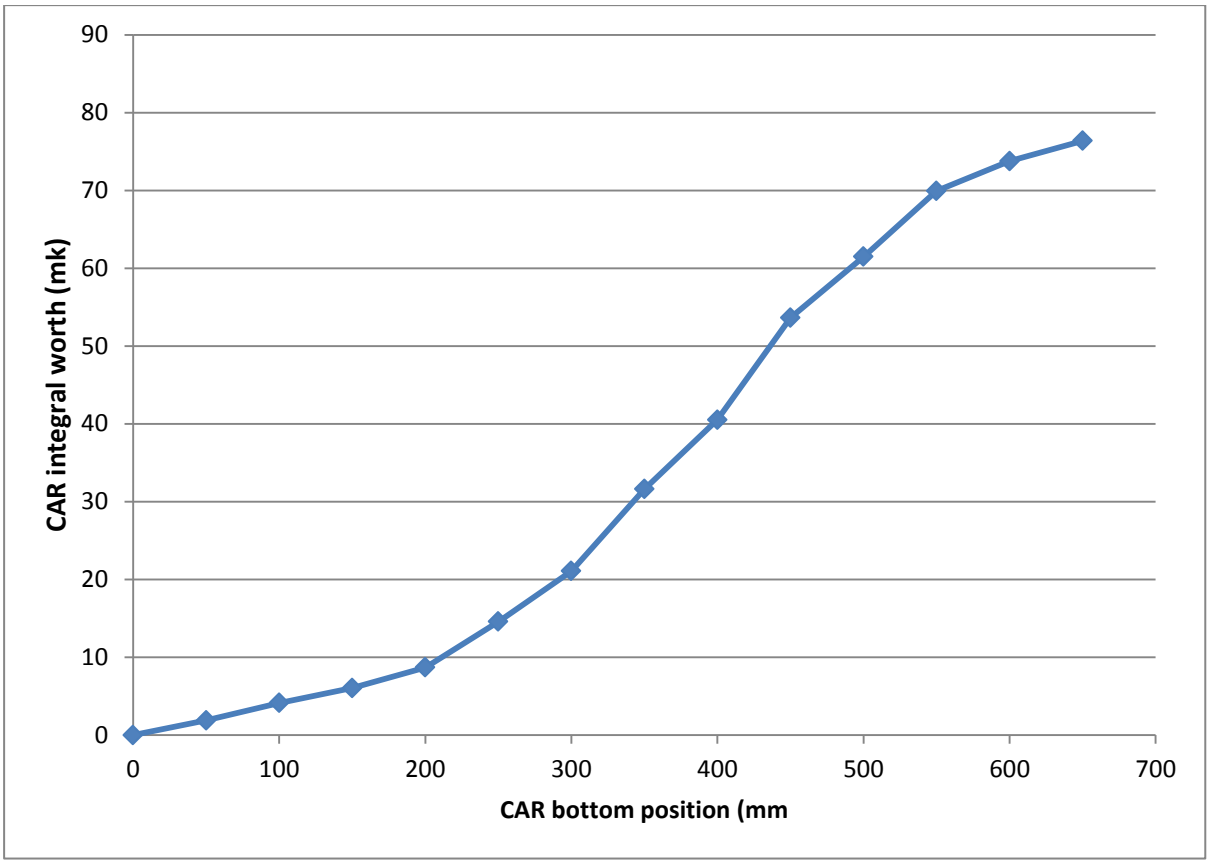

Fig. 7 Integral worth of CAR4 by rod swapping method

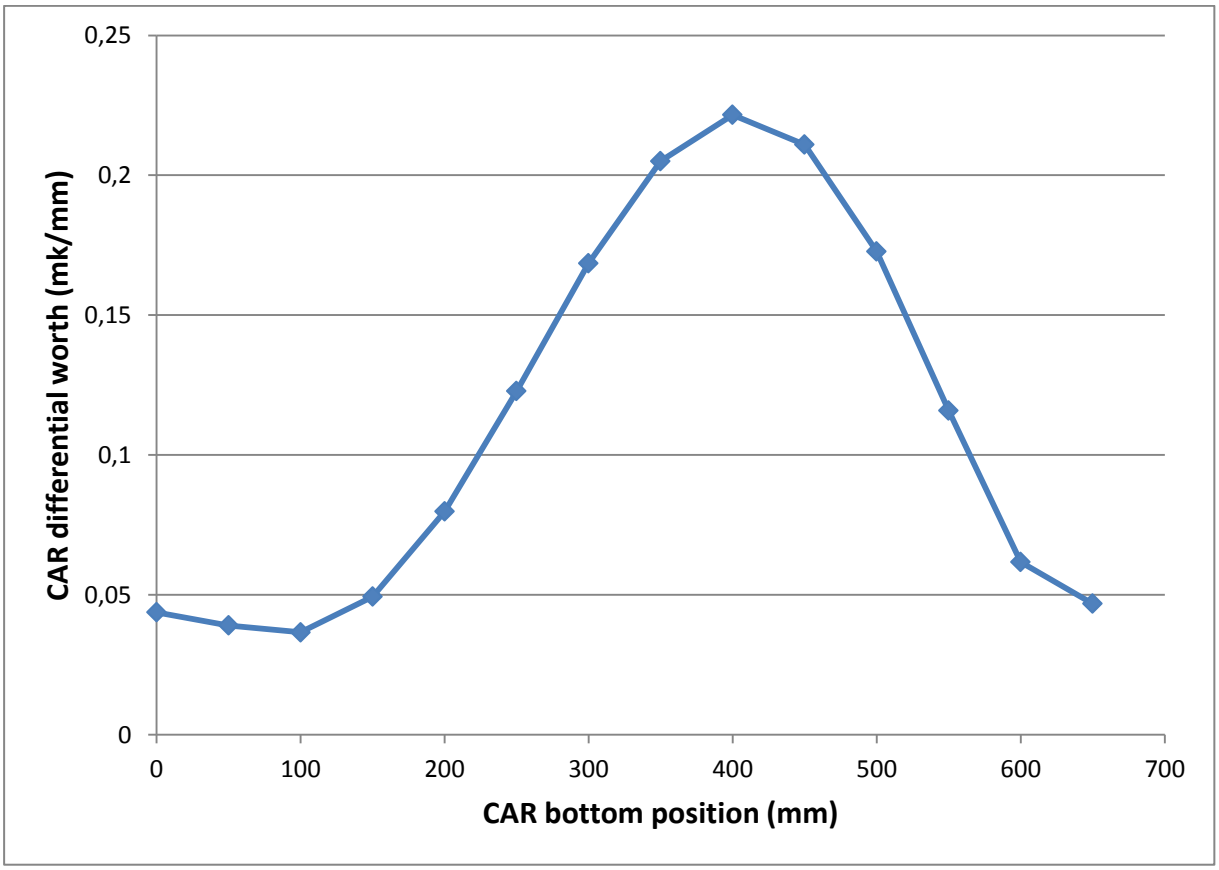

Fig. 8 Differential worth of CAR4 by rod swapping method

The total CARs worth is calculated for core with 15, 16, 17, and 18 fuel assemblies to show the change of the control rods worth with adding fuel assemblies to the core as shown in figure (9) for the integral worth and figure (10) for the differential worth.

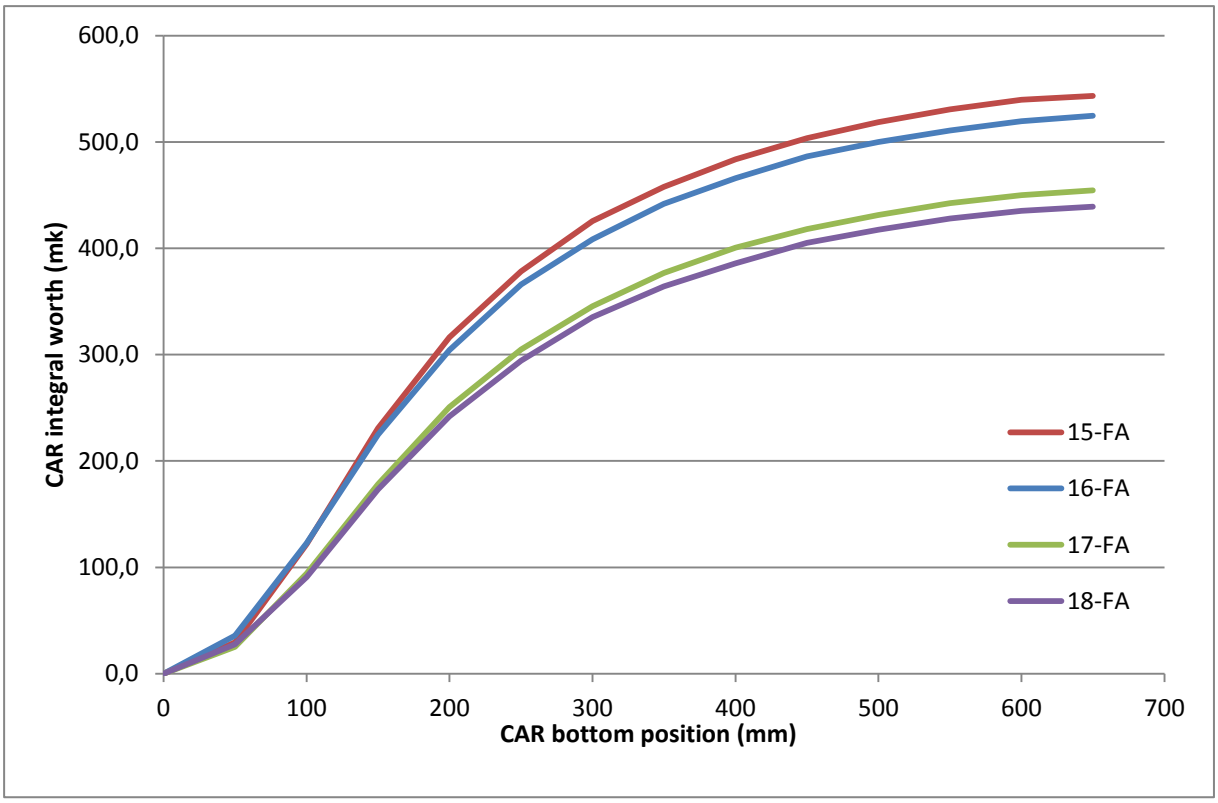

Fig. 9 Integral CARs worth for different number for FA loaded into the core

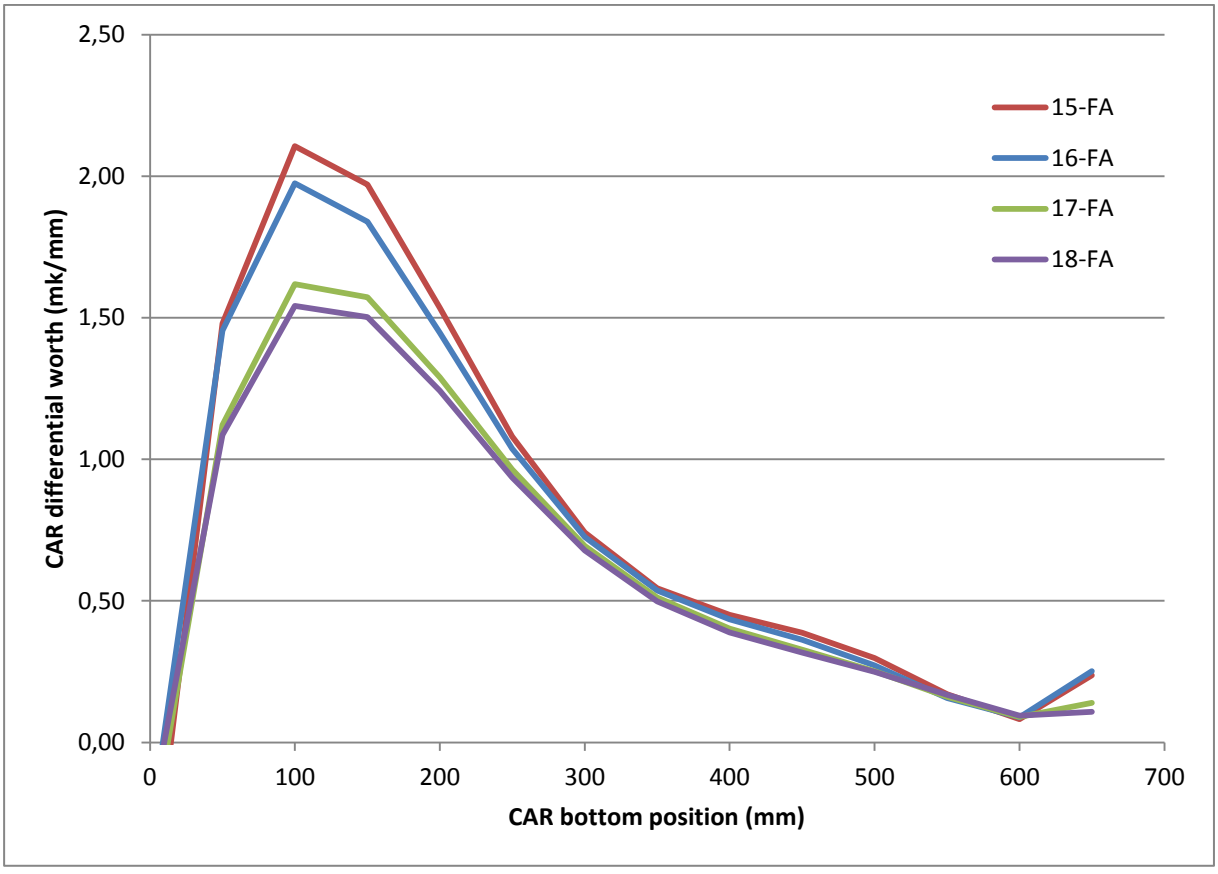

Fig. 10 Differential CARs worth for different number for FA loaded into the core

6. Conclusions

In this work the JRTR initial criticality and control rod worth calculations by rod swap method were simulated using McCARD code. Fuel loading to reach initial criticality is very important during commissioning stage of the reactor, so if the core subcriticality conditions measured during the approach to criticality deviate significantly from calculations made before the operations, further loading of the core should be stopped until the deviations are analyzed and appropriate corrective action must be taken.
For JRTR core, one fuel loading pattern was chosen based on specific criteria, and the criticality reached with 14 fuel assemblies and all control rods are fully withdrawn from the core. Also the control rods worth calculation using swap method have been modeled for a fully loaded core.
Many other tests should be simulated and the final procedures must be finished before starting the test measurement process during commissioning stage, like measuring the reactor characteristics at zero power: void coefficient, shutdown margin, delayed neutrons yield, thermal and fast neutron flux distribution at fuel and irradiation sites, neutron energy spectrum, and power distribution. Also to measure the reactor characteristics at each power level such as temperature coefficients, power defect, and xenon behavior.

References

1. JAEC, 2014, “Jordan Research & Training Reactor Final Safety Analysis Report”, Revision 0, prepared by KAERI, DAEWOO E&C.
2. IAEA, 2006, “Commissioning Of Research Reactors”, IAEA Safety Standards Series No. NS-G-4, Vienna, Austria.
3. H. Shim, B. Han, J. Jung, H. Park, C. Kim, 2012, “MCCARD: Monte Carlo Code for Advanced Reactor Design and Analysis”, Nuclear Engineering and Technology, Vol.44 No.2.

A COMPREHENSIVE ANALYSIS OF THE TECHNICAL FEASIBILITY OF THE MIR RESEARCH REACTOR CONVERSION TO LOW-ENRICHED URANIUM FUEL

A.L. IZHUTOV, V.A. STARKOV, V.V. PIMENOV, V.A. UZIKOV, V.E. FEDOSEEV
Research Reactor Complex, SSC "Research Institute of Atomic Reactors"
Dimitrovgrad-10, 433510 – Russian Federation

S.V. MAYNSKOV, T.A. OSIPOVA
National Nuclear University MEPhI (Moscow Engineering Physics Institute)
Dimitrovgrad, 433511 – Russian Federation

ABSTRACT

Presented are the results of a calculation analysis of the technical feasibility of the MIR reactor conversion to low-enriched uranium fuel. Two fuel types with 19.7% enrichment were considered: uranium dioxide UO_2 and alloy U9%Mo. The neutronic and thermal-hydraulic calculations of the reactor core parameters were performed. The analysis has shown that the reactor experimental capabilities will be preserved at conversion.
To justify safety of using LEU fuel the comprehensive calculation simulation of the accidents with the most conservative initial events was performed. Two types of the accidents were considered: LOCA and RIA with the worst possible consequences. This work was fulfilled with the financial support of Argonne National Laboratory (USA).

1. Introduction

Research reactor conversion to low-enriched uranium (LEU) fuel is one of the objectives of the Reactor Conversion Program (RERTR) under the Global Threat Reduction Initiative (GTRI). At present, an agreement has been reached between the National Nuclear Security Administration (U.S. Department of Energy) and ROSATOM State Corporation to study the technical feasibility of converting six Russian research reactors to LEU fuel including the MIR reactor [1].
The conducted analysis covered two stages. At the first stage the key objective was to obtain comparative parameters of the reactor cores with HEU and LEU fuels, i.e. to determine whether such conversion is possible. The next stage included the feasibility of safety to use a new fuel type (LEU) based on the analysis of accident consequences.

2. Brief description of the MIR reactor

The MIR reactor is located at the site of JSC “State Scientific Center – Research Institute of Atomic Reactors”, Dimitrovgrad. Its main purpose is testing of materials, items and experimental FAs, operating modes, and refinement of the next generation advanced nuclear reactor coolant technology.

The reactor core (Fig. 1) is made of hexagonal beryllium blocks. Along the axis of the blocks there are direct-flow zirconium channels to accommodate standard and experimental FAs. Such core arrangement was selected in view of the minimal mutual impact of the neighboring tested

items. For this purpose, each channel with a tested item is surrounded by six channels with standard FAs.

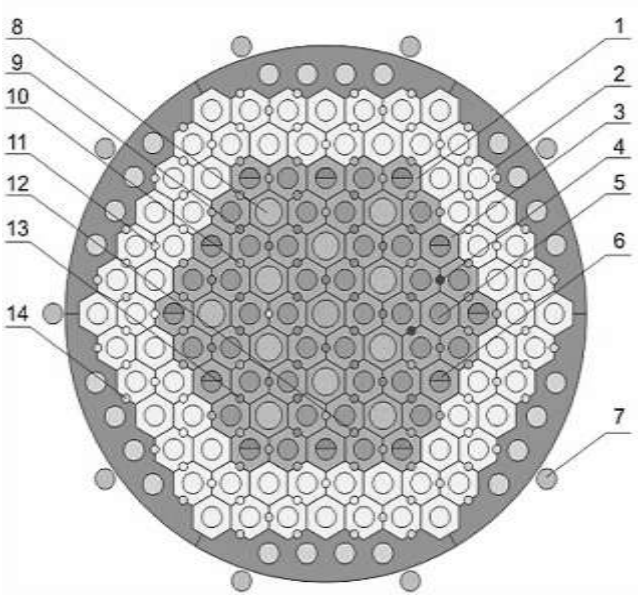

1 – Be block of the core
2 – Be block of the reflector
3 – Be block of the loop channel
4 – control rod
5 – standard channel
6 – channel with absorber
7 – ionization chamber
8 – loop channel
9 – combined safety-shim rod
10 – Be plug of the core
11 – Be plug of the reflector
12 – control rod tube
13 – control rod tube with a plug
14 – Al plug

Fig 1. MIR core arrangement

A beryllium stacking of the core and reflector is arranged along a triangular grid. It is made of 127 hexagonal blocks spaced at 150 mm with width across flats of 148.5 mm. Four central rows of Be blocks serve as a moderator, and two external rows are a reflector.

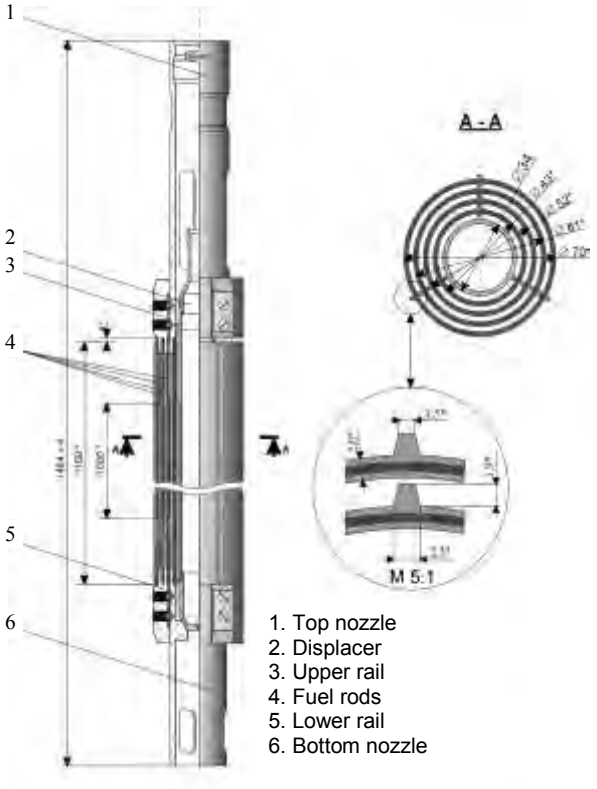

1. Top nozzle
2. Displacer
3. Upper rail
4. Fuel rods
5. Lower rail
6. Bottom nozzle

Fig 2. Standard FA

A standard FA of the MIR reactor (Fig. 2) is made of four annular coaxially positioned fuel rods. Each fuel rod is a three-layer tube. Fuel layer is enclosed on both sides in aluminum alloy

cladding. Fuel is uranium dioxide dispersed in the aluminum matrix. Enrichment in ^{235}U makes up 90%.

MIR heat removal is a two-circuit process with five circulation paths in the primary circuit, two paths in a pool cooling circuit and four paths in the secondary circuit. A cooling tower is the end user of heat.

The primary circuit is designed for heat removal from the core and its transfer to the secondary circuit (water recirculation circuit) as well as for maintaining the active medium.

The primary cooling circuit includes five circulation paths of the same type joined by inlet and pressure headers (Fig. 3). Each path consists of pipelines, stop and control valves, a heat exchanger, and the main circulation pump (MCP). From the MCP pressure header the coolant flows via two pipelines in the system consisting of circular and supply collectors connected to each other by eleven U-shape sleeves. From the supply header the coolant flows downwards to cool standard FAs. The outlet pipelines are joined in two hot collectors from which the coolant flows in an oxygen activity attenuator connected to the MCP inlet header by two pipelines. A pressurizer and a gas separator are connected to the inlet header. From the inlet header the coolant enters heat exchangers where heat is transferred to a water recirculation circuit.

Heat received from the primary circuit and pool cooling circuit by the water recirculation circuit coolant is transferred to the surrounding medium in a cooling tower.

In case of MIR primary circuit failure there is a double emergency cooling system (ECS): ECS #1 is connected to the inlet header and the core, ECS #2 supplies water from the reactor pool to the standard channels.

3. Input data

In a calculation analysis two LEU fuels were considered: UO_2 oxide and U9%Mo alloy. According to preliminary assessments, ^{235}U loading in LEU FAs shall make up approximately 460 g to preserve the reactivity margin. It is suggested to provide such ^{235}U content by taking the following measures:

- increasing fuel content in the fuel meat (for both fuels);
- increasing fuel meat thickness (for both fuels);
- increasing the amount of fuel rods (only for UO_2).

The main comparative geometry and process parameters of HEU and LEU FAs are shown in Table 1.

Parameter	HEU	LEU-1	LEU-2
Fuel	UO_2	UO_2	U9%Mo
Enrichment in ^{235}U, %	90	19.7	19.7
FA diameter, mm	70		
Fuel meat height, mm	1000		
Fuel rod thickness, mm	2		
Width of a gap between the fuel rods, mm	2.5		
The number of fuel rods in a FA	4	6	4
The total heat removal surface, m^2	1.37	1.72	1.37
^{235}U mass in a FA, g	350	460	460
Fuel meat density, g/cm^3 - ^{235}U - U	 0.91 1.01	 0.57 2.90	 1.02 5.16
Fuel volume fraction in the fuel meat, rel. units	0.11	0.317	0.33

Table 2: Comparative analysis of HEU and LEU FAs

In case of using oxide LEU fuel it is not possible to provide ^{235}U loading of 460 g only by increasing fuel meat density and thickness. This is limited by the maximum admissible UO_2 density in the meat that can be implemented in fuel rod fabrication. Therefore, the number of fuel rods in a FA with such fuel is increased up to 6 with a corresponding change in inner displacer geometry. As for U9%Mo alloy, ^{235}U loading may be provided without any changes in the amount of fuel rods in a FA.

4. Neutronic parameters

To solve the problems related to obtaining HEU and LEU fuel core parameters, a detailed neutronic calculation model was developed using the MCU-RR code (Monte Carlo Universal – Research Reactor) [2]. MCU-RR is intended to compute neutron and photon flux functionals in research reactors using the Monte Carlo method based on the assessed nuclear data without introducing any additional approximations in the description of geometry of the considered system and physics of particles-substance interaction. Changes in the fuel nuclide content were taken into account using a burnup module (BURNUP) [3].

The HEU and LEU fuel core parameters obtained in the calculations are presented in Table 2.

Parameter	Value		
	HEU UO_2	LEU UO_2	LEU U9%Mo
Average fuel burnup in the core, % ✓ reactor run beginning ✓ reactor run end	 29.5 33.3	 34.5 37.3	 33.8 36.6
Reactivity loss rate, 10^{-3} % $\Delta k/k$/MWd	4.26	3.22	2.91
Control rod performance, % $\Delta k/k$	28.7	28.3	27.4
Reactivity margin in an unpoisoned state, % $\Delta k/k$	13.0	12.8	12.6
EFA power to surrounding FAs power ratio in an unpoisoned state, rel. units	0.70	0.69	0.68

Table 2: Comparative analysis of HEU and LEU fuel neutronic parameters

The analysis of the computation results shows that in conversion to LEU fuel there is an increase in the fuel cycle duration, and as a result, an increased burnup depth in discharged FAs. A lower reactivity loss rate is explained mainly by an increased ^{235}U mass in the core. Control rod performance and reactivity margin change within the range of 3-4%. The latter parameter in the Table describing the ability to provide the necessary power in a loop channel due to power of the surrounding FAs changes insignificantly, therefore the target EFA power is provided at almost similar power of surrounding standard FAs. The annual average MIR operating parameters are specified in Table 3.

Parameter	Value		
	HEU UO_2	LEU UO_2	LEU U9%Mo
The average amount of discharged FAs at the end of the cycle, pcs	3.9	2.6	2.7
The average burnup of ^{235}U in a discharged FA, %	50.5	54.4	53.1
The annual demand in FAs	62.4	41.6	43.2
Annual consumption, kg ✓ ^{235}U ✓ U	 21.8 24.2	 19.1 97.0	 19.9 100.9
Annual fast neutron fluence (E>0.1 MeV) on the VVER fuel	3.65	3.50	3.42

cladding in the core mid plain, 10^{21} cm^{-2}			

Table 3: MIR annual average operating parameters

It should be particularly mentioned that MIR conversion to LEU fuel will lead to a considerable reduction in annual FA consumption (by 30-33%) and annual consumption of ^{235}U (by 8-12%). At that, the total uranium consumption will increase by approximately 4 times. The annual fast neutron fluence (one of the reference parameters) will decrease by 4-6%.

5. Thermal and hydraulic parameters

The thermal and hydraulic calculations were performed to show the feasibility of thermal and physical parameters of reactor safe operation. The following parameters have been calculated:

- Heat flux distribution along the fuel rod surface;
- Distribution of washed fuel rod surface temperatures, fuel-to-cladding interaction temperatures and peak fuel temperatures along the core height;
- Onset-of-surface boiling ratio and departure from nucleate boiling ratio.

To obtain the temperature of the onset of surface boiling, Bergles-Rohsenow [4] and Forster-Greif [5] correlations were used. The critical heat flux density was obtained by a Mirshak correlation [6].

Since power of a standard FA in a maneuvering mode can achieve the peak value of 3.2 MW according to the operational procedure, all thermal and hydraulic parameters were calculated taking into account this value. The coolant temperature at the FA inlet was taken equal to 40°C, and the coolant flow rate was taken equal to 70 m^3/h.

The peak temperatures of the cladding and fuel meat for each fuel type are presented in Table 4, and thermal and physical ratios – in Table 5.

Parameter	Value		
	HEU UO_2	LEU UO_2	LEU U9%Mo
Peak cladding temperature, ^0C	141	140	142
Peak fuel meat temperature, ^0C	158	156	162

Table 4: Peak temperatures of an outer fuel rod in the FA with power of 3.2 MW

Parameter	Value		
	HEU UO_2	LEU UO_2	LEU U9%Mo
Heat flux, kW/m^2	4002	3449	4042
Coolant velocity in a gap between fuel rods, m/s	9.1	7.2	9.1
Onset-of-surface boiling ratio			
• Bergles-Rohsenow correlation	1.45	1.50	1.44
• Forster-Greif correlation	1.58	1.60	1.57
Departure from nucleate boiling ratio	4.5	4.8	4.4

Table 5: Thermal and physical criteria of MIR safe operation

The data given in Table 5 were obtained for a coordinate on a fuel rod with the peak outer cladding surface temperature. The analysis of the results shows no worsening of thermal and physical parameters in MIR reactor conversion to LEU fuel.

6. Accident analysis

To show the feasibility of safe conversion to LEU fuel accident (LOCA, RIA) consequences were analyzed using the RELAP5/MOD3.2 thermal and hydraulic code [7]. As part of this work a computational model of the MIR primary circuit was developed (Fig. 3) that includes the main components of cooling and safety systems. A simulated process of the accident development is divided into two stages. At the first stage the reactor systems are brought into a stationary operating mode. The calculation of the accident mode is done at the second stage after the initiating event occurs.

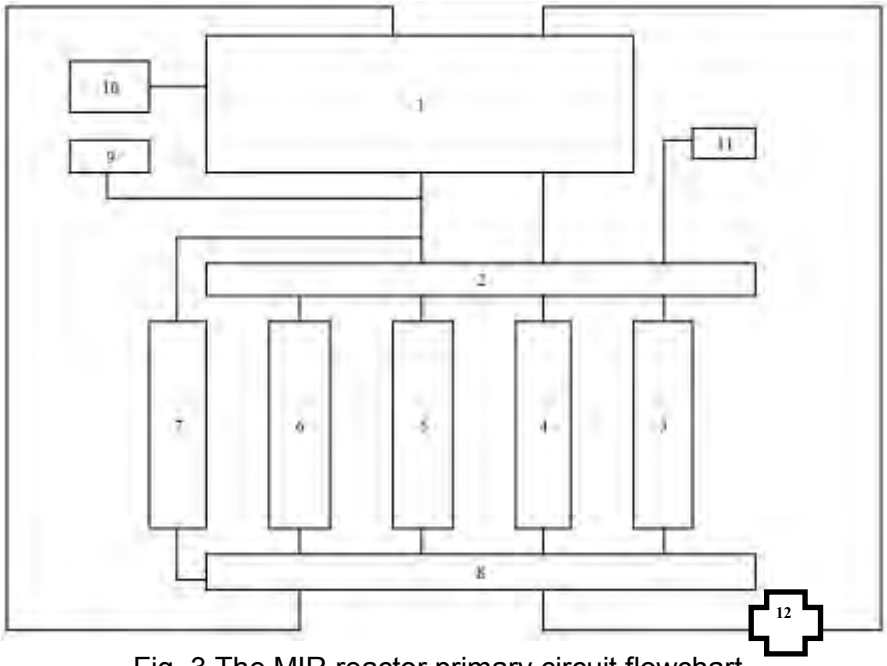

Fig. 3 The MIR reactor primary circuit flowchart

1 – reactor; 2 – inlet header; 3, 4, 5, 6, 7 – pipelines and equipment of the first, second, third, fourth and fifth legs; 8 – pressure header; 9 – pressurizer and degassing system; 10 – emergency cooling system #2 (ECS #2); 11 – emergency cooling system #1 (ECS #1); 12 – pipeline break point

6.1 MIR reactor primary circuit loss-of-coolant accident analysis

A double-ended instantaneous full cross-section pressure pipeline break is taken as a postulated initiating event of the primary circuit loss-of-coolant accident. It is assumed that the break occurs in the region between the header ring and valve P-1 at a lower height point (Fig. 3, position 12).

In accordance with [8], the overlapping on the initiating event of an undetected uncontrolled system element failure is considered (an ECS #2 pump failure) as well as one failure of any safety system element – a failure of an ECS #1 valve connecting the supply line and channels. In addition, the regulatory documents [9] postulate jamming of one of the most efficient scram rod. Thus, five control rods of six possible are inserted in the core.

The initiating event occurs in the calculation at the 1600th second.

The pipeline break leads to deterioration of the core cooling conditions caused by loss of pressure and coolant flow rate. The core is protected from dewatering by the following systems and equipment:

- ECS #1;
- ECS #2;
- MCP.

In this case a mode of coolant blowdown into the break mainly impacts these processes determining the time history of a change in pressure and coolant flow rate through the channels in the core.

There are three main phases of the accident. The first phase is reduction of the coolant flow rate through a FA and multiple circulation overturn in the FA with the highest power density. This phase is described by the high power density at a sharp loss of heat removal which can lead to departure from nucleate boiling in the maximum stressed FAs.

The second phase is described by MCP shutoff, coolant backflow through the core at rather high rates in the FA (1÷2 m/s) and ECS actuation.

The third phase is described by a significant reduction of power density in the FA and cooling quasi-steady mode with the flow rates via the channels equal to the feed flow rates.

Early after the initiating event the total coolant flow rate from the primary circuit into the break sharply increases, and there is coolant backflow from the direction of the core. An expansion wave runs along the circuit and the pressure in the core drops sharply leading to an alarm signal at the 0.2 s when a set point is achieved to reduce pressure in the hot collector up to 0.45 MPa (Fig. 4). After initial strong fluctuations the pressure in the circuit is partially restored, and then it decreases gradually.

With a 0.05 s delay the safety rods of 2.8 β_{eff} efficiency will start inserting in the core. This leads to an abrupt reactor power decrease.

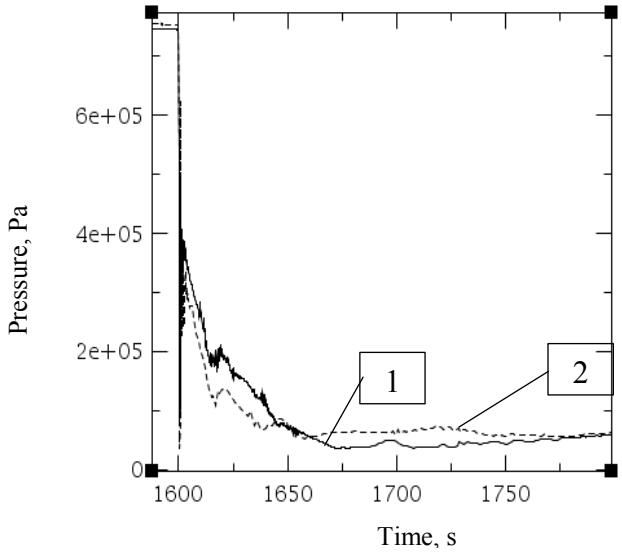

Fig. 4 Change in pressure in hot collectors
(1 – U9%Mo, 2 – UO_2)

In case of using U9%Mo+Al fuel ECS #2 is actuated at the 54th second, and in case of using UO_2+Al fuel – at the 47th second when an alarm set point is achieved to reduce the level up to 1500 mm in the pressurizer. When the emergency signal starts ECS #1 is also actuated with a 25 s delay, however, the main coolant flow from this system runs into the break, and there is the overlapping of a failure on valve KG-5 in the hot collector supply line resulting in no coolant flowing into the core. As per the same set point a signal comes to close the valve, and the pressurizer is cut off from the circuit during 33 seconds.

As a result of an abrupt drop of pressure and coolant flow rate via the maximum stressed FA, in some regions in the gaps between the fuel rods a low heat transfer factor flow mode is implemented (~100-300 W/m^{2}xK). During the 6th second of the process the melting temperature of aluminum matrix and cladding is achieved (660 ˚C (933 K)) for both FA types due to residual power density in fuel in the separate maximum stressed regions of the fuel rods. These FAs are not considered in further thermal-hydraulic calculations.

For a realistic analysis it is necessary to take into account the blistering effect of fuel rods. After achieving the temperature ~ (460-550) ˚C due to the blistering effect the outer fuel cladding contacts the channel body wall [10].

This effect increases radial thermal conductivity, and residual power density is removed to the reactor pool water. Thus, the maximal temperature that can be achieved on the fuel rods is determined by the blistering temperature (460-550 ˚C). The effect is possible due to the unique design feature of the MIR reactor (the channel-type reactor immersed in a water pool and tube-type fuel).

Out-of-pile tests of the MIR irradiated fuel showed that at the temperature of (450÷480) ºC a process of gaseous swelling and blistering starts (Fig. 5).

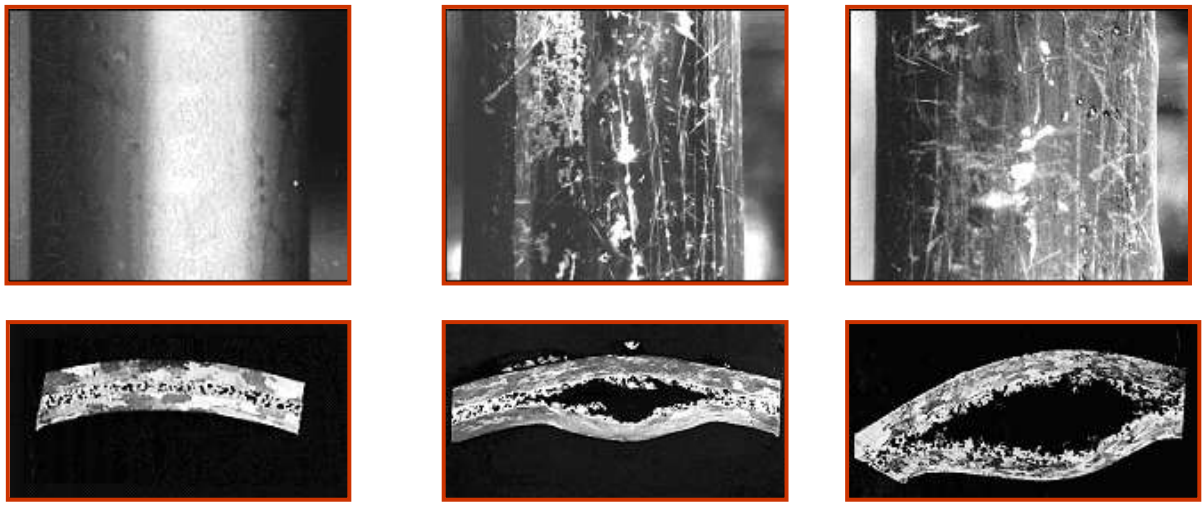

Non-heated fuel element Ø61 mm | Fuel element Ø52 mm heated to 480°C | Fuel element Ø43 mm heated to 515°C

Fig. 5 Gaseous swelling and blistering of the MIR irradiated fuel

During the first seconds after the initiating event the averaged groups of FAs with UO_2+Al fuel show a slight increase in the temperature of the fuel rod claddings (Fig. 6) not exceeding 430K (157 ˚C) due to changes in the flow mode caused by fluctuations of pressure and coolant flow rate. From the 130th second fluctuation modes of coolant flow in the channels are set leading in their turn to fuel cladding temperature fluctuations. At that, the second and third less-stressed groups of FAs show the maximal coolant heating (up to the saturation temperature) as well as coolant boiling along the entire length of the fuel rods.

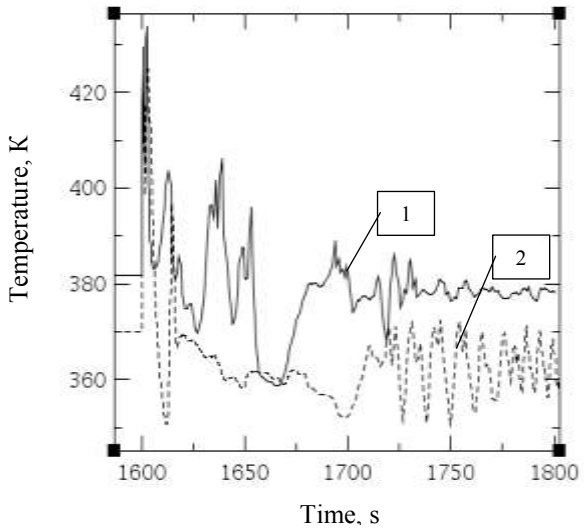

Fig. 6 Peak cladding temperature of the averaged FA groups
(1 – U9%Mo, 2 – UO_2)

In the averaged FA groups with U9%Mo+Al fuel the cladding temperature does not exceed 440K (167 ˚C). At the 150th second there is a relatively stable distribution of the coolant flow rate in the channels under calculations that results in some stabilization in the temperature mode of the fuel rods. The second less-stressed FA group shows the maximal coolant heating (up to the saturation temperature) as well as coolant boiling at the fuel rod top.
ECS #2 compensates sufficiently the coolant loss in the reactor channels, which provides safe heat removal from 5 FA groups after the 200th second under a significant decrease of power density (except for the maximum stressed FA).

Thus, as a result of the calculation analysis of the MIR reactor primary circuit pipeline break accident with actuating the emergency cooling system of the pool cooling circuit it is shown that ECS coolant supply from below into the FA operating channels ensures distillate entering the core. That is why after residual power density reduction the core will be filled with water, which provides safe heat removal from the FAs (except for the maximum stressed FA).

6.2 The results of the calculations of the accident with a non-authorized extraction of the maximum efficiency shim rod

The accident initiating event (shim rod non-authorized extraction) occurs at the 100th second. According to the calculation results the accident temporal development with moving a shim rod is practically the same for both fuels (Tab. 6).

Duration of the process for fuel U9%Mo+Al, s	Duration of the process for fuel UO_2+Al, s	Description of the event
0	0	All the reactor systems are in the stationary state.
0+	0+	Positive reactivity insertion – a shim rod is extracted.
2.2	2.28	Pre-alarm set point is achieved to actuate scram rods as reactor power increases.
3.5	3.5	Emergency set point is achieved to actuate scram rods.

Duration of the process for fuel U9%Mo+Al, s	Duration of the process for fuel UO_2+Al, s	Description of the event
3.55	3.55	Scram rods drop into the core, driving FAs with absorber start inserting into the core (taking into account the delay time).
3.6	3.8	Reactor power achieves the peak value of 97.I MW; fuel and coolant temperature increases.
4.0+	4.0+	Power decreases. The reactor is in the subcritical state.
100+	100+	New core cooling mode is stabilized.

Tab 6: Consequence of the key event during the accident development

Figure 7 presents the time history of the peak temperature of fuel and the maximum stressed fuel rod cladding as well as washing coolant temperature at the elevation with the maximal temperature of fuel and cladding for both fuels.

The temperature values for UO_2+Al at the peak load at the 3.8th second are 181 ºC (454 K) for the fuel meat and 172 ºC (445 K) for the fuel rod cladding. The temperature of the coolant washing the stressed fuel rod at that point makes up 89 ºC (362 K) not exceeding the saturation temperature at the set pressure. The minimal departure from nucleate boiling ratio (Bernat's correlation) is achieved at the maximal fuel rod heating making up K ~1.7.

The temperature values for U9%Mo+Al at the peak load at the 3.6th second make up 185 ºC (458 K) for the fuel meat and 176 ºC (449 K) for the fuel cladding. The maximal temperature of the coolant washing the stressed fuel rod at the same point is 88 ºC (361 K) that does not exceed the saturation temperature at the set pressure. The minimal departure from nucleate boiling ratio (Bernat's correlation) is achieved at the maximal fuel rod heating making up K ~1.5.

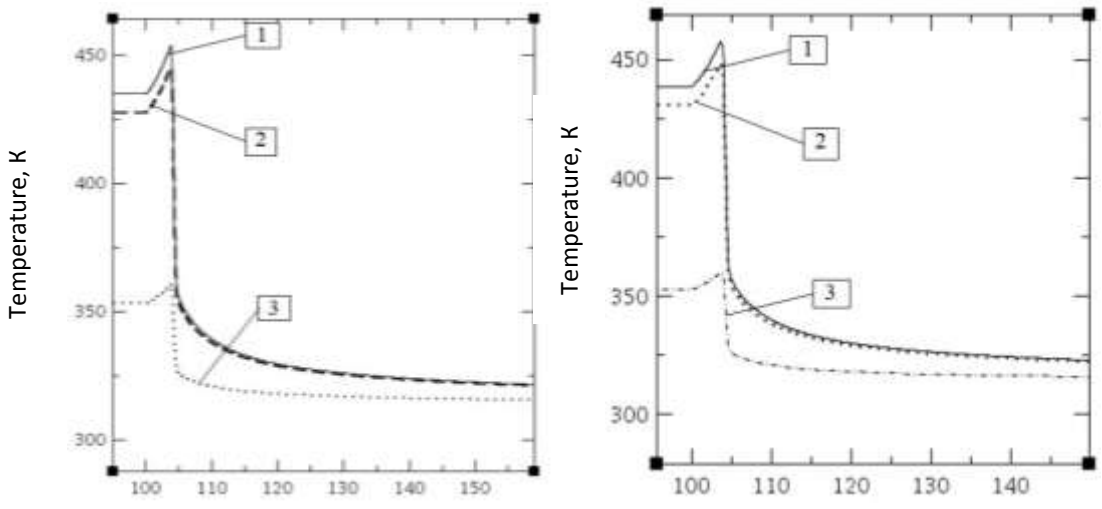

Fig. 7 Change in the maximal temperature of fuel (1), fuel rod cladding (2) and coolant (3): a - UO_2; b - U9%Mo

7. Conclusion

The calculation analysis revealed that conversion of the MIR research reactor to LEU fuel will result in the following changes of its parameters:

1. Fast neutron flux density on the test fuel rod claddings in the loop channels will decrease by 4-6%.
2. Reactivity loss rate as fuel burns up will decrease by 24-32%.
3. Uranium consumption will increase by approximately 4 times with a simultaneous decrease in ^{235}U consumption by 8-12%.
4. Annual FA consumption will decrease by approximately 30%.

In addition, the performed analysis related to accident consequences showed that the existing emergency systems are able to provide reactor cooling and its maintenance in a safe subcritical state.

Thus, the results of the calculation analysis show the possibility in principal of MIR conversion to LEU fuel with no worsening of its safety operating parameters and no significant changes in its experimental capabilities.

References

1. *Izhutov A.L., Mainskov S.V., Pimenov V.V., Starkov V.A., Svyatkin M.N.* State of Work on Calculation Studies of the MIR Reactor Conversion.33rd International Meeting on Reduced Enrichment for Research and Test Reactors. Chile. Santiago. 23-27 October.2011.
2. *Gomin E.A.* MCU-4 Status. VANT, Nuclear Reactor Physics Series, 2006. Issue 1. P.6-32.
3. *Yudkevich M.S.* BURNUP Software for Calculation of Reactor Isotopic Composition during the Reactor Run. Preprint IAE-6048/5-M.,1997.
4. *Bergles A.E., Rohsenow W.M.* The determination of forced convection surface boiling heat transfer. Transacnions ASME86//Journal of Heat Transfer. Series C. – 1964. – P. 365-371.
5. *Fabrega S.* Le calcul thermique des reacteurs de recherché refroidis par eau/Rapport CEA-R-4114, 1971.
6. *Mirshak S., Durant W.D., Towell R.H.* Heat Flux at Burnout. DuPont, DP-335, February, 1959.
7. RELAP5/MOD3, Volume 1-7. Code manual. NUREG/CR-5535 INEL-95/0174, 1995.
8. Nuclear Research Facility Safety Report Content Requirements, NP-049-03, Gosatomnadzor, Moscow, 2003.
9. Research Reactor Nuclear Safety Rules, NP-009-04, Gosatomnadzor, Moscow, 2004.
10. *A.L. Izhutov, V.V. Aleksandrov, A.Ye. Novoselov et. al.* "Results of out-of-pile tests of the MIR reactor irradiated fuel at high temperatures". Transactions of 9th International Topical Meeting on Research Reactor Fuel Management, Budapest, Hungary, April 10-13, 2005, pp.137-143.

NEUTRONIC COMPARISON OF HIGH DENSITY FUELS (U-MO-AL AND U_3SI_2-AL) FOR RESEARCH REACTORS

R. O. R. MUNIZ, A. T. SILVA, D. B. DOMINGOS, A. SANTOS, M. YAMAGUCHI
Instituto de Pesquisas Energéticas e Nucleares - Comissão Nacional de Energia Nuclear (IPEN/CNEN-SP)
Av. Professor Lineu Prestes, 2242, Cidade Universitária, 05508-000 São Paulo, SP - Brazil

ABSTRACT

The aim of this paper is to compare the infinite multiplication factor (K_∞), obtained through neutronic calculation with the code Scale 6.0, for fuel elements reflected in all directions containing U_3Si_2-Al and U-Mo-Al dispersion fuels. The U_3Si_2-Al dispersion fuels used in the calculation have a uranium density between 3.0 and 5.5 gU/cm^3 and the U-Mo-Al dispersion fuels have densities ranging from 4.0 to 7.52 gU/cm^3 and 7 and 10% Mo addition. The results show that the K_∞ calculated for U-Mo-Al fuels are smaller than that for U_3Si_2-Al fuels and increases between the uranium densities of 4 and 5 gU/cm^3 and decreases for higher uranium densities.

1. Introduction

Nuclear fuels composed by uranium metal alloys in monolithic and dispersed forms have been considered for research and power reactors due to their density properties and fast heat transfer. Among several candidates, U-Mo alloys are one of the most promising systems for plate type fuel elements owing to its broad gamma-phase stable field. This fact allows extensive fabrication capability since cubic gamma-phase shows good plasticity, higher strength and elongation [1]. Because of the high uranium density and good irradiation stability of U-Mo alloys, this fuel in the form of a dispersion in an Al matrix is the choice for the conversion of research and material test reactors currently using highly enriched uranium (HEU) to low-enriched uranium (LEU). The formation of an interaction layer between U-Mo particles and the Al matrix as a result of inter-diffusion has become a major issue for the performance of this fuel [2]. The formation of an interaction product in this dispersion fuel is unfavorable because of its low thermal conductivity and volume expansion as it consumes the Al matrix. Depending on the irradiation conditions (high burnup or high heat flux), large pores are formed at the interface of the interactions products and the Al matrix, which could eventually lead to a fuel plate failure. Many post irradiation tests have been conducted for uranium alloys with a molybdenum content between 6 to 10% by weight allowing the characterization of U-Mo-Al interaction [3], and this fuel qualification is a on-going process.

U_3Si_2-Al dispersion fuel with a uranium density of 3.5 gU/cm^3 is being considered as the fuel for the first core of the new Brazilian Multipurpose Reactor (RMB) [4]. The aim of this paper is to compare the calculated infinite multiplication factor (K_∞), obtained through neutronic calculation with the code Scale 6.0 [5], for fuel elements reflected in all directions using U_3Si_2-Al and U-Mo-Al dispersion fuels. These results will be utilized in the future to verify the core performance improvements that can be obtained for an already designed research reactor using a different fuel assembly with higher densities.

The U_3Si_2-Al dispersion fuel used in the calculation has a uranium density between 3.0 and 5.5 gU/cm^3 and the U-Mo-Al dispersion fuels have densities ranging from 4.0 to 7.52 gU/cm^3 and 7 to 10% Mo addition. The percentage by weight of molybdenum (Mo) in the dispersion changes the neutronic behavior of the fuel since the neutron absorption by Mo is considerable higher than that by Silicon (Si). Fig 1 shows a comparison between the neutron absorption cross section of Mo and Si [6].

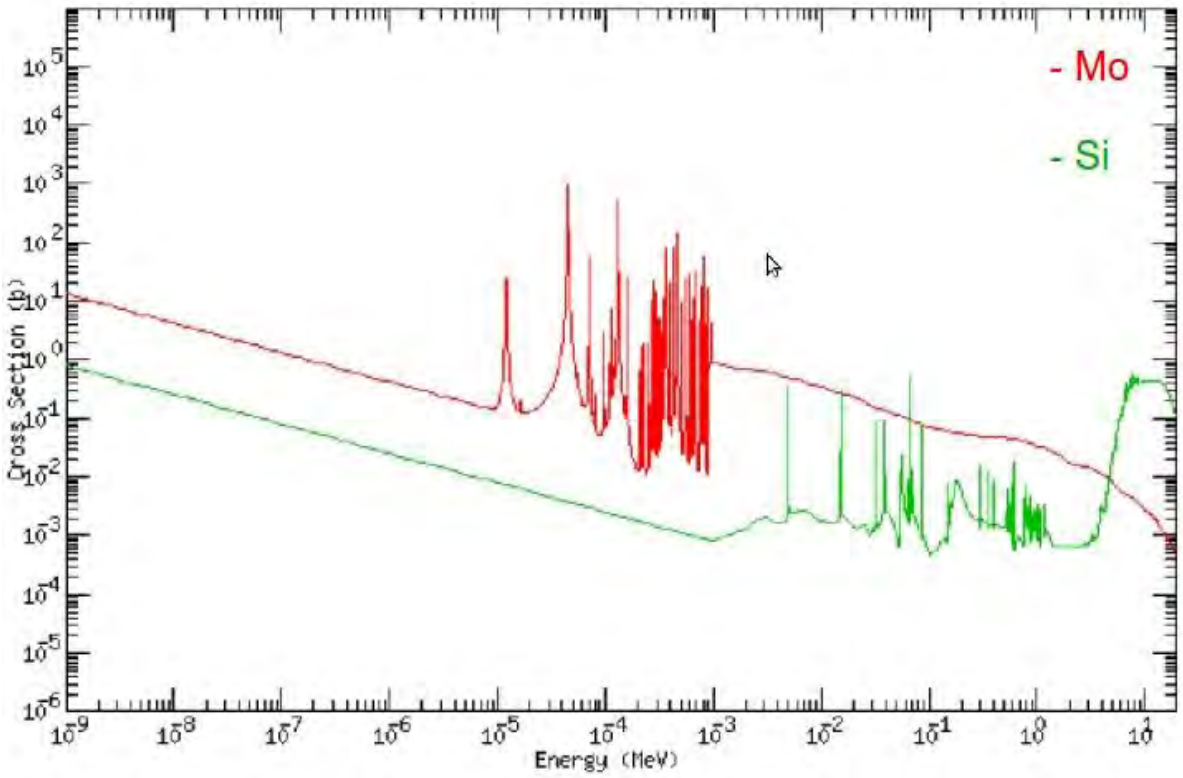

Fig 1: Neutron absorption cross section for Mo and Si.

2. Infinite multiplication factor (k_∞) calculation

2.1 Computer simulation

The computer code Scale 6.0 was used to calculate the infinite multiplication factor. The cross sections were processed with the modules Triton and Bonami that uses the Bondarenko method for calculating the self-shielding in the energy ranges of the unresolved ressonance regions. The neutron transport was calculated with KENO V.a using the Monte Carlo method for the neutron fluxes determination.

The fuel elements proposed and analyzed in this work (Fig 2) consisted of 21 rectangular aluminum coated plates and its structure is an aluminum frame where the fuel plates are fitted. The internal plates in the fuel element measure 7.049 cm x 61 cm, 0.135 mm thick, and the two external fuel plates are 0.150 mm thick. Both the U_3Si_2-Al meat and the U-Mo-Al meat are 6.5 cm x 61 cm, 0.061 cm thick. The space between the plates forms the cooling channel that is 0.245 cm thick. In the simulation this area was filled with water as well as the region around the fuel element which was modeled as a layer of 0.05 cm of water.

The concentrations used in this study are the same used in the reference [7] to simulate one U-Mo-Al plate and where only one U_3Si_2-Al uranium density was considered.

3. Results and conclusions

The calculated infinite multiplication factors (K_∞) obtained from the simulations with the code scale 6.0 are shown in Tables 1, 2 and 3. Fig 3 presents the infinite multiplication factors plotted against U_3Si_2-Al uranium density ranging from 3.0 to 5.5 gU/cm^3. Fig 4 presents the infinite multiplication factors plotted against U-Mo-Al with uranium densities from 4.0 to 7.52 gU/cm^3 and 7 and 10% Mo addition.

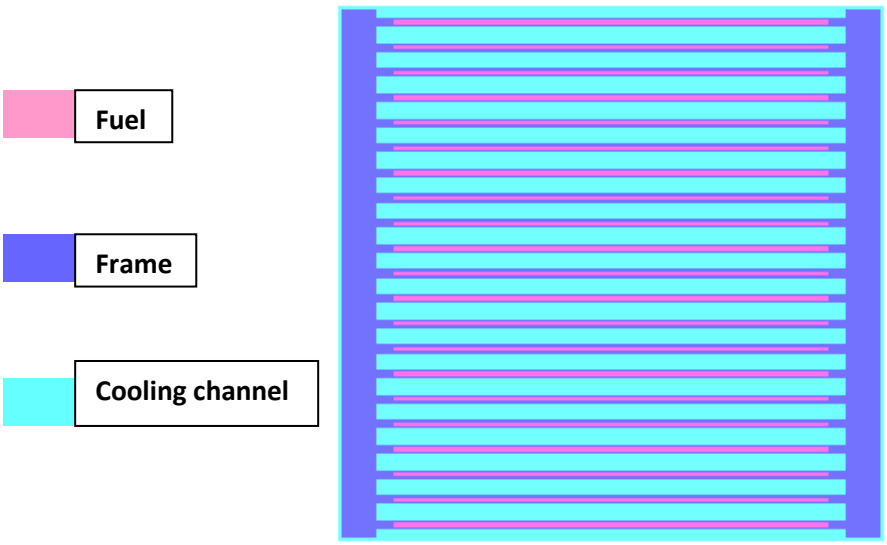

Fig 2: Fuel element cross section.

Tab 1: Infinite multiplication factors for U_3Si_2/Al fuels ranging from 3.0 to 5.5 gU/cm^3.

Uranium density (gU/cm^3)	K_∞	*σK_∞
3.00	1.60245	0.00011
3.30	1.61618	0.00011
3.50	1.62388	0.00010
3.80	1.63320	0.00010
4.00	1.63843	0.00011
4.30	1.64479	0.00010
4.50	1.64847	0.00011
4.80	1.65258	0.00010
5.00	1.65558	0.00010
5.30	1.65779	0.00010
5.50	1.65925	0.00011

* Uncertainty

Tab 2: Infinite multiplication factors for U-7wt%Mo-Al fuels ranging from 4.0 to 7.52 gU/cm^3.

Uranium density (gU/cm^3)	K_∞	σK_∞
4.01	1.62851	0.00011
4.55	1.63652	0.00010
5.02	1.64365	0.00011
5.55	1.64402	0.00011
6.02	1.64499	0.00011
6.55	1.64497	0.00011
7.02	1.64440	0.00011
7.52	1.64285	0.00011

Tab 3: Infinite multiplication factors for U-10wt%Mo/Al fuels ranging from 4.0 to 7.11 gU/cm^3.

Uranium density (gU/cm^3)	K_∞	σK_∞
4.01	1.62273	0.00011
4.52	1.63037	0.00011
5.02	1.63485	0.00010
5.56	1.63746	0.00011
6.00	1.63801	0.00011
6.54	1.63793	0.00011
7.01	1.63678	0.00011
7.11	1.63657	0.00011

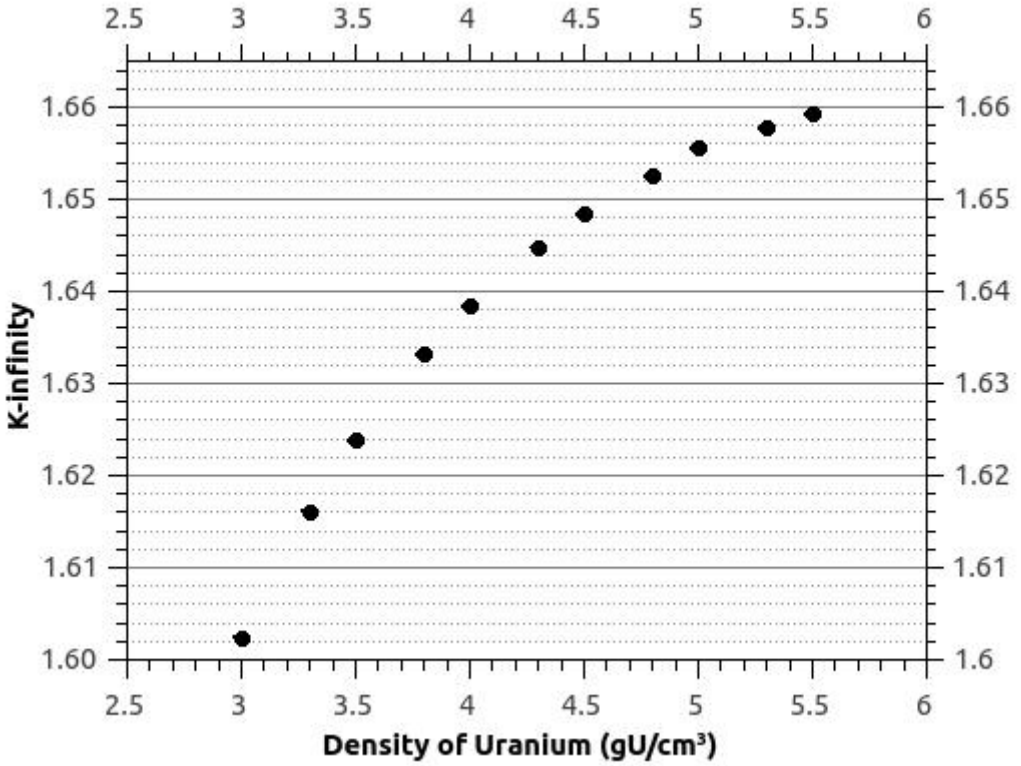

Fig 3: K_∞ for U_3Si_2-Al fuels with uranium densities ranging from 3.0 to 5.5 gU/cm^3.

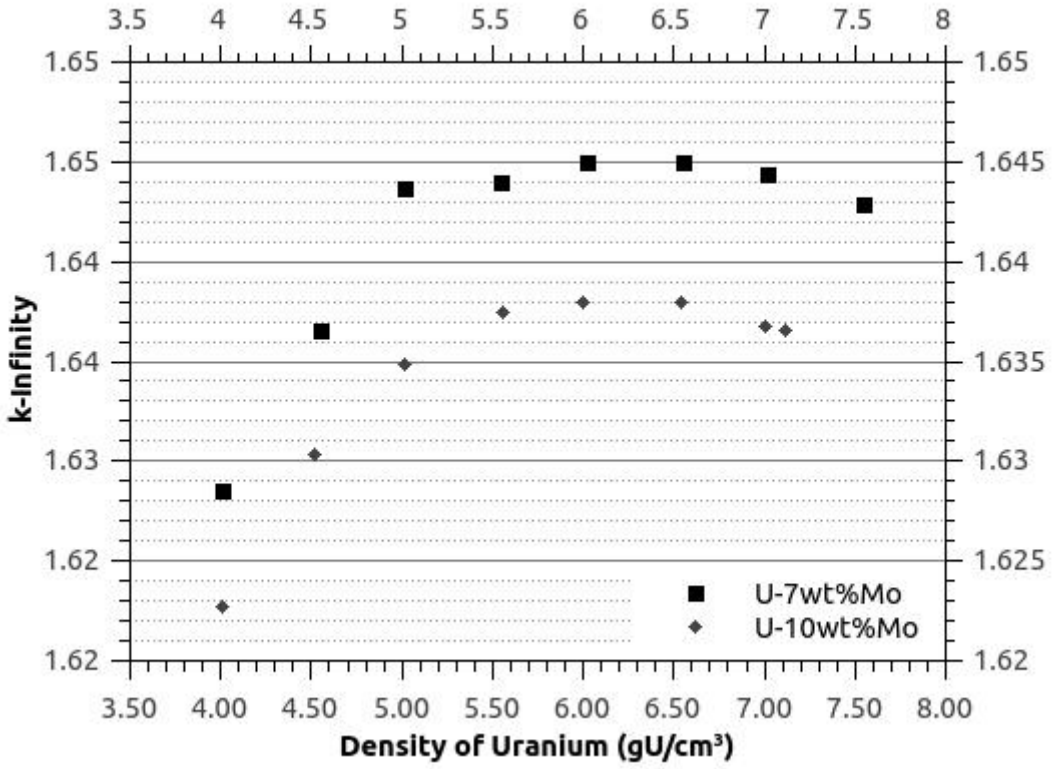

Fig 4: K_∞ for U-7wt%Mo-Al and U-10wt%Mo-Al with uranium densities ranging from 4.01 to 7.52 gU/cm^3.

It can be seen from Fig 3 that the K_∞ values obtained for different uranium densities with U-10wt%Mo/Al fuels are below those obtained with U-7wt%Mo/Al fuels. This behavior was expected due to the different absorption cross section of the two materials.

The potential benefits of the high density fuel will depend on the research reactor to be upgraded. A priory, it is difficult for potential users to clearly understand what kind of economic or improvement benefits can be expected. Further works are being conducted in order to identify improvements in core performance (higher neutron fluxes) and on the impact of fuel density on the cost of the research reactor fuel cycles (to reduce the number of fuel assemblies needed for operation) [8].

The results of this work confirm those obtained in reference 7, where was examined only a generic fuel plate. In a next step It will be analysed the performance of the U_3Si_2-Al and U-Mo-Al fuels with burnup.

Acknowledgements

The authors are grateful for financial support from CAPES.

4. References

[1] D. A. Lopes, T. A. G. Restivo, R. G. Gomide, A. F. Padilha, "Processing Window Design for U Alloys"*, Transactions RRFM 2012*, Prague, 18-22 March, pp. 46-51 (2012).

[2] H. J. Ryu, J. M. Park, J. H. Yang, C. K. Kim, Y. H. Jung and Y. S. Kim, "Interdiffusion in the Si-Rich Layer of U-Mo/Al-Si Fuel", *Transactions RERTR 2010*, Lisbon-Portugal, October 10-14, 2010.

[3] M. K. Meyer, D. M. Wachs, J. –F. Jue, D. D. Keiser, J. Gan, F. Rice, A. Robison, N. E. Wooltenhulme, P. Medvedev, G. L. Hofman, Y.-S. Kim, "U.S. Progress in the Development of Very High Density Low Enrichment Research Reactor Fuels", *Transactions RRFM 2012*, Prague, 18-22 March, pp. 10-13, 2012.

[4] J. A. Perrotta, A. J. Soares, "RMB: The New Brazilian Multipropose Research Reactor", *International Journal for Nuclear Power, atw vol. 60 (2015)*, *Issue 1, January*.

[5] *"*Scale: A Modular Code System for Performing Standardized Computer Analyses for Licensing Evaluation", ORNL/TM-2005/39, Version 5.1, Vols. I-III, November 2006. This code is available from Radiation Safety Information Computational Center at Oak Ridge National Laboratory as CCC-732.

[6] Cross Section Plotter. "http://atom.kaeri.re.kr" (2013).

[7] R. O. R. Muniz, D. B. Domingos, A. Santos, A. T. Silva, T. G. João, V. O. Aredes, "Neutronic Comparison of the Nuclear Fuels U_3Si_2/Al and U-Mo/Al", *Transactions of 2013 International Nuclear Atlantic conference – INAC 2013*, Recife, PE, Brazil, 24-29, 2013.

[8] E. A. Vilarino, "Core Performance Improvements Using High Density Fuel in Research Reactors", *Transactions RRFM 2013*, St. Petersburg-Russia, 21-25 April, pp. 68-75, 2013.

COMPARISON OF LOW ENRICHED URANIUM (UAlx-Al AND U-Ni) TARGETS WITH DIFFERENT GEOMETRIES FOR THE PRODUCTION OF MOLYBDENUM-99

D. B. DOMINGOS, A. T. SILVA, T. G. JOÃO, R. O. R. MUNIZ
Instituto de Pesquisas Energéticas e Nucleares - Comissão Nacional de Energia Nuclear (IPEN/CNEN-SP)
Av. Professor Lineu Prestes, 2242, Cidade Universitária, 05508-000 São Paulo, SP - Brazil

ABSTRACT

The IEA-R1 reactor of IPEN-CNEN/SP in Brazil is a pool type research reactor cooled and moderated by demineralized water and having Beryllium and Graphite as reflectors. In 1997 the reactor received the operating licensing for 5 MW. A new research reactor is being planning in Brazil to replace the IEA-R1 reactor. This new reactor, the Brazilian Multipurpose Reactor (RMB), planned for 30 MW, is now in the detailed design phase. Low enriched uranium (<20% ^{235}U) targets (UAl_x dispersed in Al and metallic U foils with different geometries) are being considered for the production of Molybdenum-99 (^{99}Mo) by fission in Brazil. Neutronic and thermal-hydraulics calculations were performed to determine the production of ^{99}Mo for the UAlx-Al targets irradiated in the IEA-R1 reactor core and for three different types of targets (UAlx-Al, U-Ni cylindrical and U-Ni plate) irradiated in a reactor conception with the same power of the RMB. The neutronic analyses showed that the total activity obtained for ^{99}Mo for 10 UALx-Al miniplates with a mass of 20,1 g of ^{235}U irradiated in the IEA-R1 reactor core was 1406.63 Ci. Considering that the time needed for the chemical processing and recovering of the ^{99}Mo will be seven days after the irradiation, the total ^{99}Mo activity available for distribution will be 240.48 Ci. No thermal-hydraulics design limit was overtaken. The same calculations were performed for three targets (UAl_x-Al, U-Ni cylindrical and U-Ni plate) irradiated in a reactor conception of 30 MW with a ^{235}U mass of 20.1 g. The ^{99}Mo activities produced were, respectively, 2,980.62 Ci, 3,166.6 Ci and 3495.23 Ci for the three targets. At the end of 7 days of irradiation, the total activity obtained for the targets were, respectively, 509.57 Ci, 541.36 Ci and 597.5 Ci. The thermal hydraulics analyses show that a minimum coolant speed of 7 m/s for the UAxl-Al target, 8 m/s for the U-Ni cylindrical target and 9 m/s for the U-Ni plate target will be necessary through the irradiation device to cool the targets and not exceeding the thermal-hydraulics design limits.

1. Introduction

^{99m}TC, product son of ^{99}Mo, is one of the most utilized radioisotopes in nuclear medicine in the world. Annually it is used in approximately 20 to 25 million procedures of medical diagnosis, representing about 80% of all the nuclear medicine procedures [1]. Since 2004, given the worldwide interest in ^{99}Mo production, the International Atomic Energy Agency (IAEA) has developed and implemented a Coordinated Research Project (CRP) [2] to help interested countries start a small-scale domestic ^{99}Mo production in order to meet the requirements of the local nuclear medicine. The purpose of this CRP is to provide interested countries with access to non-proprietary technologies and methods for production of ^{99}Mo using targets of thin foils of metallic low enriched uranium (LEU), UAl_x-Al miniplates of LEU type or by neutron activation reaction (n, gamma), for example, using gel generators. Brazil, through IPEN-CNEN/SP, began its CRP participation in late 2009. IPEN-CNEN/SP provides radiopharmaceuticals to more than 300 hospitals and clinics in the country, reaching more than 3.5 million medical procedures per year. The use of radiopharmaceuticals in the country over the last decade has grown at a rate of 10% per year and IPEN/CNEN-SP is primarily responsible for this distribution. ^{99m}Tc generators are the most used ones and are responsible for more than 80% of the radiopharmaceuticals applications in Brazil.

IPEN/CNEN/SP imports all the ^{99}Mo used in the country (450 Ci of ^{99}Mo per week or 24,000 Ci per year approximately). In the past, IPEN/CNEN-SP developed the ^{99}Mo production route from neutron activation of ^{98}Mo targets in the IEA-R1. However, the quantity produced does not meet the Brazilian needs of this isotope. Due to the growing need for nuclear medicine in the country and because of the short ^{99}Mo supply observed since 2008 on the world stage, IPEN/CNEN-SP has decided to develop its own project to produce ^{99}Mo through ^{235}U fission. This project has three main goals: 1) research and development of ^{99}Mo production from fission of LEU targets, 2) discussion and decision on the best production route technique, and 3) feasibility study of IPEN/CNEN-SP in reaching a routine production of ^{99}Mo. The main goal of IPEN/CNEN-SP is to accommodate the Brazilian demand for radiopharmaceuticals. Nowadays, this demand is about 450 Ci of ^{99}Mo per week and the future need, after six years, is estimated at around 1,000 Ci per week. One of the analyses planned in this project is to study the characteristics and specifications of UAl_x-Al and metallic uranium thin foils targets. The first aim of the present work was to perform neutronic calculations to evaluate the ^{99m}Mo production through fission at the IEA-R1 reactor and at a reactor conception with the same power of the RMB [3], designate in this paper as RC. The second aim of this work is to perform thermal-hydraulics calculations to determine the maximal temperatures achieved in the targets during irradiation and compared them with the design temperature limits established for UAlx-Al e uranium thin foils targets.

2. UAL_X-AL and uranium thin foil targets used in the neutronic and thermal-hydraulics analysis

The UAl_x-Al targets of LEU type proposed and analyzed in this work are aluminum coated miniplates (Fig 1). Each miniplate measures 4.7 cm x 17 cm, 0.152 cm thick, corresponding to a total volume of 12.2 cm^3. The UAl_x-Al meat is 4.0 cm x 11.8 cm, 0.076 cm thick, leading to a total volume of 3.59 cm^3. Considering this volume and a ^{235}U mass in the target equals to 2.01 g, the ^{235}U density ($\rho_{U\text{-}235}$) in the target meat is 0.58 g^{235}U/cm^3. For a 19.9% ^{235}U enrichment, the uranium density in the target is ρ_U = 2.91 gU/cm^3. This corresponds to a UAl_x volume fraction of 45% and an aluminum volume fraction of 55% in the dispersion.

A special Miniplate Irradiation Device (MID) was designed for the irradiation of the UAl_x-Al targets in the IEA-R1 and in the reflector part of the RC (Fig 2), whose external dimensions are 76.2 mm x 76.2 mm x 88.74 cm. The miniplates will be allocated in a box with indented bars placed inside the external part of the MID. Fig 3 shows the MID cross section. As seen from Fig 3, up to ten UAl_x-Al targets can be placed in the box with indented bars inside of the MID.

The targets of metallic Uranium foils with cylinder geometry analyzed at IPEN/CNEN-SP were based on targets that were examined in the Tajoura reactor in Libya to produce ^{99}Mo [4]. The targets were mounted in cylindrical geometry, in a tubular arrangement. The metallic U foil was covered with a Ni sheet before being placed concentrically inside the aluminum tubes. The dimensions of the target are (see Fig 4):

1. One foil of uranium (LEU) of 46.05 cm x 87.7 mm x 135 μm;
2. Coating nickel foil of 20 μm thickness;
3. Two aluminum cylinder having 46.05 cm length, outside diameters of 27.88 and 30.00 mm, and inside diameters of 26.44 and 28.22 mm, respectively;
4. ^{235}U mass of 20.1 g, with 19.9% enrichment of ^{235}U.

Fig 5 shows the set of concentric cylinders (Fig 6) positioned in a device with the same dimensions of the MID.

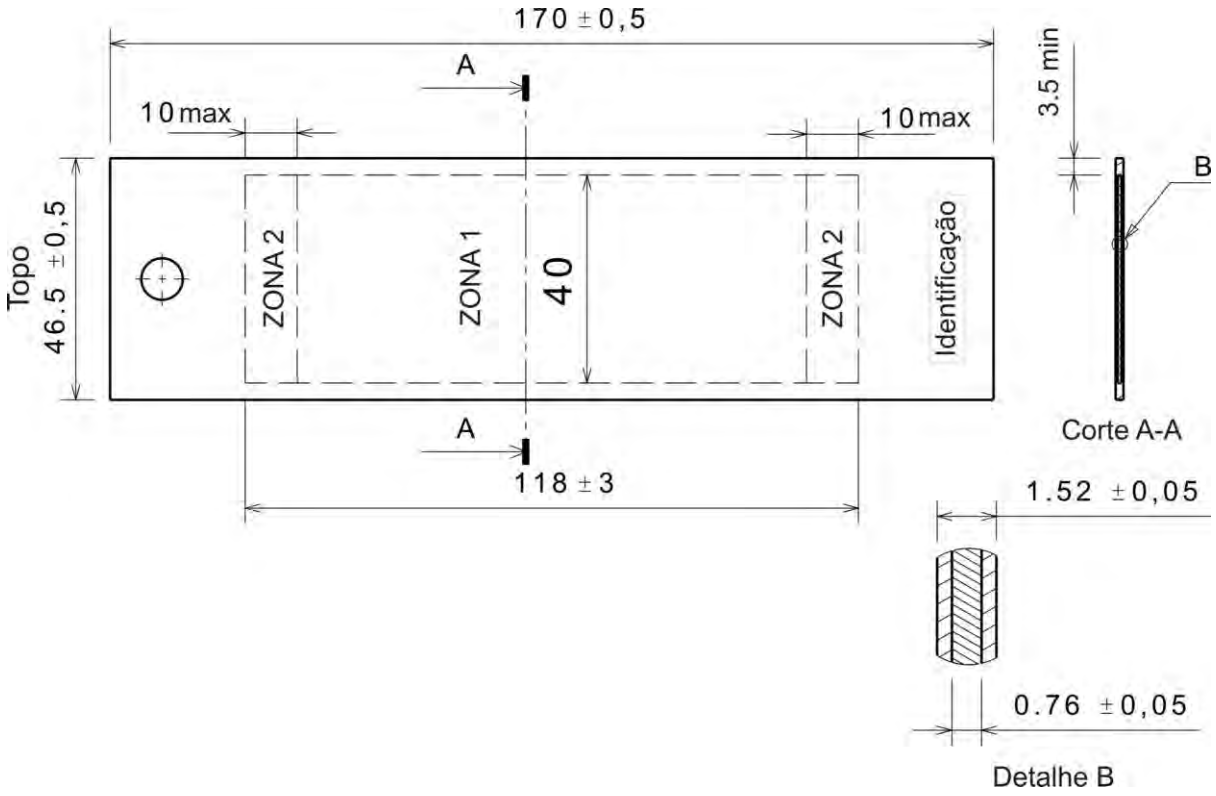

Fig 1: UAlx-Al miniplate dimensions.

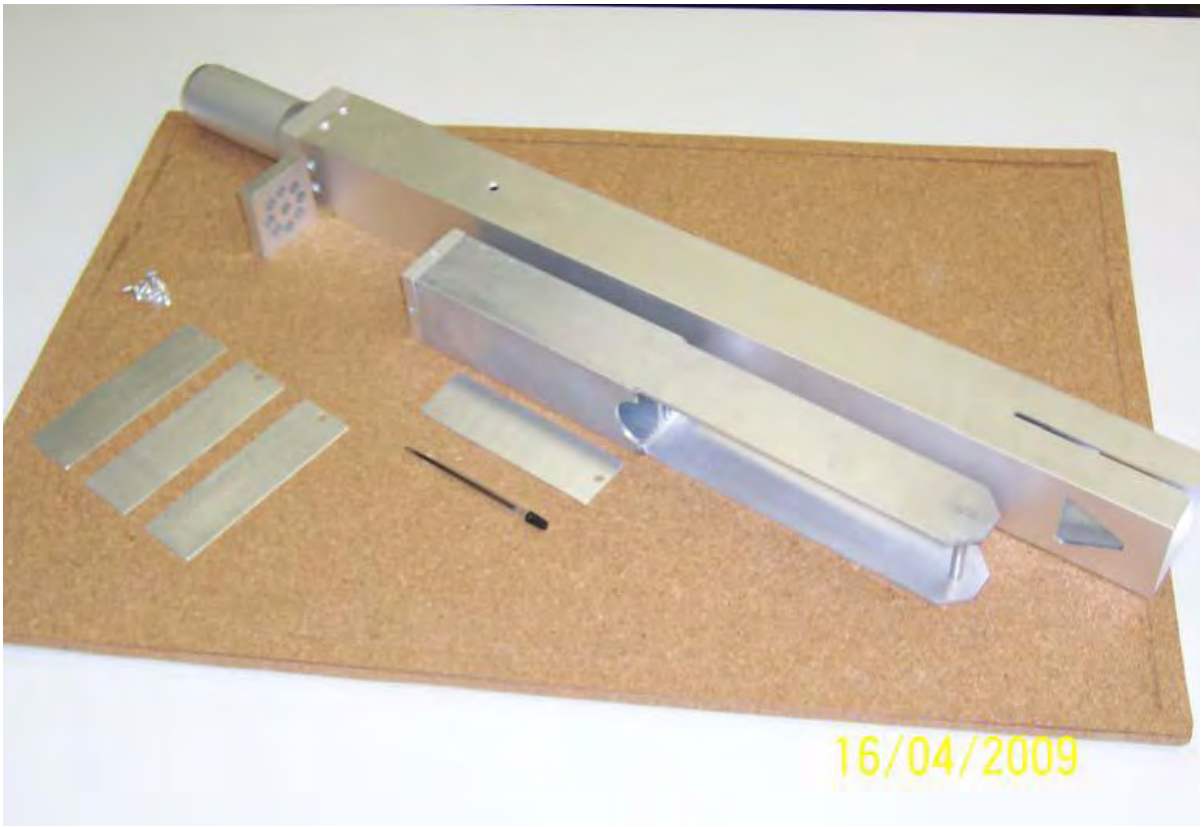

Fig 2: Miniplate irradiation device – MID.

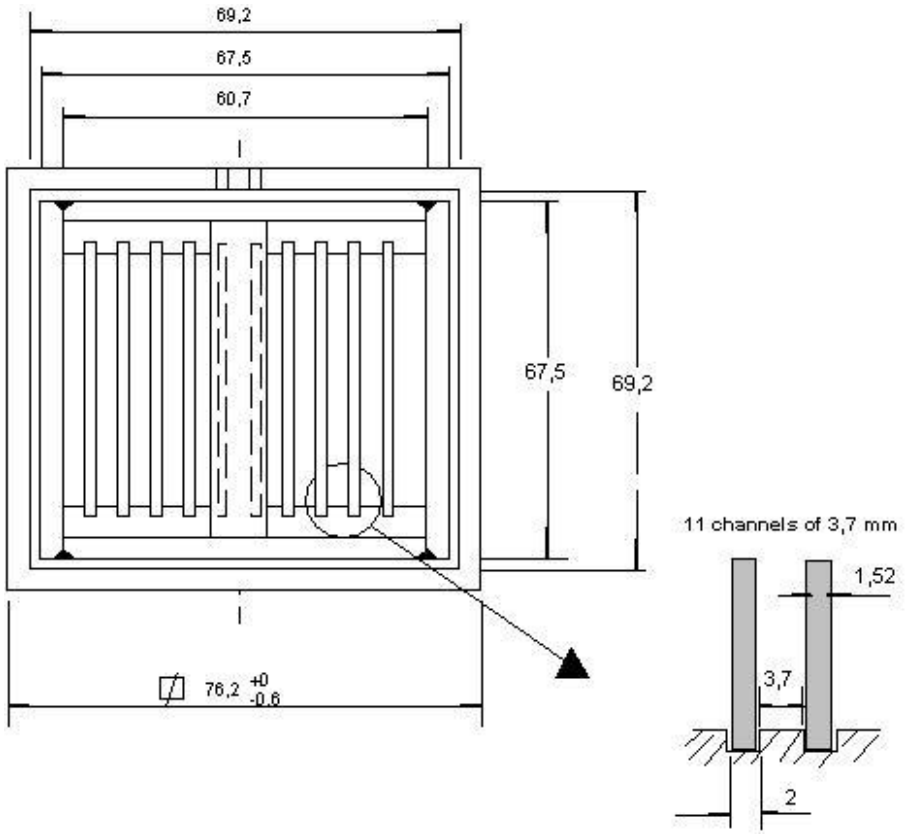

Fig 3: Cross section of the MID (dimensions in mm).

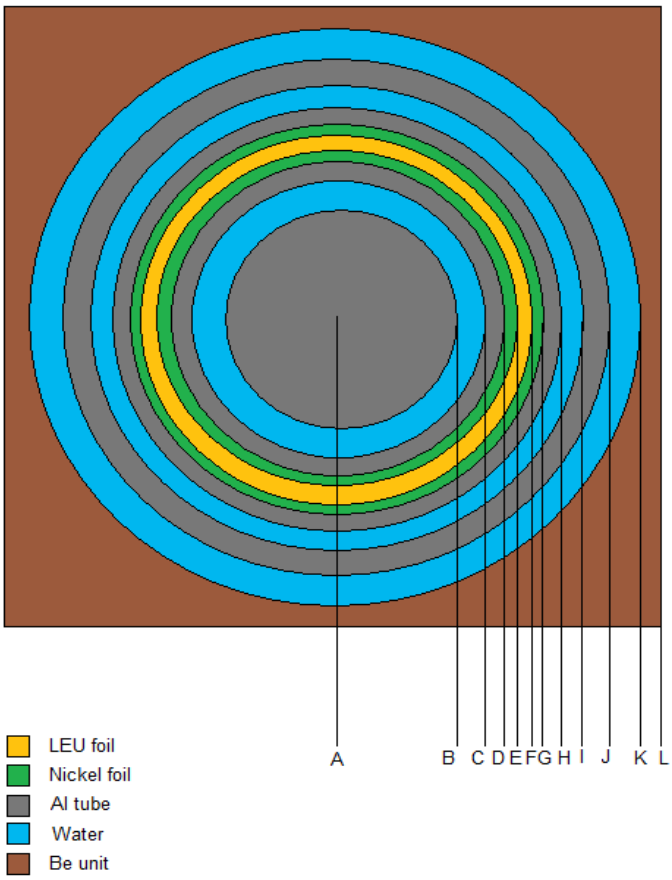

Radius	Length (cm)
AB	1.00
AC	1.322
AD	1.394
AE	1.396
AF	1.4095
AG	1.411
AH	1.5
AI	1.75
AJ	1.9
AK	2.2
AL	3.81

Fig 4: Irradiation device horizontal cross section for the U-Ni target with cylinder geometry.

Fig 5: Set of concentric cylinders positioned in the MID.

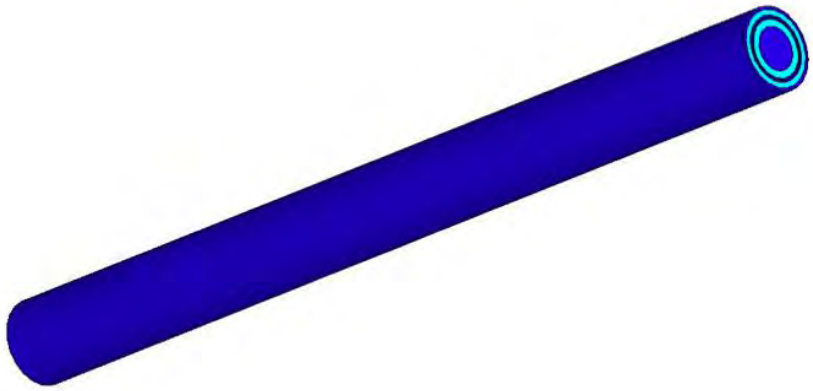

Fig 6: Set of concentric cylinders of U-Ni foil target.

The targets of metallic uranium foils with plate geometry were based on targets that were examined in the Paskitan research reactor [5] and consists of a uranium foil (19.99% ^{235}U) with a thickness of 135 μm enveloped in 20 μm thick nickel foil and placed between two aluminum plates that are welded from all sides. Each U-Ni plate has a uranium density of 2.01 g. The geometry of the foil plate target is shown in Figures 7 and 8.

For the performed calculations, the U-Ni targets (cylindrical and plate geometries) were modeled in the same irradiation device utilized for the calculations of the UAlx-Al targets.

The targets were modeled and simulated in peripheral core position of the RC, in the heavy water reflector. The target irradiation time was defined according to their current and planned operating cycle.

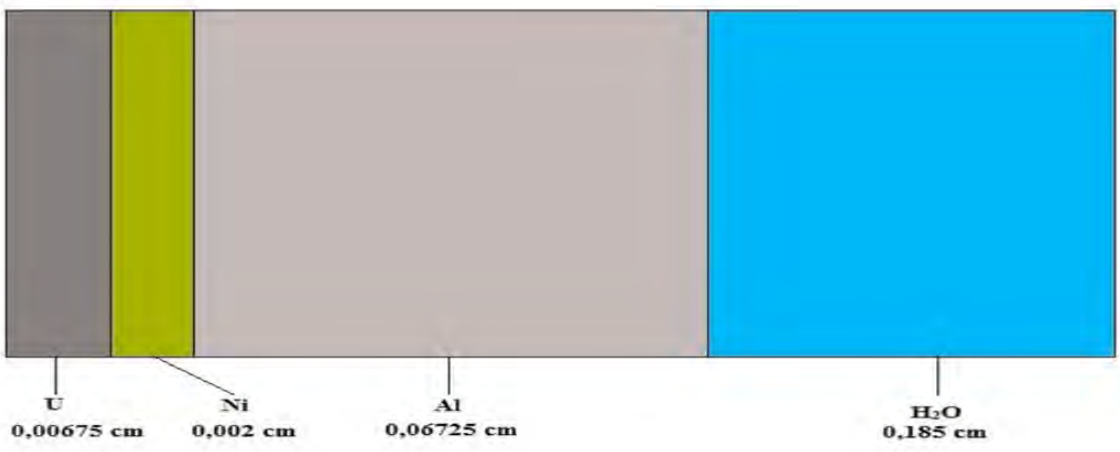

Fig 7: Half the thickness of U-Ni LEU target with plate geometry (67.5 μm), nickel foil, aluminum plate and cooling channel.

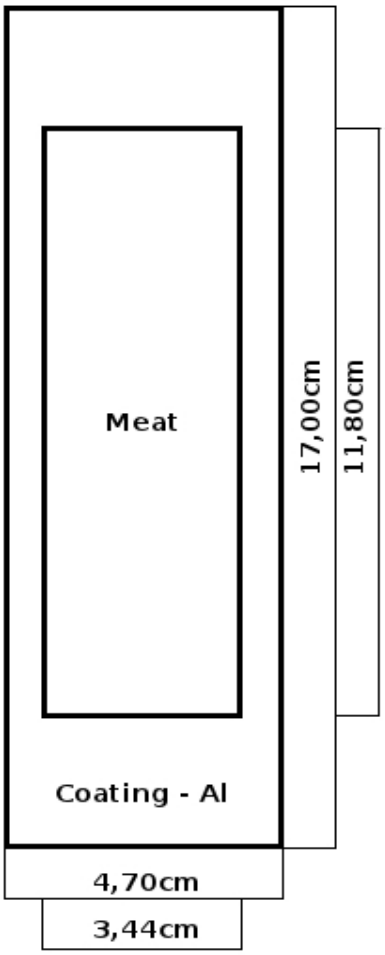

Fig 8: Width and height of the U-Ni plates.

3. Neutronic calculation for UALx-Al and U-Ni targets

The cores of the IEA-R1 and RC reactors as well as the UAlx-Al and the U-Ni targets used for the ^{99}Mo production were modeled with the HAMMER-TECHNION [6] and CITATION [7] numerical codes.

To simulate the targets in the IEA-R1 reactor, it was created a fictitious core, reflected with Beryllium, composed of 24 fuel elements of U_3Si_2-Al, 4 control elements, with density of 1.2 gU/cm^3. All fuel and control elements were taken as new and the adopted power operation was 5 MW. The cross sections of all elements were generated with HAMMER-TECHNION. The code CITATION was used to create the 3D model of the core and to determine parameters such as K-effective, neutron flux and power density. The SCALE 6.0 code system [8] was used to perform burnup calculations for each target and also to determine the ^{99}Mo activity at the end of irradiation. The target irradiation times for each reactor were defined according to their current and planned operating cycle. The UAl_x-Al targets were modeled and simulated in the IEA-R1 core central position. The target irradiation time was three (3) days. At the end of irradiation, the total activity obtained for the 10 UAl_x-Al was 1,406.63 Ci. Considering that the time needed for the chemical processing and recovering of the ^{99}Mo will be seven days after the irradiation, the total ^{99}Mo activity available for distribution will be 240.48 Ci [9].

The RC conceptual design used was an open pool type, 30 MW thermal power reactor. The RC core has a 5x6 configuration with MTR-type U_3Si_2-Al fuel elements with 19.75 wt% uranium-235 enrichment. The reactor core is light water cooled and moderated, using heavy water as reflector. The UAl_x-Al and U-Ni targets were modeled and simulated in a peripheral core position at the heavy water reflector using 30 U_3Si_2-Al fuel elements whose density was 1.9 gU/cm^3. The total activity obtained for the 10 UAl_x-Al minplates and for the U-Ni cylindrical and plate type targets were, respectively, 2,980.62 Ci, 3,166.6 Ci and 3,495.23 Ci. Considering that the time needed for the chemical processing and recovering of the ^{99}Mo will be seven (7) days after the irradiation, the total activity obtained for the 10 UAl_x-Al miniplates and for the U-Ni cylindrical and plate types targets were, respectively, 509.57 Ci, 541.36 Ci and 597.5 Ci.

4. Thermal Hydraulics Calculation for the Irradiation Device

A thermal-hydraulics model MTCR-IEA-R1 [10] was developed in 2000 at IPEN/CNEN-SP using a commercial program Engineering Equation Solver (EES). The use of this computer model enables the steady-state thermal and hydraulics core analyses of research reactors with MTR fuel elements. The following parameters are calculated along the fuel element channels: fuel meat central temperature (T_c), cladding temperature (T_r), coolant temperature (T_f), Onset of Nucleate Boiling (ONB) temperature (T_{onb}), critical heat flux (Departure of Nucleate Boiling-DNB), flow instability and thermal-hydraulics safety margins MDNBR and FIR. The thermal-hydraulics safety margins MDNBR and FIR are calculated as the ratio between, respectively, the critical heat flux and the heat flux for flow instability and the local heat flux in the fuel plate. Furthermore, the MTCR-IEA-R1 model also utilizes in its calculation the involved uncertainties in the thermal-hydraulics calculation such as: fuel fabrication uncertainties, errors in the power density distribution calculation, in the coolant flow distribution in the core, reactor power control deviation, in the coolant flow measures, and in the safety margins for the heat transfer coefficients. The calculated thermal-hydraulics core parameters are compared with the design limits established for MTR fuels: a) cladding temperature < 95°C; 2) safety margin for ONB > 1.3, or the ONB temperature higher than coolant temperature; 3) safety margin for flow instability > 2.0; and 4) safety margin for critical heat flux > 2.0. For the targets, it was considered the following design limits: 1) no material may experience a temperature greater than ½ any target material melting temperature. The lowest melting temperature for any of the proposed target materials is that of the aluminum cladding, whose melting temperature is 660°C. Therefore 330°C is the maximum allowable temperature for the LEU target; 2) the pool coolant must be kept below its saturation temperature. In this work it was adopted as target design limit the cladding temperature that initiated the coolant nucleate boiling (T_{ONB}) for a given coolant pressure and superficial heat flux given by Bergles and Rosenow correlation [11].

In order to evaluate the temperatures achieved in the targets different coolant velocities were tested through the MID. For the temperature calculations of the UAlx-Al targets the thermal-hydraulics model MTCR-IEA-R1 was used and the results were obtained for the analysis of the IEA-R1 and RC cores. The same procedure was used to calculate the temperatures achieved in the U-Ni target with plate geometry. For the calculation of the temperatures of the U-Ni targets with cylindrical geometry was utilized the software ANSYS CFX [12]. The power density (25 KW/cm^3) calculated in the ID position in the RC reflector with the code MTCR-IEAR1 was utilized as input date to determine the temperatures in the U-Ni target with cylindrical geometry.

The placement of the MID in the core central position of IEA-R1 reactor will deviate part of the reactor flow rate to cool the UAlx-Al targets. The flow rate in the core of the IEA-R1 reactor is 3,400 gpm which provides a flow rate of approximately 23 m^3/h per fuel element, and sufficient to cool a standard fuel element. The insertion of the MID in the IEA-R1 reactor core will divert part of the reactor core coolant to cool the UAlx-Al miniplates. Thus, a MID

thermo-hydraulic analysis was developed to determine the required coolant velocity to cool the miniplates, but without damaging the fuel elements in the reactor core. Coolant velocities from 5 to 15 m/s were tested through the MID. Table 1 provide the calculated UAlx-Al target temperatures for different coolant velocities through the MID in the IEA-R1 reactor core. The simulations considered the MID with ten identical UAlx-Al miniplates. Table 1 show that coolant velocities equal or higher than 5 m/s through the MID are sufficient to cool the targets without achieving ONB temperatures. The calculated cladding temperatures are below the value of 128.5 °C, indicating one-phase flow through the targets. As calculated in the reference 13, even coolant velocities of 1.78 m/s will be sufficient to cool the targets and a coolant flow restrictor (see Fig 1) was fabricated in order to maintain a MID flow rate of 12 m^3/hr in the reactor core during target irradiation.

Tab 1: Target temperatures versus DIM coolant velocities in the IEA-R1 reactor.

Coolant velocity (m/s)	UAlx-Al meat central temperature (°C)	UALx-Al aluminum cladding temperature (°C)	ONB Temperature (T_{ONB}) (°C)	Coolant Temperature (°C)
5	111.2	99.06	128.5	45.00
6	103.2	91.07	128.5	44.48
7	97.38	85,21	128.5	44.11
8	92.89	80.71	128.5	43.84
9	89.32	77.14	128.5	43.63
10	86.42	74.24	128.5	43.46
11	85.15	72.98	128.5	43.39
12	82.93	70.75	128.5	43.27
13	81.04	68.86	128.5	43.16
14	79.40	67.23	128.5	43.08
15	77.98	65.80	128.5	43.00

Table 2 provides the calculated UAlx-Al target temperature results for different coolant velocities through the MID placed in the peripheral RC core position in the heavy water reflector. The simulations considered the MID with ten identical UAlx-Al miniplates. Table 2 shows that a velocity of 7 m/s is necessary to cool the targets. For this velocity no design limit was achieved for the analyzed irradiation device. The calculated cladding temperatures are below the value of 134.7 °C, indicating one-phase flow through the targets.

Tab 2: UAlx-Al target temperatures versus different MID coolant velocities in the peripheral core position of the RC.

Coolant velocity (m/s)	UAlx-Al meat central temperature (°C)	Aluminum cladding temperature (°C)	T_{onb} (°C)	Coolant temperature (°C)
5	189.0	162.6	134.7	48.51
6	172.5	146.1	134.7	47.38
7	160.3	134.0	134.7	46.58
8	151.0	124.6	134.7	45.99
9	143.5	117.1	134.7	45.53
10	137.4	111.0	134.7	45.17
11	132.3	105.9	134.7	44.87
12	130.0	103.6	134.7	44.75
13	126.0	99.6	134.7	44.52
14	122.5	96.2	134.7	44.33
15	119.5	93.1	134.7	44.17

Tables 3 and 4 provide the calculated U-Ni target temperatures for different coolant velocities through the ID in the RC core peripheral position, respectively, for plate and cylindrical geometries. Tab 4 presents for the U-Ni target with cylindrical geometry the temperature of the aluminum tube.

Tab 3: Calculated temperatures for the U-Ni target with plate geometry versus different coolant velocities through the ID.

Coolant velocity (m/s)	Aluminum cladding temperature (°C)	T_{onb} (°C)
5	191.4	132
6	171.1	132
7	156.1	132
8	144.5	132
9	135.2	132
10	127.7	132
11	121.4	132
12	118.8	132
13	113.6	132
14	109.3	132
15	105.6	132

Tab 4: Aluminum tube temperatures for the U-Ni target with cylindrical geometry versus different coolant velocities through the ID.

Coolant velocity (m/s)	Aluminum tube temperature (°C)	T_{onb} (°C)
5	166	137
6	149	137
7	137	137
8	127	137
9	119	137
10	113	137
11	107	137
12	103	137
13	99	137
14	95	137
15	92	137
16	90	137

Tab 3 provides the calculated target temperature results for different coolant velocities through the MID placed in the peripheral core position in the heavy water reflector. A velocity of 8 m/s is necessary to cool the targets. For this velocity no design limit was achieved for the analyzed irradiation device. The calculated aluminum cladding temperatures are below the value of 132°C, indicating one-phase flow through the U-Ni targets with plate geometry.

Table 4 provides the calculated U-Ni aluminum tube temperatures for different coolant velocities through the MID placed in the peripheral core position in the heavy water reflector. A velocity of 9 m/s is necessary to cool the target. For this velocity no design limit was achieved for the analyzed irradiation device. The calculated aluminum tube temperatures are below the value of 137°C, indicating one-phase flow through the U-Ni target with cylinder geometry.

5. Conclusion

From the neutronic calculations presented here, for a uranium amount of 20.1 g in the analyzed targets a ^{99}Mo activity of 1406.63 Ci was obtained for 7 days irradiation time in the IEA-R1 core. For the UAlx-Al target and for the U-Ni targets with plate and cylindrical geometries the calculated total ^{99}Mo activity was, respectively, 2,980.62 Ci, 3,166.6 Ci and 3.495.23 Ci. Initially, ^{99m}TC generators will be distributed seven (7) days after the end of the irradiation. Consequently, the total ^{99}Mo activity is expected to reach a value of 240.48 Ci for UAl_x-Al targets irradiated in the IEA-R1 core. For the UAlx-Al target and U-Ni targets with plate and cylinder geometries irradiated in the peripheral core position of the RC the total ^{99}Mo activity is expected to reach values of 509.57 Ci, 541.36 Ci and 597.5 Ci, respectively. From these values, it is noted that the Brazilian current demand of 450 Ci of ^{99}Mo per week may be addressed irradiating the targets in a peripheral core position of the RC.

Through the thermal-hydraulics calculations it was determined the minimum flow necessary to cool the targets. No design limit was achieved for the analyzed targets. The calculated cladding temperatures are below the value of 95°C, and the coolant temperatures are below the ONB temperature, indicating one-phase flow through the irradiation devices.

Acknowledgments

The authors are grateful for financial support from CAPES and FAPESP.

6. References

[1] G. F. Wienciek, A. B. Vandegrift, A. A. Levya, and A. S. Hebden, “Status and Progress of Foil and Target Fabrication Activities for the Production of ^{99}Mo from LEU”, *RERTR 2008 – 30th International Meeting on Reduced Enrichment for Research and Test*, Washington, October 5-9, 2008.

[2] I. N. Goldman, N. Ramamoorthy, and P. Adelfang, “Progress and Status of the IAEA Coordinated Research Project: Production of Mo-99 using LEU Fission or Neutronic Activation”, *RERTR 2007, September 23-27, 2007, Prague, Czech Republic*.

[3] J. A. Perrotta, A. J. Soares, "RMB: The New Brazilian Multipropose Research Reactor", *International Journal for Nuclear Power*, atw vol. 60 (2015), Issue 1, January.

[4] F. M. Bsebsu, F. Abotweirat and S. Elwaer, “Feasibility Study Part-I Thermal Hydraulic Analysis of LEU Target for ^{99}Mo Production in Tajoura Reactor, *RERTR 2007,* September 23-27, 2007, Prague, Czech Republic.

[5] A. Mushtaq, Massod Iqbal, Ishtiaq Hussain Bokhari and Tayab Mahmood, “Low Enriched Uranium Foil Plate Target for the Production of Fission Molybdenum-99 in Pakistan Research Reactor-I, *Nuclear Instruments and Methods in Physics Research B* 267(2009) 1109-1114.

[6] J. Barhein, W. Rhotenstein, and E. Taviv, “The HAMMER Code System TECHNION”, Israel Institute of Technology, Haifa, Israel, NP-565, 1978.

[7] T. B. Fowler, D. R. Vondy, and G. W. Cunninghan, “Nuclear Reactor Core Analysis Code: CITATION”, *Oak Ridge National Laboratory, ORNL-TM-2496, Rev. 2, Suppl. 3*, July 1972.

[8] “SCALE: A Modular Code System for Performing Standardized Computer Analyses for Licensing Evaluation”, *ORNL/TM-2005/39*, Version 6.1, Vols. I–III, November 2006. The code is available from Radiation Safety Information Computational Center at Oak Ridge National Laboratory as CCC-732.

[9] D. B. Domingos, Análises Neutrônica e Termo-hidráulica de Dispositivos para Irradiação de Alvos Tipo LEU de UAlx-Al e U-Ni para Produção de Mo-99 nos Reatores IEA-R1 e RMB", *2014, Dissertação (Doutorado)* - Instituto de Pesquisas Energéticas e Nucleares, São Paulo.

[10] P. E. Umbehaun, "Metodologia para Análise Termo-hidráulica de Reatores de Pesquisa Tipo Piscina com Combustível Tipo Placa*", 2000, Dissertação (Mestrado)* – Instituto de Pesquisas Energéticas e Nucleares, São Paulo.

[11] A. E. Bergles, W. M. Rosenow, “The Determination of Forced-Convection Surface Boiling Heat Transfers”, *Trans, of the ASME 86 (Series C-J. of Heat Transfer), 365-375, Aug.* 1964.

[12] ANSYS CFX Reference Guide, release 12.0, April 2009.

[13] A. T. Silva, D. B. Domingos, T. G. João, P. J. B. O. Nishiyama, C. Giovedi, **"**Neutronic and Thermal-Hydraulics Calculations for the Production of Molybdenum-99 by Fission in Low Enriched Uranium UAlx-Al Targets", *RRFM 2015*, April 19-23, 2015, Bucharest, Romania.

NEUTRONIC AND THERMAL-HYDRAULICS CALCULATIONS FOR THE PRODUCTION OF MOLYBDENUM-99 BY FISSION IN LOW ENRICHED URANIUM UALx-AL TARGETS

A. T. SILVA, D. B. DOMINGOS, T. G. JOÃO
Instituto de Pesquisas Energéticas e Nucleares - Comissão Nacional de Energia Nuclear (IPEN/CNEN-SP)
Av. Professor Lineu Prestes, 2242, Cidade Universitária, 05508-000 São Paulo, SP - Brazil

P. J. B. O. NISHIYAMA, C. GIOVEDI
Centro Tecnológico da Marinha em São Paulo (CTMSP)
Av. Professor Lineu Prestes, 2468, Cidade Universitária, 05508-000 São Paulo, SP - Brazil

ABSTRACT

The IEA-R1 reactor of IPEN-CNEN/SP in Brazil is a pool type research reactor cooled and moderated by demineralized water and having Beryllium and Graphite as reflectors. In 1997 the reactor received the operating licensing for 5 MW. Low enriched uranium (LEU) (<20% ^{235}U) UAl_x dispersed in Al targets are being considered for production of Molybdenum-99 (^{99}Mo) by fission. Neutronic and thermal-hydraulics calculations were performed, respectively, to evaluate the production of ^{99}Mo for these targets in the IEA-R1 reactor and to determine the temperatures achieved in the UAlx-Al targets during irradiation. For the neutronic calculations were utilized the computer codes HAMMER-TECHNION and CITATION, and for the thermal-hydraulics calculations was utilized the computer code MTRCR-IEAR1. The analysis demonstrated that the irradiation will occur without adverse consequences to the operation of the reactor. The total amount of ^{99}Mo produced was calculated with the program SCALE. Considering that the time needed for the chemical processing and recovering of the ^{99}Mo will be five days after the irradiation, the total ^{99}Mo activity available for distribution will be 176 Ci for 3 days of irradiation, 236 Ci for 5 days of irradiation, and 272 Ci for 7 days of targets irradiation.

1. Introduction

^{99m}TC, product son of ^{99}Mo, is one of the most utilized radioisotopes in nuclear medicine in the world. Annually it is used in approximately 20 to 25 million procedures of medical diagnosis, representing about 80% of all the nuclear medicine procedures [1]. Since 2004, given the worldwide interest in ^{99}Mo production, the International Atomic Energy Agency (IAEA) has developed and implemented a Coordinated Research Project (CRP) [2] to help interested countries start a small-scale domestic ^{99}Mo production in order to meet the requirements of the local nuclear medicine. The purpose of CRP is to provide interested countries with access to non-proprietary technologies and methods for production of ^{99}Mo using targets of thin foils of metallic low enriched uranium (LEU), UAl_x-Al miniplates of LEU type or by neutron activation reaction (n, gamma), for example, using gel generators. Brazil, through IPEN-CNEN/SP, began its CRP participation in late 2009. IPEN/CNEN-SP provides radiopharmaceuticals to more than 300 hospitals and clinics in the country, reaching more than 3.5 million medical procedures per year. The use of radiopharmaceuticals in the country over the last decade has grown at a rate of 10% per year and IPEN/CNEN-SP is primarily responsible for this distribution. ^{99m}Tc generators are the most used ones and are responsible for more than 80% of the radiopharmaceuticals applications in Brazil. IPEN/CNEN-SP imports all the ^{99}Mo used in the country (450 Ci of ^{99}Mo per week or 24,000 Ci per year approximately). In the past, IPEN/CNEN-SP developed the ^{99}Mo production route from neutron activation of ^{98}Mo targets in the IEA-R1. However, the quantity produced does not meet the Brazilian needs of this isotope. Due to the growing need for nuclear medicine in the country and because of the short ^{99}Mo supply observed since 2008 on the world stage,

IPEN/CNEN-SP has decided to develop its own project to produce ^{99}Mo through ^{235}U fission. This project has three main goals: 1) the research and development of ^{99}Mo production from fission of LEU targets, 2) the discussion and decision on the best production route technique, and 3) the feasibility study of IPEN/CNEN-SP in reaching a routine production of ^{99}Mo. The main goal of IPEN/CNEN-SP is to accommodate the Brazilian demand for radiopharmaceuticals. Nowadays, this demand is about 450 Ci of ^{99}Mo per week and the future need, after six years, is estimated at around 1,000 Ci per week. One of the analyses planned in this project is to study the characteristics and specifications of UAl_x-Al targets. The first aim of the present work was to perform neutronic calculations to evaluate the ^{99m}Mo production through fission at the IPEN/CNEN-SP IEA-R1 nuclear reactor. The second aim of this work is to perform thermal-hydraulics calculations to determine the maximal temperatures achieved in the targets during irradiation and compared them with the design temperature limits established for UAlx-Al targets.

2. UAL_X-AL targets used in the neutronic and thermal-hydraulic analysis

The UAl_x-Al targets of LEU type proposed and analyzed in this work are aluminum coated miniplates. Each miniplate measures 52 mm x 170 mm, 1.52 mm thick, corresponding to a total volume of 13.437 mm^3. The UAl_x-Al meat is 40 mm x 118 mm, 0.76 mm thick, leading to a total volume of 3.587 mm^3. Considering this volume and a ^{235}U mass in the target equals to 2.06 g, the ^{235}U density ($\rho_{U\text{-}235}$) in the target meat is 0.58 g^{235}U/cm^3. For a 19.9% ^{235}U enrichment, the uranium density in the target is ρ_U = 2.89 gU/cm^3. This corresponds to a UAl_2 volume fraction of 45% and an aluminum volume fraction of 55% in the dispersion.

A special Miniplate Irradiation Device (MID) was designed for the irradiation of the UAl_x-Al targets in the IEA-R1 reactor. Figure 1 shows the MID which has the external dimensions of the IEA-R1 fuel element. The miniplates will be allocated in a box with indented bars placed inside the external part of the MID. Figure 2 shows the MID cross section. As seen from Figure 2, up to ten UAl_x-Al targets can be placed in the box with indented bars inside of the MID.

The UAl_x-Al targets were modeled and simulated, respectively, in the core central position in the IEA-R1 reactor. The target irradiation time was defined according to their current and planned operating cycle.

Fig 1: Miniplate irradiation device – MID.

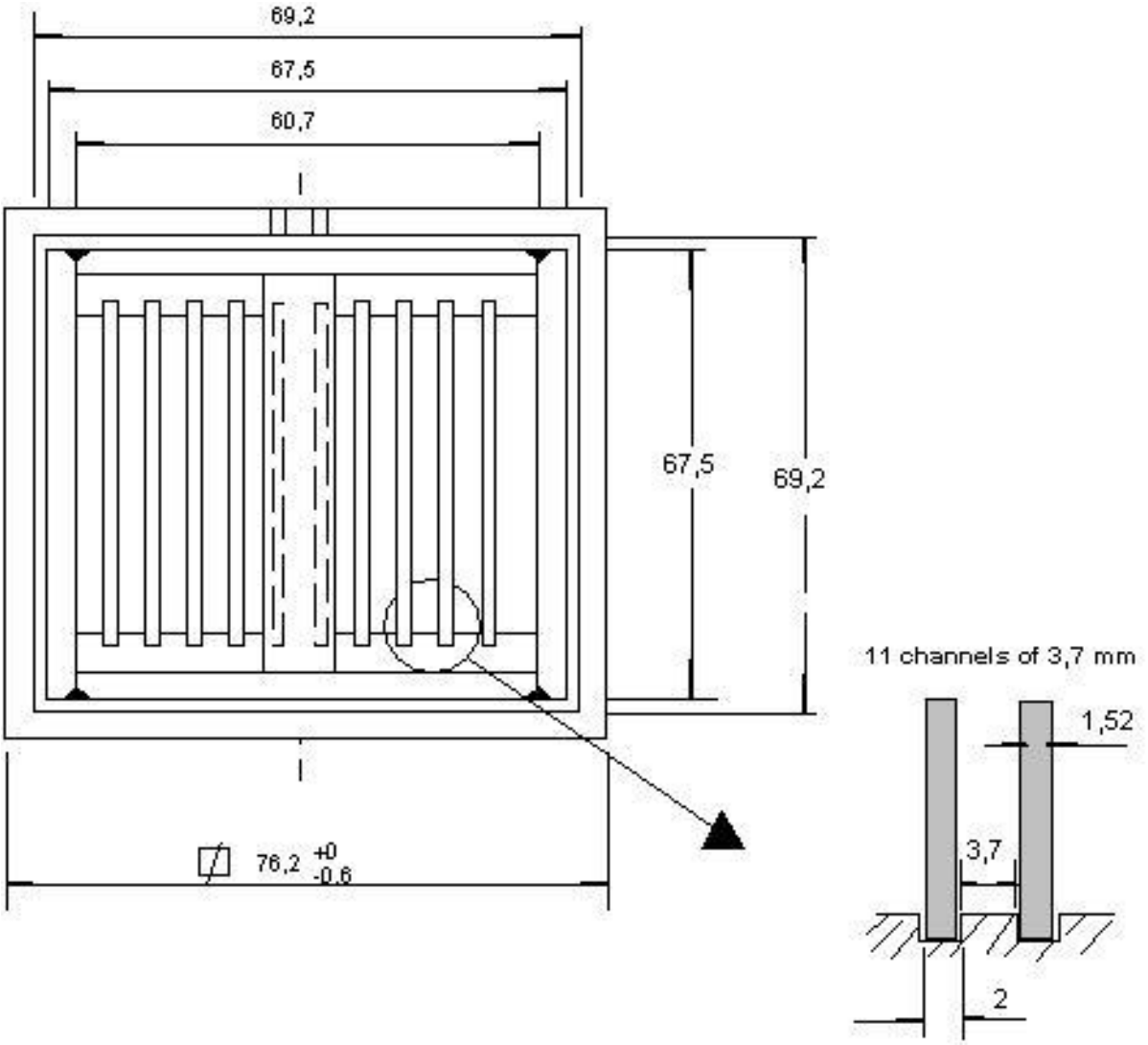

Fig 2: Cross section of the MID (dimensions in mm).

3. Neutronic calculation for the irradiation device

The IEA-R1 reactor core, as well as the UAl_x-Al targets used for the ^{99}Mo production, were modeled with the HAMMER-TECHNION [3] and CITATION [4] numerical codes. The 1D cross section for each component of the two reactors and the power distribution for any position r of the reactor cores were obtained. The SCALE 6.0 [5] code system was used to perform burnup calculations for each target and also to determine the ^{99}Mo activity at the end of irradiation.

The IEA-R1 reactor has a 5x5 configuration, 5 MW, containing 24 MTR-type fuel elements with a beryllium irradiation device at its central position. The UAl_x-Al targets were modeled and simulated in the core central position using 24 U_3Si_2-Al fuel elements whose density was 1.2 gU/cm^3. The calculations were developed for three irradiation periods: 3, 5 and 7 days. At the end of 3 irradiation days, the total ^{99}Mo activity obtained for the 10 UAl_x-Al miniplates was 620 Ci. After 5 irradiation days, the total ^{99}Mo activity obtained was 832 Ci, and after 7 irradiation days the total ^{99}Mo activity obtained was 958 Ci. Considering that the time needed for the chemical processing and recovering of the ^{99}Mo will be five days after the irradiation, the total ^{99}Mo activity available for distribution will be 176 Ci for 3 irradiation days, 236 Ci for 5 irradiation days, and 272 Ci for 7 irradiation days of the targets [6].

4. Thermal-Hydraulics calculation for the irradiation device

A thermal-hydraulics model MTCR-IEA-R1 [7] was developed in 2000 at IPEN-CNEN/SP using a commercial program Engineering Equation Solver (EES). The use of this computer model enables the steady-state thermal and hydraulics core analyses of research reactors with MTR fuel elements. The following parameters are calculated along the fuel element channels: fuel meat central temperature (T_c), cladding temperature (T_r), coolant temperature (T_f), Onset of Nucleate Boiling (ONB) temperature (T_{onb}), critical heat flux (Departure of Nucleate Boiling-DNB), flow instability and thermal-hydraulics safety margins FIR and MDNBR. The thermal-hydraulics safety margins MDNBR and FIR are calculated as the ratio between, respectively, the critical heat flux and the heat flux for flow instability and the local heat flux in the fuel plate. Furthermore, the MTCR-IEA-R1 model also utilizes in its calculation the involved uncertainties in the thermal-hydraulics calculation such as: fuel fabrication uncertainties, errors in the power density distribution calculation, in the coolant flow distribution in the core, in reactor power control deviation, in the coolant flow rate measures, and in the safety margins for the heat transfer coefficients. The calculated thermal-hydraulics core parameters are compared with the design limits established for MTR fuels: a) cladding temperature < 95°C; 2) safety margin for ONB > 1.3, or the ONB temperature (T_{onb}) higher than coolant temperature; 3) safety margin for flow instability > 2.0; and 4) safety margin for critical heat flux > 2.0.

For the targets, it was considered the following design limits: 1) no material may experience a temperature greater than ½ any target material melting temperature. The lowest melting temperature for any of the proposed target materials is that of the aluminum cladding, whose melting temperature is 660°C. Therefore 330°C is the maximum allowable temperature for the LEU target; 2) the reactor core coolant temperature must be kept below its saturation temperature. In this work it was adopted as target design limit the cladding temperature that initiated the coolant nucleate boiling (T_{ONB}) for a given coolant pressure and superficial heat flux given by Bergles and Rosenow correlation [8].

The placement of the MID in the core central position of IEA-R1 reactor will deviate part of the reactor flow rate to cool the UAlx-Al targets. The flow rate in the core of the IEA-R1 reactor is 3,400 gpm which provides a flow rate of approximately 23 m^3/h per fuel element, and sufficient to cool a standard fuel element. The insertion of the MID in the IEA-R1 reactor core will divert part of the reactor core coolant to cool the UAlx-Al miniplates. Thus, a MID thermo-hydraulic analysis was developed to determine the required flow rate to cool the miniplates, but without damaging the fuel elements in the reactor core. Flow rates from 1 to 20 m^3/hr were tested through the MID. Table 1 provide the calculated UAlx-Al target temperatures for different flow rates through the MID in the IEA-R1 reactor core. The simulations considered the MID with ten identical UAlx-Al miniplates. Table 1 show that flow rates higher than 10 m^3/h through the MID are sufficient to cool the targets without achieving ONB temperatures. The calculated cladding temperatures are below the value of 123.1°C, indicating one-phase flow through the targets. A coolant flow restrictor was fabricated in order to maintain a MID flow rate of 12 m^3/hr in the reactor core during target irradiation (see Figure 1).

Tab 1: Target temperatures versus DIM flow rates and coolant velocities.

Flow rate (m^3/h)	Coolant velocity (m/s)	UAlx-Al meat central temperature (°C)	UALx-Al aluminum cladding temperature (°C)	ONB Temperature (T_{ONB}) (°C)	Coolant Temperature (°C)
1	0.18	478.4	470.4	123.1	92.3
2	0.36	301.6	293.6	123.1	67.0

3	0.53	239	231	123.1	58.6
4	0.71	203.2	195.2	123.1	54.5
5	0.89	179.8	171.8	123.1	52.0
6	1.07	163.1	155.1	123.1	50.3
7	1.24	150.5	142.5	123.1	49.1
8	1.42	140.7	132.7	123.1	48.2
9	1.60	132.8	124.8	123.1	47.6
10	1.78	126.3	118.3	123.1	47.0
11	1.95	120.8	112.8	123.1	46.6
12	2.13	116.2	108.2	123.1	46.2
13	2.31	112.1	104.1	123.1	45.9
14	2.49	108.6	100.6	123.1	45.6
15	2.66	105.5	97.5	123.1	45.3
16	2.84	102.8	94.8	123.1	45.1
17	3.02	100.3	92.3	123.1	45.0
18	3.20	98.1	90.1	123.1	44.8
19	3.37	96.1	88.1	123.1	44.6
20	3.55	94.2	86.2	123.1	44.5

5. Conclusion

From the neutronic calculations presented for ten targets of UAlx-Al dispersion fuel with low enriched uranium (LEU) and density of 2.889 gU/cm^3, ^{99}Mo activities of 620 Ci, 832 Ci and 958 Ci were obtained, respectively for three (3), five(5) and seven (7) irradiation days in IEA-R1 reactor core at a reactor power of 5 MW. Initially, ^{99m}TC generators will be distributed five (5) days after the end of the irradiation. Consequently, the total ^{99}Mo activity is expected to reach, respectively, values of 176 Ci, 236 Ci and 272 Ci for UAl_x-Al targets irradiated during three (3), five (5) and seven (7) irradiation days in the core central position of the IEA-R1 reactor. From these values, it is noted that the Brazilian current demand of 450 Ci of ^{99}Mo per week and the future projected demand of 1,000 Ci will not be achieved with the proposed UALx-Al targets in the core central position of IEA-R1 reactor.

Acknowledgments

The authors are grateful for financial support from the CAPES, CNEN and FAPESP.

6. References

[1] G. F. Wienciek, A. B. Vandegrift, A. A. Levya, and A. S. Hebden, “Status and Progress of Foil and Target Fabrication Activities for the Production of ^{99}Mo from LEU”, *RERTR 2008 – 30th International Meeting on Reduced Enrichment for Research and Test*, Washington, October 5-9, 2008.

[2] I. N. Goldman, N. Ramamoorthy, and P. Adelfang, “Progress and Status of the IAEA Coordinated Research Project: Production of Mo-99 using LEU Fission or Neutronic Activation”, *RERTR 2007,* September 23-27, 2007, Prague, Czech Republic.

[3] J. Barhein, W. Rhotenstein, and E. Taviv, “The HAMMER Code System TECHNION”, *Israel Institute of Technology*, Haifa, Israel, NP-565, 1978.

[4] T. B. Fowler, D. R. Vondy, and G. W. Cunninghan, “Nuclear Reactor Core Analysis Code: CITATION*”*, *Oak Ridge National Laboratory,* ORNL-TM-2496, Rev. 2, Suppl. 3, July 1972.

[5] SCALE: A Modular Code System for Performing Standardized Computer Analyses for Licensing Evaluation, *ORNL/TM-2005/39*, Version 6.1, Vols. I–III, November 2006. The code is available from Radiation Safety Information Computational Center at Oak Ridge National Laboratory as CCC-732.

[6] P. J. B. O. Nishiyama, "Análises Neutrônica e Termo-hidráulica de um Dispositivo para Irradiação de Alvos Tipo LEU de UAlx-Al para Produção de ^{99}Mo no Reator IEA-R1*"*. *2012. Dissertação (Mestrado)* – Instituto de Pesquisas Energéticas e Nucleares, São Paulo.

[7] P. E. Umbehaun, "Metodologia para Análise Termo-hidráulica de Reatores de Pesquisa Tipo Piscina com Combustível Tipo Placa*"*. *2000. Dissertação (Mestrado)* – Instituto de Pesquisas Energéticas e Nucleares, São Paulo.

[8] A. E. BERGLES, W. M. ROSENOW, “The Determination of Forced-convection Surface Boiling Heat Transfers. *Trans. of the ASME 86 (Series C-J. of Heat Transfer),* 365-375, Aug. 1964.

LOW ENRICHED URANIUM FOIL TARGETS WITH DIFFERENT GEOMETRIES FOR THE PRODUCTION OF MOLYBDENUM-99

D. B. DOMINGOS, A. T. SILVA, T. G. JOÃO
Instituto de Pesquisas Energéticas e Nucleares - Comissão Nacional de Energia Nuclear (IPEN/CNEN-SP)
Av. Professor Lineu Prestes 2242, Cidade Universitária, 05508-000 São Paulo, SP - Brazil

ABSTRACT

A new research reactor is being planned in Brazil to take care of the demand of radiopharmaceuticals in the country and conduct research in various areas. This new reactor, the Brazilian Multipurpose Reactor (RMB), planned for 30 MW, is now in the detailed design phase. Two low enriched (<20% ^{235}U) metallic uranium foil targets (cylinder and plate geometries) are being considered for production of Molybdenum-99 (^{99}Mo) by fission. Neutronic and thermal-hydraulics calculations were performed to compare the production of ^{99}Mo for these targets in a reactor conception with the same power of the RMB and to determine the temperatures achieved in the targets. For the neutronic calculations were utilized the computer codes HAMMER-TECHNION, CITATION and SCALE and for the thermal-hydraulics calculations were utilized the computer codes MTRCR-IEA-R1 and ANSYS CFX.

1. Introduction

^{99m}TC, decay product of ^{99}Mo, is one of the most utilized radioisotopes in nuclear medicine in the world. Annually it is used in approximately 20 to 25 million procedures of medical diagnosis, representing about 80% of all the nuclear medicine procedures [1]. Since 2004, given the worldwide interest in ^{99}Mo production, the International Atomic Energy Agency (IAEA) has developed and implemented a Coordinated Research Project (CRP) [2] to help interested countries start a small-scale domestic ^{99}Mo production in order to meet the requirements of the local nuclear medicine. The purpose of CRP is to provide interested countries with access to non-proprietary technologies and methods for production of ^{99}Mo using targets of thin foils of metallic low enriched uranium (LEU), UAl_x-Al miniplates of LEU type or by neutron activation reaction (n, gamma), for example, using gel generators. Brazil, through IPEN/CNEN-SP, began its CRP participation in late 2009. IPEN/CNEN-SP provides radiopharmaceuticals to more than 300 hospitals and clinics in the country, reaching more than 3.5 million medical procedures per year. The use of radiopharmaceuticals in the country over the last decade has grown at a rate of 10% per year and IPEN/CNEN-SP is primarily responsible for this distribution. ^{99m}Tc generators are the most used ones and are responsible for more than 80% of the radiopharmaceuticals applications in Brazil. IPEN/CNEN-SP imports all the ^{99}Mo used in the country (450 Ci of ^{99}Mo per week or 24,000 Ci per year approximately). In the past, IPEN/CNEN-SP developed the ^{99}Mo production route from neutron activation of ^{98}Mo targets in the IEA-R1. However, the quantity produced does not meet the Brazilian needs of this isotope. Due to the growing need for nuclear medicine in the country and because of the short ^{99}Mo supply observed since 2008 on the world stage, IPEN/CNEN-SP has decided to develop its own project to produce ^{99}Mo through ^{235}U fission. This project has three main goals: 1) the research and development of ^{99}Mo production from fission of LEU targets, 2) the discussion and decision on the best production route technique, and 3) the feasibility study of IPEN/CNEN-SP in reaching a routine production of ^{99}Mo. The main goal of IPEN/CNEN-SP is to accommodate the Brazilian demand for radiopharmaceuticals. Nowadays, this demand is about 450 Ci of ^{99}Mo per week and the future need, after six years, is estimated at around 1,000 Ci per week. One of the analyses planned in this project is to study the characteristics and specifications of metallic uranium thin foils targets. The first aim of the present work is to perform neutronic calculations to

evaluate the ^{99m}Mo production through fission in a reactor conception (RC) with the same power of the RMB [3], which is in the detailed design phase. The second aim of this work is to perform thermal-hydraulics calculations to determine the maximal temperatures achieved in the targets during irradiation and compared them with the design temperature limits established for U-Ni targets.

2. U-Ni targets used in the neutronic and thermal-hydraulic analysis

The targets of metallic uranium foils with cylinder geometry analyzed at IPEN/CNEN-SP were based on targets that were examined in the Tajoura reactor in Libya to produce ^{99}Mo [4]. The targets were mounted in cylindrical geometry, in a tubular arrangement. The metallic U foil was covered with a Ni sheet before being placed concentrically inside the aluminum tubes. The dimensions of the target are (see Fig 1):

1. One foil of uranium (LEU) of 46.05 cm x 87.7 mm x 135 μm;
2. Coating nickel foil of 20 μm thickness;
3. Two aluminum cylinder having 46.05 cm length, outside diameters of 27.88 and 30.00 mm, and inside diameters of 26.44 and 28.22 mm, respectively;
4. ^{235}U mass of 20.1 g, with 19.9% enrichment of ^{235}U.

The targets of metallic Uranium foils with plate geometry were based on targets that were examined in the Paskitan research reactor [5] and consists of a uranium foil (19.99% ^{235}U) with a thickness of 135 μm enveloped in 20 μm thick nickel foil and placed between two aluminum plates that are welded from all sides. The geometry of the foil plate target is shown in Figures 2 and 3.

For the performed calculations, the U-Ni targets with cylindrical and plate geometries were modeled in the same irradiation device (ID), whose external dimensions are 76.2 mm x 76.2 mm x 88.74 cm (Fig 4).

For both targets a ^{235}U mass equals to 20.1 g was considered in the neutronic calculations. As seen from Fig 3, ten U-Ni targets with plate geometry were placed in the box with indented bars inside of the ID. Each U-Ni target with plate geometry has a ^{235}U mass equals to 2.01 g. The set of concentric cylinders of the metallic uranium foils with cylinder geometry was positioned in the same ID.

The targets were modeled and simulated in a peripheral core position of the RC, in the heavy water reflector. The target irradiation time was seven (7) days.

3. Neutronic calculations for the irradiation device

The RC core as well as the U-Ni LEU targets (cylinder and plate geometries) used for the ^{99}Mo production were modeled with the HAMMER-TECHNION [6] and CITATION [7] numerical codes. The 1D cross section for each component of the reactor was generated by the computer code HAMMER-TECHNION. The computer code CITATION was used for the three-dimensional core and radial and axial density curves calculations. These data were used as input data for the thermal-hydraulics irradiation device analysis. The power distribution for any position r of the reactor core matrix plate was obtained. The SCALE 6.0 code system [8] was used to perform burnup calculations for each target and also to calculate the ^{99}Mo activity at the end of irradiation. The target irradiation time for the reactor was defined according to their current and planned operating cycle.

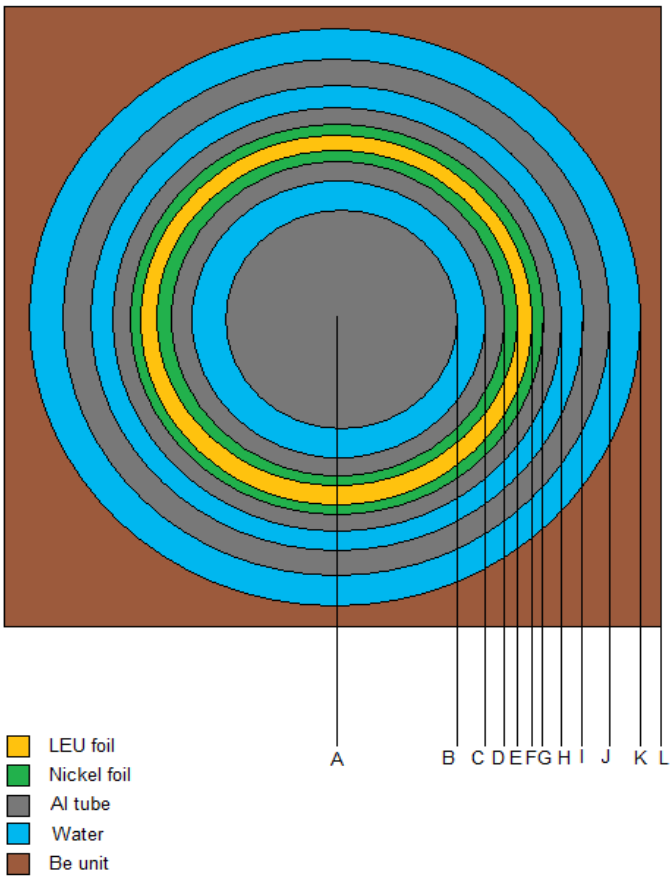

Radius	Length (cm)
AB	1.0000
AC	1.322
AD	1.3940
AE	1.3960
AF	1.4095
AG	1.4110
AH	1.5000
AI	1.7500
AJ	1.9000
AK	2.2000
AL	3.8100

Fig 1: Irradiation device horizontal cross section for the U-Ni target with cylinder geometry.

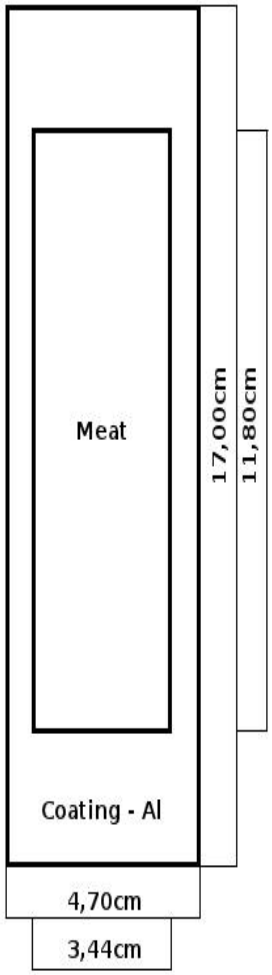

Fig 2: Width and height of the U-Ni plates.

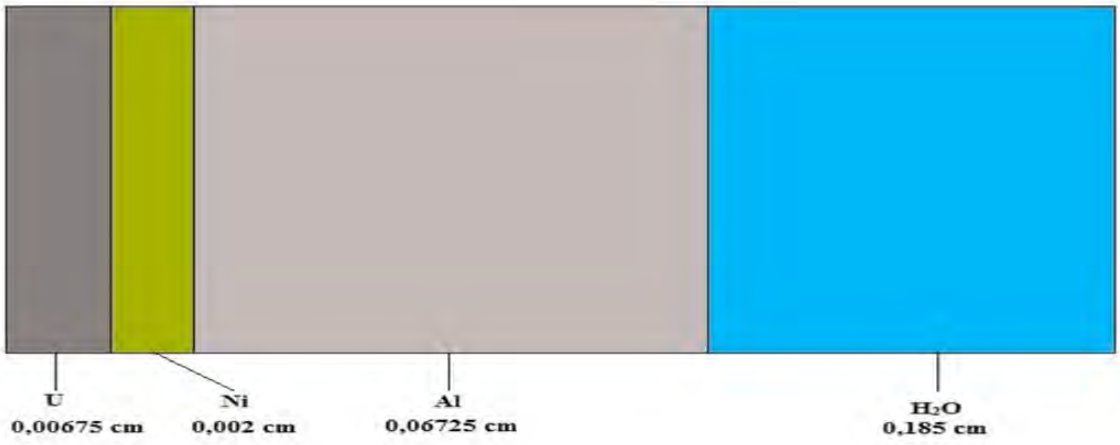

Fig 3: Half the thickness of U-Ni LEU target with plate geometry (67.5 μm), nickel foil, aluminum plate and cooling channel.

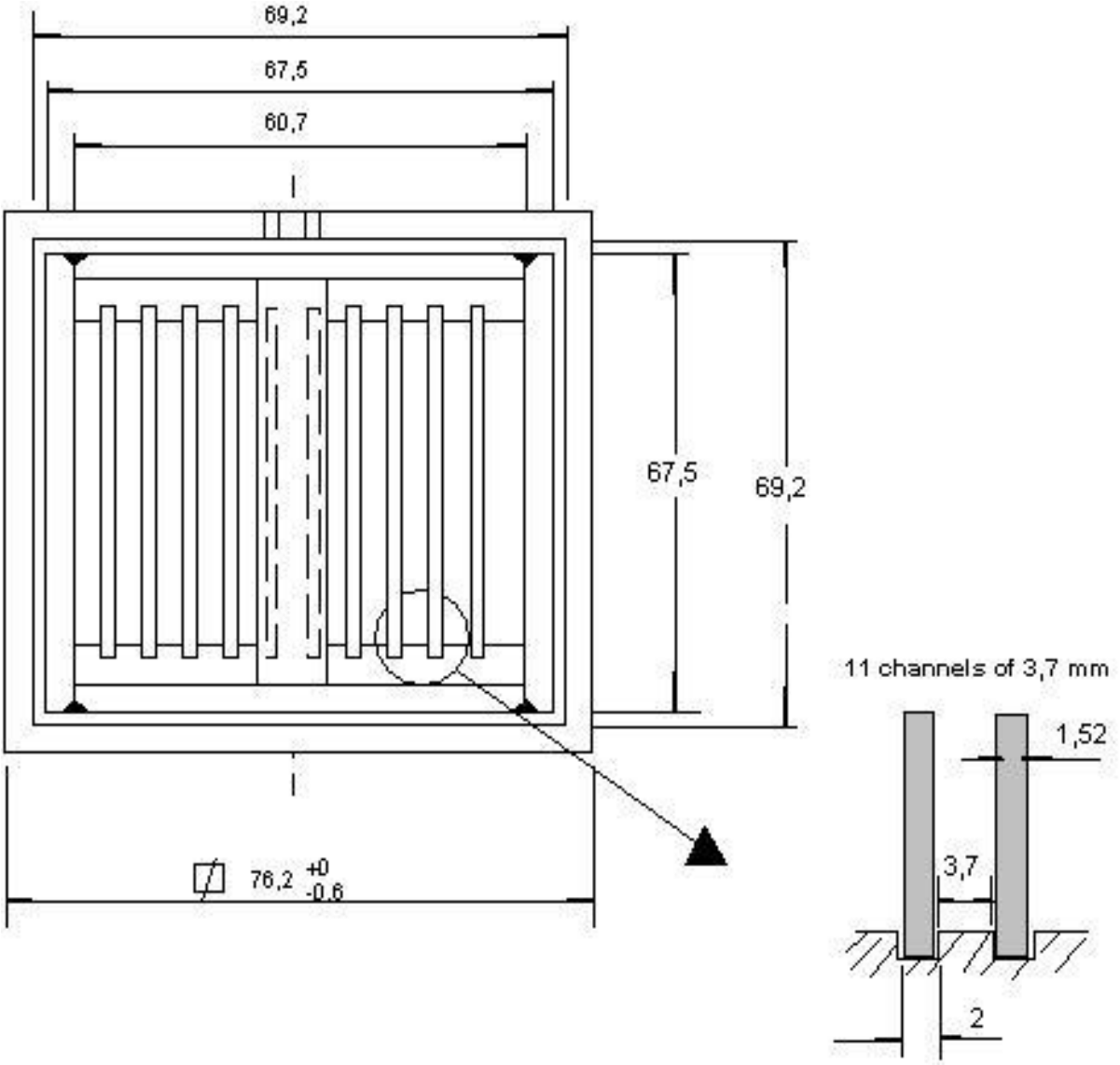

Fig 4: Irradiation device horizontal cross section for the U-Ni targets with plate geometry.

According to its conceptual design, RC is an open pool type, 30 MW thermal power reactor. The core has a 5x6 configuration with MTR-type U_3Si_2-Al fuel elements with 19.75 wt% ^{235}U enrichment. The reactor core, containing 30 U_3Si_2-Al fuel elements with a uranium density of 1.9 gU/cm^3, is light water cooled and moderated, using heavy water as reflector. The U-Ni LEU targets were modeled and simulated in a peripheral core position in the heavy water reflector. At the end of 7 days of irradiation, the total activities obtained for the U-Ni plate and cylinder geometries were, respectively, 3,495.23 Ci and 3,166.6 Ci. Considering that the time needed for the chemical processing and recovering of the ^{99}Mo will be seven days after the irradiation, the total activity obtained for the U-Ni plate and cylinder geometries were, respectively, 597.5 Ci and 541.36 Ci.

4. Thermal-Hydraulics calculation

A thermal-hydraulics model MTCR-IEA-R1 [9] was developed in 2000 at IPEN/CNEN-SP using a commercial program Engineering Equation Solver (EES). The use of this computer model enables the steady-state thermal and hydraulics core analyses of research reactors with MTR fuel elements. The following parameters are calculated along the fuel element

channels: fuel meat central temperature (T_c), cladding temperature (T_r), coolant temperature (T_f), Onset of Nucleate Boiling (ONB) temperature (T_{onb}), critical heat flux (Departure of Nucleate Boiling-DNB), flow instability and thermal-hydraulics safety margins MDNBR and FIR. The thermal-hydraulics safety margins MDNBR and FIR are calculated as the ratio between, respectively, the critical heat flux and the heat flux for flow instability and the local heat flux in the fuel plate. Furthermore, the MTCR-IEA-R1 model also utilizes in its calculation the involved uncertainties in the thermal-hydraulics calculation such as: fuel fabrication uncertainties, errors in the power density distribution calculation, in the coolant flow distribution in the core, reactor power control deviation, in the coolant flow measures, and in the safety margins for the heat transfer coefficients. The calculated thermal-hydraulics core parameters are compared with the design limits established for MTR fuels: a) cladding temperature < 95°C; 2) safety margin for ONB > 1.3, or the ONB temperature higher than coolant temperature; 3) safety margin for flow instability > 2.0; and 4) safety margin for critical heat flux > 2.0.

Thermal-hydraulics calculations were developed to determine the maximal temperatures achieved in the U-Ni targets during irradiation and to compare the temperature results with the design temperature limits established for the U-Ni targets. For the targets, it was considered the following design limits: 1) no material may experience a temperature greater than ½ any target material melting temperature. The lowest melting temperature for any of the proposed target materials is that of the aluminum cladding, whose melting temperature is 660°C. Therefore 330°C is the maximum allowable temperature for the LEU target; 2) the pool coolant must be kept below its saturation temperature. In this work it was adopted as target design limit the cladding temperature that initiated the coolant nucleate boiling (T_{ONB}) for a given coolant pressure and superficial heat flux given by Bergles and Rosenow correlation [10].

In order to evaluate the temperatures achieved in the U-Ni targets different coolant velocities were tested through the irradiation device (ID). For the temperature calculations of the U-Ni targets with plate geometry the thermal-hydraulics model MTCR-IEA-R1 was used and the results were obtained simultaneously with the RC core analysis. For the calculation of the temperatures of the U-Ni targets with cylindrical geometry was utilized the software ANSYS CFX [11]. The power density (25 KW/cm³) calculated in the ID position in the RC reflector was utilized as input date to determine the temperatures in the U-Ni target with cylindrical geometry.

Tables 1 and 2 provide the calculated U-Ni target temperatures for different coolant velocities through the ID in the RC peripheral position respectively for plate and cylindrical geometries.

Tab 1: Calculated temperatures for the U-Ni target with plate geometry versus different coolant velocities through the ID.

Coolant velocity (m/s)	Aluminum cladding temperature (°C)	T_{onb} (°C)
5	191.4	137
6	171.1	137
7	156.1	137
8	144.5	137
9	135.2	137
10	127.7	137
11	121.4	137
12	118.6	137
13	113.6	137
14	109.3	137
15	105.6	137

Tab 2: Aluminum tube temperatures for the U-Ni target with cylindrical geometry versus different coolant velocities through the ID.

Coolant Velocity (m/s)	Aluminum cladding temperature (°C)	T_{onb} (°C)
5	166	132
6	149	132
7	137	132
8	127	132
9	119	132
10	113	132
11	107	132
12	103	132
13	99	132
14	95	132
15	92	132

Table 1 provides the calculated target temperature results for different coolant velocities through the ID placed in the peripheral core position in the heavy water reflector. A velocity of 9 m/s is necessary to cool the targets. For this velocity no design limit was achieved for the analyzed irradiation device. The calculated aluminum cladding temperatures are below the value of 137°C, indicating one-phase flow through the U-Ni targets with plate geometry.

Table 2 provides the calculated U-Ni aluminum tube temperatures for different coolant velocities through the ID placed in the peripheral core position in the heavy water reflector. A velocity of 8 m/s is necessary to cool the target. For this velocity no design limit was achieved for the analyzed irradiation device. The calculated aluminum tube temperatures are below the value of 132°C, indicating one-phase flow through the U-Ni target with cylinder geometry.

5. Conclusion

From the neutronic calculations presented here, for the uranium amount of 20.1 g in the analyzed U-Ni targets with plate and cylindrical geometries, a ^{99}Mo activity of, respectively, 3,495.23 Ci and 3,166.6 Ci was obtained at the end of 7 days irradiation time. Initially, ^{99m}TC generators will be distributed seven (7) days after the end of the irradiation. Consequently, the total ^{99}Mo activity is expected to reach values of 597.5 Ci and 541.36, respectively, for U-Ni targets with plate and cylinder geometries. From these values, it is noted that the Brazilian current demand of 450 Ci of ^{99}Mo per week may be addressed for the RC conception addressed in this paper.

Acknowledgments

The authors are grateful for financial support from CAPES and FAPESP.

6. References

[1] G. F. Wienciek, A. B. Vandegrift, A. A. Levya, and A. S. Hebden, “Status and Progress of Foil and Target Fabrication Activities for the Production of ^{99}Mo from LEU”, *RERTR 2008* –

30th International Meeting on Reduced Enrichment for Research and Test, Washington, October 5-9, 2008.

[2] I. N. Goldman, N. Ramamoorthy, and P. Adelfang, “Progress and Status of the IAEA Coordinated Research Project: Production of Mo-99 using LEU Fission or Neutronic Activation”, *RERTR 2007*, September 23-27, 2007, Prague, Czech Republic.

[3] J. A. Perrotta, A. J. Soares, "RMB: The New Brazilian Multipropose Research Reactor", *International Journal for Nuclear Power*, atw vol. 60 (2015), Issue 1, January.

[4] F. M. Bsebsu, F. Abotweirat and S. Elwaer, “Feasibility Study Part-I Thermal Hydraulic Analysis of LEU Target for ^{99}Mo Production in Tajoura Reactor, *RERTR 2007, September 23-27, 2007, Prague, Czech Republic*.

[5] A. Mushtaq, Massod Iqbal, Ishtiaq Hussain Bokhari and Tayyab Mahmood, “Low Enriched Uranium Foil Plate Target for the Production of Fission Molybdenum-99 in Pakistan Research Reactor-I, *Nuclear Instruments and Methods in Physics Research B* 267 (2009) 1109-1114.

[6] J. Barhein, W. Rhotenstein, and E. Taviv, “The HAMMER Code System TECHNION”, *Israel Institute of Technology, Haifa, Israel, NP-565,* 1978.

[7] T. B. Fowler, D. R. Vondy, and G. W. Cunninghan, “Nuclear Reactor Core Analysis Code: CITATION*”, Oak Ridge National Laboratory, ORNL-TM-2496, Rev. 2, Suppl. 3*, July 1972.

[8] SCALE: A Modular Code System for Performing Standardized Computer Analyses for Licensing Evaluation, *ORNL/TM-2005/39*, *Version 6.1, Vols. I–III*, November 2006. It is available as CCC-732 from Radiation Safety Information Computational Center at Oak Ridge National Laboratory.

[9] P. E. Umbehaun, "Metodologia para Análise Termo-hidráulica de Reatores de Pesquisa Tipo Piscina com Combustível Tipo Placa*". 2000. Dissertação (Mestrado)* – Instituto de Pesquisas Energéticas e Nucleares, São Paulo.

[10] A. E. BERGLES, W. M. ROSENOW, “The Determination of Forced-Convection Surface Boiling Heat Transfers. *Trans, of the ASME 86 (Series C-J. of Heat Transfer), 365-375, Aug.* 1964.

[11] ANSYS CFX Reference Guide, release 12.0, April 2009.

HORUS3D/N NEUTRONICS CALCULATION TOOL DEDICATED TO JHR DESIGN AND SAFETY STUDIES - DEVELOPMENT, VALIDATION, BIASES AND UNCERTAINTIES QUANTIFICATION

C. VAGLIO-GAUDARD, F. JEURY*, C. D'ALETTO, J.F. VIDAL,
J.M. VIDAL, L. GAUBERT, J. POLITELLO

*CEA[1], DEN[2], Cadarache research center, Reactor Studies Department,
13108 Saint-Paul-Lez-Durance, France*

*Corresponding author: florence.jeury@cea.fr

ABSTRACT

The international Jules Horowitz Material Testing Reactor (JHR) is under construction at CEA Cadarache research center, in southern France. Its first criticality is foreseen by the end of the decade.

In order to perform JHR design and safety studies, a specific neutronics calculation tool, HORUS3D/N, based on deterministic codes and the European nuclear data library JEFF3.1.1, was developed. The purpose of this neutronics calculation tool is to predict JHR neutronics parameters: reactivity, power distribution, control rod reactivity worth,...

The calculation scheme relies on a two-level approach, with in the first level, a 2D flux calculation on restricted geometries with a fine energy meshing, and a cross section collapsing into a reduced energy meshing with the APOLLO2 lattice code. These collapsed cross sections are introduced into a full 3D core calculation with the CRONOS2 diffusion code in the second level.

The HORUS3D/N development followed the Verification & Validation – Uncertainty Quantification (V&V-UQ) process. This validation step aims at quantifying all the biases and uncertainties associated with HORUS3D/N calculations. These biases and uncertainties originate from both the nuclear data and the deterministic calculation scheme, for JHR calculations at beginning of life or during depletion (in particular for the JHR core at equilibrium).

The biases and uncertainties due to nuclear data are quantified by comparing the Monte Carlo reference TRIPOLI-4® calculations using the JEFF3.1.1 nuclear data library, with experimental data.

The biases and uncertainties due to the HORUS3D/N calculation scheme are assessed by comparing HORUS3D/N deterministic calculations with reference route calculations:

- 2D and 3D continuous-energy Monte Carlo TRIPOLI-4® calculations, for the JHR beginning of life core calculations,
- 2D APOLLO2-MOC deterministic calculations, using the Method Of Characteristics flux solver for the JHR core calculations during depletion.

Both reference routes are described with a heterogeneous geometry. They use the same JEFF3.1.1 nuclear data library as that of HORUS3D/N.

This paper describes the very latest developments implemented in the HORUS3D/N neutronics calculation tool and on the reference route considering depletion. These new developments take into account the APOLLO2.8/REL2005/CEA2005 package recommendations already applied for light water reactor studies. Moreover, the spatial meshing of the HORUS3D/N reference route was refined and optimized.

This paper also provides a synthesis of the biases and uncertainties associated with the different neutronics parameters calculated with this new version of the HORUS3D/N calculation scheme, for JHR safety studies.

[1] CEA: Commissariat à l'Energie Atomique et aux Energies Alternatives.
[2] DEN: Direction de l'Energie Nucléaire.

1 Introduction

The Jules Horowitz Reactor (JHR) [1] is the future Material Testing Reactor under construction in France. It will be a major research infrastructure in Europe designed to support existing power plant operations and lifetime extension, as well as future reactor design. Its objectives are to test the new structural material and fuel behavior under irradiation for the development of the GEN-III and GEN-IV reactors and also to demonstrate the satisfactory stainless steel behavior for current French Pressurized Water Reactor (PWR) lifetime extension. The JHR will also supply 25% to 50% of the European demand for radio-isotopes, mainly ^{99}Mo, for medical applications [2], and n-doped silicon for high power electronics.
The JHR first criticality is planned for the end of the decade.
The design and safety studies have been carried out using the neutronics calculation tool, HORUS3D/N, developed since the 2000s to meet the specific needs of JHR [3].
In this paper, after a brief description of the JHR, the HORUS3D/N calculation package will be presented. It will then focus on the very latest developments implemented in HORUS3D/N. These developments followed the Verification & Validation – Uncertainty Quantification (V&V-UQ) process, which aims at quantifying the biases and uncertainties associated with neutron calculations. At the end, the paper will provide a synthesis of the biases and uncertainties associated with the different neutronics parameters calculated using the new version of HORUS3D/N for JHR safety studies.

2 The Jules Horowitz Reactor

The JHR is a tank-in-pool type reactor using light water as its coolant and moderator. The maximum thermal power is 100 MW.
The core (600 mm. fuel active height) can contain 34 to 37 fuel elements, inserted in an aluminum alloy rack. When one of the 37 cells of the rack is free of a fuel element, an experimental device can be inserted. Up to 20 experimental devices can be loaded in the core or in the reflector and irradiated at the same time.
In order to obtain a high power density and thus reach a high fast neutron flux level (~5×10^{14} n/cm^2/s, E≥0.907 MeV), the fuel elements (see Fig.1) consist of 3 sets of curved plates assembled with aluminum stiffeners. The plates are cladded with Al-Fe-Ni. A hafnium control rod, connected to an aluminum follower (the follower is an aluminum tube replacing the absorber part of the control rod when it is withdrawn), or an experimental device can be loaded in the central hole. A boron insert is positioned 1 cm above the active height in each plate to prevent departure from nucleate boiling at the top of the core water channels.

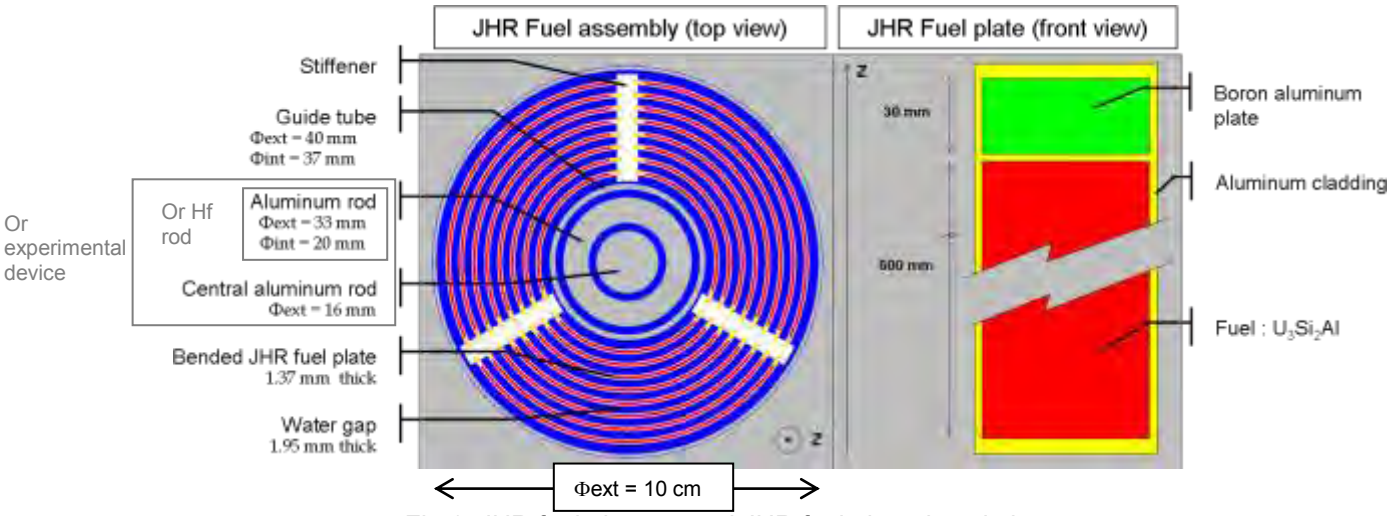

Fig.1: JHR fuel element and JHR fuel plate description

The JHR will start with a standard density low enriched U_3Si_2 fuel (e% ^{235}U = 19.75%, density 4.8 g.cm^{-3}), and with a maximum thermal power of 100MW.
The core will operate with a cold fuel (fuel temperature~100°C) and a slightly pressurized light water (pressure = 8 bars; temperature = 35°C).
The core area is surrounded by a reflector which optimizes the core cycle length and provides intense thermal fluxes in this area (~5×10^{14} n/cm^2/s, E≤0.625 eV). The reflector area is made of beryllium blocks. Experiments can be performed either in the core itself, as seen above, or in reflector static locations (Fig.2) but also on displacement systems as an effective way to investigate transient regimes occurring in incidental or accidental situations.
This provides a flexible experimental capability that can create up to 16 dpa/year - in comparison to the 2-3 dpa/year produced in industrial Light Water Reactors (LWR) - for in-core material experiments (with 275 full power operation days per year) and 600W.cm^{-1} for in reflector simple 1% ^{235}U enriched fuel experiments.

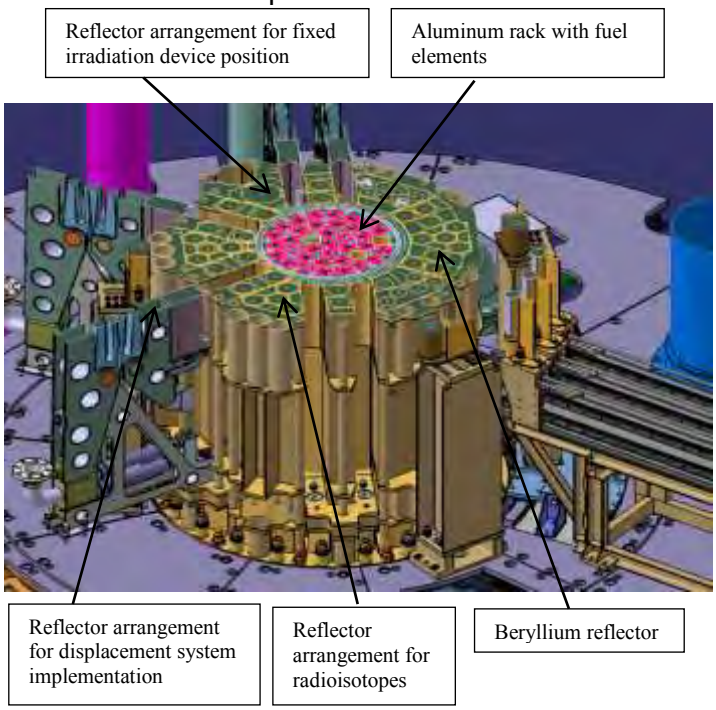

Fig.2: JHR description

3 The HORUS3D/N neutronics calculation package

The JHR innovative design led to the development of a specific neutronics tool, HORUS3D/N. The industrial route of this neutronics calculation tool is based on an APOLLO2 [4]/CRONOS2 [5] deterministic calculation scheme and the JEFF3.1.1 [6] European nuclear data library. It is a two-step calculation route (see Fig.4) with:

- ***for the first calculation step:*** several APOLLO2 two-dimensional (2D) fuel assembly calculations (one per component loaded in the center of the assembly) with fine energy-meshing to obtain self-shielded and depleted cross sections collapsed into 6 energy groups. The 1/6th assembly symmetry is used for the calculation. This first step provides libraries, tabulated versus burnup, for each kind of component present in the JHR,
- ***for the second calculation step:*** a 3D full core diffusion calculation on a hexagonal spatial meshing [3]. Despite the apparently irregular arrangement of the fuel element in the core, the assembly pattern has a hexagonal macro-symmetry (Fig.3). With the iso-parametric finite element method in the CRONOS2 code, each hexagonal mesh cell can be considered as a “Super Finite Element” (SFE). These SFEs need a conform mesh of arbitrary triangles, which form the basic finite elements. The fuel elements are meshed as dodecagons. The reflector region is modelled with a series of particular SFEs, allowing for an accurate modeling of radial and azimuthal heterogeneities.

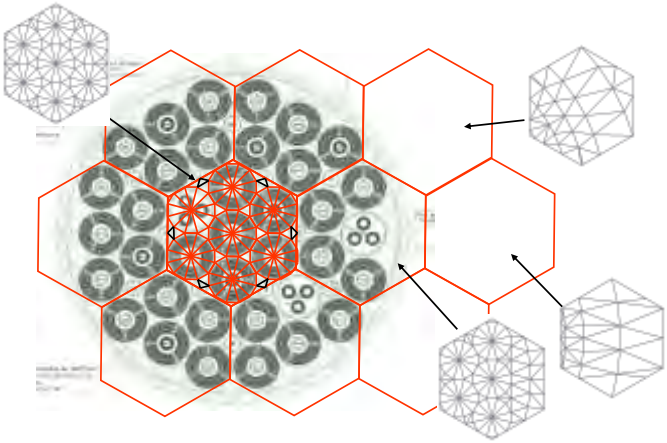

Fig.3: Division of the core by the hexagonal macro-symmetry and attribution of SFEs for the CRONOS calculation

The HORUS3D/N development follows the Verification & Validation – Uncertainty Quantification (V&V-UQ) process [9]. This validation step aims at quantifying all the biases and associated uncertainties of HORUS3D/N calculations. These biases and uncertainties originate from both the nuclear data and the deterministic calculation scheme, for JHR calculations at beginning of life or during depletion (in particular for the JHR core at equilibrium).
The biases and uncertainties due to nuclear data are quantified by comparing Monte Carlo reference TRIPOLI-4® [13] calculations using the JEFF3.1.1 nuclear data library, with experimental data.
The biases and uncertainties due to the HORUS3D/N calculation scheme are assessed by comparing HORUS3D/N deterministic calculations with reference route calculations (Fig.4):

- 2D and 3D continuous-energy Monte Carlo TRIPOLI-4® calculations, for the JHR beginning of life core calculations,
- 2D APOLLO2-MOC deterministic calculations [7], [8], for the JHR depleted core calculations.

Both reference routes are described with a heterogeneous geometry and use transport solver. They use the same JEFF3.1.1 nuclear data library as HORUS3D/N.

The very latest developments concern the APOLLO2 first step of the HORUS3D/N industrial route, and the reference route for depletion (see Fig.4).

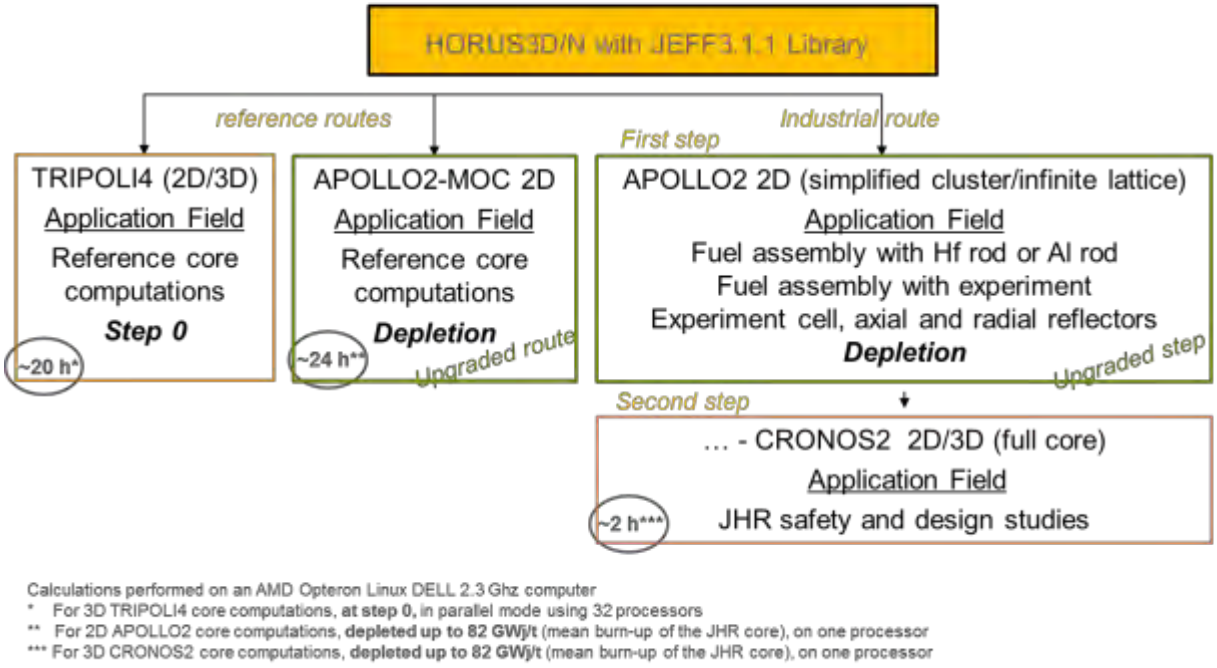

Fig.4: HORUS3D/N package calculation routes and upgraded routes

The following chapter will focus on these very latest developments.

4 HORUS3D/N package developments

Different developments were performed in HORUS3D/N last year: the reflector geometry is now updated in consistency with the JHR design evolution, the material balance with the main impurities is now considered, and, in the industrial route, new features are now available.
The main developments are presented hereafter. They take into account the APOLLO2.8/REL2005/CEA2005 package recommendations developed by CEA for light water reactor studies [10]. Moreover, the spatial meshing of the HORUS3D/N APOLLO2 core reference route was refined and optimized.

4.1 Industrial route developments

4.1.1 Self-shielding and flux computations

As mentioned above, these developments concern the first step of the industrial route, i.e. the APOLLO2 libraries[3] calculations for CRONOS2 (see Fig.4). The 2D calculation scheme for the different clusters (fuel assembly with Al rod, fuel assembly with Hf rod, fuel with experiments - Fig.1, and experiments in cell) and the radial reflector modelling, was improved by taking into account the APOLLO2.8/REL2005/CEA2005 package recommendations. The main developments for the fuel clusters are the following:

- concerning the self-shielding computations:
  - the use of the SHEM-281 group energy mesh on 1 D cylindrical simplified geometry,
  - for the U_3Si_2-Al fuel: the resonant mixture self-shielding treatment for ^{235}U, ^{238}U, ^{239}Pu and ^{240}Pu, is used in the 33-200 eV intermediate range, in order to rigorously account for resonance mutual shielding of these major actinides above 23 eV. Below 23 eV, the 281-group energy mesh (SHEM) is fine enough to avoid resonance self-shielding approximations,
  - for the Hafnium absorber: the resonant mixture self-shielding treatment for ^{177}Hf, ^{179}Hf, ^{176}Hf, ^{178}Hf, ^{180}Hf, is used up to 1keV in order to rigorously account for resonance mutual shielding of these isotopes in this energy range.

[3] Multi-group self-shielded cross sections for different fuel temperatures, moderator densities and fuel burn-ups, collapsed into 6 energy groups in the case of the JHR.

- concerning the flux computations:
  - the spatial meshing of the fuel assembly is performed with 24 angular sectors, i.e. 4 angular sectors on 1/6th of the assembly and 205 calculation regions (see Fig.5), allowing for a better assessment of the azimuthal thermal flux gradient near the stiffeners,
  - the computations are performed using the APOLLO2 Method Of Characteristics (MOC) flux solver with the SHEM-281 group energy mesh (no collapsing), at time-step zero and in depletion,
  - the calculations are based on fine tracking values: Tracking step: ΔR=0.04cm, radial direction number in [0, π]: NΦ=24, polar direction number in [0, $\pi/2$]: NΨ=3 (Bickley quadrature), associated with a P3 anisotropy scattering order,
  - neutron leakage: homogeneous B1 model with research of critical buckling.

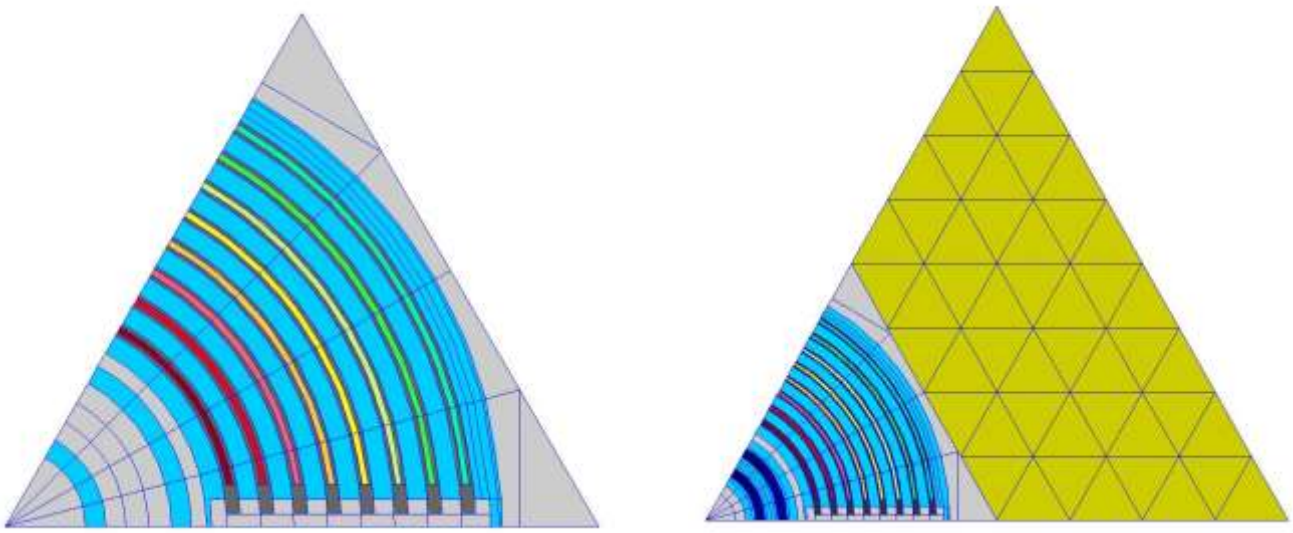

Fig.5: Flux computation geometry with APOLLO2 TDT-MOC flux solver:
1/6th of the fuel assembly with Al rod follower at the center of the assembly (205 calculation regions) (left hand side)
and 1/6th of the fuel assembly with hafnium rod with its homogenized environment in green (right hand side)

Table 1 summarizes the main developments performed on the HORUS3D/N v4.2 industrial route, in comparison with the previous versions (HORUS3D/N v4.1/v4.0). These new developments induced the adaptation of about 70 APOLLO2 procedures developed in the GIBIANE language.

Table 1: industrial route - APOLLO2 computation options - fuel clusters and reflector modellings

		HORUS3D/N v4.2 (new version)	**HORUS3D/N v4.1/v4.0** (previous versions)
APOLLO2	version	APOLLO2.8-4	APOLLO2.8-3
Library	version	JEFF3.1.1 (CEAV5.1.2, processed for APOLLO2)	JEFF3.1.1 (CEA2005V4.1.2, processed for APOLLO2)
Self-shielding	energy mesh	SHEM - 281 groups	XMAS - 172 groups
	method	Livolant-Jeanpierre + resonant mixture	Livolant-Jeanpierre + resonant mixture
	geometry	1D Cylindrical for most of the cases	
Flux calculation	energy mesh (collapsed cross sections)	**No collapsing (281 g)** *Except for:* *- axial reflector: 6 g* *- radial reflector: 22 g (t0 only)**	**6 g (collapsed from Pij 1D calculation)** *Except for:* *- fuel assembly+Hf rod: 172g* *- radial reflector: 20 g (t0 only)*
	geometry	1/6th of the fuel assembly with or without environment, "RZ" assembly for the axial reflector	
	spatial mesh	**24 angular sectors**	**6 angular sectors**
	solver	**MOC (2D)** *Except for:* *- axial reflector: SN*	**Pij (2D)** *Except for:* *- axial reflector: SN*
	Anisotropic scattering	**P3**	**P0-corrected**
	tracking	cyclic	cyclic
	Fine tracking values	- Tracking step: ΔR= 0.04 cm - radial direction number in [0, π] : NΦ = 24 - polar direction number in [0, π/2] : NΨ = 3 - polar quadrature: "Bickley"	- Tracking step: ΔR= 0.05 cm - radial direction number in [0, π] : NΦ = 24 - polar direction number in [0, π/2] : NΨ = 2 - polar quadrature: "Bickley"
	neutron leakage: homogeneous B1 model	critical buckling	geometrical buckling
Results		*self-shielded and depleted cross sections collapsed into 6 energy groups (input data for CRONOS2)*	

(*): obtained from the 2D core computations (see § 4.2), with homogenized fuel assemblies.

The number of flux calculation regions (205 for 1/6th of the assembly), and the order of anisotropic neutron scattering (P3) were optimized, i.e. a validation step (comparison of the computations with Monte Carlo TRIPOLI-4® calculations at step 0) performed on the 2 main fuel clusters (fuel assembly with Al rod, fuel assembly with Hf rod) showed that they correspond to the most computation time accuracy compromise:

- the computation region number of 205 is sufficient; finer meshing doesn't yield significant accuracy gains,
- the P3 scattering is necessary, in particular to evaluate the Hf absorption rate better; the computation time remains acceptable (~40 s with P3 to be compared to ~20 s with P0-corrected order).

4.1.1 Validation of the first step of the HORUS3D/N industrial route

An important validation step was performed on the APOLLO2 assembly scheme with the calculation options presented in Table 1. This validation step was carried out on the 2 main fuel clusters: the fuel assembly with Al rod and the fuel assembly with Hf rod.
It consisted in comparing the APOLLO2 results with the Monte Carlo TRIPOLI-4® computations at step 0 with the same JEFF3.1.1 library.
Different computations were compared: reactivity, fission rate per fuel plate, hafnium rod efficiency. The results are the following:

- the reactivity is overestimated by ~+30 pcm for the fuel assembly with Al rod,
- the hafnium rod efficiency is overestimated by +1.1%,
- the discrepancy of the fission rate per fuel plate is less than 0.4% (see Table 2).

Table 2: Fuel assembly with Hf rod – biases on the fission rate per fuel plate

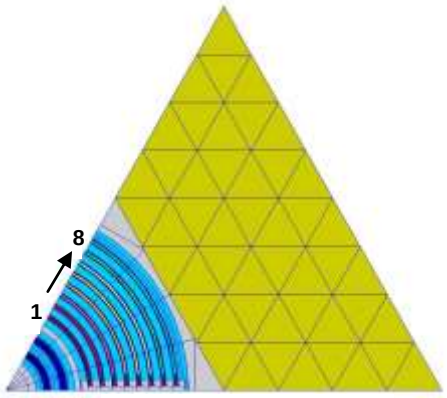

APOLLO2 modelling

Fuel plate	TRIPOLI-4®	std (%) MC unc.	(A2-T4)/T4 (%)	
			P0c	P3
1	0.503	0.008	**-0.6%**	0.1%
2	0.628	0.007	**-0.5%**	-0.1%
3	0.759	0.007	0.0%	0.3%
4	0.896	0.006	0.1%	0.3%
5	1.040	0.006	0.2%	0.2%
6	1.196	0.005	-0.1%	-0.1%
7	1.375	0.005	0.1%	0.1%
8	1.604	0.005	0.1%	-0.4%

These very good results validate the new APOLLO2 assembly scheme.

4.2 Reference route in depletion developments

4.2.1 Self-shielding and flux computations

The developments of the APOLLO2-MOC reference route (see Fig.3), follow, as APOLLO2 in the industrial route (see 4.1) the same APOLLO2.8/REL2005/CEA2005 package recommendations.
Table 3 summarizes the main developments performed on this route.

Table 3: reference route - APOLLO2-MOC computation options – 2D core

		HORUS3D/N v4.2 (new version)	**HORUS3D/N v4.1/v4.0** (previous versions)
APOLLO2	version	APOLLO2.8-4	APOLLO2.8-3
Library	version	JEFF3.1.1 (CEAV5.1.2)	JEFF3.1.1 (CEA2005V4.1.2)
Self-shielding	energy mesh	SHEM - 281 groups	XMAS - 172 groups
	method	Livolant-Jeanpierre + resonant mixture	Livolant-Jeanpierre + resonant mixture
	geometry	1D Cylindrical for most of the cases	
Flux calculation	energy mesh (collapsed cross sections)	**22 g** (collapsed from Pij 1D calculation)	**20 g** (collapsed from Pij 1D calculation)
	geometry	2D core	
	spatial mesh	Assembly: **12 angular sectors** Reflector: **new optimized spatial mesh**	Assembly: **6 angular sectors**
	solver	**MOC**	**MOC**
	Anisotropic scattering	**P3**	**P0 corrected**
	tracking	Non cycling	cyclic
	Fine tracking values	- Tracking step: ΔR= 0.04 cm - radial direction number in [0, π] : NΦ = 24 - polar direction number in [0, π/2] : NΨ = 3 - polar quadrature: "Bickley"	- Tracking step: ΔR= 0.05 cm - radial direction number in [0, π] : NΦ = 24 - polar direction number in [0, π/2] : NΨ = 2 - polar quadrature: "Bickley"

…/…

Table 3: reference route - APOLLO2-MOC computation options – 2D core (continued)

		HORUS3D/N v4.2 (new version)	**HORUS3D/N v4.1/v4.0** (previous versions)
Flux calculation	Leakage	Axial buckling No axial leakage when compared with TRIPOLI4 or CRONOS2	
Results		*Reactivity, power distribution,…* *in depletion*	

The spatial meshing of the reflector (16506 calculation regions), the assembly spatial meshing (12 angular sectors) and the anisotropic scattering order (P3) were optimized, i.e. a validation step (comparison of the computations with Monte Carlo TRIPOLI-4® calculations[4] at step 0) showed that they correspond to the most computation time accuracy compromise:

- the assembly spatial meshing with 12 angular sectors is sufficient to evaluate the azimuthal thermal flux,
- P3 anisotropic scattering enables us to reduce the reactivity discrepancy ($\Delta\rho$= -11 pcm with P3, $\Delta\rho$= -92 pcm with P0-corrected); the computation time remains acceptable (22 min. to be compared to 11 min. with P0-corrected order) (see Table 4).

Table 4: APOLLO2-MOC/TRIPOLI4 discrepancies - loaded core (37 fuel assemblies), no experiments in the core nor in the reflector, no Hafnium control rods, at JHR begin of life

	HORUS3D/N v4.2	
	P0-c	P3
Reactivity		
$\Delta\rho$ (pcm)	-92	-11
Plate power distribution		
mean deviation (%)	+1.1	+1.1
min. deviation (%)	-2.6	-2.9
max. deviation (%)	+2.9	+3.0
Computation time (Step 0)	11min.	22min.

The following paragraph focuses on the work performed to optimize the spatial meshing of the reflector, considering the REL2005 recommendation.

4.2.2 Reflector spatial meshing optimization

Before HORUS3D/Nv4.1, for APOLLO2-MOC calculations, the spatial meshing of the core and of the reflector was performed with the pre-processing user interface SILENE. The spatial meshing generation was a time-intensive task (duration of several weeks), with a serious risk of error.

Therefore, the decision was made to introduce a more modern and high performance pre-processing user interface into HORUS3D/N: the SALOME platform [14], in order to:

- generate a spatial meshing in a few minutes, and thus follow the evolution of JHR design easily,
- have the same geometric model between Monte Carlo and deterministic schemes, and thereby limit the risk of error and the computation biases,
- have a greater flexibility and thus refine areas of interest.

Up to now, only the reflector zone has been concerned with these new developments. HORUS3D/Nv4.1 was an intermediate version used to test the feasibility of the SALOME integration.

[4] Monte Carlo TRIPOLI-4® Computations are performed with 4.10^8 particles (corresponding to a standard deviation on k_{eff} of 5 pcm).

In HORUS3D/Nv4.2, thanks to SALOME, the spatial meshing of the reflector was upgraded in order to:

- follow the APOLLO2.8/REL2005/CEA2005 package recommendations (see Fig.6), i.e. refine the radial mesh near the core in order to respect the thermal neutron flux gradient:

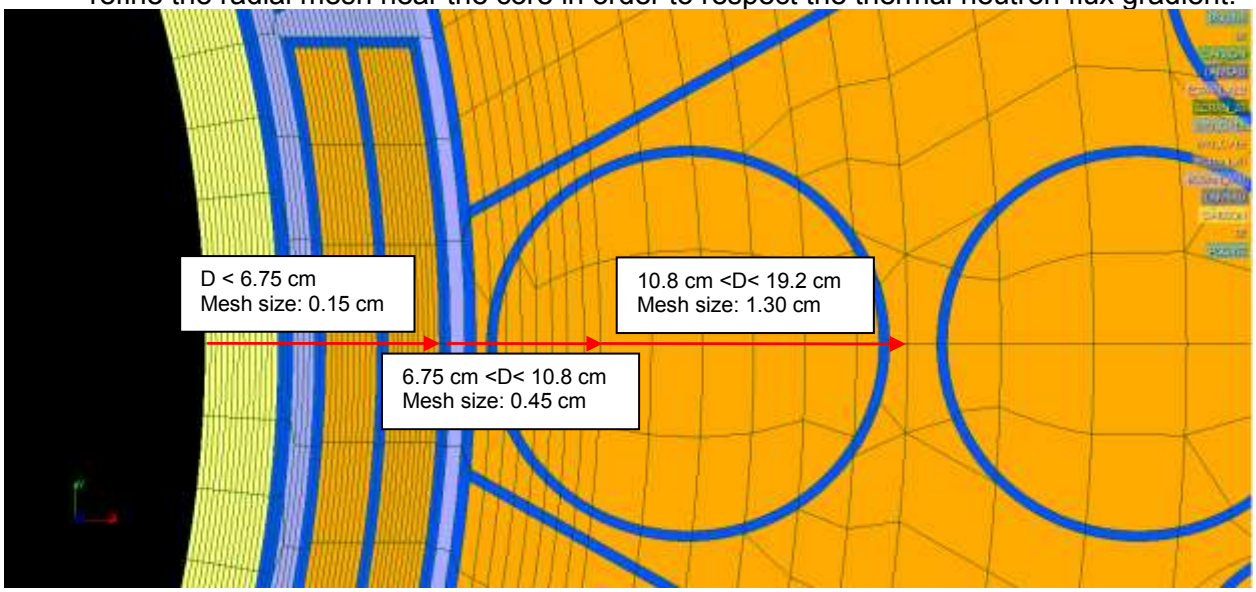

Fig.6: reflector meshing with SALOME in compliance with APOLLO2.8/REL2005/CEA2005 package recommendations

- define a specific meshing for each experiment (see Fig.7) without changing the meshing of the rest of the reflector:

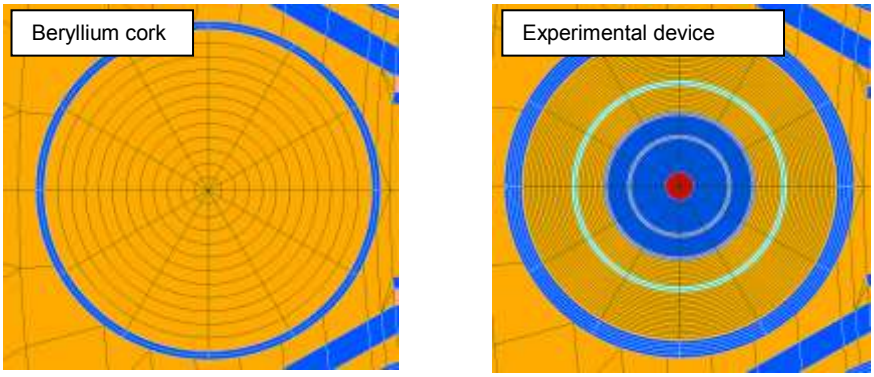

Fig.7: specific meshing with SALOME – Beryllium cork (left hand side) – experimental device (right hand side)

- optimize the mesh number (i.e. define the meshing which corresponds to the most computation time accuracy compromise).

Table 5 presents the mesh number of the two last versions of HORUS3D/N (see Fig.8). One can notice that the mesh number of the reflector is equivalent between the 2 versions. Thus, this new meshing doesn't increase the computation time, but it is optimized (refine meshing in the areas of interest) and generated much more quickly: a few minutes with SALOME, in comparison to 3 to 4 weeks with SILENE.

Table 5: mesh number of HORUS3D/N v4.2 and v4.0 versions - loaded core (37 fuel assemblies), no experiments in the core nor in the reflector

	HORUS3D/N v4.2 (reflector meshing with SALOME)	HORUS3D/N v4.0 (meshing with SILENE)
Core	25686*	16140*
Reflector	16506	13349
Total	42192	29489

(*): HORUS3D/N v4.2: 12 angular sectors for each assembly; HORUS3D/N v4.0: 6 angular sectors for each assembly.

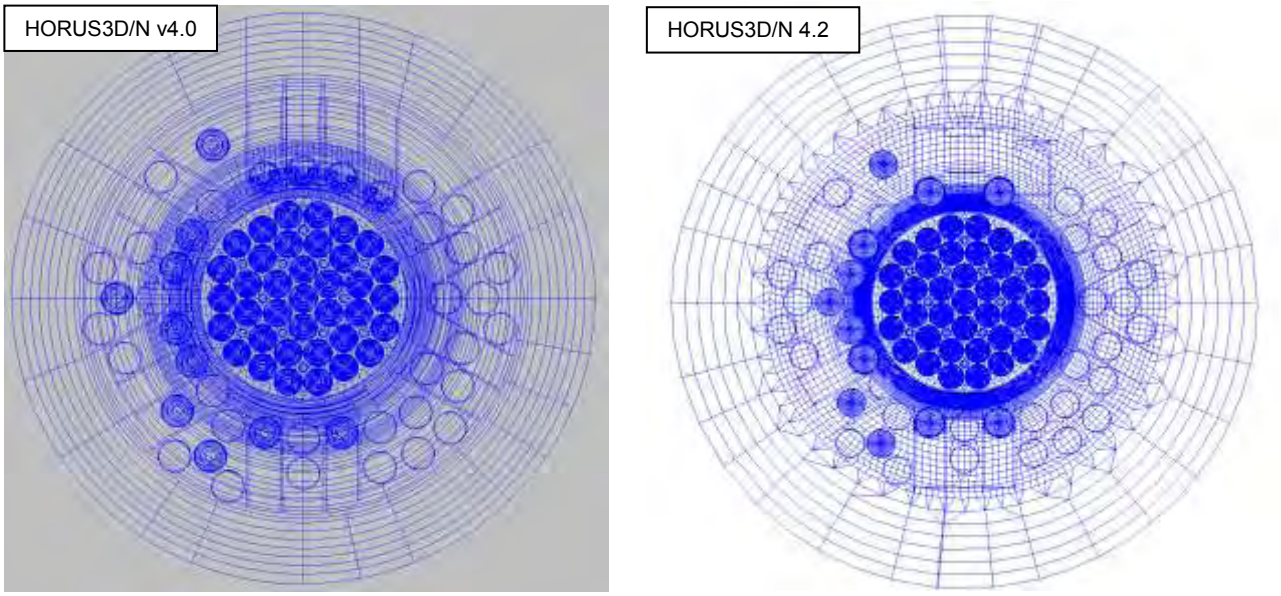

Fig.8: core and reflector meshing for v4.0 and v4.2 HORUS3D/N versions

4.2.3 Validation of the reference route in depletion

An important validation step was performed on the 2D APOLLO2-MOC core scheme of HORUS3D/N v4.2 (with the optimized meshing – see § 4.2.2, and the calculation options as presented in Table 3).
It consisted in comparing the 2D APOLLO2-MOC results versus the 2D Monte Carlo TRIPOLI-4®[5] at step 0 with the same JEFF3.1.1 library.
Different configurations were studied increasing successively the core perturbation:

- 37 Fuel Elements, without experiments, without Hafnium rod ("37FE" configuration),
- 34 Fuel Elements, maximal core experimental loading (7 Fuel elements with experiments +3 cells loaded with experiments), without Hafnium rod ("34FE" configuration),
- 34 Fuel Elements, maximal core experimental loading, with 10 Hafnium rods ("34FE_10Hf" configuration),

the reflector being loaded or not with the 12 experiments.

The results were compared to those of the previous version, the 2D APOLLO2-MOC core scheme of HORUS3D/N v4.0.

Table 6 and Table 7 summarize the discrepancy between the 2 versions when compared to the Monte-Carlo TRIPOLI-4® code, for the plate power distribution and the reactivity, respectively.
Fig.9 gives an example for the plate power distribution computation.

Table 6: Plate power distribution at JHR beginning of life - APOLLO2-MOC v4.2 and v4.0/TRIPOLI-4® discrepancies

		HORUS3D/N v4.2			HORUS3D/N v4.0		
REFLECTOR	CONFIG	mean deviation (%)	max. deviation (%)	min. deviation (%)	mean deviation (%)	max. deviation (%)	min. deviation (%)
Without experiments	*37FE*	**1.1%**	3.0%	-2.9%	**1.9%**	4.2%	-3.5%
	34FE	**1.2%**	2.7%	-4.4%	**1.9%**	4.6%	-6.0%
	34FE_10Hf	**1.5%**	3.3%	-5.4%	**2.2%**	4.8%	-6.6%
With experiments	*37FE*	**1.1%**	3.1%	-2.3%	**2.1%**	4.8%	-3.6%
	34FE	**1.2%**	2.3%	-4.6%	**2.1%**	4.7%	-6.2%
	34FE_10Hf	**1.6%**	3.3%	-5.4%	**2.5%**	5.4%	-6.8%

[5] Monte Carlo TRIPOLI-4® Computations are performed with a total number of 4.10^8 neutron histories (corresponding to a standard deviation on $k_{effectif}$ of 5 pcm).

Table 7: Reactivity at JHR beginning of life - APOLLO2-MOC v4.2 and v4.0/ TRIPOLI-4® discrepancies

		HORUS3D/N v4.2	HORUS3D/N v4.0
REFLECTOR	CONFIG	Δρ (pcm)	Δρ (pcm)
Without experiments	*37FE*	-11	-33
	34FE	61	67
	34FE_10Hf	-209	-72
With experiments	*37FE*	-8	-46
	34FE	66	62
	34FE_10Hf	-207	-85
Computation time (Step 0)		~20 min.	~10 min.

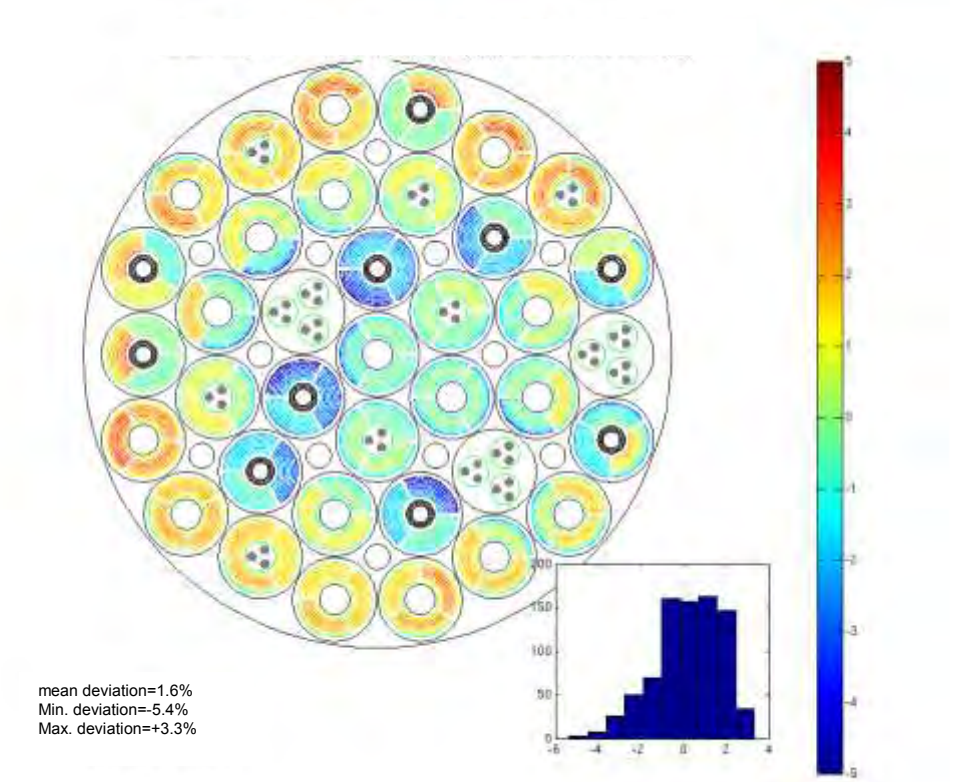

Fig.9: Plate power distribution at JHR beginning of life - APOLLO2-MOC v4.2/ TRIPOLI-4® discrepancies (in %) - 34 Fuel Elements, maximal core experimental load, 10 Hafnium rods ("34FE_10Hf" configuration), maximal reflector experimental load

Regarding the plate power distribution, APOLLO2-MOC v4.2 was improved significantly in comparison to the previous version. The mean deviation is strongly reduced: dropping from 2.5% in the v4.0 version to 1.6% in the v4.2 version in the most disturbed configuration (see Table 6).
Regarding the reactivity, APOLLO2-MOC v4.2 computations, when compared to TRIPOLI-4®, slightly underestimate the reactivity in the less disturbed configurations (-11 pcm) (see Table 7). The 10 Hafnium rods reactivity worth is overestimated by 4%.
The computation time remains acceptable (20 min. at step 0, in comparison to 10 min. for the previous version) (see Table 7).
These very good results validate the 2D APOLLO2-MOC reference core scheme of HORUS3D/N v4.2.

The development of the HORUS3D/N industrial route (see Fig.4) followed the Verification & Validation – Uncertainty Quantification (V&V-UQ) process. First, it was submitted to a Verification step including non-regression tests, and then to a Validation process in order to Quantify the biases and Uncertainties to be applied to each parameter computed with the calculation route.
The following chapter briefly presents this validation process and focuses on the main results of this step: the biases and uncertainties quantification.

5 HORUS3D/N industrial route global validation

The HORUS3D/N simulations are used to predict neutronics parameters with quantifiable confidence and across the JHR application domain. The V&V-UQ process aims at determining to what degree a calculation tool is an accurate representation of the "real world", i.e. it aims at quantifying the biases and uncertainties associated with the HORUS3D/N computations. These biases and uncertainties have two origins:

- the nuclear data which are physical parameters input and which describe all the interactions between neutrons with matter,
- the models, and more generally, all the approximations used in the APOLLO2/CRONOS2 calculation scheme (approximation of the real geometry, energy cutting, resonance self-shielding, depletion, flux solver, etc.).

5.1 Nuclear data validation

The biases and uncertainties due to nuclear data are quantified by the comparison between Monte Carlo reference TRIPOLI-4® calculations and an integral experiment.
In order to provide JHR representative measurement data the AMMON program was launched between late 2010 and early 2013 in the EOLE zero-power critical mock-up (see [9] for details). The AMMON experiment consists of an experimental zone dedicated to the analysis of the JHR neutron and photon physics surrounded by a driver zone. The experimental zone, for the reference configuration, contains 7 JHR fresh fuel standard assemblies-like (see § 2) inserted in an aluminum alloy hexagonal rack (30 cm side length). The driver zone for the reference configuration consists of 622 standard Pressurized Water Reactor (PWR) fuel pins (3.7% ^{235}U enriched UO_2), with Zircaloy-4 cladding and stainless steel overcladding. The hexagonal lattice pitch of the driver pins was optimized in order to reproduce, as well as possible, the same neutron spectrum as the one of the experimental zone. 5 configurations were studied (see Fig.10):

- a reference configuration with 7 JHR fresh fuel assemblies,
- a configuration with a hafnium control rod totally or half inserted in the middle assembly,
- a configuration with a beryllium block replacing the middle assembly,
- a configuration with water in the middle of the middle assembly (withdrawn Hf rod follower),
- a configuration with water replacing the middle assemblies.

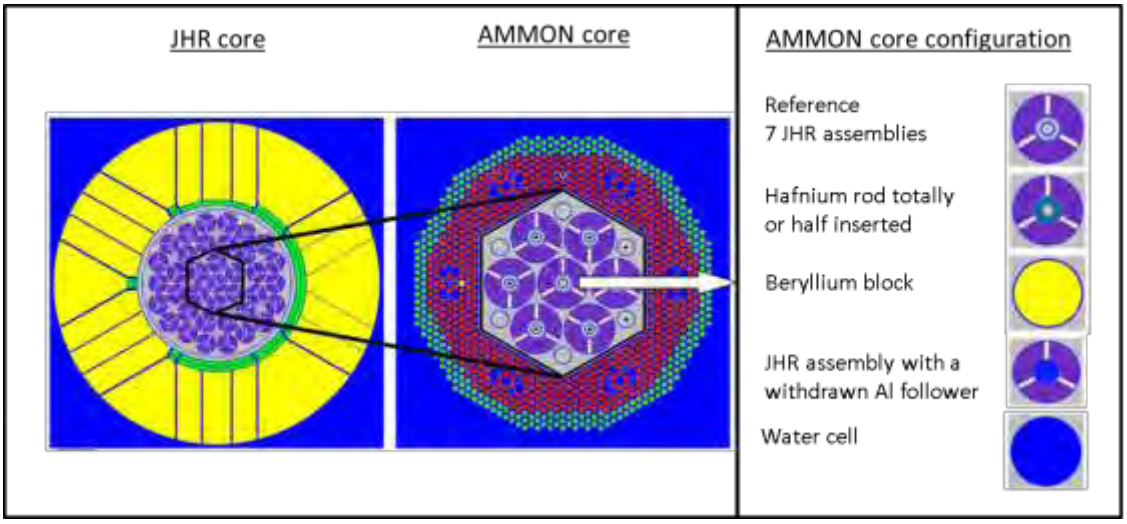

Fig.10: configurations of the AMMON experiment

The interpretation of the AMMON experiments with reference TRIPOLI-4® calculations using the JEFF3.1.1 nuclear data library, allowed us to quantify the biases and uncertainties originating from the nuclear data[6]. These results were transposed from the AMMON experiment to the real

[6] Few physical assumptions are made in TRIPOLI-4® that is why the biases are supposed to come only from nuclear data.

JHR core with the representativity methodology [11], [12], for the JHR-Beginning Of Life but also for the JHR in equilibrium. Indeed, a specific study showed that the ^{239}Pu (produced in the U_3Si_2-Al fuel thanks to ^{238}U radiative capture) contribution in assembly fission rates remains limited (<10%) compared to the ^{235}U contribution during the JHR life (the JHR neutron spectrum can be considered as constant). Thus, even if the AMMON experiments were performed on fresh JHR fuel, the results can also be transposed to the JHR in equilibrium.
The biases and uncertainties on the different neutronics parameters computed with HORUS3D/N originating from the nuclear data are summarized in [9]. They are not recalled here. Only the results of the global validation step are presented in chapter *6.*

The biases and uncertainties on the different neutronics parameters computed with HORUS3D/N, due to nuclear data <u>and</u> to the calculation scheme (see § 5.2) are summarized in chapter 6.

5.2 HORUS3D/N scheme validation

An important HORUS3D/N scheme validation step was carried out during late 2014. It consisted in assessing the biases and uncertainties due to the scheme itself (geometry approximation, energy cutting, flux solver,…) by comparing HORUS3D/N industrial route computations with reference routes calculations (see chapter 3, especially Fig.4):

- 2D and 3D continuous-energy Monte Carlo TRIPOLI-4® calculations, for the JHR beginning of life core calculations,
- 2D APOLLO2-MOC deterministic calculations, using the Method Of Characteristics flux solver, for the JHR core calculations during depletion.

The validation studies will be completed in 2015 with the use of TRIPOLI-4® in its new depletion mode, for the comparison with the HORUS3D/N calculations.

The scheme application domain matches the JHR operation domain, i.e.:

. Concerning the reactor configuration:

- fuel assembly: 34 to 37 fuel assemblies with or without Hafnium rods,
- maximal core experimental load: 7 fuel elements with experiments + 3 cells loaded with experiments
- maximal reflector experimental load: 12 experiments

. Concerning the time step:

- beginning of cycle (no xenon, samarium at saturation)
- Xenon equilibrium
- Mid cycle
- End of cycle.

Over 100 validation cases were performed to cover the JHR operation domain and to ensure statistical representativeness.
The detail of this study is not presented in this paper. Only the results of the global validation step are presented hereafter.

The biases and uncertainties on the different neutronics parameters computed with HORUS3D/N, due to the calculation scheme <u>and</u> to nuclear data (see § 5.1) are summarized in chapter 6.

6 HORUS3D/N performances: biases and uncertainties quantification

The results of the validation steps presented in chapter 5 were combined as follows for each JHR relevant parameter computed with the HORUS3D/N industrial route:

- Biases: $$\mathrm{Biases_{Global}} = \mathrm{Biases_{Scheme}} + \mathrm{Biases_{ND}} \quad (1)$$
- Uncertainties: $$\sigma_{Global} = \sqrt{(\sigma_{Scheme})^2 + (\sigma_{ND})^2} \quad (2)$$

With:
$Biases_{scheme}$: Biases of HORUS3D/N due to the calculation scheme, see § 5.2,
$Biases_{ND}$: Biases of HORUS3D/N due to Nuclear data see § 5.1,
σ_{scheme}: uncertainties of HORUS3D/N due to the calculation scheme, see § 5.2,
σ_{ND}: uncertainties of HORUS3D/N due to Nuclear data, see § 5.1.

Table 8 summarizes the results of the global validation of HORUS3D/N v4.2.

Table 8: HORUS3D/N v4.2 biases and uncertainties assessment

		Biases and uncertainties (2σ)	
		Step 0	**Depletion**
Reactivity of the critical core at nominal and cold conditions	Without control rod	-71 pcm ± 650 pcm	-233 pcm ± 827 pcm
	With control rods	-366 pcm ± 811 pcm	-663 pcm ± 911 pcm
Initial core reactivity (with 8 IA)		-862 pcm ± 640 pcm	-
Xenon equilibrium antireactivity		-	+0% ± 3.2%
Xenon antireactivity at the peak		-	+0% ± 16.9%
Samarium antireactivity		-	+0% ± 2.5%
Integral rod worth		+5.9% ± 4.7%	+6.4% ± 3.6%
Differential rod worth		+4.3% ± 3.2%	+8.9% ± 3.2%
In core experiment reactivity worth		-1.5% ± 6.0%	-3.4% ± 6.1%
In reflector experiment reactivity worth		-72 pcm ± 39 pcm	-92 pcm ± 31 pcm
Hot assembly power		+0% ± 5.4%	+0% ± 5.4%
Hot plate power		-2.6% ± 4.6%	-2.6% ± 4.6%
Burnup distribution – Assembly level		-	+0% ± 4.1%

7 Conclusion

The HORUS3D/N neutronics calculation tool, dedicated to JHR design and safety studies was upgraded in 2014 in order to take into account the APOLLO2.8/REL2005/CEA2005 package recommendations already applied for light reactor studies: HORUS3D/N v4.2 was thus released by the end of 2014. An important validation step was carried out to quantify the biases and uncertainties to be associated with each neutronics parameter computed with the new scheme. Thanks to the AMMON experiments, and to the improvement of the scheme, the performances were improved, allowing a better assessment of the JHR safety margins. Consequently, a complete validation file of the JHR neutronics calculation tool is obtained.
The development of a new neutronics deterministic calculation tool dedicated to JHR operation and loading studies will begin by the end of 2015. The objective of the tool is to deal with time constraint (a JHR loading will have to be fully calculated in a few days) and user experience (the studies will be performed routinely by JHR operators). The new HORUS3D/N v4.2 tool will serve as a starting point for these new developments.

8 REFERENCES

[1] D. Iracane, “The Jules Horowitz Reactor, a new Material Testing reactor in Europe,” *Nucl. Eng. Tech*., 38, 5, 437-442, 2006
[2] OECD/NEA, “The supply of medical radioisotopes – Implementation of the HLG-MR policy approach: results from a self-assessment by the global $^{99}Mo/^{99m}Tc$ supply chain,” NEA/SEN/HLGMR(2013)4, 2013
[3] C. Döderlein, T. Bonaccorsi, C. D’Aletto, J. Di Salvo, O. Gueton, L. Lamoine, F. Moreau, G. Naudan, P. Siréta, “The 3D neutronics scheme for the development of the Jules-Horowitz-Reactor,” Proc. Int. Conf. PHYSOR2008, Interlaken, Switzerland, September, 2008
[4] R. Sanchez, I. Zmijarevic, M. Coste-Delclaux, E. Masiello, S. Santandrea, E. Martinolli, L. Villatte, N. Schwartz, N. Guler, “APOLLO2 Year 2010,” *Nucl. Eng. Tech*., 42, 5, 474-499, 2010
[5] J.J. Lautard, S. Loubière, C. Magnaud, “CRONOS, a modular computational system for neutronic core calculations,” *Proc. IAEA Topical Meeting*, Cadarache, France, 1990
[6] A. Santamarina et al., “The JEFF-3.1.1 nuclear data library”, NEA, JEFF Report 22, 2009
[7] S. Santandrea, R. Sanchez, “Analysis and improvements of the DPN acceleration

technique for the method of characteristics in unstructured meshes," *Annals of Nuclear Energy*, 32, 163-193, 2005

[8] N. Huot, A. Aggery, D. Blanchet, C. d'Aletto, J. Di Salvo, C. Doderlein, P. Sireta, G. Willermoz, "The JHR neutronics calculation scheme based on the method of characteristics," *Proc. Int. Conf. M&C2005*, Avignon, France, 2005

[9] C. Vaglio-Gaudard, A.C. Colombier, J.P. Hudelot, O. Leray, M. Lemaire, V. Sergeyeva, J. Di Salvo, A. Gruel, P. Siréta, "Analysis of the AMMON experimental program in the EOLE facility supporting the qualification of the JHR neutron and photon tools", IEEE TNS, **61**, 4, 2014

[10] A. Santamarina, D. Bernard, P. Blaise, L. Erradi, P. Leconte, R. LeTellier, C. Vaglio, J.F. Vidal, "APOLLO2.8: a validated code package for PWR neutronics calculations," Proc. Int. Conf. ANFM2009, Hilton Head Island, South Carolina, USA, April, 2009

[11] O. Leray, C. Vaglio-Gaudard, J.P. Hudelot, A. Santamarina, G. Noguere, "Sensitivity and uncertainty analysis applied to the JHR reactivity prediction," *Proc. Int. Conf. PHYSOR2012*, Knoxville, Tennessee, USA, 2012

[12] V.V. Orlov, A.A. Van'kov, A.I. Voropaev, Y.A. Kazanskij, V.I. Matveev, V.M. Mugorov, E.A. Khodarev, "Problem of fast reactor physics related to breeding," *Atomic Energy Review*, 18. 4, 989-1077, 1980

[13] E. Brun, F. Damian, C.M. Diop, E. Dumonteil, F.X. Hugot, C. Jouanne, Y.K. Lee, F. Malvagi, A. Mazzolo, O. Petit, J.C. Trama, T. Visonneau and A. Zoia, "TRIPOLI-4, CEA, EDF and AREVA Reference Monte Carlo Code", Proc. Int. Conf. SNA+MC 2013, Paris, France, 2013

[14] www.salome-platform.org

UNCERTAINTY ASSESSMENT FOR REACTIVITY INDUCED ACCIDENT OF 5-MW POOL-TYPE RESEARCH REACTOR

SOO-BEEN YUM, SU-KI PARK
Safety Analysis Group, Korea Atomic Energy Research Institute,
989-111 Daedeokdaero, Yuseong, Daejeon, 305-353, Republic of Korea

ABSTRACT

Best estimate plus uncertainty (BEPU) is a promising approach to a safety analysis for nuclear reactors, and the uncertainty calculation is the most important concern for it. BEPU ensures realistic safety margins and secures a higher reactor effectiveness by taking the global uncertainty assessment for the parameters, whereas the previous uncertainty analysis considers each parameter separately. The reactivity induced accident (RIA) of a 5MW open-pool type research reactor was selected as a sample problem for a BEPU uncertainty assessment. We selected an insertion of cold water event, which causes a reactivity insertion by temperature feedbacks. The significant contributors to the reactor safety are identified and then input sets are sampled. 124 calculations were performed for the uncertainty evaluation, which is the number of code runs required for a 95%/95% tolerance level of the 3rd order Wilk's formula. MOSAIQUE software developed by KAERI was used for automated sampling of the uncertainty parameters, a global uncertainty calculation, and post processing of the results. We calculated the fuel centerline temperature (FCT) and the critical heat flux ratio (CHFR) with 95%/95% tolerance level and compared them with those from conservative analyses. In addition, the impact of each design parameters on the safety parameters was estimated by sensitivity analyses.

1. Introduction

1.1 Objective

US NRC revised its regulations in 1989, such that BEPU is able to replace the previous conservative approach to reactor safety analyses. Following the new regulation, ATUCHA unit 2 in Argentina recently obtained an operating license with the final safety analysis report using the BEPU approach. These two examples show the global trends of a safety analysis, which are shifting from a conservative analysis to BEPU. Figure 1 shows a comparison of the safety parameters calculated by different methodologies. BEPU estimates safety parameters more realistically compared to those by conservative analyses, reducing the excessive conservatism in a safety analysis and increasing the margin in the reactor operation.

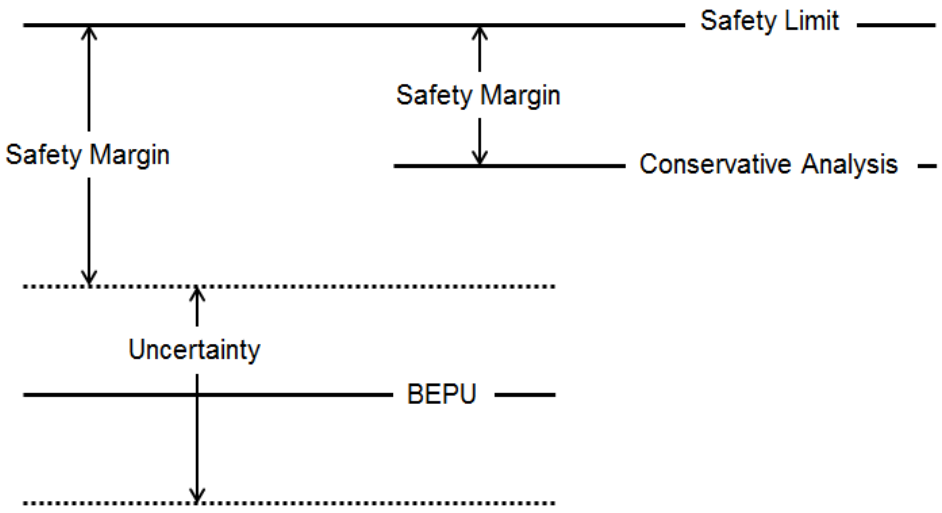

Fig 1. Comparison of different analysis methodologies

Following these international trends, we introduced the BEPU safety analysis for a reactivity induced accident of a 5-MW pool-type research reactor. The core safety parameters and input parameters affecting the parameters are selected first, and the overall uncertainties of the safety parameter are then calculated using a non-parametric uncertainty analysis. The safety parameters including uncertainties are presented and the importance of each parameter is ranked based on sensitivity analyses.

1.2 MOSAIQUE

MOSAIQUE (Module for SAmpling Input and Quantifying Estimator) software was developed in KAERI to conduct a probabilistic uncertainty analysis of computerized simulation models [1]. The software provides automated sampling, calculation and post processing, therefore reduces a lot of time and effort required to perform a BEPU analysis.
MOSAIQUE has three main functions: (1) sampling of input parameters, (2) calculating global uncertainties of the safety parameters, and (3) post processing of uncertainty bands of safety parameters and sensitivity of the input parameters.

1.3 Reactivity induced accident

For a BEPU uncertainty assessment, he RIA of a 5-MW open pool-type research reactor is selected as a sample problem. The scenario selected for the analysis is an insertion of cold water which is a RIA caused by reactivity feedbacks of coolant and fuel temperature when the primary cooling pump starts suddenly during the natural convection mode. Figure 2 shows the schematics of two cooling modes at the reactor; the natural convection mode and the forced convection mode by primary cooling pumps. During the natural convection mode, the temperature at the upper guide structure is higher than that of reactor pool since the core is cooled by the natural circulation of coolant via flap valves. When a primary cooling pump start to operate suddenly, the hot water at the upper guide structure enters the core first, but the relatively cold pool water enters soon after few second. Then the reactor power increases by the reactivity feedbacks of coolant and fuel temperature. The insertion of cold water is the most complicated event among RIAs because the thermal hydraulic variables and the reactor kinetic variables are cross-linked and change together during the event. The safety parameters investigated for the event are the maximum fuel centerline temperature (MFCT) and minimum critical heat flux ratio (MCHFR).

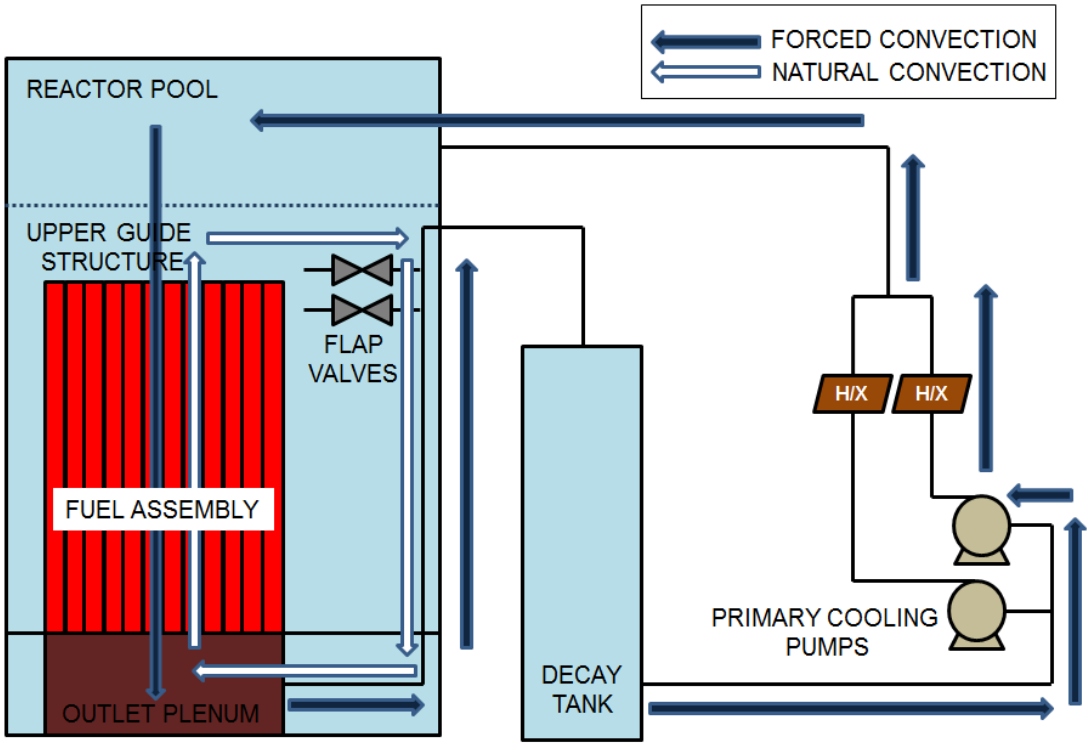

Fig 2. Schematic diagram during forced convection and natural convection mode

2. Uncertainty assessment

2.1 Frozen code selection

The behaviors of the reactor core and the systems are analyzed by the MARS-KS. MARS-KS is a consolidated and restructured version of the RELAP5/MOD3.2 and COBRA-TF codes and this code has been improved for the regulatory and best estimative purposes [2]. MARS-KS 1.3, the latest version, is used for the safety analyses of the event, since it has the best performance and accuracy at the moment.

2.2 Input parameter selection

#	Events
1	The reactor is in training operation, cooled by natural convection.
2	One PCS pump starts a sudden operation.
3	A positive reactivity is inserted by the of cold water insertion.
4	The power increases up to the power level trip set point.
5	The reactor trip signal is generated after the signal delay time.
6	The control absorber rods begin to drop into the core.

Tab 1: Sequence of event

Phenomenon	Relevant variables
Natural circulation	Initial core power, Pool inlet temperature
Forced convection	Mass flow rate, Pool level, Heat transfer coefficient,
Fuel behavior	Fuel corrosion layer, Heat flux hot channel factor
Reactivity insertion	Coolant temperature coefficient, Fuel temperature coefficient

Tab 2: Main phenomena and their relevant physical parameters

Table 1 summarizes the sequence of event during the insertion of cold water event. The important physical phenomena of the event and the relevant key design parameters expected to influence the reactor safety are summarized in Table 2.

The range of each key parameter for BEPU and conservative analysis are listed in Table 3. All parameters are assumed to have a uniform distribution. The characteristics of each input parameter are described below.

1) Initial core power: The initial core power affects the mass flow rate during natural convection mode. It determines the temperature difference through the core channel, which is related to the reactivity insertion at the event initiation. It also affects the trip time since the trip parameter of the event is the power level. In this event, the initial core power is 0.92%FP to 5.4%FP, including the operation range and sensor uncertainty.

2) Pool inlet temperature: The difference between the pool water temperature and the initial core inlet temperature determines the reactivity insertion at the event initiation. The pool inlet temperature influences the critical heat flux and the maximum fuel temperature. The possible range of pool inlet temperature is 12^{o}C to 48^{o}C. This range includes the operation range and sensor uncertainty.

3) Mass flow rate: The mass flow rate determines the cooling capability of the reactor core, and therefore, the temperature feedback effect is affected by this parameter. In the analyses, the mass flow rate is controlled by adjusting the primary coolant pump head. The possible range of the mass flow rate by a pump is 82.5kg/s to 101.5kg/s. This range includes the operation range and sensor uncertainty.

4) Pool level: The pool level determines the core pressure, which is related to the saturation temperature of the core coolant. The saturation temperature affects the inlet subcooling, which influences the critical heat flux in the fuel channel. The possible range of the pool level is 9.65m to 10.12m. This range also includes the operation range and sensor uncertainty.

5) Fuel corrosion layer: The corrosion layer on the fuel cladding has a low conductivity of less

than 2W/m·K. The fuel corrosion layer is a thermal insulator between the coolant and the fuel cladding, which affects the fuel temperature. The range of the fuel corrosion layer thickness is assumed to be 33μm to 100 μm.

6) Heat flux hot channel factor: The heat flux hot channel factor (HCF) is multiplied to the core heat flux when calculating the MFCT and MCHFR to compensate for the fuel meat fabrication tolerances. The HCF is originated from the U235 homogeneity and U235 loading per plate. The combined uncertainty of HCF is 19% including the factors and the additional core calculation uncertainty.

7) Heat transfer coefficient: The Dittus-Boelter correlation [3] in MARS-KS is used to calculate the heat transfer coefficient in the channel since the coolant is a single phase during RIA. The uncertainty of the correlation for a liquid is ±12.75%. The heat transfer coefficient is controlled by changing the heated equivalent diameter. The range of the heated equivalent diameter, which corresponds to the range of heat transfer coefficient, is 2.89×10^{-3}m to 1.04×10^{-2}m.

8) Fuel temperature coefficient: The fuel temperature coefficient is the reactivity insertion per unit temperature change of the fuel. The possible range of the coefficient is -2.7×10^{-2}mk/K to -6.3×10^{-3}mk/K.

9) Coolant temperature coefficient: The coolant temperature coefficient is the reactivity insertion per unit temperature change of the coolant. The coolant temperature range is converted into the density range adopted in MARS-KS. The coolant temperature coefficient has a range of -2.1×10^{-1}mk/K to -4.9×10^{-2}mk/K.

Number	Models/Parameters	Operating range	Distribution
1	Initial core power	0.92%FP~5.4%FP (5.4%FP)*	Uniform
2	Pool inlet temperature	12^{o}C~48^{o}C (48^{o}C)*	Uniform
3	Mass flow rate	82.5kg/s~101.5kg/s (82.5kg/s)*	Uniform
4	Pool level	9.65m~10.12m (9.65m)*	Uniform
5	Fuel corrosion layer	33μm~100μm (100μm)*	Uniform
6	Heat flux hot channel factor	0%~19% (19%)*	Uniform
7	Heat transfer coefficient	87.25%~112.75% (87.25%)*	Uniform
8	Fuel temperature coefficient	-2.7×10^{-2}mk/K~-6.3×10^{-3}mk/K (-2.7×10^{-2}mk/K)*	Uniform
9	Coolant temperature coefficient	-2.1×10^{-1}mk/K~-4.9×10^{-2}mk/K (-2.1×10^{-1}mk/K)*	Uniform

( )*: Input parameters for conservative analysis

Tab 3: Uncertainty parameters for insertion of cold water

2.3 Non-parametric uncertainty calculation

Non-parametric uncertainty calculation is a statistical technique and the required number of code runs is independent from the number of input parameters. Equation (1) shows Wilk's formula [4], which determines the number of code runs required for a certain percentile value with a certain confidence level. Table 4 shows the number of code runs to estimate a 95% probability value with a 95% confidence level, which is a 95%/95% tolerance level. The table also shows the analytical confidence level calculated from the formula.

$$\beta \le 1 - \sum_{j=n-p+1}^{n} \binom{N}{j} \gamma^{j} (1-\gamma)^{N-j} \quad (1)$$

(γ: probability, ß: confidence level, N: number of sample, p: order of Wilk's formula)

Order	Number of code runs	Analytical confidence (%)
1	59	95.1505
2	93	95.0024
3	124	95.0470
4	153	95.0555
5	181	95.0837

Tab 4: Wilk's formula

124 sets of input parameters were sampled, and the same number of code runs were conducted by the 3rd order Wilk's formula. The input sets were automatically generated by MOSAIQUE using a Simple Random Sampling (SRS) method. The safety parameters, MFCT and MCHFR, were then calculated using MARS-KS with the inputs.

2.4 Calculating the overall uncertainties

To calculate the final MFCT and MCHFR, the bias that stems from the scale effect and separate/integral effect test should be considered. However, this bias is assumed to be 0 in this analysis, and therefore, $MFCT_{95/95}$ and $MCHFR_{95/95}$ are the results of the BEPU analyses. $MFCT_{95/95}$ and $MCHFR_{95/95}$ mean the 95%/95% values of MFCT and MCHFR estimated from the analyses, by selecting the 3rd largest MFCT and the 3rd smallest MCHFR among the calculated results. Table 5 shows the comparison of the MFCT and MCHFR estimated by BEPU and conservative analyses for the event. The conservative analysis results were evaluated by MARS-KS calculation with the most conservative combinations of input parameters as shown in Table 3.

The differences of MFCT and MCHFR from two different approaches are 2.95°C and 1.09, respectively. The conservative analysis seems to show excessive conservatism in MFCT and MCHFR than those from the BEPU analyses although the bounding values of the design parameters are the same for both methods.

Output uncertainty parameter		BEPU analysis value	Conservative analysis value
MFCT	°C	68.37	71.32
MCHFR	-	7.81	6.72

Tab 5: MFCT and MCHFR from BEPU and conservative analyses

2.5 Sensitivity analysis

The impact of each design parameter on the safety parameters are estimated through sensitivity analyses. The importance of the input parameters on the safety parameters is represented quantitatively by Pearson's correlation coefficient [5]. Pearson's correlation coefficient shows the relationship between the two quantities, as shown in Equation (2).

$$Pearson = corr(X,Y) = \frac{\mathrm{cov}(X,Y)}{\sigma_X \sigma_Y} = \frac{E\left[(X-\mu_X)(Y-\mu_Y)\right]}{\sigma_X \sigma_Y} \quad (2)$$

(X,Y: parameter, μ_X, μ_Y: expected value, σ_X, σ_Y: standard deviation , conv(X,Y): covariance of X and Y)

The Pearson correlation is a measure of linear dependence between the parameters, which is +1/-1 when the variables are in a perfect linear/inverse linear relationship. The larger absolute value of the Pearson's correlation coefficient means a stronger dependency between the parameters. Figures 2 through 7 show the Pearson's correlation coefficients between the input parameters and trip time, maximum heat flux, critical heat flux (CHF),

MFCT, and MCHFR, respectively. The key design parameters relevant to MFCT and MCHFR are the initial power, the pool inlet temperature, the hot channel factor and the mass flow rate. The other design parameters, whose coefficients are between -0.2 and +0.2 [6], shows a relatively smaller relationship to MFCT and MCHFR because they are physically irrelevant, or the influence is shadowed by major parameters owing to their small uncertainty. The following are the main findings from the figures.

1) As the initial core power increases, as it can be seen in Figure 3, the reactor power reaches the trip set-point faster and the reactor trips earlier. Figure 4 shows that the maximum heat flux of the event increases as the initial core power increases because the reactivity insertion by the temperature feedback effect decreases with time. Therefore, as the initial power increases, the MFCT increases and the MCHFR decreases, as shown in Figures 6 and 7, respectively.

2) The pool inlet temperature determines the fuel temperature directly, and therefore shows a strong positive correlation with MFCT, as shown in Figure 6. The CHF is proportional to the inlet subcooling, resulting in the negative correlation shown in Figure 5. On the other hand, the maximum heat flux at the trip decreases as the pool inlet temperature increases, as shown in Figure 4. The higher inlet temperature reduces the temperature difference along the core by a higher density change per unit of temperature, and therefore the initial reactivity insertion rate decreases. However, the MCHFR shows a negative correlation with the pool inlet temperature (Figure 7), since the change in the maximum heat flux is smaller than the critical heat flux change.

3) Since the critical heat flux is divided by HCF to include the uncertainty of the fuel characteristics as shown in Equation (3), MCHFR shows a strong negative correlation with HCF (Figure 7). However, the HCF shows a negligible correlation with the MFCT (Figure 6) because the factor is multiplied with the temperature difference between the fuel surface and the fuel centerline, which is very small compared with the uncertainty of T_{clad}. T_{clad} is a function of the coolant temperature as well as the fuel temperature, and therefore, only a 2 to 4°C difference between the fuel centerline and the fuel surface can be shaded by the T_{clad} uncertainty.

$$\mathrm{CHFR} = \frac{q_{CHF}}{q_{actual} \times HCF}$$

(q_{CHF}: critical heat flux, q_{actual}: calculated actual heat flux from the fuel)

$$FCT = T_{clad} + HCF\left(T_f - T_w\right) \quad (3)$$

(T_{clad}: fuel cladding temperature, T_f: fuel centerline temperature, T_w: fuel surface temperature)

4) As the CHF is proportional to the mass flow rate (Figure 5), the MCHFR is also proportional to the mass flow rate (Figure 7). The high mass flow rate enhances the core cooling and decreases the fuel temperature; however, it increases the maximum heat flux at the same time by increasing the fuel temperature feedback. The two factors compete each other, and therefore the influence of mass flow rate on MFCT is small, as shown in Figure 6.

5) When the feedback coefficient of the coolant temperature is large in absolute value, the reactivity insertion and power increase at the event initiation becomes greater. Since the feedback coefficients are negative, the coolant temperature coefficient shows a negative correlation with maximum heat flux. However, since the change in maximum heat flux caused by a coolant temperature feedback is much smaller than the critical heat flux change, the coolant temperature coefficient shows negligible correlations with MCHFR. In the same manner, as shown in Figure 6, the coolant temperature coefficient shows a negligible correlation with MFCT. In addition, the fuel temperature coefficient does not show a clear negative correlation with the maximum heat flux, because the fuel temperature increase by higher core power is canceled with an enhanced core cooling by a cold coolant and high mass flow rate.

6) Since the corrosion layer acts as a thermal insulator between the coolant and fuel cladding, MFCT is proportional to the thickness of the corrosion layer. However, the effect of the corrosion layer on the MFCT is small because it is shaded by other strong parameters (Figure 6).

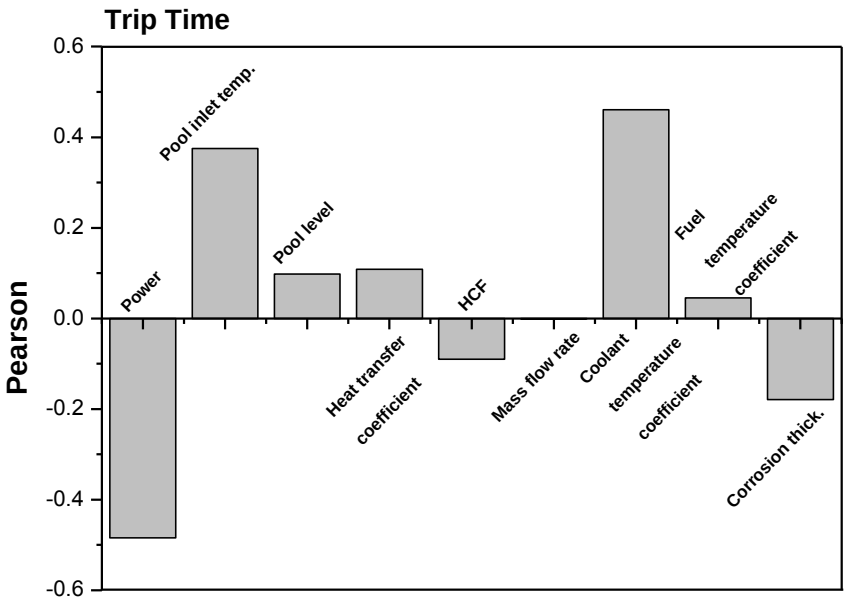

Fig 3. Pearson correlation coefficient for trip time

Fig 4. Pearson correlation coefficient for maximum heat flux

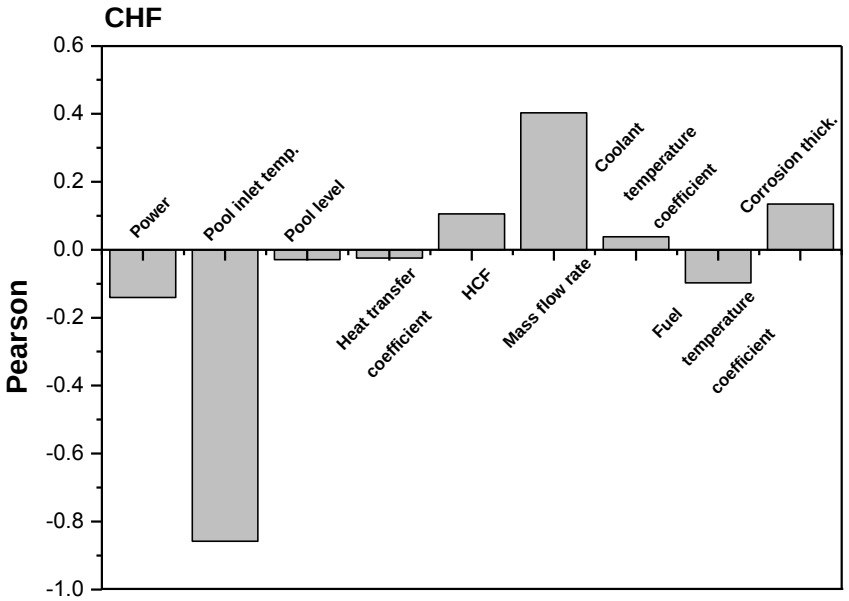

Fig 5. Pearson correlation coefficient for CHF

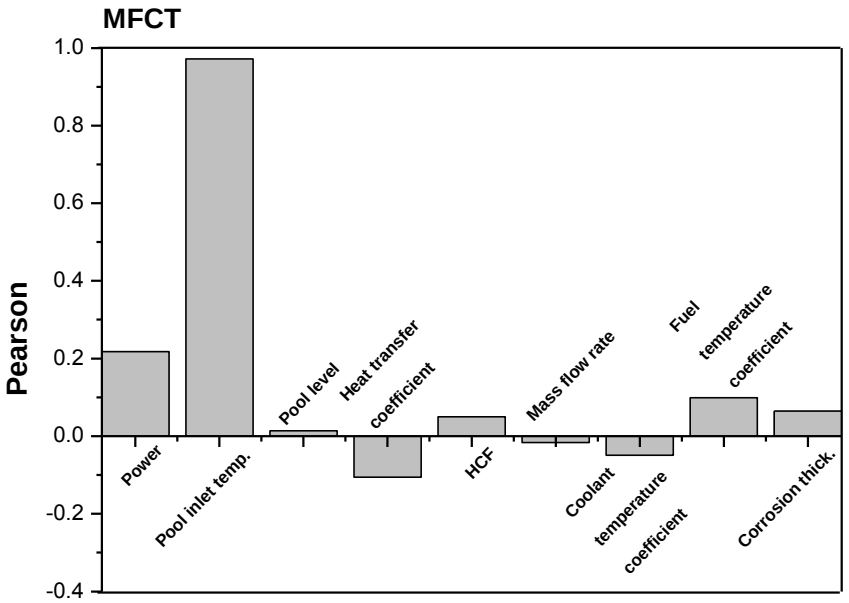

Fig 6. Pearson correlation coefficient for MFCT

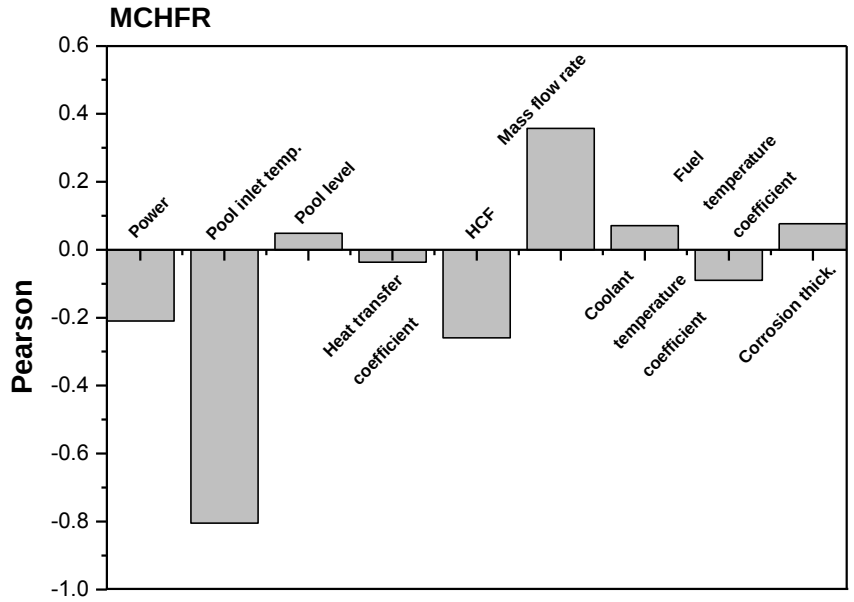

Fig 7. Pearson correlation coefficient for MCHFR

3. Conclusions

A BEPU methodology was applied to an insertion of cold water event of a 5-MW pool-type research reactor. The key input parameters for the event were identified based on the important phenomena during the event. 124 sets of input parameters were sampled, and the same numbers of code runs were used to evaluate the uncertainty of the key safety parameters, MFCT and MCHFR. The MFCT and MCHFR from the BEPU analyses were presented with a 95%/95% tolerance level. Comparing the results from BEPU and those from conservative analysis, the safety parameters show more margins from the safety limits with the BEPU approach, which means the possibility of a higher operability and enhanced efficiency. The importance of each input parameter on the safety parameters was then analyzed through sensitivity analyses. The most important parameters on MFCT and MCHFR are the pool inlet temperature, mass flow rate, HCF and initial core power. The procedures and results in this paper show the applicability and advantages of a BEPU safety analysis over conservative analysis on a research reactor.

References

[1] H.G.Lim, et al., 2011. MOSAIQUE-A network based software for probabilistic uncertainty analysis of computerized simulation models, Nuclear Engineering and Design 241, 1776-1784.

[2] Hwang, M.K. and Chung, B.D., 2011, Improvement of MARS code reflood model. In:19th International Conference on Nuclear Engineering (ICONE-19), Chiba, Japan, May 16-19.

[3] F. W. Dittus, et al., 1985. Heat Transfer in Automobile Radiators of the Tabular Type, Heat and Mass Transfer 12, 3-22.

[4] Nutt, W.T. and Wallis, G.B., 2004, Evaluation of nuclear safety from the output of computer codes in the presence of uncertainties, Rel. Eng. Sys. Saf. 83.57-77.

[5] Lehmann, E.L., 1975, Nonparametrics, Statistical Methods Based on Ranks, Holden-Day, Inc, California, USA.

[6] S.J.Son, et al., 2003, Medical statistics, Chonnam National University Medical School, Republic of Korea.

CONTRIBUTIONS TO PROBABILISTIC SAFETY ASSESSMENT STUDIES FOR TRIGA RESEARCH REACTORS

DANIELA MLADIN, MIREA MLADIN

Reactor Phys., Nucl. Safety & Fuel Performance Dept., Institute for Nuclear Research
Campului, 1, 115400 Mioveni, Romania
daniela.mladin@nuclear.ro

ABSTRACT

Probabilistic safety assessment (PSA) is used since the eighties for evaluations of the nuclear safety. It provides a method to calculate the risk to public and personnel in a complex facility such as: nuclear reactor, chemical plant, waste storage, etc. Suitable use of the PSA techniques proved to be a very strong tool to increase safety and efficiency of the design, construction, operation, modification and management of such industrial installations. During the last decades, a large volume of information and experience has accumulated from application of PSA to nuclear power plants. This information and the general PSA methodology can be very useful for the analysts working with PSA for research reactors. The trust of public in the nuclear energy does not necessarily accompany the development of scientific studies and technical methods for radioactive release prevention. The accident at Fukushima-Daichii produced significant psychological effects, even inside the nuclear community. Whatever the prevailing attitudes at a certain period of time towards the nuclear and whatever the regulation requirements, PSA stands as the main way to quantify risk and to analyze the safety of a project and of the operational configuration. Obviously, resources are directed especially where risk – defined as probability times consequences – is high, namely at nuclear power plants. However, the later years have shown an increasing presence of PSA methods inside the research reactors community. Some developed countries have already imposed PSA analyses as mandatory for the licensing of research reactors.
In Romania, approaching a PSA project for a research reactor is a scientific endeavour that was not undertaken before these studies, which aim to comply with the nowadays growing extent of safety evaluations for nuclear installations. The paper describes a wide range of PSA level 1 and level 2 aspects, applied to the Romania TRIGA 14 MW reactor. Deterministic analyses were also done for determining the radioactive inventory and release of fission product in cases where accident sequences are leading to fuel damage.

1. Introduction

Probabilistic Safety Assessment (PSA) is a method of evaluating risk to public and to personnel in a nuclear installation, such as a nuclear power plant (NPP), chemical plant, research reactor, waste disposal facility, etc. A large volume of information has accumulated in the last decades through application of PSA at power reactors. This information, in general, and PSA methodology in particular, may be useful for improving knowledge and skill of analysts working in PSA for research reactors. Anyway, due to differences between power reactors and research reactors, PSA techniques used for power reactors need to be analyzed attentively as to their applicability to research reactors. Many of research reactors have a long operating period (as well as NPPs), but also have a variety of associated experimental installations. These installations suffer ageing and obsolescence, and generally require separate consideration of their renewal at a reasonable cost. The research reactors (RRs) are more simple facilities than NPPs, having not so many systems, and are accordingly easier to analyze than a power plant. Actually, it is important to mention that the RRs are more flexible, the access to the reactor core is easier and core configuration can be changed due to

experimental requirements. The experimental aspects for RRs add a new dimension to the PSA's application.

Now a date, there are more than 300 research reactors in the world. These include a variety of constructive types and thermal power ranges, from few tens of watts up to 100 MW. Modern projects ([1], [2]) have included PSA evaluation of postulated accident sequences, while national regulatory requirements referring to design and operation of research reactors have continuously enlarged and improved as a result of international practices and recommendations.

While the methodological basis approach about PSA for RRs is known, the availability of data remains unsolved yet, due to diversity of research reactors. For this reason, IAEA, has organized a few dedicated CRPs, in order to collect failure data for PSA use for RRs ([3], [4], [5]). There is an information system called DARES (DAtabase for REsearch Reactor Safety), installed al JRC centre in Petten, Holland, for collecting information/data referring to PSA for RRs ([6]) Thirty research reactors from Europe, Argentina, Australia, Canada, South Africa and United States contributed with information to this system DARES.

2. Probabilistic Safety Assessment (PSA) for TRIGA Steady State 14 MW reactor

The purposes of the PSA analysis for TRIGA SSR are:

- Treatment of internal and external IEs;
- Evaluation and calculation of sequences that are leading to fuel failure and fission product release.

Premises of the analysis:

- Only reactor was considered as possible source of radioactive releases. Although, the fuel failure in the irradiation devices, designed for this event may represent a radiological risk for the operating personnel if particular safety barriers are inefficient, this failure is not considered as a final state in the event trees.
- Operation at maximum power (14 MW) is considered as being the bounding case in risk assessment, and PSA evaluations have been made for this situation.
- Reactor fuel was considered damaged when the fuel temperature limit is exceeded, according to the TRIGA Final Safety Report ([8]).
- Quantification analysis was performed using specific reliability data of TRIGA SSR reactor, fruit of the collection and processing of raw data for obtaining reliability data ([10]), but also generic data taken from IAEA available sources for research reactors ([3], [9]).
- For quantification of human errors it was used OAT (Operator Action Tree) ([11]) or THERP ([12]).
- The analysis of source term, inventory and transport of fission product in the primary circuit and in the reactor hall, as support of Level 2 PSA was performed.

2.1 Evaluation of initiating events for TRIGA SSR 14 MW

This subchapter presents the possible initiating events (IEs) for TRIGA SSR 14 MW reactor based on Safety Analysis Report ([8]) subsequent deterministic analysis, and initiating event list considered by IAEA ([13]) for research reactors. Initiating events frequencies together with their corresponding calculation method used are included in Table 1.

2.2 Description of the final core damage states for TRIGA reactor

According to [15], based on thermohydraulic analysis, only three final core damage states D1, D2, D3 were considered. Table 2 includes the percent of damaged core, mean frequencies and statistical confidence intervals limits (5%, 95%). The highest contribution (about 100 %) is due to D1 state, failure of 725 fuel elements in water.

Initiating Event	Method of calculation	Frequency (occ./year)
Loss of power supply LOFPS IE	Fault Tree Analysis	7.88E-03
Criticality during handling (fuel insertion error) CDHAL IE	Human Error Analysis (TESEO method) + Operating experience	2.10E-02
Loss of flow (failure of Primary Pumps Lines) LOFA IE	Fault Tree Analysis	1.74E-01
Fuel Channel Blockage FCB IE	TESEO + Maintenance Requirements	7.50E-03
Spuriously close of pool isolation valves (pneumatic valve DN 800) SP-CLOS IE	Fault Tree Analysis	1.67E-03
Loss of coolant accident (Primary Pipe Rupture) LOCA1 IE	Formula for Steel Pipes Rupture (Thomas)	1.00E-02
Loss of coolant accident through transfer gate failure followed by beam tube rupture LOCA2 IE	Fault Tree Analysis	1.67E-09
Earthquake	Safety Analysis of the Romanian TRIGA facility designer	1.00E-04

Table 1. Postulated initiating events, method of calculation, frequencies

Final core damage state	Percent of damaged core	Mean frequency / year	Confidence interval 5% / year	Confidence interval 95% / year
D1	100%, in water	7.28E-06	6.73E-06	1.07E-05
D2	80%, in air	3.98E-15	2.84E-16	2.37E-14
D3	100%, in air	2.09E-15	1.40E-16	1.33E-14

Table 2. Final core damage states for TRIGA reactor

The main contribution leading to D1 state is due to combination of initiating event, LOFA, common cause failure of control rod mechanisms (46.5%) or common cause failure of control rods (24%).

2.3 Radioactive release categories for TRIGA reactor

The radioactive release categories (Table 3) depend on the release quantities in the reactor hall, on hall isolation and on the state of radioactive products removal system (emergency ventilation system). Three reactor hall states are considered (Table 4.), depending on the successful reactor hall isolation and availability of the emergency ventilation and its associated air filters. These states combined with the three core damages states for TRIGA reactor produce nine categories of radioactive releases.

The radioactive releases states and their associated corresponding frequencies and confidence interval limits are given in the Table 5. One can note that the radioactive release state, R1 is dominant, followed by R2 state.

Contribution to R1 state is given by the LOFA IE and combination of common cause failures (CCF) of control rod (23.8%) and control rod mechanisms (46.1%). Combination of LOFPS IE and common cause failure of control rod mechanisms contributes with 12.9% to R1. Contribution to R2 fission products state is given by combinations of LOFA IE, common cause failures of control rod mechanisms, failure of dosimetry alarm unit (32.5%) or combinations of LOFA IE, common cause failures of control rod, failure of dosimetry alarm unit (16.8%). Combination of LOFPS IE, common cause failure of control rod mechanisms and failure of tri-phase inverter contributes with 12.9% to R2.

Release category	Core damage state	Containment state (reactor hall)
R1	D1	C1
R2	D1	C2
R3	D1	C3
R5	D2	C1
R6	D2	C2
R7	D2	C3
R8	D3	C1
R9	D3	C2
R10	D3	C3

Table 3. Radioactive release categories ([16])

State index	Reactor hall isolation available	Emergency ventilation available
C1	Yes	Yes
C2	Yes	No
C3	No	-

Table 4. Containment states (reactor hall) ([16])

Radioactive release category	Mean frequency / year	Confidence interval 5% / year	Confidence interval 95% / year
R1	7.28E-06	6.73E-06	9.67E-06
R2	4.40E-08	4.14E-08	7.61E-08
R3	2.54E-10	3.31E-11	7.98E-10
R5	3.98E-15	2.74E-16	2.36E-14
R6	1.81E-17	1.22E-18	9.97E-17
R7	1.69E-19	5.05E-21	9.29E-19
R8	2.09E-15	1.70E-16	1.27E-14
R9	9.45E-18	7.33E-19	5.85E-17
R10	8.90E-20	3.32E-21	5.49E-19

Table 5. Frequencies and confidence interval limits for radioactive release states

2.4 Short description of TRIGA Event Trees

Some assumptions were made for the evaluation of the event trees. These are:

- The unavailability of the emergency cooling does not lead to fuel damage. Actually, the inertia of the main pumps and the natural convection loop formed after flow reversal are able to remove the residual heat after a reactor shutdown from 14 MW power level, as the reactor commissioning tests, done in 1979, demonstrate. Moreover, safety analysis results indicate that the emergency loop is able to remove heat for a coast-down time of the main pumps larger than 2 seconds, in a scenario in which the scram is initiated at 0.2 sec. after the scram signal on flow-rate decrease ([17]).
- Natural convection is passively initiated through the emergency pump system without any dedicated components such as natural convection valves as for other research reactors.
- Secondary cooling system is not influencing upon the accident sequences because the time scale of a transient that can lead to fuel damage is quite small, making insignificant the global heat transfer to the secondary circuit. Also, if the rapid shutdown of the reactor is successful, the residual heat can be absorbed by the large volume of water in the pool and primary circuit.

LOFPS event tree

When external power supply to the reactor fails (S1 and S2 6 kV buses), the reactor should normally be scrammed by the interruption of electrical power to the control rods electromagnets. Success of the control rods insertion into the active core leads to a stable state. Next heading is the power supply in emergency mode of the TCAt bus from the tri-phase inverter by the TCC1 and TCC2 buses. These two buses are connected to the batteries B1 and B2 that feed the reactor console, the emergency lighting, the emergency pump and the emergency ventilation. Reactor hall isolation was not considered because the

loss of external power supply will automatically shutdown the normal ventilation. The difference between the final release states, R1 and R2, produced by the failure of control rods gravitational movement, is the availability of the emergency ventilation. The later can fail either because of emergency power supply or by internal causes residing in the emergency ventilation system.

CDHAL event tree

The CDHAL IE considered in the analysis refers to the manipulation and accidental reinsertion of fuel bundles into the reactor core. Actually, such an event happened during early nineties when fuel bundle handling tool uplifted 2 bundles instead of one. To avoid dropping upon the core, the operator inserted the bundles into an inappropriate double location and the reactor became critical with all rods down and no power supply at console. Fuel moving action sheet was not properly set and allowed for intermediate configuration with insufficient reactivity compensation. The frequency of this IE was calculated using the TESEO (Technique to Estimate Operator's Errors) method and the estimated number of operations on the TRIGA SSR core. In spite of the large value for this IE frequency, (2.10E-02), the event was further excluded from the IE list, based on deterministic calculation that indicates that for fuel damage to occur, a very large value for reactivity insertion would be needed because TRIGA reactor has a large negative temperature prompt coefficient of reactivity.

LOFA event tree

The LOFA IE refers to the main circulating pump lines unavailability when reactor power level is 14 MW. For the IE to happen, it is necessary that two out of two main circulating pumps in operation fail. According to deterministic analyses ([15]), the loss of forced flow is considered by failure of both main pumps in operation at 14 MW reactor power level. If the primary cooling is lost, the reactor can be cooled by the emergency pump only, after the reactor shutdown. Deterministic analyses were necessary for calculating the evolution of the reactor fuel temperature when the scram initiation does not follow the decrease of the coolant flow-rate, in other words when the automatic shutdown system fails. Thus, in the accident sequences, testing of the manual shutdown appears, too. Fission product release states are marked only on the branch with no flow-rate scram, no inlet-outlet temperature difference scram, no fuel temperature scram, and also with failure of the manual scram. Should the regulations of the reactor are to be formally fulfilled, one will be compelled to postulate that failure of the emergency pump after operation at 14 MW leads to fuel damage even after a successful scram of the reactor. Actually, as already discussed, commissioning tests demonstrated that failure of the emergency pump does not produce fuel damage. Further on, if automatic scram fails, manual scram is tested. Success of the manual scram in a reasonably short time leads to a no consequence final state, too. The release states R1, R2, imply fission product release, resulting from failure of manual scram, and are different in what concerns ventilation filters and reactor hall isolation.

Fuel channel blockage (FCB) event tree

This IE can appear due to handling during maintenance, through dropping of an object in the reactor pool. This object could block flow inside the fuel bundles or could affect locally the space between fuel elements (a subchannel). The event, with a rather large calculated appearance frequency (7.50E-03/ year) was excluded due to project of TRIGA bundle and based on deterministic analysis in SAR. Special for this type of event, the reactor design provides the existence of cooling lateral holes in the bundle walls, in case that the its surface would be blocked by an object dropped in the reactor pool. Subchannel blocking was also excluded based on SAR, which contains analysis of flow reduction effects about temperatures fuel, concluding with, that the reduction in this way of the local flow does not lead to fuel damage.

Spuriously close of pool isolation valves (SP-CLOS) event tree

The initiating event frequency was calculated as being 1.67E-03/year. The spuriously close of pool isolation valves event tree is leading to loss of flow event tree.

Loss of coolant accident – Primary pipe rupture (LOCA1) event tree

Such a transient is worth to be analyzed considering all designed protections against it (pool isolation valves, antisyphon valves). The IE supposes the rupture of primary circuit main pipe in the region of the pipe line at the lowest elevation (-18 meters), where there is enough room for water to drain from the pool. The rupture of the primary circuit pipe may lead to diminishing of the reactor pool water level down to fuel uncovering. The first heading in the event tree is “automatic shutdown (scram) due to pool level decrease”. As a result of water level decrease, automatic isolation of the pool is triggered by means of pneumatic valves at outlet and inlet of the 800 mm diameter primary pipe. These pneumatic valves are fed by two redundant compressed air systems 6 bars and 10 bars, respectively. If automatic pool isolation is not successful, manual isolation can be done using the same two valves and manual valves on the same line. Continuing on the event tree, the antisyphon system is tested. This consists in opening some floating valves letting air penetrate inside the primary line, thus interrupting the siphon and preventing the pool water decrease below the level of these valves. If the antisyphon system fails, core damage will result and reactor hall isolation is tested, which implies closing the normal ventilation air paths. As a result of fission product detection inside the reactor hall, emergency ventilation is triggered, which is the last heading in the LOCA event tree. If no automatic scram results from pool water level decrease, the operator can scram the reactor manually. This branch of the event tree further tests the same headings as above, starting with the manual pool isolation. If manual shutdown of the reactor fails and the antisyphon system is successful, the three release states will depend on the reactor hall isolation systems and on the emergency ventilation, R1, R2, R3 will be 100% underwater. If the antisyphon system is unsuccessful, the final states R8, R9, R10, will be associated with release of fission product in air.

Loss of coolant – beam tube plus transfer gate (LOCA2) event tree

There are two pneumatic fittings from the transfer gate which separate the reactor pool from the transfer pool. In case of loss of air, the pneumatic fittings will deflate and the pool water floods in the transfer pool through the transfer gate. However, this event alone will not be enough to produce core uncovering since the transfer channel is only a few meters below the pool surface. Each of two TRIGA reactors (ACPR and CCR) has two kinds of beam tubes: radial and tangential. In case of rupture of the beam tube, a water quantity floods in beam room. Against this event, protection measures were taken by design, the volume of beam room being such that about 1 m water level still remains in the pool. In these conditions the quantity of water remaining in the reactor pool is 84 m^3. The IE evaluated takes into account simultaneous possibility of loss of water from pool through transfer gate and ruptures of beam tubes. The calculation of frequency for this initiating event supposes the unavailability of the pneumatic fitting from transfer gate combined with failure of beam tubes. The frequency for this IE (1.67E-9/year) is very small and, applying a cut-off criterion, the initiating event LOCA2 was not further taken into account.

External event – earthquake

Due to Vrancea seismic zone, the site is exposed at earthquakes. Analysis was performed by the Romanian designer of the facility for a maximum earthquake intensity I= VI ½ MSK. In case of TRIGA reactor, the earthquake may initiate scenarios that can be combined in four groups, treated as scenarios for internal initiating events, as follows:

✓ If the earthquake causes a damage of reactor building, the event tree would be reduced at flow blockage case.
✓ If the reactor building falls down, two event trees would be developed, once for flow blockage and another for core damage.
✓ If in case of an earthquake pipe ruptures can appear, event tree will be treated as in case of LOCA IE, both small and large pipes ruptures.
✓ The earthquake may produce a loss of electrical power supply, the event tree will be treated as in case of LOFPS IE.
The seismic analysis for TRIGA SSR in progress.

3. TRIGA modelling with CATHARE2

The nodalization of the problem is depicted in Figure 1, and it was realized using GUITHARE v1.5.1 graphic interface of CATHARE 2 code. The reactor hall has two boundary conditions for inlet and outlet of air, simulating the air circulation done by the ventilation system (13600 m^3/h in emergency mode). The water volume is preserved but some components have been collapsed: two pumps at nominal power are represented by a single pump with mass flow rate of 500 l/s, the two heat exchangers are represented by only one composed of inlet volume (weight=2), individual thin tubes (weight=2x1262), outlet volume (weight=2). Since reactor core is not modeled, no heat transfer was considered and consequently there was no need for secondary system. The purpose of the model is to calculate the fission products transport in the primary system and containment, and the evolution of the activity in different zones. The core damage is simulated by means of a radio-chemical components source (SOURCE operator) at the axial level of the core inside the volume representing the pool. The source for the four radio-elements included in CATHARE2 (Kr-87, Xe-133, I-131 and Cs-137) had to be calculated by other means and included in the defined flow of the SOURCE operator as an activity concentration per kg of gas.

3.1 Calculation of fission product source

An average TRIGA LEU bundle was modeled (figure 2) using SAS2H module from SCALE 4.4 ([18]). Work described in ([7]) produced by General Atomic Company, gives the correlation used to calculate the release of fission products from TRIGA fuel, both gaseous and volatile metals:

$$\psi = 1.5 \cdot 10^{-5} + 3.6 \cdot 10^{3} \cdot e^{-1.34 \cdot 10^{4} / T} \quad (1)$$

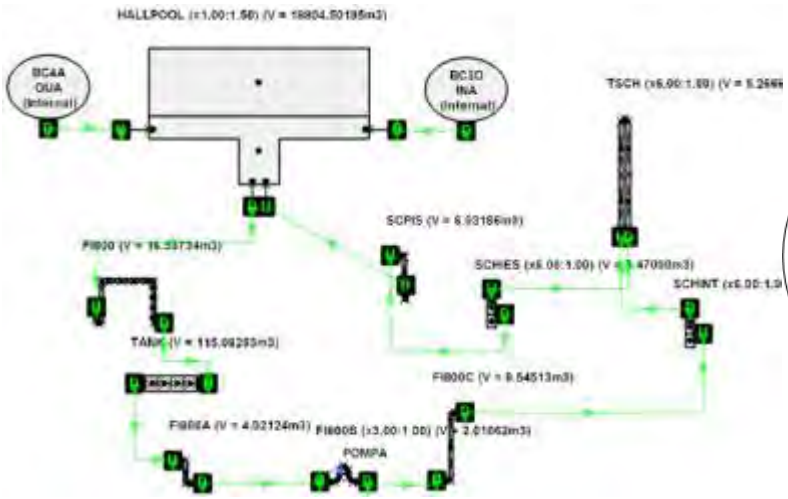

Figure 1. Nodalization of TRIGA model for fission products transport (GUITHARE v1.5.1 [14])

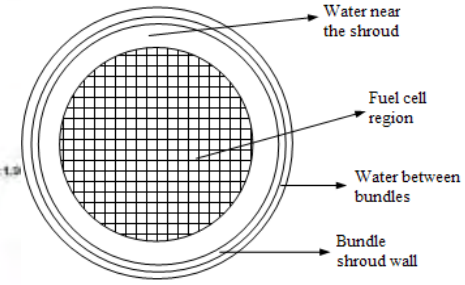

Figure 2. Regions of the TRIGA bundle model for SAS2H

, where T is the fuel temperature (K). Release fractions given by (1) assume failed or ruptured cladding. The Final Safety Analysis Report indicates 940 °C as the fuel limit temperature when cladding temperature may be at the same value as the fuel.
The calculations were done in the following assumptions:
- one hundred percent of the noble gases in the fuel-clad gap are released;
- twenty five percent of the Iodine and Cesium are released from the fuel elements, the remainder being considered deposited on the relatively cool cladding. For an underwater accident only 10.9% of the release is considered gas (10% assumed to form organic compounds that escape pool water and 1% of the balance not dissolved in the pool water). Thus, only 2.725% from the I and Cs content of the fuel-clad gap forms the CATHARE gas source for these elements, the rest (22.275% of the gap content) being introduced as liquid source;
- for fuel damage while in air, the release for noble gases (Xe and Kr) is 100% of the fuel-clad gap inventory, and for the I and Cs the release fraction is considered as 25%.

Fission product	Mass / bundle (kg)	Release / core with 29 bundles (kg)	Source in liquid phase (kg)	Source in gas phase (kg)
Kr(Kr-87)	4.45E-04	7.36E-04	0.	7.36E-04
Xe(Xe-133)	1.49E-04	2.46E-04	0.	2.46E-04
I(I-131)	1.31E-04	5.41E-05	4.82E-05	5.90E-06
Cs(Cs-137)	2.97E-02	1.23E-02	1.09E-02	1.34E-03

Table 6. Inventory per bundle and fission product sources for an underwater release. Whole core release in 100 s (100% for noble gases and 25% for I and Cs)

Fission product	Mass / bundle (kg)	Gas release from 80% of the core (kg)
Kr(Kr-87)	4.45E-04	5.89E-04
Xe(Xe-133)	1.49E-04	1.97E-04
I(I-131)	1.31E-04	4.33E-05
Cs(Cs-137)	2.97E-02	9.82E-03

Table 7. Inventory per bundle and fission product sources for release in air. Release from 80% of core in 1500 s (100% for noble gases and 25% for I and Cs)

3.2 Calculation of the radio-elements transport

Using the CATHARE2 model described above, it was investigated the capabilities of the code to calculate the concentration of each fission product in different zones of the TRIGA facility, pool, primary lines, delay tank and reactor hall. It should be mentioned that fission products are treated in CATHARE2 as pure species (i.e. no chemical interactions) and are introduced as gaseous or liquid sources at the location of reactor core in the model. The efforts were towards through support PSA calculation, in which it intended the evolution of reactor stack fission product releases, defining quantitative containment states function of CATHARE's fission product transport results and functioning of ventilation system in normal operation (unsuccessful condition) and in case of accident, emergency (successful condition). The following gives a synthesis of the results of these support analyses.

Underwater release: Maximum of the release is rapidly attained (at about 100 s) since the accident sequence with core damage involves no scram at full power. Two basic series of results are calculated, with a residual flow rate in the primary circuit: normal operation of the ventilation system with air flow rate 24360 m^3/h, and ventilation system in emergency mode: air flow rate is 18500 m^3/h, efficiency of the filters is 100% for Iodine and 10% for Cesium. Figure 3 presents, as an example of time evolution, the release rate of Krypton at LOFA with emergency ventilation and normal ventilation.

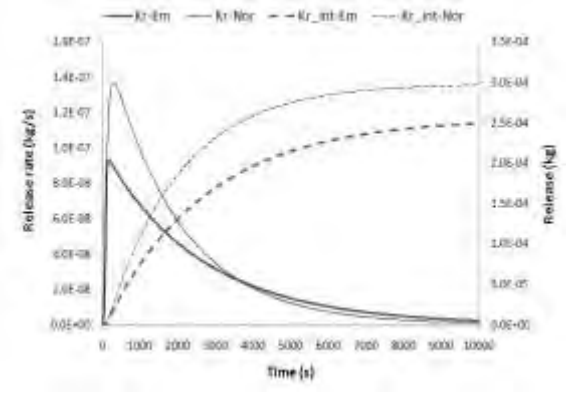

Figure 3. Instantaneous and integral stack release of Krypton at LOFA with emergency ventilation and normal ventilation

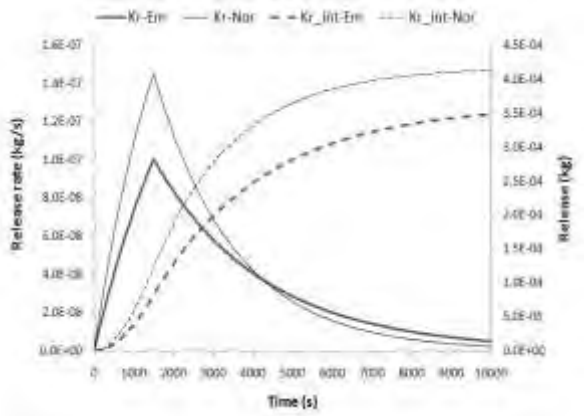

Figure 4. Instantaneous and integral Krypton stack release at LOCA with emergency ventilation and normal ventilation

Release in air: appears in case of Loss of Coolant Accident (LOCA). The maximum of instantaneous releases for all fission products is at 1500 s (end of release), the origin being the moment of fission products source opening which coincides with the damage for the maximum loaded fuel group (ppf=1.92).

The circuit here is empty (residual liquid phase), the fission products source is placed at the same elevation as before (1.5 m above the bottom of the pool) but the release is gaseous, inside the non-condensable (air). Figure 4 presents, as an example of time evolution, the release rate of Krypton with emergency ventilation and normal ventilation at LOCA.

4.Conclusions

As a result of the PSA study for the TRIGA reactor presented, several specific conclusions can be drawn regarding to the nuclear safety characteristics of the facility:

- Core Damage Frequency (CDF) is 7.28 x 10^{-6} /year and comes almost entirely from the frequency of the D1 core damage state, which is produced by the loss of flow with no scram, and has as significant contributors combination of loss of flow IE with the common cause failure of the control rods and control rods mechanisms;
- Total fission product release frequency is about 7.28 x 10^{-6} /year and is due to the release states R1 (CDF+ success of the reactor hall systems) and R2 (CDF+ success of the reactor hall systems +failure of ventilation system to switch to the emergency mode). The R1 release state is characterized by a stack release rate, on the curve's peak, of about 1 x 10^{-7} kg/s noble gases (Xe and Kr) and 1.5 x 10^{-7} kg/s Cesium. The R2 release state is characterized by a stack release rate, on the curve's peak, of about 1.9 x 10^{-7} kg/s noble gases (Xe and Kr), 1.1 x 10^{-9} kg/s Iodine and 2.5 x 10^{-7} kg/s Cesium.

5. References

[1]. ***IAEA TECDOC-517, Application of Probabilistic Risk Assessment to Research Reactors, Vienna, 1989.
[2] ***, ANSTO "Replacement Research Reactor – Probabilistic Safety Assessment (PSA)", Summary for Public Release, Australian Nuclear Science and Technology Organisation (ANSTO) document number: RRRP-7225-EBEAN-004-REV0 Revision: 0, March, 11, 2005.
[3] ***, TECDOC-636, Manual of reliability data collection for research reactor PSAs, IAEA, Vienna, 1992.
[4] ***, IAEA TECDOC-930 Generic component reliability data for research reactor PSAs, Vienna 1997.
[5] ***, IAEA Draft TECDOC "Reliability Data For Research Reactor PSA", draft, July 2005.

[6] C. Kirchsteiger, J. Kubanyi, PSA support of research reactor safety management, International Eugene Wigner Training Course on Research Reactor Safety, JRC, Petten, 2006.
[7] N. L. Baldwin, F.C. Foushee, J.S. Greenwood, Fission Product Release from TRIGA-LEU Reactor Fuels, GA-A16287, 1980.
[8] ***, General Atomic Company, 1974. Safety Analysis Report of the Triga Steady-State Research/Materials And Testing Reactor, GA E-117-323.
[9] ***, IAEA TECDOC-930, Generic component reliability data for research reactor PSAs, IAEA, Vienna, 1997.
[10] D.Mladin, M.Mladin, M. Preda, I. Prisecaru, Multiple aspects of raw data collection and processing for Romanian TRIGA SSR, Nuclear Engineering and Design 240 (2010) 1630–1643.
[11] *A. Swain,* Human Reliability Analysis, Training seminar course documentation, nov. 1993.
[12] ***, IAEA Workshop on HRA - Human Reliability Analysis in PSA, Budapest, Hungary, may, 1996.
[13] ***, IAEA Safety Series no. 35. Initiating Events at Research Reactors.
[14] S. Litonin, GUITHARE user dictionary: pre and post-processing guide, DTS/OCC/ OC2D07043/003/V0M2 OC2D07043, 2009.
[15] M. Mladin, Analiza accidentelor de tip LOFA şi LOCA la reactorul SSR, (INR's archives, in romanian language), RI 6806, SCN-Piteşti, 2003.
[16] D. Mladin, I. Prisecaru, Aspects of Probabilistic Safety Assessment for TRIGA Research Reactor, U.P.B Sci. Bull., Seria C, Vol.75, No.1, 2014.
[17] ***, General Atomic, 1980. Results of Romanian TRIGA 14 MW Startup and Commissioning Tests, Arhiva SII SCN Piteşti.
[18] O. W. Hermann, C. V. Parks, SAS2H: A Coupled One-Dimensional Depletion and Shielding Analysis Module, NUREG/CR-0200 Revision 6 Volume 1, Section S2 ORNL/NUREG/CSD-2/V2/R6, 1008.

INVESTIGATING THE SETUP FOR IRRADIATION OF MATERIAL SAMPLES IN TRIGA ROMANIA

M. MLADIN, S.D.DULUGEAC, G.A.BUDRIMAN
Reactor Phys., Nucl. Safety & Fuel Performance Dept., Institute for Nuclear Research
Campului, 1, 115400 Mioveni, Romania

M. CIOCANESCU, D. BARBOS
Reactor Dept., Institute for Nuclear Research
Campului, 1, 115400 Mioveni, Romania

ABSTRACT

The two TRIGA reactors, a 14 MW Steady State and a pulsed reactor sharing the same pool, represent the main nuclear installation at the Institute for Nuclear Research in Pitesti. The Steady State Reactor (SSR) was used for fuel and material testing in dedicated irradiation devices as well as for neutron physics methods. One its current utilization directions implies the irradiation of material samples with temperature level and flux integral prescribed and sometimes with temperature gradient constraints. The paper presents, as an example, the preliminary neutron physics and thermal calculations for the setup of generic detectors irradiation inside a dedicated capsule. Shielding was considered in order to reduce the thermal flux in some of the detectors which are mixed with unshielded detectors, sharing common holders. Geometrical dimensions and energy deposited by nuclear radiation in the materials investigated is calculated for coping with thermal constraints without any external heating. Also, it illustrates the approach for the neutron physics and thermal calculation of iron samples in TRIGA at a prescribed temperature and up to a defined irradiation limit.

1. Introduction

TRIGA Romania facility includes two independent cores sharing the same pool: a 14 MW steady state research and materials testing reactor (SSR) and an operationally independent pulsing reactor (ACPR) which can deliver pulses with a peak power up to about 20000 MW and with an energy release of about 100 MJ. Fig 1 shows a cross section through the pool and biological protection, giving some indications about the two reactors and their associated devices.

Inside the SSR core, a capsule for irradiation of structural materials was accomodated and is planned to be operated up to a fast fluence (E>1 MeV) of ~10^{21} cm^{-2}. This capsule, called C5, contains Zr–2.5%Nb CANDU pressure tube samples in a gas medium and functions at about 270 °C [1].

This paper focuses on investigating the possibilities to reach prescribed values of fast flux integral, temperature and temperature gradients in silver-ceramic detectors with and without shieding to thermal neutrons, and fast fluence and temperature in iron samples, in capsules that preserve many of the material and geometry characteristics of the present C5 capsule. Both types of irradiation experiments pertain to the fussion technology research needs.

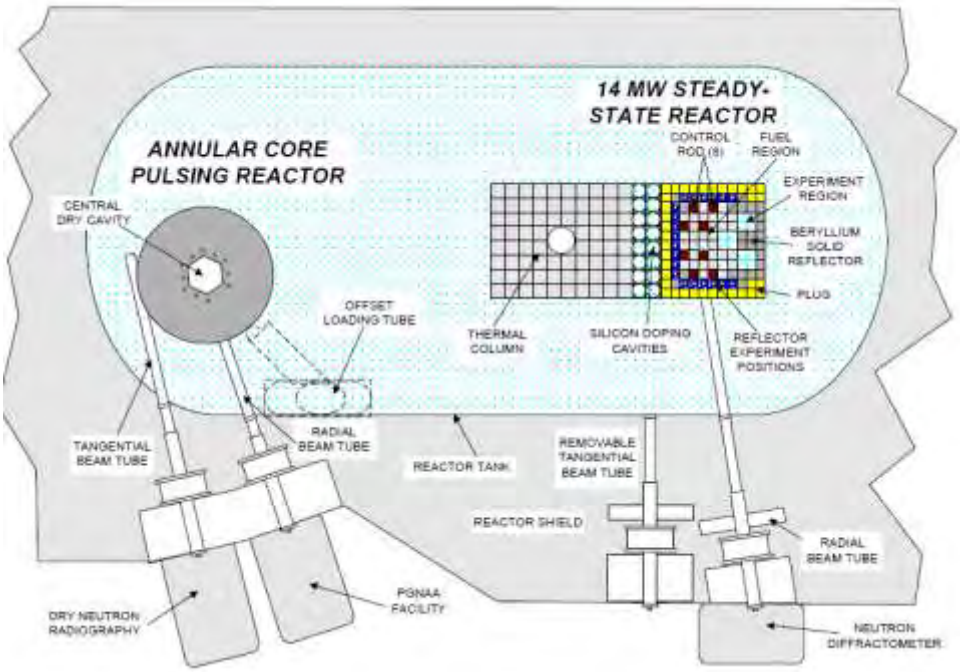

Fig 1. Schematic view of the TRIGA Romania reactors.

2. Calculation of detectors

Neutronic calculations were done with MCNPX [2] on the TRIGA SSR core model that includes a Capsule containing 3.2 x 0.7 x 4 cm detectors composed of silver on a Al_2O_3 base to determine the neutron and gamma heating in the materials. The arrangement inside the capsule included both detectors covered by Ag-In-Cd and detectors without shielding, with Aluminium holders and immersed in Helium, as revealed by the detail of modeling in Fig 2. The neutronic calculation yields the group fluxes and the heating in the location chosen and at a reactor power level (10 MW) that allows fulfilling the requirements for other experiments simultaneous with the Capsule. For a requested total flux integral of 2.34E+20 cm^{-2} , the detectors would need roughly one month of reactor operation at 10 MW.
Thermal modeling is performed with HEATING [3], nodalization of a shielded detector inside the Capsule being shown in Fig 3. It is a R-Z cross section through a R-Θ-Z model with convective boundary condition towards pool water at the outer face of the steel tube of the Capsule. Heat sources for the model resulted from a MCNP coupled neutron-photon run are given in Tab 2. Gamma heating includes prompt, capture and delayed contributions. Typical standard deviation in neutron heating tally is 1% while in gamma tallies is 0.5%. In case of Ag-In-Cd, the neutron heating tally is the major contribution to the heating source. Since there is no external heating, the temperature level and the temperature distribution across the height of the detector can be designed only using the two gap regions and the height of the lower foot of the Aluminium holder, all visible in Fig 3. The order of magnitude for these gap regions is 10^2 μm.
As an example,the thermal constraints are:
-temperature more than 100 °C but not higher than 250 °C;
-existence of a 10-100 °C temperature drop on a direction orthogonal to the neutron current in the detector.
Fig 4 presents the results for two independent arrangements. The one described as “mixed” reflects the schematics in Fig 2, where shielded and unshielded detectors (called “Device Under Testing” or DUT) coexist, sharing the same Aluminium holders, while the arrangement called

“simple” can be a separate axial region with unshielded detectors. The gap regions in these two cases are different and were searched for in order to have a good match of the temperature in unshielded detectors between “mixed” and “simple” arrangements.

Tab 1. Neutron flux in shielded and unshielded detectors in TRIGA (G4 at 10 MW at axial core mid-height) vs. their lifetime conditions.

Energy domain	ITER	TRIGA (Ag-In-Cd)	TRIGA
0. - 0.5 eV	2.03E+11	4.23E+12	1.27E+13
0.5 eV - 1 MeV	1.14E+13	6.06E+13	6.37E+13
> 1 MeV	2.52E+12	1.96E+13	1.96E+13
Total flux ($cm^{-2}s^{-1}$)	1.41E+13	8.45E+13	9.60E+13

Tab 2. Heat source density inside the Capsule for irradiation of detectors at 10 MW in G4 at axial core mid-height.

Material	Heating density ($cal \cdot sec^{-1} \cdot cm^{-3}$)
Al	0.47
Al2O3	0.92
SS	1.73
Ag(80)-In(15)-Cd(5)	13.20

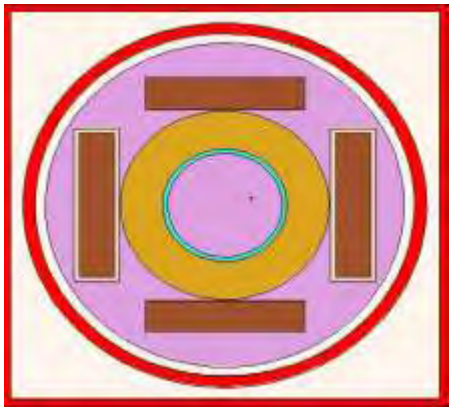

Fig 2. Detail of the neutron physics model of the Capsule accomodating the detectors.

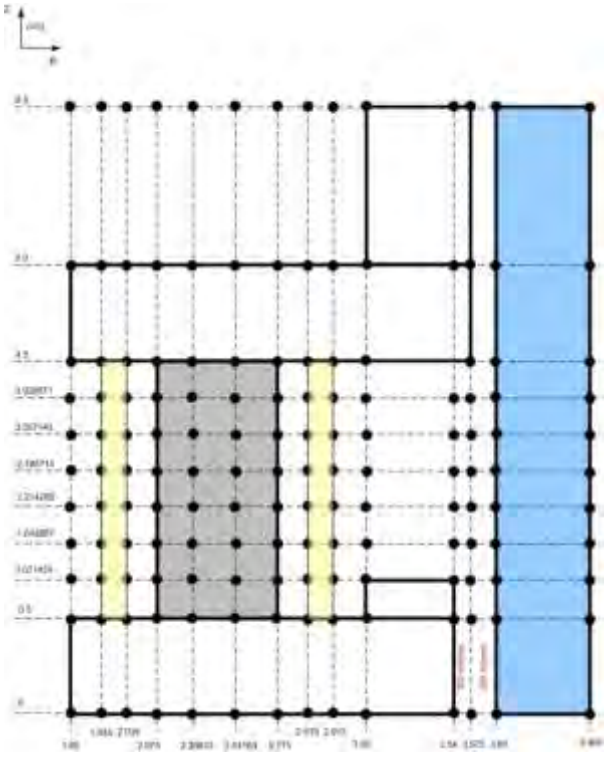

Fig 3. Example of nodalization of the heat conduction model for a covered detector inside the Capsule.

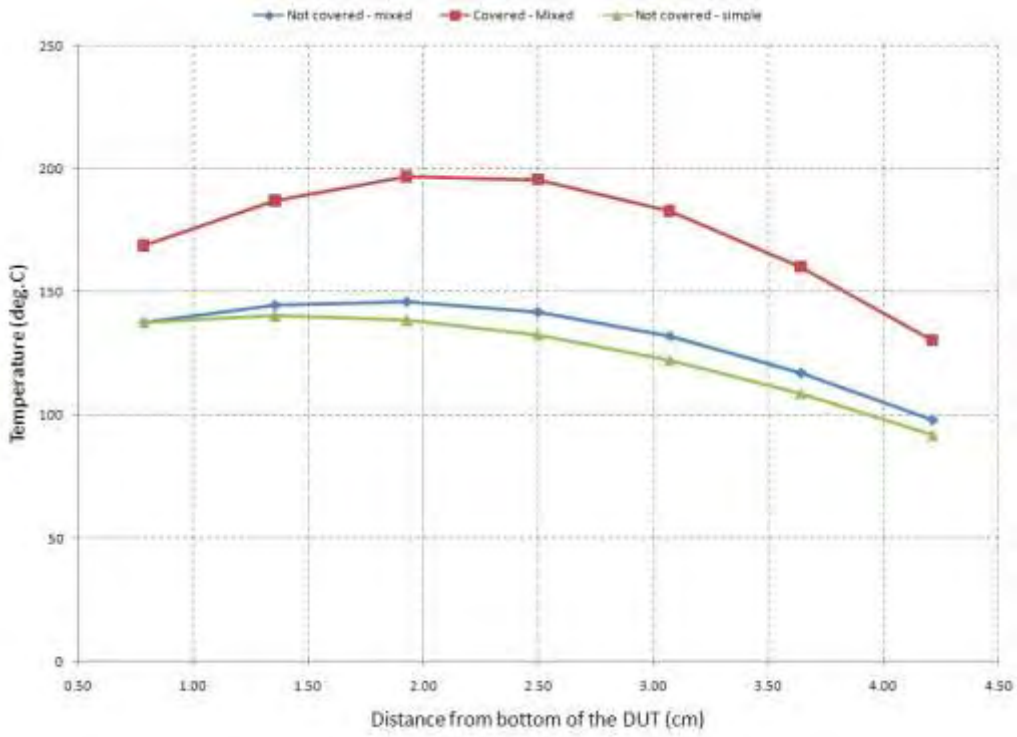

Fig 4. Temperature distribution in shielded and unshielded detectors sharing the same Aluminium holder and unshielded detectors in independent holders. Different gap sizes to match the temperature in unshielded detectors in the two arrangements.

2. Design of the iron samples irradiation

The arrangement of the Eurofer samples is quite complex, with different geometries of the samples at different floors (or axial regions inside the Capsules). A generic example for samples arrangement is provided in Fig 5. There are two different Capsules in grid positions G4 and E4, respectively (see Fig 6). The main difference between the two Capsules is the required temperature of the samples, 500 °C and 300 °C (± 50 °C), which requires holders made of different materials (i.e. Stainless Steel and Aluminium). Design of the gap thickness (between the surrounding holder and the steel tube of the Capsule) is also necessary in each case in order to obtain the targeted temperatures.

There are requirements related to extent of irradiation up to 2 DPA (or Displacement per Atom). As a first calculation, the irradiation time for the TRIGA Romania neutron spectrum (see Fig 7) inside a generic steel and gas Capsule located in G4 was obtained using the SPECTER [4] code for Stainless Steel as material. Flux input was calculated on a 96 group structure with detailed groups in the fast domain. The result is dpa 0.54 for stainless steel for one year of irradiation (200 operation days/year considered) at 10 MW reactor power level. The reactor power level is dictated by another experiment with fixed location (also visible in the core configuration presented as Fig 6). Hence, a potential project would require up to 4 years of irradiation in TRIGA Romania.

Calculations follow the same methodology: MCNPX for determining the heat source and HEATING to calculate the temperatures and design the gap thickness. Because of the complexity of the setup, homogenization of samples into rings is necessary to obtain an R-Z model of the Capsule.

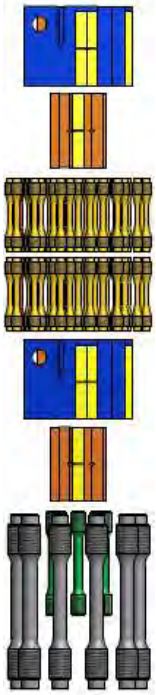

Fig 5. Example of iron samples setup inside irradiation Capsule.

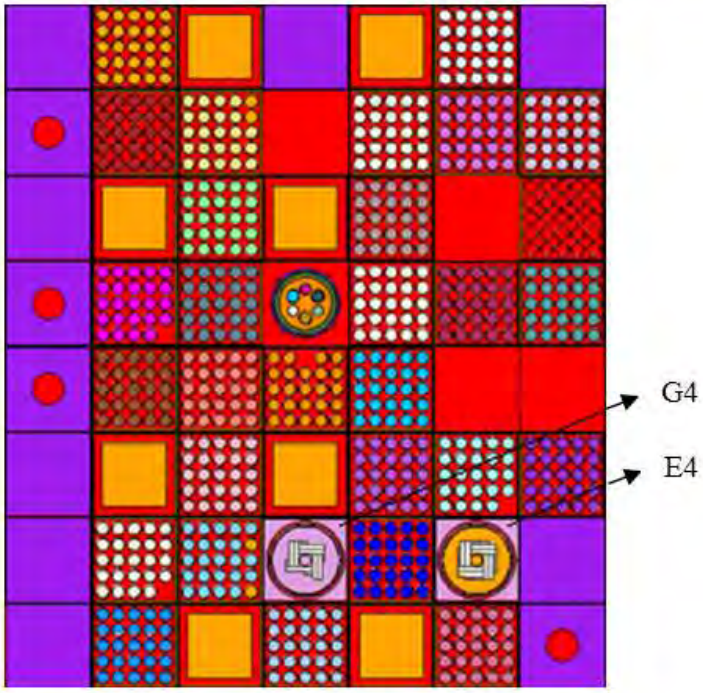

Fig 6. Core configuration with two Capsules, at 500 °C and 300 °C for iron samples irradiation (in G4 and E4, respectively).

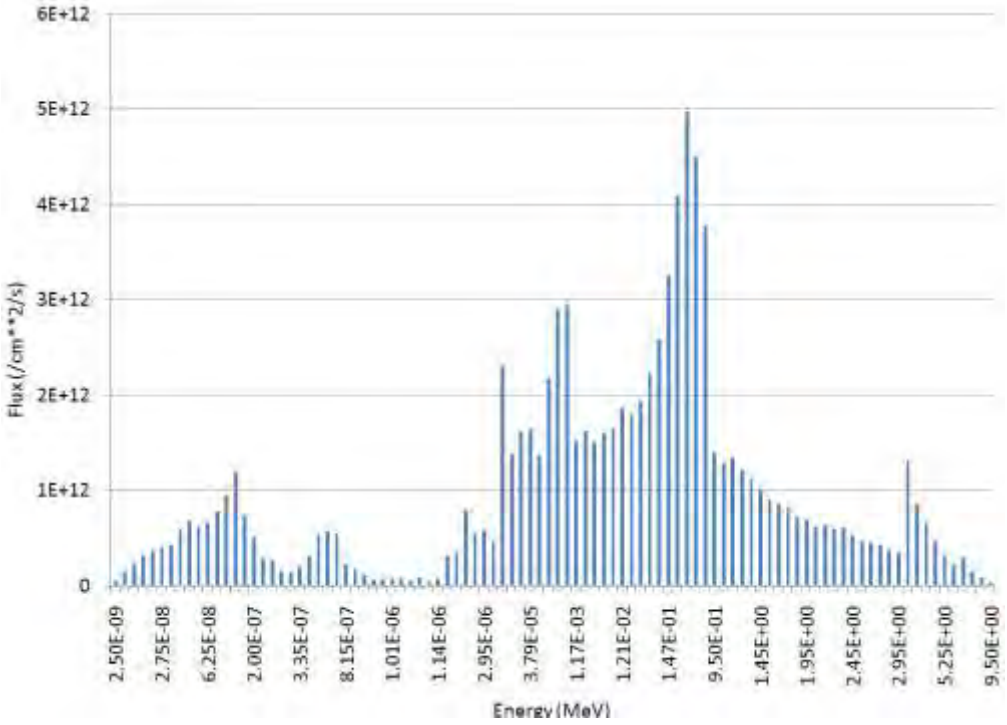

Fig 7. Neutron spectrum in steel inside a steel-gas capsule in TRIGA Romania (located in G4 grid position).

5. References

[1] Gh. Negut, M. Ancuta et al. - The irradiation effects on zirconium alloys, Journal of Nuclear Materials, 2007.
[2] Denise B. Pelowitz, editor - MCNPX™ USER'S MANUAL Version 2.6.0 April 2008.
[3] K. W. Childs - HEATING 7.2 User's Manual, NUREG/CR-0200 Rev. 6
Vol. 2, Sect F10, ORNL/NUREG/CSD-2/V2/R6
[4] L.R. Greenwood, R.K. Smither – SPECTER: Neutron Damage Calculations for Material Irradiation, ANL/FPP/TM-197.

STUDY OF MOLYBDENUM-99 PRODUCTION POSSIBILITIES IN TRIGA 14 MW REACTOR

S.D.DULUGEAC[(1)], M. MLADIN[(1)], G.A.BUDRIMAN [(1)]

Reactor Phys., Nucl. Safety & Fuel Performance Dept., Institute for Nuclear Research
Campului, 1, 115400 Mioveni, Romania
stefan.dulugeac@nuclear.ro

ABSTRACT

Molybdenum production can be a solution for the future in the utilization of the Romanian TRIGA, taking into account the international market supply needs.Techetium-99m ($T_{1/2}$ = 6.02 h) is currently the most used radio-nuclide in nuclear medicine procedures in developing countries. It labels a number of radiopharmaceuticals to assist the diagnosis of problems in different parts of the human body including heart, brain, liver, lungs, kidneys, bone, thyroid, etc. ^{99m}Tc has unique physical and nuclear properties which gives low radiation exposure to patients, high quality imaging and reliable availability in the form of ^{99}Mo/ ^{99m}Tc generators. Currently, ^{99m}Tc is exclusively produced from the decay of its 66h half-life parent Molybdenum-99.
There are two main methods to produce ^{99}Mo/^{99m}Tc in a nuclear reactor:

-Fission of an Uranium target. Producing the ^{99}Mo radioisotope by fission implies high neutron fluxes, expensive processing facilities for handling the fission products of Uranium, and creates important nuclear waste radioactivities. Neutron physics parameters are determined and presented, such as: thermal flux axial distribution for the critical reactor at 10 MW inside the irradiation location; reactivity introduced by three Uranium foil containers; neutron fluxes and fission rates in the Uranium foils; released and deposited power in the Uranium foils; Mo^{99} activity in the Uranium foils. The aim of the thermal-hydraulic analysis was to determine the flow rate, the outlet-inlet temperature difference through the irradiation device and the radial temperature distribution.

-Irradiation of a natural or ^{98}Mo enriched target, method called the neutron activation production method. It leads to low specific activities of ^{99}Mo and also low waste activities, and does not require expensive handling facilities. The calculations are performed with MCNP, searching the locations of the targets in setups that maximize the ^{99}Mo production in the present TRIGA core configuration. Calculations are done both with natural metallic Molybdenum pellets and with enriched pellets.

1. Introduction

Nuclear reactors are used for producing more than 40 activation products and 5 major fission product medical radioisotopes (I^{131}, Xe^{133}, Sr^{89}, Y^{90} and Mo^{99}). Concerning molybdenum, a target is typically irradiated for 5-7 days to reach optimal Mo^{99} production level (around 71-82% of saturation concentration) [1].
Technetium-99m is the primary medical radioisotope used today for performing diagnostic imaging procedures. 85% of all medical radioisotope procedures use Tc^{99m} and it is used in more than 30 radiopharmaceuticals.Technetium-99m is the radioactive daughter product of molybdenum-99. Tc^{99m} has a short half-life (6 hrs.) and emits a low-energy gamma ray (140 keV). It is readily “tagged” to a pharmaceutical that transports it to the location of interest in the body [2]. Generally two different techniques (Fig.1) are available for molybdenum-99 production for use in medical technetium-99 generation. The first one is based on neutron irradiation of molybdenum targets of natural isotopic composition (24.13% Mo^{98} abundance) or enriched in molybdenum-98. In these cases the Mo^{99} is generated via the nuclear reaction $Mo^{98}(n,\gamma)Mo^{99}$. Although this process can be carried out at low expenditure it gives a product of low specific activity and, hence, restricted applicability.

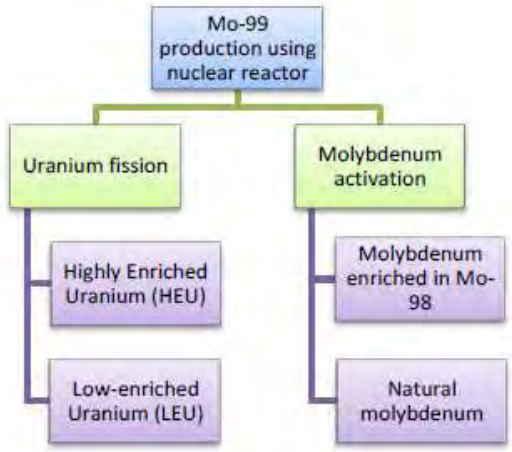

Fig.1. Summary of reactor-based Mo^{99} production technologies[1]

Two types of fission targets are in use today: highly enriched uranium (HEU) typically containing more than 90 wt% of U^{235} and low-enriched uranium (LEU) with less than 20 wt% of U^{235}. However, an international effort is currently underway to reduce and eventually eliminate the use of HEU targets given that they contain weapon-grade uranium [1].

In a second process (Fig.2) Mo^{99} is obtained as a result of the neutron induced fission of U^{235} according to $U^{235}(n,f)Mo^{99}$. For U^{235}, the thermal cross section is σ_f = 580b and the cumulative yield of Mo^{99} is 6.13% of fission product. This technique provides a product with a specific activity several orders of magnitude higher than that obtained from the $Mo^{98}(n,\gamma)Mo^{99}$ nuclear reaction and perhaps even more important up to several thousands curies of Mo^{99} per production run[3]. Neutron-activation methods of production can get up to 10 curies per gram of Mo in a target. From fission products in nuclear reactors the specific activity can be upwards of 10^4 Ci/g.

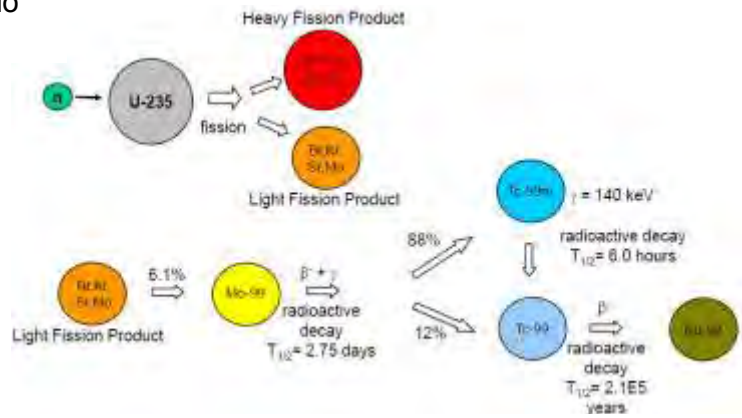

Fig.2. Diagram of Mo^{99} obtained from reaction $U^{235}(n,f)Mo^{99}$ [2]

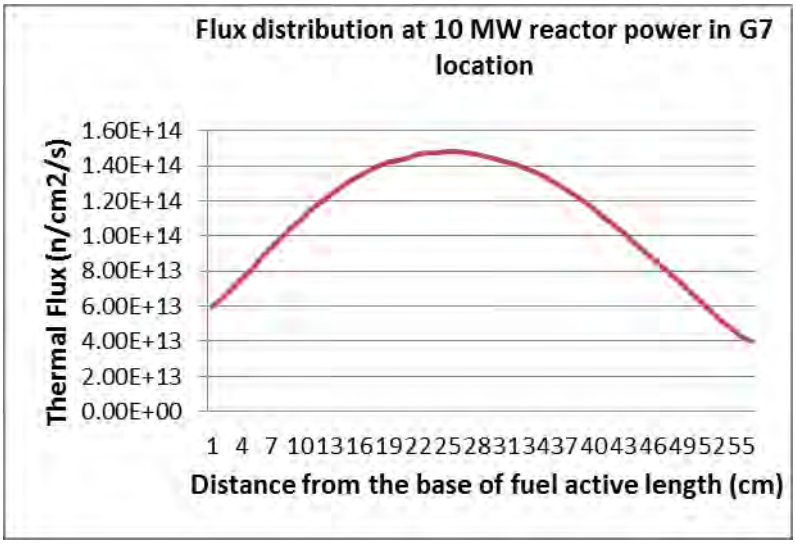

Fig.3. Axial thermal flux distribution for the critical reactor at 10 MW, Xe^{135} accumulated

The calculations use the MCNP[4] model of the TRIGA Steady State reactor, representing the current core configuration. The reactor core is composed of 29 LEU fuel bundles, each having its specific burnup resulted from MCNPX v2.6.0 core calculations.

Calculations were done at 10 MW reactor power with Xe^{135} fission product poison accumulated. The average fuel and Uranium foils temperature was considered 500K and 400K, respectively.

Control rods position (in bank) at criticality was calculated at 70% extraction length; this position will determine the axial neutrons flux distribution inside irradiation location. In these conditions, calculations were launched with the irradiation device introduced in G7 (irradiation location). The resulted axial thermal flux distribution is given in Fig.3.

2. Neutron activation method

The yield of Mo^{99} from the $Mo^{98}(n,\gamma)Mo^{99}$ reaction significantly depends of the energy spectrum of the neutron flux. The aim is to produce neutrons at the right energy, or make use of the epithermal neutrons, to get a high capture probability in Mo^{98}. This works best at large capture cross section values corresponding to resonances in Mo^{98} (Fig.4).
Unfortunately, its resonance peaks in the epithermal energy region are not productively used in water cooled reactors because fission neutrons are quickly moderated (usually by water) to thermal energies, missing the resonances, meaning a lower probability of capture.
In all cases that will be described, we used ENDFB-VII nuclear data for both Mo and isotopes entering the reactor composition zones.

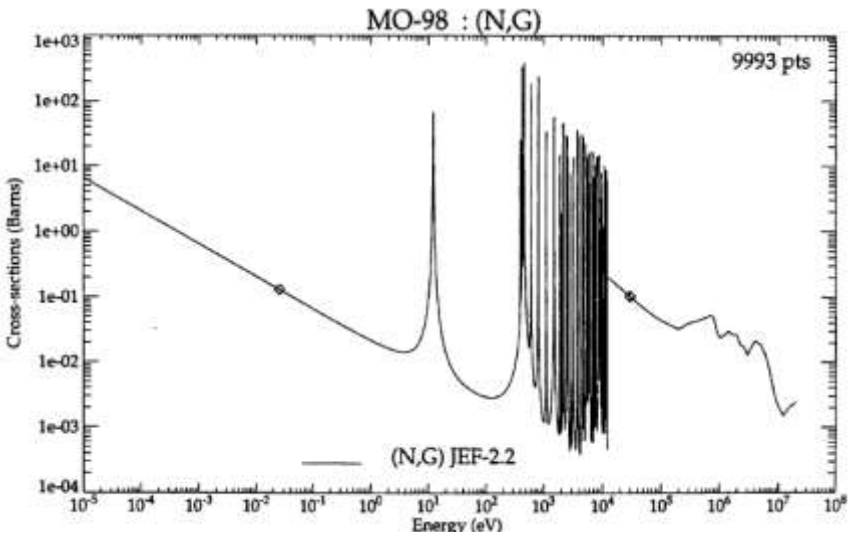

Fig.4. Cross section for neutron capture in Mo^{98} showing the resonance peaks[6]

2.1 Influence of the material surrounding the target

Different materials were studied inside the experimental location: beryllium, water, graphite, silicon, nickel. Tab.1 presents a synthesis of these results. Normalization was done to the maximum Mo^{99} activity obtained for natural Mo with beryllium around the capsules containing the pellets.

Beryllium	Water	Graphite	Silicon	Nickel
1.00	0.90	0.87	0.80	0.71

Tab.1. Relative effect of different materials surrounding the target on the Mo^{99} activity

2.2 Influence of target composition and geometry

The results in Tab.1 point to beryllium and water as the best shield materials. There are two types of geometrical arrangements inside the capsule: 40 pellets placed along the z axis (Fig.5) and 181 pellets perpendicular to the z axis (Fig.6).

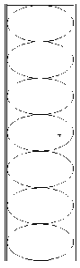

Fig.5. Setup for 40 pellets inside a capsule

Obviously, the largest total activity is in cases with 181 pellets inside one pin because of the larger mass of Mo^{98} in these cases. For beryllium around the pins, the total activity for the 98% Mo^{98} enriched pellets is lower than the corresponding activity with water, contrary to the natural Mo targets, where the maximum is reached with beryllium. This is due to the larger contribution of thermal flux, in water, for enriched pellets compared to natural Mo, coming from lack of absorbent isotopes of natural Mo other than Mo^{98} (Mo^{95}, Mo^{97}).

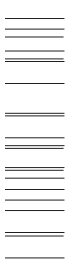

Fig.6. Setup for 181 pellets inside a capsule

The contribution of thermal, epithermal and fast regions of the neutron spectrum to Mo^{99} activity is illustrated by $Mo^{98}(n,\gamma)Mo^{99}$ reaction rate (Fig.8 through Fig.10). Fig.8 represents the reaction rate for natural Mo with water in location with 40 pellets inside a pin, while Fig.9 is 98% enriched in the same conditions. The absolute magnitude of the reaction rate in the natural Mo case is lower because of the lower atom density of Mo^{98}, and the contribution of

the thermal region to the total reaction rate is less important in the case with natural Mo. On the other hand, Fig.10 shows that in beryllium, the epithermal contribution is largely dominant because moderating properties of beryllium are not so good, the thermal flux being much lower than in water.

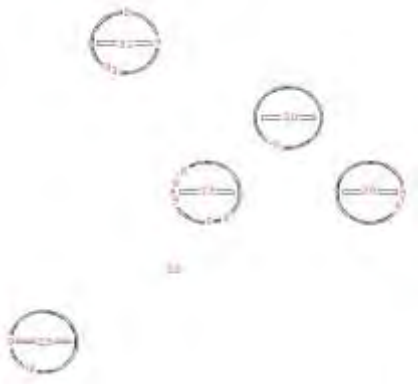

Fig.7. Placement of pins containing Mo (materials 25,28,29,30,31) in the experimental location

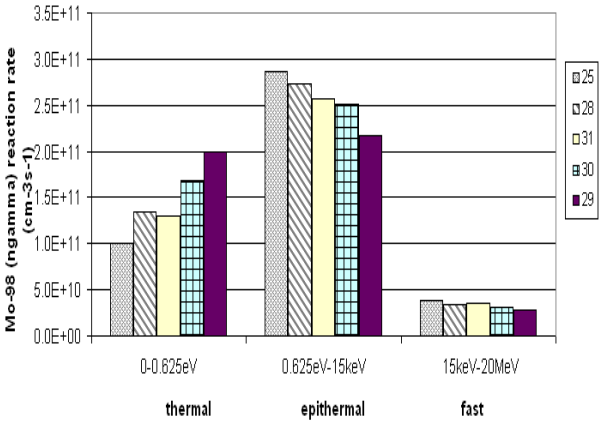

Fig.8. $Mo^{98}(n,\gamma)Mo^{99}$ avrg. reaction rate in natural Mo with water in location

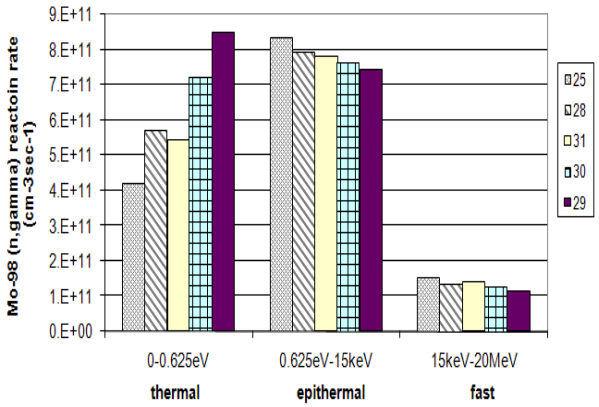

Fig.9. $Mo^{98}(n,\gamma)Mo^{99}$ avrg. reaction rate in 98% enriched for individual pins with water in location

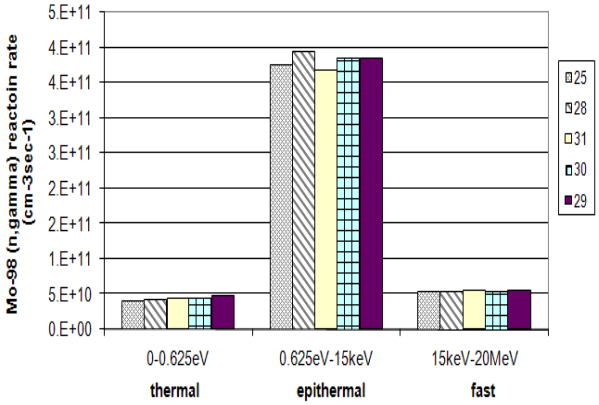

Fig.10. $Mo^{98}(n,\gamma)Mo^{99}$ avrg. reaction rate in natural Mo with beryllium in location

2.3 Influence of pin placement inside the experimental location

It can be seen (Tab.2) that the maximum activity position in the 24% ^{98}Mo in beryllium case is the corner of a TRIGA bundle followed by the center (Fig.7). For the case with 98% Mo^{98} in water, the center of the bundle is the best position followed by the corner position.

In the first calculated case (98% Mo^{98} in water) we obtained a total (5 pins) Mo^{99} activity of 623.1Ci, an activity per cubic centimeter of pellets equal to 30.73 Ci/cm^3, and a mass activity of 3.27 Ci/g Mo^{98}. In the second case (natural Mo in beryllium) we obtained a total (5 pins) Mo^{99} activity of 209.3Ci, an activity per cubic centimeter of pellets equal to 10.31Ci/cm^3 and a mass activity of 4.46 Ci/g Mo^{98}.

Material		Mat25 (corner)	Mat28 (edge-center)	Mat29 (center)	Mat30 (intermediate, 2nd row)	Mat31 (edge-corner)
H2O, 98% enrich.	Reaction rate (cm^{-3}s^{-1})	1.52E+12	1.32E+12	1.62E+12	1.36E+12	1.48E+12
	Activity (Ci)	129.	113.	139.	116.	126.
Be, 24% enrich.	Reaction rate (cm^{-3}s^{-1})	5.261E+11	5.13E+11	5.21E+11	4.74E+11	4.11E+11
	Activity (Ci)	45.1	43.8	44.5	40.5	35.2

Tab.2. Reaction rates and activities for 98% Mo^{98} pins in water and natural Mo in beryllium

2.4 Different irradiation times; corrected Mo^{98} thermal cross-section

All the results presented were calculated at 6 days irradiation time. This duration can easily be changed to obtain the activity knowing the reaction rate, using the formula[6]:

$$\Lambda = R(1 - e^{-\lambda \cdot t}) \qquad (1)$$

where:

R – the total (n,γ) reaction rate in Mo^{98} ($cm^{-3}s^{-1}$)

Λ – the Mo^{99} activity

λ – disintegration constant (s^{-1})

t – irradiation time (s)

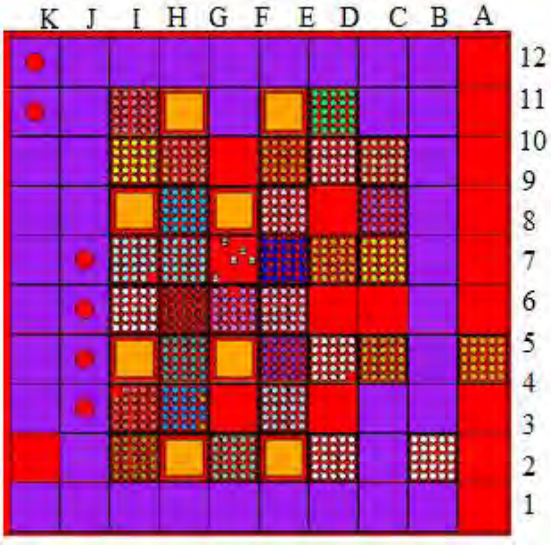

Fig.11. TRIGA core configuration

It is customary to express the irradiation spectrum for producing Mo^{99} by means of a corrected thermal $Mo^{98}(n,\gamma)Mo^{99}$ cross-section that will characterize the location inside the reactor. Thus, knowing the thermal flux, either by measurements or by calculation with a computer code, one can determine the activity of the target using ($N \cdot \sigma \cdot \Phi_{th}$) instead of R in (1). We calculate this corrected cross-section for the XC1 (G7) location inside the TRIGA reactor, in the currently existing core configuration, for 98% enriched Mo in water, and natural Mo in beryllium as:

$$\sigma_{th}^{corr.} = \frac{R}{N \cdot \Phi_{th}} \qquad (2)$$

where N=0.05777002 $barn^{-1}cm^{-1}$ (0.014224469 for natural Mo) is the atomic density of Mo^{98} in the pellets.

Φ_{th} =1.04·10^{14} $cm^{-2}s^{-1}$; R=1.46·10^{12} $cm^{-3}s^{-1}$; 98% Mo-98 in H_2O $\sigma_{th}^{corr.}$ = 0.242 b

Φ_{th} =4.99·10^{13} $cm^{-2}s^{-1}$; R=4.88·10^{11} $cm^{-3}s^{-1}$; 24% Mo-98 in Be $\sigma_{th}^{corr.}$ = 0.687 b

The 2200 m/s cross section for the $Mo^{98}(n,\gamma)Mo^{99}$ reaction is about 0.13 b. The larger is the corrected cross-section, the higher is the contribution to the total reaction rate of neutrons above 0.625 eV.

3. Fission method

3.1 Neutronic analysis

Molybdenum irradiation device is located in the grid position labeled G7 and its modelling appears in Fig.12 as well as in Fig.13, which gives a radial cut through the device, and in Fig.14, showing the materials arrangement inside one of the three Uranium foil containers.The target irradiation system (Fig.13 and Fig.14) is formed by a LEU (19.75% enriched in U^{235}) metallic uranium foil of 9 grams, 125 microns thick, wrapped in a thin (15 microns) nickel fission product-recoil barrier. The metallic uranium foil with its nickel coating surrounds an aluminum tube of 152 mm in length, 27.91 mm outer diameter and 26.44 mm inner diameter. This set, as well, is surrounded by an aluminum tube of 28.22 mm inner diameter, 30 mm outer diameter and 152 mm in length. The foil containers are vertically placed with no space between two containers, the middle one being located at the middle height of the TRIGA fuel column (active fuel length is 55.88cm).

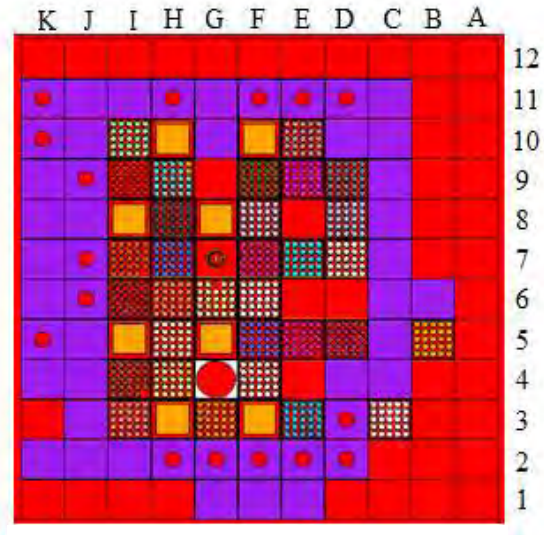

Fig.12. MCNP model of TRIGA SSR (with MCNP Visual Editor)[7]

3.1.1 Reactivity introduced by experiment

The positive reactivity introduced by the irradiation device with three foil containers was obtained by calculating the reactor with and without the irradiation device and foil containers. The resulted reactivity worth is +0.495±0.031$.

3.1.2 Neutron fluxes and fission rates in the Uranium foils

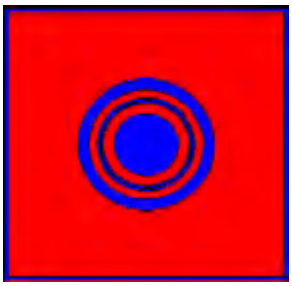

Fig.13. Radial cut through the irradiation device

Three groups neutron fluxes and fission rates were requested as tallies using the f4:n tally type in MCNP (flux averaged over a cell). Fluxes were calculated inside each of the three Uranium foils and also in exactly the same location (cell) but without the irradiation device, with water inside the experimental location. Tab.3 presents the groups boundaries and the fluxes together with their corresponding standard deviation.

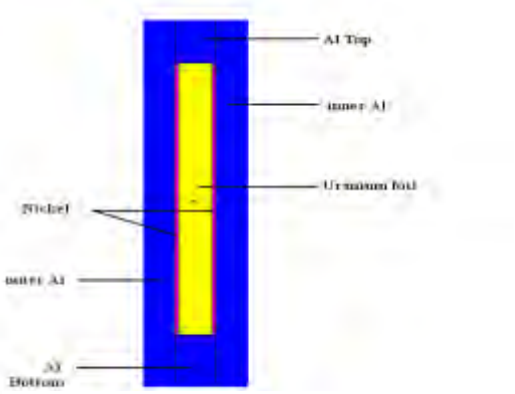

Fig.14. Axial view of one Uranium foil container

Group	Energy domain	Foil 1 ($cm^{-2}s^{-1}$)	Foil 1* ($cm^{-2}s^{-1}$)	Foil 2 ($cm^{-2}s^{-1}$)	Foil 2* ($cm^{-2}s^{-1}$)	Foil 3 ($cm^{-2}s^{-1}$)	Foil 3 ($cm^{-2}s^{-1}$)	Average standard deviation (%)
1	0eV-0.625eV	1.103E+14	1.811E+14	1.243E+14	2.049E+14	6.959E+13	1.134E+14	0.70
2	0.625e-0.5MeV	7.905E+13	6.031E+13	9.146E+13	7.014E+13	5.239E+13	4.010E+13	0.96
3	0.5Me-20MeV	7.882E+13	3.026E+13	9.146E+13	3.403E+13	5.070E+13	2.017E+13	1.27

Tab.3. Calculated fluxes in foils (foil1 in lowermost axial position) and water (*) normalized to 10 MW reactor power. The average standard deviation is the average over individual group values

Tab.4 presents the calculated fission reaction rates.The thermal flux is larger in water, when the irradiation device is not present. The fast flux is increased in the foils by their own fission reactions.The effect of control rods position on the foils thermal flux and fission rate is apparent in the ratio between foil1 and foil3. Power density in foil1 (the lowermost) is about 37% more then in foil3 (the uppermost). The power load is maximum for foil2.

Group	Energy domain	Foil 1 - ($cm^{-3}s^{-1}$)	Foil 2 - ($cm^{-3}s^{-1}$)	Foil 3 - ($cm^{-3}s^{-1}$)	Average standard deviation (%)
1	0eV - 0.625eV	4.636E+14	5.219E+14	2.906E+14	0.71
2	0.625eV – 0.5MeV	1.124E+13	1.285E+13	7.281E+12	1.77
3	0.5MeV - 20MeV	1.894E+12	2.205E+12	1.225E+12	1.23
	total	4.768E+14	5.370E+14	2.991E+14	0.70

Tab.4. Calculated fission rates in Uranium foils (foil1 in lowermost axial position) normalized to 10 MW reactor power. The average standard deviation is the average over individual group values

3.1.3 Released and deposited power in the Uranium foils

The released power was calculated using the fission rate and the energy recovered from fission, the latter being reported by MCNPX and considered adequate for water reactors with U^{235} (ε=201.7 MeV). The resulted released power values generated by each foil are:

P_{Foil1} = 7386.63 W; P_{Foil2} = 8320.06 W; P_{Foil3} = 4634.57 W

The deposited power inside the irradiation device is relevant for safety analysis. It was calculated in a neutron-photon transport problem, requesting energy deposition tallies for both neutrons and photons: F6:n, F6:p and F7:n. The deposited energy is a sum of different heating contributions inside each material:

Container no.	Power in Foil (W)	Fraction from released power	Power in Al (W)
1	6666.43	0.9025	522.92
2	7510.11	0.9026	591.26
3	4186.40	0.9032	366.27

Tab.5. Calculated deposited power in the Uranium foils and Aluminium for the three containers (container 1 in the lowermost axial position) normalized to 10 MW

$$H = H_{fp} + H_n + H_{\gamma_p} + H_{\gamma_d} + H_\beta \quad (3)$$

where: H_{fp} is due to fission products; H_n is due to neutrons; H_{γ_p} is due to prompt gammas; H_{γ_d} is due to delayed gammas; H_β is due to betas.

No MCNP tallies account for betas and delayed gammas, but these two contributions were scaled from conventional tallies as described in [5] for calculating deposited power in Uranium foils. The resulted deposited power in the Uranium foils and in the Aluminium for the three foil containers are given in Tab.5. The deposited power in the three Uranium foils seems to be 10% less than the released power. Standard deviation in both thermal fission rates and individual heating tallies is about 0.7%. The reason for the difference between released and deposited power lies in the very small gamma heating to total heating ratio (illustrated roughly by the f6:p/f7 ratio, equal to 0.006). There is a large escape probability of the gammas emitted inside the foil which can deposit their energy in the surrounding TRIGA fuel, while the foil offers a very small volume for interactions with the gamma flux in the reactor. Concerning the Aluminium in the irradiation device, an average of 1.34 W/g at 10 MW reactor power results from the calculation.

3.1.4 Mo^{99} activity in the Uranium foils

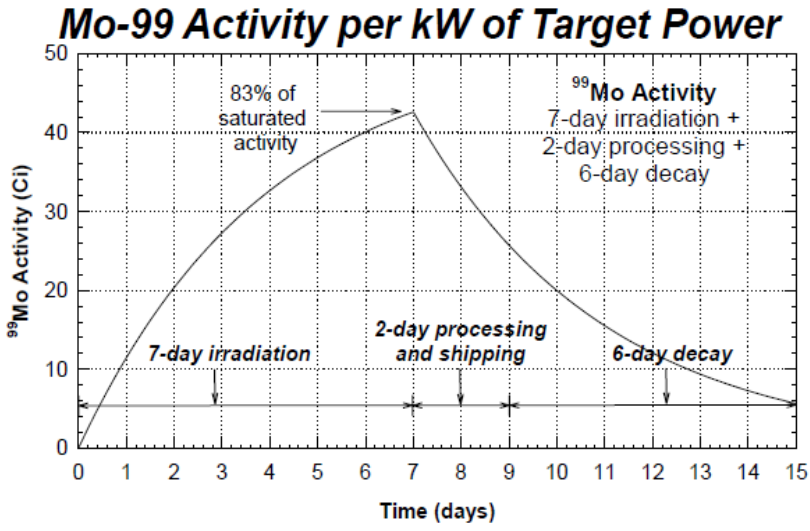

Fig.15. Mo^{99} activity per KW of target power[2]

The Mo^{99} activity as a function of the irradiation time t_i can be found from the formula:

$$\Lambda = \frac{\gamma \cdot V \cdot R_f \cdot (1 - e^{-\lambda \cdot t_i})}{3.7 \cdot 10^{10}} \quad (4)$$

where:
Λ - Mo^{99} activity (Curie)
γ - Mo^{99} fission yield (6.1%)
V – Uranium foil volume (cm^3)
R_f - fission rate ($cm^{-3}s^{-1}$)
Λ - Mo^{99} disintegration constant (2.91729E-06 s^{-1})
t_i -irradiation time (s)

Once the irradiation is over, the target is cooled for approximately 12-24 hours and then transported into the processing plant. Using data from Tab.4 for the fission rates of the foils at 10 MW reactor power, the following were obtained for each foil:
- the total Mo^{99} activity of each foil (Fig.16)
- the Mo^{99} activity per gram of Uranium present initially (Fig.17)
- the Mo^{99} activity per gram of U^{235} present initially (Fig.18)

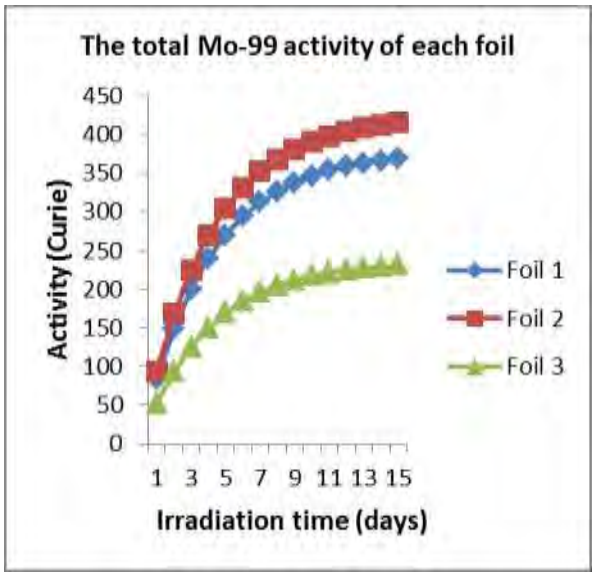

Fig.16. The total Mo^{99} activity in each of the three foils (foil1 in lowermost axial position) normalized to 10 MW

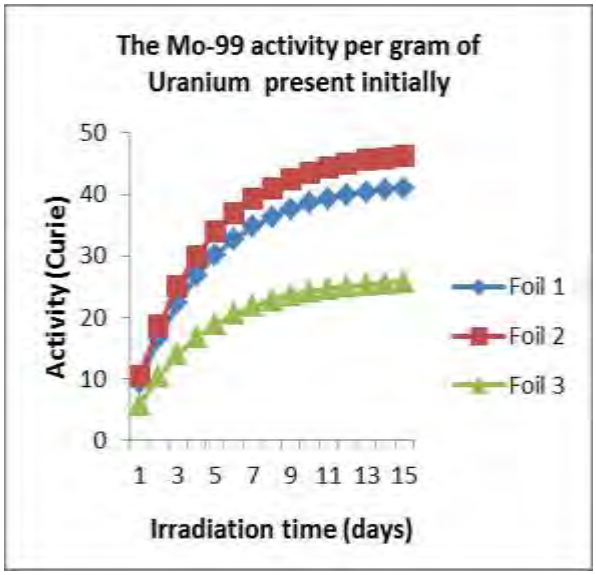

Fig.17. The Mo^{99} activity per gram of U in each of the three foils (foil1 in lowermost axial position) at 10 MW

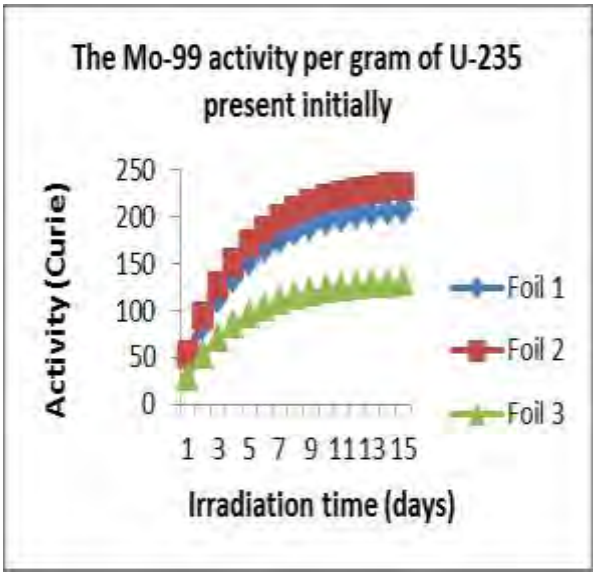

Fig.18. The Mo^{99} activity per gram of U^{235} in each of the three foils (foil1 in lowermost axial position) at 10 MW

3.2 Thermal-hydraulic analysis

The aim of the analysis was to determine the flow rate, the outlet-inlet temperature difference through the irradiation device and the radial temperature distribution. No axial temperature distribution was searched for inside one foil; the input deposited powers calculated in the previous section was provided as 3 values, for the three foils, and the thermal-hydraulic model describes each foil container as a single wall.

3.2.1 Thermal-hydraulic model

The heat producing device with U enclosed in Ni and Al was modelled a series of cylindrical walls (thermal structures) cooled on the internal face by the inner channel and on the external face by the outer channel as in the sketch included as Fig.19. There is a gap with air between the Uranium foil (tightly coated in Nickel) and the inner and outer container Aluminum. Heat is also produced in the central Al tube (radius 1 cm) on the same length and the outer Al wall (external radius 2.1 cm). The later was considered conservatively as being cooled only by the outer channel and not by the bypass channel. The central tube is internal to the inner channel. Two primary pumps are necessary for 10 MW reactor power level. The nominal flow rate given by the two pumps is 660 kg/s (from the reactor operation records).

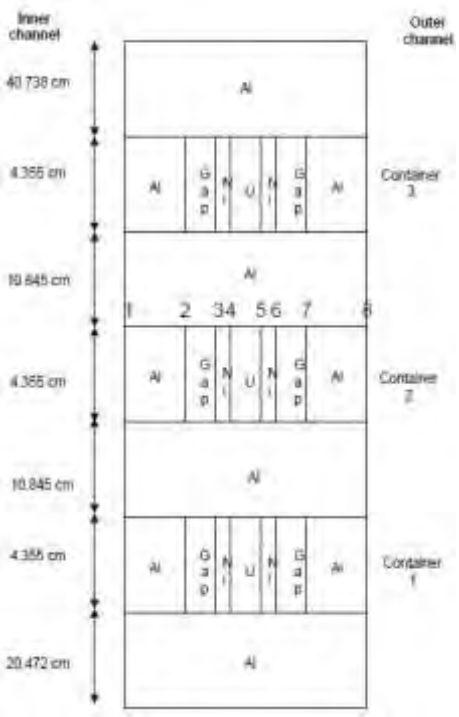

Fig.19. Arrangement of materials inside the wall. Nodes for temperature calculation are indicated

Assuming hypothetical uncertainties in calculating flow rate through the device, a sensitivity study was done also to see the effect of the flow rate on temperature distribution inside the container.

3.2.2 Results: Mass flow rate

The mass flow rates through the channels at nominal flow rate (660 kg/s) through the reactor are: inner channel Q = 1.53 kg/s; outer channel Q = 1.074 kg/s. Therefore, the heat produced by the device is removed by 2.6 kg/s of primary coolant water on a total flow area equal to 7.255 cm^2, while through the average TRIGA channel (1.3594 cm^2) passes 0.88 kg/s.

3.2.3 Results: Water temperature

Inlet water temperature was taken 22°C. The outlet water temperature in the inner channel is 22.72°C, while in the outer channel is 24.3°C. Weighting with their respective mass flow rates, it results an outlet temperature 23.075°C; outlet-inlet temperature difference is 1°C at nominal flow.

3.2.4 Results: Wall temperatures

The foil temperature as a function of gap width (considered as uniform though probably contact points will appear) is presented in Fig.20. There is a strong linear increase of the foil temperature with the gap width, for a 60 μm gap the temperature becomes close to the melting temperature of metallic Uranium (1132°C). The distribution of temperatures in different layers of the second fuel container (maximum power loaded) is presented in Fig.21 for an arbitrary gap width (25 μm).

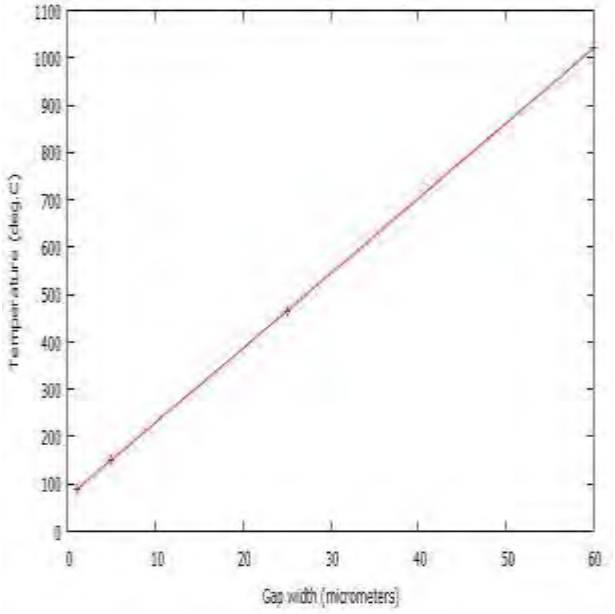

Fig.20. Uranium foil temperature (Foil2) as a function of air gap width

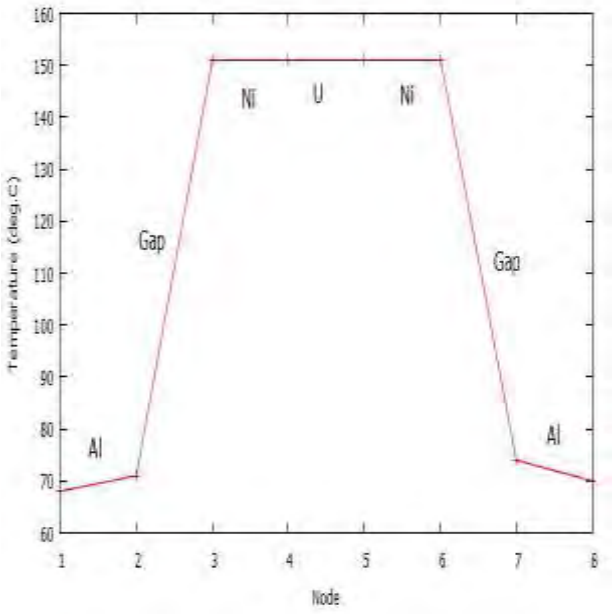

Fig.21.Temperature distribution inside container no.2; arbitrary gap width, 25 μm.

4. Conclusions

The paper focused on MCNP calculations for maximizing the ^{99}Mo activity. Two runs were done for the maximum volumetric and mass activity cases with the MCNP core model in the same arrangements of pins inside the experimental location (central, G7), at 10 MW reactor power level. We obtained, as an average over the pellets of all five pins: 30.73 Ci/cm^3 in the first case and 4.46 Ci/g ^{98}Mo.

All activities were calculated by MCNPX after 6 days irradiation time, but the paper offers the possibility to recalculate the activities for any irradiation time interval by providing the reaction rates for the two core calculations. Also, as a measure of the contribution of neutrons above thermal to the reaction rate, we calculated a thermal neutrons equivalent cross section of ^{98}Mo in each case. We have chosen the upper limit of the thermal energy region as 0.625 eV. Thus, knowing the thermal flux (either measured or calculated) one can easily obtain the reaction rate and consequently the activity in a location inside the core.

Reactor physics studies were done for the TRIGA core at 10 MW including the irradiation device placed in XC1 (G7 reactor core grid position) experimental location. The positive reactivity introduced by the irradiation device with three foil containers was obtained being +0.495±0.031$.

Three group neutron flux at the location of the Uranium foils was calculated, both perturbed (with the device) and unperturbed (without the device, in water). The average value for the perturbed thermal flux over the three foils is $1.01 \cdot 10^{14}$ neutrons/cm^2-s while the maximum thermal flux (foil 2) is $1.24 \cdot 10^{14}$ neutrons/cm^2-s. Fission rate inside the foils was also determined and used in the calculation of the released energy and Mo^{99} activity. The average foil Mo^{99} activity after 7 irradiation days is 286.86 Curie. Deposited power inside the three foils was calculated as a sum of contributions: fission products and betas energies deposited locally, and gammas and neutrons energy deposited as a result of interactions of the transported particles in a MCNP n,p problem. The average deposited power inside one foil is 6.12 kW and the maximum foil power is 7.51 kW. Gamma and neutron energy deposited in Aluminium such as structural material in the targets and irradiation device was also calculated, the average of the deposited power density being 1.34 W/g.

A thermal-hydraulic model was created, using power values inside the irradiation device calculated in reactor physics studies. Containers were modelled as multilayer walls with a variable air gap between the foil coated in Nickel and the aluminium inside the container. A 2.6 kg/s flow rate through the device was calculated at nominal primary circuit flow rate. The foil temperatures strongly increase with air gap width variation from 100^{o}C, for a 1 μm gap, to over 1000^{o}C, for a 60 μm gap. Imposing smaller flow rate values through the device does not affect dramatically the temperatures of the foil. Reducing the flow rate by a factor of three will rise the wet side temperature of the wall from 70^{o}C to 120^{o}C.

5. References

[1] The supply of Medical Radioisotopes: Review of Potential Molybdenum -99/Technetium-99m Production Technologies, Nuclear Energy Agency, November 2010

[2] The Supply of the Medical Radioisotope Tc-99m/Mo-99, Sandia National Laboratories Albuquerque, November 6, 2009

[3] A.A. Sameh, H.J. Ache, Production Techniques of fission Mo^{99}, Institut für Radiochemie, Karlsruhe, Federal Republic of Germany, 1987

[4] D. Pelowitz (editor). MCNPX User's Manual, version 2.6.0, April 2008

[5] F. B. Brown, W. R. Martin, R. Mosteller, Monte Carlo - Advances and Challenges, PHYSOR-2008 Interlaken, Switzerland, 14-19 September 2008

[6] A.I. Ryabchikov, V.S. Skuridin, E.V. Nesterov, E.V. Chibisov, V.M. Golovkov. Obtaining molybdenum-99 in the IRT-T research reactor using resonance neutrons, Nuclear Physics Institute at Tomsk Polytechnic University, 2a, Lenin Av., 634 050 Tomsk, Russia

[7] MCNP/MCNPX Visual Editor Computer Code Manual For Vised Version 22S, Released February, 2008 A.L. Schwarz , R.A. Schwarz, and L.L. Carter

THE 14 MeV NEUTRON IRRADIATION FACILITY IN MARIA REACTOR

R. PROKOPOWICZ, K. PYTEL, M. DOROSZ, A. ZAWADKA, J. LECHNIAK, M. LIPKA, Z. MARCINKOWSKA, M. WIERZCHNICKA, A. MAŁKIEWICZ, I. WILCZEK, T. KROK, M. MIGDAL, A. KOZIEŁ

Reactor Measurement and Analysis Group, Research Reactor Technology Division, National Centre for Nuclear Research
ul. Andrzeja Sołtana 7 05-400 Otwock, Poland

ABSTRACT

The MARIA reactor with thermal neutron flux density up to $3 \cdot 10^{14}$ cm-2 s-1 and a number of vertical channels is well suited to material testing by thermal neutron treatment. Beside of that some fast neutron irradiation facilities are operated in MARIA reactor as well. One of them is thermal to 14 MeV neutron converter launched in 2014. It is especially devoted to fusion devices material testing irradiation.
The ITER & DEMO research thermonuclear facilities are to be run using the deuterium - tritium fusion reaction. Fast neutrons (of energy approximately 14 MeV) resulting from the reaction are essential to carry away the released thermonuclear energy and to breed tritium. However, constructional materials of which thermonuclear reactors are to be built must be specially selected to survive intense fluxes of fast neutrons. Strong sources of 14 MeV neutrons are needed if research on resistance of candidate materials to such fluxes is to be carried out effectively. Nuclear reactor-based converter capable to convert thermal neutrons into 14 MeV fast neutrons may be used to that purpose.
The converter based on two stage nuclear reaction on lithiuim-6 and deuterium compounds leads to 14 MeV neutron production. The reaction chain is begun by thermal neutron capture by lithium-6 nucleus resulted in triton release. The neutron and triton transport calculations have been therefore carried-out to estimate the thermal to 14 MeV neutron conversion efficiency and optimize converter construction. The useable irradiation space of ca. 60 cm^3 has been obtained. The released energy have been calculated. Heat transport has been asses to ensure proper device cooling. A set of thermocouples has been installed in converter to monitor its temperature distribution on-line. Influence of converter on reactor operation has been studied. Safety analyses of steady states and transients have been done. Performed calculations and analyses allow designing the converter and formulate its operation limits and conditions.
During first tested operation of the converter the 14 MeV neutron flux density was estimated to 10^9 cm-2 s-1, whereas fast fission neutrons inside converter achieved 10^{12} cm-2 s-1, and thermal neutrons were reduced down to 10^9 cm-2 s-1.
Taking into account the feasibility of almost incessant converter operation for a number of months, its arisen as one of the most powerful (in terms of fluence), currently available 14 MeV neutron source.
Such a converter currently under operation in the MARIA reactor core will be presented.

1. Introduction

The MARIA reactor with thermal neutron flux density up to $3 \cdot 10^{14}\ cm^{-2}\ s^{-1}$ and a number of vertical channels is well suited to material testing by thermal neutron treatment. Beside of that some fast neutron irradiation facilities are operated in MARIA reactor as well. One of them is thermal to 14 MeV neutron converter launched in 2014. It is especially devoted to fusion devices material testing irradiation.

The ITER & DEMO research thermonuclear facilities are to be operate using the deuterium – tritium nuclear fusion reaction. Fast neutrons (of energy approximately 14 MeV) resulting from the reaction are essential to carry away the released thermonuclear energy and to breed tritium. However, constructional materials of which thermonuclear reactors are to be built must be specially selected to survive intense fluxes of fast neutrons. Strong sources of 14 MeV neutrons are needed if research on resistance of candidate materials to

such fluxes is to be carried out effectively. Nuclear reactor-based converter capable to convert thermal neutrons into 14 MeV fast neutrons may be used to that purpose.

2. The irradiation facility construction

The converter based on two stage nuclear reaction on lithiuim-6 and deuterium compounds leading to 14 MeV neutron production. The reaction chain is begun by thermal neutron capture by lithium-6 nucleus resulted in triton release. The nuclear reactor is used as a strong thermal neutron source.

The neutron and triton transport calculations have been therefore carried-out to estimate the thermal to 14 MeV neutron conversion efficiency and optimize converter construction. The useable irradiation space of ca. 60 cm^3 has been obtained. The released energy have been calculated. Heat transport has been asses to ensure proper device cooling. A set of thermocouples has been installed in converter to monitor on-line its temperature distribution. Influence of converter on reactor operation has been studied. Safety analyses of steady states and transients have been done. Performed calculations and analyses allow designing the converter and formulate its operation limits and conditions.

The converter construction consists of a set of concentric tubes, located inside vertical channel in reactor beryllium moderator (fig. 1). The converting layer in cylindrical shape surrounds a container with irradiated samples.

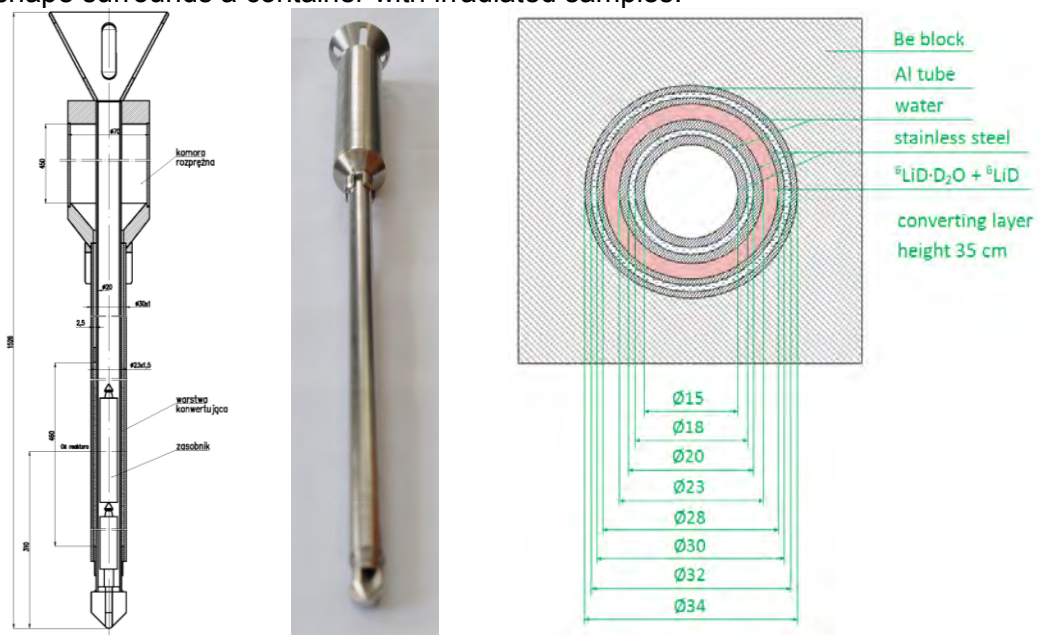

Fig. 1. Converter construction.

The neutron energy spectrum inside container depends on converter distance from nuclear fuel, and therefore on converter location in the reactor core (cf. fig. 2).

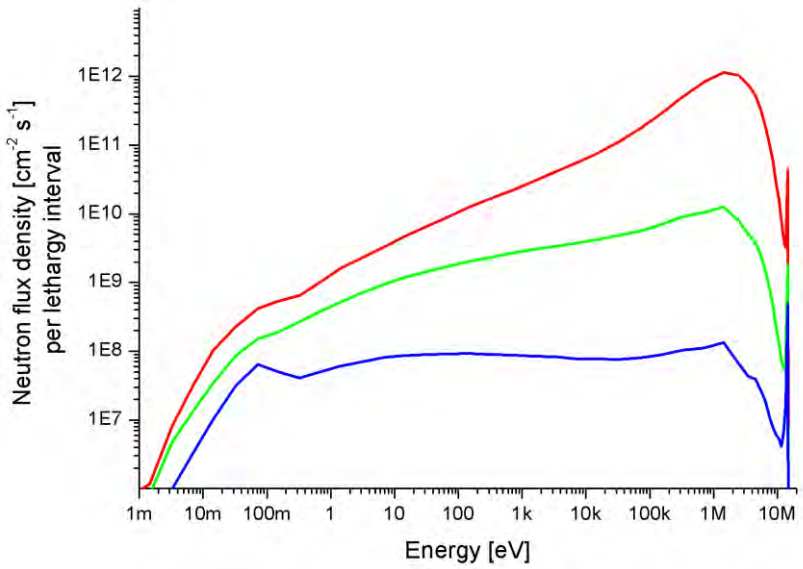

Fig. 2. Calculated neutron energy spectrum inside converter located in the middle of reactor core (red curve), in the periphery of reactor core (green curve) and in the reactor reflector (blue curve).

3. Testing Operation

During first tested operation of the converter in MARIA reactor the 14 MeV neutron flux density was estimated to over 10^9 $cm^{-2}\,s^{-1}$, whereas fast fission neutrons inside converter achieved 10^{12} $cm^{-2}\,s^{-1}$, and thermal neutrons were reduced down to 10^9 $cm^{-2}\,s^{-1}$. The neutron flux densities have been measured by means of activation method with a set of various activation foils.

A set of ITER construction steels have been irradiated in above mentioned neutron filed. Currently, they are under investigation.

4. Conclusion

Taking into account the feasibility of almost incessant converter operation for a number of months, its arisen as one of the most powerful (in terms of fluence), currently available 14 MeV neutron source.

OVERVIEW ON RRSF REPROCESSING, FROM SPENT FUEL TRANSPORTATION TO VITRIFIED RESIDUES STORAGE

J.F. VALERY, X. DOMINGO, P. LANDAU
AREVA NC
1 place Jean Millier, 92084 Paris La Défense Cedex - France

A. DUPEYRAT, P. DESCHAMPS, C. PECHARD
AREVA NC La Hague
50440 Beaumont-Hague - France

V. LALOY, M. KALIFA
AREVA TN
1 Rue des Hérons, 78180 Montigny-le-Bretonneux - France

ABSTRACT

Benefiting from its past experience, AREVA proposes to detail in pictures all the stages of a (Research Reactor Spent Fuel) RRSF reprocessing from its evacuation from reactor site to its corresponding post-reprocessing vitrified waste production and management.

1. Introduction

Reprocessing is one of the today-available options for managing back-end of Research Reactor fuel cycle.
As described in figure 1 bellow, this solution offers to RR:

- Non-proliferation: reducing ^{235}U enrichment of RRSF from 20-93% to below 2%,
- Final waste management optimisation: standardizing final waste package and reducing volume and radio-toxicity, removing IAEA safeguards on final waste,
- Sustainability of RRSF back-end management: long-lasting solution, re-use of valuable material for civilian purposes i.e. saving natural resources, cost-certainty, cost effective solution,…

Fig. 1: RRSF reprocessing basic scheme and advantages

Over the past decades, AREVA has been transporting, unloading, storing and reprocessing RRSF in its French facilities and with its equipment.
This article encompasses pictures and figures for each step of reprocessing operations by AREVA, especially in regards to transport to and reprocessing at the AREVA La Hague site.

2. Transportation of RRSF to La Hague

Since early 1990's, **around 150 MTR-type RRSF transportation casks** have been transported to AREVA La Hague.

2.1. Types of transportation cask

The first high-capacity RRSF transportation cask used by AREVA (Cogema Logistics at that time) was the IU04 cask.
As of today, AREVA proposes to its customers to use the TN-MTR transportation cask for MTR-types of RRSF, especially for transportation to the La Hague site.
This cask can contain several types of basket, generic or specialized according to the RRSF.
This cask offers the highest RRSF transportation capacity worldwide, with a 68-positions basket.
The TN-MTR cask can be loaded at RR site either under water or using a dry transfer system from pool to cask.

Fig.3: TN-MTR wet loading at RR site © AREVA

Fig.4: Transfer system for loading TN-MTR at RR site © AREVA

AREVA can also propose other types of multi-purpose transportation casks, even adapted for non-MTR-type RRSF. As an example a new package, which fabrication will be completed by mid-2015, will be proposed by AREVA: the TN-LC package [1].

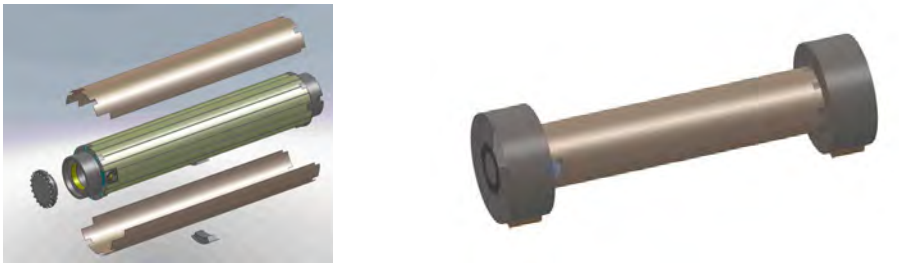

Fig.5: View of TN-LC transportation cask © AREVA

Other casks can be considered for transportation of RRSF to AREVA La Hague, after investigating the following:

- Transportation license from RR site to La Hague (i.e. French transportation license, license in the RR country, and all countries involved in this transportation),
- Receipt and unloading at La Hague (see paragraph 3.2. below).

2.2. RRSF transportation experiences

As mentioned before, **around 150 MTR-type RRSF transportation casks** have been transported to AREVA La Hague up to now.

AREVA has acquired this long-term international experience through multi-modal transportations: maritime, rail and road transportations (see Fig.6 & 7),

Fig.6: RRSF transportation on boat © AREVA

Fig.7: TN-MTR on a truck © AREVA

AREVA has notable RRSF transportation experiences in the following countries: **Australia**, **Belgium, Denmark**, **France, Indonesia**, **Italy**, **Portugal**, **Sweden**, **Taiwan**, **United States of America**, **Uruguay** and **Venezuela**.

3. Receipt and unloading of RRSF at La Hague

The AREVA La Hague plant obtained its first authorizations for receiving and unloading RRSF in the late 1990's.
Ever since and until end-of 2014, **around 150 MTR-type RRSF transportation casks** have been received and unloaded at AREVA La Hague, corresponding to **around 5 250 MTR-type RRSF assemblies**.
As mentioned before, the transportation casks used for these receipts at La Hague were the the IU04 and now the TN-MTR.
But RRSF are not only MTR-type of spent fuels. Thanks to the flexibility of its receipt-workshops, AREVA is also able to receive other types of RRSF, and other types of RRSF transportation casks.

3.1. Receipt of transportation casks at the La Hague site

At their arrival at the La Hague site (see Fig.8), and before unloading, the RRSF transportation casks are temporarily stored for a few days.
At its arrival, the transportation truck is controlled for exterior and interior contamination (see Fig.9), before control of the transportation cask itself (see Fig.10).
In preparation for unloading the cask is lifted and handled in a preparation hot-cell, next to the unloading pool (see Fig.11).
After additional controls, and notably internal shipping tests on the cask in order to detect any nuclear material leakage from RRSF assemblies, the transportation is wrapped in plastic sheet (to prevent the body of the cask from possible contamination during unloading, and consequently to facilitate the preparation of the next shipment), and moved from the preparation cell to the unloading pool (see Fig.12).

Fig.8: Truck with RRSF transportation cask arrival at La Hague © AREVA

Fig.9: Control on RRSF transportation truck at La Hague © AREVA

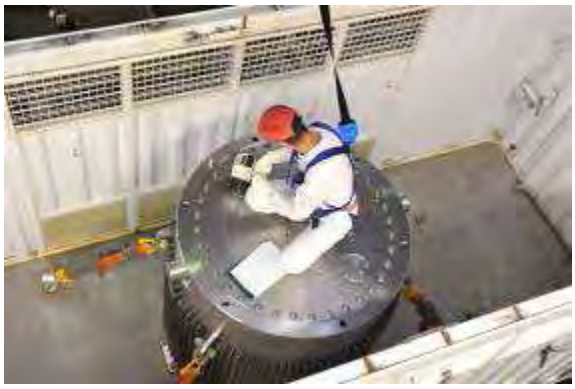

Fig.10: Radiological control on RRSF transportation cask, without shock absorber © AREVA

Fig.11: Cask handling to the preparation cell, before unloading © AREVA

Fig.12: Cask handling from preparation cell, to unloading pool © AREVA

3.2. Wet unloading of RRSF

Until 2015, the MTR-type RRSF transportation casks are unloaded in the pool *HAO-Nord*. Starting 2016, RRSF transportation casks will be unloaded in the *NPH (Nouvelle Piscine de la Hague)* pool.

Thanks to its flexibility, the *NPH* pool workshop and related tools can be adapted to a wide range of transportation casks. For example, the TN-17/2 cask, used for Fast Reactor spent fuel transportation, is also unloaded in *NPH* pool.

Nevertheless, in case a new cask needs to be received at La Hague, feasibility studies, a safety report application to Safety Authority /authorization, design and fabrication of new equipments and possible modifications to the workshop are necessary.

After introduction of the transportation cask in the pool (see Fig.13) the top-lead of the cask is removed in order to access to RRSF. All the handling operations during unloading are performed manually, by AREVA operators (see Fig.14), but are controlled by automatism and Instrumentation & Control.

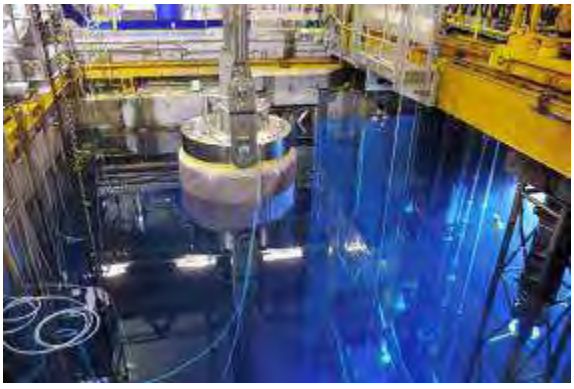

Fig.13: RRSF transportation cask introduction in HAO pool © AREVA

Fig.14: La Hague operator handling RRSF in HAO pool © AREVA

The RRSF are handled from the transportation cask to an intermediate unloading-basket, and then in a position into the interim-storage basket (see Fig. 15) to be transferred in the pools dedicated to wet interim storage (see Fig. 16), before reprocessing.

Fig.15: The baskets used for RRSF transfer to wet storage © AREVA

Fig.16: RRSF storage-basket transfer to wet storage © AREVA

4. RRSF wet interim storage at La Hague

Taking into account (i) the time needed for cooling down the RRSF, (ii) industrial reprocessing scheduling of the La Hague plant and (iii) regulatory and legal obligations related to safety authorizations and intergovernmental agreements, RRSF are stored in the La Hague storage pools for some months/years (see Fig. 17) before transfer to reprocessing facilities.

Fig.17: La Hague wet storage "piscine C" © AREVA

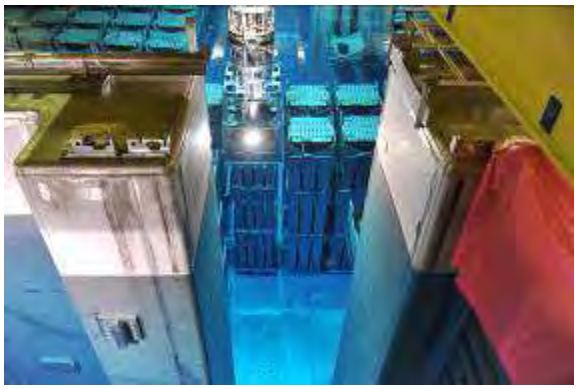

Fig.18: RRSF storage-basket transfer to reprocessing © AREVA

RRSF storage uses La Hague-standard types of baskets with dedicated inners, adapted to each type/category of RRSF.
Several designs and fuel-types of MTR RRSF are stored in La Hague pools, but other RRSF than MTR-type can be stored, if the corresponding authorization is delivered by the French Safety Authority, after review of the receipt-storage-reprocessing-related safety file.

Depending on the RRSF type, the storage capacity of one basket varies up to more than 60 fuel elements.

After storage, RRSF are transferred to the reprocessing facilities. The first operation is to bring the storage basket (see Fig. 18) to a dedicated workshop to transfer the RRSF from the storage basket to a shuttle-basket, this operation being performed by an AREVA operator (see Fig. 19). After this transfer, RRSF in shuttle basket is ready to be sent to the dissolution facility (see Fig. 20).

Fig.19: RRSF transfer from storage to shuttle basket © AREVA

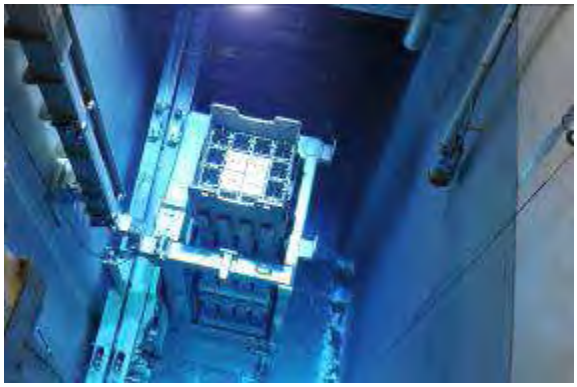

Fig.20: RRSF shuttle basket ready to go dissolution facility © AREVA

5. RRSF reprocessing operations

From the interim wet storage pool to the dissolution facility (T1 facility in La Hague UP3 reprocessing plant), the transfer of RRSF is performed with a shuttle basket.
The RRSF is inserted one by one from the storage area to the dissolution area through the *"insert-cisaille"* gate[1] (see Fig.21). The RRSF is then placed into a dedicated canister,

[1] The *« insert-cisaille »* gate is originally designed as the entry of NPP SF from wet storage to cladding-shearing equipment, before dissolution of nuclear material.

positioned on a rack, waiting for dissolution (see Fig.22). All these operations are performed by operators with dedicated cranes and tele-manipulators (see Fig.23).

Fig.21: video of RRSF going through the "insert-cisaille" gate © AREVA

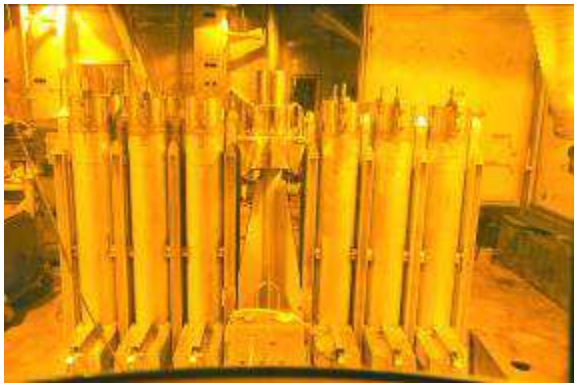

Fig.22: RRSF-canister 12-positions rack in dissolution cell © AREVA

Each canister is then positioned on the top of the dissolution pit (see Fig. 24). The RRSF are then loaded in the dissolution pit one by one by directly dropping them in the boiling nitric acid.

Fig.23: operator handling RRSF with tele-manipulator © AREVA

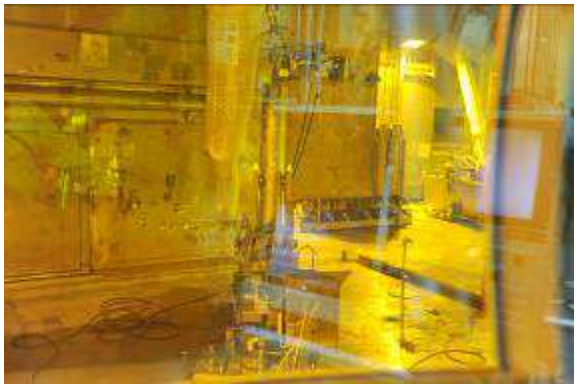

Fig.24: RRSF canister on top of the T1 dissolution pit © AREVA

The dissolution process is the same for UAl-type and USi-type of RRSF, and is controlled thanks to a dedicated camera placed on the top of the dissolution pit. The dissolution process is over once the RRSF totally disappeared from the pit (see Fig.25 & 26).

Fig.25: RRSF being dissolved © AREVA

Fig.26: dissolution pit empty © AREVA

However, after the dissolution step and prior to the mix with the LWR dissolution solution entering the liquid/liquid extraction for Al management, there is an additional operation performed in the case of USi-type RRSF. This additional operation consists in separating the silicon from the dissolution solution because the whole silicon quantity cannot proceed through the extraction. The concentrated silicon solution is managed through the “fines” line and vitrified with the fissions production solutions at the end of the process.
After dissolution of a RRSF batch, uranium and plutonium are separated from the fission products solutions thanks to the PUREX process. Fission product solutions are then concentrated before their vitrification.

The following Figure 27 & 28 give an overview of the whole reprocessing steps performed for UAl and USi RRSF.

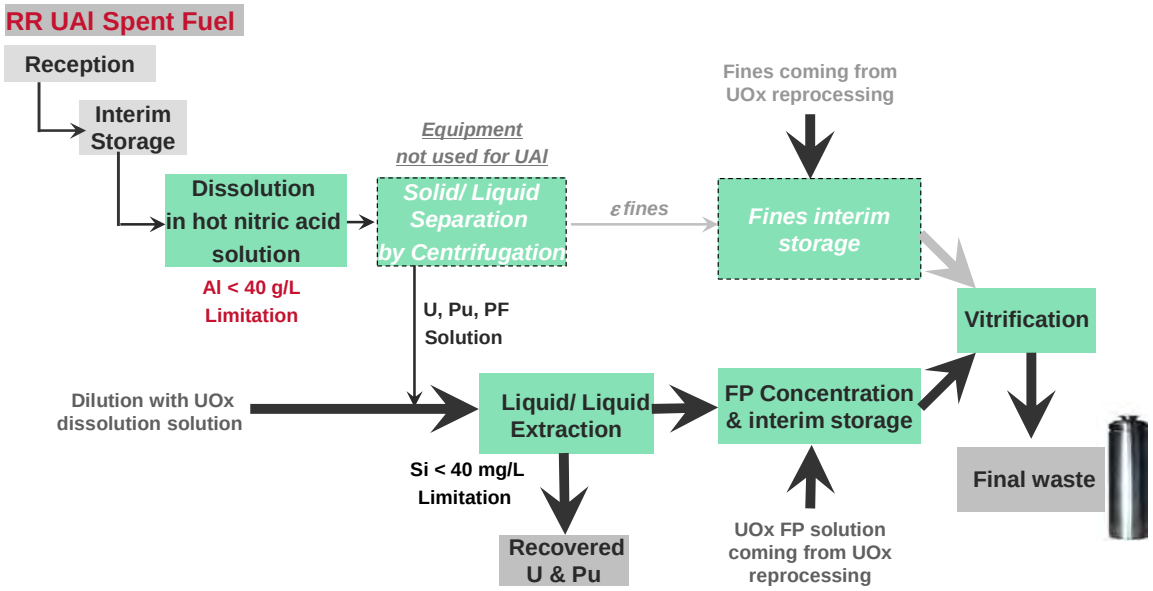

Fig. 27: Process diagram for UAl RRSF reprocessing in AREVA La Hague plant

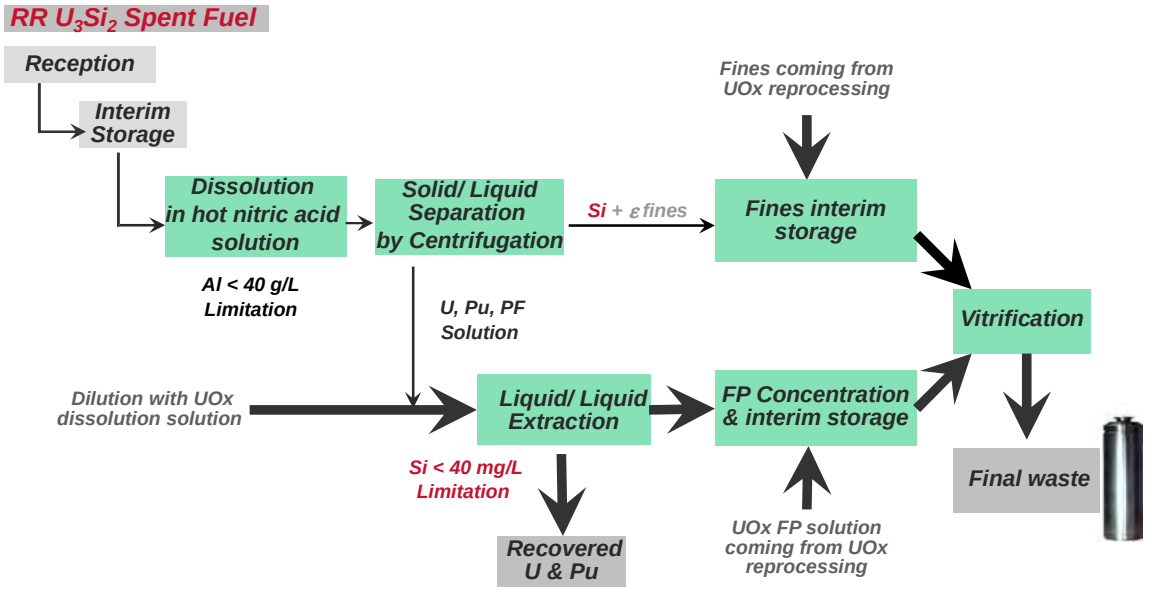

Fig. 28: Process diagram for USi RRSF reprocessing in AREVA La Hague plant

Starting at Marcoule plant and up to the 90's, **18 tons of UAl-type RRSF** from **21 reactors from 11 countries** have been reprocessed with the similar reprocessing operations as the La Hague ones.

Since 2005 and as of end-of 2014, over **7.25 tons of UAl-type RRSF** fuels have already been reprocessed at industrial scale at the AREVA La Hague plant.
AREVA is currently finalizing the studies in order to obtain the authorisation to reprocess USi-type RRSF from the French Safety Authority (réf. [2]).

6. Final waste production and management

6.1. Final waste attribution to customers

According to the applicable European Directive[2] and to French law[3], the introduction on French territory of spent nuclear fuels for a reprocessing purpose has to be framed by an intergovernmental agreement (IGA) between France and the SF country of origin. This agreement settles "a forecasted schedule for reception and processing of the material and, if any, the later planned use of the material separated during reprocessing". Article L542-2 of the French Environmental Code specifies also that disposal in France of radioactive waste from abroad is forbidden, including waste resulting from RRSF reprocessing.
In regards to spent fuel reprocessing at the AREVA La Hague plants, France already signed IGAs with Italy, the Netherlands and Belgium.

Another application of French law[4] concerns the final waste calculation method.
In order to comply with this regulation, AREVA applies a material accountancy system including a unique activity unit for waste (UAR, *Unité d'Activité de Résidu*) and a unique mass unit for waste (UMR, *Unité de Masse de Résidu*).
This system allows AREVA to calculate the amount and type of waste to be sent back to its customers. This system called EXPER (*EXPEdition des Résidus*) has been approved by decree, and has been implemented since October 2008 for all new RRSF reprocessing operations.
This system states that the UAR and UMR quantities imported in France are to be sent back from France.

In the case of silicide-type RRSF reprocessing, if all the material is dissolved, the only remaining waste corresponds to the UAR system, based on the Nd quantities imported in France in the RRSF.
The UAR system implies two possible types of vitrified residues: CSD-V (*Conteneur Standard de Déchets Vitrifiés*) and CSD-U (*Conteneur Standard de Déchets U)*.
The CSD-V concentration in FP is highly superior than the CSD-U one.
The thermal power is consequently higher in CSD-V than in CSD-U.
According the regulation of each country regulation, CSD-V and CSD-U can be considered respectively as HLW and ILW.

AREVA proposes to study the conditions under which the final waste can be managed with the RR operators and their regulatory bodies.

---

[2] Council Directive 2011/70/EURATOM of 19 July 2011 establishing a Community framework for the responsible and safe management of spent fuel and radioactive waste: http://eur-lex.europa.eu/LexUriServ/LexUriServ.do?uri=OJ:L:2011:199:0048:0056:EN:PDF

[3] French Environmental Code resulting from the law of June 28, 2006 on the sustainable management of radioactive materials and waste, and application decree no. 2008-209 of March 3, 2008 on procedures applicable to the reprocessing and recycling of foreign spent fuel and radioactive waste specifies certain conditions

Two different examples can be underlined for final waste management:

- Belgium
  After reprocessing of BR2 RRSF, corresponding CSD-Vs have been jointly sent back to Belgium with residues from Belgian utilities SF reprocessing. As the LWR SF reprocessing results in much higher volumes of CSD-V than RRSF reprocessing, the residues return was almost insignificant for the BR2 operator (SCK).
- Australia
  Australia does not operate any Nuclear Power Plant. Australia does not have any HLW to manage. The CSD-U was consequently the best option for Australia as it is managed as ILW and does not need large investments for long term management (in comparison with final HLW disposal).

Depending on each country regulations and specificities, AREVA can propose either CSD-V or CSD-U for a responsible and sustainable waste management.

6.2. Final waste production and interim storage

6.2.1. Final waste production

After the reprocessing operations, the concentrated fission products solutions are vitrified in the AREVA La Hague plant and the resulting glass matrix poured in universal canisters.

Currently there are two types of vitrified residues containing concentrated fission products solutions produced with two technologies:

- The **CSD-V**: these vitrified residues are produced thanks to the hot melter lines in AREVA NC's vitrification facility. They are mainly the result of the reprocessing operations for UOx and MOx spent fuels coming from Light Water Reactor and they represent the nominal glass residue production in the La Hague Plant.
- The **CSD-U**: these vitrified residues are produced thanks to the cold crucible line in AREVA NC's vitrification plant. They are the result of the reprocessing operations for spent fuels coming from past Gas Cooled Reactor and their production will be limited (number of items and time production). In comparison with CSD-Vs, these CSD-Us have a lower activity content and a lower related thermal power (~50 W versus 2000 W). Regarding French regulation, CSD-Us are High Level Activity Waste as CSD-Vs but, given their characteristics, these residues can be considered and managed as Intermediate Level Activity Waste in other countries (Australia for instance).

Both types of vitrified residues (CSD-V and CSD-U) are the result of the encapsulation of Fission Products in a stable, homogeneous, and durable glass matrix with a long-term predictable behaviour. Furthermore, their fissile material contents are very low and allow an exemption of safeguards for their interim storage and final disposal.

Fig. 29: Universal Waste Canister (CSD) – Vitrified wastes
© AREVA

6.2.2. Interim storage at La Hague

The interim storage of vitrified residues is performed in pits with ventilation by natural convection in the AREVA NC La Hague plant (EEVSE and EEVLH facilities).

Fig.30: Outside view of La Hague EEVSE facility © AREVA

As mentioned in paragraph 6.1, the duration of interim storage of vitrified residues coming from foreign RRSF reprocessing is agreed between France and the RR's country before starting importation in France of the RRSF, through an IGA.

De-storage of the residues and preparation for transportation, including loading in the dedicated transportation cask are performed in the *DRV* facility in AREVA La Hague. AREVA customers can witness these de-storage and preparation for transportation operations.

Fig.31: De-storage facility control room
© AREVA

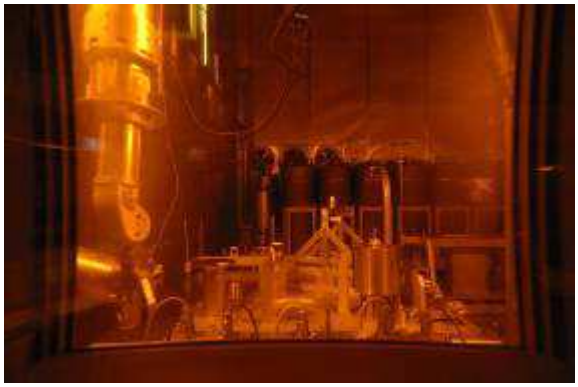

Fig.32: De-storage operations for CSD-V
© AREVA

6.3. Final waste transportation and management in the RR country

According to their UAR content (see paragraph 6.1), CSD-Vs and CSD-Us can be considered to send back final residues to foreign customers.
Transportation casks that can be used for the transport vary according to the customer's final waste interim storage policy: storage in pits/vaults, or storage in the transportation cask itself on a storage area.

6.3.1. Solutions for waste transportation

If the dedicated RR country makes the choice of interim waste management in pit/vaults, like in the AREVA La Hague plant, the TN-28 and the TN-81 residue transportation casks can be used to ship CSD-Vs or CSD-Us to the customers with a maximum of 28 universal canisters per cask. This choice has been made by Belgium for management of its final waste after RRSF reprocessing at La Hague.

In the case of an interim storage in cask, the TN-81 cask can be used as a "dual-purpose" cask ie for both residue transportation and interim storage, with a maximum of 28 universal canisters per cask. This choice has been made by Australia for management of its final waste after RRSF reprocessing at La Hague.

If needed, other types of transportation casks can be considered by AREVA for loading CSD-Vs or CSD-Us, according to customers' needs. Nevertheless, as for RRSF receipt, feasibility studies, safety report application to Safety Authority /authorization, design and fabrication of new equipments and possible modifications to the workshop are necessary.

Fig.33: AREVA TN-81 dual purpose cask
© AREVA

Fig.34: AREVA TN-28 transportation cask
© AREVA

6.3.2. Experience

AREVA has a wide experience in residues shipment to foreign customers.

In the case of residues return related to RRSF reprocessing, AREVA has already returned small quantities of CSD-V to RRSF customers, based on a joint residues management with NPP and RRSF customers (Belgian feed-back).
Indeed, in case of a nuclear power country that made the choice of reprocessing its NPP spent fuels in France, a joint return is efficient, cost effective, and reduces the number of nuclear transportations.

When there is no NPP spent fuel reprocessing in France in the RR country, and no associated return of vitrified waste, another solution can also consist in performing a CSD-U shipment CSD-U with a dedicated transport program (Australia), and benefiting from the associated advantages (see paragraph 6.2.1)

AREVA has also experience in designing, licensing and constructing the facilities dedicated to interim storage of final waste.

7. Conclusion

AREVA acquired a long-term experience on RRSF management, encompassing international and multi-modal transportation, reprocessing and waste management.
Thanks to its experience, and thanks to the high-quality of its operators, its plants and equipments, AREVA is ready to set up sustainable partnerships with its RR customers in order to robustly manage the back-end of their fuel cycle.

8. Reference

[1] “AREVA TN Transports and Logisitcs Activities - Fleet of Transport Casks for International Shipments in Support of Research Reactor and Laboratories”, N. Guibert, J. Thomas, RRFM2015, Bucharest, April 2015

[2] “Status on silicide fuel reprocessing at AREVA La Hague”, J.F. Valery, X. Domingo, P. Landau, C. Alameda-Angulo, C. Pechard, V .Laloy, RRFM2015, Bucharest, April 2015

COMPARISON BETWEEN U(Mo)/Al(Si) MINIPLATE AND U_3Si_2/Al MINIPLATE AFTER THE SAME FABRICATION PROCESS.

M. MIRANDOU [(1)*], S. ARICÓ [(1,2)], S. BALART [(1)]

(1) Gerencia Materiales, Gerencia de Área Energía Nuclear.
(2) Instituto de Tecnología "Jorge Sabato", Universidad Nacional de General San Martín.

D. PODESTÁ and J. FABRO

Departamento Elementos Combustibles para Reactores de Investigación (ECRI), Gerencia de Ciclo del Combustible Nuclear (GCCN)

Comisión Nacional de Energía Atómica (CNEA), Avda. Gral. Paz 1499, B1650KNA, San Martín, Buenos Aires, Argentina.

***corresponding author e-mail**: mirandou@cnea.gov.ar

ABSTRACT

Fuel elements based in U_3Si_2 particles dispersed in an Al matrix perform satisfactorily under irradiation. This means that phases that form the interaction layer grown during fabrication process in this kind of fuels can be considered as "*a proper interaction layer*."
In this work a comparison between dispersion plates made with U_3Si_2 particles/Al matrix and miniplates made with U-7wt%Mo atomized particles/Al-4wt%Si matrix, that underwent the same fabrication steps, is presented. The aim of this investigation is to determine similarities and differences between the phases formed during fabrication on both of them. Characterization was performed by OM, SEM, EDS and XRD.
On the other hand, and based in our experience that basic research on diffusion couples provides an important contribution to support studies as described above, an investigation on a new set of diffusion couples made with U-7wt%Mo and seven different Al(Si) binary alloys will be carried out during this year. Experimental details of the diffusion couples are presented in this work. The final purpose consists in determining which is the amount of Si that promotes the formation of an interaction layer as similar as possible to the one observed on the miniplate fabricated with U_3Si_2 particles.

1.Introduction

The use of low enriched uranium (LEU) in γU(Mo) alloys is under study in dispersion or monolithic fuel elements to convert high flux research nuclear reactors [1, 2]. In this alloy, the addition from 7 to 10 wt%Mo is used to keep, in metastable condition at room temperature, γU phase which performs well under irradiation [1, 2, 3].
U(Mo) particles dispersed in an Al-Si matrix is one of the most promising ways to fulfill the qualification of this fuel [4] as they underwent satisfactorily some of the irradiation test [5]. Post-irradiation examinations together with the analysis of the corresponding fresh plates, showed that good behavior is correlated with the formation during fabrication of a "*proper interaction layer*" around U(Mo) particles [6, 7]. However U(Mo) qualification is still ongoing because recent attempts to bring this fuel to high burnup at elevated power have not been totally successful [8, 9, 10]
In CNEA-Argentina a study is being carried out to determine how to obtain the better interaction layer (IL) characteristics (i. e. uniformity, composition, phases, etc) with the lesser modifications

to the fabrication process (currently used for silicide fuel elements) and the smallest amount of Si added to the matrix. Results of the characterization of the meats of miniplates made with atomized U-7wt%Mo dispersed in Al-2wt%Si and Al-4wt%Si matrices were presented at RRFM 2014 meeting [11]. In that work it was shown how the addition of 4wt%Si to Al behaves in an efficient way to ensure Si availability to form a uniform and very narrow IL surrounding U(Mo) particles on fully welded miniplates. This IL is only formed by Si-containing phases.
On the other hand, it is well known that fuel elements based in U_3Si_2 particles dispersed in an Al matrix are stable under irradiation in plate type configurations and are being used to convert to LEU a large number of research reactors without significant loss in performance. From this result it can be inferred that phases that form the IL grown during fabrication process in this kind of fuel elements also have a good performance under irradiation and can surely be considered as "*a proper interaction layer*."
In this work two plates fabricated with U_3Si_2 particles dispersed in an Al matrix were analyzed to obtain information about the IL that forms during fabrication process and compare it with the one obtain for the miniplates made with U-7wt%Mo dispersed in Al-4wt%Si matrices. These plates made with U-7wt%Mo are part of the set of miniplates already presented in [11]. Only the most relevant experimental details and results will be shown here to ease comparison.
To go further in U(Mo)/Al(Si) characterization, it would be important to determine which is the Si concentration in Al(Si) alloy that promotes the formation of an IL as similar as possible to the one observed on the plates fabricated with U_3Si_2 particles. With this aim, experimental details of a set of seven diffusion couples with U-7wt%Mo and seven different Al(Si) binary alloys is presented.

2.Experimental procedure

2.1.U(Mo)/Al-4wt%Si miniplates [11] and U_3Si_2/Pure Al plates.

Depleted U-7wt%Mo alloy (U-7Mo) as atomized particles provided by KAERI were used as fuel alloy. The powders used as matrices were prepared in two different ways: by mixing pure Al and pure Si particles (Al-4Si) or pure Al particles with eutectic Al-Si alloy particles (which Si concentration is 12 wt%) (Al-4Si_E). In both cases the final nominal concentration is Al-4wt%Si.
U-7Mo and matrix particles were mixed and cold pressed to obtain 7 gU/cm^3 compacts which were positioned in an AA6061 frame and **fully welded** to AA6061 covers by TIG. Hot rolling at 500 ºC up to 82 % reduction was used to obtain final size followed by a heat treatment of 1 h at 500 ºC and cold rolled.
U_3Si_2 compound was fabricated in CNEA by melting low enriched uranium (20% ^{235}U) and pure Si in an induction furnace. After melting, the material was milled and sieved to obtain the powder. Silicide particles were mixed with pure Al ones and cold pressed to obtain 4.8 gU/cm^3 compacts which were positioned in an AA6061 frame and welded, **with open corners**, to AA6061 covers by TIG. Hot rolling at 500 ºC up to 90 % reduction was used to obtain final size followed by a heat treatment of 1 h at 480 ºC and cold rolled.
Samples were cut from each miniplate or plate and one of the Al6061 cladding was removed by a rough polishing until reaching the meat followed by a final mechanical polishing up to 1 μm diamond paste. The samples were characterized by optical microscopy (OM-Olympus BX60M), scanning electron microscopy (SEM –Philips SEM 515, and FEI QUANTA 200), energy dispersive spectroscopy (EDS-EDAX Phoenix 3.2) and X-Ray diffraction (XRD- PANalytical-Empyrean with Cu *kα* radiation). Crystal structures identification and the estimation of lattice parameters were obtained by direct comparison between theoretical spectrum of each phase with the experimental spectra using POWDERCELL software [12].
Table 1 summarizes identification and characteristics of the miniplates and plates studied in this work.

TABLE 1. Identification and fabrication details of the sample taken from the miniplates and plates.

Identification	***In RRFM 2014 [11]***	***Fuel***	***Matrix***	***Fabrication process***		
				Rolling Temp	***TTF Temp. and time***	***Cooling***
U(Mo)/Al-4Si	4Si-FF-FW	U-7wt%Mo	Al-4Si	500 ºC	500 ºC – 1 h	Inside furnace
U(Mo)/Al-4Si_E	4Si_E-FF-FW	U-7wt%Mo	Al-4Si_E			
U_3Si_2/Al-IF	-	U_3Si_2	Pure Al		480 ºC – 1 h	Inside Furnace
U_3Si_2/Al-OF	-	U_3Si_2	Pure Al			Outside Furnace

2.2.Diffusion couples

Al(Si) binary alloys were made by arc melting in a small non-consumable tungsten electrode arc-furnace with a copper crucible under highly pure argon atmosphere using high purity Al and Si. Six different alloys were fabricated: Al-0.6wt%Si (Al-0.6Si); Al-2 wt%Si (Al-2Si); Al-4wt% Si (Al-4Si); Al-5.2wt%Si (Al-5.2Si); Al-6 wt%Si (Al-6Si) y Al-7.1wt%Si (Al-7.1Si). Si concentrations corresponding to 0.6; 5.2 and 7.1 were chosen in accordance to nominal Si concentration in AA6061, AA4043 and AA356 commercial Al alloys. After melting process the Al(Si) alloys were hot rolled at 480 ºC and heat treated 1 h at 550 ºC. This last temperature is the same one at which diffusion couples will be studied.

Same melting procedure is used to fabricate the U–7wt%Mo alloy. Only part of the as-cast U-7Mo alloy will be heat treated at 1000°C during 2h and quenched to room temperature to promote composition homogenization. The remaining alloy will be used in the as cast condition to represent more closely U(Mo) alloy in the miniplates. Stainless-steel mechanical clamps will be used to keep in contact the alloys. Table II shows the configuration of the seven diffusion couples.

Table II. Configuration of the seven diffusion couples.

1	Al-0.6Si	U-7Mo Non homog.	Al-5.2Si
2	Al-0.6Si	U-7Mo Non homog.	Al-7.1Si
3	Al-2Si	U-7Mo Non homog.	Al-5.2Si
4	Al-2Si	U-7Mo Non homog.	Al-6Si
5	Al-4Si	U-7Mo Non homog.	Al-6Si
6	Al-4Si	U-7Mo Non homog.	Al-7.1Si
7	U-7Mo Non homog.	Al-4Si	U-7Mo Homogenized.

As it is shown in Table II, in the first six diffusion couples U(Mo) will be positioned in between two Al(Si) alloys [i.e. Al-xSi/U-7Mo/Al-ySi]. This configuration allows comparison of relative IL

widths minimizing any effect introduced during diffusion couple fabrication. The last one will be used to study the influence of metastable γU phase decomposition [13] on IL formation.

3.Results and discussion

3.1. U-7Mo/Al-4Si miniplates characterization [11]

As previously mentioned, results presented in this section correspond to part of the investigation of a set of meats of miniplates which has already been presented in more detail in RRFM 2014 meeting. The aim of that study was to obtain an IL, formed by Si-rich phases, that completely surrounds U(Mo) particles. In the following paragraphs more relevant results concerning IL characterization will be shown to ease comparison presented in Section 3.3.

At the end of fabrication process the miniplates U(Mo)/Al-4Si and U(Mo)/Al-4Si$_E$ developed a very narrow IL which showed an important growing during thermal treatment. At the end of fabrication process almost all U(Mo) particles were completely covered by an IL which looks homogenous in thickness (dark gray in Figure 1). The IL developed even between very close particles as shown in detail in Figure 1c. IL thickness measured only on 100 μm (or higher) particles diameter was estimated in 0.5 - 2 μm.

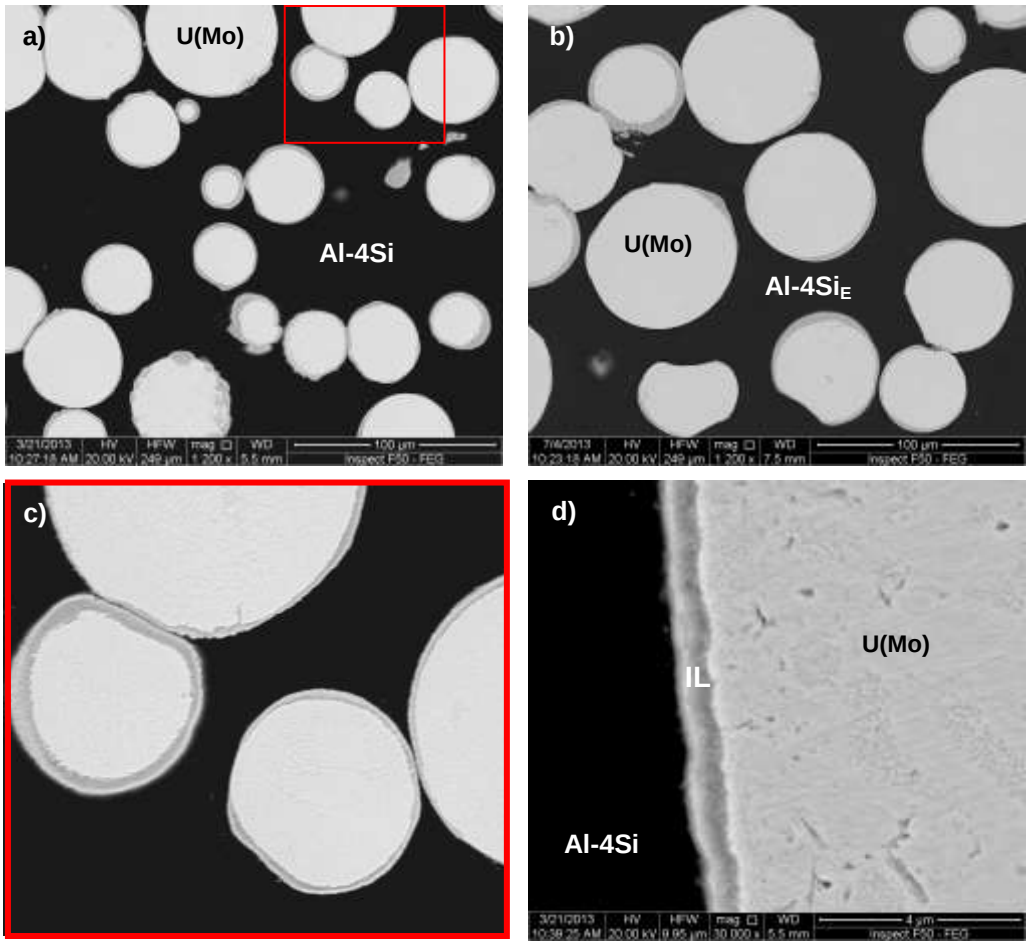

Figure 1. U(Mo) particles completely covered by an IL of homogenous thickness. a), c) and d) Miniplate U(Mo)/Al-4Si, b) Miniplate U(Mo)/Al-4Si$_E$. – SEM.

X-ray mapping was performed on both samples using Si Kα radiation to evidence IL formation around almost all U(Mo) particles, Figure 2.

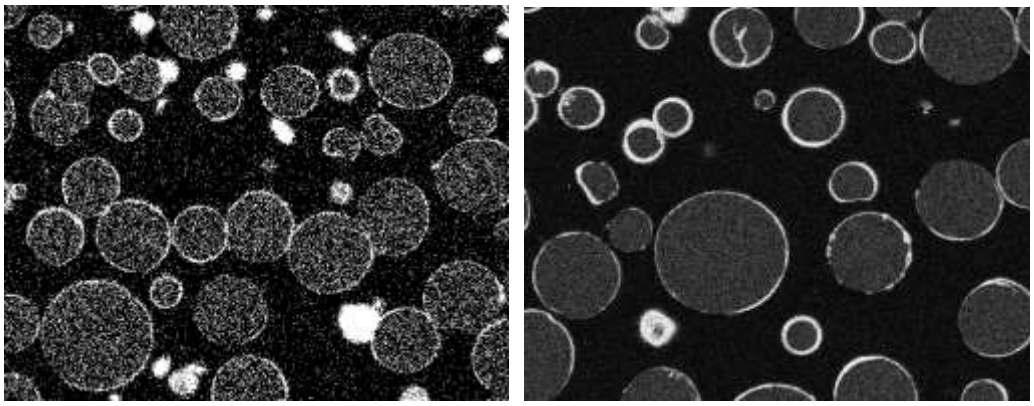

Figure 2. Si X-ray mapping. a) Miniplate U(Mo)/Al-4Si, b) Miniplate U(Mo)/Al-4Si_E. SEM - EDS.

XRD was used to identify crystalline structure of the phases that form the whole meat for both miniplates. The spectra are presented together in Figure 3a for an easy comparison and phases from the IL are only indicated for clarity. Concerning initial components of the meat, γU, αU and O_2U phases from the U-7Mo particles together with Al phase from the matrices were identified for both miniplates. Si phase was only identified for miniplate U(Mo)/Al-4Si_E (its principal reflection is marked with an arrow in Figure 3a). Concerning IL, $U(Al,Si)_3$ was clearly identified with lattice parameter *a* ~ 4.20 Å (~28 %at Si according to Dwigth [14]) meaning that IL is mainly formed by it. A deeper analysis was needed to clarify the possible presence of Si_2U and/ or Si_5U_3. With this objective two new spectra were performed on miniplate U(Mo)/Al-4Si_E. For both of them very narrow angular ranges were selected avoiding reflections from U, Al or Si phases and increasing seventeen times the scan step time. First spectrum, Figure 3b, includes reflection (001) from USi_2 phase and (001) from U_3Si_5 phase and the second one, Figure 3c, includes reflection (200) from USi_2 phase which is very near to reflection (211) from UO_2.

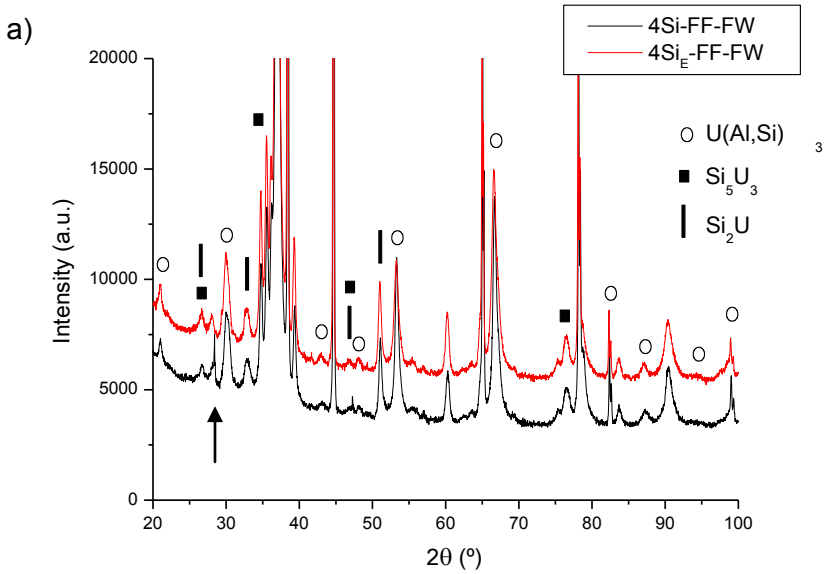

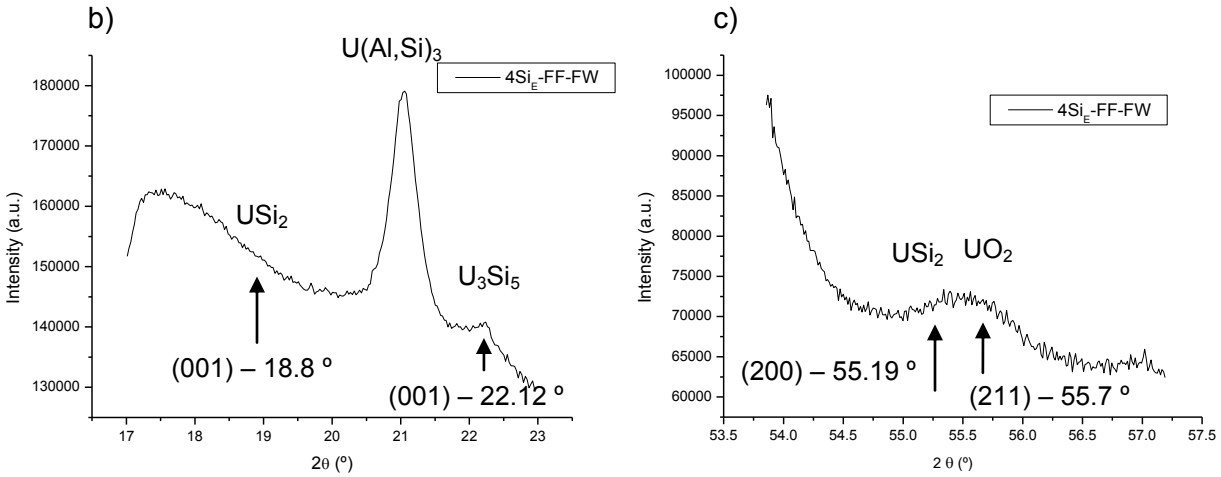

Figure 3. Spectra obtained for miniplates U(Mo)/Al-4Si and U(Mo)/Al-4Si$_E$. a) Phases corresponding to IL, b) and c) Identification of U_3Si_5 in the IL - XRD.

From Figures 3 b) and c) it can be concluded that neither (001) nor (200) reflections from USi_2 are evident in these spectra while reflection (001) from U_3Si_5 is observed. According to this the IL grown during fabrication in miniplates U(Mo)/Al-4Si and U(Mo)/Al-4Si$_E$ is formed by $U(Al,Si)_3$ and U_3Si_5 phases.

3.2. U_3Si_2/Al plates characterization

XRD was performed on both U_3Si_2 powders in the as cast condition. As shown in Figure 4 only U_3Si_2 crystalline structure was identified in both cases.

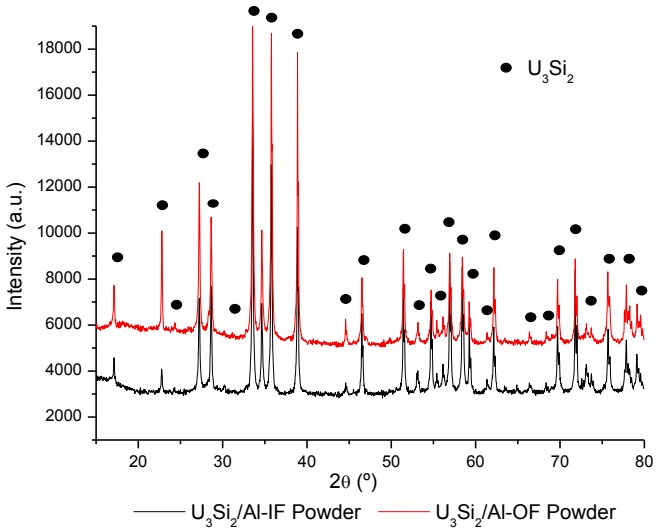

Figure 4. Crystalline structure identification in powders of U_3Si_2 compound in the as cast condition. XRD.

In Figure 5 crystalline structure identification of the meats of the plates U_3Si_2/Al-IF and U_3Si_2/Al-OF after whole fabrication process is shown. Same phases were identified for both samples meaning that different cooling process does not have any significant influence on final product.

Crystalline structure from Al and U_3Si_2 were identified which correspond to meats original components. Forming the IL, $U(Al, Si)_3$ with lattice parameter *a* ~ 4.24 Å (~12 %at Si according to Dwigth in [14]) was identified which, according to the low intensity of its reflections, is probably present in very low amount. Besides, a high intensity set of reflections was present in both spectra. From all the known aluminides, silicides and ternary U-Al-Si phases, U_3Si_2 (i.e. *t*P10) theoretical spectrum with modified lattice parameters a_{modif} ~ 7.56 Å and c_{modif} ~ 4.03 Å is the only one that matches this set.

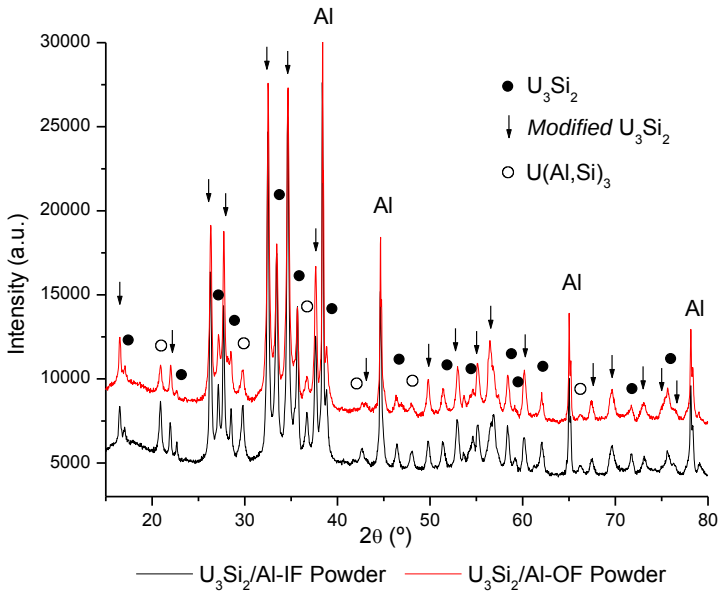

Figure 5. Crystalline structure identification in plates U_3Si_2/Al-IF and U_3Si_2/Al-OF. XRD.

High magnification observations in backscatter electron mode revealed zones of dark gray colour (i.e. rich in elements of low atomic weight) as the very narrow layer surrounding particles (more evident in smaller particles), Figure 6a, or regions at the corner of some silicide particles, Figure 6b. EDS determinations on regions as the one shown in Figure 6b evidenced the presence of ~75 %at (Al+Si). These regions would be associated to $U(Al,Si)_3$.

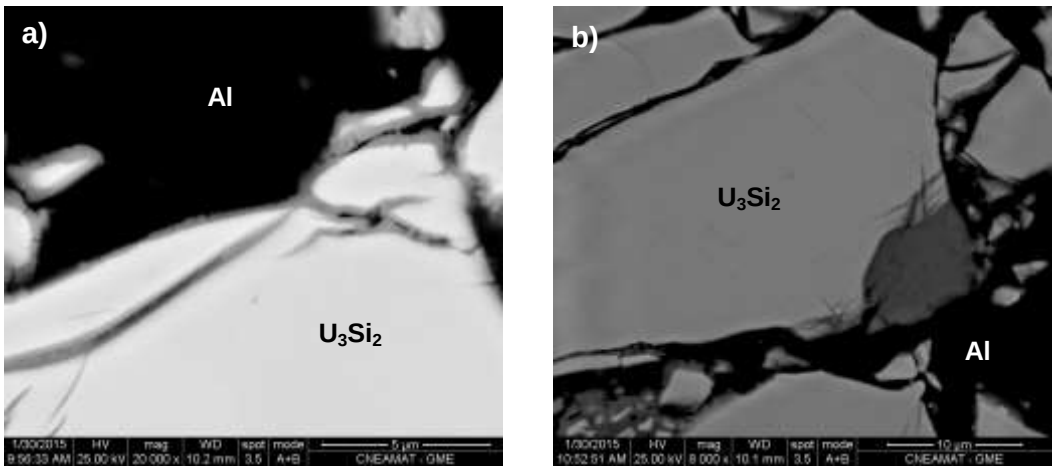

Figure 6. High magnification observations of plates U_3Si_2/Al-IF and U_3Si_2/Al-OF-SEM-BSE.

According to XRD results, fabrication process promotes the formation of a significant amount of another phase which will be called modified U_3Si_2. Although its high relative participation in the samples, it could neither be observed by OM or SEM nor obtained concentration information that accounts for its location. One possible explanation that could be proposed is that Al incorporation in solution to U_3Si_2 phase can promote an enlargement its cell volume. As Si and Al have very similar atomic weights SEM BSE images are not precise enough to evidence this. Further concentration analysis is mandatory to corroborate this assumption and define its location.

3.3. Influence of the fabrication process in IL formation for U_3Si_2/Al plates and U(Mo)/Al(Si) miniplates. Similarities and differences.

After whole fabrication process both types of fuels (U_3Si_2 and U(Mo)) reacted with matrix materials leading to the formation of an interaction layer formed by new phases. For U(Mo) these phases are $U(Al,Si)_3$ and U_3Si_5 meanwhile for U_3Si_2**,** $U(Al,Si)_3$ together with *modified* U_3Si_2 were identified.
When comparing relative participation of the IL in each meat, although an accurate calculation would be needed, it can be inferred that it is much more relevant for silicide than for U(Mo).
Crystalline structure corresponding to $U(Al,Si)_3$ was identified for both fuels but with a difference in lattice parameter. As it is well known, lattice parameter variation is correlated with Al (or Si) concentration in the Al-Si sublattice [14]. From results presented in this work Si concentration in this phase is higher for U(Mo) than for U_3Si_2**.**

4.Conclusions

In this work two plates fabricated with U_3Si_2 particles dispersed in an Al matrix were analyzed to obtain information about the IL that forms during fabrication process and compares it with the one obtain for the miniplates made with U-7wt%Mo dispersed in Al-4wt%Si matrices.
According to the results presented in this paper, and from the fact that silicide fuels have a good irradiation behavior, an IL formed only by $U(Al,Si)_3$ can be considered "*a proper interaction layer*" to be formed during fabrication process surrounding U(Mo) particles as a protective layer. Diffusion couples presented in section 2.2 will be studied in order to establish if any Si concentration (in Al matrix) favor the formation of this phase over other U-Si phases.

Acknowledgements

The authors want to thank Ricardo Sanabria for his collaboration in sample metallographic preparation together with the technical staff of Gerencia Materiales-GAEN-CNEA and Laboratorio de Difracción de Rayos X-Departamento de Física de la Materia Condensada-GAIyANN-CNEA for their support.
This work was partially financed by Project PICT-2010-1351,AgenciaNacional de Promoción Cientifica y Tecnológica (Argentina), FONCyT.

References

1.- M.K. Meyer, G.L. Hofman, S.L. Hayes, C.R. Clark, T.C. Wiencek, J.L. Snelgrove, R.V. Starin, K.H. Kim, J. Nucl. Mat. 304 (2002) 221-236.
2.- J. L. Snelgrove, G. L. Hofman, M. K. Meyer, C. L. Trybus, T. C. Wiencek, Nucl. Eng. Design 178 (1997) 119-126.

3.- Lundberg, J Nucl Mat. 167 (1989) 64-75.
4 G.L. Hofman, M.R. Finlay, Y.S. Kim, Proceedings of the 26th International Meeting on Reduced Enrichment for Research and Test Reactors (RERTR), Vienna, Austria, 2004.
5 A. Leenaers, S. Van den Berghe, J. Van Eyken, E. Koonen, F. Charollais, P. Lemione, Y. Calzavara, H. Guyon, C. Jarousse, D. Geslin, D. Wachs, D. Keiser, A. Robinson, G. Hofman, Y.S. Kim, J. Nucl. Mater. 441 (2013) 439-448.
6 D.D. Keiser Jr, A.B. Robinson, J-F Jue, P. Medvedev, D.M. Wachs, M.R. Finlay, J. Nucl. Mater. 393 (2009) 311-320.
7 D.D. Keiser Jr, J-F Jue, N.E. Woolstenhulme, E. Ashley, J. Nucl. Mater. 419 (2011) 226-234.
8.- E. Koonen, H. Guyon, P. Lemoine, C. Jarousse, D.M. Wachs, J. Stevens, 31th International Meeting on Reduced Enrichment for Research and Test Reactors, Beijing, China, 2009.
9.- F. Fréry, H. Guyon, E. Koonen, S. Van den Berghe, P. Lemoine, F. Charollais, C. Jarousse, D. Geslin, 32nd International Meeting on Reduced Enrichment for Research and Test Reactors (RERTR), Lisbon, Portugal, 2010.
10.- F. Charollais, P. Lemoine, Y. Calzavara, H. Guyon, E. Koonen, S. Van den Berghe, B. Stepnik, C. Jarousse, D. Geslin, 33rd International Meeting on Reduced Enrichment for Research and Test Reactors (RERTR), Santiago, Chile, 2011.
[11] M. Mirandou, S. Aricó, S. Balart and J. Fabro. 18th International Meeting on Research Reactor Fuel Management (RRFM), Ljubljana, Slovenia, 2014.
[12] W. Kraus, G. Nolze, U. Müller, Pulverdiffraktogramme aus Einkristalldaten und Anpassung experimenteller Beugungsaufnahmen, PowderCell 2.3., 2000.
13.- D. Blake, R. Hehemann, Transformation in Uranium Base Alloys, Session II, Physical Metallurgy of Uranium Alloys. Burke J. et al., editors. Massachusetts: Brook Hill Publishing Co., Chestnut Hill; 1976: 189-218.
14 A.E. Dwight, Report Specification Nº ANL –82-14, 1982, 1-39.

ANALYSIS OF MICROSTRUCTURE AND PRECIPITATIONS IN U-ZR METALLIC FUEL

C. T. LEE and H. L. KIM

Research Reactor Fuel Development, Korea Atomic Energy Research Institute (KAERI)

111 Deadeok-dearo 989 Beon-gil, Yuseong-gu, 305-353, Daejeon, South Korea

ABSTRACT

U-10wt.% Zr metallic fuel for releasing fast fission gas was fabricated using induction melting and sintered methods and the microstructures of the fabricated alloys were then observed through scanning and transmission electron microscopy. In particular, the selected area diffraction pattern and micro-chemical analysis were used to identify the phases. The microstructure of the induction melted U-10wt.% Zr alloy was the lamellar structure consisting of a typical α-U phase and δ-UZr_2 phase. The α-U phase was a orthorhombic crystal structure having compositions of 95.5-99.1 at.% U and 1.2-4.4 at.% Zr, and δ-UZr_2 phase was a hexagonal crystal structure. In addition, the globular precipitates were observed in the induction melted U-10wt.% Zr alloy. While the sintered U-60wt.% Zr alloy showed the inclusions of acicular-type shapes instead of a globular. A globular shape precipitate is a α-Zr with hexagonal structure including O and U elements. Rod and rectangular shape inclusions were identified as a $SiZr_2$ phase of the tetragonal crystal structure.

1. Introduction

There are renewed interests in metallic fuels for a sodium fast reactor, because of their outstanding properties such as a good breeding performance, high burn-up potential, ease of fabrication and high thermal conductivity [1, 2]. However, metallic fuels have a few serious problems which are the fuel swelling, mechanical and chemical reaction between the cladding and fuel while operating in the reactor. To overcome these problems, the ternary U-Pu-X alloys were suggested by Argonne National Laboratory (ANL). Of the alloying elements which are Mo, Nb, Ti, Zr and fissium, the Zr was found to be the most effective [2]. Thus, we examined the U-Zr binary alloy to accumulate the properties prior to irradiation testing related to its characteristics of casting, thermal stability and so on.

Previous studies have dealt only with the thermodynamic properties to understand the irradiation behavior of U-Zr alloys. Studies regarding with the microstructures of matrix and irregular phases, which are affected by impurities, have been rarely carried out. Although a few studies were previously carried out the phase identification on the microstructures of U-Zr alloys, they were mostly conducted by X-ray diffraction technique instead of transmission electron microscopy [3, 4]. However, in the case of an X-ray diffraction technique, it is difficult to determine the effects of impurities on the phase relationship because of the small amounts of impurities.

Therefore, in this study, the microstructures of the U-Zr binary alloy were observed and their phases are identified using energy dispersive spectroscopy (EDS) and a selected area diffraction (SAD) pattern of the TEM. Especially, the impurities were investigated in the microstructure of the U-Zr alloy. In addition, the dominant inclusion shapes were different according to the manufacturing methods such as induction melted and sintered processes. Thus the inclusions of U-Zr alloys were determined using SEM and TEM.

2. Experimental Procedures

The U-10wt.% Zr alloy specimens used in this study were fabricated using vacuum induction melting with depleted uranium(99.9% pure) and zirconium sponge(99.9% pure). To prevent the chemical reaction between the graphite crucible and molten fuel, a graphite

crucible coated with yttrium-stabilized zirconia was used. After holding for 30min at a temperature of 1600 ℃, molten alloy was poured into a quartz mold coated with ZrO_2. SiO_2. Meanwhile, in case of the sintered U-60wt.% Zr, the sintering was carried out at 1400 ℃ during 3hr after atomizing U and Zr powders and compacting mixed powders [5].

A chemical analysis was carried out from samples of the top, center and bottom of the casting rod using inductively coupled plasma atomic emission spectroscopy (ICP-AES). Table 1 shows the results of the chemical analysis.

Metallographic specimens were cut from the transverse section of the center segment of the alloy and then ground to a thickness of below 100 ㎛. The ground specimens were electropolished using a twin-jet thinner. Scanning electron microscopy (SEM) and transmission electron microscopy (TEM) were used to examine the microstructure. The phases were identified using a selected area diffraction (SAD) pattern and energy dispersive spectrometer (EDS).

3. Results and Discussions

Fig. 1 shows transverse-sectional microstructures of induction melted and sintered U-Zr alloys observed through scanning electron microscopy (SEM). As shown in Fig. 1 (a), the U-10 wt.%Zr alloy consisting of the α-U phase and δ-UZr_2 phase below 617℃ has eutectoid lamellar structures and globular precipitates. This lamellar structure is believed as to be the releasing paths of the fission gas during the irradiation because this microstructure has a porous crystal structure [6]. The globular precipitates were α-Zr and different with the acicular-type, which aligned the rectangular precipitates, of sintered U-60wt. %Zr alloy as shown in Fig. 1(b). The U-60wt.% Zr alloy consisted of the δ-UZr_2 matrix with acicular-type α-Zr precipitates. The acicular-type α-Zr shape was different with a globular shape of primary α-Zr formed by eutectoid reaction. It is inferred that the acicular shape inclusion was formed along preferred direction during a sintering process. The detailed characteristics of precipitates in the sintered U-Zr alloy will be studied later.

Fig. 2 shows the bright field TEM image of the lamellar structure and SAD patterns of the dark (α-U) and light (δ-UZr_2) phase in the lamellar. The average thickness of the α-U phase is two or three times larger than that of the δ-UZr_2 phase, which are 40-80 ㎚ and 20-30 ㎚, respectively (shown in Fig. 2(a)). The α-U phase is showed as an orthorhombic structure from a SAD pattern having a [010] zone axis in Fig. 2(b) and it consists of 95.5-99.1 at.% U and 1.2-4.4 at.% Zr components by EDS. While δ UZr_2 having a $[1\bar{1}02]$ zone axis in Fig. 2(c) shows a hexagonal structure. The δ-UZr_2 phases are composed of 69.4-78.6 at.% Zr and the other parts of U. Other authors observed that the expansion of the crystal lattice with increasing Zr concentration was larger along the *c*-axis than along the *a*-axis [7].

Other irregular phases, which are globular, rod and rectangular shapes, are also founded in the U-10 wt.% Zr alloy. First, a globular shape precipitate was assumed to be α-Zr stabilized by oxygen. Fig. 3 shows micrographs of the globular shape precipitate observed by SEM, TEM and SAD pattern. The size of the α-Zr globular shape is variable to 5-25 ㎛. The globular phase has a hexagonal structure like pure α-Zr from the analysis of the SAD pattern having a [0001] zone axis. The globular phase was composed of 95-99 at.% Zr concentrations, but as shown in Table 2, the lattice parameter of the globular phase, which was measured from the diffraction patterns, is slightly increased compared to pure α-Zr owing to the impurities such as a O element. The distance between the equivalent planes of the pure α-Zr and measured α-Zr of the specimens are presented in Table 2. In addition, the matrix of globular precipitate exhibited a number of small spots, as shown in Fig. 4. The black spots have a composition of 72 at.% Zr and 28 at.% U. The U elements were precipitated in the globular precipitate because of the decrease of U solubility with decreasing temperature in α-Zr. Thus, it is inferred that the globular α-Zr phase influenced by the oxygen impurity is α-Zr of hexagonal structure including a small spot with U-rich precipitate.

Fig. 5 (a), (b) shows inclusions of a rectangular shape and rod shape, which aligned rectangular inclusions, appearing in the U-Zr alloy. This rectangular shape inclusion had 33 at.% Si and 67 at.% Zr compositions (shown in Table 3). The Si elements were entered from

mold wash. The inclusion size of the rectangular type is about 10 ㎛. A TEM and SAD pattern of rectangular inclusion is presented in Fig. 5 (c). The rod type also has the same structure and compositions as a rectangular type with a tetragonal structure and $SiZr_2$, respectively.

4. Conclusions

The microstructure of the U-10wt.% Zr and U-60wt.% Zr alloy fabricated by induction melting and sintering was studied, respectively. We obtained the following results.

(1) The induction melted U-10wt.% Zr alloy consists of lamellar structure of the α-U phase and δ-UZr_2 phase having the an orthorhombic and hexagonal structure, respectively. The average thickness of the α-U phase is two- or three-times larger than that of the δ-UZr_2 phase. While the sintered U-60wt.% Zr alloy was composed of δ-UZr_2 matrix with acicular-type α-Zr precipitates.

(2) In case of U-10wt.% Zr alloy, the globular shape inclusion is α-Zr having a hexagonal structure and its lattice parameter is larger than pure α-Zr owing to impurity elements such as a O element. In addition, the globular precipitate showed a number of small spots including U-rich precipitate. Whereas the sintered U-60wt.% Zr alloy showed the acicular-type α-Zr phase formed along preferred direction

(3) The rectangular and rod shape inclusions are $SiZr_2$ with a tetragonal structure in U-10wt.% Zr alloy.

Reference

[1] J.S.Kim et. al. *Nucl. Eng. Tech*. **38** (2006) 301.

[2] J. H. Kittel, B. R. T. Frost, J. P. Mustelier, K. Q. Bagley, G. C. Crittenden and J. Van Dievoet, *J. of Nucl. Mater* **204** (1993) 1.

[3] H. L. Yakel, *Physical Metallurgical of Uranium Alloys*, Brook Hill Pub. Co., Book1 (1976) 259.

[4] A. E. Dwight and M. H. Mueller, *ANL-5581* (1957).

[5] T.K.Kim, C.T.Lee and D.S.Sohn, *J. Nucl. Mater.* **372** (2008) 394.

[6] J. Rest, *J. of Nucl. Mater* **207** (1993) 192.

[7] A.Landa, P.Soderlind and P.E.A.Turchi, *J. of Alloys Comp.* **478** (2009) 103

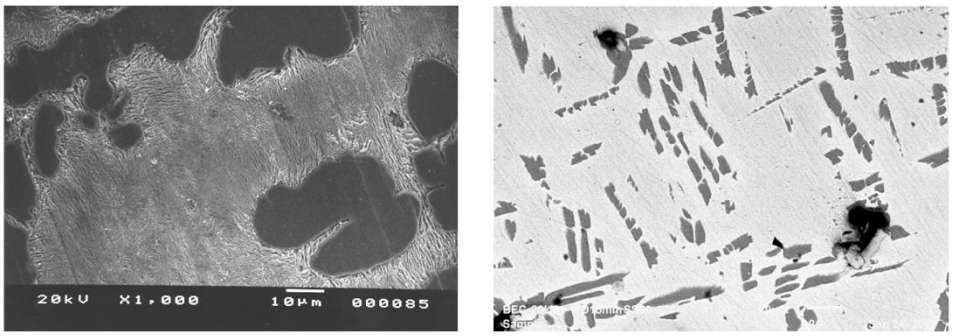

Fig. 1 SEM image of (a) the induction melted U-10 wt.% Zr alloy and (b) sintered U-60 wt.% Zr alloy

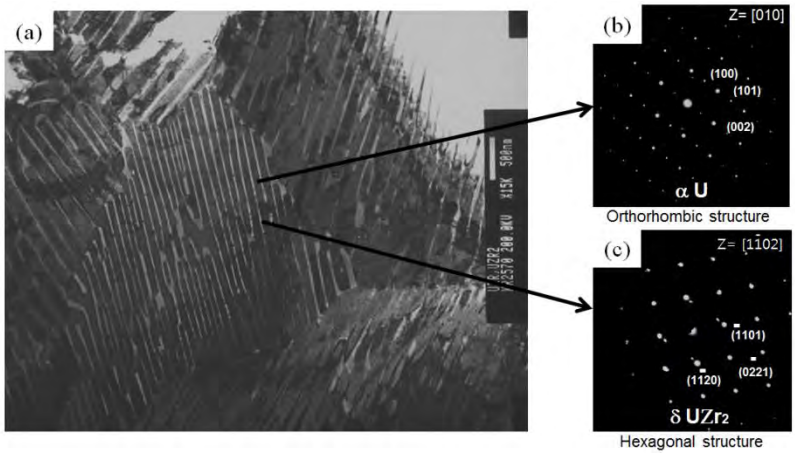

Fig. 2 (a) bright field TEM image and selected area diffraction pattern of (b) the α phase of [010] zone axis and (c) the δ phase of [1 $\bar{1}$02]zone axis in the U-10 wt.% Zr alloy

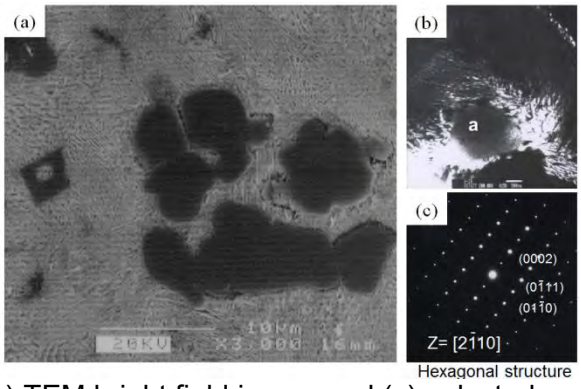

Fig. 3 (a) SEM image, (b) TEM bright field image and (c) selected area diffraction pattern of a globular shape inclusions in the U-10wt.% Zr alloy

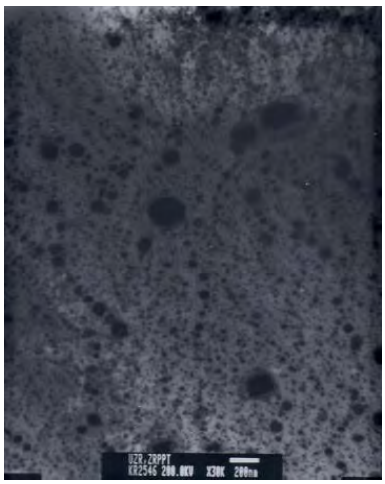

Fig. 4 . TEM bright field image in the globular shape precipitate of the U-10wt.% Zr alloy.

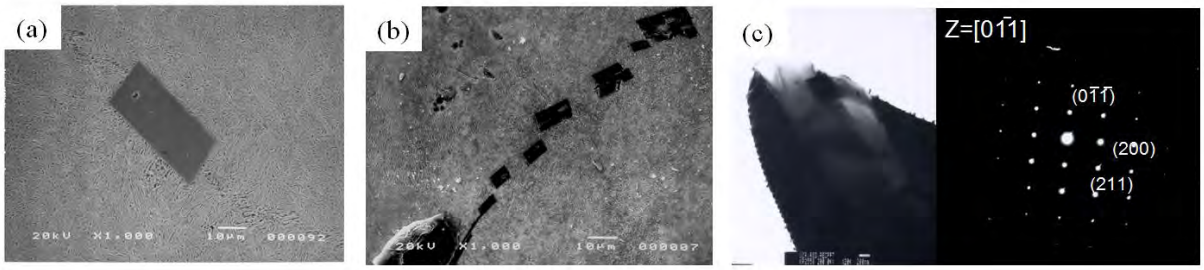

Fig. 5 SEM image of (a) a rectangular shape, (b) a rod shape inclusions and (c) BE image and SAD pattern in the U-10wt.% Zr alloy

Table 1. Chemical compositions of the U-10wt.% Zr alloy (in wt.%)

	Top	Center	Bottom	Average
U	Bal	Bal	Bal	Bal
Zr	9.05	8.95	9.10	9.03
Si	180 ppm	158 ppm	320 ppm	219 ppm
O	1825 ppm	1555 ppm	2341 ppm	1907 ppm
N	32 ppm	23 ppm	38 ppm	31 ppm
C	140 ppm	250 ppm	250 ppm	213 ppm

Table 2. Distance between equivalent planes of the pure α Zr and measured α Zr in the U-10wt.% Zr alloy

	(1010)	(0002)	(1120)	(1121)
pure α Zr	2.799	2.574	1.616	1.542
measured α Zr	2.845	2.583	1.621	1.559

Table 3. Chemical compositions of α, δ phase and precipitations in the U-10 wt.% Zr alloy

	α	δ	globular	rod	rectangular
U	99.16 at.%	30.57 at.%	97.05 at.%		
Zr		69.43 at.%	2.95 at.%	65.51 at.%	67.31 at.%
Si				33.41 at.%	32.69 at.%
O			2000ppm		

NEUTRONIC COMPARISON OF RELAP5-3D AND MCNP5 MODELS FOR THE TRIGA IPR-R1

P. A. F. MESQUITA, A. L. COSTA, C. A. M. SILVA, P. A. L. REIS, C. PEREIRA, M. A. F. VELOSO, H. V. SOARES
Departamento de Engenharia Nuclear
Universidade Federal de Minas Gerais
Av. Antônio Carlos Nº 6627, Campus Pampulha, CEP 31270-901
Belo Horizonte, MG, Brazil
Instituto Nacional de Ciências e Tecnologia de Reatores Nucleares Inovadores/CNPq, Brazil

ABSTRACT

This paper presents two models for the IPR-R1 TRIGA research reactor using the code RELAP5-3D 3.0.0 and the code MCNP5. Such models were verified according with experimental data. Results of radial relative power core distribution, average thermal flux radial core distributions and the effective multiplication factor value, k_{eff}, obtained by RELAP5-3D and MCNP5 codes calculations were compared between them and with available data for power operation of 100 kW.

1. Introduction

The increase of research reactors commercial exploitation commonly directed at neutrons generation for several types of scientific and social purposes has enlarge the interest about safety of these reactors [1]. Power generation is not the main activity of these types of reactors reaching maximum power operation of about 100 MW. In spite of this, specific features are necessary to ensure safe utilization of such installations. Therefore, several codes have been used focusing special attention for research reactors safety analysis and valuation of specific perturbation plant processes. A combination of codes for thermal hydraulic analysis, for assessment of probabilistic risk, fuel investigation and reactor physics studies are fundamental tools for an appropriate reactor behaviour definition [2]. In this work, the codes RELAP5-3D [3] and the MCNP5 [4] were used to simulate the TRIGA IPR-R1 research reactor.

TRIGA (Training, Research, Isotope, General Atomic) research reactors are constructed in a variety of configurations and capabilities, with steady-state power levels ranging from 20 kW up to 16 MW offering true “inherent safety”. In spite of this, some situations may occur disturbing the normal reactor operation. In this work two models of the TRIGA IPR-R1 have been used to simulate the reactor core behaviour. The main aim is to verify the RELAP5-3D model comparing results of k_{eff} and thermal flux distribution with a MCNP5 model, both using a Cartesian geometry. The MCNP5 was used in preceding works to simulate the IPR-R1 using cylindrical geometry model, exactly the same IPR-R1 reactor geometry and good results were obtained [5, 11].

1.1 IPR-R1 Reactor

The IPR-R1 is installed at Nuclear Technology Development Centre (CDTN) of Brazilian Nuclear Energy Commission (CNEN), in Belo Horizonte, Brazil. It is a reactor type TRIGA Mark-I housed in a 6.625 meters deep pool with 1.92 meters of internal diameter and filled with light water which has function of cooling, moderator, neutron reflector and radioactive shielding. IPR-R1 works at 100 kW but it will be briefly licensed to operate at 250 kW.

It works at low power and low pressure being applied in research, training and radioisotopes production. The core presents a radial cylindrical configuration with six concentric rings (A, B, C, D, E, F) with 91 channels able to host either fuel rods or other components like control rods, reflectors and irradiator channels. The 63 fuel elements are constituted by a cylindrical metal cladding filled with a homogeneous mixture of zirconium hydride and Uranium 20% enriched in ^{235}U isotope. There are 59 fuel elements covered with aluminum and 4 fuel elements with stainless steel. In the center of the reactor, there is an aluminum tube (central thimble) to irradiation of experimental samples. This tube is removable and when it is not in use, the reactor pool water fills its volume. The main thermal-hydraulic and kinetic characteristics of the IPR-R1 core are listed in [6, 8]. The radial relative power distribution (Fig. 1) was calculated in preceding works using the WIMSD4C and CITATION codes and also experimental data [7]. The radial factor is defined as the ratio of the average linear power density in the element to the average linear power density in the core. Fig. 1 shows also the six core concentric rings (A, B, C, D, E, F).

Furthermore, the core has an annular graphite reflector with aluminum cladding. Such annular reflector has a radial groove where a rotary rack is assembled for insertion of the samples to irradiation. In such rotary rack is possible to place the samples in 40 different positions around the core. Moreover, tangent to annular reflector, there is a pneumatic tube where the samples also can be inserted to irradiation.

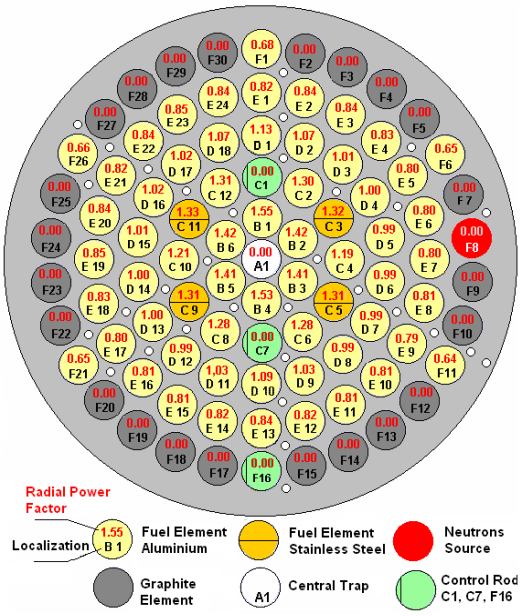

Fig 1. Radial relative power distribution

The reactor cooling occurs predominantly by natural convection governed by the water density differences. To perform the heat removal generated in the core, the water of the pool is pumped through a heat exchanger.

2. RELAP5-3D Model

There are two options for the computation of the reactor power in the RELAP5-3D code [3]. The first option is the point reactor kinetics model that was implemented in previous versions of RELAP5. The second option is a multi-dimensional neutron kinetics model based on the NESTLE code developed at North Carolina State University. RELAP5-3D was modified to call the appropriate NESTLE subroutines depending upon the options chosen by the user and this is the most prominent attribute that distinguishes the RELAP5-3D code from the previous versions. The neutron kinetics model uses the few-group neutron diffusion equations. Two or four energy groups can be utilized, with all groups being thermal groups if

desired. Core geometries modelling include Cartesian and hexagonal. Core symmetry options are available, including quarter, half and full core for Cartesian geometry and one-sixth, one-third and full core for hexagonal geometry.

To perform the IPR-R1 model in the RELAP5-3D, two energy groups were used. The full core has been simulated. As it can be verified in the Fig. 1, the IPR-R1 has circular geometry. To simulate it in the RELAP5-3D, it was chosen the Cartesian geometry. The TH regions and the NK modeling are shown in Fig. 2 for the upper axial plane, which corresponding areas coincide with those from the circular core geometry. As there are 91 nodes for each plane and there are 21 axial planes, then the core has 1911 neutron kinetic nodes. To simplify the model, the 63 fuel elements were collapsed in 13 heat structure (HS) components. These HS components were associated with the 13 corresponding hydrodynamic channels. The neutrons source (F8 in the Fig. 1) was simulated as a reflector element; the control rods (C1, C7, F16 in the Fig. 1) and the central thimble (A1) were simulated as water.

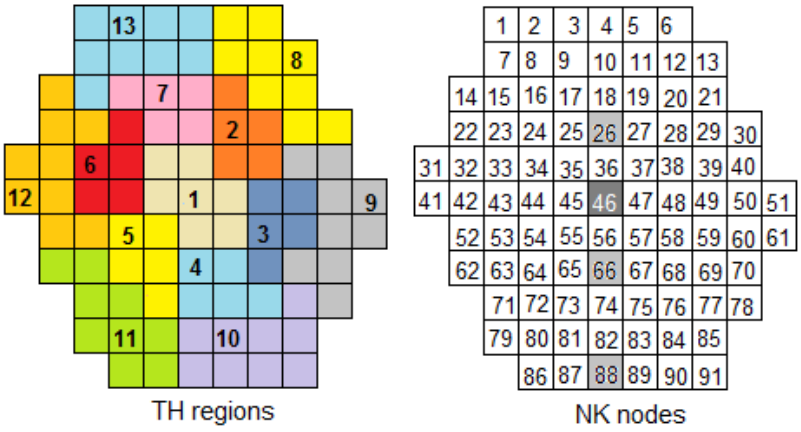

Fig 2. IPR-R1 – TH regions and corresponding NK nodes to RELAP5-3D modelling

To calculate the cross-sections sets, few compositions were considered in the model with six fuel compositions and one reflector composition (graphite element). The cross-section libraries were generated by WIMSD5 code [9] which is a general lattice cell program that uses transport theory to calculate flux as a function of energy and position in the cell. The base cross-sections were calculated according to data of the IPR-R1 exposure in year 2004.

The cross-section sets generated by WIMSD5 code were included in the RELAP5-3D. The tabular form of homogenized cross-section libraries is organized in two energy groups. Data as the scattering, absorption and fission macroscopic cross sections, and assembly discontinuity factors are tabulated for each controlled and uncontrolled composition.

The RELAP5 Mod3.3 has been used to simulate the TH behaviour of the IPR-R1 with good results [6, 8]. Then, the neutron kinetic part was incorporated to the RELAP5-3D to complete the TH-NK coupling. However, as the RELAP5 codes were developed mainly to simulate power reactors with a square geometry, it is necessary to adapt the model to simulate the cylindrical geometry of the IPR-R1.

3. MCNP5 Model

The IPR-R1 core was configured in the MCNP5 code according with neutron kinetic model of RELAP5-3D (NK nodes). This core was modeled by a square lattice with 91 cells able to host either fuel rods or other components like control rods, reflectors and irradiator channels. The

elements are surrounded by water. The control rods and the central thimble were not configured and their corresponding cells are filled with water. The neutron source (F8 in the Fig. 1) was simulated as reflector element. The fuel elements have three axial sections with upper and lower reflector (graphite), and the central portion filled with fuel. The radial reflectors elements are covered with aluminum and filled with graphite having the same dimensions of the fuel elements. Figure 3 illustrates the axial and radial view of simulated modelling and the Table 1 presents the main geometric dimensions.

Parameter	Value (cm)
Fuel radius	1.7900
Gap radius	1.7990
Cladding radius	1.8650
Fuel pitch distance	4.4025
Active length	36.1660
Axial reflector length	13.4170

Tab 1: Dimensions of MCNP5 model

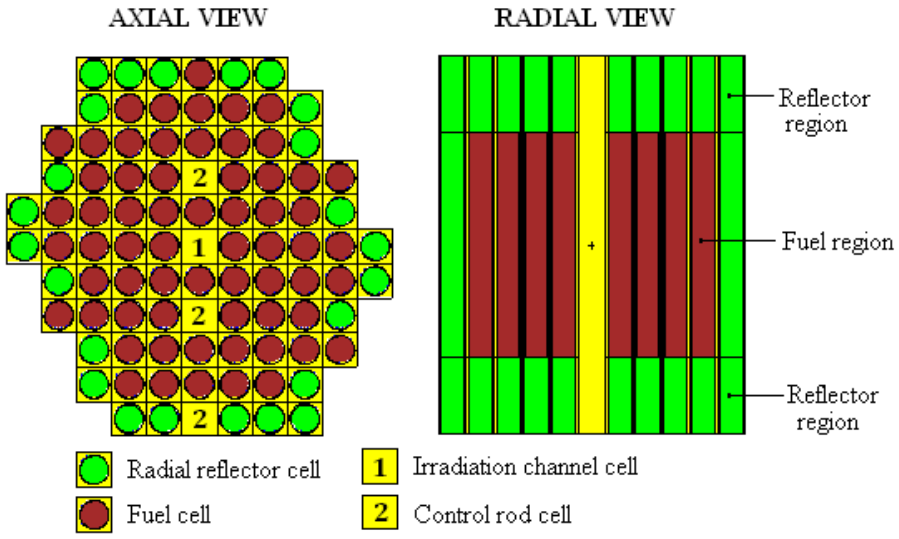

Fig 3. IPR-R1 – Core modelling using the MCNP5

The MCNP5 code apply the Monte Carlo Method that consists of actually following each of many particles from a source throughout its life to its death in some terminal category (absorption, escape, etc.). In the simulation 100 active cycles were calculated with 50000 neutrons per cycle using the ENDF/B-VI continuous neutron energy library.

The MCNP5 calculates k_{eff} values printing the respective standard deviation (*sd*) in the output file. To perform the neutron flux inside each cell the FMESH card of MCNP5 code was used. This feature allows the user to tally particles on a mesh independent of the problem geometry [4]. The MCNP5 estimates the flux using the source specified by the user. In the model, there are 91 square meshes with the same dimensions of the cell to estimate the neutron flux inside each mesh.

The flux estimation does not match the actual neutron source of the reactor. Thus, it is necessary to normalize the flux values initially calculated by MCNP5. In the simulation, this normalization was performed using the following equation [4]:

$$\phi_N = \phi_{MCNP} \times \left(\frac{P \times \nu}{Q \times k_{eff}} \right)$$

where ϕ_N is the normalized flux; ϕ_{MCNP} is the flux estimated by MCNP5; P is the reactor power level; ν is the average number of fission neutrons and Q is the recoverable energy per fission event. The values of ν, Q and k_{eff} are calculated by MCNP5 and they can be obtained in the output file of the code. The user provides the power level (P). In this case, for IPR-R1 reactor, P = 100 kW.

4. RELAP5-3D and MCNP5 Results

Fig. 4 presents the values of the average planar relative power distribution calculated by the RELAP5-3D and the MNCP5 codes; it presents also the data from the reference redistributed according to the Fig. 1 [7] and the difference found between the codes calculations and the reference data. As it can be verified, the main differences for both calculations are in the fuel elements corresponding to the last ring of the core (detached in blue color). These calculated values were considerably underestimated in relation to the reference data. This is probably because the annular graphite reflector surrounding the core was not simulated in both codes.

In fact, the MCNP5 code is capable to simulate in more details the core including the annular reflector [5]. However, as the idea is to verify the RELAP5-3D model using the MCNP5, and the RELAP5-3D is not capable to simulate exactly the same geometry of the core, both models did not consider the reflector surrounding the core. Fig. 5 shows the general result of the average relative power distribution in the core obtained by the RELAP5-3D and MCNP5 for the IPR-R1 simulations considering 100 kW of power operation.

REFERENCE

0.00	0.00	0.00	0.00	0.00	0.68	0.00	0.00	0.00	0.00	0.00
0.00	0.00	0.00	0.85	0.84	0.82	0.84	0.84	0.00	0.00	0.00
0.00	0.66	0.84	1.02	1.07	1.13	1.07	0.83	0.00	0.00	0.00
0.00	0.00	0.82	1.02	1.31	0.00	1.30	1.01	0.80	0.65	0.00
0.00	0.84	1.01	1.33	1.55	1.42	1.32	1.00	0.80	0.00	0.00
0.00	0.85	1.00	1.21	1.42	0.00	1.41	1.19	0.99	0.80	0.00
0.00	0.00	0.83	1.00	1.31	1.41	1.53	1.31	0.99	0.81	0.00
0.00	0.65	0.80	0.99	1.28	0.00	1.28	0.99	0.79	0.00	0.00
0.00	0.00	0.00	0.81	1.03	1.09	1.03	0.99	0.81	0.64	0.00
0.00	0.00	0.00	0.81	0.82	0.84	0.82	0.81	0.00	0.00	0.00
0.00	0.00	0.00	0.00	0.00	0.00	0.00	0.00	0.00	0.00	0.00

RELAP5-3D

0.0000	0.0000	0.0000	0.0000	0.0000	0.2730	0.0000	0.0000	0.0000	0.0000	0.0000
0.0000	0.0000	0.0000	0.6570	0.7935	0.7921	0.7524	0.6566	0.0000	0.0000	0.0000
0.0000	0.2847	0.7751	1.0431	1.1333	1.1270	1.0423	0.8157	0.0000	0.0000	0.0000
0.0000	0.0000	0.8355	1.1823	1.3534	0.0000	1.3522	1.1862	0.8336	0.2874	0.0000
0.0000	0.8386	1.2077	1.4451	1.3119	1.3111	1.4428	1.1986	0.7931	0.0000	0.0000
0.0000	0.6878	1.0922	1.4038	1.3227	0.0000	1.3205	1.3996	1.0880	0.6850	0.0000
0.0000	0.0000	0.8019	1.2139	1.4602	1.3239	1.3221	1.4545	1.2133	0.8405	0.0000
0.0000	0.2924	0.8521	1.2177	1.3900	0.0000	1.3811	1.2009	0.8449	0.0000	0.0000
0.0000	0.0000	0.0000	0.8486	1.0975	1.1962	1.1902	1.0775	0.7931	0.2896	0.0000
0.0000	0.0000	0.0000	0.7029	0.8515	0.8945	0.8416	0.6823	0.0000	0.0000	0.0000
0.0000	0.0000	0.0000	0.0000	0.0000	0.0000	0.0000	0.0000	0.0000	0.0000	0.0000

[(RELAP5 - Reference)*100%]/Reference

0.0	0.0	0.0	0.0	0.0	-59.9	0.0	0.0	0.0	0.0	0.0
0.0	0.0	0.0	-22.7	-5.5	-3.4	-10.4	-21.8	0.0	0.0	0.0
0.0	-56.9	-7.7	2.3	5.9	-0.3	-2.6	-1.7	0.0	0.0	0.0
0.0	0.0	1.9	15.9	3.3	0.0	4.0	17.4	4.2	-55.8	0.0
0.0	-0.2	19.6	8.7	-15.4	-7.7	9.3	19.9	-0.9	0.0	0.0
0.0	-19.1	9.2	16.0	-6.9	0.0	-6.3	17.6	9.9	-14.4	0.0
0.0	0.0	-3.4	21.4	11.5	-6.1	-13.6	11.0	22.6	3.8	0.0
0.0	-55.0	6.5	23.0	8.6	0.0	7.9	21.3	6.9	0.0	0.0
0.0	0.0	0.0	4.8	6.6	9.7	15.6	8.8	-2.1	-54.8	0.0
0.0	0.0	0.0	-13.2	3.8	6.5	2.6	-15.8	0.0	0.0	0.0
0.0	0.0	0.0	0.0	0.0	0.0	0.0	0.0	0.0	0.0	0.0

MCNP5

0.0000	0.0000	0.0000	0.0000	0.0000	0.3231	0.0000	0.0000	0.0000	0.0000	0.0000
0.0000	0.0000	0.0000	0.5676	0.7007	0.7289	0.6539	0.4541	0.0000	0.0000	0.0000
0.0000	0.2186	0.5838	0.8921	1.1015	1.2517	1.0346	0.7667	0.0000	0.0000	0.0000
0.0000	0.0000	0.8376	1.1727	1.5311	0.0000	1.4713	1.0660	0.6737	0.2392	0.0000
0.0000	0.5443	0.9855	1.3513	1.6349	1.9867	1.5874	1.2833	0.8955	0.0000	0.0000
0.0000	0.5507	1.0153	1.3927	1.8046	0.0000	1.7982	1.3741	1.0026	0.5527	0.0000
0.0000	0.0000	0.9042	1.2838	1.5834	1.9611	1.6149	1.33	0.9709	0.54	0.0000
0.0000	0.2418	0.6780	1.0686	1.4600	0.0000	1.4940	1.1468	0.8198	0.0000	0.0000
0.0000	0.0000	0.0000	0.7673	1.0277	1.2371	1.0828	0.8761	0.5758	0.2163	0.0000
0.0000	0.0000	0.0000	0.4498	0.6391	0.7569	0.69	0.5549	0.0000	0.0000	0.0000
0.0000	0.0000	0.0000	0.0000	0.0000	0.0000	0.0000	0.0000	0.0000	0.0000	0.0000

[(MCNP5 - Reference)*100%]/Reference

0.0	0.0	0.0	0.0	0.0	-52.5	0.0	0.0	0.0	0.0	0.0
0.0	0.0	0.0	-33.2	-16.6	-11.1	-22.2	-45.9	0.0	0.0	0.0
0.0	-66.9	-30.5	-12.5	2.9	10.8	-3.3	-7.6	0.0	0.0	0.0
0.0	0.0	2.1	15.0	16.9	0.0	13.2	5.5	-15.8	-63.2	0.0
0.0	-35.2	-2.4	1.6	5.5	39.9	20.3	28.3	11.9	0.0	0.0
0.0	-35.2	1.5	15.1	27.1	0.0	27.5	15.5	1.3	-30.9	0.0
0.0	0.0	8.9	28.4	20.9	39.1	5.5	1.7	-1.9	-34.0	0.0
0.0	-62.8	-15.3	7.9	14.1	0.0	16.7	15.8	3.8	0.0	0.0
0.0	0.0	0.0	-5.3	-0.2	13.5	5.1	-11.5	-28.9	-66.2	0.0
0.0	0.0	0.0	-44.5	-22.1	-9.9	-15.5	-31.5	0.0	0.0	0.0
0.0	0.0	0.0	0.0	0.0	0.0	0.0	0.0	0.0	0.0	0.0

Fig 4. Planar average relative power distribution from the reference, the RELAP5-3D and the MCNP5 codes, and the percentage differences in relation to the reference data

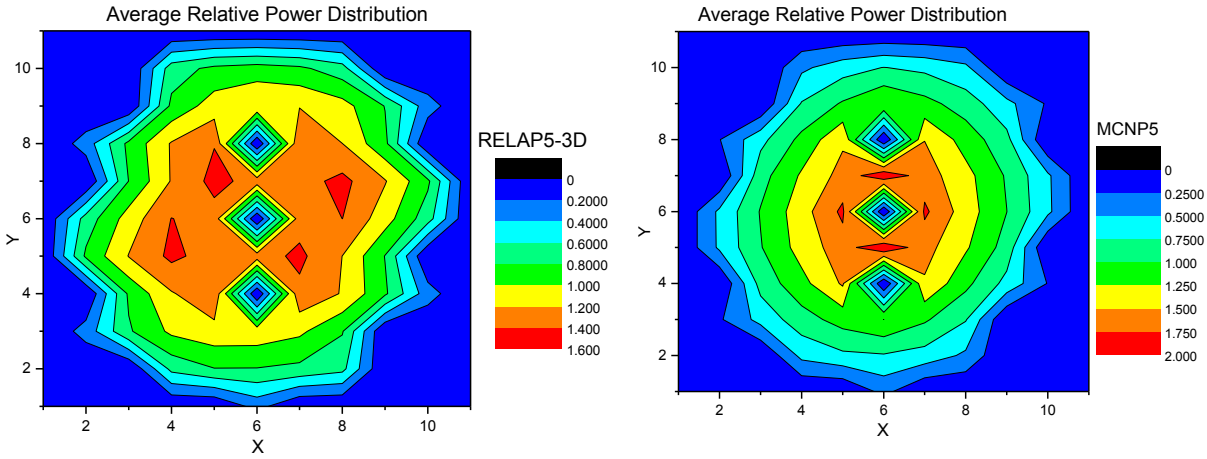

Fig 5. Planar average relative power distribution – RELAP5-3D and MCNP5 models

Fig. 6 presents the radial thermal flux distribution in the center of core (axial level 11) simulated by both codes. As it is demonstrated in Table 2, both calculations are overestimated in relation to reference data, but they are in the same order of magnitude of the experimental available data. For measuring thermal neutron flux at the central thimble it was used cobalt foil irradiated at 27 cm of the bottom of the core that is the position of maximum flux [10].

Type	**Thermal neutron flux at 100 kW (neutrons.cm^{-2}.s^{-1})**
RELAP5-3D	9.81 x 10^{12}
MCNP5	(7.11 $\pm$ 0.01) x 10^{12}
Experimental [10]	(4.1 $\pm$ 0.3) x 10^{12}

Tab 2: Calculated and experimental thermal fluxes in the central thimble

Finally, the calculated values of the effective neutron multiplication factor, k_{eff}, were compared. The values of k_{eff} given by the MCNP5 and the RELAP5-3D calculations were 0.91351 (sd =$\pm$ 3.1x10^{-4}) and 0.91670, respectively, very close each other in spite of the two different ways of neutronic calculation. However, these values are underestimated in relation to the expected value that would be next to 1.0. The explanation to such difference is probably connected to the fact that the reflector surrounding the core was not considered in the models causing a loss of neutrons that could be reflected back to the core. Then, it is necessary to find ways to simulate this part of the core in the RELAP5-3D.

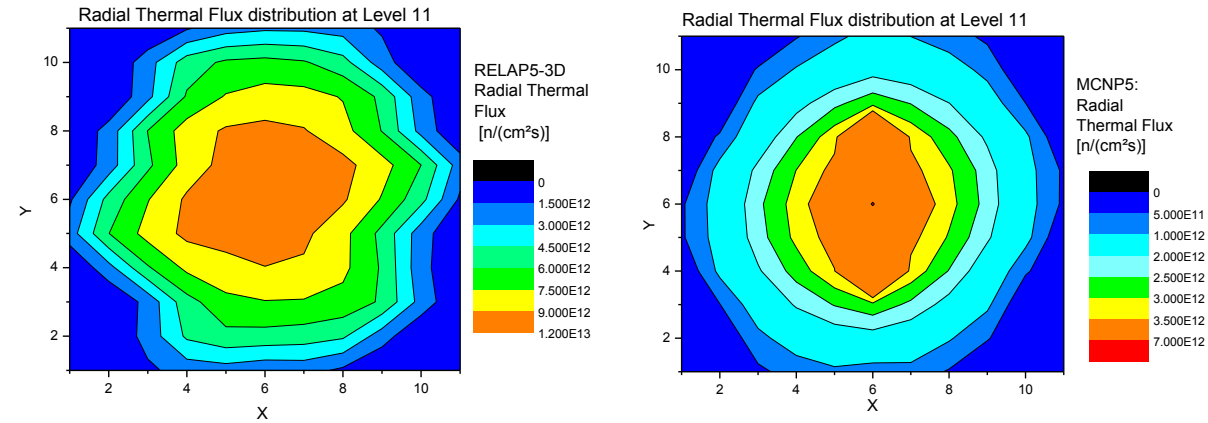

Fig 6. Radial thermal flux distribution in the center of the core (level 11) predicted by RELAP5-3D and MCNP5 models

5. Conclusions

Two models for the IPR-R1 TRIGA research reactor were considered in the RELAP5-3D and MCNP5 codes at 100 kW of power operation. Results of average radial relative power core distribution were compared with the reference data [7]. In a general way, both codes presented values next to the reference data, in spite of the difference presented in the fuel elements localized in the last ring. As the reflector surrounding the core was not considered in both models, this is possibly the cause of the neutrons loss. This also affected the prediction of k_{eff} that presented underestimated value in both models. About the thermal flux radial core distributions, the codes presented values in the same order of magnitude in comparison with the experimental data.

As it was explained, the MCNP5 is more flexible to simulate specific geometries including cylindrical one. However it is not capable to simulate transients with TH variations in nuclear systems mainly because it is not possible to perform the feedback in the cross sections. In the other hand, RELAP5-3D uses a multi-dimensional neutron kinetics model to simulate TH-NK coupled problems as steady state as transient calculations with cross sections feedback. The problem to apply the RELAP5-3D to simulate IPR-R1 TRIGA research reactors is to reproduce cylindrical geometries since it works only with hexagonal or Cartesian types. In this specific case it is necessary to adequate the model to duly simulate the core behaviour and to include aldo the external circular reflector.

Acknowledgments

The authors are grateful to CAPES, CDTN/CNEN, FAPEMIG and CNPq for the support. Thanks also to Idaho National Laboratory for the permission to use the RELAP5-3D computer software.

References

[1] IAEA. Safety Analysis for Research Reactors. IAEA Safety Standards Series, Nº 55, IAEA, Vienna, Austria, (2008).
[2] A. L. Costa et al., “Chapter 2: Safety Studies and General Simulations of Research Reactors Using Nuclear Codes”, In: Nuclear Power - System Simulations and Operation. Ed. InTech, Rijeka, Croatia, ISBN: 978-953-307-506-8, Vol. 2, p. 21-42, (2011).
[3] The RELAP5-3D© Code Development Team, RELAP5-3D© Code Manuals, *INEEL-EXT-98-00834,* (2005).
[4] T. E. Booth et al., “MCNP – A General Monte Carlo N-Particle Transport Code (version 5),” Tech. Rep. LA-UR-03-1987, Los Alamos National Laboratory, (2003).
[5] C. A. M. Silva et al., “Sensitivity Analysis of TRIGA IPR-R1 Reactor Models Using the MCNP Code”, *International Journal of Nuclear Energy* – Vol. 2014, Article ID 793934, 9 pages (2014).
[6] P. A. L. Reis et al., “Assessment of a RELAP5 model for the IPR-R1 TRIGA research reactor”, *Annals of Nuclear Energy*, 37, pp. 1341-1350, (2010).
[7] H. M. Dalle, C. Pereira, R. M. G. P., Souza, “Neutronic calculation to the TRIGA IPR-R1 reactor using the WIMSD4 and CITATION codes”, *Annals of Nuclear Energy*, 29, pp. 901–912, (2002).
[8] P. A. L. Reis et al., “Sensitivity analysis to a RELAP5 nodalization developed for a typical TRIGA research reactor”, *Nuclear Engineering and Design*, 242, pp. 300-306, (2012).
[9] RSICC Computer Code Collection WIMSD-5B.12 – Deterministic Code System for Reactor-Lattice Calculations, Oak Ridge National Laboratory (2007).
[10] R. M. G. P. SOUZA, “Thermal Neutron Flux Measurements in the Irradiation Facilities of the IPR-R1 TRIGA Reactor”, *In 3rd World TRIGA Users Conference*, Belo Horizonte, Brazil (2006).

[11] C. A. M. Silva et al., “MCNP5 modeling of the IPR-R1 TRIGA reactor for criticality calculation and reactivity determination”, *Nuclear Engineering and Design,* 241, pp. 4989-4993, (2011).

TRANSPORT OF IRRADIATED FUEL RODS AND SEGMENTS OF IRRADIATED FUEL RODS

S. MOESEN, W. BOECKX
Transnubel (TNB)
Zandbergen 1, 2480 Dessel – Belgium

ABSTRACT

The transport of irradiated fuel rods or segments of irradiated fuel rods is essential for the investigation of fuel behaviour after irradiation. The paper will focus on different aspects:

- The return of experience gained during the transport of irradiated fuel rods. More information will be given on the particularities for the loading and unloading sites.

- The return of experience gained during the transport of segments of irradiated fuel rods and identification of specific needs.

- Difficulty regarding the transport of leaking fuel rods. When utilities encounter situations of leaking fuel, it is important to investigate the causes leading to the leak. This requires the transport of leaking fuel rods to laboratories. The difficulty to obtain an approval for the transport of leaking fuel rods will be explained.

- Transport of high burnup fuel rods. The requirement for higher burnup rates in nuclear power plants leads to the need to transport fuel rods with higher burnup. The laboratories need to receive high burnup fuel rods to validate calculation codes. But this validation is needed for the validation of the transport packaging…

1. Introduction

The purpose of this paper is to share the information regarding the transport of irradiated fuel rods, segments of irradiated fuel rods and the difficulties of leaking fuel rods and higher burnup rates in fuel rods.

Until 2011, the transport of full length fuel rods or fuel segments, leaking or not, could be performed using the BG18 transport cask (see Figure 1). Due to the ever increasing demands for packagings to demonstrate compliance with the safety regulations, the older design of the BG18 could no longer guarantee this compliance. The BG18 cask has over 10 years of experience and performed about 40 transport campaigns.

Since 2011, the new R72 transport cask (see Figure 2) is being used as a replacement of the BG18 cask. The R72 packaging is designed for the transport of fuel rods or fuel segments. In this new packaging design the amount of fuel rods transported has been decreased from 30 rods, as for the BG18, to 10 rods. The R72 packaging is owned, designed and constructed by Robatel Industries and managed, operated and maintained by Transnubel. The R72 packaging is also designed but not yet approved for the transport of leaking fuel rods.

Figure 1 – BG18 cask

Figure 2 – R72 cask

2. Return of experience, transport of irradiated fuel rods

Over the years, Transnubel has performed many transports of irradiated fuel rods between research facilities and nuclear power plants in Belgium, Germany, France, Spain, Sweden, Switzerland, etc. For each research facility or power plant, specific constraints, both for the installation itself as for the operational procedures, needed to be taken into account.

Due to the transports performed in the past, Transnubel has acquired a significant experience and knowledge of these facilities. By this way, many particularities could be treated. For instance, the lifting crane may vary which calls for an adapted lifting beam to lift the packaging used for the transport of the fuel rods. Also the loading / unloading zone can have different dimensions which could make it more difficult to load / unload the packaging and ask for specific hoisting equipment or a different size of trailer.

Specific equipment has also been designed for operating the cask, for instance equipment to remove the plug or the basket both in horizontal and vertical positions. A guillotine system has been designed to secure safe working conditions to remove the plug and to guarantee the safe docking of the cask against the hot cell (see Figure 3 and Figure 4).

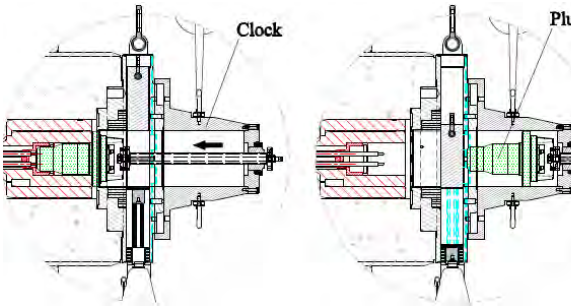

Figure 3 – Principle of guillotine system and clock for plug removal

Figure 4 – Guillotine system and clock for plug removal

A blank test or cold handling is performed by Transnubel at the loading / unloading site when “new” situations occur (other packaging, new site, etc.) to verify and adjust the equipment to perform the loading and unloading operations of the packaging. If necessary, new tools are created and tested.

The R72 packaging is designed to transport the commonly used dimensions of fuel rods. Since the fuel rods that will be transported can also differ in size depending on the loading site,

different baskets are designed to allow these other dimensions. Specific spacers are used to accommodate for different lengths.

For specific loading operations with major dimensional constraints, a Transnubel packaging has been used to act as a lead castle (see Figure 5) to transfer the fuel rods between the loading pool and the transport packaging. For this specific operation, a docking equipment (see Figure 6) was designed to facilitate the transfer of the fuel rods between the lead castle and the transport packaging.

Figure 5 – Packaging serving as lead caste

Figure 6 – Docking of lead castle onto transport packaging

3. Return of experience, transport of irradiated fuel rod segments

Despite the reduced dimensions, the packagings used for the transport of fuel rod segments are subjected to the same issues as those for the transport of irradiated fuel rods. The packaging can be selected depending on the properties of the segments.

For the loading / unloading operations of segments of fuel rods, specific requirements are needed depending on the packaging and the installation. For instance, the docking against the hot cell, the specific basket needed in the packaging or the need to encapsulate the segments which may be required by the safety analysis report of the packaging.

Figure 7 – TNB170

The R72 packaging, as described in paragraph 2, could be used for longer segments of fuel rods if these segments are loaded against a hot cell. A specific spacer has to be foreseen in order to avoid movements of the content during the transport.

For short segments of fuel rods, the TNB170 (see Figure 7) is a promising alternative. The packaging is currently under approval by the authorities and will be available by the end of 2015. Specific equipment has been designed to facilitate the loading and unloading of segments (or other sources) when docked against a hot cell.

A tilting device (see Figure 8) is foreseen to bring the packaging from the vertical to the horizontal position. The docking equipment (see Figure 10) will allow a smooth gliding of the plug when pulled

into the hot cell. In order to have an easy access from inside the hot cell, an extension tool (see Figure 9) is mounted on the plug.

Figure 8 – Tilting device

Figure 9 – Extension tool

Figure 10 – Docking part

4. Difficulty regarding the transport of leaking fuel rods

Most nuclear power plants over the world have been or will be concerned by the presence of leaking irradiated fuel rods in their pool. It is important to understand the reasons of the ruptures or damage in order to be able to take actions and avoid as much as possible the leaking fuel rods in the future. This requires a transport of these leaking fuel rods to specific laboratories for research.

The BG18 packaging was authorized in the past to transport leaking fuel rods but its approval has expired in 2011. The R72 packaging has taken over the transports performed with the BG18. The studies presented in its safety analysis report show that the packaging is able to transport leaking fuel rods, but the certificate of approval does not allow it. At the moment there is no possibility to transport leaking fuel rods as such.

During the preparation of the loaded packaging for transport, the cavity needs to be dried to limit the amount of hydrogen in it. This is done by creating a vacuum to extract the water from the cavity. With leaking fuel rods it could not be fully guaranteed that all water is removed from the fuel rod.

The following two phenomena could occur with leaking fuel rods and explain why the removal of water is not certain:

- Due to the effect of radiation, the pellets inside the fuel rods deform which may result in water trapped inside the fuel rod. One or more pellets deform and could act as a barrier between the hole in the cladding and the remaining water in the rod.
- When a fuel rod cools down after use, an existing hole in the cladding may close during this process. This results also in water trapped inside the fuel rods.

For the approval of leaking fuel rods, a radiolysis analysis is required. This analysis has to demonstrate that the amount of hydrogen remains under 4% (lower explosion limit). The determination of the leak is very difficult and the analysis is practically impossible to carry out because of the deformation of the pellets and the closure of existing holes, especially at nuclear power plants. For these reasons, the amount of hydrogen in the fuel rod could not be shown.

The concern of the authorities deals with the possible presence of water in the packaging during transport. They consider the release of the water out of the fuel rod as possible which could lead to radiolysis and risk of explosion.

5. Transport of high burnup fuel rods

Nuclear power plants ask for higher burnup rates to be able to get more power out of the fuel rods before having to replace them. This demand requires that laboratories need to receive high burnup fuel rods to validate calculation codes. The transport of this high burnup fuel rods however cannot be validated without these calculations.

The currently used calculation codes are validated to a certain limit of burnup for low enriched fuel rods. With these codes it is possible to determine the different characteristics of the irradiated fuel rods such as the thermal power and the isotopic composition. Depending on these characteristics, the operating parameters of the packaging can be determined. These parameters of the packaging are the radiation protection, the thermal analysis and the leak tightness.

With high burnup fuel, more actinides are present in the fuel. This results in lower A_2-values for the content. The leak tightness of the packaging is also more difficult to show because the limit is more restrictive. Both points reduce the total amount or the total activity to be shipped.

The current calculation codes are valid till a certain limit of burnup. To validate calculation codes for higher burnup of low enriched fuel rods, the laboratories need to receive fuel rods with higher burnup. Before a transport of high burnup fuel may be performed however, it needs validation first.

The evolution of the burnup rates in nuclear power plants leads to a need for transport of fuel rods with higher burnup. The European laboratories need to receive such high burnup fuel rods to evaluate the low enriched fuel's behaviour at high burnup and to collect radiological data in order to obtain a sufficient benchmark for the qualification of calculation codes.

To perform the safety studies on packagings intended for the transport of high burnup low enriched irradiated fuel, designers need to describe the content from the radiological point of view, to be loaded in the packaging; calculation codes need to be used out of the range of their validation.

However, the competent authorities in charge of the approval of packagings request the content to be precisely known; the usual way is to make calculations of the isotopes and activities based on of calculation codes, but these codes need to be validated by the authorities. As the validation is not granted for high burnups, long, hard and expensive discussions start about the way used for the characterization of the content and about the justification of safety margins, without possibility of demonstration.

6. Conclusion

The transports of irradiated fuel rods require in most of the situations a case by case analysis of the loading and unloading possibilities, leading to adapted procedures or specific tooling. These kind of transport campaigns remain in any case punctual operations. Due to the important experience gained by Transnubel over the years, different kinds of solutions have been successfully implemented.

For the transport of irradiated fuel rods or segments of irradiated fuel rods, a specific packaging could be used. For full length fuel rods, the cask R72 is most suited. For segments of irradiated fuel rods, the packaging TNB170 is a promising option.

The transport of leaking fuel rods and high burnup fuel remains a challenge regarding the demonstration to the competent authorities, due to the ever increasing demands for packagings to demonstrate compliance with the safety regulations.

RRFM 2015
EUROPEAN RESEARCH REACTOR CONFERENCE

19 April –23 April 2015
Bucharest, Romania

Y-12 NATIONAL SECURITY COMPLEX U-MO FABRICATION

Amy DeMint
Development Technologies
Y-12 National Security Complex
Oak Ridge, TN 37831 USA

Mike Gambrell
Uranium Metalworking Process Engineering
Y-12 National Security Complex
Oak Ridge, TN 37831 USA

Jim Henkel
Nuclear Material Applications
Y-12 National Security Complex
Oak Ridge, TN 37831 USA

Cary Langham
Uranium Metalworking Process Engineering
Y-12 National Security Complex
Oak Ridge, TN 37831 USA

Hollie A. Longmire
Nuclear Material Applications
Y-12 National Security Complex
Oak Ridge, TN 37831 USA

Alan Moore
Uranium Metalworking Process Engineering
Y-12 National Security Complex
Oak Ridge, TN 37831 USA

ABSTRACT

Y-12 National Security Complex (Y-12 NSC) participates in the Fuel Fabrication Capability (FFC) pillar of the U.S. Department of Energy's (DOE) National Nuclear Security Administration (NNSA) Global Threat Reduction Initiative (GTRI) Convert Pillar system. Y-12 NSC is primarily responsible for developing the fabrication process of a low-enriched uranium-molybdenum (LEU-Mo) feedstock. The baseline LEU-Mo fabrication process included a two-step casting process. Y-12 NSC is examining the feasibility of transitioning to a single step casting process. This presentation will focus on the transition strategy and discuss initial results from the feasibility trials.

1. Introduction

Y-12 National Security Complex (Y-12 NSC) participates in the Fuel Fabrication Capability (FFC) pillar of the U.S. Department of Energy's (DOE) National Nuclear Security Administration (NNSA) Global Threat Reduction Initiative (GTRI) Convert Pillar system. Y-12 NSC is primarily responsible for developing the fabrication process of a low-enriched uranium-molybdenum (LEU-Mo) feedstock.

The LEU-Mo Baseline Coupon Fabrication Process is a two-step casting process, as depicted in Figure 1. First, HEU is blended with a diluent and molybdenum in an initial cylindrical casting. The cylindrical casting is sampled and analyzed. Based on the analytical results, the feed is adjusted and recast or the alloy is then broken and recast into a single plate form. The LEU-Mo coupons are fabricated from the plate casting. This process has a large molybdenum distribution range, typically from 8% to 12%, resulting in a higher than desired reject rate. One theory is that the initial casting step has too many process variables in a one unit operation to provide a repeatable and predictable casting. Y-12 NSC is experimenting with an Alternate LEU-Mo Casting Process using a pre-alloyed diluent feedstock, labeled as UMoF, and a multi-plate casting form, as depicted in Figure 2.

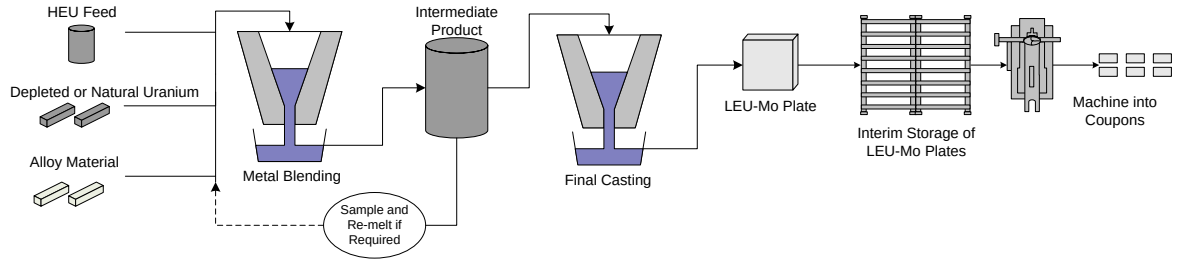

Figure 1: Baseline Coupon Fabrication Process

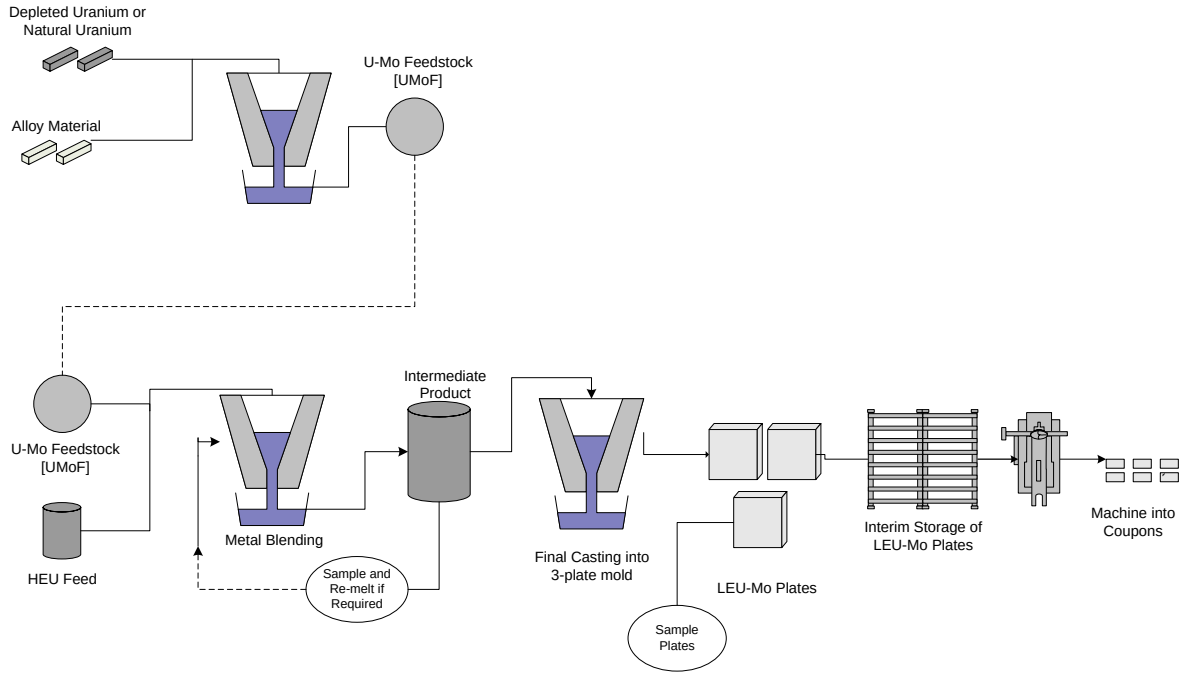

Figure 2: Alternate LEU-Mo Casting Process

Previous trials of the alternate casting process indicated there was a greater control of process parameters by pre-alloying the diluent. The alternate casting process also indicated that the Mo and uranium-235 (U235) distribution throughout the casting were more uniform, indicating a tighter process control of material constituents. In addition to using a pre-alloyed diluent, the alternate casting process indicated that a multi-plate mold could be used to increase material throughput .

In an effort for continuous improvement in both cost reduction and scrap reduction, Y-12 NSC experimented with a Proposed Optimized Casting Process, as shown in Figure 3, based on promising results from the Alternate LEU-Mo Casting Process. A series of castings were performed by eliminating the intermediate cylindrical casting step.

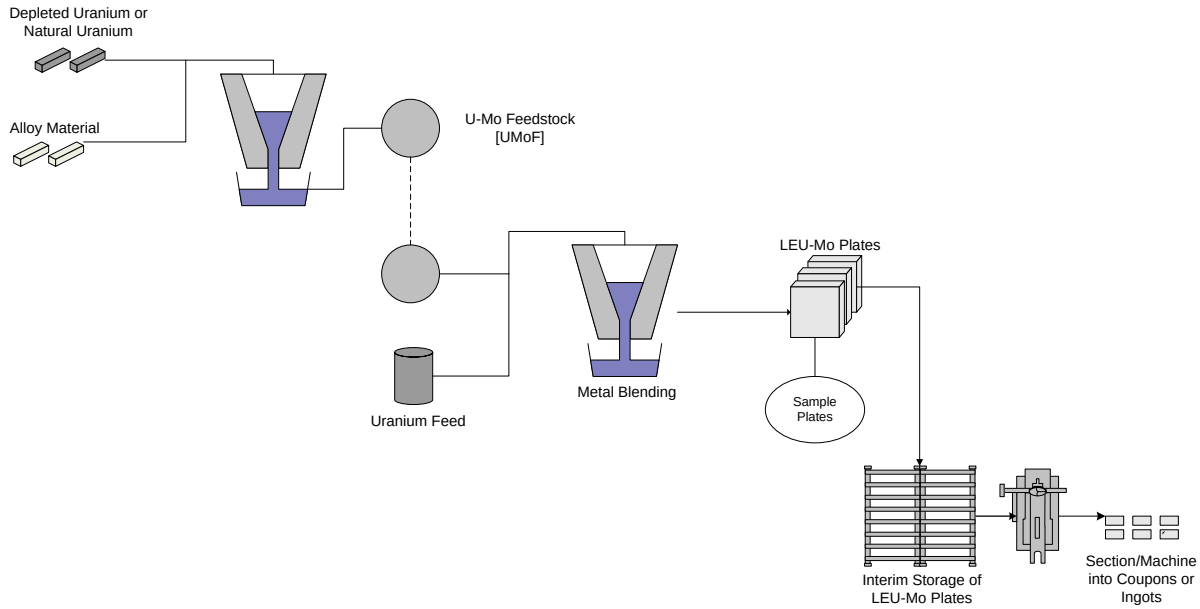

Figure 3: Proposed Optimized Casting Process

2. Description of First Trial Campaign

As part of the trial campaign, Y-12 fabricated DU-Mo plates in accordance with Figure 3. The plates were sectioned and machined into coupons as previously performed in the Baseline Coupon Fabrication Process. The first trial campaign consisted of five castings. A sixth casting was performed to account for fabrication attrition. This trial campaign assumed there was no attrition for cast surface defects. The intent of assuming no attrition was to allow the final fabricator to process all of the coupons and provide feedback to determine if coupon defects lead to foil failures during the fabrication process.

3. Results of First Trial Campaign

Y-12 completed the casting activities as described in Figure 3, which yielded eighteen plates. As the coupons were sectioned from the plates, samples were taken from the milled plate, which is representative of the coupon chemical make-up. Samples were taken from the top, middle and bottom of each plate. The chemical analyses were compared to target. For Molybdenum, the target was 10% ± 1%. For Uranium, the target was 90% ± 1%. Results for the castings are shown in Figures 4-5.

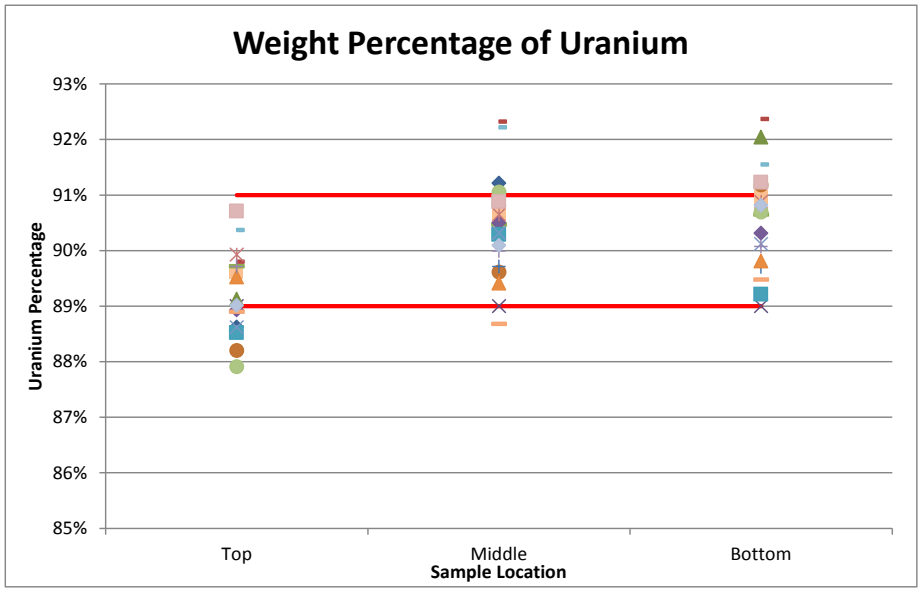

Figure 4: Uranium Weight Percentage Summary

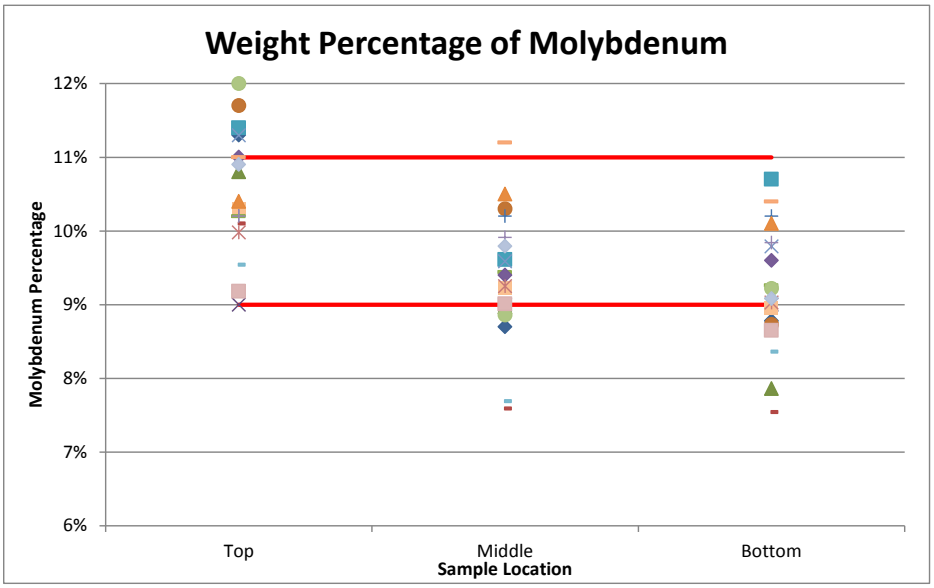

Figure 5: Molybdenum Weight Percentage Summary

The material fabricated in the trial campaign was planned at 10% Molybdenum and 90% Uranium. There were other minor constituents and impurities found in the product. However, as seen in the Figures above, when molybdenum percentages were high, the uranium percentages were lower. On the samples taken, the chemistry was out of the target range 33% of the time. Further analyses indicate that the early castings, performed in August 2013, were out of the target range 44% of the time. The last castings, performed in December 2013, were out of the target range 28% of the time. The decrease may be indicative of proficiency gained in the new process. Since this is the first time the single step casting was tested, achieving the target values for major constituents in over 65% of the trial campaign is promising. This indicates that the single step casting process is viable and may improve with process adjustments.

4. Description of Second Trial Campaign

Y-12 completed a second campaign of casting activities as described in Figure 3. This campaign consisted of nine castings. One casting was discarded, due to a mispour. The remaining castings yielded twenty-four plates. This second campaign included one additional process change. Instead of machining coupons as shown in Figure 6, the process was optimized to reduce scrap and increase material utilization. In an effort to distinguish the final products, the new product was labeled as ingots, as shown in Figure 7.

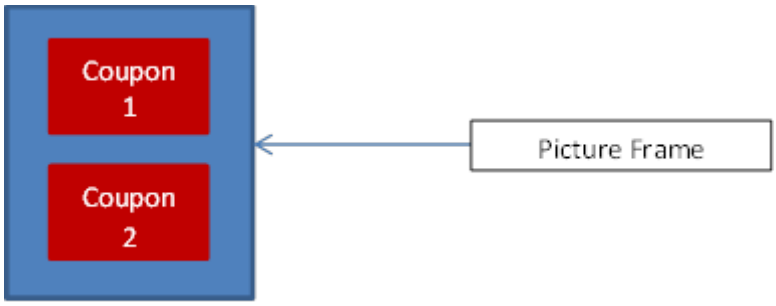

Figure 6: Baseline Machining Process

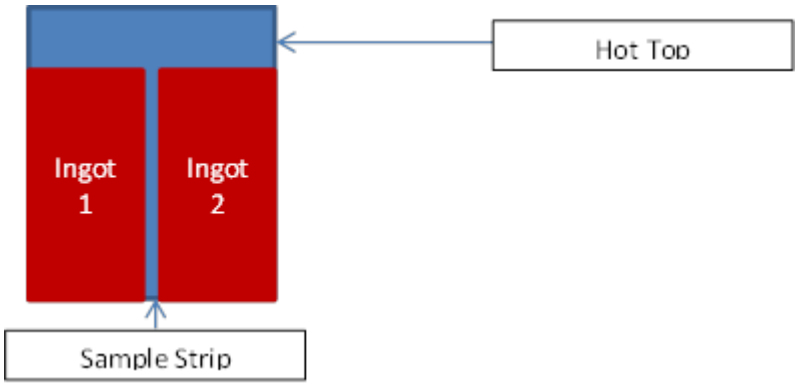

Figure 7: Optimized Machining Process

The twenty four plates were divided into two equal groups of twelve plates. One group of twelve plates (24 ingots) would have skimmed surface (i.e. minimal machining). The second group of twelve plates (24 ingots) would have an as-cast surface (i.e. no machining).

5. Results of Second Trial Campaign

As the DU-Mo ingots were sectioned from the plates, samples were taken, which is representative of the ingot chemical make-up. Samples were taken from the top, middle and bottom of each plate. The chemical analyses were compared to the target specification. For Molybdenum, the target was 10% ± 1%. For Uranium, the target was 90% ± 1%. Results for the castings are shown in Figures 8-9.

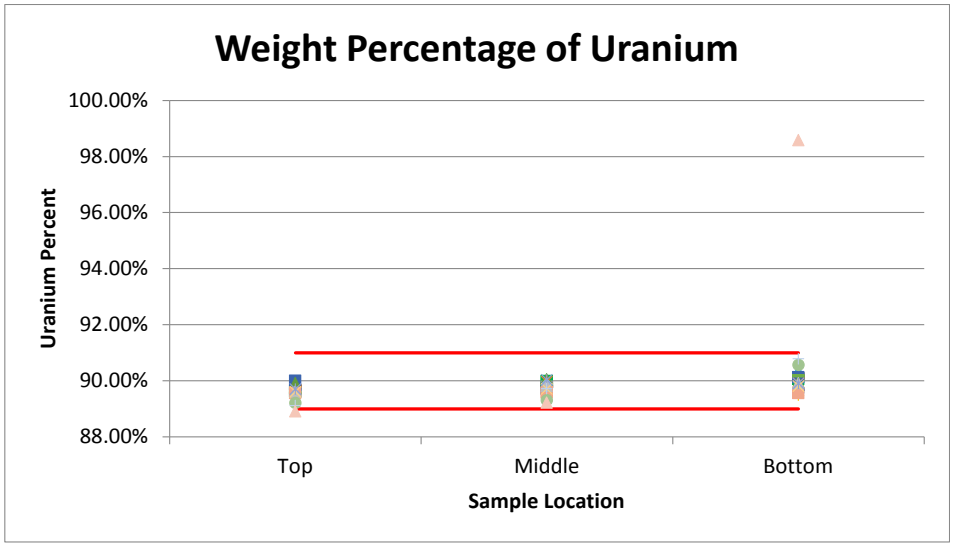

Figure 8: Uranium Weight Percentage Summary

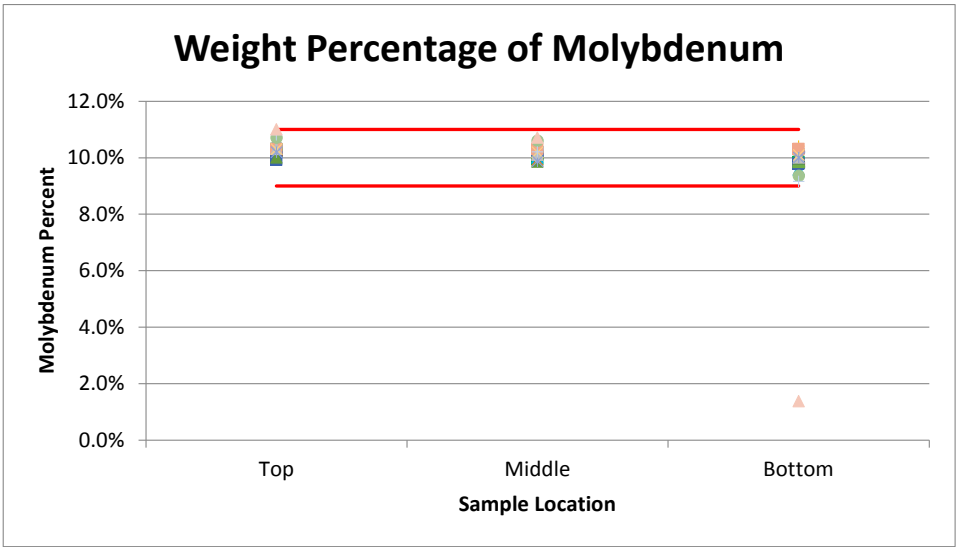

Figure 9: Molybdenum Weight Percentage Summary

The material fabricated in the trial campaign was planned at 10% molybdenum and 90% uranium. As expected, there were other minor constituents and impurities found in the product. However, as seen in the Figures above, the uranium and molybdenum were within specification in all but one sample location which indicates a casting anomaly. Further reviews are being performed on this casting data. However, the chemical analyses results from the second trial campaign further justify the feasibility of the single step casting process.

6. Summary

Y-12 NSC fabricated DU-Mo coupons and ingots using a pre-alloy diluent feedstock and a single step casting process. The trial campaigns also included a multi-plate mold. Based on the chemical analyses results, the single step casting process is a viable process. In the first trial campaign, the chemistry analysis was outside of the target 33% of the time. However, in the second trial, the chemistry analysis indicated only one sample was outside of the target, which is only 4% of the total sample population. Proficiencies were gained and the process was optimized between the first and second trials. The coupons and ingots will be processed at a commercial fuel fabrication vendor. The DU-Mo coupons and ingots will be used to prove-in the fuel fabrication equipment. Data from the fuel fabricator will provide valuable feedback to the front end casting process.

European Nuclear Society
Avenue des Arts 56
1000 Brussels, Belgium
Telephone: +32 2 505 30 50 - FAX: +32 2 502 39 02
rrfm2015@euronuclear.org
www.rrfm2015.org